

71N29405

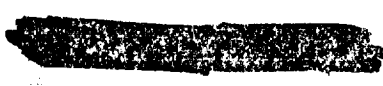
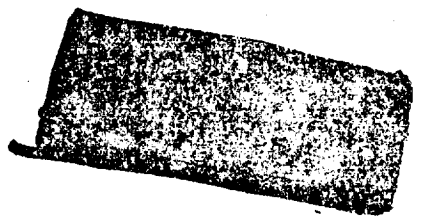


CASE FILE COPY

Declassified by authority of NASA
Classification Change Notices No. 182
Dated *~~11/30/69~~
11/30/69

[Faint, mostly illegible text, possibly bleed-through from the reverse side of the page]

[U]



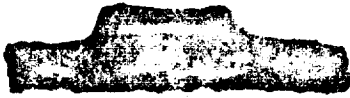
**DESIGN OF
LIQUID PROPELLANT
ROCKET ENGINES**



Dieter K. Huzel and David H. Huang
Rocketdyne Division, North American Aviation, Inc.



Scientific and Technical Information Division
OFFICE OF TECHNOLOGY UTILIZATION
NATIONAL AERONAUTICS AND SPACE ADMINISTRATION
1967
Washington, D.C.



CONFIDENTIAL

FOREWORD

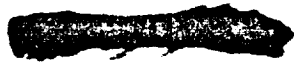
Success in space demands perfection. Many of the brilliant achievements made in this vast, austere environment seem almost miraculous. Behind each apparent miracle, however, stands the flawless performance of numerous highly complex systems. All are important. The failure of only one portion of a launch vehicle or spacecraft may cause failure of an entire mission. But the first to feel this awesome imperative for perfection are the propulsion systems, especially the engines. Unless they operate flawlessly first, none of the other systems will get a chance to perform in space.

Perfection begins in the design of space hardware. This book emphasizes quality and reliability in the design of propulsion and engine systems. It draws deeply from the vast know-how and experience which have been the essence of several well-designed, reliable systems of the past and present. And, with a thoroughness and completeness not previously available, it tells how the present high state of reliability, gained through years of research and testing, can be maintained, and perhaps improved, in engines of the future.

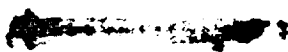
As man ventures deeper into space to explore the planets, the search for perfection in the design of propulsion systems will continue. This book will aid materially in achieving this goal.

WERNHER VON BRAUN
Director
Marshall Space Flight Center, NASA

CONFIDENTIAL



• •





PREFACE

This book intends to build a bridge for the student and the young engineer: to link the rocket propulsion fundamentals and elements (which are well covered in the literature) with the actual rocket engine design and development work as it is carried out in industry (which is very little, if at all covered in literature). The book attempts to further the understanding of the realistic application of liquid rocket propulsion theories, and to help avoid or at least reduce time and money consuming errors and disappointments. In so doing, it also attempts to digest and consolidate numerous closely related subjects, hitherto often treated as separate, bringing them up to date at the same time.

The book was written "on the job" for use by those active in all phases of engine systems design, development, and application, in industry as well as government agencies. Since it addresses itself to human beings set out to create new machines, rather than describing machines about to dominate man, the language chosen may not always be "functional" in the strict sense of the word.

The book presents sufficient detail to familiarize and educate thoroughly those responsible for various aspects of liquid propellant rocketry, including engine systems design, engine development, and flight vehicle application. It should enable the rocket engineer to conduct, independently, complete or partial engine systems preliminary detail designs and to understand and judge the activities in, and the problems, limitations, and "facts of life" of the various subsystems making up a complete engine system. It also attempts to educate those ultimately interested in specialized subsystems and component design (thrust chamber, turbopump, control valves, etc.) about their own as well as neighboring subsystems and about the complete engine system. This should enable the student to prepare realistic analytical calculations and design layouts with a long headstart toward the final specialized designs for subsystem production release.

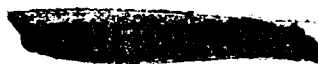
Special emphasis has been placed on engine flight application to stimulate engine systems and subsystem designers to think in these terms from the outset. The book is intended as a textbook, with specific consideration of the teacher without industry experience. We hope it will stimulate those desiring to specialize in the area of a rocket engine subsystem by supplying adequate information to enable them to benefit fully from the specialized literature. Thus it provides a realistic expert introduction for those joining the liquid propellant rocket engine field.

We gratefully acknowledge the most valuable assistance by members of the Rocketdyne and the Space Divisions of North American Aviation, Inc., Los Angeles. We are particularly indebted to R. E. Grate, C. A. MacGregor, H. M. Alexander, S. B. Macaluso and T. Holwager of Rocketdyne Division, and to R. E. G. Epple, R. W. Westrup, R. D. Hammond, and D. A. Engels of Space Division, who reviewed the various chapters of the manuscript and contributed valuable ideas.

Special recognition goes to R. F. Strauss of Astrosystems International, New Jersey, who inspired the manuscript and rendered valuable assistance during the various phases of its preparation.

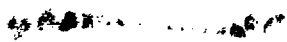
In particular, the authors are indebted to the manifold support they received from North American Aviation, Inc., and its divisions. Rocketdyne's engine technology has provided a major foundation for the book.

Dieter K. Huzel
David H. Huang





-



CONTENTS

Chapter I. INTRODUCTION TO LIQUID PROPELLANT ROCKET ENGINES	
1.1 The Generation of Thrust by a Rocket Engine	1
1.2 The Gas-Flow Processes in the Combustion Chamber and the Nozzle	4
1.3 Performance Parameters of a Liquid Propellant Rocket Engine	10
1.4 Liquid Rocket Propellants	18
1.5 The Basic Elements of a Liquid Propellant Rocket Engine System	21
Chapter II. ROCKET ENGINE DESIGN IMPLEMENTS	
2.1 The Major Rocket Engine Design Parameters	31
2.2 The Importance of Design Quality	50
2.3 Systems Analysis and Design Layout	51
2.4 Stress Analysis	56
2.5 Selection of Materials	59
Chapter III. INTRODUCTION TO SAMPLE CALCULATIONS	
3.1 Approach	63
3.2 A-1 Stage Engine	64
3.3 A-2 Stage Engine	68
3.4 A-3 Stage Engine	72
3.5 A-4 Stage Engine	74
Chapter IV. DESIGN OF THRUST CHAMBERS AND OTHER COMBUSTION DEVICES	
4.1 The Basic Thrust Chamber Elements	81
4.2 Thrust Chamber Performance Parameters	83
4.3 Thrust Chamber Configuration Layout	86
4.4 Thrust Chamber Cooling	98
4.5 Injector Design	121
4.6 Gas-Generating Devices	131
4.7 Ignition Devices	136
4.8 Combustion Instability	143
Chapter V. DESIGN OF PRESSURIZED-GAS PROPELLANT-FEED SYSTEMS	
5.1 Determination of Pressurant Requirements	151
5.2 Stored Gas Systems	156
5.3 Propellant Evaporation Systems	165
5.4 Systems Evaporating Nonpropellants	167
5.5 Systems Using Products of Chemical Reactions	167
5.6 Selection of the Pressurization System	173



	Page
Chapter VI. DESIGN OF TURBOPUMP PROPELLANT-FEED SYSTEMS	
6.1 Elements of Turbopump Propellant Feed Systems	176
6.2 Turbopump System Performance and Design Parameters	186
6.3 Design of Centrifugal Pumps	204
6.4 Design of Axial-Flow Pumps	225
6.5 Design of Turbines	238
6.6 Design of Turbopump Bearings, Seals, and Gears	257
6.7 Design Layout of Turbopump Assemblies	261
Chapter VII. DESIGN OF CONTROLS AND VALVES	
7.1 Control Methods	263
7.2 Basic Liquid Propellant Rocket Engine Control Systems	265
7.3 Engine Thrust Level Control	267
7.4 Propellant-Mixture-Ratio and Propellant-Utilization Control	268
7.5 Thrust-Vector Control	272
7.6 Design Considerations for Fluid-Flow Control Components	280
7.7 Design of Dynamic Seals for Fluid-Flow-Control Components	289
7.8 Design of Propellant Valves	294
7.9 Design of Control Pilot Valves	301
7.10 Design of Fixed-Area-Type Regulating Devices	307
7.11 Design of Servovalves	309
7.12 Design of Gas Pressure Regulators	315
7.13 Design of Liquid Flow and Pressure Regulators	321
7.14 Design of Pressure Relief Valves	322
7.15 Design of Miscellaneous Valves	325
Chapter VIII. DESIGN OF PROPELLANT TANKS	
8.1 Basic Design Configurations of Propellant Tanks	329
8.2 General Design Considerations for Propellant Tanks	332
8.3 Structural Design of Propellant Tanks	336
8.4 Design of Storable Liquid Propellant Tanks	343
8.5 Design of Cryogenic Liquid Propellant Tanks and Their Insulation	345
8.6 Design of Fiber-Glass Filament-Wound Liquid Propellant Tanks	348
8.7 Design of Propellant Tank Pressurant Diffusers	349
8.8 Propellant Expulsion Under Zero Gravity or Oscillatory G-Loading Conditions	349
Chapter IX. DESIGN OF INTERCONNECTING COMPONENTS AND MOUNTS	
9.1 The Principal Interconnecting Components and Mounts	353
9.2 Design of Tubings and Tube Fittings	358
9.3 Design of Flange Joints	360
9.4 Design of Brazed Joints for Rocket Engines	370
9.5 Design of Ducts for Rocket Engines	372
9.6 Design of Gimbal Mounts	379
Chapter X. ENGINE SYSTEMS DESIGN INTEGRATION	
10.1 Systems Engineering	383
10.2 Engine System Design Integration by Dynamic Analyses	384
10.3 Design Integration for Engine System Calibration	390
10.4 Engine System Integrated Performance Characteristics	394
10.5 Mechanical Integration of Engine Systems	399
10.6 Electrical System	403



CONTENTS

ix

	Page
10.7 Engine Instrumentation-----	411
10.8 Clustering of Liquid Propellant Rocket Engines-----	415
10.9 Engine-to-Vehicle Interface-----	419
Chapter XI. DESIGN OF LIQUID PROPELLANT SPACE ENGINES	
11.1 Principal Space Engine Applications-----	429
11.2 General Design Considerations-----	430
11.3 Design of Spacecraft Main Propulsion Systems-----	435
11.4 Design of Reaction Control Engine Systems-----	442
INDEX -----	451

1948

1948

Chapter I

Introduction To Liquid Propellant Rocket Engines

In order that the reader may better understand the basic laws and the operation of liquid propellant rocket engine systems, a brief review of the fundamentals is presented.

Combining these two fundamental relations, we obtain

$$F = \frac{m}{t} v \quad (1-3)$$

1.1 THE GENERATION OF THRUST BY A ROCKET ENGINE

The function of a chemical rocket engine system is to generate thrust through combustion; i.e., release of thermal energy derived from the chemical energy of the propellants. The generated force (pressure) imparts a momentum to the combustion products. In accordance with the basic laws of motion, a momentum in the opposite direction is also imparted to the vehicle. In practice, high temperature, high-pressure gases are produced in combustion chambers through chemical reactions of either solid or liquid propellants. These gases are ejected through a nozzle at high velocity. The operation of a rocket engine system is independent of its environment except for slight effects on performance caused by ambient air pressure. The rocket or, in a more general sense, the "reaction motor" presently is the only practical device able to propel a vehicle in space.

Let us examine briefly the process of thrust generation and summarize the most frequently used laws and formulae needed to design the shape and to predict the behavior of a rocket engine. These laws are mere adaptations of basic physical laws. We know that

$$F = ma \quad (1-1)$$

Force equals mass times acceleration. We also know that the velocity increase experienced by the accelerated mass, during the time the force is imparted, is

$$v = at \quad (1-2)$$

This expression, known as the momentum theorem, is the basic thrust equation for rocket engines. When applied to rocket engines, the term for mass, m , and the term for velocity, v , may apply either to the vehicle or to the ejected gases. The products of v and m , in opposite directions, must be equal, as prescribed by the law of action and reaction. This condition exists even in a "tiedown" static rocket firing. In this case, however, the "vehicle mass" (the earth) is so large that reaction effects are undetectable.

The vehicle designer is primarily interested in the utilization of the engine thrust available for the acceleration of the vehicle, which at any point of the trajectory may be expressed as

$$F = W_m \frac{v}{t} = W_m a \quad (1-3a)$$

The vehicle designer uses this equation for vehicle design and trajectory calculations, properly considering that thrust F and vehicle mass W_m change during flight.

In contrast, the engine designer and builder is primarily concerned with the *generation* of thrust. His attention, therefore, is focused on the efficient conversion of the chemical energy of the propellants into thermal energy, and thus into kinetic energy of the gaseous combustion products. His particular concern is to do this in the most efficient way. For the designer, the basic equation (1-3) may be rewritten as

$$\Sigma F = \frac{m}{t} v_e = \dot{m} v_e \quad (1-3b)$$

where \dot{m} is the mass flow rate of the gases, and v_e is their velocity at the nozzle exit. Even in

this simple form, it becomes clear that, for a given mass flow rate, thrust will increase with increased gas velocities obtained.

It should be remembered that the vehicle, in particular the thrust chamber of the engine, is also subject to the pressure environment, which is a function of altitude. Equation (1-3b) states that if a mass is flowing out of a container, the sum of all internal and external forces acting on all surfaces of this container is equal to the total momentum flowing out of the surface. The liquid propellant rocket thrust chamber, with the inclusion of the exit plane, is such a container (fig. 1-1).

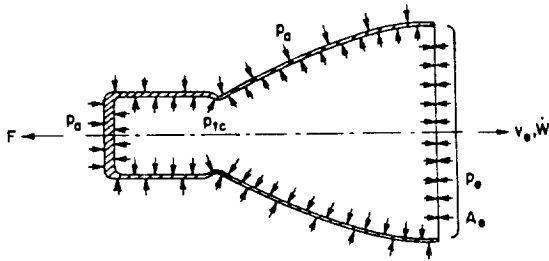


Figure 1-1

Let us first assume that the chamber is operated at an ambient pressure $P_a = 0$ (high-altitude condition). Then, the net force acting on the gas in the chamber is the sum of the reactions from the chamber walls and of the reaction of the absolute gas pressure at the exit. These two reaction forces are opposed (fig. 1-1). According to the momentum theorem, the net force on the gas must be equal to the momentum flux out of the chamber:

$$\int_{A_{tc}}^0 P_{tc} dA - A_e p_e = \frac{\dot{W}}{g} v_e$$

The integral describes that force F (lb) which acts on the thrust chamber and thus on the vehicle. We can write:

$$F - A_e p_e = \frac{\dot{W}}{g} v_e \quad (1-4)$$

or

$$F = \frac{\dot{W}}{g} v_e + A_e p_e \quad (1-5)$$

where p_e (lb/in² or psia) is the static absolute gas pressure in the exit plane A_e (in²). The equation assumes that the injection flow velocity of the propellants can be neglected and that the flow of gases through the exit plane is one-dimensional; i.e., that all molecules of the gas move on parallel lines. The expression $\frac{\dot{W}}{g} v_e$

is often referred to as the momentum thrust, and $A_e p_e$ as the pressure thrust. The pressure thrust is not a desirable form of thrust generation in rocketry. The presence of the term $A_e p_e$ indicates that not all of the pressure forces available have been converted into gas kinetic energy inside the chamber nozzle. In other words, a portion of the gas pressure generated by the release of chemical energy has not been used for the generation of gas momentum. It is the specific function of the thrust chamber nozzle to convert, at maximum efficiency, the available chamber pressure into gas momentum, and thus obtain maximum thrust for a given propellant flow rate.

We now assume that the rocket is operated at a finite ambient pressure $p_a > 0$ (lb/in²) (low-altitude condition). The resulting pressure forces acting on the outside of the chamber walls have no effect on the gas on the inside. However, these pressure forces cancel part of the pressure thrust by an amount $A_e p_a$. Since gases are flowing with supersonic velocity in the exit plane A_e , the ambient pressure p_a does not have access to it. The ambient pressure p_a thus creates a net unbalanced force onto the projected thrust chamber area (opposing the thrust) of magnitude $A_e p_a$. Including this term in equation (1-5), the general rocket thrust equation is obtained:

$$F = \frac{\dot{W}}{g} v_e + A_e (p_e - p_a) \quad (1-6)$$

The following model may extend the understanding of the nature of the terms which compose equation (1-6). Let us assume we have a movable cylinder (representing the thrust chamber and vehicle mass), a spring (representing gas pressure), a piston (representing the gas mass), and a stationary rack (representing ambient conditions) (fig. 1-2).

CONFIDENTIAL

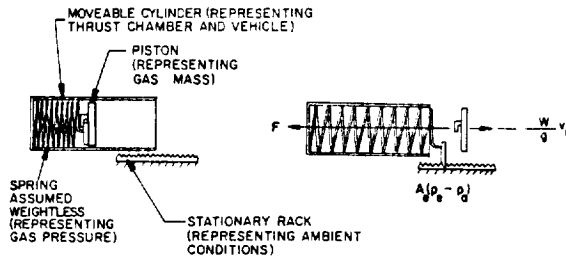


Figure 1-2

The spring is so made that its end slips sideways upon reaching the end of the cylinder and engages the stationary rack. The cylinder is suspended in a suitable manner to move freely.

When releasing the spring force (“ p_c ”), the “gas” is expelled to the rear. If, upon reaching the chamber exit, some spring force remains, the spring engages the rack and continues to act upon the cylinder, but ceases to act upon the “gas.” We find that the model works for all cases: underexpanded (as assumed above, where spring free length is longer than cylinder length); overexpanded (spring free length is less than cylinder length and the spring force is exhausted prior to the “gas” reaching the exit, the “gas” therefore being subject to deceleration within the cylinder); and ideal expansion (where spring free length equals cylinder length).

The model can also illustrate the case of the overexpanded nozzle without jet separation, which will be further explained below. This situation is equivalent to that of the inertia of piston (“gas”) and spring pulling the spring beyond its null point. The negative-loaded spring, in engaging the rack (“ambient”), will pull the cylinder backward.

Equation (1-6) is often expressed as

$$F = c \frac{\dot{W}}{g} \quad (1-7)$$

Where c is defined as the effective exhaust velocity (ft/sec) and comprises

$$c = v_e + A_e(p_e - p_a) (g/\dot{W}) \quad (1-8)$$

The effective exhaust velocity is not the actual gas velocity except when $p_e = p_a$ where c becomes equal to v_e . As explained with equation (1-6), the presence of a term $A_e(p_e - p_a)$

(g/\dot{W}) indicates that optimum v_e has not been obtained.

Sample Calculation (1-1)

The following data are given for a liquid propellant rocket engine: thrust, $F = 100\,000$ lb at sea level; propellant consumption rate, $\dot{W} = 369.3$ lb/sec; thrust chamber exit area, $A_e = 760.8$ in²; gas exit static pressure, $p_e = 10.7$ psia; ambient pressure, $p_a = 14.7$ psia (sea level); gravitational constant, $g = 32.2$ ft/sec².

From what we have just learned, we will determine (a) gas exhaust velocity, (b) engine thrust in space, and (c) the effective exhaust velocities at sea level and in space.

Solution

(a) From equation (1-6) the gas exhaust velocity

$$\begin{aligned} v_e &= [F - A_e(p_e - p_a)](g/\dot{W}) \\ &= [100\,000 - 760.8(10.7 - 14.7)](32.2/369.3) \\ &= 9040 \text{ ft/sec} \end{aligned}$$

Our calculation assumes a nozzle somewhat too long for sea-level conditions, as indicated by the fact that p_e is smaller than p_a ; a pressure “undershoot” and an exhaust velocity “overshoot” occurred. If no jet separation occurred, i.e., if the nozzle remained “filled” to the exit plane, the calculation is valid. The “penalty” of incorrect nozzle length simply appears as the negative thrust term $A_e(p_e - p_a)$. If jet separation does occur within the nozzle, or if it is combined with decelerating shock waves, the situation becomes considerably more complicated and requires elaborate mathematical treatment. However, there should be no concern at this point.

(b) From equation (1-6), we know that the difference in thrust between space and sea level is $A_e p_a$. Since the nozzle selected was too long at sea level, this thrust increase $A_e p_a$ during rocket ascent will be obtained in two distinct steps. First, by reduction of the negative thrust term $A_e(p_e - p_a)$ to zero. This will occur when $p_e = p_a$; that is, when the rising vehicle reaches an altitude where $p_a = 10.7$ psia, in our specific case. As we have learned, this represents ideal expansion. As the vehicle continues to ascend farther

and eventually reaches "empty space" where $p_a = 0$, the increase of the positive term $A_e(p_e - p_a)$ raises the thrust level farther. The combined effect of the two phases, however, is simply the elimination of $p_a A_e$, provided the nozzle is filled at all times.

Thus, we obtain engine thrust in space:

$$F = 100\,000 + 760.8 \times 14.7 = 111\,183.8 \text{ lb}$$

(c) From equation (1-8) the effective exhaust velocity at sea level results

$$\begin{aligned} c &= v_e + A_e(p_e - p_a)(g/\dot{W}) \\ &= 9040 + 760.8 \times (10.7 - 14.7) \times (32.2/369.3) \\ &= 8772 \text{ ft/sec} \end{aligned}$$

and in space

$$\begin{aligned} c &= v_e + A_e p_e (g/\dot{W}) \\ &= 9040 + 760.8 \times 10.7 \times (32.2/369.3) \\ &= 9750 \text{ ft/sec} \end{aligned}$$

1.2 THE GAS-FLOW PROCESSES IN THE COMBUSTION CHAMBER AND THE NOZZLE

Since the analytical treatment of compressible fluids flowing through cylindrical ducts and nozzles can be found in standard aerodynamics and thermodynamics textbooks, no attempt will be made here to derive basic equations governing gas flows. Rather, significant applications of those equations used in actual rocket design are presented.

The parameters and terms applicable to gas flows in a liquid propellant rocket thrust chamber are shown in figure 1-3 and table 1-1. These parameters serve to define the characteristics of gas flow at various points within the thrust chamber. Gas-flow calculations for rocket thrust-chamber design usually assume the following ideal conditions:

- (1) Homogeneous gas composition
- (2) Perfect gas
- (3) No heat transfer through the motor walls in either direction; i.e., adiabatic processes. If no increase in entropy occurs, i.e., if the process is considered revers-

ible, it is additionally called an isentropic process.

- (4) No friction
- (5) Steady flow rate
- (6) One-dimensional flow (all gas molecules move on parallel lines)
- (7) Velocity uniformity across any section normal to chamber axis
- (8) Chemical equilibrium established within the combustion chamber and not shifting in the nozzle.

Certain correction factors, usually empirically obtained, will be applied to the results derived from these ideal assumptions in the actual design of a rocket and for the prediction of its behavior.

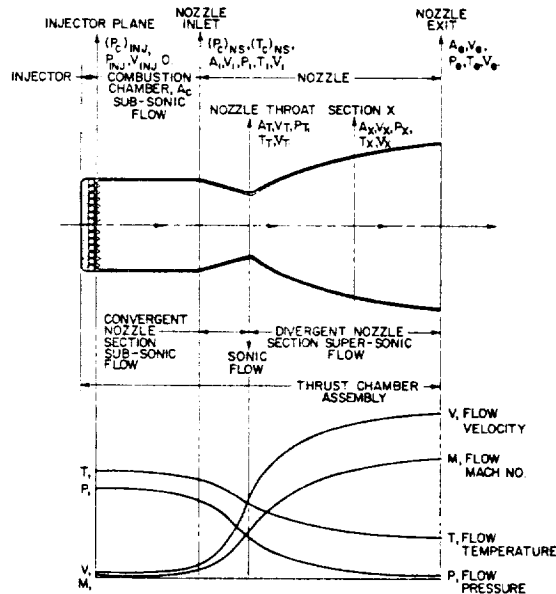


Figure 1-3.—Gas flow within liquid propellant rocket thrust chamber.

The Perfect Gas Law

At any section X the perfect gas law states:

$$144 p_x V_x = R T_x \quad (1-9)$$

The Principle of Conservation of Energy

In an adiabatic process, the increase in kinetic energy of the flowing gases between any two points is equal to the decrease in enthalpy.

CONFIDENTIAL

TABLE 1-1.—Terms Used in the Calculation of Gas Flows

a_c, a_t	Local velocity of sound in chamber and at nozzle throat (ft/sec); ($a_t = \sqrt{\gamma RT_t}$).
A_c	Cylindrical cross-sectional area of chamber (in ²).
A_i, A_t, A_e, A_x	Flow areas at nozzle inlet, throat and exit; and at any section X normal to axis (in ²).
C_p, C_v	Specific heats for constant pressure and for constant volume (Btu/lb° F).
g	Gravitational constant (32.2 ft/sec ² at sea level).
J	Energy conversion factor (778 ft-lb/Btu).
M_c, M_i, M_t, M_e, M_x	Flow Mach number (v/a) at chamber; nozzle inlet, throat and exit; and at any section X normal to axis.
\bar{M}	Molecular weight of combustion products.
$(p_c)_{inj}$	Chamber total pressure at injector end (lb/in ²). Because of the relatively low propellant injection flow velocities v_{inj} , the measurable static pressure at this station is generally treated as equivalent to the total pressure.
$(p_c)_{ns}$	Nozzle stagnation pressure or chamber total pressure at nozzle inlet (lb/in ²); ($(p_c)_{ns} = p_i [1 + \frac{1}{2}(\gamma - 1)M_i^2]^{\gamma/(\gamma - 1)}$).
P_i, P_t, P_e, P_x	Flow static pressures at nozzle inlet, throat and exit; and at any section X normal to axis (lb/in ²).
R	Gas constant (1544/ \bar{M}) (ft/°R)
$(T_c)_{ns}$	Nozzle stagnation temperature or chamber total temperature (°R). ($(T_c)_{ns} = T_i [1 + \frac{1}{2}(\gamma - 1)M_i^2]$)
T_i, T_t, T_e, T_x	Flow temperature at nozzle inlet, throat, and exit; and at any section normal to axis (°R).
v_{inj}	Injector flow velocity = 0 (by assumption).
v_i, v_t, v_e, v_x	Flow velocities at nozzle inlet, throat, and exit; and at any section X normal to axis (ft/sec).
V_i, V_t, V_e, V_x	Flow specific volumes at nozzle inlet, throat, exit; and at any section X normal to axis (ft ³ /lb).
\dot{W}	Steady weight flow rate (lb/sec).
ϵ	Nozzle expansion area ratio (A_e/A_t).
ϵ_c	Nozzle contraction area ratio (A_c/A_t).
γ	Specific heat ratio (C_p/C_v).

Applied to a nozzle, this yields for unit weight of gas flowing

$$\frac{1}{2gJ}(v_x^2 - v_i^2) = C_p(T_i - T_x) \quad (1-10)$$

The Principle of Conservation of Matter

$$\dot{W} = \frac{A_i v_i}{144 V_i} = \frac{A_x v_x}{144 V_x} = \text{constant} \quad (1-11)$$

The Isentropic Flow Process

For any isentropic flow process the following relations hold between any two points:

$$p_i V_i^\gamma = p_x V_x^\gamma = \text{constant} \quad (1-12)$$

and

$$T_i/T_x = (p_i/p_x)^{(y-1)/\gamma} = (V_x/V_i)^{\gamma-1} \quad (1-13)$$

Gas Flow Through Liquid Propellant Rocket Combustion Chambers

The function of a liquid rocket combustion chamber is to convert propellants into high-temperature, high-pressure gas through combustion which releases the chemical energy of the propellant, resulting in an increase of internal energy of the gas. Combustion chambers are generally tubular, as shown in figure 1-3. The liquid propellants are injected at the injection plane with a small axial velocity which is assumed to be zero in gas-flow calculation. The combustion process proceeds throughout the length of the chamber and is assumed to be completed at the nozzle inlet. As heat is liberated between injection plane and nozzle inlet, the specific volume of the gas is increased. To satisfy the conditions of constant mass flow, the gas must be accelerated toward the nozzle inlet with some drop of pressure. In brief, the following takes place:

The gas-flow process within the combustion chamber, that is, within the volume upstream of the nozzle entrance, is not entirely isentropic but is a partly irreversible, adiabatic expansion. Although the stagnation temperature or total temperature remains constant, the stagnation pressure or total pressure will decrease. This causes permanent energy losses, which are a function of the gas properties as expressed by γ , and of the nozzle contraction area ratio ϵ_c or (A_c/A_t). Wherever the acceleration of gases is largely effected by expansion due to heat release, rather than by a change of area as in a nozzle, the stated losses occur. The greater the

contribution of the nozzle, the more efficient is the gas acceleration. Conversely, with no nozzle attached, the losses are maximum. The great importance of ϵ_c to the thrust chamber design becomes apparent. It will be discussed further in chapter IV.

Figure 1-4 shows the loss of total pressure for two typical γ values as a function of the nozzle contraction area ratio ϵ_c . These data are generally used in rocket design, and are calculated from the Rayleigh flow process.

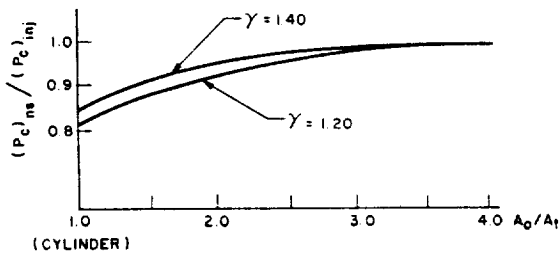


Figure 1-4

Neglecting the flow velocity at the injecting end, i.e., assuming $v_{inj} = 0$ and $(p_c)_{inj} = p_{inj}$, the total pressure ratio $(p_c)_{inj} / (p_c)_{ns}$ can also be expressed in terms of flow Mach number M_i at the nozzle inlet and of the specific heat ratio γ :

$$(p_c)_{inj} / (p_c)_{ns} = \frac{(1 + \gamma M_i^2)}{(1 + \frac{\gamma - 1}{2} M_i^2)^{\gamma / (\gamma - 1)}} \quad (1-14)$$

For the reasons mentioned above, it is desirable that the Mach number at the nozzle entrance be small. A typical value for a thrust chamber with a contraction area ratio of $A_c / A_t = 2$ is $M_i = 0.31$ ($\gamma = 1.2$). For the static pressure ratio, the expression simplifies to

$$p_{inj} / p_i = 1 + \gamma M_i^2 \quad (1-15)$$

Gas Flow Through Rocket Nozzles

The prime function of a rocket nozzle is to convert efficiently the enthalpy of the combustion gases into kinetic energy and thus high gas exhaust velocity. The nozzle is the most efficient device for accelerating gases to supersonic velocities. Rocket nozzles are conventionally

of the converging-diverging De Laval type, with the cross-sectional area decreasing to a minimum at the throat and then increasing to the exit area, as shown in figure 1-3. The flow velocity through a nozzle increases to sonic velocity at the throat and then increases further supersonically in the diverging section.

In practice it is assumed that the gas flow through a rocket nozzle is an isentropic expansion process, and that both the total temperature and the total pressure remain constant throughout the nozzle. The pressure ratio $p_t / (p_c)_{ns}$ between throat and chamber is called the critical pressure ratio and is solely a function of specific heat ratio

$$p_t / (p_c)_{ns} = [2 / (\gamma + 1)]^{\gamma / (\gamma - 1)} \quad (1-16)$$

The static pressure p_t at a nozzle throat with sonic flow, where the maximum weight flow per unit area occurs, is defined as critical pressure. The velocity of sound is equal to the velocity of propagation of a pressure wave within a medium. It is, therefore, impossible for a pressure disturbance downstream of the nozzle throat to influence the flow at the throat or upstream of the throat, provided that this disturbance will not create a higher throat pressure than the critical pressure.

It is one of the characteristic features of an attached diverging or De Laval nozzle, however, that sonic velocity in the nozzle throat is maintained even if the back pressure (ambient pressure) at the nozzle exit is greater than the pressure required at the throat for sonic velocity. As a result, a pressure adjustment (recovery) must take place between the throat and the nozzle exit (ambient pressure). This adjustment may take place through subsonic deceleration (isentropic), or by way of nonisentropic discontinuities called shock waves, or by a combination of both. Figure 1-5a represents several of the possible conditions that may occur in an overexpanded nozzle. The situations shown represent cases of an overexpanded nozzle which was mentioned earlier.

We see that pressures lower than ambient may be obtained in a supersonic nozzle. The higher ambient pressure cannot advance upstream within the nozzle, however, since the gases are flowing with supersonic velocity. An exception is along

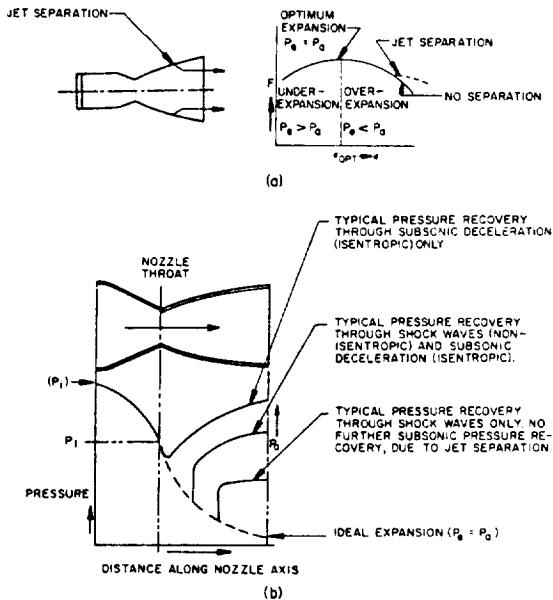


Figure 1-5.—a, Effect of incorrect nozzle length and of jet separation on thrust F ; b, pressure distribution in overexpanded De Laval nozzle.

the nozzle walls, where, due to friction, a boundary layer of slow-moving gases may exist. In this subsonic boundary layer, ambient pressure may advance for a distance, forcing the low-pressure center jet away from the walls. It might be expected that the point of separation will be at the point of optimum expansion. Actually, influenced by wall friction, nozzle divergence angle, and other factors, separation usually occurs further downstream. In fact, it rarely occurs at all in conventional rocket nozzles within their design region of operation, unless an extreme case of overexpansion exists or unless excessive nozzle divergence angles are chosen. Thus, in many cases it is correct to base all nozzle calculations on the assumption that no separation occurs; i.e., that the nozzle is "filled" at all stations (see fig. 1-5b).

Following are some significant and useful relations for an ideal gas flow through a rocket nozzle:

Theoretical exit velocity:

$$v_e = \sqrt{\frac{2g\gamma}{\gamma-1} RT_i \left[1 - \left(\frac{p_e}{p_i} \right)^{\frac{\gamma-1}{\gamma}} \right]} + v_i^2 \quad (1-17)$$

or

$$v_e = \sqrt{\frac{2g\gamma}{\gamma-1} R(T_c)_{ns} \left[1 - \left(\frac{p_e}{(p_c)_{ns}} \right)^{\frac{\gamma-1}{\gamma}} \right]} \quad (1-18)$$

Theoretical gas weight flow rate:

$$\dot{W} = A_t (p_c)_{ns} \sqrt{\frac{g\gamma [2/(\gamma+1)]^{\frac{\gamma+1}{\gamma-1}}}{R(T_c)_{ns}}} \quad (1-19)$$

Theoretical nozzle expansion ratio:

$$\epsilon = \frac{A_e}{A_t} = \frac{\left(\frac{2}{\gamma+1} \right)^{\frac{1}{\gamma-1}} \left[\frac{(p_c)_{ns}}{p_e} \right]^{\frac{1}{\gamma}}}{\sqrt{\frac{\gamma+1}{\gamma-1} \left[1 - \left(\frac{p_e}{(p_c)_{ns}} \right)^{\frac{\gamma-1}{\gamma}} \right]}}} \quad (1-20)$$

At the throat:

$$p_t = (p_c)_{ns} \left[\frac{2}{\gamma+1} \right]^{\frac{\gamma}{\gamma-1}} \quad (1-21)$$

$$v_t = \sqrt{\frac{2g\gamma}{\gamma+1} R(T_c)_{ns}} \quad (1-22)$$

At any section X between nozzle inlet and nozzle exit:

$$\frac{A_x}{A_t} = \frac{1}{M_x} \sqrt{\frac{1 + \frac{\gamma-1}{2} M_x^2}{\frac{\gamma+1}{2}}}^{\frac{\gamma+1}{\gamma-1}} \quad (1-23)$$

At any section X between nozzle inlet and the nozzle throat:

$$\frac{A_x}{A_t} = \frac{\left[\frac{2}{\gamma+1} \left(\frac{(p_c)_{ns}}{p_x} \right)^{\frac{\gamma-1}{\gamma}} \right]^{\frac{\gamma+1}{2(\gamma-1)}}}{\sqrt{\frac{2}{\gamma-1} \left[\left(\frac{(p_c)_{ns}}{p_x} \right)^{\frac{\gamma-1}{\gamma}} - 1 \right]}}} \quad (1-24)$$

At any section X between the nozzle throat and the nozzle exit:

$$\frac{A_x}{A_t} = \frac{\left(\frac{2}{\gamma+1}\right)^{\frac{1}{\gamma-1}} \left(\frac{(p_c)_{ns}}{p_x}\right)^{\frac{1}{\gamma}}}{\sqrt{\frac{\gamma+1}{\gamma-1} \left[1 - \left(\frac{p_x}{(p_c)_{ns}}\right)^{\frac{\gamma-1}{\gamma}}\right]}} \quad (1-25)$$

$$v_x = \sqrt{\frac{2g\gamma}{\gamma-1} R(T_c)_{ns} \left[1 - \left(\frac{p_x}{(p_c)_{ns}}\right)^{\frac{\gamma-1}{\gamma}}\right]} \quad (1-26)$$

$$\frac{v_x}{v_t} = \sqrt{\frac{\gamma+1}{\gamma-1} \left[1 - \left(\frac{p_x}{(p_c)_{ns}}\right)^{\frac{\gamma-1}{\gamma}}\right]} \quad (1-27)$$

Variations of isentropic pressure ratio and Mach number with the area ratio in the convergent and

divergent sections of a De Laval nozzle are shown in figure 1-6.

Useful values of functions of the specific heat ratio γ are listed in table 1-2.

Sample Calculation (1-2)

The following data are given for the thrust chamber of an ideal liquid propellant rocket engine: thrust chamber propellant flow rate, $\dot{W}_{tc} = 360.7$ lb/sec; nozzle stagnation pressure, $(p_c)_{ns} = 1000$ psia; chamber total temperature, $(T_c)_{ns} = 6540^\circ$ R; product gas molecular weight, $\bar{M} = 22.67$; gas specific heat ratio, $\gamma = 1.20$; nozzle expansion area ratio, $\epsilon = 12$. The following conditions are also assumed: flow Mach number at injecting plane, $M_{inj} = 0$; flow Mach number at the nozzle inlet, $M_i = 0.4$. (In practice, thrust chamber design values for M_i range from 0.15 to 0.45.)

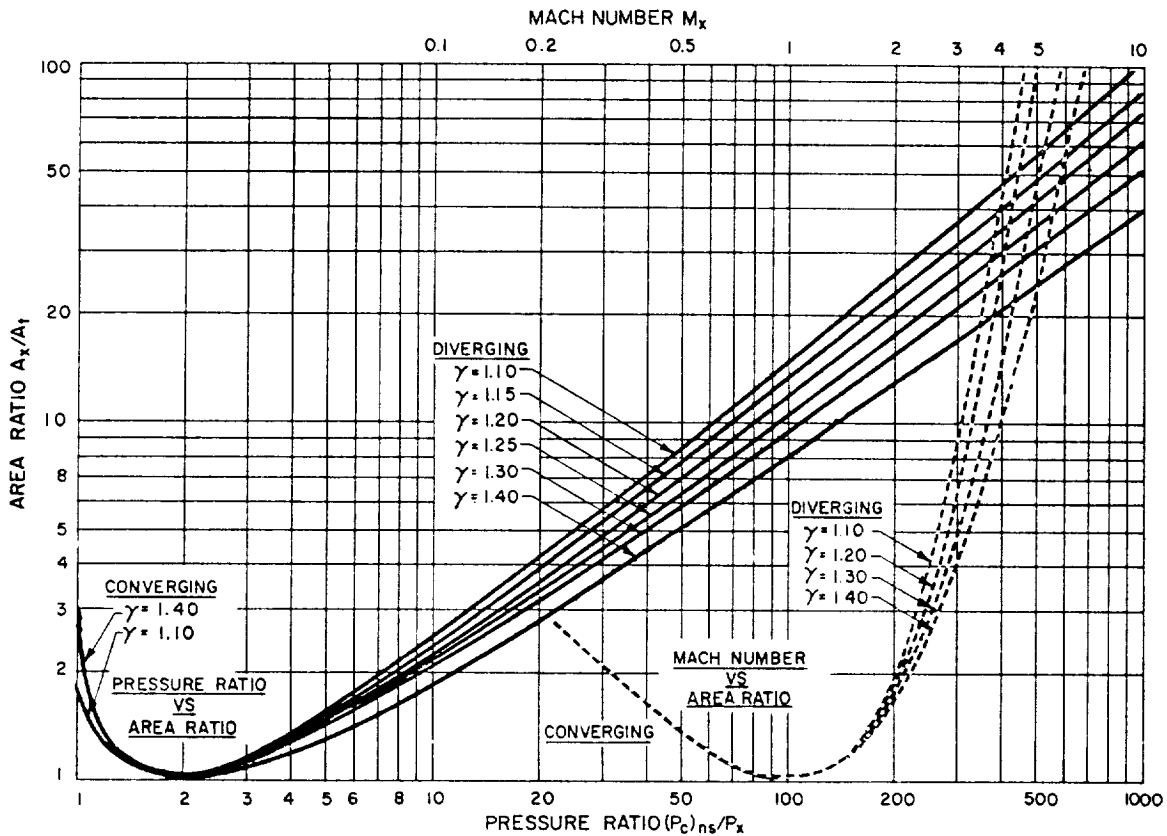


Figure 1-6.—Variations of isentropic pressure ratio and Mach number with area ratio in converging and diverging sections of De Laval nozzle.

TABLE 1-2.—Useful Values of Functions of the Specific Heat Ratio γ

γ	$\sqrt{\frac{2\gamma}{\gamma-1}}$	$\frac{\gamma-1}{\gamma}$	$\left(\frac{2}{\gamma+1}\right)^{\gamma/(\gamma-1)}$	$\gamma \sqrt{\left(\frac{2}{\gamma+1}\right)^{(\gamma+1)/(\gamma-1)}}$
1.10	26.61	0.0909	0.5847	0.6590
1.15	22.21	.1304	.5744	.6848
1.20	19.65	.1667	.5645	.7104
1.21	19.26	.1736	.5626	.7155
1.22	18.89	.1803	.5607	.7205
1.23	18.55	.1870	.5588	.7257
1.24	18.23	.1936	.5569	.7307
1.25	17.94	.2000	.5549	.7356
1.26	17.66	.2064	.5532	.7408
1.27	17.40	.2126	.5513	.7457
1.28	17.15	.2188	.5494	.7508
1.29	16.92	.2248	.5475	.7558
1.30	16.70	.2308	.5457	.7608
1.33	16.10	.2481	.5405	.7757
1.36	15.59	.2647	.5352	.7906
1.40	15.01	.2857	.5283	.8102
1.50	13.89	.3333	.5120	.8586
1.60	13.10	.3750	.4968	.9062

Determine the following: (a) flow static pressures: p_{inj} , p_i , p_t , p_x at $A_x/A_t = 4$, and p_e ; (b) flow temperatures: T_{inj} , T_i , T_t , T_x , T_e ; (c) flow specific volumes: V_{inj} , V_i , V_t , V_x , V_e ; (d) flow velocities: v_i , v_t , v_x , v_e ; flow Mach numbers: M_x , M_e ; (f) flow areas: A_c , A_i , A_t , A_x , A_e .

Solution

(a) Flow static pressures:
From equation (1-14):

$$(p_c)_{inj} = (p_c)_{ns} (1 + \gamma M_i^2) / \left(1 + \frac{\gamma-1}{2} M_i^2\right)^{\frac{\gamma}{\gamma-1}}$$

$$= 1000 \times \frac{(1 + 0.16 \times 1.20)}{\left(1 + \frac{0.2}{2} \times 0.16\right)^6} = \frac{1.192}{1.1} = 1082 \text{ psia}$$

Since, by assumption, $M_{inj} = 0$

$$p_{inj} = (p_c)_{inj} = 1082 \text{ psia}$$

From equation (1-15)

$$p_i = p_{inj} / (1 + \gamma M_i^2) = \frac{1082}{1 + 0.16 \times 1.20} = \frac{1082}{1.192} = 909 \text{ psia}$$

From equation (1-21):

$$p_t = (p_c)_{ns} \left[\frac{2}{\gamma+1}\right]^{\frac{\gamma}{\gamma-1}} = 1000 \times 0.564 = 564 \text{ psia}$$

From figure 1-6 or equation (1-25) at $A_x/A_t = 4$

$$p_x = (p_c)_{ns} \times \frac{1}{23} = \frac{1000}{23} = 43.5 \text{ psia}$$

From figure 1-6 or equation (1-20):

$$p_e = \frac{(p_c)_{ns}}{101.5} = \frac{1000}{101.5} = 9.85 \text{ psia}$$

(b) Flow temperatures:

Since $(T_c)_{inj} = (T_c)_{ns} = \text{constant}$ and $M_{inj} = 0$

$$T_{inj} = (T_c)_{inj} = (T_c)_{ns} = 6540^\circ \text{ R}$$

By definition:

$$T_i = \frac{(T_c)_{ns}}{\left[1 + \frac{1}{2}(\gamma-1)M_i^2\right]}$$

$$= \frac{6540}{1 + 0.1 \times 0.16} = \frac{6540}{1.016} = 6440^\circ \text{ F}$$

From equation (1-13):

$$T_t = (T_c)_{ns} \left[\frac{p_t}{(p_c)_{ns}}\right]^{\frac{\gamma-1}{\gamma}} = 6540 \times 0.909 = 5945^\circ \text{ R}$$

$$T_x = (T_c)_{ns} \left[\frac{p_x}{(p_c)_{ns}}\right]^{\frac{\gamma-1}{\gamma}} = 6540 \times \frac{1}{1.686} = 3880^\circ \text{ R}$$

$$T_e = (T_c)_{ns} \left[\frac{p_e}{(p_c)_{ns}}\right]^{\frac{\gamma-1}{\gamma}} = 6540 \times \frac{1}{2.16} = 3025^\circ \text{ R}$$

(c) Flow specific volumes:

$$R = \frac{1544}{\pi} = \frac{1544}{22.67} = 68$$

From equation (1-9):

$$V_{inj} = \frac{RT_{inj}}{144 p_{inj}} = \frac{68 \times 6540}{144 \times 1082} = 2.846 \text{ cu ft/lb}$$

$$V_i = \frac{RT_i}{144 p_i} = \frac{68 \times 6440}{144 \times 909} = 3.34 \text{ cu ft/lb}$$

$$V_t = \frac{RT_t}{144 p_t} = \frac{68 \times 5945}{144 \times 564} = 4.97 \text{ cu ft/lb}$$

$$V_x = \frac{RT_x}{144 p_x} = \frac{68 \times 3880}{144 \times 43.5} = 42.1 \text{ cu ft/lb}$$

$$V_e = \frac{RT_x}{144 p_x} = \frac{68 \times 3025}{144 \times 9.85} = 145.1 \text{ cu ft/lb}$$

(d) Flow velocities:

Since the sonic velocity $a_i = \sqrt{g \gamma RT_i}$

$$v_i = M_i a_i = 0.4 \times 32.2 \times 1.2 \times 68 \times 6440 = 0.4 \times 4110 = 1646 \text{ ft/sec}$$

$$v_t = M_t a_t = 1 \times 32.2 \times 1.2 \times 68 \times 5945 = 3958 \text{ ft/sec}$$

From equation (1-26):

$$v_x = \sqrt{\frac{2g\gamma}{\gamma-1} R(T_c)_{ns} \left[1 - \left(\frac{p_x}{(p_c)_{ns}} \right)^{\frac{\gamma-1}{\gamma}} \right]}$$

$$= \sqrt{6540 \times 64.4 \times 6 \times 68 \times [1 - 0.593]}$$

$$= \sqrt{64.4 \times 6 \times 68 \times 0.407 \times 6540}$$

$$= 8360 \text{ ft/sec}$$

From equation (1-18):

$$v_e = \sqrt{\frac{2g\gamma}{\gamma-1} R(T_c)_{ns} \left[1 - \left(\frac{p_e}{(p_c)_{ns}} \right)^{\frac{\gamma-1}{\gamma}} \right]}$$

$$= \sqrt{64.4 \times 6 \times 68 \times 6540 \times 0.543} = 9760 \text{ ft/sec}$$

(e) Flow Mach numbers:

Since

$$a_x = \sqrt{g \gamma RT_x} = \sqrt{32.2 \times 1.2 \times 68 \times 3880} = 3226 \text{ ft/sec}$$

$$M_x = \frac{v_x}{a_x} = \frac{8360}{3226} = 2.59$$

$$a_e = \sqrt{g \gamma RT_e} = \sqrt{32.2 \times 1.2 \times 68 \times 3025} = 2820 \text{ ft/sec}$$

$$M_e = \frac{v_e}{a_e} = \frac{9620}{2820} = 3.43$$

(f) Flow areas:

From equation (1-11):

$$A_i = \frac{144 \dot{W}_{tc} V_i}{v_i} = \frac{144 \times 360.7 \times 3.34}{1646} = 105.4 \text{ in}^2$$

$$A_c = A_i = 105.4 \text{ in}^2$$

$$A_t = \frac{144 \dot{W}_{tc} V_t}{v_t} = \frac{144 \times 360.7 \times 4.97}{3958} = 65.4 \text{ in}^2$$

$$A_x = \frac{144 \dot{W}_{tc} V_x}{v_x} = \frac{144 \times 360.7 \times 42.1}{8360} = 261.8 \text{ in}^2$$

or

$$A_x = 4 \times A_t = 261.8 \text{ in}^2$$

$$A_e = \frac{144 \dot{W}_{tc} V_e}{v_e} = \frac{144 \times 360.7 \times 145.1}{9670} = 782 \text{ in}^2$$

or

$$A_e = 12 \times A_t = 782 \text{ in}^2$$

1.3 PERFORMANCE PARAMETERS OF A LIQUID PROPELLANT ROCKET ENGINE

The performance of a rocket engine is expressed by a quantity commonly called "specific impulse," I_s . If impulse imparted to the vehicle and propellant weight consumption were measured during a given time interval, I_s would have the dimension lb-sec/lb. In practice, thrust is usually measured, in conjunction with propellant weight flow-rate measurements. This yields the same dimension: lb/(lb/sec). I_s may thus be expressed as

$$I_s = F/\dot{W} \quad (1-28)$$

Since weight is the force exerted by a mass

CONFIDENTIAL

on its rigid support under the influence of gravitation (by convention at sea level on Earth), it has become accepted practice to measure I_s in "seconds," by canceling out the terms for the forces. Obviously, the expression does not denote a time, but rather a magnitude akin to efficiency. I_s directly contributes to the final velocity of the vehicle at burnout and thus has a pronounced effect on range or size of payload, or both. This will be shown further below in connection with equation (1-30).

It is important to state whether a specific impulse quoted refers to the thrust chamber assembly only $(I_s)_{tc}$, or to the overall engine system $(I_s)_{oa}$. Often, the distinction may not be self-evident. It is important, therefore, to state accurately to what system the quoted specific impulse refers. For instance, in a turbopump fed system, overall engine specific impulse may include turbine power requirements, vernier, and attitude control devices. All of these may be fed from one or all of a given vehicle's propellant tanks. If they are properly considered, the user, in this case the vehicle builder, will obtain the correct value for his own optimization studies, which include propellant tank sizes, payload weight, and range, among other parameters.

In many instances, statement of the specific impulse $(I_s)_{tc}$ for the thrust chamber only may be desirable, such as during the component development period of this subassembly. Since, in that case, those propellant demands which are inadequately or not at all contributing to the generation of thrust are not included, the specific impulse stated will be higher than for a complete system, by 1 to 2 percent, as a rule. The specific impulse thus stated would be too high for the vehicle builder, who must consider the supply of propellants to the auxiliary devices mentioned above as well. If, due to improper identification of I_s , a thrust chamber value were used as an engine value, the consequences would be serious. This becomes clear, if one realizes that when relying on a better-than-actual value, propellant tank sizes would be designed too small, resulting in premature propellant depletion. This would eliminate the last seconds of required burning time, when the vehicle mass being accelerated is near empty weight and acceleration, therefore, is near maximum. A substantial loss of range for a given payload

would result. The situation would be further complicated by the fact that it is nearly impossible to improve the specific impulse once an engine and thrust chamber have been designed, for a given propellant combination.

Another important performance parameter is the propellant mass fraction R_p of the complete vehicle, of which the engine system is a part. The propellant mass fraction is defined as

$$R_p = \frac{\text{Usable propellant mass}}{\text{Initial rocket mass}} \quad (1-29)$$

where the initial rocket mass is equal to the sum of the masses of the engine system at burnout, the structure and guidance system, the payload, and the propellant. The significance of the propellant mass fraction can be illustrated by the basic equation for the rocket burnout velocity v_{bo} (ft/sec)

$$v_{bo} = C_{vc} \cdot g(I_s)_{oa} \ln \frac{1}{1 - R_p} \quad (1-30)$$

where the coefficient C_{vc} corrects for the effects of aerodynamic and gravitational forces. It is composed of several parameters which vary with type of trajectory and with elapsed time during flight. Although they are of no concern here, they are of great importance to the vehicle builder. Also, they cannot be neglected for rigorous engine design analyses which must include trajectory information.

Thrust Chamber Specific Impulse $(I_s)_{tc}$

The overall performance of the liquid propellant thrust chamber is a direct function of the propellant combination, the combustion efficiency of propellants in the chamber, and the product gas expansion performance in the nozzle. The expression for $(I_s)_{tc}$ may be obtained in several ways:

From equation 1-28:

$$(I_s)_{tc} = \frac{F}{W_{tc}} \quad (1-31)$$

Combine equations 1-31 and 1-7:

$$(I_s)_{tc} = \frac{c}{g} \quad (1-31a)$$

The effective exhaust velocity c may be further defined as the product of two convenient parameters, c^* and C_f

$$c = c^* C_f \quad (1-31b)$$

where the *characteristic velocity* c^* in feet per second (commonly pronounced "cee-star") is a parameter primarily used to rate the propellant combustion performance. The *thrust coefficient* C_f is a dimensionless parameter used to measure the gas expansion performance through the nozzle. Combine equations 1-31a and 1-31b:

$$(I_s)_{tc} = \frac{c^* C_f}{g} \quad (1-31c)$$

While I_s and R_p are of ultimate importance to the missile or space vehicle builder, both c^* and C_f are of great and early importance to the engine and thrust chamber designer and developer.

Characteristic Velocity c^*

In a system with sonic velocity at the throat, the quantity c^* reflects the effective energy level of the propellants and the design quality of injector and combustion chamber. It may be defined by the following expression:

$$c^* = \frac{(p_c)_{ns} A_t g}{\dot{W}_{tc}} \quad (1-32)$$

This form shows that c^* measures combustion performance in a given combustion chamber by indicating how many pounds per second of propellant must be burned to maintain the required nozzle stagnation pressure. A lower value of propellant consumption \dot{W} under the given condition indicates a combustion process of higher energy and efficiency and gives a corresponding higher value of c^* . By substituting \dot{W}_{tc} with equation 1-19 in equation 1-32, the equation for theoretical c^* may be rewritten in the following form:

$$c^* = \frac{\sqrt{g \gamma R (T_c)_{ns}}}{\gamma \sqrt{\left[\frac{2}{\gamma + 1} \right]^{\frac{\gamma + 1}{\gamma - 1}}}} \quad (1-32a)$$

This form shows that c^* is a function of the properties of the combustion product gas at the exit of the combustion chamber, i.e., at the nozzle inlet; namely, specific heat ratio γ , gas constant R , and temperature $(T_c)_{ns}$.

Thrust Coefficient C_f

The quantity C_f reflects the product gas expansion properties and design quality of the nozzle. Combining equations 1-31, 1-31c, and 1-32, the expression for theoretical C_f may be written as:

$$C_f = \frac{F}{A_t (p_c)_{ns}} \quad (1-33)$$

This form shows that C_f measures the force augmented by the gas expansion through the nozzle as compared with the force which would be generated if the chamber pressure acted over the throat area only. By combining equations 1-6, 1-18, 1-19, and 1-33, the equation for theoretical C_f at any altitude may be rewritten in the following form:

$$C_f = \sqrt{\frac{2\gamma^2}{\gamma - 1} \left[\frac{2}{\gamma + 1} \right]^{\frac{\gamma + 1}{\gamma - 1}} \left[1 - \left(\frac{p_e}{(p_c)_{ns}} \right)^{\frac{\gamma - 1}{\gamma}} \right]} + \epsilon \left[\frac{p_e - p_a}{(p_c)_{ns}} \right] \quad (1-33a)$$

Equation 1-33a shows that C_f is a function of specific heat ratio γ , chamber pressure $(p_c)_{ns}$, ambient pressure p_a , and the nozzle area expansion ratio ϵ .

As will be noted, the throat stagnation pressure $(p_c)_{ns}$ has been used in equations (1-32) and (1-33). This has been the practice in industry and in most of the literature. Briefly, the reason is that $(p_c)_{ns}$ reflects the true theoretical gas property at combustion chamber exit, i.e., at the nozzle inlet, and gives a more logical value to c^* and C_f . In actual operation the true value of $(p_c)_{ns}$ cannot be measured. $(p_c)_{ns}$ is mathematically converted from the measured value of the gas static pressure at the injector, p_{inj} . The accuracy of this calculated value has to be verified by the test results. Likewise, the gas properties, and thus the specific heat ratio γ which

CONFIDENTIAL

additionally changes along the chamber axis, affect the true values of c^* and C_f . This will have to be verified by actual test results.

To understand better the nature of C_f and the design parameters which influence it, let us first rearrange equation (1-33):

$$F = (p_c)_{ns} \cdot A_t \cdot C_f \quad (1-34)$$

The formula expresses that the thrust generated by a thrust chamber (the effect) is produced by pressure (the cause) as a function of the physical properties of the chamber itself. The relationships and effects of the principal design parameters become clearer if we proceed in steps as follows:

Assume we wish to generate a certain thrust F . Our chamber is a straight cylinder (fig. 1-7). The pressure in this chamber has a very small effect on the cylindrical wall (the forces normal to the chamber axis will cancel each other), except for effects of friction, which we will neglect. There is no part of the chamber for the pressure to act upon at the exit. The only chamber area upon which the pressure can act is the injector plate. Since, for the cylindrical chamber, the injector area A_i is equal to A_t , we can write:

$$F_{cyl} = p_{inj} \cdot A_t \quad (1-35)$$

For the reasons explained above, we rewrite to include $(p_c)_{ns}$:

$$F_{cyl} = (p_c)_{ns} \cdot A_t \cdot C_{f_1} \quad (1-36)$$

Since $(p_c)_{ns}$ is smaller than p_{inj} (fig. 1-4), the

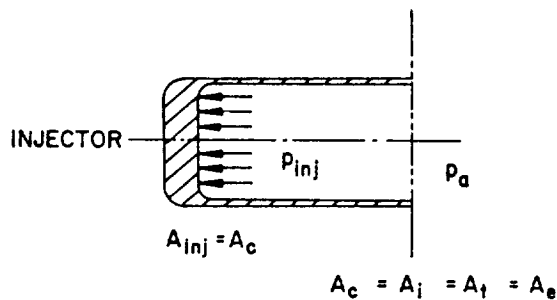


Figure 1-7

coefficient C_{f_1} is introduced to correct for this fact. For instance, if the ratio $(p_c)_{ns}/p_{inj}$ was found to be 0.8 from figure 1-4, C_{f_1} would have to be 1.25 to offset the introduction of $(p_c)_{ns}$. As will be seen, the use of a thrust coefficient of 1.25, for instance, in a straight cylinder thrust chamber for which $(p_c)_{ns}/p_{inj}$ is 0.8, is merely part of a mathematical rearrangement, but does not signify an increase in thrust for a given p_{inj} .

It is noted that the combustion chamber including injector will have to produce the required pressure $(p_c)_{ns}$ with a flow rate, the magnitude of which is determined by c^* and by the throat area A_t . Transformation of equation (1-32) shows the relationship:

$$(p_c)_{ns} = \dot{W}_{tc} \cdot c^* \cdot \frac{1}{A_t \cdot g} \quad (1-37)$$

In actual practice, the value of c^* for a given propellant combination and thrust chamber design is arrived at tentatively from existing experience and is subsequently refined during development testing.

Let us now redesign our cylindrical thrust chamber, as shown in figure 1-8. Maintaining the same throat area $A_t = A_e$, we enlarge the combustion chamber including injector to a diameter somewhat larger than that of A_t . The flow rate remains \dot{W}_{tc} .

In the straight cylindrical chamber (fig. 1-7), the gas velocity was sonic at the end of the cylindrical chamber portion, which coincided with A_t and A_e . From earlier discussions (see sec. 1-2), we know that expansion (acceleration) is nonisentropic in that case. In the redesigned chamber (fig. 1-8) by contrast, gas velocities are still well below sonic velocity at the end of the cylindrical portion. Most of the acceleration to sonic velocity will now occur in the added, convergent nozzle. Since we can make the assumption, which is essentially correct, that the combustion process is complete at the end of the cylindrical chamber portion, the subsequent expansion (acceleration) in the convergent nozzle is assumed to be isentropic; i.e., to occur without further total pressure losses. Since we keep \dot{W}_{tc} and A_t constant, and assume that c^* remains unchanged, the nozzle stagnation pressure $(p_c)_{ns}$, too, will retain the same value as in

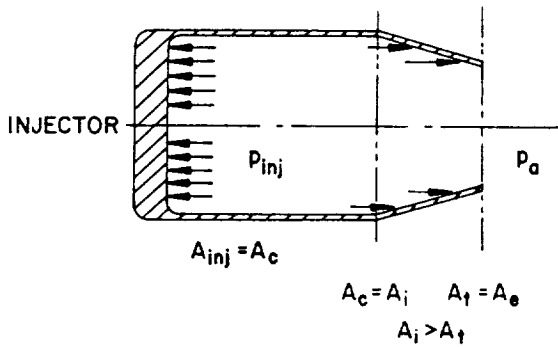


Figure 1-8

the case of the straight cylindrical chamber. However, because of the reduced pressure losses in the combustion chamber, the required total pressure at the injector end will definitely be lower.

The redesign, then, has the favorable result that, for instance, in pressurized systems, the same propellant flow rate can be sustained with lower tank pressures, thus, slightly lighter tanks can be used. In turbopump-fed systems, required turbopump horsepower will decrease. However, the forces acting upon the thrust chamber, and thus the developed thrust, can be assumed to have remained unchanged, since a lower pressure acts upon the larger injector, and since opposing forces are present at the converging nozzle.

In short, it may be stated that our redesign (fig. 1-8) results in reduced demands on the propellant feed system for the same \dot{W}_{tc} and the same thrust level.

We now proceed to further redesign the chamber to include a divergent nozzle section, as in figure 1-9. Up to the throat area, nothing changes over the preceding configuration, which includes a convergent nozzle only. Since the gas velocity in the throat area is always sonic (except for very low, subcritical chamber pressures), the attachment of the divergent nozzle section, likewise, will have no effect on the previously described gas processes and the pressures upstream of the throat. However, conditions downstream from the throat are now different.

With the cylindrical chamber, and the chamber with convergent nozzle, the static pressure energy available at the throat p_t is dissipated by

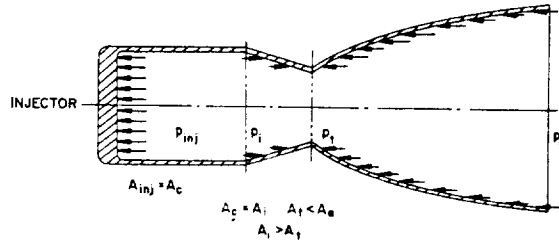


Figure 1-9

expansion to atmospheric pressure, flowing freely in all directions. By attaching a divergent nozzle, we prevent the gases from dissipating at random, and further accelerate the gases in one preferred direction only. Since this process takes place in the divergent part of the thrust chamber, the static pressures of the expanding gases produce a force on the chamber, as indicated by the arrows in figure 1-9. The expression of the thrust for the complete thrust chamber with convergent-divergent nozzle can now be written as:

$$F_{tc} = \int_0^{A_t} p dA + \int_{A_t}^{A_{inj}} p dA - \int_{A_t}^{A_i} p dA + \int_{A_t}^{A_e} p dA \quad (1-38)$$

The last expression in the equation represents the gain realized from attaching the divergent nozzle to the throat. By combining all gains into a single coefficient C_f (see eq. 1-33), we arrive again at equation (1-34):

$$F = (p_c)_{ns} \cdot A_t \cdot C_f$$

In brief, it may be stated that the redesign (fig. 1-9) results in an increased thrust level, for the same \dot{W}_{tc} and the same feed system configuration.

Summary of the Influences of p_a , ϵ , γ , R , and $(p_c)_{ns}$ on Engine Performance

The Effect of p_a

An ambient pressure p_a reduces the vacuum thrust F of an engine by the amount $p_a \cdot A_e$. (See

eq. (1-6).) C_f is similarly affected by the amount $\epsilon \cdot p_a / (p_c)_{ns}$, as shown in equation 1-33a). This may be rewritten as $C_f = (C_f)_{vac} - \epsilon \cdot p_a / (p_c)_{ns}$. The lower the ambient pressure, the higher thrust and performance. Maximum values are obtained in vacuum.

The Effect of ϵ

Optimum thrust for a given ambient pressure is obtained when the nozzle expansion area ratio $\epsilon = A_e / A_t$ is such that $p_e = p_a$. This may be seen from figure 1-10. If the divergent nozzle section is extended in the region where $p_e > p_a$, thrust will increase. Where $p_e < p_a$, however, lengthening of the nozzle will decrease thrust. Hence it would be beneficial to design the nozzle to yield $p_e = p_a$, to reach an optimum value for the thrust coefficient. The ϵ for this condition is called optimum nozzle expansion area ratio. Unfortunately, because of changing ambient pressure during flight, no one single ϵ is optimum. Optimization studies are usually made to determine the best compromise. Such a study is not required (except for weight and size considerations) for rockets which start and stop at the same ambient pressure, such as upper stages, where ambient pressure is zero or near zero at all times. For the special case of $p_a = 0$ (vacuum conditions), ϵ would become infinity, to satisfy "ideal expansion." Even for this case, however, expansion ratios over 25 contribute little. The nozzle design is usually "cut" at this point, mainly for weight considerations. This leaves a small positive pressure at the exit which is unavailable for final gas acceleration. However, it still contributes as a positive term $p_e \cdot A_e$.

The Effect of γ

The specific heat ratio is an indication of the energy storing capacity of the gas molecule. A smaller value of γ indicates a higher energy-storing capability, and in turn gives higher engine performance. As shown in equations (1-32a) and (1-33a), a smaller γ will yield a higher value for both, c^* and C_f . The influence of the properties of the selected propellants and of the combustion products is apparent.

The Effect of R ($R = 1544 / M$)

It can be seen from equation (1-32) that for constant $(T_c)_{ns}$, c^* will increase if the gas

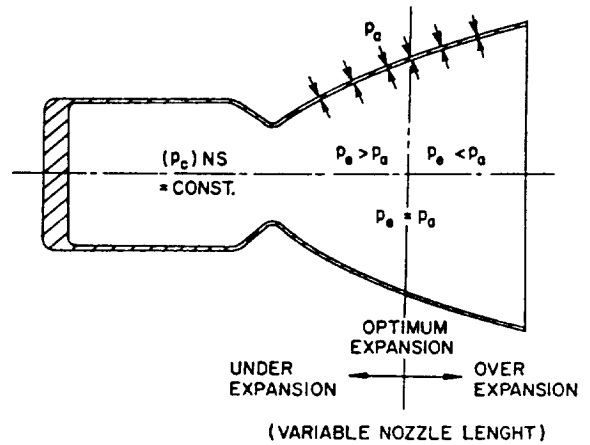


Figure 1-10

constant R increases; i.e., the gas molecular weight decreases. Thus, a higher value of R will yield a higher engine performance.

The Effect of $(p_c)_{ns}$

The effective chamber pressure or nozzle stagnation pressure $(p_c)_{ns}$ appears in equation (1-33a) for C_f in the form of two pressure ratios $p_e / (p_c)_{ns}$ and $p_a / (p_c)_{ns}$. As is evident from equation (1-20), the ratio $p_e / (p_c)_{ns}$ has a singular value, for a given ϵ and γ . $(p_c)_{ns}$ in equation (1-33), therefore, influences C_f only through the negative term $-p_a / (p_c)_{ns}$. An increase in $(p_c)_{ns}$ decreases this negative term and hence increases C_f . This effect is more pronounced when p_a is high. Since the thrust is proportional to both $(p_c)_{ns}$ and C_f , we see now clearly how an increase in $(p_c)_{ns}$ in a given thrust chamber will increase the thrust.

$(p_c)_{ns}$ also has some effect on the combustion process. Increasing $(p_c)_{ns}$ tends to increase $(T_c)_{ns}$ and to reduce γ and R . The overall result is usually an increase in c^* . However, these effects are slight, especially at $(p_c)_{ns}$ above 300 psi.

Correction Factors and Magnitudes of Engine Performance Parameters

The actual performance of a liquid propellant rocket engine differs from that of an ideal one because of friction effects, heat transfer, non-perfect gases, nonaxial flow, nonuniformity of working substance and of flow distribution, and

shifting gas composition. The latter refers to the fact that the gas properties (γ , \bar{M} , R) are not truly constant along the nozzle axis, as the isentropic treatment of the processes assumes. Therefore, correction factors have to be applied to the performance parameters which are derived from theoretical assumptions. Following are some important correction factors:

Correction factor for thrust and thrust coefficient

$$\eta_f = \frac{\text{Actual thrust coefficient}}{\text{Ideal thrust coefficient}} = \frac{\text{Actual thrust}}{\text{Ideal thrust}} \quad (1-39)$$

The values for η_f range from 0.92 to 1.00.

Correction factor for effective exhaust velocity and specific impulse

$$\eta_v = \frac{\text{Actual effective exhaust velocity}}{\text{Ideal effective exhaust velocity}} = \frac{\text{Actual specific impulse}}{\text{Ideal specific impulse}} \quad (1-40)$$

The values for η_v range from 0.85 to 0.98.

Correction factor for characteristic velocity

$$\eta_{v^*} = \frac{\text{Actual characteristic velocity}}{\text{Ideal characteristic velocity}} \quad (1-41)$$

The values for η_{v^*} range from 0.87 to 1.03.

Correction factor for propellant mass flow rate

$$\eta_w = \frac{\text{Actual propellant mass flow rate}}{\text{Ideal propellant mass flow rate}} \quad (1-42)$$

The values for η_w range from 0.98 to 1.15.

The relation between correction factors may be expressed as:

$$\eta_v = \eta_{v^*} \cdot \eta_f \quad (1-43)$$

$$\eta_v = 1/\eta_w \quad (1-44)$$

Actual ranges of liquid propellant rocket engine parameters are listed in table 1-3.

TABLE 1-3

Gas temperature, T	4000° R to 7000° R
Nozzle stagnation pressure (p_c) _{ns} ..	10 to 2500 psia
Molecular weight, \bar{M}	2 to 30
Gas constant, R	51.5 to 772
Gas flow Mach number, M	0 to 4.5
Specific heat ratio, γ	1.13 to 1.66
Nozzle expansion area ratio, ϵ	3.5 to 100
Nozzle contraction area ratio, ϵ_c ..	1.3 to 6
Thrust coefficient, C_f	1.3 to 2.0
Characteristic velocity, c^*	3000 to 8000 ft/sec
Effective exhaust velocity, c	4000 to 12 000 ft/sec
Specific impulse, I_s	150 to 480 sec (vacuum)

Values of the vacuum or altitude thrust coefficient (C_f)_{vac} plotted as functions of nozzle expansion area ratio ϵ and gas specific heat ratio γ are shown in figure 1-11.

Sample Calculation (1-3)

Assume a thrust chamber for the same ideal liquid propellant rocket engine as given in sample calculation (1-2), in which $\dot{W}_{tc} = 360.7$ lb/sec; (p_c)_{ns} = 1000 psia; (T_c)_{ns} = 6540° R; $\bar{M} = 22.67$; $\gamma = 1.20$; $\epsilon = 12$.

Determine the following: (a) Theoretical c^* ; (b) theoretical C_f at sea level and in space; (c) theoretical (I_s)_{tc} at sea level and in space; (d) actual c^* , if c^* correction factor $\eta_{v^*} = 0.97$; (e) actual C_f at sea level and in space, if sea level C_f correction factor: $\eta_f = 0.983$; (f) actual (I_s)_{tc} at sea level and in space; (g) (I_s)_{tc} correction factor at sea level; (h) thrust at sea level and in space; (i) actual A_t and A_e .

Solution

(a) From equation (1-32a):

$$\begin{aligned} \text{Theoretical } c^* &= \frac{\sqrt{g\gamma R(T_c)_{ns}}}{\gamma \sqrt{\left(\frac{2}{\gamma+1}\right)^{\frac{\gamma+1}{\gamma-1}}} \\ &= \frac{\sqrt{32.2 \times 1.2 \times \frac{1544}{22.67} \times 6540}}{0.7104} \\ &= 5830 \text{ ft/sec} \end{aligned}$$

(b) From equation (1-33a):

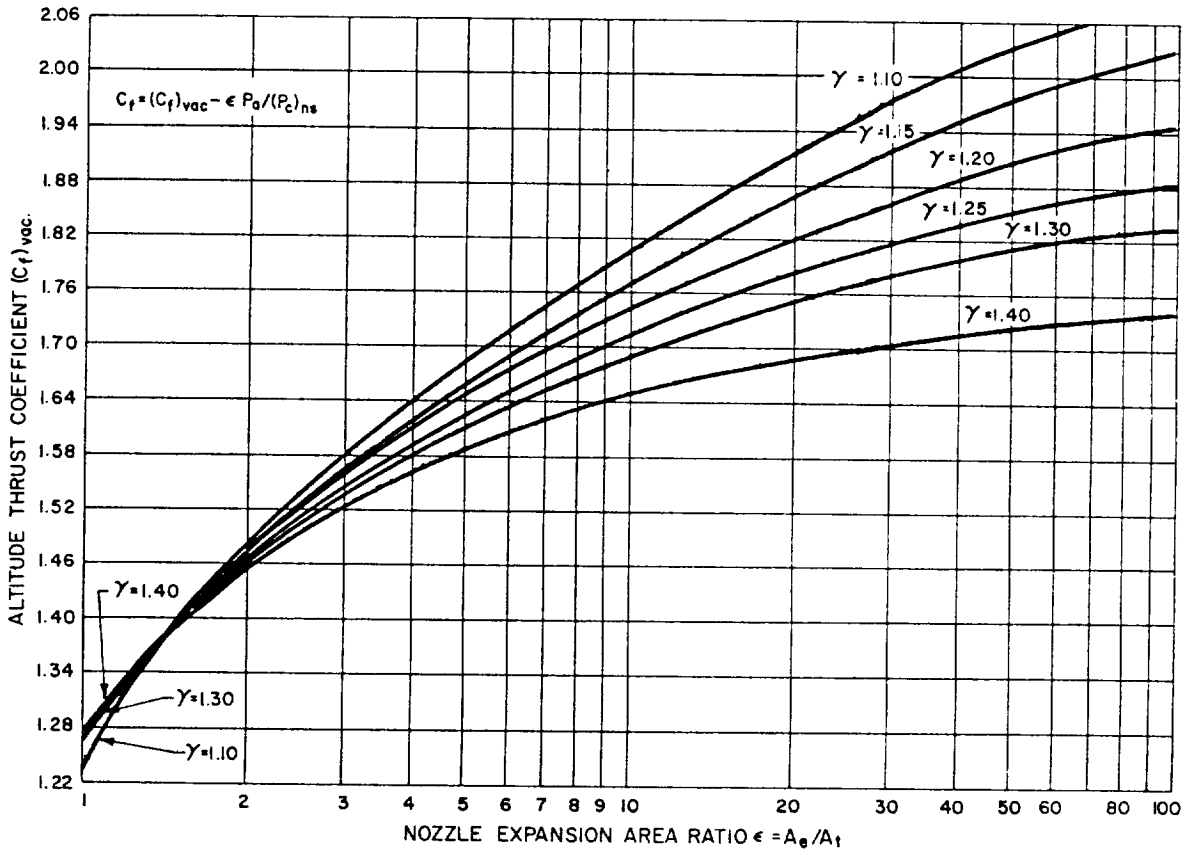


Figure 1-11.—Altitude thrust coefficient as function of area ratio and specific heat ratio.

$$\text{Theoretical } C_f = \sqrt{\frac{2\gamma^2}{\gamma-1} \left(\frac{2}{\gamma+1}\right)^{\frac{\gamma+1}{\gamma-1}} \left[1 - \left(\frac{p_e}{(p_c)_{ns}}\right)^{\frac{\gamma-1}{\gamma}}\right] + \epsilon \frac{p_e - p_a}{(p_c)_{ns}}}$$

= 1.65 - 0.0582

= 1.5918

In space:

$$\text{Theoretical } C_f = 1.5918 + 12 \times \frac{14.7}{1000} = 1.5918 + 0.1764$$

= 1.7682

From sample calculation (1-2)

$p_e = 9.85$ psia:

At sea level $p_a = 14.7$ psia:

$$\text{Theoretical } C_f = 2.247 \times \sqrt{1 - \left(\frac{9.85}{1000}\right)^{1/6}} + 12 \times \frac{9.85 - 14.7}{1000}$$

$$= 2.247 \times \sqrt{1 - 0.4625} - \frac{4.85 \times 12}{1000}$$

= 2.247 × 0.734 - 0.0582

(c) From equation (1-31):

$$\text{Theoretical } I_s = \frac{c^* \cdot C_f}{g}$$

At sea level:

$$\text{Theoretical } (I_s)_{tc} = \frac{5830 \times 1.5918}{32.2} = 288.4 \text{ lb sec/lb}$$

In space:



$$\text{Theoretical } (I_s)_{tc} = \frac{5830 \times 1.7682}{32.2} = 319.6 \text{ lb sec/lb}$$

(d) From equation (1-41):

$$\begin{aligned} \text{Actual } c^* &= \eta_v^* \cdot \text{theoretical } c^* \\ &= 0.97 \times 5830 = 5650 \text{ ft/sec} \end{aligned}$$

(e) From equation (1-39):

$$\text{Actual } C_f = \eta_f \cdot \text{theoretical } C_f$$

At sea level:

$$\text{Actual } C_f = 0.983 \times 1.5918 = 1.566$$

In space:

$$\begin{aligned} \text{Actual } C_f &= 1.566 + 12 \times \frac{14.7}{1000} \\ &= 1.566 + 0.1764 = 1.7424 \end{aligned}$$

(f) At sea level:

$$\text{Actual } (I_s)_{tc} = \frac{5650 \times 1.566}{32.2} = 275 \text{ lb sec/lb}$$

In space:

$$\text{Actual } (I_s)_{tc} = \frac{5650 \times 1.7424}{32.2} = 306 \text{ lb sec/lb}$$

(g) From equation (1-40):

$$\begin{aligned} (I_s)_{tc} \text{ correction factor} &= \frac{\text{Actual } (I_s)_{tc} \text{ at sea level}}{\eta_v \text{ at sea level} \cdot \text{Theoretical } (I_s)_{tc} \text{ at sea level}} \\ &= \frac{275}{288.4} = 0.954 \end{aligned}$$

Or from equation (1-43):

$$\eta_v = \eta_v^* \cdot \eta_f = 0.97 \times 0.983 = 0.954$$

(h) From equation (1-31):

$$\begin{aligned} \text{Thrust } F \text{ at sea level} &= \dot{W}_{tc} \cdot (I_s)_{tc} \text{ at sea level} \\ &= 360.7 \times 275 = 99\,200 \text{ lb} \end{aligned}$$

$$\begin{aligned} \text{Thrust } F \text{ in space} &= \dot{W}_{tc} \cdot (I_s)_{tc} \text{ in space} \\ &= 360.7 \times 306 = 108\,500 \text{ lb} \end{aligned}$$

(i) From equation (1-33):

$$A_t = \frac{F}{C_f \cdot (p_c)_{ns}} = \frac{99\,200}{1.566 \times 1000} = 63.4 \text{ in}^2$$

$$A_e = \epsilon \cdot A_t = 12 \times 63.4 = 760.8 \text{ in}^2$$

1.4 LIQUID ROCKET PROPELLANTS

The term "liquid propellant" is used to define both liquid oxidizers (liquid oxygen, liquid fluorine, nitric acid, etc.) and liquid fuels (RP-1, alcohol, liquid hydrogen, etc.). In some cases additives are used (water, ferric chloride, etc.). The propellants furnish the energy and the working substance for the rocket engines. The selection of the propellants is one of the most important steps in the design of an engine. It greatly affects overall engine system performance as well as the design criteria for each engine component. The propellant selection in turn is influenced by price, supply, handling, and storage considerations.

Monopropellants

Liquid monopropellants may be either a mixture of oxidizer and combustible matter, or a single compound which can be decomposed with attendant heat release and gasification. A rocket monopropellant must be stable in a natural or controlled environment, yet should produce hot combustion or decomposition gases when pressurized, heated, or fed through a catalyst. A liquid monopropellant engine system usually does have the advantage of simplicity of tankage, feed plumbing, flow control, and injection. Unfortunately, most of the practical monopropellants, such as hydrogen peroxide (H_2O_2), have a relatively low performance. Thus, they are mainly used as secondary power sources in rocket engine systems, such as for turbopump gas generators and auxiliary power drives, and for attitude and roll control jets. Certain high-performance monopropellants, such as methyl nitrate (CH_3NO_3), are rather unstable and are

CONFIDENTIAL

considered unsafe for rocket applications. However, some monopropellants promising relatively high-performance and safer operational characteristics have been under development recently. If successful, these may effect wider application of liquid monopropellant engines.

Bipropellants

In a liquid bipropellant system, two different propellants are used, usually an oxidizer and a fuel. Separate tanks hold oxidizer and fuel which are not mixed until they reach the combustion chamber. Present-day liquid propellant rocket engines use bipropellants almost exclusively because they offer higher performance, combined with safer operation.

The combustion of many bipropellant combinations is initiated by ignition devices such as: (a) chemical pyrotechnic igniters, (b) electric spark plugs, (c) injection of a spontaneously ignitable liquid fuel or oxidizer ("pyrophoric fluid") ahead of the propellant proper, (d) a small combustor wherein ignition is started by devices (a) or (b), in turn starting the main chamber by the hot gas produced.

Other bipropellant combinations ignite spontaneously upon mixing. Those combinations are defined as *hypergolics* and permit greatly simplified ignition, but pose certain hazards. For instance, accidental mixing of the fuel and oxidizer due to tank and other hardware failures could cause a violent explosion. These hazards must be considered when designing an engine system using hypergolic propellants.

Cryogenic Propellants

Some liquid propellants are liquefied gases with a very low boiling point (-230°F to -430°F) at ambient pressure and a low critical temperature (10°F to -400°F). These propellants are defined as *cryogenics*. The most common cryogenic propellants for rocket applications are liquid oxygen (O_2), liquid hydrogen (H_2), liquid fluorine (F_2), and oxygen difluoride (OF_2), or mixtures of some of them. Cryogenic propellants pose storage and handling problems. Elaborate insulation must be provided in order to minimize losses due to boiloff, the complexity depending on storage period and type of cryogenic. Recently, novel insulating techniques have been

under development which should greatly reduce these losses. Adequate venting systems are needed for the developed gases. Storage and handling equipment and their components are extremely sensitive to atmospheric or other moisture; even minute quantities may cause a jamming of, for instance, a valve. Likewise, the design criteria, including materials selection for engine systems using cryogenic propellants, must consider the very low temperatures involved. The mechanical design of engine components for cryogenic propellant applications will be discussed in subsequent chapters.

Storable Liquid Propellants

In contrast to the cryogenic propellants, certain other liquid propellants are stable over a reasonable range of temperature and pressure, and are sufficiently nonreactive with construction materials to permit storage in closed containers for periods of a year or more. These propellants are defined as *storables*. Storable liquid propellants permit almost instant readiness of the rocket engine and may result in greater reliability due to the absence of extremely low temperatures and the need to dispose of boiloff vapors. Their application to military vehicles as well as to the upper stages of space vehicles has increased significantly during recent years. The mechanical design of storable liquid engine components will be further discussed in subsequent chapters.

Additives for Liquid Rocket Propellants

Sometimes, additives are mixed into liquid propellants for one of the following reasons: (a) to improve cooling characteristics; (b) to depress freezing point; (c) to reduce corrosive effects; (d) to facilitate ignition; and (e) to stabilize combustion.

Optimum Mixture Ratio

A certain ratio of oxidizer weight to fuel weight in a bipropellant combustion chamber will usually yield a maximum performance value. This is defined as the optimum mixture ratio. As a rule, the optimum mixture ratio is richer in fuel than the stoichiometric mixture ratio, at which

theoretically all the fuel is completely oxidized and the flame temperature is at a maximum. This is because a gas which is slightly richer in fuel tends to have a lower molecular weight. This results in a higher overall engine systems performance. The optimum mixture ratio of some propellant combinations shifts slightly with changes in chamber pressure. Also, in actual application the mixture ratio may be shifted away from the optimum value for one of the following reasons: (a) lower chamber temperature to stay within the temperature limitations of chamber construction material; (b) required coolant flow; (c) improved combustion stability.

Density Impulse

In addition to the overall system-oriented specific impulse which we thoroughly discussed in paragraph 1-3, a quantity called "density impulse" is an important propellant performance parameter. It is the expression for the total impulse delivered per unit volume of the propellant. It is defined as:

$$\text{Density impulse} = I_s \cdot d \text{ (sec)} \quad (1-45)$$

wherein

d = bulk density or propellant combination, spec. weight

$$d = \frac{(r_w - 1)}{\frac{r_w}{d_o} + \frac{1}{d_f}} \quad (1-46)$$

r_w = (oxidizer/fuel) weight mixture ratio

d_o = bulk density of the oxidizer, spec. weight

d_f = bulk density of the fuel, spec. weight

The Selection of Liquid Rocket Propellants

When selecting a propellant or propellant combination for a specific application, it is well to realize that most propellants, in addition to their advantages, may have certain disadvantages. Thus, propellant selection usually includes some compromises. The more important and desirable propellant features are listed below. Order of importance may vary as a function of application.

- (1) High energy release per unit of propellant mass, combined with low molecular weight of the combustion or decomposi-

- tion gases, for high specific impulse.
- (2) Ease of ignition.
- (3) Stable combustion.
- (4) High density or high density impulse to minimize the size and weight of propellant tanks and feed system.
- (5) Ability to serve as an effective coolant for the thrust chamber (optimum combination of high specific heat, high thermal conductivity and high critical temperature).
- (6) Reasonably low vapor pressure at 160° F (a frequent specification value) for low tank weight and low net positive pump suction head requirement.
- (7) Low freezing point (preferably less than -65° F) to facilitate engine operation at low temperature.
- (8) Absence of corrosive effects; compatibility with engine construction materials.
- (9) For storables: good storability as assisted by a high boiling point (preferably above 160° F), by items 6, 7, 8 and by the resistance to deterioration during storage.
- (10) Low viscosity (preferably less than 10 cp down to -65° F) to minimize pressure drops through feed system and injector.
- (11) High thermal and shock stability to minimize explosion and fire hazard.
- (12) Low toxicity of raw propellants, their fumes, and their combustion products.
- (13) Low cost.
- (14) Availability.

Liquid Rocket Propellant Performance and Physical Properties

Detailed methods to calculate the performance for any given liquid propellant or propellant combination can be found in the standard combustion engineering or rocket propellant textbooks. For the theoretical calculations, it is generally assumed that the ideal conditions exist as described in section 1.2 (Gas Flow Processes) of this chapter. The prime objective of propellant-performance calculations is to derive the quantities c^* , C_f , and I_s through evaluation of the flame or chamber temperature $(T_c)_{ns}$; of the gas mean molecular weight \bar{M} ; and of the specific heat ratio γ for a given $(p_c)_{ns}$, p_e and p_a . The

chamber temperature can be calculated from the heat of the chemical reaction of the propellants and from the specific heat of the gases. In practice it has been found that actual test results are usually 5 to 12 percent lower than the theoretical values obtained from calculations.

In addition to the assumption of certain idealized gas conditions, the performance equations discussed assumed and employed certain singular values for the most important gas properties: γ , M , R , $(T_c)_{ns}$. For basic design information requiring greater accuracy, more rigorous calculations frequently employing electronic computers are usually conducted by specialists in the field. These consider that the gas properties are not necessarily constant along the path of flow. Two basic approaches can be taken: Calculations based on the assumption of unchanging or "frozen" gas composition along the nozzle axis, or based on the assumption of shifting composition. The applicable literature frequently uses the term "equilibrium" instead of "composition."

In calculations based on frozen composition, it is assumed that no further chemical reactions take place in the gases after leaving the combustion chamber and entering the nozzle, and that the combustion products at A_e are in the same relative proportion as they were at A_i . The remaining principal variables then are pressure and temperature at the various stations. Assuming different initial sets of mixture ratios, chamber pressures, and gas compositions, a typical set of calculations, probably involving successive approximations, may be conducted to determine the optimum values of, for instance mixture ratio, chamber length, expansion area ratio, and nozzle contour, for a given propellant combination and vehicle trajectory.

Calculations based on shifting composition take into account additional variations, mainly those of gas composition, as they result from, for instance, incomplete combustion, dissociation, and reassociation. These calculations are an attempt to consider more nearly the true physical processes. Due to their extreme complexity and unpredictability, however, the results are frequently no more reliable predictions of test results than those obtained from calculations assuming frozen composition.

Thus, it is probably a matter of preference which approach should be taken. It is noted that

the theoretical data based on a shifting composition usually give values several percent higher than those based on a frozen one. Therefore, in presenting performance data, the assumption of the type of composition assumed must be specified. As a rule, the thrust chamber designer will be supplied with the basic parameters by departments specializing in this field. We need not, therefore, concern ourselves further with this matter.

Performance and physical properties of numerous important liquid monopropellants and bipropellants are given in tables 1-4 through 1-10.

1.5 THE BASIC ELEMENTS OF A LIQUID PROPELLANT ROCKET ENGINE SYSTEM

A vehicle system has occasionally been defined as a purposeful conglomeration of subsystems. One of these is the engine system. The definition of the scope of the various vehicle subsystems has not always been uniform and probably, by necessity, never will be. For instance, for vehicle systems in which the propellant tanks simultaneously serve as the vehicle airframe, it may be a matter of opinion whether they are part of the structure or of the engine system. The decision to which subsystem they belong may well depend on the fact whether the tanks will be supplied by the engine manufacturer, or by a separate contractor. Similarly, some, notably the engine system supplier, may consider the guidance system a part of the payload, while the vehicle user will hold that anything without which the vehicle cannot fly reliably and accurately to its destination is not payload. Whatever the definitions may be, it is important that they are used uniformly and consistently in a given project.

For the purpose of this book, we will define a vehicle as being composed of the following major subsystems:

- (1) Engine system
- (2) Vehicle structure
- (3) Guidance system
- (4) Payload
- (5) Accessories

In the following, we will concern ourselves with the engine system only, except for brief references to the other systems, as required. We

TABLE 1-4.—General Data of Some Storable Liquid Rocket Propellants

Propellant	Formula	Use	Mol. wt.	Freezing point °F	Boiling point °F	Vapor press., psia	Density gm/cc	Stability	Handling hazard	Storability	Materials compatibility	Cost \$/lb
Aniline	$C_6H_5NH_2$	Fuel, coolant	93.2	21	364	0.25 at 160° F	1.022 at 68° F	Good	Good	Good	Al., steel, Teflon, Kel-F
Bromine pentafluoride	BrF_5	Oxid., coolant	174.9	-80.5	104.5	41 at 160° F	2.48 at 68° F	Up to 800° F	Reacts with fuel	Good	Al. alloy, 18-8 stainless steel, nickel alloy, copper, Teflon	4.75
Chlorine trifluoride	ClF_3	Oxid.	92.5	-105.4	53.15	80 at 140° F	1.825 at 68° F	Up to 600° F	Toxic	Good below 140° F	Al. alloy, 18-8 stainless steel, nickel alloy, copper, Teflon	0.50-2.50
92.5% E.A. (ethyl alcohol)	C_2H_5OH	Fuel, coolant	41.25	-189	172	13 at 160° F	0.81 at 60° F	Good	Flammable	Good below 130° F	Al., steel, nickel alloy, Teflon, Kel-F, polyethylene	0.15
Hydrazine	N_2H_4	Fuel, oxid., coolant	32.05	34.5	235.4	2.8 at 160° F	1.01 at 68° F	Up to 300° F	Toxic, Flammable	Good	Al., 304.307 stainless steel, less steel, Teflon, Kel-F, polyethylene	0.50-3.00
95% hydrogen peroxide	H_2O_2	Monoprop., oxid., coolant	32.57	21.9	294.8	0.05 at 77° F	1.414 at 77° F	Unstable decomp. at 285° F	Hazardous skin contact, flammable	Deteriorates at 1%/yr.	Al., stainless steel, Teflon, Kel-F	0.50
98% hydrogen peroxide	H_2O_2	Same as above	33.42	27.5	299.2	0.043 at 77° F	1.432 at 77° F	Same as above	Same as above	Same as above	Same as above	1.00
Hydrazine (40% "Delta" 60% "UDMH")	$NH(C_2H_4NH_2)_2$ $(CH_3)_2NNH_2$	Fuel, coolant	72.15	-65	140 to 400	16.5 at 160° F	0.855 at 60° F	Good	Toxic	Good	Al., stainless steel, Teflon, Kel-F	0.50-2.00
IRFNA (inhibited red fuming nitric acid)	82% HNO_3 , 15% NO_2 , 2% H_2O , 1% HF	Oxid., coolant	55.9	-57	150	17.3 at 160° F	1.57 at 68° F	Good	Toxic, hazardous skin contact	Good	Al., stainless steel, Teflon, Kel-F, polyethylene	0.08-0.10
JP-4 (jet propulsion fuel)	$C_{10}H_{18}$	Fuel, coolant	128	-76	270 to 470	7.2 at 160° F	0.747 to 0.825 at 60° F	Good	Vapor explosive	Good	Al., steel, nickel alloy, neoprene, Teflon, Kel-F	0.015
MMH (monomethylhydrazine)	CH_3NH-NH_2	Fuel, coolant	46.08	-63	187	8.8 at 160° F	0.878 at 68° F	Good	Toxic	Good	Al., 304.307 stainless steel, Teflon, Kel-F, polyethylene	0.62-6.25

TABLE 1-4. -General Data of Some Storable Liquid Rocket Propellants (Continued)

Propellant	Formula	Use	Mol. wt.	Freezing point °F	Boiling point °F	Vapor press., psia	Density gm/cc	Stability	Handling hazard	Storability	Materials compatibility	Cost \$/lb
Nitrogen tetroxide	N_2O_4	Oxid.	92.02	11	70	111 at 160° F	1.44 at 68° F	Function of temp.	Very toxic, hazardous skin contact	Good when dry	Al., stainless steel, nickel alloy, Teflon	0.075
Pentaborane	B_5H_9	Fuel	63.17	-52.28	140.11	19 at 160° F	0.61 at 68° F	Good	Explosive on exposure to air, very toxic	Good	Al., steel, copper, Teflon, Kel-F, Viton A	2.50-5.00
Propyl nitrate	$C_3H_7NO_3$	Fuel, coolant	105.09	-130.9	231	3.7 at 160° F	1.06 at 68° F	Fair	Sensitive to shock	Good	Al., stainless steel, Teflon, Kel-F
RP-1 (rocket propellant)	Mil-Spec-F25576B	Fuel, coolant	165 to 195	-47 to -64	342 to 507	0.33 at 160° F	0.82 at 68° F	Auto. ignition at 470° F	Flammable	Good	Al., steel, nickel alloy, copper, Teflon, Kel-F, Neoprene	0.015
TEA (triethylaluminum)	$(C_2H_5)_3 Al$	Fuel, start compound	114.15	-49.9	381	0.40 at 160° F	0.836 at 68° F	Decomp. over 400° F	Ignites on contact with air	Good	Al., steel, copper, Teflon
TMA (trimethylamine)	$(CH_3)_3 N$	Fuel	59.11	-179	37	108 at 160° F	0.603 at 68° F	Good	Good	Good	Al., steel, copper, Teflon
TMB-1, 3-D (NNN'-N'-tetramethylbutane-1, 3-diamine)	$(CH_3)_2 N-CH_2CH_2-CH-N(CH_3)_2$ $C'H_3$	Fuel, coolant	144.2	-131	320	1.32 at 160° F	0.795 at 68° F	Stable 1 hr. at 500° F	Good	Al., 347 stainless steel, polyethylene
TVM (tetranitromethane)	$C(NO_2)_4$	Oxid.	196.04	57.3	259	2.38 at 165° F	1.64 at 68° F	Thermal. unstable	Shock sensitive	Good below 100° F	Al., mild steel, Teflon, Kel-F	0.30
UDMH (unsymmetrical dimethylhydrazine)	$(CH_3)_2 NNH_2$	Fuel, coolant	60.08	-72	146	17.6 at 160° F	0.789 at 68° F	Good	Toxic	Good	Al., stainless steel, Teflon, Kel-F	0.50-2.00
WFNA (white fuming nitric acid)	97.5% HNO ₃ , 2% H ₂ O, 0.5% NO ₂	Oxid., coolant	59.9	-45	186	9.09 at 160° F	1.46 to 1.52 at 68° F	Decomp. above 100° F	Toxic, hazardous skin contact	Fair	Al., stainless steel, Teflon, Kel-F, polyethylene	0.15

DESIGN OF LIQUID PROPELLANT ROCKET ENGINES

TABLE 1-5.—General Data of Some Cryogenic Liquid Rocket Propellants

Propellants	Formula	Use	Mol. wt.	Freezing point, °F	Boiling point, °F	Critical press., psia	Critical temp., °F	Density at boiling point gm/cc	Stability	Handle hazard	Materials compatibility	Cost \$/lb
Ammonia	NH ₃	Fuel, coolant	17.03	-108	-28	Vapor pressure = 500 psia at 160° F		0.683	Good	Toxic, flammable	Al., steel, lead, Teflon, Kel-F, Vitron A	0.04
Liquid fluorine	F ₂	Oxid.	38.00	-364	-307	808	-200.5	1.509	Good	Very toxic, flammable	Al., 300 series stainless steel, nickel alloy, brass	6.00
Liquid hydrogen	H ₂	Fuel, coolant	2.016	-434.6	-422.9	187.8	-400.3	0.071	Good	Flammable	Stainless steel, nickel alloy, Al. alloy, Kel-F	7.00
Liquid oxygen	O ₂	Oxid.	32.00	-362	-297.4	735	-182	1.142	Good	Good	Al., stainless steel, nickel alloy, copper, Teflon, Kel-F	0.05
Oxygen difluoride	OF ₂	Oxid.	54.00	-299	719	-72.3	1.521	Good	Very toxic, flammable	Al., 300 series stainless steel, nickel alloy, brass
Ozone	O ₃	Oxid.	48.00	-420	-168	804	10.2	1.46	Above 20% explosive	Very toxic, flammable	Al., 300 series stainless steel, Teflon, Kel-F

TABLE 1-6.—Performance of Some Liquid Rocket Monopropellants

Propellant	Specific impulse I_s , lb-sec/lb ^a	Density impulse I_d , sec gm/cc	Applications	Remarks
Hydrogen peroxide (H ₂ O ₂) (95%)	140	198	Gas generators for turbopump and auxiliary drive; small control rockets	Difficult handling
Hydrazine (N ₂ H ₄)	205	207	Gas generators; small control rockets	Difficult handling (can decompose at high temperature)
Nitromethane (CH ₃ NO ₂)	180	204.8	Small ordnance rockets	Dangerous handling (can detonate unexpectedly)
Methylacetylene	160	108.6	Gas generators; small rockets	Safe handling; dangerous and very smoky exhaust fumes

^aTheoretical value at 300 psia (P_c)_{NS}, sea-level optimum expansion, frozen gas composition or frozen equilibrium.

TABLE 1-7.—Theoretical Performance of Some Medium-Energy Storable Liquid Rocket Bipropellant Combinations

Oxidizer	Fuel	r_w	r_v	d	T_c	η	c^*	C_f	I_s	I_{sd}	Applications
IRFNA (15% NO ₂)	UDMH	2.99	1.51	1.26	5340	23.7	5490	1.619	276	348	Small air-to-air, air-to-surface rockets and upper stages of space vehicles
		3.24	1.63	1.27	5315	24.2	5435	1.630	275	350	
	Hydrazine	1.47	.95	1.28	5090	20.8	5690	1.602	283	362	
		1.54	.99	1.29	5100	21.1	5665	1.608	283	365	
	50% UDMH-50% hydrazine	2.20	1.26	1.27	5250	22.4	5580	1.610	279	354	
		2.42	1.39	1.29	5220	23.0	5510	1.618	277	358	
	Hydyne	3.11	1.70	1.31	5295	24.1	5425	1.620	273	358	
		3.33	1.82	1.32	5270	24.5	5375	1.630	272	359	
	RP-1	4.80	2.48	1.35	5355	25.8	5275	1.636	268	362	
		5.14	2.65	1.36	5330	26.2	5225	1.646	267	363	
	TMB-1, 3-D	4.09	2.08	1.32	5325	25.1	5335	1.632	270	356	
		4.37	2.23	1.33	5300	25.5	5280	1.640	269	358	
	JP-X (60% JP-4, 40% UDMH)	4.13	2.16	1.33	5310	24.6	5320	1.628	269	358	
		2.89	1.47	1.26	4935	5130	1.626	259	326	
MMH	2.47	1.38	1.28	5290	5550	1.618	279	357		
	4.01	1.61	1.21	5285	5375	1.625	271	328		
95% hydrogen peroxide	UDMH	4.54	2.53	1.24	4800	21.7	5530	1.620	278	345	Manned aircraft, small air-to-air, air-to-surface rockets, and upper stages of space vehicles
		4.74	2.64	1.25	4780	21.3	5505	1.620	277	346	
	Hydrazine	2.17	1.54	1.26	4675	19.5	5655	1.604	282	355	
		2.20	1.57	1.26	4675	19.5	5655	1.604	282	355	
	50% UDMH-50% Hydrazine	3.35	2.12	1.25	4760	20.5	5580	1.610	279	349	
		3.47	2.20	1.26	4740	20.6	5560	1.615	279	351	
	Hydyne	4.68	2.83	1.27	4765	21.3	5485	1.622	276	350	
		4.87	2.95	1.28	4745	21.4	5465	1.619	275	352	
	RP-1	7.35	4.18	1.30	4785	22.1	5405	1.627	273	355	
		7.58	4.32	1.31	4765	22.2	5390	1.620	271	355	
	TMB-1, 3-D	6.20	3.49	1.28	4770	21.8	5440	1.622	274	351	
		6.45	3.63	1.29	4745	21.9	5415	1.618	272	351	

TABLE 1-7.—Theoretical Performance of Some Medium-Energy Storable Liquid Rocket Bipropellant Combinations (Continued)

Oxidizer	Fuel	r_w	r_v	d	T_c	η	c^*	C_f	I_s	I_{sd}	Applications
Nitrogen tetroxide	UDMH	2.95	1.61	1.20	5685	24.5	5555	1.632	282	339	Manned aircraft, ICBM, IRBM, ALBM, small air-to-air, surface-to-air rockets, upper stages of space vehicles
	Hydne	2.71	1.61	1.22	5650	24.1	5580	1.626	282	344	
		2.95	1.75	1.24	5655	24.7	5525	1.631	280	347	
	RP-1	4.04	2.26	1.25	5745	25.7	5440	1.636	276	345	
		4.50	2.51	1.27	5755	26.5	5385	1.639	274	348	
	TMB-1, 3-D	3.55	1.96	1.23	5715	25.2	5495	1.631	278	342	
3.90		2.15	1.24	5710	25.9	5425	1.645	277	344		
92.5% E.A.	2.59	1.45	1.19	5290	5260	1.635	267	318		
Chlorine trifluoride	UDMH	3.03	1.31	1.38	6305	25.8	5630	1.602	280	386	ICBM, IRBM, ALBM, and small air-launched rockets, upper stages of space vehicles
		3.28	1.42	1.40	6330	26.2	5605	1.589	277	388	
	Hydne	2.98	1.40	1.43	6220	26.1	5555	1.599	276	395	
		3.20	1.50	1.44	6250	26.5	5535	1.595	274	395	
	RP-1	3.20	1.42	1.41	5890	29.1	5140	1.618	258	364	
		12.80	5.66	1.68	5735	37.0	4535	1.636	230	386	
TMB-1, 3-D	3.17	1.39	1.40	6035	27.6	5330	1.608	266	373		
	3.60	1.57	1.43	6040	28.1	5280	1.592	261	374		
Bromine pentafluoride	Hydrazine	3.35	1.37	1.86	5570	5000	1.565	243	453	Small air-launched rockets

TABLE 1-8.—Theoretical Performance of Some High-Energy Storable Liquid Rocket Bipropellant Combinations

Oxidizer	Fuel	r_w	r_v	d	T_c	η	c^*	C_f	I_s	I_{sd}	Applications
95% Hydrogen peroxide	Hydrazine	2.01	1.41	1.26	4775	19.5	5735	1.601	285	359	ICBM, IRBM, ALBM
	Pentaborane	2.70	1.188	1.037	5390	19.01	6067	1.600	302	313	
Nitrogen tetroxide	UDMH	2.61	1.42	1.18	5685	23.6	5650	1.624	285	336	FBM, ICBM, IRBM, ALBM, upper stages of space vehicles
	Hydrazine	1.34	.93	1.22	5390	20.9	5845	1.610	292	357	
		1.42	.99	1.23	5415	21.3	5815	1.605	290	357	
	50% UDMH-50% Hydrazine	2.00	1.24	1.21	5590	22.6	5725	1.620	288	348	
MMH	2.15	1.33	1.21	5570	23.0	5665	1.636	288	348		
Chlorine trifluoride	Hydrazine	2.77	1.53	1.51	6550	23.2	5995	1.582	294	444	FBM, ICBM, IRBM, ALBM, upper stages of space vehicles
		2.94	1.62	1.52	6600	23.6	5980	1.572	292	444	
	50% UDMH-50% Hydrazine	2.89	1.42	1.45	6385	24.5	5795	1.596	287	416	
	MMH	3.11	1.53	1.46	6420	24.9	5770	1.598	286	417	
Hydrazine	Pentaborane	1.4	.85	.796	4430	14.7	6402	1.644	327	261	ICBM, IRBM

TABLE 1-9.—Theoretical Performance of Some High-Energy Cryogenic Liquid Rocket Bipropellant Combinations

Oxidizer	Fuel	r_w	r_v	d	T_c	\bar{M}	c^*	C_f	I_s	I_{sd}	Applications
Liquid oxygen	RP-1	2.00	1.421	0.998	5760	21.1	5898	1.605	294	293	ICBM, IRBM, large space-probe and space craft boosters
		2.40	1.708	1.012	6100	22.8	5953	1.620	300	303	
		2.56	1.82	1.02	6150	23.3	5920	1.632	300	306	
		2.73	1.94	1.03	6200	23.9	5865	1.642	299	308	
	Ammonia	1.30	.78	.88	5055	19.3	5920	1.608	296	260	
		1.40	.84	.89	5100	19.8	5865	1.612	294	261	
	95% E.A.	1.73	1.23	.99	5640	24.1	5605	1.648	287	284	
		1.80	1.28	1.00	5675	24.4	5585	1.644	285	285	
	Hydrazine90	.80	1.07	5660	19.3	6235	1.618	313	335	
		1.30	1.03	1.02	5980	20.6	6160	1.628	312	318	
	50% UDMH-50% Hydrazine	1.37	1.08	1.03	5905	20.9	6155	1.622	310	319	
		1.73	1.31	1.02	5990	21.8	6035	1.632	306	312	
	Hydyne	1.80	1.36	1.02	6030	22.2	6010	1.639	306	312	
		1.65	1.14	.98	6010	21.3	6115	1.631	310	304	
	UDMH	1.83	1.27	.99	6065	22.1	6040	1.638	307	304	
		2.28	1.60	1.01	6100	22.9	5945	1.642	303	306	
TMB-1,3-D	2.37	1.66	1.01	6120	23.2	5915	1.650	303	306		

TABLE 1-10.—Theoretical Performance of Some Very-High-Energy Cryogenic Liquid Rocket Bipropellant Combinations

Oxidizer	Fuel	r_w	r_v	d	T_c	\bar{M}	c^*	C_f	I_s	I_{sd}	Applications
Liquid oxygen	Liquid hydrogen	4.02	0.25	0.28	4935	10.0	7980	1.578	391	109	Space probe and space craft upper stage and booster
		19.50	1.20	.65	4960	23.4	5300	1.610	265	172	
Liquid fluorine	Hydrazine	2.30	1.54	1.31	7955	19.4	7245	1.615	363	476	Space probe upper stage
		2.40	1.61	1.32	7980	19.6	7235	1.614	362	478	
	Liquid hydrogen	7.60	.35	.45	6505	11.8	8365	1.578	410	185	
		23.70	1.10	.82	8230	18.5	7515	1.592	372	305	
	Ammonia	3.29	1.48	1.18	7715	19.3	7155	1.605	357	421	
	3.40	1.53	1.18	7745	19.5	7140	1.612	357	422		

NOTES FOR TABLES 1-7 THROUGH 1-10

- (1) Conditions upon which the performance calculations are based =
- (a) Combustion chamber pressure = 1000 psia
 - (b) Nozzle exit pressure = ambient pressure = 14.7 psia (optimum nozzle expansion ratio at sea-level operation)
 - (c) Chamber contraction ratio (chamber area/nozzle throat area) = infinity
 - (d) Adiabatic combustion
 - (e) Isentropic expansion of ideal gas with shifting composition or shifting equilibrium in the nozzle

(2) Symbols:

- r_w = Propellant weight mixture ratio (wt. oxidizer/wt. fuel)
- r_v = Propellant volume mixture ratio (vol. oxidizer/vol. fuel)
- d = Bulk density of propellant combination (gm/cc). (The density at boiling point was used for those oxidizers or fuels which boil below 68° F at one atmosphere pressure)
- T_c = Theoretical chamber temperature, °F
- \bar{M} = Average molecular weight of combustion products at T_c
- c^* = Theoretical characteristic velocity (ft/sec)

NOTES FOR TABLES 1-7 THROUGH 1-10 (Continued)

C_T = Theoretical thrust coefficient	900	99
I_S = Theoretical maximum specific impulse, lb-sec/lb	800	98
$I_S d$ = Theoretical maximum density impulse, sec-gm/cc	700	97
	600	95
(3) To approximate I_S and $I_S d$ at other chamber pressures.	500	93
Pressure (psia):	Multiply by—	400
1000	1.00	300
		88

further define that the engine system shall comprise all parts without which the propulsive force cannot be generated. Thus, we will include the propellant tanks and their accessories. A system thus defined frequently is called a propulsion system. We know, from the above, that by including the tanks, we may be "infringing" on the vehicle structure by other definitions.

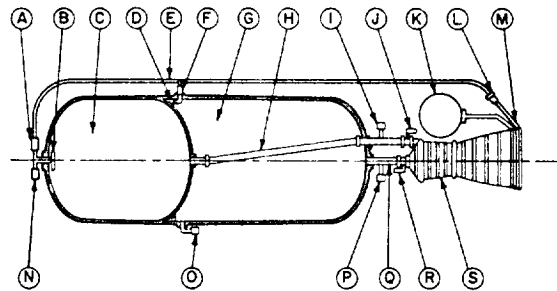
Thus prepared, we may now proceed to subdivide the engine system further into major components or subassemblies as follows:

- (1) Thrust chamber assembly
- (2) Propellant feed system: One of the following two is generally used: Pressurized gas propellant feed system and turbopump propellant feed system. The latter includes some type of tank pressurization system
- (3) Valves and control systems
- (4) Propellant tankage
- (5) Interconnect components and mounts

Depending on the engine system selected, one or another subsystem may not be required or may be integrated with another one. Typical liquid propellant rocket engine systems are shown in figures 1-12 and 1-13.

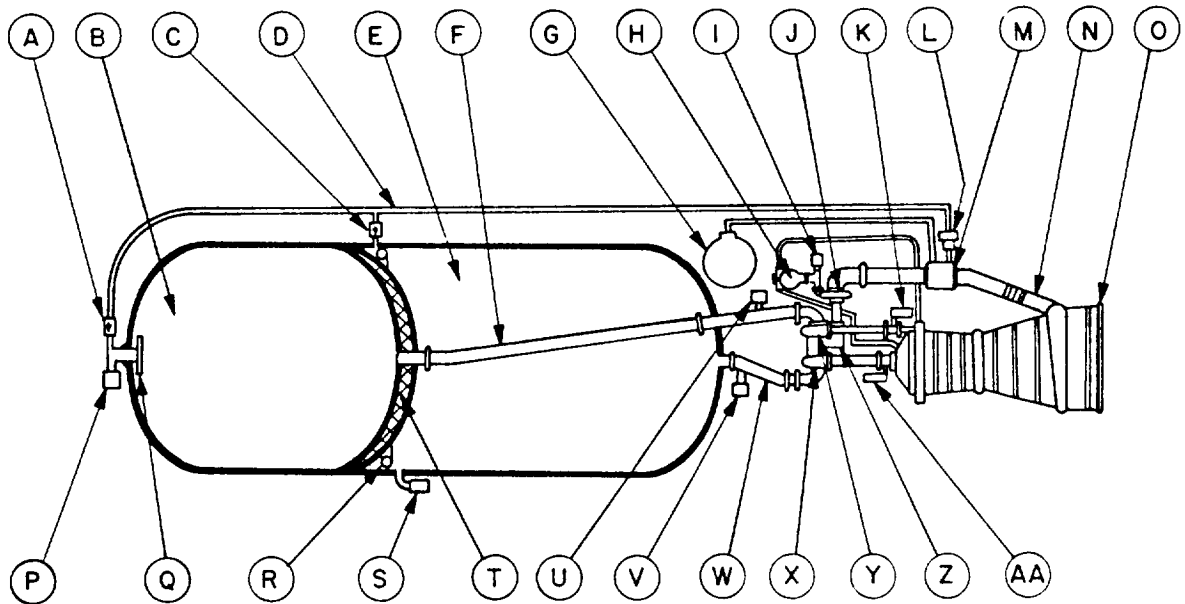
The rocket has occasionally been called the simplest propulsion system known. The simplest form of a solid propellant rocket or of a pressurized gas-fed storable liquid propellant rocket appears to come close to this ideal. Unfortunately, simplicity frequently is synonymous with inflexibility. Due to vehicle requirements, substantial departures from the basic simplicity may become necessary to meet requirements such as: light weight, high performance, thrust control, thrust vector control, restartability, cutoff im-

pulse control, propellant utilization control (sometimes called propellant management), storability, ease of handling, etc. Thus, modern rocket engines contain more subsystems than their basic principle of operation may suggest, to meet the often stringent vehicle requirements. This is true for both liquid as well as solid propellant systems. In general however, the liquid propellant engine is the more flexible one, particularly where large systems are considered.



- | | |
|----------------------------------|---------------------------------------|
| A Check valve | K High-pressure helium bottle |
| B Pressurizing gas diffuser | L Pressure regulator |
| C Fuel tank | M Heat exchanger |
| D Pressurizing gas diffuser | N Fuel tank vent and relief valve |
| E Pressurizing gas line | O Oxidizer tank vent and relief valve |
| F Check valve | P Oxidizer tank fill and drain valve |
| G Oxidizer tank | Q Oxidizer duct |
| H Fuel duct | R Main oxidizer valve |
| I Fuel tank fill and drain valve | S Thrust chamber assembly |
| J Main fuel valve | |

Figure 1-12.—Typical pressurized gas feed liquid propellant rocket engine system.



- | | | |
|------------------------------------|--|--------------------------------------|
| A Check valve | L Pressure regulator | cryogenic propellant combination) |
| B Fuel tank | M Heat exchanger | |
| C Check valve | N Turbine exhaust duct | U Fuel tank fill and drain valve |
| D Pressurizing gas line | O Thrust chamber assembly | V Oxidizer tank fill and drain valve |
| E Oxidizer tank | P Fuel tank vent and relief valve | W Oxidizer duct |
| F Fuel duct | Q Pressurizing gas diffuser | X Oxidizer pump |
| G High pressure helium bottle | R Pressurizing gas diffuser | Y Fuel pump |
| H Gas generator and valve assembly | S Oxidizer tank vent and relief valve | Z Gear box |
| I Turbine starting spinner | T Inter-tank insulation (required for cryogenic and non- | AA Main oxidizer valve |
| J Gas turbine | | |
| K Main fuel valve | | |

Figure 1-13.—Typical turbopump feed liquid propellant rocket engine system.

████████████████████

████████████████████

Chapter II

Rocket Engine Design Implements

2.1 THE MAJOR ROCKET ENGINE DESIGN PARAMETERS

To fit the engine system properly into a vehicle system, engine systems design and development specifications will have to cover the following parameters above all:

- (1) Thrust level
- (2) Performance (specific impulse)
- (3) Run duration
- (4) Propellant mixture ratio
- (5) Weight of engine system at burnout
- (6) Envelope (size)
- (7) Reliability
- (8) Cost
- (9) Availability (time table--schedule)

As the design progresses, numerous additional parameters will have to be considered. Before turning to the latter, let us briefly review and discuss those listed above. It should be noted that the last five items are closely interdependent. For instance, making an engine available in the shortest possible time ("crash program") will raise the cost and will unfavorably affect reliability. A longer design and development period may not necessarily reduce cost, but it will offer higher values in exchange for the dollar; higher reliability, refined (lower) weight, and an optimized (smaller) envelope.

Thrust Level

This engine parameter is a basic one, similar to the power rating of a gasoline engine or electric motor. It will affect most of the other engine parameters and many of the development considerations.

The total thrust requirement of a rocket-propelled vehicle is predominantly governed by--

1. The total takeoff weight of the vehicle (including engine!)
2. Minimum and maximum accelerations permissible

Selection of the proper engine thrust level

results from the decision whether a single- or a multiple-engine system is to be used. This decision is often strongly influenced by the availability of already existing engines, which would eliminate, or at least drastically reduce, the design and development cost for the propulsion system. The selection of individual engine thrust level also is--or at least should be--influenced by the general state of the art, particularly if sizes substantially larger than previously developed are considered.

More recently, largely as a result of the advent of manned rocket flight and of the high cost of very large vehicle systems, the decision to use a multiple (clustered) propulsion system consisting of several engines rather than a single one has been additionally affected by safety considerations, to permit mission completion, or at least safe return of the crew, in case of an engine failure. This "engine out" principle is analogous to the consideration of multiple-versus single-engine airplanes. Extensive studies have been conducted in this field for rocket vehicles to establish the "break-even" point regarding the minimum and maximum number of engines profitably employed in a cluster. Failure of single-engined rocket vehicles not only might destroy the vehicles themselves but also could cause severe damage to expensive ground facilities. This explains the great emphasis placed on thrust subdivision.

Thrust levels for first-stage booster engines, which start at or near sea-level altitude and stop at a specified higher altitude, are usually quoted for sea-level conditions. Additionally, the specifications may contain information on thrust level at altitudes above sea level, frequently in the form of a graph (see fig. 2-1).

The nominal thrust of engines in stages starting and operating at or near-vacuum conditions is quoted for that environment. Most engines are designed for a single nominal thrust (sea level or altitude), for which they are calibrated by

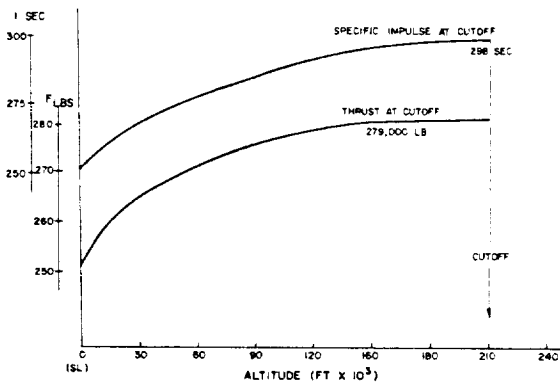


Figure 2-1.—Typical graph of rocket engine performance as function of altitude.

means of propellant line orifices or, less frequently, with the aid of regulators. Engines designed for variable thrust (throttling) always require some type of regulator. This will be discussed in section 7.3, "Engine Thrust Level Control."

Performance

Although the general term "performance" of a rocket engine in the strict sense covers a number of parameters (I_s , c^* , C_f , etc.), specific impulse (I_s) is considered the prime performance parameter. As was seen in chapter I, the specific impulse, also referred to as specific thrust, is measured in seconds, which obviously is not the dimension of time, but an abbreviation of the dimension lb-sec/lb (specific impulse), lb/(lb/sec) (specific thrust), respectively. It is important to state whether a specified value of I_s refers to the complete engine system, or to the thrust chamber only. Frequently, by stating a percentage an "actual" or "practical" value of I_s is linked to the maximum value theoretically possible. The theoretical values for the better known propellant combinations are well established and as a result practical values have become quite predictable. With less well-known combinations, disappointments have often resulted. Therefore, great caution is advisable in the use of theoretical values which have not been verified in an actual test.

In recent years, the performance of a rocket engine, as expressed by its specific impulse, has received considerable attention, far beyond

its true significance. In June 1959, Dr. von Kármán observed:

It is my personal belief that the length of the period of attaining reasonable reliability in the development process could be essentially reduced if simple design were emphasized as a leading principle, even if we had to make some sacrifice in the quantitative measure of "efficiency." Essential elements have to be designed as simply as possible, even if this means a reduction in quantitative efficiency and a certain increase of bulkiness and/or weight.

Undoubtedly, these observations were prompted by a noticeable trend on the part of both the engine builder as well as the customer, to sacrifice, or at least to compromise, nearly all other capabilities of a rocket propulsion system for I_s increases, which sometimes amounted to less than 1 percent.

Frequently, increasing emphasis on I_s during the life of a project can be traced to marginal engineering reserves in the initial vehicle design especially with weight assumptions and tank capacities. The need for competitive bidding may have contributed to this situation.

On the other hand, the highest I_s which can be obtained without compromise will pay off substantially. For instance, in the case of a typical medium-range ballistic missile, an increase of 1 second in I_s will effect a range increase of approximately 15 nautical miles. In other terms, an I_s increase of less than one-half percent results in a range increase of 1 percent. As impressive as these figures for increased flight range are, it should be kept in mind that those engine properties which will determine whether the vehicle will fly at all should not be com-

Duration

Because, by definition, a rocket vehicle carries its own complete propellant supply, including the oxidizer, its run duration is limited, as a result of an optimized balance between takeoff weight, trajectory, thrust level, and minimum and maximum accelerations. Consequently, run-duration times of most large liquid-propellant rocket engines fall into a relatively narrow band, about 50 to 400 seconds.

User specifications include a formal demonstration (such as preliminary flight rating tests (PFRT) and qualification tests) requiring accumulated duration times, without breakdown, of

CONFIDENTIAL

many times the comparatively short rated flight duration (typical: six full duration tests for PFRT of an ICBM).

These specifications, therefore, govern most engine design considerations, with the exception of the following areas, which for weight considerations are tailored to the flight-run duration:

- (1) Auxiliary tank capacity, for systems which employ a separate turbine power supply
- (2) Propellant-tank pressurization supply, if it is part of the engine system
- (3) Lube oil tank capacity, if applicable
- (4) Temperature nonequilibria, such as those of uncooled nozzles

Closely related to the run duration are the start and shutdown characteristics of an engine system, the requirements for both of which may be very stringent in a given vehicle system.

The characteristics and the quality of the "start," or "thrust buildup," of a liquid rocket engine are judged by—

- (1) Compliance with specified thrust versus time characteristics
- (2) Maximum rate of increase at any time during buildup
- (3) Freedom from surges and thrust overshoots
- (4) Smoothness (freedom from damaging oscillations)
- (5) Repeatability from run to run and from engine to engine

These characteristics will be discussed in greater detail in chapter X, "Engine Systems Design Integration." Suffice it to state, at this point that a rocket engine is not easy to adapt with special thrust buildup requirements. Difficulties in this area can arise from inadequate communication between the vehicle contractor and the engine contractor. Thorough understanding of the problems by both contractors is vital.

The characteristics of engine "shutdown" or "thrust decay" are predominantly influenced by guidance considerations. To understand this better, let us consider the case of a single-stage, ground-to-ground, ballistic missile. As the term "ballistic" implies, the missile is designed to impart a desired speed to a known payload, in a desired direction from a desired point, after which the payload coasts freely to the target.

This is analogous to a cannon, where muzzle exit velocity of the projectile, gun-barrel attitude, and location of the gun emplacement will determine the point of impact (neglecting environmental influences such as wind). With a ballistic rocket, the gun barrel is literally replaced by the guidance system, the intricate components of which not only predetermine the three basic parameters mentioned but also have the capability to compensate for deviations of any or all of them. If, for instance, the trajectory angle near the point of cutoff is too steep, the guidance system will compensate accordingly, by calling for a higher final velocity, by slightly delaying the cutoff signal, simultaneously considering the distance over ground already covered.

It is obvious that a prompt and repeatable execution of the cutoff signal is imperative. However, for several reasons, it is impossible to effect a truly instantaneous thrust cessation: time is required to sense and then transmit the cutoff signal; closing of valves requires a finite time; structural (hydraulic hammer) considerations are superimposed; residual propellants below the valves have an effect. Figure 2-2 shows a typical thrust decay diagram.

Let us recall:

$$Ft = m\Delta v$$

Thrust multiplied by time equals mass times velocity increase, or

$$\Delta v = \frac{Ft}{m}$$

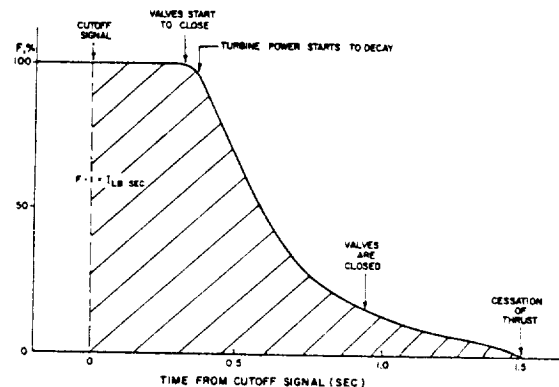


Figure 2-2.—Typical thrust decay diagram.

The velocity increase following cutoff signal is a function of the residual thrust acting on the vehicle mass m , and is integrated over the time from cutoff signal to final thrust cessation; this integral is commonly referred to as the "cutoff impulse." A typical value for a well-known earlier rocket (Redstone) was 16 000 lb-sec ± 2500 . Note the tolerance. This deviation will obviously influence missile accuracy. Reduction of the tolerance is thus an important design and development goal.

It might be concluded that a substantial reduction of the tolerance is the principal task, zero deviation being the optimum. This is unfortunately not so because the final vehicle mass m , on which the decaying thrust force acts, is unpredictable within certain limits, due to weighing tolerances of the initial vehicle mass, and to flow rate and mixture ratio tolerances. The engine designer and developer will have to concentrate on reducing both: base value and tolerance.

A glance at figure 2-2 shows that the area under the thrust curve is a function of not only decay time but also of main-stage thrust level. In fact, the major portion of the shaded area is accumulated prior to the beginning of thrust decay. This observation has led to the utilization of vernier thrust systems.

A vernier cutoff system is characterized by a substantial thrust reduction before final cutoff. This can be accomplished by thrust reduction, for a few seconds, of the main engine itself (V-2 fashion) or by shutdown of the main engines, while much smaller engines continue for a brief period (typical: 0-25 seconds, depending on final Δv required).

It should be emphasized that any components that must be added to improve cutoff characteristics are basically undesirable, since engine complexity is drastically increased. The addition of such components should be avoided at all costs. Here again, close coordination between the vehicle (guidance) designer and engine designer, and thorough understanding of their common problems, is vital.

Mixture Ratio

As is well known, complete combustion of a given amount of fuel requires a corresponding

amount of oxidizer. That mixture ratio which effects complete combustion, with no leftover of either fuel or oxidizer, is called the stoichiometric mixture ratio. This ratio depends on the type of propellants used. Theoretical temperature and heat release are maximum at this ratio. In rocket engines, however, where the highest possible exhaust velocity is desired, optimum conditions often prevail at other than stoichiometric ratios. Equation 1-18 indicates that the gas properties strongly affect exhaust velocity. The expression for the specific gas constant, R , in equation 1-18 may be rewritten as—

$$R = \frac{R'}{\mu}$$

where R' is the universal gas constant and μ is the molecular weight of the gas (see table 1-1).

The lower the molecular weight, the higher the exhaust velocity, other things being equal. Analytical and experimental investigations will determine the optimum point of balance between energy release (heat) and composition (molecular weight) of the gas, a portion of which will consist of gasified but unburnt propellants. The optimum point may also be affected by—

- (1) *Stay time of the burning gas in the combustion chamber.*—Stay time is a function of combustion chamber volume and of gas volumetric flow rate. Complete combustion, even though desirable, requires a finite time which is not available unless the chamber is relatively large, and correspondingly heavy. A compromise in chamber size, therefore, is often made. This leaves unburned a small percentage even of those propellants entering the nozzle, which could have burned given sufficient time (chamber volume). This percentage must be considered for accurate determination and optimization of the composition of the combustion gases and when optimizing the gas properties with energy release and system weight.
- (2) *Cooling considerations.*—The temperatures resulting from stoichiometric or near-stoichiometric mixture ratios, dependent on propellant type, may impose severe demands on the chamber-wall cooling

system. A lower temperature, therefore, may be desired and obtained by selecting a suitable ratio.

Once the optimum mixture ratio has been determined for a given engine system, based on the major factors just discussed, it is obvious that deviations from it would result in engine performance penalties. Since the vehicle powered by an engine will have been sized and tanked to conform with the specified engine mixture ratio, it is important to know that deviations will also result in reduced vehicle performance, namely:

- (1) Reduced engine duration, due to premature exhaustion of one of the propellants
- (2) Reduced mass ratio, due to excessive residual amounts of the other propellant (increased burnout weight)

Since the relationship between engine performance (I_s) and mixture ratio for many systems is usually relatively flat near the optimum point (fig. 2-3), the effects from duration and burnout weight may well be the most influential ones for vehicle range.

The effects of even minor discrepancies in mixture ratio (propellant utilization) are substantial. For instance, in a typical single-stage medium-range ballistic missile, each pound of excess burnout weight will result in a range decrease of approximately 0.2 nautical miles. For long-range vehicles, the penalty is still higher. The close target tolerances that have occasionally been reported for test flights illustrate the remarkable degree of accuracy which can be achieved from all contributing subsystems.

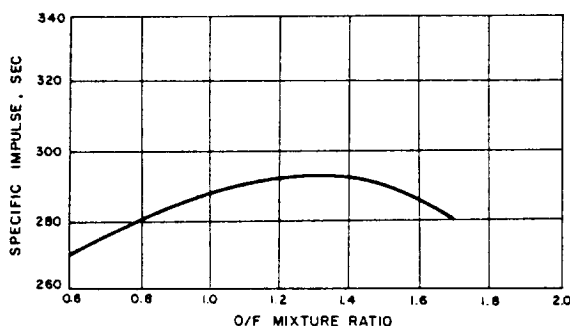


Figure 2-3.—Theoretical thrust chamber performance vs mixture ratio for N_2O_4/N_2H_4 at $p_c = 1000$ psia shifting equilibrium and optimum sea level expansion.

Weight

The parameter of weight, as no other, dominates the thinking of those employed in rocketry. Weight of payload flown over a distance, or placed into orbit, is the ultimate accomplishment. Success is often gaged directly in pounds of payload flown per dollar spent.

The importance weight rightfully carries does not necessarily mean that it is all important. For instance, a somewhat smaller payload placed into orbit more reliably, or at a lower cost per pound, may be preferred. By and large however, weight is a most important consideration.

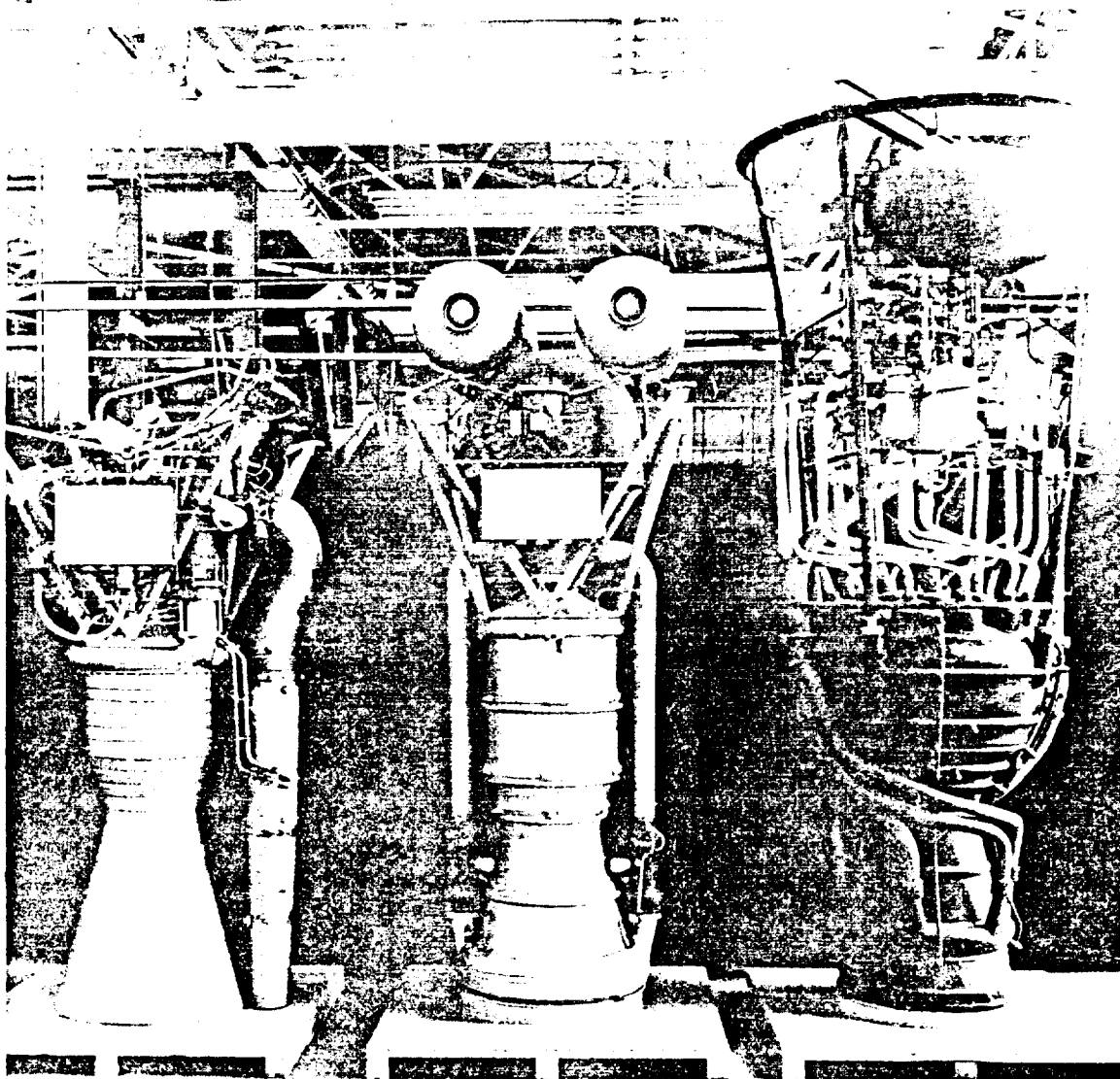
As we have seen earlier, a vehicle's final velocity is a function of, among other parameters, its mass ratio. The smaller the final mass, the higher the final velocity. However, since payload mass should be as high as possible, the weight squeeze is applied to all those vehicle components which are not payload. This includes the engine.

To isolate the influence of vehicle-structures weight, a parameter called "propellant fraction" has come into increased usage. This factor expresses the ratio of the total propellant weight to the fueled vehicle weight without payload. Typical values are 0.94 for turbopump-fed systems, and 0.89 for pressure-fed systems. For turbopump-fed engines, the ratio of thrust to engine weight is a useful additional yardstick. Larger modern liquid rocket engines may fall into a range from 75 to 125 pounds of thrust/lb of engine weight. These figures represent a substantial progress over the past (see fig. 2-4).

As was seen with residual propellants, excessive dead weight at burnout imposes penalties. Therefore, whenever rocket engines can be made lighter without compromising reliability and structural integrity, the payoff in range and payload will be sizable.

Engine and vehicle builders usually distinguish several types of engine weight:

- (1) *Dry weight*.—The net weight of the engine as it leaves the factory.
- (2) *Burnout weight*.—The engine dry weight plus residual, measurable propellants remaining in the engine at cutoff. In a typical engine design, burnout weight may be 4 percent higher than dry weight. Burnout weight is significant for vehicle mass ratios (eq. 1-30).



(a)	(b)	(c)
↑	↑	↑
Early Navaho Engine (Rocketdyne 1953) Thrust _{SL} : 120,000 lb Dry Weight: 1230 lbs I _{SSL} = 230 sec	Early Redstone Engine (Rocketdyne 1952) Thrust _{SL} : 75,000 lb Dry Weight: 1475 lb I _{SSL} = 215 sec	German V-2 Engine (1942) Thrust _{SL} : 56,000 lb Dry Weight: 2484 lb I _{SSL} = 199 sec

Figure 2-4.—Substantial progress has been made in ratio of thrust to engine weight as demonstrated by: (a) postwar engine (1953), thrust_{SL}: 120 000 lb, dry weight: 1230 lb, I_{SSL} = 230 sec; (b) postwar engine (1952), thrust_{SL}: 75 000 lb, dry weight: 1475 lb, I_{SSL} = 215 sec; (c) German V-2 engine (1942), thrust: 56 000 lb, dry weight: 2484 lb, I_{SSL} = 199 sec.

CONFIDENTIAL

- (3) *Wet weight.*—The engine dry weight plus all propellant within it, during main stage. In a typical design, engine wet weight may be 6 percent higher than dry weight. Wet weight is significant for vehicle in-flight center-of-gravity location and moments of inertia.
- (4) *Wet gimbale weight.*—That portion of wet weight representing engine mass which is gimbale for steering purposes. In earlier designs this meant essentially the thrust chamber and injector wet weight. In later designs it often refers to the entire engine less a relatively small amount of stationary parts. This weight is significant for gimbal actuator loads and guidance control loop response characteristics.

Ideally, dry weight and burnout weight should be equal; that is, no propellants should be trapped in the engine at shutdown. In practice, this will not always be possible. However, the engine designer can do much through proper design, siz-

ing and routing of lines, avoidance of traps, and location of valves.

Because of the importance of weight control, rocket engine manufacturers employ engineers specifically in charge of this area. Table 2-1 shows a typical weight progress form, as it is used by the Rocketdyne Division of North American Aviation. It is revised and reissued periodically. Thus it becomes a useful tool to raise early danger warnings. In our arbitrary example a slight underweight is shown. However, the table also shows that the data are based almost entirely on estimated and calculated figures, rather than on actual weighing results. This is characteristic for the earlier phases of design and development of a rocket engine. More often than not, the weight advantage will disappear gradually as the design firms up; then the squeeze will be on. For convenient display of the weight tendencies over time, a graph such as shown in figure 2-5 will be useful.

The weight changes of the various components as well as of the entire engine affect centers of gravity and moments of inertia. Through

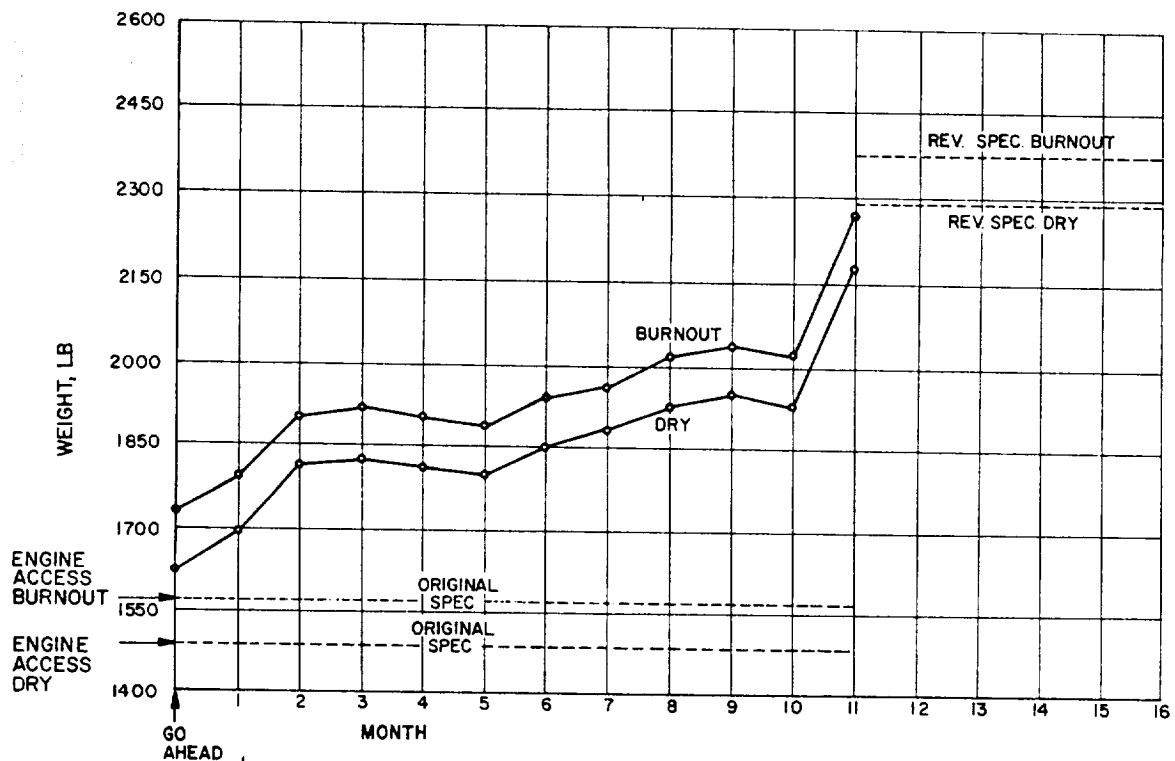


Figure 2-5.—A-2 stage rocket engine and accessory weight history.

TABLE 2-1.-A-2 Stage Engine Weight Report

	Spec. weight per original design	Con-tractor changes (rev. spec. weight)	Current status	Last status (Report No. 11)	Changes last to current status (col. 4 minus col. 5)	Basis for current data			Notes
						Percent, estimated			
						7	8	9	
1	2	3	4	5	6	7	8	9	10
Model: A-2 stage. Contract: Issue: 1 Date: Feb. 28, 1964. Enclosure: Page: 1 Report No. 12									
Rocket engine and accessories (at burnout) (A+D+E) (1580) (2380) (2292) (2112) (+180)									
Rocket engine and accessories (dry) (B+D) (1485) (2280) (2181) (2011) (+170) (18)									
A Rocket engine (at burnout) (B+C) (1365) (2000) (1923) (1763) (+160)									
B Rocket engine (dry) (1300) (1930) (1850) (1700) (+150) (24) (59) (17)									
Thrust chamber 500 730 730 640 +90 7 62 31									
Gimbal bearing 40 55 52 217 +33 6 94 0									
Turbopump, fuel 200 260 250 217 +33 1 97 2									
Mount, fuel pump 25 30 27 202 +22 1 87 12									
Turbopump, oxidizer 190 230 224 202 +22 0 33 67									
Mount, oxidizer pump 25 30 28 26 +2 3 82 15									
Fuel feed system 70 100 95 96 +1 72 28 0									
Oxidizer feed system 60 90 87 87 0 75 25 0									
Controls (ignit. elect. pneu.) 100 130 114 114 0 65 33 2									
Exhaust system 70 100 96 96 0 60 39 1									
Propellant utilization system 10 15 12 10 +2 4 96 0									
Start system 0 140 135 135 0 100 0 0									
C Fluid at burnout (rocket engine) (65) (70) (73) (63) (+10)									
D Accessories (185) (350) (331) (311) (+20) (2)									
Inlet line, fuel pump 50 85 79 74 +5 33 65 2									
Inlet line, oxidizer pump 50 85 81 75 +6 30 64 6									
Helium bottle 0 24 21 21 0 100 0 0									
Heat exchanger, oxygen 30 34 31 27 +4 12 82 6									
Flowmeters 5 6 5 5 0 100 0 0									
Instrumentation 50 80 78 73 +5 100 0 0									
Vehicle connection provision 0 36 36 36 0 100 0 0									
E Fluid at burnout (accessories) (30) (30) (38) (38) (0)									

~~CONFIDENTIAL~~

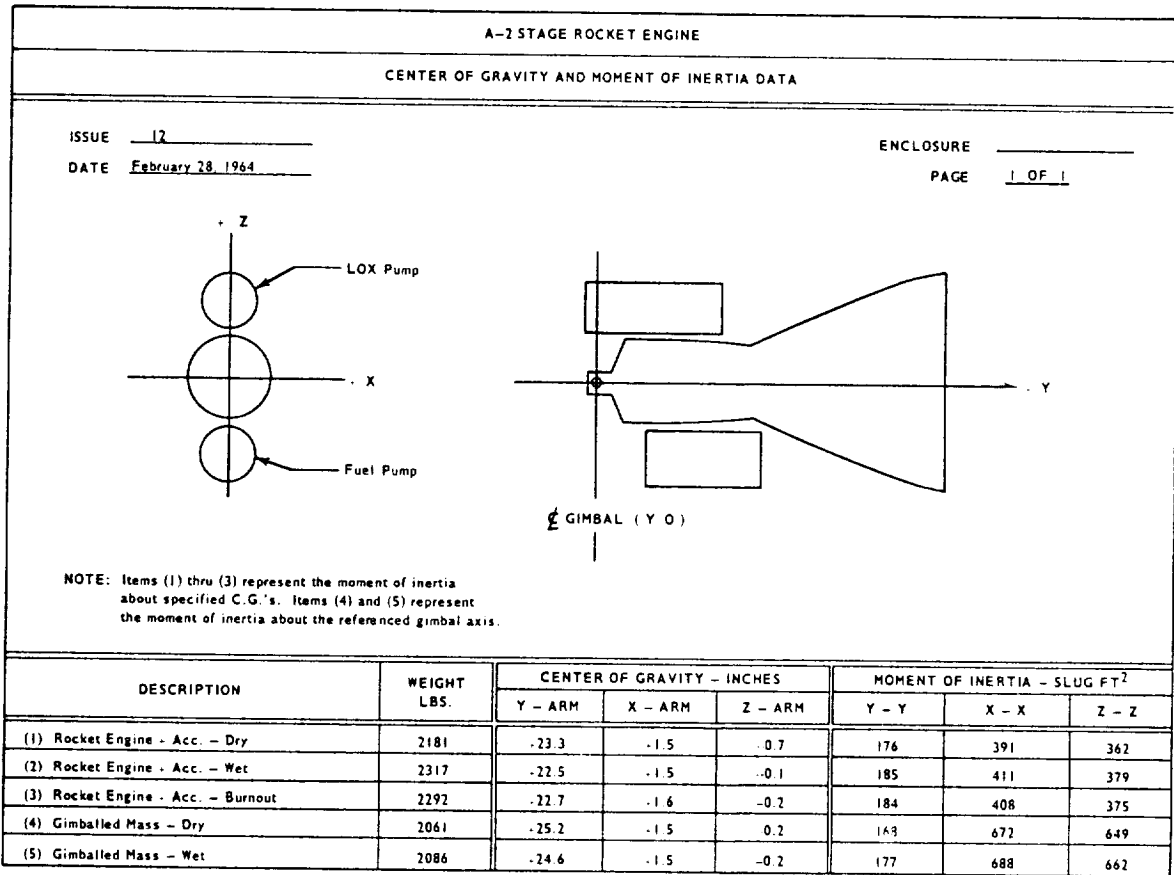


Figure 2-6.—Typical data sheet for center of gravity and moment of inertia.

issue of a data sheet as shown in figure 2-6, all parties concerned can be kept informed on changes as they occur.

Note that the data presented in table 2-1 and figures 2-5 and 2-6 are for the 150K A-2 stage engine system which is a part of an assumed multistage space vehicle configuration treated in later chapters.

Let us now explore the influence structural weight has on the performance and gross takeoff weight of a rocket vehicle system, and how its magnitude varies with the design parameters of different vehicle systems. The quantitative relationships will be evaluated individually for each case.

Equation (1-30) can be rewritten for the stage burnout velocity of a single-stage vehicle, or the stage velocity increment, of any individual stage of a multistage vehicle system as:

$$V_{bo} = C_{vc} \cdot g \cdot (I_s)_{oa} \ln$$

$$\left(\frac{\text{Stage usable propellant weight} + \text{Stage payload weight} + \text{Stage inert weight}}{\text{Stage payload weight} + \text{Stage inert weight}} \right) \quad (2-1)$$

where

$$\text{Stage inert weight} = \frac{\text{Stage residual propellant weight at burnout}}$$

$$+ \text{Stage engine system weight} + \text{Stage structure, guidance and other weights, which are not payload} \quad (2-2)$$

It can be concluded from these equations that for a given burnout velocity, there is an even weight trade off between stage engine system

weight and stage payload weight. If the weight of all other items were kept constant, a pound decrease in the stage engine system weight will increase the stage payload capacity by 1 pound.

For a fixed payload, and assuming other items except engine weight to be constant, the relation between the stage velocity increment, V_{bo} , and stage engine system weight for a given system can be written as

$$V_{bo} = k_1 \ln \left(\frac{k_3 + \text{Stage engine system weight}}{k_2 + \text{Stage engine system weight}} \right) \quad (2-3)$$

where

$$k_1 = C_{vc}g(I_s)_{oa} = \text{constant}$$

$$k_2 = \frac{\text{Stage payload weight}}{\text{Stage residual propellant weight at burnout}} + \frac{\text{Stage structure, guidance and other weight}}{\text{Stage usable propellant weight}} = \text{constant}$$

$$k_3 = \text{Stage usable propellant weight} + k_2 = \text{constant}$$

Since $k_2 < k_3$, the denominator will decrease more rapidly than the numerator, with decreasing engine weight. Thus for fixed payloads, an increase in burnout velocity is realized which will pay off in longer range or higher orbit.

For a given burnout velocity and for a fixed payload, the required stage average overall specific impulse $(I_s)_{oa}$ in terms of stage engine system weight can be established as

$$(I_s)_{oa} = k_4 / \ln \left(\frac{k_3 + \text{Stage engine system weight}}{k_2 + \text{Stage engine system weight}} \right) \quad (2-4)$$

where

$$k_4 = \frac{V_{bo}}{C_{vc}g} = \text{constant}$$

Equation (2-4) shows that with decreasing engine-system weight, the overall specific impulse requirements decrease.

Another parameter illustrating the importance of weight is the growth factor of a rocket vehicle system. For instance, if the weight of a component increases, it is possible to adjust for this by increasing the weight of the propellants loaded and thus possibly that of other components, such as a pump, to maintain the same required vehicle performance; i.e., payload and

vehicle trajectory. Therefore, if one part of the vehicle system exceeds its weight allotment by 1 pound, an increase of the total vehicle system weight at takeoff by a certain number of additional pounds will result. Growth factor is defined as the total vehicle system (including payload) weight increase at takeoff, divided by the causal increment of added inert and/or payload weight. It is emphasized that the growth factor, for a given vehicle system, is not a precise value, but varies within a band. For instance, a small weight increase of a component in an existing system may only require the addition of a corresponding small amount of propellants, but not require enlargement of the tanks, valves, etc. Accordingly, the growth factor will be small. In another case, the weight increase may be "the straw that breaks the camel's back," requiring the use of the next larger valve size, duct size, or the like. The growth factor will then be large.

In general, however, the growth factor of a vehicle system is a useful tool during the preliminary design of an engine system, because it attaches a tangible value to the importance of the engine-system weight. A systems weight increase may be considered "uninvited payload." For single-stage vehicles, and relatively small weight changes, the value of the growth factor then can be expressed with sufficient accuracy as

$$\text{Growth factor} = \frac{\text{Total vehicle system weight at takeoff}}{\text{Payload weight}} \quad (2-5)$$

For any stage of a multistage vehicle, the approximate value of the growth factors against total vehicle system weight at takeoff can be expressed as

$$\text{Growth factor} = \frac{\text{Total vehicle system weight at takeoff}}{\text{Stage payload weight}} \quad (2-6)$$

The growth factors of any stage against the vehicle system weight at ignition of the same or lower stage can be expressed as

$$\text{Growth factor} = \frac{\text{Vehicle system weight at same or lower stage ignition}}{\text{Stage payload weight}} \quad (2-7)$$

~~CONFIDENTIAL~~

Sample Calculation (2-1)

A three-stage rocket vehicle system has the following weight data: Total vehicle system weight at takeoff, 40 000 pounds. Vehicle system weight at second-stage ignition, 7500 pounds; vehicle system at third-stage ignition, 2200 pounds; payload weight, 700 pounds. For each pound increase of engine system weight of first, second, and third stages, respectively, determine (at a constant vehicle performance): (a) increases of total vehicle system weight at takeoff; (b) increases of vehicle system weight at second- and third-stage ignition.

Solution

(a) Payload weight of first stage = vehicle system weight at second-stage ignition = 7500 pounds

Payload weight of second stage = vehicle system weight at third stage ignition = 2200 pounds

Payload weight of third stage = actual system payload weight = 700 pounds

From equation (2-6):

(1) Growth factor of first stage against vehicle system takeoff weight =

$$\frac{\text{Vehicle system takeoff weight}}{\text{First-stage payload weight}} = \frac{44\,000}{7500} = 5.86$$

(2) Growth factor of second stage against vehicle system takeoff weight =

$$\frac{\text{Vehicle system takeoff weight}}{\text{Second-stage payload weight}} = \frac{44\,000}{2200} = 20$$

(3) Growth factor of third stage against vehicle system takeoff weight =

$$\frac{\text{Vehicle system takeoff weight}}{\text{Third-stage payload weight}} = \frac{44\,000}{700} = 62.9$$

Therefore:

For each pound increase of first-stage engine-system weight, the increase on vehicle system takeoff weight = 5.86 pounds

For each pound increase of second-stage engine-system weight, the increase on vehicle system takeoff weight = 20 pounds

For each pound increase of third-stage engine-system weight, the increase on vehicle system takeoff weight = 62.9 pounds

(b) Note that the weight growth of lower stages will not affect the upper stage weight growth. For an increase of first-stage vehicle system weight, there will be no weight changes on second and third stages, and for an increase on second-stage vehicle system weight, no weight change is required for third stage.

From equation (2-7):

(1) Growth factor of second stage against vehicle system weight at second-stage ignition =

$$\frac{\text{Vehicle system weight at second-stage ignition}}{\text{Second-stage payload weight}} = \frac{7500}{2200} = 3.41$$

(2) Growth factor of third stage against vehicle system weight at second-stage ignition =

$$\frac{\text{Vehicle system weight at second-stage ignition}}{\text{Third-stage payload weight}} = \frac{7500}{700} = 10.72$$

(3) Growth factor of third stage against vehicle system weight at third-stage ignition =

$$\frac{\text{Vehicle system weight at third-stage ignition}}{\text{Third-stage payload weight}} = \frac{2200}{700} = 3.14$$

Therefore:

For each pound increase of second-stage engine system weight, the increase on vehicle system weight at second-stage ignition = 3.41 pounds

For each pound increase of third-stage engine system weight, the increase on vehicle system weight at second-stage ignition = 10.72 pounds, and the increase on vehicle system weight at third-stage ignition = 3.14 pounds

The correctness of results can be checked by recombining the individual stage growth factors to obtain the growth factor for the entire vehicle system:

$$3.14 \times 3.41 \times 5.86 = 62.9$$

Envelope (Size)

The linear dimensions of liquid propellant rocket engines require relatively elaborate description and frequently cannot be made clear without a drawing. In those cases where only approximate values are required for comparison or for overall estimates, the term "envelope" is preferred. For instance, definition of a hypothetical smallest cylinder, cube, or sphere into which the engine would fit conveys a good feeling of engine size or bulkiness.

Obviously, engine size directly affects engine weight, the importance of which was emphasized above (fig. 2-4). Aside from the engine itself, numerous other areas are directly affected by increasing engine size:

- (1) The vehicle structure, which becomes heavier, especially with upper stages. Engine size directly affects the size and thus weight of the aft end and/or inter-stage structure.
- (2) Handling equipment and procedures become more costly
- (3) Servicing becomes more difficult
- (4) Manufacturing machinery becomes larger
- (5) Storage and transportation means become more bulky

In several of these areas, there is a definite upper limit, such as railroad tunnel sizes, clearances on bridges and underpasses, and available machine tools.

The selection of the thrust-chamber expansion-area ratio has a very pronounced effect on engine envelope. When optimizing the thrust chamber expansion area ratio, which is also influenced by performance, weight, pressure drop, heat transfer, and other considerations, its effect on envelope, and thus on other vehicle systems, must be considered (section 10.9).

Reliability

The subject of reliability has become almost a branch of science by itself. In addition to the designer, to the development engineer, and to the user, mathematicians, statisticians, and "human factor" and "man rating" specialists are involved. Numerous books have been written on the subject and manufacturers maintain entire groups to predict, monitor, tabulate, and evaluate

the reliability of their products. This emphasis on reliability is well justified and is of particular significance to rocket engines. The advent of manned space flight has placed even greater emphasis on rocket-engine reliability.

Reliability may be defined as the capability of the engine to perform according to specifications, whenever "the button is pushed." The degree to which this is met can be expressed in figures and graphs. If the evaluation is made following a test series, reliability can be simply expressed as the ratio of success to failure, say 98 percent (2 failures and 98 successes in 100 runs). As there is no guarantee, however, that the system under test will perform identically in subsequent tests, reliability predictions are made, the accuracy ("confidence level") of which increases with the amount of previous information available. The interrelation of reliability and its confidence level is something the statisticians have much to say and write about.

What can the rocket engine designer do to achieve the highest possible reliability, as early as possible? Below are compiled a few pointers and thoughts which have proven valuable, not only in rocket engine design. They will be followed by specific details for the implementation of a reliability-assurance program.

First of all, painstaking execution of all calculations and drawings that are part of a given design is an obvious requirement. This includes the thorough study of previous experience, one's own as well as that of others; familiarity with and correct application of accepted and proven design standards and procedures; clearly written statements and instructions; clear line drawings. It cannot be overemphasized: it pays to spend that extra hour in carefully checking repeatedly every detail of a design and its contemplated mode of operation, before its commitment to manufacture and subsequent use. Neglect may have to be paid for by many months of toilsome, tearful, embarrassed "corrective action," often causing losses of hundreds of thousands, even millions of dollars. When making these checks, the most pessimistic assumptions of what someone else may do wrong during manufacture, assembly and use, are not out of place.

The designer should not rely solely on his own judgement. Careful and independent checking of all calculations and designs by superiors

and by independent checkers is important. Early availability of a wooden (or "soft") mockup of the engine under design will be an invaluable tool to avoid costly errors that subsequently may seriously affect schedules and reliability. Specific recommendations for design and checking techniques will be made in section 2.2.

"Reliability" is sometimes treated as being synonymous with "simplicity." Undeniably, simplicity of a design contributes significantly to increased reliability. Parts which do not fulfill a truly useful purpose should be omitted. This may include many of the so-called safety features and interlocking devices, which often cause more trouble than they prevent. Early designs of liquid-propellant rocket engines have indeed frequently suffered from such an overdose of sophistication and safety devices. Many of the more recent designs have been substantially improved in this area, to a point where caution must be exercised not to overshoot the target and not to lose that flexibility which only liquid-propellant systems can provide, as compared to solid-propellant systems. Simplifications, like all other design features, must be carefully planned and evaluated. Simplification by elimination of a useful component must not become an excuse for failure to improve that component if its absence could severely penalize other sub-systems, or maintenance and servicing procedures.

For instance, to avoid a troublesome sealed connection it may be decided to omit flanges and seals and to weld it. However, if one of the lines thus connected were inadvertently pinched in the field, removal of the entire engine from a vehicle under preparation for launch would become necessary. Thus, a simple replacement may be magnified into a major operation. To be sure, welding or preferably brazing may indeed be the best solution for many problem connections. The point is, this will not be true for all connections. Careful analysis of all aspects including handling and in particular mishandling by the user, is necessary.

In another example, tests may have shown that an engine could readily be set up and calibrated to specifications by means of orifices, eliminating previously-used regulators. Engines are delivered accordingly. With rocket engines, it is entirely normal that many months, if not

several years, may elapse between delivery and final use. Much can happen during this period. For instance, changes of plans for the mission may have made another thrust level more desirable. In this case, the adjustment by means of orifices, in particular its verification, becomes a major operation. While the omission of a strategic regulator was indeed an engine simplification, for the vehicle system it turned out to be a complication. The point here again is; the careful evaluation of a planned omission must consider *all* aspects, including changes of plans.

Reliability Assurance

The emphasis on reliability must not remain an empty slogan. Fortunately, implements are available to the rocket engine designer which can assist him effectively to achieve the highest degree of reliability. One of these, an effective failure reporting and correction system, will be discussed in section 2.2. Equally, if not more important, is a most effective failure prevention system. The numerous activities contributing to the latter may all be considered part of a reliability assurance program. The quality of design, without question, is the program's foundation upon which all subsequent phases rest. The characteristics of a reliability-assurance program, then is that its most significant steps (analyses, design reviews, design improvements) are taken before the design of a component is finalized; before the development test program is initiated; and again before the first vehicle is committed to launch.

Definitions

The definitions used in rocket vehicle reliability assurance programs vary widely with individual preferences, with the object under design and development, and with the missions contemplated. The definitions given below are typical, have been used in actual rocket engine and vehicle programs, and can be readily adapted to others. For the sake of clarity, irrelevant jargon and detail have been omitted.

Reliability

The probability that a part or system will

function properly and if necessary repeatedly under rated operating conditions, within the specified load and time limits.

Mission Success

Completion of the rocket vehicle mission objectives within specified tolerances. All subsystems, including the engine, contribute to the success. It is an inherent characteristic of mission-success analysis and assurance that they anticipate the probability of certain part and subsystem malfunctions, offsetting them with appropriate countermeasures (such as redundancies, emergency power sources, power and propellant reserves, and others).

Mission Failure

Failure of the rocket vehicle to complete the mission objectives. Mission failures can be classified as: a) Catastrophic, b) Critical, and c) Deferred.

Catastrophic Failure

A failure in which the time between the failure event and a subsequent crew hazard is less than 500 milliseconds. Abort sequence must be automatically initiated.

Critical Failure

A failure in which the time between the failure event and the hazard ranges from 500 milliseconds to five seconds. Abort sequence may be initiated automatically or manually.

Deferred Failure

A failure in which the time between the failure event and the hazard is five seconds or greater. Action to cope with the failure is deferred to allow analysis by the pilot or an automatic logic, to decide whether corrective action can be taken or an abort sequence should be initiated. Typical example: shutting off an engine with a feathered propeller in a four engine airplane and reaching destination safely though with a delay. Analogous provisions are anticipated for manned rocket flight.

Man Rating

Design and operational provisions to assure crew survival even in case of mission failure. Thus, man-rated reliability must be higher than mission reliability. For instance, overall vehicle reliability to achieve mission success may be 95 percent. By the addition of an escape mechanism, man-rated reliability may be increased to 99.5 percent. Caution is advised not to become entirely "wrapped up" in man rating, at the expense of mission reliability. A single launch of a man-carrying space vehicle costs several hundred million dollars, all told. Investment in means to save the mission as well as the man, therefore, appears to be prudent. Table 2-2 illustrates this clearly. For optimum reliability of spacecraft and launch vehicle including the engines, the need for a crew escape system is minimized. Both, mission and crew survival are assured with high reliability.

TABLE 2-2.—*Relationship of Vehicle Reliability to Flight Safety*

Reliability		Flight safety
Spacecraft and launch vehicle	Escape system	Probability of crew survival
0.50	0.998	0.999
0.90	0.99	
0.999	0.00	

Engine Out

Design and operational provisions to permit limited or complete mission continuance in case one engine fails to fire, or malfunctions and is shut down. Possible only with vehicles having engine clusters. See airplane analogy under "Deferred Failure," above.

Failure Mode

The manner in which a part or system malfunctions. This may be a "short" or "open" circuit, an incorrectly "closed" or "open" valve, an engine out, or similar malfunction.

Order of Failure

The number of components in a system which

~~CONFIDENTIAL~~

would have to fail, regardless of their failure mode, to cause systems or mission failure. First-order failures are failures caused by a malfunction of a single component or part. Second- and higher-order failures are defined in a like manner. Typical example: a stuck pressurizing valve causing overpressure in a vessel would rupture it only if the safety valve failed to open; this would be second-order failure. However, continuous venting of a properly opening vent valve may prematurely deplete gas supply. A thorough failure-effect analysis will reveal all ramifications. In the example, depletion would not occur instantaneously, this would be deferred failure. The designer can do something about it in advance: provide an overriding closing valve for the pilot, which remains completely inactive when not needed, but adds weight.

Failure-Mode-Effect Analysis

An orderly and qualitative listing of the modes in which components or parts of a system can fail; the effects of the failures on the engine's or vehicle's ability to complete the mission; and the order of the failures. Such an analysis should distinguish between the pre-launch, launch, and cutoff phases. Also, all identified failures should be classified as catastrophic, critical, or deferred.

Failure Mode Cause Analysis

An analysis listing all the conceivable reasons why each mode of failure could occur. Likewise, reasons for each potential cause not occurring should be explained in detail.

Emergency Detection System (EDS)

The EDS comprises the electromechanical devices, including sensors and discriminators, to detect an imminent malfunction. Depending on the type of failure (catastrophic, critical or deferred) it may initiate immediate action, or defer but store and/or display it in a suitable manner (timer; visual gage or light). Inputs to the EDS must be analyzed, selected and provided by the designer, in particular the engine designer, at the outset.

Failure Modes of Engine Components

The failures of rocket engine components may be attributed to one or a combination of several of the following principal modes:

- (1) Functional failures
- (2) Fatigue failures
- (3) Over-stress and over-strain
- (4) Failures pertaining to combustion devices
- (5) Failures pertaining to electrical devices
- (6) Manufacturing and material defects
- (7) Unexplained failures
- (8) Human errors

Functional Failures

These are malfunctions of parts or components due to reasons other than structural failures. For instance, an "O" ring may fail to seal due to improper groove depth specified in the design. Or, a plunger may freeze in the bore of a guiding bushing, because of improper surface finish and/or noncompatibility of materials. To minimize possible function failures in the design of engine components the following precautions are recommended:

- (1) Choose proven designs with an established service record.
- (2) Use standard mechanical elements (bolts, nuts, threads, gears, pins, rivets, springs, seals, tube fittings, pistons, keys, shafts, bearings) wherever possible.
- (3) Select simple designs, but without impairing flexibility. In particular, minimize the number of moving parts and sealing surfaces.
- (4) Allow adequate functional margins in the design of components (spring forces, actuating powers, supply of lubricants, supply of coolants).
- (5) Subject newly-designed parts to extensive functional testing, under simulated working and environmental conditions, before "freezing" the final configuration.
- (6) Provide redundancy. This is a "buddy plan": where one component would be sufficient, two of the same type are actually provided. If one fails, the other takes over. This can be achieved in two ways: by noncomplex and by complex redundancy. Intelligently applied,

redundancy can significantly increase reliability.

- (7) At all times, pursue a rigorous program of product improvement.

Noncomplex Redundancy

The simultaneous function of identical equipment. Application depends upon the particular failure mode which is to be eliminated. For a typical example, see figures 2-7 and 2-8. Other examples are: dual (series) seals, parallel valves.

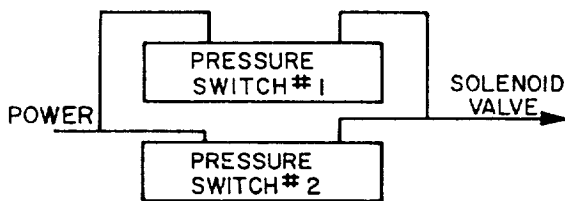


Figure 2-7.—Noncomplex parallel redundancy. (This type of redundancy guards against failure to close when called upon to close.)



Figure 2-8.—Noncomplex series redundancy. (This type of redundancy guards against inadvertent closing, i.e., closing when not called upon to close.)

Complex Redundancy

The original function carried out by one component. Failure sensors, logic circuits and switching devices energize an identical standby component, when needed. The advantages obtained can be completely offset by the additional complexity of sensing and switching circuitry. The potential problem area may be merely shifted from the equipment to the failure-detection components. However, this standby redundancy may be advantageous when long mission times are involved (e.g., days or weeks) and where it may be undesirable to also subject the backup equipment to prolonged operation.

A typical example is an electric power emergency battery with voltage sensor and switchover circuitry.

Fatigue Failures

Fatigue failures are fractures caused by repeated load applications at stresses considerably lower than those causing failures in a single load application. They are the most common type of mechanical failure. The ability of a part to resist fatigue failure cannot be checked without destroying the part. Checking is possible, however, through destructive endurance tests with representative samples selected at random.

Most fatigue failures start with a crack at or near an outside surface because stresses are apt to be greatest there. The actual failure will result from gradual propagation of these cracks.

The point at which the crack will start will depend upon the geometry of the part and on surface conditions. Any notch or other stress raiser, being a point of highest stress concentration, is a potential starting point for fatigue cracks. Fillet radii that are too small, threads, oil holes, keyways and similar surface irregularities are all potential sources of fatigue failure. Although a part may be designed to be free of geometric irregularities, having no shoulders, grooves or the like, it may still contain a great number of minute stress raisers. These may be tool marks, scratches, identification stamp marks, or various inherent discontinuities in the material itself, such as inclusions of foreign matter and quenching cracks. The design engineer should make every effort to avoid stress concentrations in a highly-stressed part subject to repeated load applications. In the design, rigid specifications should be called out for surface finishes. For repeated load services, forgings are generally preferred to castings. Ductile materials are preferred to material prone to become brittle.

In welded constructions, the joints are subject to almost all types of stress concentration and fatigue failure. Wherever possible, welded joints should be minimized in the design of parts subject to repeated loads. Rigid procedures for welding and inspection must be called out in the design.

Over-Stress and Over-Strain

Stress analysis in mechanical design to prevent over-stress and over-strain will be discussed in section 2-4. The interrelationship of stress and reliability of mechanical parts is illustrated in figure 2-9.

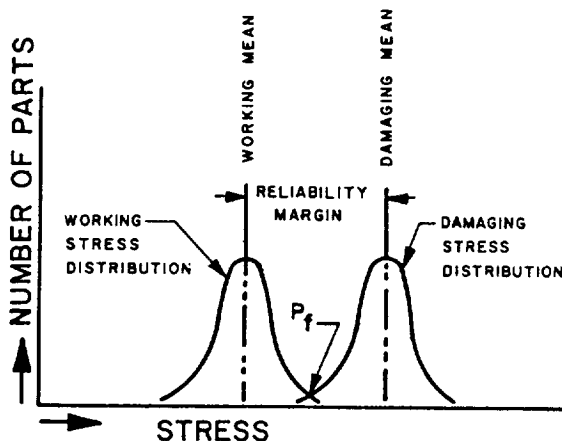


Figure 2-9.—Interrelationship of stress and reliability as related to mechanical parts.

Two stress levels exist for every part in a given engine component: the working stress, and the damaging stress at which failure occurs. The failure may be either a fracture, or a deformation beyond allowable tolerances. Each of the two stresses are mean values of a distribution about a mean. The difference between the working and the damaging stress mean values is indicative of the stress reliability margin of the part.

The deviations from the mean working stress result mainly from variations in the dimensions of the part, and from operational and environmental conditions. The distribution about the mean damaging stress results from variations in material properties, fabrication processes, quality control and maintenance practices. The area P_f , where the two distributions overlap represents the probability of failure, or unreliability.

Close control of functional and environmental loads may decrease the variation of the working stress about the mean. Likewise, better materials and strict quality control should increase the damaging-stress mean value, and decrease the variation about the mean. Thus, the area of overlap may be substantially reduced or eliminated, and reliability increased.

Failures of Combustion Devices

Under steady-state operating conditions, combustion devices in liquid-propellant rocket engines are exposed to hot gases with temperatures ranging from 1000° F to 6000° F. The walls of these devices are either made from high-temperature-resisting (refractory) materials, or are provided with effective cooling, through heat-absorbing effects, ablative cooling, propellant film and/or regenerative cooling. Structural failure may occur because of erosion, from wall temperatures exceeding the values assumed during design. Or failure may occur from a combination of excessive temperatures and pressures.

Under certain transient or unstable conditions, such as during engine start or stop, combustion instability or abrupt pressure surges may occur and cause a failure. See chapter IV, "Design of Thrust Chambers and Combustion Devices."

Electrical Failures

Although predominantly an assembly of mechanical parts, a modern rocket engine employs a number of electrical devices without which it cannot function reliably. Among the electrical components used most widely are: power sources (batteries), converters (DC to AC), wires and harnesses, connectors, switches, relays (electromechanical and solid-state), timers, pressure switches, diodes, solenoid valves, servomotors and position indicators.

All of these devices are, to various degrees, potential sources of failure, the consequences of which are just as detrimental as failure of mechanical parts. By proper design and assembly instructions, and by careful selection of the elements, the designer can forestall electrical failures and thus assure overall systems reliability. Most common potential electrical failures which must be prevented are:

Cold solder spots in connectors, wirings and electrical elements. They result in often sporadic discontinuities, particularly under vibration.

Short circuits in wirings, connectors and other electrical devices. This may be due to poor design, leaving insufficient separation between connector pins, lugs and the like; excessive solder; damaged insulation due to

poor harness installation, chafing under vibration and poor handling; overload and/or overheating in solenoids; moisture in connectors.

Fused relay contacts, due to overload and/or incorrect current rating of the elements.

Relay and switch contact loss under vibration. This is really an electromechanical malfunction. It can be prevented by proper relay selection, shockmounting, orientation of installation, replacement by solid-state circuitry where possible.

Power failure resulting from one or more of the causes listed above. Prevention means include emergency batteries and overload switches, combined with subcircuit isolation through diodes.

A liquid-propellant rocket engine usually includes additional electrical elements as required for instrumentation and telemetry. These may include instrumentation power supplies, end organs (sensors, pickups, thermocouples, accelerometers, position indicators), signal conditioners (analog-to-digital), and wiring. Although, as a rule, instrumentation is not required directly for proper function of the engine system, its failure may indirectly cause engine malfunction, by interference with engine operation. For instance, a pressure pickup may rupture and cause premature depletion of a gas supply; the same event in the fuel system may cause an engine-compartment fire; improper installation of a thermocouple may block a vital lubricant or other line.

The engine designer's task includes engine instrumentation. It is obvious, therefore, that this peripheral system, too, will require his full attention.

Manufacturing and Material Defects

Manufacturing and material defects of engine component parts directly affect the reliability of the components. These defects can be prevented only by strict quality control. The areas of quality control may be subdivided as follows:

- (1) Materials inspection. The extent of inspection and testing conducted with raw materials depends upon the nature of the part for which they will be used. Inspection of materials includes testing of their composition, uniformity, mechani-

cal properties, fabrication and heat-treating characteristics, and possibly of other properties as the application may demand.

- (2) Traceability. By the time a materials defect is detected, many more parts may have been made from the same lot or batch of raw material. If accurate records have been kept, for what parts which numbered material lots have been used, it will be possible, without a "panic," to withdraw and replace all parts made from the faulty lot. The importance of accurate and complete records is obvious.
- (3) Process inspection. This refers to all shop inspections made of the parts as they are being processed. Its purpose is to check the performance of the operators and tools or equipment, and to sort out faulty parts as soon as errors are detected.
- (4) Salvage. This includes the decision whether defective materials or parts can be corrected or will be scrapped.
- (5) Final inspection. This is the inspection of the completed component parts to insure they are within the limits required by the design.
- (6) Checking of actual service performance. This includes investigation of complaints and studies of actual service performance of the part in the engine system (see "Failure Reporting System").

Unexplained Failures

From time to time failures occur which cannot readily be isolated as having originated in a given component or part. This may be because several causes were present simultaneously and could not be separated. Or instrumentation was inadequate, recording only the ultimate effects but not the cause. Or that an incomplete investigation was conducted, maybe in the hope it would not happen again.

Classification of a failure as "unexplained" should never be done as a matter of convenience, but only as a last resort if the most thorough investigation did not establish a clear cause. Complete and accurate records must be kept of

CONFIDENTIAL

the details associated with the failure. Through special statistical methods it may be possible to isolate the cause or causes at a later date.

Also, special instrumentation may immediately be added in the areas of suspected but unproven causes. But the most sophisticated explanation of a failure cannot transform it into a success.

Human Error

Experience with early manned rocket flights has shown that certain functions could be performed better by trained men than by automatic devices. It appears certain that future space-flight efforts will continue to employ combinations of automatic and manual systems, the ratio of the two depending on mission requirements. Even in those missions which are unmanned and therefore appear to be fully automatic, man is still directly involved: during launch preparations, and through postlaunch commands for trajectory-correction maneuvers, information playback, and similar actions.

We must realistically recognize that even a fully-trained, and very alert individual is subject to error. He may commit an error at a desk while using a slide rule, or while connecting a number of hydraulic lines, or under stress while pushing buttons. The history of rocketry is full of glaring examples. Whenever it happens, the most eloquent regrets are probably voiced by the designers of the system involved: if someone had not done something to their perfect creation, it would have worked faultlessly. The reaction is understandable, but wrong.

For whatever reason a system failed, it obviously was not perfect. Its designer did not consider human nature, nonideal operating conditions, nor emergency situations. Clear and complete drawings, specifications and other written instructions are important but they will not prevent, by themselves, human errors, because they can be misplaced, misread, or not read at all.

It is not surprising that the elimination of human error, or more positively, the perfection of the integration of man with the machine, is becoming an independent branch of engineering. It would be beyond the scope of this book to go into the details of "Human Engineering" or "Human Factors Analysis." Simply by applying

mostly known methods and common sense, the rocket-engine designer can do much to prevent human error by the design of his parts and by mandatory actions during their building, checking and handling. The following are only typical examples of a probably infinite number of possibilities of preventing human error by design.

Clear marking of bolts, lines, connectors, wires, etc.

Use of dissimilar connectors, dissimilar threads, a variety of keyways, and the like, to make incorrect electrical and mechanical connections impossible.

Safety wiring; electrical and mechanical interlocks.

Painting bright red, and/or attaching bright red streamers to, auxiliary devices which must be removed before operation.

Storing of components and systems which have successfully passed all inspections and checkouts, in locked rooms requiring two different keys from two different individuals.

Intentional attempts at improper handling, assembly, checkout and operation of components and systems, to assist "foolproofing," during development.

None of these and numerous similar steps will eliminate human errors completely. However, they will substantially reduce their possibility and thus contribute to overall reliability.

Design Reviews for Reliability

The reliability of rocket engines and their components depends on many factors. Design reviews are among the most potent methods for increasing reliability. In practice, a design review is the progressive evaluation of a design. It starts with the preliminary schematics, layouts and specifications and extends through the release of all final drawings. Those conducting reliability design reviews should include: reliability specialists, design engineers, development, test and service engineers, and various specialists for structures, materials, manufacturing, and quality control.

A minimum of three design reviews is recommended for each design:

Preliminary design review.—This is preliminary review of work statements, basic concepts, schematics, layouts, and analyses.

It determines development needs and results in decisions for the next design phases. This review should uncover misapplications, critical areas and marginal designs at an early stage, when changes can be effected without difficulty.

Critical design review.—This is the most important review for decisions and approvals. It includes formal review of all reliability aspects of layouts, analyses, planned development tests and procurement specifications.

Final design review.—This is the final review of overall design layouts, detail and assembly drawings, analyses, process specifications, and R&D test results, before production release.

The reviews should emphasize:

- (1) Structural integrity
- (2) Function and performance
- (3) Customer (vehicle) connections and envelope
- (4) Materials compatibility and component interfaces
- (5) Produceability and cost
- (6) Reliability and repeatability; malfunction effects
- (7) Environment and servicing
- (8) Special requirements

It is highly recommended that the agreed-to layout bear the approval signatures of the groups involved.

A reliability checklist tailored to the individual designs may be used as a guide during the various design review phases. The "Design Check-Off Sheet" shown in section 2-2 may be used for this purpose.

Design reviews are valuable and cost-saving tools for improving reliability. A well organized and staffed review group will assure a meaningful review and instigate effective recommendations and actions. Complete documentation of all review details will provide valuable data for future reference.

Under "Manrating" the cost of a single launch was mentioned. Press releases give the cost of a major space program as about 3.5 billion dollars a year—10 millions a day! To save a mission, or just a single day of preparation, by improved reliability, quite clearly, is worth the effort.

Likewise, the loss of a launch, or a day in

the program, is very costly indeed. The rocket-engine design can contribute substantially to prevent it.

Cost

Cost considerations should enter a design at the very beginning. Not only from the viewpoint of competitive bidding and narrow profit margins but of available and/or developed national resources as well. A major rocket vehicle program quite possibly may tax the resources of certain materials, facilities, and services to the limit. Moreover, it should be ascertained that the program does not rely on facilities, and on supply of materials and of propellants that may not become available for several years. The rocket engine under design may well be for a project costing a total of hundreds of millions of dollars. Savings of even fractions of a percent can therefore amount to millions of dollars.

Cost, as far as the designer is concerned, will be affected by the selection of materials; by the machinery required to make the parts; by the time and skill required to make them; by the difficulty of assembling, testing, and servicing the parts; and last, but not least, by the experience of the people making the design.

Availability (Scheduling)

The best design, the most perfect device, may be useless if it is not available when needed. In a way, the design of (in our case) a rocket engine is a product by itself. It must be planned, prepared, and made. It results in physical products: drawings, written instructions, and procedures, which all must be faultless and available when needed. Delays in the release of drawings can become very costly indeed. In a manufacturer's overall plan of action, the design will be timed and synchronized with other activities. If the drawings are not available on schedule, sizable portions of a machine shop or an assembly plant may be forced to stand idle.

2.2 THE IMPORTANCE OF DESIGN QUALITY

Even today many people still regard the design of technical objects as not much more than the act of putting pencil lines on large

pieces of paper. Of course, the general concept of design is much broader. Many a designer may not even occupy a drawing board, since he may be completely devoted to the creation of basic ideas and solutions, to the numerical checking of their validity, or to the planning, direction, and integration of a design team. By contrast, many of the most successful designers always retain their board, their most valuable tool of creation, however advanced their position in the organization may be.

It is a commonplace to state that a technical project will stand or fall with the quality of its design. Obviously, no device can be built, tested, or used until and unless it has been specified first how to build, test, and operate it. With this in mind, a completed design can be considered a set of instructions for shop actions to follow. For instance, final drawings are only the end product of an extensive, diversified effort which preceded their release. All this is well known, yet sometimes forgotten in the daily grind of a project. May it suffice to state that the design and the designer are principal links of the chain in a project.

This book attempts to supply some of the necessary special tools required to arrive at a detailed "set of instructions" to the shop foreman, from which an engine could be actually built and prepared for test. The following chapters are devoted to the necessary technical detail, based on the latest state of the art in the field of liquid propellant rocket engines.

There are numerous areas which the designer should consider early and keep in mind at all times, for overall increase of quality and reliability, and for reduction of cost. Among these are:

- (1) Experience, reliability, and reputation of subcontractors and their products
- (2) Adequate receiving inspection
- (3) Clear and complete instructions for inspection and quality control
- (4) Full use of the experience of others: in-plant and out-of-plant
- (5) Use of suitable existing designs, from small parts to subsystems
- (6) Availability and application of an effective failure analysis and correction system
- (7) Last, but not least, the experience,

knowledge, analytical capabilities, and judgment of the designer himself.

A number of time-proven tools are available to the designer to optimize his design and the end product it describes. Among these are:

Design checkoff sheets.—Checkoff sheets force the designer to check his design systematically from all imaginable angles, before release. See sample sheet on next page.

Design change checkoff sheets.—Used for systematic evaluation of design changes for effects on all potentially affected systems, including the user and the vehicle. A sample sheet is shown below.

Failure reports.—The feedback to the designer of failures of his product in the field, for immediate corrective action.

Change control.—A projectwide effort to scrutinize and minimize proposed changes; and to establish and monitor implementation by engine serial number, if the change must be made.

Specifications.—Detailed specifications, often based on applicable Government specifications, to establish the exact execution of all manufacturing processes, materials used, parts purchased, tests to be performed, and so on.

2.3 SYSTEMS ANALYSIS AND DESIGN LAYOUT

So far, numerous important basic considerations for rocket engine design have been discussed. The detailed engine design procedures and the treatment of typical examples as they may occur in practice will now follow. The questions are where to start, how to proceed, and what are the expected results.

It would be beyond the scope of this book to describe the detailed mechanics of the generation of design drawings, their breakdown, their execution, and the system for their release. The young engineer, who uses this book and already works in industry, knows. The student reader can be assured that the future employer has a manual (usually voluminous) covering this subject exhaustively, and which is slanted to his specific needs. The following are specific design techniques as they are used in liquid rocket engine design. Many of these techniques will be

LIQUID ROCKET ENGINE DESIGN CHECK-OFF SHEET

Project: _____

Subsystem: _____

Supervisor: _____

Item	Answer & initials of designer	Date	Answer & initials of supervisor	Date
1. Have designs for similar earlier projects been thoroughly reviewed and understood?				
2. Have principal participants in those projects been contacted? Has their advice been solicited?				
3. Has a list been prepared of all problems which were encountered in previous, related projects, including their solutions?				
4. Has the new engine system schematic diagram been reviewed for hidden "won't works?"				
5. Has the number of components and their complexity been reduced to a minimum, without loss in flexibility and serviceability, for maximum reliability? (In particular: has minimum of moving parts been achieved?)				
6. Has a thorough malfunction analysis been made? (Assessment of malfunction effects of each component on all other parts and on the complete system. Include external systems, such as the vehicle and GSE.)				
7. Have all existing detail designs been reviewed for possible inclusion and/or adaptation to the new design?				
8. Have standard parts been used wherever possible; permissible; or as prescribed by customer specifications?				
9. Has the number of external connections ("customer connections") been held to a minimum?				
10. Has the location and type of customer connections been chosen in the best interest of the customer? Has he been consulted?				
11. Has the need for ground support equipment (GSE) been reduced to a minimum, by number as well as by complexity?				
12. Are there good reasons if support equipment used during R&D is different from the one supplied to the field?				
13. Have all environmental conditions been considered, including those not likely but possible to occur? (Salt spray, sand, fungus, humidity, temperature, etc.)				
14. Has resistance to vibration and shock effects been considered? In all planes? Including improper handling?				
15. Have acceleration effects been considered? In all planes?				

LIQUID ROCKET ENGINE DESIGN CHECK-OFF SHEET—Continued

Item	Answer & initials of designer	Date	Answer & initials of supervisor	Date
16. Has the use of critical materials been held to a minimum? (Chromium, Molybdenum, Tungsten, Cobalt, etc.?)				
17. Has it been made absolutely certain that no cheaper materials will do?				
18. Has it been assured that no electrolytic action can occur due to attachment of dissimilar metals?				
19. Can the engines be gimballed according to specifications?				
20. Can the engine be clustered, if necessary?				
21. Can the engine be attached to air frames other than the one presently contemplated?				
22. Has it been confirmed that all parts can be made?				
23. Has it been confirmed that there is no cheaper way of making these parts?				
24. Can the parts readily be assembled, with a minimum of special tools?				
25. Has it been made impossible to incorrectly assemble and install any part? (Or incorrectly reassemble and reinstall them in the field?)				
26. Will all parts requiring service be readily accessible, prior to and following mating of the engine with the vehicle?				
27. Have all markings been called out completely and correctly?				
28. Do instructions for inspection and quality control leave no gap?				
29. Has it been ascertained that (without penalty) the design cannot save further weight?				
30. Is the envelope the smallest possible?				
31. Can the system be drained, readily and completely? (Avoidance of traps, low spots, etc.)				
32. Have engine propellant feed system components, including pumps and thrust chamber been designed for minimum trapped propellants after cutoff? (Minimum wet weight)				
33. Has the purchasing department been appraised of the significance of mandatory (proven) sources, where applicable?				
34. Can it be transported? In one or several pieces?				

LIQUID ROCKET ENGINE DESIGN CHANGE CHECK-OFF SHEET

Project: _____

Change No.: _____

Supervisor: _____

Item	Initials of designer	Date	Initials of supervisor	Date
Assuming that it has been ascertained beyond doubt (has it?) that a design change must be made, check that the effect of this change is fully understood and implemented in the following areas:				
1. Interchangeability of changed parts.				
2. "Chain Reaction" to other parts and systems, including vehicle, test facilities, and GSE.				
3. Engine start and stop sequence.				
4. Engine performance, including gain factors.				
5. Conformance with <i>all</i> specifications.				
6. Weight, envelope, c.g., moments of inertia, loads.				
7. Reliability.				
8. Instrumentation, data recording, telemetry.				
9. Packaging, shipping, storage.				
10. Development and qualification.				
11. Human factors: skills, training, notification of persons concerned.				
12. Field service equipment and procedures.				
13. Handbooks and other user documents.				
14. Logistics (spare parts maintenance).				
15. Manufacturing tooling and processes.				
16. Purchased materials.				
17. Subcontractor-supplied parts.				
18. Funding.				
19. Agreed-to delivery dates.				
20. Customer notification and approval.				

applied in subsequent chapters, in connection with the discussion and demonstration of various component designs.

The activities discussed below are not clearly separated phases, following one another in a rigid sequence. Rather, they overlap, frequently occur in parallel, and are tightly interwoven. One of the first drawings the liquid-rocket designer will most likely prepare is a schematic diagram of the engine system. A typical example is shown in figure 2-10. This diagram shows how the principal components are linked together. The schematic may be accompanied by a sequence diagram, showing the operation of each compo-

nent in relation to the other as a function of time (fig. 2-11).

Concurrently, analyses will have been conducted to establish preliminary engine performance parameters and operating characteristics, as well as individual component configurations and operating principles. A typical example of a performance diagram is shown in figure 3-1. Engine and component starting and operating characteristics can be analytically predicted with a high degree of accuracy by computers. Thus, important knowledge required for optimum design is obtained long before the part is actually built and tested. Savings in time and cost are

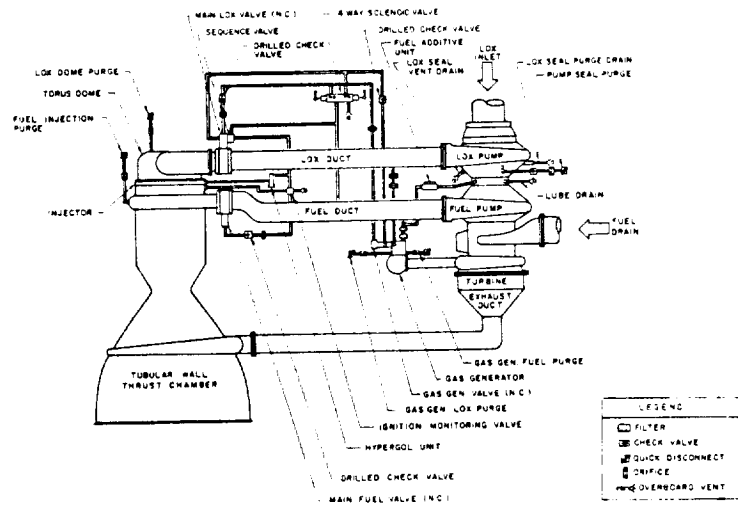


Figure 2-10.—Typical engine system schematic diagram.

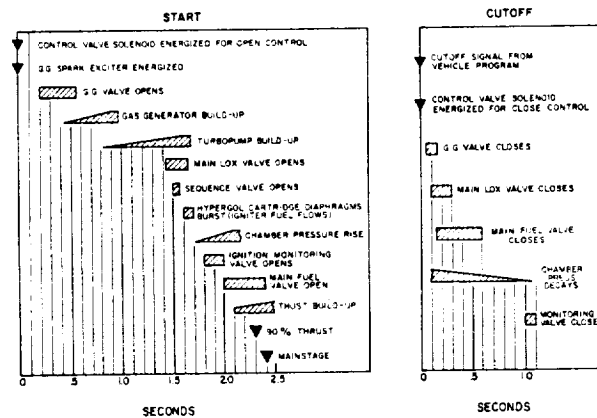


Figure 2-11.—Typical engine system sequence diagram.

substantial. These analyses and computer programs will draw heavily upon experience with earlier systems and on advanced design studies.

Once the prototype schematic diagram is considered completed, and performance parameters have been established by the analysis, the first actual "engine picture" will be drawn. This very likely will be a general, in-scale preliminary layout of the engine system and components. A typical example of an engine system preliminary layout is shown in figure 3-2.

Through continued analyses, calculations, consultations, and joint reviews by all participants, the layout will gradually take final shape. In this process, nothing should be left to chance.

Consultations with specialists in their fields and rigorous calculations doublechecked for accuracy and presented in a readily understood form, will contribute materially. Layout drawings should be made accurately and to true scale. In this manner, all components of the engine system will have been designed and optimized for one another, rather than "hung on a mounting frame in Christmas-tree fashion."

Before working drawings are made from the layouts, they should again be reviewed, and revised as necessary, taking into consideration all design aspects, the basic considerations, and the reliability assurance aspects, which were discussed earlier.

2.4 STRESS ANALYSIS

Stringent reliability and weight requirements call for rigorous and complete stress analyses during the mechanical design of engine components. Stress analyses predict the manner in which a mechanical part is likely to fail under anticipated working conditions. They also generate means to prevent failure. The goal is to design a part with sufficient, but not excessive, strength in every detail.

In conjunction with the engine design layouts, the approximate shape of the parts will be established, based on functional requirements and on similar satisfactory designs of the past. First, a preliminary design sketch is made. Subsequently, the determination of probable working loads, environmental effects, deflections, stresses, and determination of the final dimensions is made step by step, together with the selection of materials. The following steps are typical for stress analyses:

- (1) Analyze and determine the loads and environmental effects to be expected during the useful life of the part.
- (2) Evaluate the various possible modes of part failure from stress and strain induced within the part by the working loads and from other effects.
- (3) Select the materials and establish their mechanical properties under anticipated working conditions. Applying a likely theory of failure, arrive at the final dimensions of the part.
- (4) Apply experimental stress analyses to refine the above procedure. Redesign the part if necessary, depending on the results.

In certain cases, such as with highly stressed lightweight members, further stress analysis refinement must be obtained. The greater the refinement desired, the more nearly the methods of stress analysis must indicate the true strength of the member. This requires consideration of complex states of stress, residual stresses, stress concentrations, dynamic effects, inelastic effects, and other influences which determine the true stresses within the member. The following is a discussion of the four steps of stress analysis enumerated above.

Analysis of Working Loads and Environmental Effects

In stress analyses for mechanical design, working loads and environmental effects should be considered jointly. Stresses and strains induced in mechanical parts by external forces, which we will call loads, are affected significantly by environmental effects such as temperature, chemical reactions, corrosion, etc. Furthermore, the mechanical properties of most materials are affected by temperature. Sometimes, thermal stresses are induced as a result of temperature gradients within the part. Chemical reactions or corrosion can change the mechanical properties of the material, as well as the size and shape of the part.

For the analysis of working loads and environmental effects, determination of the following is essential:

- (1) The type of load: constant, impact, or repeated
- (2) The maximum value and duration of a constant load; the maximum and the minimum value for repeated or varying loads
- (3) The nature of load application: concentrated or uniform; rate per unit of time and, for repeated loads, total number of working cycles
- (4) Vibration load effects
- (5) Load effects with respect to the nature of material: ductile or brittle
- (6) Load effects with respect to the shape of a part: effect of geometry on stress concentration
- (7) Temperature effects: thermal stresses, high-temperature creep and reduction of strength, low-temperature embrittlement
- (8) Chemical reaction or corrosion effects: embrittlement, stress concentration

A part will have a proper margin of safety if it is designed with a design limit load larger than the maximum expected working load. The design limit load in turn should be smaller than the calculated damaging loads because of the uncertainty and inaccuracy involved in stress analyses. Damaging loads include: endurance limit load, yield load, and ultimate load, which are defined below. The more accurate the analysis, the smaller the allowable margin between the design limit loads and damaging loads.

~~CONFIDENTIAL~~

Below are given typical recommended criteria for the working loads, the design limit loads, and the damaging loads (yield and ultimate loads). The proof-testing loads applied to component design are also defined.

- (1) Design limit load: Select the largest of the following:

$$\begin{aligned} &1.2 \times \text{load (A)} \\ &1.2 \times \text{load (B)} \\ &1.1 \times \text{load (C)} \\ &1.0 \times \text{load (D)} \end{aligned} \quad (2-8)$$

where

Load (A) = Working load under normal steady operating conditions

Load (B) = Working load under normal transient operation conditions, such as during normal engine start and stop

Load (C) = Working load under occasional transient operation condition, such as load during irregular starts

Load (D) = Mandatory malfunction load which must be taken into account. For example, in a clustered engine configuration, certain mount members may carry the greatest load when one engine ceases to fire while the others are still operating (engine-out capability). In certain instances it is mandatory that an individual rocket engine continue to operate when a given component fails. If this causes significant structural loads, these are considered mandatory malfunction loads.

- (2) Yield load = $1.1 \times$ design limit load (2-9)

Yield load is the load which will induce a stress equal to the yield strength of the material used under rated ambient conditions.

- (3) Ultimate load = $1.5 \times$ design limit load (2-10)

Ultimate load is the load which will induce a stress equal to the ultimate strength of the material used under rated ambient conditions.

- (4) Proof test load =

$$1.0 \times \text{design limit load} \quad (2-11)$$

Proof test load is the load which is applied to test the part during the acceptance inspection. Its value can be adjusted for material properties if the rated ambient conditions cannot be duplicated for the test.

When a part is subjected to an indefinite number of cycles during service life, such as in rotating machinery, the endurance limit of a material should be applied instead of the ultimate strength. The endurance limit is the stress which can be repeated an infinite number of times without causing failure of the material from progressive fracture or fatigue. The endurance limit of metals, depending largely on range of stress variation, is as low as between 20 to 60 percent of their ultimate strength in tension. An additional design margin of safety should also be allowed for dynamic impact loads. When the shape of a part changes abruptly, as with a groove, a notch, a hole, or where a small section joins a large one, the value of unit stress at points close to the abrupt change or discontinuity increases steeply. The amount of stress increase generally ranges from 100 to 300 percent of the mean stress in the section.

Sample Calculation 2-2

The hydraulic accumulator of a large liquid-propellant rocket engine has the following design parameters: (a) Required volume (fluid capacity), 7238 cu in.; (b) working pressure (load) under normal steady and transient operating conditions, 2000 psia; (c) occasional surge pressure, 2200 psia; (d) mandatory malfunction pressure, 2450 psia; (e) maximum ambient temperature, 300° F; (f) material selected, AISI 4340 H.T.-180. (Strength at room temperature: Ultimate, 185 000 psi; yield, 170 000 psi. Strength at 300° F: Ultimate, 178 000 psi; yield, 150 000 psia.)

Determine the following: (a) Lightest possible configuration and resulting dimensions; (b) required proof test pressure at room temperature.

Solution

(a) Since a sphere is the lightest pressure vessel for a given volume and pressure, we will use this configuration. For a 7238-cu-in. volume

Required inside diameter of the sphere

$$\begin{aligned} &= \sqrt[3]{\frac{6}{\pi} \text{volume}} = \sqrt[3]{\frac{6}{\pi} \times 7238} \\ &= 24 \text{ inch} \end{aligned}$$

From equation (2-8), design limit pressure = largest of the following:

$$\begin{aligned} 1.2 \times 2000 &= 2400 \text{ psia;} \\ 1.1 \times 2200 &= 2420 \text{ psia;} \\ 1.0 \times 2450 &= 2450 \text{ psia} \\ \text{Selected: } &2450 \text{ psia} \end{aligned}$$

From equation (2-9), yield pressure = $1.1 \times 2450 = 2695$ psia

Thickness of sphere wall

$$\begin{aligned} &= \frac{\text{Yield pressure} \times \text{diameter of sphere}}{4 \times \text{yield strength at } 300^\circ \text{ F}} \\ &= \frac{2695 \times 24}{4 \times 150\,000} = 0.108 \text{ inch} \end{aligned}$$

or from equation (2-10):

$$\text{Ultimate pressure} = 1.5 \times 2450 = 3675 \text{ psia}$$

Thickness of sphere wall

$$\begin{aligned} &= \frac{\text{Ultimate pressure} \times \text{diameter of sphere}}{4 \times \text{ultimate strength at } 300^\circ \text{ F}} \\ &= \frac{3675 \times 24}{4 \times 178\,000} = 0.124 \text{ inch} \end{aligned}$$

We will use the higher value 0.124 inch.

Therefore, the sphere dimensions = 24-inch inside diameter \times 0.124-inch wall thickness.

(b) From equation (2-11), nominal proof test pressure at 300° F

$$\begin{aligned} &= \text{Design limit pressure} \\ &= 2450 \text{ psia} \end{aligned}$$

Proof test pressure corrected for room temperature conditions:

$$\begin{aligned} &= 2450 \times \frac{\text{Yield strength at room temperature}}{\text{Yield strength at } 300^\circ \text{ F}} \\ &= 2450 \times \frac{170\,000}{150\,000} = 2780 \text{ psig} \end{aligned}$$

Evaluation of Failure Modes

There are three basic types of failure modes: elastic deflection, permanent plastic deformation, and fracture. Although the first type is not

a material failure, it may cause a part to perform improperly with resulting malfunction of a component or system. The other two—plastic deformation and fracture—are material failures influenced by material properties, load and environmental conditions, and by the shape of the part.

Each of the three failure modes is characterized by certain criteria. For elastic deflection, strain is the criterion. For plastic deformation and fracture, the criterion is stress. In the process of stress analyses, following load determination, the possible modes of failure of the part can be established in relation to the criteria induced by the loads. Failure cause can thus be determined, and the failure prevented through design changes. Some of the possible combinations of failure modes and criteria are listed in table 2-3 together with suggested design remedies.

Selection of Materials and Dimensions

For the process of finalizing the dimensions of a part to endure all working loads and environmental conditions without failure, the strength or ability of the selected material to withstand these loads must be known. Material properties are determined through materials tests conducted with specimens. In these tests, all conceivable loads such as tension, compression, torsion, and shear are applied, often with simultaneous application of temperature, vibration, or chemical environment. The results are compiled in graphs and tables. From these tables, materials with properties most suitable for a particular application can be selected.

Experimental Stress Analyses

A rocket engine part may be of such shape, or may be loaded in such a way, that design based on theoretical analysis alone is difficult and unreliable. In such cases experimental stress analyses can supplement the theoretical methods. Many recent advances in stress analysis can be attributed to the development of effective experimental methods.

Applying loads simulating as closely as possible those expected to occur in actual use, measurements of strains and stresses are made. These loads can be applied to full-size prototype

TABLE 2-3.—Failure Modes and Their Criteria

Failure mode	Conditions	Criteria	Design remedies
1. Elastic deflection:			
a. Stable equilibrium	Loads within elastic limits	Strain; linear or angular displacement (stretch or bending)	Change of shape or dimensions (stiffening); material selection
b. Unstable equilibrium	Loads within elastic limits	Buckling; ratio of applied vs. critical load	Change of shape or dimensions
c. Vibration	Within elastic limits; abrupt changes of loads; repeated application of load at or near natural frequency	Amplitude, frequency transmissibility, resonance	Stiffening; change of natural frequency; damping
2. Plastic deformation:			
a. Yield	Loads exceed elastic limits	Stress; permanent set	Change of dimensions and/or material
b. Creep	Loads may or may not exceed elastic limits; elevated temperatures	Stress; slow permanent set	Change of dimensions and/or material
3. Fracture:			
a. Overload	Load increase beyond yield point to ultimate strength	Stress; elongation; area reduction; rupture	Change of dimensions and/or material
b. Brittleness	Load above ultimate strength	Stress; rupture with little or no yield	Change of dimensions and/or material; change of heat treatment; change of contour
c. Impact or shock	Abrupt load application to ductile materials	Stress; behavior like brittle materials	Selection of most ductile material; increased margin of safety
d. Fatigue	Many repeated load applications within elastic limits	Stress; number of load applications	Change of shape and dimensions; change of material; increase of endurance limits

parts, to scale models made from the real material or from special plastic material, or to portions of full-scale parts. Not infrequently, applied loads are intentionally increased beyond rated levels, until failure of the part occurs. These "tests to failure" will establish the actual margin of safety achieved in the design.

The tools used in experimental stress analyses include electrical, mechanical, and optical strain gages; photoelastic plastic models, lacquers, and paints.

2.5 SELECTION OF MATERIALS

The selection of the most suitable material for a given rocket engine part will be governed by—

- (1) The function, size, and shape of the part
- (2) Required mechanical properties; strength, stiffness or rigidity, hardness, and ductility, with particular consideration

of the extreme temperature conditions in liquid rocket engines

- (3) Required physical and chemical properties; density, thermal conductivity, specific heat, coefficient of expansion, Poisson's ratio, strength-to-weight ratio, corrosion resistance, compatibility with propellants as a function of temperature
- (4) Considerations related to fabrication, such as forgeability, castability, weldability, machinability, and formability
- (5) Cost and availability
- (6) Existing industry and Government standards

Extreme temperature and corrosion conditions combined with the need for very-high-strength-to-weight ratios drastically narrow the choice of available materials. In particular, the extremely low temperatures encountered with cryogenic liquids have introduced serious materials problems. As a rule, tensile strength and yield

strength increase with decreasing temperature. However, ductility is seriously affected. Apart from selecting the best alloys for extremely low temperatures, highest purity of the metals is mandatory.

The increased usage of liquid hydrogen has introduced additional problems which further narrow the selection of available materials. Specifically for the LH₂ application, metals must exhibit:

Resistance to Low-Temperature Embrittlement

This can also be referred to as toughness or resistance to brittle fracture. Toughness, in general, describes resistance to fracture under shock-type loads and stresses. Most rocket engine parts are exposed to these loads; however, conditions are much more severe at the extremely low liquid-hydrogen temperatures. The tendency of various alloys to brittle failure is measured experimentally by the notched/unnotched tensile strength ratio. Typically, for 2014-T6 aluminum at -423° F, the ratio is 0.94 (longitudinal) and 0.83 (transverse).

Resistance to Thermal Shock

This is a measure of a material's ability to resist weakening or fracture as a result of sudden heating or cooling. The following properties appear to be requirements for high thermal shock resistance: High tensile strength (F_{tu}), high thermal conductivity (k), low modulus of elasticity (E), and a low coefficient of thermal expansion (α). The ratio $F_{tu}k/E\alpha$ provides a relative measure of thermal shock resistance for comparison of different metals. Typical values are 5 to 8 for stainless steel and 40 to 48 for 2014-T6 aluminum.

Resistance to Hydrogen Embrittlement

Certain metals, such as steels and titanium alloys, have a tendency to embrittlement in a hydrogen atmosphere. This tendency is greatest in the intermediate-temperature range, but disappears at low and high temperatures. The effect is often delayed until a critical hydrogen concentration in the metal is reached when cracks start to appear, as a result of a marked decrease in ductility. Also, the embrittlement effect decreases with increasing strain in the metal. Heat-treated steels are more susceptible to it than annealed ones.

Resistance to Chemical Reactions

While low-temperature hydrogen is considered essentially noncorrosive, gaseous hydrogen forms hydrides with some metals, such as uranium and titanium.

For up-to-date detail on material properties, the reader is referred to material handbooks, industry (material supplier) information, and Government publications (Bureau of Standards).

The principal groups of materials used for liquid rocket engines are as follows:

Low-Alloy Steels

Uses for rocket engine components include pins, bolts, shafts, brackets, mounts, thrust chamber structure members, ducts, injector bodies, and certain pressure vessels. The standard grades AISI 4130, AISI 4140, AISI 4340, MAS 6434 are prominent in this group of steels.

The low-alloy steels are normally used in the temperature range from -60° F to 600° F. They are not suitable for corrosive environments. Elevated temperatures produce excessive creep, thus reducing the strength. Also, very low temperatures tend to induce brittleness in most of them. An exception is AMS (SAE 9310).

Austenitic Stainless Steels (300 Series)

Steels in this group possess the highest corrosion resistance in the family of stainless steels and are highly qualified for storable liquid propellant application. They are inherently tough and well adapted for fabrication by deep drawing and other similar means. They can be welded easily, can be soldered by proper technique, and are well suited for machining and forming under normal conditions. Ordinary sand castings, precision investment castings, and forgings can also be produced from these steels. They are widely employed in rocket engines using cryogenic and storable propellants. Parts such as regenerative-cooled thrust-chamber tubes and manifolds, injector bodies and domes, valve poppets and bodies, propellant ducts and tanks are made from these steels.

Martensitic-Type Stainless Steels (400 Series)

The steels in this group are hardenable, in

which condition they exhibit their best mechanical as well as corrosion-resisting properties. The thermal conductivity of these steels is low but still the best of the stainless-steel family. They are specially suitable for hot working or forging. Their cold-forming characteristics are fair. They are well suited for most applications requiring high strength, hardness, and resistance to abrasion, wet and dry erosion, and moderate corrosion. They are not suitable for cryogenic applications, because of brittleness and shock sensitivity under these conditions. They are used for turbopump ball bearings and shafts, gears, valve actuators, and cams.

Semiaustenitic Stainless Steels

The steels in this group can be formed in the soft state and then precipitation hardened. They are intended for use in parts requiring corrosion resistance and high strength at operating temperatures up to 800° F, and where such parts may require welding and soldering during fabrication. However, the corrosion resistance of this type of steel is not as good as that of the austenitic stainless steels. Rocket engine component parts, such as thrust chambers, pump shafts, levers, brackets, bellows, ducts, springs, clamp rings, valve poppets, housings, and pressure vessels, have been made from the steels of this group.

Aluminum Alloys

Pure metallic aluminum has a relatively low strength. However, the strength can be greatly increased by alloying aluminum with one or more metals or metalloids. This can be accomplished without affecting appreciably the other desirable properties of aluminum, such as low weight, corrosion resistance, ductility, good thermal and electric conductivity.

Wrought alloys of aluminum are generally of two types: one group that can be hardened by cold-working only (non-heat-treatable), such as 1100, 3003, 3004, 5050, and 5052 and a second group that will respond to both cold-working and heat-treatment, such as 2011, 2014, 2017, 2024, 6061, 6066, and 7075. Wrought-aluminum alloys are suitable for fabrication processes such as machining, shearing, drawing, stretch forming,

spinning, stamping, and shape bending. Most of them are also adaptable for forging, welding, brazing, and soldering. Aluminum alloys can be cast by all three common casting methods: sand, permanent mold, and pressure die casting. Mechanical properties and workability of aluminum castings are excellent.

Aluminum alloys are the most widely used materials in rocket engine construction except where elevated temperatures are encountered. Typical applications are valve bodies and poppets, injector domes, propellant tanks and ducts, pump housings, impellers and inducers, and structure mounts.

Magnesium Alloys

Magnesium alloys have found many applications in rocket engines and vehicles because of their excellent strength-to-weight, fatigue and stiffness characteristics. These alloys are used to make pump housings, valve bodies, and structure mounts and are available in sheets, rods, and castings.

Magnesium sheet alloys can be formed at elevated temperatures. They are also suitable for various machining processes. They can be joined by fusion and resistance welding as well as by adhesive bonding. Magnesium alloys can be cast by all three common casting methods: sand, permanent mold, and pressure die casting. Certain cast alloys can also be welded and heat treated.

High-Temperature Nickel-Base Alloys

The metals included in this group are used primarily for their strength at temperatures up to 1700° F. The majority of them contain aluminum or titanium as precipitation-hardening agents and are vacuum melted. Their resistance to oxidation and corrosion is excellent. These alloys have found wide application in rocket engine components such as: turbine housings, wheels, and blades; thrust chamber tubes and injectors; gas generators; high-temperature gas ducts, bolts, and fasteners.

Special Alloys

The ever-present extreme temperature condi-

tions in liquid rockets calls for continued and intensive materials research, particularly with the advent of liquid hydrogen systems. In addition to the metals discussed in the preceding paragraphs, other metals and alloys are receiving increasing attention. Among these are:

Copper base alloys.—These metals exhibit excellent ductility and toughness at very low temperatures. Typical representatives are Berylco-10, -25 alloys, and Fe-Si bronze.

Cobalt base alloys.—The properties of these metals, such as Haynes-25, are similar to those of the nickel alloys.

Tantalum.—Tantalum, when pure, has good properties at both low and elevated temperatures.

Columbium.—This metal has been considered for cryogenic application, but is liable to become embrittled at very low temperatures.

Titanium-base alloys.—These alloys have attracted considerable attention because of their high strength-to-density ratios, particularly at very low temperatures.

Nonmetallic Materials

For gaskets, seals, lubricants, thread compounds, and the like, liquid rocket engines require compatible nonmetallic materials. A great variety of commercial products is available.

In advanced LOX-pump designs, as well as in liquid-hydrogen pumps, the pumped fluid is used as the lubricant.

Chapter III

Introduction to Sample Calculations

3.1 APPROACH

It is a major goal of this book to familiarize the student with the detailed techniques used by industry in liquid propellant rocket engine systems and component design. The authors feel that to convey a feeling for this subject effectively, nothing serves better than a set of realistic sample calculations. To promote a good feeling for the interrelationship between major subsystems, the principal calculations were made for the engines of a hypothetical multistage space vehicle. These calculations and their associated designs were especially prepared for this book and are not related to existing or planned engines. As the various subsystems of liquid rocket engines are discussed in subsequent chapters, most of the supporting sample calculations will be for the engines of that assumed vehicle, which thus will appear throughout the entire book. For simplicity of reference, the space vehicle will be called the "Alpha" vehicle; it is assumed to be composed of four stages: A-1, A-2, A-3, and A-4. Table 3-1 lists the major parameters of the Alpha vehicle.

The Alpha vehicle combination is realistic, though not necessarily optimized. For instance, a different propellant combination has been chosen for each stage to permit sample calculations and designs for a number of typical propel-

lant combinations, feed systems, and thrust levels. In practice for logistics reasons, or to permit multiple use of parts, fewer combinations would be chosen. In fact, the student and the teacher using this book may find it interesting and instructive to modify the designs chosen by the authors.¹ For instance, the student may wish to determine what engine-design parameters would result if stages A-2 and A-3 were to use the same propellant combination; or, what design parameters would be obtained if stages A-3 and A-4 were combined into one, capable of restart and throttling to 30 percent nominal thrust.

It is not intended to suggest a specific mission for the Alpha vehicle. However, a "primary mission" for it could be the landing of an unmanned scientific payload on the Moon to gather samples and return them to Earth. The staging sequence may then be as follows:

Stage A-1: Boost to 250 000-foot altitude.

Stage A-2: Boost to 300-nautical-mile altitude and inject into Earth parking orbit.

Stage A-3: Accelerate to escape velocity and inject into a translunar trajectory.

Stage A-4:

First start: Deceleration for lunar orbit and soft Moon landing of scientific payload

Second start: Moon takeoff for return to Earth

In addition to its main powerplant, stage A-4 will require very-low-thrust attitude-control jets.

Even if designed for a given "primary mission," a vehicle combination retains a certain degree of

TABLE 3-1.—4-Stage Space Alpha Vehicle

Takeoff weight, 2 100 000 lb;
Payload^a for 300-n.mi. orbit, 109 500 lb.

Stage	Stage thrust, lb	Number of engines	Engine thrust, lb	Propellant
A-1	3 000 000	4	750 000	LO ₂ /RP-1
A-2	600 000	4	150 000	LO ₂ /LH ₂
A-3	48 000	3	16 000	LF ₂ /LH ₂
A-4	15 000	2	7500	N ₂ O ₄ /N ₂ H ₄

^a Consisting of stages 3 and 4, and of the mission payload.

¹ Several good books on astronautics and space dynamics are available from which student and teacher may gather mission data for their own engine selection and design. Among them is a little book by Dr. Wernher von Braun, "The Mars Project" (University of Illinois, Urbana, 1962, \$0.95). Most of the calculations in this book were made as early as 1948, yet are still fundamentally applicable. They appear ideally suited for the reader to design his own up-to-date engine system for the manned Mars mission described, for which all necessary vehicle data are presented.

flexibility. Within the limits of existing propellant tank configurations, the following principal possibilities of modification exist:

Omission of the upper two stages, for Earth-orbital tankers, shuttle vehicles, space-station assembly, and supply ships.

Omission of stage A-4, for unmanned deep space probe assignments, with no return intended.

Off-nominal tanking of one or more stages. This may yield some overall performance gains for special missions.

It is emphatically not intended to say that the stated modifications can be made a few days before launch. Rather, the stages and certain of their subsystems, in particular the engines, should be regarded as building blocks. Their availability can permit meeting a new requirement within, for example, a year, as compared to several years when "starting from scratch." In such ways, substantial gains have been obtained in practice. The earlier Thor, and the Redstone and Atlas Mercury boosters are well-known such cases.

Brief mention should be made here of a special type of system: experimental engine systems, sometimes referred to as breadboard engines. Because of time and fund limitations, the design and development of liquid rocket engines for a given mission rarely permit the investigation of novel ideas and principles. New ideas must then be tried out independently, detached from rigid schedules. Here the test effort can be conducted with full awareness that many of the principles under investigation will not "make the grade." However, while those that succeed can be applied to advanced operational systems, the eliminated marginal ones are just as valuable, as they were early prevented from finding their way into operational engines. If experimentally verified advances are selected for operational use with strong emphasis on vehicle application, true progress will have been made. The major U.S. liquid propellant engine manufacturers have been conducting experimental engine programs with excellent results for a number of years.

The reader will now be acquainted with some of the characteristics of the engines which have been selected for the different stages of the Alpha vehicle. While discussing and implementing these in greater detail in subsequent chap-

ters, and through calculations and layouts, this summarizing description can serve as a guide and reference, throughout the book.

3.2 A-1 STAGE ENGINE

Four engines of 750 000-pound thrust each were selected for a combined thrust of 3 million pounds (3000K), as a compromise between number of engine systems, and thus complexity on one hand, and flexibility on the other. Flexibility is offered through the possibility of including engine-out capabilities; of using existing smaller systems or designs; and for guidance and packaging considerations.

The propellant combination of liquid oxygen and kerosene type RP-1 fuel was selected for the A-1 engine. The selection was guided by the consideration that high performance is not as critical for first booster stages as it is for upper stages. Both propellants are abundantly available and comparatively inexpensive. The fluids and their combustion products are "docile"; their corrosivity is nil. Both fluids are relatively dense. Liquid propellant rocket engine systems using these propellants are well developed and reliable, and many "off the shelf" components and designs are available for them.

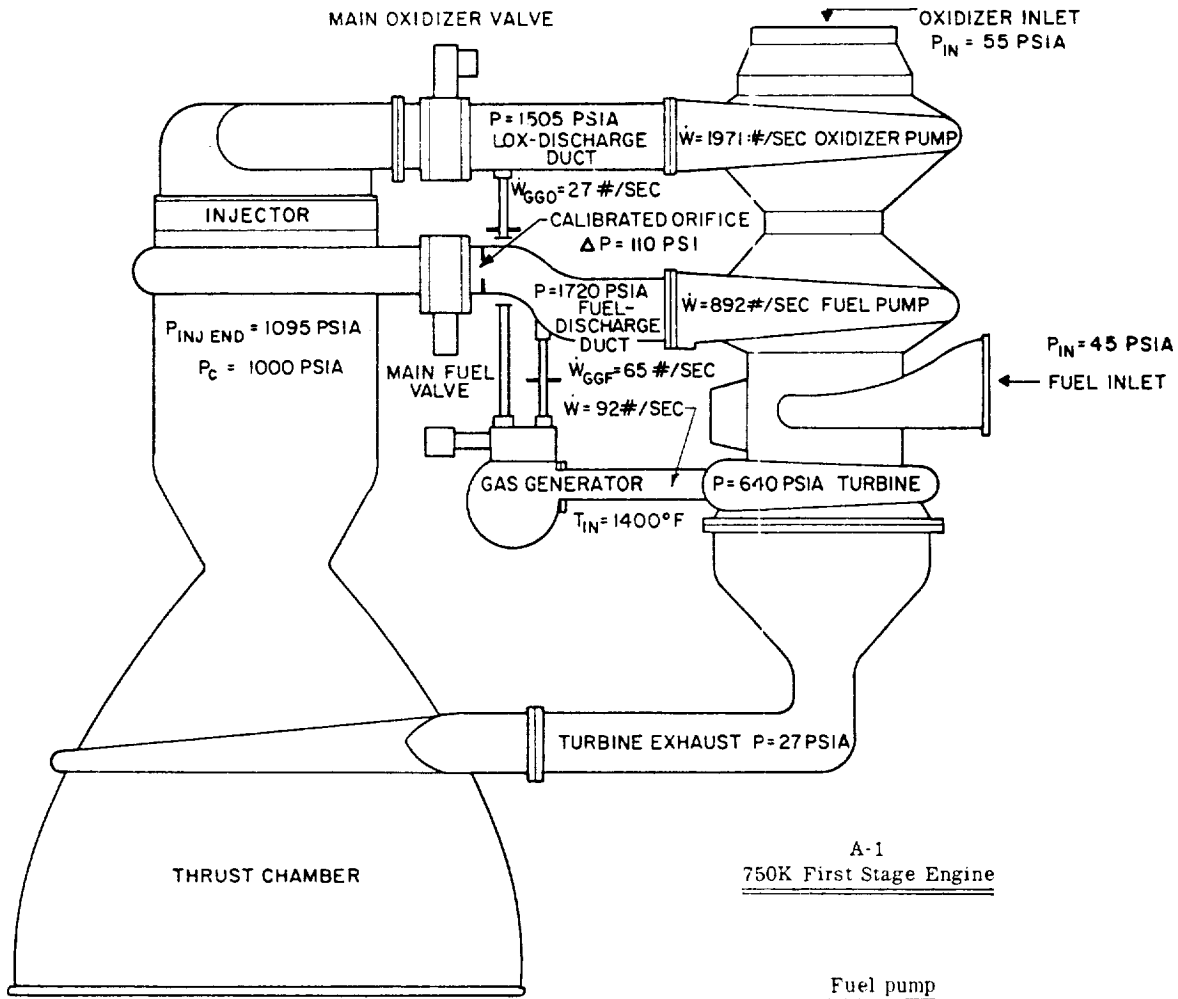
General Engine System Description

The A-1 engine is a single-start, fixed-thrust, gimbaled, bipropellant system. The fuel, RP-1, is also used as the turbopump lubricant and as the engine control system actuating fluid. The major components of the A-1 engine are a regeneratively fuel-cooled, double-pass, tubular-wall thrust chamber with bolt-on injector; a direct-drive turbopump consisting of two centrifugal pumps and a single-stage, two-wheel turbine; an uncooled gas generator with dual-ball valve; butterfly main valves; and required controls. The gas generator uses the same propellant combination as the thrust chamber. Table 3-2 presents all necessary operating parameters on which engine component designs will be based for the A-1 engine system.

The A-1 engine system schematic diagram is shown in figure 2-7. This diagram identifies clearly all major engine components and their interconnecting plumbing. For the various

TABLE 3-2.—750K A-1 Stage Engine Operating Parameters
[Sea-level conditions]

Engine (turbopump feed):		Line pressure drop	psi	10
Thrust	lb	Main valve pressure	psi	15
Nominal single-firing duration	sec	Calibration orifice pressure drop	psi	110
Specific impulse	sec	Pump:		
Oxidizer LO ₂ :		Inlet pressure	psia	45
Flow rate	lb/sec	Discharge pressure	psia	1720
Density	lb/ft ³	Developed pump head	ft	4790
Fuel RP-1:		Pump:		
Flow rate	lb/sec	Flow rate	lb/sec	892
Density	lb/ft ³	Shaft power	bhp	11 790
Mixture ratio	O/F	Efficiency	Percent	65.8
		Shaft speed	rpm	7000
Thrust chamber (tubular wall construction regeneratively cooled by fuel):		Turbine:		
Thrust	lb	Inlet pressure	psia	640
Specific impulse	sec	Inlet temperature	°F	1400
Injector end pressure	psia	Pressure ratio		23.7
Nozzle stagnation pressure	psia	Gas flow rate	lb/sec	92
Oxidizer flow rate	lb/sec	Shaft power	bhp	27 140
Fuel flow rate	lb/sec	Efficiency	Percent	58.2
Mixture ratio	O/F	Shaft speed	rpm	7000
c* efficiency	Percent	Shaft torque	in-lb	20 380
c*	ft/sec	Auxiliary drive:		
C _f efficiency	Percent	Shaft power	bhp	500
C _f		Gas generator system:		
Contraction ratio	A _c /A _t	Oxidizer side:		
Expansion ratio	A _e /A _t	Flow rate	lb/sec	26.7
Throat area A _t	in ²	Entrance loss	psi	25
L*	in	Line pressure drop	psi	25
Nozzle contour	80 percent bell	Control-orifice pressure drop	psi	615
		Valve pressure drop	psi	10
		Injector pressure drop	psi	120
		Fuel side:		
Oxidizer side:		Flow rate	lb/sec	65.3
Injector pressure drop	psi	Entrance loss	psi	25
Torus dome pressure drop	psi	Line pressure drop	psi	25
Line pressure drop	psi	Control-orifice pressure drop	psi	800
Main valve pressure drop	psi	Valve pressure drop	psi	20
Pump inlet pressure	psia	Injector pressure drop	psi	140
Pump discharge pressure	psia	Gas generator:		
Developed pump head	ft	Mixture ratio	O/F	0.408
Pump:		Injector end pressure	psia	710
Flow rate	lb/sec	Combustor pressure drop	psi	70
Shaft power	bhp	Thrust vector control:		
Efficiency	Percent	Minimum acceleration	rad/sec ²	1
Shaft speed	rpm	Maximum velocity	deg/sec	10
Heat exchanger	lb/sec	Displacement	deg	±14
Fuel side:				
Injector pressure drop	psi			
Jacket and manifold pressure drop	psi			



A-1
750K First Stage Engine

		<u>Fuel pump</u>	
		Developed head	4790 ft
		Flow rate	892 lb/sec
		Efficiency	65.8%
		Horsepower	11 790 bhp
		Speed	7000 rpm
<u>Nominal engine parameters</u>		<u>Oxidizer pump</u>	
Propellants:			
Liquid oxygen density	71.38 lb/ft ³	Developed head	2930 ft
RP-1 density	50.45 lb/ft ³	Flow rate	1971 lb/sec
Thrust (sea level)	750 000 lb	Efficiency	70.7%
Specific impulse	262.4 sec	Horsepower	14 850 bhp
Mixture ratio	2.20	Speed	7000 rpm
<u>Thrust chamber</u>		<u>Turbine</u>	
Expansion area ratio	14	P _{in}	640 psia
Throat area	487 in ²	Pressure ratio	23.7
Thrust	747 000 lb	Temp _{in}	1400° F
Specific impulse	270 sec	Efficiency	58.2%
Mixture ratio	2.35	Horsepower	27 140 bhp
Flow rates:		Exhaust thrust	3000 lb
oxidizer	1941 lb/sec		
fuel	827 lb/sec		

Figure 3-1.—A-1 engine performance diagram.

phases of engine design and development, it has been found useful to work from an "engine performance diagram." This is a combination of the basic engine schematic and the principal performance parameters. The A-1 engine diagram is shown in figure 3-1. It is suggested that the reader prepare his own performance diagrams for the other three stages.

For simplicity of mounting and compactness, the turbopump is attached directly to the thrust

chamber. All other components are either mounted on these two assemblies, or are located in the plumbing system between them. This arrangement permits engine gimbaling without pump-discharge high-pressure propellant-duct flexure. Rather, thrust-vector control is achieved by gimbaling the entire engine. The engine weighs approximately 7500 pounds dry, 7900 pounds wet, and 7830 pounds at burnout. The preliminary design layout of the A-1 engine system and its overall dimensions are shown in figure 3-2.

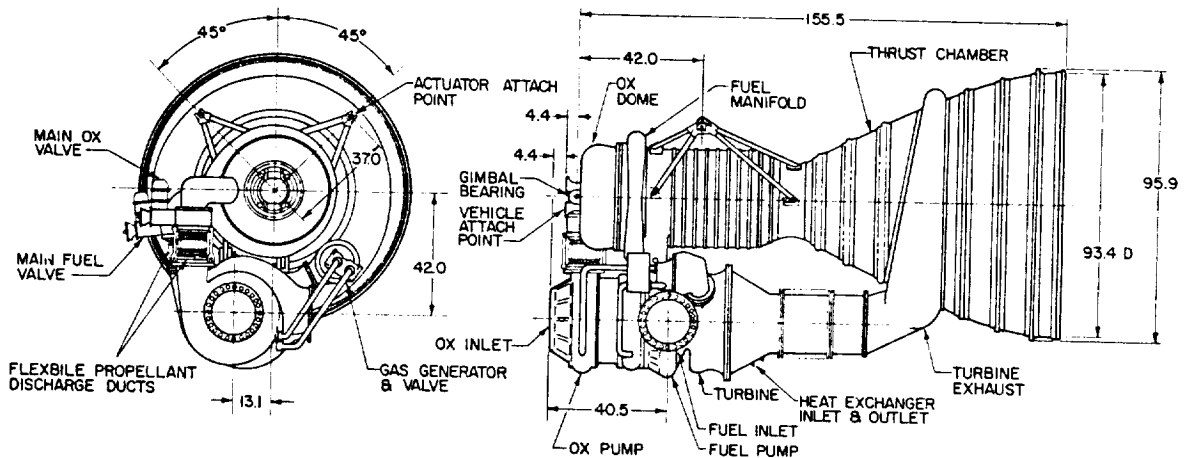


Figure 3-2.—A-1 750K first stage engine system preliminary layout.

System Operation

The starting method of the A-1 engine is the "main-tank-head start," combined with pressure ladder sequence (figs. 2-7 and 2-8). Propellants are used under vehicle-tank-head pressures to initiate gas generator operation. As the turbopump starts to accelerate, main propellant pressures "bootstrap" the system to mainstage level.

Starting Sequence

After all vehicle launch preparations are completed and the main propellant tanks are pressurized, the gas generator dual sparkplugs are activated upon a given signal and the engine four-way control valve is energized to open. The closing side is vented and fuel pump outlet pressure (50 psia from tank head) is admitted to the opening side of the main oxidizer and gas generator valve actuators. The gas generator valves open and admit both propellants to the gas generator combustor, where they are ignited by the

spark plugs. At this point, the main oxidizer valve remains closed, since the valve spring prevents opening until substantially higher actuating fuel pressures are developed by the pump later in the sequence.

The low initial gas generator power level is sufficient to start and accelerate the turbopump. This, in turn, increases the propellant pressures available to the gas generator, which is connected upstream of the still closed main valves. As a result, the gas generator-turbine system "bootstraps" itself.

At a predetermined fuel pump outlet pressure (valve spring rate selection), the main oxidizer valve opens. During the oxidizer valve stroke, an integral and mechanically linked igniter fuel sequence valve is actuated. The sequence valve in turn admits fuel pressure to the hypergol igniter cartridge, rupturing its diaphragms. Hypergol (such as triethylaluminum) enters the combustion chamber igniter elements and ignites with the oxidizer just being admitted by the main

oxidizer valve. Fuel following the hypergol sustains the igniter flame.

The chamber pressure resulting from igniter combustion is sufficient to actuate the ignition monitor valve. This valve admits fuel pressure to the main fuel valve opening actuator, opening the valve, which is the last step in the sequence. Main fuel enters the combustion chamber; chamber pressure and thrust climb to the rated level.

Cutoff Sequence

Upon receipt of a cutoff signal, the engine four-way control valve is deenergized to close. The opening pressures of all valves vent; the valves close. Turbine power and main chamber pressure decay. While the main propellant tanks vent, all valves are held in their closed position by springs. Note that the gas generator valve and the main oxidizer valve are closed by admitting actuation pressure to their closing port, while the main fuel valve is closed by spring force only. Experience has shown that cutoff precision is largely influenced by turbopump decay characteristics and by cessation of that propellant flow which has the smallest duct volume below the valve, in this case the oxidizer (no cooling jacket). The fast closing valves need some timing, however, from water-hammer considerations.

3.3 A-2 STAGE ENGINE

For the same reasons as with the A-1 stage, a four-engine cluster has been chosen, having a total vacuum thrust of 600 000 pounds (150 000 pounds per engine). Because of the substantial vehicle performance gains obtainable through the use of high-energy propellants in upper booster stages, liquid oxygen (LO_2) and liquid hydrogen (LH_2) have been selected as propellants. For decades this combination has attracted the attention of rocket experimenters and developers. However, only relatively recently has the art of hydrogen engines reached maturity. Several major systems are in active development or in early flight application.

Through the years, the production and handling of the cryogenic propellant liquid oxygen (LO_2 or "LOX") has become a routine matter; its price has come down considerably. It can be reasonably expected that in the near future this will be

equally true for liquid hydrogen. Both elements are abundantly available. Their combustion product—water vapor—is the most harmless of all propellant combinations, solid or liquid. Telemetry engineers like it because of the low attenuation effects of the exhaust gases on RF signals, an important aspect for vehicle guidance and telemetry. Most important, the yield in specific impulse of this combination is close to the theoretical maximum for chemical reactions. Only certain fluorine/hydrogen combinations are slightly higher (approximately 4 percent). However, the extreme toxicity of fluorine and fluorine compounds, both as a liquid and as components of combustion products, makes fluorine less attractive for operational use. By building the A-1 and A-2 stage a little larger, the same payload can be obtained as with fluorine. However, all advantages of liquid oxygen and hydrogen are retained, including the great amount of available experience.

Hydrogen does have its drawbacks. The principal one is low density, resulting in rather bulky tanks. For a typical oxygen-to-hydrogen mixture ratio of 5:1, the corresponding volume ratio is inverted: 1:3. This disadvantage, however, is successfully offset for upper stages by the high energy yield (I_s). It can be expected that the improved state of the art of ultralightweight vehicle and tank constructions will further increase the superiority of hydrogen systems for upper stages.

A secondary effect of low density is a high boiloff rate, unless tanks and lines are properly insulated. Because of the low density, and of the resulting large surface area of the containers, the heat input per unit hydrogen mass is high. Furthermore, the temperature of liquid hydrogen is sufficiently low to liquefy air on the tank surfaces. This sharply increases heat transfer rates, resulting in extreme boiloff rates. Tank and line insulation, therefore, is vital. Although techniques of rocket vehicle insulation are highly developed, some weight penalties are incurred.

Overall, however, a substantial net performance gain can be obtained for upper stages.

General Engine System Description

The A-2 engine is a single-start, fixed-thrust,

TABLE 3-3.-150K A-2 Stage Engine Operating Parameters

[Vacuum conditions]

Engine (turbopump feed):		Shaft speed rpm	8600
Thrust lb	150 000	Turbine:	
Nominal single-firing duration sec	250	Inlet pressure psia	700
Specific impulse sec	434	Inlet temperature °F	1200
Oxidizer LO ₂ :		Pressure ratio	16
Flow rate lb/sec	288	Gas flow rate lb/sec	1.58
Density lb/ft ³	71.38	Shaft power bhp	1940
Fuel LH ₂ :		Efficiency Percent	54.3
Flow rate lb/sec	57.6	Shaft speed rpm	8600
Density lb/ft ³	4.42	Shaft torque in-lb	14 200
Mixture ratio O/F	5		
Thrust chamber (tubular wall construction regeneratively cooled by fuel. Nozzle extension film cooled by turbine exhaust gas):		Fuel side:	
Thrust lb	149 500	Injector pressure drop psi	100
Specific impulse sec	440	Jacket and manifold pressure drop psi	325
Injector end pressure psia	875	Line pressure drop psi	20
Nozzle stagnation pressure psia	800	Main valve pressure drop psi	20
Oxidizer flow rate lb/sec	285.2	Calibration orifice pressure drop psi	60
Fuel flow rate lb/sec	54.5	Pump inlet pressure psia	25
Mixture ratio O/F	5.22	Pump discharge pressure psia	1400
c* efficiency Percent	97.5	Developed pump head ft	44 800
c* ft/sec	7480	Pump weight flow rate lb/sec	59.8
C _f efficiency Percent	101	Pump volumetric flow rate gpm	6080
C _f	1.895	Heat exchanger bleed lb/sec	2.2
Contraction ratio A _c /A _t	1.60	Pump:	
Expansion ratio A _e /A _t	40	Shaft power bhp	6100
Throat area, A _t in ²	98.6	Efficiency Percent	80
L* in	26	Shaft speed rpm	27 000
Nozzle contour	75 percent bell	Chamber coolant passage bleed for fuel tank pressurization lb/sec	2.2
Oxidizer side:		Turbine:	
Injector pressure drop psi	160	Inlet pressure psia	700
Torus dome pressure drop psi	40	Inlet temperature °F	1200
Line pressure drop psi	20	Pressure ratio	16
Main valve pressure drop psi	20	Gas flow rate lb/sec	4.32
Calibration orifice pressure drop psi	60	Shaft power bhp	6100
Pump inlet pressure psia	35	Efficiency Percent	62.5
Pump discharge pressure psia	1175	Shaft speed rpm	27 000
Developed pump head ft	2305	Shaft torque in-lb	14 250
Pump weight flow rate lb/sec	290.5	Tapoff gas from thrust chamber for turbine drive:	
Pump volumetric flow rate gpm	1830	Pressure lb/in ²	750
Heat exchanger bleed (oxidizer tank pressurization) lb/sec	2.5	Temperature °F	1200
Pump:		Weight flow rate lb/sec	5.9
Shaft power bhp	1910	Mixture ratio O/F	0.90
Efficiency Percent	64	Thrust vector control:	
		Minimum acceleration rad/sec ²	2
		Maximum velocity deg/sec	15
		Displacement deg	±6

gimbaled, bipropellant system. The thrust chamber features a combination of fuel regenerative cooling, and film cooling with turbine exhaust gas. The chamber assembly is fed by two independent, direct-drive centrifugal turbopumps. For the fuel, an alternative axial pump may be chosen. Each operates at optimum speed. Hot gases are tapped off from the main combustion chamber to power the turbines. A hot gas orifice in the tapoff duct controls the engine thrust level. The turbines are gas coupled in parallel. Their exhaust gases are routed to the thrust chamber and injected in the 30:1 expansion area ratio plane. Thus the gases provide film cooling for the nozzle portion from there to the 40:1 area ratio plane. The remainder of the chamber, above the 30:1 plane, is regeneratively cooled (1½ pass). Helium gas is used to actuate the controls. No lubricants or any other fluids are used which could freeze at low temperatures. The engine is started by the hot gases generated by a solid-grain turbine spinner. Chlorine trifluoride (ClF_3), which is hypergolic with LH_2 , is used to ignite the combustion chamber. Both turbine spinner and igniter fluid are insulated and electrically temperature conditioned from a ground source until first-stage takeoff. Gaseous hydrogen is bled from the thrust chamber coolant

passage to pressurize the vehicle main fuel tank. A small portion of liquid oxygen bled from the oxidizer pump discharge is heated in a heat exchanger and used for vehicle main oxidizer tank pressurization.

A listing of the A-2 engine operating parameters is presented in table 3-3. The engine schematic diagram is shown in figure 3-3. Note that engine parameters are based on vacuum conditions. This is justified and customary, if a stage starts and performs in vacuum for its entire duration. In the case of the A-2 stage, the starting altitude of 250 000 feet is not an absolute vacuum, but for all practical purposes may be considered absolute.

Thrust-vector control is achieved by gimballing the entire engine. It weighs approximately 2181 pounds dry, 2317 pounds wet, and 2292 pounds at burnout. The overall dimensions and the preliminary design layout of the A-2 engine are shown in figure 3-4.

System Operation

The starting method of the A-2 engine (figs. 3-3 and 3-5) is a "turbine spin start," for very fast buildup (less than 2 seconds from start signal to main stage). Starting power is furnished

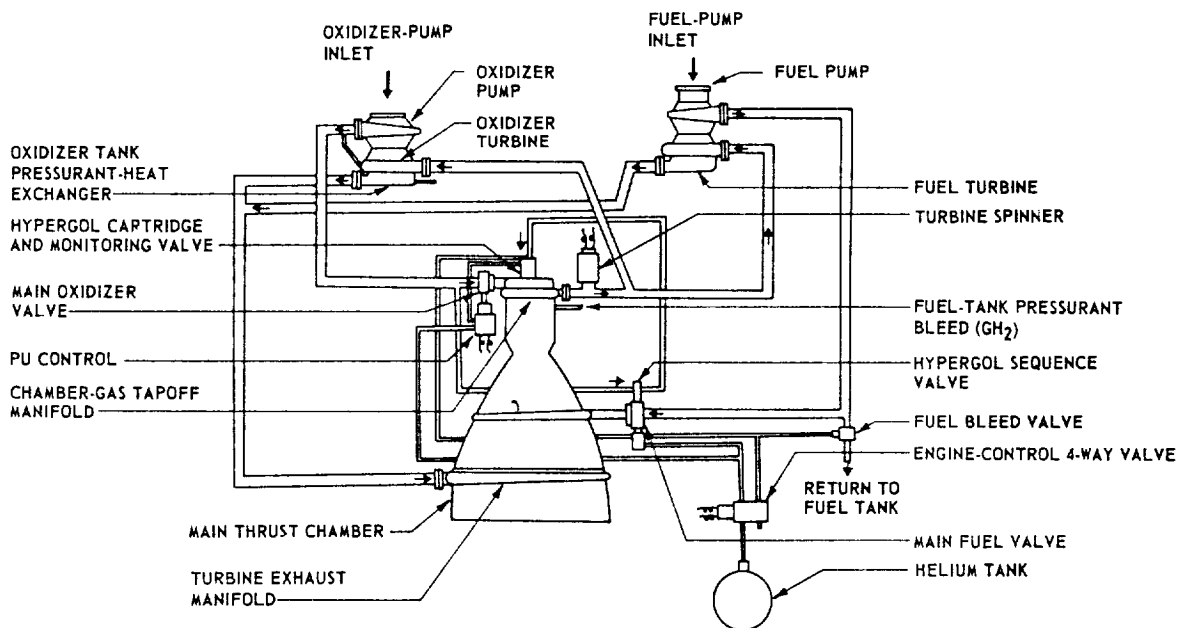


Figure 3-3.—A-2 stage engine system schematic diagram.

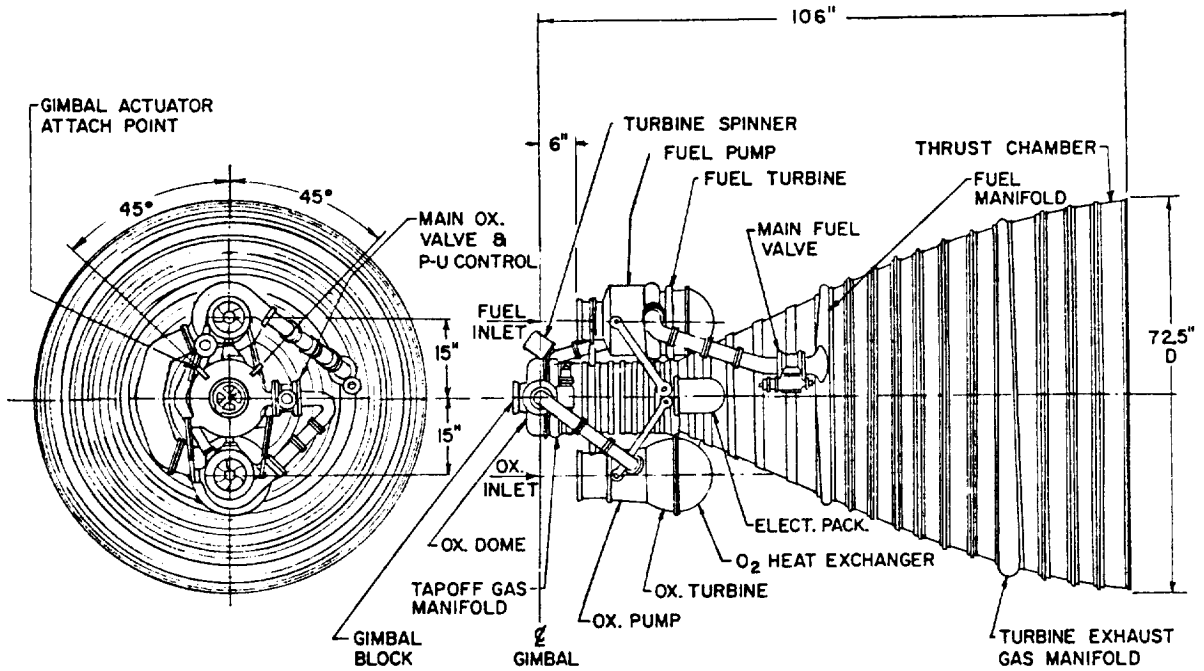


Figure 3-4.—150K A-2 stage engine system preliminary layout.

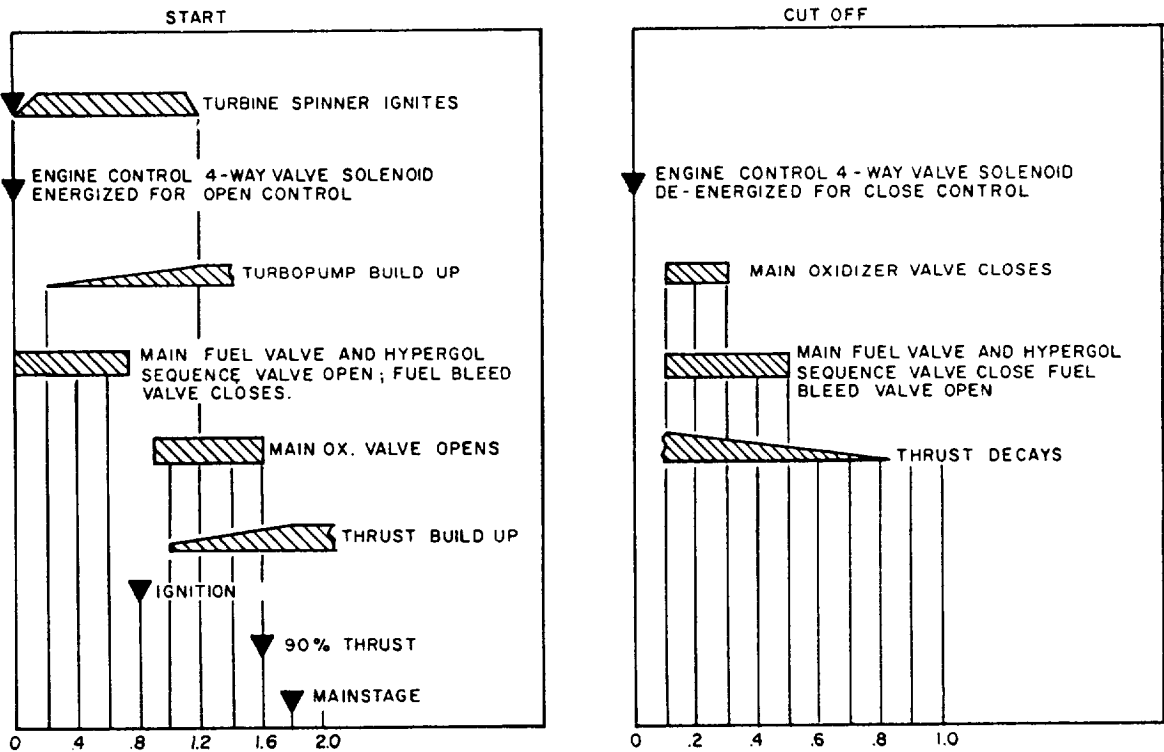


Figure 3-5.—A-2 engine system sequence diagram.

by a turbine spinner. Chamber tapoff gases then bootstrap the turbine and main stage operational level is established.

Starting Sequence

As part of the separation and staging sequence, a vehicle programmer furnishes a start signal to the engine, which ignites the turbine spinner and supplies hot gases at 2000° F to turbines and combustion chamber. This signal also energizes the solenoid of the engine control valve, which vents the closing side of both main propellant valve actuators and pressurizes the opening side of the fuel valve actuator with helium gas. Simultaneously, the hypergol sequence valve, which is mechanically linked to the main fuel valve, is opened and the actuator of the normally open fuel bleed valve is pressurized to close. The fuel flows through the chamber cooling jacket under increasing pump discharge pressure and injects into the combustion chamber. Ignition is achieved by the hypergolic reaction between hydrogen and the slug of chlorine trifluoride forced into the chamber by increased oxidizer-pump discharge pressure.

When the main fuel valve reaches the 90-percent open position, ports integral with the actuating piston open and permit helium gas to flow through the hypergol monitor valve and to pressurize the open side of the main oxidizer valve actuator. The main oxidizer valve opens, admitting oxidizer to the chamber where pressure builds up rapidly. Chamber tapoff gases bootstrap the turbines to main stage operation. The spinner will burn for about 1.2 seconds. After the main stage is achieved, the propellant-utilization servo system will begin to function.

Cutoff Sequence

The cutoff signal, received from the vehicle programmer, deenergizes the engine control valve causing it to close. This vents the open side and pressurizes the closing side of the main propellant valve actuators. The main oxidizer valve is made to close faster than the main fuel valve, by proper orificing of the helium lines, to assure a fuel-rich cutoff. Engine thrust decays. The fuel bleed valve opens after the helium pressure in its actuator is vented.

3.4 A-3 STAGE ENGINE

The total thrust of 48 000 pounds is subdivided into three engines of 16 000-pound thrust each. This effects a shorter overall propulsion system and a shorter, lighter vehicle interstage. Furthermore, the liquid fluorine/liquid hydrogen propellant combination was chosen because of the relatively stringent performance requirements for upper stages.

Fluorine is the most reactive and energetic chemical element. It has vigorous and reliable hypergolic ignition characteristics, and superior specific impulse capabilities with most fuels. The high density of liquid fluorine, combined with high performance with liquid hydrogen, results in maximum payloads. As mission requirements become more ambitious, payload advantages from the fluorine-oxidized propellant combination should compensate for handling problems caused by fluorine toxicity and corrosiveness. Past experience has indicated that the operation of a fluorine-oxidized engine is practical at this thrust level (50 000 pounds or less). Fluorine when used for gaseous passivation of metals renders a metallic surface resistant to future chemical reaction. Thus, once a metallic fluoride film is formed, further action by the liquid fluorine is either prevented or significantly retarded, making handling or storing of liquid fluorine less of a problem. No known elastomer is completely compatible with fluorine; however, flow tests of liquid fluorine with Teflon have given satisfactory results.

General Engine System Description

The A-3 engine is a multiple-start, gimballed, bipropellant system. The basic system includes a thrust chamber assembly using a combination of fuel-film (LH_2) and radiation cooling; propellant ducts; valves; and a control subsystem. Ignition is achieved by the hypergolicity of the propellants. These are fed directly from pressurized propellant tanks, through main propellant valves, to the thrust chamber inlets. The propellant tanks and their gas pressurization system are considered part of the engine propellant feed system. Gaseous helium supplied from a high-pressure helium bottle located inside the main fuel tank is used for main oxidizer tank

CONFIDENTIAL

pressurization. The main fuel tank is pressurized by gaseous hydrogen supplied from a liquid hydrogen bottle which is pressurized by helium and which is also located inside the main fuel tank. Both pressurants are heated in heat exchangers located at the thrust chamber nozzle extensions before they are expanded through pressure regulators and transferred to the propellant tanks. Helium gas is used to operate the main valves and the gimbal actuators, and to purge the propellant manifolds during start.

A-3 engine operating parameters, for vacuum conditions, are presented in table 3-4. The propulsion system schematic diagram is shown in figure 3-6.

The design of the entire propulsion system is governed by simplicity and minimum number of components. This is essential because of the

highly reactive and toxic nature of fluorine. Welded joints are used extensively. No rotating seals are employed. Sliding seals are of the metal-bellows type.

A preliminary design layout of the A-3 propulsion system and dimensions are shown in figure 3-7.

The fuel tank is pressure stabilized rather than mechanically stabilized. The thrust loads are transmitted to the payload through the fuel tank. Both tanks are insulated, as are the ducts between tanks and engine systems.

Thrust-vector control is achieved by gimbaling the thrust chambers. Each basic engine weighs approximately 330 pounds dry and 365 pounds at burnout. It has a cylindrical space envelope of 5 feet 4 inches diameter by 7 feet 6 inches length. The propulsion system (including the three engines and the tankage) weighs

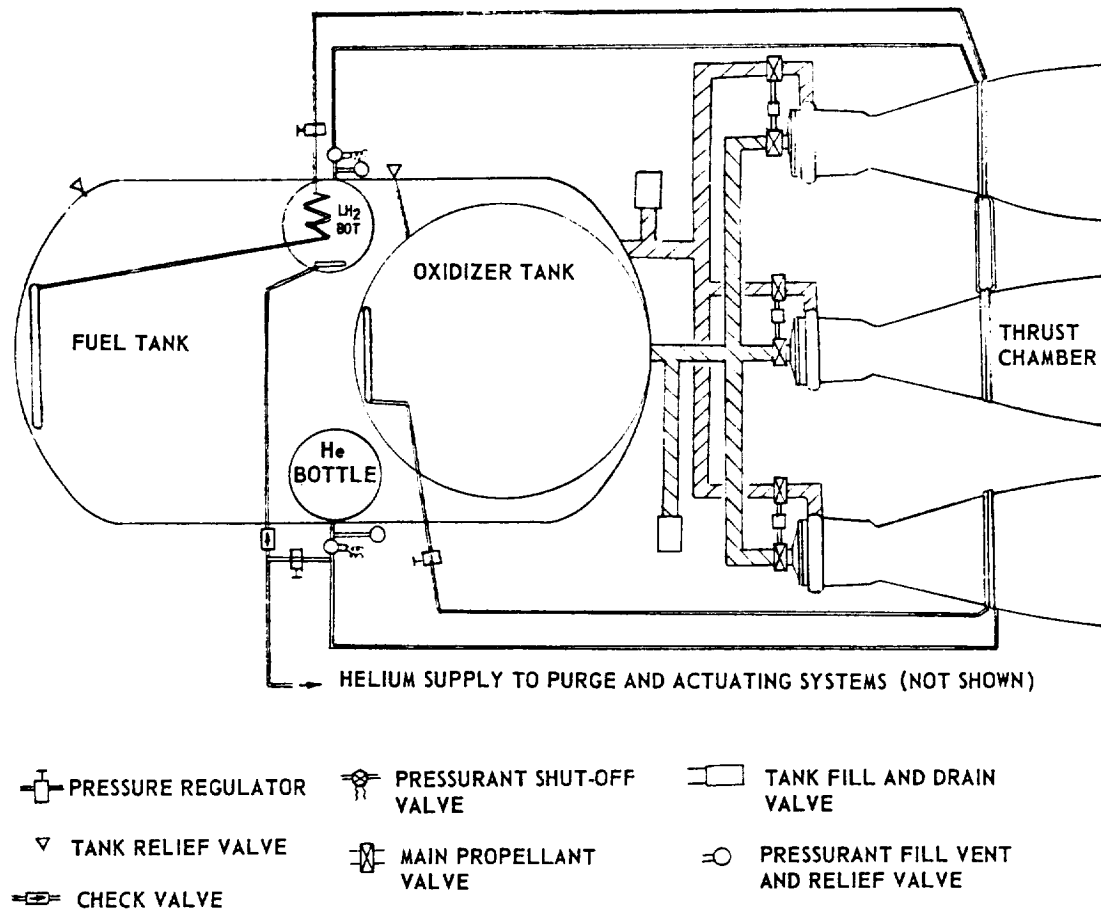


Figure 3-6.—A-3 stage propulsion and engine system schematic diagram.

TABLE 3-4.—16K A-3 Stage Engine Operating Parameters
[Vacuum conditions]

Engine (pressurized gas-feed):		Calibration orifice pressure drop psi	17
Thrust lb	16 000	Oxidizer tank pressure psia	170
Nominal total multiple-firing duration sec	300	Total oxidizer weight (300 sec duration for 3 engines, plus 1 percent residual) lb	27 950
Specific impulse sec	446	Oxidizer tank volume (including 3 percent ullage volume) ft ³	305
Oxidizer LF ₂ :		Pressurant (helium) flow rate (assuming tank gas temperature 400° R) lb/sec	0.1555
Density lb/ft ³	94.16	Total pressurant weight (including other requirements in the system) (assume storage bottle final pressure 350 psi, plus 2 percent reserve) lb	60
Flow rate lb/sec	30.78	Pressurant storage tank, volume (assume 200° R storage temperature, including 3 percent ullage volume) ft ³	7.35
Fuel LH ₂ :		Pressurant storage tank, initial pressure psia	4500
Density lb/ft ³	4.42		
Flow rate lb/sec	5.13	Fuel side (pressurized by heated hydrogen):	
Mixture ratio O/F	6	Injector pressure drop psi	25
Thrust chamber (solid wall film cooled by fuel and radiation cooled on nozzle extension):		Inlet manifold pressure drop psi	10
Thrust lb	16 000	Main valve pressure drop psi	10
Specific impulse sec	446	Line pressure drop psi	5
Injector end pressure psia	110	Fuel tank pressure psia	160
Nozzle stagnation pressure psia	100	Total fuel weight (300 sec duration for 3 engines, plus 1 percent residual) lb	4660
Oxidizer flow rate lb/sec	30.78	Fuel tank volume (including 3 percent ullage volume) ft ³	1087
Fuel flow rate lb/sec	5.13	Pressurant (hydrogen) flow rate (assuming tank vapor temperature 300° R) lb/sec	0.346
Mixture ratio O/F	6	Total pressurant weight (assuming storage bottle final pressure 350 psia, plus 4 percent reserve) lb	108
c* efficiency Percent	98	Pressurant storage tank, volume (liquid hydrogen including 3 percent ullage volume) ft ³	25.2
c* ft/sec	7910	Pressurant storage tank, pressure psia	350
C _f efficiency Percent	102		
C _f	1.817		
Contraction ratio A _c /A _t	2		
Expansion ratio A _e /A _t	35		
Throat area A _t in ²	88		
L* in	28		
Nozzle contour	70 percent bell		
Thrust vector control:			
Minimum acceleration rad/sec ²	2		
Maximum velocity deg/sec	15		
Displacement deg	±7		
Oxidizer side (pressurized by heated helium):			
Injector pressure drop psi	25		
Oxidizer dome pressure drop psi	5		
Main valve pressure drop psi	8		
Line pressure drop psi	5		

approximately 5130 pounds dry, 37 900 pounds wet, and 5530 pounds at burnout.

System Operation

The A-3 propulsion system is designed for automatic start, on receipt of a signal from the guidance system. A similar signal effects automatic engine shutdown. One or more restarts can be made by merely sending additional start and shutdown signals to the propulsion system.

Figure 3-8 shows the operational sequence of the A-3 stage engine. In conjunction with figure 3-6, this illustrates the system starting and shutdown operations.

3.5 A-4 STAGE ENGINE

For the A-4 stage, two engines of 7500-pound thrust each were selected, for a combined thrust of 15 000 pounds. It is assumed that the mission assigned to this fourth and last stage of

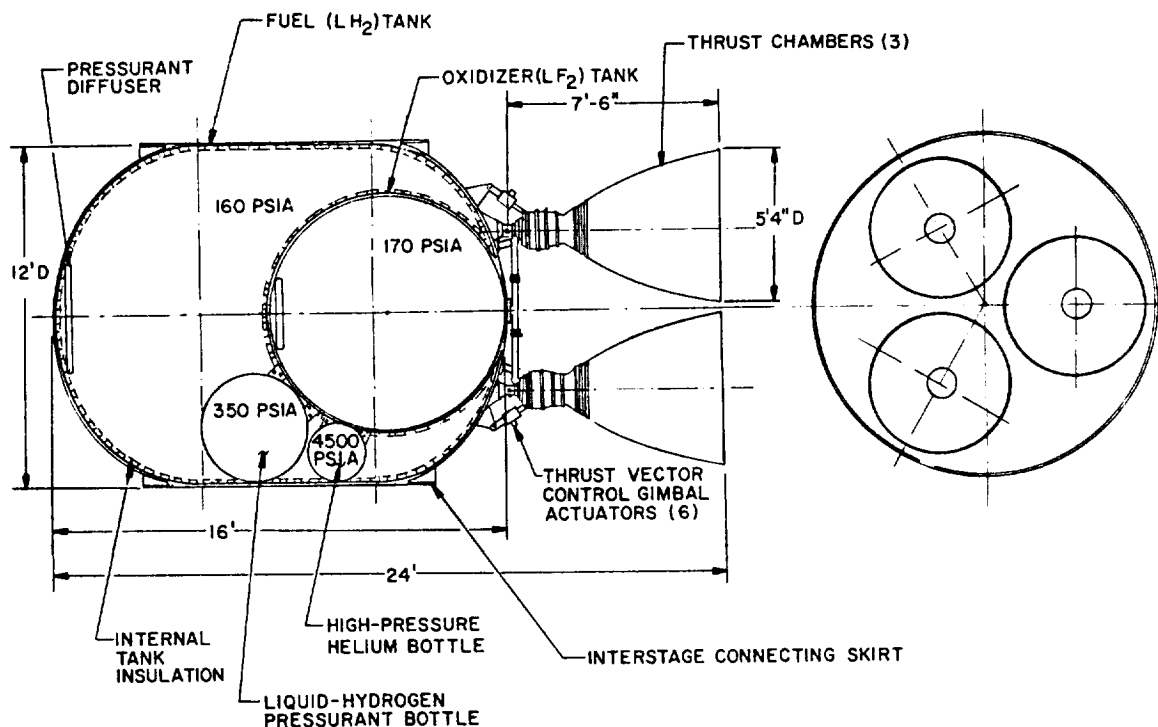


Figure 3-7.—48K A-3 stage propulsion system preliminary design layout.

our space vehicle may require prolonged cruising periods prior to ignition and possibly even longer waiting periods prior to reignition. While it would be desirable to utilize the high-energy propellants of the second and third stages, the fact that they are cryogenics poses some prob-

lems. Although cryogenic propellants could probably be used with refined insulation techniques, they were not selected because of the systems complication for a vehicle of this size. Solid propellants were also ruled out because of the need for repeated starts and throttling.

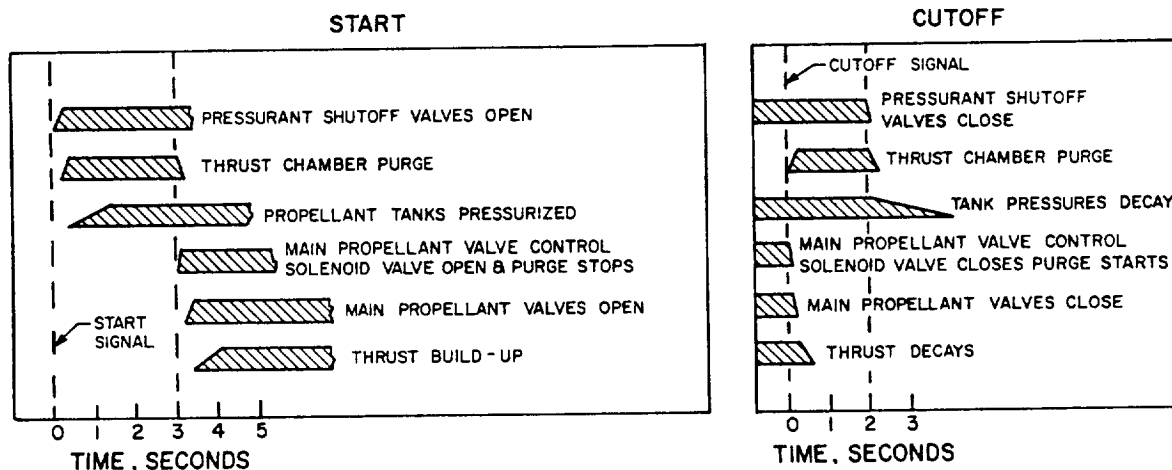


Figure 3-8.—A-3 stage engine and propulsion system operational sequence.

A hypergolic, storable propellant combination possesses certain characteristics which contribute to high reliability. Among these are simplicity of ignition and ease of propellant maintenance, since the propellants can be contained in closed vessels over reasonable temperature ranges for considerable periods of time without developing excessively high pressures, or undergoing unacceptable changes in composition.

Among the applicable storable propellant combinations with high performance are chlorine trifluoride (ClF_3)/hydrazine (N_2H_4) and nitrogen tetroxide (N_2O_4)/hydrazine. Hydrazine, as a monopropellant, is prone to explosive thermal decomposition. However, the condition can be remedied by certain additives. The $\text{ClF}_3/\text{N}_2\text{H}_4$ combination has slightly higher performance than the $\text{N}_2\text{O}_4/\text{N}_2\text{H}_4$ combination. Handling of ClF_3 , however, requires special design provisions because of its thermal characteristics. For this reason, the $\text{N}_2\text{O}_4/\text{N}_2\text{H}_4$ propellant combination was chosen for the A-4 engine. It is worthy of note that the performance of $\text{N}_2\text{O}_4/\text{N}_2\text{H}_4$ is comparable to that of $\text{LO}_2/\text{RP-1}$.

Teflon and Teflon 100X can be used as seal material in the A-4 engine system. Kel-F, while a satisfactory material for use with N_2H_4 , degrades after short-term service in N_2O_4 . Most series 300 stainless steels, aluminum alloys, nickel, and nickel-base brazing alloys can be used as construction materials.

General Engine System Description

The A-4 engine is a multiple-start, variable-thrust, gimballed, bipropellant system. The basic system includes a thrust chamber assembly utilizing combined ablative and radiation cooling, propellant ducts, valves, and control subsystems. Thrust chamber ignition is achieved by the hypergolicity of the propellants. One significant feature of this engine system is the clustering of two thrust chambers to one propellant feed system and one set of propellant controls. The propellants are fed by pressurants directly from the propellant tanks through the main propellant valves to the thrust chamber inlets. Gaseous helium supplied from high-pressure bottles is used for pressurization of both tanks. The pressurant is heated in heat exchangers located at the thrust chamber nozzle extensions

before expansion through a pressure regulator and transfer to the propellant tanks. Helium gas is also used to operate the main valves and the gimbal actuators.

A-4 engine operating parameters at vacuum condition are presented in table 3-5. The engine and propulsion system schematic diagram is shown in figure 3-9.

The engine gimbal blocks are fastened to thrust mounts which are attached to the aft end of the oxidizer tank. The fuel tank is attached forward of the oxidizer tank to form an integral vehicle structure. As in the A-3 system, the thrust loads are transmitted to the payload through the pressure-stabilized tank assembly. The propellant ducts between fuel tank and engine systems are routed outboard and covered by fairings for protection against aerodynamic heating and for lower air resistance during first-stage boost.

Both throttling and propellant-utilization control are achieved by varying the degree of opening of both propellant valves. The positions of the valves are controlled by the vehicle guidance system in conjunction with a vehicle propellant quantity measuring system. Thrust vector control is accomplished by gimbaling the thrust chambers. The basic single engine weighs approximately 150 pounds dry and 170 pounds at burnout. It has a cylindrical space envelope of 3 feet 6 inches diameter by 5 feet 9 inches length. The complete propulsion system (including the two engines and the tanks) weighs approximately 725 pounds dry, 19 649 pounds wet, and 795 pounds at burnout. The preliminary design layout of the A-4 propulsion system is shown in figure 3-10.

Note that for the A-3 and A-4 engines a slightly smaller nozzle expansion area ratio has been specified than for the A-2. While all three upper stages operate in the vacuum and can use the largest practical expansion area ratio for best performance, other considerations will influence the ratio actually chosen.

System Operation

The propulsion system is designed to start automatically upon a signal from the guidance system. During main-stage operation, engine

TABLE 3-5.—7.5K A-4 Stage Engine Operating Parameters
[Vacuum conditions]

Engine (pressurized gas-feed and throttlable):		Main valve pressure drop psi 4
Thrust lb 7500		Calibration orifice pressure drop psi 8
Nominal total multiple-firing duration at full thrust sec 410		Mixture ratio control reserve psi 10
Specific impulse sec 320		Oxidizer tank pressure psia 165
Oxidizer N ₂ O ₄ :		Total oxidizer weight (410 sec full thrust duration for 2 engines, plus 0.8 percent residual) lb 10 560
Density lb/ft ³ 90.88		Oxidizer tank volume (including 2.5 percent ullage volume) ft ³ 120
Flow rate lb/sec 12.78		Nominal pressurant (helium) flow rate (assuming tank ullage temperature 700° R) lb/sec 0.0225
Fuel N ₂ H ₄ :		Total pressurant weight (assuming storage bottle final temperature 191° R, pressure 400 psia, plus 2 percent reserve) lb 12.95
Density lb/ft ³ 63.25		Pressurant storage tank:
Flow rate lb/sec 10.65		Volume ft ³ 4.3
Mixture ratio O/F 1.2		Pressure psia 4500
Thrust chamber (ablatively cooled and radiation cooled on nozzle extension):		Temperature °R 560 max.
Thrust lb 7500		Fuel side (pressurized by heated helium):
Specific impulse sec 320		Injector pressure drop psi 25
Injector end pressure psia 110		Inlet manifold pressure drop psi 4
Nozzle stagnation pressure psia 100		Line pressure drop psi 4
Oxidizer flow lb/sec 12.78		Main valve pressure drop psi 4
Fuel flow lb/sec 10.65		Calibration orifice pressure drop psi 8
Mixture ratio O/F 1.2		Fuel tank pressure psi 155
c* efficiency Percent 98		Total fuel weight (410 sec full thrust duration for 2 engines, plus 1.2 percent residual) lb 8840
c* ft/sec 5540		Fuel tank volume (including 2.5 ullage volume) ft ³ 143.5
C _f efficiency Percent 101		Nominal pressurant (helium) flow rate (assuming tank ullage temperature 700° R) lb/sec 0.025
C _f 1.858		Total pressurant weight (assuming storage bottle final temperature 191° R, pressure 400 psia, plus 2 percent reserve) lb 14.4
Contraction ratio A _c /A _t 2		Pressurant storage tank:
Expansion ratio A _e /A _t 35		Volume ft ³ 4.77
Throat area, A _t in ² 40.4		Pressure psia 4500
L* in 32		Temperature °R 560 max.
Nozzle contour 70 percent bell		
Thrust vector control:		
Minimum acceleration rad/sec ² 2		
Maximum velocity deg/sec 15		
Displacement deg ±7		
Oxidizer side (pressurized by heated helium):		
Injector pressure drop psi 25		
Oxidizer dome pressure drop psi 3		
Line pressure drop psi 5		

thrust level and mixture ratio are controlled continuously through the engine control package by the guidance and propellant utilization systems. Upon a shutdown signal, engine shutdown is effected. The propulsion system is capable of

restart an indefinite number of times. It can be operated at any thrust level between 10 percent and full thrust. Figure 3-11 shows the operational sequence of the A-4 stage engine.



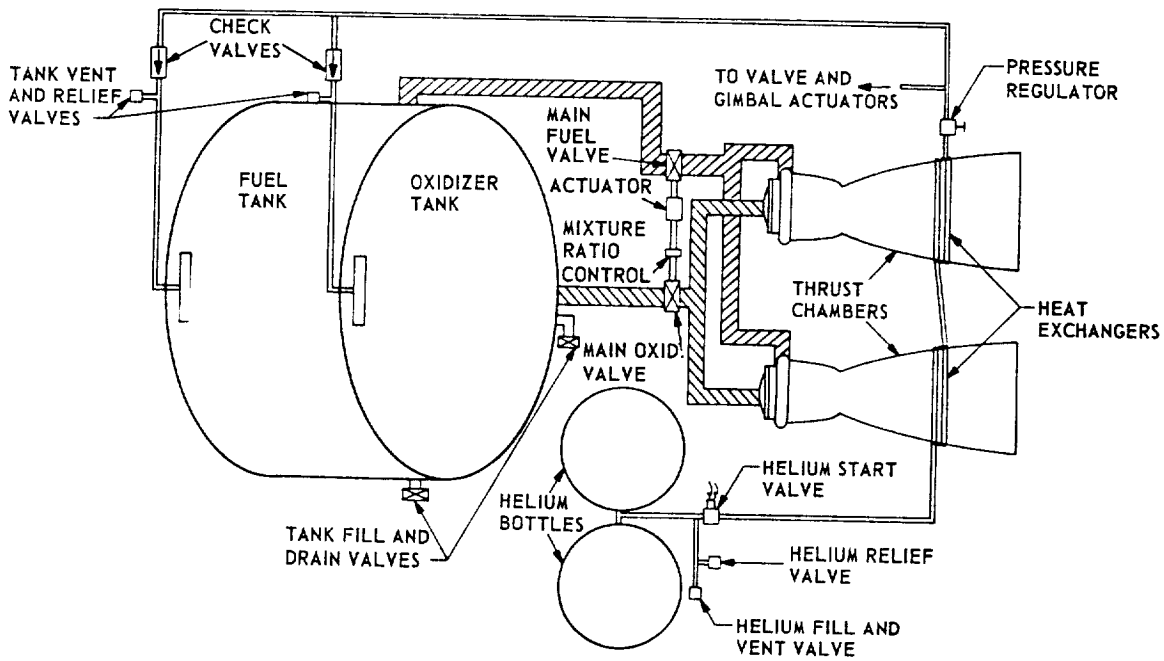


Figure 3-9.—A-4 stage engine and propulsion system schematic diagram.

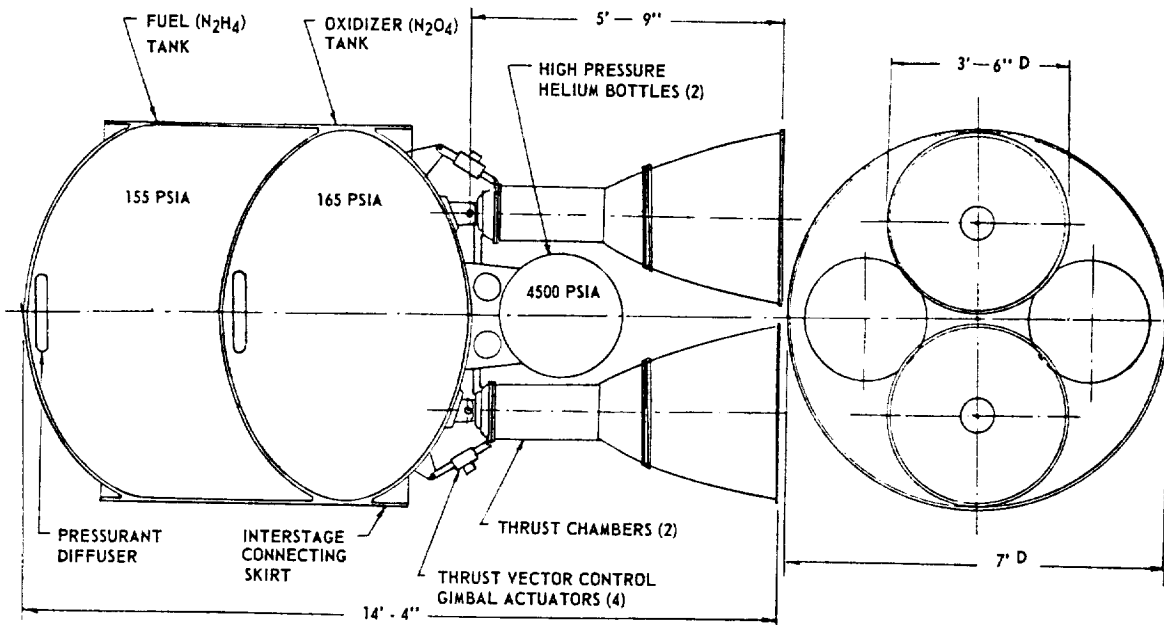


Figure 3-10.—15K A-4 stage propulsion system preliminary design layout.

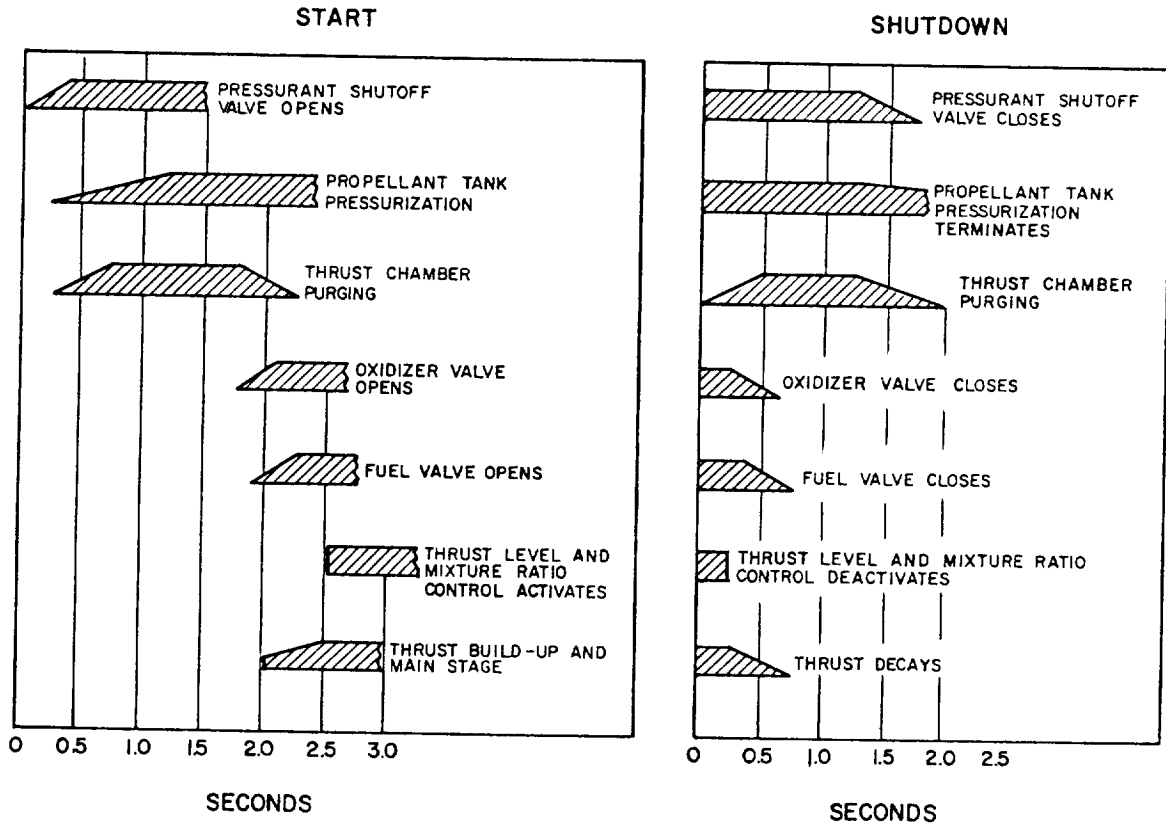
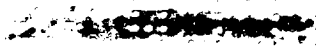


Figure 3-11.—A-4 stage engine operational sequence.



Chapter IV

Design Of Thrust Chambers And Other Combustion Devices

While the proud designers of the various sub-systems of a rocket engine each consider their product as "the heart of the engine," the thrust chamber assembly undeniably embodies the essence of rocket propulsion: the acceleration and ejection of matter, the reaction of which imparts the propulsive force to the vehicle. The designer's goal is essentially to accomplish this with a device of maximum performance, stability and durability, and of minimum size, weight, and cost.

The design of thrust chambers is one of the more complex subjects in the field of liquid propellant rocket engineering. This is primarily due to the fact that the basic processes, especially the combustion within the thrust chamber, are comparatively difficult to define and to study analytically. Thus, during most engine development programs, a major effort must be expended toward the design and development of the thrust chamber. A rational approach to this effort is attempted here.

4.1 THE BASIC THRUST CHAMBER ELEMENTS

The thermodynamic processes governing the generation of thrust within a thrust chamber have been treated in chapter I. The primary function of the thrust chamber is to convert the energy of propellants into thrust. In a liquid bipropellant rocket engine, this process is characterized by the following basic functional steps:

1. The liquid propellants, at their proper mixture ratio, are injected into the combustion chamber through orifices in an injector, as jets at velocities ranging from 20 to 150 feet per second. These jets either impinge to form a mixed droplet spray, or run straight into the chamber hot gas as a series of droplets. Part of the combustion reaction may already take place in the liquid state.

2. The droplets are subsequently vaporized by heat transfer from the surrounding gas. The size and velocity of the droplets change continuously during their entrainment in the combustion gas flow.

3. The vaporized propellants are mixed rapidly, further heated and promptly reacted at their stoichiometric mixture ratio where ever they are formed, thus effecting a continuous increase of the gaseous mass flow rate within the combustion chamber. This gas reaction is further aided by the high-speed diffusion of active molecules or atoms. The combustion is essentially complete upstream of the chamber throat, when all liquid droplets have been vaporized. Under certain conditions, shock and detonation waves may be generated by local disturbances in the combustion front, possibly caused by instability of mixing process and propellant flow prior to reaction. These effects may trigger sustained pressure oscillations at certain frequencies within the thrust chamber, resulting in destructive combustion instability. A major portion of the design and development effort, therefore, is directed toward achievement of stable combustion.

4. As the gaseous products of the combustion process pass toward and through the throat, they are accelerated to sonic, and then to supersonic, velocities within the diverging nozzle section, and are finally ejected to the rear.

The basic elements of a thrust chamber required for its function, include a combustion chamber section, an expansion nozzle section, an injector, an ignition device (for nonhypergolic propellant combinations), propellant inlets and distributing manifolds, and interconnecting surfaces for component and thrust mounts. The construction of the various thrust chamber elements depends largely on their specific operational function. However, low weight and simplicity, which make manufacturing easier, are two important factors to be considered at all times.

Figures 4-1 and 4-2 illustrate a typical liquid bipropellant rocket engine thrust chamber assembly. The illustrated thrust chamber assembly is composed of four major subassemblies or basic elements; namely, thrust chamber body, injector, liquid oxygen dome, and igniter.

The thrust chamber body subassembly is of a venturi shape, consisting of a cylindrical section in which the combustion occurs; a section narrowing toward a throat; and a bell-shaped, expanding nozzle section through which the combustion gases are expelled (fig. 4-1). The body wall of this chamber is constructed of nickel tubes running longitudinally, joined by silver brazing, and retained by external tension bands. The tubes, of 0.012-inch wall thickness, are of rectangular cross section of varying area, to conform to the thrust chamber shape. This construction permits simple thrust chamber cooling during operation, by flowing fuel through the tubes which form the chamber wall. The fuel, under pressure, enters the thrust chamber body at the fuel manifold inlet and is distributed to alternate thrust-chamber tubes. It then flows down toward the thrust chamber nozzle exit where the fuel return manifold reverses the flow

into the return tubes. The fuel then flows through an injector fuel screen into the radial injector passages, and finally through the fuel injector orifices into the thrust chamber combustion zone. The fuel manifolds of this chamber are made of 4130 steel or 347 stainless steel. Other structural members, such as tension bands, stiffening rings, and outriggers were all made of 4130 steel. The oxidizer (liquid oxygen) enters the LOX dome under pressure through a screened central port and is distributed within the dome directly to the liquid oxygen passages and orifices (fig. 4-2).

The following are the operating characteristics and principal dimensions of a hypothetical thrust chamber similar to the one shown in figure 4-1:

1. Propellants LOX/RP-1
2. O/F mixture ratio 2.30
3. Characteristic velocity, c^* , ft/sec 5400
4. Thrust coefficient, C_f (sea level) 1.489
5. Specific impulse (I_{sp})_{tc} (sea level),
sec. 249
6. Total propellant flow rate, lb/sec 402
7. Thrust (sea level), lb 100 000
8. Chamber pressure (injector end), psia .520
9. Chamber pressure (nozzle stagnation),
psia 480

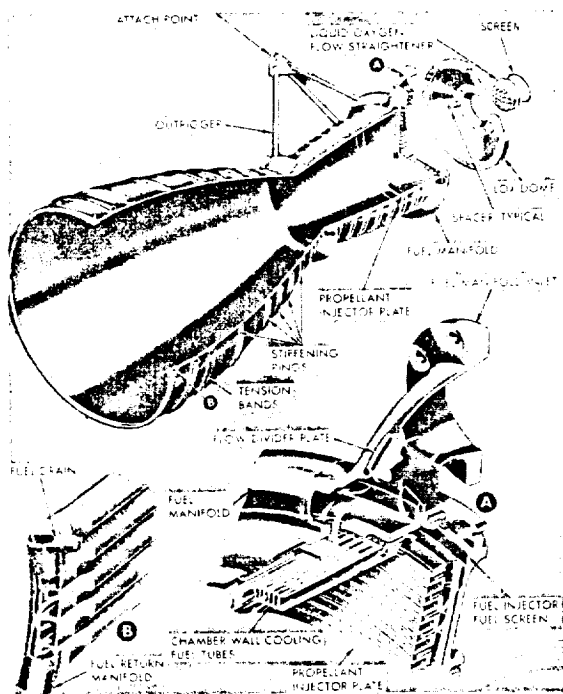


Figure 4-1.—Thrust chamber assembly.

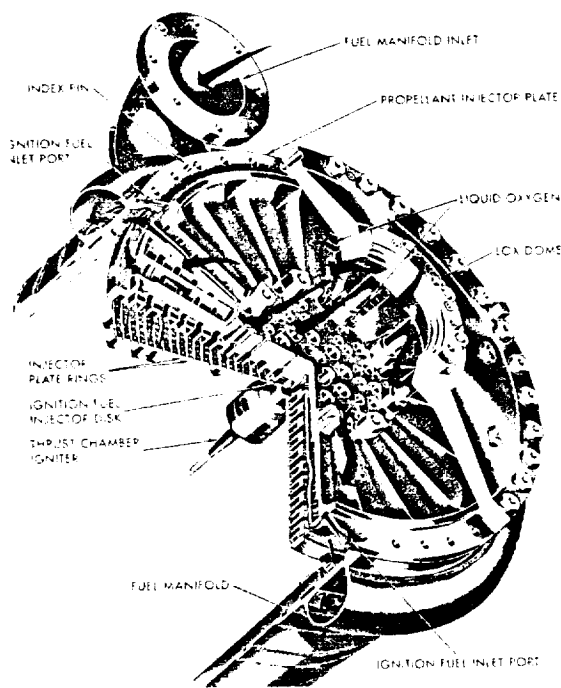


Figure 4-2.—Thrust chamber injector.

- 10. Average gas specific heat ratio (γ) 1.233
- 11. Combustion chamber cross-section area, in² 244
(at injector)
- 12. Throat area, in² 140
- 13. Nozzle exit area, in² 1120
- 14. Combustion chamber volume, in³ 5320
(above the throat)
- 15. Combustion chamber length, in 28.5
(injector to throat)
- 16. Characteristic chamber length, L^* , in 38
- 17. Overall thrust chamber length, in 73
- 18. Design contraction area ratio, ϵ_c 1.60:1
- 19. Design expansion area ratio, ϵ_e 8:1

The thrust chamber injector (fig. 4-2) is a round plate, honeycombed with circular and radial inner passages, leading to drilled orifices. It is constructed of 4130 steel with nickel-plated surfaces, and held in position at the fuel manifold below the liquid oxygen dome with high-strength bolts. The seals between injector and thrust chamber body are of the O-ring type, made of rubber selected for compatibility with the fuel (RP-1). A threaded hole is provided in the center of the injector face to permit pyrotechnic thrust chamber igniter installation. The injector has 20 circular concentric copper rings which contain the injection orifices and are fed from the main propellant systems. Fuel and oxidizer are kept separate by an elaborate distribution system, feeding alternate rings. Fuel flows through the outermost ring, through each alternate inner ring, and through a central fuel disk which is separately fed from an igniter fuel valve through an ignition fuel inlet port. Liquid oxygen emerges from the remaining rings. The injection orifices are so angled that the propellants impinge in the thrust-chamber combustion zone in a like-on-like pattern (liquid oxygen on liquid oxygen and fuel on fuel). The primary orifices are arranged in pairs, with a 0.416-inch distance between centerlines and a 40° included impingement angle, for both propellants. In other designs, impingement angles or orifice separations are made different for the two propellants, so as to effect their impingement in different planes (multiplanar impingement as opposed to uniplanar).

The liquid oxygen dome is a single-piece, 2014-T6 aluminum-alloy die forging. It provides the inlet for the liquid oxygen. It also serves as the thrust-chamber-to-vehicle attachment interface. The flanges of the liquid oxygen dome and

the injector are sealed by a spiral-wound gasket made of 304 stainless-steel strips with asbestos fillers. This type of gasket is designed specifically for cryogenic and elevated-temperature applications.

The electrically fired pyrotechnic igniter is secured centrally to the injector surface by means of a threaded joint. It is designed for one start only and must be replaced after each firing. It receives an electrical firing signal from wires connected through the nozzle exit.

4.2 THRUST CHAMBER PERFORMANCE PARAMETERS

The significance of the parameters which express or influence the efficiency of thrust chamber operation has been discussed in section 1.3 of chapter I. Before discussing the details of actual thrust chamber design, the following summarizes these parameters and illustrates their use for design calculations by applying them to the engine systems of the Alpha vehicle which was discussed in chapter III.

Specific Impulse, I_s (sec)

From equations 1-31 and 1-31c:

$$(I_s)_{tc} = \frac{F}{\dot{W}_{tc}} = \frac{c^* C_f}{g}$$

The specific impulse figure indicates the overall quality of the thrust-chamber design. As was learned earlier, it shows how much thrust is generated for what "running propellant expenditures."

Characteristic Velocity, c^* (ft/sec)

From equation 1-32a:

$$c^* = f(\gamma, R, (T_c)_{ns}) \quad (4-1)$$

Assuming that the propellant and mixture ratio selection has been made, it can be expected that the gas properties (γ, R) will fall into a known band. From there on, c^* almost entirely depends on the temperature of the gases. Obviously, this temperature has a theoretical maximum for a selected propellant combination. How close

to this maximum the chamber will operate depends on influences discussed for mixture ratio in chapter II. Figures 4-3, 4-4, 4-5, and 4-6 illustrate this. It is seen that c^* peaks at combustion temperatures somewhat lower than maximum. Other considerations, such as bulk densities, which affect vehicle tank sizes, may cause further adjustments of the mixture ratio for optimum overall vehicle performance. Within these boundaries, the quality of the combustion process greatly depends on the design efficiency of a thrust chamber assembly, in particular the injector.

Thrust Coefficient, C_f (dimensionless)

From equation 1-33a:

$$C_f = f(\gamma, \epsilon, p_a) \quad (4-2)$$

Let us assume that the performance of energy generation through the combustion process, the effects of which were just summarized for c^* , has been determined. Then, with a given gas property (γ), the performance of the remaining thrust generating functions of the thrust chamber, essentially those of the divergent nozzle, will depend on the nozzle geometry (mainly ϵ which determines the pressure ratio $(p_e/(p_c)_{ns})$ and the ambient pressure (p_a).

Performance Calculation

In actual design practice, the calculation of the thrust chamber performance is based on theoretical propellant combustion data and the application of certain correction factors as explained in chapter I. The theoretical propellant combustion data are derived from thermochemical computations which equate the heat of reaction of the propellant combination and the rise in enthalpy of the combustion gases. Typical propellant combustion data at frozen composition are presented in figures 4-3 through 4-6. For given propellant combinations and chamber-nozzle stagnation pressures $(p_c)_{ns}$, the values for the combustion gas temperature $(T_c)_{ns}$, molecular weight M , and specific heat ratio γ are plotted against the O/F mixture ratio r_w . Performance correction factors are determined by the theoretical assumptions and from earlier test data, as

well as from the chosen design configurations. Typical performance calculation methods have

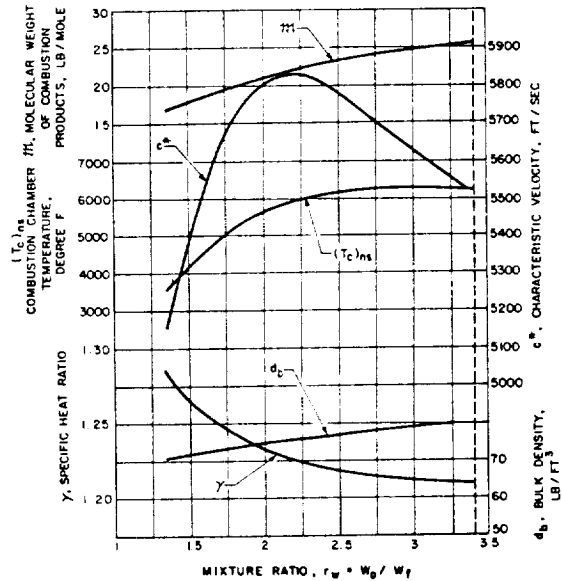


Figure 4-3.—Theoretical $O_2/RP-1$ combustion data (frozen composition), $(p_c)_{ns} = 1000$ psia.

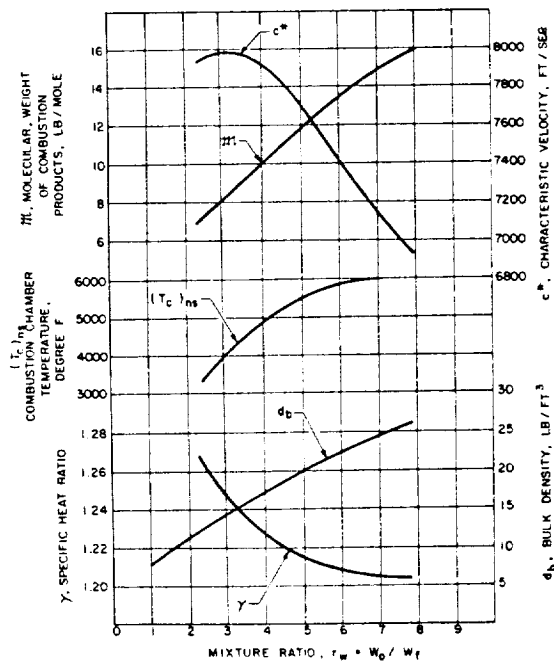


Figure 4-4.—Theoretical O_2/H_2 combustion data (frozen composition), $(p_c)_{ns} = 800$ psia.

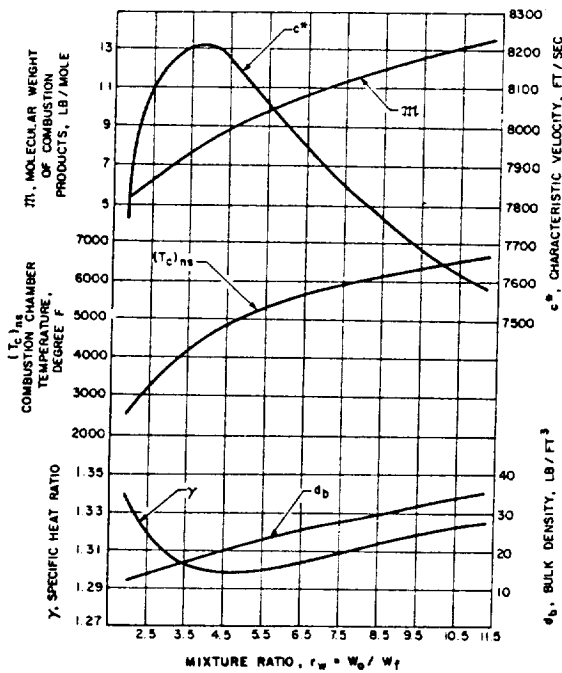


Figure 4-5.—Theoretical F_2/H_2 combustion data (frozen composition), $(p_c)_{ns} = 100$ psia.

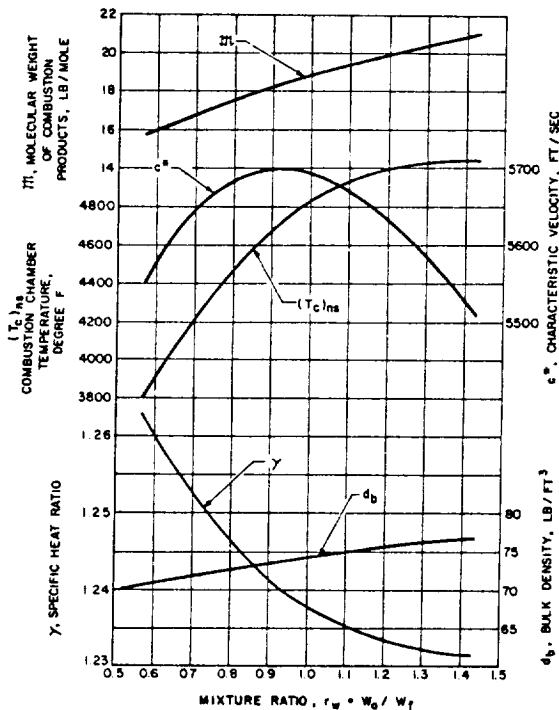


Figure 4-6.—Theoretical N_2O_4/N_2H_4 combustion data (frozen composition), $(p_c)_{ns} = 100$ psia.

been demonstrated earlier by sample calculation (1-3). The following sample calculations illustrate the more specific approaches.

Sample Calculation (4-1)

Determine the design values of c^* , C_f , and $(I_s)_{tc}$ for the engine thrust chambers of the stages of the hypothetical Alpha vehicle, with the following assumed design parameters:

(a) 750K A-1 Stage Engine:

Propellants, $LO_2/RP-1$; thrust chamber O/F mixture ratio, 2.35; $(P_c)_{ns}$, 1000 psia; propellant combustion data, figure 4-3; nozzle expansion area ratio, $\epsilon = 14$.

(b) 150K A-2 Stage Engine:

Propellants, LO_2/LH_2 ; thrust chamber O/F mixture ratio, 5.22; $(p_c)_{ns}$, 800 psia; propellant combustion data, figure 4-4; nozzle expansion area ratio, $\epsilon = 40$.

Solutions

(a) A-1 Stage Engine:

From figure 4-3 for $LO_2/RP-1$ at $(P_c)_{ns} = 1000$ psia and a mixture ratio of 2.35, the following values are derived for the chamber product gases:

$$(T_c)_{ns} = 6000^\circ F \text{ or } 6460^\circ R, \\ M = 22.5 \text{ lb/mol}, \quad \gamma = 1.222$$

Substitute into equation (1-32a):

$$\text{Theoretical } c^* = \frac{\sqrt{32.2 \times 1.222 \times 6460 \times 15.44 / 22.5}}{0.7215} \\ = 5810 \text{ ft/sec}$$

This value for c^* can also be derived from figure 4-3.

For a good combustion chamber and injector design, the c^* correction factor for $LO_2/RP-1$ and frozen composition will be about 0.975.

$$\text{Design } c^* = 5810 \times 0.975 = 5660 \text{ ft/sec}$$

For $\gamma = 1.222$, $\epsilon = 14$, a theoretical vacuum C_f value of 1.768 can be derived from figure 1-11:

$$\text{Theoretical } C_f \text{ at sea level} = (C_f)_{vac} - \frac{\epsilon p_a}{(P_c)_{ns}} \\ = 1.768 - \frac{14 \times 14.7}{1000} = 1.562$$

Sea level C_f can also be calculated using equation (1-33a), with the aid of equation (1-20).

With effective nozzle contour design, an overall C_f correction factor of 0.98 for $\text{LO}_2/\text{RP-1}$ frozen composition can be used.

$$\text{Design sea level } C_f = 1.562 \times 0.98 = 1.531$$

From equation (1-31c):

$$\text{Design sea level } (I_s)_{tc} = \frac{5660 \times 1.531}{32.2} = 270 \text{ sec}$$

(b) *A-2 Stage Engine:*

From figure 4-4 for LO_2/LH_2 at $(P_c)_{ns} = 800$ psia and a O/F mixture ratio of 5.22, the following values are derived for the chamber product gases:

$$(T_c)_{ns} = 5580^\circ \text{ F or } 6040^\circ \text{ R,} \\ \mu = 12 \text{ lb/mole, } \gamma = 1.213$$

Substitute into equation (1-32a):

$$\text{Theoretical } c^* = \frac{\sqrt{32.2 \times 1.213 \times 6040 \times 1544/12}}{0.717} \\ = 7670 \text{ ft/sec}$$

Based on experimental data, a c^* correction factor can be assumed for the LO_2/LH_2 frozen-composition data of about 0.975.

$$\text{Design } c^* = 7670 \times 0.975 = 7480 \text{ ft/sec}$$

For $\gamma = 1.213$, $\epsilon = 40$, a theoretical vacuum C_f value of 1.876 can be derived from figure 1-11. C_f can also be calculated using equations (1-33a) and (1-20). With effective nozzle contour design, an overall C_f correction factor value of 1.01 can be used for LO_2/LH_2 frozen-composition data:

$$\text{Design vacuum } C_f = 1.876 \times 1.01 = 1.895$$

From equation (1-31c):

$$\text{Design vacuum } (I_s)_{tc} = \frac{7480 \times 1.895}{32.2} = 440 \text{ sec}$$

The reader should perform his own calculations for the A-3 and the A-4 engines, with the aid of tables 3-4 and 3-5, and figures 4-5 and 4-6.

4.3 THRUST CHAMBER CONFIGURATION LAYOUT

After major thrust chamber operating parameters such as type of propellants, thrust level, chamber pressure, C_f , c^* , and I_s have been established from engine system requirements and performance calculations, one of the fundamental dimensions of the thrust chamber, the throat area A_t , can be readily derived (eq. (1-33)). The throat area A_t or throat diameter D_t usually is the starting point of a thrust chamber configuration layout. The combustion chamber and nozzle section are commonly designed as an integral thrust chamber body. For light weight and ease of manufacture, thrust chambers will have the general shape of a pressure vessel with wall surfaces of rotation and smooth contours.

Combustion Chamber Volume

The combustion chamber serves as an envelope to retain the propellants for a sufficient period (stay time) to assure complete mixing and combustion before entering the nozzle. The volume of the combustion chamber thus has a definite effect on combustion efficiency. The theoretical required chamber volume is a function of the mass flow rate of the propellants and their average density, and of the stay time needed for efficient combustion. The relationship can be expressed by the following equation:

$$V_c = \dot{W}_{tc} V t_s \quad (4-3)$$

where:

$$V_c = \text{chamber volume, ft}^3 \\ \dot{W}_{tc} = \text{propellant mass flow rate, lb/sec} \\ V = \text{average specific volume, ft}^3/\text{lb} \\ t_s = \text{propellant stay time, sec}$$

A useful parameter, the characteristic length L^* (commonly pronounced "L-star"), can be used to specify the propellant stay time in the combustion chamber. L^* is defined as the ratio of chamber volume to nozzle throat area, and can be expressed by the following equation:

$$L^* = \frac{V_c}{A_t} = \frac{\dot{W}_{tc} V t_s}{A_t} \quad (4-4)$$

Since the value of A_t is in nearly direct proportion to the product of \dot{W}_{tc} and V , L^* is essentially a function of t_s . The effect of L^* on c^* in an experimental combustion chamber is shown in figure 4-7. The c^* value increases with L^* to an asymptotic maximum. Increasing L^* beyond a certain point tends to decrease overall engine system performance because of the following:

- (1) Larger L^* results in higher thrust chamber volume and weight.
- (2) Larger L^* creates more surface area in need of cooling.
- (3) Larger L^* increases friction losses at the chamber walls.

In actual design practice, optimization analyses will determine the minimum possible combustion chamber L^* consistent with efficient combustion.

Under a given set of operating conditions, such as type of propellants, mixture ratio, chamber pressure, injector design, and chamber geometry, the value of the minimum required L^* can only be evaluated by actual firings of experimental thrust chambers. L^* values of 15 to 120 inches for corresponding propellant stay-time values of 0.002-0.040 second have been used in various thrust chamber designs. Typical L^* values for different propellants are given in table 4-1. With A_t and minimum required L^* established, the required combustion chamber volume V_c can be calculated by equation (4-4).

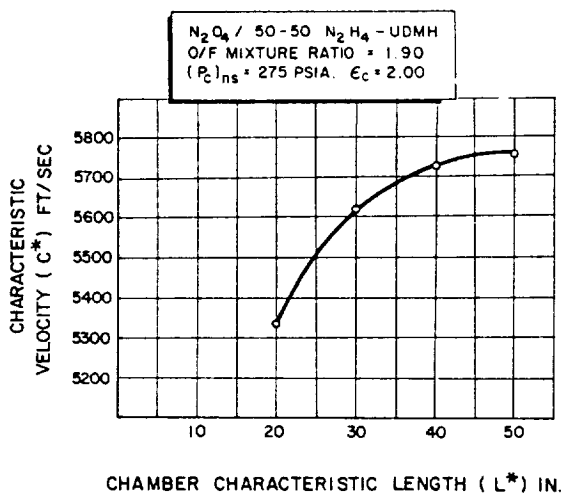


Figure 4-7.—Effect of L^* on c^* value of experimental thrust chamber.

TABLE 4-1.—Recommended Combustion Chamber Characteristic Length (L^*) for Various Propellant Combinations

Propellant combination	Combustion chamber characteristic length (L^*), in.
Chlorine trifluoride/hydrazine-base fuel	30-35
Liquid fluorine/hydrazine	24-28
Liquid fluorine/liquid hydrogen (GH_2 injection)	22-26
Liquid fluorine/liquid hydrogen (LH_2 injection)	25-30
Hydrogen peroxide/RP-1 (including catalyst bed)	60-70
Nitric acid/hydrazine-base fuel	30-35
Nitrogen tetroxide/hydrazine-base fuel	30-35
Liquid oxygen/ammonia	30-40
Liquid oxygen/liquid hydrogen (GH_2 injection)	22-28
Liquid oxygen/liquid hydrogen (LH_2 injection)	30-40
Liquid oxygen/RP-1	40-50

Combustion Chamber Shape

As can be seen from equation (4-3), the stay time t_s is independent of the combustion chamber geometry. Theoretically, for a given required volume, the chamber can be of any shape. In actual design, however, the choice of the combustion chamber configuration is limited. In a long chamber with a small cross section, higher nonisentropic gas flow pressure losses will result as explained in chapter I. This approach also dictates a longer thrust chamber space envelope and imposes certain space limitation on the injector design to accommodate the necessary number of injector holes. With a short chamber of large cross section, the propellant atomization or vaporization zone occupies a relatively large portion of the chamber volume, while the mixing and combustion zone becomes too short for efficient combustion. Other factors, such as heat transfer, combustion stability, weight, and ease of manufacturing, are to be considered in determining the final combustion chamber configuration.

Three geometrical shapes which have been used in combustion chamber design are shown in figure 4-8. While the spherical and the near-spherical chambers were used in earlier European

designs, the cylindrical chamber has been used most frequently in the United States.

The spherical or nearly-spherical chamber, as compared to the cylindrical one of the same volume, offers the advantage of less cooling surface and weight. A sphere has the smallest surface-to-volume ratio. For equal strength of material and chamber pressure, the structural walls of the spherical chamber are about half the thickness of the walls of a cylindrical chamber. However, the spherical chamber is more difficult to manufacture and has poorer performance under most circumstances. For these practical reasons, the design details of the cylindrical combustion chamber will be treated in this book. Several

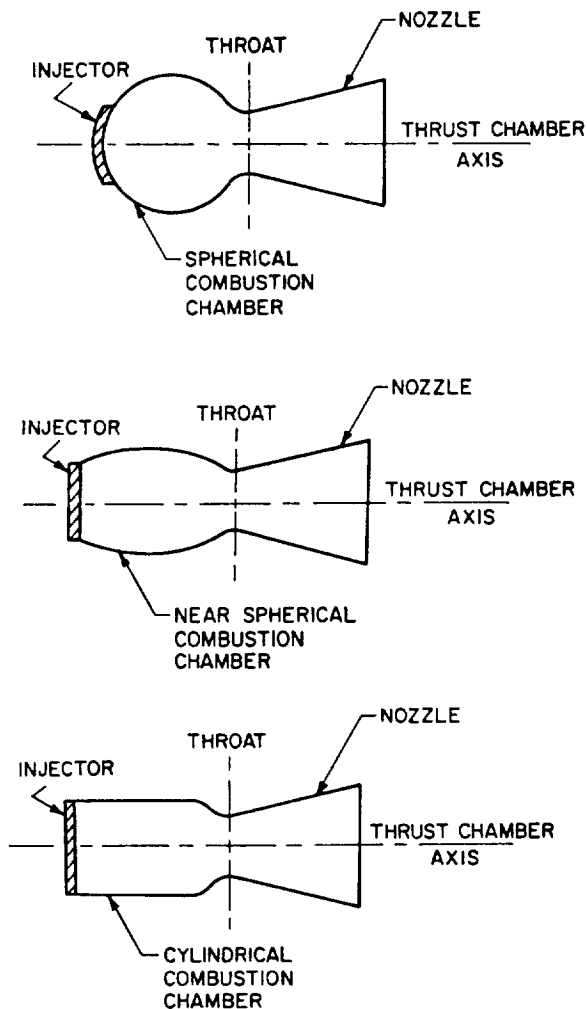


Figure 4-8.—Frequently used geometrical shapes for combustion chambers.

novel thrust chamber designs will also be discussed.

In the design layout of the cylindrical combustion chamber of a given A_t and L^* , the value of the contraction area ratio, ($\epsilon_c = (A_c/A_t)$) can be optimized through careful studies of the following factors:

- (1) Combustion performance in conjunction with the injector design
- (2) Chamber gas flow pressure drop
- (3) Chamber wall cooling requirements
- (4) Combustion stability
- (5) Weight
- (6) Space envelope
- (7) Ease of manufacturing

For pressurized-gas propellant feed, low-thrust engine systems contraction area ratio values of 2 to 5 have been used. For most turbo-pump propellant feed, high thrust and high chamber pressure engine systems lower ratio values of 1.3 to 2.5 are employed. The reader is also referred to section 1.2 chapter I, "The Gas-flow Processes in the Combustion Chamber and the Nozzle."

The basic elements of a cylindrical combustion chamber are identified in figure 4-9. In design practice, it has been arbitrarily defined that the combustion chamber volume includes the space between injector face I-I and the nozzle throat plane II-II. The approximate value of the combustion chamber volume can be expressed by the following equation

$$V_c = A_t \left[L_c \epsilon_c + \frac{1}{3} \sqrt{\frac{A_t}{\pi}} \cot \theta (\epsilon_c^{1/3} - 1) \right] \quad (4-5)$$

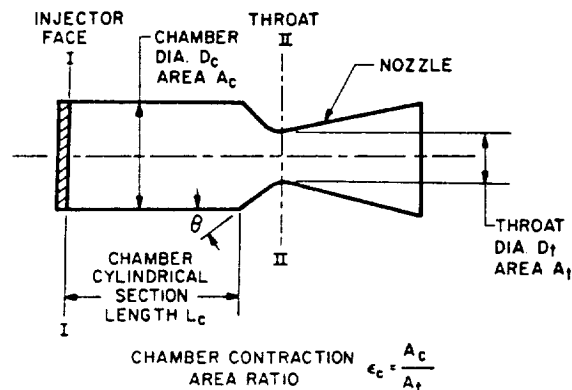


Figure 4-9.—Elements of basic cylindrical combustion chamber.

The total surface area of the combustion chamber walls excluding injector face can be approximated by the following expression:

$$\text{Total area} = 2L_c \sqrt{\pi \epsilon_c A_t} + \csc \theta (\epsilon_c - 1) A_t \quad (4-6)$$

Nozzle Expansion Area Ratio

It was learned earlier that with all other parameters fixed, in particular chamber pressure, there is only one optimum nozzle expansion area ratio for a given altitude or, more specifically, ambient pressure. Except for those systems which start in vacuum, ambient pressure will have to be considered. This is especially true for boosters which start at or near sea-level conditions.

It is the ultimate purpose of a rocket engine to lift vehicles to altitudes. Inherently, then, ambient pressure will not be a constant (except for high-altitude starts, as mentioned). It is, therefore, extremely important for the designer to know the trajectory of the vehicle to be propelled or, more specifically, its altitude-versus-time characteristics. With this information, the designer is in a position to make a first, optimizing selection of a nozzle expansion area ratio, for best results throughout the entire trajectory. As shown earlier, area ratio will be truly optimum for only one specific altitude. The optimization for ambient pressure then is essentially an averaging process.

Other considerations usually cause the designer to deviate from the "paper optimum" for the nozzle expansion area ratio. Some of the most common are: weight, size, ease of manufacturing, handling, and cooling (heat transfer) considerations.

Nozzle Shape

Most rocket nozzles are of the converging-diverging De Laval type. Since the flow velocity of the gases in the converging section of rocket nozzle is relatively low, any smooth and well-rounded convergent nozzle section will have very low energy losses. By contrast, the contour of the diverging nozzle section is very important to performance, because of the very high flow velocities involved.

The selection of an optimum nozzle shape for a given expansion area ratio is generally influenced by the following design considerations and goals:

- (1) Uniform parallel axial gas flow at the nozzle exit for maximum momentum vector
- (2) Minimum separation and turbulence losses within the nozzle
- (3) Shortest possible nozzle length for minimum space envelope, weight, wall friction losses, and cooling requirements
- (4) Ease of manufacturing

In actual design practice, any abrupt change or discontinuity in the nozzle wall contour should be avoided to eliminate the possibility of shock waves or turbulence losses. Theoretically, the nozzle throat is simply the unique plane of minimum cross-section area. In practice, a well-rounded throat section is employed. Only at the nozzle exit plane is a sharp edge used because a rounded one would permit overexpansion and flow separation.

1. Conical Nozzle

In early rocket engine applications, the conical nozzle, which had proved satisfactory in most respects, was used almost exclusively. The advantages of a conical nozzle are ease of manufacturing and flexibility of converting an existing design to higher or lower expansion area ratios without major redesign of the nozzle contour.

The configuration of a typical conical nozzle is shown in figure 4-10. The nozzle throat section has the contour of a circular arc with a radius R ranging from 0.5 to 1.5 times the throat radius R_t . The half angle of the nozzle convergent cone section can range from 20° to 45° . The

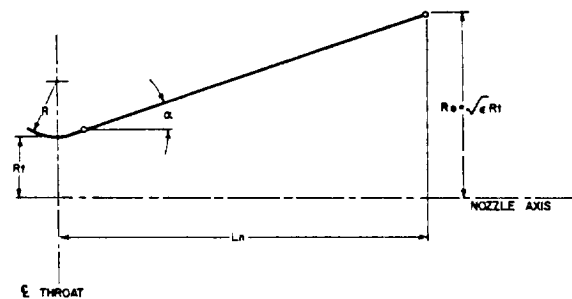


Figure 4-10.—Conical nozzle contour.

divergent cone half angle α varies from approximately 12° to 18° . The length of the conical nozzle section can be expressed by the equation

$$L_n = \frac{R_t(\sqrt{\epsilon} - 1) + R(\sec \alpha - 1)}{\tan \alpha} \quad (4-7)$$

The conical nozzle with a 15° divergent half angle has become almost a standard, as it is a good compromise on the basis of weight, length, and performance.

Since in a conical nozzle certain performance losses occur as a result of the nonaxial component of the exhaust gas velocity, a correction factor λ is applied for the calculation of the exit gas momentum. This factor or thrust efficiency is the ratio between the exit gas momentum of the conical nozzle and that of an ideal nozzle with uniformly parallel axial gas flow. The value of λ can be expressed by the following equation:

$$\lambda = \frac{1}{2}(1 + \cos \alpha) \quad (4-8)$$

where α = half angle of the conical nozzle.

For an ideal nozzle, λ would be unity. For a conical nozzle with $\alpha = 15^\circ$ and $\lambda = 0.983$, the exit gas momentum or the exit velocity will be 98.3 percent of the ideal nozzle exit velocity calculated by equation (1-18). The value of the vacuum thrust coefficient of a nozzle is in direct proportion to the thrust generated by the nozzle, or to the nozzle exit gas velocity. Therefore, the theoretical vacuum thrust coefficient (neglecting friction and other flow losses) of a conical nozzle with 15° half angle will be 98.3 percent of the ideal nozzle thrust coefficient calculated by equation (1-33a).

2. Bell Nozzle

For increased performance and shorter length, bell-shaped nozzles have been developed. This nozzle design employs a fast expansion or radial flow section in the initial divergent region, which then leads over to a uniform, axially directed flow at the nozzle exit. The wall contour is changed gradually enough so that oblique shocks will not form.

Figure 4-11 shows the contour of a bell nozzle. A circular arc of selected radius R_1 is

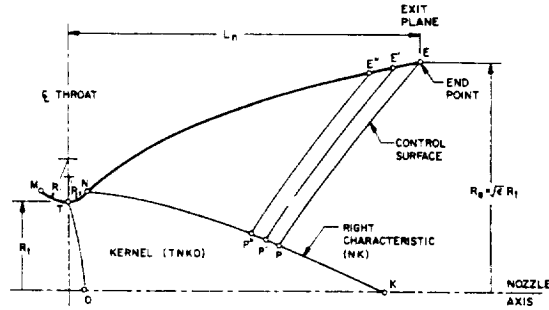


Figure 4-11.—Bell nozzle contour.

chosen for the nozzle contour MT upstream of the throat. Contour TNE is the diverging portion of the nozzle. The initial expansion occurs along contour TN; contour NE turns the flow over to a direction nearer to axial. For design convenience, the contour TN is also a circular arc, with a smaller radius R_2 .

For those familiar with compressible flow theories, it is noted that, using transonic flow analyses, a constant-Mach-number line TO can be defined at the throat. Given the flow condition along TO and the solid boundary TN, a kernel flow field TNKO can be generated by the method of characteristics developed in gas dynamics. The kernel of the rocket nozzle contour is defined as that portion of the supersonic flow field determined entirely by throat conditions. The last right characteristic line NK of kernel TNKO, and thus the location of the point N along contour TN, is to be determined by specific design criteria.

The location of the end point E along contour NE is defined by the given nozzle expansion area ratio and nozzle length (distance between throat and exit plane). Then the right characteristic line NK can be determined by satisfying the following conditions concurrently:

- (1) A control surface PE can be generated between the point E and a selected point P along the line NK
- (2) Mass flow across PE equals the mass flow across NP
- (3) Maximum thrust by the nozzle is attained.

By selecting points P' , P'' , etc., along line NK, a series of control surfaces $P'E'$, $P''E''$, etc., can be generated to define points E' , E'' , etc., along the contour NE. Calculations for the nozzle contour can be effectively performed by a computer.

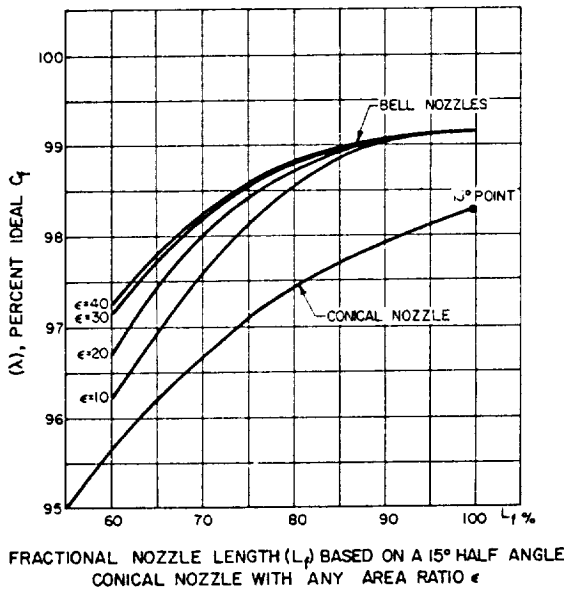


Figure 4-12.—Thrust efficiency versus bell nozzle length. (Shown for comparison: effect of shortening conical nozzle, increasing half angle.)

Commonly, an equivalent 15° half-angle conical nozzle is used as a standard to specify bell nozzles. For instance, the length of an 80-percent bell nozzle (distance between throat and exit plane) is 80 percent, or 0.8 of that of a 15° half-angle conical nozzle having the same throat area, radius below the throat, and area expansion ratio.

Figure 4-12 shows the thrust efficiency λ versus fractional nozzle length L_f for conical and bell nozzles.

As may be seen, bell nozzle lengths beyond approximately 80 percent do not significantly contribute to performance, especially when considering weight penalties.

3. Parabolic Approximation of Bell Nozzles

One convenient way to design a near-optimum-thrust bell nozzle contour is through the use of the parabolic approximation procedures as suggested by G.V.R. Rao. The design configuration of a parabolic approximation bell nozzle is shown in figure 4-13. The nozzle contour immediately upstream of the throat T is a circular arc with a radius of $1.5 R_t$. The divergent section nozzle contour is made up of a circular entrance

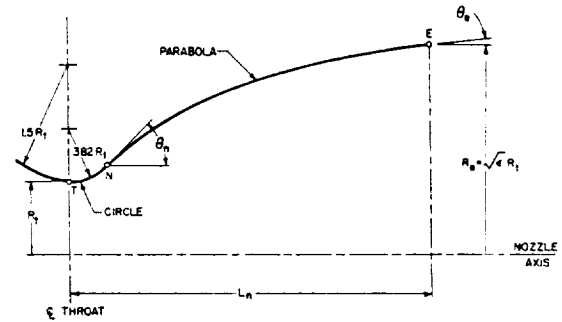


Figure 4-13.—Parabolic approximation of bell nozzle contour.

section with a radius of $0.382 R_t$ from the throat T to the point N and a parabola from there to the exit E .

For the design of a specific nozzle, the following data are required:

- (1) Throat diameter, D_t , inches
- (2) Axial length of the nozzle from throat to exit plane, L_n , inches (or the desired fractional length L_f based on a 15° conical nozzle)
- (3) Expansion area ratio ϵ
- (4) Initial wall angle of the parabola, θ_n , degrees
- (5) Nozzle exit wall angle, θ_e , degrees

The wall angles, θ_n and θ_e are shown in figure 4-14 as a function of the expansion area ratio ϵ .

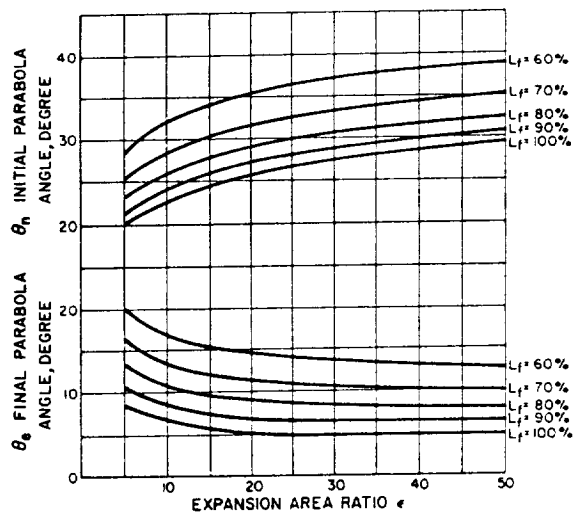


Figure 4-14.— θ_n and θ_e as function of expansion area ratio ϵ .

Optimum nozzle contours can be approximated quite accurately by selecting the proper inputs. Although no allowance is made for different propellant combinations, experience has shown that the effect of specific heat ratio γ upon the contour is small. A computer program can be readily set up to perform the calculation.

4. Annular Nozzles

Based on the momentum theorem, for ideal expansion the thrust generated by a thrust chamber depends only upon the mass flow conditions (velocity and direction) at the nozzle exit. In some nozzle designs, such as annular nozzles, the gas flow at the throat is not necessarily parallel to the axis, but the exit flow is similar to that of a conical or bell nozzle and thus produces the same thrust results.

There are two basic types of annular nozzles: the radial in-flow type (spike nozzle) and the radial out-flow type (expansion-deflection or E-D; reverse-flow or R-F; and horizontal-flow or H-F nozzles). They are shown in figure 4-15, together with conventional conical and bell noz-

zles. For comparison of the effect of nozzle type on size, all nozzles shown are scaled to the same thrust level, nozzle expansion area ratio, and theoretical nozzle efficiency. These nozzles show potential of adapting their geometry to space vehicle application, because shortened nozzles reduce interstage structure weight and will permit an increase in payload through increased performance for a given length.

The nozzle expansion area ratio ϵ for an annular nozzle is defined by equation (4-9):

$$\epsilon = \frac{\text{Projected area of the contoured nozzle wall}}{\text{Throat area}} = \frac{A_e - A_p}{A_t} \quad (4-9)$$

where the projected area of the contoured nozzle wall equals nozzle exit plane area A_e , less the centerbody projected area A_p . Another convenient design parameter for annular nozzles is the annular diameter ratio, D_p/D_t , where D_t is the throat diameter of an equivalent circular throat, and D_p the centerbody diameter. The parameter D_p/D_t is an index of the annular nozzle design

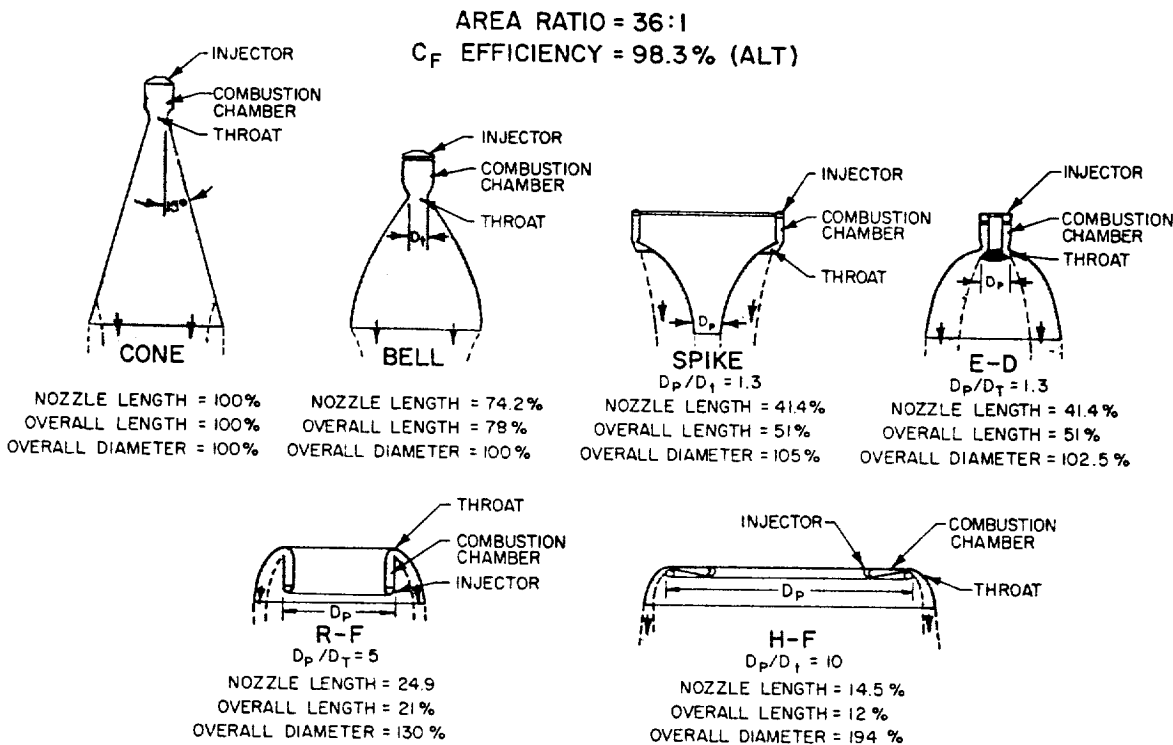


Figure 4-15.—Comparison of nozzle shapes.

geometry as compared to a conventional nozzle. The contour-calculating methods for annular nozzles are similar to those for bell nozzles.

In a conical or bell nozzle, the gases may expand to pressures well below the ambient (sea-level or low-altitude operation) before flow separation from the nozzle wall occurs. As explained in chapter I, for nozzles with large area ratios, this overexpansion results in thrust losses at low altitudes. Annular nozzles, because of their special characteristics, are not subject to these losses. As shown in figure 4-16 for an E-D nozzle (and equally applicable to other annular nozzles), the back pressure P_b at the back face of the centerbody plays an important role in regulating the nozzle flow. The value of P_b is a function of the ambient pressure and generally is lower than ambient. Downstream of the throat, the expansion of the gases around the centerbody shoulder C will continue unaffected until this base pressure is reached. After the initial gas expansion through the constant-Mach line CD , the downstream flow of the gases is controlled by the following two boundary conditions:

- (1) The nozzle wall contour DE which turns the gases to near-axial flow.
- (2) The base pressure P_b which influences the free stream surface of the inner jet boundary.

Because of the curved-wall contour, the gases are deflected, which leads to some compression and local increases in wall pressure. A typical nozzle wall pressure distribution for low-altitude operation is shown in figure 4-16. This com-

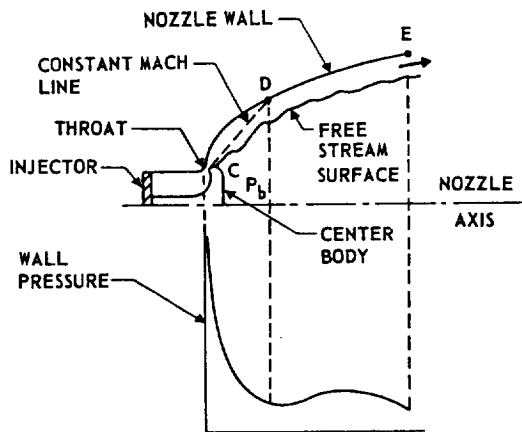


Figure 4-16.—E-D nozzle at low altitude operation.

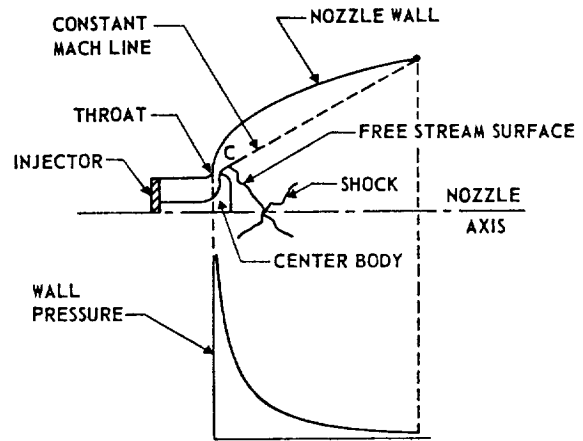


Figure 4-17.—E-D nozzle at high altitude operation.

pressive turning at the nozzle wall, which is also typical for the spike nozzle, is responsible for improved nozzle performance at low altitude. Because of the self-adjusting nature of the inner jet boundary, there is no flow separation from the nozzle wall, as is the case for a conventional nozzle.

At high-altitude operation the base pressure P_b becomes so low that the nozzle flow converges behind the centerbody, as shown in figure 4-17. Since the flow at the closure point must be axial, a shock wave may occur depending on the flow conditions. However, the expansion of the gases may continue unaffected up to the end of the nozzle. The nozzle wall pressure distribution under this condition is also shown in figure 4-17.

An improved spike nozzle concept is the *aerodynamic spike nozzle*.¹ This nozzle concept is a truncated annular spike nozzle (radial inflow type), which utilizes a small amount of secondary flow introduced into the nozzle base region.

Performance of the aerodynamic spike nozzle is a function of various nozzle geometric parameters, the amount of secondary flow, the manner in which this secondary flow is introduced, and the relative energy between the primary and secondary streams. To describe the flow field and interrelated effect of truncating the spike nozzle,

¹Source: AIAA Paper No. 66-828, "Liquid Rocket Engines: Their Status and Their Future" By S. F. Iacobellis.

the base pressure and the base pressure increase achieved through the secondary flow addition requires a lengthy, detailed discussion; only the basic operation can be presented here.

The primary flow (high-pressure gases) which produces the major portion of the engine thrust is exhausted from an annular-type combustion chamber and expands against the metal surface of the center truncated-spike nozzle (fig. 4-18). The characteristics of the primary flow field upstream of the base, shown as region 1 in figure 4-18, are determined by the annular throat geometry, the nozzle wall contour, and the ambient pressure. The annular primary flow continues to expand beyond the nozzle surface and encloses a subsonic, recirculating flow field in the base region (region 2). The pressure acting on the nozzle base contributes additional thrust to the nozzle.

When a small amount of secondary flow is introduced into the base (added to the recirculating flow), the base pressure is increased further. As the secondary flow is increased, the overall nozzle efficiency (considering the additional flow) increases because of this increase in base pressure. There is a limit to this gain in efficiency, and an optimum secondary flow exists for each configuration.

The outer surface of the annular primary flow is a free-jet boundary, which is influenced by ambient pressure. This ambient pressure influence on the primary nozzle flow endows this type of nozzle with altitude compensation. In operation at high-pressure ratios (i.e., altitude conditions), the outer free-jet boundary of the primary flow expands outward, governed by the Prandtl-Meyer turning angle at the throat. At low-pressure ratios (i.e., sea level operation), the relatively higher ambient pressure com-

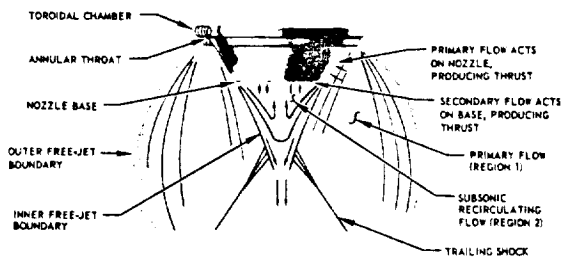


Figure 4-18.—Aerodynamic spike flow field illustrated under altitude conditions.

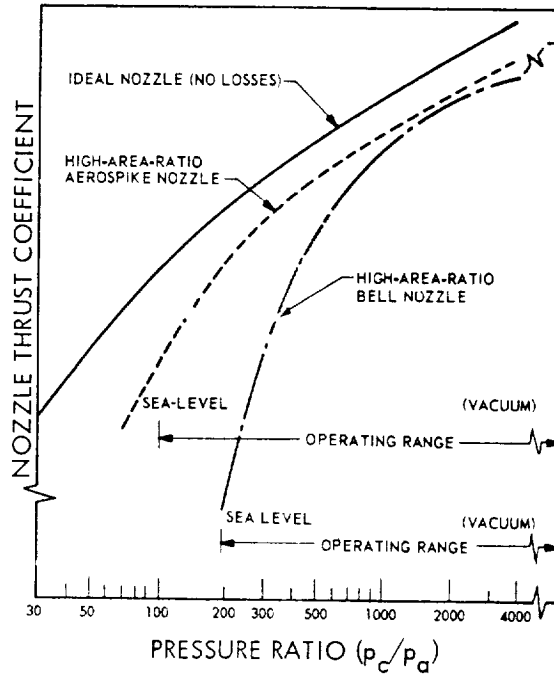


Figure 4-19.—Nozzle performance comparison.

presses the outer free-jet boundary of the primary flow field. This compression increases the static pressure on the nozzle wall and partially offsets the negative effect of the higher ambient pressure on the back side of the nozzle. The base pressure also is increased with the higher ambient, because the compressed primary flow field, which influences the base pressure, has higher static pressures. This combination of flow field effects provides the altitude compensation inherent to the aerodynamic spike nozzle.

Figure 4-19 presents the performance comparison of various nozzle designs. The nozzle thrust coefficient C_f for an ideal nozzle (i.e., a variable-area-ratio nozzle having the optimum expansion for each chamber pressure to ambient pressure ratio, p_c/p_a) is shown together with those of the high-area-ratio aerodynamic spike and bell nozzle. As is evident, the C_f curve of the aerodynamic spike follows the ideal nozzle performance (altitude-compensation), rather than dropping off rapidly like the bell design at low p_c/p_a (i.e., sea level) operating points. All nozzles have a higher C_f at a high p_c/p_a (i.e., vacuum).

The development of the annular-nozzle concept may influence the design of rocket vehicles,

especially in the areas of boattail structure and mission staging optimization. The advantages and disadvantages of annular nozzles are summarized as follows:

Advantages

- (1) Shortened nozzle length for the same performance, or increased performance (higher expansion area ratios) for a given length.
- (2) Improved performance at sea level or low altitudes. (Annular nozzles with high expansion area ratios can be used for a single-stage sea level to vacuum vehicle mission.)
- (3) The relatively stagnant region in the center of the nozzle can possibly be used for installation of gas generators, turbo-pumps, tanks, auxiliary equipment, and turbine gas discharges.
- (4) A segmented combustion chamber design approach can be used, easing development effort (individual segments can be built and tested during the early phases) and improving combustion stability.

Disadvantages

- (1) Relatively high cooling requirements, because of higher heat fluxes and greater surface areas to be cooled.
- (2) Heavier structural construction in some applications.
- (3) Manufacturing difficulties.

Sample Calculation (4-2)

Lay out the thrust chamber internal configuration (cylindrical combustion chamber with bell nozzle) for the engines on the Alpha vehicle with the data derived from sample calculation (4-1) and the following required chamber thrusts F_{tc} :

- (a) A-1 stage engine: $F_{tc_1} = 747\,000$ lb at sea level
- (b) A-2 stage engine: $F_{tc_2} = 149\,500$ lb at altitude
- (c) A-3 stage engine: $F_{tc_3} = 16\,000$ lb at altitude
- (d) A-4 stage engine: $F_{tc_4} = 7\,500$ lb at altitude

The detailed calculations and their results are presented in the following for the first-stage engine only. For the other stages, the calculation results are summarized in figures 4-21 to

4-23. The reader is urged to conduct his own calculations using the first stage as a guide, and to compare his results with those shown.

Solution

A-1 Stage Engine:

From sample calculation (4-1):

Design sea level $C_f = 1.531$;

$$(P_c)_{ns} = 1000 \text{ psia}; \epsilon = 14$$

Substitute into equation (1-33):

$$\text{Throat area: } A_t = \frac{747\,000}{1.531 \times 1000} = 487 \text{ in}^2$$

$$\text{Throat diameter: } D_t = \sqrt{\frac{4}{\pi} \times 487} = 24.9 \text{ in}$$

$$R_t = \frac{24.9}{2} = 12.45 \text{ in}$$

$$\text{Exit diameter: } D_e = \sqrt{14} \times 24.9 = 93.4 \text{ in}$$

$$R_e = \frac{93.4}{2} = 46.7 \text{ in}$$

Use a combustion chamber L^* of 45 in for $\text{LO}_2/\text{RP-1}$ application. Substitute into equation (4-4):

$$\text{Chamber volume: } V_c = 487 \times 45 = 21\,915 \text{ cu in}$$

Use a nozzle convergent half angle of 20° , a contraction area ratio $\epsilon_c = 1.6$, and a circular arc of radius $R = 1.5 R_t$, or 18.68 in, for nozzle contour upstream of the throat.

$$\text{Chamber diameter: } D_c = \sqrt{1.6} \times 24.9 = 31.5 \text{ in}$$

$$R_c = \frac{31.5}{2} = 15.75 \text{ in}$$

Use equation (4-7) to calculate the chamber convergent cone length

Convergent cone length

$$= \frac{12.45(\sqrt{1.6} - 1) + 18.68(\sec 20^\circ - 1)}{\tan 20^\circ}$$

$$= \frac{4.515}{0.364} = 12.4 \text{ in}$$

DESIGN OF LIQUID PROPELLANT ROCKET ENGINES

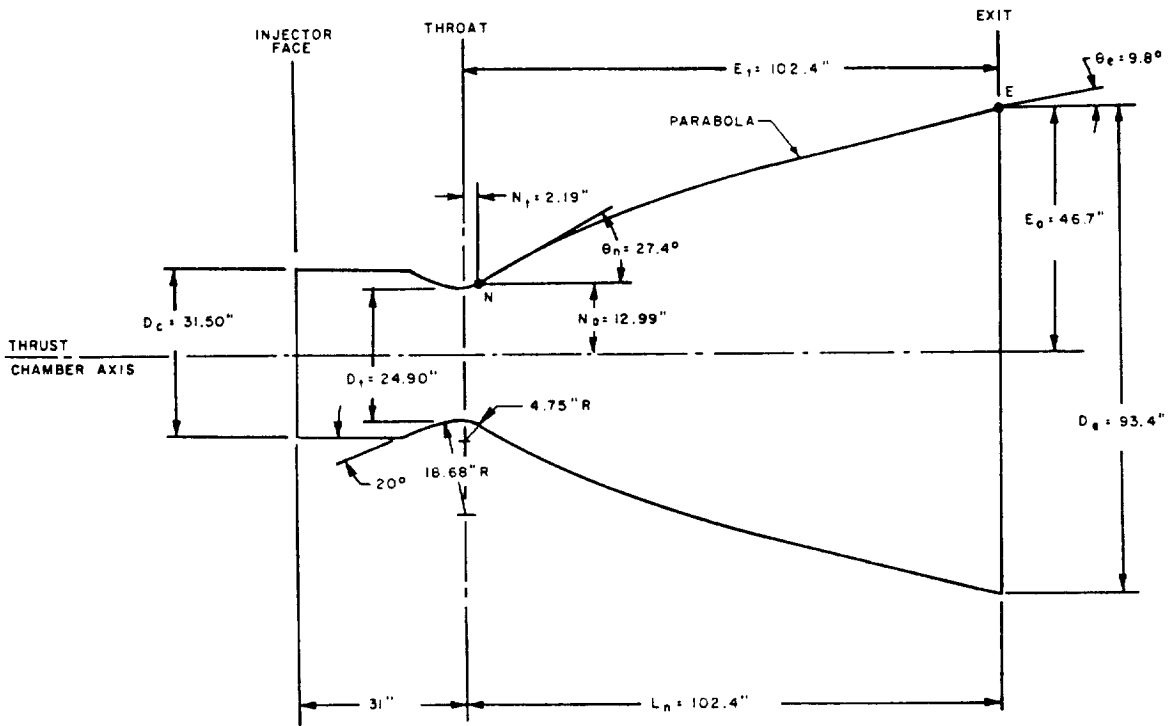


Figure 4-20.—A-1 stage engine thrust chamber internal configuration layout:
 $\epsilon = 14$, 80% bell, $L^* = 45$ ", $\epsilon_c = 1.6$.

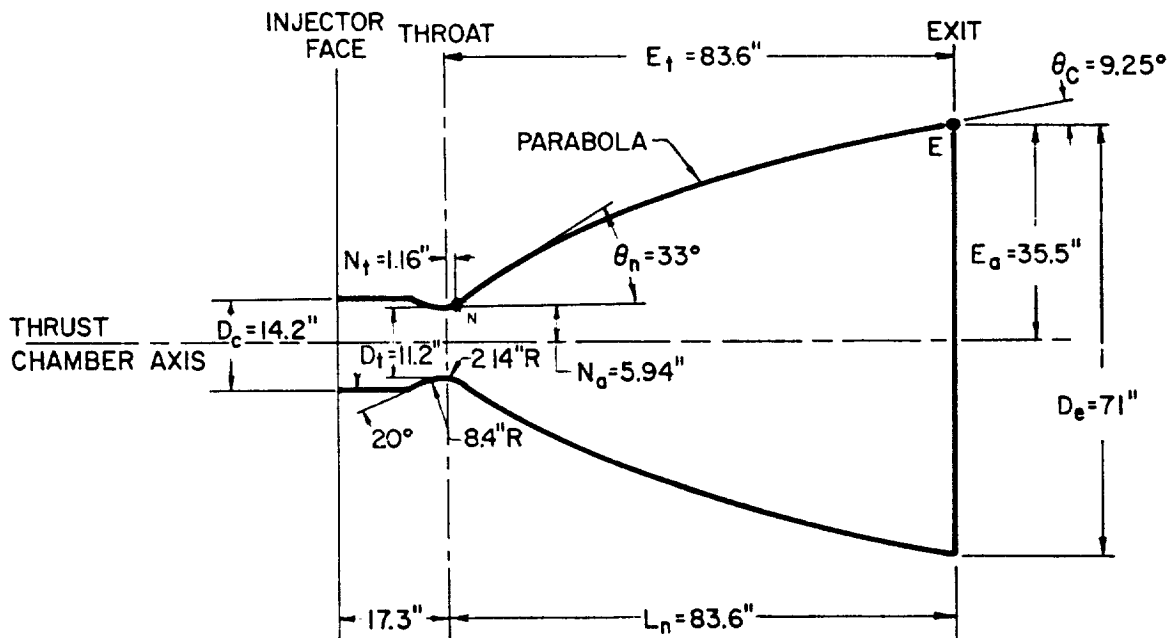


Figure 4-21.—A-2 stage engine thrust chamber, internal configuration layout:
 $\epsilon = 40$, 75% bell, $L^* = 26$ ", $\epsilon_c = 1.6$.

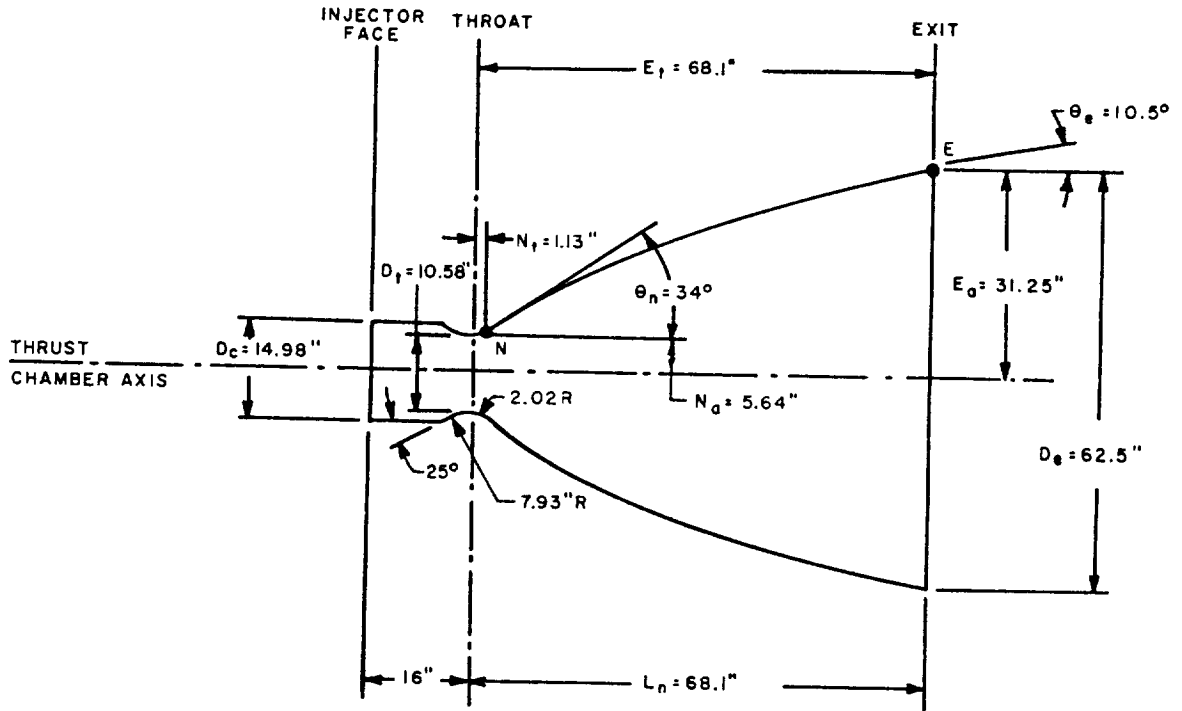


Figure 4-22.—A-3 stage engine thrust chamber, internal configuration layout:
 $\epsilon = 35$, 70% bell, $L^* = 28$ ", $\epsilon_c = 2$.

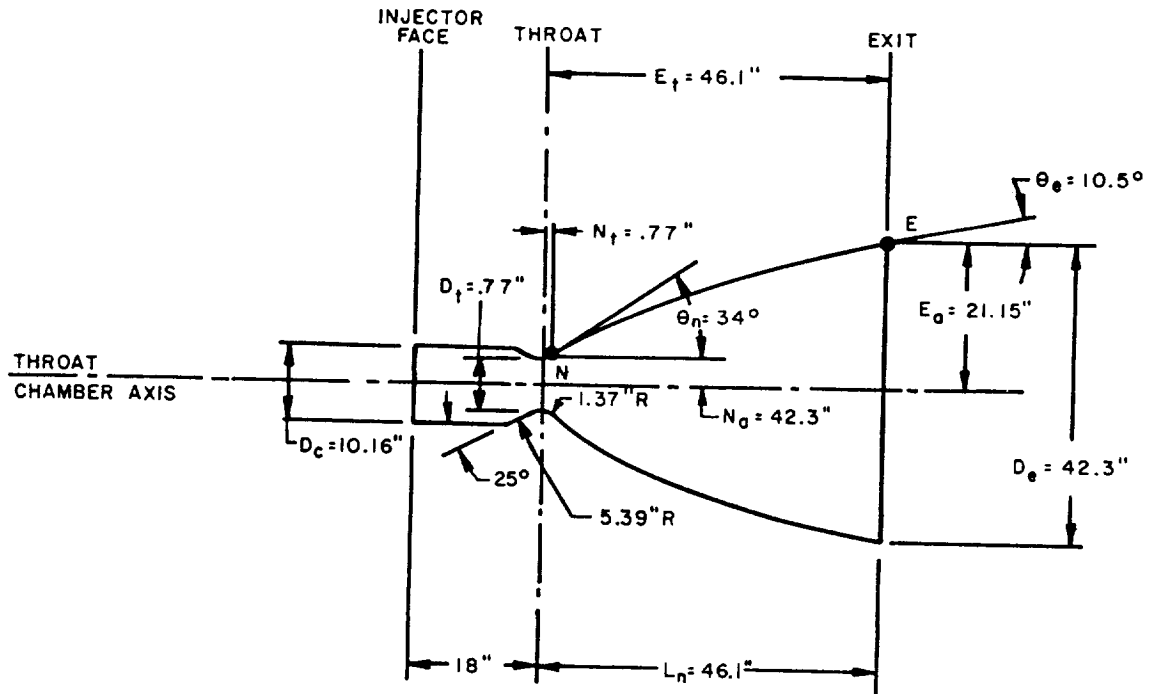


Figure 4-23.—A-4 stage engine thrust chamber, internal configuration layout:
 $\epsilon = 35$, 70% bell, $L^* = 32$ ", $\epsilon_c = 2$.

Using the frustrum cone volume equation and neglecting the slight rounding of the throat, the approximate convergent cone volume is obtained:

$$\begin{aligned} \text{Volume} &= \frac{\pi}{3} \times 12.4 \left[(15.75)^2 + (12.45)^2 + 15.75 \times 12.45 \right] \\ &= 7760 \text{ cu in} \end{aligned}$$

$$\begin{aligned} \text{Required volume for cylindrical chamber section} \\ &= 21\,915 - 7760 = 14\,155 \text{ cu in} \end{aligned}$$

$$\begin{aligned} \text{Required length for cylindrical chamber section} \\ &= 14\,155 / 1.6 A_t = 18.17 \text{ inches} \end{aligned}$$

$$\begin{aligned} \text{Distance from injector face to throat} \\ &= 18.17 + 12.40 = 30.57, \text{ say } 31 \text{ inches} \end{aligned}$$

Design an "80-percent bell" nozzle configuration using the parabolic approximation procedure. The nozzle contour downstream of the throat will be a circular arc of radius $0.382 R_t$, or 4.75 inches. By definition, the nozzle length L_n will be 80 percent of the length for an equivalent 15° half-angle conical nozzle. Substitute into equation (4-7)

$$\begin{aligned} L_n &= 0.8 \times \left[\frac{12.45(\sqrt{14} - 1) + 4.75(\sec 15^\circ - 1)}{\tan 15^\circ} \right] \\ &= 0.8 \times 128 = 102.4 \text{ inches} \end{aligned}$$

The parabolic contour wall angles θ_n and θ_e can be derived from figure 4-14, for $\epsilon = 14$ and $L_t = 0.8$; $\theta_n = 27.4^\circ$ and $\theta_e = 9.8^\circ$. The location of N and E along the nozzle contour, with respect to throat and nozzle axis, can be calculated

$$N_t = 0.382 R_t \sin \theta_n = 2.19 \text{ inches}$$

$$N_a = R_t + 0.382 R_t (1 - \cos \theta_n) = 12.99 \text{ inches}$$

$$E_t = L_n = 102.4 \text{ inches}$$

$$E_a = R_e = 46.7 \text{ inches}$$

With the aid of the established coordinates for points N and E, and the angles θ_n and θ_e , a parabola can be fitted to complete the contour. The general layout of the A-1 stage engine thrust chamber is shown in figure 4-20. With the aid of a computer program, more accurate calculations of the divergent nozzle contour can be made by the method of characteristics.

Since the calculations for the thrust chamber configuration are based on the calculated design C_f value which has to be verified by later actual testing, a slight change of chamber pressure is usually allowed to compensate for C_f deviations in order to meet the required thrust value.

4.4 THRUST CHAMBER COOLING

Techniques and Their Selection

Because of the high combustion temperatures (4000° to 6000° F) and the high heat transfer rates from the hot gases to the chamber wall (0.5 to 50 Btu/in²-sec), thrust chamber cooling becomes a major design consideration. For short-duration operation (up to a few seconds), uncooled chamber walls can be used. In this case, the heat can be absorbed by the sufficiently heavy chamber wall material which acts as a heat sink, before the wall temperature rises to the failure level. For most longer duration applications, a steady-state chamber cooling system has to be employed. One or a combination of the following chamber cooling techniques is often used:

1. *Regenerative cooling.*—Regenerative cooling is the most widely applied method and utilizes one or possibly both of the propellants, fed through passages in the thrust chamber wall for cooling, before they are injected into the combustion chamber. (See par. 4.1 and fig. 4-1.)

2. *Dump cooling.*—With this principle, a small percentage of the propellant, such as the hydrogen in a LO_2/LH_2 engine, is fed through passages in the thrust chamber wall for cooling and subsequently dumped overboard through openings at the rear end of the nozzle skirt. Because of inherent problems, this method has only limited application.

3. *Film cooling.*—Here, exposed chamber wall surfaces are protected from excessive heat with a thin film of coolant or propellant which is introduced through manifolded orifices in the chamber wall near the injector, and usually in several more planes toward the throat. The method has been widely used, particularly for high heat fluxes, either alone or in combination with regenerative cooling.

4. *Transpiration cooling.*—Transpiration cooling is accomplished by introducing a coolant

(either gaseous or liquid propellants) through porous chamber walls at a rate sufficient to maintain the desired combustion gas side chamber wall temperature. This method is essentially a special type of film cooling and has been widely used.

5. *Ablative cooling.*—In this process a sacrifice of combustion-chamber gas-side wall material is made by melting and subsequently vaporizing it to dissipate heat. As a result, relatively cool gases flow over the wall surface, thus creating a cooler boundary layer, assisting the cooling process. Ablative cooling has been used in numerous designs, initially mainly for solid propellant systems, but later equally successfully for low P_c , pressure-fed liquid systems.

6. *Radiation cooling.*—With this method, heat is radiated away from the surface of the outer thrust chamber wall. It has been successfully applied to low heat flux regions, such as nozzle extensions.

The selection of the best cooling method for a given thrust chamber depends on many design considerations. There are no simple-and-fast rules. However, the following are the main factors which influence the selected design approaches:

1. *Propellants.*—The properties of the combustion products, such as temperature, specific heat, specific weight, viscosity, etc., have a direct bearing on the heat transfer rate and in turn affect the chamber cooling requirements and methods. The cooling properties of the propellants and their relative flow rate decide whether they are suitable or sufficient for regenerative or film cooling. Therefore, in evaluating a chamber cooling system, the propellants involved will be one of the primary design considerations.

2. *Chamber pressure.*—High chamber pressure is linked with higher combustion gas mass flow rates per unit area of chamber cross section and thus raises the heat transfer rate. Combined regenerative and film-cooling methods are usually employed for the stringent requirement of higher chamber pressure applications.

3. *Propellant feed system.*—The type of propellant feed used in an engine system determines the pressure budget for the system. In a turbopump-fed engine system, more pressure drop is usually available for chamber cooling. The

availability of this pressure drop permits the use of regenerative cooling which requires propellant pressure sufficient to force the coolant through the cooling passage before entering the injector. A pressurized-gas-fed engine system usually has more stringent pressure limitations and operates on relatively low chamber pressures. This suggests the application of film, ablative, or radiation cooling.

4. *Thrust chamber configuration.*—The geometric shape of the chamber affects local combustion gas mass flow rates and wall surface areas to be cooled. This influences the choice of cooling method. It can also limit the design arrangements for regeneratively cooled tubular wall thrust chambers.

5. *Thrust chamber construction material.*—The properties of the thrust chamber materials will affect the cooling system design profoundly. Strength at elevated temperature, combined with heat conductivity properties of a metal, will determine suitability for regenerative cooling systems. For film-cooled chambers higher allowable material working temperatures are desired to reduce heat transfer rates and thus film coolant flow rates. The application of radiation-cooling to a chamber depends largely on the availability of high temperature (3000° F and up) refractory alloys. The success of ablative cooling depends entirely on the availability of suitable composite plastic materials.

In practice, the design of thrust chamber cooling systems is a major link in the complete engine system design. It cannot be treated independently, without due consideration of other engine system aspects. For instance, optimization of the chamber pressure value for a high-performance engine system is largely limited by the capacity and efficiency of the chamber cooling system. In turn, chamber pressure will affect other design parameters such as nozzle expansion area ratio, propellant feed pressure, and weight. Because of the complex interrelation between these factors, the complete analysis of chamber cooling systems is a specialized field and requires thorough knowledge of heat transfer, fluid mechanics, thermodynamics, and thermal stresses. The engine system designer, therefore, will enlist the services of heat transfer specialists.

Gas-Side Heat Transfer

One of the primary steps in the design of a thrust chamber cooling system is the analysis of the heat transfer from the combustion gases to the chamber walls (gas-side heat transfer). Because of the very high surface velocity of the gases along the chamber walls, the heat transfer occurs mainly through forced convection; i.e., through the transfer of heat energy resulting from the relative motion of different parts of a fluid. Before the gases can transfer heat to the wall, the heat energy must pass through a layer of stagnant gas along the wall, called the boundary layer.

The basic correlation for this complicated convective heat transfer can be expressed by the following equation:

$$q = h_g(T_{aw} - T_{wg}) \quad (4-10)$$

where

q = Heat flux or heat transferred across the stagnant gas film per unit surface area per unit time, Btu/in²-sec

h_g = Gas-side heat transfer coefficient, Btu/in²-sec-deg F

T_{aw} = Adiabatic wall temperature of the gas, deg R = $(T_c)_{ns} \times$ turbulent boundary layer recovery factor (ranging from 0.90 to 0.98)

T_{wg} = Hot-gas-side local chamber-wall temperature, deg R

The determination of the gas-side heat transfer coefficient h_g is a rather complex problem. The convection phenomenon as it occurs in rocket thrust chambers eludes complete understanding. Attempts to compare analytical results with experimental heat-transfer data obtained on rocket thrust chambers have often shown disagreement. The differences are largely attributed to the initial assumptions for analytical calculations. For example, there is good evidence that oxidizing and reducing atmospheres covering a wide range of temperature exist locally in the combustion product gases within the thrust chamber, because of the imperfect mixing of the propellants at the injector face. This results in deviations from calculations based on the assumption of homogeneous product gases.

However, it has been established by experiment that the heat-transfer coefficient is pre-

dominantly influenced by the mass velocity or the mass flow rate per unit area of the gas, subject to the exponent 0.8. In comparison, all other factors are relatively minor. A rough approximation of h_g can thus be expressed by the following equation:

$$h_g = (\rho' V)^{0.8} \quad (4-11)$$

where

ρ' = Free stream value of local gas density, lb/cu in

\bar{V} = Free stream value of local gas velocity, in/sec

Thus, under normal circumstances, the heat-transfer coefficient varies with the chamber pressure to the 0.8 power and throughout a given chamber inversely with the local chamber diameter to an exponent of 1.8.

Based on experience with turbulent boundary layers, some relatively simple correlations for the calculation of the gas-side heat-transfer coefficient have been developed. A much-used form is that credited to Colburn

$$Nu = C Re^{0.8} P_r^{0.34} \quad (4-12)$$

where

Nu = Nusselt number = $h_g D/k$

C = Dimensionless constant

Re = Reynolds number = $\rho' \bar{V} D/\mu$

\bar{V} = Free stream velocity, in/sec

P_r = Prandtl number = $\mu C_p/k$

D = Hydraulic diameter, in

k = Gas thermal conductivity, Btu/sec-in²-deg F/in

μ = Viscosity, lb/in sec

C_p = Specific heat at constant pressure, Btu/lb-deg F

or as Bartz has shown

$$h_g = \left[\frac{0.026}{D_t^{0.2}} \left(\frac{\mu^{0.2} C_p}{P_r^{0.6}} \right)_{ns} \left(\frac{(p_c)_{ns} g}{c^*} \right)^{0.8} \left(\frac{D_t}{R} \right)^{0.1} \right] \left(\frac{A_t}{A} \right)^{0.9} \sigma \quad (4-13)$$

where

R = Radius of curvature of nozzle contour at throat, in

σ = Correction factor for property variations across the boundary layer

~~CONFIDENTIAL~~

A = Area under consideration along chamber axis
 The value of σ can be evaluated in terms of nozzle stagnation temperature, local gas-side chamber wall temperature, and local Mach number.

$$\sigma = \frac{1}{\left[\frac{T_{wg}}{(T_c)_{ns}} \left(1 + \frac{\gamma-1}{2} M^2 \right) + \frac{1}{2} \right]^{0.68} \left[1 + \frac{\gamma-1}{2} M^2 \right]^{0.12}} \quad (4-14)$$

values of σ for various $T_{wg}/(T_c)_{ns}$ and γ , as computed by Bartz, are shown in figure 4-24.

If P_r and μ data are not available for particular combustion gas mixtures, the following equations can be used for approximate results:

$$P_r = \frac{4\gamma}{9\gamma - 5} \quad (4-15)$$

$$\mu = (46.6 \times 10^{-10}) \mathbb{M}^{0.5} T^{0.6} \quad (4-16)$$

where T = temperature of gas mixture, °R

Equations (4-13), (4-14), (4-15), and (4-16) can be used to calculate the approximate h_g values along the thrust chamber walls. However, the calculated values can be expected to be lower than the actual ones if the following conditions exist:

- (1) A substantial fraction of the combustion gases are strong radiators.
- (2) There is substantial dissociation, with subsequent recombination near the wall.
- (3) There are strong high-frequency flow instabilities.

The calculated values may be higher than the actual ones, because of the following:

- (1) The combustion reactions may not be completed in the chamber.
- (2) The combustion gases may deposit solids on the chamber walls, which act as insulators.

In certain propellant combinations, the combustion products contain small amounts of solid particles. These solids tend to deposit on the chamber walls, and form a rather effective insulating layer. A quantitative evaluation of the insulation effectiveness of this layer, necessary for correct heat transfer calculations, has been accomplished only experimentally.

In the case of the LO₂/RP-1 combination, carbon solids are deposited on the chamber walls. After a firing, the carbon gives the interior of the thrust chamber the appearance of being freshly painted black. The outer surface of the carbon appears sooty and can easily be removed by light rubbing. Underneath the exterior soot layer is a harder, graphitelike layer which can also be removed, but is more tenacious. This carbon deposit significantly increases the gas-side thermal resistance. The temperature of the carbon deposit at the hot gas-side interface approaches the gas temperature as the carbon thickness increases.

The values of the thermal resistance of the carbon deposit based on actual experimental testing results of a thrust chamber burning LO₂/RP-1 are shown in figure 4-25.

For the heat transfer calculation of the gas-side heat transfer with solid deposit on chamber walls, the following equations can be used

$$q = h_{gc} (T_{aw} - T_{wg}) \quad (4-17)$$

where h_{gc} = overall gas-side thermal conductance, Btu/in²-sec-deg F

$$h_{gc} = \frac{1}{\frac{1}{h_g} + R_d} \quad (4-18)$$

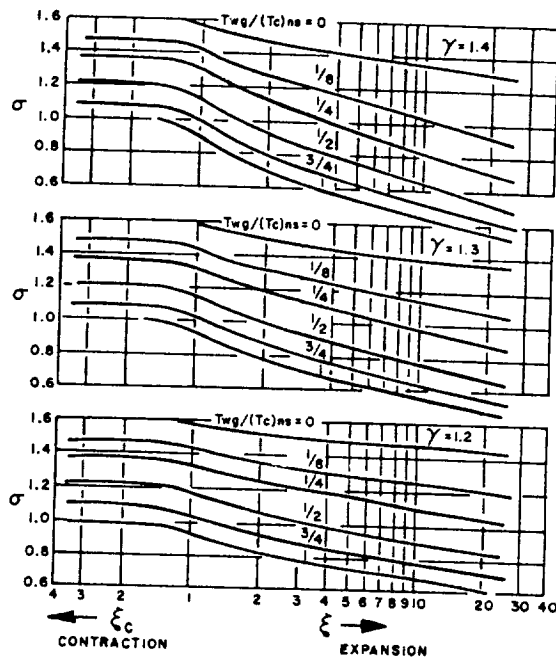


Figure 4-24.—Values of correction factor σ for property variation across boundary layer.

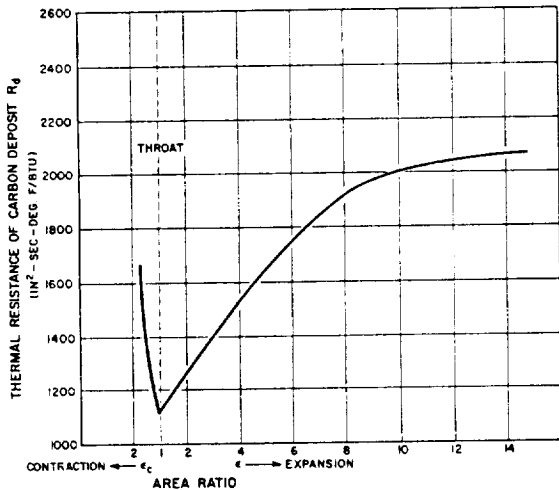


Figure 4-25.—Thermal resistance of carbon deposit on chamber walls $LO_2/RP-1$, mixture ratio = 2.35, $(p_c)_{ns} = 1000$ psia.

where R_d thermal resistance caused by the solid deposit, $\text{in}^2\text{-sec-deg F/Btu}$

When there is no solid deposit, $R_d = 0$ and $h_{gc} = h_g$, and equation (4-10) is used for heat transfer calculations.

Sample Calculation (4-3)

Determine the approximate design gas-side overall thermal conductance h_{gc} in the combustion chamber, at the throat, and at the exit nozzle point of $\epsilon = 5$, for the regeneratively cooled thrust chambers on the A-1 and A-2 stage engines.

Solution

(a) A-1 Stage Engine

First, let us consider equation (4-13). The combustion reactions are assumed to be homogeneous and complete. From figure 4-3 the following values are derived for the chamber product gases, for $LO_2/RP-1$ at $(p_c)_{ns} = 1000$ psia and a mixture ratio of 2.35:

$$(T_c)_{ns} = 6000^\circ \text{F or } 6460^\circ \text{R}, \quad \mathcal{M} = 22.5 \text{ lb/mol}, \quad \gamma = 1.222$$

The design $(T_c)_{ns}$

$$= \text{Theoretical } (T_c)_{ns} \times (c^* \text{ correction factor})^2$$

$$= 6460 \times (0.975)^2 = 6140^\circ \text{R}$$

(See eq. 1-32a and 1-41).

From sample calculation (4-1):

$$\text{Design } c^* = 5660 \text{ ft/sec}$$

From sample calculation (4-2):

$$D_t = 24.9 \text{ in}$$

Mean radius of the throat contour

$$= \frac{18.68 + 4.75}{2} = 11.71 \text{ in}$$

$$C_p = \frac{\gamma R}{(\gamma - 1)J} = \frac{1.222 \times \left(\frac{1544}{22.5}\right)}{(1.222 - 1) \times 778} = 0.485 \text{ Btu/lb-deg F}$$

From equation (4-15):

$$P_r = \frac{4 \times 1.222}{(9 \times 1.222) - 5} = 0.816$$

From equation (4-16):

$$\begin{aligned} \mu &= (46.6 \times 10^{-10}) \times (22.5)^{0.5} \times (6140)^{0.6} \\ &= 46.6 \times 10^{-10} \times 4.76 \times 188 \\ &= 4.18 \times 10^{-6} \text{ lb/in-sec} \end{aligned}$$

From equation (4-13):

$$\begin{aligned} h_g &= \left[\frac{0.026}{24.9^{0.2}} \times \left(\frac{(4.18 \times 10^{-6})^{0.2} \times 0.485}{0.816^{0.6}} \right) \right. \\ &\quad \left. \times \left(\frac{1000 \times 32.2}{5660} \right)^{0.8} \times \left(\frac{24.9}{11.71} \right)^{0.1} \right] \left(\frac{A_t}{A} \right)^{0.9} \sigma \\ &= 0.01366 \times 0.046 \times 4.02 \times 1.078 \times \left(\frac{A_t}{A} \right)^{0.9} \sigma \\ &= 0.0027 \times \left(\frac{A_t}{A} \right)^{0.9} \sigma \end{aligned}$$

Since the carbon deposit temperature approaches the gas temperature, a $(T_{wg}/(T_c)_{ns})$ value of 0.8 is used to determine the σ values from figure 4-24 ($\gamma \approx 1.2$).

At the combustion chamber:

$$\left(\frac{A_t}{A}\right)^{0.9} = \left(\frac{1}{1.6}\right)^{0.9} = 0.655, \sigma = 1.05$$

$$h_g = 0.0027 \times 0.655 \times 1.05 = 0.00185 \text{ Btu/in}^2\text{-sec-deg F}$$

At the throat:

$$\left(\frac{A_t}{A}\right)^{0.9} = 1, \sigma = 1$$

$$h_g = 0.0027 \times 1 \times 1 = 0.0027 \text{ Btu/in}^2\text{-sec-deg F}$$

At the exit nozzle point of

$$\epsilon = 5, \left(\frac{A_t}{A}\right)^{0.9} = \left(\frac{1}{5}\right)^{0.9} = 0.235, \sigma = 0.8$$

$$h_g = 0.0027 \times 0.235 \times 0.8 = 0.000507 \text{ Btu/in}^2\text{-sec-deg F}$$

The experimental data of figure 4-25 can be used to determine the values of thermal resistance R_d , for the carbon deposit. The thermal resistances are

$$1670 \frac{\text{in}^2\text{-sec-deg F}}{\text{Btu}}, \quad 1125 \frac{\text{in}^2\text{-sec-deg F}}{\text{Btu}},$$

and $1645 \frac{\text{in}^2\text{-sec-deg F}}{\text{Btu}}$

for points at the combustion chamber, the throat, and the exit nozzle area ratio of $\epsilon = 5$.

Substitute into the equation (4-18); at the combustion chamber

$$h_{gc} = \frac{1}{\frac{1}{0.00185} + 1670} = 0.00045 \text{ Btu/in}^2\text{-sec-deg F}$$

at the throat

$$h_{gc} = \frac{1}{\frac{1}{0.0027} + 1125} = 0.00067 \text{ Btu/in}^2\text{-sec-deg F}$$

At the exit nozzle of $\epsilon = 5$.

$$h_{gc} = \frac{1}{\frac{1}{0.000507} + 1645} = 0.000276 \text{ Btu/in}^2\text{-sec-deg F}$$

(b) A-2 Stage Engine

Again, the combustion reactions are assumed to be homogeneous and complete. From figure 4-4, the following values are derived for the chamber product gases, for LO_2/LH_2 at $(p_c)_{ns} = 800$ psia and a mixture ratio of 5.22:

$$(T_c)_{ns} = 5580^\circ \text{ F or } 6040^\circ \text{ R},$$

$$\bar{M} = 12 \text{ lb/mol}, \quad \gamma = 1.213$$

The design $(T_c)_{ns} =$

$$\text{Theoretical } (T_c)_{ns} \times (c^* \text{ correction factor})^2 = 6040 \times (0.975)^2 = 5740^\circ \text{ R}$$

From sample calculation (4-1):

$$\text{Design } c^* = 7480 \text{ ft/sec}$$

From figure 4-21:

$$D_t = 11.2 \text{ in}$$

Mean radius of the throat contour =

$$\frac{8.4 + 2.14}{2} = 5.27 \text{ in}$$

$$C_p = \frac{\gamma R}{(\gamma - 1)J} = \frac{1.213 \times \frac{1544}{12}}{(1.213 - 1) \times 778} = 0.943 \text{ Btu/lb-deg F}$$

From equation (4-15):

$$P_r = \frac{4 \times 1.213}{(9 \times 1.213) - 5} = 0.820$$

From equation (4-16):

$$\begin{aligned} \mu &= (46.6 \times 10^{-10}) (12)^{0.5} (5740)^{0.6} \\ &= 46.6 \times 10^{-10} \times 3.47 \times 180 \\ &= 2.92 \times 10^{-6} \text{ lb/in-sec} \end{aligned}$$

From equation (4-13):

$$\begin{aligned} h_g &= \left[\frac{0.026}{11.2^{0.2}} \times \left(\frac{(2.92 \times 10^{-6})^{0.2} \times 0.943}{0.820^{0.6}} \right) \right. \\ &\quad \left. \times \left(\frac{800 \times 32.2}{7480} \right)^{0.8} \times \left(\frac{11.2}{5.27} \right)^{0.1} \right] \left(\frac{A_t}{A} \right)^{0.9} \sigma \end{aligned}$$

$$= 0.01605 \times 0.0828 \times 2.69 \times 1.078 \times \left(\frac{A_t}{A}\right)^{0.9} \sigma$$

$$= 0.00385 \times \left(\frac{A_t}{A}\right)^{0.9} \sigma$$

Since there is no solid deposit on the chamber walls, an average gas-side wall temperature of 1500°R is assumed, and a $(T_{wg}/(T_c)_{ns})$ value of $(1500/5740)$ or 0.26 is used to determine the σ values from figure 4-24.

At the combustion chamber:

$$\left(\frac{A_t}{A}\right)^{0.9} = \left(\frac{1}{1.6}\right)^{0.9} = 0.655, \sigma = 1.38$$

$$h_{gc} = h_g = 0.00385 \times 0.655 \times 1.38 \\ = 0.00348 \text{ Btu/in}^2\text{-sec-deg F}$$

At the throat:

$$\left(\frac{A_t}{A}\right)^{0.9} = 1, \sigma = 1.35$$

$$h_{gc} = h_g = 0.00385 \times 1 \times 1.35 \\ = 0.00520 \text{ Btu/in}^2\text{-sec-deg F}$$

At the exit nozzle point of $\epsilon = 5$:

$$\left(\frac{A_t}{A}\right)^{0.9} = \left(\frac{1}{5}\right)^{0.9} = 0.235, \sigma = 1.16$$

$$h_{gc} = h_g = 0.00385 \times 0.235 \times 1.16 \\ = 0.00105 \text{ Btu/in}^2\text{-sec-deg F}$$

Regenerative Cooling

The heat transfer in a regeneratively cooled chamber can be described as the heat flow between two moving fluids, through a multilayer partition. Figure 4-26 shows this process schematically. The general steady-state correlation of heat transfer from the combustion gases through the layers, which include the metal chamber walls, to the coolant can be expressed by the following equations:

$$h_{gc}(T_{aw} - T_{wg}) = q = \left(\frac{k}{t}\right)(T_{wg} - T_{wc}) \quad (4-19)$$

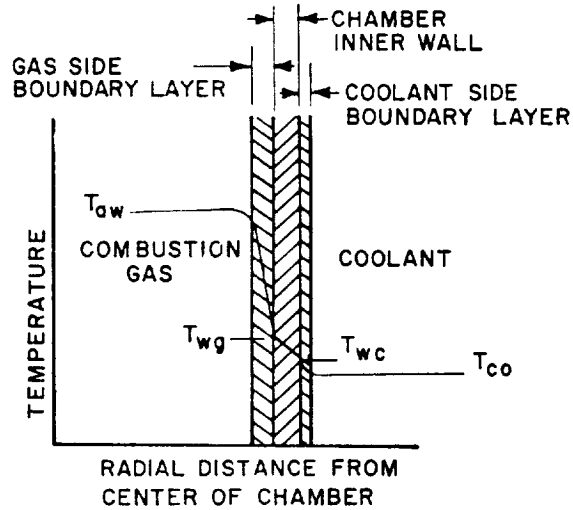


Figure 4-26.—Heat transfer schematic for regenerative cooling.

$$= h_c(T_{wc} - T_{co}) \quad (4-20)$$

$$= H(T_{aw} - T_{co}) \quad (4-21)$$

$$H = \frac{1}{\frac{1}{h_{gc}} + \frac{t}{k} + \frac{1}{h_c}} \quad (4-22)$$

where

q = Heat flux, Btu/in²-sec

h_{gc} = Overall gas-side thermal conductance, Btu/in²-sec-deg F (see eq. 4-18; without deposits, $h_{gc} = h_g$)

h_c = Coolant side heat-transfer coefficient, Btu/in²-sec-deg F

k = Thermal conductivity of chamber wall, Btu/in²-sec-deg F/in

t = Chamber wall thickness, in

T_{aw} = Adiabatic wall temperature of the gas, deg R

T_{wg} = Gas-side wall temperature, deg R

T_{wc} = Coolant side wall temperature, deg R

T_{co} = Coolant bulk temperature, deg R

H = Overall heat-transfer coefficient, Btu/in²-sec-deg F

The bulk temperature T_{co} of the coolant increases from the point of entry until it leaves the cooling passages, as a function of the heat absorbed, and of the coolant flow rate. Proper balance of these parameters, to maintain the chamber walls at temperatures below those at

which failure might occur because of melting or stress, is one of the major criteria for the design of regeneratively cooled thrust chambers. For metals commonly used in thrust-chamber walls, such as stainless steel, nickel, and Inconel, the limiting hot-gas-side wall temperature is around 1500°-1800° F. The resultant differences between combustion gas temperature and wall temperature range from 2500° to 6000° F.

Assume a station in the thrust chamber with gas temperature T_{aw} and coolant bulk temperature T_{co} . Referring to equation 4-21, it is seen that the heat flux q , which must be the same through all layers, is a function of the temperatures, and of overall heat transfer coefficient H . The value of H is composed of the individual coefficients for the boundary layers and the chamber metal wall (eq. 4-22). The smaller H , the smaller is q . However, it is one of the major design goals to keep coefficient h_{gc} low, but heat transfer coefficient h_c and conductivity t/k high, in relation to h_{gc} . Since the temperature differentials are inversely proportional to the heat-transfer coefficients of the heat flow paths, the temperature drop will then be steepest between hot gas and inner chamber wall. The effect is analogous to voltage drops along resistors in electrical circuits.

It is noted that the heat absorbed by the propellant used for regenerative cooling raises temperature of the propellant, and thus the energy level before it is injected into the combustion chamber. However, this effect on overall engine performance is slight, the gain usually being less than 1 percent. On the other hand, regenerative cooling with attendant pressure losses requiring additional turbopump power or higher gas pressurization levels imposes a performance penalty.

Coolant Side Heat Transfer

The coolant side heat-transfer coefficient h_c is influenced by many factors. At the high heat fluxes and temperatures encountered in thrust chamber operation, the propellants used for cooling may become corrosive, may decompose or deposit impurities upon the heated surface, thereby reducing cooling effectiveness. It is impossible to calculate the h_c values under these conditions without experimental data.

The characteristics of coolant side heat transfer depend largely on the coolant pressure and coolant side wall temperature. In figure 4-27, the heat flux is plotted versus wall temperature for a constant coolant pressure, bulk temperature, and flow velocity. Curve A indicates the behavior of heat transfer at coolant pressures below critical. Line segment A_1 - A_2 represents the heat transfer without boiling when the wall temperature is below the saturation temperature of the coolant corresponding to the fluid pressure. As the wall temperature at A_2 exceeds the saturation temperature by a certain margin (50° to 100° F), bubbles will form within the coolant layer close to the wall. The bubbles grow continuously out into the colder liquid stream until condensation at the vapor to liquid surface begins to exceed the rate of vaporization at the base of the vapor bubble, whereupon the bubbles start to collapse. This process, which occurs at high frequencies, is described as "nucleate boiling." It substantially increases the heat-transfer coefficient, resulting in little increase in wall temperature for a wide range of heat fluxes. The heat transfer with nucleate boiling is represented by line A_2 - A_3 . At A_3 , further increase in the heat flux abruptly leads to such a dense bubble population that the bubbles combine into a vapor film with an attendant large decrease in heat-transfer coefficient. The region of heat transfer with film boiling is represented by line A_3 - A_4 . The resulting increase in

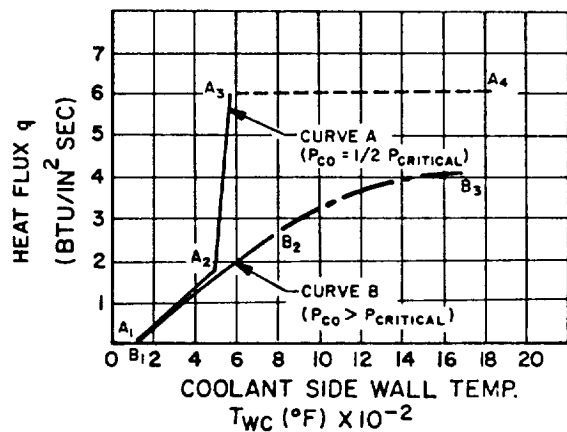


Figure 4-27.—Heat flux versus coolant side wall temperature of typical propellant in various heat transfer regions.

wall temperature is so high that failure of the wall material often occurs. The heat flux at A_3 is defined as the upper limit of nucleate boiling of the coolant q_{ul} , which therefore should be used as the design limit for a regenerative cooling system.

Curve B indicates the heat transfer behavior of a coolant above critical pressure. Since no boiling can occur, the wall temperature continually increases with increasing heat flux. Line B_1 - B_2 represents the heat-transfer region, when the wall temperature is below the coolant critical temperature. The heat-transfer coefficient remains essentially constant. As the wall temperature reaches the critical temperature B_2 and higher, a gradual transition to a stable supercritical vapor-film boundary layer begins, which results in somewhat lower heat-transfer coefficients. Line B_2 - B_3 represents the heat transfer in this region. Wall failure temperatures are usually reached at lower temperatures when the coolant is above the critical pressure than when it is below it. Where possible, a coolant operating pressure between 0.3 to 0.7 of critical pressure should be used to take advantage of the high heat-transfer coefficients available with nucleate boiling. However, in most systems, particularly those which are fed from a turbo-pump, the cooling jacket pressure, which is equal to or larger than the sum of chamber pressure and injection pressure, is supercritical. For the nonboiling subcritical temperature regions of both, subcritical and supercritical coolant pressures (A_1 - A_2 and B_1 - B_2 in fig. 4-27), the relationship between wall temperature and heat flux, which depends on the heat transfer coefficient h_c , can be predicted with sufficient accuracy for design purposes with the help of the Sieder-Tate equation (eq. 4-23) for turbulent heat transfer to liquids flowing in channels:

$$Nu = C_1 Re^{0.8} P_r^{0.4} \left(\frac{\mu}{\mu_w} \right)^{0.14} \quad (4-23)$$

where

C_1 = a constant (different values for various coolants)

Nu = Nusselt number = $h_c d / k$

Re = Reynolds number = $\rho V_{co} d / \mu$

P_r = Prandtl number = $\mu C_p / k$

μ = coolant viscosity at bulk temperature

μ_w = coolant viscosity at coolant sidewall temperature

d = coolant passage hydraulic diameter, in

k = coolant thermal conductivity, Btu/sec-in²-deg F/in

ρ = coolant density, lb/in³

V_{co} = coolant velocity, in/sec

C_p = coolant specific heat at constant pressure, Btu/lb-deg F

The heat flux at the upper limit of nucleate boiling q_{ul} can be estimated from

$$\frac{q_{ul}}{q_{nonboiling}} = \frac{C_2 \times 10^4}{p_{co} G} \quad (4-24)$$

where

C_2 = constant, its value depending on coolant used

$q_{nonboiling}$ = heat flux without nucleate boiling, Btu/in²-sec

p_{co} = coolant pressure, psia

G = coolant maximum flow rate per unit area, lb/in²-sec

When the heat is transferred through a vapor-film boundary layer (coolant at supercritical pressure and temperature, region B_2 - B_3 in fig. 4-27), the coolant-side heat-transfer coefficient h_c can be estimated from

$$h_c = \frac{0.029 C_p \mu^{0.2}}{P_r^{2/3}} \left(\frac{G^{0.8}}{d^{0.2}} \right) \left(\frac{T_{co}}{T_{wc}} \right)^{0.55} \quad (4-25)$$

where

C_p = coolant specific heat at constant pressure, Btu/lb-deg F

μ = coolant viscosity, lb/in-sec

P_r = Prandtl number

G = coolant weight flow rate per unit area, lb/in²-sec

d = coolant passage hydraulic diameter, in

T_{co} = coolant bulk temperature, deg R

T_{wc} = coolant side wall temperature, deg R

The bulk temperature of most coolants should be kept below the critical temperature, since the vapor-film heat-transfer coefficient would be too low to cool the wall effectively. The cooling capacity of the liquid-state regenerative coolant system can be estimated by

$$Q_c = \dot{w}_c C_p (T_{cc} - T_{ci}) \quad (4-26)$$

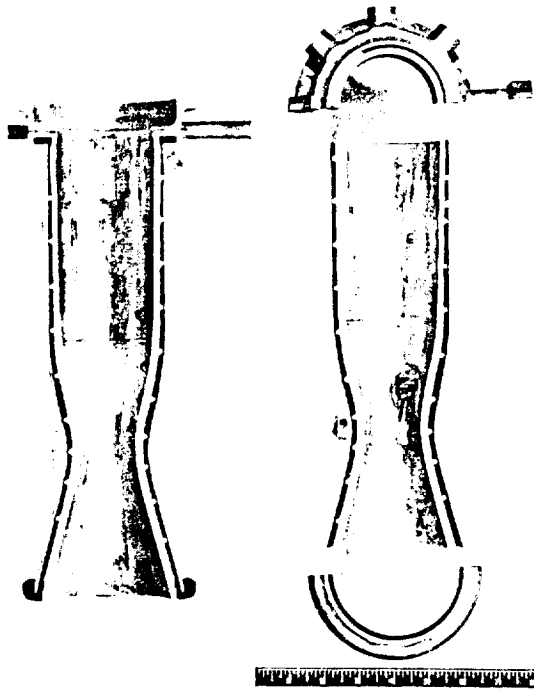


Figure 4-28.—Coaxial shell thrust chamber cutaway. Note overheated and burnt-through spot on chamber wall.

where

Q_c = coolant capacity, Btu/sec

\dot{w}_c = coolant mass flow rate, lb/sec

C_p = coolant specific heat at constant pressure, Btu/lb-deg F

T_{cc} = coolant critical temperature, deg R

T_{ci} = coolant inlet temperature, deg R

The allowed value of the total chamber wall gas heat-transfer rate Q should be kept below Q_c by a safe margin ($Q < Q_c$).

However, there is no such limitation for hydrogen when used as a coolant. Hydrogen has excellent heat-transfer characteristics with a reasonably high heat-transfer coefficient even in the supercritical pressure and temperature region. Usually liquid hydrogen enters the chamber coolant passage under supercritical pressure and reaches supercritical temperature a short distance from the inlet.

The coolant passage areas at various points along the chamber walls are designed to maintain the proper coolant velocity dictated by the heat-transfer coefficients determined by the heat-

transfer calculation. There are several basic design approaches for regenerative-cooled thrust chambers. Axial-flow cooling jackets, made up of tubes, are used in the design of large thrust chambers (3000 pounds of thrust and up); coaxial shells separated by helical ribs or wires are typical of the smaller thrust chamber designs. Figure 4-1 shows a large regenerative cooled tubular wall thrust chamber. Figure 4-28 represents a typical coaxial shell design for a smaller thrust chamber.

In this design, the coolant passage is defined as the rectangular area between inner and outer shell and two adjacent ribs, which are wrapped helically around the inner shell or liner.

Tubular Wall Thrust Chamber Design

In the design of tubular wall thrust chambers, the number of coolant tubes required is a function of the chamber geometry, the coolant weight flow rate per unit tube area, the maximum allowable tube wall stress, and fabrication considerations. The critical cooling region is near the throat where the heat flux is highest. It is this region, then, which determines the number of tubes required for a given coolant flow rate. For easier fabrication and lower stress, tube cross sections of circular shape are preferred. However, other shapes are often used to meet certain flow-area requirements. The stress analysis of the tubes is based upon three primary considerations: the hoop stress caused by coolant pressure, the thermal stress caused by temperature gradient across the tube section and the wall, and the bending stress caused by distortion induced by the pressure differential between adjacent tubes (if any) or by other effects such as discontinuities. The tube design stress is based on the combined stress from the above three considerations. It has been found that the maximum combined stress will occur at the throat region.

As shown in figure 4-29, the maximum combined tangential stresses of the circular-tube will be at section A-A and can be expressed by

$$S_t = \frac{(p_{co} - p_g)r}{t} + \frac{E\alpha qt}{2(1-\nu)k} + \frac{6MA}{t^2} \quad (4-27)$$

where

S_t = combined tangential tensile stress, lb/in²

- q = heat flux, Btu/in²-sec
- r = tube radius, in
- t = tube wall thickness, in
- p_{co} = coolant pressure, lb/in²
- p_g = combustion gas pressure, lb/in²
- E = modulus of elasticity of tube wall material, lb/in²
- a = thermal expansion coefficient of tube wall material, in/in-deg F
- k = thermal conductivity of tube wall material, Btu/in²-sec-deg F/in
- ν = Poisson's ratio of tube wall material
- M_A = bending moment caused by discontinuity, in-lb/in (no effect of pressure differential between adjacent tubes for circular tube design)

Since the combustion-gas-side portion of the tube (zone I) has a much higher mean temperature than that of the back side tube portion and chamber outer shell (zone II), the thermal expansion of zone I will be restrained by zone II. Because of the considerably greater mass of zone II, thermal inelastic buckling is induced under certain conditions, in zone I, in the longitudinal direction. The longitudinal thermal stress can be estimated by

$$S_1 = Ea \Delta T \quad (4-28)$$

where

- S_1 = longitudinal thermal stress, lb/in²
- ΔT = mean temperature difference between zone I and zone II, deg F
- S_1 should be kept at a level not higher than $0.9 S_c$, below.

The critical stress for longitudinal inelastic buckling on zone I can be estimated by

$$S_c = \frac{4 E_t E_c t}{(\sqrt{E_t} \sqrt{E_c})^2 \sqrt{3(1-\nu^2)} r} \quad (4-29)$$

where

- S_c = critical stress for longitudinal inelastic buckling in zone I, lb/in²
- E_t = tangential modulus of elasticity at wall temperature, lb/in²
- E_c = tangential modulus of elasticity from compression stress-strain curve, at wall temperature, lb/in²

An elongated cross section tube design is shown in figure 4-30. Equations (4-27), (4-28),

and (4-29) can be also applied to calculate the stresses for this design. Here again the maximum combined stress is at section A. The bending moment at section A, M_A , should take into consideration the pressure differential (if any) between adjacent tubes.

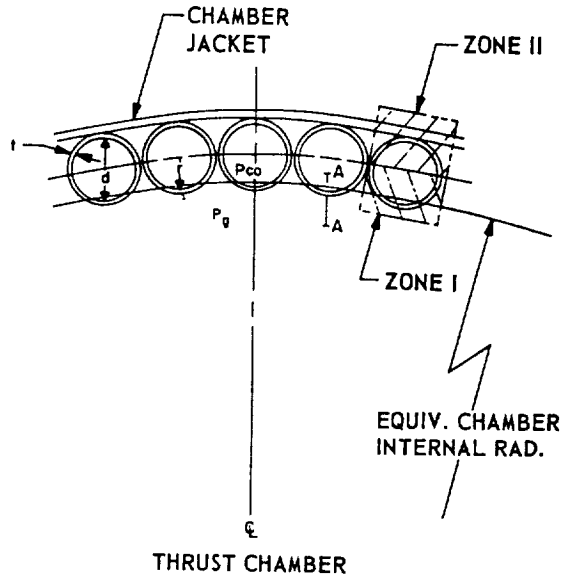


Figure 4-29.—Circular tube wall of regeneratively cooled thrust chamber.

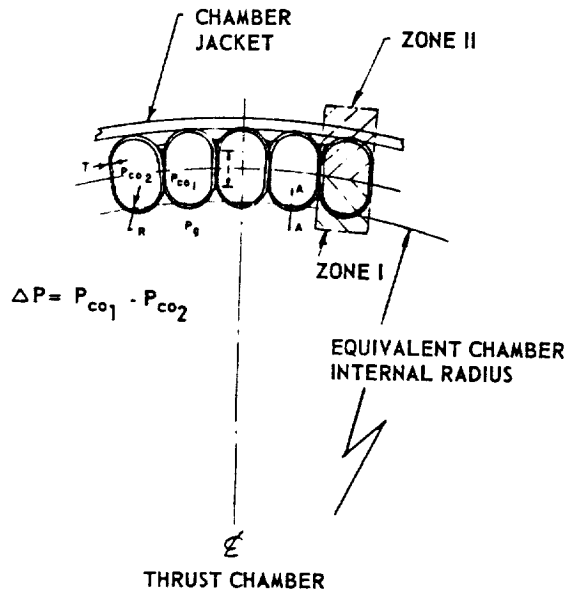


Figure 4-30.—Elongated tube wall of regeneratively cooled thrust chamber.

$$M'_A = M_A + K_A \frac{l \Delta p}{2} \quad (4-30)$$

where

M'_A = combined bending moment at section A, in-lb/in

M_A = bending moment due to discontinuity

K_A = dimensionless design constant based on test results (range 0.3-0.5)

l = length of flat portion on tube wall, in

Δp = pressure differential between adjacent tubes, lb/in²

Substituting equation (4-30) into equation (4-27), the maximum stress of the elongated tube can be calculated.

The working loads induced in a regenerative tubular wall chamber by the chamber pressure are designed to be absorbed by a chamber jacket or tension bands wrapped around the tube bundle.

Coaxial Shell Thrust Chamber Design

In a coaxial-shell-type thrust chamber as shown in figure 4-28, the outer shell is subjected only to the hoop stress induced by the coolant pressure. The inner shell, however, is subjected to the combination of compressive stress caused by the pressure differential between the coolant and combustion gases, and of the thermal stress caused by the temperature gradient across the wall. The maximum stress occurs at the inner-wall surface of the inner shell and can be calculated from the following equation.

$$S_c = \frac{(p_{co} - p_g) R}{t} + \frac{E a q t}{2(1 - \nu) k} \quad (4-31)$$

where

S_c = combined maximum compressive stress, lb/in²

q = heat flux, Btu/in²-sec

R = radius of the inner shell, in

t = thickness of the inner shell, in

p_{co} = coolant pressure, lb/in²

p_g = combustion gas pressure, lb/in²

E = modulus of elasticity of inner shell material, lb/in²

a = thermal expansion coefficient of inner shell material, in/in-deg F

k = thermal conductivity of inner shell material, Btu/in²-sec-deg F/in

ν = Poisson's ratio of inner shell material

Pressure Drop in Cooling Passages

It is desirable to design a cooling passage with minimum pressure drop. Abrupt change of flow direction and sudden expansion or contraction of flow areas should be avoided. The inner surface of cooling passages should be smooth and clean. The pressure drop in a cooling passage can be treated as that in a hydraulic conduit and be calculated accordingly.

$$\Delta p = f \frac{L}{d} \frac{\rho V_{co}^2}{2g} \quad (4-32)$$

where

Δp = coolant pressure drop through the portion of cooling passage under consideration, lb/in²

L = length of that portion, in

d = equivalent average diameter of that portion, in

ρ = average density of the coolant, lb/in³

V_{co} = average coolant flow velocity, in/sec

g = mass conversion factor, equal to gravitational constant, 32.2 × 12 in/sec²

f = friction loss coefficient, which is a function of the Reynolds number, and of cooling passage conditions such as surface smoothness, geometric shape, etc. This can be determined only experimentally (also see fig. 7-20 and table 7-3)

Sample Calculation (4-4)

Determine the cooling passage and the tube design at the throat for the thrust chambers of the A-1 and A-2 stage engines.

Solution

(a) A-1 Stage Engine

The fuel, RP-1, is used as the coolant. Since the cooling requirement is most stringent at the throat, the tube design for this station will serve as the starting point for the entire chamber. For high strength, Inconel X is chosen as the tube

material. Based on experimental test results which showed good solid carbon deposits, design values not exceeding 1000° F or 1460° R may be permitted for gas-side tube-wall temperature. Specifically for the throat region, a T_{wg} value of 1188° R is taken. Using the results of sample calculation 4-3, the value for the adiabatic wall temperature T_{aw} can be calculated by multiplying $(T_c)_{ns}$ by the estimated stagnation recovery factor of 0.923, $T_{aw} = 6140 \times 0.923 = 5667^\circ \text{R}$. From the same calculation, the overall gas-side thermal conductance at the throat region is $h_{gc} = 0.00067 \text{ Btu/in}^2\text{-sec-deg F}$. Substitute into equation (4-10), to obtain the heat flux at the throat:

$$q = (5667 - 1188) \times 0.00067 = 3.00 \text{ Btu/in}^2\text{-sec}$$

From supplier's specifications, the following average data are obtained for Inconel X at 1000°-1200° R: Coefficient for thermal expansion, $a = 8 \times 10^{-6} \text{ in/in-deg F}$; modulus of elasticity, $E = 28 \times 10^6 \text{ psi}$; thermal conductivity, $k = 3.19 \times 10^{-4} \text{ Btu/in}^2\text{-deg F/in}$; Poisson's ratio, $\nu = 0.35$.

A circular tube configuration with an internal diameter d and a wall thickness t of 0.020 inch is used. The assumption for thickness is to be verified by heat transfer and stress calculations. From equation (4-19), the coolant side wall temperature then is:

$$T_{wc} = T_{wg} - \frac{qt}{k} = 1188 - \frac{3.00 \times 0.02}{3.19 \times 10^{-4}} \approx 1000^\circ \text{R}$$

A double pass design is used; i.e., the coolant passes down through alternating tubes and up through adjacent tubes.

For an "up" tube, assume a coolant bulk temperature $T_{co} = 600^\circ \text{R}$ at the throat (the more severe case, since the coolant has passed the throat region before, on the way down). This temperature is well below the critical one and can be expected to remain so for the remainder of the passage. Total temperature increase for a typical thrust chamber design is of the order of 100° F between cooling jacket inlet and outlet. The heat-transfer coefficient required to permit the calculated heat flux for the temperature differential assumed can now be calculated from equation (4-20):

$$h_c = \frac{q}{T_{wc} - T_{co}} = \frac{3.00}{1000 - 600} = 0.0075 \text{ Btu/in}^2\text{-sec-deg F}$$

The relationship between required h_c and correct tube diameter is established by equation (4-23), and experimental data for RP-1 ($C_1 = 0.0214$):

$$Nu = 0.0214 Re^{0.8} Pr^{0.4} \left(\frac{\mu}{\mu_w} \right)^{0.14}$$

or, substituting corresponding terms:

$$\frac{h_c d}{k} = 0.0214 \left(\frac{\rho V_{co} d}{\mu} \right)^{0.8} \left(\frac{\mu C_p}{k} \right)^{0.4} \left(\frac{\mu}{\mu_w} \right)^{0.14} \quad (a)$$

The following additional relationships exist:

$$\begin{aligned} \text{Number of tubes } N &= \frac{\pi [D_t + 0.8(d + 0.04)]}{(d + 0.04)} \\ &= \frac{(0.8d + 24.93)}{(d + 0.04)} \quad (b) \end{aligned}$$

From sample calculation (4-2), $D_t = 24.9$ inches. The factor 0.8 considers the fact that the tube centers are located on a circle, rather than a straight line.

For our double-pass design, the coolant velocity then is

$$V_{co} = \frac{\dot{w}_t}{N \frac{\pi d^2}{4}} = \frac{827 \times 8}{\pi N d^2 \rho} = \frac{2106}{N d^2 \rho} \quad (c)$$

From table 3-2: $\dot{w}_t = 827 \text{ lb/sec}$; $\rho = \text{local value of fluid density}$.

RP-1 at 600° R has the following properties:

$$\mu = 4.16 \times 10^{-5} \text{ lb/in-sec}$$

$$k = 1.78 \times 10^{-6} \text{ Btu/in}^2\text{-sec-deg F/in}$$

$$C_p = 0.5 \text{ Btu/lb-deg F}$$

For RP-1 at 1000° R, $\mu_w = 0.416 \times 10^{-5} \text{ lb/in-sec}$.

Now substitute known values and equation (c) into equation (a)

$$\frac{0.0075 d}{1.78 \times 10^{-6}} = 0.0214 \times \left(\frac{\rho d \frac{2106}{Nd^2 \rho}}{4.16 \times 10^{-5}} \right)^{0.8}$$

$$\times \left(\frac{0.5 \times 4.16 \times 10^{-5}}{1.78 \times 10^{-6}} \right)^{0.4} \times \left(\frac{4.16 \times 10^{-5}}{0.416 \times 10^{-5}} \right)^{0.14}$$

$$4220 d = 115\,000 \left(\frac{1}{Nd} \right)^{0.8}$$

$$N = 62.4 d^{-2.25}$$

Substitute equation (d) into equation (b)

$$62.4 d^{-2.25} = \frac{\pi(0.8d + 24.93)}{(d + 0.04)}$$

$$d = 0.85 \text{ in}$$

Substitute (d) into equation (b)

$$N = 94.5$$

Since for two-pass design a whole, even tube number is needed, the design value of $N = 94$ is used. Substituting this into equation (b)

$$d = 0.855 \text{ in}$$

For the determination of a new tube design, repeated calculations, with varied assumptions, will be required. An experienced designer will require fewer approaches, particularly if test results of prior, comparable designs are available. However, even for complicated conditions, great amounts of data can be generated in a relatively short time if an electronic computer is available.

From table 3-2:

$$\rho = \frac{50.45}{1728} = 0.0292 \text{ lb/in}^3$$

Substitute into equation (c)

$$V_{co} = \frac{2106}{94 \times (0.855)^2 \times 0.0292}$$

$$= 1051 \text{ in/sec or } 87.6 \text{ ft/sec}$$

At the throat $p_{co} = 1500$ psia is established,

as an interpolation between fuel pump outlet pressure and injector manifold pressure.

Combustion gas pressure at the throat

$$p_g = p_t = (p_c)_{ns} \left(\frac{2}{\gamma + 1} \right)^{\frac{\gamma}{\gamma - 1}} = 1000 \times 0.562 = 562 \text{ psia}$$

($\gamma = 1.222$ from sample calculation (4-2); use table 1-2).

Thus maximum tensile stress at the inner tube wall face can be determined using equation (4-27):

$$S_t = \frac{(1500 - 562) \times 0.427}{0.020}$$

$$+ \frac{28 \times 10^6 \times 8 \times 10^{-6} \times 3.0 \times 0.02}{2 \times (1 - 0.35) \times 3.19 \times 10^{-4}} + 6 \frac{M_A}{t^2}$$

$$= 20\,000 + 32\,500 + 15\,000 M_A$$

$$= 52\,500 + 15\,000 M_A$$

Based on suppliers' recommendation, $F_{ty} = 82\,000$ was used for Inconel X at 1000°R .

$$\text{Maximum allowable } M_A = \frac{82\,000 - 53\,700}{15\,000}$$

$$= 1.88 \text{ in-lb/in}$$

From experience it can be assumed that the bending moment due to discontinuity in this case will be less than 1.88 in-lb/in. Thus the assumption of 0.020 in thickness for the tube wall is sufficient. Summarizing the tube configuration at the throat:

$$d = 0.855 \text{ in, } t = 0.020 \text{ in, } N = 94$$

(b) A-2 Stage Engine

The fuel, hydrogen, is used as the coolant. Again, Inconel X is chosen as the tube material. To avoid the "hot shortness" or low-ductility properties of Inconel X in the range 1200° - 1400°F , the mean temperature of the tube wall must be kept under 1000°F (or 1460°R). The value for adiabatic wall temperature T_{aw} of the gas can be calculated using an assumed stagnation recovery factor of 0.92.

$$T_{aw} = (T_c)_{ns} \times 0.92 = 5740 \times 0.92 = 5270^\circ \text{R}$$

From sample calculation (4-3) the overall gas-side conductance at the throat region $h_{gc} = 0.00520$ Btu/in²-sec-deg F. Substitute into equation (4-19), to obtain the heat flux at the throat:

$$q = (5270 - 1600) \times 0.00520 = 3670 \times 0.00520 = 19.10 \text{ Btu/in}^2\text{-sec}$$

A value of 1600° R will be used for the gas-side wall temperature T_{wg} at the throat region. From supplier's specifications the following data is obtained for Inconel X at 1600° R or 1140° F:

$$a = 8.2 \times 10^{-6} \text{ in/in-deg F}; \quad E = 24 \times 10^6 \text{ psi}; \\ k = 3.86 \times 10^{-4} \text{ Btu/in}^2\text{-sec-deg F/in}$$

$$\nu = 0.35.$$

Use a circular tube configuration with an internal diameter d and a wall thickness t of 0.008 inch.

From equation (4-19) the coolant side wall temperature

$$T_{wc} = 1600 - \frac{19.10 \times 0.008}{3.86 \times 10^{-4}} = 1600 - 396 = 1204^\circ \text{R}$$

A mean value will be used for the wall temperature

$$T_{wc} = \frac{1600 + 1204}{2} = 1402^\circ \text{R} < 1460^\circ \text{R}$$

Assume a coolant bulk temperature, $T_{co} = 135^\circ \text{R}$ at the throat; then, from equation (4-20),

$$h_c = \frac{19.10}{1204 - 135} = 0.0179 \text{ Btu/in}^2\text{-sec-deg F}$$

Substitute into equation (4-25),

$$0.0179 = \frac{0.029 C_p \mu^{0.2}}{P_r^{2/3}} \frac{(G^{0.8})}{(d^{0.2})} \left(\frac{T_{co}}{T_{wc}} \right)^{0.55} \quad (a)$$

From figure 4-21, $D_t = 11.2$ in. The following relationships exist:

$$\text{Number of tubes } N = \frac{\pi [D_t + 0.8(d \times 0.016)]}{(d + 0.016)} \\ = \frac{\pi(0.8d + 11.213)}{(d + 0.016)} \quad (b)$$

A 1½-pass design is used (i.e., the coolant enters the fuel manifold at the $\epsilon = 8$ nozzle plane, flows to $\epsilon = 30$ and back, then passes through the throat and combustion chamber zone before it enters the injector). From table 3-3:

$$\dot{w}_f = 54.5 \text{ lb/sec}$$

Coolant weight flow rate per unit area

$$G = \frac{\dot{w}_f}{N \left(\frac{\pi d^2}{4} \right)} = \frac{54.5 \times 4}{\pi N d^2} = \frac{69.3}{N d^2} \quad (c)$$

For hydrogen at 135° R:

$$P_r = 0.82; \quad C_p = 3.5 \text{ Btu/lb-deg F}; \\ \mu = 0.367 \times 10^{-6} \text{ lb/in-sec}$$

Substitute these values and equation (c) into equation (a):

$$0.0179 = \frac{0.029 \times 3.5 \times (0.367 \times 10^{-6})^{0.2}}{(0.82)^{2/3}} \\ \times \left[\frac{(69.3)^{0.8}}{N d^2} \right] \times \left(\frac{135}{1204} \right)^{0.55}$$

or

$$N = 3.91 d^{-2.25}$$

Substitute equation (d) into equation (b)

$$3.91 d^{-2.25} = \frac{\pi(0.8d + 11.213)}{(d + 0.016)}$$

$$d = 0.185 \text{ in}$$

Substitute into equation (b)

$$N = \frac{\pi(0.8 \times 0.17 + 11.213)}{(0.17 + 0.016)} = 178$$

CONFIDENTIAL

Maximum tensile stress is now checked at the inner wall surface using equation (4-27):

At the throat, estimated $P_{co} = 1200$ psia;
 $P_g = P_t = (p_c)_{ns} (2/(\gamma + 1))^{\gamma/(\gamma - 1)} = 800 \times 0.554 = 443$ psia ($\gamma = 1.213$ from sample calculation (4-1))

$$S_t = \frac{(1200 - 443) \times 0.0925}{0.008} + \frac{24 \times 10^6 \times 8.2 \times 10^{-6} \times 19.10 \times 0.008}{2(1 - 0.35) \times 3.86 \times 10^{-4}} + 6 \frac{M_A}{(0.008)^2}$$

$$= 68750 + 93900 M_A$$

Based on suppliers' recommendations,

$F_{ty} = 81000$ psi for Inconel X at $1200^\circ R$

Maximum allowable $M_A = \frac{81000 - 68750}{93900}$
 $= 0.131$ in-lb/in

From experience, it can be assumed that the bending moment due to discontinuity will be less than 0.131 in-lb/in. Thus the selection of 0.008-inch tube thickness is valid. Summarizing the tube configuration at the throat:

$d = 0.185$ inch, $t = 0.008$ inch, $N = 178$.

As a general design aid, figures 4-31 and 4-32 present construction detail for a typical regeneratively cooled thrust chamber. The chamber shown is very similar to the one presented in figures 4-1 and 4-2. Figure 4-31 shows clearly how the tube shape changes along the longitudinal axis. In a typical manufacturing process, tubes of uniform circular cross-section area are first cut to length, then swaged. The latter operation can best be accomplished by internal hydraulic pressure in a die. The tubes are filled with wax, and are then bent (preshaped), in a special fixture, to the thrust-chamber contour.

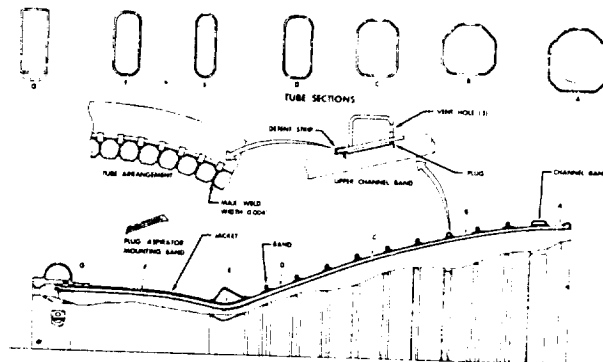


Figure 4-31.—Typical regeneratively cooled tube wall thrust chamber.

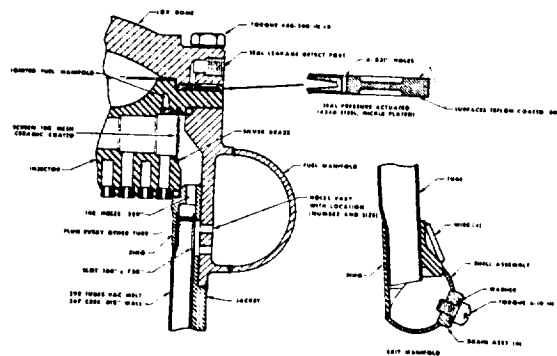


Figure 4-32.—Detail of injector manifold and return manifold of typical regeneratively cooled tube wall thrust chamber.

The tube is then placed in a die of varying cross-sectional area. Hydraulic pressure applied to the inside of the tube forces it to align with the die and to assume final shape. In preparation for assembly, a trimming process usually follows.

In preparation for assembly into a chamber, the tubes are arranged on a brazing fixture (core). For proper brazing great care is required to assure even distribution of the gaps between tubes. Earlier chamber models were then hand brazed, a process requiring many weeks and considerable skill. More recently, furnace brazing has been successfully applied, drastically cutting chamber-assembly time.

Dump Cooling

The dump cooling technique may be particularly effective for applications in hydrogen-fueled, low-pressure systems ($p_c < 100$ psia), or for nozzle extensions of high-pressure hydrogen systems. A small amount of the total hydrogen flow is diverted from the main fuel feed line, fed through cooling passages and ejected. The heat transfer mechanism is similar to that of regenerative cooling. The coolant, however, becomes superheated as it flows toward the nozzle exit, where it is expanded overboard at reasonably high temperatures and velocities, thus contributing some thrust. Application of dump cooling is often limited, however, by various technical difficulties, such as discharge nozzle design at low coolant flow rates.

The type of coolant path for a dump-cooled thrust chamber is selected to assure maximum overall engine system performance. Two possible paths are shown in figure 4-33:

- (1) Axial flow: a one-pass longitudinal passage, using double-wall (fig. 4-33A) or tube-wall designs (fig. 4-33C). Both are open ended, with provision for expansion of the dumped superheated hydrogen gas at the nozzle exit.
- (2) Circumferential flow: a double-wall design having a spiral flow path for the coolant and provision for expansion of the dumped superheated hydrogen gas in the axial direction (fig. 4-33B). A spiral-wound tube design may also prove advantageous (fig. 4-33D).

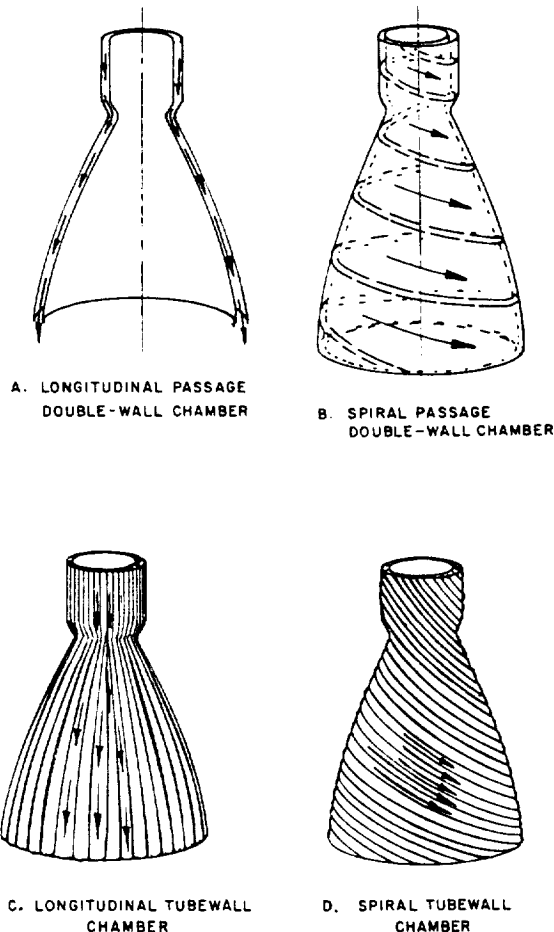


Figure 4-33.—Typical dump-cooled chamber fabrication methods.

The various constructions differ considerably in complexity and fabrication cost. Selection will depend on an optimum tradeoff between reliability, performance, cost, and weight. The longitudinal passage designs are often employed for larger coolant flow rates, as related to the physical size of the thrust chamber. The spiral passage designs are used for smaller coolant flow rates to alleviate the difficulties in maintaining proper flow velocities and dimensional clearances in the coolant passage.

Because the hydrogen coolant gas can be discharged at relatively high temperatures (1000° R and up), overall engine system performance will not be affected appreciably by the dump-coolant flow.

Film Cooling

Porous wall materials, or slots and holes provided in thrust chamber walls, can serve to introduce a coolant, a process commonly referred to as film cooling. Because of interaction between coolant film and combustion gases, as a result of heat and mass transfer, the effective thickness of the coolant film decreases in the direction of flow. In most cases, therefore, additional coolant must be injected at one or more downstream chamber stations. Figure 4-34 shows a model of the film-cooling process. The coolant is introduced through rows of holes. The fluid introduced through row "A" will cover the wall surface between "A" and "B." Fluid from row "B" will cover the surface between "B" and "C," etc. In an optimum design a flow rate from each row is provided which is just sufficient to cover the area to be cooled.

Although heat protection exclusively by film cooling has not been applied in the past for the major operational rocket engines, it is significant that in practice regenerative cooling is nearly always supplemented by some form of film cooling. In most instances, a fuel-rich gas boundary layer is created by the injection of fuel from the outermost circle of injector orifices, toward the chamber wall.

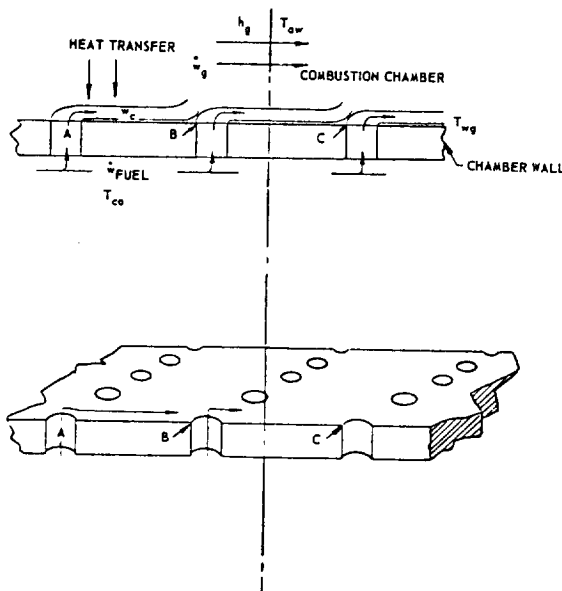


Figure 4-34.—Film-cooling model.

An important advantage of film cooling is the fact that it reduces heat transfer through the wall. Consequently, thermal stresses become less critical. This is an important consideration, as thermal stresses may establish the feasibility limits of conventional regenerative cooling.

Liquid Film Cooling

It would appear, and has been verified experimentally, that for simply reducing the heat transfer to the wall, film cooling would be more effective with the coolant injected as a liquid rather than a gas. When the coolant film is liquid, it should behave essentially as an isothermal heat sink, as it evaporates and diffuses into the free stream. However, this process results in two-phase flow, consisting of an annular liquid-coolant film and a combustion gas core. This effect introduces coolant losses which reduce the theoretical cooling potential. Disturbances in the form of capillary waves appear on the surface of the liquid film adjacent to the combustion gases and cause accelerated coolant loss.

The theoretical equation by Zucrow and Sellers can be used for design calculations of liquid-film-cooled thrust chambers.

$$\frac{G_c}{G_g} = \frac{1}{\eta_c} \cdot \frac{H}{a(1 + bC_{pvc}/C_{pg})} \quad (4-33)$$

where

G_c = film coolant weight flow rate per unit area of cooled chamber wall surface, lb/in²-sec

G_g = combustion gas weight flow rate per unit area of chamber cross section perpendicular to flow, lb/in²-sec

η_c = film cooling efficiency

H = film coolant enthalpy

$$= \frac{C_{pvc}(T_{aw} - T_{wg})}{C_{plc}(T_{wg} - T_{co}) + \Delta H_{vc}}, \text{ Btu/lb}$$

C_{plc} = average specific heat at constant pressure of the coolant in the liquid phase, Btu/lb-deg F

C_{pvc} = average specific heat at constant pressure of the coolant in the vapor phase, Btu/lb-deg F

C_{pg} = average specific heat at constant pressure of the combustion gases, Btu/lb-deg F

T_{aw} = adiabatic wall temperature of the gas, deg R

T_{wg} = gas-side wall temperature and coolant film temperature, deg R

T_{co} = coolant bulk temperature at manifold, deg R

ΔH_{vc} = heat of vaporization of coolant, Btu/lb

$a = 2V_d/V_m f$

$b = (V_g/V_d) - 1$

f = applicable friction coefficient for the two-phase flow between combustion gases and liquid film coolant

V_d = axial stream velocity of combustion gases at edge of boundary layer, ft/sec

V_m = average axial stream velocity of combustion gases, ft/sec

V_g = axial stream velocity of combustion gases at the center line of the thrust chamber, ft/sec

In practice the theoretically determined film coolant flow would be inadequate because of losses. Therefore, the film-cooling efficiency η_c is introduced to correct for this. Liquid-film-cooling efficiency values range from about 30 to 70 percent. They are determined experimentally in actual hot firings of a specific design or test model.

Hydrocarbon fuels have been found to be very effective liquid film coolants. Their effectiveness is attributed to their action as both film and deposition cooling agents. As was mentioned earlier, these fuels deposit carbon on the wall, which serves as an effective heat insulator.

Gaseous Film Cooling

With the increasing use of hydrogen, gaseous-film cooling has become important. Even if hydrogen were injected as a liquid for film-cooling purposes, the film between the combustion gases and the chamber wall would be heated within a very short distance to temperatures above the critical, after which the film would behave as a gas.

For design calculation of gaseous-film-cooled thrust chambers, the theoretical equation of Hatch and Papell can be used. This equation can be written as follows:

$$\frac{T_{aw} - T_{wg}}{T_{aw} - T_{co}} = e^{-\left(\frac{h_g}{G_c C_{pvc} \eta_c}\right)} \quad (4-34)$$

where

T_{aw} = adiabatic wall temperature of the gas, deg R

T_{wg} = maximum allowable gas side wall temperature, deg R

T_{co} = initial film-coolant temperature, deg R

e = base of natural logarithms, 2.718

h_g = gas-side heat-transfer coefficient, Btu/in²-sec-deg F

G_c = film-coolant weight flow rate per unit area of cooled chamber wall surface, lb/in²-sec

C_{pvc} = average specific heat at constant pressure of the gaseous film coolant, Btu/lb-deg F

η_c = film-cooling efficiency

The film-cooling efficiency η_c corrects for the amount of gaseous-film coolant lost into the combustion gas stream without producing the desired cooling effect. Values range from about 25 to 65 percent, depending upon coolant injection geometry and on flow conditions.

The above equation assumes that a balance exists between heat input and coolant temperature rise. The heat input is based upon the gas-side heat-transfer coefficient h_g and the difference between the adiabatic gas temperature at the wall and the coolant film temperature. The heat absorbed is proportional to the heat capacity of the coolant film from initial to final temperature values. Once equilibrium is reached, no heat is transferred to the wall (adiabatic condition) and the chamber wall surface will have achieved the film-coolant temperature corresponding to the various axial locations. Accordingly, the wall-surface temperature will range axially from the value of initial coolant temperature to a maximum allowable design wall temperature, at which point the next film-coolant injection station must be provided. It is the specific aim of film-cooled thrust chamber design to accomplish cooling with an optimum number of coolant injection stations.

Figure 4-35 shows an experimental hydrogen film-cooled thrust chamber. Cooling is provided by four film-coolant injecting rings upstream, and one downstream of the throat. Axial coolant injection, in the direction of combustion gas

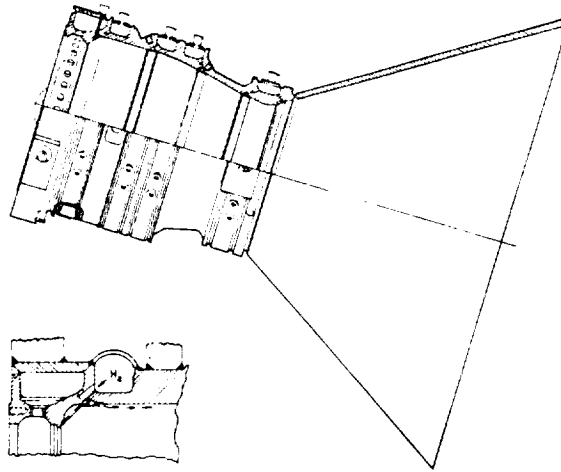


Figure 4-35.—Experimental hydrogen/oxygen, film-cooled thrust chamber.

flow, greatly improves film-cooling efficiency, whereas normal injection results in the escape, without any benefit, of large portions of the coolant into the combustion gas stream. In a typical case, the film coolant flow was approximately 3 percent of the propellant.

Sample Calculation (4-5)

For the design of the hydrogen film-cooling system for the thrust chamber of the A-3 stage engine, the following data are given at the throat section:

$$\begin{aligned} h_g &= 0.0011 \text{ Btu/in}^2\text{-sec-deg F} \\ T_{aw} &= 5240^\circ \text{ R} \\ T_{wg} &= 1900^\circ \text{ R max} \\ T_{co} &= 50^\circ \text{ R} \\ C_{pvc} &= 3.6 \text{ Btu/lb-deg F average} \end{aligned}$$

Assuming a value of 0.5 for film-cooling efficiency, determine the film-coolant weight flow rate per unit area of cooled chamber surface in the throat section.

Solution

Substitute the given data into equation (4-34):

$$\frac{5240 - 1900}{5240 - 50} = e^{-\left(\frac{0.0011}{G_c \times 3.6 \times 0.5}\right)}$$

$$1.554 = e^{\left(\frac{0.00061}{G_c}\right)}$$

$$G_c = \frac{0.00061}{\ln 1.554} = \frac{0.00061}{0.439} = 0.001392 \text{ lb/in}^2\text{-sec}$$

To calculate the heat flux for a regenerative cooling system, with added film cooling, a corrected value (T_{aw}) must be used in equation (4-10) or (4-17). This corrected adiabatic wall temperature can be determined experimentally under the specific thrust chamber operation and film-cooling conditions. As to the gas-side heat-transfer coefficient, it was found that there is practically no difference with and without film cooling. Thus, the normal gas-side heat-transfer coefficient h_g can be used in equation (4-10). Note that if a hydrocarbon fuel is used as the film coolant, the effect of carbon deposition must be taken into account (eq. 4-17).

Transpiration Cooling

Figure 4-36 shows the principle of transpiration cooling. The coolant is introduced through numerous drilled holes in the inner chamber wall. In other designs, the wall may be made of porous material. In both cases, the permeable chamber inner liner is enclosed by an outer shell (similar to fig. 4-28), forming a jacket from which the coolant emerges. For adequate design, the total coolant flow requirement and coolant weight flow rate per unit area of cooled chamber wall (lb/in²-sec) must be determined and then implemented by a practical method.

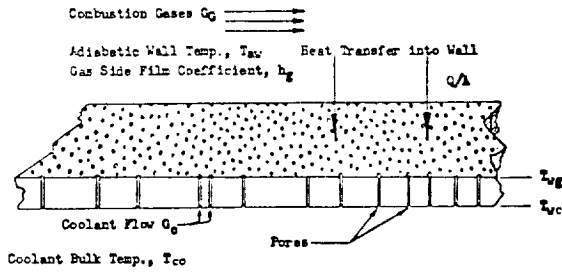


Figure 4-36.—Transpiration cooling model.

Transpiration coolant flow requirements determined from theoretical equations turn out to be significantly lower than those for film cooling. This is due to the more efficient coolant distribution. The Rannie equation for transpiration cooling can be used to calculate the theoretical coolant flow requirements:

$$\frac{T_{aw} - T_{co}}{T_{wg} - T_{co}} = \left[1 + \left\{ 1.18 (Re_b)^{0.1} - 1 \right\} \left\{ 1 - e^{-37 \left(\frac{G_c}{G_g} \right) (Re_b)^{0.1}} \right\} \right] \left[e^{37 \left(\frac{G_c}{G_g} \right) (Re_b)^{0.1} Pr_m} \right] \quad (4-35)$$

where

- T_{aw} = adiabatic wall temperature of the gas, deg R
- T_{wg} = gas-side wall temperature, deg R
- T_{co} = coolant bulk temperature, deg R (entering)
- G_c = transpiration coolant weight flow rate per unit area of cooled chamber wall surface, lb/in²-sec
- G_g = combustion gas weight flow rate per unit area of chamber cross section perpendicular to flow, lb/in²-sec
- Pr_m = mean film Prandtl number
- e = base of natural logarithms, 2.718
- Re_b = bulk combustion-gas Reynolds number

Test data from various transpiration-cooling experiments have been in good agreement with the Rannie equation. However, the equation predicts coolant flows slightly lower than those required in experiments. It is recommended that

an efficiency factor of approximately 0.85 is used for calculations.

The porous material used for the transpiration-cooled chamber walls must be selected and dimensioned for correct hydraulic resistance to render the required coolant flow rate per unit surface area. It must also be able to withstand the stresses caused by the pressure differential between coolant and combustion gases, and thermal stresses. These requirements impose certain limitations on the selection of materials and on construction methods. The mechanical design of the coolant distribution system, therefore, is an important factor for successful application of transpiration cooling.

Ablative Cooling

Ablatively cooled thrust chambers have many advantages for upper-stage applications. They are designed to meet accumulated duration requirements varying from a few seconds to many minutes. Most designs are limited to lower chamber pressure applications, 300 psia or less. When assisted by film cooling, or by throat inserts made from refractory materials, successful firings have been made up to a chamber pressure level of 1000 psia. In general, ablative chamber construction is rugged, exterior wall temperatures are held to a minimum and the cost is low.

Ablative cooling is accomplished by the pyrolysis of resins contained in the chamber wall material. The thrust chamber construction will vary with mission requirements. As shown in figure 4-37, chamber and nozzle are composed of an ablative liner, a thin layer of insulation, and a high-strength outer shell. The ablative liner is fabricated from a phenolic-resin-impregnated high-silica fabric which is wrapped in tape form on a mandrel at optimum orientation. The thickness is programed as a function of chamber station to provide adequate strength, char thickness, and minimum weight for a particular mission. A wrap of oriented phenolic-impregnated asbestos is placed on the outer (far) surface of the ablative liner as an insulator.

The high-strength outer shell is composed of layers of unidirectional glass cloth for longitudinal strength, and of circumferential-wound glass filaments for hoop strength. The glass wrap is bonded with epoxy resin. Aluminum alloy and

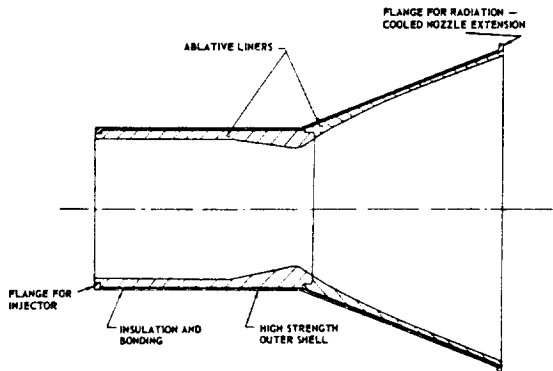


Figure 4-37.—Ablatively cooled thrust chamber.

stainless steel also are sometimes used for the outer shell. The combined thermal resistance of the ablative liner and of the insulation layer protects the outer shell and keeps it at moderate temperatures.

Figure 4-38 shows an ablatively-cooled thrust chamber fitted with a throat insert. Both 98 percent tungsten/2-percent molybdenum alloy and pyrolytic graphite have been successfully employed as insert materials. The tungsten-molybdenum alloy has given the best results. Although pyrolytic graphite has a much lower density than tungsten alloy, and therefore has a substantial weight advantage, it is vulnerable to fracture from thermal shock, making design and installation critical. The throat insert is installed with heavy graphite backups for better structural results. Insert and backups are bonded to the thrust chamber main ablative liner with epoxy adhesives. These adhesives have performed satisfactorily up to 500° F. Certain ceramic materials, such as silicon carbide, also have been used successfully as throat inserts in space engine applications.

The design of an ablative thrust chamber for a given mission depends on the accuracy of predicting the depth of char during exposure, and on the soak-back temperature variation in the insulation surrounding the charred portion of the thrust chamber wall during and after the hot firing. Test data from hot firings with various ablative thrust chambers indicate that the charring process in the combustion chamber (including throat), that is, the relation between mass pyrolyzed and heat absorbed, can be expressed by the following equation:

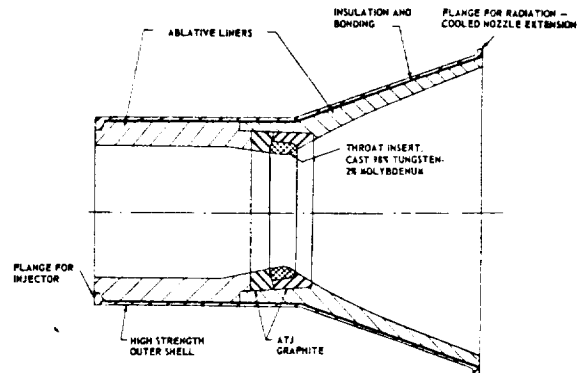


Figure 4-38.—Ablatively cooled thrust chamber with throat insert for high chamber pressure applications.

$$a = c \left[\frac{2kt}{R_r R_v C_p \rho} \ln \left(1 + \frac{R_r R_v C_p (T_{aw} - T_d)}{L_p} \right) \right]^{0.5} \left[\frac{(P_c)_{ns}}{100} \right]^{0.4} \quad (4-36)$$

where

- a = char depth, in
- c = correction factor based on experimental data for the specific design at the throat section, and on a nozzle stagnation pressure of 100 psia
- R_r = weight fraction of resin content in the ablative material
- R_v = weight fraction of pyrolyzed resin versus total resin content R_r
- C_p = heat capacity at constant pressure of pyrolysis gases, Btu/lb-deg F
- ρ = density of ablative material, lb/in³
- k = heat conductivity of char, Btu/sec-in²-deg F/in
- t = thrust chamber firing duration, sec
- L_p = latent heat of pyrolysis, Btu/lb
- T_{aw} = adiabatic wall temperature of the gas, deg F
- T_d = decomposition temperature of resin, deg F
- $(P_c)_{ns}$ = nozzle stagnation chamber pressure, psia

Results predicted by equation (4-36) have been compared with char depth data obtained from firings of Refrasil-filled phenolic chambers. They were found to agree very closely with the experimental data. However, for areas downstream of the throat, char depths were found to

be somewhat greater than predicted, and when using the equilibrium gas temperature. Temperature recovery in the boundary layer may be one cause for the discrepancy. A modified equation is used, therefore, to predict char depths in the nozzle areas:

$$a = bt^{0.5} e^{-0.0247\epsilon} \quad (4-37)$$

where

b = a constant depending upon the nature of the ablative shield (to be determined experimentally)

ϵ = nozzle expansion area ratio at the investigated section

e = base of natural logarithms, 2.718

The char-rate analysis is characterized by physical dimensions and the formation of a char layer that progresses from the heated surface toward the supporting wall. During the pyrolysis of the resin, the formation of a hard carbonaceous surface of increasing thickness is vital because it resists thermal and mechanical ablation and chemical attack. At the charring interface, which slowly travels away from the hot chamber gases, a large amount of heat energy is absorbed by pyrolysis; i.e., melting and vaporization of the bonding material. As gaseous pyrolysis products flow through and out of this char layer, they control the heat flux to the walls by their own endothermic decompositions, and by migration into the boundary layer.

No gross dimensional change occurs due to energy considerations throughout most of the thrust chamber; however, mechanical erosion is evidenced in some designs in the throat region, due to the high prevailing shear stresses. At chamber pressures below 150 psia, throat erosion is generally reduced. Throat erosion rates vary from 0.0005 to 0.00005 in/sec

The adaptation of ablative thrust chamber technology to the special field of space engines has been significantly advanced during recent years. Approaches typical for this type of engine will be discussed in chapter XI.

Sample Calculation (4-6)

The following design data are given for the ablatively cooled thrust chamber of the A-4 stage engine:

$C = 1.05$; $R_r = 0.3$; $R_v = 0.41$; $C_p = 0.38$ Btu/lb-deg F; $\rho = 0.061$ lb/in³; $k = 9.8 \times 10^{-6}$ Btu/in²-sec-deg F/in; $L_p = 686$ Btu/lb; $T_{aw} = 5060^\circ$ R; $T_d = 1460^\circ$ R; $b = 0.0335$

Determine the char thickness at the throat and combustion chamber section, and in the nozzle at station $\epsilon = 5$, after firing for the design duration of 410 seconds.

Solution

From table 3-5: $(p_c)_{ns} = 100$ psia

Substitute this and given data into equation (4-36). The char thickness at the throat and combustion section results as:

$$\begin{aligned} a &= 1.05 \left[\frac{2 \times 9.8 \times 10^{-6} \times 410}{0.3 \times 0.41 \times 0.38 \times 0.061} \right. \\ &\quad \left. \times \ln \left(1 + \frac{0.3 \times 0.41 \times 0.38 (5060 - 1460)}{686} \right) \right]^{0.5} \times (1)^{0.4} \\ &= 1.05 \times [2.82 \times \ln 1.245]^{0.5} = 0.828 \text{ in} \end{aligned}$$

Char thickness at nozzle station $\epsilon = 5$, using equation (4-37):

$$\begin{aligned} a &= bt^{0.5} e^{-0.0247\epsilon} = 0.0335 \times (410)^{0.5} \times (2.718)^{-0.0247 \times 5} \\ &= 0.0335 \times 20.248 \times (2.7182)^{\frac{1}{8.1}} \\ &= 0.599 \text{ in} \end{aligned}$$

Radiation Cooling

Cooling by radiation heat transfer is practical only for thrust chamber nozzle extensions, where pressure stresses are lowest. High metal-wall temperatures are required to attain the heat fluxes needed. Assuming negligible temperature drop through the metal and coatings, if any, the steady-state heat transfer for a radiation-cooled nozzle, as shown schematically in figure 4-39, can be expressed by the following correlation:

$$h_{gc} (T_{aw} - T_{wg}) = \epsilon \sigma T_{wg}^4 \quad (4-38)$$

where

h_{gc} = overall gas-side thermal conductance, Btu/in²-sec-deg R

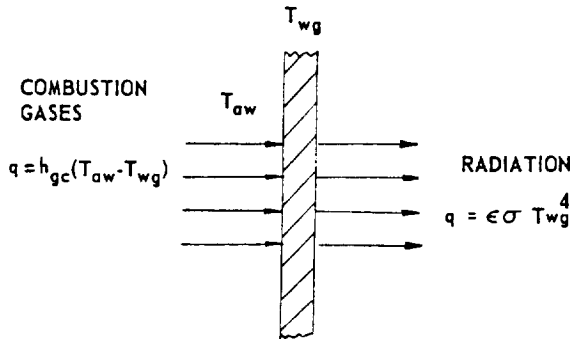


Figure 4-39.—Schematic of radiation cooling.

- T_{aw} = adiabatic wall temperature of the gas, deg R
 T_{wg} = gas-side wall temperature = bulk wall temperature, deg R
 ϵ = total emissivity of outer wall surface
 σ = Stefan-Boltzmann radiation heat transfer constant, 0.3337×10^{-14} Btu/in²-sec-(deg R)⁴

The design approach to radiation cooling is to determine a T_{wg} value which will satisfy both equation (4-38) and the structural capability of the wall material used under operational conditions.

Only alloys which possess short-time strength in the temperature range of 2600° R to 3500° R have been successfully applied to radiation cooling. A molybdenum alloy containing 0.5 percent titanium, and a 90 percent tantalum-10 percent tungsten alloy appear to have sufficient short-time strength for use at 3500° R. Because of the low emissivity of molybdenum and also for resistance against oxidation, a coating of MoSi₂ is required on both sides of the metal. Titanium alloys and other commercial alloys, such as Haynes 25, have been operated successfully at 2600° R. If a temperature capability higher than the working range of bare metals is required, insulating coatings of ceramic materials on the gas-side wall surface may be needed. Because of their brittleness and coefficient of thermal expansion relative to that of the alloys, experienced judgment is advised before using these coatings for a specific application.

Sample Calculation (4-7)

The following design data are given for the A-4 stage chamber nozzle extension at station of area ratio = 8:

$$h_{gc} = 7.1 \times 10^{-5} \text{ Btu/in}^2\text{-sec-deg R}; T_{aw} = 4900^\circ \text{R}$$

Assuming a total emissivity of 0.95 of outer wall surface, determine the bulk temperature and heat-radiated flux.

Solution

Substitute data into equation (4-37):

$$7.1 \times 10^{-5} (4900 - T_{wg}) = 0.95 \times 0.3337 \times 10^{-14} \times (T_{wg})^4$$

$$(T_{wg})^4 = 22.4 \times 10^9 \times (4900 - T_{wg})$$

$$T_{wg} = 2660^\circ \text{R}$$

$$\text{Heat flux} = 7.1 \times 10^{-5} (4900 - 2660) = 0.159 \text{ Btu/in}^2\text{-sec}$$

4.5 INJECTOR DESIGN

The function of an injector, which is located in general, at the forward end of the combustion chamber as shown in figures 4-1 and 4-2, is similar to that of the carburetor of an internal combustion engine. The injector introduces and meters the propellant flow to the combustion chamber, and atomizes and mixes the propellants for satisfactory combustion.

Design Objectives

A great number of injectors have been developed and many details of successful injector designs are now available. However, there still are no hard-and-fast rules to assure a successful design. In the past, most injectors were designed by a trial-and-error approach, with the help of previous test data. While good results have eventually been obtained, it was usually at the expense of large amounts of time and money. A more rational approach toward the design of injectors is through understanding and prediction of the chemical and physical processes that are encountered within the combustion chamber, and using this information as a basis for initial injector design. For a given propellant combination, the chemical reactions and the kinetics of stream breakup, mixing, droplet formation, and heat transfer should be studied and clearly understood, before the approach to the design of an injector is established.

There are numerous requirements to qualify a given injector for operational use. The following are the most important objectives for injector design:

1. *Combustion stability.*—In combination with a given combustion-chamber configuration and for a given propellant combination, an injector should give smooth combustion, during engine start and stop transients as well as during steady-state operation.

Depending upon the propellants and their ignition characteristics, the arrival sequence of oxidizer and fuel streams during start is of great importance. Any accumulation of unburned propellants in the combustion chamber prior to ignition must be prevented to avoid destructive chamber-pressure surges. Similarly, during engine shutoff, chamber overheating and burnout may be prevented by maintaining a fuel-rich mixture. Arrival sequences are best controlled by propellant valve timing. Furthermore, minimum feed-line and injector-manifold volumes between propellant valves and injector face will materially improve propellant sequencing during start and stop.

To prevent chamber-pressure fluctuations from affecting the propellant flows and thus from inducing combustion instability, sufficient pressure drop through injector orifices must be maintained. Effective and even mixing of the propellants will be achieved through the choice of a suitable injector impingement pattern. This will help to minimize accumulation within the combustion chamber of unburned propellants which could cause local detonations and thus trigger combustion instability. Under certain conditions, combustion instabilities of the tangential oscillation mode can be prevented by isolating local detonations by partitioning the injector face into several compartments, as shown in figure 4-40.

2. *Performance.*—Combustion performance of an injector is influenced by: propellant mass distribution; local mixture ratios; degree of mixing of injected propellants, in either the liquid or the gaseous phase, or both; droplet atomization and vaporization; rate of heat input; and chemical reaction rates. These are predominantly a function of suitable manifolding and proper selection of injector-hole patterns. The more

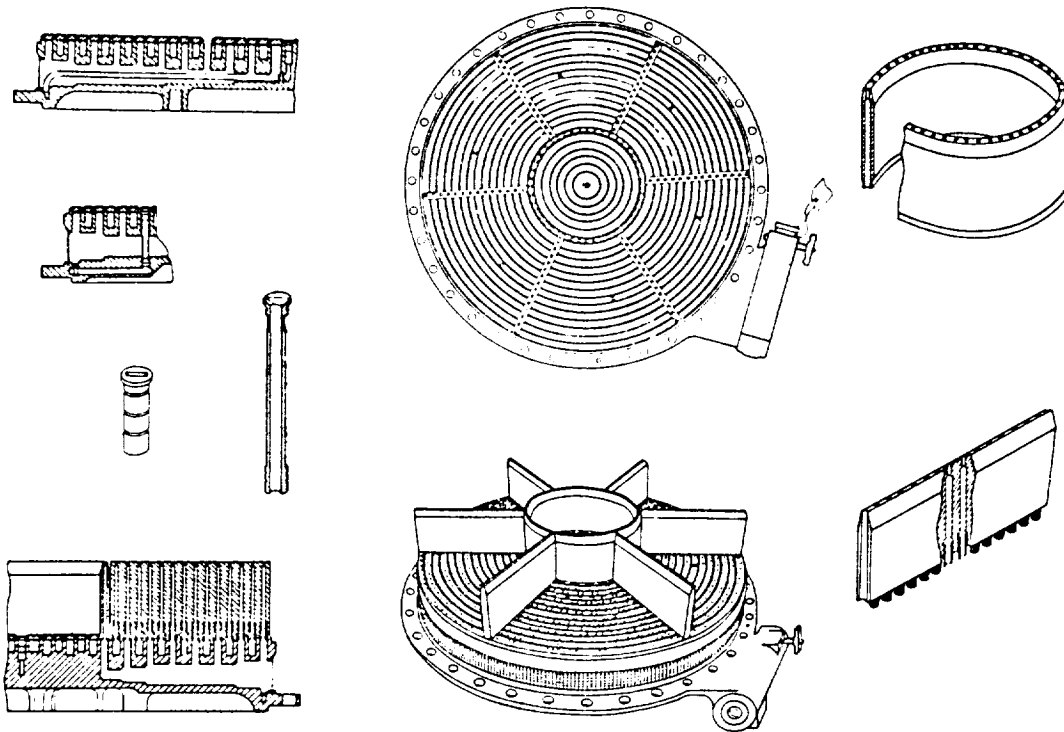


Figure 4-40.—Baffled injector.

through the mixing and uniform the distribution of the oxidizer relative to the fuel, produced by the injector, the more rapidly will the combustion products reach the equilibrium composition necessary for optimum performance. Although turbulence induced by the combustion probably contributes a major portion of the energy required for gas-phase mixing, thorough premixing of the liquid propellants must be accomplished by the injector if maximum performance is to be achieved. Furthermore, reaction between certain specific propellant combinations such as hypergolic propellants cannot reliably be initiated and maintained without it, since the energy released by liquid-phase reactions supplements the kinetic energy available for the process of atomization through combustion-gas evolution. In addition, the heat release from liquid-phase reaction accelerates the process of vaporization.

Experience has shown that for a given injection velocity, propellant-droplet size is reduced with decreasing injector-orifice size. Smaller droplet size, in turn, results in a higher overall vaporization rate, as a function of increased total droplet surface area. This is true whether the heat of vaporization is supplied internally via liquid phase reaction or externally by heat transfer from the hot gaseous combustion products. Consequently, injector designs with the largest practical number of injection elements can be expected to be the most efficient ones in a given combustion chamber volume.

3. *Structural integrity.*—An injector should be able to withstand the maximum loads incurred during all phases of engine operation. Sufficient cooling must be provided to prevent the injector face or any other portion from overheating.

4. *Hydraulic qualities.*—The holes or orifices of the injector must be designed to effect predetermined pressure drops at specific flow rates, and to atomize the propellants properly. A low injector pressure drop is desirable from the standpoint of overall engine-system performance. However, minimum pressure drop is determined from combustion-stability considerations.

5. *Combustion chamber heat protection.*—An injector should be designed to avoid formation of hot spots or streaks on the combustion chamber wall. Complete mixing of the propellants will prevent oxidizer-rich peak temperature zones from forming, although this may not prevent

streaks of high mixture ratio (O/F) from occasionally reaching the chamber wall. To offset this, a special set of fuel holes is often provided at the periphery of the injector, close to the chamber wall. Excess fuel along the chamber wall is thus provided which tends to lower the O/F mixture ratio of any errant streak. It also assists in cooling the chamber wall.

6. *Special requirements.*—Certain engine systems are required to operate at off-nominal conditions, such as at lower thrust levels during throttling, or other than nominal mixture ratios as a result of propellant-utilization control. In these cases, injectors must be capable of operating reliably under modified as well as rated conditions.

Injector Configurations

A typical injector design construction and propellant-distribution method is illustrated in figure 4-2. Different distribution methods are shown in figures 4-41 and 4-42. The injector in figure 4-42 uses an integral faceplate. This plate is secured to the main injector body by brazing it at the periphery and at posts which are an integral part of the main body. A fuel compartment is located immediately behind the faceplate, and fed from an inlet passage. The oxidizer compartment is separated from the fuel by a partition. The fuel is injected through orifices drilled in the faceplate, while the oxidizer is injected through orifices drilled in the posts.

The injector construction for a typical liquid-bipropellant gas generator is illustrated in figure 4-43. The copper injector body is secured to the stainless-steel outer shell by brazing. The oxidizer inlet forms an integral part of the injector body. Fuel is supplied through a manifold in the outer shell. In this injector, 2 fuel streams impinge on each oxidizer stream, producing a total of 44 impingement points.

A variety of injector patterns have been designed to satisfy the needs of various propellant combinations. In most cases, for good mixing the injected streams are made to impinge at a predetermined point. The impingement point should be as close to the injector face as heat-transfer conditions permit. The arrangement in which all impinging points are the same distance from the injector face is called uniplanar

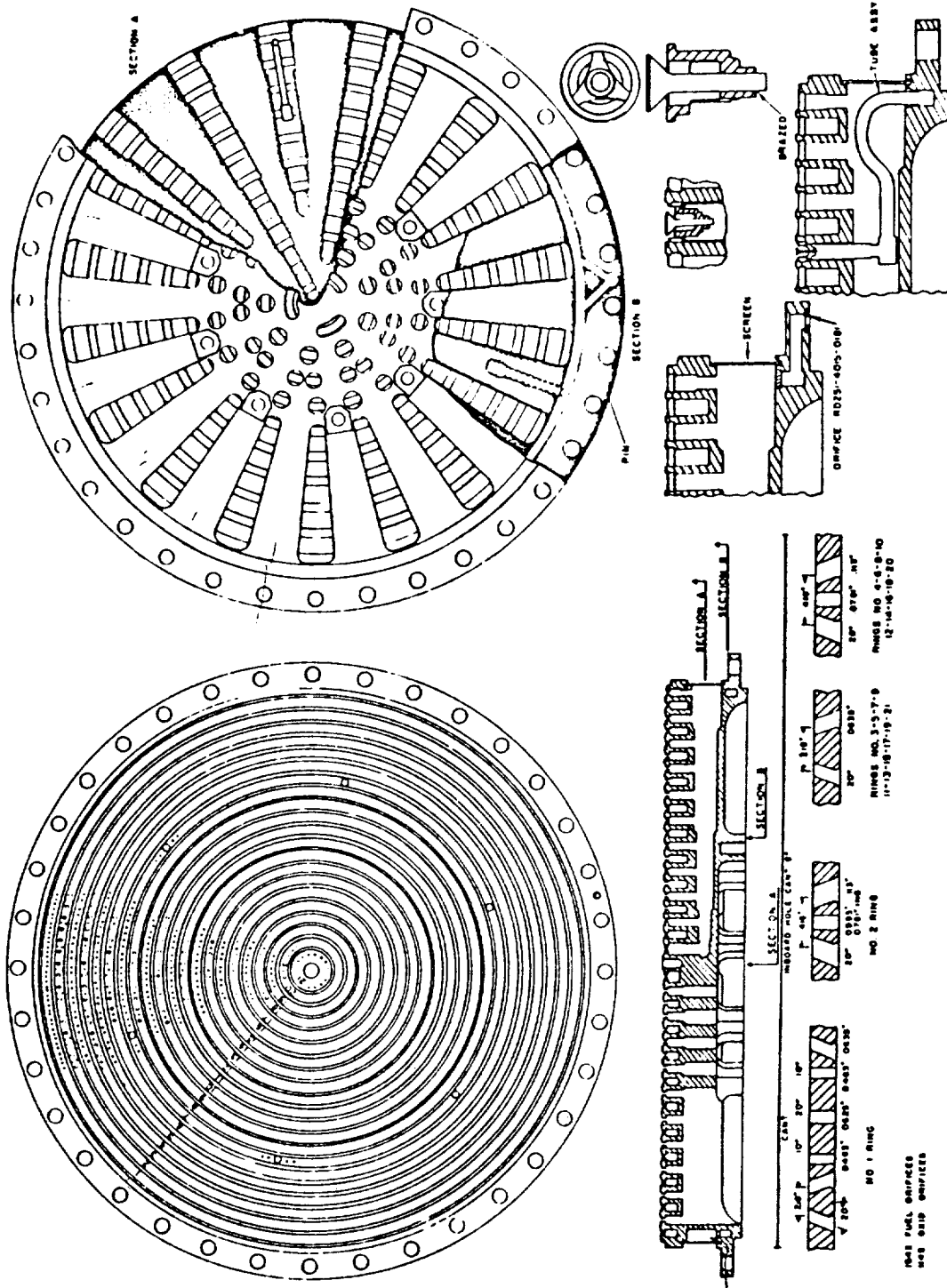


Figure 4-41.—Concentric ring injector.

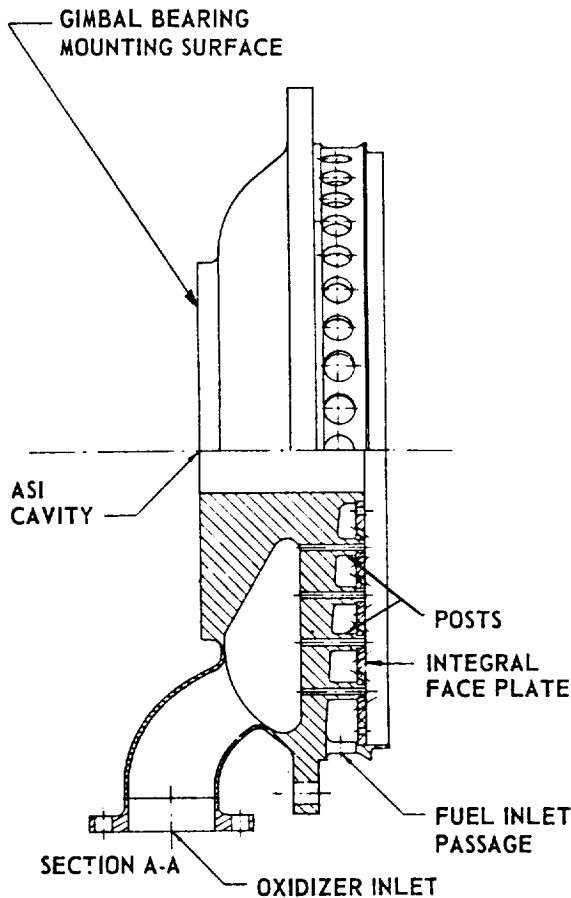


Figure 4-42.—Integral face plate injector.

impingement. If two or more different impinging-point distances are used (fig. 4-44), the arrangement is called biplanar or multiplanar impingement. Numerous tests have been conducted to determine impingement-angle and distance effects. Large included angles will enhance stability, but can result in some of the propellants splashing back on the injector face, which can cause burnouts. Close spacing of the impinging holes in a pair has similar advantages and disadvantages, as has increased spacing between pairs. The satisfactory design value for the included angle is usually found to be between 20° and 45° . The injector face can be further protected against overheating by circulating the propellants on the back side of the faceplate or by introducing film coolant (propellant) on the surface. Some of the impingement patterns used are described below:

1. *Showerhead* (fig. 4-44a).—This pattern em-

plains nonimpinging oxidizer and fuel streams which emerge normal to the injector face. It relies entirely on combustion chamber turbulence for mixing. While being the simplest to fabricate, the showerhead injector exhibits poor performance in most applications, with the exception of certain cryogenic propellant combinations.

2. *Doublet* (fig. 4-44b).—In this design, oxidizer and fuel jets are made to impinge in pairs. Thus good liquid-phase mixing and atomization is obtained. One of the disadvantages of this doublet arrangement is that even if the injector holes have been accurately drilled, the resultant angle of momentum vector, or beta angle, β , will vary with mixture ratio, particularly if a large impinging angle is used. This variation can adversely affect combustion performance and chamber-wall heat transfer. The doublet design is frequently used in systems using liquid oxygen.

3. *Triplet* (fig. 4-44c).—Two streams of one propellant impinging symmetrically on one stream of the other propellant will eliminate the change of vector angle β , as a result of mixture-ratio variations. This arrangement also provides intimate mixing. Application and propellant combination will determine whether two oxidizer jets will impinge on one fuel jet, or vice versa. Injectors using this triplet pattern have given high combustion performance. These injectors have been widely used for various propellant combinations.

4. *Quintuplet* (fig. 4-44d).—Four streams of one propellant impinging on one stream of the other propellant in a symmetrical quintuplet pattern provide excellent mixing and performance. This design has been applied for various propellant combinations.

5. *Self-impinging* (fig. 4-45a).—This pattern, also known as a like-on-like impingement, generally employs self-impinging pairs of fuel and oxidizer. Mixing is accomplished in the combustion chamber by volatilization of the propellants and by turbulence. This design usually provides good inherent combustion stability, at a moderate performance level. Applications have been successful for both cryogenic and storable hypergolic propellant combinations. A modification of this design provides for secondary impingement of the two propellants following self-impingement.

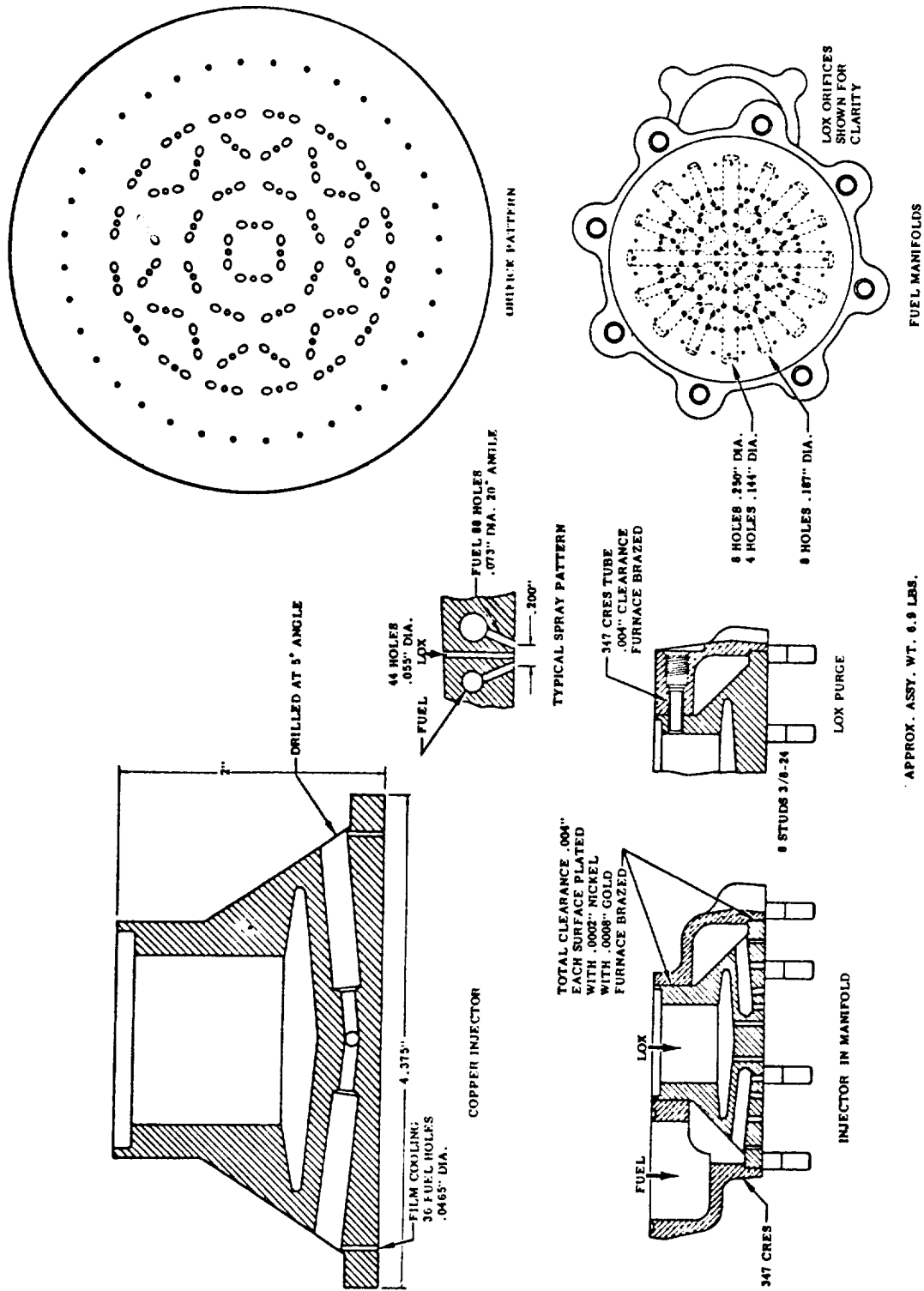


Figure 4-43. — Bipropellant gas generator injector.

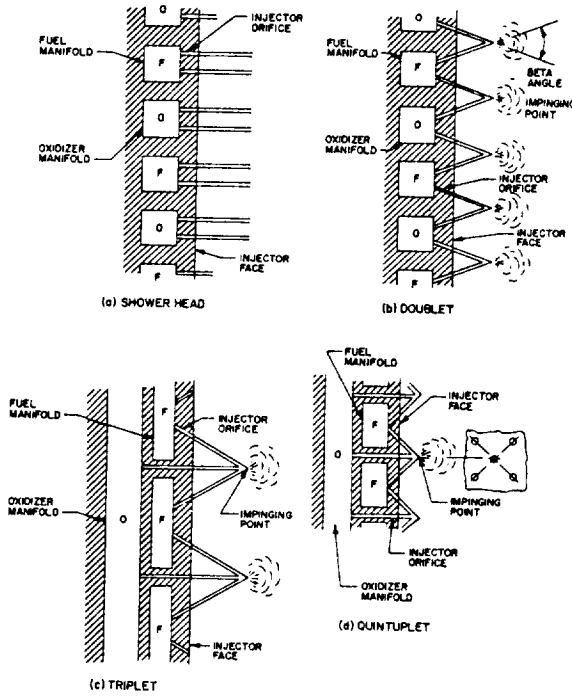


Figure 4-44.—Injector impinging patterns.

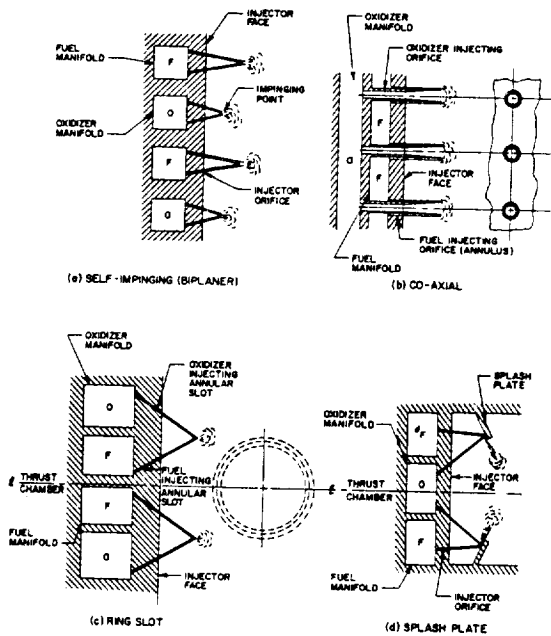


Figure 4-45.—Injector impinging patterns.

6. *Coaxial* (fig. 4-45b).—This injector employs two concentric tubes for the two propellants, which are injected coaxially.

7. *Ring slot* (fig. 4-45c).—The ring-slot injector employs concentric pairs of annular slots which eject the propellants as conical sheets. The slots are so arranged that fuel and oxidizer sheets impinge much in the same manner as in the doublet-type injector.

8. *Splash plates* (fig. 4-45d).—This injector is designed for good propellant mixing while the propellants are still in the liquid state. For this purpose, injected propellants are deflected by the splash plates. The plates will be kept cool by the impinging liquid propellants which do not ignite until they have left the plate.

9. *Premix*.—Figure 4-46 shows a typical premix-type injector. Fuel and oxidizer are injected radially into the premixing chamber, where they are intimately mixed before entering the combustion chamber by a gas jet introduced tangentially at the chamber end. The length and diameter of the premixing chamber with relation to the mass flow of propellants is critical, as is the reaction time of the propellants.

10. *Throttleable injector*.—Certain requirements for space vehicle missions, such as orbit corrections, rendezvous and docking maneuvers, and lunar soft landings, demand engine systems capable of thrust control. Figure 4-47a shows a typical throttleable injector with variable injection-slot areas. This is a very effective means of controlling the propellant flows and injector pressure drops at various engine thrust levels. The addition of moving parts, however, causes design complications. Another approach to a throttleable injection system is the "aeration method," as shown in figure 4-47b.¹ An inert gas is introduced into the injector propellant manifold for reduced thrust levels. Through variation of the propellant/gas mixture ratio, the effective density of the propellants can be varied over a wide range to achieve any desired thrust level without affecting combustion stability. The gas can be supplied by the same source used to pressurize the propellant tanks. This method has increased the range of rocket-engine throttling up to a ratio of 100 to 1.

Design Calculations

For the design of injectors, various parameters, such as injector pressure drop, impingement

¹Astronautics magazine, December 1962, pp. 36-37.

and resultant vector angle relationship, and structural loads, can be calculated with reasonable accuracy.

Injection Velocity

The propellant (oxidizer or fuel) injection velocity V (in/sec) can be calculated from the basic relation:

$$V = \frac{\dot{w}}{A\rho} \quad (4-39)$$

where \dot{w} is the propellant weight flow rate, lb/sec; A is the calculated injector orifice area, in²; and ρ is the propellant density, lb/in³.

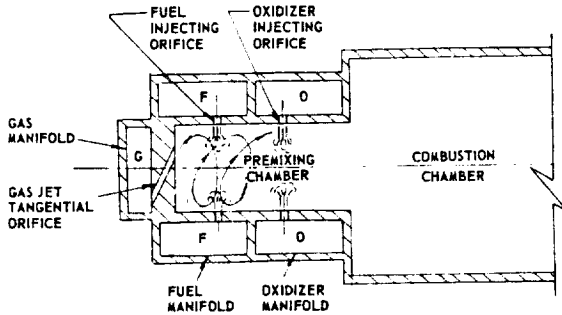


Figure 4-46.—Premixing type injector.

Injection Pressure Drop

The injection pressure drop ΔP_i (lb/in²) can be calculated as

$$\Delta P_i = \frac{\rho}{2g} \left(\frac{V}{C_d} \right)^2 = \frac{1}{2g\rho} \left(\frac{\dot{w}}{C_d A} \right)^2 \quad (4-40)$$

where g is the gravitational constant, in/sec²; C_d is a dimensionless discharge (velocity and jet contraction) coefficient which is a function of injector orifice configuration.

The value of this coefficient ranges from 0.5 to 0.92 and can be determined accurately by experiment (water flow tests). Injector orifices with well-rounded entrance and smooth bore give high values of the discharge coefficient. For a given injection velocity, a higher value of discharge coefficient gives a lower injection pressure drop. The rule-of-thumb design value for injector pressure drop varies from 15 to 20 percent of the chamber-nozzle stagnation pressure.

Resultant Angle of Impinging Streams

The angle between the thrust chamber axis and the resultant momentum vector of a pair of impinging streams is defined as the beta angle, β . By definition when the vector is directed toward the chamber wall, the beta angle is positive, and when the vector is directed toward the

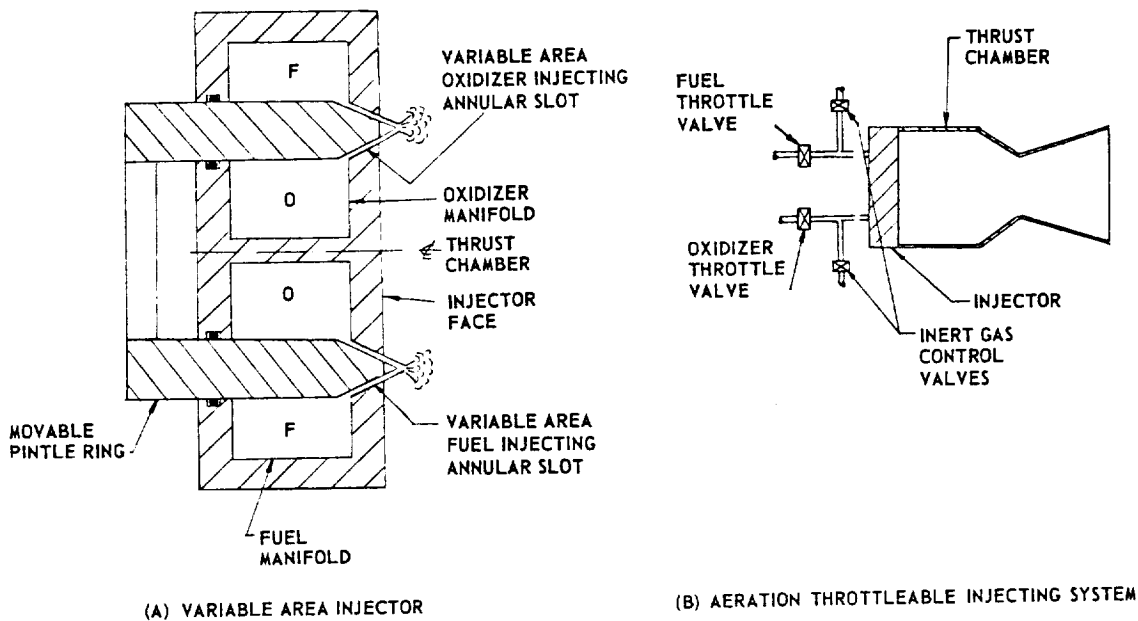


Figure 4-47.—Throttleable injecting methods.

central axis of the thrust chamber, the beta angle is negative. With a hypergolic-type propellant combination, a positive beta angle (2° to 5°) tends to increase the combustion performance by causing recirculation and better mixing of the liquid propellants along the chamber wall. However, in a cryogenic propellant combination, where gaseous mixing is predominant, the combustion performance will not be noticeably affected by the beta angle. A negative beta angle should be used in this case to avoid the possibility of hot streaks on the chamber wall caused by excessive heat transfer.

The beta angle may be readily calculated, from the principle of conservation of momentum:

$$\tan \beta = \frac{\dot{w}_1 V_1 \sin \alpha_1 - \dot{w}_2 V_2 \sin \alpha_2}{\dot{w}_1 V_1 \cos \alpha_1 + \dot{w}_2 V_2 \cos \alpha_2} \quad (4-41)$$

For the impinging streams shown in figure 4-48, α_1 and α_2 are the respective angles between the thrust chamber axis and the streams; \dot{w}_1 and \dot{w}_2 are the weight flow rates; and V_1 and V_2 are the injection velocities.

Injection Momentum Ratio

The injection momentum ratio can be defined by the expression

$$R_m = \frac{\dot{w}_o V_o}{\dot{w}_f V_f} \quad (4-42)$$

where \dot{w}_o and \dot{w}_f are weight flow rates, and V_o and V_f are injection velocities for oxidizer and fuel. The injection momentum ratio is a useful injector design parameter for the prediction of combustion stability and performance of certain propellant combinations. In the design of oxygen-hydrogen injectors, the value of the momentum ratio varies from 1.5 to 3.5 for liquid hydrogen injection, and from 0.5 to 0.9 for gaseous hydrogen injection.

Structural Loads

The main loads to be considered in the structural design of injectors result from propellant pressures behind the injector face, and in the manifolds. During steady-state main-stage operation, the pressure load on the injector face is equal to the injector pressure drop:

$$P_f = \Delta P_i \quad (4-43)$$

The pressure load in the injector manifolds is equal to the sum of the injector-end chamber pressure and the injector pressure drop:

$$P_m = (P_c)_i + \Delta P_i \quad (4-44)$$

where P_f is the pressure load on the injector face, P_m is the pressure load in the manifold; ΔP_i is the injector pressure drop; and $(P_c)_i$ is the injector-end chamber pressure.

During start transients, however, maximum pressure loads on the injector may be substantially higher than during steady state. When the propellant valves are opened rapidly, propellants rushing into the empty injector passages can cause severe hydraulic ram. This pressure load can be estimated empirically as

$$P_f = P_m = 4 P_p \quad (4-45)$$

where P_p is the propellant pressure at time of valve opening.

Sample Calculation (4-8)

Using data given in tables 3-2 and 3-3, determine the injector orifice sizes, injection velocities and momentum ratios for the A-1 and A-2 engines.

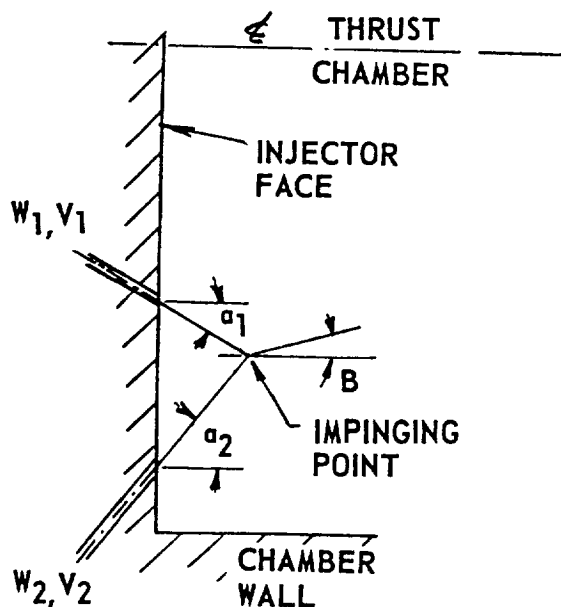


Figure 4-48.—Resultant angle of impinging streams.

Solution(a) A-1 Engine

Thrust chamber propellant flow rates are 1941 lb/sec (oxidizer) and 827 lb/sec (fuel); propellant densities are 71.38 lb/ft³ (oxidizer) and 50.45 lb/ft³ (fuel); injector pressure drops are 200 psi for both propellants. Based on component test results an injector orifice discharge coefficient C_d of 0.75 is used for both sides. Substituting it into equation (4-40), and converting feet to inches:

For the oxidizer side:

$$200 = \frac{1}{2 \times 32.2 \times 12 \times 71.38 \times \frac{1}{1728}} \left(\frac{1941}{0.75 \times A_o} \right)^2$$

Total oxidizer injector orifice area: $A_o = 32.4 \text{ in}^2$

For the fuel side:

$$200 = \frac{1}{2 \times 32.2 \times 12 \times 50.45 \times \frac{1}{1728}} \left(\frac{827}{0.75 \times A_f} \right)^2$$

Total fuel injector orifice area: $A_f = 16.4 \text{ in}^2$

An injector pattern of 700 pairs of self-impinging streams is used for both oxidizer and fuel. The following orifice areas and diameters result:

$$a_o = \frac{32.4}{1400} = 0.0232 \text{ in}^2 \quad d_o = 0.172 \text{ in}$$

$$a_f = \frac{16.4}{1400} = 0.0117 \text{ in}^2 \quad d_f = 0.122 \text{ in}$$

From equation (4-39), and using orifice areas obtained above for available ΔP and C_d , mean injection velocities are determined:

For the oxidizer:

$$V_o = \frac{\dot{w}_o}{A_o \rho_o} = \frac{1941}{32.4 \times \frac{71.38}{1728}} = 1452 \text{ in/sec or } 121 \text{ ft/sec}$$

For the fuel:

$$V_f = \frac{\dot{w}_f}{A_f \rho_f} = \frac{827}{16.4 \times \frac{50.45}{1728}} = 1728 \text{ in/sec or } 144 \text{ ft/sec}$$

In support of the injector development engineer, who may wish to compare with earlier test data, the injection momentum ratio is determined, using equation (4-42):

$$R_m = \frac{121 \times 1941}{144 \times 827} = 1.97$$

(b) A-2 Engine

From table 3-3, the propellant flow rates for the thrust chamber are 285.2 lb/sec (oxidizer) and 54.5 lb/sec (fuel); the propellant densities are 71.38 lb/ft³ (oxidizer) and 0.72 lb/ft³ (fuel); gaseous hydrogen at 180° R; the injector pressure drops are 160 psi (oxidizer) and 60 psi (fuel). With the coaxial injecting pattern (fig. 4-45b), experimental tests give a value of 0.62 for the oxidizer-side discharge coefficient and a value of 0.9 for the fuel side. Substitute these into equation (4-40).

For the oxidizer side:

$$160 = \frac{1}{2 \times 32.2 \times 12 \times 71.38 \times \frac{1}{1728}} \left(\frac{285.2}{0.62 \times A_o} \right)^2$$

Total injector oxidizer orifice area: $A_o = 6.43 \text{ in}^2$

For the fuel side:

$$60 = \frac{1}{2 \times 32.2 \times 12 \times 0.72 \times \frac{1}{1728}} \left(\frac{54.5}{0.9 \times A_f} \right)^2$$

Total injector fuel orifice area: $A_f = 13.79 \text{ in}^2$

Use a total of 300 coaxial elements for the injector. The individual orifice areas and diameters will be

$$a_o = \frac{6.43}{300} = 0.0214 \text{ in}^2 \quad d_o = 0.165$$

$$a_f = \frac{13.79}{300} = 0.0459 \text{ in}^2$$

Use a tube inner wall thickness of 0.025 inch. The diameters for the annular fuel orifice will be

$$d_{f_1} = d_o + 2 \times 0.025 = 0.215 \text{ in}$$

$$d_{f_2} = \sqrt{\left(\frac{4}{\pi} a_f + d_{f_1}^2 \right)} = 0.323 \text{ in}$$

From equation (4-39), the injecting velocities are

For the oxidizer:

$$V_o = \frac{\dot{w}_o}{A_o \rho_o} = \frac{285.2}{6.41 \times \frac{71.38}{1728}} = 1076 \text{ in/sec or } 89.6 \text{ ft/sec}$$

For the fuel:

$$V_f = \frac{\dot{w}_f}{A_f \rho_f} = \frac{54.5}{13.79 \times \frac{0.72}{1728}} = 9500 \text{ in/sec or } 790 \text{ ft/sec}$$

From equation (4-42), the injection momentum ratio

$$R_m = \frac{285.2 \times 89.6}{54.5 \times 790} = 0.593$$

Experimental Evaluation of Injector Designs

The design of an injector can be improved through experimental testing. Three types of tests are usually employed: hydrostatic pressure, water flow, and hot firing. The hydrostatic pressure tests are used to determine whether the injector structure will withstand the required pressure loads. The water flow tests are used to evaluate the following design characteristics:

1. *Effective injector pressure drop.*—The data from the water-flow tests can be used to determine the orifice-discharge coefficient and to predict the injector pressure drop for the design propellant, with corrections for density and viscosity.

2. *Injection pattern.*—Injection pattern and impingement can be observed, and faulty operation can be detected and corrected.

3. *Atomization.*—Water-flow tests at velocities corresponding to those employed in actual service indicate the quality of atomization to be expected with the actual propellants.

The true injector operational characteristics, such as performance, combustion stability, and heat-transfer characteristics for main-stage conditions, as well as start-and-stop transients, can only be fully evaluated by hot firing tests, in a thrust chamber of representative design or a "workhorse" equivalent.

It is often beneficial if during the hot-firing tests of a given injector configuration, certain operational parameters such as injector pressure drops, thrust chamber shape, and L^* can be changed to determine the effects on performance and stability. In such an experimental evaluation program injector, orifice hole patterns can be redrilled or holes plugged, until an optimum configuration is obtained.

Heat-transfer characteristics are an important factor when evaluating an injector design. Temperature-measuring instruments embedded in chamber walls and injector face are required to measure heat-transfer rates and to detect local hot spots. Instrumentation for measuring propellant flows, chamber pressure, and combustion vibration characteristics are similarly important for determining the true levels of injector performance and stability.

4.6 GAS-GENERATING DEVICES

In liquid propellant rocket engine systems, gases are required to power the propellant feed systems and other subsystems. Bottled compressed gases such as helium can be employed for these purposes; however, the use of higher temperature gases generated by suitable devices gives much higher overall system performance. Gases at temperatures ranging from 400° to 1000° F have been generated for pressurizing propellant tanks. Gases in the range from 1200° to 1700° F are used to drive gas turbines for pump-fed systems. Where ever possible, the engine system primary propellants are used for gas-generating purposes in the interests of overall system simplicity. However, for certain applications, such as for a pressurized gas-fed system or for starting a turbopump-fed system, high-pressure propellants other than those tapped off the primary system are required to supply the gas-generating systems.

Most operational engine systems use special devices for gas generation. However, tapping hot gases from the main chamber has shown promise for certain applications. The following is a list of design objectives for operational gas generators:

- (1) Ability to produce gases safely, with required properties (temperature, pressure,

- nonexplosive) in a compact unit, at the required flow rate.
- (2) Ability to start and stop smoothly, without abrupt temperature surges, pressure oscillations, or overflow of unburned propellants.
 - (3) Ability to operate over a wide range of propellant flow rates and (in the case of bipropellants) mixture ratios, and to respond closely to the control system.
 - (4) Ability to maintain safe shutdown without complicated purging and draining systems.
 - (5) Ability to restart safely (restartable engine systems only).

Additional design requirements depend on the particular engine system involved.

Gas generators can be classified according to the propellants employed:

- (1) Solid propellant systems
- (2) Liquid monopropellant systems
- (3) Liquid bipropellant systems.

Solid Propellant Gas Generators

Solid propellant gas generators are applied to liquid propellant engine systems for limited-duration applications only, such as for turbine spinners for engine start, or as pressurants for

short-duration pressure-fed systems. The temperature of the gases generated by solid propellants is generally in excess of 2000° F and is not suitable for uncooled components over extended durations. Diluents can be used with a loss of basic simplicity.

Figure 4-49 shows the typical design of an operational solid-propellant gas generator used to supply power to the turbine for engine start. It is built in the form of a cartridge that bolts to a flange at the liquid bipropellant gas generator (shown in fig. 4-51). The particular cartridge shown is a disposable type that cannot be reloaded and reused. Upon an engine start signal, two initiators or igniters set off solid propellant combustion.

Twenty milliseconds after start, the solid grain produces a gas-flow rate of approximately 4.68 pounds per second. It will maintain this flow rate for approximately 1.0 second. This gas generator operates at 2500° F and at a chamber pressure of 1000 psia. The product gas renders an approximate characteristic velocity of 4000 ft/sec. A burst diaphragm located just upstream of the gas generator orifice is used to seal the unit during storage. It is ruptured by the increased gas pressure at start. Body and end cap are made of 4130 steel.

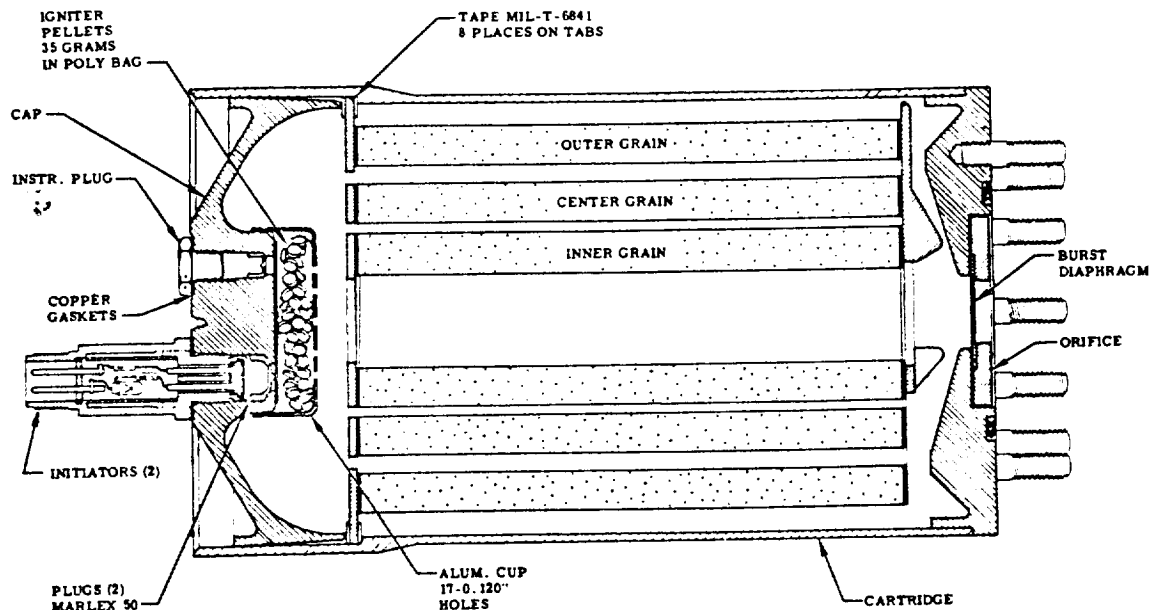


Figure 4-49.—Disposable solid propellant gas generator (SPGG).

Solid propellants burn uniformly at the exposed surfaces at a rate which is primarily a function of the temperature and the pressure of the surrounding gases. The correlation for a given propellant can be expressed as

$$R = k_1 \left(\frac{P_c}{1000} \right)^n \quad (4-46)$$

where

- R = propellant linear burning rate, in/sec
- k_1 = constant representing the linear burning rate of a given propellant, at a given initial temperature and a chamber pressure of 1000 psia
- P_c = chamber pressure, psia
- n = constant allowing for the sensitivity of the propellant burning rate to changes in pressure, at a given temperature.

The weight flow rate of a solid propellant gas generator can be calculated by

$$\dot{w}_g = A_b R \rho_p \quad (4-47)$$

where

- \dot{w}_g = weight flow rate through gas generator, lb/sec
- A_b = burning area, in²
- ρ_p = propellant density, lb/in³

It can be seen that a solid propellant gas generator of constant flow requires a propellant grain design which assures constant burning area. The correlation between P_c , A_b , and gas generator orifice area can be expressed as

$$P_c = k_2 \left(\frac{A_b}{A_0} \right)^{\frac{1}{1-n}} \quad (4-48)$$

where

- A_0 = gas generator orifice area, in²
- k_2 = constant characteristic for a given propellant at a given temperature.

Liquid Monopropellant Gas Generators

Monopropellants such as hydrogen peroxide (H₂O₂) and hydrazine (N₂H₄) have been used as gas generants in many applications. They permit a simple generator system and do not require mixture-ratio adjustments. The advantage of

these systems is that they are relatively easy to control and that the gases are generated at predictable temperatures. However, unless the monopropellant is also employed as one of the engine system main propellants, the monopropellant gas generator system introduces a third propellant often requiring special handling and tankage.

Figure 4-50 shows the schematic of a typical monopropellant gas generator using 90 percent hydrogen peroxide. The catalytic screen pack or bed consists of alternate layers of stainless-steel mesh and silver-plated brass wire screens secured by perforated end plates or grids, which are applied with a preload of approximately 800-1000 pounds per square inch of bed cross-sectional area. The length of the catalytic bed generally ranges from 2 to 3 inches. The allowable design throughput, that is, propellant flow rate per unit cross-sectional area of catalytic bed, is about 0.4 lb/in²-sec. The propellant pressure drop across the bed can be approximated by

$$\Delta P_b = \frac{C_1 G_b^{1.95}}{P_c^{0.9}} + C_2 t \quad (4-49)$$

where

- ΔP_b = pressure drop through the catalytic bed, psi
- G_b = throughput, lb/in²-sec
- P_c = gas generator chamber pressure at the end of the catalytic bed, psia
- t = accumulated running time, sec
- C_1, C_2 = design constants determined experimentally for a given bed configuration.

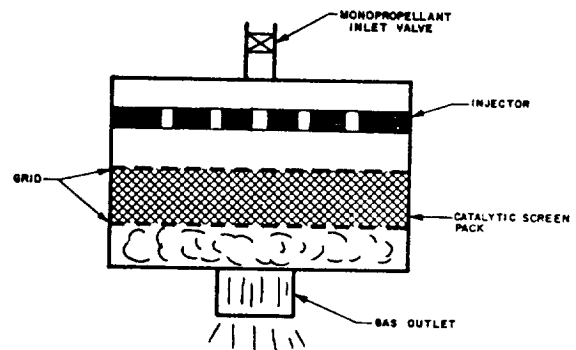


Figure 4-50.—Schematic of monopropellant gas generator.

Sample Calculation (4-9)

A hydrogen peroxide monopropellant gas generator attached directly to the inlet flange of a turbine has the following design data: Turbine inlet pressure, 340 psia; total turbine nozzle throat area, 0.776 in². Assume a c^* value of 3080 ft/sec for 90 percent H₂O₂ and catalytic bed design constants $C_1 = 7.2 \times 10^4$ and $C_2 = 0.021$ psi/sec. Determine the gas generator propellant flow rate \dot{w}_g , catalytic bed area, and pressure drop after 480 seconds of accumulated running time.

Solution

Gas generator pressure = turbine inlet pressure = 340 psia. Equivalent gas generator throat area = total turbine nozzle throat area = 0.776 in². Substitute into equation (1-32):

$$3080 = \frac{340 \times 0.776 \times 32.2}{\dot{w}_g}$$

$$\text{Propellant flow rate } \dot{w}_g = 2.76 \text{ lb/sec}$$

Use a design value for catalytic bed throughput, G_b , of 0.4 lb/in²-sec

$$\text{Catalytic bed area} = \frac{2.76}{0.4} = 6.9 \text{ in}^2$$

Substitute given data into equation (4-49):

$$\begin{aligned} \text{Bed pressure drop } \Delta P_b &= \frac{7.2 \times 10^4 \times (0.4)^{1.95}}{(340)^{0.9}} \\ &\quad + 0.021 \times 480 \\ &= 63.5 + 10 = 73.5 \text{ psi} \end{aligned}$$

Liquid Bipropellant Gas Generators

This gas-generating system is used more widely in liquid rocket engine systems than any other, since it makes use of the primary rocket engine propellants. Bipropellant gas generators react in the same manner as the main thrust chamber, except that the oxidizer-fuel-mixture ratio will be adjusted to yield the desired gas temperatures and chemical properties. The gases generated may be either fuel rich or oxi-

dizer rich, depending on the propellant combination. Oxidizer-rich gases tend to accelerate erosion of structural members, while fuel-rich gases continue to burn with ambient air after discharge, requiring special measures to prevent damage.

Figure 4-51 and table 4-2 describe a typical liquid bipropellant gas generator system. It is designed to produce hot gases using primary engine propellants (LO₂/RP-1) for driving the turbine of a pump-fed system. The control system consists of two normally closed, linked poppet valves that control the flow of propellants to the gas generator injector. The valve assembly includes an oxidizer strainer, oxidizer poppet, fuel poppet, timing orifice, actuating piston, and valve main body. The valve assembly is actuated by gas pressure which forces the piston on the fuel side down to open the fuel poppet. A yoke integral with the piston actuates the oxidizer poppet. The valve design, through a combination of manifold volumes and LOX poppet adjustment, effects a slight oxidizer lead to prevent detonations, and a fuel-rich cutoff to eliminate the possibility of turbine burning. The propellants flow through the poppets to the injector and into the gas generator combustor, are mixed, and burn within the inner chamber and combustor body. Ignition of the propellants is accomplished by two pyrotechnic igniters. A gas duct with two flanges opposite to each other is located at the end of the combustor body. These flanges connect with the solid propellant gas generator turbine spinner and the turbine inlet.

The basic design parameters for bipropellant gas generators are similar to those for thrust chambers. The total throat area of the turbine nozzles may be considered to be the equivalent throat area of the gas generator combustion chamber. In calculating combustion chamber characteristic length L^* , the volume between injector and turbine nozzle throats is used, with a correction factor allowing for the specific design configuration. Because of temperature limitations of the turbine construction materials, gas generators are rarely operated at gas temperatures higher than 1800° F. In most designs no cooling is provided for the combustion-chamber wall and other surfaces exposed to the hot gases.

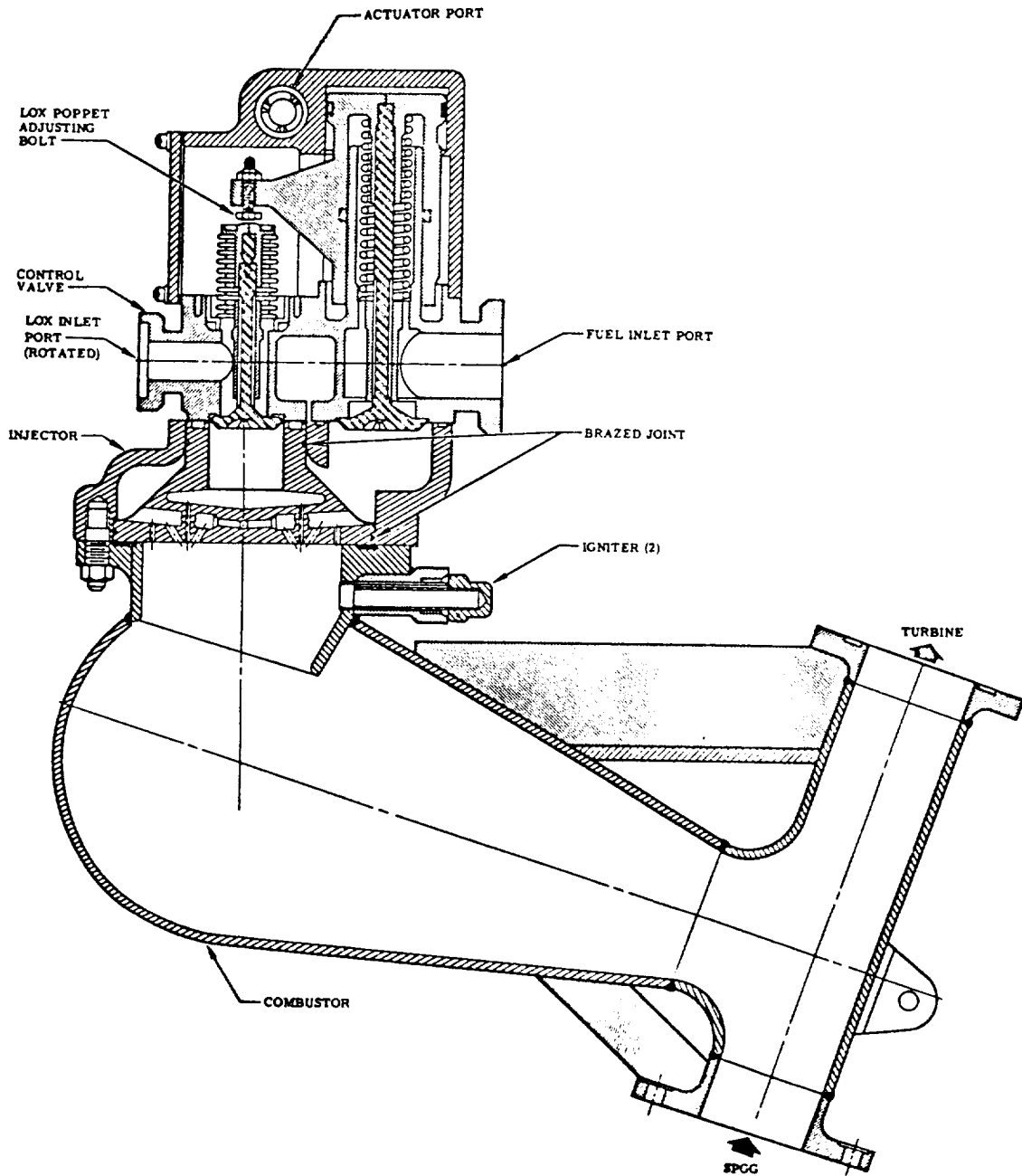


Figure 4-51.—Liquid bipropellant gas generator.

The maximum available energy per pound of gas generator propellants is obtained when the products of combustion are expanded isentropically through a supersonic nozzle to ambient

pressure. This quantity of energy is termed the available energy content ΔH_t , and is expressed by the correlations in equations (6-16), (6-17), and (6-18).

TABLE 4-2.—Operating Characteristics of a Typical Liquid Bipropellant Gas Generator System, as Shown in Fig. 4-51

Oxidizer	Liquid oxygen
Fuel	RP-1
Total propellant flow rate	17.34 lb/sec
O/F mixture ratio	0.342
Oxidizer flow rate	4.42 lb/sec
Fuel flow rate	12.92 lb/sec
GG chamber pressure (injector end)	612.1 psia
GG chamber temperature	1200° F
Oxidizer-side pressure drop of line, valve, and injector	114 psi
Oxidizer side pressure drop across orifice	121 psi
GG oxidizer supply line takeoff pressure (total at main oxidizer pump discharge)	846 psia
Fuel side pressure drop of line, valve, and injector	216 psi
Fuel side pressure drop across orifice	80 psi
GG fuel supply line takeoff pressure (total at main fuel pump discharge)	907 psi

Thrust Chamber Gas Tapoff Systems

With these systems, combustion product gases are bled from the main thrust chamber and ducted to the turbine, where they are used as the working fluid. This arrangement eliminates the need for a separate gas generator system and contributes significantly to the simplicity and its reliability potential of the engine system. The technique has been successfully developed by North American Aviation's Rocketdyne Division and appears to be particularly promising for hydrogen engines requiring throttling. Figure 4-52 shows a schematic of a tapoff system.

In a separate gas generator system, gases are produced and "tailormade" for turbine-power purposes only, with the benefit of relatively high liquid supply pressures. In a tapoff system, the bulk of the extremely hot gases of the main chamber would not be suitable as the turbine drive fluid, in view of the limitation of the turbine construction materials. It has been successfully demonstrated, however, that by withdrawing chamber gases from the boundary zones only, and through proper shaping and location of the bleedports, any desired turbine inlet temperature (usually less than 1700° F) can be reliably and repeatably produced, for a given thrust chamber and injector design. The bleed gases thus withdrawn have been found to possess thermodynamic properties comparable to the products of a liquid bipropellant gas generator utilizing the

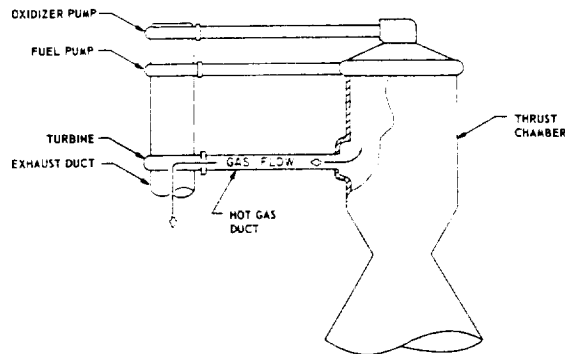


Figure 4-52.—Schematic diagram of thrust chamber gas tapoff system.

same primary propellants. However, a tapoff turbine must be designed to operate at an inlet pressure lower than the thrust chamber pressure. Furthermore, a tapoff engine system will require some sort of simple starting device, such as gas spinner. With the aid of a hot gas regulating valve placed at the turbine inlet, hydrogen tapoff engine systems have been successfully throttled to thrust ratios of 10:1 or better.

4.7 IGNITION DEVICES

The initiation of the release of the chemical energy stored in liquid rocket propellants is accomplished by a number of methods from which the engine designer will select the most suitable for a particular system:

- (1) Igniters
- (2) Hypergolic ignition
- (3) Catalysts

All of these methods have been in use for both thrust chambers and gas generators. Note that in liquid propellant rocketry, gas generators have been used not only for turbine power but for propellant-tank pressurization as well. The selection of the preferred ignition method depends on the chosen type of propellants, whether bipropellants or monopropellants are used, on the size of the combustion chambers, the heat release per unit time required in relation to the amount of propellants entering, and on a number of other considerations which will be discussed.

All ignition methods, particularly those for bipropellant systems, have one overriding requirement in common: minimum ignition delay.

If the propellants entering the combustion chamber are not promptly ignited, explosive mixtures can form and detonate with damaging results. The assurance of faultless ignition is dependent on the selection of the ignition method, the quality of design, and on adequate heat release.

Igniters

These are defined as devices which release heat and thus initiate the reaction of the main propellants which subsequently sustains itself. Igniters derive their power from an outside source or from a limited amount of energy stored as solid propellants within themselves. Following ignition, igniters do not participate further in the combustion process. Some of the principal igniter types are discussed below.

Pyrotechnic Igniters

These are literally slow-burning fire crackers, somewhat modified for rocket engine application. Burning time is in the range of a few seconds. For thrust chamber use they can be mounted to the injector face or inserted from below at the end of a wooden or plastic stick (fig. 4-2). For better heat distribution, multiple units firing in different directions, have been used, as a rule radially outward from the center across the injector face. In other designs they have been mounted to pinwheels, achieving distribution through rapid rotation.

Although pyrotechnic igniters are used, they should be considered obsolescent. To achieve adequate heat release for modern large engines, their size becomes impractical. Also, ejection of their inert parts can cause damage to the delicate thin-walled tubes of modern chamber walls. Under cryogenic conditions, they have exhibited a tendency to cause ignition delays, complete duds, or explosive popping.

Pyrotechnic igniters for gas generators and small thrust chambers have been mounted in recesses as screw-in-type plugs. (See figs. 4-53 and 4-54.) The igniters are initiated by electrically triggered squibs, of which there are a variety of types in use. The need to connect wires to the pyrotechnic igniters is another inconvenience. Furthermore, checkout of the integrity and readiness of pyrotechnic igniters is

difficult. It is one of the inherent shortcomings of solid propellants that they cannot be switched on briefly for checkout and then stopped again.

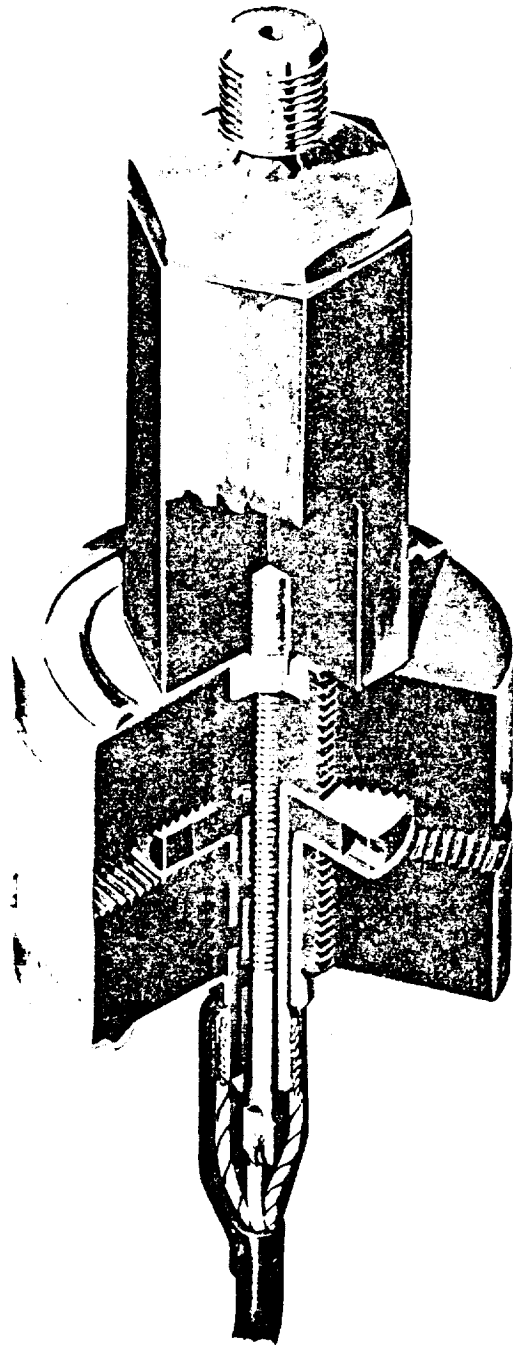


Figure 4-53.—Radially outward firing pyrotechnic igniter for center of injector mounting.

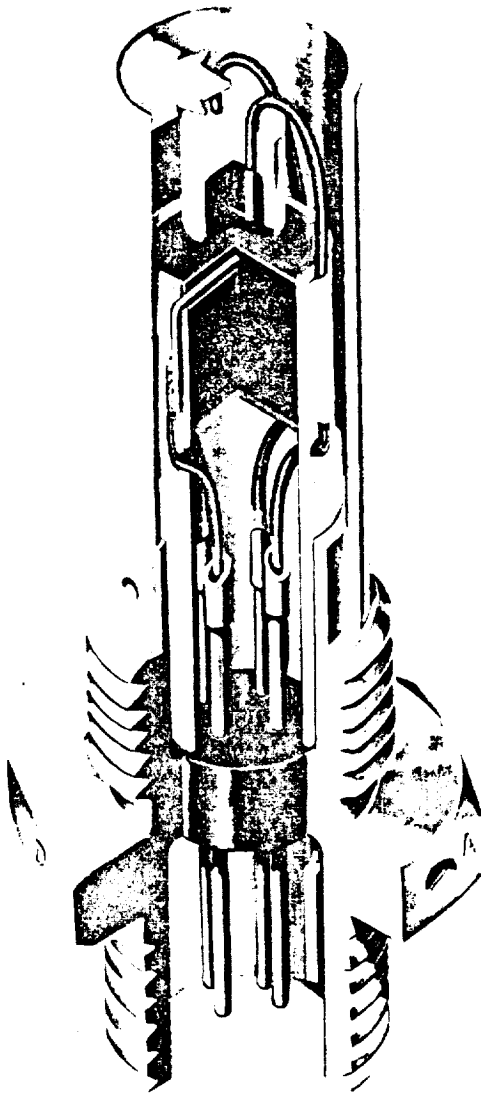


Figure 4-54.—Gas generator igniter with built-in fusible link.

Assurance of their reliability, therefore, is by statistical and sampling methods. For operational application, additional safety margins are secured by redundancy. However, this tends to increase bulkiness further. Also, pyrotechnic igniters are unsuitable for repeated starts.

Engine manufacturers have been procuring pyrotechnic igniters from sources specializing in this field. Typical examples of selected parameters are as follows:

For a 150 000-pound thrust, LOX/RP-1 engine:

Main chamber: centrally mounted unit; propellant weight, 33 gms; 4.5 sec burning time; heat release, 45 Btu/sec; perchlorate-type fuel. Electrically initiated. (Later models of this engine used hypergolic slugs.)

Gas generator: Pyrotechnic: propellant weight, 2 gms; 8 sec burning time; heat release, 1.6 Btu/sec; perchlorate-type fuel.

Vernier engines (earlier models only): Similar to gas generator units.

It is vital that certain of the specifications fall within a stated band. For instance, it can be specified that in a family of samples no igniter will fire at currents below 1 amp, and that all must fire below 4 amp. The first condition concerns the avoidance of accidental firing due to stray currents introduced by extraneous RF signals or other sources; the latter is simply a reliability requirement. Similarly, minimum and maximum burning times, i.e., tolerances of the nominal times, will be dictated by start-sequence conditions.

In operational designs, the pyrotechnic igniters frequently do not ignite the main propellants directly, but ignite a pilot flame fed by a small portion of the main fuel. The pilot flame then ignites the main propellants.

Hypergolic Igniters

The term "hypergolic" was coined by the German chemist Noeggerath about 1942 and is composed of elements of the Greek words for "high energy liquid." The term now denotes a bipropellant combination which ignites spontaneously when the two components meet. Such a system was used as an ignition source for the earlier German A-4 engine (later called V-2 engine), utilizing hydrazine-hydrate ($N_2H_4 \cdot H_2O$) and 80 percent hydrogen peroxide (H_2O_2). Thin tubes supported by a wooden stick were inserted into the thrust chamber from below. Upon an "ignition" signal, a ground-mounted supply unit, including remotely operated valves, fed the two components to near the injector elements where they burned with a spontaneously igniting hot flame. This method may also have been used temporarily on other systems. However, its clumsiness, the frequent clogging of feed lines,

and the need to eject a considerable amount of inert solid material made it undesirable. Also, adaptation to repeated starts would be complex and would require vehicle mounting, thus adding inert flight weight.

Hypergolic Slugs

A more elegant way of using the hypergolic effect for main-propellant ignition is through use of a hypergolic slug. In this design a small amount of fluid is used which is hypergolic with one of the main propellants but not with the other. The fluid is stored in a cylindrical cartridge which has burst diaphragms at either end. The cartridge, in turn, is loaded into a housing which is part of a bypass line paralleling a high-pressure main propellant feed line (fig. 4-55). If a fluid is chosen which is hypergolic with the oxidizer but neutral to the fuel, it is installed in the fuel system, and vice versa. The former type is the more common one. Here a fuel bypass line feeds an injection element in the center of the injector, or a set of elements evenly distributed over the injector face. When the pumps start and outlet pressures rise, the oxidizer valve is opened. As pressures rise further, the burst diaphragms in the hypergolic-fluid container rupture and the fluid meets with the oxidizer in the chamber, igniting spontaneously. The fuel following the slug sustains the ignition flame. The main fuel valve is then opened and all parameters reach main-stage level. Since the igniter elements carry fuel fed from the main source following ignition, they continue to participate in the combustion, undistinguished from the remainder of the main injector. (See schematic, fig. 2-13.)

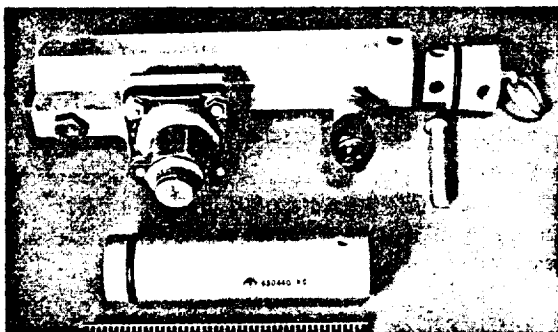


Figure 4-55.—Hypergolic slug cartridge and housing.

Typical of fluid hypergolic with oxygen is triethyl aluminum. For optimum behavior, i.e., for minimum ignition delays and avoidance of undesirable deposits in fuel and sensing lines, optimum mixtures of the two have been successfully established experimentally. In a typical application, an amount of 6 cubic inches has been found adequate, although 9 cubic inches are actually used for maximum safety margin. By comparison, a 1.5-million-pound thrust engine uses 35 cubic inches. The hypergolic slug method, first explored at the German Peenemünde installation, is well developed and has found wide application. Limited design and development work has been done more recently toward repeated-start units, using a device resembling an automobile brake master cylinder with its replenishing features. However, the hypergolic slug is truly a single-start device. Because of relative bulkiness, the hypergolic slug is not recommended for small units such as gas generators, where pyrotechnic igniters or spark plugs are preferred.

Spark Plugs

Spark plugs and their accessories have been developed to high levels of efficiency and reliability for liquid rocket engine use. They are eminently suitable for repeated starts. For direct ignition, however, they are confined to relatively small combustion devices. (See fig. 4-56.) In a typical 200 000-pound thrust engine, the gas-generator spark plugs fire at the rate of 50 sparks per second, releasing approximately 1/10 joule per spark. This corresponds to 5 joules/sec or 0.005 Btu/sec per plug. The efficiency of spark generation from the electrical

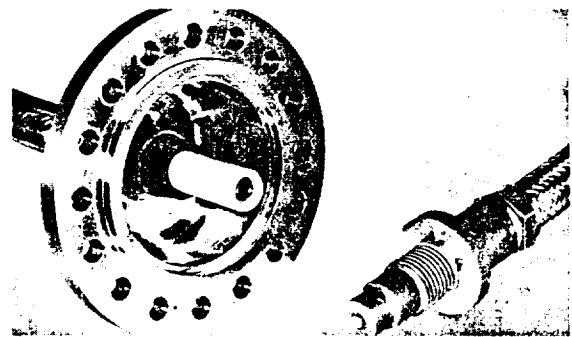


Figure 4-56.—Spark igniter assembly. At right, screw-in spark plug; at left, cable connector.

storage device is approximately 20 percent. The overall efficiency of the spark ignition system is approximately 10 percent. Thus, 100 watts of electrical power is required. If a 28-V source is used, the nominal current is 4 amp when two redundant systems are used in parallel. A Typical voltage at the spark plug is 15 000 V.

Augmented Spark Igniters

The limitation of direct spark ignition to small units has led to the design and development of augmented spark igniters (ASI). In this design a spark plug, similar to the above, fires into a small chamber about the size of a gas generator. A small amount of the main propellants is fed into this chamber where they ignite. The hot flame generated in turn ignites the main propellants. Figure 4-57 shows the principles of an earlier augmented spark igniter design. Permanently located at the injector end of the thrust chamber, this igniter directs its products of combustion across the face of the main injector. It is film cooled by the tangential injection of fuel. The oxidizer is injected through two copper tubes which impinge at the centerline of the igniter, resulting in a hot-core type of combustion. The igniter is made of 4130 steel and has a convergent, throatless nozzle. This results in a wide dispersion angle of gases emanating from the nozzle. The igniter is capable of an unlimited number of starts, since the spark plug is so located that the combustion does not seriously affect its life. The igniter has proven operable over a wide range of mixture-ratio and pressure conditions. It continues to operate throughout

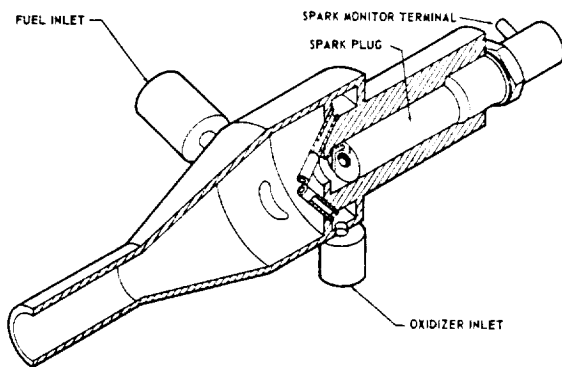


Figure 4-57.—Augmented spark igniter.

main stage, which prevents any of the main chamber gases from backing up into the igniter. Approximately one-half percent of the main propellant flow rates has been found adequate for the augmented spark igniters.

Special Designs

For the engine used in the Saturn S-I booster, gas-generator ignition by the solid-propellant turbine spinner has been successfully developed. The turbine spinner will be discussed in a later chapter.

Hypergolic Main Propellant Ignition

In preceding paragraphs it was learned that hypergolic fluids are being used as ignition sources for main propellant combinations which by themselves are not hypergolic (i.e., "anergol" propellants). Hypergolic liquid main propellants have attracted attention since the early days of modern rocketry. Their use permits a substantial simplification of the engine system through elimination of the entire ignition system, leaving entry timing the only functional requirement. This gain however, is not entirely without penalties. The practical hypergolic propellant combinations have a somewhat limited specific impulse. Furthermore, some are highly corrosive and/or pose handling and storage problems which the engine designer has to consider.

A number of hypergolic main propellant combinations have been in successful operational use for many years. During World War II, several guided-missile systems using hypergolic propellants, were under development in Germany. Hydrazine hydrate ($N_2H_4 \cdot H_2O$) and high-percentage hydrogen peroxide were used in certain Messerschmitt rocket fighters and the anti-aircraft missile Enzian. Amines and nitric acid were used for the AA rocket Schmetterling. Optolines and nitric acid with sulfuric acid additives (approximately 10 percent) were applied in the Peenemünde developments of the anti-aircraft rocket Wasserfall (17 000-pound thrust) and the small 1300-pound Taifun. "Optoline" was a generic term for various mixtures of aniline, hydrocarbons, and other substances.

In the United States, several propulsion systems utilizing hypergolic propellants have been developed.

CONFIDENTIAL

To make available to the high performing but anergol propellant combinations the simplicity of hypergolic behavior, the effectiveness of small amounts of additives ("sweeteners") has been successfully demonstrated.

Catalysts

In a general sense, catalysts are not igniters but initiators and sustainers of reactions, which themselves remain unchanged during these reactions. In rocketry, catalysts have been used predominantly to initiate and sustain the composition of monopropellants ("Monergols"), notably that of hydrogen peroxide. Several operational or near-operational systems existed during World War II, such as the earlier Messerschmitt Me-163 which used hydrogen peroxide with potassium permanganate solution as the catalyst. Probably the most widely used application of this principle during that period was for the turbine steam-generating system of the German A-4 (later called V-2) ballistic missile, which employed 80 percent hydrogen peroxide with either potassium permanganate or sodium permanganate as catalysts.

Because of the need for relatively elaborate timing, valving, and interlocking devices, the use of liquid catalysts was soon found to be cumbersome and undesirable. Application of solid catalysts, therefore, as they were being used for underwater torpedoes, led to design and development work toward use of these systems for rocket application. They never reached maturity for the German World War II systems, but were perfected after the war by the British and to a limited degree by the United States. The Redstone rocket steam plant, using solid catalysts, has consistently and successfully operated in many flights, among them the first U. S. manned rocket flight by Commander Shepard. Another successful development are the AR airplane superperformance rockets. Analogous to certain British systems, the AR systems decompose hydrogen peroxide fed through a solid catalyst bed consisting of impregnated wire screens. Since the specific impulse of decomposed hydrogen peroxide alone is low (below 200, depending on concentration and design parameters), RP fuel is injected below the decomposition chamber. Because of the sufficiently high temperature of

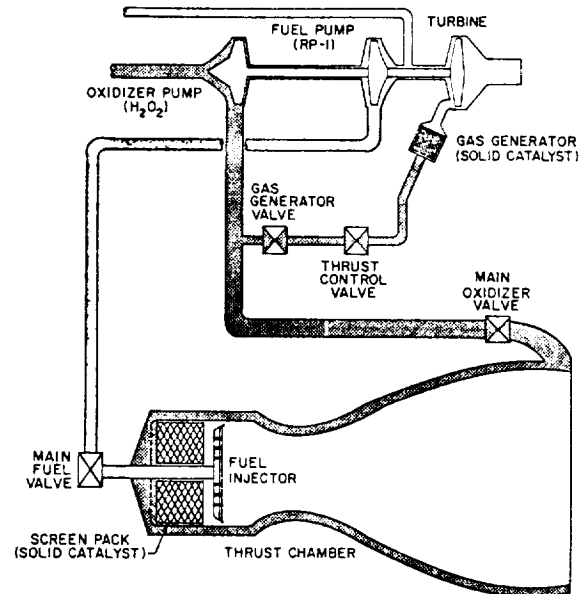


Figure 4-58.—Schematic of a Rocketdyne AR-1 superperformance rocket engine.

the decomposition gases (1400° F), the RP ignites and burns spontaneously with the free oxygen of the decomposed H_2O_2 . (See fig. 4-58.) In this manner, the solid catalyst indirectly serves as an ignition system. While the specific impulse with RP afterburner is still moderate (approximately 245 seconds for the AR), these systems offer great versatility, storability, and extreme simplicity, including throttling to low levels and restartability.

More recently, it has been successfully demonstrated that catalytic operation offers a simple alternative to augmented spark ignition for hydrocarbon systems.

In a process patented for Engelhard Industries, Newark, N. J., a gaseous mixture of oxygen and hydrogen is fed through a catalyst bed of palladium-impregnated alumina (Al_2O_3) pellets, by which the mixture is ignited. Installation of this igniter is similar to an augmented spark igniter.

Ignition Detection

The reader familiar with the news stories about rocket launchings over the past years is well aware of the consequences of rocket stages failing to ignite: loss of mission. This is

equally true for liquid- and for solid-propellant systems. With the former, however, an additional hazard exists in case of ignition failure: that of accumulation of explosive propellant mixtures which can be accidentally set off with catastrophic consequences. This consideration has always been a concern with unmanned vehicles, but has become even more important for manned ones.

Recognition of these potential dangers has prompted extensive investigation of means to detect reliably absence or presence of ignition in liquid propellant rocket engines. Only upon an "ignition OK" signal should the engine-start sequence be permitted to proceed. This refers mainly to the thrust chamber. For gas generators, redundancy appears to be adequate protection for most applications. Desirable detection systems must judge ignition both qualitatively (absence or presence) and quantitatively (adequate heat release). Not all methods are equally good in both respects.

In some form or another, the engine designer will have to provide means for ignition detection. A survey follows of several which have found operational application.

Visual Detection

For the German A-4 (V-2) and the early U. S. Redstone missiles, visual observation by the test conductor was used. Man in this case was the interlocking device and would initiate the next sequence step only if, in his judgment, ignition was adequate. This simple procedure was satisfactory because these early systems employed a prestage, during which the main propellants were admitted under tank head only. The resulting relatively low flow rates were then increased by starting the turbopump upon a "prestige OK" signal.

With the increasing size of modern rocket engines, visual observation became unreliable. The type of installation of these systems in static firing stands and on launch tables made direct observation difficult. Furthermore, improved igniters, developed to keep the ignition flame concentrated where it should be, i.e., at the injector face, resulted in little or no visible fire emerging at the chamber exit. With the disappearance of the prestage step, the visual

problem increased because of the large amount of oxidizer present in full flow ignitions which shrouds the ignition flame. Thus, means had to be found to detect ignition by other means.

Optical Detection

Ground-mounted optical devices can be moved up close to the chamber exit. A number of types have been investigated, such as simple light or infrared-sensitive cells. They were found, however, to be subject to the limitations mentioned for human observers. It is possible to mount the optical devices into the chamber wall facing toward the inside near the injector face; however, the devices used thus become vehicle mounted and require interfaces to ground-support equipment. Also, "windows" in the chamber wall represent undesirable surface discontinuities. It is unlikely, therefore, that optical devices will find wide application for ignition detection.

Pyrometers

Heat-sensitive pyrometers are closely related to the optical devices and subject to the same limitations.

Fusible Wire Links

For many applications these are simple and reliable devices. A wire is strung across the chamber exit which, when fused by the ignition flame, interrupts a circuit and signals "ignition OK." Through proper selection of wire gage, material and distance from the chamber exit and/or center, some quantitative judgment is obtained. The wire can be ground mounted or chamber mounted. It must be isolated and should have spring loading, like the well-known electric fuses, to assure positive separation.

Wire links have a number of shortcomings. The fused wire ends may touch other metal parts and thus reconnect the circuit before the relay drops out. Suitable circuitry and mounting must therefore be applied. If a pyrotechnic igniter is used, the wire can be broken by inert particles, or even by a dud igniter coming out of the chamber, giving an incorrect "ignition OK" signal. This has been overcome by providing redundancy using several wires in parallel, all of which

must be broken before the sequence can proceed. In another design the wire has been mounted as a loop placed in a groove on a wooden or plastic stick. It is thus supported against all reasonably expected mechanical damage and adequate insulation is maintained after fusion.

Pressure-Sensing Devices

Because of the need to mount the fusible wires at the exit of the thrust chamber, they are subject to some of the limitations noted for visual and optical methods. It has been attempted, therefore, to sense the pressure rise in the combustion chamber resulting from the burning igniter flame. However, since the pressure rise is small (a few psi at best), reliable discrimination is difficult. Furthermore, the sensing-pressure switches must be able to withstand the much higher pressures during subsequent main stage. Pressure-sensing devices have potential for multistart engines.

Resistance Wires

Another method designed to overcome the shortcomings of fusible wire links is the application of resistance wires. Constructed like a glow plug and connected to a bridge circuit, the resistance wire will signal by a distinctly different resistance in the presence or absence of ignition. The art is to find that spot in the thrust chamber or gas generator which experiences a clear temperature rise as a function of ignition, yet remains cool enough to prevent fusion of the wire. Resistance-wire sensors are ideally suited for repeatable start engines.

Indirect Methods

In conjunction with hypergolic slug ignition, other approaches to ignition sensing have been developed. In one design an electric contact assures that a cartridge is actually installed. This does not assure, however, that the cartridge is loaded or completely loaded, nor that the downstream lines are not clogged or that the diaphragms will burst. Weighing of the cartridge and purging of all lines must be included in the firing preparation.

In another arrangement a pressure switch

senses pressure buildup in the igniter injection line upon rupture of the hypergolic fluid cartridge burst diaphragms. The switch signal then initiates the next sequential step. A modification of the system substitutes a pressure-actuated valve for the switch with similar effects. This method does not assure, however, that the cartridge is properly filled with the right amount of the correct fluid.

Spark igniters use electric devices which ascertain that the plug is sparking based on conductivity effects due to ionization near the electrodes.

The methods in the above list, which undoubtedly is not complete, are described as indirect because none of them directly and reliably detects ignition; i.e., the release of adequate heat. This is a drawback and cannot entirely be offset by weighing, certifying, and inspecting.

4.8 COMBUSTION INSTABILITY

"Combustion instability" is defined in terms of amplitude of pressure fluctuations in the combustion chamber. Chamber-pressure fluctuations are always present during normal, stable operation of a rocket engine system. These fluctuations are generally quite random, showing frequency spectra which are essentially continuous in nature, with few, if any, recognizable peaks. However, in case of instability, large concentrations of vibratory energy appear at one or more frequencies in the spectrum. They can easily be recognized against the normal random-noise background.

It has been found experimentally that the amplitude of the chamber pressure oscillations which will cause detrimental physical or operational effects varies widely for different thrust chambers and engine systems. Also, in a given chamber or system the effects of various types of instability can be quite different at the same amplitude. Thus it is difficult to assign a quantitative value to the amplitude at which the combustion chamber should be considered as running unstable.

It is an interesting observation that the first large liquid-propellant rocket-propulsion system, the German A-4 (V-2) rocket, never experienced combustion instability in over 4000 launchings and in several times as many static chamber and

engine firings. The term "combustion instability" was literally unknown. It has been suggested that the Germans may have had instability, but did not know it because of their poor high-speed recorders. To this it can be said that for those instabilities which have caused today's real difficulties, the high-speed recorder chart is merely a postmortem confirmation of the cause of often very costly failures, which did not require any special instrumentation but were unmistakable even to the untrained visual observer. It is much more likely that there is a relationship between the low performance level of the A-4 or the chamber geometry, or both, and the inherent stability.

Experimentally it has been found that as long as the ratio of the peak-to-peak amplitude of pressure oscillation to average chamber pressure is kept below 0.10, there is usually no physical damage to the chamber. However, while a 10-percent variation in pressure for any class of instability may not appear to have detrimental physical effects instantly or within a short period, it would be unacceptable for longer range rocket vehicle missions. One practical way to detect combustion instability and to prevent it from causing damage during engine operation is by monitoring the vibratory acceleration of the system. Accelerometers are mounted on the system to monitor in all three coordinates. They are connected to discriminator circuits which are set to specific g-load limits. When these limits are exceeded, a counting instrument begins to record. As soon as an allowable cumulative number of oscillations is exceeded, an engine cutoff signal is automatically triggered to prevent damage.

Types of Instability

For proper remedial action, it will often be important to know whether the observed oscillations are of a longitudinal, radial, or tangential mode, or a combination of these. These three modes and their normal acoustic frequency are indicated in figure 4-59. Furthermore, in certain cases, it will be extremely valuable to know whether the oscillations originated in the thrust chamber, or in the feed system, or whether they originate in an interaction of characteristics, harmless when separate but destructive when

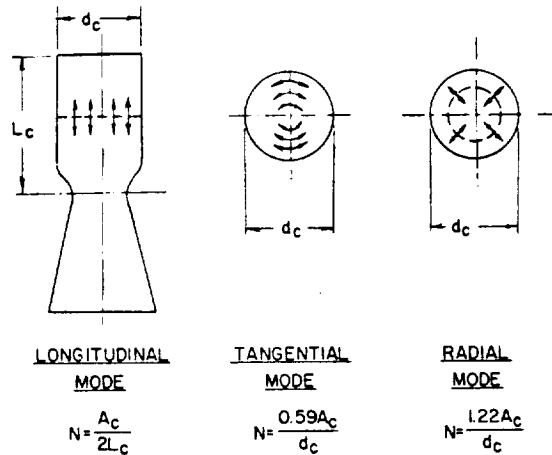


Figure 4-59.—Three modes of instability. L_c = combustion chamber length (injector face to throat); d_c = combustion chamber diameter; N = normal acoustic frequency; A_c = velocity of sound in chamber.

combined, of both feed system and chamber. This will be further discussed in connection with methods to improve stability.

The effects of the oscillations on an engine system are very much dependent on frequency. These effects may range from simple shaking (usually at the lower frequencies), possibly resulting in an eventual mechanical failure after sometimes prolonged exposure, to "acoustic" vibrations (usually at the higher frequencies) capable of destroying the entire system in a few hundred milliseconds. But, how low is "low" and how high is "high"? As pointed out earlier, the general field of combustion stability is extremely complex and it would be far beyond the scope of this book to attempt to present a generalized theory of the subject. Each system, because of configuration and dimensions, behaves somewhat differently and requires special treatment. The thrust chamber designer must have a basic understanding of the stability problem, and it is felt that this can best be conveyed by describing it in terms of a typical system, for which a substantial amount of experimental data exists.

The frequency of the chamber pressure oscillations in a given chamber is determined by the geometry of the system as well as by complex interactions between the fluid flow in the propellant lines, the physical and chemical process

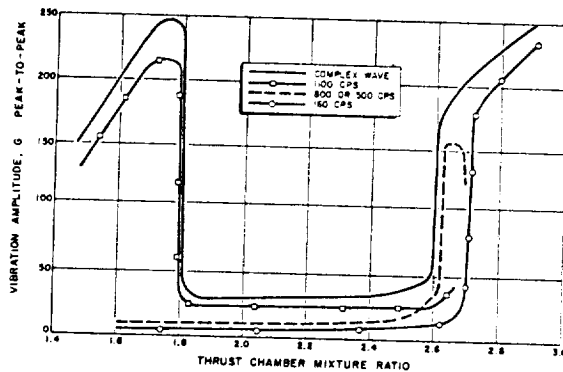


Figure 4-60.—Approximate vibration characteristics at 150 000 lb thrust level.

of combustion, and the dynamics of the combustion gases in the chamber. It has been found that each of the frequency components in the instability spectrum of a thrust chamber is predominantly influenced by only one physical process so that it is possible to group the observed instabilities in broad general classes, which are: high frequency or gas dynamics, low frequency or hydrodynamics, and intermediate frequency or combustion dynamics, listed in the order of their relative importance. Figure 4-60 presents vibration amplitudes of various frequencies versus mixture ratio of a typical $LO_2/RP-1$ engine at the 150 000-pound thrust level. The graph indicates the large difference in vibration amplitude between a stable and an unstable region.

High-Frequency Instabilities

High-frequency instabilities at frequencies of approximately 1000 cps and over are sometimes referred to as "damaging acoustic," or "screaming" modes of instability. They are gas-dynamic instabilities which are both sustained and initiated by the combustion process and are believed to be concentrated in the uppermost portion of the combustion chamber where they cause increased heat-transfer rates to the injector sufficient to melt and burn it through within a few hundred milliseconds. They also frequently have serious damaging effects upon other parts of the rocket engine system. High-frequency instabilities are further characterized by instantaneous initiation (a few milliseconds from absence to full amplitude), and by extreme difficulty in

eliminating them once they are initiated. They do not occur at, nor can they be generally damped to, low-amplitude levels. They are either present at high amplitudes or not at all. It is believed that these oscillations are predominantly of the radial and tangential types.

In many systems extremely unpredictable high-frequency instability has occurred. It is often, but by no means always, connected with the buildup phase to main stage. Systems which ran stably during numerous successive tests can become unstable without warning or subsequent clear indication of a cause. Figure 4-61 shows the starting of a typical high-frequency instability, indicated by the sudden shift in the accelerometer trace due to high-amplitude chamber pressure oscillations. All types of rocket propulsion systems, including solid systems, have been plagued by high-frequency instability. A considerable amount of research and engineering has been devoted to the explanation and elimination of this phenomenon.

Unless a run in which instability is encountered is terminated within fractions of a second, serious damage to the engine hardware almost always occurs. It is assumed that the rapid gas pulsations directly interface with propellant injection, their mixing, and with the combustion process, upsetting the condition in the boundary zones, in particular at the injector face, to such an extent that the heat transfer to the metal parts increases at a high rate. Within seconds, or even fractions thereof, the injector can burn through, permitting propellant mixing behind the injector face. This, in turn, leads to explosions which often completely destroy the system.

It has been observed that the degree and speed of damage is somewhat related to the level of energy release occurring in the combustion chamber. This may explain why "bursts of

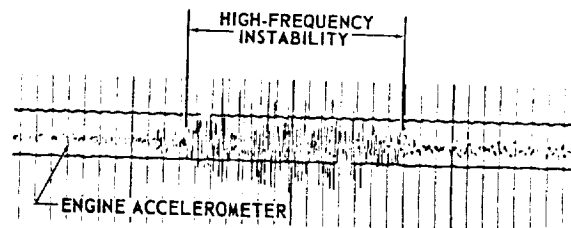


Figure 4-61.—High frequency combustion instability shown on oscillograph for engine accelerometer.

instability" during shutdown cause damage less frequently than they do during buildup and main stage.

Low-Frequency Instabilities

This type of instability, at frequencies below approximately 180 cps, is a hydrodynamic oscillation, characterized by a cause-and-effect-type coupling between combustion process and propellant feed system flow processes. The phenomenon is sometimes referred to as "chugging." Its secondary effects can be serious indeed. "Chugging" may trigger destructive high-frequency instability. Also, prolonged chugging can lead to loosening of bolts and other vital connections and to ruptures in general. Low-frequency instability is self-sustaining but may damp out. As a rule, it is predictable from analytical and from test result studies. In figure 4-62 the high-speed-pressure instrumentation measurements indicating chugging clearly show that the oscillations of propellant feed system pressures are at the same frequency as the "rough combustion cutoff accelerometer" reading.

Chugging occurs most frequently during buildup and shutdown of an engine system, or when operating at off-rated operating levels, such as at incorrect mixture-ratio values. Likewise, too high, and particularly, too low a thrust level can lead to chugging. This is especially important for systems requiring throttling to a lower-than-rated thrust level during flight. If sustained, chugging will cause measurable performance losses, which are attributable to widely fluctuating mixture ratios.

The chugging phenomenon is frequently associated with the quality and promptness of ignition of the entering propellants. This can be described as "flame holding characteristics," "combustion timelags," "flame propagation velocity," or other terms, which ultimately are all traceable to the excessive accumulation of unburned fuel, with subsequent detonation or cyclic higher-than-rated combustion. The resulting excessive chamber-pressure spikes effect a reduction, or even reversal, of the propellant flows. This will cause rapid collapse of the chamber pressure, allowing propellants to rush in again, thus repeating the cycle. It is readily evident that the physical dimensions of the com-

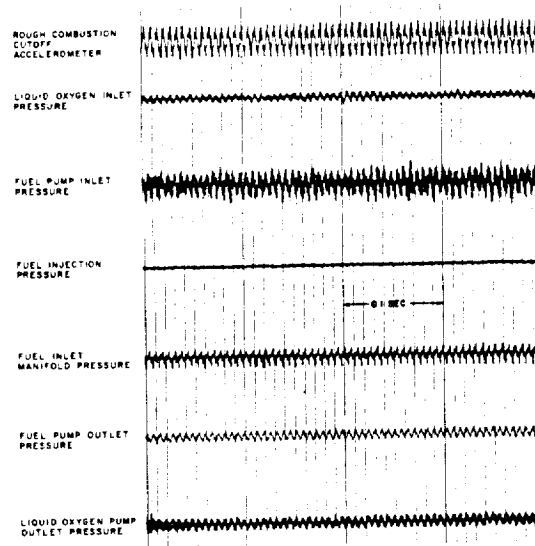


Figure 4-62.—High-speed pressure measurements of low-frequency instability.

bustion chamber and of the propellant ducts, and the magnitude of the propellant flow rates and their ratio to one another (in a bipropellant system), are critical to the phenomenon of low-frequency system oscillations.

Intermediate-Frequency Instabilities

This instability, with frequencies ranging from 200 to 1000 cps, is sometimes referred to as combustion dynamics or "buzzing." It is characterized by a spring-and-mass-type coupling between combustion process and propellant feed system flow processes. It is often present in only a portion of the feed system, or is confined to the combustion chamber, or, in a bipropellant system, to one of the two propellant systems only. It appears to be initiated by the combustion process and to be sustained by acoustic resonance of a critical portion of the system. Some researchers have shown that in a system having a pump, the pump may be the prime source of these oscillations.

This type of instability has not appeared to be a problem in the development of large engines. While it can occur occasionally in large engines, it appears to be much more prevalent in small-scale low-thrust systems. Systems oscillations of the buzzing type are undesirable because of their adverse effects on engine reliability and

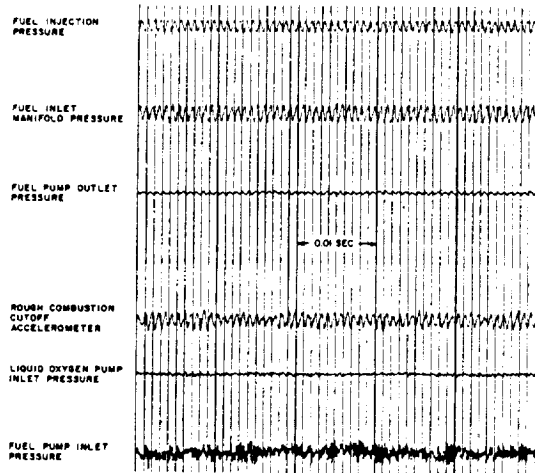


Figure 4-63.—High-speed pressure measurements of intermediate frequency instability.

performance. When exposed to prolonged buzzing, critical parts of the engine may fail because of material fatigue, and thus cause secondary major failures. In addition, measurements have shown that a performance (I_s) loss of up to approximately 7 percent can be incurred, which is largely attributed to widely fluctuating mixture ratios.

Figure 4-63 is the record of high-speed-pressure measurements of a typical test afflicted by buzzing. The oscillation is attenuated in the fuel pump outlet pressure, and nonexistent in the pump inlet pressure. This indicates that the buzzing is limited to only a part of the feed system.

Field of Stability

For a given engine system, combustion stability limits can be defined experimentally in terms of certain operational parameters such as chamber pressure, injection ΔP , and mixture ratio. Figure 4-64 presents the stability field for a typical $LO_2/ RP-1$, 150 000-pound nominal thrust engine system. The stability field, together with heat transfer limits, can serve as a guide to the design of a safely operating engine system.

Design Approaches Toward Control of Combustion Instability

The problem of controlling combustion insta-

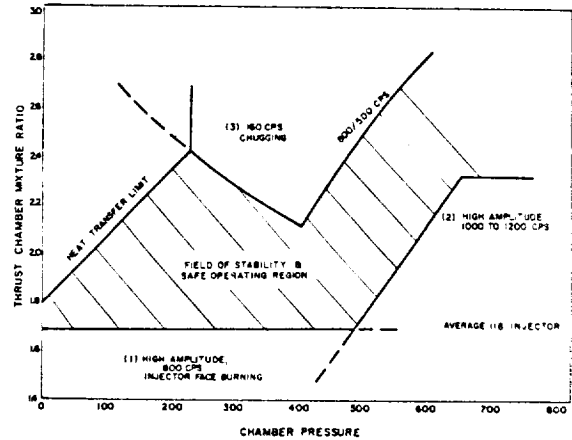


Figure 4-64.—Field of stability and safe operating region of a typical engine system.

bility in liquid propellant rocket engine systems can be attacked in several ways, including systems design, choice of propellant combination, and operating conditions, and through the use of special control devices. Two basic approaches toward eliminating combustion instability are employed. The first is to eliminate triggering processes and/or to limit the driving energy per cycle to a value below the damping per cycle inherent to the system. This approach is typified by design investigations in which injector configurations are varied to give different atomization and propellant distribution characteristics with varying resistance to initiation of instability, or in which propellant additives are used which modify the physical properties controlling spray formation, chemical kinetics, etc. Experimental studies, both with full-scale engines and with research model thrust chambers, have shown that injector modification yields relative stability ratings, differing by a factor from 5 to 6 from the most stable to the least stable configuration.

The second approach is to introduce additional damping in the system through the use of mechanical or other devices so that any operational disturbance, or oscillation triggered by the disturbance, are sufficiently and rapidly damped out. Experience over the past several years has shown that the destructive transverse acoustic modes of instability can be most effectively combated through the use of this second approach. Mechanical devices, such as baffles or a divergent wall gap, have been found to

introduce sufficient damping into the system so that it will recover from an instability triggered by an explosive charge as large as can be used without damaging the thrust chamber in some other manner. This ability of a system to recover from a triggered instability has been designated as "dynamic stability." A prerequisite for any propulsion system to operate reliably is that it should exhibit dynamic stability with respect to all modes of instability. As a minimum requirement it should be "dynamically stable" at least with respect to the destructive transverse (radial and tangential) acoustic modes.

The successful application of the above methods has been based primarily on criteria established empirically in research model thrust chambers, together with testing in actual engine systems. However, the understanding of the fundamental physical principles of the damping processes is still limited.

Prevention of Triggering Processes

The most desirable design method of controlling instability is the prevention of those physical or chemical processes which trigger and/or sustain the resonant modes of the combustion chamber or engine system. While a great number of studies, in which different design parameters were varied systematically, have been made by various investigators, the results have failed to yield truly generalized design criteria. This can be traced to the fact that basic processes which trigger and sustain the various types of instability have not been isolated. Thus, while a parameter which controls one type of instability may have been established on an engineering basis, this same design criterion may be enhancing another type of instability. The following is a general discussion of the prevention of triggering instability in various component and subsystem designs:

1. *Propellant feed system design.*—Past experience has indicated that certain combustion instabilities, such as buzzing, are sustained through an interaction between feed system and combustion dynamics. It is believed that hydraulic resonances are a major factor in sustaining this type of instability. The requirement is to design a feed system whose hydraulic charac-

teristics will not trigger the interaction with the combustion process.

2. *Combustion chamber design.*—Analytical studies and experimental results have indicated that the geometrical configuration of the combustion chamber will determine the type of frequency of the acoustic modes of instability. Chambers having large length-to-diameter ratios appear to be quite prone to large-amplitude longitudinal instability. On the other hand, chambers having small length-to-diameter ratios appear to be sensitive to the transverse modes. Also, small-diameter chambers are much more stable than large-diameter chambers. The requirement is to design a chamber geometry which will have least tendency to trigger instability, in conjunction with other considerations.

3. *Injector design.*—The injector design appears to be a most critical factor in triggering instability. In turn, it offers great potential for controlling instability-triggering processes through variation of parameters. Of the most common types of injectors, the self-impinging injector (fig. 4-45a) has been chosen by many investigators as the best compromise between performance and stability. There is some indication that longitudinal instability may be enhanced if the propellant travel time from the injector face to the point of impingement is close to the half-period (or an odd multiple of the half-period) of the longitudinal mode oscillations. There are strong indications that increasing the injection ΔP to too great a value may cause the thrust chamber to operate unstably in the transverse acoustic modes. The effect of injection ΔP on the longitudinal acoustic modes and on hydrodynamic instabilities appears to be just the opposite, with stability improving as ΔP increases. The propellant distribution across the injector face has a significant relation to triggering transverse modes of instability.

4. *Propellant combination and mixture ratio.*—Control tests with various propellants have shown that there are certain oxidizers or fuels which can be triggered into instability more easily than others, in general or at certain mixture ratio conditions. In LO_2/LH_2 systems, a lower hydrogen injection temperature tends to trigger instability.

5. *Engine system operating characteristics.*—In some cases, combustion instability can be

CONFIDENTIAL

avoided by modification of engine-system operating characteristics. For instance, if the chamber pressure buildup period during engine start is excessive, "chugging" may have time to develop. This low-frequency instability, in turn, can trigger the destructive acoustic modes of instability by contaminating one propellant system with the other propellant by driving it back through the injector ports. The triggering chugging can be eliminated through a fast chamber pressure buildup.

Application of Damping Devices

In further support of design for stability, special damping devices can be provided for "dynamic stability" in the combustion chamber and engine system. The following are several devices which have been applied with good results:

1. *Feed system hydraulic capacitor.*—Self-sustained combustion and feed system instabilities of the buzzing type can be eliminated by introducing hydraulic capacitors in the feed system. A hydraulic capacitor is any device which will increase the effective compressibility at a given point in the liquid system. Figure 4-65 shows the schematic of an experimental hydraulic capacitor. It is an isolation-type capacitor with large capacitance and zero resistance between it and the system. Its function is to isolate the transmission of pressure disturbances through the system above a given frequency. Another type is called absorption capacitor, which has small capacitance and high resistance between it and the system. Its function is to absorb the oscillatory energy of the system by damping or attenuating the resonant frequencies of the system.

2. *Combustion-chamber baffles.*—The use of combustion-chamber baffles has been found to be

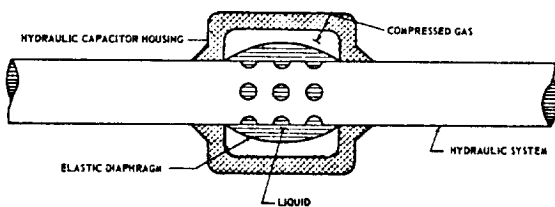


Figure 4-65.—Schematic of experimental isolation type hydraulic capacitor.

the most effective method of suppressing transverse acoustic modes of combustion instability. This has been demonstrated in both full-scale thrust chamber and small-scale models, operating with various propellant combinations. These baffles are usually designed to be secured to the injector face as shown in figure 4-40. Adequate cooling means should be provided to keep the baffles from burnout. The depth or height of the baffles is a function of the distance of the combustion-flame front from the injector face. Experimental evaluations should be conducted to support the design and development effort.

3. *Chamber divergent wall gap.*—It was found experimentally that leaving blank an annular portion of the propellant injection area adjacent to the combustion chamber wall, as shown in figure 4-66, improved the capability of the combustion chamber to recover from triggered instabilities. It was further determined that by filling this "wall gap" with a contoured filler block, "dynamic stability" could be drastically improved in most cases. The exact shape of the contour is critical, and experimental evaluations are required to determine the most effective design configuration.

4. *Acoustic chamber liners.*—The feasibility of using resonant and nonresonant acoustic suppressing liners on the combustion chamber walls has been demonstrated in turbojet engine applications. In this case the principle of suppression is similar to the use of patches of acoustic tile to reduce the sound level in a room, whereby the energy absorbed from the mode will reduce its amplitude. Figure 4-67 shows a typical arrangement. The combined area of the suppressor openings must be of the order of from 3

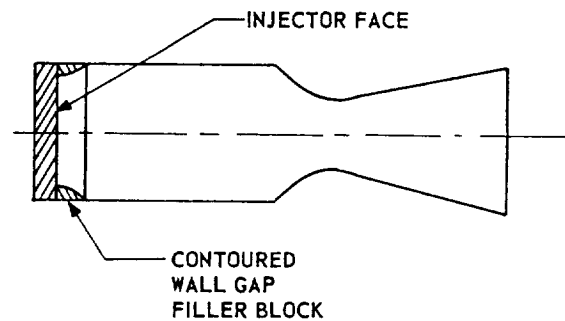


Figure 4-66.—Combustion chamber divergent wall gap.

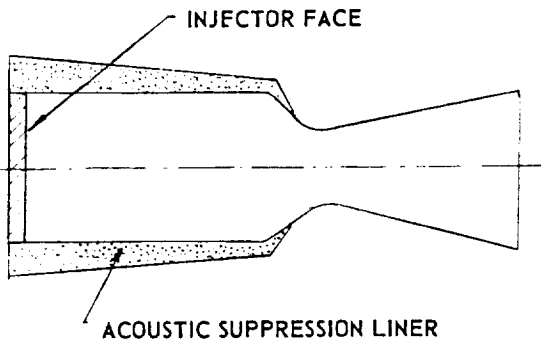


Figure 4-67.—Combustion chamber acoustic liner.

to 4 percent of the total chamber wall surface area. Furthermore, the suppressor thickness should be maximum in the area of maximum pressure variation; i.e., near the injector face.

Rating Stability

It is desirable to establish the combustion stability level of a particular engine system without an excessive number of tests. This can be accomplished by perturbing a normally stable system by suitable means until instability is initiated. The relative stability of various systems is then judged as a function of the magnitude of perturbation needed to reduce the instability. The larger the perturbation, the more stable the system. The perturbation can be introduced in either the propellant feed system or in the combustion chamber. Several effective methods exist for inducing different types of instability.

Feed System Perturbations

Perturbation in the propellant feed system to induce disturbances in the chamber of the low-frequency hydrodynamic type, can be introduced by—

- (1) Explosive charges in the fuel feed system
- (2) Single-stroke positive displacement pistons
- (3) Oscillating pistons

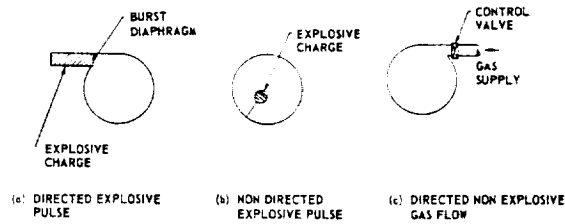


Figure 4-68.—Combustion chamber perturbation methods.

Combustion Chamber Disturbances

The introduction of disturbance in the chamber proper offers a simpler method of inducing instability. Transverse acoustic modes have been initiated most successfully by the following methods:

1. *Directed explosive pulses.*—The directed explosive pulse method of inducing instability, as shown in figure 4-68a, uses a high explosive charge mounted in an external fixture which is attached to the combustion chamber in such a way that the gas pulse resulting from the detonation enters the chamber with any desired orientation.
2. *Nondirected explosive pulses.*—The closest simulation of localized random detonations which can occur in a chamber during normal operation due to accumulation of unburned propellants is achieved by the nondirectional explosive pulse method as shown in figure 4-68b. An explosive is placed into a thin-walled Micarta shell which is designed to be mounted at any desired position in the chamber.
3. *Directed nonexplosive gas flows.*—In this method, as shown in figure 4-68c, a flow of gas from a regulated high-pressure source is controlled by a fast-acting valve. This valve is placed as near to the chamber as possible. This method additionally permits a better definition of the parameters associated with the disturbance.

Chapter V

Design Of Pressurized-Gas Propellant-Feed Systems

For the transfer of the rocket propellants from the tanks to the thrust chamber at the required flow rates and pressures, a suitable feed system is required. The selection of the feed system will depend on the mission of the vehicle, its size and weight, thrust level and duration, space available for the propulsion system, on reliability considerations, and on other factors. There is no simple rule for the choice between a pressurized gas feed system (fig. 1-12) or a turbopump feed system (fig. 1-13). The advancement in the state of the art of lightweight pressurized gas feed systems, in conjunction with the availability of high-strength tank construction materials, has enlarged their field of applications to engine thrust levels of approximately 100 000 pounds, and total impulse values of over 5 million pound-seconds. For large vehicle applications, turbopump feed systems are predominant. However, some type of pressurized gas feed system is always required even in a turbopump feed system to supply propellants to the pump at the correct inlet conditions.

Classified according to their power sources, four major types of pressurized feed systems can be distinguished:

- (1) Stored gas systems
- (2) Propellant evaporation systems
- (3) Systems evaporating nonpropellants
- (4) Systems using products of chemical reactions

Selection depends largely upon engine system design, type of propellants, mission requirements, and available experience.

Among the considerations for selection of the type of pressurized gas propellant feed system are—

- (1) Compatibility of pressurant gases with propellants and tank materials, considering chemical interactions, temperature, solubility, etc.
- (2) Expected pressurization system reliability and complexity, considering the state

- of the art of systems components used.
- (3) Molecular weight of the pressurant gases: Lower molecular weight reduces required pressurant weight per unit pressure and per unit tank volume, and thus results in lower vehicle system weight at burnout and thus improved mass ratio.
 - (4) Pressurization system specific weight; i.e., required pressurization system gross weight (including system components and pressurant), per unit of weight of useful pressurant.

5.1 DETERMINATION OF PRESSURANT REQUIREMENTS

The physical and chemical processes which take place during the expulsion of a liquid propellant from a tank by a gas or gas mixture are numerous and difficult to analyze. Applicable experimental data for a selected system are often limited. Thus, the basis for the analytical approach is frequently narrow and uncertain. As a result, the initial design calculations of the quantity of pressuring gas required must be considered approximate until verified experimentally. The refinement of the analytical approach to minimize discrepancies between theoretical predictions and actual test results is an art requiring experience and thorough understanding of the physical processes.

Basic considerations and necessary procedures for the calculation of pressurant requirements are described below.

Required Engine System Data and Assumptions

Before starting calculations of pressurant requirements, the following significant engine operating parameters must be known or assumed:

- (1) Design operating temperature range of the propellants and the feed system including pressurant

- (2) Type of propellants, their weights and corresponding volumes at the extremes of the operating temperature range
- (3) Total tank volumes: Nominal value and tolerances
- (4) Initial tank ullage volume, percent of total tank volume at the temperature limits. (The term "ullage" denotes that portion of a propellant tank not occupied by the liquid propellants.)
- (5) Trapped propellant volumes, percent of total propellant load, at engine burnout
- (6) Operating tank pressure: Nominal value and tolerances
- (7) Operating duration of the engine systems: Nominal value and variations.

To avoid later marginal conditions, calculations should assume that pressurization must be supplied for maximum systems operating duration even though some missions may require shorter durations. Realistic assumptions for the temperature of tanks and propellants at burnout must be made. If a mission calls for several system restarts and coasting periods, the environmental conditions during the coasting periods must also be given or assumed.

Factors Influencing Pressurant Requirements

Several important factors which will influence considerably the final state of a pressurizing gas or gases, and thus their required quantity, are discussed below.

1. *Propellant vaporization.*—Propellants evaporate to various degrees from the gas-liquid interface within the tank. The amount depends upon the volatility of the propellant, the temperature of the entering gas, the turbulence of the gas, the sloshing of the liquid, the tank geometry including internal structural members, and the rate of propellant expulsion. To whatever degree vaporization takes place, it lowers the temperature of the gas and adds propellant vapor as a component of the pressurizing gases. Also, as the liquid propellant level recedes, a film of liquid may be left on the tank wall surface, further contributing to propellant evaporation.

2. *Tank wall temperature.*—If the pressurizing gas is hotter than the tank walls, cooling of the gas and heating of the wall may result. On the other hand, aerodynamic heating of the tank

walls in flight may cause heating of the pressurizing gas. It may also heat the propellant and thus increase vaporization effects and raise NPSH requirements in turbopump-fed systems.

3. *Vapor condensation.*—Certain components of the pressurizing gas, such as water vapor, may condense. Even if the bulk of the gas remains above the dew point for the condensible component, local condensation may occur at the tank walls, or at the propellant surface.

4. *Solubility of the pressurizing gas.*—If the pressurizing gas contains components which are soluble in the propellant, diffusion of these components into the propellant can occur. Solubility is generally affected by temperature and pressure conditions.

5. *Ullage gas compression.*—If, before start, the tank ullage space is filled with low-pressure gas, onset of pressurization will cause adiabatic compression. This can raise the ullage space temperature considerably during the initial few seconds of operation.

6. *Chemical reaction.*—If any components of the pressurizing gas are chemically reactive with the propellant, the reaction products may become a component of the gas.

7. *Pressurizing gas turbulence.*—The heat exchange between pressurizing gas and propellant would be extremely large if the gas were permitted to agitate the liquid propellant surface. This effect can be prevented through the use of a diffuser which spreads the gas in a gentle flow toward the top and sides of the tank.

Design Calculations of Pressurant Requirements

If the system operating duration is relatively short, or if the pressurant temperature is close to or lower than the propellant temperature, heat- and mass-transfer effects can be neglected. The required pressurant weight can then be calculated by the perfect gas law:

$$W_g = \frac{P_T V_T}{R_g T_g} \quad (5-1)$$

where

W_g = required pressurant weight in the tank, lb

P_T = propellant tank pressure, lb/ft²

V_T = total volume of the empty propellant tank, ft³

CONFIDENTIAL

R_g = gas constant of the pressurant, ft-lb/lb-deg R

T_g = mean temperature of entering pressurant, °R

However, in cases where longer systems duration and higher pressurant temperatures are involved, the pressurant requirement can best be determined by the following procedure, keeping in mind the limitations set forth at the beginning of section 5.1.

Considering first a single-start operation (not requiring coast periods and restarts), and neglecting heat transfer from the tank walls, the total heat transferred from the pressurant gas to the vaporized propellant can be approximated by equation (5-2).

$$Q = HAt(T_u - T_e) \quad (5-2)$$

where

Q = total heat transferred, Btu

H = experimentally determined heat transfer coefficient at the gas-liquid interface, Btu/sec-ft²-deg R

A = area of the gas-liquid interface (in case of a cylindrical tank, the cross-section area of the tank), ft²

t = operating duration, sec

T_u = temperature of the gases at burnout, °R

T_e = temperature of the propellant, °R

Both T_u and T_e are treated as constant values at the interface between liquid and gas.

This heat, Q , is assumed to have heated and vaporized the propellant according to the equation

$$Q = W_v [C_{pl}(T_v - T_e) + h_v + C_{pv}(T_u - T_v)] \quad (5-3)$$

where

W_v = total weight of vaporized propellant, lb

C_{pl} = specific heat of the liquid propellant, Btu/lb-deg R

h_v = heat of vaporization of the propellant, Btu/lb

C_{pv} = specific heat of the propellant vapor, Btu/lb-deg R

T_v = vaporization temperature of the liquid propellant, °R

The value of W_v can now be obtained from equations (5-2) and (5-3) with an assumed value for T_u .

The partial volume occupied by the vaporized propellant is given by

$$V_v = \frac{W_v Z R_p T_u}{P_T} \quad (5-4)$$

where

V_v = total volume occupied by the vaporized propellant, ft³

Z = compressibility factor evaluated at the total pressure (P_T) and the temperature (T_u) of the gaseous mixture at burnout

R_p = gas constant of the propellant vapor, ft-lb/lb-deg R

The remaining tank volume at burnout, neglecting residual propellants, can be assumed to be occupied by the pressurant gas

$$V_g = V_T - V_v \quad (5-5)$$

where V_g = volume of pressurant gas at burnout, ft³

The weight of pressurant is calculated by the perfect gas law

$$W_g = \frac{P_T V_g}{R_g T_u} \quad (5-6)$$

In order to maintain the heat balance, the value for Q should satisfy the following equation:

$$Q = W_g C_{pg} (T_g - T_u) \quad (5-7)$$

where C_{pg} = specific heat at constant pressure of pressurant gas, Btu/lb-deg R

From equation (5-7) the required value of T_g for the assumed T_u can thus be calculated. If however, T_g is a predetermined fixed value, then the values of W_g , W_v , and T_u must satisfy the following as well as other correlated equations:

$$W_g C_{pg} (T_g - T_u) = W_v [C_{pl}(T_v - T_e) + h_v + C_{pv}(T_u - T_v)] \quad (5-8)$$

Thus far, heat transfer from the tank walls has been neglected. However, if there is a considerable temperature differential between pressurizing gases, propellant, and tank walls, the total heat transferred between them during the mission must be taken into consideration for the determination of vaporized propellant at burnout.

Equation (5-3) can be rewritten as

$$Q \pm Q_{W_1} = W_v [C_{pl}(T_v - T_e) + h_v + C_{pv}(T_u - T_v)] \quad (5-9)$$

where Q_{W_1} = total heat transferred between tank walls and liquid and gaseous propellant during the mission, Btu. The positive (+) or negative (-) sign indicates whether Q_{W_1} is contributed by, or lost to, the tank walls.

Furthermore, equation (5-7) becomes

$$Q = W_g C_{pg}(T_g - T_u) \pm Q_{W_2} \quad (5-10)$$

where Q_{W_2} = total heat transferred between pressurizing gases and tank walls during a mission, Btu. Again the positive (+) or negative (-) sign indicates whether heat is contributed by, or lost to, the tank walls.

Combining equations (5-9) and (5-10), the heat balance considering heat transfer from the tank walls can be written as

$$[W_g C_{pg}(T_g - T_u)] \pm Q_{W_2} = W_v [C_{pl}(T_v - T_e) + h_v + C_{pv}(T_u - T_v)] - (\pm Q_{W_1}) \quad (5-11)$$

If the vehicle mission includes several powered flight and coasting periods, the calculation of the heat transfer across the gas-liquid interface should take the total mission time into consideration. Equation (5-2) can be rewritten as

$$Q = H A t_m (T_m - T_e) \quad (5-12)$$

where

t_m = total mission time including powered flight and coasting period, sec

T_m = mean temperature of the pressurizing gases during the entire mission, °R.

This is a function of many factors such as length of coasting periods, heat transfer between gases and tank wall, etc.

Other effects such as vapor condensation, solubility of the pressurizing gas in the propellant, and chemical reactions of the pressurizing gas with the propellant can be included, based

on experimental data. However, no set of equations can be applied directly.

In some cases, the uncertainties in pressurizing system design can be reduced by providing adjustability of the pressurant temperature at the propellant tank inlet. In this approach, the temperature of the pressurizing gas at system burnout is assumed or targeted from the beginning. Based on this and other given or assumed data, the values of required pressurant quantity and inlet temperature can be calculated by equations (5-1) through (5-11). Certain correction factors such as pressurant solubility, etc., can be applied later. If the required pressurant quantity in experimental engine system evaluation deviates from the calculations, because of temperature discrepancies of the pressurizing gas at system burnout, an adjustment of the pressurant temperature at the propellant tank inlet can often be made to correct for this difference, such as through an adjustment of the pressurant supply from a heat exchanger, or from a gas generator. Because of the narrow safety margins employed in rocket vehicle design, the effect of varied gas temperatures on structural members must be carefully weighed.

The following is a sample calculation to demonstrate this design approach:

Sample Calculation 5-1

From table 3-5, the following data are obtained for the oxidizer tank of the A-4 stage propulsion system:

Oxidizer, N_2O_4

Pressurant, gaseous He

Tank volume, neglecting the volume of residual propellant, (V_T) = 119 ft³

Average tank cross-section area, (A) = 20 ft²

Tank pressure, (P_T) = 165 psia, or 23 760 psfa

Propellant temperature, (T_e) = 520° R

Calculate the following:

(a) The total pressurant weight (W_g) and required temperature (T_g) at the tank inlet, for a single operation time (t) of 500 seconds, with an experimentally determined heat transfer coefficient (H) at the gas-liquid interface of 0.002 Btu/sec-ft²-deg R. It is assumed the ullage gas temperature T_u at burnout is 700° R and that there is no heat transferred at the tank wall surfaces.

(b) The required pressurant weight (W_g) and temperature (T_g) at the tank inlet, for a mission consisting of several powered flight and coasting periods, with a total mission duration (t_m) of 18 000 seconds. The mean temperature of the pressurizing gases during the mission (T_m) is 526° R. The total heat transferred between propellant and tank walls (Q_{W_1}) is -2000 Btu. The total heat transferred between pressurizing gas and tank walls (Q_{W_2}) is -600 Btu. The temperature (T_u) of the ullage gases at final burnout is 660° R.

Solution

(a) From standard propellant references, the following data are obtained for N_2O_4 at a pressure of 165 psia:

Vaporization temperature, $T_v = 642^\circ R$

Heat of vaporization, $h_v = 178$ Btu/lb

Mean value of specific heat in liquid state,

$C_{pl} = 0.42$ Btu/lb deg F

Mean value of specific heat in vapor state,

$C_{pv} = 0.18$ Btu/lb-deg F

Compressibility factor, $Z = 0.95$

Molecular weight = 92

The specific heat of helium, C_{pg} , is 1.25 Btu/lb-deg F, and its molecular weight is 4.

From equation (5-2), total heat transferred at the gas-liquid interface:

$$Q = HAt(T_u - T_e) \\ = 0.002 \times 20 \times 500(700 - 520) = 3600 \text{ Btu}$$

Substitute this into equation (5-3):

$$3600 = W_v [C_{pl}(T_v - T_e) + h_v + C_{pv}(T_u - T_v)] \\ = W_v [0.42(642 - 520) + 178 + 0.18(700 - 642)] \\ = W_v \times 239.6$$

Total weight of vaporized propellant, $W_v = 15.1$ lb

Substitute into equation (5-4), to obtain the volume occupied by the vaporized propellant:

$$V_v = \frac{W_v Z R_p T_u}{P_T} \\ = \frac{15.1 \times 0.95 \times \frac{1544}{92} \times 700}{23760} \\ = 7.13 \text{ ft}^3$$

Substitute this into equation (5-5), to obtain the volume occupied by pressurant gas

$$V_g = V_T - V_v = 119 - 7.13 = 111.87 \text{ ft}^3$$

From equation (5-6), the required pressurant weight results:

$$W_g = \frac{P_T V_g}{R_g T_u} \\ = \frac{23760 \times 111.87}{\left(\frac{1544}{4}\right) \times 700} \\ = 9.79 \text{ lb}$$

Substitute results into equation (5-7),

$$Q = 9.79 C_{pg}(T_g - T_u) \\ 3600 = 9.79 \times 1.25(T_g - T_u)$$

The required pressurant temperature at tank inlet is:

$$T_g = \frac{3600}{9.79 \times 1.25} + 700 = 995^\circ R$$

(b) From equation (5-12), the total heat transferred at the gas-liquid interface:

$$Q = HAt_m(T_m - T_e) \\ = 0.002 \times 20 \times 18000(526 - 520) \\ = 4320 \text{ Btu}$$

Substitute into equation (5-9):

$$4320 - 2000 = W_v [0.42(642 - 520) \\ + 178 + 0.18(660 - 642)]$$

$$W_v = 10.0 \text{ lb}$$

Substitute into equation (5-4):

$$V_v = \frac{10.0 \times 0.95 \times \left(\frac{1544}{92}\right) \times 660}{23760} \\ = 4.45 \text{ ft}^3$$

Substitute into equation (5-5):

$$V_g = 119 - 4.45 = 114.5 \text{ ft}^3$$

Substitute into equation (5-6):

$$W_g = \frac{23760 \times 110.76}{\left(\frac{1544}{4}\right) \times 660} = 10.65 \text{ lb}$$

Substitute into equation (5-10):

$$4320 = 10.65 \times 1.25 (T_g - 660) - 600$$

$$T_g = \frac{4320 + 600}{10.65 \times 1.25} + 660 = 1030^\circ \text{ R}$$

5.2 STORED GAS SYSTEMS

Stored gas pressurization systems are widely used in numerous combinations. The gas is usually stored in a vessel at pressures ranging from 3000 to 5000 psi and supplied to the propellant feed system at a specified pressure level controlled by a regulator. These systems have achieved a high level of reliability. In earlier systems, compressed nitrogen gas was frequently used or even air (German V-2), mainly for logistics and supply reasons. As it became more readily available, helium gas found increased usage because of its substantially lower molecular weight and thus reduced total pressurant weight, and its superiority as an inert agent, with very low boiling point. For hydrogen-fueled engine systems, reliable compressed hydrogen gas systems have been successfully developed. In general, the most important design requirements for a stored gas system are: low molecular weight of the gas, high gas density under storage conditions, minimum residual gas weight, and high allowable stress-to-density ratio of the storage vessel material. Since helium systems are now the most widely used ones, the following discussions will be based on them.

Discussion of Commonly Used Configurations

1. *Helium system without heating.*—This pressurization system is shown schematically in figure 5-1. It consists of a high-pressure storage vessel, a start and shutoff valve, and a pressure regulator. Regulated helium is ducted directly

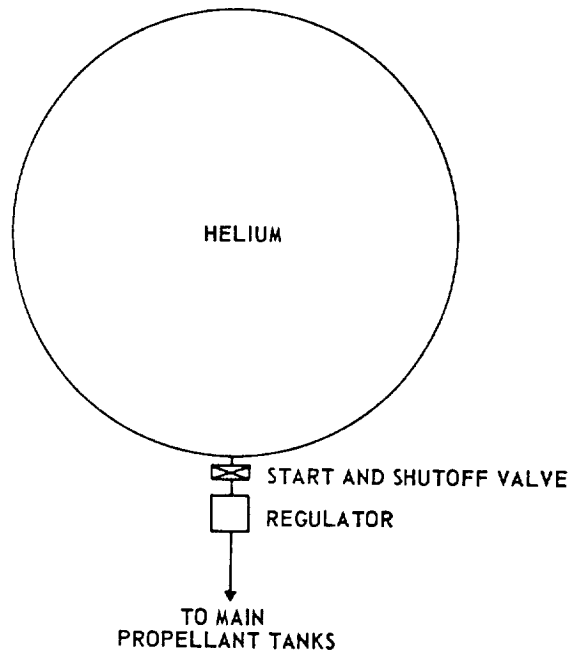


Figure 5-1.—Helium pressurization system without heating.

to the main propellant tanks. This has the advantage of great simplicity. However, the weight of the system is relatively high because of the lower temperature and thus lower specific volume of the gas.

2. *Helium system using thrust chamber heat exchangers.*—This system, which is used in the design for the A-3 and A-4 stage propulsion systems, consists of a high-pressure helium storage vessel, a start and shutoff valve, manifolded thrust chamber heat exchangers, and a pressure regulator. A typical schematic is shown in figure 5-2. The heat exchangers are part of the thrust chamber divergent nozzle section and absorb heat from the thrust chamber combustion process. From overall performance and weight considerations it is considered preferable to locate the heat exchanger in the high-pressure portion of the system. The volume increase of the gas due to heating reduces the mass required for tank pressurization. However, a considerable quantity of cold, high-density helium still remains in the storage vessel at the end of the system operation.

3. *Helium cascade system.*—The cascade system shown schematically in figure 5-3 is an

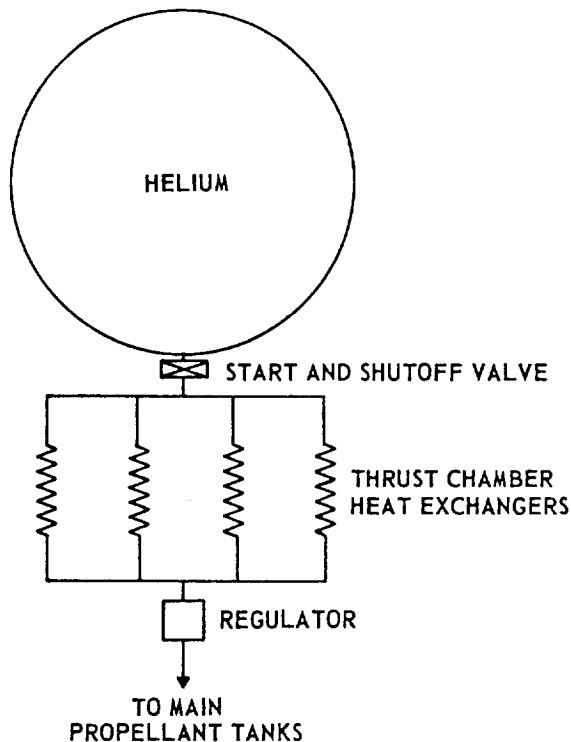


Figure 5-2.—Helium pressurization system using thrust chamber heat exchangers.

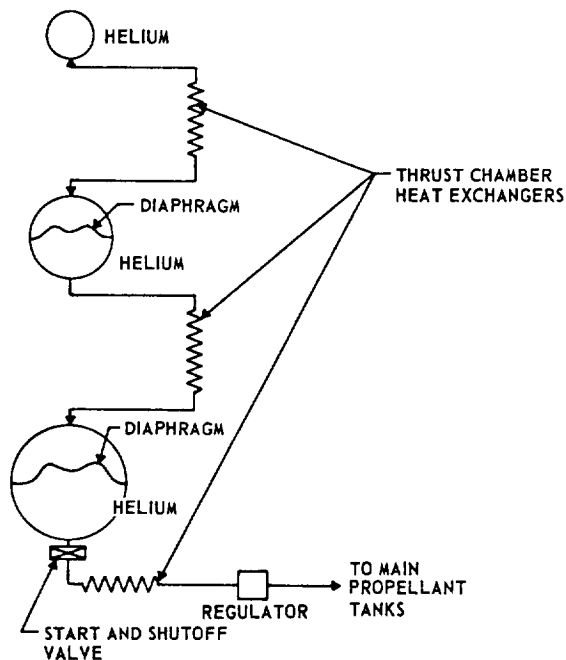


Figure 5-3.—Helium cascade system.

all-helium pressurization system designed to minimize the weight penalty resulting from cooling of the helium during expansion. System components include helium storage vessels of equal high-pressure level but of different sizes, two of which are divided internally by a flexible diaphragm, three thrust chamber heat exchangers, a start and shutoff valve, and a pressure regulator. During operation of the system, helium flows from the first and smallest vessel, through a heat exchanger, and displaces completely the helium in the intermediate vessel. The helium in the intermediate vessel in turn flows through a second heat exchanger and completely displaces the helium in the last and largest vessel. The latter flows through a third heat exchanger and pressurizes the main propellant tanks. At the end of the operation, only the small storage vessel contains low-temperature, high-density helium, while the two large storage vessels contain relatively warm low-density helium. This contrasts with the preceding systems in which one large storage vessel remains partially filled with low-temperature, high-density helium. The disadvantages of cascade systems are high weight and complexity.

4. *Helium system with heating inside the storage vessel.*—This system is shown schematically in figure 5-4 and consists of a high-pressure helium storage vessel containing a heat exchanger or other heat-generating device mounted internally, a start and shutoff valve, and a pressure regulator. This system provides higher temperature helium to the main propellant tanks, simultaneously assuring relatively warm residual gas in the storage vessel. Disadvantages are the need for larger and more complex high-pressure storage vessels and the possibility of control problems during operation.

For the pressurization of liquid hydrogen propellant tanks, stored hydrogen gas can be used in place of helium for the systems described above.

Calculations for Stored Gas Requirements

The design calculations discussed in section 5.1 apply only to the net or effective quantity of gas required to pressurize the propellant tanks. However, the gross weight of the stored gas required for a given system depends also on the

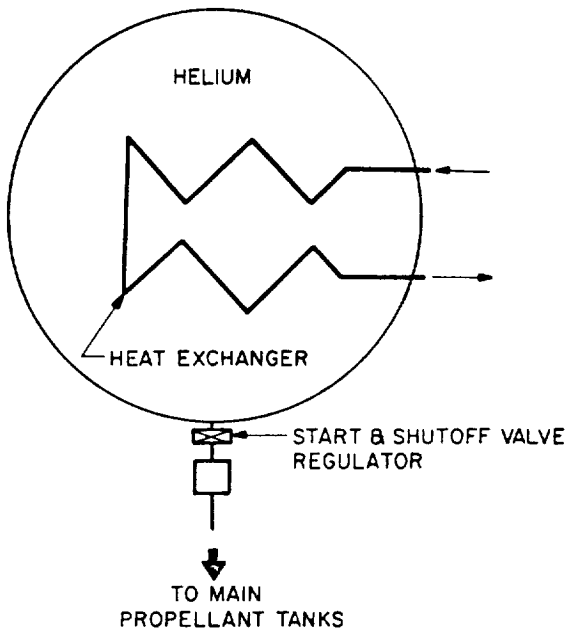


Figure 5-4.—Helium pressurization system using heaters in storage vessel.

system design, on the expansion process during operation, and on the environmental temperature range within which the system must function. Based on conditions at systems burnout, the total or gross stored gas requirement can be expressed by the following correlation:

$$\text{Stored gas gross requirement} = \frac{\text{Net system pressurant requirement}}{\text{pressurant use factor}} \quad (5-13)$$

$\frac{\text{Residual gas in storage vessel} + \text{Residual gas in various lines, heat exchangers, etc.}}{\text{pressurant use factor}}$

A parameter to define these additions is the pressurant use factor, defined as the ratio of gross stored gas requirement or initial gas weight in the storage vessel to the net weight of pressurant utilized:

$$\text{pressurant use factor} = \frac{\text{Gross stored gas requirement}}{\text{System pressurant net requirement}} \quad (5-14)$$

The lowest pressure level in a storage vessel required to safely operate the pressurization system is determined by the individual system pres-

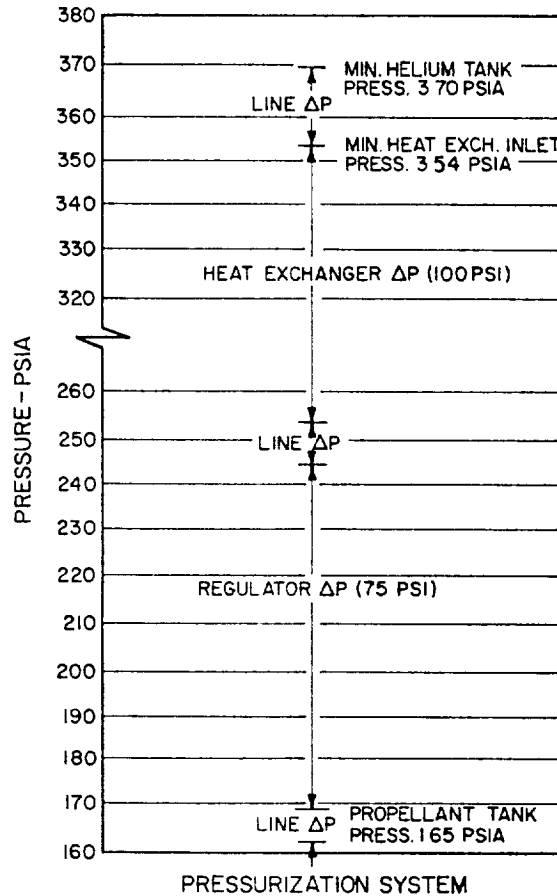


Figure 5-5.—Estimated pressure drops for A-4 stage oxidizer tank pressurization system.

sure drops. Figure 5-5 shows estimated pressure drops for the stored helium pressurization system with thrust chamber heating which was selected for the A-4 stage engine oxidizer tank. In addition, a safety margin is usually provided. In this case, the mission is assumed to be completed when the storage vessel pressure decays to 400 psia.

If a heating source is provided inside the vessel, as shown in figure 5-4, the expansion process of the gas within would be polytropic. For a system without heating inside the storage vessel, the expansion process of the gas can be

assumed to be isentropic; i.e., no heat is transferred between gas and vessel walls. From equation (1-13) the following correlation can be derived to calculate the final gas temperature in the storage vessel:

$$\frac{T_2}{T_1} = \left(\frac{P_2}{P_1} \right)^{\frac{n-1}{n}} \quad (5-15)$$

where

T_1 = initial helium temperature in the vessel, °R

T_2 = final helium temperature in the vessel, °R

P_1 = initial helium pressure in the vessel, psia

P_2 = final helium pressure in the vessel, psia

n = exponent for the polytropic expansion process

The exponent n is estimated during analytical treatment and verified experimentally. For isentropic expansion of helium, $n = 1.67$.

For most analyses it has been found adequate to assume an adiabatic flow process through regulator and lines. It is a characteristic of this process that the total (or "stagnation") temperature remains constant. Since the gas essentially comes to rest in the propellant tank and no further compression takes place following initial propellant tank pressurization, it is assumed that propellant tank temperature is equal to heat exchanger outlet temperature.

If an operating temperature range is specified for a system, the lower temperature limit must be used to calculate the weight of pressurant required, while the upper limit determines the volume of the gas storage vessel for a given storage pressure. Thus, for a stated propellant tank net pressurant gas requirement, a wider environmental temperature range results in a heavier pressurization system, regardless of the expansion process followed by the gas.

Sample Calculation 5-2

The following data are given for the stored helium pressurization system of the A-4 stage oxidizer tank:

Temperature range in the storage vessel at system start, 500°-560° R

Storage vessel pressure at system start, 4500 psia

Pressure in the storage vessel at system burnout, 400 psia

Volume of the helium lines downstream of regulator, 0.4 ft³

Volume of heat exchangers, 1.0 ft³

Volume of lines between storage vessel, heat exchangers and regulator, negligible

Pressurant reserve, 2 percent

Assuming an isentropic expansion process, calculate the following:

(a) Oxidizer tank pressurant gross weight, storage-vessel volume, and use factor, for case (a) of sample calculation (5-1).

(b) Oxidizer tank pressurant gross weight, storage-vessel volume, and use factor, for case (b) of sample calculation (5-1).

(c) Oxidizer tank pressurant gross weight, storage-vessel volume, and use factor for single start operation but without heat exchangers.

(d) Same as (c), but assuming a polytropic expansion process with $n = 1.2$ in the storage vessel.

Solution

The following calculations establish the requirements for the oxidizer tank, which in the A-4 stage has the higher minimum storage pressure requirement. To this required pressurant mass and volumes for fuel tank pressurization, purges and valve actuations will have to be added.

(a) A net pressurant requirement of 9.79 pounds is obtained from sample calculation (5-1), case (a). Temperature and pressure of the residual pressurant in the lines downstream of the regulators following shutdown are assumed to be the same as those of the propellant tank ullage gases at system burnout (700° R and 23 760 psfa). Residual gas weight in these lines then is

$$\frac{0.4 \times 23\,760}{\left(\frac{1544}{4} \right) \times 700} = 0.035 \text{ lb}$$

It is further assumed that the temperature of the residual pressurant in the heat exchangers is at run tank inlet conditions, or 995° R, and that the pressure is that of the residual helium in the storage vessel, or 400 psia. Thus a value of

$$\frac{1 \times 400 \times 144}{\left(\frac{1544}{4}\right) \times 995} = 0.15 \text{ lb}$$

is obtained for these residuals.

Substituting the lower limit of the system operating temperature, and the initial and final helium pressures into equation (5-15), the temperature of the residual helium in the storage vessel at system burnout is obtained:

$$T_2 = 500 \times \left(\frac{400}{4500}\right)^{\frac{1.67-1}{1.67}} = 500 \times (0.089)^{0.4} = 191^\circ \text{R}$$

Using equation (5-13), the pressurant volume V_L required for oxidizer tank pressurization can now be calculated, based on the lower storage temperature limit of 500°R :

$$\frac{4500 \times 144 \times V_L}{\left(\frac{1544}{4}\right) \times 500} = 9.79 + \frac{400 \times 144 \times V_L}{\left(\frac{1544}{4}\right) \times 191} + 0.035 + 0.15$$

$$V_L = \frac{9.975}{0.374 \times 6.9} = 3.78 \text{ ft}^3$$

Gross pressurant weight:

$$\frac{4500 \times 144 \times 3.78}{\left(\frac{1544}{4}\right) \times 500} \times 1.02 = 12.95 \text{ lb}$$

including 2 percent reserve.

Using the upper start temperature limit (560°R), the required volume of the storage vessel for oxidizer pressurization is calculated:

$$V_u = \frac{\left(\frac{1544}{4}\right) \times 560 \times 12.95}{4500 \times 144} = 4.3 \text{ ft}^3$$

From equation (5-14), LOX tank pressurant use factor:

$$\frac{12.95}{9.79} = 1.325$$

(b) From sample calculation (5-1), case (b), the net pressurant requirement is given as 10.65 pounds. Assuming temperature and pressure in

the lines are the same as those in the propellant tank at system burnout (660°R and 23 760 psfa), residual gas weight in these lines is

$$\frac{0.4 \times 23760}{\left(\frac{1544}{4}\right) \times 660} = 0.037 \text{ lb}$$

The temperature of the residual pressurant in the heat exchangers is assumed to be at the run tank inlet level, or 1030°R , and that the pressure is that of the residual helium in the storage vessel, or 400 psia. The gas weight in the heat exchangers then amounts to:

$$\frac{1 \times 400 \times 144}{\left(\frac{1544}{4}\right) \times 1030} = 0.145 \text{ lb}$$

From equation (5-13), pressurant volume V_L and mass are obtained, using the lower temperature limit:

$$\frac{4500 \times 144 \times V_L}{\left(\frac{1544}{4}\right) \times 500} = 10.65 + \frac{400 \times 144 \times V_L}{\left(\frac{1544}{4}\right) \times 191} + 0.037 + 0.145$$

$$V_L = \frac{10.832}{2.58} = 4.2 \text{ ft}^3$$

Gross pressurant weight:

$$\frac{4500 \times 144 \times 4.2}{\left(\frac{1544}{4}\right) \times 500} \times 1.02 = 14.45 \text{ lb}$$

including 2 percent reserve.

Required volume of the storage vessel:

$$V_u = \frac{\left(\frac{1544}{4}\right) \times 560 \times 14.45}{4500 \times 144} = 4.82 \text{ ft}^3$$

Pressurant use factor:

$$\frac{14.45}{10.65} = 1.36$$

(c) Without heat exchangers, the bulk temperature of helium in the propellant tank at system burnout can be expected to be the average of the

initial and final helium temperatures in the storage vessel, or

$$T_g = \frac{500 + 191}{2} = 346^\circ \text{R}$$

Since this temperature is lower than the propellant temperature, no heat loss from pressurant to propellant is assumed. The net pressurant weight required may then be calculated by equation (5-1):

$$W_g = \frac{23\,760 \times 119}{\left(\frac{1544}{4}\right) \times 346} = 21.2 \text{ lb}$$

The weight of residual helium in the lines at system burnout:

$$\frac{0.4 \times 23\,760}{\left(\frac{1544}{4}\right) \times 346} = 0.071 \text{ lb}$$

From equation (5-13), pressurant volume V_L and mass are obtained, based on the lower ambient temperature limit:

$$\frac{4500 \times 144 \times V_L}{\left(\frac{1544}{4}\right) \times 500} = 21.2 + \frac{400 \times 144 \times V_L}{\left(\frac{1544}{4}\right) \times 191} + 0.071$$

$$V_L = \frac{21.27}{2.58} = 8.25 \text{ ft}^3$$

Gross pressurant weight =

$$\frac{4500 \times 144 \times 8.25}{\left(\frac{1544}{4}\right) \times 500} \times 1.02 = 28.2 \text{ lb}$$

including 2 percent reserve.

The required volume of the storage vessel is

$$V_u = \frac{\left(\frac{1544}{4}\right) \times 560 \times 28.2}{4500 \times 144} = 9.4 \text{ ft}^3$$

Pressurant use factor:

$$\frac{28.2}{21.2} = 1.33$$

(d) The expansion process of helium in the storage vessel is assumed to be polytropic, with $n = 1.2$. From equation (5-14), the temperature of residual helium in the vessel at system burnout:

$$T_2 = 500 \times \left(\frac{400}{4500}\right)^{\frac{1.2-1}{1.2}} = 500 \times \frac{2.73}{4.07} = 336^\circ \text{R}$$

The helium bulk temperature in the propellant tank at system burnout:

$$T_g = \frac{500 + 336}{2} = 418^\circ \text{R}$$

The required net pressurant weight:

$$W_g = \frac{23\,760 \times 119}{\left(\frac{1544}{4}\right) \times 418} = 17.5 \text{ lb}$$

The residual helium weight in the lines at system burnout:

$$\frac{0.4 \times 23\,760}{\left(\frac{1544}{4}\right) \times 418} = 0.059 \text{ lb}$$

Pressurant volume and mass, based on the lower ambient temperature limit:

$$\frac{4500 \times 144 \times V_L}{\left(\frac{1544}{4}\right) \times 500} = 17.5 \text{ lb} + \frac{400 \times 144 \times V_L}{\left(\frac{1544}{4}\right) \times 336} + 0.059$$

$$V_L = \frac{17.56}{2.92} = 6.01 \text{ ft}^3$$

Gross pressurant weight:

$$\frac{4500 \times 144 \times 6.01}{\left(\frac{1544}{4}\right) \times 500} \times 1.02 = 20.6 \text{ lb}$$

including 2 percent reserve.

The required volume of the storage vessel:

$$V_u = \frac{\left(\frac{1544}{4}\right) \times 560 \times 20.6}{4500 \times 144} = 6.88 \text{ ft}^3$$

Pressurant use factor:

$$\frac{20.6}{17.5} = 1.178$$

Design of Stored Gas System Components

Since system components can be expected to require relatively extensive development effort to achieve satisfactory performance and reliability, they require careful design considerations. This is especially true for large, high-pressure, lightweight, pressurant storage vessels, pressure regulators, and thrust chamber nozzle skirt-type heat exchangers.

Storage Vessels

Because of the combined requirement of high pressure and light weight, pressurant storage vessels are generally spherical in shape and made of high-strength-to-weight materials. PH-15-7-MO stainless steel, 6Al-4V-titanium, and light aluminum liners wound with plastic filaments for strength, such as fiber glass, have been successfully employed as construction materials for the vessels. Design details for pressurant storage vessels will be further discussed in chapter VIII.

For weight estimates in preliminary designs, it is assumed that the vessel is made of two hemispherical shells, and that the thickness of the weld lands can be accounted for by assuming a 3-inch-wide band of one-half the wall thickness placed over the weld seam. Hence, the total weight of the vessel can be estimated as:

$$W_v = \pi d^2 \rho_m (pd/4s) + 3\pi d \rho_m (0.5 pd/4s) \quad (5-16)$$

where

- W_v = weight of the vessel, lb
- d = inside diameter of the vessel, in
- p = maximum storage pressure, psia
- s = allowable working stress of the material, psi
- ρ_m = density of the material, lb/in³

It is of prime importance in the design of stored gas systems that the storage vessel be capable of containing the gas at high pressure for long periods of time without loss by leakage. Frequent checking of the storage pressure or recharging is undesirable in most applications.

Experimental data indicate that gases of low molecular weight such as helium and hydrogen will not leak through homogeneous metals such as good-quality, hot-rolled stock or forgings. However, they can leak through porous metals such as may exist in castings and in welded joints. Good welding workmanship and effective leakage inspection are most important in the fabrication of storage vessels.

Pressure Regulators

For most pressurization systems a regulator of high accuracy is a necessity. Regulation becomes particularly difficult if gases with temperatures higher than 1200° R have to be handled, or if high flow rates or large pressure differentials are involved. Design detail of pressure regulators will be discussed in chapter VII. For some applications, a control system combining a pressure switch, a solenoid valve, and an orifice may be preferred.

Thrust Chamber Heat Exchangers

For helium systems using thrust-chamber heat

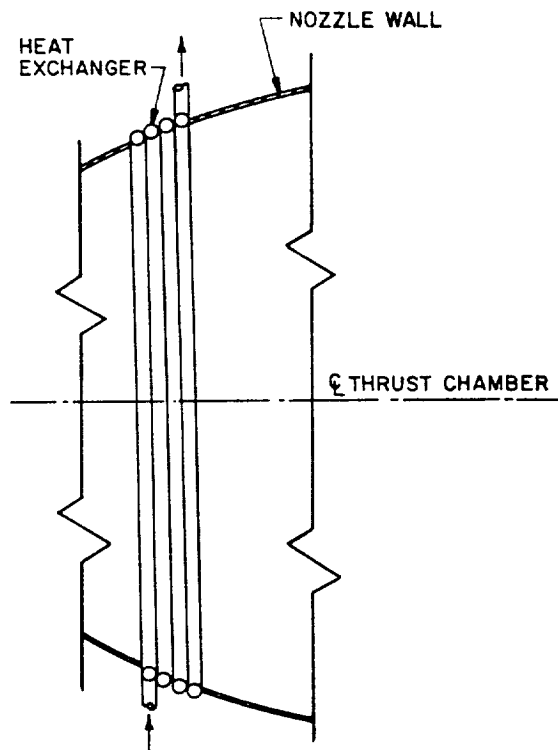


Figure 5-6.—Thrust chamber heat exchanger.

exchangers as shown in figure 5-2, the heat exchanger should be designed as an integral part of the thrust chamber expansion nozzle. As a rule, the heat exchanger is made of coiled tubing formed to fit the nozzle contour (fig. 5-6).

The combustion-gas side heat-transfer coefficient can be determined by methods described in chapter IV. The heat conducted through the wall of the heat exchanger is assumed to be totally absorbed by the pressurant helium, raising its temperature. The determination of the helium-side heat-transfer coefficient and the design of the heat exchanger tubing are similar to the regeneratively cooled tubular wall thrust chamber analyses. The number of tube turns for the heat exchanger is a function of the helium temperature rise required and of the heat exchanger location at the nozzle. The various operating parameters of a thrust chamber heat exchanger can be correlated by the following equation:

$$\dot{W}_h C_p (T_o - T_i) = A \left(\frac{1}{\frac{1}{h_g} + \frac{t}{k} + \frac{1}{h_h}} \right) \left(T_{aw} - \frac{T_i + T_o}{2} \right) \quad (5-17)$$

where

- \dot{W}_h = helium flow rate, lb/sec
- C_p = specific heat at constant pressure of helium, Btu/lb-deg F
- T_i = mean helium temperature at heat exchanger inlet, °R
- T_o = mean helium temperature at heat exchanger outlet, °R
- A = effective area of the heat exchanger, in²
- h_g = combustion-gas side heat transfer coefficient, Btu/in²-sec-deg F
- h_h = helium-side heat transfer coefficient, Btu/in²-sec-deg F
- t = heat exchanger tube wall thickness, in
- k = thermal conductivity of the tube material, Btu/in²-sec-deg F/in
- T_{aw} = combustion-gas side adiabatic wall temperature, °R

Heat exchanger design must consider that the temperature of the helium leaving the heat exchanger at any given time depends on the storage vessel exit temperature.

The choice of heat exchanger tube material must be made with consideration of its brazing

compatibility with the main chamber nozzle wall. Firm attachment of the heat exchanger to the nozzle wall is mandatory, since heat exchanger efficiency depends on intimate contact. Selection of tube thickness must be based on pressure and thermal stress conditions.

Sample Calculation (5-3)

The following data are given for the design of the pressurant heat exchangers for the A-4 stage engine thrust chamber nozzle extension, when located at the station of area ratio = 10, and used in parallel:

Helium flow rate through each heat exchanger,

$\dot{W}_h = 0.024$ lb/sec (considers requirements for both tanks and for other uses)

Helium specific heat ratio, $\gamma = 1.67$

Helium specific heat at constant pressure, $C_p = 1.25$

Mean temperature of helium at heat exchanger inlet, $T_i = 346^\circ$ R

Mean temperature of helium at heat exchanger outlet, $T_o = 1030^\circ$ R (from sample calculation (5-1), case (b))

Combustion-gas side adiabatic wall temperature, $T_{aw} = 4900^\circ$ R

Combustion-gas side heat transfer coefficient, $h_g = 5.7 \times 10^{-5}$ (Btu/in²-sec-deg F)

Calculate:

(a) Heat exchanger tube dimensions, assuming it to be made of 13V-11Cr-3AC titanium alloy with the following physical characteristics, at a recommended maximum working temperature range of 1400°-1550° R:

Minimum yield strength, $S_y = 40\,000$ psi

Modulus of elasticity, $E = 12 \times 10^6$ psi

Thermal conductivity, $k = 2.04 \times 10^{-4}$ Btu/in²-sec-deg F/in

Coefficient of thermal expansion, $\alpha = 5.0 \times 10^{-6}$ in/in-deg F

Poisson's ratio, $\nu = 0.33$

(b) Number of turns of the heat exchanger tubing.

Solution

(a) The wall temperature at given sections of the heat exchanger will vary directly with the bulk temperature of the helium in these sections. Maximum wall temperature occurs at the heat

exchanger outlets. A mean combustion-gas side wall temperature (T_{wg}) at the outlets of 1400°R is allowed. From equation (4-10), the heat flux at that section is:

$$q = h_g (T_{aw} - T_{wg}) \\ = 5.7 \times 10^{-5} \times (4900 - 1400) = 0.2 \text{ Btu/in}^2 \text{ sec}$$

A tube wall thickness (t) of 0.05 inch is used. This will be checked further below for compatibility with pressure and thermal stresses. From equation (4-19), the mean helium-side wall temperature is

$$T_{wc} = T_{wg} - \frac{tq}{k} = 1400 - \frac{0.05 \times 0.2}{2.04 \times 10^{-4}} = 1350^\circ\text{R}$$

Using equation (4-20), the helium-side heat transfer coefficient is calculated as

$$h_h = h_c = \frac{q}{(T_{wc} - T_{co})} = \frac{0.2}{(1350 - 1030)} \\ = 6.25 \times 10^{-4} \text{ Btu/in}^2\text{-sec-deg F}$$

Equation (4-15) permits determination of the Prandtl number of the flowing helium:

$$Pr = \frac{4\gamma}{9\gamma - 5} = \frac{4 \times 1.67}{9 \times 1.67 - 5} = 0.665$$

The viscosity of the helium according to equation (4-16) is:

$$\mu = (46.6 \times 10^{-10}) \times \mathcal{M}^{0.5} T^{0.6} \\ \mu = 46.6 \times 10^{-10} \times 4^{0.5} \times (1030)^{0.6} \\ = 60.2 \times 10^{-8} \text{ lb/in-sec}$$

From equation (4-25)

$$h_h = \frac{0.029 C_p \mu^{0.2} \left(\frac{G^{0.8}}{d^{0.2}}\right) \left(\frac{T_{co}}{T_{wc}}\right)^{0.55}}{Pr^{2/3}} \\ 6.25 \times 10^{-4} = \frac{0.029 \times 1.25 \times (60.2 \times 10^{-8})^{0.2}}{(0.665)^{2/3}} \\ \times \left(\frac{4 \dot{W}_h}{\pi d^2}\right)^{0.8} \times \left(\frac{1030}{1350}\right)^{0.55}$$

$$d^{1.8} = 0.235$$

Inside tubing diameter, $d = 0.44$ inch.

Check for combined pressure and thermal stresses at the heat exchanger outlet (neglecting bending stress), using equation (4-27), and assuming bending stress due to discontinuities to be negligible

$$S_t = \frac{(P_{co} - P_g)r}{t} + \frac{Eaq t}{2(1-\nu)k} \\ = \frac{4500 \times \left(\frac{0.44}{2}\right)}{0.05} + \frac{12 \times 10^6 \times 5.0 \times 10^{-6} \times 0.2 \times 0.05}{2(1-0.33) \times 2.04 \times 10^{-4}} \\ = 19800 + 2200 = 22000 \text{ psia}$$

The combined pressure and thermal stresses at the heat exchanger inlet are now checked. It can be assumed that the difference between the combustion-gas side wall temperature and the helium bulk temperature remains approximately constant throughout the heat exchanger. Then:

$$T_{wg} \text{ at the inlet} = 1400 - (1030 - 346) = 716^\circ\text{R} \\ \text{(mean temperature)}$$

$$\text{Heat flux } q \text{ at the inlet} = 5.7 \times 10^{-5} (4900 - 716) \\ = 0.239 \text{ Btu/in}^2\text{-sec}$$

Combined stress S_t at the inlet

$$= 19800 + 2200 \times \left(\frac{0.239}{0.2}\right) \\ = 19800 + 2630 = 22430 \text{ psi}$$

Therefore, it is safe to use the selected tube size of 0.440-inch inside diameter and 0.050-inch wall thickness, with sufficient margin for the fact that the heat exchanger helium inlet temperature will be higher than the maximum at the beginning of the process.

(b) From equation (5-17), the required effective area for each heat exchanger element

$$A = 0.024 \times 1.25 (1030 - 346) \\ \times \frac{\left(\frac{1}{5.7 \times 10^{-5}} + \frac{0.05}{2.04 \times 10^{-4}} + \frac{1}{6.25 \times 10^{-4}}\right)}{4900 - \frac{1030 + 346}{2}} = 95 \text{ in}^2$$

The nozzle diameter at area ratio = 10 of the A-4 chamber is:

$$D = D_t \times \sqrt{10} = 7.18 \times \sqrt{10} = 22.7 \text{ in}$$

Assuming 40 percent of the internal tube surface as the effective heat exchanger area, the number of heat exchanger tube turns required is:

$$N = \frac{A}{\pi D \times \pi d \times 0.4} = \frac{95}{\pi^2 \times 22.7 \times 0.44 \times 0.4} = 2.42 \text{ turns}$$

5.3 PROPELLANT EVAPORATION SYSTEMS

This concept is practical only for thermally stable, low normal boiling point propellants, such as cryogenics and near cryogenics, for which it is widely used. It is particularly suitable for cryogenics of low molecular weight, such as hydrogen.

Application in Pump-Fed Systems

Propellant evaporation systems for pump-fed engines usually employ propellants tapped off downstream of the pump and vaporized in a heat exchanger, after which they are used to pressurize the main propellant tank from which they were withdrawn. Figure 5-7 shows a typical heat exchanger design used in an LO₂/RP-1 pump-fed engine system. The turbine exhaust gases are used as the heat source. Sometimes the vaporized propellant is bled directly from the manifold downstream of the chamber cooling passage if it is the coolant in a regeneratively cooled thrust chamber. As shown schematically in figures 3-3 and 5-8, the pressurant for the A-2 stage main oxidizer tank is provided by oxygen tapped off downstream of the oxidizer pump and vaporized in a heat exchanger located at the turbine exhaust duct of the oxidizer turbopump. The main fuel tank of this stage is pressurized by bleeding hot hydrogen from the thrust chamber fuel manifold downstream of the thrust chamber cooling tubes. The pressure of both tanks can be regulated by pressure switch/solenoid valve combinations, as shown in figure 5-8, or by regulators. The latter are often preferred, particularly if a narrow band of regulation is essential. In both cases, flow limiting orifices may be used in series, for increased reliability, with valve or regulator design-biased to fail open.

The required propellant flow rate bled for vaporization and main tank pressurization is determined by the main propellant flow rate at the pump inlet (or tank outlet), and by the heat

and mass transfer processes within the main propellant tank, which in turn are influenced by pressurant and environmental temperatures. For a given rate of evaporation of the propellant in the tank, average flow rate through the tank vent, and tank ullage gas or vapor condition, the following steady-state correlation can be established:

$$\dot{W}_p = \frac{\dot{W}P_T}{\rho RT} - \frac{(\dot{W}_e - \dot{W}_v)}{N} \quad (5-18)$$

where

\dot{W}_p = required flow rate per engine bled off for propellant tank pressurization, lb/sec

\dot{W}_e = rate of propellant evaporation in the tank, lb/sec

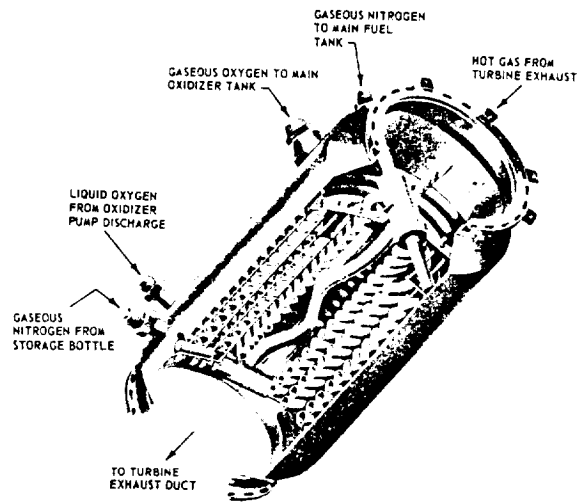


Figure 5-7.—Typical heat exchanger design.

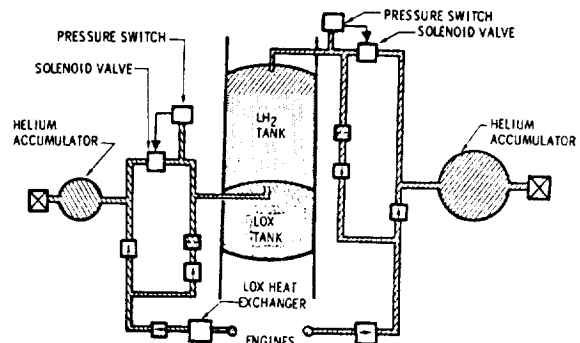


Figure 5-8.—A-2 stage propellant tank pressurization system schematic.

\dot{W}_v = average flow rate through the tank vent, lb/sec
 \dot{W} = main propellant flow rate (per engine) at pump inlet, lb/sec
 ρ = density of the liquid propellant, lb/ft³
 P_T = propellant tank pressure, lb/ft²
 R = gas constant of the propellant vapor, ft-lb/lb-deg R
 T = temperature of the tank ullage gas, °R
 N = number of engines in the system

Sample Calculation (5-4)

The following data were established for the A-2 stage engine and vehicle systems during steady-state operation conditions:

Main oxidizer flow rate at pump inlet, per engine, 290.5 lb/sec (table 3-3)
 Main oxidizer tank pressure, 45 psia
 Rate of oxidizer evaporation in the tank, 1.6 lb/sec
 Average flow rate through the oxidizer tank vent,¹ 1.64 lb/sec
 Temperature of the oxidizer tank ullage gas, 220° R
 Main fuel flow rate per engine, at pump inlet, 59.8 lb/sec (table 3-3)
 Main fuel tank pressure, 38 psia
 Rate of fuel evaporation in the tank, 4.2 lb/sec
 Average fuel flow rate through the fuel tank vent,¹ 6.6 lb/sec
 Temperature of the fuel tank ullage gas, 120° R
 Number of engines in the vehicle system, 4

Calculate:

(a) The required steady-state flow rate, per engine, bled off for oxidizer tank pressurization.

¹For fire hazard reasons, vehicle design very likely will require provisions to prevent venting during first stage boost. Also, during regulated A-2 stage operation, venting should normally not occur, as it would be a performance loss. However, as a pressurization system performance margin it is well to lay out the system on the basis of some vent losses. Also, in cryogenic systems it may be desirable to increase the tank pressures toward the end of stage operation to improve pump NPSH conditions, when the upper tank layer, in which somewhat warmer liquid may have accumulated, is about to reach the pump. This can be simply done by opening an orificed by-pass around the regulator, using the vent valve liftoff pressure as the regulating factor.

(b) The required steady-state flow rate, per engine, bled off for fuel tank pressurization.

Solution

(a) The density of liquid oxygen is 71.38 lb/ft³, the gas constant of the gaseous oxygen is 1544/32 = 48.2 ft-lb/lb-deg R.

Substitute this and data given above into equation (5-18) to obtain the required steady-state flow rate of evaporated oxidizer pressurant:

$$\dot{W}_p = \frac{290.5 \times 45 \times 144}{71.38 \times 48.2 \times 220} - \frac{(1.6 - 1.64)}{4} = 2.50 \text{ lb/sec}$$

(b) The density of the liquid hydrogen is 4.42 lb/ft³, and the gas constant of the gaseous hydrogen is 1544/4 = 386 ft-lb/lb-deg R.

Substitute this and data given above into equation (5-18) to obtain the required steady-state flow rate of the evaporated fuel pressurant:

$$\dot{W}_p = \frac{59.8 \times 38 \times 144}{4.42 \times 386 \times 120} - \frac{(4.2 - 6.6)}{4} = 2.2 \text{ lb/sec}$$

It is noted that some engine specialists prefer to use slightly lower propellant densities; for instance, 71.0 for LOX and 4.4 for LH₂. These values consider the fact that storage and vehicle containers, even when vented to atmosphere, have small positive pressures because of vent valve resistance, resulting in slightly increased propellant temperatures. However, since later engine calibration-run evaluations will require corrections for a number of run-to-run engine input deviations, consistent usage of design parameters is probably more important than their absolute value. It is further pointed out that tank pressure regulation through venting, particularly if used throughout the systems duration, is not an efficient method, since onboard gas storage must allow for the maximum vent rate anticipated.

Applications in Pressurized Gas Propellant Feed Systems

The application of propellant evaporation systems to pressurized propellant feed systems is somewhat limited. Evaporation systems can result in lower pressurant storage vessel weight,

as compared to stored gas systems, because of higher storage densities and lower storage pressures. However, this can be offset by the higher required pressurant weight per unit volume, particularly for propellants with higher molecular weight. For hydrogen, the principal propellant with low molecular weight, another limitation exists because of the low critical pressure. To obtain reasonable volume increases due to vaporization, the tank pressure must be kept sufficiently below the critical pressure.

It must be further considered that the propellant evaporation concept, when applied to pressure-fed systems, requires a pressurization system within a pressurization system, since a separate stored gas is required to expel the pressurant from the storage vessel as a liquid, after which it is vaporized in a heat exchanger. This system comprises a relatively complicated array of components, line assemblies, heat exchangers, and support structures. It is further complicated because of the auxiliary pressurization system required to initiate the main propulsion system operation. As shown schematically in figure 3-6, the main fuel tank of the A-3 stage propulsion system is pressurized by evaporated hydrogen supplied from a separate liquid hydrogen storage vessel which in turn is pressurized by the stored helium gas. The hydrogen pressurant is vaporized in the heat exchangers, located at the thrust chamber nozzle extensions.

For the various reasons stated, the propellant vaporization principle will be used only for the fuel tank of the A-3 stage, for which it still appears attractive because of the relatively low pressure levels selected, and the low molecular weight of hydrogen. The A-3 oxidizer tank will be pressurized by stored helium gas. This decision was further influenced by the difficulty in handling gaseous fluorine and by its toxicity.

5.4 SYSTEMS EVAPORATING NONPROPELLANTS

This type of pressurization system has not been employed frequently. Two types of inert cryogenics could be considered applicable: liquid nitrogen and liquid helium. Both have definite disadvantages which would generally preclude their use in nonpropellant evaporation systems. The main disadvantages are their

solubility in the propellants (nitrogen in liquid oxygen) and a storage temperature significantly lower than that of the propellants (liquid helium). The system design for this concept is similar to that of the propellant evaporation systems.

5.5 SYSTEMS USING PRODUCTS OF CHEMICAL REACTIONS

Pressurization systems using hot gaseous products generated from solid or liquid propellants have been successfully developed for the storable liquid propellant engine systems. Another technique used with noncryogenics is the main propellant tank injection pressurization system. Here a hypergolic fluid is injected into the tank and pressurization is provided by the products of the reaction occurring within the tank.

These methods are not applicable to cryogenic propellants because the products of reaction, such as water, will solidify, and because the heat of combustion will raise undesirably the bulk temperature of the cryogenic propellant. Especially in the case of liquid hydrogen, bulk heating cannot be tolerated because of its limited liquid range (normal boiling point to critical point).

Two important considerations for the application of combustion products for pressurization are: propellant compatibility and gas temperature level. Except for very short operating durations (few seconds), fuel-rich hot gases are used for fuel tanks, to prevent reactions. Similarly, oxidizer-rich hot gases are applied to oxidizer tanks. The temperature of the product gas pressurant should be maintained at, or should be cooled to, a level below 1200° F.

Solid Propellant Gas Generator Pressurization Systems

Several effective solid-propellant gas-generator systems have been developed for tank pressurization of prepackaged storable liquid propulsion systems. Pressurant gas temperatures up to 3000° F and tank pressures up to 2000 psia have been proven successful for short-duration applications. This pressurization method is primarily employed for its inherent simplicity, low production cost, long-term storability, relatively light

system weight, and compactness. The system is usually composed of two electrically fired initiators, or squibs, a charge of igniter pellets, safety and arming devices, a pressure-relief-type regulator, and the propellant grains. A device to cool the hot gases may be required in specific applications.

Figure 5-9 shows a typical design. The solid-propellant gas-generator assembly is enclosed in an insulated steel housing. This housing is installed within an aluminum casing, which in turn is an integral part of the propellant tank constructed of aluminum alloy. The gas generator unit is completely integrated into a compact package ready for testing, storage, and installation into the propulsion system, with minimum effort and maximum safety. All gas outlets are hermetically sealed with burst dia-

phragms to maintain system reliability even after long storage periods.

Upon ignition, the propellant grains are ignited by the igniter pellets. Combustion starts and produces pressurization gases for the duration for which the propellant grains were designed. The burning rate of the grain, and in turn the gas pressure level of a solid propellant system, is affected by grain bulk temperature. Within a given service temperature range, the grain is designed to produce required gas pressures and flow rates at the lower temperature limit. When operating at a higher temperature, the pressure level will be maintained by a regulator which vents all excess gases overboard. The required grain charge is sized for full propulsion system operating duration at the upper temperature limit, at which maximum grain burning rate occurs.

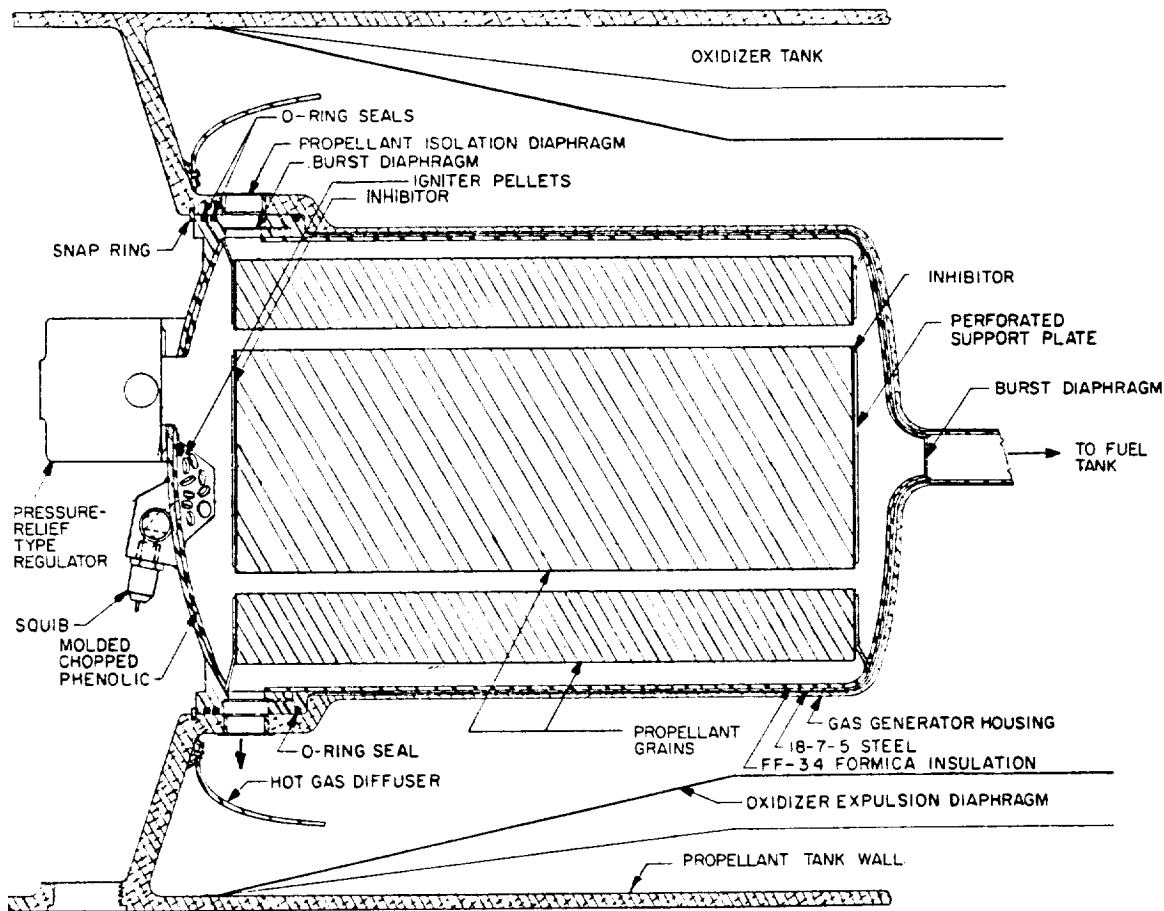


Figure 5-9.—Typical solid propellant gas generator pressurization system.

The selection and design of solid propellant gas generator pressurization systems must consider potential problem areas, notably the following:

- (1) Chemical and temperature compatibility of the gases with the propellants
- (2) Pressure regulation difficulties
- (3) System clogging by solid particles carried in the gas stream
- (4) Lack of restart capability
- (5) Requirement to vent gas rapidly in the event of premature engine cutoff.

A brief discussion of several commonly used solid propellant systems follow:

1. *Solid propellant gas generator system without cooling.*—This system is shown schematically in figure 5-10 and consists of a solid propellant charge, including igniter, filter, and hot gas regulator or orifice. This system is suitable mainly for relatively short durations. Upon ignition, hot gases are fed through the filter, regulated, and ducted to the main propellant tanks. The regulator dumps excess gas overboard, for which a vent line must be provided. As an alternate, an orifice may be installed in place of the regulator. In the latter case, the engine thrust level is a direct function of the solid gas generator pressure which in turn is a function of environmental temperature.

2. *Solid propellant gas generator system with solid coolant.*—This system (fig. 5-11) consists of a solid propellant charge and igniter, a sublimating solid coolant, a filter and a regulator. In operation, the hot gases generated are cooled as they pass through a bed of solid material, subjecting it to decomposition or sublimation. Thus the cooling process simultaneously results in additional gases available for pressurization. The gases finally pass through a filter and are regulated and ducted to the main propellant tanks.

In a typical design an ammonium nitrate base propellant is used with a theoretical flame temperature of 2320° F. Oxalic acid pressed into pellets is the solid coolant. This chemical decomposes endothermically at temperatures above 250° F, producing a mixture of CO, CO₂, and H₂O. The desired temperature level of the mixed product gases is achieved through selection of the propellant to coolant ratio. Final gas temperatures as low as 400° F have been obtained.

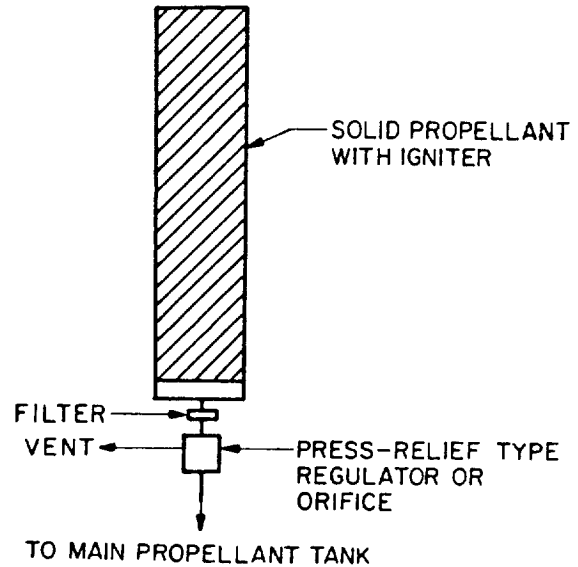


Figure 5-10.—Solid propellant gas generator without cooling.

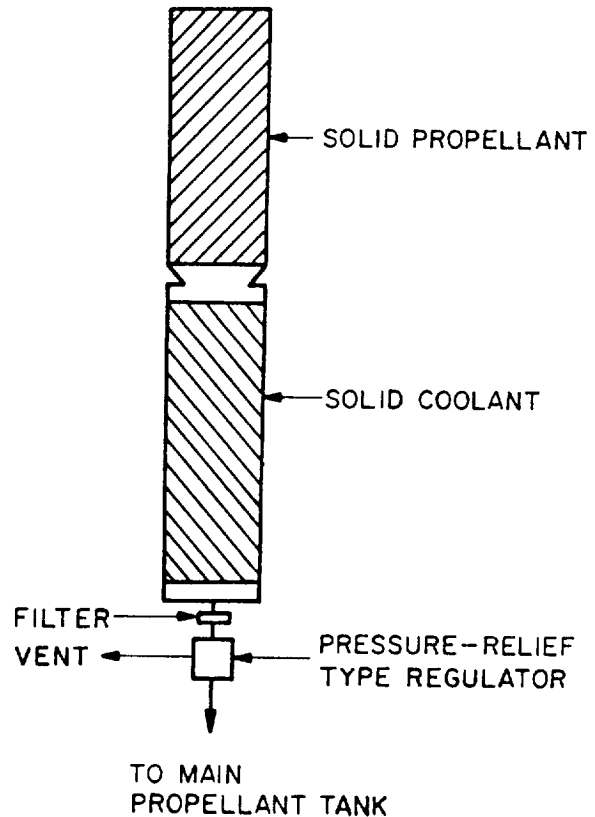


Figure 5-11.—Solid propellant gas generator system with solid coolant.

3. *Solid propellant gas generator system with azide cooling pack.*—The principal components of this system are shown in figure 5-12. Here, hot gases are cooled when passing through a bed of azide material which decomposes and yields essentially pure nitrogen. However, the gas leaving the azide pack is often contaminated with metal particles resulting from the decomposition of the azide. These have to be removed in a cyclone separator. The gases are filtered to remove any remaining particles, then regulated, and directed to the main propellant tanks.

The advantage of these pressurization sys-

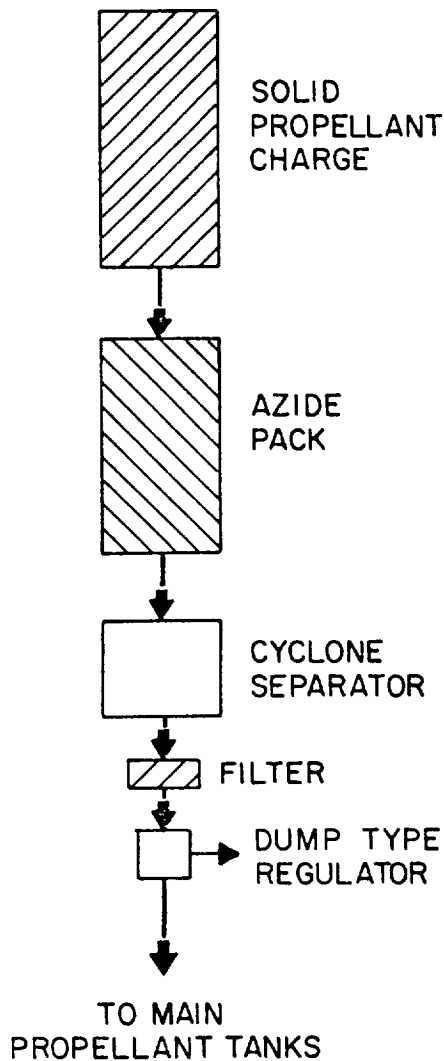


Figure 5-12.—Solid propellant gas generator system with azide cooling pack.

tems is in providing relatively pure nitrogen gas at a reasonable temperature level (as low as 600° F).

4. *Helium system with solid propellant gas generator heating.*—This system (fig. 5-13) consists of a high-pressure helium storage vessel with a solid-propellant gas generator mounted internally, a filter, and a pressure regulator. The solid-propellant charge provides both heat for helium expansion and additional pressurizing gas. A disadvantage of this system is the need for a relatively large, high-pressure storage vessel.

Liquid Propellant Gas Generator Pressurization Systems

Both liquid monopropellant and liquid bipropellant gas generators have been used successfully for generating pressurant gases in

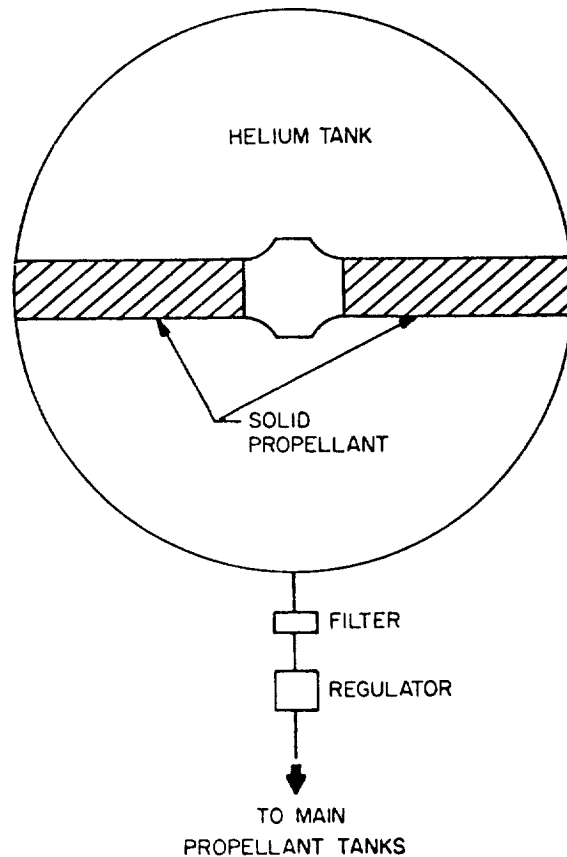


Figure 5-13.—Helium system with solid propellant gas generator heating.

engine systems with relatively long operating durations. The selection and design of a gas generation system must consider propellant compatibility, operating temperature limits of propellants and tank materials, and gas molecular weight.

Among the monopropellants, hydrazine is considered the most satisfactory with respect to chemical characteristics and molecular weight of the product gases. The decomposition products of hydrazine can be made even lighter by catalytic decomposition of the ammonia component. The gases contain no carbon, deposits of which could lower the heat transfer rate if a heat exchanger is used for cooling. The theoretical gas decomposition temperature of pure hydrazine is 1800° F. Additives can be used to reduce the temperature level.

To meet the requirement for compatibility with the propellant, bipropellant gas generators possess the flexibility of operation at either fuel-rich or oxidizer-rich conditions. Thus the same propellant combination can be used to produce both a fuel-compatible and an oxidizer-compatible pressurant gas. For instance, nitrogen tetroxide in combination with hydrazine, UDMH, and various other amine fuels permits hypergolic starting and stable operation in either fuel- or oxidizer-rich modes.

Several avenues are open to meet the pressurant gas temperature requirement. The aforementioned flexibility to operate at either fuel- or oxidizer-rich conditions has the additional advantage to combust well off stoichiometric mixture ratios, resulting in lower temperatures. A limitation exists if one of the bipropellants is also a monopropellant which continues to decompose exothermically. The cooling effect can also be obtained by injecting into the hot gases a given amount of noncombustible liquid which absorbs heat when evaporating. A third method of cooling is heat exchange with one of the liquid propellants in a heat exchanger. This can be applied with essentially any propellant combination, provided the cooling liquid can safely absorb the heat transferred from the gas.

The requirement of low molecular weight will be met by most fuel-rich product gases if they are at approximately 1000° F, where the complex organic compounds composing most fuels are cracked into simple gases of low molecular

weight. However, if excess fuel is injected to lower the temperature to well below 1000° F, this benefit is not obtained, resulting in a gas with high molecular weight which readily condenses.

Liquid-propellant gas-generator pressurization systems, some of which will now be discussed, require relatively complex components and controls. Their selection and application is determined mainly from vehicle mission requirements, such as long operating duration, restart, etc.

1. *Single gas generator system with injection cooling.*—Here, a single generator provides pressurant gas for both the fuel and the oxidizer tank. The liquids employed consist of either a monopropellant and a nonreacting injection coolant, or a bipropellant combination with cooling achieved by injecting an excess of one propellant. As shown in figure 5-14, system components include a small, high-pressure helium gas storage vessel assembly (including start, relief, and fill valves), a pressure regulator, two liquid storage vessels, and a gas generator assembly (including controls).

This system is potentially simple and reliable. The product gases are cool enough for use in the propellant tanks. The difficulty is to find a combination of liquids that will produce a product gas meeting all requirements, including compatibility with both propellants. It has been demonstrated, however, that fuel-rich gases can

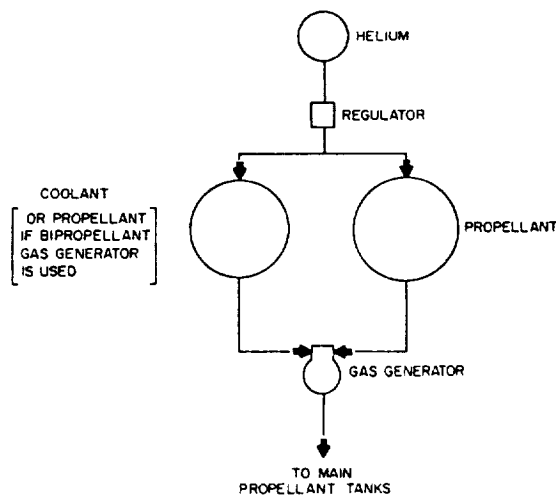


Figure 5-14.—Single liquid propellant gas generator system with injection cooling.

be used to pressurize storable oxidizers. For instance, ammonia-rich, ammonia-nitrogen tetroxide gas generator products and hydrazine decomposition products with either water or ammonia injection have been successfully applied as the pressurant for storable oxidizers.

2. Single gas generator-helium system.-

Figure 5-15 shows the main components comprising this system. The number of propellant tanks depends on whether a monopropellant or bipropellant gas generator is used. The hot gas generator products are ducted to a heat exchanger where heat is transferred to the cold helium. The heated and expanded helium gas is then used to pressurize the main oxidizer tanks, while the gas generator gases are used to pressurize the main fuel tank. While the system efficiently uses the available heat for both tanks, it has the disadvantages of requiring a moderate-size, high-pressure helium storage vessel and of pressure regulation problems.

3. Dual bipropellant gas generator system with injection cooling.-

The major components for this system are shown in figure 5-16. During operation, fuel and oxidizer are fed to the gas generators by pressurizing the auxiliary propellant tanks with helium. One gas generator operates with excess fuel injection to produce relatively cool, fuel-rich gases which are used directly to pressurize the main fuel tank. The second gas generator operates with excess oxi-

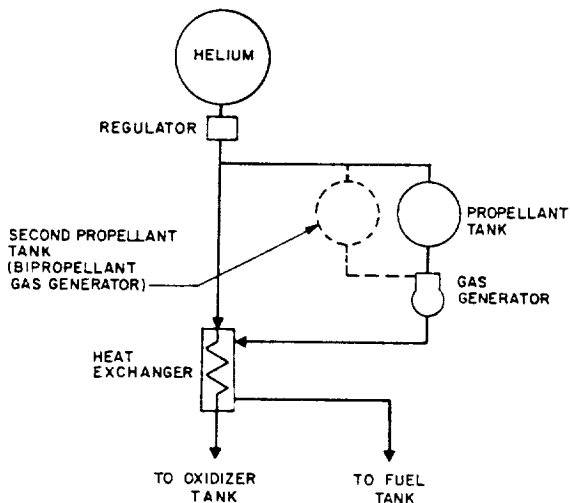


Figure 5-15.—Single liquid propellant gas generator helium system.

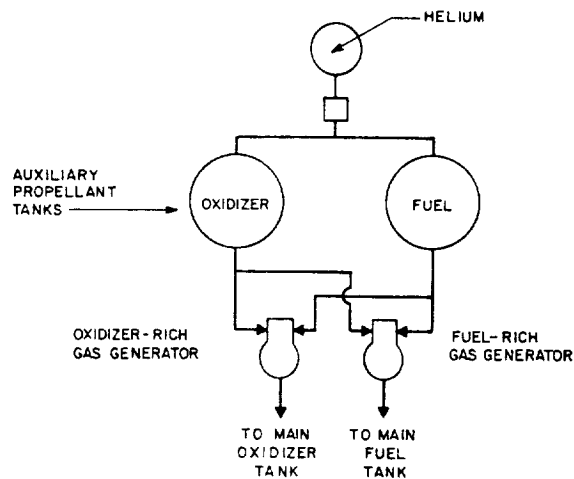


Figure 5-16.—Dual bipropellant gas generator system with injection cooling.

dizer injection to produce relatively cool, oxidizer-rich gases which are used directly to pressurize the main oxidizer tank. A design problem is produced by the need to balance the output of the two gas generators and to provide proper pressure control in both tanks. Gas temperatures as low as 600° F have been successfully generated with these systems.

Main Propellant Tank Direct Injection Pressurization Systems

The direct injection systems employ injection of small quantities of fuel and oxidizer into the main oxidizer and fuel tanks, respectively. Following hypergolic reaction, the pressurizing gases are thus produced within the main propellant tanks themselves. The fuel system (fig. 5-17) includes a small, high-pressure helium storage vessel assembly, a helium pressure regulator, and two small auxiliary propellant tanks from which propellants are injected into the main tanks. The series injection system (fig. 5-18) consists of only one auxiliary oxidizer tank for main fuel tank pressurization, or vice versa, instead of two separate auxiliary tanks for each main tank. The series system takes advantage of the situation where one of the main propellant tanks can operate at a slightly lower pressure than the other. In the case shown in Figure 5-18, a small quantity of the main fuel supply is fed through a regulator to the main

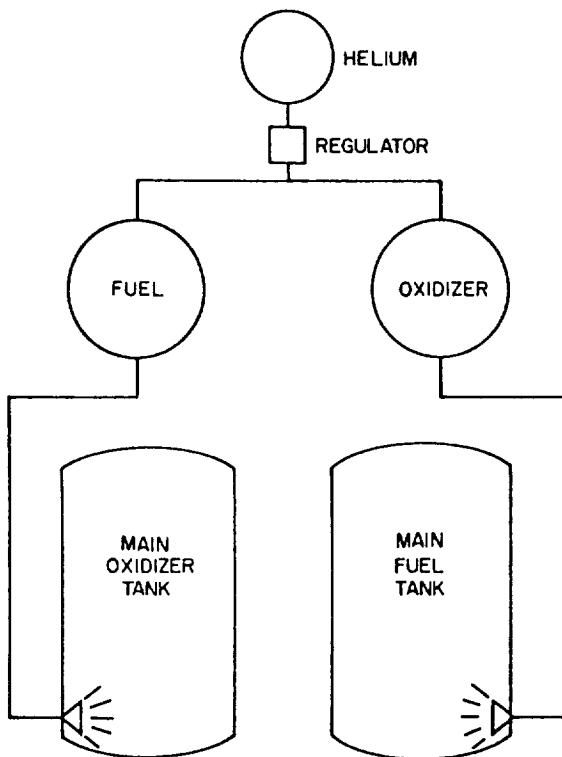


Figure 5-17.—Main propellant tank dual direct injection system.

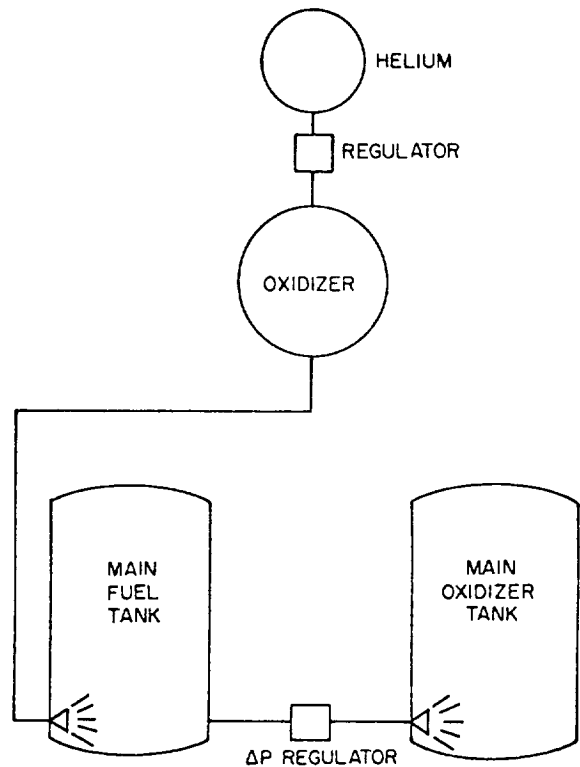


Figure 5-18.—Main propellant tank series direct injection system.

oxidizer tank. Although these systems appear to offer the lightest and simplest method of pressurization by number of components, system safety, reliability, and ability to produce steady regulated tank pressures are questionable.

5.6 SELECTION OF THE PRESSURIZATION SYSTEM

At the beginning of the design of a pressurization system, a preliminary study of the various design approaches is conducted. This will provide a technical basis for systems selection, but can become a relatively complex task in view of the great number of tank pressurization techniques developed. In the course of the study, all information pertinent to the wide range of systems is gathered. A standard vehicle configuration and uniform assumptions for mission and performance, structural materials, and other factors affecting the pressurization system design are adopted to permit valid weight and size comparisons of the various systems studied.

The four principal selection criteria are: vehicle mission requirements, propellant and material compatibility, system reliability, and system performance. Mission requirements include storability, system instant start and restart, and closely controllable pressure levels (constant or variable). Compatibility includes chemical inertness, freedom from excessively condensible and soluble gas products, and proper pressurant temperature level. Reliability is evaluated on the basis of system complexity, number of failure modes, and number of system components the reliability level of which must be attained economically within the limits of development time and funds allotted. Components which can be expected to require considerable development effort toward satisfactory reliability levels include gas generator assemblies, thrust chamber heat exchangers, large high-pressure storage vessels, and hot-gas ducting and regulators. System performance is determined entirely on the basis of gross pressurization system weight which is influenced by

TABLE 5-1.—Comparisons of Various Tank Pressurization Systems for the A-4 Stage Propulsion System

System	Stored gas and generants	Gas produced	Total quantity of system components	Number of complex component designs	System overall weight, percent	System overall volume, percent
Helium with thrust chamber heating (fig. 5-2)	Helium	Helium at 995° R average	11	3	100	100
Helium—no heating (fig. 5-1)	Helium	Helium at 354° R average	9	2	182	183
Helium cascade (fig. 5-3)	Helium	Helium at 1000° R average	17	7	81	75
Solid propellant gas generator heating helium (fig. 5-12)	Helium, ammonium nitrate base grain	^a Mixed helium and solid propellant products at 1000° R average	15	4	79	72
Solid propellant gas generator with solid subliming coolant (fig. 5-10)	Ammonium nitrate base grain, oxalic acid pellets	^a Solid propellant products at 1000° R	9	3	53	12
Solid propellant gas generator with azide cooling (fig. 5-11)	Viton azide propellant, lithium azide coolant	Nitrogen at 1000° R	11	4	70	11
Single liquid propellant gas generator—helium (fig. 5-14)	Helium, hydrazine	^b Helium at 1000° R on oxidizer, hydrazine products at 1200° R on fuel	11	4	63	51
Dual liquid propellant gas generator with injection cooling (fig. 5-15)	Helium, nitrogen tetroxide, ammonia	^a Ammonia-rich gas generator products at 1000° R on fuel; N ₂ O ₄ -rich gas generator products at 1000° R on oxidizer	16	6	48	16

^aQuestionable compatibility of pressurant with propellants.

^bMarginal pressurant temperature level on fuel.

pressurant molecular weight and specific system weight. The gross weight of the pressurization system is treated as inert weight, since the entire pressurant and system components are part of the vehicle system weight at burnout.

A sample preliminary design study was conducted for the tank pressurization system for the A-4 stage propulsion system. The vehicle mission was assumed to require single-start, constant-thrust, full-duration operations. Eight different pressurization systems were compared.

The results presented in table 5-1, "Total Quantity of System Components" include components of like design; i.e., two identical storage vessels or check valves are considered a quantity of two. "Complex Component Designs" refers to parts requiring relatively long development time and high production cost. Instead of absolute values for overall weight and volume of the various systems, percentages of the selected system (stored helium with thrust chamber heating) are used for comparison.

Design of Turbopump Propellant-Feed Systems

In high-thrust, long-duration liquid propellant rocket engine applications, turbopump feed systems, as shown in figures 1-13, 2-10, 3-3, and 4-58, generally result in lower systems weight and higher performance when compared to pressurized gas feed systems. Turbopump feed systems require only relatively low pump-inlet pressures, and thus propellant-tank pressures, while the major portion of the pressure required at the thrust chamber inlets is supplied by the pumps. This saves considerable tank weight, particularly in large vehicles.

As the overall trend toward higher chamber pressure of liquid propellant rocket engines continues, the role of turbopumps in an engine system becomes of even greater importance, particu-

larly with the introduction of high-performance hydrogen-fueled engines. As shown in figure 6-1 for two propellant combinations, the proportional turbopump-assembly weight in an engine system rises with increasing chamber pressure, as does the required turbopump power expressed as a percentage of total engine propellant flow rate.

A representative range of pump operating parameters for various liquid propellant rocket engine applications is shown in figure 6-2. Figure 6-3 depicts an envelope of turbine power requirements for a number of actual turbine designs.

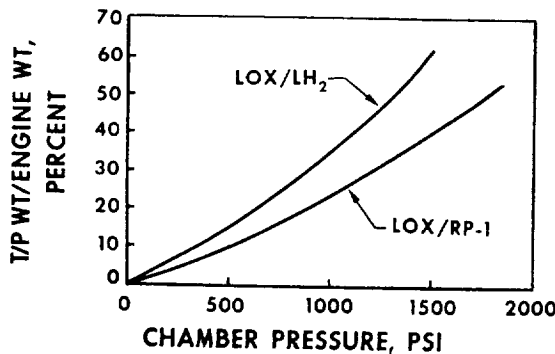
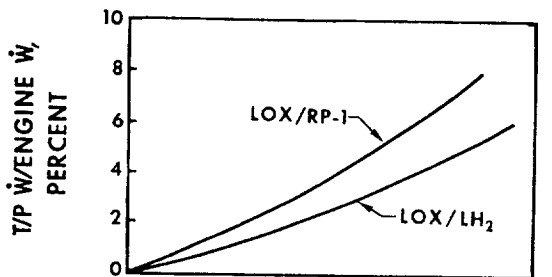


Figure 6-1.—Variation of turbopump/engine weight and flow ratios with change of chamber pressure.

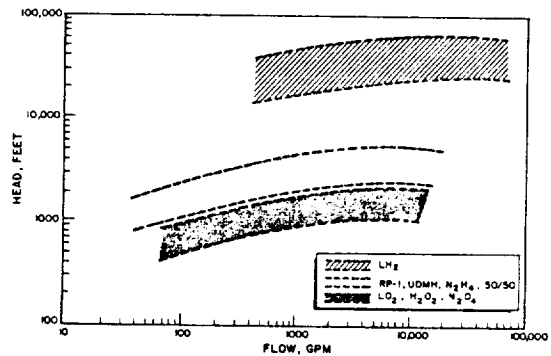


Figure 6-2.—Range of operation for typical propellant pumps.

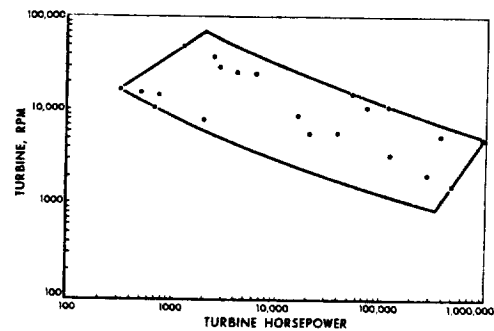


Figure 6-3.—Envelope of rocket engine turbine designs.

6.1 ELEMENTS OF TURBOPUMP PROPELLANT FEED SYSTEMS

The supply of propellants to the inlet of the pumps at required minimum pressures is customarily considered the responsibility of the vehicle propellant system and thus of the vehicle designer. The main function of the turbopump feed system then is to raise the pressure of the propellants received from the vehicle tanks and deliver them to the main thrust chamber, through ducts and valves, at pressures and flow rates commensurate with rated engine operation. A turbopump feed system may consist of the following basic elements:

- (1) Propellant pumps
- (2) Turbine(s) to drive them
- (3) A power source for the turbine(s) (during engine start as well as main stage)
- (4) Speed reduction gear transmissions (if any)
- (5) Lubrication system for bearings and gears (if any)
- (6) Shaft-speed pickup for instrumentation and for safety purposes (overspeed cutoff)
- (7) Accessory drives (if any)
- (8) Propellant inlet and discharge ducts (if any)
- (9) Turbopump mounts

Propellant Pumps

The principal requirements of a rocket engine propellant pump are reliability, optimum speed, light weight, high delivery rate at maximum pressure head, smooth flow for a wide range of operating conditions, and high efficiency. The most widely used pump types are centrifugal (or radial) flow, axial flow, and mixed flow pumps. Centrifugal pumps are generally designed with a single stage, while axial pumps are primarily of multistage design. However, multistage centrifugal pumps with crossover-type volutes have also been considered. Various pump configurations are shown schematically in figure 6-4.

1. *Centrifugal pumps.*—Almost all operational rocket propellant pumps (except those for high-flow, high-pressure liquid hydrogen applications) are of this type. They can handle large flows at high pressures efficiently as well as economically in terms of weight and size. The elements of a centrifugal pump are shown in figures 6-5,

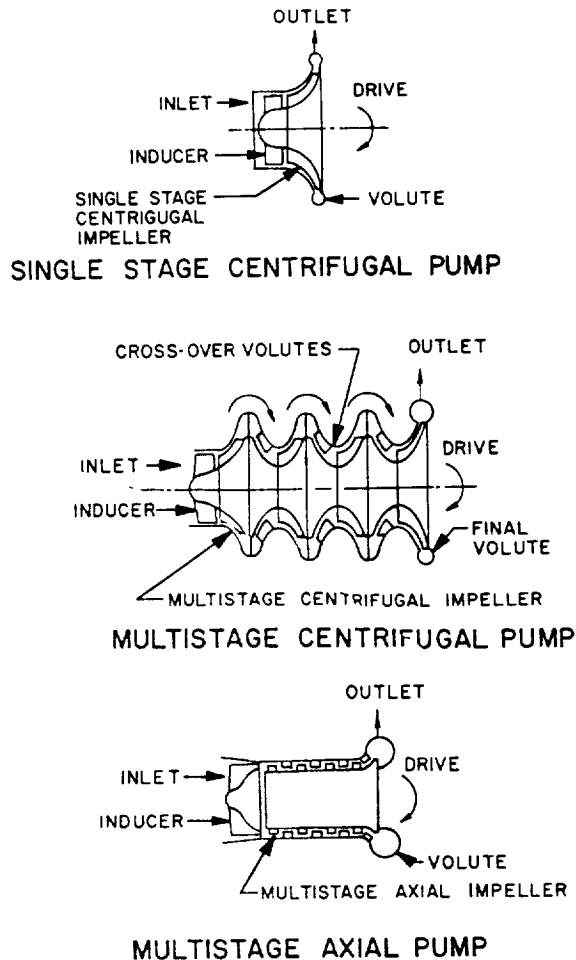


Figure 6-4.—Schematics of various pump configurations.

6-14, 6-43, 6-47, and 6-48. Centrifugal pumps, like other steady-flow rotating machinery, consist essentially of two basic elements: the rotor and the stator. Their working principle is the acceleration of the fluid flow by imparting kinetic energy to it in the rotor and then decelerating or "diffusing" it in the stator. This results in increased fluid pressure head. The rotor assembly usually includes an inducer, an impeller, and a shaft. The stator assembly consists of a casing with stationary diffuser vanes, a volute with discharge outlet, shaft bearings, and seals.

An inducer is an axial-flow-type impeller. Its main function is the increase of the static pressure of the entering fluid sufficiently to permit normal operation of the main impeller. An inducer can reduce the pump inlet pressure net-positive suction head (NPSH) requirements

CONFIDENTIAL

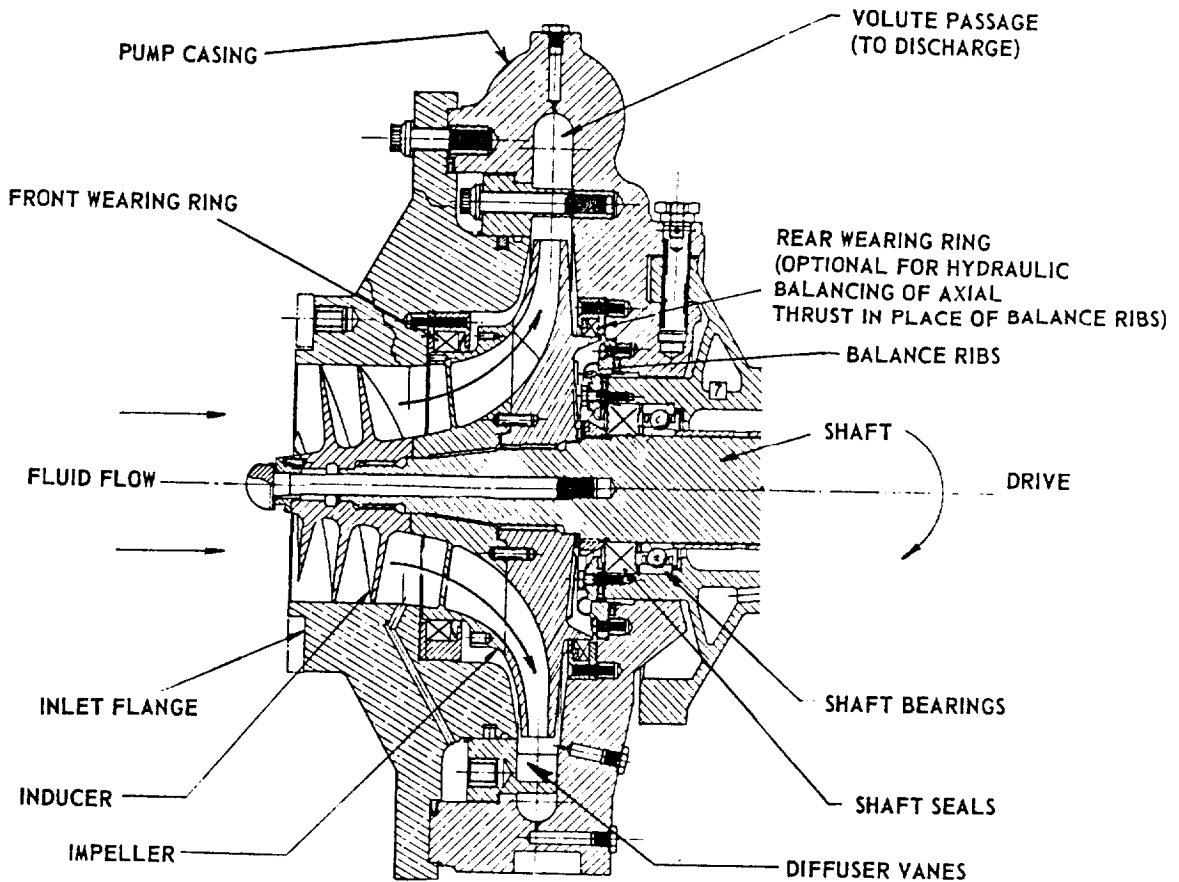


Figure 6-5.—Elements of a centrifugal-flow pump.

substantially. The impeller of a centrifugal (or radial) pump basically is a rotating wheel with radial vanes. Fluid is admitted axially to the impeller which, when rotating in an enclosure, ejects it at the periphery with increased velocity (fig. 6-5).

The primary functions of the pump stator assembly are: diffusing (i.e., decelerating) the fluid to convert the velocity head into pressure head, collecting and redirecting the fluid to the pump discharge outlet, and providing structural support and a pressure enclosure for the pump. The main function of the wearing rings shown in figure 6-5 is to provide axial thrust control and to minimize internal leakage, or circulating of the fluid between the high-pressure (discharge) and the low-pressure (inlet or suction) zones. External leakage along the shaft is prevented by the use of dynamic shaft seals.

2. *Multistage centrifugal pumps.*—For higher pressure rises, multiple-stage centrifugal pumps can be designed if a single stage proves limited. The basic construction of a multistage pump is similar to that of a single-stage pump, except that proper channeling of the fluid between stages is added.

3. *Multistage axial pumps.*—This design is well suited to liquid hydrogen service which entails the problems of extremely low fluid temperature and density. Low fluid density results in high-volume flow and in high pressure-head rise requirements. For applications at either flow rates higher than 60 lb/sec or pressure-head rises above 1400 psi, a multistage axial flow pump is generally superior with respect to construction and performance.

Elements of an axial flow pump are shown in figures 6-6, 6-51, and 6-53. The rotor assembly

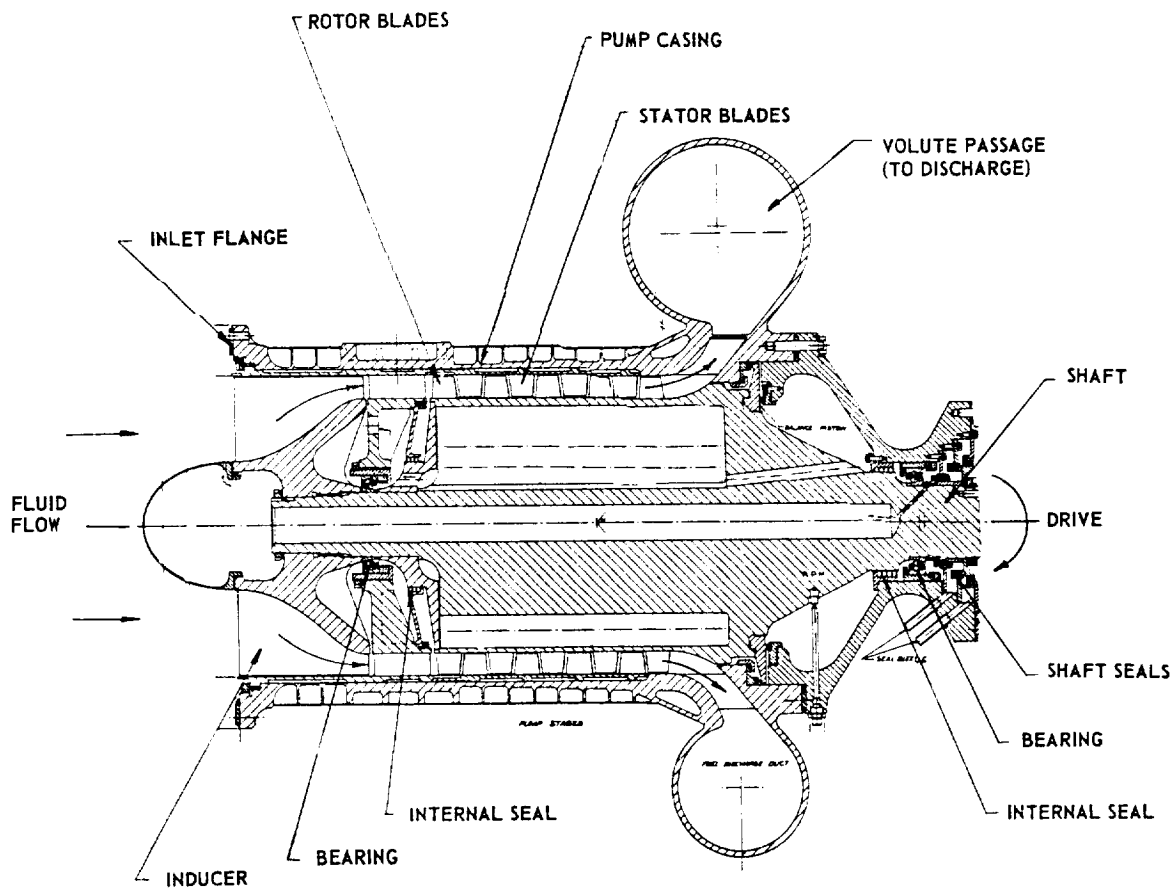


Figure 6-6.—Elements of an axial-flow pump.

consists of an inducer, a cylindrical rotor with multiple rows of rotating blades, and a rotor shaft. The stator assembly includes a cylindrical casing with rows of stationary blades spaced between inducer and rotating blades, a volute casing, bearings, and seals.

An inducer is placed at the pump inlet to supply the fluid to the main-pump section at the required pressure and velocity. Both rotor and stator blades have a hydrofoil shape. The main function of the rotor blades is to accelerate the flow relative to the stator and thus to increase the kinetic energy of the fluid, while the stator blades, acting as diffusers, convert the velocity head of the fluid into pressure head. However, the velocity vector of the fluid in the axial direction is kept constant throughout the various stages of the pump.

Turbines

The turbines which provide shaft power to the propellant pumps derive their energy from the expansion of a high-pressure, high-temperature gas to lower pressures and temperatures. The basic elements of a turbine are shown in figures 6-7, 6-14, and 6-54. Turbines can be divided into two major types: impulse turbines and reaction turbines. Impulse turbines can be either single or multiple stage. Reaction turbines are usually multistage. Various turbines employed in rocket engine applications are described as follows:

1. *Single-stage, single-rotor impulse turbine.*—This turbine consists of a single-rotor disk or turbine wheel to which is attached a row of turbine blades or buckets. Gas is fed to the rotating blades through stationary nozzles (fig. 6-8).

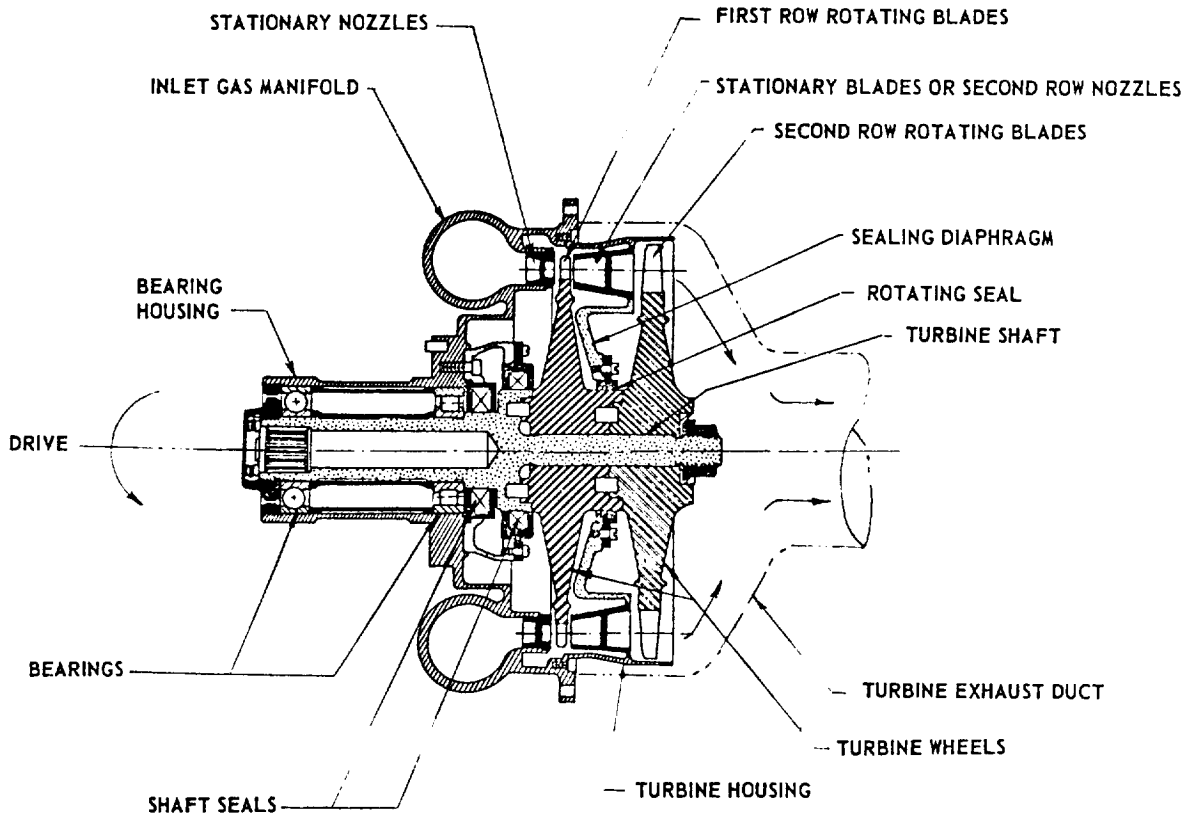


Figure 6-7.—Elements of a turbine.

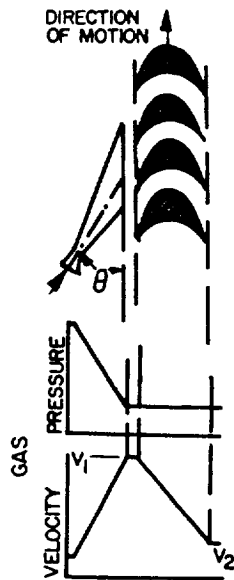


Figure 6-8.—Schematic of a single-stage, single-rotor impulse turbine.

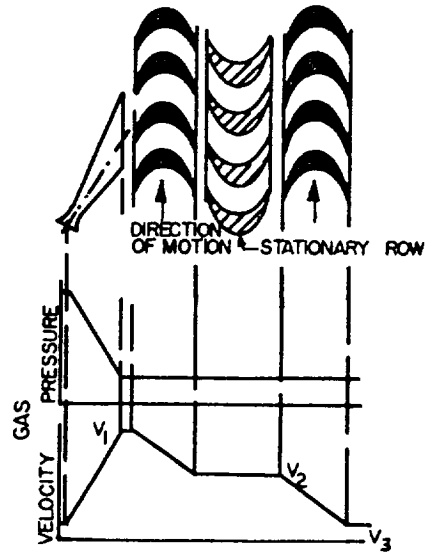


Figure 6-9.—Schematic of a single-stage, two-rotor, velocity-compounded impulse turbine.

In the nozzles, the gas pressure is converted into kinetic energy (velocity head) with attendant static pressure drop. The gas flow velocity is maximum upon entering the rotating blades, where the kinetic energy of the gas is imparted to the turbine rotor as mechanical energy of rotation. Ideally, the static pressure of the gas remains constant when it passes through the rotating blades (except for the effects of friction).

2. *Velocity-compounded impulse turbine.*—Figure 6-9 shows a schematic of this turbine type. Here, two separate rows of rotating blades instead of one are used to transfer the kinetic energy of the gas discharged from the set of stationary nozzles. A row of stationary blades is placed between the wheels to guide the gas into the second set of moving blades. This principle is credited to Curtis who originally developed it. Ideally, the entire pressure drop occurs in the stationary nozzles. The gas velocity decreases during passage through the first row of rotating blades, remains constant through the stationary blades, and decreases further as it passes through the second rotating row. Velocity-compounded turbines are considered single stage, since only one pressure step is involved.

3. *Pressure-compounded impulse turbine.*—As shown schematically in figure 6-10, the expansion of the gas is accomplished in steps, through two or more rows or stages of stationary nozzles, each set being followed by a row of rotating blades. A design objective is that the velocity, and thus the kinetic energy, of the gas flow is the same at the entrance of each row of rotating blades. This results in equal energy transferred to each rotating blade row, while the pressure drop in each stationary nozzle row will vary. Since the pressure is greater in region A than in region B, it is necessary to separate the stages by a sealing diaphragm to prevent bypass flows (fig. 6-7). However, because of clearances required at the rotating seal between diaphragm and turbine shaft, some losses do occur at this point due to leakage from stage to stage.

4. *Reaction turbine.*—The main difference between an impulse turbine and a reaction turbine (shown schematically in fig. 6-11) is that in an impulse turbine no static pressure drop occurs (no expansion) while the gas passes through the rotating blades, whereas in a reaction turbine the pressure does drop (expansion occurs). Both

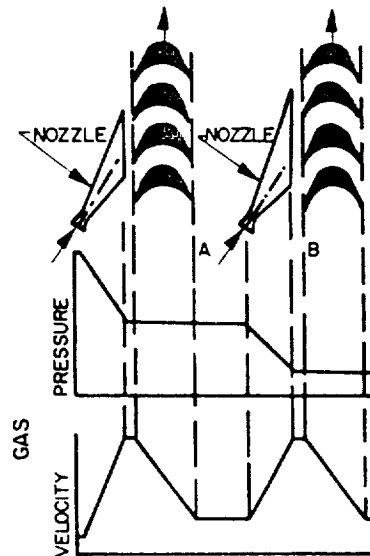


Figure 6-10.—Schematic of a two-stage, pressure-compounded impulse turbine.

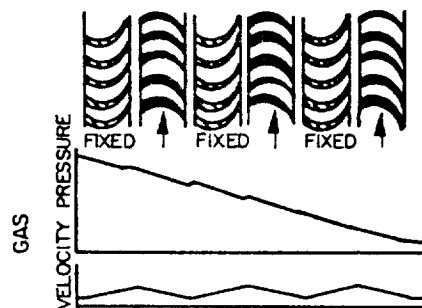


Figure 6-11.—Schematic of a reaction turbine.

impulse and reaction wheels are driven by a change in momentum of the gas. In a pure reaction-type turbine, the driving force is derived entirely from the reaction due to gas expansion within the rotating blades (similar to the gas expansion in a rocket nozzle). In actual reaction turbine designs, however, a portion of the driving force is derived from impulse due to gas impingement on the rotating blades.

Turbine Power Sources

In most applications the turbine is driven by gas produced in either bipropellant or monopropellant gas generators. Other turbine power sources have also been used, such as "tapoff"

and "topping" systems. Typical turbine power sources are shown in figure 6-12 and are described briefly as follows:

1. *Bipropellant gas generator.*—This is the most widely used system since it has the advantage of using the engine main propellants.

2. *Monopropellant gas generator.*—This provides the simplest gas-generating system. However, it requires a third propellant if neither one of the main propellants is suitable for monopropellant application.

3. *Thrust chamber bleed.*—This is applied in "tapoff" engine systems. Gases are bled off directly from the main combustion chamber to drive the turbine.

4. *Topping.*—In a topping cycle, such as with a hydrogen-fueled engine system, the heated hydrogen gas emerging from the thrust chamber cooling jacket is used as the turbine working fluid before being injected into the main combustion chamber. In systems using a monopropellant as one of the main propellants, the monopropellant can be decomposed and used to drive the turbine prior to injection into the main combustion chamber. Topping gas turbine drives render the highest possible theoretical cycle efficiency.

5. *Dual combustion.*—The entire fuel flow reacts with a portion of the oxidizer in a bipropellant gas generator and thus provides the gas to drive the turbine. The usually fuel-rich exhaust gas is then ducted into the main combustion chamber and reacts with the balance of the oxidizer. Dual combustion cycle efficiency equals that of the topping cycle.

For most systems, an auxiliary power source is required during engine start to drive the turbine until the main power source takes over. The energy and its rate of delivery required for the start transient depend to a large extent on the engine system design. Several common turbine power sources for engine start are as follows:

1. *Monopropellant.*—In systems using a liquid monopropellant gas generator, the fluid is supplied by an independently pressurized tank, such as in the German V-2 engine. Thus, no additional turbine power source for engine start is required.

2. *Bipropellant start tanks.*—In a system using a liquid-bipropellant gas generator, fed from the main propellant system, bipropellant

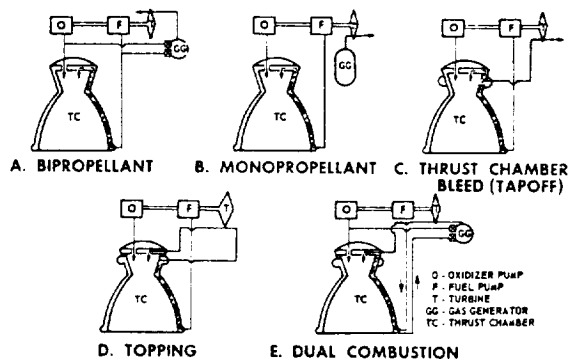


Figure 6-12.—Typical turbine power sources.

start tanks pressurized to up to 90 percent of rated pump outlet pressures supply the propellants to the gas generator during engine start until main propellant pump discharge pressures build up. In some applications (first stages), the start tanks have been made a part of the ground-support equipment.

3. *Main propellant tanks.*—Experimental engine systems have been successfully started with the propellants supplied directly from the vehicle main propellant tanks, thus initiating gas generator and main thrust chamber operation until pump "bootstrap" occurred. In a hydrogen-fueled topping cycle engine, hydrogen vapor is used under tank head pressure to start the turbine directly.

4. *Stored gas.*—Stored gas under high pressure has been used to spin the turbine during engine start. In the case of hydrogen-fueled engines, hydrogen gas stored in a rechargeable bottle is used to drive the turbine during initial as well as restarts.

5. *Solid propellant gas generator.*—Solid propellant gas generators or turbine spinners, as shown in figure 4-49, have also been widely used to power turbines during engine start.

Turbopump Drive Arrangements

The specific type of coupling between turbine and pumps depends not only upon the propellants being pumped but also on the design of the overall engine system. Various turbopump drive arrangements are shown schematically in figure 6-13. Where a single turbine directly drives both propellant pumps through a common shaft, the turbine can be located either on the shaft end

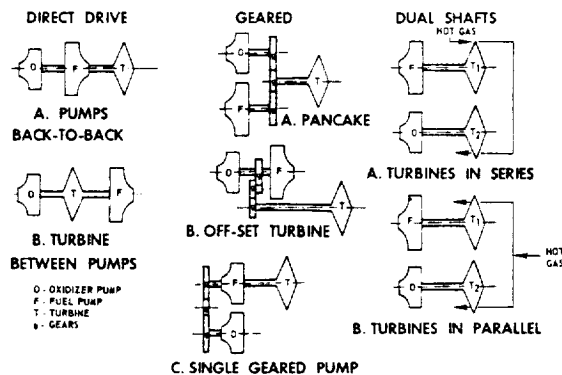


Figure 6-13.—Principal turbopump drives.

(with back-to-back pump arrangement), or between pumps. In this case both pumps and turbine will operate at the same shaft speed. Gear-driven turbopump arrangements include: the pancake type, which uses different reduction gears and is applied where there are speed differentials between pumps and turbine; the offset turbine, with both pumps on one shaft but driven through a gear train; and the single-gear pump where one pump is mounted with the turbine on the same shaft, while the other is driven through a reduction gear. Dual-shaft turbopump arrangements with pump and turbine for each propellant on separate shafts include: two gas turbines in series with the discharge gas from the first turbine driving the second turbine; and two gas turbines in parallel, both receiving gas directly from the power source.

Description of Developed Turbopump Systems

Figures 6-14 and 6-15 illustrate a typical liquid bipropellant rocket engine turbopump system. It was developed for a 188 000-pound-thrust LOX/RP-1 booster engine. Figure 6-14 shows the major elements of this turbopump design. Figure 6-15 is a cutaway view of an actual assembly with the inlet elbow ducts attached. This assembly is a dual-pump unit consisting of an oxidizer pump, a fuel pump, a reduction gearbox, an accessory drive adapter, and a turbine. The turbine is started by hot gases from a turbine spinner (solid propellant gas generator) and powered from a liquid propellant gas generator during mainstage. The turbine shaft drives a series of reduction gears, which in turn drive the

pump shaft. The turbopump gears and bearings are cooled and lubricated either by a separate oil supply system, or by a fuel additive subsystem (fig. 6-17). During mainstage operation, the turbopump supplies oxidizer and fuel to the main thrust chamber as well as to the gas generator at the required pressures and flow rates. Operating characteristics and materials of construction for this turbopump are listed in table 6-1.

Both oxidizer and fuel pumps are of single-entry, centrifugal-flow type. They are mounted back to back on a common shaft, one on each side of the gearbox. The fuel pump is bolted to the gearbox, while the oxidizer pump is secured to it by radially inserted steel pins. These pins allow the oxidizer pump housing to expand and contract during extreme temperature changes without distortion and misalignment. Each pump has an axial-flow inducer, a radial-flow impeller with backward curved vanes, stationary diffuser vanes, and a volute. The propellants pass from the inducers to the guide vanes in the impeller inlets through the impeller rotor vanes into stationary diffuser vanes in the pump casing and into the pump volutes. The diffuser vanes assure uniform pressure distribution and reduction of fluid velocity around the impellers. Balance ribs are provided on the back side of the impellers to neutralize pump shaft axial thrust.

The gearbox includes a series of full-depth reduction spur gears with integral bearing inner races, gear carrier and main shaft bearings, accessory drives, pump shaft bearing seals, and a bearing heater on the oxidizer pump shaft. A drain manifold is provided for horizontal drainage. The gears reduce the speed of rotation between turbine and pump shaft by an overall ratio of 4.88 to 1. Details of typical turbopump gears and bearings are shown in figure 6-16. The pump shaft turns clockwise as viewed from the oxidizer pump. The sequence of power transmission is as follows: turbine to high-speed pinion gear, to intermediate shaft gear, to intermediate pinion gear, and to pump shaft gear. Power is also transmitted to a main accessory drive gear from a drive pinion gear mounted on the intermediate gear shaft.

The turbine is an impulse-type, two-stage pressure-compounded unit (fig. 6-10). It is bolted to the fuel pump housing and consists of hot gas inlet manifold, stationary nozzles and

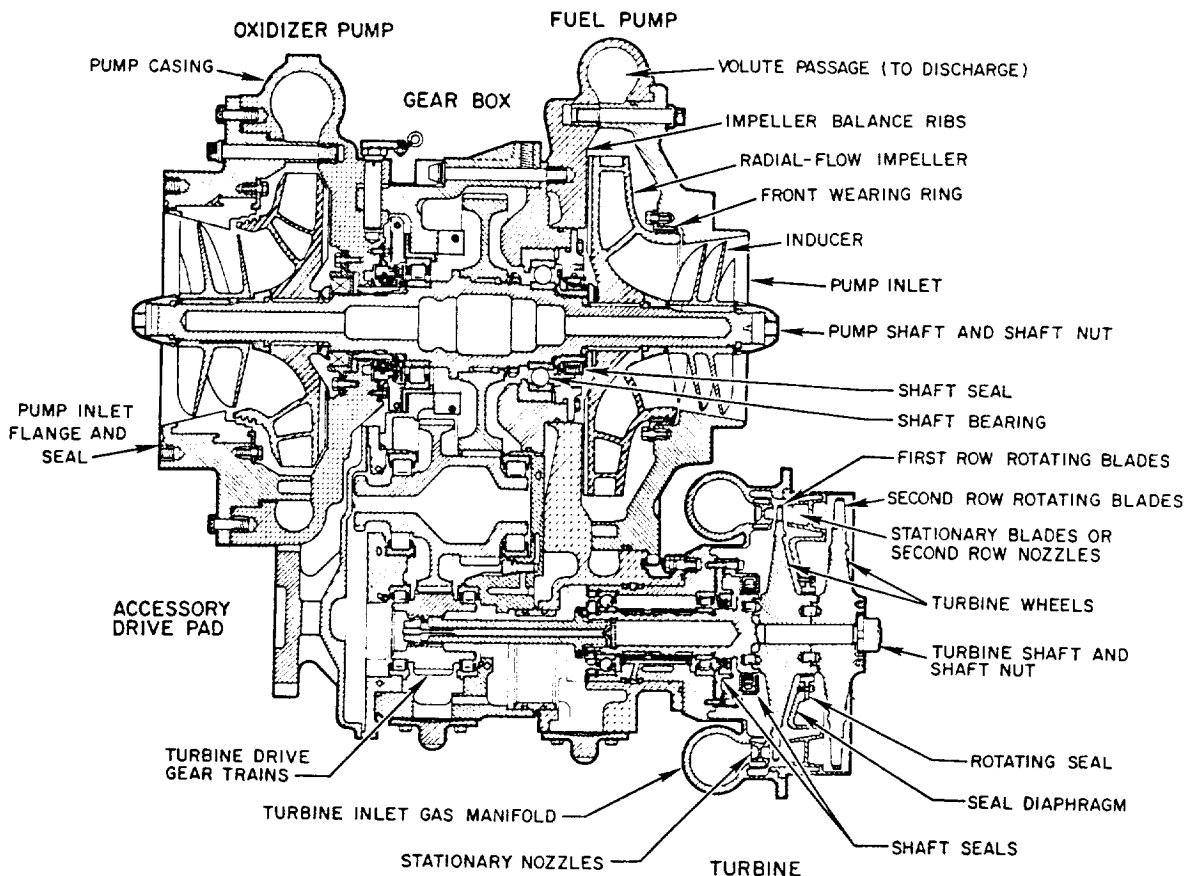


Figure 6-14.—Major elements of a typical turbopump.

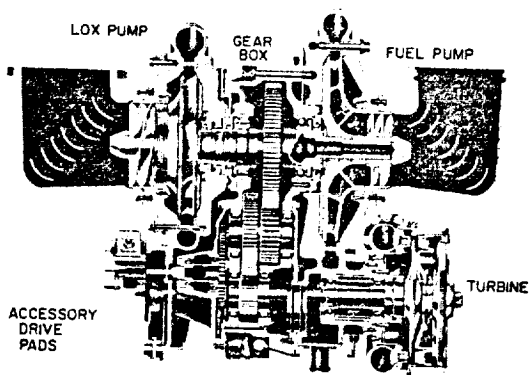


Figure 6-15.—Cutaway view of a turbopump assembly.

blades, first- and second-stage turbine wheels, a turbine shaft, and a splined quill shaft connecting the turbine shaft to the high-speed pinion

gear. The turbine shaft is supported on the in-board side by a ball bearing; on the outboard side, by a roller bearing. Carbon-ring shaft seals are used to prevent hot-gas leaks. The turbine inlet manifold distributes the gases to the first row of stationary nozzles which, in turn, distribute the gases to the first row of rotating blades. When leaving these, the gases again increase their velocity when passing through the second row of stationary nozzles. They finally pass through the second row of rotating blades and leave the turbine through an exhaust duct. A sealing diaphragm between the first and second turbine wheel prevents the hot gas from bypassing the second row of stationary nozzles.

In later systems, a fuel additive blender unit (fig. 6-17) was substituted for the oil lubrication system to increase reliability and to reduce weight by eliminating the separate oil tank, its pressurizing equipment, plumbing, and controls

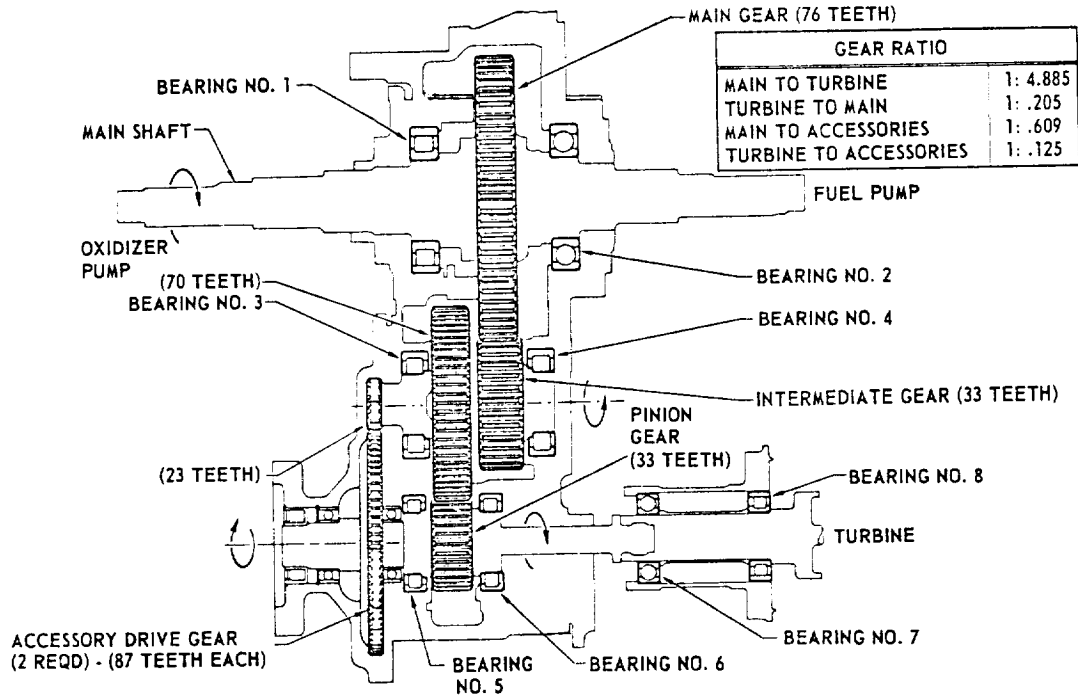


Figure 6-16.—Typical turbopump gears and bearings.

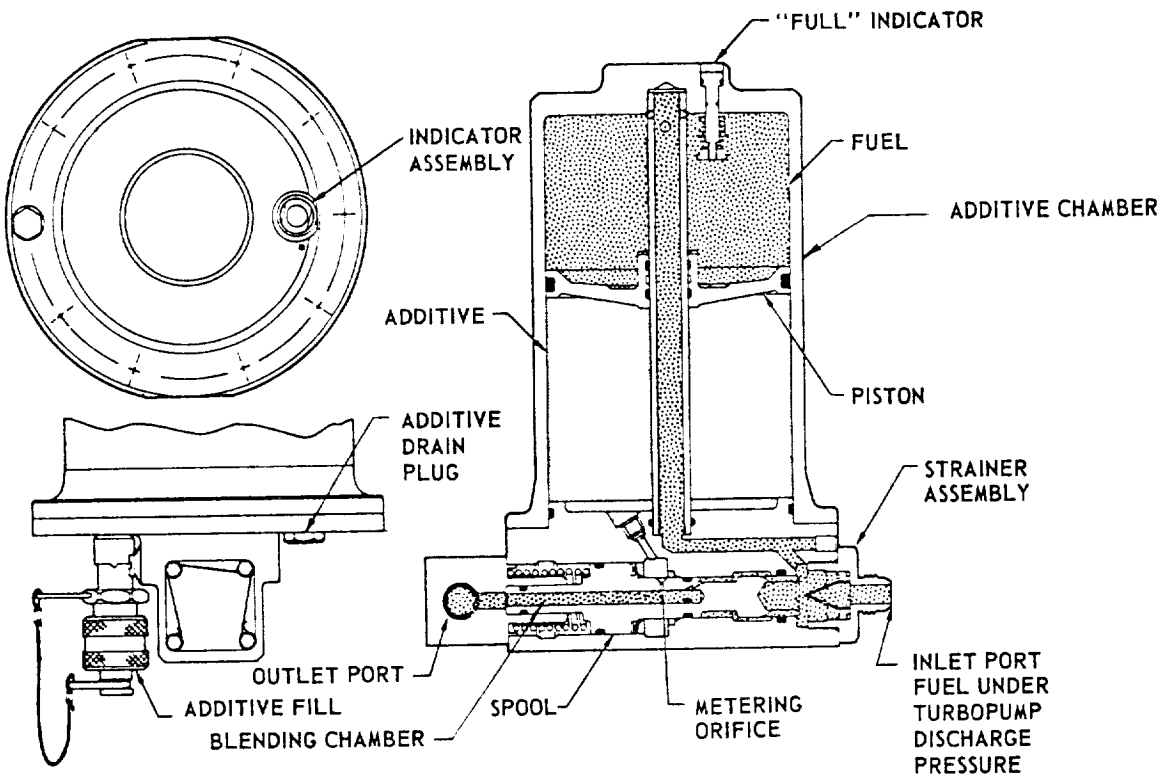


Figure 6-17.—Fuel additive blender unit.

TABLE 6-1.—Operating Characteristics and Materials of Construction for the Turbopump Shown in Figure 6-14

	Oxidizer	Fuel
Pumps:		
Fluid	Liquid oxygen	RP-1
Inlet density	71.38 lb/ft ³	50.45 lb/ft ³
Inlet pressure (total)	80.0 psia	57.0 psia
Discharge density	70.95 lb/ft ³	50.55 lb/ft ³
Discharge pressure (total)	915.2 psia	1023.0 psia
Pressure rise in pump	835.2 psi	966.0 psi
Pump developed head	1696.2 ft	2751.0 ft
Volume flow	3257.4 gpm	2007.6 gpm
Flow rate	518.0 lb/sec	225.7 lb/sec
Shaft speed		6537 rpm
Efficiency	75.5 percent	72.1 percent
Shaft power	2117 bhp	1565 bhp
NPSH required	35.0 ft	35.0 ft
Casing material	TENS 50-T6 aluminum alloy sand casting	
Inducer material	7075-T6 aluminum alloy die forging	2024-T351 aluminum alloy plate
Impeller material	TENS 50-T6 aluminum alloy sand casting	9669-48230-3 aluminum alloy sand casting
Shaft material	4340 alloy steel	
Bearing material	9310 alloy steel	
Turbine:		
Inlet gas pressure (total)	597.6 psia	
Exit gas pressure (static)	32.86 psia	
Pressure ratio: Total inlet/static exhaust	18.21	
Inlet gas pressure (static)	517.8 psia	
Inlet gas temperature	1200° F	
Exit gas temperature	938° F	
Gas flow rate	17.34 lb/sec	
Brake horsepower	3793 hp	
Shaft speed	31740 rpm	
Efficiency	66.2 percent	
Housing material	Hastelloy "B"	
Nozzle block material	Hastelloy "B"	
Wheel material	Timken alloy 16-25-6 AMS-5727 steel	
Shaft material	4340 alloy steel	
Bearing material	9310 alloy steel	
Gearbox:		
Reduction speed ratio	1/4.855	
Gearbox material	TENS 50-T6 aluminum alloy sand casting	
Gear and-shaft material	9310 alloy steel die forging	
Bearing material	9310 alloy steel	

previously required. The blender works on the principle of adding a small amount of a chemical to the fuel tapped off through metering orifices at the fuel pump outlet and of using this mixture as the lubricant. The fuel entering the blender inlet port is admitted to the top side of the additive chamber and to the blending chamber. The fuel pressure causes the piston to displace and

to inject a proportionate amount (2.75 percent) of additive into the fuel flowing through the blending chamber. The mixture then flows to the turbopump where it lubricates and cools the gears and bearings.

Figure 6-18 and table 6-2 illustrate another turbopump system. It was developed for a 6000-pound-thrust aircraft superperformance rocket

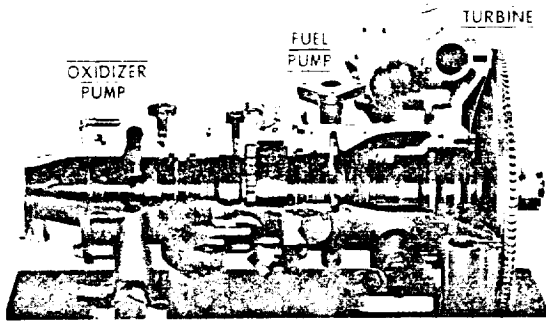


Figure 6-18.—Cutaway view of an aircraft rocket turbopump assembly.

engine (shown schematically in fig. 4-60). Pumped fluids are 90 percent hydrogen peroxide and JP-4 fuel. The turbopump consists of two centrifugal pumps mounted back to back on a single shaft which is directly driven by a single-stage, single-rotor impulse turbine. The shaft is supported by antifriction bearings located between the two pumps, and just forward of the overhung turbine. The bearings are lubricated by a pressure-fed lube oil system. Inducers are used on both pumps to permit operation at a low

TABLE 6-2.—Aircraft Rocket Turbopump Operating Characteristics

	Oxidizer	Fuel
Pumps:		
Fluid	90% H ₂ O ₂	JP-4
Density	86.7 lb/ft ³	50.5 lb/ft ³
Inlet pressure (total)	25 psia	15 psia
Discharge pressure (total) ..	862 psia	657 psia
Pressure rise in pump	837 psi	642 psi
Pump developed head	1382 ft	1910 ft
Volume flow	106.8 gpm	26.4 gpm
Flow rate	20.52 lb/sec	2.84 lb/sec
Shaft speed	30 000 rpm	
Efficiency	60 percent	40 percent
Shaft power	87 bhp	25 bhp
Turbine:		
Inlet gas pressure (total) ...	510 psia	
Exit gas pressure (static) ...	25.5 psia	
Pressure ratio:		
Total inlet/static exhaust	20	
Inlet gas temperature	1364° F	
Exhaust gas temperature ...	910° F	
Gas flow rate	0.54 lb/sec	
Brake horsepower	112 hp	
Shaft speed	30 000 rpm	
Efficiency	40 percent	

NPSH. Pump inducers, impellers, shaft and cast housings are fabricated from 300 series stainless steel. Turbine manifold, housing and nozzle blocks form an integral Hastelloy-X weldment. The turbine wheel is made of Timken alloy.

6.2 TURBOPUMP SYSTEM PERFORMANCE AND DESIGN PARAMETERS

Turbopump performance and design parameters are closely related. Variation of the turbopump design and operating parameters will contribute to the optimization of both turbopump and engine system performance. The turbopump system design procedure includes the evaluation of all possible design approaches and mechanical configurations which can satisfy engine system specifications. From this, the selection of the best design with respect to overall systems reliability and performance is made.

Turbopump System Performance

The "best performing" turbopump system is simply defined as that which affords the heaviest payload for a vehicle with a given thrust level, range or velocity increment; gross stage takeoff weight; and thrust chamber specific impulse (based on propellant combination, mixture ratio, and chamber operating efficiency). Turbopump performance affects the vehicle payload in three ways:

1. *Turbopump component weight.*—Since the weight of the turbopump components is part of stage burnout weight, it directly affects stage payload.
2. *Required pump-inlet suction pressure head.*—Required suction pressure directly translates into required main propellant tank pressure level. If it is raised, tank and pressurization system weights increase and thus reduce the stage payload for a given burnout weight.
3. *Turbine gas flow rate.*—Since the turbine drive gases, the flow rate of which is a function of propellant types and flow rates, pump discharge pressures, and of pump and turbine efficiencies, are usually ejected at a lower specific impulse than the thrust chamber gases (except in the case of the topping cycle), their flow rate decreases the overall engine system specific impulse and thus decreases the allowable vehicle

stage burnout weight. For a fixed weight of engines, tanks, guidance, and other equipment, a decrease in allowable stage burnout weight results in decrease of payload weight.

The relation between turbine gas flow rate and stage payload weight can be expressed by an equivalent-weight factor, EWF, which is defined as the decrease of payload weight (lb) as a function of turbine flow rate (lb/sec). EWF is proportional to the ratio between turbine exhaust specific impulse $(I_s)_{te}$ and thrust chamber specific impulse $(I_s)_{tc}$.

$$EWF \approx \left(1 - \frac{(I_s)_{te}}{(I_s)_{tc}}\right) \quad (6-1)$$

The total effect of the turbopump on allowable vehicle stage payload, i.e., the equivalent weight of the turbopump, EW, is the sum of turbopump component weight, W_{tb} , and the product of EWF and the turbine weight flow rate, \dot{w}_t :

$$EW = W_{tb} + (EWF)(\dot{w}_t) \quad (6-2)$$

Equation (6-2) permits a quantitative definition of the "best performing" turbopump system possessing the lowest equivalent weight. Values for the turbopump equivalent-weight factor EWF range from 5(lb/lb/sec) for booster stage engines to 200(lb/lb/sec) for upper stage engines. The equivalent-weight EW helps to establish the optimized point between turbine and pump efficiencies, and corresponding turbopump component weights. It is not practical to include the effects of pump inlet pressure on vehicle tank weights, since the required information is usually unavailable to the turbopump designer. It is advisable however, that the pumps should be designed for the lowest possible inlet pressure.

Sample Calculation (6-1)

The following design data are set forth for the hypothetical A-1 stage engine:

Turbopump weight, W_{tb} , 1900 lb

Turbine gas flowrate, \dot{w}_t , 92 lb/sec

Turbopump equivalent-weight factor EWF,
55 lb/lb/sec

Determine the turbopump equivalent weight (EW) per engine.

Solution

From equation (6-2):

$$\begin{aligned} \text{Turbopump equivalent weight per engine} \\ &= 1900 + 92 \times 55 \\ &= 6960 \text{ lb} \end{aligned}$$

Turbopump System Design Parameters

In the design of turbopump systems the following parameters, which are often interdependent, are considered paramount and will be discussed:

- (1) Propellant properties
- (2) Pump developed heads and flow rates
- (3) Pump specific speeds
- (4) Pump net positive suction head (NPSH)
- (5) Pump efficiencies
- (6) Turbine overall performance and operating efficiency
- (7) Turbopump system cycle efficiency
- (8) Turbopump system calibration and off-design characteristics

No simple rules are available for optimizing the correlations of these parameters when designing a specific type of turbopump for a given engine systems application. Generally speaking, however, available pump suction pressure together with the basic pump flow characteristics will determine the maximum shaft speed at which the unit can operate. The higher this shaft speed, the lower the turbopump weight is likely to be. Once the pump speed is determined, turbine type, turbine driving arrangement, and turbine power source are selected on the basis of efficiency, weight, simplicity, and other factors.

Propellant Properties

General data for some propellants used in liquid rocket engines are given in tables 1-3 to 1-5. Table 6-3 lists those properties of commonly used liquid propellants which have specific significance in the design of pumps. These propellants include Earth-storable liquids such as RP-1 and N_2O_4 , cryogenics such as LO_2 and LH_2 , and liquids having a wide range of physical and chemical properties.

The low temperature of cryogenic liquids creates problems with turbopump construction materials, seals, bearings, lubricants, and through the danger of ice formation. The total temperature range to which the structural elements of a cryogenic turbopump may be exposed varies from

TABLE 6-3.—Fluid Properties of Commonly Used Liquid Propellants

Liquid	^a Data at normal conditions					
	Temperature, °F	Vapor pressure, psia	Density, lb/ft ³	Conversion factors		Viscosity, lb-sec/sq in
				Head, ft Pressure, psi	gpm lb/sec	
N ₂ O ₄	60	11.1	90.7	1.59	4.96	0.637 × 10 ⁻⁷
H ₂ O ₂ (90 percent)	60	.026	87.8	1.64	5.12	1.868 × 10 ⁻⁷
N ₂ H ₄	60	.158	63.3	2.28	7.12	1.49 × 10 ⁻⁷
RP-1	60	.031	50.8 (max) 49.8 (min)	2.83(min) 2.89(max)	8.84(min) 9.00(max)	3.22 × 10 ⁻⁷
Ethyl-alcohol (95 percent)	60	.62	50.4	2.85	8.91	2.22 × 10 ⁻⁷
UDMH	60	1.83	49.66	2.90	9.06	.842 × 10 ⁻⁷
50 percent UDMH/N ₂ H ₄	60	1.77	56.66	2.54	7.94	1.378 × 10 ⁻⁷
LO ₂	-297.6	14.7	71.17	2.02	6.32	.2765 × 10 ⁻⁷
LF ₂	-307	14.7	94.21	1.54	4.79	.353 × 10 ⁻⁷
LH ₂	-422.9	14.7	4.43	32.5	101.5	.0208 × 10 ⁻⁷
^b LN ₂	-320.4	14.7	50.44	2.86	8.92	.226 × 10 ⁻⁷
^b Water	60	.256	62.37	2.31	7.2	1.64 × 10 ⁻⁷

^aNormal conditions do not necessarily imply standard conditions, if tank pressures have been applied.

^bIncluded here because these fluids are frequently used as pump calibration media.

-300 to -430° F at the pumps to 1200°-1700° F at the turbine. This induces temperature gradients between the various turbopump components which must be accommodated and requires structural flexibility or suitable devices to permit the required thermal expansion and contraction. Radial connecting pins are often employed to permit a cryogenic pump to contract independently of a turbine and/or of a normal-temperature pump.

The vapor pressure of the propellants under normal engine operation conditions directly influences total suction pressure requirements at the pump inlet. This will be further discussed in conjunction with the pump inlet net positive suction head (NPSH).

The density variations of different propellants produce substantially different pump head-rise requirements, as well as large differences in volume flow. The power required per unit weight flow and pressure rise of a pump is inversely proportional to the density of the fluid. This is shown dramatically in the case of liquid hydrogen which has a density of less than 10 percent of that of other propellants. For the same weight flow and pressure rise, a liquid

hydrogen pump requires more than 10 times the volume flow and driving power as compared to other propellant pumps. Thus the design of liquid hydrogen pumps requires specific considerations.

The viscosity of the pumped fluids effects a boundary layer along the surface of the flow passages within the pump. There is a minimum size of the impeller cross-section below which pump performance will fall off rapidly. As the passage clearances in the impeller are decreased, a point will be reached where the flow is predominantly boundary layer, and viscous rather than turbulent forces become predominant. This completely changes the performance of a pump. The drag effect of the boundary layers, together with the rotation of the fluid in certain pump passages from an axial to a radial direction, such as in the impeller of a centrifugal pump, results in secondary flows being set up. This, together with friction losses which also are in direct proportion to the viscosity of the fluid, and with leakage losses, constitutes a major portion of the energy losses in a pump. It is seen that a high propellant viscosity tends to lower pump efficiency.

Some liquid propellants, such as LF_2 and N_2H_4 , are highly reactive chemically, and thermally unstable, beyond certain temperature limits. In the design of turbopumps for these propellants, special consideration must be given to the selection of compatible materials as well as to the construction of mechanical parts. Seals, bearings, and the protection (insulation) of the pump section against heat influx from the turbine section following engine shutdown, are typical problem areas.

Pump Developed Heads and Flow Rates

The term "pump developed head," ΔH (ft), is defined as the difference between pump discharge head and pump suction head. The relationship between developed fluid pressure Δp (psi) and fluid head ΔH (ft) is given by

$$\Delta H \text{ (ft)} = \frac{144 \times \Delta p \left(\frac{\text{lb}}{\text{in}^2} \right)}{\text{Fluid density} \left(\frac{\text{lb}}{\text{ft}^3} \right)} \quad (6-3)$$

The required pump developed head at the design propellant flow rate (i.e., engine thrust level) is dictated by the sum of the hydraulic resistances within the engine propellant flow system. These resistances include the pressure drops across injector, thrust chamber manifold, cooling jacket, propellant valves and ducts, as well as the injector end thrust chamber pressure. An additional pressure margin is usually allowed for systems calibration. An engine propellant flow system hydraulic resistance curve representing the resistance head to flow-rate relationship at various pump operating levels is shown in figure 6-19.

Any value for developed fluid head of a given pump is tied to a corresponding level of fluid flow at any impeller rotating speed. At the maximum flow rates, the entire pump drive energy is consumed by internal flow losses and kinetic energy imparted to the fluid. Thus the measured head rise at the pump outlet is zero. At the other extreme, where fluid flow is zero (except for secondary flows), head rise is a maximum. A pump developed head versus flow capacity curve, commonly called *H-Q curve*, is derived by connecting the pump operating points between the two extremes for constant speeds. A family of

curves is thus obtained experimentally for the range of speeds through which the pump may operate, all of them having similar parabolic shape. Typical *H-Q* curves of a pump at various speeds are shown in figure 6-19, along with the system flow resistance curve. Together they form the design operating range of a system.

Two dimensionless coefficients are frequently used to indicate the head and flow characteristics of a given pump. They are the pump head coefficient ψ and the pump flow coefficient ϕ . The *pump head coefficient* is the ratio of rated pump head (ft) to the maximum theoretical head at zero flow for meridional (axial) inlet (no pre-rotation) expressed as

$$\psi = \frac{\Delta H}{\frac{u_2^2}{g}} \quad (6-4)$$

where

ψ = overall pump head coefficient at rated design point (range is 0.2 to 0.7 for single stage centrifugal pumps and up to 1.5 to 2.0 for multistage axial pumps, depending on number of stages)

ΔH = pump rated developed head, ft

u_2 = mean tip velocity of pump impeller at rated design rotating speed, ft/sec

g = gravitational constant, 32.2 ft/sec²

The *pump flow coefficient* can be expressed as

$$\phi = \frac{C_{m2}}{u_2} \quad (6-5)$$

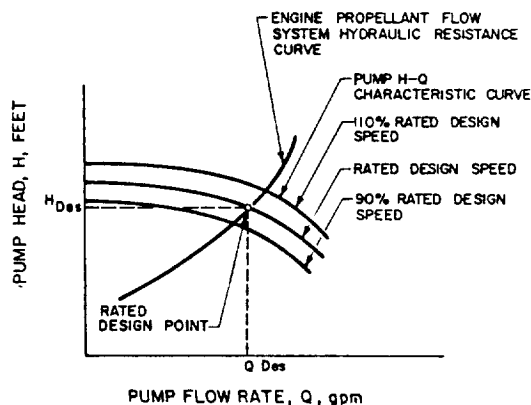


Figure 6-19.—Engine system resistance and pump characteristic curves.

where

ϕ = overall pump flow coefficient at rated design point (range 0.01 to 0.15 in rocket engine application)

c_{m2} = velocity of pump flow in meridional direction at rated design point, ft/sec

$$= \frac{\text{Rated pump flow, ft}^3/\text{sec}}{A_2}$$

A_2 = discharge area normal to meridional direction, ft²

Pump Specific Speeds

For any given pump design, the relation between fluid flow rate Q , developed fluid head ΔH , required driving power hp , and rotating speed N can be defined by three expressions called the affinity laws of a pump. These laws state:

- (1) Pump volume flow rate varies directly with speed:

$$\frac{Q_1}{Q_2} = \frac{N_1}{N_2} \quad (6-6a)$$

- (2) Pump developed head varies directly as the square of the speed:

$$\frac{\Delta H_1}{\Delta H_2} = \frac{N_1^2}{N_2^2} \quad (6-6b)$$

- (3) Pump driving power varies directly as a cube of the speed:

$$\frac{hp_1}{hp_2} = \frac{N_1^3}{N_2^3} \quad (6-6c)$$

The affinity laws are based on the assumption that the pump efficiency is independent of the rotating speed. Actual pump operation has shown, however, that pump efficiency does change with speed. The degree depends on the individual pump design, but is usually not more than 2 or 3 percent within a reasonable range from the rated design point. Furthermore, it affects only the power requirements rather than the relationship between developed head and flow rate. Thus the pump affinity laws hold quite well in most cases.

The relationships established in equations (6-6a), (6-6b), and (6-6c) permit us to derive a useful pump design parameter, the pump specific speed, N_s :

$$N_s = \frac{N(Q)^{0.5}}{(\Delta H)^{0.75}} \quad (6-7)$$

where

N_s = pump specific speed (dimensionless)

N = pump rotating speed, rpm

Q = pump flow rate, gpm

ΔH = pump developed head, feet

Pump specific speed is a characteristic value defined as the rpm required to produce 1-gpm flow at 1-foot head rise across the pump impeller (or across the combination of inducer and impeller). In pump design, this term is very useful to classify inducers or impellers on the basis of their performance and geometric proportions regardless of the actual size or speed at which they operate. N_s is a function of design configuration; it does not vary significantly for a series of geometrically similar impellers (having the same angles and proportions), or for one particular impeller operating at any speed.

Since the H-Q characteristic curve of a pump ranges from zero flow at shutoff to zero head at maximum flow, the specific speed for one curve varies from zero to infinity. To make the term definite, it is necessary to relate it to a defined condition. The logical point is that of maximum efficiency, usually the rated design point. It is generally understood that this point is meant when specific speed is stated.

Figure 6-20 indicates typical pump specific speeds for various impeller geometries. For a given speed, a low value of specific speed is characteristic for low-volume flow, high-head-rise pumps. Higher specific speed indicates a higher volume flow, low-head-rise pump.

1. *Radial-type impeller.*—The head is largely developed by the action of centrifugal force. This type is used for heads above 200 feet. Specific speed ranges from 500 to 1200. Geometric proportion, r_2/r_1 , varies from 2 to 3.

2. *Francis-type impeller.*—This type has an axial inlet, a radial discharge, and is used for lower heads. Specific speed ranges from 1200 to 2400. Geometric proportion, r_2/r_1 , varies from 1.3 to 1.8.

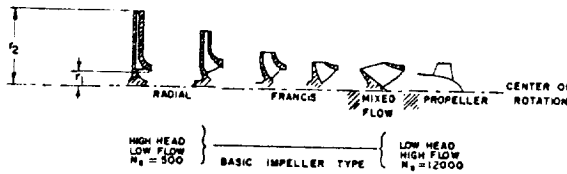


Figure 6-20.—Relationship between the pump specific speeds and pump impeller geometries.

3. *Mixed-flow type impeller.*—The head developed in this impeller is due partly to change in tangential velocity and partly to change in fluid velocity relative to the rotor. The discharge is partly radial and partly axial. The impeller vanes are doubly curved. Specific speed varies from 2200 to 3500.

4. *Propeller-type impeller.*—The head developed by this type is through push of the vanes only. Flow direction is axial. Specific speeds range from 3000 to 6000 for multistage impellers, and from 6000 to 12 000 for inducers.

Sample Calculation (6-2)

The following data are given for the propellant pumps of the hypothetical A-1 stage engine at the rated design point:

Pump	Fluid density, lb/ft ³	Pump inlet suction pressures, psia (total)	Pump discharge pressure, psia	Pump weight flow rate, lb/sec	Pump speed, rpm
Oxidizer.	71.38	55	1505	1971	7000
Fuel	50.45	45	1720	892	7000

Determine the pump specific speeds.

Solution

Oxidizer pump developed pressure,

$$\Delta p = 1505 - 55 = 1450 \text{ psi}$$

From equation (6-3):

Oxidizer pump developed head,

$$\Delta H = \frac{144 \times 1450}{71.38} = 2930 \text{ ft}$$

Since 1 ft³/sec = 449 gpm

Oxidizer pump volume flow rate,

$$Q_o = 1971 \times 449 / 71.38 = 12\,420 \text{ gpm}$$

From equation (6-7):

Oxidizer pump specific speed,

$$N_s = \frac{7000 \times (12\,420)^{0.5}}{(2930)^{0.75}} = \frac{7000 \times 111.7}{395} = 1980$$

Fuel pump developed pressure,

$$\Delta p = 1720 - 45 = 1675 \text{ psi}$$

From equation (6-3):

Fuel pump developed head,

$$\Delta H = \frac{144 \times 1675}{50.45} = 4790 \text{ ft}$$

Fuel pump volume flow rate,

$$Q_f = 892 \times 449 / 50.45 = 7960$$

From equation (6-7):

$$N_s = \frac{7000 \times (7960)^{0.5}}{(4790)^{0.75}} = \frac{7000 \times 89.1}{576} = 1083$$

Pump Net Positive Suction Head; Cavitation

Steady flow operation of a pump creates a low-pressure area at the pump inlet, thus allowing the static head upstream of the pump to push fluid into the inlet at a continuous rate. There are local regions within the pump which are at static pressures even lower than the inlet static pressure. If the static pressure of the fluid at the pump inlet or any regions within the pump is allowed to drop below the local fluid vapor pressure level, these regions will cavitate; i.e., the fluid will pass from liquid to vapor and form bubbles. The formation of vapor alters the effective flow passages of the fluid and hence seriously affects normal pump performance. The

subsequent collapse of these vapor regions creates local pressure forces which can result in flow instabilities and/or substantial damage.

To avoid cavitation during operation of a propellant pump, the pump-inlet available net positive suction head, $(NPSH)_a$, furnished by the propellant feed system upstream of the pump, must be higher than the suction head above the propellant vapor pressure at which cavitation would set in. $(NPSH)_c$ is the difference between the propellant inlet total pressure head and the propellant vapor pressure. This can be expressed as:

$$(NPSH)_a = \frac{P_t \times 144}{\rho} + Z - \frac{\Delta p_f \times 144}{\rho} - \frac{p_v \times 144}{\rho} \quad (6-8)$$

where

$(NPSH)_a$ = available net positive suction head, ft

P_t = propellant tank pressure, psia

ρ = density of propellant, lb/ft³

Z = height of propellant above the pump inlet and within the tank (corrected in flight for vehicle acceleration and gravity effects), ft

Δp_f = pressure drop due to friction losses within the propellant suction ducts, psi

p_v = propellant vapor pressure for the propellant temperature at the pump inlet, psia

In design practice the term "critical net positive suction head," or $(NPSH)_c$, is used to indicate the minimum suction head required above the propellant vapor pressure to assure suppression of cavitation. This critical net positive suction head is defined by convention, as that value which will result in a 2-percent head-generation loss at the rated design speed and flow rate of a given pump. Usually further reduction in inlet NPSH below the $(NPSH)_c$ point results in rapidly increasing cavitation. In turn, the developed head is further reduced, and non-steady flow can result. This fluctuation of propellant flow can cause erratic combustion in the thrust chamber. Figure 6-21 represents the cavitation characteristics of a typical pump operated at rated design speed. To insure a margin of safety for pump operation, the $(NPSH)_a$

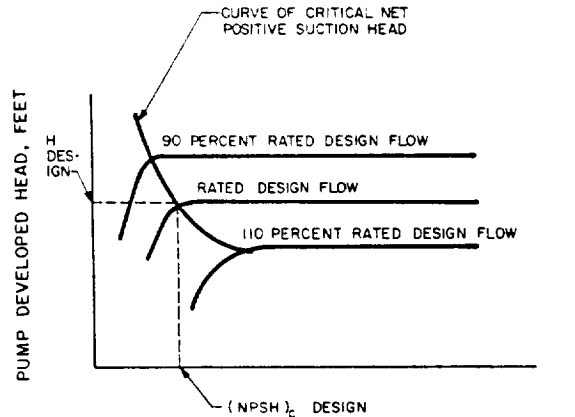


Figure 6-21.—Typical cavitation characteristics of a pump operated at rated design speed.

supplied by the vehicle must be larger than the $(NPSH)_c$ of the propellant pumps, or

$$(NPSH)_a > (NPSH)_c \quad (6-9)$$

It is useful to compare the suction characteristics of various pump designs on the basis of a design parameter called suction specific speed, N_{SS} , which is defined as follows:

$$N_{SS} = \frac{N(Q)^{0.5}}{(NPSH)_c^{0.75}} \quad (6-10)$$

where

N_{SS} = pump suction specific speed

N = pump rated design speed, rpm

Q = pump rated design volume flow rate, gpm

$(NPSH)_c$ = pump critical net positive suction head, ft

Suction specific speed is related to the critical net positive suction head in the same manner the specific speed is related to overall pump developed head. Design values of suction specific speeds for rocket propellant pumps range from 10 000 without inducers approximately to 55 000 with inducers.

Another coefficient describing pump suction characteristics is the Thoma parameter τ . It is the ratio of critical net positive suction head $(NPSH)_c$ and rated pump developed head ΔH , or

$$\tau = \frac{(NPSH)_c}{\Delta H} = \left(\frac{N_s}{N_{SS}} \right)^{1.333} \quad (6-11)$$

The Thoma parameter is a function of pump design quality and specific speed.

For a given vehicle $(NPSH)_a$, the pump suction characteristics (N_{SS}) determine the maximum permissible rpm at the design flow rate. A high pump N_{SS} or vehicle $(NPSH)_a$ permits a higher pump rpm, lower turbopump weight, and possibly higher turbine performance. It is desirable to operate a pump at the highest practicable speed. Figure 6-22 represents the results of a parametric turbopump system design study for a typical $LO_2/RP-1$ booster stage rocket engine system, such as the A-1 stage engine. The study reflects the effects of N , $(NPSH)_c$, and N_{SS} on the selection of turbopump configuration.

In addition to the pump $(NPSH)_c$ values during steady-state operation, the engine starting transient pump $(NPSH)_c$ must be determined and specified to permit satisfactory engine acceleration from zero to nominal design speed and flow rate in the desired time and manner. The starting $(NPSH)_c$ depends on the rate of acceleration and on the control system of the engine, as well as on vehicle acceleration, gravity effects, and propellant suction duct geometry. Therefore, sufficient tank pressure must be provided to accelerate the propellant and to overcome the hydraulic resistance in the suction duct, as well as to supply the necessary pump $(NPSH)_c$ during all phases of system operation.

Sample Calculation (6-3)

(a) The following test data are given for the propellant pumps of the A-1 stage:

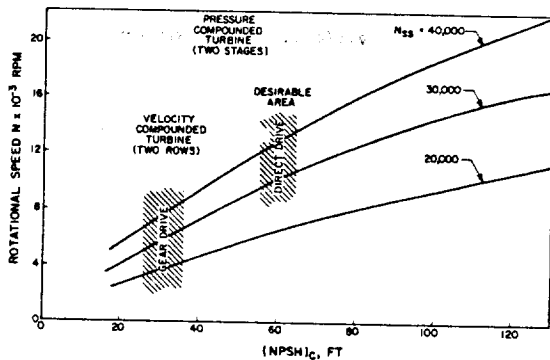


Figure 6-22.—Effects of N , $(NPSH)_c$, and N_{SS} on turbopump configuration selection for a typical $LO_2/RP-1$ booster stage rocket engine system.

Pump	Pump speed, rpm	Fluid pumped	Pump volume flow rate, gpm	Pump developed head, ft	Pump $(NPSH)_c$, ft
Oxidizer..	7000	LO_2	12 420	2930	58
Fuel	7000	RP-1	7960	4790	70

Determine pump suction specific speeds and Thoma parameters.

(b) The following system design data are given for the A-1 stage vehicle:

Pump	Fluid density, lb/ft ³	Tank pressure, psia	Longitudinal distance between tank and pump inlet, ft	^a Permanent static pressure loss in suction duct, including valves, psi	Propellant temperature at pump inlet, °F
Oxidizer	71.38	60	3.5	5	-297.6
Fuel ...	50.45	50	25	8	60

^aThe dynamic head at the pump inlet is considered a part of the available NPSH and thus is not subtracted from the tank pressure.

Determine the available NPSH at the pump inlets.

Solution

(a) Substitute given data into equation (6-10):

Oxidizer pump suction specific speed,

$$N_{SS} = \frac{7000 \times (12\,420)^{0.5}}{(58)^{0.75}} = \frac{7000 \times 111.7}{21} = 37\,230$$

Fuel pump suction specific speed,

$$N_{SS} = \frac{7000 \times (7960)^{0.5}}{(70)^{0.75}} = \frac{7000 \times 89.1}{24.2} = 25\,790$$

Substitute given data into equation (6-11):

Thoma parameter of the oxidizer pump,

$$\tau = \frac{58}{2930} = 0.0198$$

Thoma parameter of the fuel pump,

$$\tau = \frac{70}{4790} = 0.0146$$

(b) From table 6-3:

Vapor pressure of liquid oxygen
= 14.7 psia at -297.6° F

Vapor pressure of RP-1 = 0.031 psia at 60° F

Assume the vehicle is at sea-level holddown condition and substitute given data into equation (6-8):

Available NPSH at oxidizer pump inlet

$$\begin{aligned} (\text{NPSH})_a &= \frac{(60-5-14.7) \times 144}{71.38} + 3.5 \\ &= 81.5 + 3.5 = 85 \text{ ft} \end{aligned}$$

Available NPSH at fuel pump inlet

$$\begin{aligned} (\text{NPSH})_a &= \frac{(50-8-0.031) \times 144}{50.45} + 25 \\ &= 120 + 25 = 145 \text{ ft} \end{aligned}$$

Pump Operational Efficiency; Losses

Several types of energy losses occur during pump operation which affect efficiency.

1. *Hydraulic losses.*—These include friction losses in the passages and flow turbulence losses. The friction losses are a function of the "wetted areas" in the passages and of the roughness of their surfaces. The turbulence losses are caused by disturbances in certain regions of the pump, such as at the inlet and outlet edge of the vanes of both impeller and diffuser and in the return guide vanes.

2. *Disk friction losses.*—The energy required to rotate a disk, such as an impeller or inducer, in a fluid is known as disk friction loss. The disk friction losses are due to two actions: namely, (a) the actual friction of the fluid on the

disk, which is relatively minor, and (b) a pumping action on the fluid in contact with the disk, whereby the fluid is circulated locally by centrifugal action. The energy loss due to disk friction is transformed into heat and can appreciably increase the temperature of the fluid.

3. *Mechanical losses.*—These are losses in bearings and seals caused by mechanical friction.

4. *Leakage losses.*—To prevent the pumped fluid from leaking back to the suction side after it has passed the impeller and is at outlet pressure levels, close-clearance labyrinth-type seals or wearing rings are provided. Leakback lowers the flow capacity of a pump and thus increases required pumping power.

For a new design, losses are difficult to predict and are usually estimated from data derived during actual testing and other past experience with similar designs.

The overall efficiency of a pump, η_p , can be expressed by the ratio of pump fluid horsepower output, fhp, to brake horsepower input by the pump drive, bhp:

$$\eta_p = \frac{\text{fhp}}{\text{bhp}} \quad (6-12)$$

The pump fluid horsepower fhp is the actual usable output delivered by the pump. It is the product of delivered propellant weight flow, \dot{w}_p (lb/sec), times the actual head ΔH (ft) developed by the pump, divided by a conversion factor:

$$\text{fhp} = \frac{\dot{w}_p \Delta H}{550} \quad (6-13)$$

The brake horsepower bhp represents the mechanical horsepower delivered to the pump by the drive. This delivered brake horsepower is consumed in the pump as fluid horsepower and as the various losses.

$$\text{bhp} = \text{fhp} + (\text{hp})_h + (\text{hp})_{df} + (\text{hp})_m + (\text{hp})_l \quad (6-14)$$

where

bhp = brake horsepower

fhp = fluid horsepower

$(\text{hp})_h$ = horsepower required to overcome hydraulic losses

- (hp)_{df} = horsepower required to overcome disk friction losses
- (hp)_m = horsepower required to overcome mechanical losses
- (hp)_l = horsepower required to overcome leakage loss

The efficiency of a pump is related to the volume flow rate Q , the developed head ΔH , and the rotating speed N , all of which are included in the pump specific speed N_s . Of these, the most important one is the design volume flow rate or capacity of the pump. There is a definite trend toward increased efficiency with higher pump capacities, because hydraulic, disk friction, and mechanical losses represent a smaller percentage of the total brake horsepower when large capacities are being handled. On the other hand, increased pump-developed head and rotating speed for a pump of given capacity results in lower efficiency because of increased disk friction and mechanical losses. The overall efficiency of rocket engine propellant pumps of high

developed head and rotating speed ranges from 60 to 85 percent. This is about 10 percent lower than that of industrial pumps. The variation of pump efficiency with specific speed, at various pump capacities, is shown in figure 6-23. Figure 6-24 shows the correlation between pump flow rate and the following three parameters: developed head, efficiency, and required brake horsepower, for a typical centrifugal pump.

Sample Calculation (6-4)

The following test data are given for the propellant pumps of the A-1 stage engine:

Pump	Fluid pumped	Pump volume flow rate, gpm	Pump developed head, ft	Drive shaft power, hp
Oxidizer	LO ₂	12 420	2930	14 850
Fuel	RP-1	7960	4790	11 790

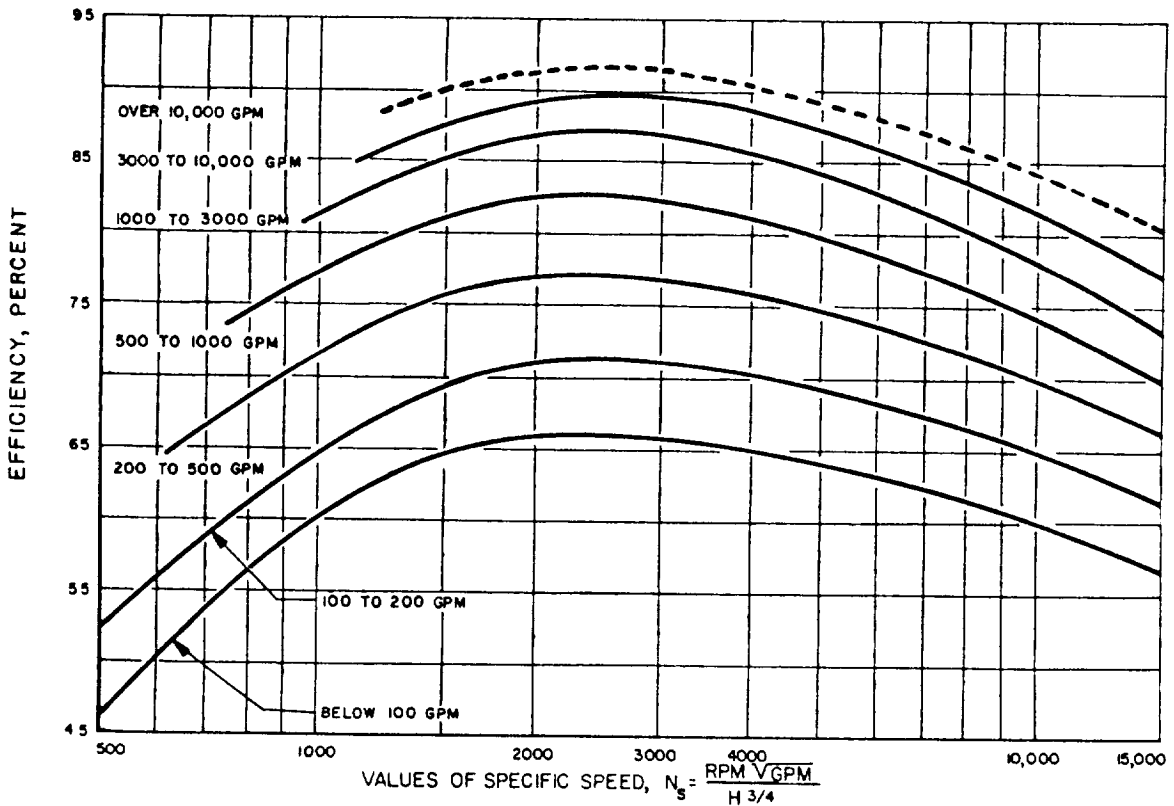


Figure 6-23.—Variation of pump efficiency with specific speed.

Determine the overall efficiencies η_p of both pumps.

Solution

Substitute given data and flow rates from sample calculation (6-2) into equation (6-13):

Oxidizer pump fluid horsepower

$$f_{hp} = \frac{1971 \times 2930}{550} = 10\,500 \text{ hp}$$

Fuel pump fluid horsepower

$$f_{hp} = \frac{892 \times 4790}{550} = 7760 \text{ hp}$$

Substitute into equation (6-12):

Oxidizer pump overall efficiency

$$\eta_p = \frac{10\,500}{14\,850} = 70.7\%$$

Fuel pump overall efficiency $\eta_p = \frac{7760}{11\,790} = 65.8\%$

PUMP DEVELOPED HEAD H , FEET
PUMP EFFICIENCY η_p , PERCENT
PUMP REQUIRED POWER, Bhp

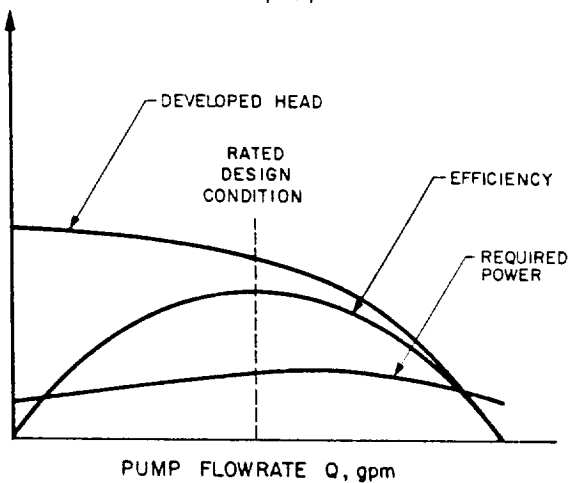


Figure 6-24.—H-Q, efficiency, and required power characteristic curves of a typical centrifugal pump.

Turbine Overall Performance and Operating Efficiency

The overall performance of a turbine is defined as the ratio of turbine shaft horsepower output, thp, and required turbine working-fluid flow rate, \dot{w}_t , in pounds per second or

Overall turbine performance

$$= \frac{\text{thp}}{\dot{w}_t} \text{ (hp/lb/sec)} \quad (6-15)$$

In general, turbine overall performance depends upon two variables: the available energy content per pound of turbine working-fluid, ΔH_t , and the overall turbine operating efficiency, η_t .

The available energy content of the turbine working fluid is defined as the enthalpy drop per pound of working fluid in the turbine

$$\Delta H_t = H_o - H_e \quad (6-16)$$

where

ΔH_t = available energy content of the working fluid, Btu/lb

H_o = enthalpy per unit weight of the working fluid at turbine-inlet, Btu/lb

H_e = enthalpy per unit weight of the working fluid at exhaust pressure, Btu/lb, assuming isentropic expansion

Using equations (1-10) and (1-13), equation (6-16) can be rewritten as

$$\Delta H_t = C_p(T_o - T_e) = C_p T_o \left[1 - \left(\frac{p_e}{p_o} \right)^{\frac{\gamma-1}{\gamma}} \right] \quad (6-17)$$

where

C_p = working fluid specific heat at constant pressure, Btu/lb-F

T_o = working fluid total temperature at turbine inlet, °R

T_e = working fluid static temperature at turbine exhaust, °R

p_o = working fluid total pressure at turbine inlet, psia

p_e = working fluid static pressure at turbine exhaust, psia

γ = working fluid specific heat ratio

The ratio of turbine inlet and exhaust pressures, p_1/p_2 , can be expressed as the turbine pressure ratio R_t , which is a frequently used parameter in turbine design.

$$\Delta H_t = C_p T_0 \left[1 - \left(\frac{1}{R_t} \right)^{\frac{\gamma-1}{\gamma}} \right] \quad (6-18)$$

It is seen that the available energy in the turbine working fluid is a function of gas properties and inlet temperature, and of the turbine pressure ratio. Most of the turbine working fluids for rocket engine application are fuel-rich product gases generated by bipropellant combustion. Typical working fluid properties are listed in table 6-4.

Figure 6-25 shows the relationship between turbine-inlet temperature and available working fluid energy for a turbine pressure ratio of 20 for the two propellant combinations LO₂/RP-1 and LO₂/LH₂. Turbine inlet temperatures are limited by the high-temperature properties of the turbine construction materials. A practical design limit is around 1700° F. Above certain levels the gain from a higher turbine-inlet tem-

perature is offset by the turbine efficiency losses (blade losses; see below) resulting from higher gas jet speed (spouting velocity C₀) which is proportional to the turbine-inlet temperature.

Figure 6-26 shows the relationship between turbine pressure ratio and available energy of the working fluid for a turbine-inlet temperature of 1200° F, again for the propellant combinations LO₂/RP-1 and LO₂/LH₂. Although a large amount of energy may be available in a working fluid, it may be difficult to convert it efficiently into turbine shaft horsepower because of the severe weight limitations on rocket engine turbopumps. Thus the available pressure ratio of a turbine often cannot be fully used.

The overall efficiency of a turbine, η_t , is defined as the ratio of turbine shaft horsepower,

TABLE 6-4.—Properties of Typical Fuel-Rich Combustion Product Gases

Fluid	Inlet temperature °F	C _p , Btu/lb °F	γ	R, ft/°R	Mixture ratio, O/F
LOX/RP-1	1100	0.635	1.097	43.3	0.303
	1150	.639	1.100	45.1	.320
	1200	.643	1.106	47.1	.337
	1250	.646	1.111	58.6	.354
	1300	.648	1.115	50.4	.372
	1350	.651	1.119	51.8	.390
	1400	.653	1.124	53.6	.408
	1450	.655	1.128	55.4	.425
	1500	.657	1.132	58.0	.443
	1550	.659	1.137	59.0	.460
N ₂ O ₄ /CH ₃ (UDMH)	1400	.380	1.420	87.5	.110
	1500	.398	1.420	91.6	.165
	1600	.416	1.420	95.7	.220
	1700	.434	1.420	99.9	.274
	1800	.452	1.420	104.0	.328
	1900	.470	1.420	108.2	.382
LOX/LH ₂	1000	2.05	1.374	434	.785
	1200	1.94	1.364	403	.903
	1400	1.86	1.354	378	1.025
	1600	1.80	1.343	358	1.143
	1800	1.73	1.333	336	1.273
	2000	1.69	1.322	320	1.410

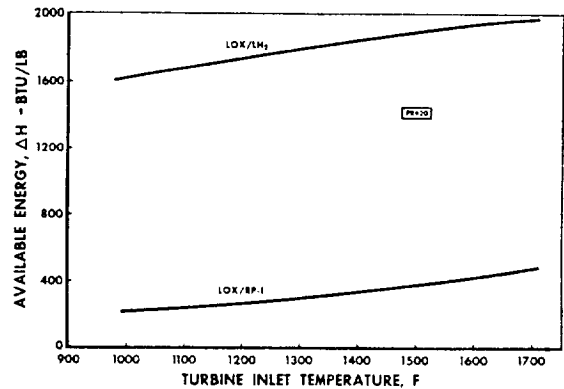


Figure 6-25.—Effect of turbine-inlet temperature on working fluid available energy.

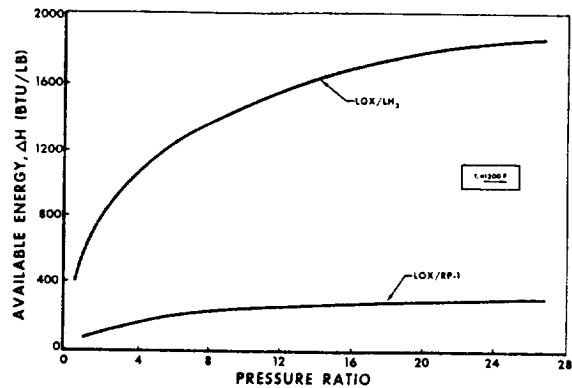


Figure 6-26.—Effect of turbine pressure ratio on working fluid available energy.

thp, to enthalpy drop rate or the available energy delivered rate of the working fluid.

$$\eta_t = \frac{550 \text{ thp}}{778 \dot{w}_t \Delta H_t} = 0.707 \frac{\text{thp}}{\dot{w}_t C_p T_0 \left[1 - \left(\frac{1}{R_t} \right)^{\frac{\gamma-1}{\gamma}} \right]} \quad (6-19)$$

Combining equations (6-15) and (6-19):

Turbine overall performance

$$= \frac{\eta_t \Delta H_t}{0.707} = \frac{\eta_t C_p T_0 \left[1 - \left(\frac{1}{R_t} \right)^{\frac{\gamma-1}{\gamma}} \right]}{0.707} \quad (6-20)$$

In turbine operation efficiency can be affected by—

1. *Nozzle losses.*—Similar to those in thrust chamber nozzles, these losses are due to the gas leaving the nozzle at a lower velocity as compared to that of an ideal nozzle. The losses are due to flow turbulence, fluid friction, and loss of heat to and through the turbine nozzle blocks.

2. *Blade losses.*—These are caused by residual velocity of the gas as it leaves the rotor blades, the obliquity of the nozzle (i.e., the nozzle angle θ in fig. 6-8 cannot be made zero), flow turbulence, and fluid friction. Losses due to residual gas velocity can be reduced by optimizing the turbine blade-to-gas velocity ratio U/C_0 , where U is the pitch speed of the rotor blades, and C_0 is the ideal spouting velocity of the gas based on available energy and isentropic expansion. These conditions can be analyzed quantitatively by means of turbine gas flow velocity diagrams which will be discussed in section 6.5. Flow turbulence can be reduced through improved blade shape and through full turbine nozzle admission.

3. *Leakage or clearance losses.*—The clearance required between rotor blade tips and casing permits some gas to leak past the blades without doing work, thus causing energy losses. The gas leakage from stage to stage in a multi-stage pressure-compounded turbine due to required clearance between shaft and sealing diaphragm results in similar losses.

4. *Disk friction losses.*—Fluid friction occurs at the interface of gas and rotor disk surface.

Also, centrifugal action of the rotor disk causes some of the gas to flow radially to the casing and to be dragged along the face of the casing by the rotor blades.

5. *Mechanical losses.*—These result from the mechanical friction in bearings and rotating seals.

The design of turbines for rocket turbopumps tends toward the simpler and lighter impulse types, with most of the expansion occurring in the stationary elements. Figure 6-27 shows the typical efficiency curves of various impulse-type turbines. The design problem becomes one of balancing efficiency (optimum velocity ratio U/C_0 , weight (number of stages or rows), and structural considerations. A higher performance can be achieved by employing a working fluid with high available energy, and by matching its high gas spouting velocity C_0 with a high rotor blade pitch speed U . However, the blade speed is often limited by the required pump rpm, by the practical size of the rotor wheel, and by the strength of materials. The optimum velocity ratio (or optimum value of blade speed for a given gas spouting velocity) is reduced by the use of velocity or pressure-compounded arrangements (shown schematically in fig. 6-9 and 6-10). However, these designs increase weight and complexity.

In general, for a direct-drive configuration (fig. 6-13) with an rpm lower than ideal, a low value of U/C_0 results, and a velocity compounded turbine will be used because of its low overall weight and simplicity. Where a reduction gear is

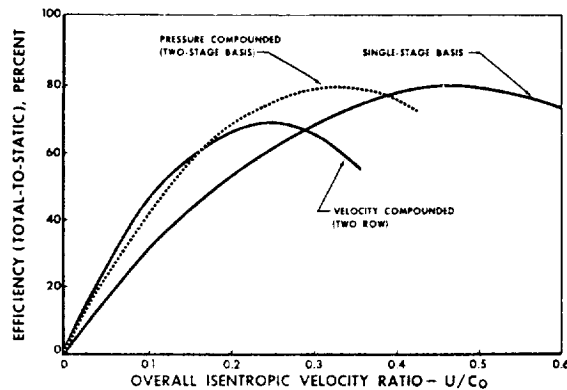


Figure 6-27.—Typical efficiency curves of impulse-type turbines.

provided between pumps and turbine, a higher value of U/C_0 is possible and a more efficient pressure-compounded turbine can be used.

Since the turbine pressure ratio has only a small effect upon available energy content of the working fluid (fig. 6-26), the power level of a turbine is usually regulated by controlling the inlet pressure p_0 and in turn the flow rate \dot{w}_t of the turbine.

Sample Calculation (6-5)

The following test data are given for the turbine of the A-1 stage engine turbopump:
 Turbine gas mixture ratio, $LO_2/RP-1 = 0.408$
 Gas total temperature at turbine-inlet,
 $T_0 = 1860^\circ R$ ($1400^\circ F$)
 Gas total pressure at turbine-inlet, $p_0 = 640$ psia
 Gas static pressure at turbine exhaust, $p_e = 27$ psia
 Turbine gas flow rate, $\dot{w}_t = 92$ lb/sec
 Turbine shaft speed, 7000 rpm
 Turbine shaft torque, 20 380 ft-lb
 Determine the overall turbine efficiency in percent and the performance in horsepower per lb/sec of turbine flow \dot{w}_t .

Solution

From table 6-4, for a $LO_2/RP-1$ mixture ratio of 0.408, we derive a specific heat $C_p = 0.653$ and a specific heat ratio $\gamma = 1.124$.

Substitute the above and other given data into equation (6-17) to obtain the available energy content of the turbine gas:

$$\begin{aligned}\Delta H_t &= 0.653 \times 1860 \left[1 - \left(\frac{27}{640} \right)^{\frac{1.124-1}{1.124}} \right] \\ &= 0.653 \times 1860 [1 - 0.705] \\ &= 359 \text{ Btu/lb}\end{aligned}$$

Turbine shaft horsepower

$$\begin{aligned}\text{thp} &= \frac{\text{Turbine shaft torque} \times 2\pi N}{33\,000} \\ &= \frac{20\,380 \times 2\pi \times 7000}{33\,000} \\ &= 27\,150 \text{ hp}\end{aligned}$$

Total shaft horsepower required by the pumps (sample calculation (6-4)):

$$14\,850 + 11\,790 = 26\,640 \text{ hp}$$

Thus a margin of 510 hp is available for auxiliary drives and contingencies.

Substitute the values for thp, ΔH_t , and \dot{w}_t into equation (6-19):

$$\begin{aligned}\text{Overall turbine efficiency } \eta_t &= \frac{0.707 \times 27\,150}{92 \times 359} \\ &= 58.2\%\end{aligned}$$

From equation (6-15):

$$\text{Overall turbine performance} = \frac{27\,150}{92} = 295 \frac{\text{hp}}{\text{lb/sec}}$$

Turbopump System Cycle Efficiency

Turbopump system cycle efficiency is an indicator of the energy losses and their effect on overall engine systems performance because of turbopump operation. It can be defined as the ratio of the specific impulse of the complete turbopump-fed engine system, $(I_s)_{\text{eng}}$, to the thrust chamber specific impulse, $(I_s)_{\text{tc}}$.

$$\text{Turbopump cycle efficiency } \eta_c = \frac{(I_s)_{\text{eng}}}{(I_s)_{\text{tc}}} \quad (6-21)$$

Generally, two types of energy cycles are employed in rocket turbopump applications: the separate-flow cycle and the topping-flow cycle. Because of certain systems-design limitations the second type is used less frequently than the former.

In the separate-flow cycle the turbine exhaust gas flow is discharged separately or is ducted into the low-pressure region of the main thrust chamber exit nozzle. This is shown schematically for cases (A), (B), and (C) in figure 6-12, and for the A-1 and A-2 stage engines in figures 2-10 and 3-3. The separate-flow cycle system design affords a lower discharge pressure by the propellant pumps and yields a higher pressure ratio for the turbine. Generally, this results in a simpler and lighter system. However, the turbine exhaust gas of a separate-flow cycle is usually not utilized efficiently to generate thrust.

Thus, it has a relatively low cycle efficiency. The separate-flow cycle efficiency can be expressed as

$$\eta_{sc} = \frac{(I_s)_{eng}}{(I_s)_{tc}} = \frac{\dot{w}_{tc}(I_s)_{tc} + \dot{w}_t(I_s)_{te}}{\dot{w}_{eng}(I_s)_{tc}} \quad (6-22)$$

$$= \frac{F_{tc} + F_{te}}{\dot{w}_{eng}(I_s)_{tc}}$$

where

- η_{sc} = separate-flow cycle efficiency
- $(I_s)_{eng}$ = engine system specific impulse, sec
- $(I_s)_{tc}$ = main thrust chamber specific impulse, sec
- $(I_s)_{te}$ = turbine exhaust specific impulse, sec
- \dot{w}_{eng} = engine system total propellant flow rate, lb/sec
- \dot{w}_{tc} = thrust chamber propellant flow rate, lb/sec
- \dot{w}_t = turbine gas flow rate, lb/sec

The efficiency of the separate-flow cycle can be increased somewhat by better utilization of the turbine exhaust gases to generate thrust. A higher expansion area nozzle may be attached to the turbine exhaust duct for upper stage engine applications, for a higher $(I_s)_{te}$, or the turbine exhaust gases may be burned with additional propellant in an afterburner similar to that in a jet engine. Separate-flow-cycle efficiencies range from 0.96 to 0.99.

In the topping flow cycle the turbine exhaust gases, before being expanded and ejected through the thrust chamber nozzle, are ducted into the thrust chamber combustion zone for further reaction with one of the main propellants. This is illustrated schematically in cases (D) and (E) of figure 6-12. Because this system requires a turbine exhaust pressure higher than the thrust chamber pressure, it results in higher propellant pump discharge pressures and a much lower turbine pressure ratio. Also, for bipropellant combinations, two-stage combustion is required. Usually combustion products of 100 percent of one propellant and a portion of the other are used as the turbine drive fluid. This method results in higher cycle efficiency, but tends to be heavier and less flexible.

Since the residual kinetic and chemical energies of the turbine exhaust gas are generating thrust as efficiently as the main propellants, the

topping flow cycle is sometimes considered a "no loss" cycle. However, that net energy which is required to lift the propellants from their respective pump inlet pressures to the thrust chamber nozzle stagnation pressure must be considered. The topping flow cycle efficiency may be approximated as

$$\eta_{tc} = \frac{(I_s)_{eng}}{(I_s)_{tc}} = \sqrt{1 - \frac{E_p}{C_p(T_c)_{ns}}} \quad (6-23)$$

$$= \sqrt{1 - \frac{MR\Delta H_0 + \Delta H_f}{778(1 + MR)C_p(T_c)_{ns}}}$$

where

- η_{tc} = topping flow cycle efficiency
- E_p = ideal energy required to pump 1 pound total propellant flow of an engine system from pump inlet to main chamber nozzle stagnation pressures
- C_p = specific heat of the thrust chamber gases, Btu/lb-F
- $(T_c)_{ns}$ = thrust chamber nozzle stagnation temperature, °R
- MR = propellant mixture ratio of the engine system, O/F
- ΔH_0 = pressure head, based on the difference between thrust chamber nozzle stagnation and oxidizer pump inlet pressures, ft
- ΔH_f = pressure head, based on the difference between thrust chamber nozzle stagnation and fuel pump inlet pressures, ft

Topping flow cycle efficiencies may range from 0.996 to 0.9996. Typical cycle efficiency versus chamber pressure curves of various propellants are illustrated in figure 6-28.

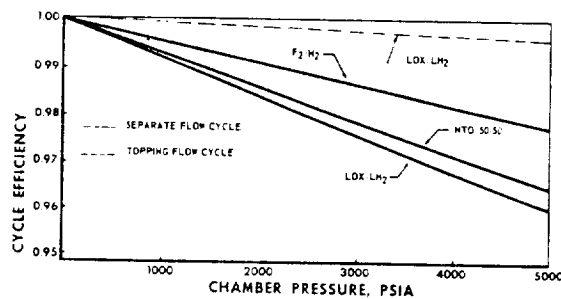


Figure 6-28.—Typical cycle efficiency versus chamber pressure curves of various propellants.

Sample Calculation (6-6)

(a) The following component test results are given for the A-1 stage engine, as schematically shown in figure 2-10, for sea level and rated design conditions:

- Thrust chamber oxidizer flow rate, 1941 lb/sec
- Thrust chamber fuel flow rate, 827 lb/sec
- Thrust chamber nozzle stagnation pressure, 1000 psia
- Thrust chamber thrust, 747 300 lb
- Gas generator oxidizer flow rate, 26.7 lb/sec
- Gas generator fuel flow rate, 65.3 lb/sec
- Thrust generated by turbine exhaust, 2700 lb

Determine the cycle efficiency of the turbopump system, engine system sea-level specific impulse and thrust, and overall engine system propellant mixture ratio at rated conditions.

(b) Assume that, as an alternate, a topping flow cycle is used for the turbopump of the A-1 stage engine and that this engine system is to be operated at the same engine system thrust and mixture ratio as in case (a). Estimate the ideal turbopump cycle efficiency and engine system sea-level specific impulse with the following assumptions: (1) no change in $(p_c)_{ns}$, combustion-produced gas properties, and performance of the thrust chamber due to the minor changes in mixture ratio and two-stage combustion; (2) oxidizer pump inlet pressure = 55 psia; and (3) fuel pump inlet pressure = 45 psia.

Solution

(a) Thrust chamber mixture ratio = $\frac{1941}{827} = 2.35$

Thrust chamber propellant flow rate

$$\dot{w}_{tc} = 1941 + 827 = 2768 \text{ lb/sec}$$

Sea-level thrust chamber specific impulse

$$(I_s)_{tc} = \frac{747\,300}{2768} = 270 \text{ sec}$$

Turbine gas flow rate $\dot{w}_t = 26.7 + 65.3 = 92 \text{ lb/sec}$

Sea-level turbine exhaust specific impulse

$$(I_s)_{te} = \frac{2700}{92} = 29.34 \text{ sec}$$

Total engine system propellant flow rate

$$= 2768 + 92 = 2860 \text{ lb/sec}$$

Substitute the above data into equation (6-22) to obtain the flow cycle efficiency of the turbopump

$$\eta_{sc} = \frac{2768 \times 270 + 92 \times 29.34}{2860 \times 270} = \frac{747\,300 + 2700}{772\,200} = 0.971$$

From equation (6-21), the engine system specific impulse at sea level

$$(I_s)_{eng} = 0.971 \times 270 = 262.2 \text{ sec}$$

Total engine system thrust

$$F_{eng} = 262.2 \times 2860 = 750\,000 \text{ lb}$$

$$\text{Engine system mixture ratio} = \frac{1941 + 26.7}{827 + 65.3} = 2.20$$

The calculations can also be made by first combining F_{tc} and F_{te} to derive F_{eng} . Then F_{eng} and \dot{w}_{eng} are used to calculate $(I_s)_{eng}$. η_{sc} can be calculated by forming the ratio $(I_s)_{eng}$ to $(I_s)_{tc}$.

(b) Use the combustion product gas properties from sample calculation (4-1) (a):

$$(T_c)_{ns} = 6460^\circ \text{ R}, \quad \gamma = 1.222$$

$$\begin{aligned} \mathcal{M} = 22.5 \text{ lb/mol: } C_p &= \frac{1544 \gamma}{778 \mathcal{M} (\gamma - 1)} \\ &= 0.486 \text{ Btu/lb-deg F} \end{aligned}$$

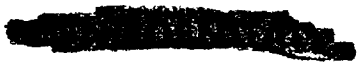
Pressure head difference between chamber pressure and oxidizer pump inlet:

$$\Delta H_o = (1000 - 55) \times 144 / 71.38 = 1910 \text{ ft}$$

Pressure head difference between chamber pressure and fuel pump inlet:

$$\Delta H_f = (1000 - 45) \times 144 / 50.45 = 2728 \text{ ft}$$

Substitute these data into equation (6-23) for the topping flow cycle efficiency of the turbopump



$$\eta_{tc} = \sqrt{1 - \frac{2.2 \times 1910 + 2728}{778 \times (1 + 2.2) \times 0.486 \times 6460}}$$

$$= \sqrt{0.9991} = 0.9996$$

Since $(I_s)_{tc} = 270$ sec, substitute η_{tc} and $(I_s)_{tc}$ into equation (6-21); the ideal engine system specific impulse

$$(I_s)_{eng} = 0.9996 \times 270 = 269.9 \text{ sec}$$

Turbopump System Calibration and Off-Design Characteristics

Ideally, an engine system is designed to operate at a single set of conditions, specifically at rated thrust and mixture ratio. Each of its components in turn is designed for optimum function at that rated thrust level. In addition, however, most of these engine components, notably pumps and turbines, are also required to operate satisfactorily within a certain range away from the design point. This may be caused by—

- (1) System and component calibration characteristics
- (2) System operational deviations
- (3) System start and shutdown transients
- (4) Special system requirements, such as throttling

Figure 6-29 illustrates typical operating ranges for the turbopump of a rocket engine system. The elliptically shaped areas represent ranges of operational probability. For instance, the 95-percent ellipse envelopes those values at which the pumps or turbine will operate with a 95-percent probability.

Because of engine and component performance tolerance requirements and to correct for hydrodynamic variations within the components, it is

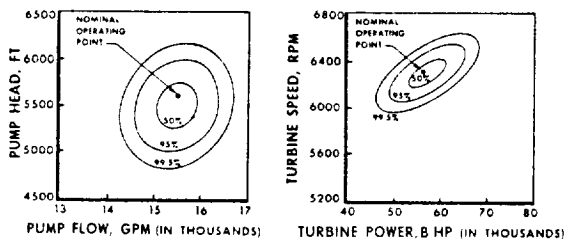


Figure 6-29.—Typical pump and turbine operating ranges of a rocket engine system.

necessary to calibrate a turbopump prior to its integration into an engine system. Here, the performance of each pump is determined experimentally. By modifying the pump geometry (impeller trimming) and varying the discharge hydraulic resistances, the desired operating characteristics required by the engine system are achieved. For turbopumps with a single direct or geared turbine drive (as shown in fig. 6-13), the calibration procedure begins with the experimental determination of that shaft speed at which one of the pumps (usually the oxidizer pump) develops the required head and flow. Simultaneously, the suction characteristics of this pump are determined at this speed. The other pump is then operated at the same speed and the discharge adjusted for the required flow. Based on the pressure readings, the diameter of the pump impeller is trimmed on a lathe until the desired head is produced at rated speed and flow. The pump suction characteristics at these conditions are also determined. Figure 6-30 shows the trimming effects of a typical pump. The trimming procedure requires that the pump impellers be made sufficiently large initially, since addition of material is not feasible. The calibrated pumps are then combined with a turbine. The amount of turbine working fluid which must be bled from the pump discharges to operate

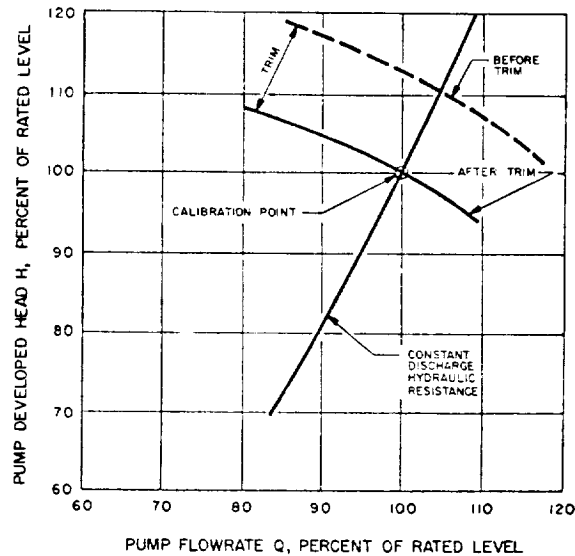


Figure 6-30.—Trimming effects of a typical pump.

the gas generator is now established experimentally at the required operating point. This procedure considers the influence of turbine variations. The turbopump is then matched with the remaining engine system in complete engine systems calibrations. Adjustments in engine mixture ratio can be made by orificing the discharge of one of the pumps. Orifice installation considerations and type of propellant often make it desirable to assure that orificing is always done for the same propellant; in LOX/RP systems, usually the fuel. For this reason, the pump for that system is trimmed for a slight excess head. Adjustments in engine thrust level are made by varying the turbopump speed.

An engine system is frequently required to operate at certain off-design levels. For instance, upper stage vehicles often require an effective propellant utilization system based on variation of the engine mixture ratio. (See ch. II.) This involves control of the discharge of one pump and possibly the control of turbine supply gas if correction of thrust due to the shifting of mixture ratio is desired. Design and development of the turbopump must consider these operational requirements.

During the start and shutdown transients of an engine system, propellant flow and pressure characteristics are determined by engine system design characteristics. Figure 6-31 shows the propellant flows and chamber pressure buildup history for a typical engine start transient. Note temporary oxidizer flow drop as a result of LOX

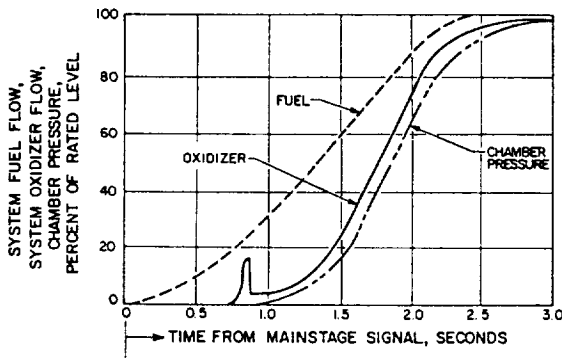


Figure 6-31.—Propellant flow and chamber pressure transient characteristics during engine system start.

dome priming. The time in which a rocket turbopump must attain full-power level is substantially shorter than that of conventional turbomachinery. Frequently, full-power operation must be achieved in less than 1 second. This is dictated by the need for propellant consumption economy in flight and for avoiding the possibility of flow instability in thrust chamber and other components. This, together with other transient requirements such as throttling, must be satisfied by the off-design characteristics of a turbopump. The latter substantially influence selection of type. Basically, the problem is that of coupling the pump characteristics with those of the rest of the engine system under off-design operating conditions. Figure 6-32 shows typical off-design characteristics of various types of pumps.

One of the most significant pump off-design characteristics is the pump stalling point which usually occurs in the low-flow region. The pump operation tends to be erratic at this point, resulting in the abrupt loss of developed head and the danger of overspeeding.

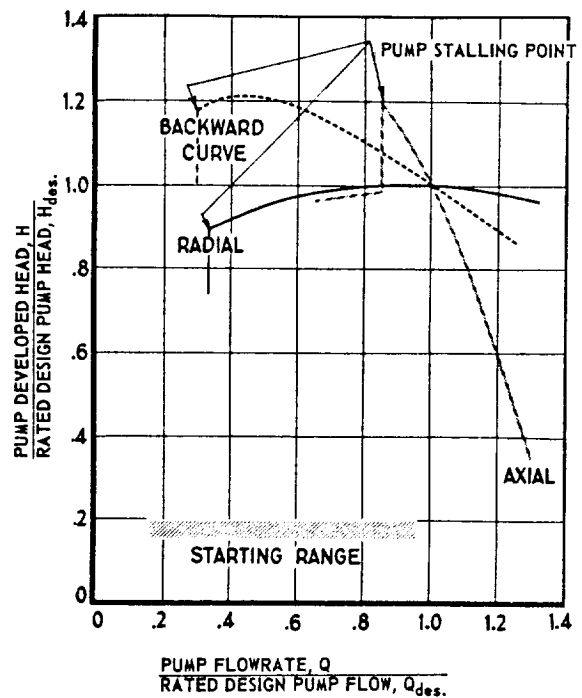


Figure 6-32.—Typical off-design characteristics of various types of pumps.

6.3 DESIGN OF CENTRIFUGAL PUMPS

Because of its specific needs, the rocket industry has developed its own pump design approaches which may differ from those for conventional applications. In addition, designers may employ their individual methods of analysis and calculation. However, the broad underlying principles are quite similar. The range of speeds, proportions, design coefficients, and other mechanical detail for rocket engine pumps has been well established by earlier designs as well as through experiments.

General Design Procedures

As a rule, rated pump head-capacity (H - Q) requirements and expected available NPSH at the pump inlets will be established by engine system design criteria. The first step then is to choose a suitable suction specific speed (N_{SS}) and the type of inducer which will yield the highest pump speed (N) at design conditions (eq. (6-10)). The pump specific speed (N_s) or type of impeller can now be established from the chosen pump speed and required head-capacity characteristics. Owing to its relatively light weight and simplicity of construction, a single-stage centrifugal pump may be given first consideration.

With suction specific speed and specific speed of the proposed pump design established, the designer can now look for a suitable "design model" among comparable existing pumps which approximate the desired performance. The latter includes satisfactory suction requirements, suitable head-capacity characteristics, and acceptable efficiency. If a suitable model is available, the design calculations of the new pump will include application of a scaling factor to the parameters of the existing model. The following correlations are valid for pumps with like specific speed, based on the pump affinity laws (eqs. (6-6a) and (6-6b)):

$$\frac{N_1 Q_1^{0.5}}{\Delta H_1^{0.75}} = \frac{N_2 Q_2^{0.5}}{\Delta H_2^{0.75}} \quad (6-24a)$$

$$Q_2 = Q_1 f^3 \left(\frac{N_2}{N_1} \right) \quad (6-24b)$$

$$\Delta H_2 = \Delta H_1 f^2 \left(\frac{N_2}{N_1} \right) \quad (6-24c)$$

where

N_1 , Q_1 , and ΔH_1 = rotating speed (rpm), flow rate (gpm), and developed head (ft) of the existing model at rated conditions

N_2 , Q_2 , and ΔH_2 = rotating speed (rpm), flow rate (gpm), and developed head (ft) of the new pump at rated conditions

$f = D_2/D_1$ = scaling factor

D_1 = impeller diameter of the existing model, ft

D_2 = impeller diameter of the new pump, ft

This approach assumes that other dimensions of the pump are in approximately linear proportion to the impeller diameter.

If a suitable model is not available for the design of a new pump, the designer can use "design factors" established experimentally by other successful designs. These may permit establishing relations between rated pump developed head and flow rate, and such parameters as velocity ratios. However, best results are obtained through experimental testing of proposed design itself. The test results then are used for design revisions and refinements.

In the discussions below, the following basic symbols are used:

c = flow velocities, absolute (relative to ducts and casing)

v = flow velocities, relative to inducer or impeller

u = velocities of points on inducer or impeller

Subscript:

0 = inducer inlet

1 = inducer outlet = impeller inlet

2 = impeller outlet

3 = pump casing

prime 1 = actual or design

Operating Principles of the Centrifugal Pump Impeller

In its simplest form, the impeller of a centrifugal pump can be regarded as a paddle wheel with radial vanes, rotating in an enclosure, with the fluid being admitted axially and ejected at

CONFIDENTIAL

the periphery. This is shown schematically in figure 6-33. The tangential velocity component of each fluid element increases as it moves out radially between the vanes. Therefore, the centrifugal force acting on these fluid elements increases as the fluid moves out radially. Assuming constant flow velocity in the radial direction and no energy losses, the ideal head rise due to centrifugal force between the central entrance (1) and the peripheral exit (2) is

$$\Delta H_{ic} = \frac{\omega^2}{2g} (r_2^2 - r_1^2) \quad (6-25)$$

where

- ΔH_{ic} = ideal head rise due to centrifugal forces, ft
- ω = angular velocity of the wheel, rad/sec
- r_1 = vane radius at the entrance, ft
- r_2 = vane radius at the periphery, ft
- g = gravitational constant, 32.2 ft/sec²

For optimum performance, most impellers in high-speed centrifugal rocket engine pumps have shrouded, backward curved vanes. The impeller width is tapered toward the periphery to keep the cross-sectional area of the radial flow path near constant. A typical impeller design of this type is shown in figure 6-34.

Velocity diagrams may be constructed to analyze the fluid flow vector correlations at various points of an impeller. Let us assume the following ideal conditions:

- (1) There are no losses, such as fluid-friction losses
- (2) The impeller passages are completely filled with actively flowing fluid at all times

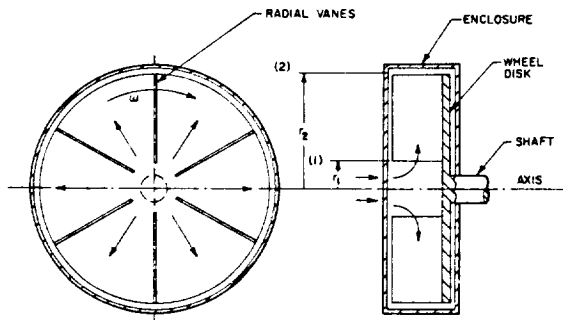


Figure 6-33.—Paddle wheel (schematic).

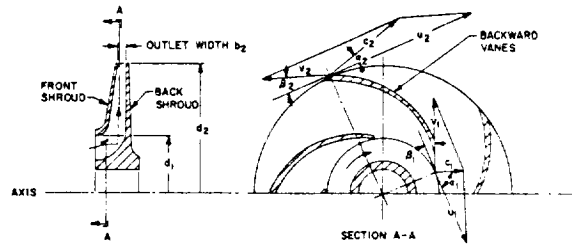
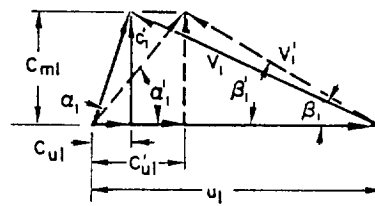


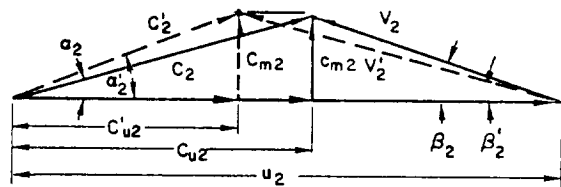
Figure 6-34.—Typical shrouded centrifugal impeller with backward curved vanes.

- (3) The flow is two dimensional (velocities at similar points on the flow lines are uniform)
- (4) The fluid leaves the impeller passages tangentially to the vane surfaces (complete guidance of the fluid at the outlet)

The ideal inlet (point (1)) and outlet (point (2)) flow velocity diagrams of the impeller described in figure 6-34 are shown in figure 6-35. At this point with corresponding fluid velocities u , v , and c (as identified above), α is the angle between c and u , and β is the angle enclosed by a



INLET VELOCITY DIAGRAM



OUTLET VELOCITY DIAGRAMS

Figure 6-35.—Flow velocity diagrams for the impeller shown in figure 6-34 (draw in a plane normal to the impeller axis).

tangent to the impeller vane and a line in the direction of vane motion. The latter is equal to the angle between v and u (extended).

Based on these velocity diagrams, the following correlations have been established:¹

$$\Delta H_{ip} = \frac{u_2^2 - u_1^2 + v_1^2 - v_2^2}{2g} \quad (6-26a)$$

$$\Delta H_i = \frac{u_2^2 - u_1^2 + v_1^2 - v_2^2 + c_2^2 - c_1^2}{2g} = \frac{1}{g}(u_2 c_{u2} - u_1 c_{u1}) \quad (6-26b)$$

$$Q_{imp} = 448.8 c_{m1} A_1 = 448.8 c_{m2} A_2 \quad (6-27)$$

$$c_{u2} = u_2 - \frac{c_{m2}}{\tan \beta_2} \quad (6-28)$$

where

ΔH_{ip} = ideal static pressure head rise of the fluid flowing through the impeller due to centrifugal forces and to a decrease of flow velocity relative to the impeller, ft

ΔH_i = ideal total pressure head rise of the fluid flowing through the impeller = the ideal developed head of the pump impeller, ft

Q_{imp} = impeller flow rate at the design point (rated conditions), gpm

A_1 = area normal to the radial flow at the impeller inlet, ft²

A_2 = area normal to the radial flow at the impeller outlet, ft²

d_1 = vane diameter at the impeller inlet, in

d_2 = vane diameter at the impeller outlet = outside diameter of the impeller, in

u_1 = $\pi \times \text{rpm} \times d_1 / 720$ = impeller peripheral velocity at inlet, ft/sec

u_2 = $\pi \times \text{rpm} \times d_2 / 720$ = impeller peripheral velocity at outlet = impeller tip speed, ft/sec

v_1 = inlet flow velocity relative to the impeller, ft/sec

v_2 = outlet flow velocity relative to the impeller, ft/sec

c_1 = absolute inlet velocity of the flow, ft/sec

c_{u1} = tangential component of the absolute inlet flow velocity, ft/sec

c_{m1} = "meridional" or (by definition for radial flow impellers) radial component of the absolute inlet flow velocity, ft/sec

c_2 = absolute outlet velocity of the flow, ft/sec

c_{u2} = tangential component of the absolute outlet flow velocity, ft/sec

c_{m2} = meridional or radial component of the absolute outlet flow velocity, ft/sec

β_1 = impeller inlet vane angle

β_2 = impeller discharge vane angle

For pumping low-density propellants (such as liquid hydrogen), which is associated with very high developed heads, straight radial vanes are frequently used in centrifugal impellers, since they permit a higher obtainable head coefficient ψ . Figure 6-36 presents a typical radial vane impeller and its outlet velocity diagram. The vane discharge $\beta_2 = 90^\circ$ and $c_{u2} = u_2$. The ideal developed head of a radial vane impeller becomes

$$\Delta H_i = \frac{u_2^2 - u_1 c_{u1}}{g} \quad (6-29)$$

For centrifugal pumps of the noninducer type (which are now rarely used in rocketry), proper selection of the impeller inlet vane angle β_1 or the provision of guide vanes at the inlet minimizes the absolute tangential component of fluid flow at the inlet, c_{u1} , which for best efficiency should be zero. This is defined as no prerotation, where $\alpha_1 = 90^\circ$. Thus, equation (6-26) becomes

$$\Delta H_i = \frac{u_2 c_{u2}}{g} \quad (6-30)$$

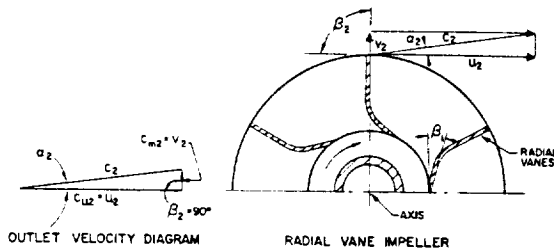


Figure 6-36.—Typical radial vane impeller and its outlet velocity diagram.

The above discussions assumed ideal conditions. For most rocket applications, centrifugal pumps are designed with an inducer upstream of and in series with the impeller. The flow conditions at the impeller inlet thus are affected by the inducer discharge flow pattern. In addition, two types of flow usually take place simultaneously in the flow channels; namely, the main flow through the passages, and local circulatory flows (eddy currents). The latter are relatively small but modify the former. The resultant effect at the impeller inlet is to make the flow enter at an angle β_1' , larger than the impeller inlet vane angle β_1 . The fluid is also caused to leave the impeller at an angle β_2' , less than the impeller discharge vane angle β_2 , and to increase the absolute angle α_2 to α_2' . This and the hydraulic losses in the impeller correspondingly change the relative flow velocities v_1 and v_2 to v_1' and v_2' , the absolute flow velocities c_1 and c_2 to c_1' and c_2' , and the absolute tangential components c_{u1} and c_{u2} to c_{u1}' and c_{u2}' . Since the radial flow areas A_1 and A_2 , and the impeller flow rate Q_{imp} remain constant, the absolute radial or meridional components c_{m1} and c_{m2} also remain unchanged. The inlet and outlet flow velocity diagrams in figure 6-35 may now be redrawn as represented by the dotted lines.

The correlation established in equation (6-26b) may be rewritten as

$$\Delta H_{imp} = \frac{u_2 c_{u2}' - u_1 c_{u1}'}{g} \quad (6-31)$$

where

- ΔH_{imp} = impeller actual developed head, ft
- c_{u1}' = tangential component of the design absolute inlet flow velocity, ft/sec
- c_{u2}' = tangential component of the design absolute outlet flow velocity, ft/sec

The ratio of the design flow velocity c_{u2}' to the ideal flow velocity c_{u2} can be expressed as

$$e_v = \frac{c_{u2}'}{c_{u2}} \quad (6-32)$$

where e_v = impeller vane coefficient. Typical design values range from 0.65 to 0.75.

Referring to figure 6-35, equation (6-28) may be rewritten as

$$c_{u2}' = u_2 - \frac{c_{m2}}{\tan \beta_2'} \quad (6-33)$$

By definition, the required impeller developed head can be determined as

$$\Delta H_{imp} = \Delta H + H_e - \Delta H_{ind} \quad (6-34)$$

where

- ΔH = rated design pump developed head, ft
- ΔH_{ind} = required inducer head-rise at the rated design point, ft
- H_e = hydraulic head losses in the volute, ft. Typical design values of H_e vary from 0.10 to 0.30 ΔH .

The required impeller flow rate can be estimated as

$$Q_{imp} = Q + Q_e \quad (6-35)$$

where

- Q_{imp} = required impeller flow rate at the rated design point, gpm
- Q = rated delivered pump flow rate, gpm
- Q_e = impeller leakage losses, gpm. Most of these occur at the clearance between impeller wearing rings and casing. Typical design values of Q_e vary from 1 to 5 percent of Q_{imp} .

Centrifugal Impeller Design Elements

After general pump design parameters, such as developed head ΔH , capacity Q , suction specific speed N_{ss} , rotating speed N , and specific speed N_s have been set forth or chosen, the design of a centrifugal (radial) pump impeller may be accomplished in two basic steps. The first is the selection of those velocities and vane angles which are needed to obtain the desired characteristics with optimum efficiency. Usually this can be achieved with the help of available design or experimental data such as pump head coefficient ψ , impeller vane coefficient e_v , and leakage loss rate Q_e . The second step is the design layout of the impeller for the selected angles and areas. Considerable experience and skill are required from the designer to work out graphically the best-performing configuration based on the given design inputs.

The following are considered minimum basic design elements required for proper layout of a radial-flow impeller:

1. *Radial velocity at the impeller entrance or eye, c_{m1} .*—This is a function of inlet conditions such as inducer discharge velocity and inlet duct size. For best performance, the value of c_{m1} should be kept reasonably low. Typical design values of c_{m1} range from 10 to 60 ft/sec.

2. *Radial velocity at the impeller discharge, c_{m2} .*—Its value is a function of the impeller peripheral velocity u_2 and the flow coefficient ϕ . Typical design values for c_{m2} range from 0.01 to 0.15 u_2 .

3. *Diameter of the impeller at the vane entrance, d_1 .*—Its value is determined by the inducer design as well as by impeller shaft and hub size.

4. *The impeller peripheral velocity at the discharge, u_2 .*—The value of u_2 can be calculated by equation (6-4) for a given pump developed head H and a selected overall pump head coefficient, ψ . The maximum design value of u_2 is often limited by the material strength which thus determines the maximum developed head that can be obtained from a single-stage impeller. Typical design values of u_2 range from 200 to 1500 ft/sec. With u_2 and N known, the impeller discharge diameter d_2 (in) can be calculated readily.

5. *The inlet vane angle β_1 .*—The value of β_1 is affected by the inlet flow conditions. Generally, β_1 should be made equal or close to the inlet flow angle β_1' which can be approximated by

$$\tan \beta_1' = c_{m1} / (u_1 - c_{u1}') \quad (6-36)$$

Typical design values for β_1 range from 8° to 30°.

6. *The discharge vane angle β_2 .*—In the special case of radial vane impeller designs $\beta_2 = 90^\circ$. For backward curved vane impellers, β_2 is the most important single design element. Usually the selection of β_2 is the first step in determining the other impeller design constants, since most of them depend on β_2 . Pump efficiency and head-capacity characteristics are important considerations for the selection. For a given u_2 , head and capacity increase with β_2 . Typical design values for β_2 range from 17 to

28°, with an average value of 22.5° for most specific speeds.

Figure 6-37 presents the basic layout of a typical radial-flow impeller with backward curved vanes. The shaft diameter d_s may be determined by the following correlations

$$S_s = \frac{16 T}{\pi d_s^3} \quad (6-37)$$

$$S_t = \frac{32 M}{\pi d_s^3} \quad (6-38)$$

$$S_{sw} = \frac{1}{2} \sqrt{4 S_s^2 + S_t^2} \quad (6-39)$$

$$S_{tw} = \frac{1}{2} S_t + \frac{1}{2} \sqrt{4 S_s^2 + S_t^2} \quad (6-40)$$

where

d_s = impeller shaft diameter, in

T = shaft torque corresponding to yield or ultimate loads as defined by equations (2-9) and (2-10), lb-in

M = shaft bending moment corresponding to yield or ultimate loads as defined by equations (2-9) and (2-10), lb-in

S_s = shear stress due to torque, lb/in²

S_t = tensile stress due to bending moment, lb/in²

S_{sw} = allowable working shear stress (yield or ultimate) of the shaft material, lb/in²

S_{tw} = allowable working tensile stress (yield or ultimate) of the shaft material, lb/in²

Impeller hub diameter d_h and eye diameter d_e may be equal to hub diameter and tip diameter of the inducer. The maximum tensile stress induced in an impeller by the centrifugal forces

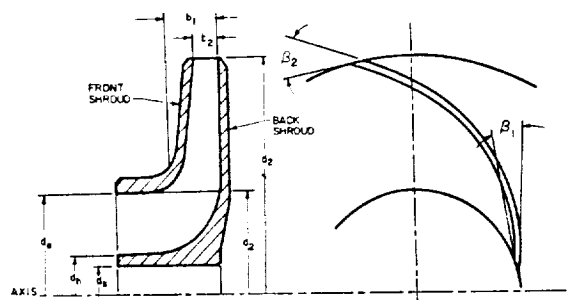


Figure 6-37.—Basic layout of a typical radial-flow impeller with backward curved vanes.

occurs as the tangential stress at the edge of the shaft hole. It may be checked by

$$S_{t\max} = \frac{\rho u_{2\max}^2 (3 + \mu)}{576 g} \left[1 + \frac{1 - \mu}{3 + \mu} \left(\frac{d_s}{d_2} \right)^2 \right] K_s \quad (6-41)^1$$

where

- $S_{t\max}$ = maximum tensile stress, lb/in² (should be less than the allowable working tensile stress of the impeller material)
- ρ = density of the impeller material, lb/ft³
- μ = Poisson's ratio of the impeller material
- d_s = impeller shaft hole diameter, in
- d_2 = impeller outside diameter, in
- $u_{2\max}$ = maximum allowable peripheral impeller speed, ft/sec = 1.25 × design value of u_2 , for most rocket engine applications
- g = gravitational constant, 32.2 ft/sec²
- K_s = design factor, determined experimentally. Typical values vary from 0.4 to 1.0, depending on impeller shape.

The surface finish and contour of the impeller shaft hole should be free of stress concentrations. First-class splines are preferred rather than ordinary keyways.

The width of the impeller can be calculated by the following correlations:

$$b_1 = \frac{Q_{\text{imp}}}{3.12 \pi d_1 c_{m1} \epsilon_1} \quad (6-42)$$

$$b_2 = \frac{Q_{\text{imp}}}{3.12 \pi d_2 c_{m2} \epsilon_2} \quad (6-43)$$

where

- b_1 = impeller width at the vane inlet, in
- b_2 = impeller width at the discharge, in
- ϵ_1 = contraction factor at the entrance. It considers effective flow area reduction from vane thickness and other effects such as local circulatory flows. Typical design values range from 0.75 to 0.9.
- ϵ_2 = contraction factor at the discharge. Typical design values range from 0.85 to 0.95.

Q_{imp} = impeller flow rate at the rated design point, gpm

After the vane angles and other dimensions at inlet and discharge have been established, no set rule is available for designing the backward curved vanes. However, the number of vanes is usually between 5 and 12, and may be determined empirically by

$$z = \frac{\beta_2}{3} \quad (6-44)$$

where

- β_2 = discharge vane angle
- z = number of vanes

If there is a space limitation at the impeller entrance, every other vane may be made a partial vane, starting at a larger radius. The contour of the vanes is designed to afford a gradual change of flow cross-sectional area (total divergence of 10° to 14°), at reasonably short flow passage length. The flow passage shape should be as close to a square as possible. The vanes should be as thin as material strength and manufacturing processes will permit. They may be of constant thickness; i.e., a contour similar for both sides may be used. This allows a thinner edge (typical value: 0.12 inch) at the inlet and results in better efficiency if the angle β_1 has the correct value. The impeller is usually a high-quality aluminum-alloy casting, the vanes being integral with the shrouds. In some high-speed applications, forged aluminum alloys or titanium alloys are used. A typical aluminum forging, the 7075 alloy with a T73 heat treat, has a yield strength of 63 000 psi and an ultimate strength of 74 000 psi. In this case a two-piece construction might be preferred to facilitate machining operations.

Mixed-flow-type vanes which extend into the impeller entrance or eye (shown in fig. 6-38a) are frequently used in radial-flow impellers or centrifugal pumps. This is done to match the impeller inlet flow path with the inducer discharge flow pattern and to provide more efficient turning of the flow.

The mixed-flow-type impeller as shown in figure 6-38b is also frequently used in a "centrifugal flow pump." The velocity correlations and design constants of a mixed-flow impeller are essentially the same as those of a radial-flow impeller. Mean effective impeller diameters

¹ According to S. Timoshenko.

are used in the calculations for head rise, flow velocities, etc. They are presented in figure 6-38 a and b as:

$$d_1^2 = \frac{(d_{1o}^2 + d_{1i}^2)}{2} \quad (6-45)$$

$$d_2^2 = \frac{(d_{2o}^2 + d_{2i}^2)}{2} \quad (6-46)$$

where

d_1 = mean effective impeller diameter at the inlet, in

d_{1o} = outer vane diameter at the inlet, in

d_{1i} = inner vane diameter at the inlet, in

d_2 = mean effective impeller diameter at the discharge, in

d_{2o} = outer vane diameter at the discharge, in

d_{2i} = inner vane diameter at the discharge, in

Effective impeller widths at inlet and discharge, b_1 and b_2 , are also presented in figure 6-38 a and b. They are equal to the diameter of a circle which is tangent to the contours of both front and back shrouds. γ is the angle between the meridional flow vectors (c_{m1} and c_{m2}) and the plane normal to the axis of rotation. It is also the angle between the plane of the velocity

diagrams and the plane normal to the axis. The value of γ varies along the flow passage. The layout of a mixed-flow impeller on the drawing board is a rather complicated drafting problem. This is due to the three-dimensional vane curvature and other complexities. The method of "error triangles" suggested by Kaplan may be used. Details of this method can be found in standard pump reference books.

Design of Cavitating Inducers

The cavitating inducer of a centrifugal propellant pump is a lightly loaded axial-flow impeller operating in series with the main pump impeller as shown in figure 6-5. The term "cavitating" refers to the fact that the inducer is capable of operating over a relatively broad range of incipient cavitation prior to a noticeable pump head dropoff. It produces from 5 to 20 percent of the total head rise of a pump. The conditions of pump critical NPSH at the 2-percent dropoff point may correspond to a 10- to 30-percent inducer-developed-head reduction, depending upon its match to the main pump impeller. The required inducer head rise for a given design is expressed by the correlation

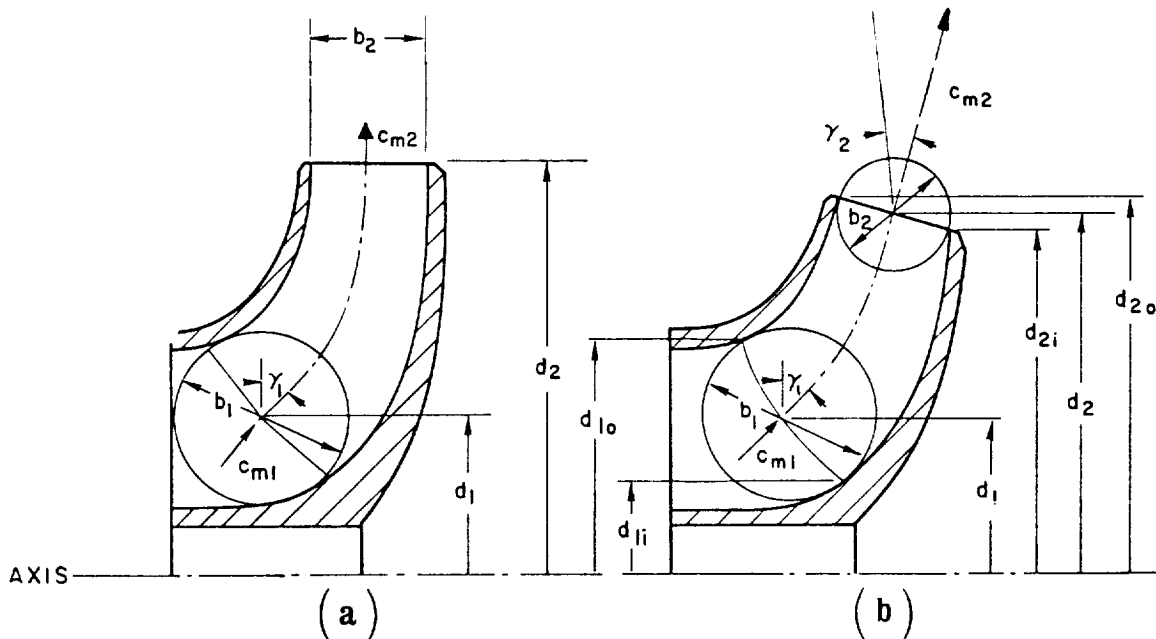


Figure 6-38.—(a) Radial-flow impeller with mixed-flow vanes at the impeller entrance; (b) Mixed-flow impeller.

$$\Delta H_{ind} = (NPSH)_{imp} - (NPSH)_{ind} \quad (6-47)$$

or

$$\left[\frac{N(Q)^{0.5}}{(N_s)_{ind}} \right]^{1.333} = \left[\frac{N(Q)^{0.5}}{(N_{ss})_{imp}} \right]^{1.333} - \left[\frac{N(Q)^{0.5}}{(N_{ss})_{ind}} \right]^{1.333} \quad (6-48)$$

where

- ΔH_{ind} = required inducer head rise at the design point, ft
- $(NPSH)_{ind}$ = inducer critical NPSH = pump critical NPSH or $(NPSH)_c$
= Thoma parameter $\tau \times$ pump total developed head H
- $(NPSH)_{imp}$ = impeller critical NPSH
- N = pump shaft speed, rpm (same for inducer and impeller)
- Q = rated pump flow rate, gpm
- $(N_s)_{ind}$ = inducer specific speed
- $(N_{ss})_{imp}$ = impeller suction specific speed
- $(N_{ss})_{ind}$ = inducer suction specific speed = pump suction specific speed N_{ss}

Figure 6-39 presents the basic elements of a typical inducer design. The primary increase in static pressure occurs at the leading (upstream) edge of the vane through free stream diffusion; i.e., through a reduction of relative speed and by operating at a small angle of attack between relative inlet flow and inducer inlet vane. The cavitation performance of an inducer depends strongly on the inlet flow coefficient ϕ_{ind} (ratio of inlet axial flow velocity c_{mo} to inlet tip speed u_{ot}). To obtain high suction specific speeds (for highest pump speed N), the inducer must have a low flow coefficient. This results in small angles (θ_t, θ_h) between vanes and the plane normal to the axis of rotation. As a rule, the inducer vane angle θ varies radially according to a constant

$$c = d \tan \theta = d_t \tan \theta_t = d_h \tan \theta_h \quad (6-48a)$$

It also often varies axially, according to the variation of the axial or meridional component c_m of the absolute flow velocity. Inducer inlet flow coefficient ϕ_{ind} , inducer diameter ratio r_d (ratio of hub diameter d_h to tip diameter d_t), and

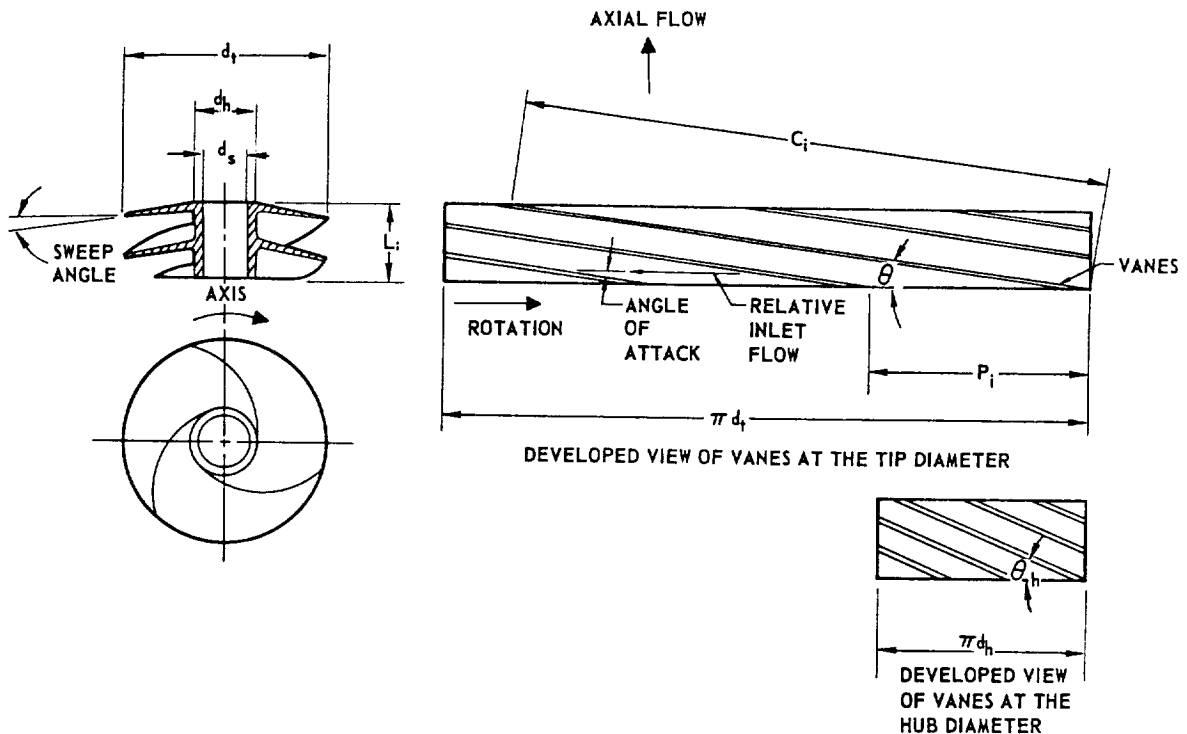


Figure 6-39.—Elements of a typical inducer design (three-vanes; cylindrical hub and tip contour).

suction specific speed $(N_{ss})_{ind}$ are related, based on theoretical one-dimensional fluid cavitation considerations, by the expression

$$\frac{(N_{ss})_{ind}}{(1-r_d^2)^{0.5}} = \frac{8150(1-2\phi_{ind}^2)^{0.75}}{\phi_{ind}} \quad (6-49)$$

Figure 6-40 shows this relationship graphically. The actual performance of a typical inducer is also shown for comparison.

The three vanes shown in figure 6-39 are equally spaced at a tip distance P_i . This is defined as "pitch" and can be expressed as

$$P_i = \frac{\pi d_t}{z} \quad (6-50)$$

where

- P_i = pitch or vane spacing, in
- d_t = inducer tip diameter, in
- z = number of vanes

The ratio of vane tip chord length C_i to vane pitch P_i is an important design element. It is defined as "vane solidity at the tip" of an inducer. Vane solidity S_v is a descriptive term relating the vane area (actual or projected) to the area of the annuli normal to the axial flow. It can be expressed as

$$S_v = \frac{C_i}{P_i} \quad (6-51)$$

The ratio of inducer length L_i to inducer tip diameter d_t , (L_i/d_t) is another important design

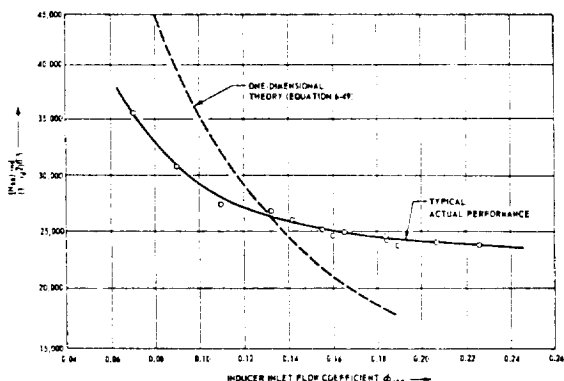


Figure 6-40.—Relation between inducer inlet flow coefficient and inducer suction specific speed.

element used to describe the proportions of an inducer.

Frequently the design of high suction performance inducers dictates a relatively large inlet eye diameter, while the pump main impeller inlet eye diameter must remain small for best performance. This condition can be accommodated by tapering the inducer tip to lead over from one diameter to the other (as shown in fig. 6-41). To minimize the tip taper, tapering of the inducer inlet hub diameter may be added to maintain the desired inducer inlet flow area. In the calculation of tapered inducers, mean values may be used for d_t and d_h . For structural reasons, the inducer vane elements sometimes are designed to cant forward instead of being normal to the axis of rotation. The angle between the canted vane and the plane normal to the axis is defined as the sweep angle.

Table 6-5 contains typical values for inducer design parameters and variables. Figure 6-42 presents inducer inlet and outlet velocity diagrams based on the mean effective diameters. For the design calculations of inducers, the following correlations may be used (figs. 6-39, 6-41 and 6-42). For inducers with cylindrical hub and tip contour:

$$d_o^2 = d_i^2 = \frac{d_t^2 + d_h^2}{2} \quad (6-52)$$

(assume $c_{u0}' = 0$)

$$c_o' = c_{m0} = c_{m1} = \frac{Q_{ind}}{3.12 \times \frac{\pi}{4} (d_t^2 - d_h^2)} \quad (6-53)$$

$$u_o = u_1 = \frac{\pi N}{720} d_o = \frac{\pi N}{720} d_1 \quad (6-54)$$

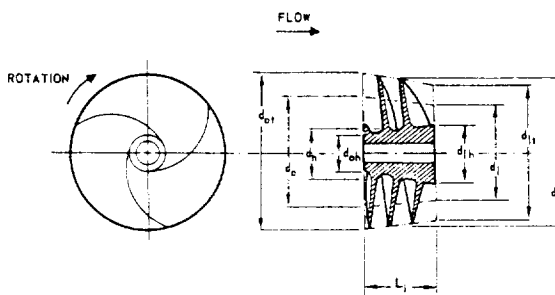
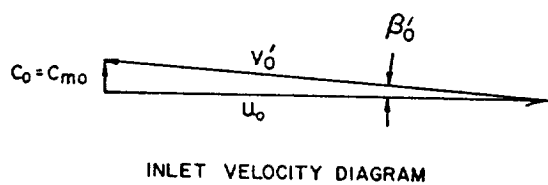


Figure 6-41.—Taper contour inducer.

TABLE 6-5.—Cavitating Inducer Design Parameters and Variables

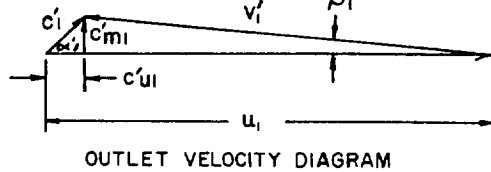
Parameter or variable	Typical design values	Design requirement
Specific speed, $(N_s)_{ind}$	6000 to 12 000	Head-capacity characteristics
Suction specific speed, $(N_{ss})_{ind}$	20 000 to 50 000	Suction characteristics
Head coefficient, ψ_{ind}	0.06 to 0.15	Head rise
Inlet flow coefficient, ϕ_{ind}	0.06 to 0.20	Cavitation performance
Inlet vane angle, θ	8° to 16° (measured from plane normal to axis)	Flow coefficient, angle of attack
Angle of attack, i	3° to 8°	Performance, flow coefficient, vane loading
Diameter ratio, r_d	0.2 to 0.5	Performance, shaft critical speed
Vane solidity, S_v	1.5 to 3.0 at the tip	Desired flow area
Number of vanes, z	3 to 5	Desired solidity
Hub contour	Cylindrical to 15° taper	Compatibility with main impeller and shaft geometry
Tip contour	Cylindrical to 15° taper	Compatibility with main impeller and shaft geometry
Vane loading	Leading edge loading, channel lead	Performance
Leading edge	Swept forward, radial, swept back (shown in fig. 6-39)	Vane stress, performance
Sweep angle	Normal to shaft to 15° forward	Vane stress
Vane thickness	0.070 to 0.300 chord length C_i	Vane stress
Tip clearance (between inducer outside diameter and casing)	0.5 to 1 percent of inducer outside diameter	Shaft axial and radial deflections
Length to tip diameter ratio (L_i/d_t)	0.3 to 0.6	Head-capacity characteristics



$$d_1^2 = \frac{d_{1t}^2 + d_{1h}^2}{2} \quad (6-56)$$

$$d_t = \frac{d_{0t} + d_{1t}}{2} \quad (6-57)$$

$$d_h = \frac{d_{0h} + d_{1h}}{2} \quad (6-58)$$



$$c'_0 = c_{m0} = \frac{Q_{ind}}{3.12 \times \frac{\pi}{4} (d_{0t}^2 - d_{0h}^2)} \quad (6-59)$$

(no prerotation)

Figure 6-42.—Typical flow velocity diagrams of an inducer based on the mean effective diameters.

$$c_{m1} = \frac{Q_{ind}}{3.12 \times \frac{\pi}{4} (d_{1t}^2 - d_{1h}^2)} \quad (6-60)$$

For inducers with tapered hub and tip contour:

$$u_0 = \frac{\pi N}{720} d_0 \quad (6-61)$$

$$d_0^2 = \frac{d_{0t}^2 + d_{0h}^2}{2} \quad (6-55)$$

$$u_1 = \frac{\pi N}{720} d_1 \quad (6-62)$$

For all inducers:

$$Q_{\text{ind}} = Q + Q_{ee} + \frac{1}{2} Q_e \quad (6-63)$$

$$r_d = \frac{d_h}{d_t} \quad (6-64)$$

$$u_t = \frac{\pi N}{720} d_t \quad (6-65)$$

$$u_{ot} = \frac{\pi N}{720} d_{ot} \quad (6-65a)$$

$$\Delta H_{\text{ind}} = \psi_{\text{ind}} \frac{u_t^2}{g} = \frac{u_1 c_{u1}'}{g} \quad (6-66)$$

$$\Delta H_{\text{ind}t} = \frac{H_{\text{ind}}}{\eta_{\text{ind}}} = \frac{u_1 c_{u1}'}{g} \quad (6-67)$$

$$\phi_{\text{ind}} = \frac{c_{m0}}{u_{ot}} \quad (6-68)$$

where

- Q = rated pump flow rate, gpm
 Q_{ind} = required inducer flow rate at the rated design point, gpm
 Q_e = impeller leakage losses at the rated design point, gpm
 Q_{ee} = inducer leakage loss rate through the tip clearance, gpm. Typical design values vary from 2 to 6 percent of Q
 ΔH_{ind} = required inducer head rise at rated conditions, ft
 $\Delta H_{\text{ind}t}$ = ideal inducer head rise at rated conditions, ft
 η_{ind} = inducer efficiency
 d_t = inducer mean tip diameter, in
 d_{ot} = inducer tip diameter at the inlet, in
 d_{1t} = inducer tip diameter at the outlet, in
 d_h = inducer mean hub diameter, in
 d_{oh} = inducer hub diameter at the inlet, in
 d_{1h} = inducer hub diameter at the outlet, in
 d_0 = inducer mean effective diameter at the inlet, in
 d_1 = inducer mean effective diameter at the outlet, in
 u_0 = inducer peripheral velocity at mean effective inlet diameter, ft/sec

- u_1 = inducer peripheral velocity at mean effective outlet diameter, ft/sec
 u_t = mean tip speed of the inducer, ft/sec
 u_{ot} = inducer inlet tip speed, ft/sec
 u_{1t} = inducer outlet tip speed, ft/sec
 v_0' = inlet velocity of the flow relative to the inducer, ft/sec
 v_1' = outlet velocity of the flow relative to the inducer, ft/sec
 c_0' = absolute inlet velocity of the flow, ft/sec
 c_{u0}' = tangential component of the absolute flow velocity, ft/sec
 c_{m0} = meridional or axial component of the absolute inlet flow velocity, ft/sec
 c_1 = ideal absolute outlet flow velocity, ft/sec
 c_1' = absolute outlet flow velocity, ft/sec
 c_{u1}' = tangential component of the absolute outlet flow velocity, ft/sec
 c_{m1} = meridional component of the absolute outlet flow velocity, ft/sec
 r_d = hub to tip diameter ratio
 ψ_{ind} = inducer head coefficient (for range, see table 6-5)
 ϕ_{ind} = inducer inlet flow coefficient (for range, see table 6-5)

The inducer is generally made from a high-quality aluminum-alloy forging of single-piece construction. For manufacture, special machines and tooling are required for best results.

Experimental results have indicated that a high-pressure fluid-injection system can be designed to increase the suction performance of a pump with inducer by imparting an inlet "prewhirl" to the fluid entering the inducer. Fluid injection provides a tangential component c_{u0}' in the proper direction to the absolute fluid inlet velocity c_0' and thereby lowers the fluid inlet velocity v_0' relative to the inducer. Jet momentum and directed whirl in the direction of blade rotation combined should serve to reduce the tendency for the blade tips to cavitate as a result of high relative velocities and low static pressure. The suction specific speed of one typical inducer design was increased from 34 000 to 44 000 by applying "prewhirl." Fluid injection is introduced tangentially (at a small angle with the plane normal to the axis of rotation) several inches upstream of the inducer inlet. It is fed from the pump outlet fluid pressure.

Sample Calculation (6-7)

The following required design data and experimental model test results are given for the oxidizer pump of the A-1 stage engine:

Required pump developed head, $\Delta H = 2930$ ft

Required pump flow rate, $Q = 12420$ gpm

Pump shaft speed, $N = 7000$ rpm

Pump specific speed, $N_s = 1980$

Pump critical NPSH, $(NPSH)_c = 58$ ft

Pump actual suction specific speed, N_{ss}
 $= 37230$ (from experimental tests)

Pump overall head coefficient, $\psi = 0.46$

Basic inducer configuration (tip and hub taper contours) (similar to fig. 6-41)

Inducer head coefficient, $\psi_{ind} = 0.06$

Inducer diameter ratio, $r_d = 0.3$

Inducer ratio, $L_i/d_t = 0.4$

Angle of attack at inducer inlet tip, $i = 4^\circ$
 maximum

Inducer tip contour taper half angle = 7°

Inducer hub contour taper half angle = 14°

Inducer solidity based on mean tip diameter,
 $d_t = 2.2$

Inducer leakage loss rate, $Q_{ee} = 0.032 Q$

Basic impeller configuration = radial-flow type
 with mixed flow vanes at the inlet (similar
 to fig. 6-38a)

Impeller suction specific speed, $(N_{ss})_{imp}$
 $= 11000$

Impeller discharge vane angle, $\beta_2 = 24^\circ$

Impeller contraction factor at the entrance,
 $\epsilon_1 = 0.82$

Impeller contraction factor at the discharge,
 $\epsilon_2 = 0.88$

Impeller coefficient, $e_v = 0.74$

Impeller leakage loss rate, $Q_e = 0.035 Q$

Pump volute head loss, $H_e = 0.19 H$

Design and calculate the basic parameters and dimensions of: (a) pump inducer, (b) pump impeller.

Solution

(a) Oxidizer pump inducer

Modifying equation (6-10), the impeller critical NPSH can be calculated as

$$(NPSH)_{imp} = \left[\frac{NQ^{0.5}}{(N_{ss})_{imp}} \right]^{1.333}$$

$$= \left[\frac{7000 \times (12420)^{0.5}}{11000} \right]^{1.333} = 293 \text{ ft}$$

Substitute $(NPSH)_{imp}$ into equation (6-47) to obtain the required inducer head rise

$$\Delta H_{ind} = (NPSH)_{imp} - (NPSH)_{ind}$$

$$= (NPSH)_{imp} - (NPSH)_c = 293 - 58 = 235 \text{ ft}$$

From equation (6-66), inducer mean tip speed

$$u_t = \sqrt{\frac{235 \times 32.2}{0.06}} = 355 \text{ ft/sec}$$

Inducer mean tip diameter

$$d_t = \frac{720}{\pi N} u_t = \frac{720 \times 355}{\pi \times 7000} = 11.62 \text{ in}$$

(from eq. (6-65)).

For the given (L_i/d_t) ratio of 0.4, the axial length of the inducer becomes

$$L_i = 11.62 \times 0.4 = 4.65 \text{ in}$$

For a given tip contour taper half angle of 7° , the tip diameter at the inducer inlet

$$d_{ot} = d_t + 2 \times \frac{L_i}{2} \times \tan 7^\circ$$

$$= 11.62 + 4.65 \times 0.1228 = 12.19 \text{ in}$$

Tip diameter at the inducer outlet

$$d_{it} = d_t - 2 \times \frac{L_i}{2} \times \tan 7^\circ = 11.62 - 0.57 = 11.05 \text{ in}$$

Mean hub diameter

$$d_h = d_t r_d = 11.62 \times 0.3 = 3.49 \text{ in}$$

(from eq. (6-64)).

For the given hub contour taper half angle of 14° , the hub diameter at the inducer inlet

$$d_{oh} = d_h - 2 \times \frac{L_i}{2} \tan 14^\circ = 3.49 - 4.65 \times 0.2493 = 2.33 \text{ in}$$

The hub diameter at the inducer outlet

$$d_{ih} = d_h + 2 \times \frac{L_i}{2} \tan 14^\circ = 3.49 + 1.16 = 4.65 \text{ in}$$

Substitute the given leakage loss rates $Q_{ee} = 0.032$ for the inducer and $\frac{1}{2}Q_e = 0.0175$ for the impeller into equation (6-63) to obtain the required inducer flow rate

$$Q_{ind} = Q + Q_{ee} + \frac{1}{2}Q_e \\ = 12\,420(1 + 0.032 + 0.0175) = 13\,040 \text{ gpm}$$

From equation (6-59), the actual inducer absolute inlet flow velocity c_0' (= its meridional component c_{m0} , assuming its tangential component $c_{u0} = 0$; $\alpha_0' = 0$)

$$c_0' = c_{m0} = \frac{Q_{ind}}{3.12 \times \frac{\pi}{4}(d_{0t}^2 - d_{0h}^2)} \\ = \frac{13\,040}{3.12 \times \frac{\pi}{4} \times (148.6 - 5.43)} = 37.2 \text{ ft/sec}$$

From equation (6-60), the meridional component of the inducer absolute outlet flow velocity

$$c_{m1} = \frac{Q_{ind}}{3.12 \times \frac{\pi}{4}(d_{1t}^2 - d_{1h}^2)} \\ = \frac{13\,040}{3.12 \times \frac{\pi}{4} \times (122.1 - 21.6)} = 53.1 \text{ ft/sec}$$

From equation (6-55), the inducer mean effective diameter at the inlet

$$d_0 = \sqrt{\frac{d_{0t}^2 + d_{0h}^2}{2}} = \sqrt{\frac{148.6 + 5.43}{2}} = \sqrt{77} = 8.76 \text{ in}$$

From equation (6-61), the inducer peripheral velocity at d_0

$$u_0 = \frac{\pi \times 7000}{720} \times 8.76 = 268 \text{ ft/sec}$$

From equation (6-56), the inducer mean effective diameter at the outlet

$$d_1 = \sqrt{\frac{d_{1t}^2 + d_{1h}^2}{2}} = \sqrt{\frac{122.1 + 21.6}{2}} \\ = \sqrt{71.85} = 8.45 \text{ in}$$

From equation (6-62), the inducer peripheral velocity at d_1

$$u_1 = \frac{\pi \times 7000}{720} \times 8.45 = 258.5 \text{ ft/sec}$$

From equation (6-66), the tangential component of the inducer absolute outlet velocity

$$c_{u1}' = \Delta H_{ind} \frac{g}{u_1} = \frac{235 \times 32.2}{258.5} = 29.2 \text{ ft/sec}$$

Refer to figure 6-42 for the flow velocity diagrams of the inducer, based on the mean effective diameters d_0 and d_1 . Inducer design relative inlet flow velocity

$$v_0' = \sqrt{c_{m0}^2 + u_0^2} = \sqrt{1384 + 71\,825} = 270.6 \text{ ft/sec}$$

Inducer design relative inlet flow angle

$$\sin \beta_0' = \frac{c_{m0}}{v_0'} = \frac{37.2}{270.6} = 0.135; \beta_0' = 7^\circ 45'$$

Inducer design absolute outlet flow velocity

$$c_1' = \sqrt{c_{u1}'^2 + c_{m1}^2} = \sqrt{852.64 + 2819.61} = 60.5 \text{ ft/sec}$$

Inducer design absolute outlet flow angle

$$\tan \alpha_1' = \frac{c_{m1}}{c_{u1}'} = \frac{53.1}{29.2} = 1.82; \alpha_1' = 61^\circ 13'$$

Inducer design relative outlet flow velocity

$$v_1' = \sqrt{(u_1 - c_{u1}')^2 + c_{m1}^2} \\ = \sqrt{52\,578 + 2820} = 235 \text{ ft/sec}$$

Inducer design relative outlet flow angle

$$\tan \beta_1' = \frac{c_{m1}}{u_1 - c_{u1}'} = \frac{53.1}{229.3} = 0.232; \beta_1' = 13^\circ 3'$$

Since the cavitation performance of an inducer depends largely on the angle of attack of the vane leading edge at the inducer inlet tip, and on the inducer inlet flow coefficient ϕ_{ind} , we now proceed to determine the vane angle θ_{0t} at the inducer inlet tip, and to check ϕ_{ind} with the help of equation (6-49).

From equation (6-65a) the inducer inlet tip speed

$$u_{ot} = \frac{\pi \times N}{720} d_{ot} = \frac{\pi \times 7000}{720} \times 12.19 = 372.5 \text{ ft/sec}$$

The relative flow angle at the inducer inlet tip

$$\tan \beta_{ot}' = \frac{c_{m0}}{u_{ot}} = \frac{37.2}{372.5} = 0.0998; \quad \beta_{ot}' = 5^\circ 42'$$

If we use a vane angle $\theta_{ot} = 9^\circ$ at the inducer inlet tip, the angle of attack at the inlet tip

$$\theta_{ot} - \beta_{ot}' = 9^\circ - (5^\circ 42') = 3^\circ 18' (< 4^\circ, \text{ as desired})$$

The vane angle θ_0 at the inducer inlet mean effective diameter d_0

$$\tan \theta_0 = \frac{d_{ot}}{d_0} \tan \theta_{ot} = \frac{12.19}{8.76} \times \tan 9^\circ = 0.220; \quad \theta_0 = 12^\circ 25'$$

(see eq. (6-48a)).

The vane angle θ_{oh} at the inducer inlet hub diameter d_{oh}

$$\tan \theta_{oh} = \frac{d_{ot}}{d_{oh}} \tan \theta_{ot} = \frac{12.19}{2.33} \times \tan 9^\circ = 0.829; \quad \theta_{oh} = 39^\circ 40'$$

From equation (6-68), the inducer inlet flow coefficient

$$\phi_{ind} = \frac{c_{m0}}{u_{ot}} = \frac{37.2}{372.5} = 0.0998$$

Substitute this into equation (6-49), to obtain the theoretical inducer suction specific speed

$$\begin{aligned} (N_{ss})_{ind} &= \frac{8150(1 - 2\phi_{ind}^2)^{0.75}}{\phi_{ind}} (1 - r_d^2)^{0.5} \\ &= \frac{8150 \times (0.9601)^{0.75}}{0.0998} \times (0.91)^{0.5} \\ &= \frac{8150 \times 0.97 \times 0.954}{0.098} = 75700 > N_{ss} = 37300 \end{aligned}$$

Our inducer exhibits characteristics similar to those shown in figure 6-40 for a typical inducer. If we use a vane angle θ_1 of $14^\circ 30'$ at the inducer outlet mean effective diameter d_1 , the difference between θ_1 and the relative outlet flow angle β_1'

$$\theta_1 - \beta_1' = (14^\circ 30') - (13^\circ 3') = 1^\circ 27'$$

This allows for the effect of local circulatory flow (boundary effects).

The vane angle θ_{1t} at the inducer outlet tip diameter d_{1t}

$$\tan \theta_{1t} = \frac{d_1}{d_{1t}} \tan \theta_1 = \frac{8.45}{11.05} \tan (14^\circ 30') = 0.198; \quad \theta_{1t} = 11^\circ 12'$$

The vane angle θ_{1h} at the inducer outlet hub diameter d_{1h}

$$\tan \theta_{1h} = \frac{d_1}{d_{1h}} \tan \theta_1 = \frac{8.45}{4.65} \tan 14^\circ 30' = 0.471; \quad \theta_{1h} = 25^\circ 13'$$

We will use three vanes ($z=3$). The vane pitch at the mean tip diameter d_t can be calculated from equation (6-50)

$$P_i = \frac{\pi d_t}{z} = \frac{\pi \times 11.62}{3} = 12.18 \text{ in}$$

The chord length at vane tip can be calculated as

$$C_i = \frac{L_i}{\sin\left(\frac{\theta_{ot} + \theta_{1t}}{2}\right)} = \frac{4.65}{\sin 10^\circ 6'} = \frac{4.65}{0.175} = 26.57 \text{ in}$$

From equation (6-51) the inducer solidity based on the mean tip diameter d_t

$$S_v = \frac{C_i}{P_i} = \frac{26.57}{12.18} = 2.18$$

A-1 Stage Engine Oxidizer Pump Inducer Design Summary

Following completion of calculations it is advisable to compile the results systematically

in a summary, prior to start of layouts. This gives an opportunity for cross checks and reduces the probability of errors.

Required head rise and capacity, ΔH_{ind}

$$= 235 \text{ ft}, Q_{ind} = 13\,040 \text{ gpm}$$

Inlet velocity diagram (at inlet mean effective diameter d_0)

$$\alpha_0' = 90^\circ, \beta_0' = 7^\circ 45'$$

$$u_0 = 268 \text{ ft/sec}, v_0' = 270.6$$

$$c_0' = c_{m0} = 37.2 \text{ ft/sec}, c_{u0} = 0$$

Outlet velocity diagram (at outlet mean effective diameter d_1)

$$\alpha_1' = 61^\circ 13', \beta_1' = 13^\circ 3'$$

$$u_1 = 258.5 \text{ ft/sec}, v_1' = 235 \text{ ft/sec}$$

$$c_1' = 60.5 \text{ ft/sec}, c_{u1}' = 29.2 \text{ ft/sec}$$

$$c_{m1} = 53.1 \text{ ft/sec}$$

Axial length of inducer, $L_i = 4.65$ in

Taper half angle at tip: 7° ; at hub: 14°

Inlet dimensions

$$d_{ot} = 12.19 \text{ in}, d_{oh} = 2.33 \text{ in}, d_0 = 8.76 \text{ in}$$

$$\text{vane angle at } d_{ot}, \theta_{ot} = 9^\circ$$

$$\text{vane angle at } d_{oh}, \theta_{oh} = 39^\circ 40'$$

$$\text{vane angle at } d_0, \theta_0 = 12^\circ 25'$$

Outlet dimensions

$$d_{1t} = 11.05 \text{ in}, d_{1h} = 4.65 \text{ in}, d_1 = 8.45 \text{ in}$$

$$\text{vane angle at } d_{1t}, \theta_{1t} = 11^\circ 12'$$

$$\text{vane angle at } d_{1h}, \theta_{1h} = 25^\circ 13'$$

$$\text{vane angle at } d_1, \theta_1 = 14^\circ 30'$$

Number of vanes, $z = 3$

Solidity at vane tip, $S_v = 2.18$

Inlet flow coefficient, $\phi_{ind} = 0.0998$

(b) *Oxidizer pump impeller*

We will use a radial-flow-type impeller with mixed-flow-type vanes extending into the impeller entrance eye, as shown in figure 6-38a. The flow path and velocity conditions at the impeller inlet can be assumed to be the same as those at the inducer outlet.

From equation (6-4), the tip or peripheral speed at the impeller discharge

$$u_2 = \sqrt{\frac{gH}{\psi}} = \sqrt{\frac{32.2 \times 2930}{0.46}} = 453 \text{ ft/sec}$$

The impeller outlet diameter

$$d_2 = \frac{720 \times u_2}{\pi \times N} = \frac{720 \times 453}{\pi \times 7000} = 14.8 \text{ in}$$

Substitute the given hydraulic head losses $H_e = 0.19 \Delta H$ into equation (6-34), to obtain the required impeller developed head

$$\begin{aligned} \Delta H_{imp} &= \Delta H + H_e - \Delta H_{ind} \\ &= 2930(1 + 0.19) - 235 = 3252 \text{ ft} \end{aligned}$$

From equation (6-35), the required impeller flow rate

$$Q_{imp} = 12\,420(1 + 0.035) = 12\,855 \text{ gpm}$$

From equation (6-31), the tangential component of the impeller design absolute outlet flow velocity

$$\begin{aligned} c_{u2}' &= \frac{g\Delta H_{imp} + u_1 c_{u1}'}{u_2} \\ &= \frac{32.2 \times 3252 + 258.5 \times 29.2}{453} = 248 \text{ ft/sec} \end{aligned}$$

From equation (6-32), the tangential component of the impeller ideal absolute outlet flow velocity

$$c_{u2} = \frac{c_{u2}'}{e_v} = \frac{248}{0.74} = 335 \text{ ft/sec}$$

Referring to figures 6-34 and 6-35, and to equation (6-28), the meridional component of the impeller design absolute outlet flow velocity

$$\begin{aligned} c_{m2} &= (u_2 - c_{u2}) \tan \beta_2 \\ &= (453 - 335) \tan 24^\circ = 52.5 \text{ ft/sec} \end{aligned}$$

The impeller design absolute outlet flow velocity

$$c_2' = \sqrt{c_{u2}'^2 + c_{m2}^2} = \sqrt{248^2 + 52.5^2} = 253.4 \text{ ft/sec}$$

Impeller design absolute outlet flow angle:

$$\tan \alpha_2' = \frac{c_{m2}}{c_{u2}'} = \frac{52.5}{248} = 0.212; \quad \alpha_2' = 11^\circ 58'$$

Impeller design relative outlet flow velocity

$$\begin{aligned} v_2' &= \sqrt{(u_2 - c_{u2}')^2 + c_{m2}^2} \\ &= \sqrt{205^2 + 52.5^2} = 211.6 \text{ ft/sec} \end{aligned}$$

Impeller design relative outlet flow angle:

$$\tan \beta_2' = \frac{c_{m2}}{(u_2 - c_{u2}')} = \frac{52.5}{205} = 0.256; \quad \beta_2' = 14^\circ 22'$$

Referring to figure 6-38a, and to equation (6-42), the width of the impeller at the vane inlet

$$b_1 = \frac{Q_{\text{imp}}}{3.12 \pi d_1 c_{m1} \epsilon_1} = \frac{12855}{3.12 \times \pi \times 8.45 \times 53.1 \times 0.82} = 3.56 \text{ in}$$

From equation (6-43), the width of the impeller at the discharge

$$b_2 = \frac{Q_{\text{imp}}}{3.12 \pi d_2 c_{m2} \epsilon_2} = \frac{12855}{3.12 \times \pi \times 14.8 \times 52.5 \times 0.88} = 1.91 \text{ in}$$

From equation (6-5) the overall pump flow coefficient

$$\phi = \frac{c_{m2}}{u_2} = \frac{52.5}{453} = 0.116$$

A-1 Stage Engine Oxidizer Pump Impeller Design Summary

Required impeller developed head and $\Delta H_{\text{imp}} = 3252 \text{ ft}$, $Q_{\text{imp}} = 12855 \text{ gpm}$ flow capacity

Inlet velocity diagram (at mean inlet effective diameter d_1)

$$\begin{aligned} \alpha_1' &= 61^\circ 13', \quad \beta_1' = 13^\circ 3' \\ u_1 &= 258.5 \text{ ft/sec}, \quad v_1' = 235 \text{ ft/sec} \\ c_1' &= 60.5 \text{ ft/sec}, \quad c_{u1}' = 29.2 \text{ ft/sec}, \\ c_{m1} &= 53.1 \text{ ft/sec} \end{aligned}$$

Outlet velocity diagram (at outlet diameter d_2)

$$\begin{aligned} \alpha_2' &= 11^\circ 58', \quad \beta_2' = 14^\circ 22' \\ u_2 &= 453 \text{ ft/sec}, \quad v_2' = 211.6 \text{ ft/sec} \\ c_2' &= 253.4 \text{ ft/sec}, \quad c_{u2}' = 248 \text{ ft/sec}, \\ c_{m2} &= 52.5 \text{ ft/sec} \end{aligned}$$

Inlet dimensions

$$\begin{aligned} \text{inlet eye diameter} &= d_{1t} = 11.05 \text{ in} \\ \text{inlet hub diameter} &= d_{1h} = 4.65 \text{ in} \\ \text{inlet mean effective diameter} &= d_1 = 8.45 \text{ in} \\ \text{inlet vane angle at diameter } d_1 &= \beta_1' = 13^\circ 3' \\ \text{inlet vane width } b_1 &= 3.56 \text{ in} \end{aligned}$$

Outlet dimensions

$$\begin{aligned} \text{outside diameter } d_2 &= 14.8 \text{ in} \\ \text{discharge vane angle } \beta_2 &= 24^\circ \\ \text{impeller outlet width } b_2 &= 1.91 \text{ in} \\ \text{Number of impeller vanes (eq. 6-44)} \quad z_i &= \beta_2'/3 \\ &= 24/3 = 8 \end{aligned}$$

Design of Casings

The main function of a pump casing is to convert the kinetic energy of high flow velocity at the impeller discharge into pressure. It does not contribute to the generation of head. The construction of a typical centrifugal pump casing is shown in figure 6-5. The front section of the casing, which provides the pump inlet and houses the inducer, is called the suction nozzle. The rear section of the casing, which collects the fluid from the impeller and converts the velocity head into pressure prior to discharge, is called the volute.

Since the flow path in a suction nozzle is short and the flow velocities are relatively low, the head loss in a suction nozzle due to friction is very small. The contour of the suction nozzle is designed to suit the inducer configuration. A tapered suction nozzle (as shown in fig. 6-14), also known as an end suction nozzle, together with a tapered inducer, yields best results in most respects. This nozzle, the area of which gradually decreases toward the impeller eye, greatly steadies the flow and assures uniform feed to the impeller. In liquid oxygen pumps, frequently a liner made of a material such as Kel-F is inserted between inducer and suction nozzle wall. This eliminates the possibility of metal-to-metal rubbing in the presence of narrow inducer tip clearances. Rubbing in liquid oxygen pumps may cause dangerous explosions. In turbopumps of the single-shaft type (fig. 6-18), the fuel is introduced to the fuel pump in a radial direction. Special guide devices are required in the inlet to minimize pressure drops because of the need of turning the flow axially into the inducer.

Two types of volute casing are used in rocket centrifugal pumps, the plain volute and the diffusing vane volute (see fig. 6-43). In the first, the impeller discharges into a single volute channel of gradually increasing area. Here, the

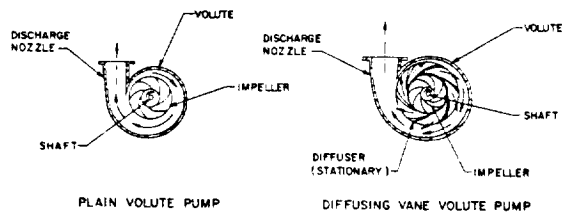


Figure 6-43.—Plain volute and diffusing vane volute centrifugal pump casings.

major part of the conversion of velocity to pressure takes place in the conical pump discharge nozzle. In the latter, the impeller first discharges into a diffuser provided with vanes. A major portion of the conversion takes place in the channels between the diffusing vanes before the fluid reaches the volute channel. The main advantage of the plain volute is its simplicity. However, the diffusing volute is more efficient. Head losses in pump volutes are relatively high. Approximately 70 to 90 percent of the flow kinetic energy is converted into pressure head in either volute type.

The hydraulic characteristics of a plain volute are determined by several design parameters which include: volute throat area a_v and flow areas a_θ , included angle θ_s between volute side walls (fig. 6-44), volute tongue angle α_v , radius r_t at which the volute tongue starts, and volute width b_3 . Their design values are somewhat influenced by the pump specific speed N_s and are established experimentally for best performance.

All of the pump flow Q passes through the volute throat section a_v , but only part of it passes through any other section, the amount depending on the location away from the volute tongue. One design approach is to keep a constant average flow velocity c_3' at all sections of the volute. Thus

$$c_3' = \frac{Q}{3.12 a_v} \frac{1}{3.12} \frac{\theta}{360} \frac{Q}{a_\theta} \quad (6-69)$$

where

c_3' = average flow velocity in the volute, ft/sec
 Q = rated design pump flow rate, gpm
 a_v = area of the volute throat section, in²
 a_θ = area of a volute section (in²), at an angular location θ (degrees) from the tongue

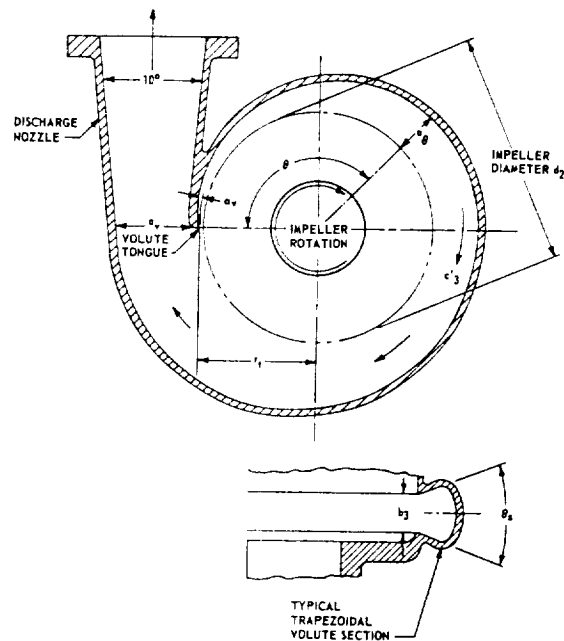


Figure 6-44.—Plain volute casing of a centrifugal pump.

The design value of the average volute flow velocity c_3' may be determined experimentally from the correlation

$$c_3' = K_v \sqrt{2g\Delta H} \quad (6-70)$$

where

K_v = experimental design factor; typical values range from 0.15 to 0.55. K_v is lower for higher specific speed pumps

ΔH = rated design pump developed head, ft
 g = gravitational constant, 32.2 ft/sec²

In order to avoid impact shocks and separation losses at the volute tongue, the volute angle α_v is designed to correspond to the direction of the absolute velocity vector at the impeller discharge: $\alpha_v \approx \alpha_2'$. Higher specific speed pumps have higher values of α_2' and thus require higher α_v . The radius r_t at which the tongue starts should be 5 to 10 percent larger than the outside radius of the impeller to suppress turbulence and to provide an opportunity for the flow leaving the impeller to equalize before coming into contact with the tongue.

The dimension b_3 at the bottom of a trapezoidal volute cross section is chosen to minimize losses due to friction between impeller

discharge flow and volute side walls. For small pumps of lower specific speeds, $b_3 = 2.0 b_2$, where b_2 is the impeller width at the discharge, in. For higher specific speed pumps, $b_3 = 1.6$ to $1.75 b_2$. The maximum included angle θ_s between the volute side walls should be about 60° . For higher specific speed pumps, or for higher impeller discharge flow angles a_2' , the value of θ_s should be made smaller.

The pressure in the volute cannot always be kept uniform, especially under off-design operating conditions. This results in a radial thrust on the impeller shaft. To eliminate or reduce the radial thrust, double-volute casings have been frequently used (fig. 6-45). Here, the flow is divided into two equal streams by two tongues set 180° apart. Although the volute pressure unbalances may be the same as in a single-volute casing, the resultant of all radial forces may be reduced to a reasonably low value, owing to symmetry.

The diffusing vane volute has essentially the same shape as a plain volute, except that a number of passages are used rather than one. This permits the conversion of kinetic energy to pressure in a much smaller space. The radial clearance between impeller and diffuser inlet vane tips should be narrow for best efficiency. Typical values range from 0.03 to 0.12 inch, depending upon impeller size. The width of the diffuser at

its inlet can be approximated in a manner similar to that used for the width of a plain volute (i.e., 1.6 to 2.0 impeller width b_2). A typical diffuser layout is shown in figure 6-46. The vane inlet angle a_3 should be made equal or close to the absolute impeller discharge flow angle a_2' . The design value of the average flow velocity at the diffuser throat c_3' may be approximated by

$$c_3' = \frac{d_2}{d_3} c_2' \quad (6-71)$$

where

c_3' = average flow velocity at the diffuser throat, ft/sec

d_2 = impeller discharge diameter, in

d_3 = pitch diameter of the diffuser throats, in

c_2' = absolute flow velocity at impeller discharge, ft/sec

Since each vane passage is assumed to carry an equal fraction of the total flow Q , the following correlation may be established:

$$b_3 h_3 z = \frac{Q}{3.12 c_3'} \quad (6-72)$$

where

b_3 = width of the diffuser at the throat, in

h_3 = diffuser throat height, in

z = number of diffuser vanes

Q = rated design pump flow rate, gpm

The number of diffuser vanes z should be minimum, consistent with good performance, and should have no common factor with the number of impeller vanes to avoid resonances. If possible,

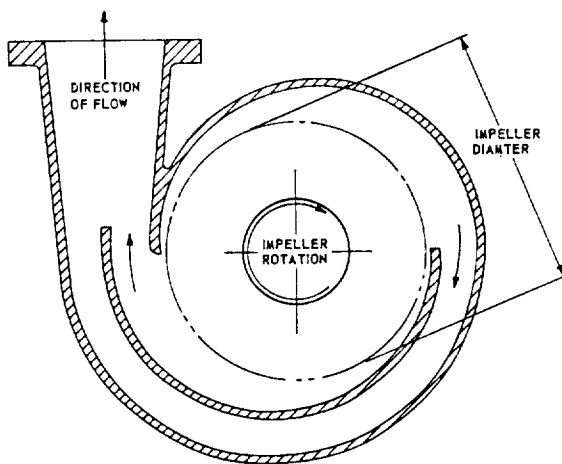


Figure 6-45.—Typical single discharge, 180° opposed double-volute casing of a centrifugal pump.

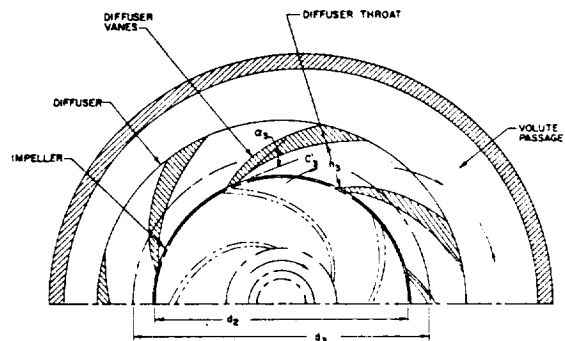


Figure 6-46.—Typical layout of the diffuser for a centrifugal pump volute casing.

the cross section of the passages in the diffuser are made nearly square; i.e., $b_3 = h_3$. The shape of the passage below the throat should be diverging, with an angle between 10° to 12° . The velocity of the flow leaving the diffuser is kept slightly higher than the velocity in the pump discharge line.

Rocket pump casings are frequently made of high-quality aluminum-alloy castings. In low-pressure pumps, the casing wall thickness is held as thin as is consistent with good foundry practice. Owing to the intricate shape of the castings, stress calculations are usually based upon prior experience and test data. For a rough check, the hoop stress at a casing section may be estimated as

$$S_t = p \frac{a}{a'} \quad (6-73)$$

where

S_t = hoop tensile stress, lb/in²

p = local casing internal pressure, psia (or pressure difference across the casing wall, psi)

a = projected area on which the pressure acts, in²

a' = area of casing material resisting the force pa , in²

The actual stress will be higher, because of bending stresses as a result of discontinuities and deformation of the walls, and thermal stresses from temperature gradients across the wall.

Sample Calculation (6-8)

The flow conditions at the outlet of the A-1 stage engine oxidizer pump impeller were derived in sample calculation (6-7). Calculate and design a double-volute (spaced 180°), single-discharge-type casing (as shown in fig. 6-45) for the same pump, assuming a design factor K_V of 0.337.

Solution

From equation (6-70), the average volute flow velocity may be calculated as

$$c_3' = K_V \sqrt{2g\Delta H} = 0.337 \times \sqrt{2 \times 32.2 \times 2930} = 146 \text{ ft/sec}$$

Referring to figures 6-44 and 6-45, and from equation (6-69), the required volute flow area at

any section from 0° to 180° away from the volute tongue may be calculated for both volutes as

$$a\theta = \frac{\theta Q}{3.12 \times 360 \times c_3'} = \frac{12420}{3.12 \times 360 \times 146} \theta = 0.076 \theta$$

At $\theta = 45^\circ$, $a_{45} = 3.42 \text{ in}^2$; at $\theta = 90^\circ$, $a_{90} = 6.84 \text{ in}^2$; at $\theta = 135^\circ$, $a_{135} = 10.26 \text{ in}^2$; and at $\theta = 180^\circ$, $a_{180} = 13.68 \text{ in}^2$.

Total volute throat area at the entrance to the discharge nozzle

$$a_v = 2 \times 13.68 = 27.36 \text{ in}^2$$

The volute angle α_v can be approximated as

$$\alpha_v = \alpha_2' = 11^\circ 58', \text{ say } 12^\circ$$

The radius r_t at which the volute tongues start can be approximated as (assuming 5 percent clearance)

$$r_t = \frac{d_2}{2} \times 1.05 = \frac{14.8}{2} \times 1.05 = 7.77 \text{ in}$$

The width at the bottom of the trapezoidal volute section shall be

$$b_3 = 1.75 b_2 = 1.75 \times 1.91 \text{ in} = 3.34 \text{ in}$$

Allowing for a transition from the shape of the volute to round, we use a diameter of 6.25 inches, or an area of 30.68 in^2 , for the entrance to the discharge nozzle. With a 10° included taper angle and a nozzle length of 10 inches, the exit diameter of the discharge nozzle can be determined as

$$\begin{aligned} d_e &= 6.25 + 2 \times 10 \times \tan 5^\circ \\ &= 6.25 + 2 \times 10 \times 0.0875 = 6.25 + 1.75 \\ &= 8 \text{ in (or an area of } 50.26 \text{ in}^2) \end{aligned}$$

Flow velocity at the nozzle inlet:

$$\frac{12420}{3.12 \times 30.68} = 130 \text{ ft/sec}$$

Flow velocity at the nozzle exit:

$$\frac{12420}{3.12 \times 50.26} = 79.4 \text{ ft/sec}$$

Balancing the Axial Thrust of Centrifugal Pumps

Unbalanced axial loads acting on the inducer-impeller assembly of centrifugal pumps are primarily the result of changes in axial momentum, and of variations in pressure distribution at the periphery of the assembly. These unbalanced forces can be reduced by mounting two propellant pumps back to back, as shown in figures 6-14 and 6-18. More subtle balancing of the axial loads can be accomplished by judicious design detail, which is especially important in high-pressure and high-speed pump applications. Either one of the following two methods is frequently used.

With the first method (as shown in fig. 6-47), a balance chamber is provided at the back shroud of the impeller, between back wearing ring diameter d_{br} and shaft seal diameter d_s . Balancing of axial loads is effected by proper selection of the projected chamber area and of the admitted fluid pressure. The pressure level p_c in a balance chamber can be controlled by careful adjustment of the clearances and leakages of the back wearing ring and the shaft seals. The required p_c may be determined by the following correlation:

$$p_c \pi (d_{br}^2 - d_s^2) = p_v \pi (d_{br}^2 - d_{fr}^2) + p_1 \pi (d_{fr}^2 - d_t^2) + p_0 \pi d_h^2 + \frac{4 \dot{w}_i c_{m_0}}{g} \pm T_e \quad (6-74)$$

where

- p_c = balance chamber pressure, psia
- p_v = average net pressure in the space between impeller shrouds and casing walls, psia
- p_1 = static pressure at the inducer outlet, psia
- p_0 = static pressure at the inducer inlet, psia
- d_s = effective shaft seal diameter, in
- d_h = hub diameter at the inducer inlet, in
- d_t = inducer tip diameter = eye diameter at the impeller inlet, in
- d_{fr} = front wearing ring diameter, in
- d_{br} = back wearing ring diameter, in
- \dot{w}_i = inducer weight flow rate, lb/sec
- c_{m_0} = axial flow velocity at the inducer inlet, ft/sec (converts to radial)
- g = gravitational constant, 32.2 ft/sec²
- T_e = external axial thrust due to unbalanced axial loads of the other propellant and/or

the turbine; lb. A positive sign indicates a force which tends to pull the impeller away from the suction side, a negative sign indicates the opposite.

The static pressure at the inducer outlet, p_1 , can be either measured in actual tests, or approximated by

$$p_1 = k_i p_0 \quad (6-75)$$

where

k_i = design factor based on experimental data (ranging from 1.1 to 1.5)

p_0 = static pressure at the inducer inlet, psia

The average pressure in the space between impeller shrouds and casing side walls, p_v , may be approximated by

$$p_v = p_1 + \frac{3}{576} \frac{u_2^2 - u_1^2}{2g} \rho \quad (6-76)$$

where

u_2 = peripheral speed at the impeller outside diameter d_2 , ft/sec

u_1 = peripheral speed at the impeller inlet mean effective diameter d_1 , ft/sec

ρ = density of the pumped medium, lb/ft³

The main advantage of the balance chamber method is flexibility. The final balancing of the turbopump bearing axial loads can be accomplished in component tests by changing the value of p_c through adjustment of the clearances at the wearing ring and shaft seals. However, this tends to increase leakage losses.

In the second method (as shown in fig. 6-48), straight radial ribs are provided at the back shroud of the impeller to reduce the static pressure between the impeller back shroud and casing wall through partial conversion into kinetic energy. This reduction of axial forces acting on the back shroud of the impeller may be approximated by the following correlation:

$$F_a = \frac{3\pi}{4608} (d_r^2 - d_s^2) \frac{(u_r^2 - u_s^2)}{2g} \rho \frac{(s+t)}{2s} \quad (6-77)$$

where

F_a = reduction of the axial forces acting on the back shroud of impeller, lb

d_r = outside diameter of the radial ribs, in

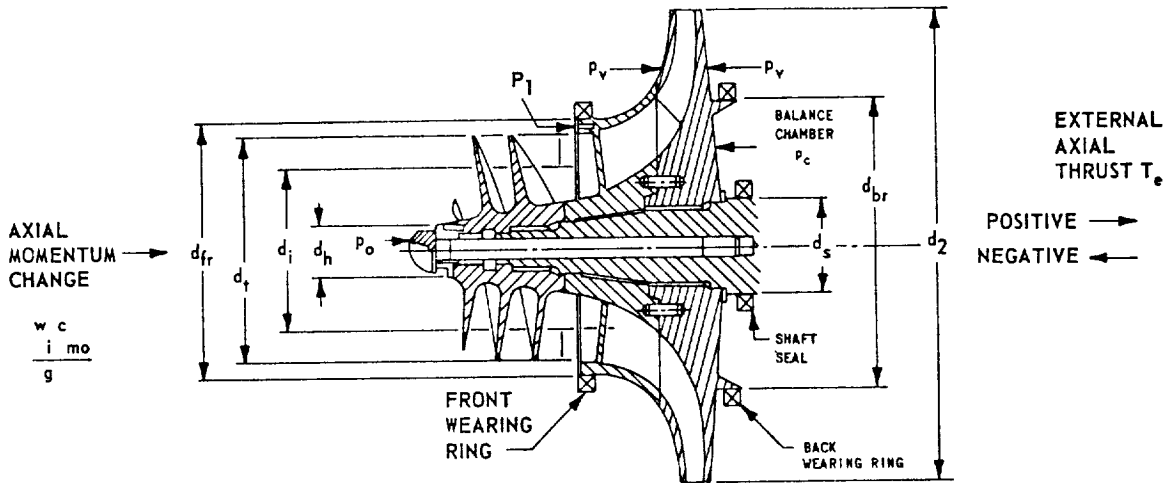


Figure 6-47.—Balancing axial thrusts of a centrifugal pump by the balance chamber method.

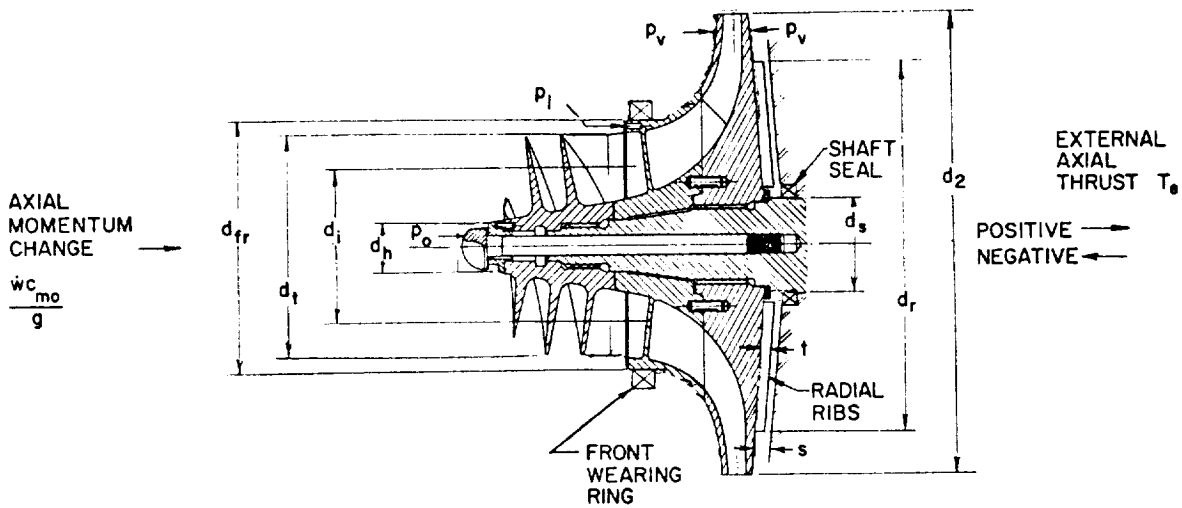


Figure 6-48.—Balancing axial thrusts of a centrifugal pump by the radial rib method.

- d_s = effective shaft seal diameter \approx inside diameter of the radial ribs, in
- u_r = peripheral speed at diameter d_r , ft/sec
- u_s = peripheral speed at diameter d_s , ft/sec
- g = gravitational constant, 32.2 ft/sec²
- ρ = density of the pumped medium, lb/ft³
- t = height or thickness of the radial ribs, in
- s = average distance between casing wall and impeller back shroud, in

The required F_a may be determined by the following correlation:

$$p_v \pi (d_{fr}^2 - d_s^2) - 4 F_a = p_1 \pi (d_{fr}^2 - d_t^2) + p_o \pi d_h^2 + \frac{4 \dot{w} c_{m0}}{g} \pm T_e \quad (6-78)$$

The pressures p_1 and p_v may be approximated by equations (6-75) and (6-76). See equation (6-74) for other terms.

Sample Calculation (6-9)

Radial ribs (similar to those in fig. 6-48) are used on the back shroud of the A-1 stage engine

oxidizer pump impeller, with the following dimensions:

- Outside diameter of the radial ribs, $d_r = 14.8$ in (equal to d_2)
- Inside diameter of the radial ribs, $d_s = 4.8$ in
- Height of the radial ribs, $t = 0.21$ in
- Width of the radial ribs, $w = 0.25$ in (not critical)

Average distance between the casing wall and impeller back shroud, $s = 0.25$ in

Estimate the reduction of the axial forces acting on the back shroud of the impeller, due to the radial ribs.

Solution

The peripheral speed at diameter d_r

$$u_r = \frac{\pi N}{720} d_r = \frac{\pi \times 7000}{720} \times 14.8 = 452 \text{ ft/sec}$$

The peripheral speed at the diameter d_s

$$u_s = \frac{\pi N}{720} d_s = \frac{\pi \times 7000}{720} \times 4.8 = 147 \text{ ft/sec}$$

From equation (6-77), the reduction of the axial forces

$$F_a = \frac{3\pi}{4608} (219.04 - 23.04) \frac{(204304 - 21609)}{2 \times 32.2} \times 71.38 \times \frac{(0.25 + 0.21)}{2 \times 0.25} = 74680 \text{ lb}$$

6.4 DESIGN OF AXIAL-FLOW PUMPS

Except when used as inducers, application of axial-flow pumps in rocket engines is essentially limited to liquid hydrogen systems in a multistage configuration. Thus, the following discussions are applicable to axial-flow hydrogen pumps only. Multistage axial-flow hydrogen pumps are applied in regions which are beyond the capability of a single-stage centrifugal pump, since their construction is comparatively simple (fig. 6-4). As can be seen in figure 6-6, the fluid in an axial-flow pump flows from one stage to the next with a minimum of connecting passages.

The head rise of a typical single-stage centrifugal hydrogen pump is limited to about 65 000 ft (2000 psi). Beyond this point, a multistage

axial-flow pump is selected. For each stage of an axial-flow pump, head rises of 5000 to 9000 feet can be obtained.

The capacity of an axial-flow hydrogen pump is usually limited to about 5500 gpm as a minimum. This is due to the minimum practical height h_v of the vanes (fig. 6-49). For heights below 0.5 inch, the tip clearance required for efficient performance becomes critical, causing manufacturing problems. A reduction in rotor diameter below certain values is not practical either, because of the high rpm required for proper blade speed.

Figure 6-50 presents typical operating regions of various liquid hydrogen pump types. These include centrifugal pumps of $(N_s)_1 = 500$ per

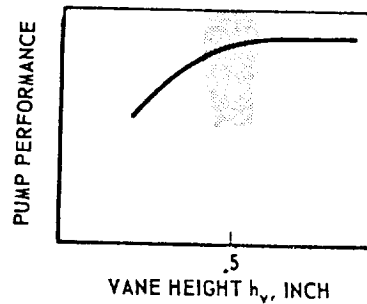
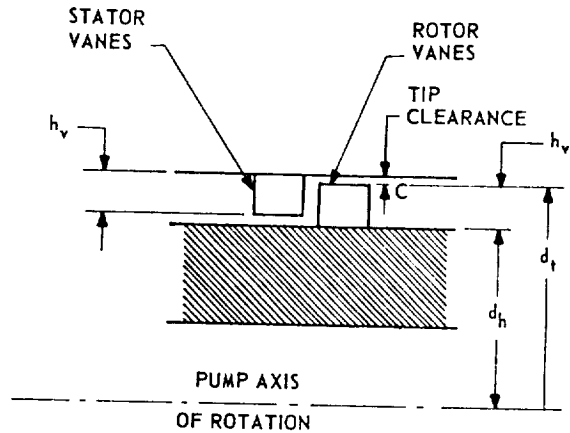


Figure 6-49.—Effect of vane height on the performance of an axial-flow pump.

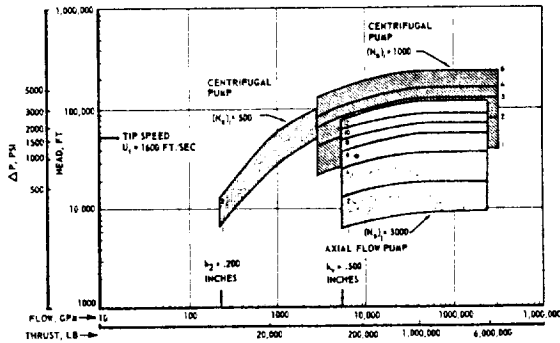


Figure 6-50.—Typical operating regions of various pump types for liquid-hydrogen-fueled rocket engine applications.

stage (1 and 2 stages); centrifugal pumps of $(N_s)_1 = 1000$ per stage (1 to 6 stages; not recommended for rocket engine use); and axial-flow pumps of $(N_s)_1 = 3000$ per stage (1 to 12 stages). For any given operating region, there is usually a best-suited design configuration. However, overlapping regions occur which could be fulfilled by either a multistage axial-flow pump or by a single-stage centrifugal pump. The best solution then is dictated by other considerations, such as space envelope, mounting and ducting arrangement, and others. For instance, the requirements for the region above 5500 gpm, and head rises from 30 000 to 65 000 feet, could be met by either a single-stage centrifugal pump or a multistage axial-flow pump. The centrifugal pump also has its dimensional limitations. A value of less than 0.2 inch for the impeller discharge width, b_2 (fig. 6-34), would complicate manufacture of shrouded impellers and make critical the tip clearance of an open-faced impeller. This establishes the lower capacity limit for centrifugal hydrogen pumps at about 250 gpm.

Basic Assumptions for Axial-Flow Pumps

During operation of an axial flow pump, it is assumed that the meridional or axial component of the absolute flow velocity c_m is constant throughout all stages of the impeller rotor and the stator. To satisfy the flow continuity equation, the cross-sectional areas of the various flow passages at right angles to c_m must also remain constant. This assumption is reasonable, except for the effects of frictional drag at the casing walls and the vanes.

Operation of the Impeller Rotor

The main function of the impeller rotor of an axial-flow pump is to impart kinetic energy to the fluid by increasing the tangential component of the absolute flow velocity. This is accomplished by the action of airfoil-shaped rotor vanes (figs. 6-51 and 6-52). It is convenient to describe the vanes on several developed cylindrical sections. Three sections are of particular interest: at the impeller tip diameter d_t , at the impeller hub d_h , and at its mean effective diameter d_m (inches). The mean effective diameter is defined by

$$d_m^2 = \frac{d_t^2 + d_h^2}{2} = \frac{d_t^2(1 + r_d^2)}{2} \quad (6-79)$$

where r_d = impeller hub ratio or d_h/d_t .

For simplicity, vane characteristics and flow conditions are discussed here only with respect to the mean effective diameter d_m . The vanes are equally spaced at a circumferential distance P_r

$$P_r = \frac{\pi d_m}{z_r} \quad (6-80)$$

where

P_r = pitch or rotor vane spacing at the mean effective diameter d_m , in

z_r = number of rotor vanes

The ratio of the rotor vane chord length C_r to the pitch P_r is called rotor vane solidity S_r

$$S_r = \frac{C_r}{P_r} \quad (6-81)$$

where S_r = rotor vane solidity at the mean effective diameter d_m .

The chord to pitch ratio generally increases from rotor tip diameter d_t to hub diameter d_h for structural reasons. The profile of the vane can be represented by the vane mean line (fig. 6-52) which determines most of the important hydraulic properties of the vane. The thickness of the vane varies along the mean line for better performance and for structural strength. To impart effectively the driving action to the fluid, the angle of the vane mean line, or rotor vane angle,

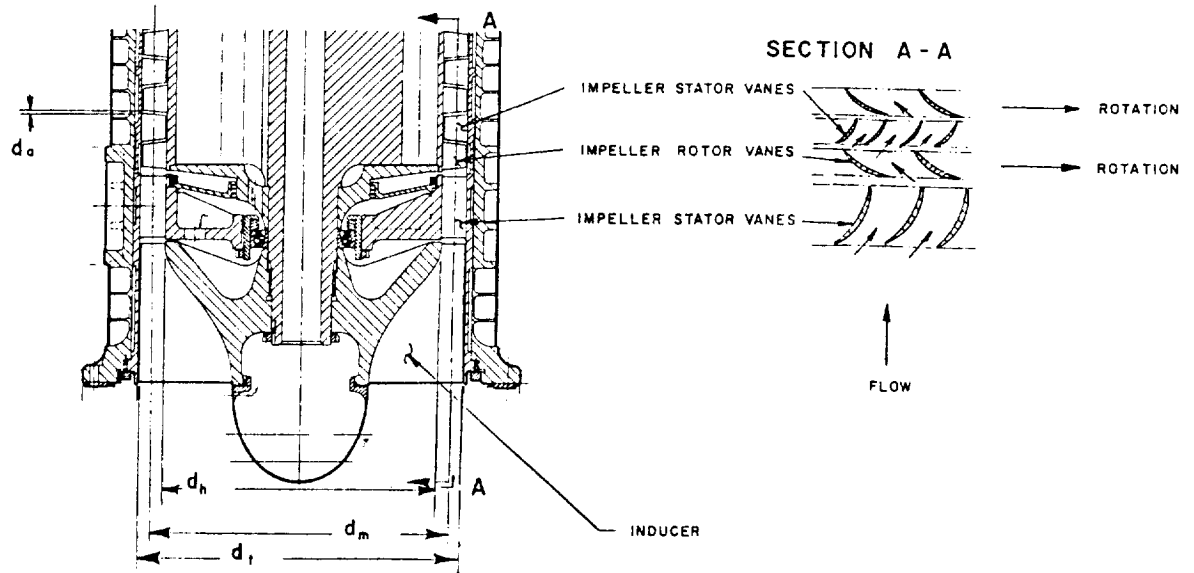


Figure 6-51.—Inducer, inducer stator, impeller rotor, and impeller stator of an axial-flow pump.

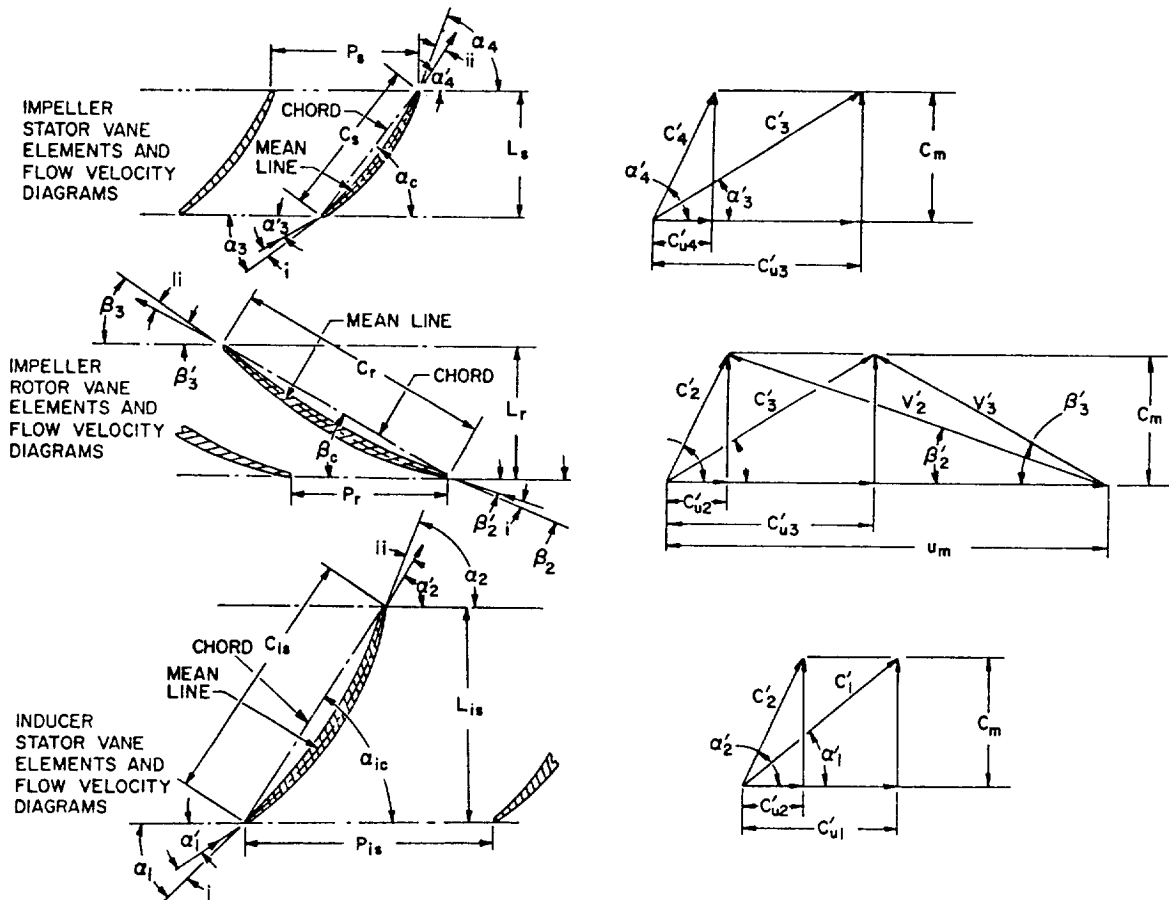


Figure 6-52.—Vane elements and flow velocity diagrams of axial-flow pumps.

is gradually increased from β_2 to β_3 . The difference between the two, $\beta_3 - \beta_2$, is a measure of the vane curvature along any particular vane section. Generally, in axial-flow pump designs, all vane mean lines can be approximated by a circular arc. The following correlations can be established:

$$\beta_c = \frac{\beta_2 + \beta_3}{2} \quad (6-82)$$

$$C_r = 2 R_r \sin \left(\frac{\beta_3 - \beta_2}{2} \right) = \frac{L_r}{\sin \beta_c} \quad (6-83)$$

where

β_c = chord angle of the rotor vane, deg

β_2 = vane angle at the rotor inlet, deg

β_3 = vane angle at the rotor outlet, deg

C_r = chord length of the rotor vane, in

R_r = radius of the rotor vane curvature, in

L_r = axial length of the rotor vane, in

(All parameters refer to the mean effective diameter, d_m)

An angle of attack or incidence angle "i" between rotor inlet vane angle β_2 and the direction of the relative velocity of the flow entering the rotor, β_2' , is allowed for more effective driving of the fluid. Also, an angle "ii" is allowed for circulatory flow between the rotor outlet vane angle β_3 and the direction of the relative velocity of the flow leaving the rotor, β_3' . For the design of impeller rotors, velocity diagrams of the flows at the inlet and outlet of rotor vanes can be constructed (fig. 6-52) with the following correlations:

$$\beta_2 = \beta_2' + i \quad (6-84)$$

$$\beta_3 = \beta_3' + ii \quad (6-85)$$

$$c_m = \frac{Q_{\text{imp}}}{3.12 \times \frac{\pi}{4} (d_t^2 - d_h^2) \epsilon} \quad (6-86)$$

$$Q_{\text{imp}} = Q + Q_e \quad (6-87)$$

$$u_m = \frac{\pi N}{720} d_m \quad (6-88)$$

$$\Delta H_{\text{imp}} = (\Delta H)_1 + H_e = \frac{u_m c_{u3}' - u_m c_{u2}'}{g} \quad (6-89)$$

$$(\psi)_1 = \frac{(\Delta H)_1}{\frac{u_m^2}{g}} \quad (6-90)$$

$$c_m = c_{u2}' \tan \alpha_2' = c_{u3}' \tan \alpha_3' = c_2' \sin \alpha_2' \\ = c_3' \sin \alpha_3' = v_2' \sin \beta_2' = v_3' \sin \beta_3' \quad (6-91)$$

where

i = angle of attack, deg

ii = angle allowed for circulatory flow at the outlet, deg

β_2', β_3' = relative flow angles at the rotor inlet and outlet, deg

α_2', α_3' = absolute flow angles at the rotor inlet and outlet, deg

c_m = meridional or axial component of the absolute flow velocities, ft/sec

u_m = rotor peripheral velocity at mean effective diameter d_m , ft/sec

c_2', c_3' = design absolute flow velocities at the rotor inlet and outlet, ft/sec

c_{u2}', c_{u3}' = tangential components of the design absolute rotor inlet and outlet flow velocities, ft/sec

v_2', v_3' = design relative flow velocities at the rotor inlet and outlet, ft/sec

Q_{imp} = required impeller flow rate at the rated design point, gpm

Q = rated design pump flow rate, gpm

Q_e = impeller leakage loss rate, gpm (2 to 10 percent of Q)

ϵ = contraction factor of vane passage (0.85 to 0.95)

ΔH_{imp} = required developed head per impeller stage, ft

$(\Delta H)_1$ = rated design developed head per axial-flow pump stage, ft

H_e = hydraulic head losses per stage of impeller stator, ft

$(\psi)_1$ = head coefficient per axial flow pump stage

(All applicable parameters refer to the mean effective diameter, d_m)

At various cylindrical sections between vane tip diameter d_t and hub diameter d_h , the following correlations between vane angles and flow velocities are established:

$$d_m \tan \beta_2 = d_t \tan \beta_{2t} \\ = d_h \tan \beta_{2h} = d_x \tan \beta_{2x} \quad (6-92)$$

$$d_m \tan \beta_3 = d_t \tan \beta_{3t} \\ = d_h \tan \beta_{3h} = d_x \tan \beta_{3x} \quad (6-93)$$

$$\frac{u_m}{d_m} = \frac{u_t}{d_t} = \frac{u_h}{d_h} = \frac{u_x}{d_x} \quad (6-94)$$

$$\frac{c_{u2}'}{d_m} = \frac{c_{u2t}'}{d_t} = \frac{c_{u2h}'}{d_h} \quad (6-95)$$

$$\frac{c_{u3}'}{d_m} = \frac{c_{u3t}'}{d_t} = \frac{c_{u3h}'}{d_h} \quad (6-96)$$

where

- β_{2t}, β_{2h} = rotor inlet vane angles at tip and hub diameter, deg
- β_{3t}, β_{3h} = rotor outlet vane angles at tip and hub diameter, deg
- u_t, u_h = rotor peripheral velocities at tip and hub diameter, ft/sec
- c_{u2t}', c_{u2h}' = tangential components of the design absolute rotor inlet flow velocities at tip and hub diameter, ft/sec
- c_{u3t}', c_{u3h}' = tangential components of the design absolute rotor outlet flow velocities at tip and hub diameter, ft/sec

Function of the Stator

The purpose of the stator of an axial-flow pump is to convert a major portion of the tangential component of the absolute flow velocity leaving the rotor into static pressure. This is accomplished by "straightening" the flow as it leaves the rotor. The stator vane curvature is designed so that the fluid enters the vanes with minimum loss, and leaves the stator with a reduced tangential component of the absolute flow velocity. The cross-sectional areas of the stator flow passages normal to the axial direction are equal to those of the rotor. Thus, the axial component of the absolute flow velocity is maintained. The dimensions d_t and d_h of the stator can be treated as equal to the tip and hub diameters of the rotor. The chord-pitch ratio of the stator vanes generally increases from hub diameter d_h to tip diameter d_t . The axial length L_s of the stator vane at the mean effective diameter is usually made equal to that of the rotor, L_r .

Referring to figure 6-52, the velocity diagrams at the stator inlet and outlet are constructed with the assumption that the absolute flow velocities and angles at stator inlets and outlets are equal to the corresponding ones at the rotor outlets and inlets. This facilitates the design of multi-stage axial-flow pumps using uniform rotor and stator stages.

To deflect the fluid effectively, the stator inlet vane angles α_3 should be greater by a few degrees than the inlet absolute flow angles α_3' ; i.e., an angle of attack "i" should be allowed. Also, an angle "ii" should be allowed between outlet vane angle α_4 and outlet absolute flow angle α_4' for the circulatory flow (boundary condition). The following correlations can be established for the vane and flow velocity diagrams of the stator (fig. 6-52):

$$P_s = \frac{\pi d_m}{z_s} \quad (6-97)$$

$$S_s = \frac{C_s}{P_s} \quad (6-98)$$

$$\alpha_c = \frac{\alpha_3 + \alpha_4}{2} \quad (6-99)$$

$$C_s = 2 R_s \sin \left(\frac{\alpha_4 - \alpha_3}{2} \right) = \frac{L_s}{\sin \alpha_c} \quad (6-100)$$

$$\alpha_3 = \alpha_3' + i \quad (6-101)$$

$$\alpha_4 = \alpha_4' + ii \quad (6-102)$$

$$c_m = c_{u3}' \tan \alpha_3' = c_{u4}' \tan \alpha_4' \\ = c_3' \sin \alpha_3' = c_4' \sin \alpha_4' \quad (6-103)$$

$$d_m \tan \alpha_3 = d_t \tan \alpha_{3t} \\ = d_h \tan \alpha_{3h} = d_x \tan \alpha_{3x} \quad (6-104)$$

$$d_m \tan \alpha_4 = d_t \tan \alpha_{4t} \\ = d_h \tan \alpha_{4h} = d_x \tan \alpha_{4x} \quad (6-105)$$

where

- P_s = pitch or stator vane spacing, in
- z_s = number of stator vanes
- S_s = stator vane solidity
- C_s = stator vane chord length, in
- α_c = stator vane chord angle, deg

a_3, a_4	= vane angles at stator inlet and outlet, deg
R_S	= radius of the stator vane curvature, in
L_S	= axial length of the stator vane, in
i	= angle of attack, deg
ii	= angle allowed for circulatory flow at the outlet, deg
a_3', a_4'	= absolute flow angles at stator inlet and outlet, deg
c_m	= axial component of the absolute flow velocities, ft/sec
c_3', c_4'	= design absolute flow velocities of stator inlet and outlet, ft/sec
c_{u3}', c_{u4}'	= tangential components of the design absolute velocities at stator inlet and outlet, ft/sec
a_{3t}, a_{3h}, a_{3x}	= stator inlet vane angles at tip, hub and any intermediate diameter, deg
a_{4t}, a_{4h}, a_{4x}	= stator outlet vane angles at tip, hub and any intermediate diameter, deg

(All parameters refer to the mean effective diameter d_m , unless specified differently.)

Design of Impeller Rotors and Stators

A number of design factors directly affect the performance and characteristics of an axial flow pump. Evaluation of test information, on the basis of specific speed per stage $(N_s)_1$, shows definitely the following correlations:

1. *Impeller hub ratio, r_d .*—The ratio of impeller hub diameter d_h to tip diameter d_t (fig. 6-51) has a direct bearing on the specific speed per stage $(N_s)_1$. Higher specific speed pumps have smaller hubs or hub ratios which results in greater free flow area, and thus greater capacity, but lower head (H/Q characteristics). On the other hand, a higher hub ratio tends to yield a higher head coefficient per stage $(\psi)_1$. Typical values of r_d in rocket engine hydrogen pump designs range from 0.76 to 0.86. Typical design values for $(N_s)_1$ and $(\psi)_1$ range from 3000 to 5000, and from 0.25 to 0.35, respectively.

2. *Vane solidities S_r, S_s .*—The vane solidities or chord-spacing ratios of the rotor and stator are important design parameters. They are selected on the basis of previous experience.

A higher pump specific speed is linked with lower solidity. Typical design values for vane solidities for the rotor and stator at the mean effective diameter d_m range from 1 to 1.3, and 1.5 to 1.8, respectively.

3. *Number of vanes z_r, z_s .*—A lower pump specific speed generally results in a larger number of vanes. Design values of z_r range from 14 to 20. Design values of z_s vary between 35 and 45. Their number should have no common factor with z_r .

4. *Vane curvature and vane setting.*—Experiments indicate that the head developed by an impeller rotor is essentially determined by the vane curvature; i.e., $\beta_3 - \beta_2$. Changes in vane settings, i.e., outlet vane angle β_3 and inlet vane angle β_2 , by the same amount ($\beta_3 - \beta_2 = \text{const}$) will not affect head rise and efficiency materially.

The design procedure for the impeller rotors and stators of a multistage axial-flow pump is essentially the same as that for a single-stage centrifugal pump, except for the determination of the number of pump stages. Design parameters and coefficients established experimentally with earlier successful designs should be utilized to the fullest. Special development tests are still required to verify the characteristics of the new design. The design procedure includes the following steps:

1. To meet a given set of engine system requirements such as rated design pump developed head H , flow rate Q , and rated pump $(NPSH)_c$, the pump rotating speed N is determined first through selection of a suitable inducer of a given suction specific speed $(N_{ss})_{ind}$.

2. With N established, selection of impeller rotor and stator of a given specific speed per stage $(N_s)_1$, combined with the determination of the number of pump stages, can now proceed with the aid of the following correlations.

$$(N_s)_1 = \frac{N(Q)^{0.5}}{(H)_1^{0.75}} \quad (6-106)$$

$$\Delta H = \Delta H_{ind} = H_{ee} + n(\Delta H)_1 \quad (6-107)$$

where

$(N_s)_1$ = specific speed per axial-flow pump stage

N = rated design pump rotating speed, rpm

- Q = rated design pump flow rate, gpm
- $(\Delta H)_1$ = rated design pump developed head per axial-flow pump stage, ft
- ΔH = rated design pump overall developed head, ft
- ΔH_{ind} = inducer rated head rise, ft
- H_{ee} = hydraulic head loss at the inducer stator, ft
- n = number of axial-flow pump stages

3. For the specific speed per stage $(N_s)_1$ thus obtained, various design factors and coefficients such as impeller hub ratio r_d , vane solidities S_r and S_s , number of vanes z_r and z_s , head coefficient per stage $(\psi)_1$, etc., are selected based on past designs with comparable $(N_s)_1$ values.

4. The required impeller rotor and stator diameters, velocity diagrams and vane profiles can now be derived from equations (6-79) through (6-105).

Impeller rotor and stator vanes are generally machined from forgings (fig. 6-51 and 6-53) using aluminum alloys or nickel-base alloys such as K-Monel. In view of the relatively low head produced by an individual axial-flow impeller stage, reduction of skin friction and flow turbulence losses are more important than with centrifugal pumps. A high degree of vane streamlining and polishing is required for high efficiency.

The axial distance d_a between impeller rotor vanes and stator vanes (fig. 6-51) has some bearing on performance. Typical design values of d_a range from 0.02 to 0.05 d_t , where d_t = the

impeller tip diameter. Design values for tip clearances, c , between rotor and stator (fig. 6-49) range from 0.005 to 0.010 inch.

The vane thickness along the mean line is mainly determined by structural considerations, since experiments indicate that there is very little effect on performance from variation of vane thickness. The problems with stressing pump rotor vanes are similar to those with turbine blades. The methods given in section 6-5 for turbines can be applied here also. Vane stresses include centrifugal stresses, bending stresses due to lift and drag loadings on the vanes, and vibrational stresses.

Design of Cavitating Inducers for Axial-Flow Pumps

The design procedures and parameters for cavitating inducers in axial-flow pumps are essentially the same as those for a centrifugal pump (fig. 6-51). Usually, the inducer has a cylindrical tip contour and the same tip diameter d_t as the impeller. The contour of the inducer hub is highly tapered from a relatively small diameter at the inlet to a diameter close to that of the impeller at the outlet.

An inducer stator, which also serves as the front bearing support, is positioned behind the inducer rotor. It is designed to convert into pressure, a portion of the tangential component of the absolute flow velocity leaving the inducer, and to discharge the fluid at an absolute flow velocity and angle equal to that at the outlet of an impeller stator ($c_2' = c_u'$). The inducer stator has the same d_h and d_t as the impeller, and thus the same effective passage cross-sectional area normal to the axial velocity component c_m . The inlet and outlet velocity diagrams for the inducer stator are shown in figure 6-52. The following correlations can be established for the design of an inducer stator:

$$P_{is} = \frac{\pi d_m}{z_{is}} \quad (6-108)$$

$$S_{is} = \frac{C_{is}}{P_{is}} \quad (6-109)$$

$$a_{ic} = \frac{a_1 + a_2}{2} \quad (6-110)$$

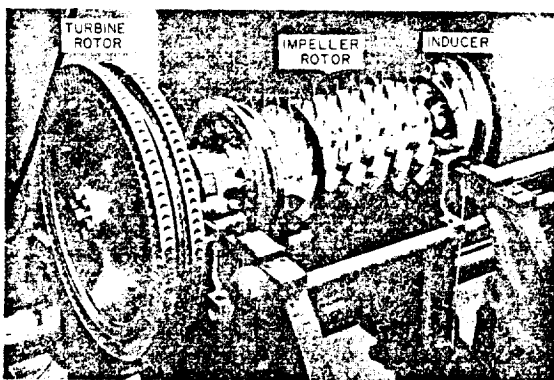


Figure 6-53.—Inducer, impeller rotor, and turbine rotor assembly of a typical multi-stage axial-flow pump.

$$C_{is} = 2 R_{is} \sin \left(\frac{\alpha_2 - \alpha_1}{2} \right) = \frac{L_{is}}{\sin \alpha_{ic}} \quad (6-111)$$

$$\alpha_1 = \alpha_1' + i \quad (6-112)$$

$$\alpha_2 = \alpha_2' + ii \quad (6-113)$$

$$c_m = c_{u1}' \tan \alpha_1' = c_{u2}' \tan \alpha_2' \\ = c_1' \sin \alpha_1' = c_2' \sin \alpha_2' \quad (6-114)$$

$$d_m \tan \alpha_1 = d_t \tan \alpha_{1t} \\ = d_h \tan \alpha_{1h} = d_x \tan \alpha_{1x} \quad (6-115)$$

$$d_m \tan \alpha_2 = d_t \tan \alpha_{2t} \\ = d_h \tan \alpha_{2h} = d_x \tan \alpha_{2x} \quad (6-116)$$

where

- P_{is} = pitch or inducer stator vane spacing, in
 z_{is} = number of inducer stator vanes
 S_{is} = inducer stator vane solidity
 C_{is} = inducer stator vane chord length, in
 α_{ic} = chord angle of the inducer stator vane, deg
 α_1, α_2 = vane angles at inducer stator inlet and outlet, deg.
 R_{is} = radius of the inducer stator vane curvature, in
 L_{is} = axial length of the inducer stator vane, in
 i = angle of attack, deg
 ii = angle allowed for circulatory flow at the outlet, deg
 α_1', α_2' = absolute flow angles at inducer stator inlet and outlet, deg
 c_m = axial component of the absolute flow velocity, ft/sec
 c_1', c_2' = design absolute flow velocities at inducer stator inlet and outlet, ft/sec
 c_{1u}', c_{2u}' = tangential components of the design absolute velocities at inducer stator inlet and outlet, ft/sec
 α_{1t}, α_{1h} = inducer stator inlet vane angles at tip and hub diameters, deg
 α_{2t}, α_{2h} = inducer stator outlet vane angles at tip and hub diameters, deg
 α_{1x}, α_{2x} = vane angles at any diameter d_x
 (All parameters refer to the mean effective diameter d_m , unless specified differently.)

Inducer stator vane solidity design values range from 1.5 to 1.8; the number of vanes z_{is} , ranges from 15 to 20. The number z_{is} should have no common factor with the number of impeller rotor vanes, z_r .

Design of Casings for Axial-Flow Pumps

As shown in figures 6-6 and 6-54, the casing of an axial-flow pump consists of a cylindrical section which houses the inducer stage and the impeller stages. It also includes a volute section with radial guide vanes which is located behind the last impeller rotor stage. In addition to converting the tangential flow velocity component into pressure, the volute section also serves to reduce the axial velocity component by gradually increasing the flow area toward the volute discharge.

The radial guide vanes of the volute section are designed such that the fluid enters them with minimum losses and that it leaves them in a radial plane, analogous to a centrifugal pump (fig. 6-46). The number of radial guide vanes usually ranges from 17 to 23. They should have no common factor with the number of impeller rotor vanes. Vane angle α_v can be determined by constructing the flow velocity diagram for that section.

The calculations of the required areas at the various sections of an axial flow pump volute are essentially identical to those for a centrifugal pump (eqs. 6-69 and 6-70). For liquid hydrogen, design values for volute flow velocities range from 100 to 150 ft/sec. The section of the volute is generally circular in shape to accommodate the high pressures. First-class thermal insulation should be applied to the pump outside surfaces. This will prevent excessive hydrogen boiloff.

Balancing the Axial Thrust of Multistage Axial-Flow Pumps

Balancing of the combined axial thrust of a multistage axial-flow pump is an important function, in view of the high pressures involved. Special balancing devices, such as automatic balance pistons, are frequently used. The balance piston is secured to the rotor assembly, as

shown in figure 6-54. It consists of a disk having small clearances with a pair of seal rubs, located on either side of the disk. A forward movement (toward the inlet) of the rotor assembly, and thus the balance piston, reduces the clearance at the front seal rub, simultaneously increasing it at the rear seal rub. As a result, the pressure in the control chamber between front and rear seal rubs is reduced. This effect counteracts the forward hydraulic axial thrust of the rotor assembly and restrains its forward motion. Similarly, a rearward movement (reverse thrust) of the rotor assembly is counteracted by a pressure increase in the control chambers. The volume to the rear of the control chamber, through cavities in the rotor, communicates with the low-pressure region of the pump inlet. The variation in forward axial thrust can be expressed as

$$\Delta T_a = \Delta p_c \frac{\pi}{4} (d_f^2 - d_r^2) \quad (6-117)$$

where

ΔT_a = variation of the forward hydraulic axial thrust, lb

Δp_c = variation of the fluid pressure in the control chamber, psi

d_f = diameter of the front seal rub, in

d_r = diameter of the rear seal rub, in

Sample Calculation (6-10)

The following design data, based on engine system requirements and on experimental model test results, are given for the alternative A-2 stage engine fuel (liquid hydrogen) pump, based on an axial-flow, multistage configuration (similar to figs. 6-51 and 6-54).

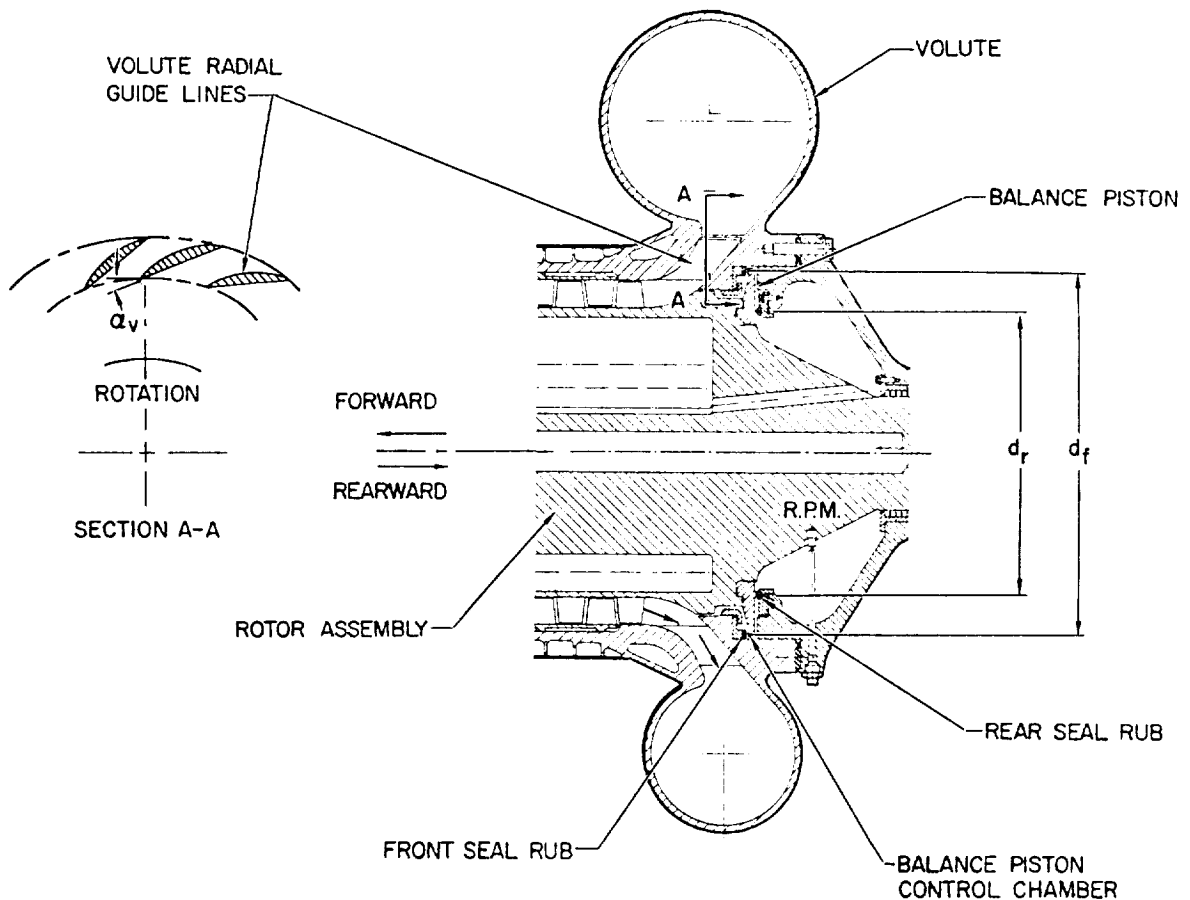


Figure 6-54.—Axial-flow pump volute casing and balance piston arrangement.

Rated design pump developed head, ΔH
= 44 800 ft

Rated design pump flow rate, $Q = 6080$ gpm

Rated design pump (NPSH)_c = 135 ft

Inducer general configuration = cylindrical tip
contour; tapered hub contour

Inducer suction specific speed, $(N_{SS})_{ind}$
= 53 400

Inducer inlet flow coefficient, $\phi_i = 0.09$ max

Inducer head coefficient, $\psi_{ind} = 0.307$

Inducer leakage loss rate, $Q_{ee} = 0.03 Q$

Inducer stator head loss, $H_{ee} = 0.08 \Delta H_{ind}$

Inducer stator vane solidity, $S_{is} = 1.53$

Number of inducer stator vanes, $z_{is} = 17$

Specific speed per axial-flow pump stage,
 $(N_s)_1 = 3200$

Head coefficient per axial-flow pump stage,
 $(\psi)_1 = 0.304$

Impeller hub ratio, $r_d = 0.857$

Impeller leakage loss rate, $Q_e = 0.06 Q$

Head loss per stage of the impeller stator,
 $H_e = 0.08 (\Delta H)_1$

Impeller rotor vane solidity S_r at the mean
effective diameter = 1.05

Number of impeller rotor vanes, $z_r = 16$

Impeller stator vane solidity S_s at the mean
effective diameter = 1.61

Stator and rotor vane passage contraction
factor, $\epsilon = 0.88$

Angle of attack at the vane inlet, $i = 4^\circ$

Angle allowed for circulatory flow at the vane
outlet, $ii = 5^\circ$

Calculate and design basic pump dimensions
and vane detail of: (a) inducer stator, and (b)
impeller rotor and stator.

Solution (refer to fig. 6-52)

(a) Inducer stator

From equation (6-10), the rated pump rotating
speed can be determined:

$$N = \frac{N_{SS} (NPSH)_c^{0.75}}{Q^{0.5}}; \quad (N_{SS} = (N_{SS})_{ind} = 53\,400)$$

$$N = \frac{53\,400 \times (135)^{0.75}}{(6080)^{0.5}} = 27\,000 \text{ rpm}$$

From equation (6-106), the pump developed
head per stage

$$\begin{aligned} (\Delta H)_1 &= \left[\frac{N(Q)^{0.5}}{(N_s)_1} \right]^{1.333} \\ &= \left[\frac{27\,000 \times (6080)^{0.5}}{3250} \right]^{1.333} = 5580 \text{ ft} \end{aligned}$$

From equation (6-90), the peripheral speed at
the impeller mean effective diameter d_m

$$u_m = \sqrt{\frac{g(\Delta H)_1}{(\psi)_1}} = \sqrt{\frac{32.2 \times 5580}{0.304}} = 768 \text{ ft/sec}$$

From equation (6-88), the impeller mean effec-
tive diameter

$$d_m = \frac{720 u_m}{\pi N} = \frac{720 \times 768}{\pi \times 27\,000} = 6.52 \text{ in}$$

From equation (6-79), the impeller rotor tip
diameter (cylindrical tip contour)

$$d_t = d_m \sqrt{\frac{2}{(1+r_d^2)}} = 6.52 \sqrt{\frac{2}{1+0.734}} = 7 \text{ in}$$

The impeller rotor hub diameter

$$d_h = r_d \times d_t = 0.857 \times 7 = 6 \text{ in}$$

The rotor vane height

$$h_v = \frac{d_t - d_h}{2} = \frac{7 - 6}{2} = 0.5 \text{ in}$$

Seven main pump stages and one inducer
stage are used. From eq. (6-107), the required
inducer head rise

$$\begin{aligned} \Delta H_{ind} (1 - 0.08) &= \Delta H - n(\Delta H)_1 \\ \Delta H_{ind} &= \frac{(44\,800 - 7 \times 5580)}{0.92} \\ &= 6240 \text{ ft} \end{aligned}$$

Use an inducer tip diameter of 7 inches, equal
to the impeller rotor tip diameter. Inducer head
rise:

$$u_t = \frac{N \pi d_t}{720} = \frac{27\,000 \times \pi \times 7}{720} = 826 \text{ ft/sec}$$

Substitute this into equation (6-66):

$$\Delta H_{\text{ind}} = \psi_{\text{ind}} \frac{u_t^2}{g} = 0.307 \times \frac{(826)^2}{32.2} = 6500 \text{ ft}$$

This is slightly more than the minimum of 6240 feet required.

The required impeller and inducer flows are obtained from equations (6-35) and (6-63):

$$Q_{\text{imp}} = Q + Q_e = 6080(1 + 0.06) = 6450 \text{ gpm}$$

$$Q_{\text{ind}} = Q + Q_{ee} + \frac{1}{2} Q_e \\ = 6080(1 + 0.03 + 0.03) = 6450 \text{ gpm}$$

We use a hub diameter $d_{oh} = 2.9$ inches at the inducer inlet. Considering that we are using a cylindrical tip contour, the absolute inlet velocity and its meridional component of the inducer flow result from equation (6-59) as:

$$c_o' = c_{mo} = \frac{Q_{\text{ind}}}{3.12 \times \frac{\pi}{4} (d_t^2 - d_{oh}^2)} \\ = \frac{6450}{3.12 \times \frac{\pi}{4} (49 - 8.41)} = 64.8 \text{ ft/sec}$$

Check for inducer inlet flow coefficient:

$$\phi_{\text{ind}} = \frac{c_{mo}}{u_t} = \frac{64.8}{826} = 0.0784 (< 0.09 \text{ max. specified})$$

Use identical values c_m for the meridional component of the absolute flow velocities through the inducer outlet, the stators and the rotors. From equation (6-86)

$$c_m = \frac{Q_{\text{imp}}}{3.12 \times \frac{\pi}{4} (d_t^2 - d_h^2) \epsilon} \\ = \frac{6450}{3.12 \times \frac{\pi}{4} (49 - 36) \times 0.88} = 230 \text{ ft/sec}$$

From equation (6-60), the required hub diameter at the inducer outlet

$$d_{1h} = \sqrt{d_t^2 - \frac{Q_{\text{ind}}}{3.12 \times \frac{\pi}{4} \times c_m}}$$

$$= \sqrt{49 - \frac{6450}{3.12 \times \frac{\pi}{4} \times 230}} = 6.13 \text{ in}$$

The mean effective diameter at the inducer outlet

$$d_1 = \sqrt{\frac{d_t^2 + d_{1h}^2}{2}} = \sqrt{\frac{49 + 37.58}{2}} = 6.57 \text{ in}$$

The peripheral speed at d_1

$$u_1 = \frac{N\pi d_1}{720} = \frac{27000 \times \pi \times 6.57}{720} = 774 \text{ ft/sec}$$

From equation (6-66), the tangential component of the inducer design absolute outlet flow velocity,

$$c_{u1}' = \Delta H_{\text{ind}} \frac{g}{u_1} = \frac{6500 \times 32.2}{774} = 270 \text{ ft/sec}$$

The inducer design absolute outlet flow velocity

$$c_1' = \sqrt{c_{u1}'^2 + c_m^2} = \sqrt{72900 + 52900} = 354.7 \text{ ft/sec}$$

The inducer design absolute outlet flow angle

$$\tan \alpha_1' = \frac{c_m}{c_{u1}'} = \frac{230}{270} = 0.852; \quad \alpha_1' = 40^\circ 26'$$

We use an inducer stator with a meridional flow area equal to that of the impeller rotors and stators (i.e., $d_t = 7$ in, $d_h = 6$ in, $d_m = 6.52$ in, and $\epsilon = 0.88$). We also assume that the absolute flow conditions at the inducer stator inlet are identical to those at the inducer outlet. From equation (6-112), the stator inlet vane angle at d_m

$$\alpha_1 = \alpha_1' + i = 40^\circ 26' + 4^\circ = 44^\circ 26'$$

For a design absolute flow angle at the stator outlet, α_2' of 65° , equation (6-113) yields a vane angle at the stator outlet

$$\alpha_2 = \alpha_2' + ii = 65^\circ + 5^\circ = 70^\circ$$

The tangential component of the stator absolute outlet flow velocity

$$c_{u2}' = \frac{c_m}{\tan \alpha_2'} = \frac{230}{\tan 65^\circ} = \frac{230}{2.145} = 107.2 \text{ ft/sec}$$

The stator absolute outlet flow velocity

$$c_2' = \sqrt{c_{u2}'^2 + c_m^2} = \sqrt{11490 + 52900} \\ = \sqrt{65350} = 253.8 \text{ ft/sec}$$

From equation (6-108), the pitch of the inducer stator vanes at d_m

$$P_{is} = \frac{\pi d_m}{z_{is}} = \frac{\pi \times 6.52}{17} = 1.205 \text{ in}$$

From equation (6-109), the chord length of the inducer stator at d_m

$$C_{is} = S_{is} P_{is} = 1.53 \times 1.205 = 1.844 \text{ in}$$

From equation (6-110), the chord angle of the inducer stator vanes at d_m

$$\alpha_{ic} = \frac{\alpha_1 + \alpha_2}{2} = \frac{44^\circ 26' + 70^\circ}{2} = 57^\circ 13'$$

From equation (6-111), the axial length of the inducer stator vanes at d_m

$$L_{is} = C_{is} \sin \alpha_{ic} = 1.844 \times \sin 57^\circ 13' = 1.55 \text{ in}$$

The radius of the inducer stator vane curvature at d_m

$$R_{is} = \frac{C_{is}}{2 \sin \left(\frac{\alpha_2 - \alpha_1}{2} \right)} = \frac{1.844}{2 \times \sin (12^\circ 47')} = 4.16 \text{ in}$$

A-2 Stage Engine Fuel Pump Inducer Stator Design Summary

(Unless specified otherwise, all data are at the mean effective diameter d_m .)

Inlet flow velocity diagram (fig. 6-52), $\alpha_1' = 40^\circ 26'$; $c_1' = 354.7 \text{ ft/sec}$; $c_m = 230 \text{ ft/sec}$; $c_{u1}' = 270 \text{ ft/sec}$

Outlet flow velocity diagram (fig. 6-52), $\alpha_2' = 65^\circ$; $c_2' = 253.8 \text{ ft/sec}$; $c_m = 230 \text{ ft/sec}$; $c_{u2}' = 107.2 \text{ ft/sec}$

Nominal tip diameter, $d_t = 7 \text{ in}$

Nominal hub diameter, $d_h = 6 \text{ in}$

Nominal vane height, $h_v = 0.5 \text{ in}$

Nominal mean effective diameter, $d_m = 6.52 \text{ in}$
Vane elements (fig. 6-52), $\alpha_1 = 44^\circ 26'$; $\alpha_2 = 70^\circ$; $\alpha_{ic} = 57^\circ 13'$; $S_{is} = 1.53$; $z_{is} = 17$; $P_{is} = 1.205 \text{ in}$; $C_{is} = 1.844 \text{ in}$; $L_{is} = 1.55 \text{ in}$; $R_{is} = 4.16 \text{ in}$

(b) Impeller rotor and stator

Assume that the design absolute flow conditions at the impeller rotor inlets and at the impeller stator outlets are identical to those at the inducer stator outlet. Thus

$$\alpha_2' = \alpha_4' = 65^\circ$$

$$c_2' = c_4' = 253.8 \text{ ft/sec}$$

$$c_m = 230 \text{ ft/sec}$$

$$c_{u2}' = c_{u4}' = 107.2 \text{ ft/sec}$$

The design relative flow angle at the impeller rotor inlets

$$\tan \beta_2' = \frac{c_m}{u_m - c_{u2}'} = \frac{230}{768 - 107.2} = 0.344; \beta_2' = 19^\circ$$

The relative flow velocity at the impeller rotor inlets

$$v_2' = \sqrt{(u_m - c_{u2}')^2 + c_m^2} \\ = \sqrt{436700 + 52900} = 699.6 \text{ ft/sec}$$

From equation (6-84), the rotor inlet vane angle at d_m

$$\beta_2 = \beta_2' + i = 19^\circ + 4^\circ = 23^\circ$$

From equation (6-89), the required developed head for the impeller rotor

$$\Delta H_{imp} = (\Delta H)_1 + H_e = 5580(1 + 0.08) \\ = 6026 \text{ ft per stage}$$

From equation (6-89), the tangential component of the design absolute flow velocity at the impeller rotor outlet

$$c_{u3}' = \frac{g \Delta H_{imp}}{u_m} + c_{u2}' = \frac{32.2 \times 6026}{768} + 107.2 \\ = 359.6 \text{ ft/sec}$$

The impeller rotor design absolute outlet flow velocity

$$c_3' = \sqrt{c_{u3}'^2 + c_m^2} = \sqrt{129\,300 + 52\,900} = 426.9 \text{ ft/sec}$$

The impeller rotor design absolute outlet flow angle

$$\tan \alpha_3' = \frac{c_m}{c_{u3}'} = \frac{230}{359.6} = 0.641; \quad \alpha_3' = 32^\circ 40'$$

The impeller rotor design relative outlet flow velocity

$$v_3' = \sqrt{(u_m - c_{u3}')^2 + c_m^2} = \sqrt{166\,800 + 52\,900} = 468.7 \text{ ft/sec}$$

The impeller rotor design relative outlet flow angle

$$\tan \beta_3' = \frac{c_m}{(u_m - c_{u3}')} = \frac{230}{408.4} = 0.564; \quad \beta_3' = 29^\circ 26'$$

From equation (6-85), the rotor outlet vane angle at d_m

$$\beta_3 = \beta_3' + ii = 29^\circ 26' + 5^\circ = 34^\circ 26'$$

From equation (6-80), the rotor vane pitch

$$P_r = \frac{\pi d_m}{z_r} = \frac{\pi \times 6.52}{16} = 1.281 \text{ in}$$

From equation (6-81), the chord length of the rotor vanes at d_m

$$C_r = S_r P_r = 1.05 \times 1.281 = 1.346 \text{ in}$$

From equation (6-82), the chord angle of the rotor vanes at d_m

$$\beta_c = \frac{\beta_2 + \beta_3}{2} = \frac{23^\circ + 34^\circ 26'}{2} = 28^\circ 43'$$

From equation (6-83), the axial length of the rotor vanes

$$L_r = C_r \sin \beta_c = 1.346 \times \sin 28^\circ 43' = 0.645 \text{ in}$$

The radius of the rotor vane curvature at d_m

$$R_r = \frac{C_r}{2 \sin \frac{\beta_3 - \beta_2}{2}} = \frac{1.346}{2 \sin 5^\circ 33'} = 6.95 \text{ in}$$

Assume that the design absolute flow conditions at the impeller stator inlet are identical to those at the impeller rotor outlet. From equation (6-101), the impeller stator inlet vane angle at d_m

$$\alpha_3 = \alpha_3' + i = 32^\circ 40' + 4^\circ = 36^\circ 40'$$

From equation (6-102), the impeller stator outlet vane angle at d_m

$$\alpha_4 = \alpha_4' + ii = 65^\circ + 5^\circ = 70^\circ$$

The axial length of the stator vanes at d_m is equal to that of the rotor vanes; thus

$$L_s = L_r = 0.645 \text{ in}$$

From equation (6-99), the chord angle of the stator vanes at d_m

$$\alpha_c = \frac{\alpha_3 + \alpha_4}{2} = \frac{36^\circ 40' + 70^\circ}{2} = 53^\circ 20'$$

From equation (6-100), the chord length of the stator vanes at d_m

$$C_s = \frac{L_s}{\sin \alpha_c} = \frac{0.645}{\sin (53^\circ 20')} = 0.805 \text{ in}$$

The radius of the stator vane curvatures at d_m

$$R_s = \frac{C_s}{2 \sin \left(\frac{\alpha_4 - \alpha_3}{2} \right)} = \frac{0.805}{2 \sin (16^\circ 40')} = 1.41 \text{ in}$$

From equation (6-98), the stator vane pitch at d_m

$$P_s = \frac{C_s}{S_s} = \frac{0.805}{1.61} = 0.5 \text{ in}$$

From equation (6-97), the number of the stator vanes

$$z_s = \frac{\pi d_m}{P_s} = \frac{\pi \times 6.52}{0.5} = 41$$

A-2 Stage Engine Fuel Pump Impeller Rotor and Stator Design Summary

(Unless otherwise specified, data are all at the mean effective diameter d_m .)

Rotor inlet flow velocity diagram (fig. 6-52),
 $\alpha_2' = 65^\circ$; $\beta_2' = 19^\circ$; $u_m = 768$ ft/sec; v_2'
 $= 699.6$ ft/sec; $c_2' = 253.8$ ft/sec; $c_{u2}' = 107.2$
 $c_m = 230$ ft/sec

Rotor outlet flow velocity diagram (fig. 6-52),
 $\alpha_3' = 32^\circ 40'$; $\beta_3' = 29^\circ 26'$; $u_m = 768$; v_3'
 $= 468.7$ ft/sec; $c_3' = 426.9$ ft/sec; $c_{u3}' = 359.6$
 ft/sec; $c_m = 230$ ft/sec

Stator inlet flow velocity diagram (fig. 6-52),
 $\alpha_3' = 32^\circ 40'$; $c_3' = 426.9$ ft/sec

Stator outlet flow velocity diagram (fig. 6-52),
 $\alpha_4' = 65^\circ$; $c_4' = 253.8$ ft/sec; $c_{u4}' = 107.2$
 ft/sec; $c_m = 230$ ft/sec

Nominal rotor and stator tip diameter, $d_t = 7$ in

Nominal rotor and stator hub diameter, $d_h = 6$ in

Nominal rotor and stator vane height, $h_v = 0.5$
 in

Nominal mean rotor and stator effective diam-
 eter, $d_m = 6.52$ in

Rotor vane elements (fig. 6-52), $\beta_2 = 23^\circ$;
 $\beta_3 = 34^\circ 26'$; $\beta_c = 28^\circ 43'$; $S_r = 1.05$; $z_r = 16$;
 $P_r = 1.281$ in; $C_r = 1.346$ in; $L_r = 0.645$ in;
 $R_r = 6.95$ in

Stator vane elements (fig. 6-52), $\alpha_3 = 36^\circ 40'$;
 $\alpha_4 = 70^\circ$; $\alpha_c = 53^\circ 20'$; $S_s = 1.61$; $z_s = 41$;
 $P_s = 0.5$; $C_s = 0.805$ in; $L_s = 0.645$ in;
 $R_s = 1.41$ in

6.5 DESIGN OF TURBINES

For rocket engine applications, impulse turbines are preferred, for their simplicity and light weight. Our discussion will be confined to these turbines only. Figure 6-55 shows the general arrangement of a typical single-stage two-rotor velocity-compounded impulse turbine.

General Design Procedure

The following steps are essential in the design of a rocket engine impulse turbine:

1. The first item of importance is the selection of the proper type. A single-stage single-rotor turbine (fig. 6-8) is used if the required turbine power is low, since in this case the efficiency of the turbine has less effect on overall engine systems performance. When the avail-

able energy of the turbine working fluid and thus the gas spouting velocity C_0 is relatively low, a higher turbine velocity ratio U/C_0 may be achieved with a moderate turbine rotor blade speed U . As shown in figure 6-27, this suggests the use of a relatively simple single-stage single-rotor impulse turbine. We have selected this type for the A-2 stage oxidizer turbopump, at the same time taking advantage of its overall simplicity.

In most direct-drive turbopump configurations, such as the A-1 stage engine turbopump (fig. 6-63), where turbine rotating speed N and consequently turbine velocity ratio U/C_0 tends to be lower than ideal, a single-stage two-rotor velocity-compounded impulse turbine (figs. 6-9 and 6-55) is selected for best results. Figure 6-27 indicates that the optimum efficiency of a velocity-compounded turbine can be achieved at a relatively low U/C_0 value.

On the other hand, if a reduction gear train is provided between pumps and turbine, such as in the turbopump shown in figure 6-14, the turbine can be operated at a much higher rotating speed (over 25 000 rpm). A higher value of U/C_0 can be achieved with reasonable turbine wheel size. Then a higher performance, two-stage, two-rotor, pressure-compounded impulse turbine (fig. 6-10) may be used.

2. After the type of impulse turbine has been selected, the next step is the determination of the turbine rotor size. Once the characteristics of the turbine working-fluid (i.e., inlet temperature T_0 , specific heat ratio γ , etc.), the turbine pressure ratio R_t , and the pump or turbine rotative speed N have been set forth, a larger diameter for the turbine rotor tends to result in a higher velocity ratio U/C_0 , or higher efficiency. However, it also results in higher assembly weight, larger envelope, and higher working stresses. Thus, the final selection of the turbine rotor size, and consequently the U/C_0 ratio, is often a design compromise.

3. The required power output from the turbine shaft must be equal to the net input to the propellant pumps, plus the mechanical losses in the gear train (if any), plus the net power required for auxiliary drives. The required flow rate of the turbine working fluid can then be calculated by equation (6-19) after required turbine power, available energy of the working fluid (eq. 6-18), and overall turbine efficiency (estimated from

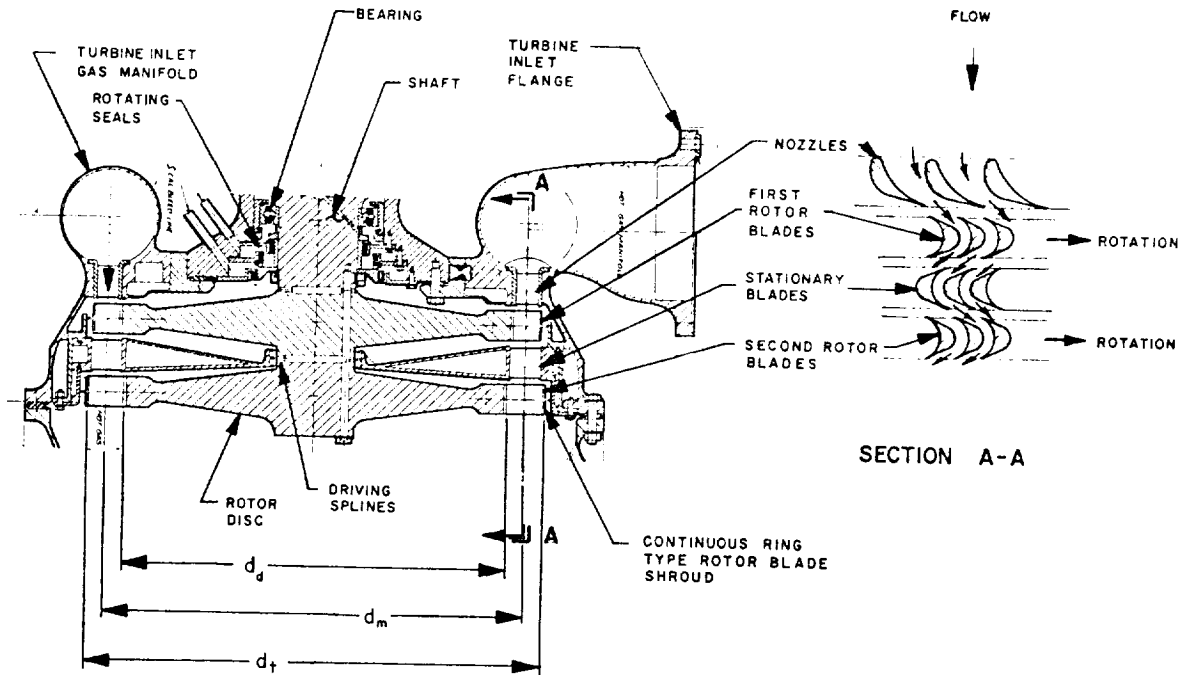


Figure 6-55.—Typical single-stage, two-rotor velocity compounded impulse turbine.

figure 6-27 for a given U/C_0 ratio and turbine type), have been established.

4. Now the dimensions of the stationary nozzles, as well as those of the rotor blades, can be calculated based on the characteristics and the flow rate of the turbine working fluid.

Design of Turbine Nozzles

The nozzles of most rocket engine turbines are basically similar to those of rocket thrust chambers. They are of the conventional converging-diverging De Laval type. The main function of the nozzles of an impulse-type turbine is to convert efficiently the major portion of available energy of the working fluid into kinetic energy or high gas spouting velocity. The gas-flow processes in the thrust chamber nozzles are directly applicable to turbine nozzles. However, the gas flow in an actual nozzle deviates from ideal conditions because of fluid viscosity, friction, boundary layer effects, etc. In addition, the energy consumed by friction forces and flow turbulence will cause an increase in the temperature of the gases flowing through a nozzle,

above that of an isentropic process. This effect is known as reheat. As a result of the above effects, the actual gas spouting velocity at the turbine nozzle exit tends to be less than the ideal velocity calculated for isentropic expansion (from stagnation state at the nozzle inlet to the static pressure at the rotor blade inlet). Furthermore, the effective flow area of a nozzle is usually less than the actual one, because of circulatory flow and boundary layer effects. The following correlations are established for the design calculations of turbine nozzles:

Nozzle velocity coefficient k_n

$$k_n = \frac{\text{Actual gas spouting velocity at the nozzle exit, ft/sec}}{\text{Ideal gas velocity calculated for isentropic expansion from stagnation state at the nozzle inlet to static pressure at the rotor blade inlet, ft/sec}}$$

$$k_n = \frac{C_1}{C_0} \tag{6-118}$$

Nozzle efficiency η_n

$$\begin{aligned} &= \frac{\text{Actual gas kinetic energy at the nozzle exit}}{\text{Ideal gas kinetic energy (isentropic expansion)}} \\ &= \frac{\frac{C_1^2}{2g}}{\frac{C_0^2}{2g}} = k_n^2 \end{aligned} \quad (6-119)$$

Nozzle throat area coefficient ϵ_{nt}

$$= \frac{\text{Effective area of the nozzle throat}}{\text{Actual area}} \quad (6-120)$$

Actual gas spouting velocity at the nozzle exit, ft/sec:

$$\begin{aligned} C_1 &= k_n C_0 = k_n \sqrt{2gJ C_p T_0 \left[1 - \left(\frac{p_1}{p_0} \right)^{\frac{\gamma-1}{\gamma}} \right]} \\ &= k_n \sqrt{2gJ \Delta H_{0-1}''} \end{aligned} \quad (6-121)$$

Amount of nozzle reheat:

$$q_{nr} = \frac{(1 - k_n^2) C_1^2}{k_n^2 2gJ} = \frac{(1 - \eta_n) C_1^2}{\eta_n 2gJ} \quad (6-122)$$

Required total nozzle throat area, in²:

$$A_{nt} = \frac{\dot{w}_t}{\epsilon_{nt} p_0 \sqrt{\frac{g\gamma}{RT_0} \left[\frac{2}{\gamma+1} \right]^{\frac{\gamma-1}{\gamma}}}} \quad (6-123)$$

where

- C_p = turbine gas (working fluid) specific heat at constant pressure, Btu/lb-deg F
- γ = turbine gas specific heat ratio
- R = turbine gas constant (1544/molecular weight), ft²/°R
- T_0 = turbine gas total (stagnation) temperature at the nozzle inlet, °R
- \dot{w}_t = turbine gas mass flow rate, lb/sec
- p_0 = turbine gas total pressure at the nozzle inlet, psia
- p_1 = turbine gas static pressure at the rotor blade inlet, °R

$\Delta H_{0-1}''$ = isentropic enthalpy drop of the gases flowing through the nozzles, due to expansion, Btu/lb

The performance of a turbine nozzle, as expressed by its efficiency or velocity coefficient, is affected by a number of design factors, such as

- (1) Exit velocity of the gas flow
- (2) Properties of the turbine gases
- (3) Angles and curvatures at nozzle inlet and exit
- (4) Radial height and width at the throat
- (5) Pitch or spacing, and number of nozzles

Design values for the efficiency and velocity coefficients of a given turbine nozzle may be determined experimentally, or estimated from past designs. Design values of nozzle efficiency η_n range from 0.80 to 0.96. Design values of nozzle velocity coefficient k_n vary from 0.89 to 0.98. The nozzle throat area coefficient ϵ_{nt} generally will increase with nozzle radial height, with design values ranging from 0.95 to 0.99.

The cross-sectional shape (fig. 6-56) of rocket turbine nozzles is square, or, more frequently, rectangular. They are closely spaced on a circular arc extending over a part of (partial admission), or all (full admission), the circumference. Most high-power turbines use full admission for better performance.

While the gases are passing through a nozzle and expanding, the direction of flow is changing from an approximately axial direction to one forming the angle α_1 (fig. 6-56) with the plane of rotation, at the nozzle exit. Thus the turning angle is $90^\circ - \alpha_1$. The angle θ_n of the nozzle centerline at the exit usually is the result of a design compromise. Theoretically, better efficiency is obtained through the use of a smaller nozzle exit angle, since the rotor blading work is larger and the absolute flow velocity at the rotor blade exit is smaller. However, a smaller nozzle exit angle means a larger angle of flow deflection within the nozzle, which causes higher friction losses. Design values of θ_n range from 15° to 30° . The actual effective discharge angle α_1 of the gas jet leaving the nozzle tends to be greater than θ_n , because of the unsymmetrical nozzle shape at the exit.

A sufficiently large nozzle passage aspect ratio, h_{nt}/b_{nt} , is desirable for better nozzle

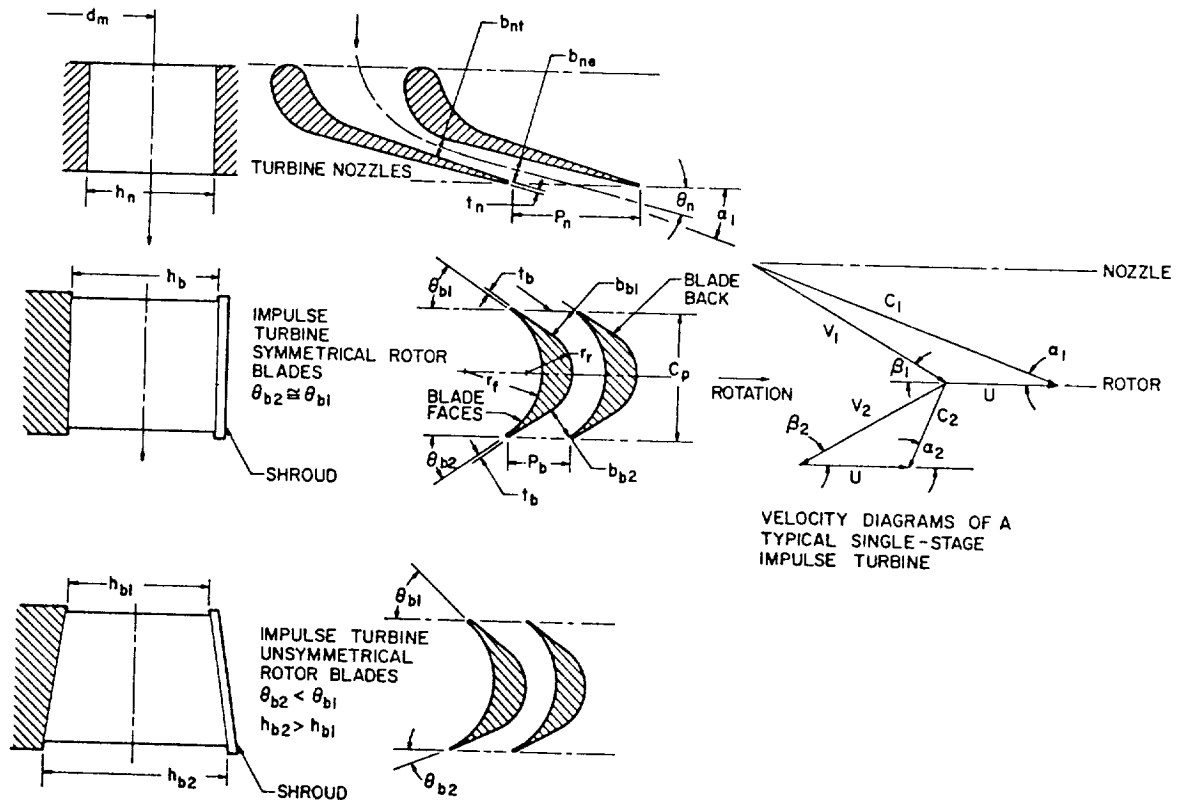


Figure 6-56.—Nozzles, rotor blades, and velocity diagrams of a typical single-stage impulse turbine.

efficiency. For a given nozzle height, an increase in aspect ratio can be secured by decreasing the nozzle pitch, P_n . However, a small pitch, and consequently a large number of nozzles, z_n , with attendant increase in wall surface, tends to increase friction losses. The determination of nozzle pitch thus also requires a design compromise. The following correlations are established for the calculation of nozzle flow areas:

Total nozzle throat area, in²:

$$A_{nt} = z_n b_{nt} h_{nt} \quad (6-124)$$

Total nozzle exit area, in²:

$$A_{ne} = \frac{144 \dot{w}_t}{\rho_1 C_1 \epsilon_{ne}} = z_n b_{ne} h_{ne} = z_n h_{ne} (P_n \sin \theta_n - t_n) \quad (6-125)$$

Pitch or nozzle spacing:

$$P_n = \pi \frac{d_m}{z_n} \quad (6-126)$$

where

- \dot{w}_t = turbine gas mass flow rate, lb/sec
- ρ_1 = density of the gases at nozzle exit, lb/ft³
- C_1 = gas spouting velocity at nozzle exit, ft/sec
- ϵ_{ne} = nozzle exit area coefficient
- h_{nt} = radial height at nozzle throat, in
- h_{ne} = radial height at nozzle exit, in
- b_{nt} = width normal to flow at nozzle throat, in
- b_{ne} = width normal to flow at nozzle exit, in
- z_n = number of nozzles
- θ_n = angle between nozzle exit centerline and plane of rotation, deg
- t_n = thickness of nozzle partition at exit, in
- d_m = mean diameter of nozzles and rotor blades, in

Turbine nozzle block and inlet gas manifold assembly can be made of, for instance, welded sections of forged Hastelloy C. However, the airfoil surfaces should be blended smoothly between the defined contour and the sections.

Design of Impulse Turbine Rotor Blades

The function of the rotor blades in an impulse turbine (figs. 6-55 and 6-56) is to transform a maximum of the kinetic energy of the gases ejected from the nozzles into useful work. Theoretically, there should be no change of gas pressure, temperature, or enthalpy in the rotor blades. In actual operation however, some gas expansion, i.e., reaction, usually occurs. Furthermore, the actual gas flow through the rotor blades deviates from ideal flow conditions because of friction, eddy currents, boundary layers, and reheating.

The velocity vector diagram shown in figure 6-56 describes graphically the flow conditions at the rotor blades of a single-stage, single-rotor turbine, based on the mean diameter d_m . The gases enter the rotor blades with an absolute velocity C_1 , and at an angle α_1 with the plane of rotation. The tangential or peripheral speed of the rotor blades at the mean diameter is U . V_1 and V_2 , the relative velocities at the blade inlet and outlet, differ, i.e., $V_1 > V_2$, due to friction losses. Ideally, the gas should leave the blades at very low absolute velocity C_2 and in a direction close to axial for optimum energy conversion in the blades. The forces generated at the rotor blades are a function of the change of momentum of the flowing gases. The following correlations may be established for design calculations of the rotor blades of a single-stage, single-rotor turbine.

Tangential force acting on the blades (lb/lb of gas flow/sec):

$$F_t = \frac{1}{g}(C_1 \cos \alpha_1 + C_2 \cos \alpha_2) \\ = \frac{1}{g}(V_1 \cos \beta_1 + V_2 \cos \beta_2) \quad (6-127)$$

Work transferred to the blades (ft-lb/lb of gas flow/sec):

$$E_b = \frac{U}{g}(C_1 \cos \alpha_1 + C_2 \cos \alpha_2) \\ = \frac{U}{g}(V_1 \cos \beta_1 + V_2 \cos \beta_2) \quad (6-128)$$

$$U = \frac{\pi d_m N}{720} \quad (6-129)$$

For subsequent calculations, the following relation will be useful:

$$\tan \beta_1 = \frac{C_1 \sin \alpha_1}{C_1 \cos \alpha_1 - U} \quad (6-130)$$

Axial thrust at blades, lb/lb of gas flow/sec

$$F_a = \frac{C_1 \sin \alpha_1 - V_2 \sin \beta_2}{g} \quad (6-131)$$

Blade velocity coefficient:

$$k_b = \frac{V_2}{V_1} \quad (6-132)$$

Blade efficiency:

$$\eta_b = \frac{\text{Work transferred to blades}}{\text{Kinetic energy input}} = \frac{E_b}{\frac{C_1^2}{2g}} \quad (6-133)$$

Ideally, η_b is a maximum for a single-rotor impulse turbine, when the turbine velocity ratio:

$$\frac{U}{C_1} = \frac{\cos \alpha_1}{2}$$

i.e., when $U = \frac{1}{2} C_{1t}$

where C_{1t} is the tangential component of C_1 .

$$\text{Max. ideal } \eta_b = \frac{\cos^2 \alpha_1}{2} \left(1 + k_b \frac{\cos \beta_2}{\cos \beta_1} \right) \quad (6-134)$$

If there is some reaction or expansion of the gas flowing through the blades, the relative gas flow velocity at the rotor blade outlet can be calculated as

$$V_2 = \sqrt{k_b^2 V_1^2 + 2gJ\eta_n \Delta H_{1-2}} \quad (6-135)$$

Amount of reheat in the rotor blades, Btu/lb of gas flow:

$$q_{br} = (1 - k_b^2) \frac{V_1^2}{2gJ} + (1 - \eta_n) \Delta H_{1-2}' \quad (6-136)$$

where

α_1, α_2 = absolute gas flow angles at the inlet and outlet of the rotor blades, deg

β_1, β_2 = relative gas flow angles at the inlet and outlet of the rotor blades, deg

C_1, C_2 = absolute gas flow velocities at the inlet and outlet of the rotor blades, ft/sec

V_1, V_2 = relative gas flow velocity at the inlet and outlet of the rotor blades, ft/sec

U = peripheral speed of the rotor, ft/sec

d_m = mean diameter of the rotor, in

η_n = equivalent nozzle efficiency applicable to the expansion process in the blades

$\Delta H_{1-2}'$ = isentropic enthalpy drop of the gases flowing through the rotor blades due to expansion or reaction, Btu/lb;
 $\Delta H_{1-2}' = 0$ if only impulse is exchanged

All parameters refer to the mean diameter d_m , unless specified otherwise. The turbine overall efficiency η_t defined by equation (6-19) can be established for a single-stage, single-rotor impulse turbine as

$$\eta_t = \eta_n \eta_b \eta_m \quad (6-137)$$

where

η_n = nozzle efficiency

η_b = rotor blade efficiency

η_m = machine efficiency indicating the mechanical, leakage, and disk-friction losses in the machine.

Equation (6-134) shows that the blade efficiency η_b improves when β_2 becomes much smaller than β_1 . Reduction of β_2 without decreasing the flow area at the blade exit can be achieved through an unsymmetrical blade design (fig. 6-56), where the radial blade height increases toward the exit. In actual designs, the amount of decrease of β_2 , or the increase of radial height, is limited considering incipient flow separation and centrifugal stresses. Generally, the β_2 of an unsymmetrical blade will be approximately $\beta_1 - (5^\circ \text{ to } 15^\circ)$. Equation (6-134) also indicates that η_b improves as α_1 is reduced.

Design values of k_b vary from 0.80 to 0.90. Design values of η_b range from 0.7 to 0.92.

Referring to figure 6-56, the radial height at the rotor inlet, h_b , is usually slightly larger (5 to 10 percent) than the nozzle radial height h_n . This height, together with the blade peripheral speed U , will determine the centrifugal stress in the blades. The mean diameter of the rotor blades is defined as $d_m = d_t - h_b$, where d_t is the rotor tip diameter. Pitch or blade spacing, P_b , is measured at the mean diameter d_m . There is no critical relationship between blade pitch P_b and nozzle pitch P_n . There just should be a sufficient number of blades in the rotor to direct the gas flow. The number of blades z_b to be employed is established by the blade aspect ratio, h_b/C_b and the solidity C_b/P_b , where C_b is the chord length of the rotor blades. The magnitude of the blade aspect ratio ranges from 1.3 to 2.5. Design values of blade solidity vary from 1.4 to 2. Best results will be determined by experiment. The number of rotor blades should have no common factor with the number of nozzles or of stator blades.

The blade face is concave, with radius r_f . The back is convex, with a circular arc of small radius r_f concentric with the face of the adjoining blade ahead. Two tangents to this arc to form the inlet and outlet blade angles θ_{b1} and θ_{b2} complete the blade back. The leading and trailing edges may have a small thickness t_b .

The inlet blade angle θ_{b1} should be slightly larger than the inlet relative flow angle β_1 . If $\theta_{b1} < \beta_1$, the gas stream will strike the backs of the blades at the inlet, exerting a retarding effect on the blades and causing losses. If $\theta_{b1} > \beta_1$, the stream will strike the concave faces of the blades and tend to increase the impulse. The outlet blade angle θ_{b2} is generally made equal to the outlet relative flow angle β_2 .

The mass flow rate \dot{w}_t through the various nozzle and blade sections of a turbine is assumed constant. The required blade flow areas can be calculated by the following correlations. Note that the temperature values used in calculating the gas densities at various sections must be corrected for reheating effects from friction and turbulence.

$$\dot{w}_t = \frac{\rho_1 V_1 A_{b1} \epsilon_{b1}}{144} = \frac{\rho_2 V_2 A_{b2} \epsilon_{b2}}{144} \quad (6-138)$$

Total blade inlet area, in²:

$$A_{b1} = z_b b_{b1} h_{b1} = z_b h_{b1} (P_b \sin \theta_{b1} - t_b) \quad (6-139)$$

Total blade exit area, in²:

$$A_{b2} = z_b b_{b2} h_{b2} = z_b h_{b2} (P_b \sin \theta_{b2} - t_b) \quad (6-140)$$

where

- P_b = pitch or rotor blade spacing
= $\pi d_m / z_b$, in (6-140a)
- ρ_1, ρ_2 = density of the gases at the inlet and outlet of the rotor blades, lb/ft³
- V_1, V_2 = relative gas flow velocities at the inlet and outlet of the rotor blades, ft/sec
- $\epsilon_{b1}, \epsilon_{b2}$ = area coefficients at inlet and outlet of the rotor blades
- z_b = number of blades
- h_{b1}, h_{b2} = radial height at the inlet and outlet of the rotor blades, in
- b_{b1}, b_{b2} = passage widths (normal to flow) at the inlet and outlet of the rotor blades, in
- θ_{b1}, θ_{b2} = rotor blade angles at inlet and outlet, deg
- t_b = thickness of blade edge at inlet and outlet, in

Typical constructions of rocket turbine rotor blades and disks are shown in figures 6-53, 6-55, 6-56, and 6-57. Usually, blades are designed with a shroud, to prevent leakage over the blade tips and to reduce turbulence and thus improve efficiency. Frequently the shroud forms an integral portion of the blade, the shroud sections fitting closely together when assembled. In other designs the shroud may form a continuous ring (fig. 6-55) which is attached to the blades by means of tongues at the blade tip, by rivets, or is welded to the shrouds. The blades may be either welded to the disk, or attached to it using "fir-tree" or other dovetail shapes.

The main loads to which a rotor blade is exposed can be divided into three types:

1. *Tension and bending due to centrifugal forces.*—The radial component of the centrifugal forces acting on the blade body produces a centrifugal tensile stress which is a maximum at the root section. As a remedy, blades are often tapered, with the thinner section at the tip, for lower centrifugal root stresses. The centroids

of various blade sections at different radii generally do not fall on a true radial line. Thus the centrifugal forces acting upon the offset centroids will produce bending stresses which also are a maximum at the root section.

2. *Bending due to gas loading.*—The tangential driving force and the axial thrust produced by the momentum change of the gases passing over the blades may be treated as acting at the midheight of the blade to determine the amount of bending induced.

3. *Bending due to vibration loads.*—The gas flow in the blade passages is not a uniform flow as assumed in theory, but varies cyclically from minimum to maximum. The resultant loads represent a dynamic force on the blades, having a corresponding cyclic variation. If the frequency of this force should become equal to the natural frequency of the blades, deflections may result which will induce bending stresses of considerable magnitude.

Detail stress analyses for rotor blades can be rather complex. A basic approach is to counteract a major portion of the bending moments from gas loading with the bending moments induced by the centrifugal forces at nominal operating speeds. This can be accomplished by careful

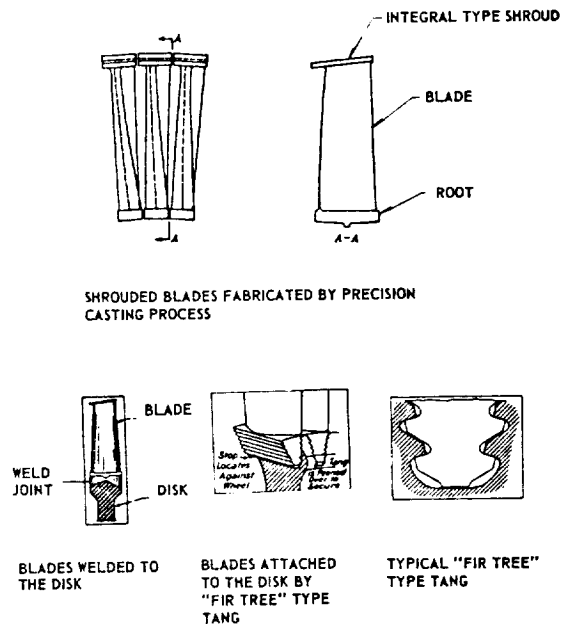


Figure 6-57.—Typical rotor blade constructions.

blade design. Thus the centrifugal tensile stresses become a first consideration in blade design, while other details such as centroid location and root configuration are established later to fulfill design requirements. The following correlations are established at the blade root section where stresses are most critical.

Centrifugal tensile stress at the root section of blade of uniform cross section, psi:

$$S_c = 0.0004572 \frac{1}{g} \rho_b h_b d_m N^2 \quad (6-141)$$

Centrifugal tensile stress at the root section of a tapered blade, psi:

$$S_{ct} = 0.0004572 \frac{1}{g} \rho_b h_b d_m N^2 \left[1 - \frac{\left(\frac{a_t}{a_r}\right)}{2} \left(1 + \frac{h_b}{3d_m}\right) \right] \quad (6-142)$$

Bending moment due to gas loading at the root section, in-lb:

$$M_g = \frac{h_b \dot{w}_t}{2 z_b} \sqrt{F_t^2 + F_a^2} \quad (6-143)$$

where

- ρ_b = density of the blade material, lb/in³
- h_b = average blade height, in
- d_m = mean diameter of the rotor, in
- N = turbine speed, rpm
- a_r = sectional area at the blade root, in²
- a_t = sectional area at the blade tip, in²
- \dot{w}_t = turbine gas flow rate, lb/sec
- z_b = number of blades
- F_t = tangential force acting on the blades, lb/lb/sec (eq. (6-127))
- F_a = axial thrust acting on the blades, lb/lb/sec (eq. (6-131))

The bending stresses at the root can be calculated from the resultant bending moment. The vibration stresses can be estimated from past design data. If the blade is fitted with a separate shroud, its centrifugal force produces additional stresses at the root. The total stress at the root section is obtained by adding these stresses to those caused by the centrifugal forces acting on the blades.

The stresses in a turbine rotor disk are induced by (1) the blades, and (2) the centrifugal forces acting on the disk material itself. In addition, there will be shear stresses resulting from the torque. As seen in figure 6-55, turbine disks are generally held quite thick at the axis, but taper off to a thinner disk rim to which the blades are attached. In single-rotor applications, it is possible to design a disk so that both radial and tangential stresses are uniform at all points, shear being neglected. In multi-rotor applications, it is difficult to do this because of the greatly increased axial length and the resulting large gaps between rotor and stator disks.

Equation (6-144) may be used to estimate the stresses in a uniform stress turbine disk, neglecting rotor blade effects:

$$S_d = 0.000114 \frac{1}{g} \rho_d \frac{d_d^2 N^2}{\log_e \left(\frac{t_0}{t_r}\right)} \quad (6-144)$$

where

- S_d = centrifugal tensile stress of a constant stress turbine disk, psi
- ρ_d = density of the disk material, lb/in³
- d_d = diameter of the disk, in
- N = turbine speed, rpm
- t_0 = thickness of the disk at the axis, in
- t_r = thickness of the disk rim at d_d , in

Equation (6-144a) permits estimation of the stresses in any turbine disk, neglecting effects of the rotor blades:

$$S_d = 0.0004425 \frac{1}{g} W_d r_i \frac{N^2}{a_d} \quad (6-144a)$$

where

- S_d = centrifugal tensile stress of the turbine disk, psi
- W_d = weight of the disk, lb
- r_i = distance of the center of gravity of the half disk from the axis, in
- a_d = disk cross-sectional area, in²
- N = turbine speed, rpm

For good turbine design, it is recommended that at maximum allowable design rotating speed, the S_d calculated by equation (6-144a) should be about 0.75 to 0.8 material yield strength.

Turbine rotor blades and disks are made of high-temperature alloys of three different base

materials: iron, nickel, and cobalt, with chromium forming one of the major alloying elements. Tensile yield strength of 30 000 psi minimum at a working temperature of 1800°F is an important criterion for selection. Other required properties include low creep rate, oxidation and erosion resistance, and endurance under fluctuating loads. Haynes Stellite, Vascojet, and Inconel X are alloys frequently used. The rotor blades are fabricated either by precision casting or by precision forging methods. Rotor disks are best made of forgings for optimum strength.

Design of Single-Stage, Two-Rotor Velocity-Compounded Impulse Turbines (figs. 6-9, 6-55, and 6-58)

In most impulse turbines, the number of rotors is limited to two. It is assumed that in a single-stage, two-rotor, velocity-compounded impulse turbine, expansion of the gases is completed in the nozzle, and that no further pressure change occurs during gas flow through the moving blades. As mentioned earlier, the two-rotor, velocity-compounded arrangement is best suited for low-speed turbines. In this case, the gases ejected from the first rotor blades still possess considerable kinetic energy. They are, therefore, redirected by a row of stationary blades into a second row of rotor blades, where additional work is extracted from the gases, which usually leave the second rotor blade row at a moderate velocity and in a direction close to the axial.

The velocity diagrams of a single-stage, two-rotor, velocity-compounded impulse turbine are shown in figure 6-58, based on the mean rotor diameter. The peripheral speed of the rotor blades at this diameter is represented by U . The gases leave the nozzles and enter the first rotor blades with an absolute velocity C_1 , at an angle α_1 with the plane of rotation. V_1 and V_2 are the relative flow velocities in ft/sec at the inlet and outlet of the first rotor blades. The gases leave the first rotor blades and enter the stationary blades at an absolute flow velocity C_2 , and at an angle α_2 . After passing over the stationary blades, the gases depart and enter the second rotor blades at an absolute flow velocity C_3 , and at an angle α_3 . V_3 and V_4 are the relative inlet and outlet flow velocities at the second rotor

blades. Angles β_1 , β_2 , β_3 , and β_4 represent the flow directions of V_1 , V_2 , V_3 , and V_4 .

As with single-rotor turbines, the exit velocity from any row of blades (rotary or stationary) is less than the inlet velocity, because of friction losses. It can be assumed that the blade velocity coefficient k_b has the same value for any row of blades:

$$k_b = \frac{V_2}{V_1} = \frac{C_3}{C_2} = \frac{V_4}{V_3} \quad (6-145)$$

In a multirotor turbine, the total work transferred is the sum of that of the individual rotors:

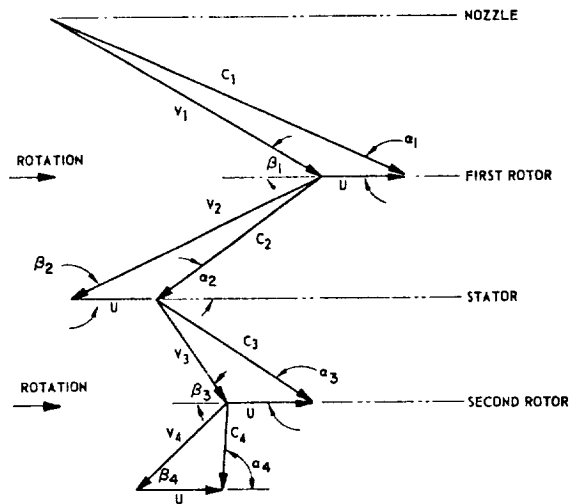


Figure 6-58.—Velocity diagrams of a typical single-stage, two-rotor, velocity-compounded impulse turbine.

Total work transferred to the blades of a two-rotor turbine, ft-lb/lb of gas flow/sec

$$\begin{aligned} E_{2b} &= \frac{U}{g} (C_1 \cos \alpha_1 + C_2 \cos \alpha_2 \\ &\quad + C_3 \cos \alpha_3 + C_4 \cos \alpha_4) \\ &= \frac{U}{g} (V_1 \cos \beta_1 + V_2 \cos \beta_2 \\ &\quad + V_3 \cos \beta_3 + V_4 \cos \beta_4) \quad (6-146) \end{aligned}$$

Combined nozzle and blade efficiency of a two-rotor turbine:

$$\eta_{nb} = \frac{E_2 b}{J\Delta H} \quad (6-147)$$

where

ΔH = overall isentropic enthalpy drop of the turbine gases, Btu/lb
 = total available energy content of the turbine gases (eq. 6-17)

Equation (6-137) can be rewritten for the turbine overall efficiency η_t of a two-rotor turbine as

$$\eta_t = \eta_{nb} \eta_m \quad (6-148)$$

Ideally, η_{nb} is a maximum for the single-stage, two-rotor, velocity-compounded impulse turbine velocity ratio

$$\frac{U}{C_1} = \frac{\cos \alpha_1}{4}$$

i.e., when $U = \frac{1}{4} C_{1t}$. The workload for the second rotor of a two-rotor, velocity-compounded turbine is designed at about one-fourth of the total work.

The design procedures for the gas flow passages of the rotor and stationary blades of a single-stage, two-rotor turbine are exactly the same as those for a single-rotor turbine. However, velocities and angles of flow change with each row of blades. As a result, the radial height of symmetrical blades increases with each row, roughly as shown in figure 6-55. The effects of reheating (increase of gas specific volume) in the flow passages must be taken into account when calculating the gas densities at various sections. Equation (6-136) may be used to estimate the amount of reheat at each row of blades. Also see sample calculation (6-11) and figure 6-60 for additional detail.

In the calculations for multirow unsymmetrical blades, the radial heights at the exit side of each row are determined first by equation (6-140). The radial heights at the blade inlets are then made slightly larger, approximately 8 percent, than those at the exit of the preceding row.

Design of Two-Stage, Two-Rotor Pressure-Compounded Impulse Turbines (figs. 6-10, 6-14 and 6-59)

An operational schematic of a typical two-stage, two-rotor, pressure-compounded impulse turbine and its velocity diagrams at the mean diameter are shown in figures 6-10 and 6-59. Each stage of a pressure-compounded impulse turbine may be regarded as a single-stage impulse turbine rotating in its own individual housing. Most of the design characteristics of a single-stage turbine are applicable to the individual stages. The gas-spouting velocities C_1 and C_3 , at flow angles α_1 and α_3 , of the first- and second-stage nozzles, are designed to be approximately the same. V_1, V_2, V_3 , and V_4 represent the relative flow velocities at inlets and outlets of the rotor blades. $\beta_1, \beta_2, \beta_3$, and β_4 are the corresponding flow angles for V_1, V_2, V_3 , and V_4 . The second-stage nozzles are designed to receive the gas flow discharged from the first-stage rotor blades at an absolute velocity C_2 , and to turn it efficiently to a desired angle α_3 . Simultaneously, the gases are accelerated to a desired velocity C_3 , through expansion to a lower pressure. The flow at the outlet of the second rotor has an absolute velocity C_4 and a flow angle α_4 . U is the rotor peripheral speed at the mean effective diameter d_m .

The total work performed in the turbine is the sum of that of the separate stages. These may be designed to divide the load equally (i.e., the

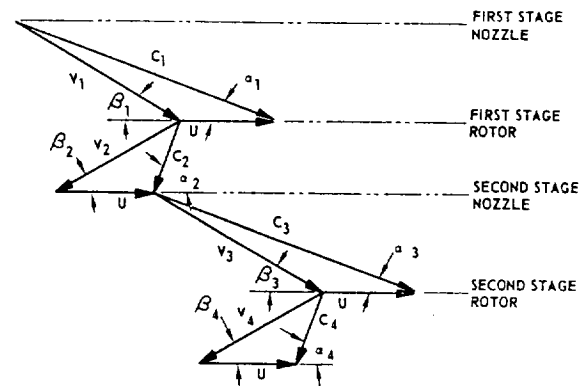


Figure 6-59.—Velocity diagrams of a typical two-stage, two-rotor, pressure-compounded impulse turbine.

velocity diagrams of each stage are identical or $C_1 = C_3$, $C_2 = C_4$, $a_1 = a_3$, $a_2 = a_4$, etc.). The friction losses occurring in the first stage is passed on in the gas stream as additional enthalpy and increases the available energy for the second stage. Also, the kinetic energy of the gases leaving the first stage is largely used and not entirely lost as with a single-stage turbine. The carryover ratio r_c , i.e., the ratio of the kinetic energy actually utilized as inlet energy by the second-stage nozzles to the total kinetic energy of the gases leaving the first stage, can vary from 0.4 to close to unity. The axial distance between the first-stage rotor and the second-stage nozzle, as well as the leakages through the sealing diaphragm between stages, should be minimized for optimum carryover.

The determination of the right enthalpy drop resulting in equal work for each stage may require a trial-and-error approach, in view of the effects of reheating. Or, the proper enthalpy drop may be estimated from previous designs and test data. With the velocity coefficients for nozzles and blades given by past or concurrent experiments, equations (6-122) and (6-136) can be used to estimate the amount of reheating.

Most equations established for the single-stage turbines may be employed in the design calculations for two-stage turbines. The following additional correlations are available for the design of second stage nozzles:

$$T_{2t} = T_2 + r_c \frac{C_2^2}{2gJC_p} \quad (6-149)$$

$$P_{2t} = P_2 \left(\frac{T_{2t}}{T_2} \right)^{\frac{\gamma}{\gamma-1}} \quad (6-150)$$

$$C_3 = k_n \sqrt{2gJC_p T_{2t} \left[1 - \left(\frac{p_3}{p_{2t}} \right)^{\frac{\gamma-1}{\gamma}} \right]} \\ = k_n \sqrt{r_c C_2^2 + 2gJ\Delta H_{2-3'}} \quad (6-151)$$

$$(A_{nt})_2 = \frac{\dot{w}_t}{\epsilon_{nt} p_{2t} \sqrt{\frac{g\gamma}{RT_{2t}} \left[\frac{2}{\gamma+1} \right]^{\frac{\gamma+1}{\gamma}}}} \quad (6-152)$$

where

- T_{2t} = turbine gas total (stagnation) temperature at second-stage nozzle inlet, °R
- T_2 = turbine gas static temperature at second-stage nozzle inlet, °R
- p_{2t} = turbine gas total pressure at second-stage nozzle inlet, psia
- p_2 = turbine gas static pressure at second-stage nozzle inlet, psia
- C_2 = absolute gas flow velocity at first-stage rotor blade outlet, ft/sec
- C_3 = gas-spouting velocity at second-stage nozzle exit, ft/sec
- r_c = second-stage carryover ratio of kinetic energy
- C_p = turbine gas specific heat at constant pressure, Btu/lb-deg F
- γ = turbine gas specific heat ratio
- $\Delta H_{2-3'}$ = isentropic enthalpy drop of the gases flowing through the second-stage nozzles due to expansion, Btu/lb
- $(A_{nt})_2$ = required total second-stage nozzle area, in²
- k_n = nozzle velocity coefficient
- ϵ_{nt} = nozzle throat area coefficient

Sample Calculation (6-11)

From sample calculation (6-5), the following data have been obtained for the turbine of the A-1 stage engine turbopump.

Turbine gas mixture ratio, $LO_2/RP-1 = 0.408$

Turbine gas specific heat at constant pressure, $C_p = 0.653$ Btu/lb-deg F

Turbine gas specific heat ratio, $\gamma = 1.124$

Turbine gas constant, $R = 53.6$ ft/°R

Gas total temperature at turbine inlet, $T_0 = 1860$ °R

Gas total pressure at turbine inlet, $p_0 = 640$ psia

Gas static pressure at turbine exhaust, $p_e = 27$ psia

Total available energy content of the turbine gases, $\Delta H = 359$ Btu/lb

Turbine gas flow rate, $\dot{w}_t = 92$ lb/sec

Turbine shaft speed, $N = 7000$ rpm

Overall turbine efficiency (when using velocity-compounded wheels), $\eta_t = 58.2$ percent

In addition, the following design data are set forth:

- Nozzle aspect ratio = 9.7
- Nozzle velocity coefficient, $k_n = 0.96$
- Nozzle throat area coefficient, $\epsilon_{nt} = 0.97$
- Nozzle exit area coefficient, $\epsilon_{ne} = 0.95$
- Rotor and stator blade velocity coefficient, $k_b = 0.89$
- Rotor and stator blade exit area coefficient, $\epsilon_{b2} = 0.95$
- Chord length of rotor and stator blades, $C_b = 1.4$ in
- Partition thickness at the exit of nozzles and blades, $t_n = t_b = 0.05$ in
- Solidity of first rotor blades = 1.82
- Solidity of stator blades = 1.94
- Solidity of second rotor blades = 1.67

(a) Determine the velocity diagrams and principal dimensions of the single-stage, two-rotor, velocity-compounded, impulse-type turbine for the A-1 stage engine turbopump, with about 6 percent reaction in rotor and stator blades downstream of the nozzles.

(b) Determine the velocity diagrams of an alternate two-stage, two-rotor, pressure-compounded, impulse-type turbine for the A-1 stage engine turbopump, with equal work in each stage and about 3 percent reaction in the rotor blades downstream of the nozzles of each stage.

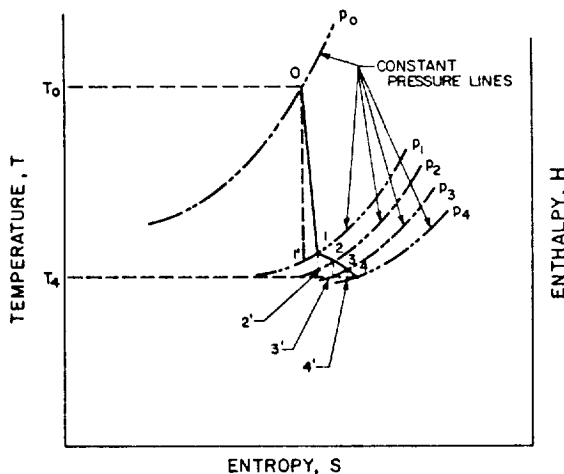


Figure 6-60.—Temperature-entropy-enthalpy diagram of the gas processes in a single-stage, two-rotor, velocity-compounded impulse turbine with small amount of reactions downstream of the nozzles.

Solution

(a) Single-stage, two-rotor, velocity-compounded impulse turbine.

A representative velocity diagram for this turbine is shown in figure 6-58. Figure 6-60 represents the temperature-entropy-enthalpy diagram for the gas processes involved in the operation of this turbine. The following subscripts denote the various points and processes listed:

- 0, 1, 2, 3, 4 = Points representing inlet conditions at the nozzles; first rotor blades; stator blades; second rotor blades; and the exit conditions of the second rotor blades.
- 1', 2', 3', 4' = Points representing exit conditions at the nozzles; first rotor blades; stator blades; and second rotor blades, for an ideal isentropic expansion process.
- 0-1', 1-2', 2-3', 3-4' = Path of an ideal isentropic expansion process in the nozzles; first rotor blades; stator blades; and second rotor blades.
- 0-1, 1-2, 2-3, 3-4 = Path of actual processes in the nozzles; first rotor blades; stator blades; and second rotor blades.
- 1'-1, 2'-2, 3'-3, 4'-4 = Differences along constant pressure lines, between ideal isentropic expansion processes and actual processes, due to friction losses and reheating in the nozzles, first rotor blades, stator blades, and second rotor blades

Point "0"—Nozzle Inlet

- T_0 = nozzle inlet total temperature = turbine inlet total temperature = 1860°R
- p_0 = nozzle inlet total pressure = turbine inlet total pressure = 640 psia
- ΔH = overall isentropic enthalpy drop of the turbine gases = total available energy content of the turbine gases = 359 Btu/lb
- η_n = nozzle efficiency = $k_n^2 = (0.96)^2 = 0.92$

Point "1"—Nozzle exit = First Rotor Blade Inlet

Since about 6 percent of the overall isentropic enthalpy drop ΔH is assumed to occur in the rotor and stator blades, the isentropic enthalpy drop in the nozzles

$$\Delta H_{0-1'} = \Delta H(1 - 0.06) = 359 \times 0.94 = 337.5 \text{ Btu/lb}$$

We can write:

$$\Delta H_{0-1'} = C_p T_0 \left[1 - \left(\frac{p_1}{p_0} \right)^{\frac{\gamma-1}{\gamma}} \right]$$

From this, the gas static pressure at the nozzle exit

$$\begin{aligned} p_1 &= p_0 \left[1 - \frac{\Delta H_{0-1'}}{C_p T_0} \right]^{\frac{\gamma}{\gamma-1}} \\ &= 640 \times \left[1 - \frac{337.5}{0.653 \times 1860} \right]^{\frac{1.124}{0.124}} \\ &= 640 \times (0.722)^{9.06} = 640 \times 0.053 = 33.94 \text{ psia} \end{aligned}$$

From equation (6-121), the gas spouting velocity at the nozzle exit

$$C_1 = k_n \sqrt{2gJ\Delta H_{0-1'}} = 0.96 \sqrt{16.9 \times 10^6} = 3940 \text{ fps}$$

From equation (6-122), the amount of reheat in the nozzles

$$q_{nr} = \frac{(1 - k_n^2) C_1^2}{k_n^2 2gJ} = \frac{0.08 \times 15524000}{0.92 \times 64.4 \times 778} = 27 \text{ Btu/lb}$$

Referring to figure 6-60, the gas temperature at the nozzle exit, following an isentropic expansion

$$T_{1'} = T_0 - \frac{\Delta H_{0-1'}}{C_p} = 1860 - \frac{337.5}{0.653} = 1344^\circ \text{R}$$

The actual gas static temperature at the nozzle exit

$$T_1 = T_{1'} + \frac{q_{nr}}{C_p} = 1344 + \frac{27}{0.653} = 1385^\circ \text{R}$$

The gas density at the nozzle exit

$$\rho_1 = \frac{p_1}{T_1} \times \frac{144}{R} = \frac{33.94 \times 144}{1385.4 \times 53.6} = 0.0658 \text{ lb/ft}^3$$

We will use an angle α_1 of 25° for the spouting-gas-flow direction at the nozzle exit.

Ideally, the efficiency η_{nb} of a two-rotor, velocity-compounded impulse turbine is a maximum when the turbine velocity ratio

$$\frac{U}{C_1} = \frac{\cos \alpha_1}{4}$$

From this, the peripheral speed at the mean diameter of the rotor

$$\begin{aligned} U &= C_1 \frac{\cos \alpha_1}{4} = 3940 \times \frac{\cos 25^\circ}{4} \\ &= 3940 \times 0.226 = 890 \text{ fps} \end{aligned}$$

From equation (1-129), the turbine rotor mean diameter

$$d_m = \frac{720 U}{\pi N} = \frac{720 \times 890}{\pi \times 7000} = 29.1 \text{ in}$$

From equation (1-130), the relative gas flow angle β_1 at the inlet to the first rotor blade can be calculated:

$$\begin{aligned} \tan \beta_1 &= \frac{C_1 \sin \alpha_1}{C_1 \cos \alpha_1 - U} = \frac{3940 \times 0.423}{3940 \times 0.906 - 890} = 0.622 \\ \beta_1 &= 31^\circ 53' \end{aligned}$$

Referring to figure 6-58, the relative gas flow velocity at the first rotor blade inlet

$$\begin{aligned} V_1 &= \frac{C_1 \sin \alpha_1}{\sin \beta_1} = \frac{3940 \times \sin 25^\circ}{\sin 31^\circ 53'} \\ &= \frac{3940 \times 0.423}{0.528} = 3156 \text{ fps} \end{aligned}$$

Point "2"—First Rotor Blade Exit = Stator Blade Inlet

Assume that the given 6 percent reaction downstream of the nozzles is equally divided between the two rotors and the stator. Then the isentropic enthalpy drop in the first rotor blade can be approximated as

$$\Delta H_{1-2'} = \frac{0.06}{3} \times 359 = 7.18 \text{ Btu/lb}$$

Using equation (6-135), the relative gas flow velocity at the exit of the first rotor blades

$$\begin{aligned}
 V_2 &= \sqrt{k_b^2 V_1^2 + 2gJ\eta_n \Delta H_{1-2}'} \\
 &= \sqrt{(0.89 \times 3156)^2 + 64.4 \times 778 \times 0.92 \times 7.18} \\
 &= 2866 \text{ fps}
 \end{aligned}$$

From equation (6-136), the amount of reheat in the first rotor blades,

$$\begin{aligned}
 q_{br1} &= (1 - k_b^2) \frac{V_1^2}{2gJ} + (1 - \eta_n) \Delta H_{1-2}' \\
 &= [1 - (0.89)^2] \times \frac{(3156)^2}{64.4 \times 778} + (1 - 0.92) \times 7.18 \\
 &= 41.975 \text{ Btu/lb}
 \end{aligned}$$

The static gas pressure at the first rotor blade exit

$$\begin{aligned}
 p_2 &= p_1 \left[1 - \frac{\Delta H_{1-2}'}{C_p T_1} \right]^{\frac{\gamma}{\gamma-1}} \\
 &= 33.94 \times \left[1 - \frac{7.18}{0.653 \times 1385} \right]^{9.06} \\
 &= 33.94 \times 0.93 = 31.6 \text{ psia}
 \end{aligned}$$

The gas static temperature at the exit of the first rotor blade row following an isentropic expansion

$$T_2' = T_1 - \Delta H_{1-2}' / C_p = 1385 - 7.18 / 0.653 = 1374^\circ \text{ R}$$

The actual static gas temperature at the first rotor blade row exit

$$T_2 = T_2' + \frac{q_{br2}}{C_p} = 1374 + \frac{41.975}{0.653} = 1438^\circ \text{ R}$$

Gas density at the first rotor blade exit

$$\rho_2 = \frac{144 p_2}{RT_2} = \frac{144 \times 31.6}{53.6 \times 1438} = 0.059 \text{ lb/ft}^3$$

We use an angle β_2 of 25° for the relative gas flow direction at the first rotor blade exits (unsymmetrical blades). The absolute flow angle α_2 at the first rotor blade exits can be calculated from

$$\begin{aligned}
 \tan \alpha_2 &= \frac{V_2 \sin \beta_2}{V \cos \beta_2 - U} = \frac{2866 \times \sin 25^\circ}{2866 \times \cos 25^\circ - 890} = 0.707 \\
 \alpha_2 &= 35^\circ 15'
 \end{aligned}$$

The absolute flow velocity at the first rotor blade exit

$$C_2 = \frac{V_2 \sin \beta_2}{\sin \alpha_2} = \frac{2866 \times \sin 25^\circ}{\sin 35^\circ 15'} = \frac{1210}{0.577} = 2080 \text{ fps}$$

Point "3"—Stator Blade Exit = Second Rotor Blade Inlet

The isentropic enthalpy drop in the stator blades

$$\Delta H_{2-3}' = \Delta H_{1-2}' = 7.18 \text{ Btu/lb}$$

Analogous to equation (6-135), the absolute gas flow velocity at the stator blade inlets

$$\begin{aligned}
 C_3 &= \sqrt{k_b^2 C_2^2 + 2gJ\eta_n \Delta H_{2-3}'} \\
 &= \sqrt{(0.89 \times 2080)^2 + 64.4 \times 778 \times 0.92 \times 7.18} \\
 &= 1938 \text{ fps}
 \end{aligned}$$

Reheat in the stator blades

$$\begin{aligned}
 q_{bs} &= (1 - k_b^2) \frac{C_2^2}{2gJ} + (1 - \eta_n) \Delta H_{2-3}' \\
 &\quad \text{(Analogous to eq. (6-136))}
 \end{aligned}$$

$$\begin{aligned}
 &= [1 - (0.89)^2] \times \frac{(2080)^2}{64.4 \times 778} + (1 - 0.92) \times 7.18 \\
 &= 18.53 \text{ Btu/lb}
 \end{aligned}$$

The static gas pressure at the stator blade exits

$$\begin{aligned}
 p_3 &= p_2 \left[1 - \frac{\Delta H_{2-3}'}{C_p T_2} \right]^{\frac{\gamma}{\gamma-1}} = 31.6 \times \left[1 - \frac{7.18}{0.653 \times 1438} \right]^{9.06} \\
 &= 29.42 \text{ psia}
 \end{aligned}$$

Gas static temperature at the stator blade exits following an isentropic expansion

$$T_3' = T_2 - \Delta H_{2-3}' / C_p = 1438 - 7.18 / 0.653 = 1427^\circ \text{ R}$$

Actual static gas temperature at the stator blade exits

$$T_3 = T_3' + \frac{q_{bs}}{C_p} = 1427 + \frac{18.53}{0.653} = 1456^\circ \text{R}$$

Gas density at the stator blade exit

$$\rho_3 = \frac{144 p_3}{R T_3} = \frac{144 \times 29.42}{53.6 \times 1456} = 0.0544 \text{ lb/ft}^3$$

We use an angle α_3 of 35° for the absolute gas flow direction at the stator blade exit ($\alpha_3 \cong \alpha_2$). The relative flow angle β_3 at the stator blade exit can be calculated from

$$\tan \beta_3 = \frac{C_3 \sin \alpha_3}{C_3 \cos \alpha_3 - U} = \frac{1938 \times 0.574}{1938 \times 0.819 - 890} = 1.596$$

$$\beta_3 = 57^\circ 56'$$

The relative flow velocity at the stator blade exit

$$V_3 = \frac{C_3 \sin \alpha_3}{\sin \beta_3} = \frac{1938 \times 0.574}{0.847} = 1312 \text{ fps}$$

Point "4" - Second Rotor Blade Exit

The isentropic enthalpy drop in the second rotor blades

$$\Delta H_{3-4'} = \Delta H_{1-2'} = 7.18 \text{ Btu/lb}$$

The relative gas flow velocity at the second rotor blade exit

$$V_4 = \sqrt{k_b^2 V_3^2 + 2 g J \eta_n \Delta H_{3-4'}}$$

$$= \sqrt{(0.89 \times 1312)^2 + 64.4 \times 778 \times 0.92 \times 7.18}$$

$$= 1306 \text{ fps}$$

The amount of reheat in the second rotor blades

$$q_{br2} = (1 - k_b^2) \frac{V_3^2}{2 g J} + (1 - \eta_n) \Delta H_{3-4'}$$

$$= [1 - (0.89)^2] \times \frac{(1312)^2}{64.4 \times 778} + (1 - 0.92) \times 7.18$$

$$= 7.73 \text{ Btu/sec}$$

Gas static pressure at the second rotor blade exit

$$p_4 = p_3 \left[1 - \frac{\Delta H_{3-4'}}{C_p T_3} \right]^{\frac{\gamma}{\gamma-1}}$$

$$= 29.42 \times \left[1 - \frac{7.18}{0.653 \times 1456} \right]^{9.06}$$

$$= 27.46 \text{ psia} > 27 \text{ psia } (p_e)$$

p_4 is slightly higher than the turbine exit pressure (underexpansion), because of the reheating effects.

The gas static temperature at the second rotor blade exits following an isentropic expansion

$$T_4' = T_3 - \Delta H_{3-4'} / C_p = 1456 - \frac{7.18}{0.653} = 1445 \text{ Btu/lb}$$

The actual gas static temperature at the second rotor blade exit

$$T_4 = T_4' + \frac{q_{br2}}{C_p} = 1445 + \frac{7.73}{0.653} = 1457^\circ \text{R}$$

Gas density at the second rotor blade exits

$$\rho_4 = \frac{144 p_4}{R T_4} = \frac{144 \times 27.46}{53.6 \times 1457} = 0.0506 \text{ lb/ft}^3$$

We use an angle β_4 of 44° for the relative gas flow direction at the second rotor blade exits (unsymmetrical blades). The absolute flow angle α_4 at the second rotor blade exits can be calculated from

$$\tan \alpha_4 = \frac{V_4 \sin \beta_4}{V_4 \cos \beta_4 - U} = \frac{1306 \times 0.695}{1306 \times 0.719 - 890} = 18.5$$

$$\alpha_4 = 86^\circ 55'$$

The absolute flow velocity at the second rotor blade exits

$$C_4 = \frac{V_4 \sin \beta_4}{\sin \alpha_4} = \frac{1306 \times 0.695}{0.9985} = 908 \text{ fps}$$

Nozzle Dimensions

From equation (6-123), the required total nozzle throat area

$$A_{nt} = \frac{\dot{w}_t}{\epsilon_{nt} p_0 \sqrt{\frac{g \gamma \left[\frac{2}{\gamma+1} \right]^{\frac{\gamma+1}{\gamma-1}}}{RT_0}}}$$

$$= \frac{92}{0.97 \times 640 \sqrt{\frac{32.2 \times 1.124 (0.94)^{17.15}}{53.6 \times 1860}}}$$

$$= 13.22 \text{ in}^2$$

We use a radial height h_{nt} of 1.5 inches at the nozzle throat. Thus the nozzle width at the throat

$$b_{nt} = \frac{h_{nt}}{\text{Nozzle aspect ratio}} = \frac{1.5}{9.7} = 0.1548 \text{ in}$$

The number of nozzles

$$z_n = \frac{A_{nt}}{b_{nt} h_{nt}} = \frac{13.22}{0.1548 \times 1.5} = 57$$

Pitch or nozzle spacing

$$P_n = \frac{\pi d_m}{z_n} = \frac{\pi \times 29.1}{57} = 1.604 \text{ in}$$

We allow 2° between nozzle exit angle θ_n and nozzle spouting-gas flow angle α_1 ; thus

$$\theta_n = \alpha_1 - 2 = 25 - 2 = 23^\circ$$

From equation (6-125), the required total nozzle exit area,

$$A_{ne} = \frac{144 \dot{w}_t}{\rho_1 C_1 \epsilon_{ne}} = \frac{144 \times 92}{0.0658 \times 3940 \times 0.95} = 53.75 \text{ in}^2$$

Combining equations (6-125) and (6-126), we obtain radial height and width at the nozzle exit:

$$h_{ne} = \frac{A_{ne}}{\pi d_m \sin \theta_n - z_n t_n} = \frac{53.75}{\pi \times 29.1 \times 0.391 - 57 \times 0.05}$$

$$= 1.64 \text{ in}$$

$$b_{ne} = \frac{A_{ne}}{z_n h_{ne}} = \frac{53.75}{57 \times 1.64} = 0.576 \text{ in}$$

First Rotor Blade Dimensions (at d_m)

The pitch or blade spacing

$$P_{br1} = \frac{\text{Blade chord length } C_b}{\text{Blade solidity}} = \frac{1.4}{1.82} = 0.769 \text{ in}$$

From equation (6-140a), the number of blades

$$z_{br1} = \frac{\pi d_m}{P_{br1}} = \frac{\pi \times 29.1}{0.769} = 119$$

Allow $2^\circ 7'$ between inlet blade angle θ_{b1r1} and inlet relative flow angle β_1 ; thus

$$\theta_{b1r1} = \beta_1 + 2^\circ 7' = 31^\circ 53' + 2^\circ 7' = 34^\circ$$

Make exit blade angle θ_{b2r1} equal to exit relative flow angle β_2

$$\theta_{b2r1} = \beta_2 = 25^\circ$$

We select a blade radial height at the inlet

$$h_{b1r1} = h_{ne} (1 \times 0.08) = 1.64 \times 1.08 = 1.77 \text{ in}$$

The blade passage width at the inlet

$$b_{b1r1} = P_{br1} \sin \theta_{b1r1} - t_b = 0.769 \times 0.559 - 0.05$$

$$= 0.379 \text{ in}$$

From equation (6-138), the required total blade exit area

$$A_{b2r1} = \frac{144 \dot{w}_t}{\rho_2 V_2 \epsilon_{b2}} = \frac{144 \times 92}{0.059 \times 2866 \times 0.95} = 82.5 \text{ in}^2$$

Combining equations (1-139) and (1-140a), we obtain the blade radial height at the exit

$$h_{b2r1} = \frac{A_{b2r1}}{\pi d_m \sin \theta_{b2r1} - z_{br1} t_b}$$

$$= \frac{82.5}{\pi \times 29.1 \times 0.423 - 119 \times 0.05} = 2.52 \text{ in}$$

The blade passage width at the exit

$$b_{b2r1} = P_{br1} \sin \theta_{b2r1} - t_b = 0.769 \times 0.443 - 0.05$$

$$= 0.291 \text{ in}$$

The mean blade radial height

$$h_{br1} = \frac{1.77 + 2.52}{2} = 2.145 \text{ in}$$

Assume a tapered blade with shroud, and that it is subject to approximately the same tensile stresses from centrifugal forces, as would be a uniform blade without shroud. The blades shall be made of Timken alloy, with a density $\rho_b = 0.3 \text{ lb/in}^3$. Check the centrifugal tensile stresses at the root section using equation (6-141).

$$\begin{aligned} S_{cr1} &= 0.0004572 \frac{1}{g} \rho_b h_{br1} d_m N^2 \\ &= 0.0004572 \times \frac{0.3}{32.2} \times 2.145 \times 29.1 \times (7000)^2 \\ &= 13\,050 \text{ psi} \end{aligned}$$

Stator Blade Dimensions

Pitch or blade spacing

$$P_{bs} = \frac{\text{Blade chord length } C_b}{\text{Blade solidity}} = \frac{1.4}{1.94} = 0.721 \text{ in}$$

From equation (6-140a), the number of blades

$$z_{bs} = \frac{\pi d_m}{P_{bs}} = \frac{\pi \times 29.1}{0.721} = 127$$

Allowing $2^\circ 24'$ between inlet blade angle θ_{b1s} and inlet absolute flow angle α_2

$$\theta_{b1s} = \alpha_2 + 2^\circ 24' = 34^\circ 36' + 2^\circ 24' = 37^\circ$$

We hold exit blade angle θ_{b2s} equal to exit absolute flow angle α_3 :

$$\theta_{b2s} = \alpha_3 = 35^\circ$$

From equation (6-149), blade radial height at the inlet

$$h_{b1s} = 1.08 \times 2.52 = 2.72 \text{ in}$$

The blade passage width at the inlet

$$\begin{aligned} h_{b1s} &= P_{bs} \sin \theta_{b1s} - t_b = 0.721 \times 0.602 - 0.05 \\ &= 0.384 \text{ in} \end{aligned}$$

Using equation (6-138), we obtain the required total blade exit area

$$A_{b2s} = \frac{144 \dot{w}_t}{\rho_3 C_3 \epsilon_{b2}} = \frac{144 \times 92}{0.0544 \times 1938 \times 0.95} = 132.5 \text{ in}^2$$

Combining equations (6-139) and (6-140a), we calculate the blade radial height at the exit

$$\begin{aligned} h_{b2s} &= \frac{A_{b2s}}{\pi d_m \sin \theta_{b2s} - z_{bs} t_b} \\ &= \frac{132.5}{\pi \times 29.1 \times 0.574 - 127 \times 0.05} = 2.87 \text{ in} \end{aligned}$$

The blade passage width at the exit

$$\begin{aligned} h_{b2s} &= P_{bs} \sin \theta_{b2s} - t_b = 0.721 \times 0.574 - 0.05 \\ &= 0.364 \text{ in} \end{aligned}$$

Second Rotor Blade Dimensions

Pitch or blade spacing

$$P_{br2} = \frac{\text{Blade chord length } C_b}{\text{Blade solidity}} = \frac{1.4}{1.67} = 0.838 \text{ in}$$

From equation (6-140a), the number of the blades

$$z_{br2} = \frac{\pi d_m}{P_{br2}} = \frac{\pi \times 29.1}{0.838} = 109$$

Allow $2^\circ 4'$ between the inlet blade angle θ_{b1r2} and the inlet relative flow angle β_3 ; thus

$$\theta_{b1r2} = \beta_3 + 2^\circ 4' = 57^\circ 56' + 2^\circ 4' = 60^\circ$$

We make the exit blade angle θ_{b2r2} equal to the exit relative flow angle β_4

$$\theta_{b2r2} = \beta_4 = 44^\circ$$

From equation (6-149), the blade radial height at the inlet is

$$h_{b1r2} = 1.08 \times 2.87 = 3.10 \text{ in}$$

The blade passage width at the inlet

$$\begin{aligned} h_{b1r2} &= P_{br2} \sin \theta_{b1r2} - t_b = 0.838 \times 0.866 - 0.05 \\ &= 0.677 \text{ in} \end{aligned}$$

From equation (6-138), the required total blade exit area

$$A_{b2r2} = \frac{144 \dot{w}_t}{\rho_4 V_4 \epsilon b_2} = \frac{144 \times 92}{0.0506 \times 1306 \times 0.95} = 211 \text{ in}^2$$

Combining equations (1-139) and (1-140a), we obtain the blade radial height at the exit

$$h_{b2r2} = \frac{A_{b2r2}}{\pi d_m \sin \theta_{b2r2} - z_b t_b} = \frac{211}{\pi \times 29.1 \times 0.695 - 119 \times 0.05} = 3.66 \text{ in}$$

The blade exit passage width

$$b_{b2r2} = P_{br2} \sin \theta_{b2r2} - t_b = 0.838 \times 0.695 - 0.05 = 0.533 \text{ in}$$

The mean blade radial height

$$h_{br2} = \frac{3.10 + 3.66}{2} = 3.38 \text{ in}$$

Check the centrifugal tensile stress at the root section using equation (6-141)

$$\begin{aligned} S_{cr2} &= 0.0004572 \frac{1}{g} \rho_b h_{br2} d_m N^2 \\ &= 0.0004572 \times \frac{0.3}{32.2} \times 3.38 \times 29.1 \times (7000)^2 \\ &= 20550 \text{ psi} \end{aligned}$$

Turbine Efficiencies

From equations (6-146) and (6-147), the combined nozzle and blade efficiency

$$\begin{aligned} \eta_{nb} &= \frac{U(C_1 \cos \alpha_1 + C_2 \cos \alpha_2 + C_3 \cos \alpha_3 + C_4 \cos \alpha_4)}{gJ\Delta H} \\ &= \frac{890(3940 \times 0.906 + 2080 \times 0.817 + 1938 \times 0.819 + 908 \times 0.055)}{32.2 \times 778 \times 359} \\ &= 0.683 \end{aligned}$$

From equation (6-148), the turbine machine efficiency

$$\eta_m = \frac{\eta_t}{\eta_{nb}} = \frac{0.582}{0.683} = 0.852$$

A-1 Stage Engine Turbine (Single-Stage, Two-Rotor, Velocity-Compounded Impulse Type) Design Summary

For velocity diagrams at mean diameter d_m , see figure 6-58.

$U = 890$:

$\alpha_1 = 25^\circ$; $\beta_1 = 31^\circ 53'$; $C_1 = 3940$ fps; $V_1 = 3156$ fps; $\alpha_2 = 35^\circ 15'$; $\beta_2 = 25^\circ$; $C_2 = 2080$ fps; $V_2 = 2866$ fps; $\alpha_3 = 35^\circ$; $\beta_3 = 57^\circ 56'$; $C_3 = 1938$ fps; $V_3 = 1312$ fps; $\alpha_4 = 86^\circ 55'$; $\beta_4 = 44^\circ$; $C_4 = 908$ fps; $V_4 = 1306$ fps

Isentropic enthalpy drops:

Nozzles, $\Delta H_{0-1} = 337.5$ Btu/lb

First rotor blades, $\Delta H_{1-2} = 7.18$ Btu/lb

Stator blades, $\Delta H_{2-3} = 7.18$ Btu/lb

Second rotor, $\Delta H_{3-4} = 7.18$ Btu/lb

Total $\Delta H = 359$ Btu/lb

Working efficiencies:

$\eta_t = 58.2\%$; $\eta_n = 92\%$; $\eta_{nb} = 68.3\%$; $\eta_m = 85.2\%$

Mean diameter of nozzles and blades:

$d_m = 29.1$ in

Nozzle dimensions (at d_m):

Aspect ratio = 9.7; $z_n = 57$; $P_n = 1.604$ in;

$\theta_n = 23^\circ$; $h_{nt} = 1.5$ in; $a_{ne} = 1.64$ in; $b_{nt} = 0.1548$ in; $b_{ne} = 0.576$ in

First rotor blade dimensions (at d_m):

Solidity = 1.82; $C_b = 1.4$ in; $z_{br1} = 119$;

$P_{br1} = 0.769$ in; $\theta_{b1r1} = 34^\circ$; $\theta_{b2r1} = 25^\circ$;

$h_{b1r1} = 1.77$ in; $h_{b2r1} = 2.52$ in; $b_{b1r1} = 0.379$ in; $b_{b2r1} = 0.291$ in

Stator blade dimensions (at d_m):

Solidity = 1.94; $C_b = 1.4$ in; $z_{bs} = 1.27$;

$P_{bs} = 0.721$ in; $\theta_{b1s} = 37^\circ$; $\theta_{b2s} = 35^\circ$;

$h_{b1s} = 2.72$ in; $h_{b2s} = 2.87$ in; $b_{b1s} = 0.384$ in; $b_{b2s} = 0.364$ in

Second rotor blade dimensions (at d_m):

Solidity = 1.67; $C_b = 1.4$ in; $z_{br2} = 109$;

$P_{br2} = 0.838$ in; $\theta_{b1r2} = 60^\circ$; $\theta_{b2r2} = 44^\circ$;

$h_{b1r2} = 3.10$ in; $h_{b2r2} = 3.66$ in; $b_{b1r2} = 0.677$ in; $b_{b2r2} = 0.533$ in

(b) Two-stage, two-rotor, equal-work, pressure-compounded impulse turbine. (For velocity diagrams, see fig. 6-59.)

From prior trial-and-error calculations, the following isentropic enthalpy drops resulting in (approximately) equal work for each stage were obtained. We assume a stage carryover ratio $r_c = 0.91$.

First-stage nozzles:

$$\Delta H_{0-1'} = 50\%; \Delta H = 0.5 \times 359 = 179.5 \text{ Btu/lb}$$

First-stage rotor blades:

$$\Delta H_{1-2'} = 3\%; \Delta H = 0.03 \times 359 = 10.75 \text{ Btu/lb}$$

Second-stage nozzles:

$$\Delta H_{2-3'} = 44\%; \Delta H = 0.44 \times 359 = 158 \text{ Btu/lb}$$

Second-stage rotor blades:

$$\Delta H_{3-4'} = 3\%; \Delta H = 0.03 \times 359 = 10.75 \text{ Btu/lb}$$

Point "0"—First-Stage Nozzle Inlet

$$T_0 = 1860^\circ\text{R}$$

$$p_0 = 640 \text{ psia}$$

Point "1"—First-Stage Nozzle Exit = Rotor Blade Inlet

From equation (6-121), the gas-spouting velocity at the first-stage nozzle exit

$$C_1 = k_n \sqrt{2gJ\Delta H_{0-1'}} = 0.96 \times 223.8 \times \sqrt{179.5} \\ = 2880 \text{ fps}$$

We use a value of 25° for the spouting-gas flow angle α_1 . For optimum efficiency, the peripheral speed at the rotor mean diameter

$$U = \frac{\cos \alpha_1 C_1}{2} = \frac{0.906 \times 2880}{2} = 1308 \text{ fps}$$

Using equation (6-130), the relative gas flow β_1 at the first-stage rotor blade inlet can be calculated as

$$\tan \beta_1 = \frac{C_1 \sin \alpha_1}{C_1 \cos \alpha_1 - U} = \frac{2880 \times 0.423}{2880 \times 0.906 - 1308} = 0.936$$

$$\beta_1 = 43^\circ 8'$$

The relative gas flow velocity at first-stage rotor blade inlet

$$V_1 = \frac{C_1 \sin \alpha_1}{\sin \beta_1} = \frac{2880 \times 0.423}{0.683} = 1784 \text{ fps}$$

Point "2"—First-Stage Rotor Blade Exit = Second-Stage Nozzle Inlet

From equation (6-135), the relative gas flow velocity at the first-stage rotor blade exit

$$V_2 = \sqrt{k_b^2 V_1^2 + 2gJ\eta_n \Delta H_{1-2'}} \\ = \sqrt{(0.89 \times 1784)^2 + 64.4 \times 778 \times 0.92 \times 10.75} \\ = 1736 \text{ fps}$$

We chose a relative exit gas flow angle $\beta_2 = 38^\circ$ for the first-stage rotor blades. The absolute gas flow angle, α_2 , can then be calculated as

$$\tan \alpha_2 = \frac{V_2 \sin \beta_2}{V_2 \cos \beta_2 - U} = \frac{1736 \times 0.616}{1736 \times 0.788 - 1308} = 17.25$$

$$\alpha_2 = 86^\circ 40'$$

The absolute gas flow velocity at the first-stage rotor blade exits

$$C_2 = \frac{V_2 \sin \beta_2}{\sin \alpha_2} = \frac{1736 \times 0.616}{0.998} = 1070 \text{ fps}$$

Point "3"—Second-Stage Nozzle Exit = Second Rotor Blade Inlet

From equation (6-151), the second-stage nozzle gas-spouting velocity

$$C_3 = k_n \sqrt{r_c C_2^2 + 2gJ\Delta H_{2-3'}} \\ = 0.96 \sqrt{0.91 \times (1070)^2 + 64.4 \times 778 \times 158} \\ = 2880 \text{ fps}$$

Since $C_3 = C_1$, the remainder of the second-stage velocity diagram is the same as that of the first stage, i.e., $\alpha_3 = \alpha_1 = 25^\circ$; $\beta_3 = \beta_1 = 43^\circ 8'$; $V_3 = V_1 = 1784 \text{ fps}$; $\alpha_4 = \alpha_2 = 86^\circ 40'$; $\beta_4 = \beta_2 = 38^\circ$; $C_4 = C_2 = 1070 \text{ fps}$; $V_4 = V_2 = 1736 \text{ fps}$.

From equation (6-129), the turbine rotor mean diameter

$$d_m = \frac{720 U}{\pi N} = \frac{720 \times 1308}{\pi \times 7000} = 42.7 \text{ in}$$

From equation (6-147), the combined nozzle and blade efficiency

$$\eta_{nb} = \frac{U(C_1 \cos \alpha_1 + C_2 \cos \alpha_2 + C_3 \cos \alpha_3 + C_4 \cos \alpha_4)}{gJ\Delta H}$$

$$= \frac{1308(2880 \times 0.906 + 1070 \times 0.058) + 2880 \times 0.906 + 1070 \times 0.058}{32.2 \times 778 \times 359}$$

$$= 0.78$$

The turbine machine efficiency is assumed to be the same as that used in design (a):

$$\eta_m = 0.852$$

From equation (6-148), the overall turbine efficiency

$$\eta_t = \eta_{nb}\eta_m = 0.78 \times 0.852 = 0.664$$

A-1 Stage Engine Alternate Turbine Design Summary (Two-Stage, Two-Rotor, Pressure-Compounded, Impulse Type)

For velocity diagrams at mean diameter d_m , see figure 6-59.

$U = 1308$ fps:

$\alpha_1 = 25^\circ$; $\beta_1 = 43^\circ 8'$; $C_1 = 2880$ fps; $V_1 = 1784$ fps; $\alpha_2 = 86^\circ 40'$; $\beta_2 = 38^\circ$; $C_2 = 1070$ fps; $V_2 = 1736$ fps; $\alpha_3 = 25^\circ$; $\beta_3 = 43^\circ 8'$; $C_3 = 2880$ fps; $V_3 = 1784$ fps; $\alpha_4 = 86^\circ 40'$; $\beta_4 = 38^\circ$; $C_4 = 1070$ fps; $V_4 = 1736$ fps

Isentropic enthalpy drops:

First-stage nozzles, $\Delta H_{0-1} = 179.5$ Btu/lb

First-stage rotor blades, $\Delta H_{1-2} = 10.75$ Btu/lb

Second-stage nozzles, $\Delta H_{2-3} = 158$ Btu/lb

Second-stage rotor blades, $\Delta H_{3-4} = 10.75$ Btu/lb

Working efficiencies:

$\eta_t = 66.4\%$; $\eta_n = 92\%$; $\eta_{nb} = 78\%$; $\eta_m = 85.2\%$

Mean diameter of nozzles and blades:

$d_m = 42.7$ in

Comment: The overall efficiency of the pressure compounded turbine is higher than that of design (a). However, a relatively large d_m is required (weight, size).

6.6 DESIGN OF TURBOPUMP BEARINGS, SEALS, AND GEARS

Turbopump Bearing Design

A turbopump shaft is supported by two or more bearings. The loads on the bearings are the

result of forces which act on the shaft or on the parts supported by the shaft. These forces may be divided into two classes: those which act at right angles to the shaft axis (radial forces), and those which act parallel to the shaft axis (thrust loads).

Radial loads on turbopump bearings may result from one or more of the following sources:

- (1) Weights of parts such as shafts, pump impellers, turbine rotors, gears
- (2) Centrifugal forces due to unbalance of these rotating parts
- (3) Forces due to inertia, resulting from rapid acceleration
- (4) Resultant radial forces on the impeller due to nonuniform pressure distribution in the discharge volute of the pump
- (5) Tangential or torque forces induced by the gears

Thrust loads on turbopump bearings may result from one or more of the following sources:

- (1) Weight of rotating parts mounted on a vertical shaft
- (2) Unbalanced axial thrust of the pumps
- (3) Resultant axial thrust on the turbine rotor blades

For the turbopumps of liquid rocket engines, high-speed ball and roller bearings are used almost exclusively. A typical two-bearing design is shown in figure 6-7. A ball bearing carries both radial and thrust loads. It is paired with a roller bearing which carries only radial loads, however, of a higher magnitude. A typical three-bearing arrangement is shown in figure 6-63. The shaft radial loads are carried by a single roller bearing at the turbine end and by a roller and a ball bearing on the pump side. The ball bearing also absorbs the thrust loads. As a rule, the shaft thrust loads in a turbopump are carried by a single or dual bearing located at one end of the shaft. Thus loads from thermal expansion or contraction of the shaft are avoided.

Bearing design data with regard to load-carrying capacity, operating speed, and service life are usually furnished by the manufacturers. The useful life of a bearing is dependent upon its speed and load, and may be expressed by the correlation:

$$\text{Life, hours} = K_b \left(\frac{\text{Rated speed, rpm}}{\text{Actual operating speed, rpm}} \right) \times \left(\frac{\text{Rated capacity, lb}}{\text{Actual working load, lb}} \right)^4 \quad (6-153)$$

where K_b = design factor usually furnished by manufacturer.

If a bearing is subjected to both thrust and radial loads, the two can be combined into a single equivalent radial load:

$$P = R + xA \quad (6-154)$$

where

P = equivalent radial load used for bearing selection, lb

R = actual radial load, lb

A = actual thrust load, lb

x = design coefficient usually furnished by manufacturer

Rocket turbopump bearings quite commonly are cooled and lubricated by the propellants pumped. They are usually operated at very high "DN" values, a parameter which is the product of the bearing bore D (millimeters), and the bearing rotative speed N (rpm).

Propellant lubrication has the advantage of eliminating an additional lubricant supply system, and of simplifying bearing sealing problems. The following are important design considerations for propellant-lubricated bearings:

- (1) Characteristics of the propellants, such as thermal stability, operating temperature, chemical inertness, viscosity.
- (2) Compatibility of the bearing materials with the propellants. The application of certain high-strength alloys is sometimes limited by the propellants used.

The "DN" rating is convenient when selecting high-speed ball or roller bearings. As the rotative speed of a bearing increases, contact fatigue of the outer race caused by centrifugal loads of the balls or rollers may cause failures. In addition, bearing contact speeds will result in non-rolling phenomena with attendant failures caused by overheating. Through proper selection of the bearing geometry, these problems can be minimized, and the DN rating increased. Note that for a given horsepower rating, the shaft size based on allowable stress does not decrease

proportionally with the increase of shaft design speed. Thus the required bearing DN value rapidly increases for high-speed turbopumps. As a result, especially for liquid hydrogen application, the turbopump rpm is often determined by the DN limits of the bearings.

A most important bearing design consideration is the expected operating life of the rocket engine. The bearings must have adequate statistical probability of conforming with this requirement. A generally accepted life rating for ball and roller bearings is the "B-10 life." The term denotes the operating life (hours) of a "population" of bearings at a given load and speed, at the expiration of which statistically 10 percent of them will have failed. Of course, in actual rocket engine operation, component reliability must be much higher. Bearing life at a given load and speed varies inversely with reliability. For instance, the B-1 life (99 percent reliability) is one-tenth of the B-10 life (90 percent reliability), or one-fiftieth of the B-50 life (50 percent reliability). Therefore, turbopump bearings are generally designed for a B-10 life of at least 100 hours. This corresponds to a B-1 life of 10 hours, or a B-0.1 life (99.9 percent reliability) of 1 hour, the latter by order of magnitude being the life the bearing most likely will actually see. For critical applications, an even higher life rating may be selected.

Figure 6-61 presents the centrifugal load DN limits in terms of 10, 100, and 1000 hours of B-10 life for a typical ball bearing design (extra-light series).

The stress-limiting DN values of roller bearings are much higher than for ball bearings; however, it is extremely difficult to control the temperature rise in a roller bearing, if the DN value is above 1.5×10^6 , due to excessive cage slip. Generally, rocket turbopump bearings have been successfully operated at DN values up to 1.5×10^6 . Limited test information indicates possible satisfactory operation at 2.0×10^6 DN.

Dynamic Seal Design

The principal dynamic, i.e., rotating seal types used in liquid rocket turbopumps are the labyrinth, face-riding, and shaft-riding seals. Satisfactory seal operation depends upon good design which considers many factors, including

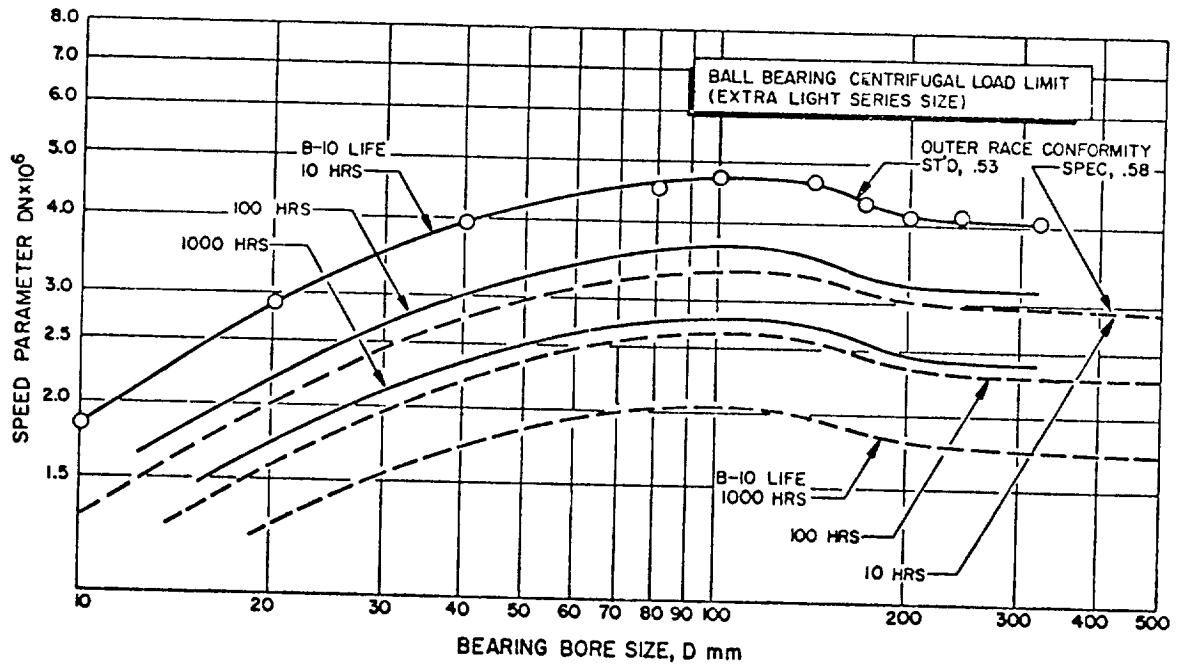


Figure 6-61.—Ball bearing centrifugal load DN limits.

fluid pressure surges, vibration, expansion and contraction of sealing components, contact pressure between sealing surfaces, rubbing velocities of the sealing surfaces, smooth and friction-free operation of internal sealing parts, and on squareness of the sealing surfaces. Any influence which directly or indirectly subsequently alters these factors can cause improper operation of the seal.

As shown in figure 6-62, the labyrinth seal is a clearance-type seal. The fluid tending to pass through the sealing interface is throttled many times and is forced to follow a devious path. The function of a labyrinth seal is not to prevent fluid leakage entirely, but rather to reduce leakage to a reasonable level at a minimum of friction and wear. The amount of leakage through a labyrinth seal can be estimated by the correlation

$$Q_e = C_s A_c \sqrt{24 g \Delta p_s / \rho} \quad (6-155)$$

where

Q_e = leakage rate, in³/sec

A_c = seal clearance area, in²

Δp_s = pressure differential across the seal, lb/in²

ρ = density of the fluid lb/in³

C_s = seal leakage coefficient, established experimentally

Labyrinth seals are used for the wearing rings of pump impellers, as well as for the rotating seals attached to the sealing diaphragm between two turbine stages.

In a face-riding-type seal the sealing is accomplished through rubbing contact between the precision-lapped faces of a floating seal washer and a shoulder ring. The mating faces are at a right angle to the axis of rotation. As shown in figure 6-62, the floating seal washer is attached to a metal bellows. The bellows, in turn, is welded to a stationary seal housing which is secured and statically sealed to the casing. The bellows provides flexibility and spring force to the contact face, permitting it to follow axial and angular movement without leakage. Sometimes a lip seal is used in conjunction with a spring-loaded floating washer, instead of a bellows.

The shaft-riding seal (fig. 6-62) consists of a seal housing, a seal retaining plate, and several seal segments. The segments form a ring around the shaft and are held against it by garter springs.

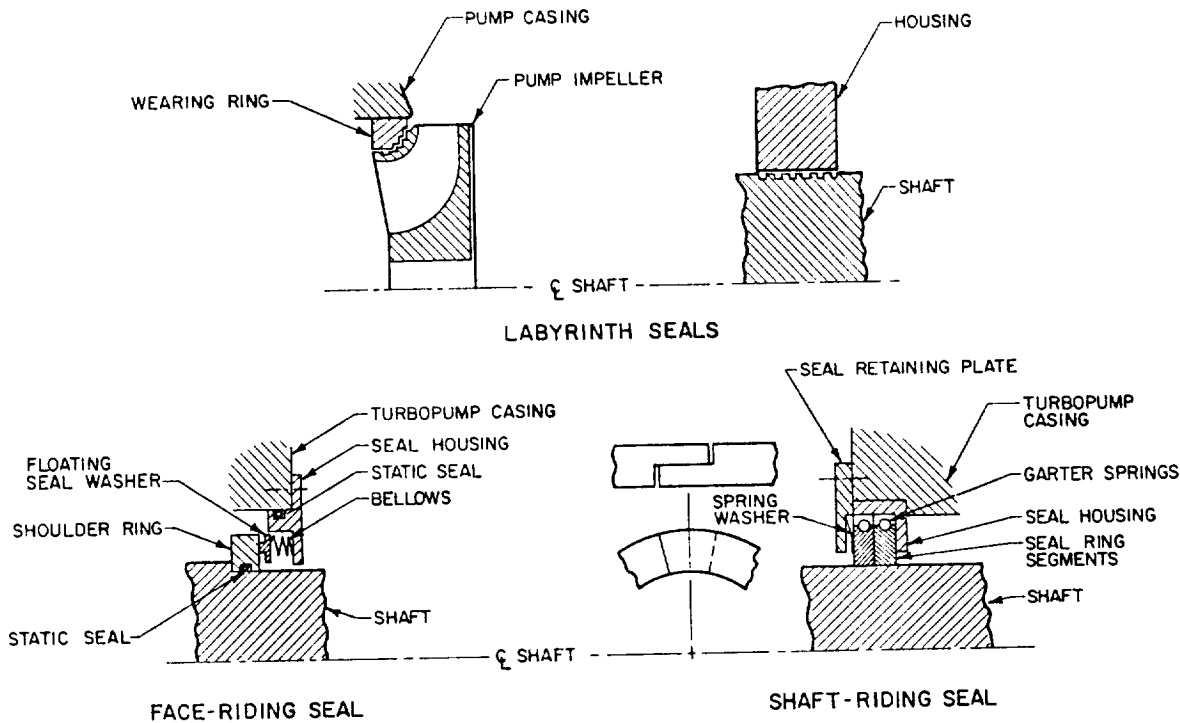


Figure 6-62.—Principal turbopump dynamic seal types.

Thus self-adjusted dynamic sealing is accomplished between shaft outside diameter and segment inside diameter. Axially, the segments are forced against a flat surface of the seal housing by a retaining plate and a spring washer, thus providing a static seal. Shaft-riding seals tend to occupy less space than the face-riding seals.

A wide variety of materials is available for floating seal washers and seal ring segments. Carbon is used most frequently. The rubbing seal faces on shoulder ring or shaft must be hardened or plated, and lapped to a very smooth finish. The seal face rubbing speed should not exceed 300 fps. Frequently, vent or purge lines are connected to the cavities between two or more dynamic seals installed in series. This assures positive sealing for critical applications such as interpropellant seals.

Turbopump Gear Design

The gear trains used in liquid rocket turbopumps (fig. 6-16) afford speed differentials between turbine, pumps and accessory drives, and also sometimes between a pump impeller and a

low-speed inducer. Gear arrangement and geometry depend upon power transmitted, propellants, speed ratio, and other factors. During operation, the gears are cooled and lubricated with oil, or with the propellant being pumped.

The gears are usually housed in an aluminum casing. To minimize weight further, webs are held as thin as possible as are cross sections at the rim and hub. The hubs are often internally splined for best results. Spur gears are most widely used, since they minimize thrust on bearings. Tooth loads and speeds in turbopump gears are very high. The designer, therefore, must achieve high tooth strength and high resistance to wear. Turbopump gears are usually made of high-alloy steel, with the tooth surfaces hardened by either case carburizing or induction hardening. If possible, the tooth surface should be accurately finished by a grinding process. Materials and dimensional tolerances of turbopump gears must be held under very close control during manufacturing.

To improve gear life and load-carrying stability, certain modifications to standard design practices can be applied. Pinions are frequently

made with long addendum and gears with short addendum to adjust tip-sliding velocities and to strengthen the pinion. Furthermore, pinion tooth thicknesses are often increased, at the expense of gear tooth thickness. High pressure angles as high as $22\frac{1}{2}^\circ$, 25° , or $27\frac{1}{2}^\circ$ may be applied to reduce contact stresses on the tooth surface and to increase the width of the tooth at the base. Involute-profile modifications are often also made to compensate for bending and to keep the tips from cutting the mating part.

6.7 DESIGN LAYOUT OF TURBOPUMP ASSEMBLIES

Figure 6-63 presents the design layout of the A-1 stage engine turbopump assembly. Logical packaging and arranging of the basic mechanical elements of the turbopump are among the

considerations in preparing the layout. For instance, one of the more important criteria which influences the selection or arranging of the turbopump mechanical elements is the ease of development. Standard or proven mechanical detail should be extensively adopted in the layouts. The following is a list of important turbopump design layout considerations:

- (1) Compatibility with engine systems packaging and plumbing
- (2) Structural integrity
- (3) Positive interpropellant sealing
- (4) Compensation for thermal expansion and contraction
- (5) Ease of development
- (6) Ease of assembly
- (7) Ease of manufacturing

Considerable experience and skill are required in turbopump design layout work for best results.

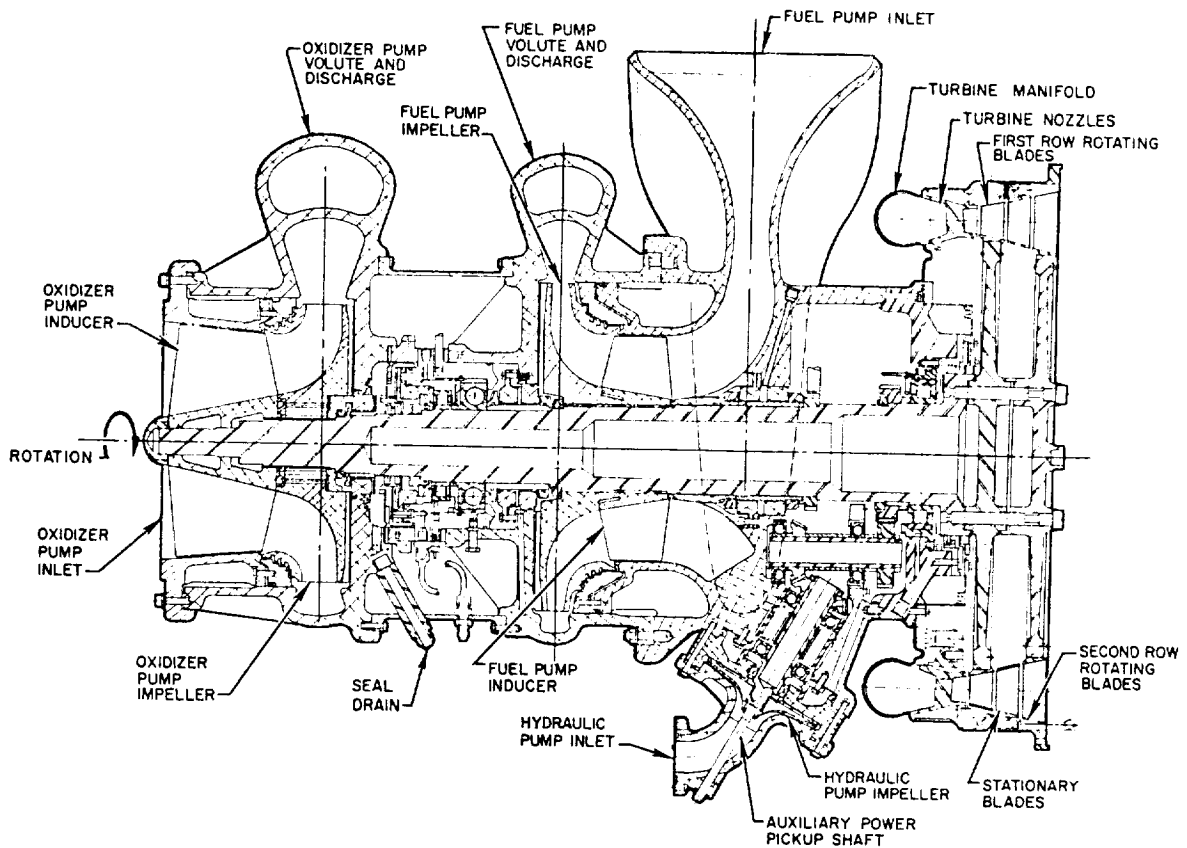
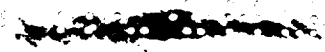


Figure 6-63.—Assembly design layout of the hypothetical A-1 stage engine turbopump.



Chapter VII

Design of Controls and Valves

7.1 CONTROL METHODS

The foremost design requirements for any control system are accuracy, stability, and reliability. Two basic control methods are available: open-loop (no feedback) and closed-loop (feedback) control systems. Both have found wide application in liquid propellant rocket propulsion systems. Open-loop control is confined to those systems which are designed to operate at a fixed, steady-state level over a narrow range of environmental conditions. Most other applications require one of the many forms of closed-loop control. For these, mathematical models can be constructed with which the functions and dynamics, such as gain factors and stability of a proposed system, can be analyzed.

The selection of the best-suited method then is an important first step in control systems design. It will be influenced by the required accuracy, the dynamic characteristics of the system being controlled, and by allowable time-lags. Once the method is determined, the basic elements for the proposed system must be selected, such as type of components of the power supply or working fluid (electric, hydraulic, or pneumatic), and of the operating mechanism for the specific control, which all depend on the specific application. Ideally, the basic theories and past experience should permit design without experiment or development work. However, some development work with attendant redesign will always be required in the process of perfecting a new system.

Open-Loop Control

With this system, control is accomplished by preset control means, such as orifices, and on-off command devices. A typical example of open-loop control is an engine propellant flow system, calibrated to a fixed set of conditions. The propellant flows are controlled simply by

opening and closing the propellant valves. Minor deviations from the design mixture ratio or propellant flow rates, such as from fabrication tolerances of engine components, are corrected beforehand by insertion of accurately sized orifices into the propellant flow lines to effect the desired pressure drops (also see ch. II). The extent of correction is determined from systems preflight calibration test data. Open-loop control has the advantage of simplicity. However, it is limited to a specific set of operating parameters, and is unable to compensate for variable conditions during operation.

Accurate sequencing of an open-loop control system such as is used for engine start and stop is usually accomplished with the aid of interlocks. Mechanical interlocks are preferred for their high reliability. For instance, the propellant valves of many small engines or gas generators are mechanically linked and are operated by a single actuator. Proper sequencing between fuel and oxidizer valves is achieved by adjusting the relative positions of the valve gates or poppets, with respect to the mechanical linkage. Interlock requirements can also be furnished by other means (electric, hydraulic, or pneumatic). In high-thrust engines, sequencing between main propellant valves and ignition system is often accomplished by the combination of various interlock designs. A typical example is the A-1 stage engine, for which the start and stop sequence and their interlocks were described in detail in chapter III.

Closed-Loop Control

Closed-loop control is also called automatic or feedback control. This system usually includes sensing means, computing means to detect errors, and control means to correct them. An accurately sensed feedback is compared with a fixed or variable reference by a computer, which

then generates signals to correct for any deviations. The main system thus does not require precise calibration for a specific set of conditions. Unlike open-loop control, closed-loop control depends on sensing absence or presence of an error to maintain a desired condition or to bring about a correction. In general, the objective of closed-loop control is to minimize errors during operation and reduce system sensitivity to environmental changes and changes in component characteristics. It is applied to areas such as engine-thrust control and/or throttling, propellant mixture-ratio control, and thrust-vector control.

For rocket engine application, closed-loop control systems usually employ one or a combination of the following modes of operation:

1. *Simple "on" and "off" type.*—(Example: pressure switch/valve combination for tank pressure control.)

2. *Proportional type.*—Employs a continuous control signal which is proportional to the error. (Example: transducer output for chamber pressure control.)

3. *Derivative type.*—Employs a continuous control signal which is a function of the error and its time derivative(s) (rate of change). This is principally used when systems stability is critical. (Example: thrust vector control system with phase lead.)

4. *Integral type.*—Employs a continuous signal which is proportional to the cumulative integral of one or more errors. (Example: two flow-meter outputs for mixture-ratio control.)

Closed-loop or feedback control systems are essentially dynamic systems. Their design characteristics may be analyzed according to the basic laws of physics. Figure 7-1 shows a typical example. Its function is to maintain the controlled variable p_c equal to the desired value p_r , by manipulating the variable \dot{w}_g . Maintaining p_c equal to p_r is assumed to maintain the indirectly controlled quantity F . In a typical turbopump fed engine control system, p_c would be the combustion chamber pressure, maintained equal to a fixed reference pressure p_r by means of a valve controlling the gas generator propellant flow \dot{w}_g . F then would be engine thrust, which is indirectly maintained at a desired value.

In this control system which consists of a sensor (chamber pressure transducer), a computer

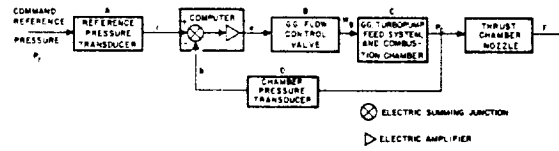


Figure 7-1.—Schematic of a typical closed-loop control system.

(electric summing junction and amplifier), and a controller (gas generator flow control valve), the command reference input r is compared with the sensor feedback b . The controller then manipulates \dot{w}_g in response to an error signal e from the computer. Ideally, r should be in linear proportion to p_r and b to p_c , save for constants required to convert one physical quantity into the other. However, this ideal condition is difficult to attain because of the dynamic characteristics of the pressure transducers. These characteristics are influenced by physical properties such as mass inertia, fluid compressibility and viscosity, and frictional resistance. Instead of r being directly proportional to p_r , the two parameters are actually related through a differential equation which represents the dynamic behavior of the elements involved. The same is true for the feedback b and the controlled variable p_c . It is also applicable to other systems components. Hence, the analysis of a closed-loop control system usually involves the solution of sets of often complicated differential equations.

Refer again to figure 7-1, where p_c is the controlled variable, \dot{w}_g the manipulated variable, e the error signal, b the feedback, r the reference input, and p_r the desired value. A , B , C , and D symbolically represent the dynamic relation between input and output of the respective components. The following terms representative of the differential equations for this closed-loop control system can be written:

$$\begin{aligned} r &= Ap_r & e &= r - b & p_c &= C\dot{w}_g \\ b &= Dp_c & \dot{w}_g &= Be \end{aligned} \quad (7-1)$$

The solution of these equations in combination with a systematic experimental program will suffice to analyze the dynamic performance of the system.

The continuous corrective action of a closed-loop control system may promote dangerously

unstable operation when control elements or components are employed having high gain and significant response lags. An unstable control system is one that is no longer effective in maintaining a variable at its desired value. Instead, large divergent oscillations may set in. The requirements for control accuracy and for stability are often difficult to combine. Higher accuracy requires high amplification; i.e., high gain. The high amplification results in overshoot during corrective action, thus promoting various degrees of system instability. However, through appropriate means of compensation, such as "anticipatory" phase leads (time derivatives), it is possible to obtain a high gain control system with satisfactory stability. Additional information on compensation will be presented in connection with thrust-vector control.

7.2 BASIC LIQUID PROPELLANT ROCKET ENGINE CONTROL SYSTEMS

Most engine systems require several or all of the basic control systems summarized in the following paragraphs. Typical applications are found in chapter III, for the A-1, A-2, A-3, and A-4 propulsion systems (figs. 2-10, 3-3, 3-6, and 3-9).

Engine System Start Control

The prime objective of a start-sequence control is to bring the engine system safely from start signal to main-stage operation. A typical sequence may consist of systems preconditioning (purging, chilldown); application of start energy, if required (start tanks, turbine spinner); and introduction and ignition of the propellants in the main combustion chamber. Secondary sequences may be required for certain subsystems such as the gas generator system. A reliable engine-start sequence is maintained through interlocks and by monitoring each functional step of engine operation during the start transient. The propellant-valve opening sequence is set to effect either an oxidizer-lead or a fuel-lead start. This is usually dictated by propellant type and chamber ignition and cooling methods. Figures 2-11, 3-5, 3-8, and 3-11 present typical engine system start and cutoff sequences.

Engine System Cutoff Control

Rapid and safe engine shutdown, during normal operation as well as in an emergency, is desirable for minimum and repeatable cutoff impulse, and to enhance reliable systems operation. The cutoff sequence usually consists of shutoff of subsystems power (gas generator, etc.); shutoff of main chamber power; and, in case of test firings, postfiring securing (purges, flushes). As a rule, the propellant valve-closing sequence is adjusted to provide a fuel-rich cutoff in the main combustion chamber. This prevents damaging temperature spikes and results in smooth and rapid thrust termination.

Engine Main Stage Duration Control

Important considerations governing engine duration have been discussed in section 2.1. The signal for engine in-flight cutoff, unless it is the result of a malfunction, will be supplied by the vehicle and fed directly into the cutoff control system discussed in a preceding paragraph. For lower stages, where optimum utilization of the propellants is desired, a tank low-level sensor is often employed. In final stages, where precise cutoff velocity is essential, an integrating accelerometer or equivalent device will signal cutoff.

Engine System Safety Controls

Special monitoring devices, such as combustion stability monitors for detecting combustion instability, gas generator overtemperature sensors, or turbopump overspeed trips, are frequently employed to prevent undesired or unsafe conditions by effecting prompt, automatic, nonhazardous, fail-safe system shutdown during all phases of engine operation. In addition, most engine control systems are designed so that an interruption of electrical power supply will cause the system to shutdown safely. (For certain missions it may be desirable to switch to an emergency power source, or prevent shutdown by mechanical latching, for continued operation.) Mechanical and electrical interlock devices are extensively used in the control system to assure the reliability of the safety control systems.

Propellant Tank Pressurization Control

Various propellant tank pressurization systems have been discussed in chapter V. The design requirements for the control of these systems must consider—

- (1) Means to maintain the required tank pressure level within an allowable range during all phases of vehicle and engine systems operation, including steady-state engine mainstage; start or dynamic throttle transients; and vehicle coasting periods between restarts.
- (2) Effective safety devices such as pressure relief valves to prevent overpressurization and rupture of the propellant tanks.
- (3) Compatibility with other subsystem controls, such as propellant-utilization-control and thrust-control systems.

Most propellant tank pressurization control systems are of the closed-loop type.

Engine System Control Calibration

The systems described in the preceding paragraphs require proper adjustment and calibration for desired engine operating characteristics and performance. This includes the setting of timing devices, pressure switches, position switches, and the sizing of orifices. The correct values for each of these are verified during engine calibration and checkout firings. Of the orifices, some are placed in propellant lines for performance parameter calibration. Others are used in pneumatic or hydraulic lines as timing and restricting devices. Specific orifice applications for thrust and mixture ratio control will be discussed in sections 7.3 and 7.4; orifice design

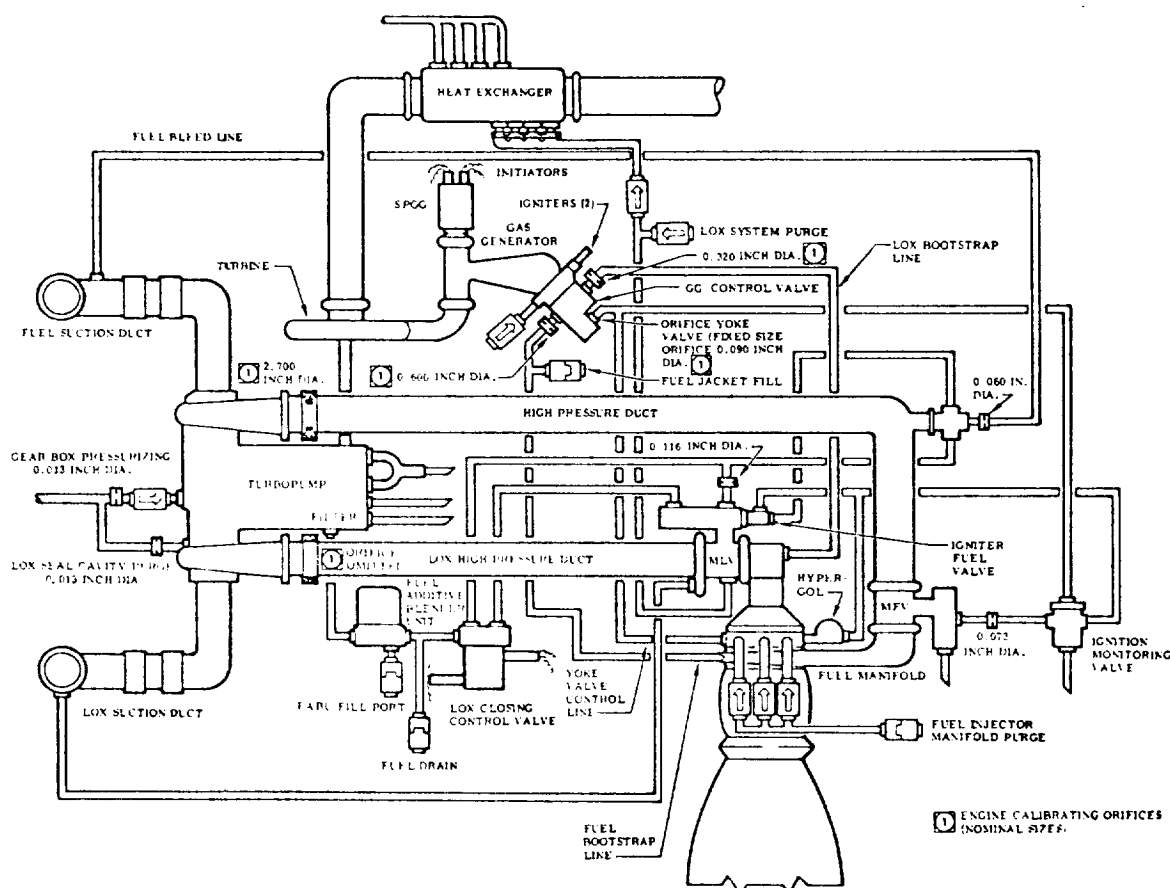


Figure 7-2.—Control orifice locations and sizes of a typical engine system.

elements will be presented in section 7.10. Following sizing, orifices must be properly identified, by stamping or banding, and their actual sizes recorded in the engine logbook. Control and calibration orifice locations and sizes of a typical system are shown in figure 7-2.

Engine Systems Checkout and Test Controls

To verify operational readiness of the engine system and its subsystems, suitable control means are required for postassembly and pre-firing checkouts. These permit simulation of the operation of the engine and its critical control components, without actually firing the engine system. Utilizing suitable ground-support equipment (GSE), an engine checkout control system should include—

- (1) Provisions to conduct leak checks and electrical-continuity checks of the entire engine system.
- (2) Provisions for verifying proper operation of all instrumentation pickups, such as dc bus voltage and spark plug firing monitors; open, closed, and continuous position signals for valves; propellant flowmeters; and pressure transducers.
- (3) Provisions for verifying the proper function and operating range of all control devices and subsystems, such as flow control valves, pressure regulators, and thrust and mixture ratio control devices.
- (4) Provisions to simulate vehicle signals for "cold" checkout of the engine system operating sequence, such as for start and cutoff.

In addition to the checkout equipment, the engine ground-support system must include equipment to permit control of static test firings. This often requires additional instrumentation.

7.3 ENGINE THRUST LEVEL CONTROL

The significance of the thrust level of a liquid rocket engine (sea level or vacuum) has been explained in section 2.1. It is usually specified with a tolerance; for instance, " $\pm 3\%$." It is possible, with modern "fixed thrust level" engines, to guarantee this band with simple orifice calibrations in the various propellant subsystems of the engine, without resort to regu-

lators, and with a minimum of calibration firings. However, "thrust" regulators or "controllers" are employed in vehicle systems which require a higher degree of precision and repeatability, such as in single-stage vehicles starting at sea level, or in final stages of a multistage system. Thrust regulators are actually chamber pressure regulators. At altitude (vacuum), their effect is identical to thrust regulation, since at altitude thrust for a given engine and mixture ratio is solely a function of chamber pressure. The same is essentially true for systems starting at sea level, because the relationship of thrust to chamber pressure as a function of altitude is predictable with high accuracy.

Occasionally, vehicle missions will require in-flight thrust control over a wider range. Usually, in such cases, the need is for a planned reduction of thrust, or "throttling," during the last portion of propelled flight. Two basic procedures are possible:

- (a) Stepwise reduction of chamber pressure, p_c
- (b) Continuous reduction of p_c

Each of them can be accomplished by control of—

- (1) Turbine power (in the case of turbopump fed systems), through regulation of gas generator propellant flow rate or hot gas flow rate (preferred method).
- (2) Main propellant flow rate
- (3) Variation of main tank pressures (in the case of pressure-fed systems).

Additionally, in multiple (clustered) engine systems, stepwise thrust reduction can be effected by shutoff of one or more engines of the subsystems.

The example chosen in section 7.1 to illustrate a closed-loop control system is typical for a system effecting thrust control through turbine power variation. Figure 7-3 shows the thrust control system proposed for our A-4 stage engine, which relies on main propellant flow variation. Here, the closed-loop control system operates on the principle of variable fluid resistances in the main oxidizer and fuel feed lines to achieve propellant flow-rate modulation. Engine reaction is determined by sensing chamber pressure, the parameter most indicative of thrust level, and by comparing the feedback b with the command reference pressure input r . Any resultant error e ,

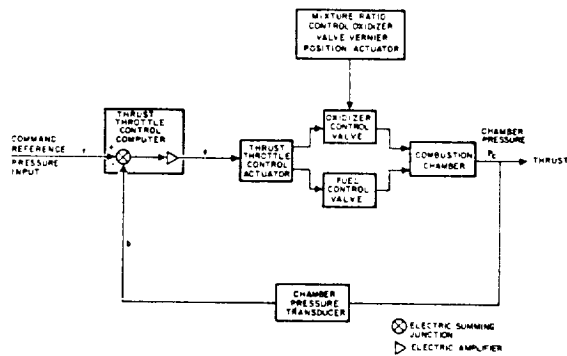


Figure 7-3.—Main-stage thrust throttle control loop for the A-4 stage engine.

following amplification and compensation as required, is used to drive the thrust throttle control actuator of the main propellant control valves in a direction which reduces the error. Ideally, the system operates over the entire thrust throttle range with minimal disturbances to other critical engine parameters; in particular, the propellant mixture ratio. In practice, these disturbances are not entirely avoidable, but can be minimized by maintaining a given resistance ratio between the two main propellant control valves throughout the control range. A most reliable method toward this objective would be mechanical coupling of the two propellant valves (fig. 7-4).

Orifices, propellant valves, and servovalves required for thrust control will be described in subsequent chapters.

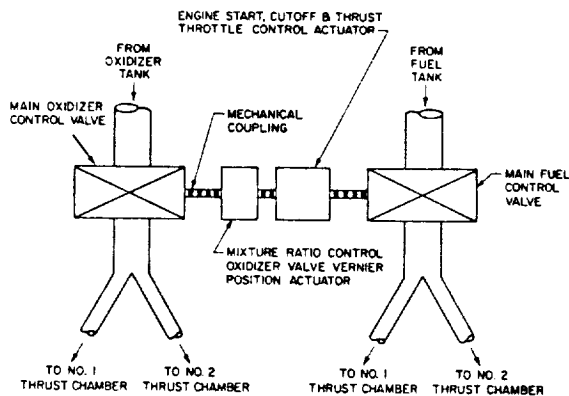


Figure 7-4.—Schematic of the propellant control system for A-4 stage engine start, cutoff, throttle and mixture ratio control.

7.4 PROPELLANT-MIXTURE-RATIO AND PROPELLANT-UTILIZATION CONTROL

The significance of propellant mixture ratio and its control have been discussed in section 2.1. The principal reasons for mixture-ratio control are recalled:

- Optimum engine performance (important)
- Complete propellant utilization; i.e., minimum residuals (most important)

Both goals are closely interrelated and essentially inseparable.

Open-Loop Mixture Ratio Control

The simplest form of engine mixture ratio control is obtained by the installation of properly sized calibration orifices in the main propellant lines. Acceleration effects during flight are usually accurately predictable as a function of trajectory and flight time. Thus, simple averaging of flight mixture ratio and selection of the corresponding orifice size reduces mixture ratio deviations over the duration of flight to a level acceptable for optimum total propellant utilization in many missions.

Open-loop mixture-ratio control can often be further refined by the following procedures:

1. *Weighing of the propellants loaded; i.e., accurate determination of the tanked propellant mixture ratio.*—The vehicle to be launched rests on load cells, thus permitting weighing of the propellants actually loaded. In mixed systems, the noncryogenic component is loaded and weighed first. The cryogenic component follows and is subsequently maintained at level through a topping line. The mass of both propellants is determined from on-the-spot temperature and ambient pressure readings while the tanking procedure is progressing.

2. *Use of adjustable, rather than fixed, orifices in one or both propellant lines.*—As close to vehicle takeoff as possible, and as a function of tanked weight and temperature readings, a hand or remotely ground-controlled prestart-orifice adjustment is made. This method is usually confined to noncryogenic fluids.

For systems where engine operation closely follows that obtained during final calibration, remarkable accuracy of targeted mixture ratio and thus propellant utilization can be obtained

with the open-loop method, approaching that of a closed-loop system (single stages; first stages).

In certain applications, however, the variation of mixture ratio as a function of increasing acceleration may exceed tolerable limits. Acceleration in most vehicle tank arrangements affects predominantly the propellant in the forward tank. Because of the long supply line, acceleration continues to act upon a relatively large fluid column, even near the end of powered flight (tank depletion). By comparison, the effect on the fluid in the rear tank is often nearly completely offset by the simultaneous decrease in fluid head (short liquid column).

To offset excessive acceleration effects on the fluid from the forward tank and thus on mixture ratio, head-suppression valves are sometimes used at the pump inlet of turbopump fed systems. Here, pump inlet pressure increase is sensed as a function of acceleration. Corresponding signals are fed through a logic device to the head-suppression valve which will gradually close, thus acting as a throttling device. This valve also protects the pump structurally.

Closed-Loop Mixture Ratio Control

In certain cases, such as in last stages, or in missions requiring engine restart following extensive cruising periods involving propellant boiloff, a closed-loop system may be required. In figure 7-5 we see the A-4 stage engine mixture ratio control loop which operates on the basis of continuous propellant mass flow sensing. Both fuel and oxidizer mass flow rates are monitored and integrated to establish the ratio of either the propellants consumed or the propellants remaining. The mixture ratio feedback, $(MR)_b$, is then compared with a command reference mixture ratio input, $(MR)_r$, in the propellant utilization control computer. The resulting error signal, $(MR)_e$, is fed to the mixture ratio control oxidizer valve vernier position actuator, which forms a link in the mechanical coupling between the two main propellant control valves, as shown in figure 7-4. The oxidizer flow rate is thus modified to eliminate the error. In high-thrust turbopump-fed engine systems such as the A-2 stage engine, where the propellant valves are independently actuated, the system propellant mixture ratio control can be accomplished by varying the main

oxidizer flow in a similar manner. For instance, a propellant-utilization servo control valve, which regulates the pneumatic pressure to the main oxidizer valve actuator, may control the oxidizer flow by adjusting the angular position of the oxidizer valve gate during engine main-stage operation. In certain applications it may be desirable to integrate the propellant flow rates and to compare the masses consumed to one another and to those tanked for optimum propellant utilization.

It is readily seen that control systems, based on propellant flow-rate measurements, are a refinement of open-loop systems using fixed orifices. They are basically still mixture-ratio controls and thus merely "assume," but do not measure directly, the amount of propellants actually remaining in the tanks and their unbalance. To accomplish this function, usually referred to as "propellant utilization" (*PU*), additional control elements must be employed in the form of vehicle tank-level sensors. Numerous principles are known: point sensing, sonar, acoustic, radiation sensing, differential pressure, and capacitance probes.

Figure 7-6 presents the propellant utilization control system for the A-4 stage propulsion system. The residual propellant quantities in the main tanks are continuously monitored, summed, and compared with a *PU* control reference in the propellant utilization control computer. Any error detected is used to modify the command reference mixture ratio input, $(MR)_r$, to the mixture-ratio control computer. This method isolates the mixture ratio control from the propellant utilization control, and thus prevents interaction between them. The bandwidth of the

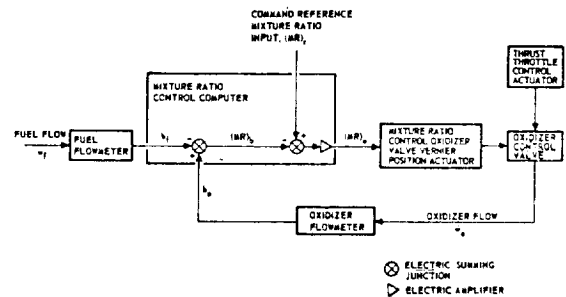


Figure 7-5.—Propellant mixture ratio control loop for the A-4 stage engine.

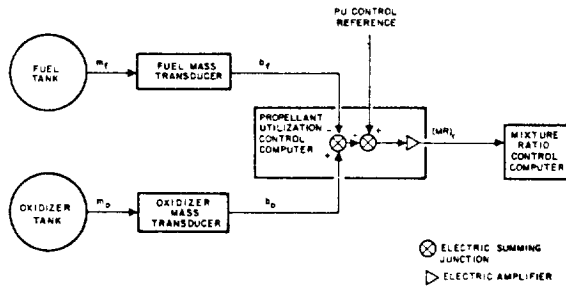


Figure 7-6.—Propellant utilization control system for the A-4 stage propulsion system.

propellant utilization control system is made narrow as compared to that of the mixture-ratio control system, because propellant residual errors may be expected to develop slowly; i.e., initial tanking errors can be corrected over the entire duration of engine operation.

The sensors used in the vehicle tanks may serve additional purposes. In combination with suitable ground equipment, they may permit an automatically controlled loading, high-level limiting and topping procedure. In static firings and flight, they may serve as redundant low-level sensors to initiate engine cutoff. For such a complete system, the term "propellant management system" has come into increased usage.

Apart from throttle valves placed in the main propellant lines, bypass lines have been successfully applied to vary mixture ratio. Here, a line is tapped off the pump outlet and ducted back to the pump inlet. A servo valve, possibly supported by an orifice, can be varied so that the bypass flow is adjusted from no flow to full bypass flow.

The implementation of closed-loop propellant-utilization control through mixture-ratio control is a major vehicle-to-engine interface area. The requirements or criteria will usually be established by the vehicle builder and/or user. Close coordination between engine and vehicle designer is essential.

A closed-loop mixture-ratio- and propellant-utilization-control system may not only be used for accurate maintenance of a fixed mixture ratio but it also has the potential for programed mixture ratio control (*PMR*). Here, the mixture ratio is varied during flight, either continuously or in steps. It must be kept in mind that the average mixture ratio still must be equal to the tanked

mixture ratio to assure simultaneous propellant depletion. However, by programing a mixture ratio in favor of the heavier component during the early portion of flight, and then switching it in favor of the lighter one, the accelerated vehicle mass is reduced faster. Also, mixture ratio may be programed to provide a higher thrust level during the steeper portion of a trajectory. This provides a better thrust-to-weight ratio in the presence of gravitation, with attendant velocity increase benefits. These methods, possibly in combination, may substantially increase stage payload capacity, since the effects of mixture ratio on performance (I_s) are usually small within a reasonable range (see table 7-1). Optimization can readily be made with the aid of an electronic computer program. In a number of applications, programed mixture ratio control without *PU* control, i.e., open loop mixture ratio control with *PMR*, may give best results, simultaneously reducing complexity.

Valves suitable for mixture ratio control will be discussed in section 7.8.

TABLE 7-1

	Mixture ratio, O/F	Thrust	NPSH	I_s	Flow rates	
					Fuel	Oxidizer
Change, percent	+10 -10	+11 -11	+12 -12	-1.3 +1.3	+4 -4	+14 -14

General Design Considerations

The precision with which a desired mixture ratio is obtained or maintained is affected considerably in open-loop systems, and to some extent in closed-loop systems, by the following:

- (1) Instrumentation accuracies (in particular, flow and tank-level metering)
- (2) Machining tolerances of orifices
- (3) Operating tolerances of regulators
- (4) Temperature influences on orifices and regulators
- (5) Density tolerances of the propellants, as a function of temperature and of purity (composition according to specifications; contamination and dilution)

- (6) Acceleration effects during flight
- (7) Propellant tank pressure deviations
- (8) Turbopump speed deviations
- (9) Differences between fuel and oxidizer pump characteristics as a function of speed
- (10) Line resistance changes as a function of temperature and for miscellaneous mechanical reasons
- (11) Temperature effects in rotating machinery

In the following we will discuss important steps toward maintenance of high quality, and toward further improvement in the listed areas, for highest accuracy of mixture-ratio (and propellant-utilization) control.

First, continued improvement of propellant flow-metering devices is imperative. Here, turbine-type flowmeters have achieved a high degree of accuracy (conformance with truth) and precision (repeatability).

The accurate calibration of these meters to most reliable standards is important. Since engine inlet pressures also affect the mixture ratio, pressure measurements of the highest reliability are equally necessary. Wherever possible, the rocket engine design should include vital metering and measuring elements from the outset. Dynamic sensing devices, in particular flow meters, are drastically influenced by their installation configuration. If these end organs, following accurate calibration, remain with the engine through its entire life cycle, including flight, a maximum degree of accuracy is obtained.

The design and machining of all calibration orifices should closely follow accepted standards (see section 7.10). Selection of suitable materials to eliminate or at least to reduce to a minimum, temperature influences and corrosion, is important. The design of orifice holders must prevent the possibility of incorrect (upside down) installation and of distortion of the orifices.

Regulators, if any are used, must be designed for highest accuracy and precision with particular consideration of the medium to be controlled. More detail will be presented in section 7.12.

The purity and composition of the better known propellants are regulated by official government specifications. The designer can expect that approved sources will deliver the propellants in conformance with these. However, subsequent contamination, dilution or alteration is

always a possibility and must be prevented by proper design and handling procedures. Many of these, such as cleaning procedures, will be called out in the shop drawings. Furthermore, the design, where applicable, will have to include filters, check valves, and suitable line routing in order to prevent contamination and/or contact with incompatible materials. Note that some propellants may change their properties merely as a function of time, such as hydrogen-peroxide, which loses its concentration due to (very slow) decomposition (with attendant gas development), even if absolute cleanliness has been maintained. This affects design conditions in addition to contamination considerations since proper venting devices must be provided. The latter, in turn, have to be designed in such a way that no contaminants, including moisture, can enter the propellant system.

Since mass flow rates delivered by pumps and/or regulated by orifices will be a function of the fluid densities, mixture ratio may be affected accordingly. The densities, in turn, aside from conformance with specifications, will be affected by temperature (noncryogenic fluids) or ambient pressure; i.e., boiling point (cryogenic fluids). To overcome these effects, it may be necessary to temperature-condition the propellants. This may be done by heating or cooling. Or, it may be accomplished by suitable storage, such as shielding against solar radiation. For cryogenic propellants, it is usually sufficient to keep the containers vented to atmosphere until immediately prior to use, since the possible changes of atmospheric pressure at a given altitude can only introduce relatively minor temperature changes. The designer, through a suitable operating sequence (engine schematic) and through provision of vent valves, recirculators, heaters, and other components, can minimize temperature effects.

The actuation of mixture ratio control devices affects the nominal engine performance parameters. Depending on the type of engine, in particular its turbopump characteristics, these effects may be significant. In an actual case, the effects shown in table 7-1 were observed.

It is clear that the vehicle thrust structure must be capable of absorbing the higher thrust loads. Also, the vehicle tanks and their operating pressures must be capable of meeting the

NPSH requirements for extreme mixture ratio excursions. Furthermore, chamber cooling may be affected. During sea-level testing, nozzles with high expansion area ratios may experience jet separation at the lower thrust levels (low p_c), resulting in vibration, destructive to engine as well as vehicle structure.

Since vehicles are tanked for their nominal mixture ratio, and since engines are calibrated to this ratio, mixture-ratio valve excursions should be small for vehicles which are expended within a few minutes after takeoff. For stages, with long cruising periods prior to operation or reignition, and which use one or two cryogenic propellants, boiloff may have altered the ratio of the propellants in the tanks to such a degree that the *PU* system may be called upon to operate at or near its maximum excursion. It is, therefore, vital that the engine designer appraise the vehicle builder of all performance variations as a result of mixture-ratio adjustments, beyond the standard tolerances of the nominal performance values. Also, engine turbopumps must be capable of operating for extended periods with the valve in either extreme position.

A propellant utilization system is a complex system. If required, it must be of the highest quality. Otherwise, it will do more harm than good. Only closest cooperation between vehicle and engine designer will assure optimum quality. Areas of particular significance to teamwork are:

Selection of the mixture ratio control method.—For instance, should the *PU* system be active during the entire flight duration, or only for the last, say, 30 percent. (Both methods have been successfully used.)

Selection of the mixture ratio control valve specifications.—Should it be a variable orifice, or a bypass valve? What should be the permissible pressure drops, required response rates, and accuracies? In case of sensor failure, should the valve return to the neutral position or remain in its last working position? (Self-locking.)

Selection of the sensors.—Should it be one of several available continuously reading types, such as capacitance gages or differential pressure (tank top to bottom) gages? Or should point sensors be employed, such as hot wires (change of heat loss as a function of being immersed in fluid or exposed); switches triggered magnetically by floats; voltage pips induced in station-

ary coils by a passing magnet, or others? (The engine designer will be involved in this selection only if the generated signals affect engine components.)

Selection of the best-suited electronic control system.—This will be largely influenced by sensors and control-valve selections.

A propellant utilization system is not a malfunction prevention system. It does not add to vehicle reliability, possibly subtracts from it. Rather, it is a system required to live with a marginal preliminary vehicle design. It is a safe assumption, however, that the first flights of a new vehicle will not be for its ultimate mission. *PU*, therefore, will not be a vital necessity for these flights.

Thus, enough time is available to thoroughly investigate, analyze, select, and develop the *PU* system. This time should be utilized. Both engine and vehicle builder have facilities and test programs to permit mutual exposure of their selected systems to flight and simulated-flight environment.

7.5 THRUST-VECTOR CONTROL

To steer a vehicle over its trajectory, thrust-vector control is applied. The following methods have found application:

- (1) Gimbale thrust chamber or engine assembly (widely used)
- (2) Jet vanes (obsolescent)
- (3) Jetevator
- (4) Gimbale thrust chamber nozzle (rare with liquid propellants)
- (5) Secondary injection (into the thrust chamber)
- (6) Auxiliary jets

The first method is used most frequently, due to its inherent reliability and performance. The first four systems require actuators which may be operated by hydraulic, pneumatic, or electric means. The remaining systems are controlled by flow regulation.

Thrust Vector Control Systems Using Actuators

Figure 7-7 presents a simplified schematic for a thrust vector control system, employing hydraulic or pneumatic actuators. It may serve to explain the fundamentals of closed-loop thrust

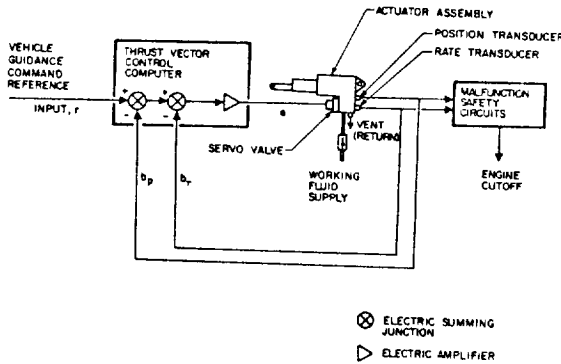


Figure 7-7.—Typical schematic of a thrust vector control system using hydraulic or pneumatic actuators.

vector control, even though the systems used in practice may differ significantly in detail. The actuators are controlled by commands, originating in the vehicle guidance system, which are a function of the vehicle's deviations from a prescribed path and of its response to corrective steering action. These signals are fed through an electronic thrust vector control logic to servo valves. In the system shown in figure 7-7, each servovalve modulates the fluid flow to its respective actuator assembly in response to an electrical error signal which is proportional to the difference between desired actuator position and its actual position. Feedback of the actual position is obtained through a transducer attached to the actuator. Additionally, the actuating speed is sensed by a rate transducer and applied to the control computer to stabilize the closed-loop control through adequate damping. Instead of a rate transducer, electronic differentiation of the position transducer output may be applied

toward the same end. Malfunction safety circuits are included to effect engine cutoff in the event of erratic operation.

A typical schematic for a thrust vector control system using electromechanical actuators is shown in figure 7-8. Here, the actuator is powered by a continuously operating, constant-speed, 28 volt dc motor, fitted with dry-powder metal bidirectional clutches. The control computer consists of summing junctions and an amplifier as in the case of hydraulic actuators. The dc motor drives the actuator through the bidirectional clutches which are controlled by the error signal generated through comparing guidance command reference input with systems position feedback. To provide adequate systems damping, the actuating speed is sensed by a rate generator or through differentiation of the position signal.

Apart from electrical feedback and compensation systems, mechanical feedback systems coupled with hydromechanical compensation "networks" are coming into increased usage. They are inherently simpler and thus offer higher reliability. Two basic types of hydromechanical compensating devices may be distinguished: piston-bypass devices and load-pressure-sensing devices.

Piston-bypass devices utilize leakages past the actuator piston to introduce system damping and may make use of dynamic relationships to control time constants (a hole drilled through the piston is an example).

Load-pressure-sensing devices, commonly called "pressure feedback" (PQ) valves or "derivative pressure feedback" (DPQ) valves, are widely used.

Figure 7-9 shows a typical servovalve and actuator schematic with derivative pressure feedback (DPQ) and mechanical feedback. The only electrical signal required is the input to the "torque motor" (an electromagnetic actuator) resulting in deflection of the flapper of a differential valve, which drains to the sump. If the flapper is deflected, as indicated in figure 7-9 by the arrow, nozzle flow on side B decreases, with an attendant pressure rise. The reverse is true for side A. The resulting pressure differential forces the power-stage spool to the left, blocking the return line on side B, and opening it on side A. As a result, pressure P_b increases,

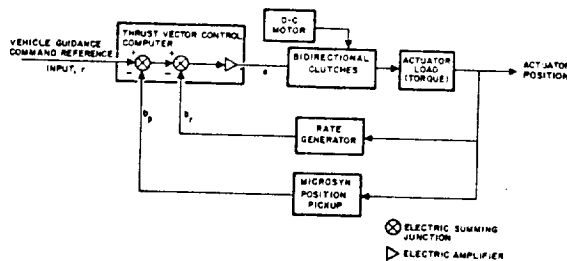


Figure 7-8.—Typical schematic for a thrust vector control system using electromechanical actuators.

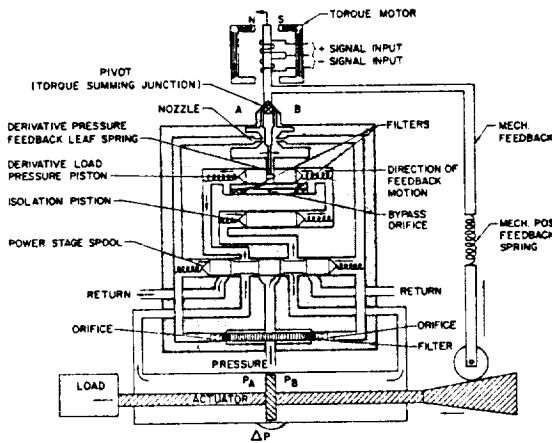


Figure 7-9.—DPQ valve with actuator.

and P_a decreases, forcing the actuator piston to the left to apply the desired load force. Attached to the actuator piston rod is a tapered extension which acts upon the mechanical feedback linkage, including a roller and a spring. The mechanical feedback attaches to the torque motor. The pivot point of the valve flapper becomes the error torque summing junction. Note that the nozzle jets also have a feedback effect. The time derivative of the actuator motion, i.e., the hydromechanical compensation, is obtained through action of a derivative load pressure piston. This piston is affected by the same pressure differential that acts upon the actuator piston; i.e., by the load pressure. However, by inserting an isolation piston and permitting flow through an orifice bypassing the derivative pressure piston, the pressures affecting the latter can equalize. The degree of this effect is a function of the actuator pressure differential and its rate of change and of the bypass orifice size (shock absorber principle). As seen in figure 7-9, the derivative load pressure piston acts upon the valve flapper when displaced. Thus it provides the required time derivative of the actuator motion for compensation.

As has been seen, it is possible to provide compensation in thrust-vector-control systems by either electrical or hydromechanical means, the latter now being often preferred for actuators. Conceivably, other control systems could be converted from electrical to hydromechanical networks. The analogies between the differential equations of the two network types often permit the use of existing electrical networks

and transfer functions by substituting the equivalent hydromechanical time constants.

Table 7-2 may be found valuable by those who wish to familiarize themselves with some fundamentals in this field. Detail on the design of servovalves will be found in section 7.11.

Demonstration Example

Two basic types of electrical compensation networks exist: current output for voltage input, and voltage output for voltage input networks. Figure 7-10 shows a simple form of a current output for voltage input network. Find the analogous hydromechanical network.

Solution

The transfer function for the electrical network is

$$\frac{i}{V} = \frac{1 + RCS}{R} \text{ Amp/volt}$$

where

- i = electrical current (amps)
- V = voltage (volts)
- R = resistance (ohms)
- C = capacitance (farads)
- S = LaPlace transform operator ($= j\omega$ for sinusoidal forcing functions)

From table 7-2, we obtain the equivalent hydromechanical parameters for i , V , R , and C . The new transfer function then is

$$\frac{Q}{\Delta P} = \frac{1 + \left(\frac{A_p^2}{C_x K}\right)S}{\frac{1}{C_x}}$$

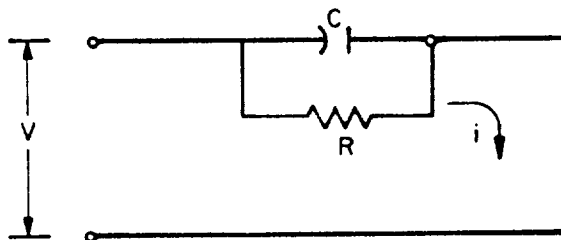
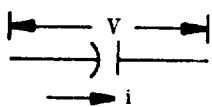
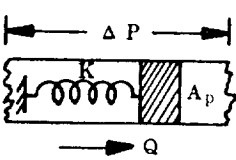
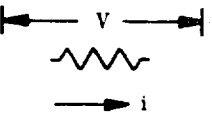
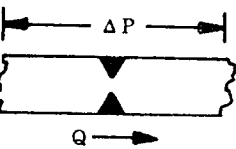
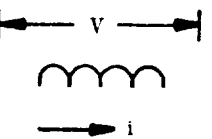
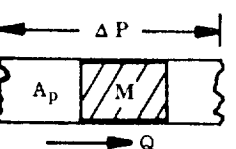


Figure 7-10.—Current output for voltage input network.

TABLE 7-2.—Electrical-Hydraulic Component Analogies

Electrical quantity or component	Describing equation	Hydraulic component or quantity	Describing equation	Analogy	Remarks
V , voltage drop, volts	$V = V_A - V_B$	ΔP , pressure drop, psi	$\Delta P = P_A - P_B$	$V \rightarrow \Delta P$	
i , current coulombs/sec	$i = \frac{dq}{dt}$ $q = \text{coulomb charge}$	Q , flow, in ³ /sec	$Q = \frac{dV}{dt}$ $V = \text{volume}$	$i \rightarrow Q$	
 Capacitor, farads	$i = C \frac{dv}{dt}$	 $A_p = \text{piston area, in}^2$ $K = \text{spring constant, lb/in}$	$Q = \frac{(A_p)^2}{K} \frac{d(\Delta P)}{dt}$	$C \rightarrow \frac{A_p^2}{K}$	Massless piston assumed
 Resistor, ohms	$i = \frac{V}{R}$	 Orifice, $\frac{\text{in}^3/\text{sec}}{\sqrt{\text{psi}}}$	$Q \approx C_X \sqrt{\Delta P}$ $\approx C_X \Delta P$	$R \rightarrow \frac{1}{C_X}$	Parabolic flow curve linearized about operation point
 Inductor, henries	$i = \int \frac{V}{L} dt$	 $A_p = \text{piston area, in}^2$ $M = \text{piston mass}$	$Q = \frac{A_p^2}{M} \int (\Delta P) dt$	$L \rightarrow \frac{M}{A_p^2}$	Piston mass not negligible

Source: D. A. Engels, "A Method of Synthesizing Electro-Mechanical Compensation Networks for Hydraulic Servomechanisms," Proceedings of the IEEE, PTGAC, October 1964.

The correct hydromechanical network, which is of the piston-bypass type, is shown in figure 7-11.

Engine-to-Vehicle Interfaces With Actuator Systems

Engine Installation and Alinement

For minimum demands on the vehicle guidance and engine actuation systems, it is required that the engine thrust vector be properly pre-aligned with respect to the vehicle attachment point in all three planes. Typical specified tolerances are: ± 0.25 inch laterally, $\pm 0.5^\circ$ vertically.

The significance of good thrust alinement can be seen from the fact that in an engine cluster, at the randomly distributed maximum of these tolerances, a trim deflection of close to 0.5° would be required from all engines to offset the misalignment.

For larger (looser) alinement tolerances, the trim deflection would be further increased. Even if the trim deflections seem to reduce effective thrust and guidance capability only slightly, the need to apply them for the full duration of powered flight results in appreciable payload reductions.

It is customary to aline the engine thrust vector to the upper face of the gimbal bearing prior to shipment. Both optical and dynamic

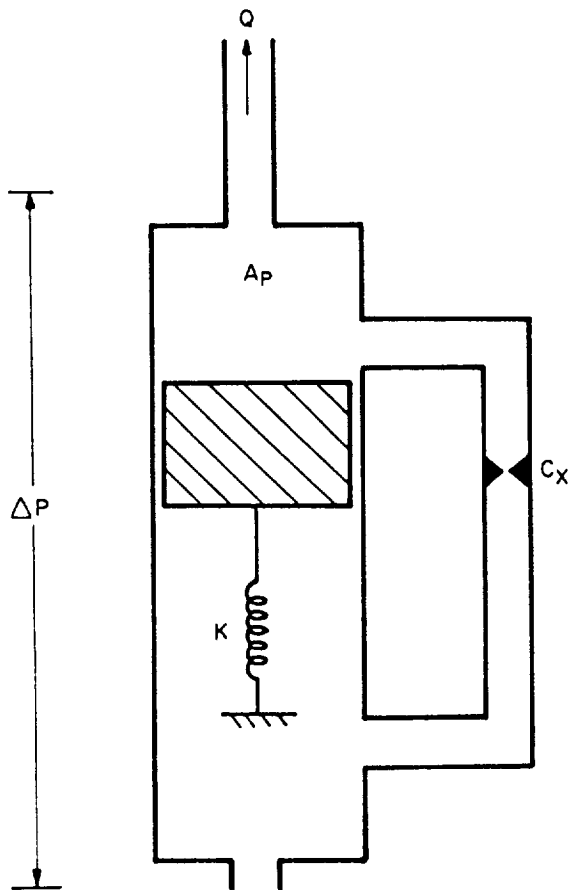


Figure 7-11.—Piston bypass hydromechanical network.

methods (load cells) are used. The optical or cold alinement establishes the geometrical location of the thrust vector in the shop, through finding the centers of nozzle throat and nozzle exit, and alining their connecting line perpendicular to the gimbal plane. A simple plumb attached to the injector center may be used in support of this operation. Subsequently, during engine firing, this measurement may be confirmed dynamically using side load cells in lieu of gimbal actuators. As a rule, after a few engines have been alined in this manner, experience will permit meeting specification by optical means alone. The vertical alinement can be simply documented as the eye-to-eye distance of the actuator attach points, or as the line through two index points (fig. 7-12). Lateral dimensions can be marked in a suitable manner at or on the gimbal bearing face. If the mating vehicle face had been properly alined to the vehicle axes,

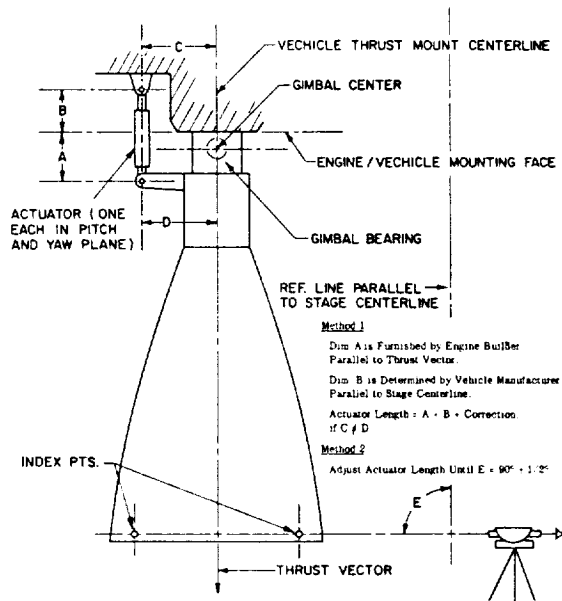


Figure 7-12.—Engine alignment.

installation of the engine then simply consists of attaching it, observing the engine logbook specifications. Figure 7-12 shows installation methods of a prealined engine into the vehicle. For the first vehicles of a new type produced, it is advisable to specify verification of engine alinement following transportation to the launching site.

Actuators, Loads

Actuators are usually of the hydraulic-piston type. Hydraulic-rotary, electromechanical, and pneumatic turbine-driven types have also been investigated.

Engine gimbal actuators are attached to the engine at one end, and to the vehicle at the other (fig. 7-13). They may be procured by the vehicle builder or by the engine builder, and must be properly dimensioned. The attachment points at either end must be capable of absorbing the forces encountered with an adequate reserve. As a rule, two actuators are required for each engine. Together, they permit deflection of the engine in all directions. It is important to note that if the maximum deflection effected by an individual actuator, for instance, is 7° , the combined maximum angle ("corner deflection") of a pair is approximately 10° . Inlet ducts, flex lines, gimbal bearing, and possibly

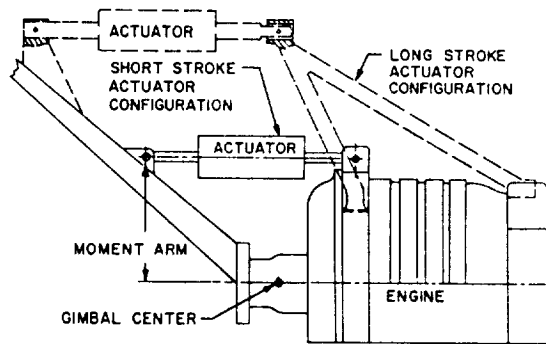


Figure 7-13.—Engine actuator installations.

other components affected, must be able to "take" this deflection. If their capability is limited, proper gimbaling restriction (stops or snubbers) must be provided (circular gimbaling pattern instead of square).

Selection and design of the actuators is based on the gimbaling forces required. In a typical case, the actuator force may be 25 percent of the engine thrust level. The force is determined by considering the following:

- Inlet duct reactions
- Flexible service line reactions
- Gimbaling bearing friction
- Heat shield reaction (if any)
- Correction for misalignments
- Aerodynamic loading (if any)
- Vehicle acceleration effects
- Inertia of gimbaling mass
- Miscellaneous minor effects

It is stressed that the engine design should reduce these forces to a minimum for smallest size and lightest weight of hydraulic pump, actuators, and associated equipment. Recognition of this need and careful design can do much toward this goal. The system must be capable of stable, well-damped response when cold gimbaling, such as during prelaunch checkout, even though the loads encountered here may be quite different from those occurring during engine firing. This dual-load situation may pose serious problems.

During startup of the engine, brief peak side loads in excess of those occurring during normal gimbaling can be generated by the thrust chamber itself. This is especially true for high expansion area nozzles being developed at sea level (for engines designed for altitude operation),

where filling of the nozzle takes a longer time during buildup than with shorter ones. Unless these loads can be eliminated or at least reduced, they must be considered for the design of actuators and attach points at both ends (notification of vehicle builder).

Crosstalk and Spring Rate

Since engine and vehicle designer are not entirely free regarding actuator installation, a situation may exist wherein motion of the actuator in one plane affects the other actuator in its plane. This is referred to as "crosstalk." If it is excessive, control instabilities may develop. Therefore, close coordination between engine designer and vehicle builder to minimize crosstalk is essential.

The actuator must be able to translate its motion without delay into engine deflection. If the control loop formed by actuator, engine structure, and vehicle thrust structure is "soft," i.e., if it has a low spring rate (lb/in), the engine does not react promptly to an actuator motion as called for by the guidance system. A delay with subsequent overshoot and continued oscillation may result. The natural frequency of this oscillation is a function of actuator stroke per degree engine deflection, feedback gains, and compensation network parameters.

Figure 7-13 shows two typical engine actuator installations. The short-stroke configuration has the advantage of high spring rate and high stiffness, and of compactness. However, the effective gimbaling mass is high, requiring larger actuators and a more powerful hydraulic system. Resolution is low (gain, expressed in degrees deflection per inch actuator stroke, is high). The long-stroke design results in low effective gimbaling mass and reduces actuator size and hydraulic system dimensions. However, the spring rate is low and so is the stiffness. Moreover, the arrangement is bulky and requires extra structural members. Only a detailed design analysis conducted jointly by engine and vehicle designer will determine which configuration is best for the flight system.

Hydraulic System

Until other means are available, a hydraulic system is probably required to power the engine actuators. Its basic elements are:

- Hydraulic pump
- Reservoir (low pressure, or "sump")
- Accumulator (high pressure)
- Servo valve
- Actuators
- Feedback (electric or mechanical)
- Lines, check valves, filters, connectors, instrumentation

If continuous hydraulic power is required prior to engine start, such as for recirculation of the hydraulic fluid or for gimbal tests, an electrically driven auxiliary pump is also provided. In most instances, the auxiliary pump will be operated until vehicle liftoff only, and can, therefore, be ground powered. For upper stages, the accumulator will then provide, for a limited time, the hydraulic power required during staging and turbopump buildup following its unlocking.

Since some of these components will be part of the engine system, while others are stage mounted, an important vehicle/engine interface exists. Through an auxiliary drive shaft, the main hydraulic pump may be driven from the engine turbopump. It is connected to the other hydraulic equipment and to the actuator through high-pressure lines, several of which must be flexible. These other elements may be mounted on the vehicle at the expense of longer lines which also must cross the gimbal plane and must therefore be flexible. Or, they may be engine mounted. This, however, increases the engine gimballed mass and may pose space and envelope problems. To compensate for misalignments and thermal expansion and contraction, a certain amount of flexibility must be provided for the lines even in this case. It is possible to connect an electric generator to the main turbopump, and drive electrically a stage-mounted hydraulic pump. Only electrical wires will then cross the gimbal plane, with the exception of the hydraulic lines to the actuators which always must be flexible. Another possible simplification is to combine servo valve and actuator into one single unit. Figure 7-14 shows a typical hydraulic engine actuation system. Figures 7-15 and 7-16 may serve to identify the major components of this system.

From the above it becomes apparent that numerous hydraulic connections will have to be made when installing the engine into the vehicle. All of them must fit, and permit adequate flexure,

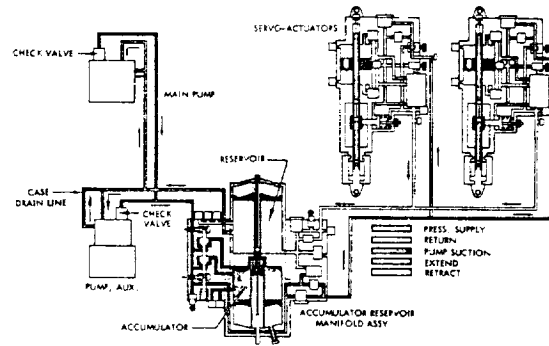


Figure 7-14.—Engine actuation system schematic (hydraulic).

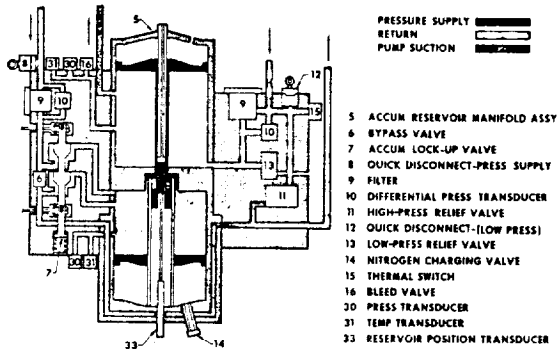


Figure 7-15.—Accumulator-reservoir schematic.

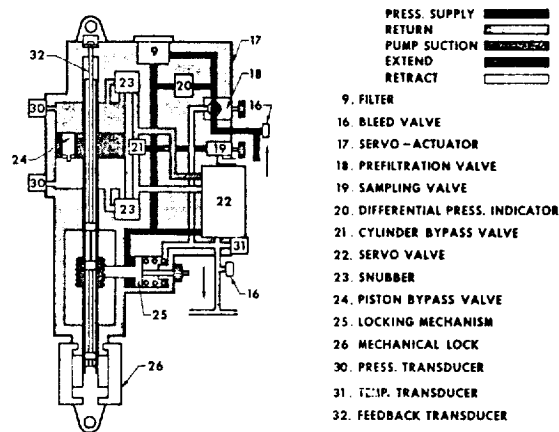


Figure 7-16.—Servoactuator schematic.

must be long enough and of the proper pressure rating, and, above all, must have a mating part on the vehicle.

Furthermore, the designer must know and consider the environment in which the hydraulic system will perform. The narrow-tolerance components and the hydraulic fluid are very temperature and contamination sensitive. Thus, the designer will have to specify extreme cleanliness requirements and adequate temperature conditioning for maximum reliability of this vital system. On cryogenic engine systems, heating of the more sensitive components of the hydraulic system is often required. Ground supplied and thermostat-controlled electric heaters, which disconnect at liftoff, are a favored temperature-conditioning method. Continuous recirculation of the hydraulic fluid by means of the aforementioned ground electrically driven auxiliary pump is another.

Secondary Injection

Thrust vector control through secondary injection of matter into the thrust chamber nozzle (SITVC) has been successfully applied to solid motors. It has found only limited, predominantly experimental application in liquid propulsion systems, where it appears especially promising for upper stage engines, in which the lateral forces required are smaller than with boosters. The principal methods of secondary injection are—

- (1) Gas injection, using—
 - (a) Inert stored gas
 - (b) Thrust chamber tapoff (fig. 7-17A)
 - (c) Gas generator (fig. 7-17B)
- (2) Liquid injection (fig. 7-17C), using—
 - (a) Inert fluid
 - (b) Propellants

Other methods, such as injection of preheated hydrogen, have been investigated but proven uneconomical.

In a gimbale thrust chamber, the side force is located approximately at the injector end. With an SITVC system, the applied side force is located downstream of the nozzle throat and approximately at the point of injection, resulting in an increased moment arm which decreases the required side force.

Performance Evaluations

The performance of any type of secondary injection system is based upon two performance

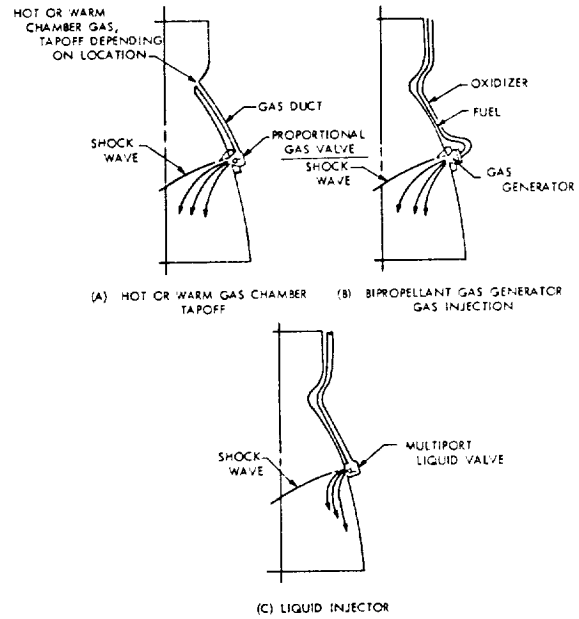


Figure 7-17.—Secondary injection systems.

factors: amplification (K) and axial thrust augmentation (K_1). These factors are defined as follows:

$$K = \frac{I_{S_s}}{I_{S_p}} = \frac{F_s/\dot{w}_s}{F_p/\dot{w}_p} = \frac{F_s/F_p}{\dot{w}_s/\dot{w}_p} \quad (7-1a)$$

$$K_1 = \frac{I_{S_a}}{I_{S_p}} = \frac{\Delta F_a/\dot{w}_s}{F_p/\dot{w}_p} = \frac{\Delta F_a/F_p}{\dot{w}_s/\dot{w}_p} \quad (7-1b)$$

where

- \dot{w}_s = secondary flow rate, lb/sec
- \dot{w}_p = primary flow rate, lb/sec
- F_s = side force, pounds
- F_p = undisturbed axial primary thrust, pounds
- ΔF_a = axial thrust increase, pounds
- I_{S_p} = undisturbed axial specific impulse of the primary chamber (seconds) = F_p/\dot{w}_p
- I_{S_s} = side specific impulse (seconds) = F_s/\dot{w}_s
- I_{S_a} = secondary axial specific impulse (seconds) = $\Delta F_a/\dot{w}_s$

Essentially, the K factor determines the quantity of fluid required to obtain the side force, and the K_1 factor determines the penalty on the overall system I_s to obtain the required side force. If both of these factors are known, the total effect of a given secondary injection system on a propulsion system may be determined.

The K factor determines the quantity of secondary injectant fluid required (for a known duty cycle); the maximum flow rate; the additional tankage, pressurization fluid, and secondary injection hardware weight; and the effect of the added inert weight on vehicle trajectory. The K_1 factor evaluates the I_s penalty on the propulsion system. If K_1 is equal to 1, the specific impulse of the secondary fluid is equal to that of the primary fluid and, therefore, the propulsion system suffers no specific impulse penalty due to the SITVC system.

Both the amplification factor K and the thrust augmentation factor K_1 are influenced by the secondary injection orientation. For each application, a tradeoff must be made between the two factors to determine the optimum injection orientation for maximum propulsion efficiency. Let the force of an external jet of comparable geometry at right angles to the primary nozzle be unity. Then amplification factors greater than 2 are obtained if secondary injection is made with the nozzles pointing upstream, rather than in a normal or downstream direction. Side forces for a given \dot{w}_s are further increased if injection is made through a series of holes arranged on a horizontal arc, rather than through a single orifice. Note that the manifolds required in this case may adversely affect response, however. Test experience suggests that overall pressure ratio and injector size appear to have little effect, while gas temperature does, optimum values being a function of propellant combination.

For an oxygen/hydrogen tapoff system, the range between 3000° and 4000° F appears most favorable; however, as with turbines drives, material strength and cooling problems will dictate values substantially lower, say 1800° F. In a typical tapoff SITVC system, the gas flow rate may be 1.5 to 2.5 percent of the primary flow rate, the upper value indicating the situation of maximum force required between two injection stations (two jets operating). The tapoff system offers simplicity and good performance. However, with low-duty cycles, a continuous bleed may be necessary to maintain temperatures at the valves.

The performance of a gas generator SITVC system is comparable to that of a tapoff system, probably slightly better. This is offset by higher complexity (valves, injectors, ignition, cooling).

Liquid injection systems (inert fluid or propellants) offer the simplest arrangement. This is offset by their low performance, K -factors being in the order of unity, at flow rates from 5 to 6 percent of the primary flow. However, in systems with low-duty cycles, they may still be very attractive.

As a rule, four elements are required for a given system, equally spaced on the main chamber circumference, of which no more than two adjacent ones would be operating at a given time. The control of the required valves is accomplished through a logic and a servosystem analogous to that of a hydraulic gimbal actuator system.

7.6 DESIGN CONSIDERATIONS FOR FLUID-FLOW CONTROL COMPONENTS

By their very nature, liquid propellant rocket engines use many control elements for regulating and measuring of fluid flows, such as valves, pressure regulators, and flowmeters. Some of the design considerations governing these components are discussed below.

Basic Flow Characteristics of an Ideal Fluid

Fluids, by definition, include both liquids and gases. A liquid is an incompressible fluid which is characterized by a tendency to retain a fixed density or volume; but not shape. A gas is a compressible fluid which has no tendency to either a definite shape or volume. Its density or volume will vary according to the basic gas laws (eqs. 1-9, 1-12, and 1-13). In general, the same fundamental laws of force, mass, and velocity apply to matter in all forms, and thus are also applicable to the flow of fluids.

The analysis of fluid-flow controls may be simplified by initially assuming ideal conditions. For the calculation of physical dimensions and functional characteristics of specific control components, the results can then be modified by additional assumptions and empirical factors, which often are the result of extensive testing. A frictionless (zero viscosity), incompressible fluid which is nonturbulent and loses no mechanical energy as heat is referred to as an ideal fluid. For steady, ideal-fluid flow in a closed conduit, Bernoulli's energy equation applies:

CONFIDENTIAL

$$z_1 + \frac{144 p_1}{\rho} + \frac{v_1^2}{2g} = z_2 + \frac{144 p_2}{\rho} + \frac{v_2^2}{2g} = \text{constant} \quad (7-2)$$

Assuming $z_1 = z_2$, and rearranging the expressions, we obtain

$$\frac{144(p_1 - p_2)}{\rho} = \frac{v_2^2 - v_1^2}{2g} \quad (7-3)$$

In conformance with the continuity law of fluid flow

$$\dot{w} = \frac{C_v \rho v_1 A_1}{144} = \frac{C_v \rho v_2 A_2}{144} \quad (7-4)$$

and

$$\frac{v_1}{v_2} = \frac{A_2}{A_1} \quad (7-5)$$

where

- z_1, z_2 = elevations at sections 1 and 2, ft
- p_1, p_2 = static pressures of the fluid at sections 1 and 2, psia
- v_1, v_2 = velocities of the fluid flow at sections 1 and 2, fps
- ρ = density of the fluid, lb/ft³
- g = gravitational constant, 32.2 ft/sec²
- \dot{w} = weight flow rate of the fluid-flow, lb/sec
- C_v = venturi or orifice flow velocity coefficient. This is a function of the design configuration and of the fluid-flow characteristics, and is determined by tests.
- A_1, A_2 = cross-sectional areas of the fluid-flow conduit at sections 1 and 2, in²

The above basic fluid-flow characteristics can be used to measure or sense the flow rate in flow control systems. An accurately sized restriction, such as an orifice, nozzle, or venturi, is inserted in the conduit. Pressure taps are provided for reading the static pressure p_1 and p_2 at the inlet (sec. 1) and at the minimum area of the restriction (sec. 2). If the flow areas A_1, A_2 and the fluid density ρ are known, the flow velocities v_1 and v_2 , and the flow rate \dot{w} can be calculated with the aid of equations (7-3), (7-4), and (7-5). The venturi or orifice meter should be preceded by a straight length of pipe equivalent

to at least 10 times its diameter for repeatable results. For liquid flows, this flow-measuring method is fairly accurate, if friction losses are compensated for by the velocity coefficient C_v . For gaseous flows, however, pressure and temperature have a significant influence on the density of the fluid and must be taken into account for calculations.

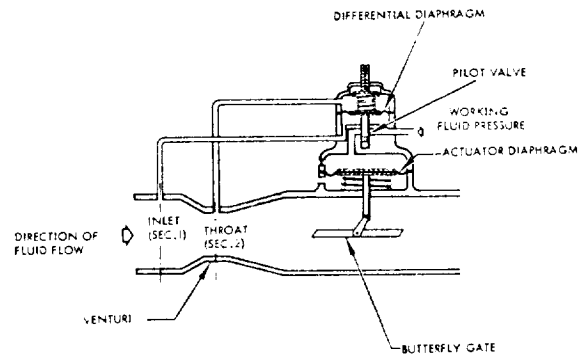


Figure 7-18.—Schematic of a typical closed-loop, fluid-flow control system.

Figure 7-18 is the schematic of a typical closed-loop fluid-flow control system, in which the static pressure differential across a venturi is sensed and used to control fluid flow. The flow is regulated by means of a butterfly gate which is positioned by a fluid-powered actuator diaphragm. The working fluid pressure to the diaphragm is controlled by a pilot valve. Its position in turn is controlled by the pressure differential between venturi inlet (sec. 1) and throat (sec. 2). Because of the dynamic characteristics of the venturi sensing ports, diaphragms, springs, butterflies, and other parts, the relationship between flow rate \dot{w} and venturi pressure differential ($p_1 - p_2$) is not exactly linear. However, theoretical analyses usually permit good approximations of these dynamic functions. The empirical factors thus obtained will permit design calculations resulting in a reasonable degree of control accuracy. Flow-bench calibrations, including adjustments of, for instance, spring forces, serve to further increase this accuracy. The control of fluid flow and pressure by means of orifices and regulators will be further discussed in subsequent sections.

Sample Calculation (7-1)

The following data are given for a horizontal venturi meter, measuring liquid oxygen flow:
 Venturi inlet diameter, $d_1 = 6$ in
 Venturi throat diameter, $d_2 = 3$ in
 Venturi flow velocity coefficient, $C_v = 0.92$
 Pressure differential between inlet and throat
 ($p_1 - p_2$) = 22.5 psi
 Density of LOX, $\rho = 71.38$ lb/ft³
 Determine flow rate \dot{w} .

Solution

From equation (7-5):

$$\frac{v_1}{v_2} = \frac{A_2}{A_1} = \left(\frac{d_2}{d_1}\right)^2 = \frac{1}{4}$$

$$v_1 = \frac{1}{4} v_2$$

Substitute this into equation (7-3):

$$\frac{144(p_1 - p_2)}{\rho} = \frac{v_2^2 - (\frac{1}{4}v_2)^2}{2g}$$

$$v_2 = \sqrt{\frac{2 \times 32.2 \times 144 \times 22.5}{71.38 \left(1 - \frac{1}{16}\right)}} = 55.9 \text{ fps}$$

Substitute this into equation (7-4):

$$\text{Flow rate } \dot{w} = \frac{C_v \rho v_2 A_2}{144} = \frac{0.92 \times 71.38 \times 55.9 \times \frac{\pi}{4} \times 9}{144}$$

$$= 180.2 \text{ lb/sec}$$

Real Fluid Flows Involving Pressure Drops

All real fluids possess the physical property of viscosity; i.e., they offer resistance to shear stresses. The viscosity of the fluid directly affects friction. The basic correlation is given by Newton's law of viscosity (see fig. 7-19):

$$\tau = \frac{\mu U}{gt} \quad (7-6)$$

where

τ = shear stress = F/A , lb/ft²

F = shear or friction force of the fluid tangent to the surface in consideration, lb

A = area of the surface in consideration, ft²
 μ = viscosity of the fluid, lb/ft-sec
 (viscosity conversions:

$$1 \text{ lb/ft-sec} = \frac{1}{32.2} \text{ lb-sec/ft}^2$$

$$= \frac{1}{4636.8} \text{ lb-sec/in}^2 = 14.84 \text{ poise})$$

U = velocity of a fluid particle at the surface in consideration, ft/sec
 t = distance from the point where the velocity of a fluid particle is zero, to the surface in consideration, ft
 U/t = rate of angular deformation of the fluid

When a fluid is forced to flow through a closed conduit, its flow is laminar or nonturbulent below certain "critical" velocities. In a laminar flow, the fluid moves in layers, or laminae, one layer gliding smoothly over an adjacent layer, with only a molecular interchange of momentum. The velocity of the fluid is greatest at the center of the conduit and decreases sharply to zero at the conduit wall. As the flow velocity is increased above the "critical" point, the flow becomes turbulent. In turbulent flow an irregular random motion of the fluid exists, in directions transverse to the direction of the main flow. The turbulent flow velocity distribution is more uniform across the conduit than with laminar flow. Even in turbulent flow there is always a thin layer at the conduit wall, the boundary layer, which moves as a laminar flow.

Experiments and theoretical considerations have shown that the Reynolds number, R_e of a given fluid flow can be used as a criteria to indicate whether a flow is laminar or turbulent.

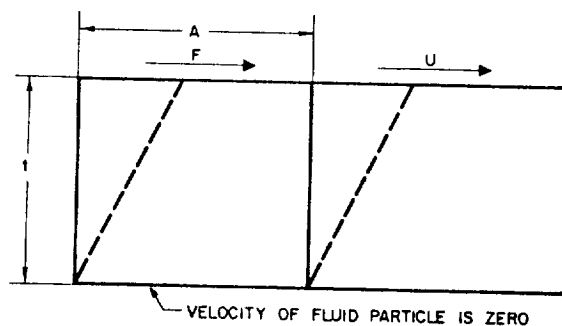


Figure 7-19.—Angular deformation of a real fluid.

($R_e = Dv\rho/\mu$, where D = equivalent diameter of the conduit, ft; v = flow velocity, fps; ρ = fluid density, lb/ft³; and μ = fluid viscosity, lb/ft-sec.) For most calculations, it is assumed that the flow is laminar for Reynolds numbers less than 1200, and turbulent for Reynolds numbers greater than 1200.

Real fluid flows always involve friction caused by rubbing of the fluid particles against one another and against the conduit wall. Consequently, there is a loss of energy; i.e., drop in pressure in the direction of the flow. This energy loss is converted into heat energy. The heat thus produced may be entirely absorbed by the fluid, in one extreme case (adiabatic flow), or it may be entirely dissipated through the conduit wall, in the other extreme (constant-temperature or isothermal flow). Generally—at ambient temperature—the flow of liquids and gases through pipes is assumed to be isothermal. However, adiabatic flow is assumed to take place in nozzles, orifices, short tubes, and valves through which the fluid is moving at high velocities.

The pressure drop Δp (psi) of a fluid flowing in straight conduits (ducts or tubes) in a horizontal position can be estimated by equation (7-7). This is essentially the same as equation (4-32), except for the dimensions.

$$\Delta p = f \frac{L}{d} \frac{\rho v^2}{288 g} \quad (7-7)$$

where

- L = length of the conduit, in
- ρ = density of the fluid, lb/ft³
- v = flow-velocity of the fluid, fps
- d = equivalent diameter of the duct or tube, in

$$= \frac{4 \times \text{duct cross-sectional area (any shape)}}{\text{Wetted perimeter}}$$

f = friction factor, determined experimentally

Equation (7-7) is valid for laminar or turbulent flow of any incompressible fluid in ducts or tubes. With suitable restrictions it may also be used when compressible fluids are being handled. The density of compressible fluids changes considerably as a function of pressure; therefore, if the pressure drop between two points is great, density and velocity will change appreciably.

Also, there will be a slight change in the friction factor. Consequently, it is recommended that equation (7-7) be used with compressible fluids only where the pressure drop Δp is less than 10 percent of the fluid static pressure at the outlet point. To calculate higher pressure drops of compressible fluids, other methods should be used.

If the flow is laminar ($R_e < 1200$), the friction factor is a function of the Reynolds number, and can be arrived at by Poiseuille's equation for laminar flow

$$f = \frac{64}{R_e} \quad (7-8)$$

When the flow is turbulent ($R_e > 1200$), the friction factor depends not only upon the Reynolds number but also upon the roughness of the duct or tube walls. The friction factors of turbulent flows may be found by means of the Moody diagram¹ shown in figure 7-20. The dimensionless term, "relative roughness" (ϵ/D), is a measure of the size of the surface roughness projections relative to the duct diameter. Average values of surface roughness projections ϵ for rocket engine flow control components are given in table 7-3.

For a curved-flow passage or for other shapes, the friction factor f obtained from figure 7-20 has to be modified by an empirical correction factor, which is a function of the Reynolds number and

TABLE 7-3.—Average Values of Surface Roughness Projections for Rocket Engine Fluid-Flow Control Component Designs

Surface description	Roughness projection, ϵ , ft
Drawn tubing with very clean surface	0.000005
Smooth machined and clean surface00001
Machined or commercial cold-rolled surface00005
Rough machined surface0001
Smooth cast or forged surface0003
Commercial cast, forged and welded surface0008

¹Moody, L. F., Friction Factors for Pipe Flows, Trans. ASME, Nov. 1944.

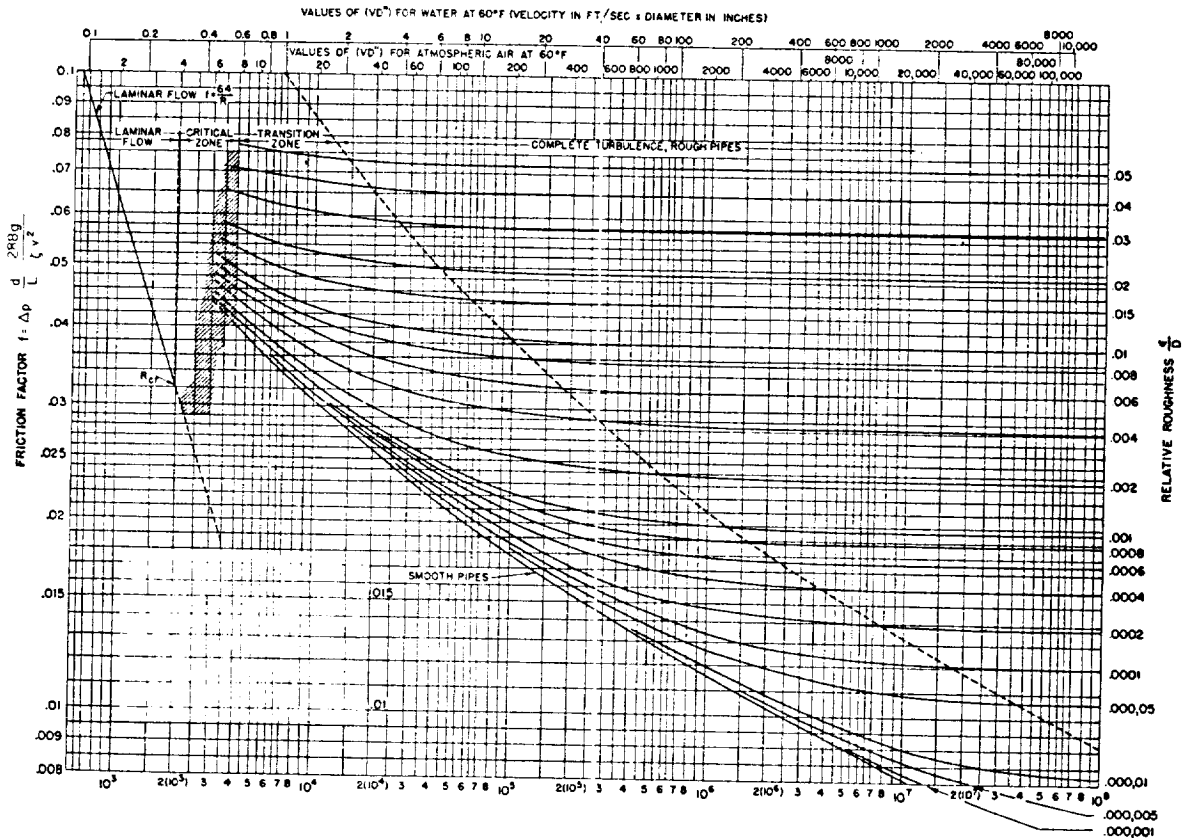


Figure 7-20.—Moody diagram.

of the design configuration. Sometimes the increased resistance of a specific flow passage can be accounted for by assigning to it a fictitious or equivalent length L_e , of straight duct which is arrived at empirically. The sum of this equivalent length and the actual passage length, ($L_e + L$), is then used in equation (7-7) for the calculation of turbulent flow. Figure 7-21 presents typical resistance characteristics of 90° bends.

Because flow-control components such as valves and fittings disturb the flow pattern, they produce an additional pressure drop in a duct or line of tubing. The loss of pressure produced by a flow-control component consists of the pressure drop within the component itself, as well as the pressure drop in the upstream and downstream ducting or tubing in excess of that which would normally occur if there were no component in the line. With certain exceptions, the fluid

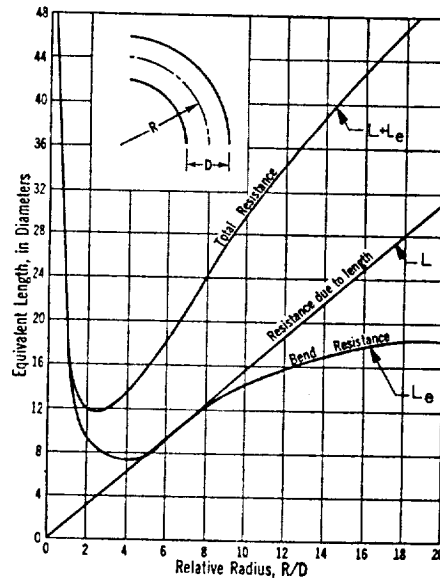


Figure 7-21.—Typical resistance characteristics of 90° bends.

flows through rocket engine control components are usually treated as being turbulent. The true pressure drops chargeable to the components can only be evaluated accurately through actual flow tests.

Figure 7-22 shows a typical test setup for fluid-flow-control components. Pressure taps are located 4 diameters upstream and 10 diameters downstream of the component to be evaluated. This minimizes the flow disturbances at the pressure tapoff points caused by the components. The combination of pressure gages, U-tube manometer, and weighting tank produces quite accurate and repeatable test data. The net pressure drop caused by the component is obtained by subtracting from the measured Δp that pressure drop which is caused by an uninterrupted straight pipe of the same size and length $(a + b) = 14$ diameters, at the same flow conditions.

Because of the large number of fluid-flow-control components used in rocket engines and the great variety of service conditions, it is virtually impossible to obtain individual test data for every type and size of a component for the determination of pressure drop. It is desirable instead to extrapolate from test data which may be already available. This can be done by employing a component resistance coefficient K when calculating pressure drop using the correlation

$$\Delta p = K \frac{\rho v^2}{288 g} \quad (7-9)$$

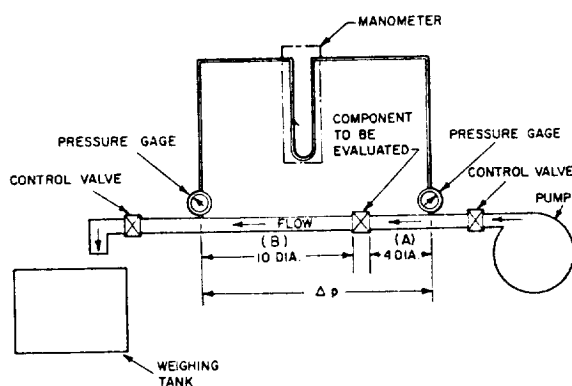


Figure 7-22.—Typical test setup for fluid-flow control components.

where

Δp = pressure drop chargeable to the component as defined by the test method shown in figure 7-22, psi

ρ = density of the fluid, lb/ft³

$v = \frac{144 \dot{w}}{\rho A^*}$ = characteristic flow velocity of the component, fps

\dot{w} = flow rate of fluid passing through the component, lb/sec

A^* = characteristic flow area of the component. This is the minimum cross-sectional area in the flow path of the component when fully open, in². Usually this area is designed to have about the same cross-sectional area as the duct leading to the component.

The coefficient K is essentially constant for any given component over a large range of Reynolds numbers, providing the flow is turbulent. For a given type of component configuration, K may vary with its size. A smaller size tends to have a higher K value. In general, the higher the flow resistance of the component, the more nearly independent of size is the resistance coefficient K . If a series of flow-control components of different sizes were geometrically similar (constant ratio in all the linear dimensions), the resistance coefficient K would then depend upon the Reynolds number only and would not be influenced by component size. However, the design of a component is influenced by design standards, economy of material, structural strength, available space, etc. None of these considerations necessarily require geometric similarity of the various sizes of a given design. Average resistance coefficients for various fluid-flow-control components of liquid propellant rocket engines are presented in table 7-4.

For minimum pressure drop across a flow-control component, the following flow-passage design considerations should be observed:

- (1) Allow sufficient characteristic flow area for the component
- (2) Avoid abrupt changes of flow area
- (3) Avoid abrupt changes of wall contour, and sharp turns in the flow path
- (4) Minimize the length of the flow path within the component
- (5) Provide a smooth surface finish for the flow passages

TABLE 7-4.—Typical Resistance Coefficients for Various Fluid-Flow-Control Components of the Liquid Propellant Rocket Engines

Component description	Resistance coefficient K
Butterfly-type valves (fig. 7-33):	
90° open.....	0.31
80° open.....	.41
70° open.....	.77
60° open.....	1.98
50° open.....	5.68
40° open.....	15.45
30° open.....	44.7
20° open.....	124.2
Ball-type valves (fig. 7-38):	
90° open.....	0.81
70° open.....	1.58
50° open.....	3.6
30° open.....	18.2
20° open.....	63
10° open.....	362
Poppet-type valves (fig. 7-40): Full open	2.5-3.5
Venturi-type valves (noncavitation) (fig. 7-41)	0.8-1.5
Gate-type valve (fig. 7-42):	
Full open.....	0.18
¾ open.....	1.20
½ open.....	5.6
¼ open.....	24
Poppet-type check valve (fig. 7-60)	2 to 4
Swing-gate-type check valve (fig. 7-61)	1 to 2.5
Standard tee.....	1.8
Standard elbow (90°).....	.90
Medium sweep elbow.....	.75
Long sweep elbow.....	.60
45° elbow.....	.42
Sudden enlargement:	
$d_1/d_2 = ¼$	0.92
$d_1/d_2 = ½$56
$d_1/d_2 = ¾$50
Ordinary entrance.....	.50
Sudden contraction:	
$d_2/d_1 = ¼$	0.42
$d_2/d_1 = ½$33
$d_2/d_1 = ¾$19

The characteristics of fluids flowing through orifices will be further discussed in section 7.10.

Sample Calculation (7-2)

The following design data are given for the oxidizer pump discharge flexible duct and the

main oxidizer valve (butterfly type) of the A-1 stage engine.

Liquid oxygen flow rate, $Q = 12\,420$ gpm
 Liquid oxygen density, $\rho = 71.38$ lb/ft³
 Flexible duct inside diameter, $d = 8$ in
 Flexible duct actual length, $L = 16$ in
 Flexible duct equivalent length considering resistance due to flow passage contour deviation, $L_e = 6d$
 Main oxidizer valve characteristic flow area = 78 percent of duct area

Estimate:

- The pressure drop chargeable to the duct
- The pressure drop chargeable to the valve

Solution

(a) Oxidizer flexible duct

The average flow velocity in the flexible duct

$$v = \frac{Q}{3.12 \times \pi \frac{d^2}{4}} = \frac{12\,420}{3.12 \times \pi \times 16} = 79.4 \text{ fps}$$

From table 6-3, the viscosity of liquid oxygen is 0.277×10^{-7} lb-sec/in²; thus $\mu = 0.277 \times 10^{-7} \times 4636.8 = 0.1282 \times 10^{-3}$ lb/ft-sec (see eq. 7-6).

The Reynolds number of the flow in the duct

$$R_e = \frac{Dv\rho}{\mu} = \frac{8}{12} \times 79.4 \times 71.38}{0.1282 \times 10^{-3}} = 2.94 \times 10^7$$

Use a surface roughness projection size ϵ of 0.00005 or a relative roughness

$$\frac{\epsilon}{D} = \frac{0.00005}{\frac{8}{12}} = 0.000075$$

for the duct. From figure 7-20, friction factor, $f = 0.0112$. Substitute the equivalent total length ($L_e + L$) into equation (7-7). The pressure drop chargeable to the oxidizer flexible duct then is

$$\Delta p = \frac{f(L_e + L)\rho v^2}{288gd} = \frac{0.0112(6 \times 8 + 16) \times 71.38 \times (79.4)^2}{288 \times 32.2 \times 8} = 4.34 \text{ psi}$$

(b) Main oxidizer valve

The characteristic velocity of the valve

$$v = \frac{79.4}{0.78} = 101.6 \text{ fps}$$

From table 7-4, the resistance coefficient for butterfly valves $K = 0.31$. Substitute this into equation (7-9) to obtain the pressure drop chargeable to the main oxidizer valve:

$$\Delta p = K \frac{\rho v^2}{288 \text{ g}} = \frac{0.31 \times 71.38 \times (101.6)^2}{288 \times 32.2} = 24.65 \text{ psi}$$

Control Fluid Pressure Level

The working pressure level and the temperature of compressible fluid-flow-control system are important factors, since both govern the density of the fluid. Means of compensation for changes of pressure in a compressible fluid control system must always be provided. With an incompressible fluid, the pressure has relatively little influence on density.

The working pressure level of the fluid determines the selection of the structural design of the components as well as of the sealing methods, especially for dynamic seals. Special provisions are often made to meet the stringent requirements in high-pressure applications. For example, the cutoff events in a high-pressure turbopump-feed engine system may be sequenced so that turbine power is cut first; thus the main propellant valves are not required to shut off against the high main-stage discharge pressures.

Fluid-Flow Velocity

The requirements for smooth component-flow-passage contours are more critical with controls for compressible, or low-density, fluids such as hydrogen than for incompressible fluids, because their design flow velocities usually are much higher than those of the denser liquids. Also, in general the design trend for high-thrust, high-pressure engine systems is toward smaller propellant duct and valve sizes, and consequently toward higher flow velocities (over 100 fps).

An important consideration in the design of high velocity flow-control components is the high-impact loading imposed upon the control

surfaces by the fluid stream. This is especially acute with the higher density liquids. To obtain reliable control performance characteristics with liquids at high velocities, the control components subject to impact loading must be designed to withstand the stresses involved. Also, they should be contoured so as to maintain small impingement angles with the fluid stream and to keep impact forces to a minimum.

Fluid-Flow Temperature

Temperature is an important consideration for the design of fluid-flow controls. This is especially true if the controls are for fluids at temperatures in excess of, or far below, normal ambient.

In liquid propellant rocket engines, fluid-flow controls may have to handle hot gases at temperatures up to about 1700° F. Example: the control of a turbine working fluid. Hot liquids need not be considered, since none of the liquid propellants have sufficiently low vapor pressures to permit handling at high temperatures. Ability to operate at elevated temperatures without any form of lubrication is a prime objective in the mechanical design of fluid-flow control. This can be accomplished by using bearings of either extremely hard, wear-resistant alloys, such as stellite and sintered carbides (high loading condition), or relatively soft materials such as graphite (low loading condition). Bearings are usually subject to compression loads only and are therefore not subject to failure if the materials used are of low ductility. For structural members not subject to wear or bearing loads, conventional high-temperature alloys such as stainless steels and other nickel-base alloys may be used. For static and dynamic seals, metal gaskets and bellows, carbon or graphite face seals, and labyrinth-type seals are suitable at high temperatures.

At the other end of the scale, liquid propellant rocket engine controls may see extremely low-temperature levels, such as in liquid hydrogen service (-425° F). Here, two principal conditions must be considered: (1) The physical characteristics of the fluids which at these low temperatures may affect control performance; and (2) the physical characteristics of the materials from which the control components are made and

which may affect the operation and, thus, the performance characteristics of the control devices.

Many of the cryogenic fluids, i.e., liquefied gases, experience somewhat unpredictable phase changes (two-phase conditions) for relatively small temperature changes. No serious difficulties need to be expected, however, if the heat-transfer rate from components in critical control areas is low enough to prevent vaporization of the liquid. This is particularly important in liquid hydrogen service, where insulation may pose difficult design problems. At any rate, except for viscosity changes, nearly all liquids exhibit more stable physical characteristics with large temperature variations, within the range between their freezing and boiling points, than do gases if the temperature range reaches to their liquefaction temperatures.

The construction materials for fluid-control components for low-temperature applications must be especially carefully selected. Practically every metal undergoes irregular phase changes at low temperatures which may seriously affect its physical properties. While the strength of metals generally increases with a decrease in temperature, further temperature decrease beyond certain limits may result in a decrease in strength. Many metals also become brittle at very low temperatures. Most of the aluminum alloys and the 300-series stainless steels exhibit much better stability at temperatures in the cryogenic range than do others. Elastomers such as Teflon, Kel-F, and Mylar, when used for sealing purposes, exhibit satisfactory mechanical characteristics at extremely low temperatures. Teflon-coated surfaces additionally have good anti-icing characteristics. For further detail on materials, see chapter II.

Fluid-flow-control components for operation at cryogenic temperatures should be designed to be free of external icing effects. In addition to insulation, moisture-preventing purges should be provided internally in critical areas such as bearing interfaces. Also, actuators and/or bearings may require heating.

Rate of Response in Fluid-Flow Controls

Response rate is an important design consideration in any control system. Basically, the

limiting factors governing response rate are (1) the speed with which signals can be transmitted, and (2) the mass/force ratio or its function, the inertia/force ratio of the main control organ.

In many fluid-control systems the controlled fluid is used to transmit the sensed signal. In others, part of the sensing link employs electrical or mechanical means. However, in most cases, part or all of the sensing loop utilizes an impulse generated by a pressure change. This impulse is transmitted at the speed of sound in the fluid. As a typical example, the velocity of sound in water is five times that in air; accordingly, a control signal would be transmitted five times faster in water.

The actuators for most fluid-flow-control mechanisms use pistons or diaphragms, powered by fluid pressure which, in turn, is regulated by some form of pilot valve. If suitable, the controlled fluid may be used as the actuating fluid. The response and flow capacity of the pilot valve, the effective area of actuator piston or diaphragm, and the actuating fluid pressure level influence directly the response rate of the control mechanism for given mass inertia and frictional or other resistances.

To satisfy certain operating conditions and to attain stable control it sometimes becomes necessary to introduce simple damping devices. In most control systems, stability is inversely proportional to sensitivity or response rate. Thus, the design of a fluid-flow-control system should reflect a realistic balance between sensitivity or response rate, control accuracy, and system stability.

Figure 7-23 illustrates the schematic of a typical piston-type actuator for fluid-flow-control devices. The piston when actuated moves against the spring in the direction of the arrow. The basic correlation between the response rate or acceleration of the piston, and other operational parameters, can be expressed by

$$\frac{Ma_p}{g} = A_1 p_1 - A_2 p_2 - F_f - F_t - F_s - Cx \quad (7-10)$$

where

M = effective mass accelerated by the actuator piston, lb. It consists of piston mass, that of moving parts mechanically connected to the piston, and of the mass of all the fluid columns in the system

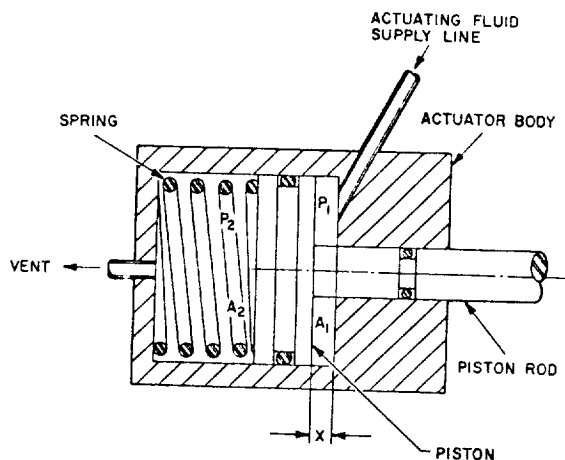


Figure 7-23.—Schematic of a typical piston-type actuator.

a_p = acceleration of the piston, ft/sec²

A_1 = area of the piston actuating side, in²

A_2 = area of the piston vent side, in²

P_1 = actuating pressure, psia. This is the pressure at the actuating fluid source, less the supply-line pressure drop which depends on the flow rate (a function of acceleration a_p)

P_2 = vent pressure, psia. This is the ambient pressure, plus the vent-line pressure drop which also depends on flow rate (again a function of acceleration a_p)

F_r = resistance force of the control function, lb, which also may be a function of acceleration a_p

F_f = friction forces (seals, sliding surfaces, etc.), lb

F_s = initial spring force, lb (at $x = 0$)

C = spring rate, lb/in

x = distance traveled by the piston from its initial position, in

Since the relations between p_1 , p_2 , F_r , and a_p are not linear, equation (7-10) may become complex and require a high-speed computer for solution.

7.7 DESIGN OF DYNAMIC SEALS FOR FLUID-FLOW-CONTROL COMPONENTS

Apart from the static seals, which will be treated in chapter IX, two basic types of dynamic seals are required for fluid-flow-control components: seals for moving (reciprocating and rotating) cylindrical elements such as actuator pis-

tons, shafts, and rods; and seals for valve seats. Here, too, temperature is one of the most important design considerations. Seals can be classified into those for medium-temperature service (-60° to 400° F), low-temperature service (-60° to -425° F), and high-temperature service (400° F and up). The selection of the configurations and the materials for these seals is based to a large extent on service conditions and type of fluid involved. Generally, soft nonmetallic or elastomeric seals are used wherever possible. The outstanding advantage of these seals is that they function satisfactorily despite minor imperfections in the seal or the mating part.

Design of Dynamic Seals for Medium-Temperature Services

Elastomeric O-rings have been widely applied as dynamic seals for moving cylindrical parts as well as for valve seats. However, proper design techniques must be observed to assure success. Figure 7-24 and table 7-5 represent recommended design practices for diametral-squeeze-type O-ring seals for typical dynamic and static applications. Figure 7-26 shows a typical O-ring seal used for a valve seat. Important design considerations for dynamic O-ring seals are summarized as follows:

1. *Design correlations between fluid pressure, O-ring compound hardness and diametral clearance.*—A frequent cause of seal failure is the extrusion of diametral-squeeze-type O-rings into the clearance gap adjacent to the O-ring groove (when under pressure) (fig. 7-25), leaving a permanent deformation after the pressure is reduced. Fluid pressure influences O-ring seal design because it affects the choice of compound hardness. The combination of fluid pressure and chosen hardness will determine the maximum clearance E that can be tolerated safely. A proper combination of clearance and O-ring hardness may prevent O-ring extrusion (table 7-5). In general, the O-ring nominal section diameter is chosen as large as space and installation considerations will permit. Past designs usually will provide a useful guide. In addition, Teflon backup rings as shown in figure 7-25 are recommended for dynamic O-ring seals at sealing pressures over 800 psi and for static O-ring seals at pressures above 1500 psi.

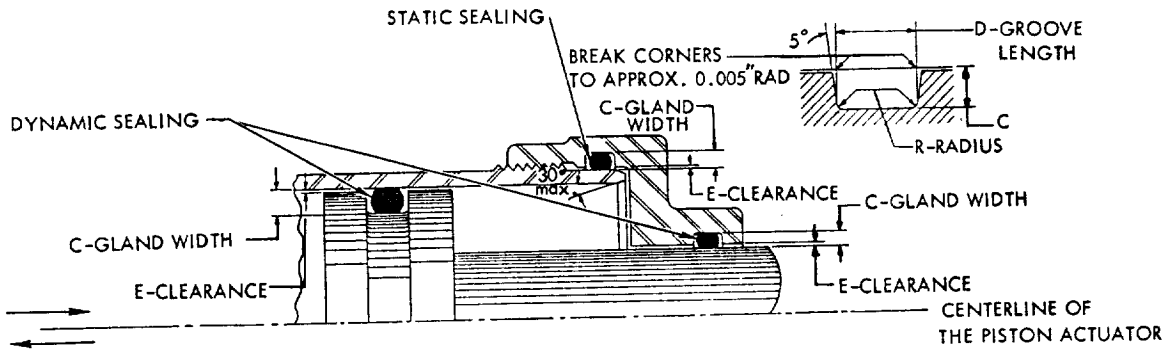


Figure 7-24.—Diametral-squeeze-type O-ring seals in typical dynamic and static applications.

2. *Surface finish requirements.*—The finish of the sliding surfaces in contact with dynamic O-ring seals should be as smooth as possible. They should be ground, honed, or polished to a microinch finish of 8 to 10 rms. It has been found that a finish within this range yields a longer life than either rougher or smoother finishes. Codirectional patterns, as produced by honing, have been proven to be the best surface finish for any type of dynamic sliding seal. For still better results, after an initial finishing, the surface could be hard chrome or nickel plated and again finished. The plating provides a hard, slippery surface that resists corrosion, wear, and scratching. A microinch finish of 60 rms or bet-

ter is recommended for surfaces in contact with static diametral-squeeze-type O-ring seals.

3. *Friction of dynamic O-ring seals.*—The breakaway friction of a dynamic O-ring seal is usually about three times the running friction. Breakaway and running frictions increase with fluid pressure, O-ring hardness, diametral squeeze, and decrease of temperature. Accurate values of O-ring frictions can only be obtained experimentally for a given design.

4. *Selection of O-ring compounds.*—A great variety of O-ring elastomer compounds is available, with trade names such as Silicone rubber, Buna N, Butyl, Viton, Teflon, and Kel-F. The selection of an O-ring compound and its physical

TABLE 7-5.—Recommended Design Practice for Diametral-Squeeze-Type O-Ring Seals

[See fig. 7-15 for explanation of dimensions; all dimensions in inches]

O-ring nominal section diameter	O-ring section diameter	Diametral squeeze, min		C-gland width		D-groove length	R-radius, min	2 × E-diametral clearance, max
		Dynamic	Static	^a Dynamic	^b Static			
1/16	0.070 ± 0.003	0.010	0.015	0.057	0.052	3/32	1/64	0.005
3/32	0.103 ± 0.003	.010	.017	.090	.083	9/64	1/64	.005
1/8	0.139 ± 0.004	.012	.022	.123	.113	3/16	1/32	.006
3/16	0.210 ± 0.005	.017	.032	.188	.173	9/32	3/64	.007
1/4	0.275 ± 0.006	.029	.049	.240	.220	3/8	1/16	.008
		Fluid pressure		O-ring compound hardness				
		0-1000 psi		70 Shore "A" Durometer				
		1000-2000 psi		80 Shore "A" Durometer				
		2000 psi and higher		90 Shore "A" Durometer				

^aTolerance = +0.000, -0.001.

^bTolerance = +0.000, -0.005.

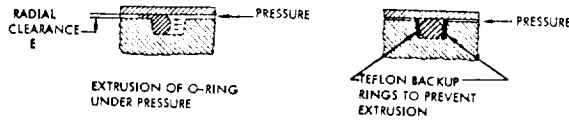


Figure 7-25.—Extrusion of the diametral-squeeze-type O-ring under pressure and the application of backup rings.

properties (furnished by the producer) is based on operating conditions such as type of fluid or propellant, pressure, temperature, and type of seal (dynamic or static).

5. *Installation of diametral-squeeze-type O-ring seals.*—Proper installation of O-rings during component assembly is extremely important to assure an effective seal. Generous chamfers or radii should be provided on all edges and corners in contact with O-rings to minimize the possibility of cutting or scratching during the assembly process.

6. *O-ring seals for valve seats.*—O-rings can be applied effectively as seals for valve seats (fig. 7-26). The resiliency of the O-ring absorbs shock loads and seals tightly at all pressures, even when some dirt and grit are present in the system. One design problem is to prevent the O-ring from being blown out of the groove. This can be prevented by providing a dovetail O-ring groove in a two-piece valve poppet (see fig. 7-26).

Design of Dynamic Seals for Low-Temperature Services

For cryogenic or low-temperature services, lip-type seals made of elastomer sheets (figs.

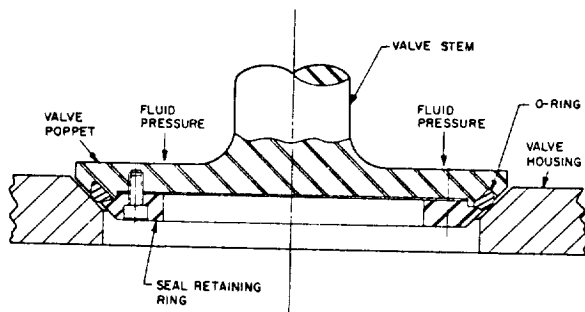


Figure 7-26.—Typical valve seat O-ring seal design for poppet-type valves.

7-27, 7-28, and 7-29) are used effectively as dynamic seals for moving cylindrical parts and valve seats. This type of seal has been applied successfully at sealing pressures over 2000 psi, and at temperatures as low as -425°F . They are also reasonably effective when sealing low-molecular-weight gases such as helium and hydrogen.

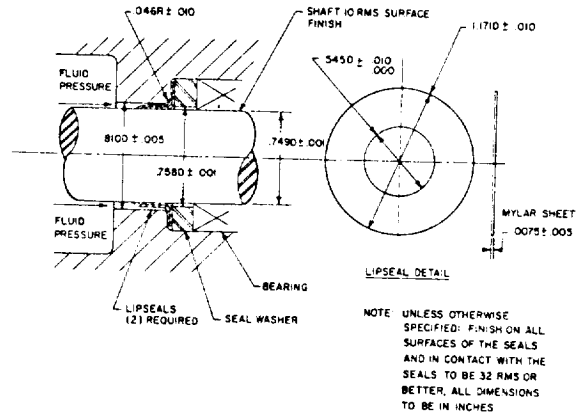


Figure 7-27.—Typical rotating lip-seal design for valve actuator shaft.

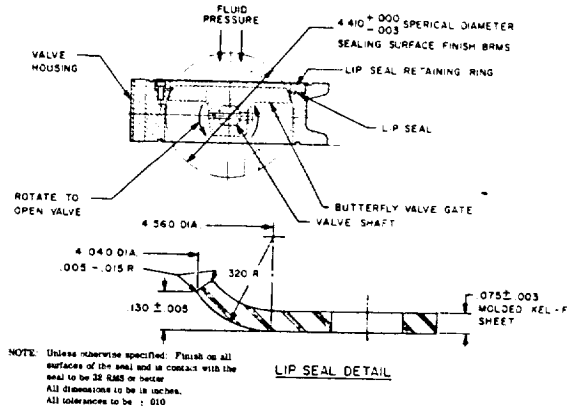


Figure 7-28.—Typical valve seat lip-seal design for butterfly-type valves.

The basic design principle of lip seals is to employ the fluid pressure to increase the contact pressure at the sealing surfaces. Due to their lip configuration, the resilience of these seals is maintained even at very low temperatures. Design considerations for lip seals are similar

to those for O-ring seals. The design approaches can best be illustrated by examples. Figure 7-27 shows a typical valve shaft rotating lip seal arrangement, including dimensions and surface finishes, for liquid oxygen and hydrogen service. Figure 7-28 presents the valve seat lip seal of a butterfly valve for use with the same liquids. Valve seat O-ring seals (fig. 7-26) made of Kel-F have also been successfully applied in poppet-type valves for liquid oxygen. The design of lip seals for piston-type actuators using low-temperature helium gas as the actuating fluid is shown in figure 7-29.

In liquid hydrogen service, metallic bellows (as shown in fig. 7-30) have been used to a great extent to achieve positive dynamic sealing. However, pressure levels and available space impose limitations on their application.

Design of Dynamic Seals for High-Temperature Services

The metallic bellows (fig. 7-30) is most frequently used as reciprocating-type dynamic seals for high-temperature services. Two types of metallic bellows are distinguished: the hydraulic-formed and the multidisk welded type. The former is made of one to three plies of sheet metal and is designed for all pressure ranges. The latter is for relatively low-pressure services and for high flexibility.

A metallic bellows of any type behaves, in part, like a helical spring. The spring rate (lb/in of movement) is a direct function of the

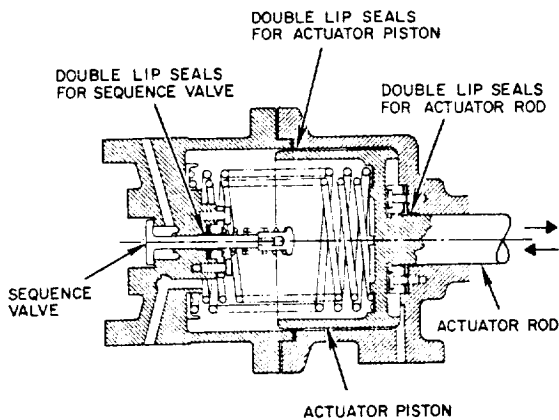


Figure 7-29.—Lip seals for piston-type actuators. Double lip seals seal pressures both ways.

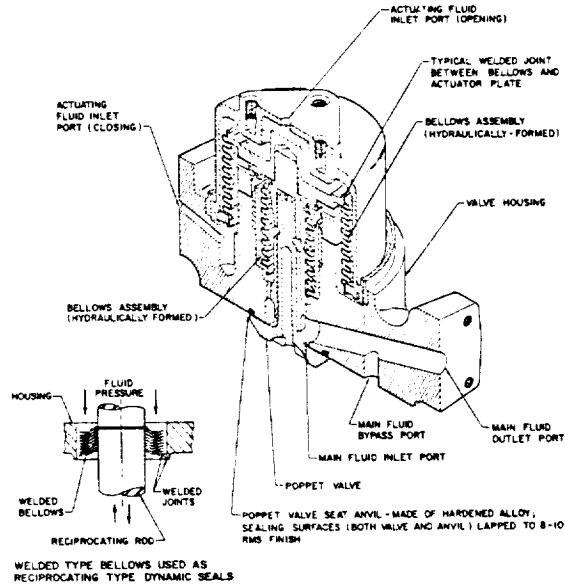


Figure 7-30.—Metallic bellows used as reciprocating-type dynamic seals in a typical poppet valve for high- and low-temperature services.

elastic modulus, and of approximately the square of the thickness of the material. It is also a function of the outside-inside diameters and of the number of convolutions and their curvature. For maximum flexibility (inches of stroke/lb of load), a minimum inside diameter combined with a maximum outside diameter should be used. Also, material thickness (within stress limitations) and modulus of elasticity should be minimum.

Generally, bellows design data, such as stock size, allowable working pressure, spring rate, materials and service temperature, are supplied by the manufacturers. Important design considerations are discussed in the following:

1. *Application of pressure.*—When a bellows is subjected to a differential pressure between interior and exterior, it is preferable to apply the higher pressure to the exterior. This reduces stress, and permits higher pressures and longer life for a given design.

2. *Provision of mechanical stops.*—These should always be provided to prevent extension of the bellows beyond its permissible extended length and compression beyond its "bottomed" height.

3. *Selection of materials.*—Selecting of bellows material should be governed by fluid compatibility or corrosion considerations, operating temperature ranges, and spring characteristics. Some high-temperature alloys such as stainless steels, Monel, Inconel, and Hastelloy B have proven suitable.

4. *Effective area.*—This is that area which, when multiplied by a change in bellows length, yields the actual displaced volume. This area can be approximated by

$$\text{Bellow effective area} = 0.1963 \times (\text{inside diameter} + \text{outside diameter})^2 \quad (7-11)$$

5. *End attachment.*—Typical welded joints for the end attachment of bellows are illustrated in figure 7-30. Silver brazing and soft soldering can also be employed for low-temperature services.

A typical design of a rotating-type dynamic seal for high-temperature services is illustrated in figure 7-31. The dynamic sealing is achieved through the spherical mating surfaces between the graphite seal ring and the steel shaft collar. The contact force of the sealing surfaces is maintained by the shaft thrust spring. Any misalignment between the thrust bearing and the shaft is compensated by the spherical seal face and side movement of the seal ring. This seal arrangement has been applied to a turbine hot

gas throttle valve which was operated successfully at temperatures ranging from 1200° to 1800° F at pressures up to 700 psia. An alternate design is to attach a flat-face graphite seal ring to the end of a metallic bellows which is welded to the shaft (fig. 7-31). Here, the shaft misalignment is compensated by the flexibility of the bellows.

The sealing of valve seats for high-temperature services is usually achieved by metal-to-metal contact, as shown in figures 7-30 and 7-32. This seal design has two basic requirements. Firstly, a finish of 10 rms or better is required for the sealing surfaces. Secondly, a high-enough unit loading must be applied to create a compensating deformation of the sealing surfaces and to achieve the intimate contact required to overcome manufacturing tolerances, distortion of the

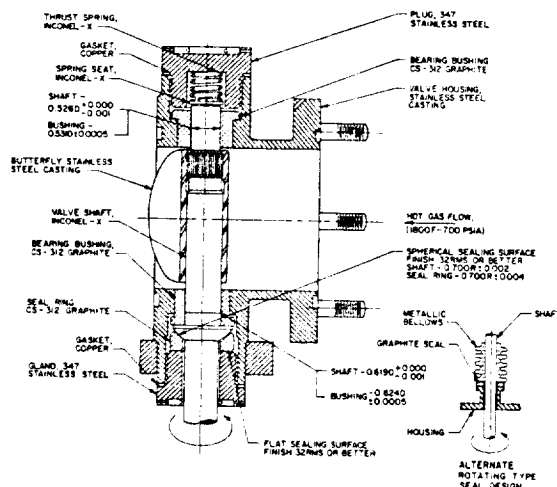
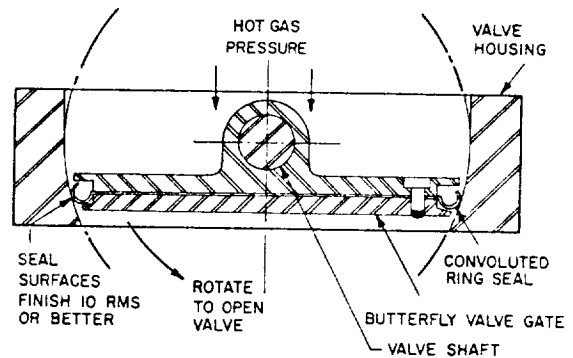
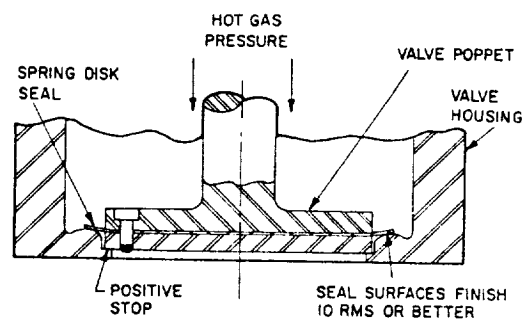


Figure 7-31.—Turbine hot gas throttle valve with typical rotating-type dynamic seals.



(a) CONVOLUTED RING TYPE VALVE SEAT SEAL USED IN A HOT GAS SHUTOFF BUTTERFLY VALVE



(b) SPRING DISK TYPE VALVE SEAT SEAL USED IN A HOT GAS SHUTOFF POPPET VALVE

Figure 7-32.—Valve seat seals for high-temperature services.

valve parts due to temperature, internal stress, and mechanical loading of the mating parts.

Figure 7-32(a) shows a convoluted-ring-type valve seat seal used in a hot gas shutoff butterfly valve. Depending upon the specific application, the convoluted ring may be made of high-temperature alloys such as Inconel-718. The rings effect a leakproof seal in the closed position, since the upstream fluid pressure tends to expand the convolute and produces a high contact unit force at the sealing surfaces. The curvature of the convolute ring tends to maintain a continuous contact with the valve seat. Figure 7-32(b) presents a metallic-spring-disk-type valve seat seal used in a hot gas shutoff poppet valve. Again, the upstream gas pressure produces a high contact unit load on the sealing surfaces. The valve seat has a curved contour which effects a continuous contact with the flat face of the seal disk.

Sealing Specifications

The degree of sealing (or the allowable leak rate) is a very important specification which will dictate the type of seal to be selected for a specific fluid-flow-control component design. The basic reference for leak rates is Specification MIL-S-8484. It states that a Grade A seal, the highest quality seal, shall have a leakage rate not to exceed 1 standard cubic centimeter of air/year/inch of seal at a pressure differential of 1 atmosphere. This corresponds to a leakage rate of 3.171×10^{-8} cc/sec/inch of seal. It is a design assumption that any seal leak rate below or equal to this value is considered zero leakage. For many applications, higher leak rates are permissible. For instance, a check valve may be specified with a leak rate of 5 scim's (standard cubic inches of gas per minute). This is still a relatively tight specification.

7.8 DESIGN OF PROPELLANT VALVES

Propellant valves are used to initiate and terminate propellant flows to main thrust chambers and gas generators. They are usually open-closed, two-position, normally-closed valves. To meet specific sequencing requirements, other designs may provide for an intermediate opening position. For thrust-throttle or mixture-ratio-

control purposes, ability for continuously variable opening position may be required.

In addition to propellant compatibility and structural integrity, prime design considerations for propellant valves are:

- (1) No leakage of propellant through the valve when closed
- (2) Proper actuating time during opening and closing in accordance with the requirements of the control system
- (3) Minimum pressure drop

A great variety of propellant valve types is available. Each design has certain characteristics which make it suitable for a specific application. Frequently used propellant valves, classified according to their design configurations, are:

- (1) Butterfly valves
- (2) Ball valves
- (3) Poppet valves
- (4) Venturi valves
- (5) Gate valves
- (6) Needle valves

Butterfly-Type Propellant Valves

The butterfly valve is one of the most widely used propellant valve types in large liquid propellant rocket engines. It has established a reliable operational record in $LO_2/RP-1$, LO_2/LH_2 , storable, and other liquid propellant services. Existing butterfly valve designs range from 2 to 17 inches nominal diameter, for use at propellant pressures from 20 to over 1500 psia. With improvements in sealing and structural details, successful designs for higher capacities and propellant pressures are certain to be achieved.

Figure 7-33 presents a typical butterfly valve design. Sealing is provided by a lip seal, which engages a spherical surface on the valve gate, similar to figure 7-28. The valve gate pivots on the valve shaft, the axis of which passes through the geometric center of the spherical sealing surface. In most designs, the valve gate rotates 90° from the closed to the fully opened position. The valve is operated by a piston-type actuator, through a connecting link and shaft crank arm. Lip seals are used as dynamic seals for the rotating valve shaft (fig. 7-27). The actuating power is furnished either by noncryogenic propellant pressure, or by an inert gas supply, and

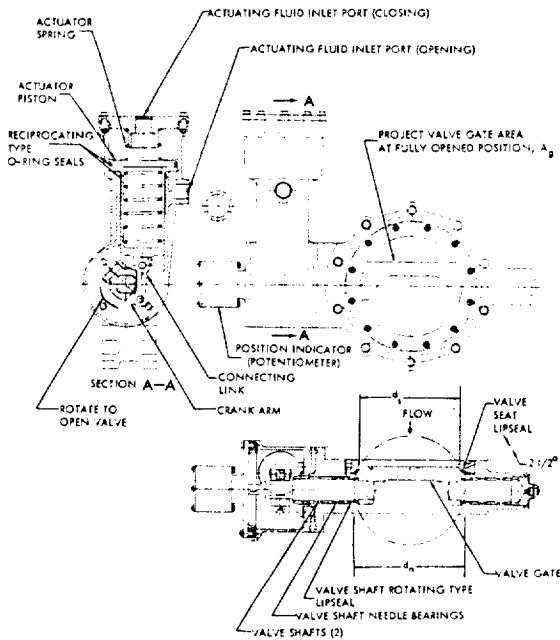


Figure 7-33.—Typical butterfly-type propellant valve design (shown in the closed position).

controlled by a pilot valve. The valve shown is designed to be normally closed by a spring which is installed on the closing side of the actuator piston. Except for shaft and pins which are made of stainless steels, most of the other parts are made of aluminum-alloy forgings. Figure 7-34 shows a 4-inch, butterfly-type, liquid oxygen valve used on the Rocketdyne Atlas ICBM booster engine.

Butterfly valves have relatively low resistance to fluid flow. They are compact, light, and easy to service. They have a high characteristic area which can be expressed as

$$A^* = \frac{\pi}{4} d_s^2 - A_g \quad (7-12)$$

where (see fig. 7-33 for dimension references)

A^* = characteristic area of the valve, in²

d_s = inside diameter of the valve seat lip seal, in

A_g = projected valve gate area at the fully open position, in²

Values for A^* range from 65 percent of the duct area (duct area = $\pi/4 d_n^2$, where d_n = valve nominal diameter, in) on a 2-inch size valve, to about 87 percent of the duct area on a 12-inch

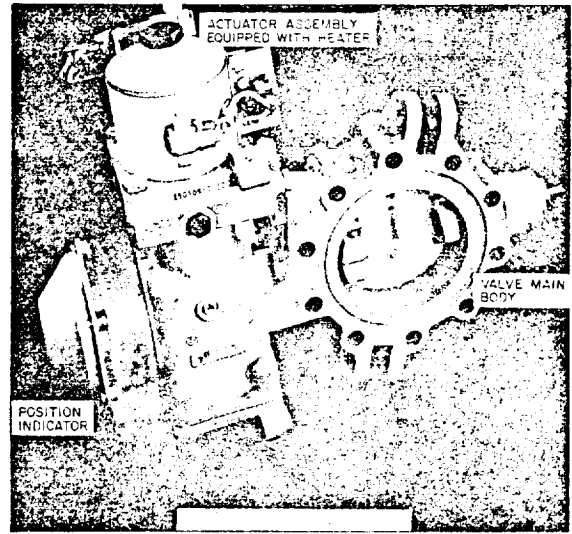


Figure 7-34.—Four-inch butterfly-type main liquid oxygen valve used on Rocketdyne Atlas ICBM booster engines.

valve. A butterfly valve maintains a relatively smooth fluid-flow stream over a wide range of valve-gate angular positions. Thus, when used as a throttle valve, it has little tendency toward turbulence with attendant adverse effects such as local propellant cavitation. Typical fluid-flow resistance coefficients K at various opening positions of a butterfly valve are listed in table 7-4.

When RP-1 is used as the actuating fluid for the liquid oxygen valve, in a LO₂/RP-1 system such as the A-1 stage engine, a heater may be required at the actuator to keep the RP-1 from freezing. The actuator-valve arrangement of the butterfly valve shown in figure 7-33 provides flexibility for specific engine control system needs: the valve may be normally open or normally closed; position indicators may be added; closing of the valve may be accomplished by means of a pyrotechnic squib, rather than by pneumatic pressure. Figure 7-35 illustrates the linkage between the main oxidizer valve and the igniter fuel sequence valve of the A-1 stage engine. During the opening stroke, the cam attached to the main oxidizer valve shaft actuates the igniter fuel sequence valve to open. Frequently, a potentiometer is also attached to the shaft for continuous indication of the angular position of the valve gate.

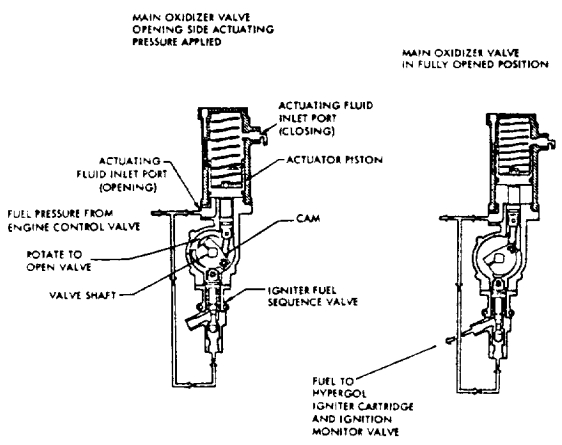


Figure 7-35.—Mechanically linked arrangement between the main oxidizer valve and the igniter fuel sequence valve of the A-1 stage engine.

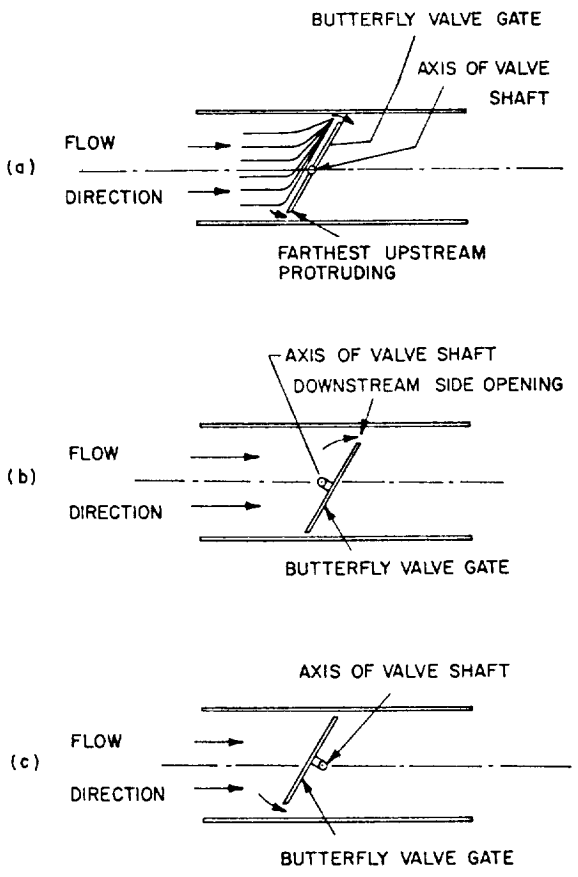


Figure 7-36.—Various locations of valve shaft axis with respect to butterfly valve gate.

The amount of torque required to turn valve shaft and gate is determined by the summation of hydraulic and friction torques. Hydraulic torque is the unbalance of forces on the valve gate caused by the flow of fluid around it. If the axis of the valve shaft is located as shown in figure 7-36(a), the fluid striking the gate portion protruding farthest upstream is deflected more than that at a point near the other end of the gate. This produces an unbalanced force which tends to close the gate. Offsetting the valve gate as shown in figure 7-36(b) would further increase the closing torque, because the fluid velocity rises as it approaches the downstream side opening. Consequently, the resulting low-pressure area tends to increase the unbalance in the closing direction. For this reason, butterfly valves are usually designed offset as shown in figure 7-36(c) (also see fig. 7-33). This produces a fluid velocity effect tending to ease opening of the gate, because of the lower net closing hydraulic torque acting on the valve gate.

Nevertheless, the net hydraulic torque will still be acting in the closing direction for most angular gate positions (9°-80°), unless the valve gate is further offset. Friction torque always opposes rotation. For most operational valve designs

$$T_o = T_f + T_h \quad (7-13)$$

$$T_c = T_f - T_h \quad (7-14)$$

where

- T_o = required opening torque, in-lb
- T_c = required closing torque, in-lb
- T_f = friction torque, in-lb
- T_h = hydraulic torque, in-lb (assumed to act in the closing direction)

The friction torque T_f varies with the pressure differential across the valve gate, and with the valve gate projected area which is a function of gate angular position. Friction torque can be estimated by

$$T_f = K_f t_s f_m d_s^2 \Delta p \quad (7-15)$$

where

- K_f = friction torque coefficient, which is a function of gate angular position (to be determined experimentally)

- r_s = radius of valve shaft at the bearing section, in
- f_m = coefficient of friction between shaft and bearing (0.20 for aluminum journal and steel shaft; 0.05 for needle bearing and steel shaft)
- d_s = inside diameter of valve seat lip seal, in
- Δp = pressure differential across the valve gate, psi

Hydraulic torque T_h may be estimated by

$$T_h = K_h d_s^3 \Delta p \quad (7-16)$$

where K_h = hydraulic torque coefficient, which is a function of gate angular position (to be determined experimentally)

Figure 7-37 shows plots of required opening and closing torques versus gate angular positions for a typical butterfly valve. In actual design practice, the actuator of a butterfly valve will provide two to three times the maximum

estimated opening and closing torques. In addition, at the start of the opening stroke, the actuator has to overcome the static friction forces of all seals. Butterfly-type propellant valves are relatively fast acting. Opening and closing times range from 20 to 200 milliseconds.

Sample Calculation (7-3)

The following design and experimental data are given for the main oxidizer valve (butterfly type) of the A-1 stage engine.

Design Data

- Radius of valve shaft at bearing section, $r_s = 0.8$ in
- Inside diameter of the valve seat lip seal, $d_s = 7.7$ in
- Coefficient of friction between shaft and needle bearing, $f_m = 0.05$

Test Data

Valve gate angular position, deg	Δp , psi	K_f	K_h
5	1058	0.78	1.11×10^{-3}
15	769	0.78	2.55×10^{-3}
40	87.5	1.57	12.50×10^{-3}
85	25	3.61	-11.64×10^{-3}

Determine the required opening and closing torques at the 5°, 15°, 40°, and 85° angular positions of the valve gate.

Solution

From equation (7-15), the friction torques

$$T_f = K_f r_s^2 f_m d_s^2 \Delta p$$

- at 5°: $T_f = 0.78 \times 0.8 \times 0.05 \times (7.7)^2 \times 1058 = 1960$ in-lb
- at 15°: $T_f = 0.78 \times 0.8 \times 0.05 \times (7.7)^2 \times 769 = 1425$ in-lb
- at 40°: $T_f = 1.57 \times 0.8 \times 0.05 \times (7.7)^2 \times 87.5 = 326$ in-lb
- at 85°: $T_f = 3.61 \times 0.8 \times 0.05 \times (7.7)^2 \times 25 = 214$ in-lb

From equation (7-16), the hydraulic torques

$$T_h = K_h d_s^3 \Delta p$$

- at 5°: $T_h = 1.11 \times 10^{-3} \times (7.7)^3 \times 1058 = 535$ in-lb
- at 15°: $T_h = 2.55 \times 10^{-3} \times (7.7)^3 \times 769 = 895$ in-lb

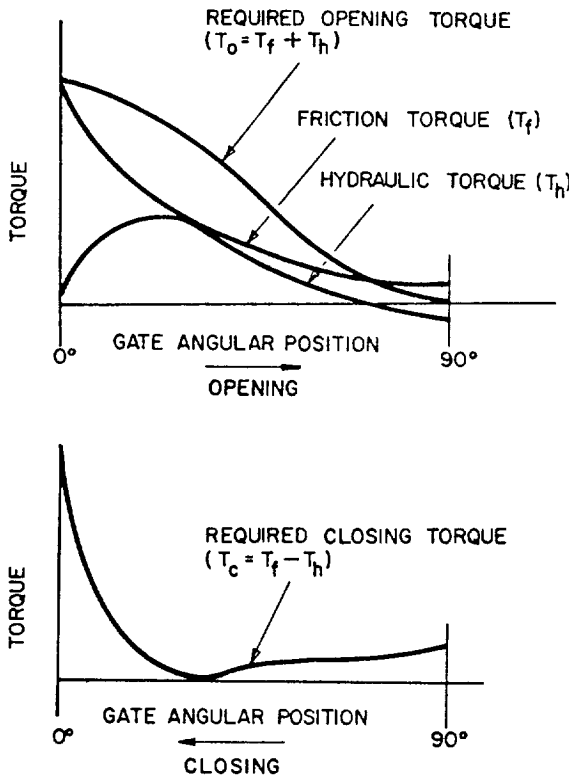


Figure 7-37.—Typical required opening and closing torques versus gate angular position for a butterfly valve.

$$\begin{aligned} \text{at } 40^\circ: T_h &= 12.50 \times 10^{-3} \times (7.7)^3 \times 87.5 \\ &= 500 \text{ in-lb} \end{aligned}$$

$$\begin{aligned} \text{at } 85^\circ: T_h &= -11.64 \times 10^{-3} \times (7.7)^3 \times 25 \\ &= -133 \text{ in-lb} \end{aligned}$$

From equation (7-13), the required opening torques

$$T_o = T_f + T_h$$

$$\text{at } 5^\circ: T_o = 1960 + 535 = 2495 \text{ in-lb}$$

$$\text{at } 15^\circ: T_o = 1425 + 895 = 2320 \text{ in-lb}$$

$$\text{at } 40^\circ: T_o = 326 + 500 = 826 \text{ in-lb}$$

$$\text{at } 85^\circ: T_o = 214 + (-133) = 81 \text{ in-lb}$$

From equation (7-14), the required closing torques

$$T_c = (T_f - T_h)$$

$$\text{at } 5^\circ: T_c = 1960 - 535 = 1425 \text{ in-lb}$$

$$\text{at } 15^\circ: T_c = 1425 - 895 = 530 \text{ in-lb}$$

$$\text{at } 40^\circ: T_c = 326 - 500 = -174 \text{ in-lb}$$

$$\text{at } 85^\circ: T_c = 214 - (-133) = 347 \text{ in-lb}$$

Ball-Type Propellant Valves

The major advantage of a ball valve is its low-pressure drop, since it permits in-line, unrestricted fluid flow. Its use also enhances structural soundness for high-pressure service. It has a reliable record in cryogenic and some storable propellant applications, for high-capacity gas generators as well as for lower thrust main chambers (up to about 50 000-lb thrust). Up to a nominal diameter of 3 inches, ball valves are comparable to other valve types with respect to space envelope and weight. For larger diameters, ball valves are used only infrequently, because it becomes increasingly difficult to meet flight weight and envelope requirements. However, for ground service applications where weight and size are not critical, the ball valves, in all sizes, are used quite frequently. Many ball-type propellant valves are designed in a mechanically linked, dual-valve arrangement, operated by a single actuator.

Figure 7-38 illustrates the design of such a valve. Here, the valve elements are mechanically linked, controlling both oxidizer and fuel flows. The valves can be sized either individually as shown, and according to the specific volumetric propellant flows, or be designed to have a common size. The sealing of a ball valve is accomplished by lip- or O-ring-type seals, riding on the spherical sealing surface of the valve ball. In our specific case, the valve seal

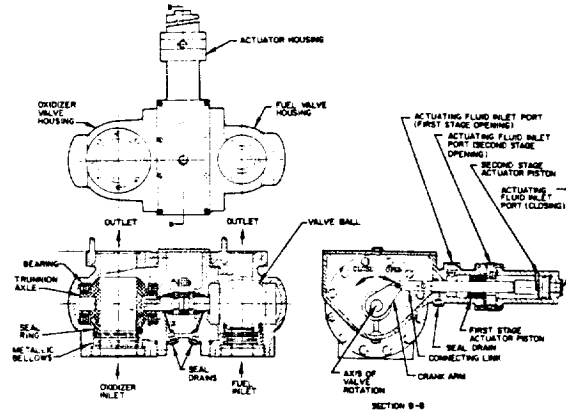


Figure 7-38.—Typical ball-type propellant valve design.

assembly consists of a seal ring and an attached metallic bellows. The area enclosed within the effective seal diameter, $\left(\frac{\pi}{4} d_s^2\right)$, is designed to be less than the effective area of the bellows. During valve closing, this creates an unbalanced force acting on the sealing surface, as affected by the fluid pressure within the bellows.

Each valve ball is trunnion mounted using two integral axles on antifriction bearings. The axis of valve rotation passes through the geometric center of the spherical sealing surface. In most designs, the valve ball rotates 90° from the closed to the fully open position. Typical fluid-flow resistance coefficients K for ball-type valves, as determined at the fully open position, are listed in table 7-4. Ball-type valves can readily be used as flow-regulating devices, such as for propellant throttling. Flow characteristics for constant pressure drops of a typical ball valve at various angular positions are presented in figure 7-39.

The activation of the ball valves shown in figure 7-38 is provided by a piston-type actuator, which could be powered by either fuel pressure or inert gas pressure. The reciprocating motion of the actuator is translated to a rotary motion of the balls by means of a connecting link and crank arm arrangement. The opening sequence of the two valves can be adjusted by varying the relative angular positions between the valve axles and the crank arm. The actuator shown has two stages. First, the valves are opened to an intermediate position (partial opening), then to the

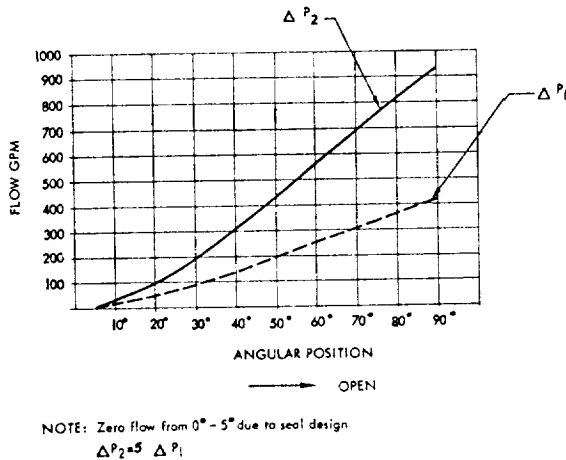


Figure 7-39.—Flow characteristics for constant pressure drops of a typical ball-type valve at various angular positions.

fully open position using separate pistons for each stage. The closing of the valve is effected by venting both opening ports and pressurizing the closing port. Dual seals with a drain between them are provided for all dynamic seals sealing to ambient.

Poppet-Type Propellant Valves

Figure 7-30 shows a typical poppet valve with metal-to-metal seats. This valve is designed to be pneumatically operated and normally closed. All sealings are achieved without the use of elastomers. Because of the nonwiping characteristics of all dynamic seals, this design is particularly suitable for use with fluorine and other highly reactive propellants. A main advantage of poppet valves is their relative simplicity. This is largely due to the reciprocating operation which permits the direct, in-line connection of an actuator. However, this arrangement requires turning of the flow inside the passage, and consequently results in relatively high-pressure drops. Typical fluid-flow resistance coefficients K for poppet valves are given in table 7-4.

Figure 7-40 presents the design of a typical, large size (6 to 10 inches nominal diameter), poppet-type propellant valve. To reduce the unbalanced hydrodynamic forces, and thus the size of the actuator, a balance chamber is provided. The effective area and the fluid pressure

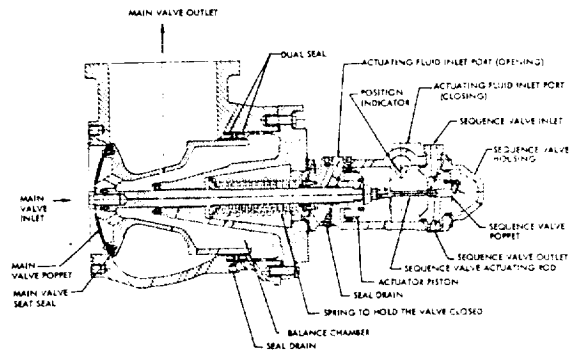


Figure 7-40.—Typical large-size poppet-type propellant valve design.

in the balance chamber are dimensioned so as to result in the proper counteracting force which varies as a function of the unbalanced force at various positions of the valve. A small sequence valve is mechanically attached to the main valve. This type of poppet valve is suitable for high-flow and high-pressure, storable as well as cryogenic, propellant services.

Venturi-Type Propellant Valves

Figure 7-41 presents a typical design for a venturi-type propellant valve. In certain installations, it may be desirable, for various reasons, to use a valve of a nominal size smaller than that of the main duct. A valve installed in the throat of a venturi is a possible solution. The smooth contours of the venturi limit pressure drop penalties to a few psi. Adjacent ducting permitting, it is conceivable that the venturi may simultaneously be used for flow measurements. Typical resistance coefficients K for venturi valves are given in table 7-4.

The venturi may be designed to operate as a cavitating venturi. Based on Bernoulli's energy equation (eq. (7-2)), the minimum pressure of a liquid is made to fall below its vapor pressure. As a result, a gaseous region forms at the throat. If this gas moves through the throat at the velocity of sound, downstream pressure variations and disturbances cannot advance beyond the throat. Up to minimum pressure differentials across the venturi (say 20 percent of upstream pressure), flow rate is dependent on upstream pressure only. When used as a throttling device, the cavitating venturi affords smaller pressure drops,

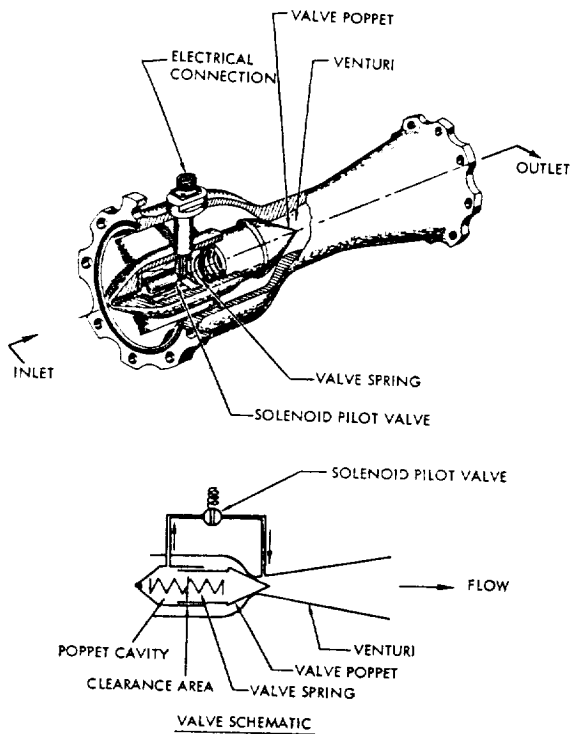


Figure 7-41.—Typical venturi-type propellant valve designed and manufactured by Fox Valve Development Co.

since the gaseous characteristics at the throat effect a near linear relationship between flow rate and supply pressure, rather than according to a square law. The fluid-flow venturi valves have been applied successfully in cryogenic and storable propellant services.

In fluid-flow systems which require flow limitation as well as a shutoff control valve, the venturi valve with a cavitating diffuser will provide both, at a weight of only the valve and at a pressure drop of only the venturi.

Venturi valves occupy a relatively long space in the direction of flow, between 4 to 6 times of the line nominal diameter. This length imposes limitations on size and application in engine systems. However, venturi valves up to 10 inches nominal diameter have been successfully built for rocket vehicle systems.

Figure 7-41 presents a typical venturi-type propellant valve designed and manufactured by Fox Valve Development Co. It is a pilot-operated shutoff valve which consists of a convergent-divergent venturi section with a simple, spring-

loaded poppet seated at the throat. Propellant line pressure controlled by a solenoid pilot valve is used to actuate the valve open or closed. As shown in the valve schematic (fig. 7-41), the normally closed pilot valve is inserted in a passageway interconnecting the poppet cavity and an opening in venturi throat. Normally, upstream propellant pressure fills the poppet cavity and provides additional seating force on the poppet in the same direction as the valve spring to assure valve closure. When the pilot valve is energized to open, propellant pressure behind the valve poppet is vented out at a greater rate than it can be replaced by leakage through the poppet clearance area. This results in a reduced pressure overcoming the valve spring and causes the main valve poppet to open. The venturi valve contains no dynamic seals. Since the valve body is not pierced by a shaft or actuator rod and there are no dynamic seals, no pathways exist for leakage to ambient. The small number of moving parts further enhances reliability.

Gate-Type Propellant Valves

Figure 7-42 shows a typical design of a propellant gate valve. Its major advantage is unrestricted fluid flow, resulting in low-pressure drop. It also provides a relatively short distance between the valve inlet and outlet in the direction of the flow. The design shown in figure 7-42 uses elastomer O-rings as the valve-seat

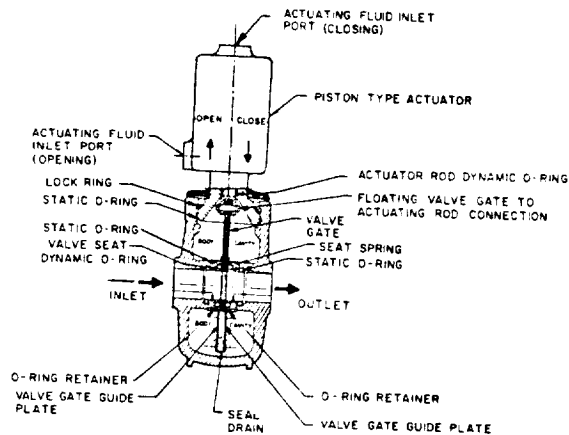


Figure 7-42.—Typical gate-type propellant valve design.

seal. These are suitable only for medium-temperature services. In cryogenic application other seal types are required. Gate valves are designed for propellant line pressures up to 3000 psi. Because of their relative bulkiness, gate valves are limited to low propellant-flow applications such as for gas generator control and ground-support services.

Needle-Type Propellant Valves

A typical needle-type propellant valve is shown in figure 7-43. This valve type is used for extremely low flow applications such as for attitude-control thrust chambers. The assembly shown is a dual-valve arrangement, positively linked by a mechanical yoke. The valve body is an integral part of the thrust chamber injector assembly. Both valves are normally closed. Their actuation is provided by a quick-response electric solenoid.

Sealing at the valve seat is achieved by the elastomer tip of the valve needle. Dynamic sealing at the actuator rods is achieved by means of metallic bellows. This seal design is compatible with cryogenic as well as storable propellants. The pintle vanes provide a guide for the reciprocating motion of the valve needle.

In chapter XI we will discuss other special valve types, as they are needed for very low propellant flow service in miniature-size space engines.

7.9 DESIGN OF CONTROL PILOT VALVES

The main function of a pilot valve is to control a fluid which in turn is used to control or

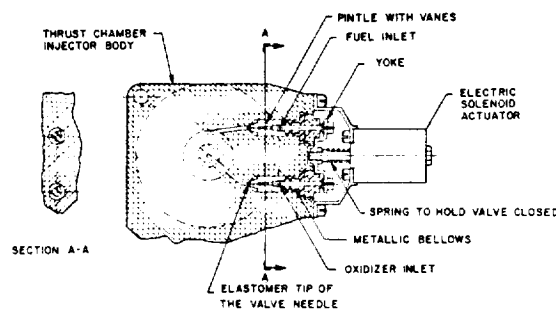


Figure 7-43.—Typical needle-type propellant valve design.

actuate other fluid-flow-control components, such as propellant valves, or to control engine sequence events, such as the admission of igniter fuel. There is a great variety of control pilot valves available for liquid propellant rocket engine services. Basically, they can be grouped into two categories: the on-off type and the proportional type. We confine our discussion here to the on-off type. Since the proportional-type pilot valves are used widely in closed-loop control systems, they will be treated as regulating devices, and discussed in section 7.11. Proportional-type pilot valves are also known as servo valves.

A pilot valve may be operated electrically or by fluid pressure, or through a mechanical connection with other control components. Important design considerations for pilot valves are:

- (1) Fast response
- (2) No leakage of control fluid through the valve when closed
- (3) Required actuating power source compatible with systems design
- (4) Sufficient output at the design point

The output of a pilot valve can be defined as

$$W = p_d \dot{v} \quad (7-17)$$

where

W = pilot valve output at the design point, in-lb/sec

p_d = valve control fluid discharge pressure at the design point, psig

\dot{v} = valve volumetric flow rate at the design point, in³/sec

The most frequently used on-off pilot valves may be classified according to their design configurations into

- (1) Two-way types
- (2) Three-way types
- (3) Four-way types

Two-Way-Type Pilot Valves

The term "two-way" refers to the number of ports. A two-way pilot valve is basically a two-port, open-close-type shutoff valve, similar to a propellant valve. The sequence valves shown in figures 7-35 and 7-40 are typical examples of two-way-type pilot valves. Both examples use a mechanical link, actuated from the main valves.

Solenoid or fluid pressure operated two-way pilot valves are also frequently used.

Three-Way-Type Pilot Valves

A three-way pilot valve (fig. 7-44) has three ports: inlet or pressure port, outlet or cylinder (actuator) port, and vent or return port. If the valve is designed normally closed (N.C.), the fluid path between pressure and cylinder ports is closed, while the path between cylinder and return ports is open. Actuation of the valve effects closing of one fluid path and opening of the other. The reverse is true for a normally open (N.O.) valve; i.e., the fluid path between pressure and cylinder ports is normally open.

Most of the standard pilot valves furnished by specializing manufacturers are solenoid valves, actuated by electrical energy. A direct-acting solenoid valve (fig. 7-44) is one in which opening and closing is controlled by solenoid only. A pilot-operated solenoid valve (fig. 7-45) is one in which the solenoid controls the flow of a small portion of the pressure fluid, which in turn operates the valve. This results in a smaller electrical current required to operate a smaller solenoid for a high-capacity valve. The pilot-operated solenoid valve, necessarily, requires a certain minimum actuating fluid pressure to overcome friction and spring loads before it will open or close.

Figure 7-44 presents a typical direct-acting solenoid, three-way normally closed pilot valve

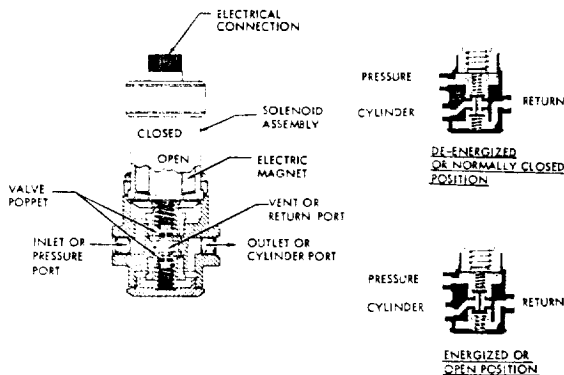


Figure 7-44.—Typical direct-acting solenoid three-way normally closed pilot valve developed by General Controls.

developed by General Controls. Figure 7-45 shows a typical design of a pilot-operated solenoid, three-way pilot valve developed by Skinner. It uses a solenoid to control fluid flow to a diaphragm which opens or closes the valve. The valve may be normally closed or normally open. The selection of standard pilot valves is based on the design data furnished by their manufacturer. For specific applications, modifications can be incorporated into standard designs.

A typical fluid-pressure-actuated, three-way pilot valve design is shown in figure 7-46. This valve may be used as the ignition monitor valve in the A-1 stage engine control system. The valve is held normally closed by a spring. The valve diaphragm is designed as a combined sensing and actuating diaphragm. During engine start and when satisfactory main thrust chamber ignition has been achieved, the pressure buildup sensed at the thrust chamber injector fuel manifold will cause the ignition monitor valve to open

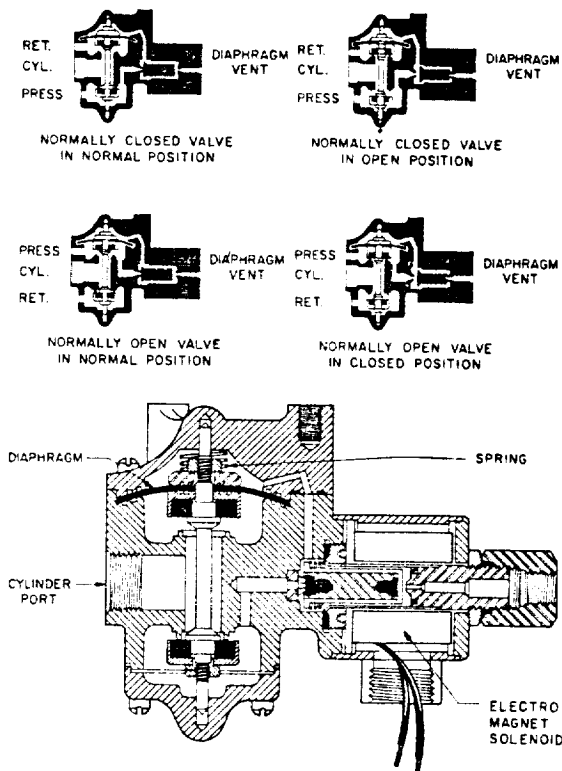


Figure 7-45.—Typical design of a pilot-operated solenoid, three-way pilot valve developed by Skinner.

by pressurizing its diaphragm. The opening of the ignition monitor valve, in turn, directs the fuel pressure to the main fuel valve actuator opening port. The valve spring can be calibrated corresponding to the effective diaphragm area, so that the valve will open at a predetermined sensed pressure. During engine cutoff, decreasing fuel pressure allows the ignition monitor valve to close. This, in turn, vents the opening side of the main fuel valve actuator, closing the valve.

The valve poppet is balanced by internal fluid pressure acting on a dynamic O-ring seal which has the same diameter d_s as the poppet. The valve diaphragm is made of multilayer, thin (0.01 inch) Mylar sheets which are pressure formed with heat added. The effective diaphragm area can be determined experimentally. The required preload of the valve spring may then be estimated by

$$\frac{\pi}{4} d_d^2 p_s = F_f + S_p \quad (7-18)$$

where

- d_d = effective diaphragm diameter, in
- p_s = rated sensed threshold pressure to open the valve, psig
- F_f = static friction of the valve poppet, lb
- S_p = required preload of the valve spring, lb

Sample Calculation (7-4)

The following design data are given for the ignition monitor valve of the A-1 stage engine (fig. 7-46):

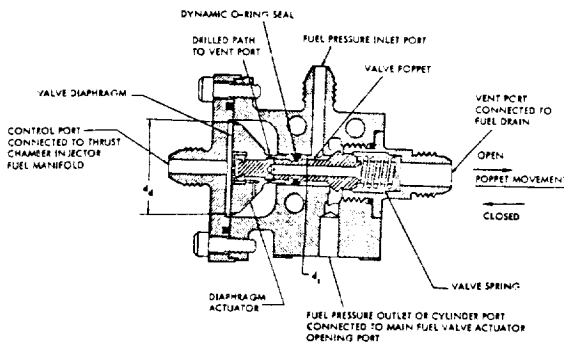


Figure 7-46.—Typical fluid pressure actuated three-way pilot valve used as the ignition monitor valve in the A-1 stage engine.

- Valve characteristic flow area in the fully open position, $A^* = 0.19 \text{ in}^2$; $d_d = 2.1 \text{ in}$;
- $p_s = 20 \text{ psig}$; $F_f = 14 \text{ lb}$
- Valve resistance coefficient at the fully open position, $K = 3.5$
- Required valve volumetric flow rate, $\dot{v} = 200 \text{ in}^3/\text{sec}$
- Inlet port fuel pressure = 350 psig
- Determine the required preload of the valve spring, S_p . Also, calculate the valve output W in the fully open position.

Solution

From equation (7-18), the required valve spring preload

$$S_p = \frac{\pi}{4} d_d^2 p_s - F_f = \frac{\pi}{4} (2.1)^2 \times 20 - 14 = 69.2 - 14 = 55.2 \text{ lb}$$

The characteristic flow velocity of the valve

$$V = \frac{\dot{v}}{A^*} = \frac{200}{0.19} = 1052 \text{ in/sec} = 87.6 \text{ fps}$$

The density of the fuel (RP-1) is 50.45 lb/ft³. Substitute this and other data into equation (7-9). The pressure drop through the valve at the design point

$$\Delta p = K \frac{\rho V^2}{288 g} = \frac{3.5 \times 50.45 \times (87.6)^2}{288 \times 32.2} = 146.5 \text{ psi}$$

The fuel pressure at the valve discharge

$$p_d = 350 - 146.5 = 203.5 \text{ psig}$$

Substitute into equation (7-17), the valve output

$$W = p_d \dot{v} = 203.5 \times 200 = 40700 \text{ in-lb/sec}$$

Four-Way-Type Pilot Valves

A four-way-type pilot valve can replace two three-way valves, for control of double-acting (two-directional) actuators, as shown in figures 7-33 and 7-40. Figure 7-47 presents the basic schematic of a four-way pilot valve. The ports are arranged so that one side is venting while the other is pressurizing.

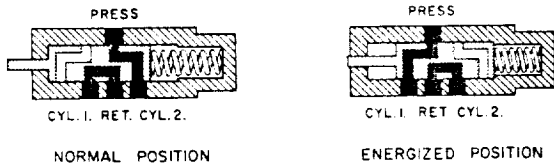


Figure 7-47.—Basic schematic of a four-way pilot valve.

The typical design of a pilot-operated four-way solenoid pilot valve, developed by Valvair, is shown in figure 7-48. This valve type is used to control pneumatic actuators.

Figure 7-49 presents the schematic of a typical self-locking-type, four-way pilot valve. It is held normally closed (cylinder 1 port) by springs S_1 and S_2 . When an actuating pressure p_a is applied to the opening port, the pintle moves and connects the pressure port to cylinder 1 port, and cylinder 2 port to the return port. An unbalanced self-locking force, $\pi/4(d_3^2 - d_1^2)p_i$, acting in the opening direction, causes the valve to stay open, even after the actuating pressure p_a is removed

from the opening port. The valve can be closed only by pressurizing the closing port, and venting the opening port.

Sample Calculation (7-5)

The following data are given for the self-locking-type, four-way pilot valve shown in figure 7-49.

- S_1 spring: Preload = 35 lb, rate = 210 lb/in
- S_2 spring: Preload = 25 lb, rate = 250 lb/in
- Static friction of the valve poppet, $F_f = 24$ lb
- Pressure port pressure, $p_i = 400$ psig
- Actuating fluid pressure, $p_a = 250$ psig
- Return port pressure = ambient
- Poppet guide diameter, $d_1 = 0.5$ in
- Valve poppet total travel = 0.05 in
- Determine diameters d_2 , d_3 , and d_4 (using an actuating-force contingency factor of 1.5).

Solution

Calculate diaphragm diameter d_2 for the required actuating force to open the valve:

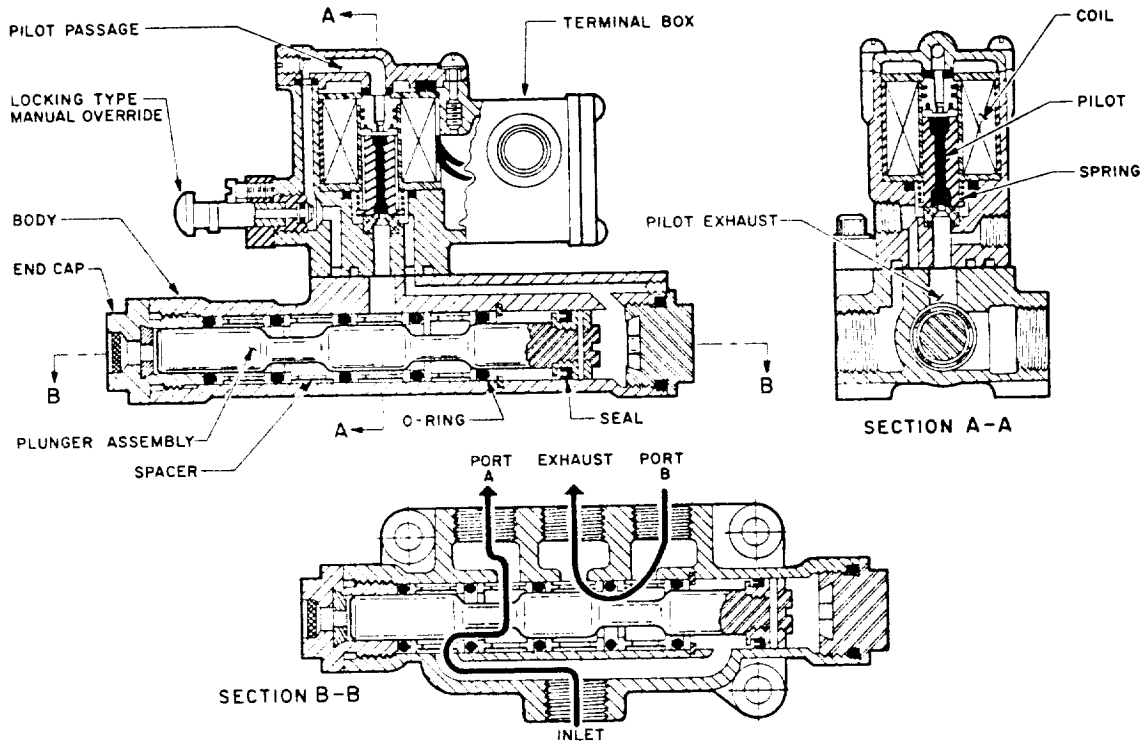


Figure 7-48.—Typical design of a pilot-operated, four-way solenoid pilot valve, developed by Valvair.

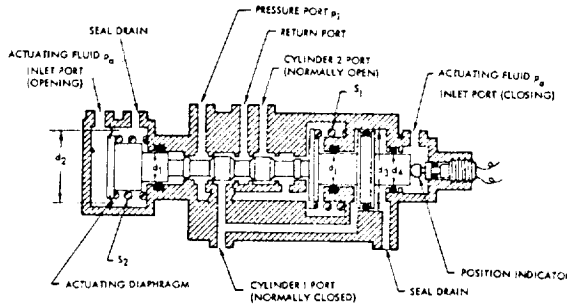


Figure 7-49.—Schematic of a typical self-locking-type, four-way pilot valve.

$$\frac{\pi}{4} d_2^2 p_a = (S_1 \text{ preload} + S_2 \text{ preload} + F_f) \times \text{contingency factor}$$

$$d_2^2 = \frac{(35 + 25 + 24) \times 1.5}{\frac{\pi}{4} \times 250} = 0.64$$

$$d_2 = 0.8 \text{ in}$$

Determine piston diameter d_3 , based on the required force to lock the valve in the open position, in the event the actuating pressure p_a is lost:

$$\frac{\pi}{4} (d_3^2 - d_1^2) p_i = (\text{spring forces} - F_f) \times \text{contingency factor}$$

$$d_3^2 = \frac{(35 + 25 + 210 \times 0.05 + 250 \times 0.05 - 24) \times 1.5}{\frac{\pi}{4} \times 400} + (0.5)^2$$

$$= 0.281 + 0.25 = 0.531$$

$$d_3 = 0.73 \text{ in}$$

Calculate diameter d_4 for the required force to close the valve:

$$\frac{\pi}{4} d_4^2 p_a = \left(\frac{\pi}{4} (d_3^2 - d_1^2) p_i + F_f - \text{spring forces} \right) \times \text{contingency factor}$$

$$d_4^2 = \frac{0.222 \times 400 + 24 - (35 + 25 + 210 \times 0.05 + 250 \times 0.05)}{\frac{\pi}{4} \times 250} \times 1.5 = 0.22$$

$$d_4 = 0.47 \text{ in}$$

Design of Solenoid Actuators

Solenoid actuators are usually applied to the sliding stem of pilot valve poppets, for on-off, two-position operation (figs. 7-44, 7-45, and 7-48). Solenoids are electromagnets, containing an armature or plunger which moves in a coil of wire. When the coil is energized, a magnetic force is exerted on the plunger. The magnitude of the force is proportional to the cross-sectional area of the plunger, the number of the coil turns, the electric current applied to the coil, and the gap G between plunger and core. It increases as the gap narrows.

Figure 7-50 shows a typical direct-current solenoid actuator as frequently used in two-position-type, pilot valve services. Its magnetic current consists of a stationary core, the case, a base, and the plunger. When the coil is energized, the plunger, along with the valve stem connected to it by a bolt, is pulled toward the core, against a compression spring. This spring pushes the plunger back to the normal position when the coil is deenergized.

The following are general correlations for flat-faced, plunger-type magnets of the type shown in figure 7-50.

$$F = \frac{B^2 A}{C} \quad (7-19)$$

$$B = \frac{f P N I}{C} \quad (7-20)$$

where

F = pull force on the plunger in its normal position, lb

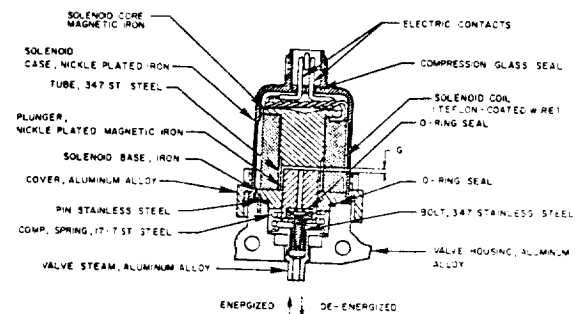


Figure 7-50.—Typical direct-current solenoid actuator design frequently used in two-position-type pilot valves.

B = magnetic flux density in the air gap, kilomaxwells/in²

A = plunger cross-sectional area, in²

C = a factor comprising constants and allowances for stray flux. A value of 72 is applicable to round, flat-faced, plunger-type magnets

P = a factor comprising constants and the permeability of the fluid in gap G between core and plunger; a value of 0.00319 applies if an airgap is assumed

f = flux leakage factor. It is determined by analyzing the magnetic circuit

N = number of coil turns

I = electric current applied to the coil, amperes

G = gap between core and plunger, in

Solenoid actuators, particularly if energized for extended periods, must be designed with sufficient radiating surface to prevent the temperature from becoming excessive. To give the required current, the resistance of the coil should be based on its maximum temperature. Suitable protection, such as seals, should be provided to prevent the solenoid from becoming contaminated with propellants. If the plunger is designed to bottom-out against the core when energized, it is advisable to provide for a thin wafer of nonmagnetic material at its face to prevent sticking.

Sample Calculation (7-6)

The following data are given for the solenoid actuator of the A-2 stage engine four-way pilot control valve:

Required actuating force at start of stroke,
 $F = 27$ lb

Nominal electric supply: 28 volts dc; 2.0 amperes maximum

Valve poppet travel = Air gap between solenoid core and plunger, $G = 0.05$ in

Plunger diameter = 0.56 in

Assumed flux leakage factor, $f = 0.7$

Determine the ampere-turn requirements of the solenoid.

Solution

Plunger area:

$$A = \frac{\pi}{4} \times (0.56)^2 = 0.246 \text{ in}^2$$

Substitute this and other values into equation (7-19):

$$F = \frac{B^2 A}{C}; \quad 27 = \frac{B^2 \times 0.246}{72}$$

The required flux density:

$$B = \sqrt{27 \times 72 / 0.246} = 88.8 \text{ kilomaxwells/in}^2$$

Substitute this into equation (7-20):

$$B = \frac{fPNl}{G}; \quad 88.8 = \frac{0.7 \times 0.00319 \times NI}{0.05}$$

The required ampere-turns for the solenoid coil

$$NI = \frac{88.8 \times 0.05}{0.7 \times 0.00319} = 1990 \text{ ampere-turns}$$

Assume a current of 1.4 amperes for the solenoid; then the required number of turns

$$N = \frac{1990}{I} = \frac{1990}{1.4} = 1425 \text{ turns}$$

The required electric resistance of the solenoid coil, at operating temperature

$$R = \frac{E}{I} = \frac{28}{1.4} = 20 \text{ ohms}$$

The wire can now be selected for the required resistance. For instance, we may choose a No. 26 AWG copper wire (0.017-inch diameter, enameled) and wind it to an average coil diameter of 1.05 inches.

Resistance = 51 ohm/1000 ft, warm.

Total length = $1.05 \times \pi \times 1425 / 12 = 391$ ft.

$R = 391 \times 51 / 1000 = 20$ ohms.

Lay wires 22 deep, 65 high.

Thickness of coil: $22 \times 0.017 = 0.374$ in.

Inside diameter = $1.05 - 0.374 = 0.676$ in.

This leaves $0.676 - 0.56 = 0.116$ for insulation, sleeves, and plunger clearance. Height of coil: $65 \times 0.017 = 1.1$ inches. Outside diameter = 1.424 inches.

7.10 DESIGN OF FIXED-AREA-TYPE REGULATING DEVICES

Fixed-area-type regulating devices, such as orifices, nozzles, and venturis, are frequently used in rocket engines for fluid system calibration and for control purposes. Although the energy loss caused by an orifice is high, as compared to that of nozzles or venturis, orifices are extensively used because of their compactness and simplicity (fig. 7-2).

Orifices and Nozzles for Liquid Flow

The basic correlations for liquid flow through orifices and nozzles are (assuming uniform flow distribution):

$$\dot{V} = 0.0438 C d_o^2 \sqrt{\Delta h} = 0.525 C d_o^2 \sqrt{\frac{\Delta p}{\rho}} \quad (7-21)$$

$$\dot{w} = 0.0438 C d_o^2 \rho \sqrt{\Delta h} = 0.525 C d_o^2 \sqrt{\Delta p \rho} \quad (7-22)$$

$$k = \frac{\Delta p_o}{\Delta p} \quad (7-23)$$

where

- \dot{V} = volumetric flow rate, ft³/sec
- \dot{w} = weight flow rate, lb/sec
- ρ = density of the fluid, lb/ft³
- Δh = static pressure head drop across the orifice or nozzle, ft
- Δp = static pressure drop across the orifice or nozzle, psi
- d_o = diameter of the orifice or nozzle throat, in
- d_1 = diameter of the duct leading to the orifice or nozzle, in
- C = flow coefficient for orifices or nozzles.
Considers the effects of discharge jet contraction in orifices, velocity of approach, diameter ratio d_o/d_1 , friction and flow profile
- Δp_o = total (or permanent) pressure drop chargeable to the orifice or nozzle, psi
- k = factor, correcting nozzle or orifice working pressure to permanent pressure loss

The correlations are still reasonably accurate for gas flows, if the pressure drop across the control orifice is small (<10 percent).

The value of flow coefficients C is a function of the design configurations and flow Reynolds

number and can only be evaluated by experiments. Typical designs and flow coefficients of frequently used orifices and flow nozzles are presented in figures 7-51(a), 7-51(b), and 7-51(c). Orifices of the VDI type are preferred because their behavior is more predictable. This is attributable to the bevel at the backside, which prevents erratic wall reattachment of the contracted jet within the orifice. It is important that the leading edge be absolutely sharp. The value of k is a function of the diameter ratio (d_o/d_1). The $(\Delta p_o/\Delta p)$ versus (d_o/d_1) relationship is plotted in figure 7-52.

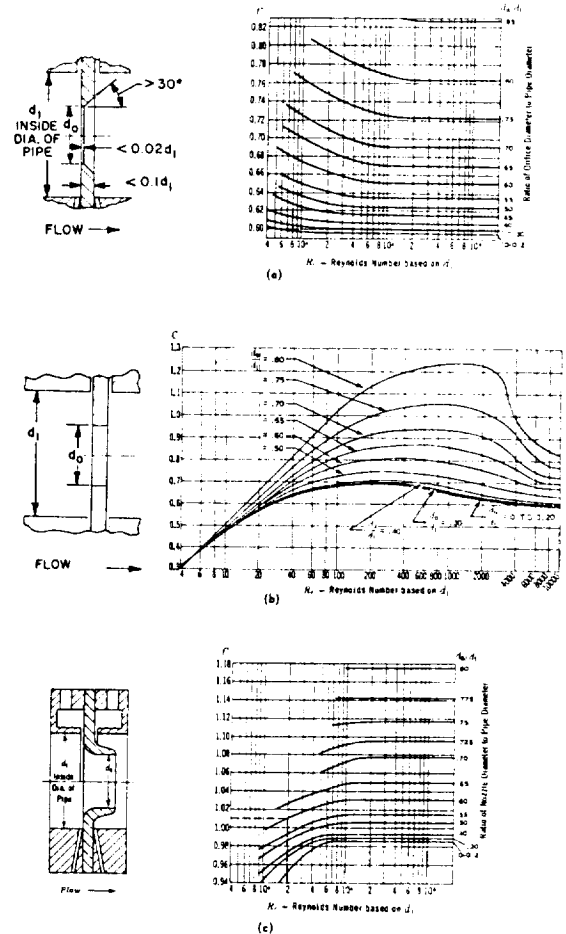


Figure 7-51.—Typical designs and flow coefficients C of flow regulating orifices. A, VDI type; B, square edged; C, VDI type flow nozzles.

Sample Calculation (7-7)

The following data are given for the fuel pump discharge duct of the A-1 engine:

Required fuel weight flow rate, $\dot{w} = 892$ lb/sec

Fuel pump discharge duct diameter, $d_1 = 7$ in

Selected design value of total pressure drop for orifice or flow nozzle installed in the fuel duct, $\Delta p_o = 100$ psi

Estimate the required diameter d_o , (a) for a VDI-type orifice, and (b) for a VDI-type flow nozzle (figs. 7-51(a) and 7-51(c)).

Solution

The average flow velocity in the fuel duct

$$v = \frac{\dot{w}}{\rho \frac{\pi}{4} (d_1)^2} = \frac{892}{50.45 \times \frac{\pi}{4} \times \left(\frac{7}{12}\right)^2} = 66.3 \text{ fps}$$

From table 6-3, we obtain the viscosity of RP-1 = 3.22×10^{-7} lb-sec/in², or $\mu = 3.22 \times 10^{-7} \times 4636.8 = 1.494 \times 10^{-3}$ lb/ft-sec (see eq. 7-6).

The Reynolds number, based on duct diameter d_1 ,

$$R_e = \frac{Dv\rho}{\mu} = \frac{\frac{7}{12} \times 66.3 \times 50.45}{1.494 \times 10^{-3}} = 1.306 \times 10^6$$

From equations (7-22) and (7-23)

$$\dot{w} = 0.525 Cd_o^2 \sqrt{\Delta p \rho} = 0.525 Cd_o^2 \sqrt{\Delta p_o \rho / k}$$

$$\begin{aligned} \frac{Cd_o^2}{\sqrt{k}} &= \frac{\dot{w}}{0.525 \sqrt{\Delta p_o \rho}} = \frac{892}{0.525 \times \sqrt{100 \times 50.45}} \\ &= \frac{892}{0.525 \times 71} = 23.9 \end{aligned} \quad (a)$$

(a) For the VDI-type orifice, we determine by trial and error that d_o , which will simultaneously satisfy equation (a), figure 7-51(a), and figure 7-52. A value of 4.47 inches is found for d_o . Confirm:

$$\frac{d_o}{d_1} = \frac{4.47}{7} = 0.638$$

From figure 7-51(a), a value of $C = 0.67$ is derived for $R_e = 1.306 \times 10^6$. A corresponding

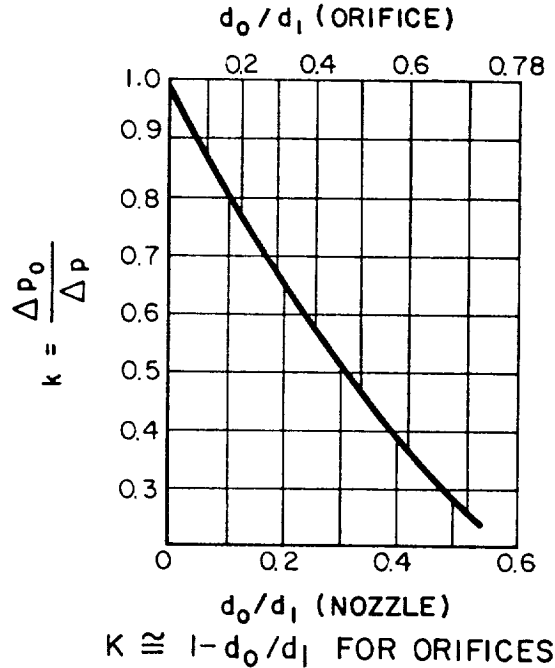


Figure 7-52. $-(\Delta p_o/\Delta p)$ versus (d_o/d_1) for orifices and nozzles.

value of 0.32 for k is obtained from figure 7-52. Substitute this into equation (a):

$$\frac{Cd_o^2}{\sqrt{k}} = \frac{0.67 \times (4.47)^2}{\sqrt{0.32}} = 23.9$$

(b) For the VDI-type flow nozzle, the same approach can be used to determine d_o . A value of 3.55 inches is found for d_o ; thus

$$\frac{d_o}{d_1} = \frac{3.55}{7} = 0.506$$

From figure 7-51(c), a value of $C = 1.005$ is obtained, for $R_e = 1.306 \times 10^6$. From figure 7-52, the corresponding value for k is 0.28. Substitute this into equation (a):

$$\frac{Cd_o^2}{\sqrt{k}} = \frac{1.005 \times (3.55)^2}{\sqrt{0.28}} = 23.9$$

Thus, for the VDI orifice, $d_o = 4.47$ in; for the VDI flow nozzle, $d_o = 3.55$ in.

Orifices for Gas Flow

The basic correlations for an isentropic, compressible gas flow through an orifice are:

$$\dot{w} = \frac{CAp_1Z}{\sqrt{RT}} \tag{7-24}$$

If $(p_2/p_1) \leq$ Critical ratio, i.e.,

$$\leq \left(\frac{2}{\gamma+1}\right)^{\frac{\gamma}{\gamma-1}}, Z = \sqrt{g\gamma \left(\frac{2}{\gamma+1}\right)^{\frac{\gamma+1}{\gamma-1}}} \tag{7-25}$$

If $(p_2/p_1) >$ Critical ratio,

$$Z = \sqrt{\frac{2g\gamma}{\gamma-1} \left[\left(\frac{p_2}{p_1}\right)^{\frac{2}{\gamma}} - \left(\frac{p_2}{p_1}\right)^{\frac{\gamma+1}{\gamma}} \right]} \tag{7-26}$$

where

- \dot{w} = gas weight flow rate, lb/sec
- A = orifice area, in²
- p_1 = gas pressure upstream of the orifice, psia
- p_2 = gas pressure downstream of the orifice, psia
- R = gas constant, ft/°R
- T = gas temperature upstream of the orifice, °R
- Z = compressibility factor, ft^{0.5}/sec
- γ = gas specific heat ratio
- C = flow coefficient, a function of design configuration and flow Reynolds number.
May be approximated from figure 7-51(a) and 7-51(b)
- g = gravitational constant, 32.2 ft/sec²

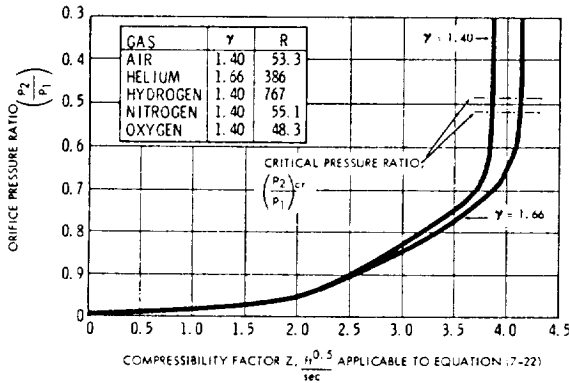


Figure 7-53.—Compressibility factors for an isentropic compressible flow through an orifice.

Values for Z applicable to equation (7-24) for various pressure ratios (p_2/p_1) are presented in figure 7-53.

Sample Calculation (7-8)

The following data are given for an orifice:

- Orifice diameter, $d_o = 0.06$ in
- Flow coefficient, $C = 0.6$
- Helium gas pressure = 500 psig
- Helium gas temperature = 100° F

Calculate the orifice flow rates for downstream pressure, $p_2 = 14.7$ (ambient) and $p_2 = 350$ psia.

Solution

For a downstream pressure of 14.7 psia, the orifice pressure ratio

$$\left(\frac{p_2}{p_1}\right) = \frac{14.7}{500 + 14.7} = 0.0286$$

From figure 7-53, the compressibility factor Z is derived as 4.11 for $\gamma = 1.66$. Substitute this and other parameters into equation (7-24):

$$\begin{aligned} \dot{w} &= \frac{CAp_1Z}{\sqrt{RT}} = \frac{0.6 \times \frac{\pi}{4} (0.06)^2 \times (500 + 14.7) \times 4.11}{\sqrt{386 \times (460 + 100)}} \\ &= \frac{0.6 \times 0.00283 \times 514.7 \times 4.11}{\sqrt{386 \times 560}} = 0.00774 \text{ lb/sec} \end{aligned}$$

For a downstream pressure of 350 psia, the orifice pressure ratio

$$\left(\frac{p_2}{p_1}\right) = \frac{350}{514.7} = 0.682$$

From figure 7-53, we obtain a compressibility factor $Z = 3.88$; thus

$$\dot{w} = \frac{3.88}{4.11} \times 0.0077 = 0.00726 \text{ lb/sec}$$

7.11 DESIGN OF SERVOVALVES

Fixed-area-type regulating devices have definite limitations. For instance, an orifice regulates flow and pressure only under specific conditions of flow, but does not function under

other conditions. By contrast, variable-area-type devices will function under both dynamic and static conditions. Classified according to their function, the most frequently used variable-area-type pressure and flow regulating devices for rocket engines can be grouped into—

- (1) Throttle valves (including valves for thrust and *PU* control)
- (2) Gas pressure regulators
- (3) Liquid flow regulators

Throttle valves have been discussed in section 7.8. Detail on gas pressure and liquid flow regulators will be found in sections 7.12 and 7.13. Many of these devices use some form of fluid-pressure-operated actuator. The position of the actuator, and thus the area of the controlling valve opening, is effected by applying a pressure differential across the actuator piston or diaphragm, by means of various types of servo pilot valves, which will be discussed. The function of a servovalve is similar to that of an on-off pilot valve, except that it can continuously vary the pressure or flow rate of the actuating fluid to control the desired actuator position. In a pneumatic actuating system, the servovalve operates as a pressure control device. It functions as a flow control device in hydraulic systems. In rocket engine applications, where usually only low-power electrical signals or sensing pressure forces are available to operate the valves, servovalves with very high gain characteristic are required. Three basic servovalve types are most frequently used: the flapper-nozzle type (fig. 7-55), the spool type (fig. 7-56), and the poppet type (fig. 7-57). They are used independently, or jointly, to form a two-stage servovalve in which the flapper-nozzle valve acts as a pilot valve for the spool valve. A typical example was presented in figure 7-9.

General Design Considerations for Servovalves:

- (1) Type of control fluid (gas or liquid) and its conditions (pressure and temperature)
- (2) Systems gain: In some applications the ratio between electrical quiescent input power to the valve coils and the maximum valve output (as defined by eq. (7-17)) is as high as 1600-2000
- (3) Bandwidth and frequency response; dynamic stability
- (4) Minimum bleed of control fluid
- (5) Simplicity of construction and line connections
- (6) Compatibility with environmental conditions: temperature, humidity, acceleration, and vibration.

The open-loop gain and phase shift versus frequency characteristics of a typical servovalve and driving amplifier combination are shown in figure 7-54. These characteristics are obtained by applying an input signal to the servoamplifier from an oscillator. The amplifier drives the valve by means of a current input to the valve transducer coil (torque motor). In turn, the valve controls the flow of working fluid to the actuator which produces the desired load force. The voltage output from a potentiometer attached to the actuator is then compared to the amplifier input. Instead of electrical feedback, mechanical feedback may be employed. (See sec. 7.5, "Engine Thrust Vector Control.")

Flapper-Nozzle-Type Servovalves

The flapper-nozzle-type servovalve is essentially a variable orifice or nozzle. Figure 7-55 illustrates schematically the operation of a typical double-bleed unit. Actuating fluid is supplied at a constant pressure or flow rate. When an input signal is fed to the torque motor from a servoamplifier, the electric signal is converted into a mechanical force. The resultant deflection of the flapper is proportional to the input signal and causes the flow of actuating fluid to increase at one nozzle, and to decrease at the

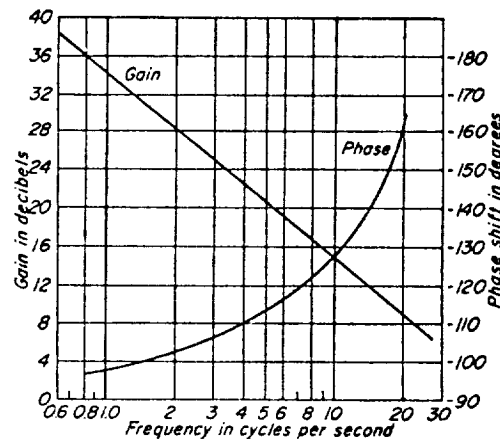


Figure 7-54.—System characteristics of a typical servovalve and driving amplifier combination.

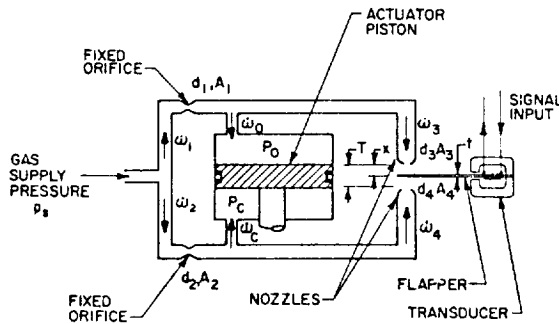


Figure 7-55.—Schematic of a typical flapper-nozzle-type pneumatic servovalve.

other. An increased flow reduces the fluid pressure (compressible fluid) or fluid volume (incompressible fluid) on the corresponding side of the actuator piston. Correspondingly, the fluid pressure or fluid volume on the other side of the piston increases. The resultant pressure differential across the actuator piston causes it to move in the desired direction. The flapper-nozzle valve is also applicable to servo systems with single-control nozzle bleed. Here, the actuator position is controlled by regulating the actuating fluid on one side of the piston or diaphragm only. This is analogous to the single-bleed pneumatic poppet servovalve (fig. 7-57).

Flapper-nozzle valves are particularly suitable as pilot valves for larger servovalves (see fig. 7-9). Because the transducers or torque motors for these valves require rather low power levels, they usually consist of coil relays exerting forces of only a few ounces. The effect of the flapper spring rate is often counterbalanced by the gradient of the magnetic force developed in a properly designed transducer or by mechanical means. To prevent spreading of the jets leaving the nozzles and to ease the rate balancing between flapper spring and transducer magnetic forces, the travel of the flapper should be kept reasonable small.

Equations (7-22) and (7-24), which describe the flow of liquids and gases through orifices and nozzles, are applicable to the design calculations of flapper-nozzle valves. Two conditions may exist for the flow through the nozzles of a flapper-nozzle valve: first, when the restriction is determined by the position of the flapper; and secondly, when the flapper has moved far enough from the nozzle for the flow to be restricted by

the throat area of the nozzle. Most designs are based on the first condition. The effective (ring shaped) flow area then is

$$A_n = \pi d_n X \quad (7-27)$$

where

A_n = effective flow area, in²

d_n = diameter of the nozzle, in

X = displacement of the flapper from the nozzle, in. (Maximum value should be less than $d_n/5$.)

Sample Calculation (7-9)

The following dimensions and data are defined for a flapper-nozzle pneumatic servovalve (schematically shown in fig. 7-55), which is used as a pilot valve of the servo *PU* control valve attached to the main oxidizer valve of the A-2 stage engine:

Helium supply pressure, $p_s = 500$ psia, and temperature $T = 560^\circ R$

$d_1, A_1, d_2, A_2, d_3, A_3, d_4, A_4$ = corresponding diameters and flow areas of fixed orifices and nozzles

$$d_1 = d_2 \quad d_3 = d_4$$

$w_1, w_2, w_3, w_4, w_0, w_c$ = flow rates through fixed orifices and nozzles, and to and from the actuator, lb/sec

Z_1, Z_2, Z_3, Z_4 = compressibility factors of the flows through the orifices and nozzles

Flow coefficient of the orifices and nozzles, $C = 0.7$

Distance between the two nozzles,

$$T = (d_3/4) + t$$

t = thickness of the flapper = 0.004 in

At the neutral or equilibrium position of the servovalve:

The pressures in the actuators, $p_c = p_0 = 450$ psia

The bleed through nozzles, $w_3 = w_4 = 0.000778$ lb/sec

Determine:

(a) The dimensions of fixed orifices and nozzles, and of distance T .

(b) The pressure differential across the actuator piston when the flapper is deflected downward 0.001431 inch from its neutral position, and the flow rates w_0 and w_c to and from the actuator are 0.00021 lb/sec (as governed by the speed of the piston).

Solution

(a) Since the gas flow through the nozzles is discharged to ambient, it is assumed that the pressure ratio across the nozzles will always be less than critical (sonic flow).

From figure 7-53, $Z_3 = Z_4 = 4.11$.

From equation (7-24), the following correlations are established:

$$\dot{w}_1 = \frac{CA_1 p_s Z_1}{\sqrt{RT}} = \frac{0.7 \times 500}{\sqrt{386 \times 560}} A_1 Z_1 = 0.753 A_1 Z_1$$

$$\dot{w}_2 = \frac{CA_2 p_s Z_2}{\sqrt{RT}} = 0.753 A_2 Z_2$$

$$\dot{w}_3 = \frac{CA_3 p_0 Z_3}{\sqrt{RT}} = \frac{0.7 \times 4.11}{\sqrt{386 \times 560}} A_3 P_0 = 0.0062 A_3 P_0$$

$$\dot{w}_4 = \frac{CA_4 p_c Z_4}{\sqrt{RT}} = 0.0062 A_4 P_c$$

The flow areas of fixed orifices and flapper nozzles (eq. (7-27)) are:

$$A_1 = \frac{\pi}{4} d_1^2, \quad A_2 = \frac{\pi}{4} d_2^2,$$

$$A_3 = \pi d_3 X, \quad A_4 = \pi d_4 (T - t - X)$$

When the valve is at neutral position, the actuator is at rest, and

$$\dot{w}_c = \dot{w}_0 = 0; \quad \dot{w}_1 = \dot{w}_2 = \dot{w}_3 = \dot{w}_4 = 0.000778 \text{ lb/sec};$$

$$X = \frac{T - t}{2} = \frac{d_3}{8}$$

Since $p_c = p_0 = 450$ psia under these conditions, the pressure ratio across the fixed orifices is $450/500 = 0.9$.

From figure 7-53, $Z_1 = Z_2 = 2.418$

$$A_1 = A_2 = \frac{\dot{w}_1}{0.753 Z_1} = \frac{0.000778}{0.753 \times 2.418} = 0.000427 \text{ in}^2$$

$$d_1 = d_2 = \sqrt{\frac{0.000427}{\frac{\pi}{4}}} = \sqrt{5.44 \times 10^{-4}} = 0.0233 \text{ in}$$

$$A_3 = A_4 = \frac{\dot{w}_3}{0.0062 p_0} = \frac{0.000778}{0.0062 \times 450} = 0.000279 \text{ in}^2$$

Since $A_3 = \pi d_3 X = \pi d_3^2 / 8$

$$d_3 = d_4 = \sqrt{\frac{8 \times 0.000279}{\pi}} = \sqrt{7.095 \times 10^{-4}} = 0.0266 \text{ in}$$

$$T = \frac{d_3}{4} + t = \frac{0.0266}{4} + 0.004 = 0.01065 \text{ in}$$

(b) When the flapper is deflected downward 0.001431 inch from its neutral position, the displacement of the flapper from the upper nozzle

$$X = \frac{T - t}{2} + 0.001431 = 0.003325 + 0.001431$$

$$= 0.004756 \text{ in}$$

With the flapper deflected

$$A_3 = \pi d_3 X = \pi \times 0.0266 \times 0.004756 = 0.000397 \text{ in}^2$$

The flow rate through the upper nozzle, \dot{w}_3 , is now equal to the fixed orifice flow rate \dot{w}_1 , plus the flow rate from the actuator \dot{w}_0 ; thus

$$\dot{w}_3 = \dot{w}_1 + \dot{w}_0$$

$$0.0062 A_3 p_0 = 0.753 A_1 Z_1 + 0.00021$$

$$0.0062 \times 0.000397 p_0 = 0.753 \times 0.000427 Z_1 + 0.00021$$

$$p_0 = \frac{0.753 \times 0.000427 Z_1 + 0.00021}{0.0062 \times 0.000397} = 130.6 Z_1 + 85.4$$

We use a trial-and-error method to find these values for p_0 and Z_1 , which will satisfy the above correlations and figure 7-53. We find that

$$p_0 = 436.5 \text{ psia}$$

$$Z_1 = 2.687$$

Checking the results for a pressure ratio of

$$\frac{p_0}{p_s} = \frac{436.5}{500} = 0.875,$$

a Z_1 value of 2.687 is derived from figure 7-53; thus

$$p_0 = 130.6 \times 2.687 + 85.4 = 436.5 \text{ psia}$$

With the flapper deflected

$$\begin{aligned}
 A_4 &= \pi d_4 (T - t - X) \\
 &= \pi \times 0.0266 (0.01065 - 0.004 - 0.004756) \\
 &= 0.0001583 \text{ in}^2
 \end{aligned}$$

The flow rate through the lower nozzle, \dot{w}_4 , is equal to the fixed orifice flow rate \dot{w}_2 , minus the flow rate to the actuator, \dot{w}_c :

$$\begin{aligned}
 \dot{w}_4 &= \dot{w}_2 - \dot{w}_c \\
 0.0062 A_4 p_c &= 0.753 A_2 Z_2 - 0.00021 \\
 p_c &= \frac{0.753 \times 0.000427 Z_2 - 0.00021}{0.0062 \times 0.0001583} = 328 Z_2 - 214
 \end{aligned}$$

We use again a trial-and-error method to obtain the values for p_c and Z_2 which will satisfy the above correlations and figure 7-53. We have found that

$$\begin{aligned}
 p_c &= 464 \text{ psia} \\
 Z_2 &= 2.0808
 \end{aligned}$$

Thus the pressure differential across the actuator piston

$$p = p_c - p_0 = 464 - 436.5 = 27.5 \text{ psi}$$

Spool-Type Servovalves

The spool-type servovalve (schematically shown in fig. 7-56) is basically a four-way valve. A cylindrical valve spool is accurately fitted into valve inserts, which in turn are shrunk into the valve body. Both inserts and spool are made of hardened alloy steels. The thickness of the inserts in the axial direction, and thus the location of the ports, is held to very close tolerances by lapping their faces. The outside diameter of the inserts is accurately ground for a tight seal with the valve body. The surfaces of their axial passages are also lapped. The diametral clearance between insert and spool is of the order of 0.0002 inch, at which the spool must still slide freely. The axial location of the spool lands must also be closely controlled. To minimize leak flow in the neutral position, the spool lands may be designed for slight overlap. As a rule, leak flows are less when the spool is displaced, due to better isolation of the drain lines. A typical leak flow rate in neutral position is 0.5 gpm.

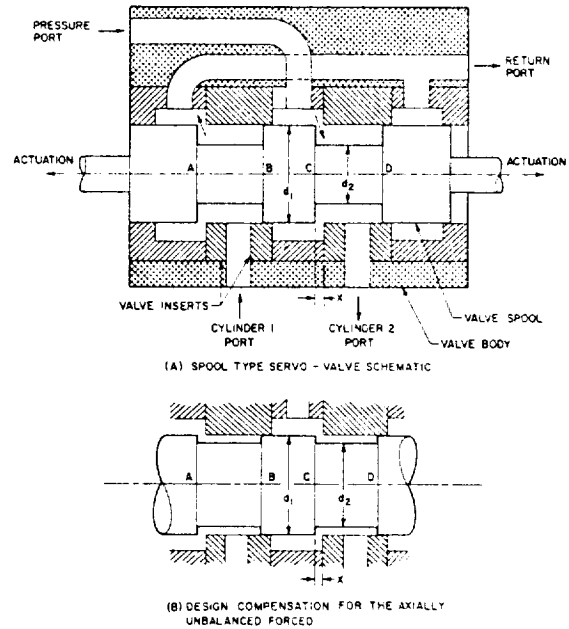


Figure 7-56.—Spool-type servovalve.

Although the spool valve theoretically is force balanced, hydrodynamic and friction forces cause relatively large loads which must be overcome. Refer to figure 7-56(a). Due to the difference in flow velocities, the static pressure at face A will be less than that at face B. Similarly, the pressure is less at face C than at face D. This results in two approximately equal axial forces, both of which tend to move the valve spool to the right so as to close the valve. These unbalanced axial forces can be compensated by design remedies. One is to increase diameter d_2 (as shown in fig. 7-56(b)). It is recommended that the maximum control port flow area $\pi d_1 X$ (where X = spool displacement, in) be just less than twice the annular area between spool diameters d_1 and d_2 . As a result, the flow velocity along the spool is substantially increased and the axial forces on faces B and D are considerably reduced.

The difference between minimum flow rate (leak flow in neutral position) and maximum flow rate (actuator in motion) is substantial. Various means of adjustment may be employed, such as simple relief bypass valves, or the pump output may be adjusted. For instance, in a piston pump operated by a wobble plate, the pitch of the plate may be adjusted as a function of pressure to give strokes varying from maximum to zero.

The correlation between pressure drop and flow in a spool valve is not as predictable as one might expect from a sharp-edged orifice. Experimental data are required to verify a design. Equation (7-24) for gas flow orifices may be used to approximate the flow through a pneumatic spool valve, where orifice area $A = \pi d_1 X$ and flow coefficient $C = 0.8$. For a spool valve using hydraulic oil or RP-1 as the actuating fluid, the following empirical equation applies:

$$\Delta p = \left[\frac{\dot{v}}{a} + \left(\frac{1}{b} + \frac{c}{X^2} \right) \dot{v}^2 \right] \rho^2 \quad (7-28)$$

where

- Δp = valve pressure drop, psi
- \dot{v} = valve volumetric flow rate, in³/sec
- X = spool displacement, or valve opening, in
- ρ = density of the liquid, lb/ft³
- a, b, c = empirical constants depending on the design

Sample Calculation (7-10)

The following design data are given for a spool-type hydraulic servovalve (shown schematically in fig. 7-56):

RP-1 is supplied at pressure $p_s = 2000$ psia
 Valve pressure drop and flow characteristics may be obtained from equation (7-28), for the following design constants:

- $a = 254$
- $b = 1270$
- $c = 1.79 \times 10^{-7}$

Maximum spool displacement, $X = 0.009$ in

Determine the flow rate \dot{v} , pressure drop Δp , and output W of the valve at maximum displacement.

Solution

Substitute $a, b, c, X,$ and ρ into equation (7-28)

$$\Delta p = \left[\frac{\dot{v}}{254} + \left(\frac{1}{1270} + \frac{1.79 \times 10^{-7}}{(0.009)^2} \right) \dot{v}^2 \right] \times (50.45)^2$$

$$\Delta p = 10 \dot{v} + 7.62 \dot{v}^2$$

From equation (7-17), the valve output

$$W = p_d \dot{v} = (p_s - \Delta p) \dot{v} = 2000 \dot{v} - 10 \dot{v}^2 - 7.62 \dot{v}^3$$

To find the maximum valve output design point, this expression is differentiated and set equal to zero

$$\frac{dW}{d\dot{v}} = 2000 - 20 \dot{v} - 22.86 \dot{v}^2 = 0$$

or

$$22.86 \dot{v}^2 + 20 \dot{v} - 2000 = 0$$

$$\dot{v} = \frac{-20 + \sqrt{20^2 - 4 \times 22.86 \times (-2000)}}{2 \times 22.86}$$

$$= \frac{-20 + \sqrt{400 + 183\,000}}{45.72} = 8.95 \text{ in}^3/\text{sec}$$

$$\Delta p = 10 \times 8.95 + 7.62 \times (8.95)^2 = 89.5 + 610 = 699.5 \text{ psi}$$

$$W = (2000 - 699.5) \times 8.95 = 11\,620 \text{ in-lb/sec} = 1.764 \text{ hp}$$

It should be noted that stabilized flow conditions rarely exist, because of mass inertias limiting acceleration and deceleration, and feedback effects.

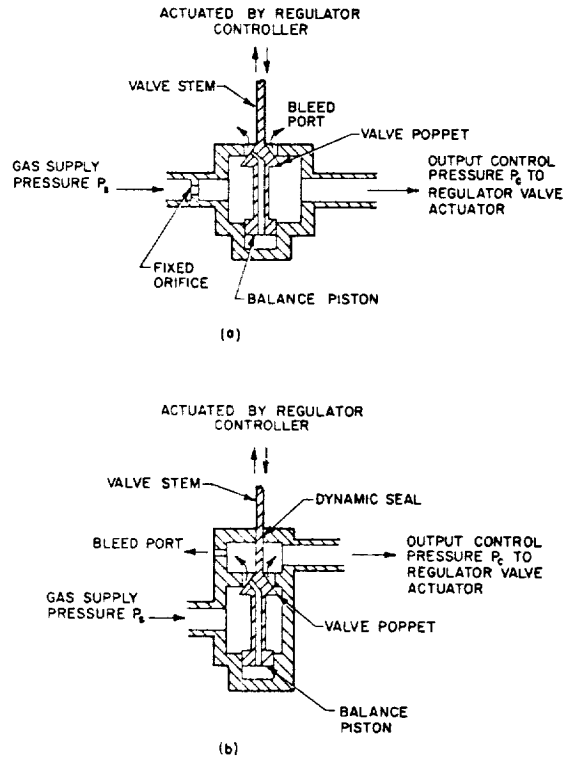


Figure 7-57.—Schematics of typical single-bleed, poppet-type, pneumatic servovalves used in gas pressure regulators.

Single-Bleed, Poppet-Type Servovalves

The single-bleed, poppet-type servovalve operates as a variable orifice like the flapper-nozzle valve. Figure 7-57 presents, schematically, the principle of operation of typical single-bleed, poppet-type, pneumatic servovalves as used in gas pressure regulating services. Two basic configurations are in use. The first (fig. 7-57(a)) effects output control pressure p_c regulation through variation of bleed port flow area. In the second (fig. 7-57(b)), the bleed port area is fixed. Here, p_c is regulated by varying the supply gas flow rate.

The selection of configuration depends on application. To minimize unbalance forces, a balance piston is usually attached to the valve poppet. The area of the balance piston is made equal to the projected area of the poppet seat diameter, less that of the valve stem.

7.12 DESIGN OF GAS PRESSURE REGULATORS

Basically, gas pressure regulators are variable-area-type pressure-reducing valves. Their prime function is to maintain constant pressure at their outlet, or in a downstream region, even though the pressure at their inlet may vary (decrease). Gas pressure regulators may be operated independently, or in conjunction with pressure relief devices, under either dynamic or static conditions. For example, the gas pressure regulator for the A-4 stage propulsion system (fig. 3-9) is designed to maintain a constant main oxidizer tank pressure of 165 psia, while the helium gas pressure at the regulator inlet varies from 4500 to 245 psia. Additional protection is provided by a tank relief valve, should the tank pressure continue to rise with the regulator completely closed, because of such effects as aerodynamic heating.

Elements of Gas Pressure Regulators

Most pressure regulators include two basic elements: the regulator controller and the regulator valve. The former controls the regulator valve opening, which in turn regulates the gas flow through the regulator.

A regulator controller essentially is a sensing-computing unit which measures the difference

between actual and desired pressure. Its output, called the error signal, can be directly applied mechanical force, or control pressure output to a servovalve. Figure 7-58 presents the schematic of a typical gas pressure regulator controller. Here, the pressure being regulated is sensed externally by a bellows which is internally evacuated, or vented to atmosphere. The vacuum establishes an absolute pressure reference, while a vented bellows uses ambient pressure for reference ("gage pressure"). As the regulated pressure (the sensing pressure) changes, the bellows deflects against the calibrated internal spring load, simultaneously positioning a directly connected servovalve (fig. 7-57), which in turn regulates a control pressure output.

A regulator valve consists of the control valve and an actuator. If only limited accuracy is required, or very small capacities are involved, it suffices if the regulator controller develops the error signal directly as a mechanical force to position the regulator valve. Such a directly spring-loaded pressure regulator is represented schematically in figure 7-59(a).

Where greater accuracy is required, the regulator valve actuator is positioned by controlled pressure from a servovalve connected to the regulator controller.

Since the servovalve amplifies the regulated pressure errors, small errors in regulated pressure will cause large changes in its control pressure output. This control pressure p_c can then be applied to control the regulator valve position in the following ways:

- (1) Control pressure p_c is used as the loading pressure for a simple dome-loaded pressure regulator, as shown schematically

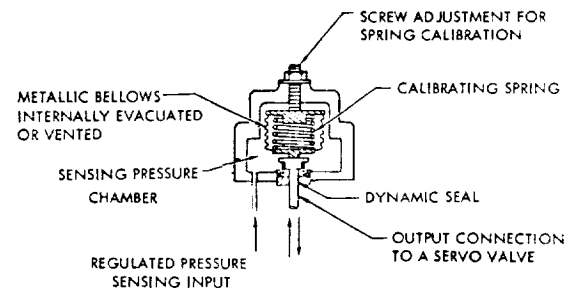


Figure 7-58.—Schematic of a typical gas pressure regulator controller.

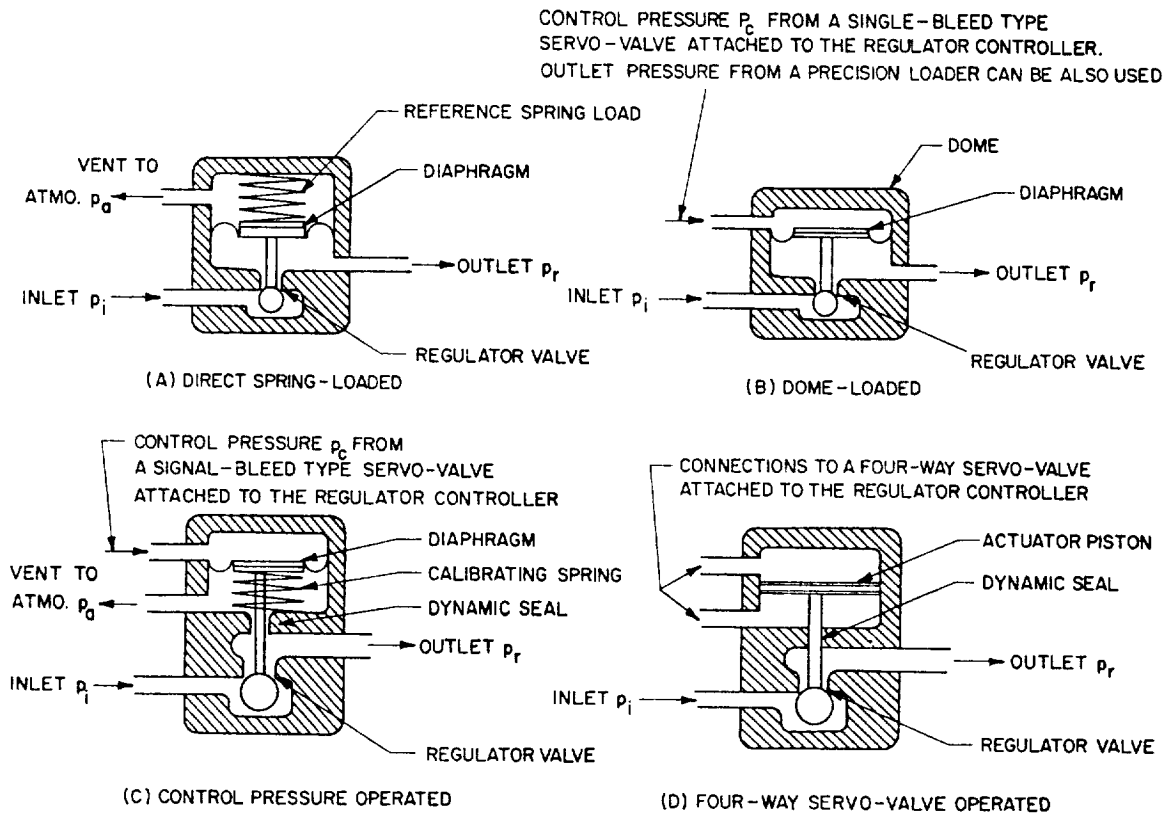


Figure 7-59.—Schematics of various gas pressure regulator designs.

in figure 7-59(b). A large-capacity, dome-loaded pressure regulator can also be loaded by a separate, small-capacity precision pressure regulator (precision loader).

- (2) Control pressure p_c is used as the input to a mechanism that positions the regulator valve as a linear function of control pressure. In its simplest form, this mechanism consists of a spring and a diaphragm (fig. 7-59(c)).

In some designs, a four-way servovalve (as in figs. 7-55 and 7-56) operates the double-acting piston-type actuator of the regulator controller to control the position of the regulator valve (fig. 7-59(d)). This design is known as an integrating-type pressure regulator.

When a single-bleed servovalve is used with the regulator controller, the supply pressure p_s to the control servo circuit must be isolated from the inlet pressure p_i to the main regulator valve, because of the steady-state error that would be

introduced by the often extreme variation of p_i . A simple, directly spring-loaded, low-capacity regulator similar to figure 7-59(a) is required to reduce p_i to a reasonably constant supply pressure p_s for the control servo circuit. This regulator is commonly known as the bleed regulator and can be a part of the main regulator controller.

Design Considerations for Gas Pressure Regulators

The following are basic considerations for the design of gas pressure regulators.

1. The principal causes of error in a pressure regulator are—
 - a. Variation in inlet pressure
 - b. Variation in flow demand
 - c. Variation in temperature
 - d. Mechanical hysteresis and friction
 - e. Creep of stress members
 - f. Variation in effective length of members because of angular displacement

- g. Variation in vehicle acceleration
- h. Vibration
- i. The fact that pressures are not sensed at the point at which control of pressure is desired (influence of pressure drops caused by flow through downstream systems)

The basic test of a good regulator design is whether these errors have been held within allowable tolerances, without mechanisms (including diaphragms and springs) of unreasonable complexity and size.

2. Where feasible, proven concepts and control mechanisms of previous designs should be utilized. This is especially important for dynamic characteristics, stability and transient response, and for mechanical details such as poppets, seals, diaphragms, and springs.

3. Balance of the regulator valve poppet should be provided to minimize the forces imparted to the valve by inlet pressure p_i . This may be achieved by attaching a balance piston, similar to that of the poppet servovalves (fig. 7-57). However, this will require some type of dynamic seal, which are known trouble sources. In certain applications, therefore, an unbalanced valve may be preferred.

4. In most cases, the regulator must lend itself to the alternate mode of operation as a shutoff valve, until a start pilot valve is opened.

5. The various gas pressure regulator designs shown in figure 7-59 regulate pressure by admitting additional gas, as required to the regulated pressure region. If the flow demand on the regulator is reduced to zero (dead-end conditions), the regulator valve shuts off. However, the pressure in the regulated region may increase above the design point, even with the regulator valve closed, due to—

- a. A timelag in closing, following reduction of demand to zero
- b. Inevitable regulator valve leakage
- c. Thermodynamic effects, such as increase in temperature of the gas in the regulated pressure region, or from vaporization of a liquid.

This condition is known as a lockup, and often poses problems. Lockup can be eliminated by incorporating a relief valve downstream of the regulator valve as part of the regulator assembly. In the A-4 stage propulsion system, individual

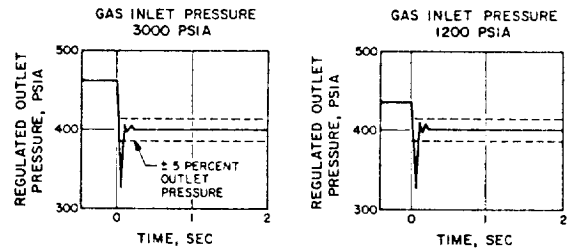


Figure 7-60.—Dynamic response characteristics of a typical pneumatic pressure regulator.

relief valves are provided for the main propellant tanks to prevent possible intermixing of propellant vapors.

6. Other design considerations for gas pressure regulators are—

- a. Type of regulated gas
- b. Gas inlet-pressure and temperature range
- c. Regulated gas outlet pressure level with respect to ambient or vacuum, its tolerance or accuracy of regulation, and range of adjustment
- d. Required maximum flow capacity
- e. Required response time and allowable overshoot
- f. Type of line connections
- g. Environmental conditions (temperature, vibration, humidity, etc.)

Figure 7-60 presents the dynamic response characteristics of a typical pneumatic pressure regulator upon initiation of a demand. The regulator was set at a regulated outlet pressure of 400 psia. The gas used (helium) is discharged into a system of approximately 60-cubic-inch volume.

Sizing of the Gas Pressure Regulator

The required flow area across the regulator valve when fully open, i.e., the characteristic flow area of a pressure regulator, may be calculated for required flow capacity and regulated outlet pressure, at minimum allowable gas inlet pressure.

The following correlation derived from equation (7-24) for gas flow orifices is applicable to gas pressure regulator design:

$$A^* = \frac{\dot{w}\sqrt{RT}}{C p_i Z} \quad (7-29)$$

where

- A^* = characteristic area of the pressure regulator, in²
- \dot{w} = design weight flow rate of the pressure regulator, lb/sec
- R = gas constant, ft²/°R
- T = gas inlet temperature at minimum inlet pressure condition, °R
- Z = compressibility factor, ft^{0.5}/sec, a function of pressure ratio p_r/p_i and specific heat ratio (fig. 7-53)
- C = flow coefficient, a function of design configuration. Design values range from 0.6 to 0.7
- p_i = minimum allowable gas inlet pressure, psia
- p_r = required regulated outlet pressure, psia

Sample Calculation (7-11)

The following design data are given for the helium gas pressure regulator of the A-4 stage propulsion system:

- Design weight flow rate, $\dot{w} = 0.048$ lb/sec
- Minimum allowable gas inlet pressure, $p_i = 245$ psia
- Gas inlet temperature at minimum inlet pressure condition, $T = 1030^\circ$ R
- Required regulated outlet pressure, $p_r = 168$ psia
- Regulator flow coefficient, $C = 0.65$

Determine the characteristic area A^* of the pressure regulator.

Solution

At minimum inlet pressure conditions, the pressure ratio across the regulator

$$\frac{p_r}{p_i} = \frac{168}{245} = 0.685$$

From figure 7-53, the compressibility factor Z is 3.9 for helium. Substitute this and other data into equation (7-29). The characteristic area

$$A^* = \frac{\dot{w}\sqrt{RT}}{Cp_iZ} = \frac{0.048 \times \sqrt{386 \times 1030}}{0.65 \times 245 \times 3.9} = 0.0487 \text{ in}^2$$

Dome-Loaded Pressure Regulators

This regulator type (fig. 7-57(b)) is one of the most frequently used. The main actuator usually

employs a metallic diaphragm for low friction. The dome pressure p_c , which determines the force to the actuator diaphragm, and thus regulates valve position and outlet pressure, can be regulated either internally by a pressure controller, or externally by a low-capacity pressure regulator or loader. There are many variations of dome-loaded regulators. Design approaches may best be illustrated by typical examples.

Figure 7-61 presents the schematic of a typical dome-loaded gas pressure regulator which has an alternate mode of operation as a shutoff valve. The prime purpose of the regulator is to maintain a regulated outlet pressure at a pre-selected value called the set point. The regulator is composed of four elements: the start pilot valve, the bleed regulator, the sensing-control unit, and the main regulator valve. The combination of bleed regulator and sensing-control unit forms the function of main regulator controller.

The start pilot valve is a solenoid-actuated poppet valve which is normally held closed by a spring. In the closed position, it locks up the outlet pressure of the bleed regulator. The latter is a normally closed, directly spring-loaded-type, pressure-reducing valve and supplies an approximately constant preset pressure p_s to the sensing-control unit. This pressure is greater than the main regulator outlet pressure p_r . It is the sensing-control unit, then, which establishes the main regulator outlet pressure. It detects small deviations from the set point and magnifies the error signals by means of a single-bleed, flapper-nozzle servovalve linked to a sensor

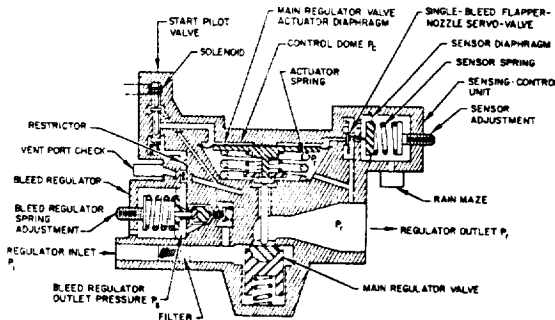


Figure 7-61.—Schematic of a typical dome-loaded, negative-gain-type gas regulator with an alternate mode of operation as a shutoff valve.

diaphragm by increasing or decreasing the control pressure p_c which operates the actuator diaphragm of the main regulator valve. This valve is a normally closed, dome-loaded pressure reducing valve.

In operation, the following sequence of events occurs. Gas enters the regulator through a filter located at the regulator inlet port, but is prevented from entering the main regulator control pressure dome by the closed start pilot valve. Upon opening of the latter by energizing its solenoid, gas flows through the bleed regulator and is reduced to pressure p_s , as determined by the preset reference spring force. The gas then flows through a fixed restrictor and passes into the control dome. This tends to open the main regulator valve against the actuator spring. Dome pressure p_c is controlled by varying the flow area of the flapper-nozzle servovalve which bleeds the loading gas into the main regulator outlet manifold. When the sensed regulated outlet pressure p_r and the sensor spring force are in equilibrium, the servovalve flapper is positioned a sufficient distance off the nozzle seat and maintains a steady-state control pressure p_c . This pressure is always greater than p_r , as determined by the main regulator valve actuator

spring preload. Under these steady-state conditions, gas continues to flow from the bleed regulator through the servovalve at a rate determined by the restrictions and out to the outlet manifold. The regulator controller circuitry has what is called a negative gain. A sensed increase in pressure p_r causes an amplified decrease in control pressure p_c , with attendant decrease of the main regulator valve opening. Similarly, a decrease in p_r causes an increase of valve opening.

The controller gain can be defined as

$$G = - \frac{\Delta p_c}{\Delta p_r} \quad (7-30)$$

where

- G = controller gain
- Δp_c = change in control pressure, psi
- Δp_r = change in sensed pressure, psi

The principal design parameters of the gas pressure regulator shown in figure 7-61 are listed in table 7-6.

Figure 7-62 presents the design layout of a typical dome-loaded, zero-gain-type gas pressure regulator. The main regulator controller consists of a spring-loaded bleed regulator and a fixed-area bleed orifice, which gives a constant

TABLE 7-6.—Principal Design Parameters of a Typical Dome-Loaded, Negative-Gain-Type Gas Pressure Regulator (Fig. 7-61)

Parameter	Design data
Regulated gas	Helium
Inlet gas pressure, p_i	4500 psia nominal, 5800 psia maximum, 500 psia minimum
Inlet gas temperature, T	110° to 360° R
Regulated outlet pressure, p_r	400 psig \pm 25 psi
Flow demand	a. Maximum: 0.1 lb/sec at 500 psia inlet pressure and 160° R inlet temperature b. Minimum: zero
Modes of operation	a. Start pilot valve solenoid deenergized: regulator remains shut off. Outlet pressure = 0 b. Start pilot valve solenoid energized: regulator functions normally
Controller bleed	a. None when start pilot valve solenoid deenergized b. 0.0002 lb/sec at 530° R when solenoid energized
Main regulator valve	Seating diameter, 0.205 in; characteristic area, 0.0281 in ²
Main regulator valve actuator	Effective area, 7.55 in ² ; bias spring preload, 75.5 lb; rate, 500 lb/in
Start pilot valve	Seating diameter, 0.025 in; characteristic area, 0.000437 in ²
Bleed regulator valve	Seating diameter, 0.028 in; characteristic area, 0.000301 in ²
Bleed regulator sensor	Effective area, 0.185 in ² ; reference spring preload, 93.5 lb; rate, 1500 lb/in
Bleed flow restrictor	Diameter, 0.0116 in; area, 0.000105 in ²
Main regulator controller sensor	Effective area, 0.315 in ² ; reference spring preload, 126 lb; rate, 702 lb/in
Flapper-nozzle servovalve	Seating diameter, 0.043 in (2 holes); maximum stroke, 0.011 in; maximum flow area, 0.003 in ² ; bias spring preload, 1.0 lb; rate, 5.0 lb/in

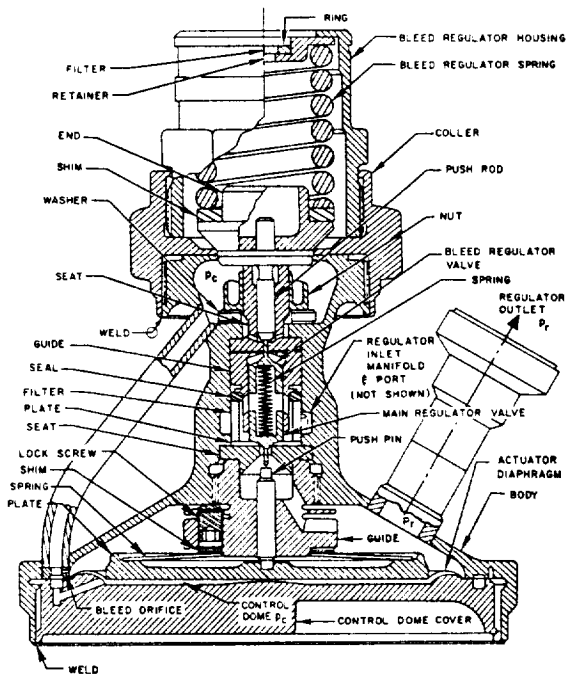


Figure 7-62.—Typical dome-loaded, zero-gain-type gas pressure regulator loaded by a bleed regulator.

bled from the control dome to the regulator outlet. The control dome pressure p_c is maintained at a constant level by the bleed regulator. This is known as a zero-gain-type control circuit. Here, too, control pressure p_c is higher than the regulated outlet pressure p_r by an amount determined by the main regulator valve actuator spring preload. The regulator shown is designed to maintain an outlet pressure p_r of 282 psig \pm 5 psi, at inlet pressures ranging from 5000 to 375 psig. The actuator diaphragms are made of a 0.0025-inch 17-7 PH high-strength stainless-steel sheet. 440C stainless steel is used for all sliding members, such as regulator valve poppets and guides, to eliminate the surface galling problem. Regulator main body and housing are made of aluminum-alloy forgings.

Integrating-Type Pressure Regulators

Figure 7-63 presents the design of a typical integrating-type gas pressure regulator, designed to regulate the propellant tank pressures of a pressurized gas propellant feed system such as the A-4 stage propulsion system. Main oxidizer

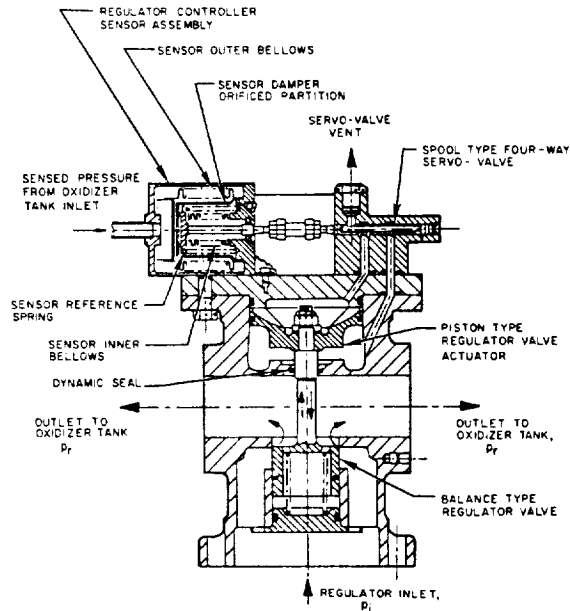


Figure 7-63.—Integrating-type, gas pressure regulator with spool-type, four-way servovalve.

tank pressure is to be sensed through a relatively short external line. Fuel tank pressure is maintained at 10 psi below the oxidizer tank pressure by different pressure settings of line check valves and tank relief valves. A spool-type, four-way servovalve, which is directly connected to the sensor of the regulator controller, controls the regulator valve actuator. Supply pressure p_s of the servovalve is taken from the regulator outlet pressure p_r ; i.e., $p_s = p_r$. The sensor contains two bellows with an oil-filled damper in between. The damper consists of a partition having a properly sized orifice. The outer bellows, which is exposed to the propellant vapors, is hydroformed from thin 321 stainless-steel tubing, because the pressure differential across it is small and because it contains fluid. The inner bellows must withstand a pressure differential equal to full tank pressure, since the interior of this bellows is vented directly to atmosphere. For this reason, the bellows is machined from 17-4 PH stainless-steel stock. This regulator is called an integrating type because a constant tank pressure error will produce a constant actuator piston velocity (neglecting extraneous forces). This, in turn, gives a constant regulator valve opening (or closing) velocity and a constantly increasing (or decreasing)

gas flow rate. Tank pressure is then the integral of tank pressure error versus time. The integrating-type pressure regulator provides the constantly increasing regulator valve flow area required for decreasing supply pressures, with minimum error in tank pressure, but may be unstable if the gain of the servovalve-actuator combination is too high. A suitable gain value should be determined by computer studies of the regulator dynamic characteristics.

7.13 DESIGN OF LIQUID FLOW AND PRESSURE REGULATORS

Liquid flow and pressure regulators basically are variable-area-type, pressure-reducing valves. A liquid flow regulator maintains a constant rate of flow, or limits the maximum rate of a flow. A liquid pressure regulator, like a gas pressure regulator, maintains a constant fluid pressure at its outlet under variable flow conditions. Design considerations for liquid flow and pressure regulators are similar to those for gas regulators.

Design of Liquid Flow Regulators

Liquid flow control can be obtained with a venturi. The pressure at the throat is proportional to the velocity of the (incompressible) fluid and thus the flow rate. The pressure differential between throat and inlet can be used to control the position of a butterfly valve, and thus the flow rate, by means of a servocontrol circuit. A regulator of this type is shown schematically in figure 7-18.

Figure 7-64 presents the principle of another type flow regulator which is frequently used in rocket engine systems, because of its simplicity. It consists of two restrictors, one of fixed and the other of variable area. This combination automatically maintains a constant pressure drop across the fixed restrictor, and thus a constant flow. The fixed restrictor consists of a disk containing a number of orifices and mounted in a piston. The variable restrictor is formed by variable throttle ports located around the piston periphery. The pressure differential across the fixed orifices causes the piston to move against the regulator reference springs. Piston throttle ports and reference spring rate are designed so

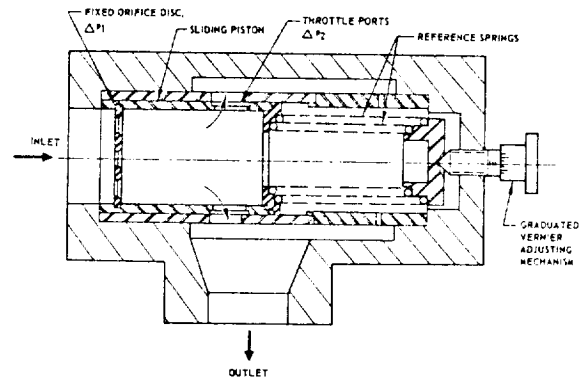


Figure 7-64.—Schematic of a typical sliding-piston-type liquid flow regulator.

that a constant pressure drop is maintained across the orifice disk.

As the fluid inlet pressure increases, or the back pressure decreases, the flow rate tends to increase also. However, the attendant increase is pressure differential, i.e., pressure force on the piston, moves it against the reference springs, simultaneously increasing the flow restriction. A new equilibrium is achieved as the inlet pressure increase is absorbed by an increase in pressure drop across the piston throttle port.

The following design correlations are established for this flow regulator:

$$F_s = (\Delta p_1 + \Delta p_2) A_p \quad (7-31)$$

$$K_s = \frac{\Delta p}{\Delta l} A_p \quad (7-32)$$

where

F_s = regulator reference spring preload, for a given flow rate, lb

Δp_1 = pressure drop across the fixed orifice disk at that flow rate, psi

Δp_2 = pressure drop across the piston throttle ports at that flow rate, psi

A_p = effective piston area, in²

K_s = regulator reference spring rate, lb/in

$(\Delta p/\Delta l)$ = change of pressure drop across the piston throttle ports per inch of movement of piston, lb/in²-in

Adjustment of the regulated flow rate is made by adjusting the reference spring force, using a graduated vernier mechanism.

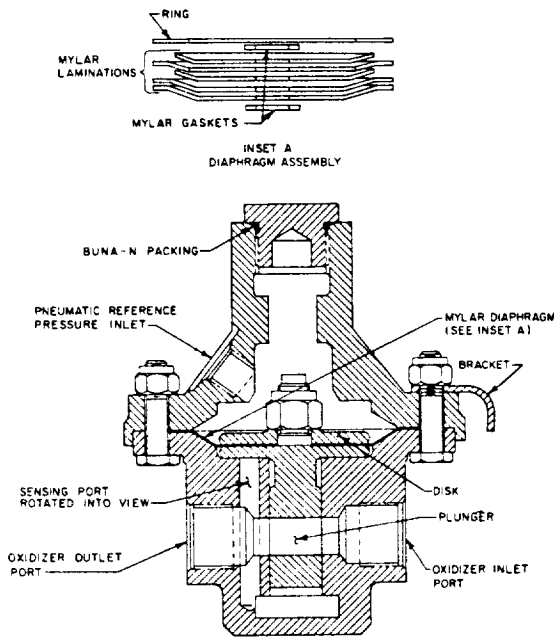


Figure 7-65.—Typical liquid pressure regulator design for liquid oxygen service.

Design of Liquid Pressure Regulators

Figure 7-65 presents a liquid pressure regulator design frequently used in rocket engine systems. The actuator diaphragm of the regulator valve (plunger) can be loaded either by a pneumatic reference pressure (as shown), or by a reference spring.

Regulated outlet pressure is sensed directly. An increase in outlet pressure tends to reduce the flow area of the regulator valve until an equilibrium is reached between outlet pressure and reference pressure. The actuator diaphragm is made of Mylar laminations which are compatible with cryogenic propellants such as liquid oxygen.

7.14 DESIGN OF PRESSURE RELIEF VALVES

The prime function of pressure relief valves is to protect fluid systems and pressure vessels from being overpressurized. There are two basic types of pressure relief valves; the direct operated and the pilot operated. In the first, the valve poppet is loaded directly by a properly

calibrated reference spring. The valve opens as the pressure force acts against the spring force. In the second, the main relief valve actuator is controlled by a pilot valve which is calibrated for the desired relief pressure setting. The direct-operated relief valves are used for large-tolerance, low-capacity services. For large flow requirements, pilot-operated relief valves are used for quick response and to avoid excessive size.

Most pressure relief valves are used in gas pressure systems. Important design considerations are—

- (1) Type of gas and its conditions
- (2) Pressure relief level, its tolerance and range of adjustment
- (3) Required response time, dead band (differential between actuation or opening, and deactuation or closing pressure), and other dynamic characteristics
- (4) Required maximum flow capacity
- (5) Simplicity of construction and line connections
- (6) Environmental conditions, such as temperature, humidity, acceleration, and vibration

The required flow area for a gas pressure relief valve at its maximum opening position, i.e., its characteristic flow area, can be calculated from equation (7-24) for gas flow orifices.

Direct-Operated Gas Pressure Relief Valves

Figure 7-66(a) shows the design of a typical low-capacity, direct-operated gas pressure relief valve. The valve poppet is loaded directly by a coil spring. This is one of the simplest designs. It may, however, become dynamically unstable under externally introduced vibration.

Figure 7-66(b) is the schematic of an improved design of a direct-operated relief valve. It assures a predictable dead band and eliminates chatter under vibration. This design employs coned-disk-type (Belleville) springs, operating between positive stops, in the negative rate portion of the force-deflection curve of the spring. As shown in figures 7-66(b) and 7-67, the spring remains against pretravel stop C, until the applied force (valve inlet pressure $p_i \times$ valve poppet seat area $\pi d^2/4$) reaches a level A. The spring then snaps from C to the

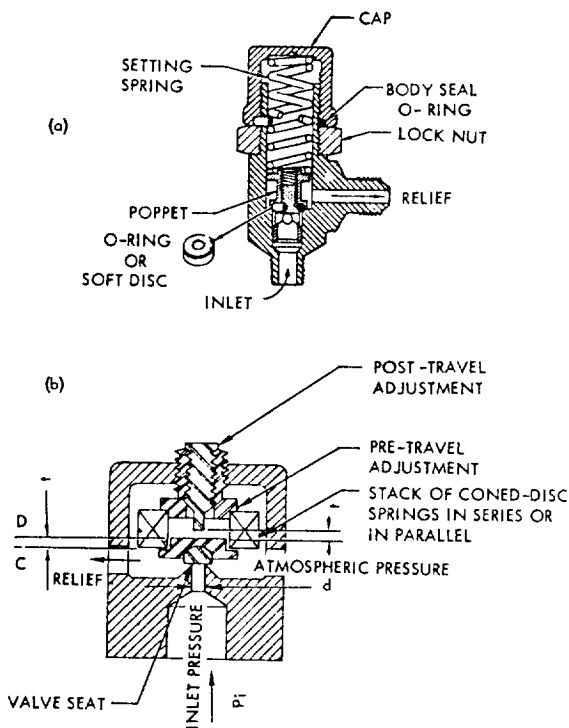


Figure 7-66.—Low-capacity, direct-operated gas pressure relief valves. (a) Coil-spring-loaded, direct-operated relief valve; (b) Snap-action, coned-disk, spring-loaded, direct-operated relief valve.

posttravel stop *D*, with no further increase in applied force. Reduction of the applied force to *B* will cause the spring to snap back from *D* to *C*. The positions of the pre- and posttravel stops can be adjusted for constant actuation and deactuation forces, independent of spring manufacturing tolerances. The coned-disk spring washers are usually made of beryllium copper or 17-7 PH stainless steel. This type of relief valve is suitable for high-pressure helium storage bottle services, such as in the A-4 stage propulsion system.

Pilot-Operated Gas Pressure Relief Valves

Figure 7-68 presents the schematic of a typical high-capacity, pilot-operated tank gas pressure relief valve. Normally, both main and pilot valves, are held closed by valve spring forces F_{sm} , F_{s3} , and pressure p_c . The pilot valve

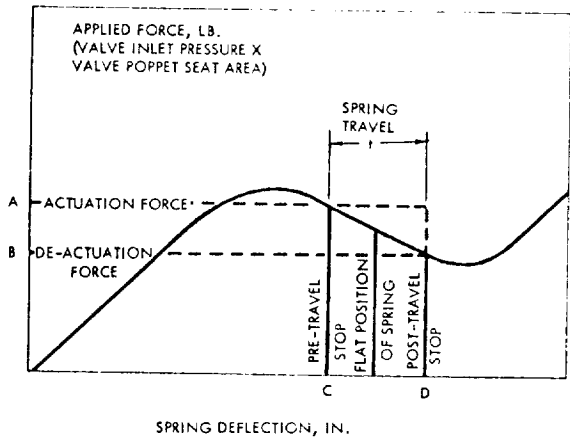


Figure 7-67.—Coned-disk-spring, force-deflection curve.

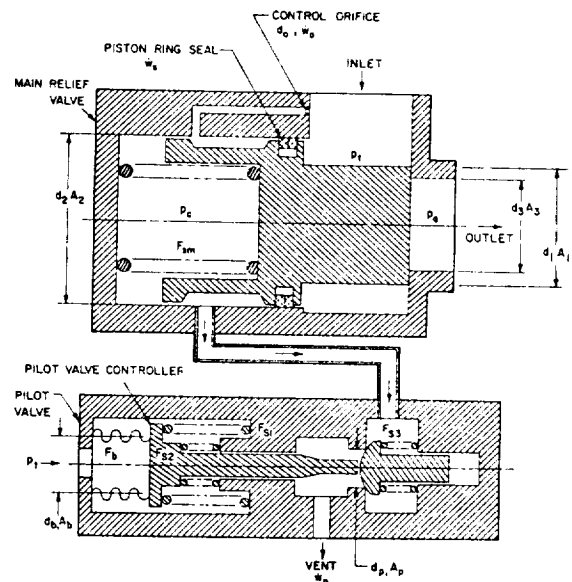


Figure 7-68.—Schematic of a typical high-capacity, pilot-operated tank gas pressure relief valve.

controller also senses the tank pressure p_t . When the latter reaches or exceeds the preset level, the pilot valve is actuated to crack. This vents the main relief valve actuator control pressure p_c and, in turn, permits opening of the main valve. Main valve poppet position is a function of the control pressure, which in turn is controlled by the position of the pilot valve poppet

and by the tank pressure. This correlation can best be illustrated by the following sample calculation.

Sample Calculation (7-12)

The following design data are given for the A-4 stage propulsion system main oxidizer tank relief valve (schematically shown in fig. 7-68):

Tank pressurant temperature, $T = 700^\circ \text{R}$ (helium gas)

Relief pressure set point, $p_t = 165 \text{ psia}$

Required maximum flow capacity, $\dot{w} = 3 \text{ lb/sec}$

Main valve flow coefficient, $C = 0.75$

Estimated leakage past the main valve actuator piston seal, $\dot{w}_s = 0.003 \text{ lb/sec}$

Control orifice diameter, $d_o = 0.080 \text{ in}$

Flow coefficient for control orifice and pilot valve, $C_o = 0.6$

$d, A =$ Diameters and areas of various elements, in; in^2

$p_c =$ Control pressure, psia

$p_a =$ Ambient pressure (14.7 psia maximum)

Determine:

- (a) Dimensions of the main relief valve and force balance equations for various conditions
- (b) Dimensions of pilot valve poppet and actuator, and force balance equations

Solution

(a) *Main relief valve.*—The valve is sized for an isentropic compressible flow through an orifice. From equation (7-24), the main relief valve port area

$$A_3 = \frac{\dot{w} \sqrt{RT}}{C p_t Z}$$

Since $p_a/p_t = 14.7/165 = 0.089$, $Z = 4.11$ (from fig. 7-53)

$$A_3 = \frac{3 \times \sqrt{386 \times 700}}{0.75 \times 165 \times 4.11} = 3.07 \text{ in}^2$$

$$d_3 = 1.98 \text{ in} \approx 2 \text{ in}$$

Required minimum travel of the main valve to the fully opened position

$$X_{mo} = \frac{A_3}{\pi d_3} = \frac{3.07}{\pi \times 2} = 0.487 \text{ in} \approx 0.5 \text{ in}$$

Force balance equations of the main relief valve poppet at various conditions:

(1) Basic equation:

$$F_{sm} + p_c A_2 - p_t (A_2 - A_1) - p_a A_3 = F_{seat}$$

(2) Condition at cracking:

$$F_{sm} + p_{cc} A_2 - p_{tc} (A_2 - A_1) - p_a A_3 = 0$$

(3) Condition at any intermediate valve position:

$$F_{sm} + K_{sm} X_m + p_c A_2 - p_t (A_2 - A_1) - p_a A_3 = 0$$

(4) Fully open condition:

$$F_{sm} + K_{sm} X_{mo} + p_{co} A_2 - p_{to} (A_2 - A_1) - p_a A_3 = 0$$

(5) Condition at start to reseal:

$$F_{sm} + K_{sm} X_{mo} + p_{cr} A_2 - p_{tr} (A_2 - A_1) - p_a A_3 = 0$$

(6) Fully reseated:

$$F_{sm} + p_{cr} A_2 - p_{tr} (A_2 - A_1) - p_a A_3 = 0$$

where

- F_{seat} = main valve seating force, lb
 F_{sm}, K_{sm} = preload and rate of main valve spring, lb; lb/in
 X_m, X_{mo} = main valve poppet travel intermediate and fully open position
 $p_{cc}, p_{co},$ and p_{cr} = control pressures at cracking, full open, and reseal of the main valve, psia
 $p_{tc}, p_{to},$ and p_{tr} = tank pressures at cracking, full open and reseal of the main valve, psia

(b) *Pilot valve.*—The pilot valve flow capacity must be larger than the combined flow rate of control orifice and leakage past the main valve actuator piston seal for adequate venting of p_c . From equation (7-24), the flow rate of the control orifice

$$\begin{aligned} \dot{w}_o &= \frac{C_o \pi d_o^2 p_t Z}{4 \sqrt{RT}} = \frac{0.6 \times 0.00503 \times 165 \times 4.11}{\sqrt{386 \times 700}} \\ &= 0.00394 \text{ lb/sec} \end{aligned}$$

The total flow into the control cavity, $\dot{w}_0 + \dot{w}_s = 0.00394 + 0.003 = 0.00694$ lb/sec.

Setting the flow capacity of the pilot valve 50 percent higher, its flow capacity results as

$$\dot{w}_p = 1.5 \times 0.00694 = 0.0104 \text{ lb/sec}$$

It is desirable that this flow be maintained freely at all points, independent of back pressures. This is achieved by maintaining sonic velocity, i.e., critical or supersonic pressure ratios, at the restrictions. Thus, the maximum allowable control pressure

$$p_c = p_t \left(\frac{2}{\gamma + 1} \right)^{\frac{\gamma}{\gamma - 1}} = 165 \left(\frac{2}{2.67} \right)^{\frac{1.67}{0.67}} = 80.6 \text{ psia}$$

Based on this pressure, and using equation (7-24), the required minimum pilot valve port area results as

$$A_p = \frac{\dot{w}_p \sqrt{RT}}{C_o p_c Z} = \frac{0.0104 \sqrt{386 \times 700}}{0.6 \times 80.6 \times 4.11} = 0.0272 \text{ in}^2$$

$$d_p = 0.186 \text{ in} \approx 0.2 \text{ in}$$

Required travel of the pilot valve to the fully open position

$$X_{p0} = \frac{A_p}{\pi d_p} = \frac{0.0272}{\pi \times 0.2} = 0.0433 \text{ in}$$

Force balance equations of the pilot valve poppet and actuator:

(1) Poppet:

$$(p_c - p_a) A_p + F_{s3} = F_p$$

(2) Actuator:

$$(p_t - p_a) A_b - F_b - F_{s1} - F_{s2} = F_a$$

where

- F_p = pilot valve poppet seating force, lb
- F_a = pilot valve actuating force, lb
- F_b = sensor bellows force, lb
- F_{s1}, F_{s2}, F_{s3} = forces of the various springs

When $F_a > F_p$, pilot valve starts to open.

7.15 DESIGN OF MISCELLANEOUS VALVES

Check Valves

The prime function of check valves is to allow fluid flow in only one direction. There are two basic check valve types: the poppet and the swing-gate type. The selection depends to a great extent on application. General design considerations for check valves are—

- (1) Type of fluid and its pressure and temperature
- (2) Required flow capacity
- (3) Allowable pressure drop
- (4) Allowable rate of leakback (including zero leakage)
- (5) Space envelope and line connection
- (6) Simplicity of construction

Figure 7-69 presents the design of a typical poppet-type check valve. A light, compression return spring normally holds the poppet in the closing position. This prevents any possibility of fluid leaking back. When fluid pressure is introduced upstream, the poppet will open against the return spring. Because of their relatively high-pressure drop, check valves of this type are used only in low-capacity services. Either elastomer O-rings or metal to metal seals are used.

Figure 7-70 presents a swing-gate-type check valve. The valve consists of two elements: the inlet and the outlet body. The swing gate is secured to the inlet body. A torsional-type return spring holds the gate in the closing position. Swing-gate check valves minimize pressure drop. However, positive sealing against back-flow is more difficult. In some applications,

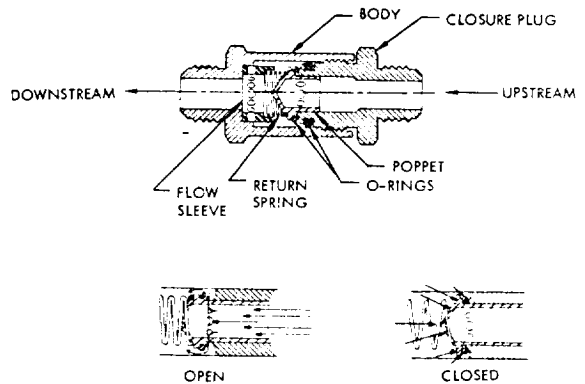


Figure 7-69.—Typical poppet-type check valve.

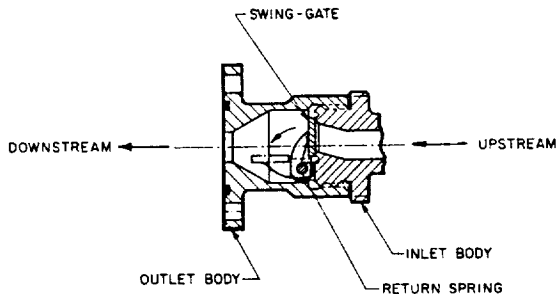


Figure 7-70.—Typical swing-gate-type check valve.

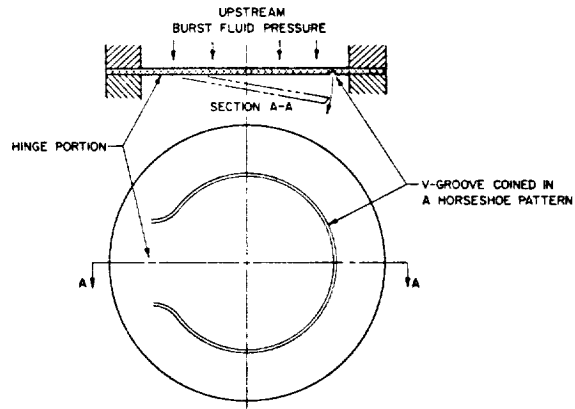
orifice holes are drilled in poppets or swing gates to allow a controlled backflow for specific control purpose.

Burst Diaphragms

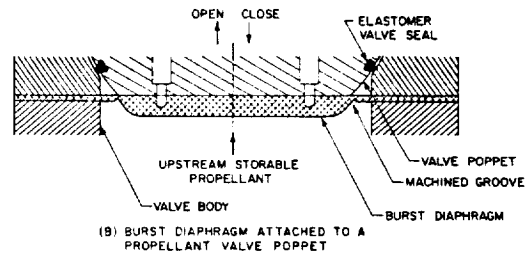
When positive, hermetic sealing is essential, in fluid-flow systems burst diaphragms are used. They are especially useful in storable liquid propellant engine system applications; they also serve as safety valves to prevent excessive pressures, or to initiate flow at a predetermined pressure. Burst diaphragms can be ruptured either by the upstream fluid pressure or mechanical means. General design considerations for burst diaphragms are—

- (1) Type of fluid and its corrosive characteristics
- (2) Duration of storage (especially with corrosive storable liquid propellants)
- (3) Method of diaphragm installation in duct or valve body
- (4) Method of rupture (upstream fluid pressure or other means)
- (5) Burst pressure level (if upstream fluid pressure is used) and its tolerance; environmental temperature effects
- (6) Retention of the diaphragm after rupture (no metal particles must be ejected)
- (7) Allowable pressure drop across the burst diaphragm

Figure 7-71(a) presents a typical flat-disk type burst diaphragm. A V-groove has been coined into it in a horseshoe pattern. The depth of the groove will determine the burst pressure. The uncoined section serves as a hinge during rupture and as a retainer. The diaphragm can be



(A) FLAT DISC BURST DIAPHRAGM



(B) BURST DIAPHRAGM ATTACHED TO A PROPELLANT VALVE POPPET

Figure 7-71.—Typical burst diaphragm designs.

joined to the duct by welding, brazing, or bolting. This design has been satisfactory for many applications.

Figure 7-71(b) presents a poppet-type, storable propellant valve with built-in burst diaphragm. The latter assures a positive, hermetic seal of zero leakage during long storage periods; it also protects the elastomer seal of the valve seat. Rupture of the diaphragm occurs during valve opening, either from valve actuation or from upstream propellant pressure. When closing, satisfactory valve sealing is provided by the elastomer seal only.

Burst diaphragms are made from a wide variety of metals. Annealed aluminum alloys such as 1100-0 and 6061-0 are among the most easily controlled. Burst diaphragms rupture in a combination of shearing, bending, and tearing. The exact burst pressure of a specific diaphragm design can only be evaluated experimentally. Variations of material ultimate strength have a pronounced effect. Consistency of the desired diaphragm burst pressure level will be greatly

enhanced by the following precautions in manufacturing and quality control:

- (1) Grinding of raw sheet or diaphragm to insure uniform and accurate thickness
- (2) Close control of groove depth, by precision coining or machining, and by stress relieving before and after coining
- (3) Continuous testing of the diaphragm material for hardness
- (4) Close control of the clamping pressure with bolted diaphragms
- (5) Close control of the welding or brazing processes to minimize heat effects
- (6) Proper dimensioning of diaphragm thickness and groove depth to allow for corrosive effects of the propellant during storage

It is possible to hold burst pressure variations of a specific diaphragm design to within ± 2 percent for diaphragms of over 1 inch diameter and design burst pressures greater than 300 psi. For diaphragms of smaller size and lower burst pressure, this tolerance may increase up to ± 5 percent.

Explosive-Actuated Valves

In certain applications, a valve may only be required to operate once (to either open or close). In these cases, explosive-actuated valves provide the smallest possible size and weight. Since the power of the explosive actuation is virtually unlimited, a rigid, hermetic zero-leakage-type seal can be used with this type of valve.

Figure 7-72 presents a typical explosive-actuated pilot valve developed and produced by the Conax Corp. The actuator of this normally closed valve consists of an explosive charge "A," and a ram "B" including a shearing head

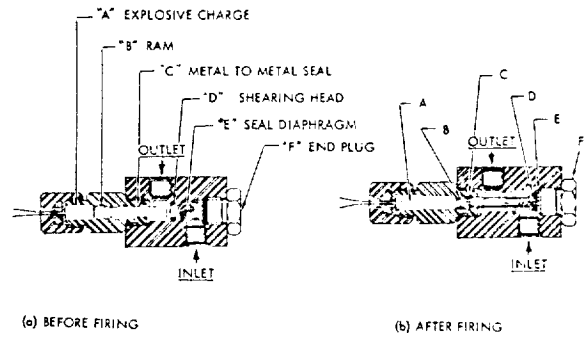


Figure 7-72.—Typical explosive-actuated pilot valve.

"D." The seal of the valve is provided by a solid metal diaphragm "E," machined as an integral part of the valve body. Upon an electrical signal the explosive charge detonates and drives the ram forward to cut out the seal diaphragm as a single piece of metal and hold it firmly against the end plug "F." Ram "B" has a tapered head, which rams into the guide-hole edge and causes a perfect metal-to-metal seal at point "C." This prevents contamination of the working fluid with gases from the explosive charge. The input current required for this valve is about 0.5 ampere; actuation of the valve takes about 0.002 second.

Explosive cartridges may also be used to actuate valves of larger size, such as the main propellant valves. In the form of threaded plugs, they can be attached to the valve actuator ports in lieu of pneumatic lines. For maximum reliability, two separate cartridges are often installed. The pressures produced by the cartridges range from approximately 2000 to 10 000 psi. The valve designer will have to determine the required pressure and volume of the gases at the end of the actuator stroke, which then serve as the specification to the cartridge supplier.

Chapter VIII

Design of Propellant Tanks

Liquid propellant rocket engines and the tanks feeding them, together with certain auxiliary systems such as pressurization, form the propulsion system. For reasons set forth in section 1.5, a discussion of tank design is included here. The need for close coordination between engine and tank designer is reemphasized, particularly if they are members of different contractors.

8.1 BASIC DESIGN CONFIGURATIONS OF PROPELLANT TANKS

The configuration of propellant tanks depends largely on vehicle mission and size. In most modern designs, the tanks form an integral part of the vehicle structure. Propellant tanks can be categorized, according to vehicle application, as follows:

- (1) Prepackaged storable liquid systems
- (2) Booster stage systems
- (3) Upper stage systems

Propellant Tanks for Prepackaged Storable Liquid Systems

Figure 8-1 presents the configuration of a typical prepackaged storable liquid propulsion system. The tanks are arranged in tandem, with a common bulkhead between. This system is designed for long storage periods, perhaps 5 to 10 years. A main characteristic of these systems is that the propellants are factory loaded and are hermetically sealed in the tanks by burst diaphragms. Both tank and diaphragm construction materials must be compatible with the propellants for the storage duration. In the example, the propellants are expelled by pressurized gases produced by a solid propellant gas generator. The tank walls form an integral part of the vehicle structure and are designed to withstand the internal pressure loads as well as the vehicle

dynamic loads. In some designs the tanks are further stabilized by the internal pressure against buckling; i.e., the walls are always kept under tension loads by a specified pressure level maintained during storage and handling. In smaller units, the walls are usually capable of taking external loads without being pressurized internally. Operational tank pressures for these range from 400 to 2000 psia.

Prepackaged storable liquid systems are usually employed to relatively short-duration, low-thrust applications. Since the tanks form an integral part of the propulsion system, they are designed and furnished by the engine builder. In one design, the thrust chamber is located inside the aft tank and welded directly to the tank bulkhead.

Propellant Tanks for Booster Stage Systems

Figure 8-2 presents the propellant tank design configuration of a typical propulsion system as used in the booster stages of a large launch vehicle such as the Saturn V. The system shown can be used for either storable or cryogenic propellants. The tanks are arranged in tandem; their walls form an integral part of the vehicle structure. For booster application, overall vehicle systems optimization usually dictates use of a turbopump-fed engine system. This permits relatively low operational tank pressures, ranging from 30 to 100 psia.

Since the tanks represent a large percentage of the vehicle structural (inert) weight, advantage is taken of the low-pressure levels by constructing the tanks with extremely thin-wall thicknesses. However, the often huge tank structures thus become sensitive to external buckling loads. To stabilize the tank structures of large booster stage systems, two basic design avenues are open: pressure-stabilization and self-supporting structures. In the pressure-stabilized systems, such as the Atlas ICBM, the

DESIGN OF LIQUID PROPELLANT ROCKET ENGINES

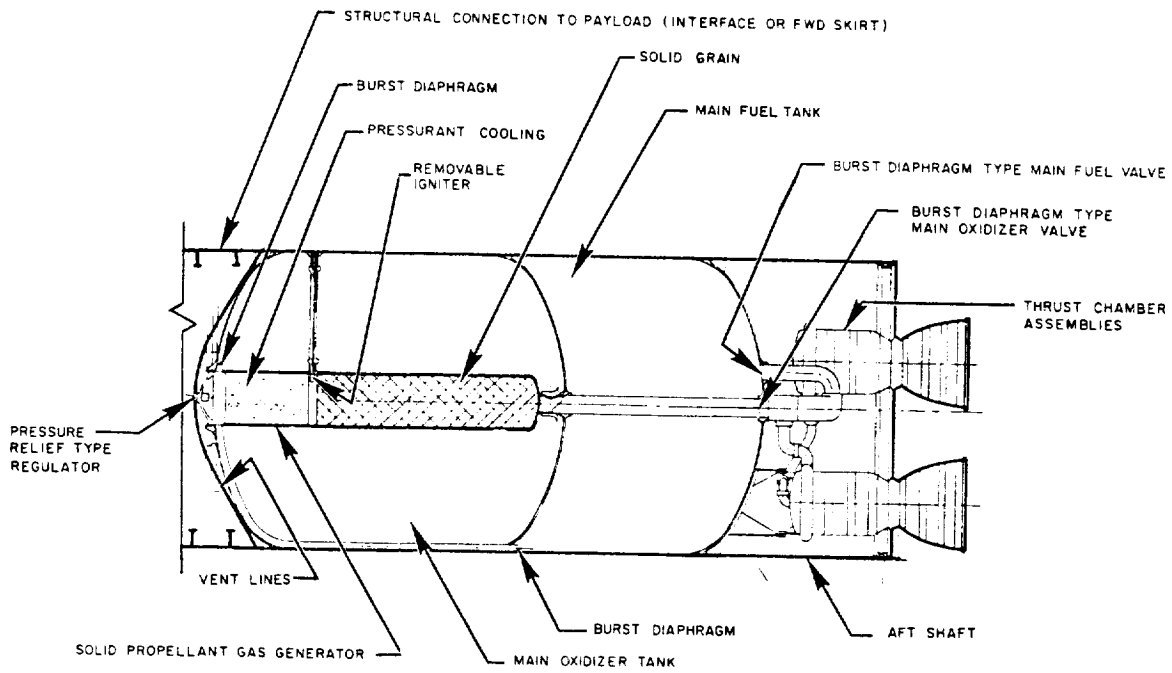


Figure 8-1.—Propellant tank design configuration of a typical prepackaged storable liquid propulsion system.

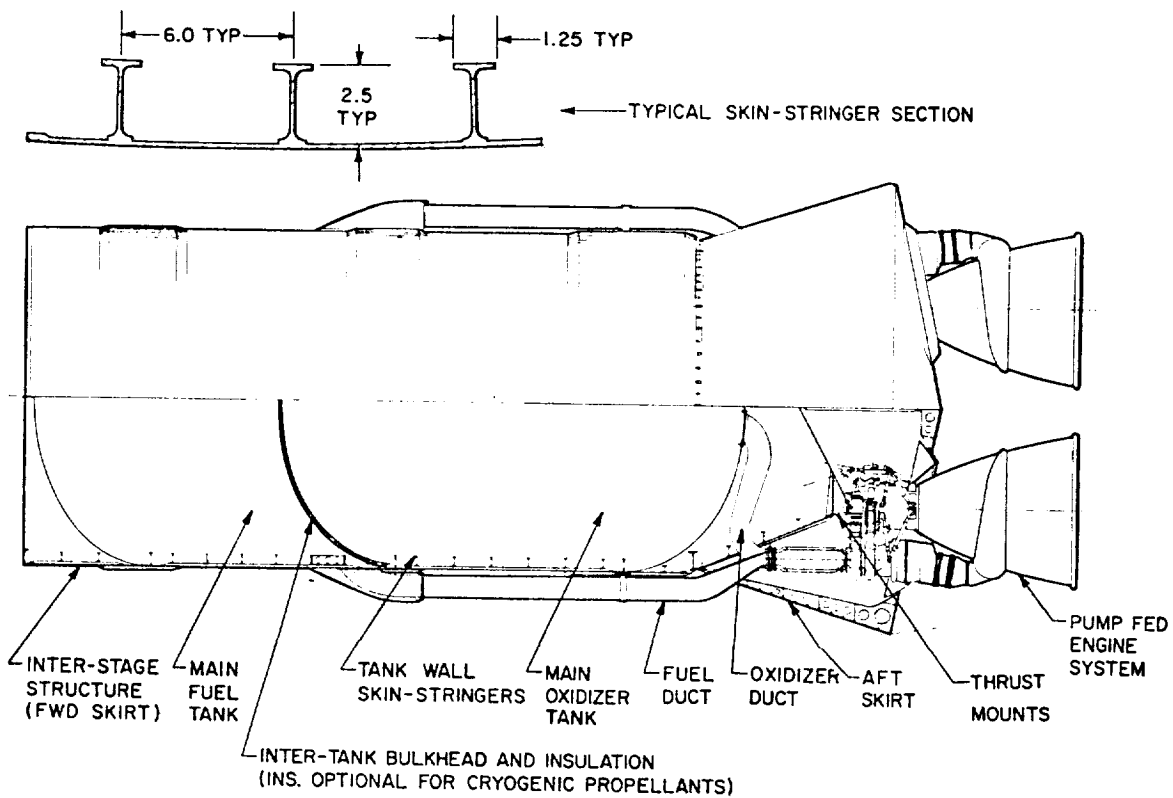


Figure 8-2.—Propellant tank design configuration of a typical booster stage propulsion system.

CONFIDENTIAL

tank pressures must be constantly maintained above a specified minimum by elaborate controls. This tank structure basically is a thin-wall monocoque, requiring special handling procedures. In most booster-stage systems, the propellant tanks are self-supporting types, the tank walls being reinforced by skin stringers (fig. 8-2), or by other structural means, such as waffle grid patterns.

When cryogenic propellants are used, tank insulation may be required. Insulation is mandatory in liquid hydrogen system to prevent ambient air liquefaction which causes high heat transfer rates with attendant high boiloff rates, and safety hazards.

Propellant Tanks for Upper Stage Systems

Figure 8-3 presents the propellant tank design configuration of a typical pressure-fed, upper stage propulsion system. Here, the tanks

are contained within an outer cylindrical shell, through which thrust is transmitted to the payload. The shell is designed to withstand all anticipated boost and flight loads. The propellant tankage consists of two individual units. The main fuel tank is located forward, and the main oxidizer tank near the aft end. The two welded aluminum-alloy tanks are modified spheres, faired into conical sections at the bottom, for propellant discharge. The tanks are bolted to the shell structure around their support ring. The thrust chamber assembly is located just below, and closely coupled to, the oxidizer tank. Thrust is transmitted to the outer shell through the aft half of the oxidizer tank. Both tanks may be insulated independently, for cryogenic propellant service.

Many upper-stage vehicles employ a pressurized gas feed propulsion system. Tank pressures range from 100 to 400 psia. The system shown in figure 8-3 uses stored helium gas for

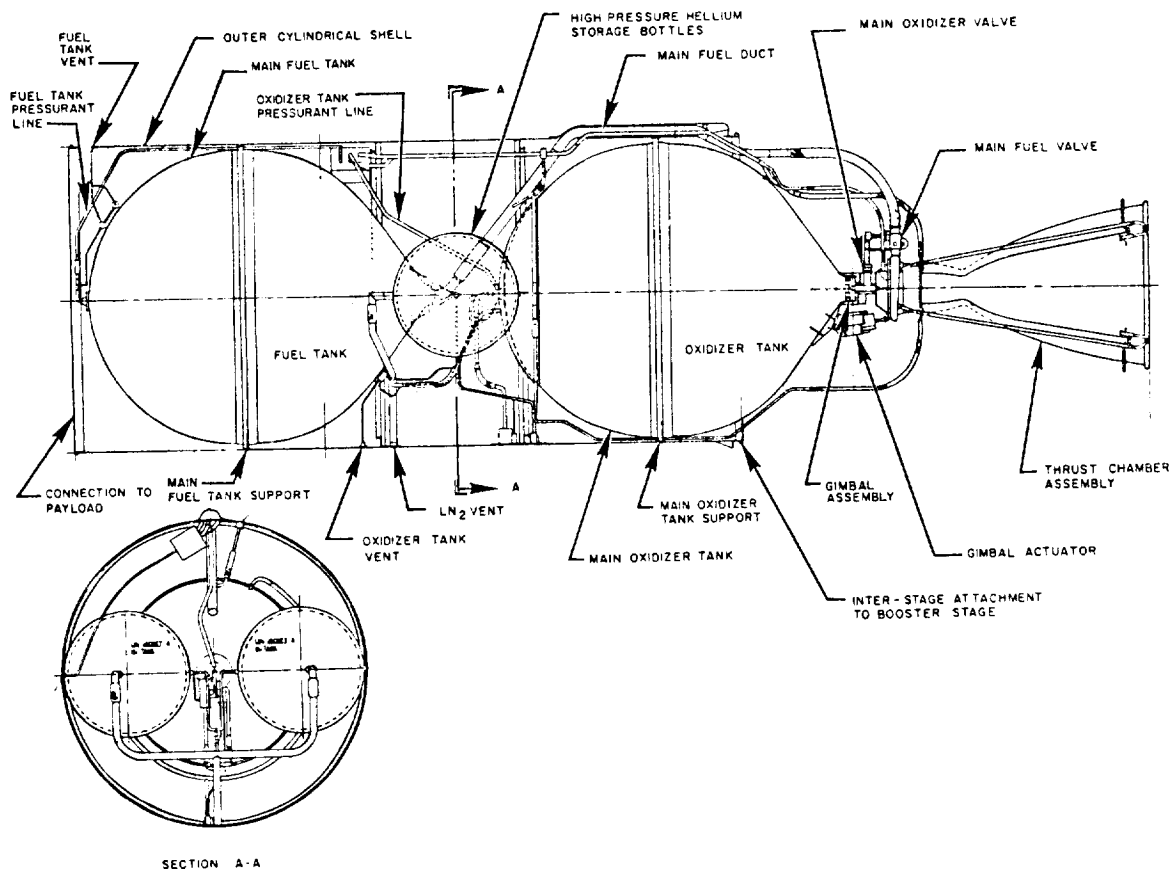


Figure 8-3.—Propellant tank design configuration of a typical upper stage propulsion system.

pressurization. The gas is stored at an initial pressure level from 4500 to 5500 psia at -300°F in two liquid-nitrogen-jacketed, high-pressure spherical bottles located between the two main propellant tanks.

It is for upper stage propulsion systems that the engine designer may most likely also design the tankage. The following discussions, therefore, will confine themselves to these systems. By contrast, the design of booster tanks will probably always be made by an independent group. However, many of the design principles presented here are equally applicable to booster tanks and may thus further the understanding of their design problems.

8.2 GENERAL DESIGN CONSIDERATIONS FOR PROPELLANT TANKS

The tank design is greatly influenced by systems optimization within the overall vehicle design. A principal design objective is for the vehicle to yield the highest payload and/or velocity increment with maximum possible reliability. Design details depend largely upon type of propellants, vehicle mission requirement and configuration, propulsion system design, and available construction materials and fabrication techniques. Some of the most important considerations follow.

Propellant Properties

Propellants affect tank design mainly by their physical and chemical characteristics. The boiling point or storage temperature of a propellant determines the operating temperature range of the tank assembly. Cryogenic propellants cause tank design problems from thermal gradients, from the need for insulation and from the need for construction materials capable of remaining ductile at very low temperatures. The very low density of some propellants, such as liquid hydrogen, requires tanks of considerable volume. The highly corrosive and reactive properties of other propellants severely limit the selection of tank materials.

Shape and Size of Propellant Tanks

Propellant tanks are pressure vessels. Disregarding other factors, the lightest pressure

vessel for a given volume is a spherical shell, since it has the smallest surface to volume ratio. It also has the smallest shell stress for a given internal pressure. While a sphere may be the lightest pressure vessel, the combination of several spheres into the generally cylindrical envelope typical for most rocket vehicles would cause a sizable volume penalty. Furthermore, a sphere would preclude the use of the tank wall as a load-carrying member of the vehicle structure (figs. 8-1 and 8-2), resulting in further weight and volume penalties.

Thus both vehicle configuration and tank pressure level will determine the shape of propellant tanks. For vehicles of relatively large length-to-diameter ratios and of limited space envelopes, cylindrically shaped tanks are used. For relatively high tank pressures and less stringent space conditions, spherical tanks may be employed to best advantage (fig. 8-3). The ends of cylindrical tanks can have either spherical or ellipsoidal shapes. The basic cylindrical tank with spherical ends is lighter than one with ellipsoidal ends. However, the overall weight of an ellipsoidally ended tank may be less when the shorter interstage structure required is considered. In some designs the propellant tank aft ends are faired into conical or other special shapes to accommodate the thrust loads from engine assemblies as well as to minimize trapped propellants.

The required size or volume of a propellant tank is the sum of usable propellant volume and other volume requirements:

$$V_t = V + T + B + U \quad (8-1)$$

where

V_t = propellant tank design volume, ft^3

V = usable propellant volume calculated from propulsion system requirements, ft^3 (may include a "usable residual" term representing design reserves, mixture ratio shift effects, etc.)

T = trapped propellant volume. This is a function of system design configuration and includes propellants trapped in tank, ducts, thrust chamber cooling jacket, etc., ft^3

B = boiled-off propellant volume (applicable only to cryogenic propellants), ft^3

U = tank ullage volume, ft^3

The calculation of propellant volume is based on the propellant density at specific temperatures. A standard temperature of 68° F is used for storable propellants. Boiling point conditions at ambient pressure are used for the cryogenic propellants. The tank ullage-volume calculations should allow for propellant volume changes due to temperature change of the tanked propellant, and for tank deformation when pressurized. This is especially important for pre-packaged storable liquid systems to prevent excessive tank ullage pressures when the system is exposed to a specified upper temperature limit during storage. Adequate ullage volume is also required to maintain tank pressure at starting when the relative ullage volume increase is large and may tax the response of the pressurization system.

Sample Calculation (8-1)

The following data are given for the A-4 stage propulsion system, including two engines:
 Oxidizer (N₂O₄) density, 90.12 lb/ft³
 Oxidizer weight flow rates, 12.78 lb/sec/engine
 Fuel (N₂H₄) density, 63.17 lb/ft³
 Fuel weight flow rate, 10.65 lb/sec/engine
 Nominal engine firing duration at full thrust, 410 sec
 Trapped oxidizer volume, T_o = 0.9 ft³
 Trapped fuel volume, T_f = 1.8 ft³
 Tank ullage volume, U = 2.5% of propellant volume

Determine the volume of the propellant tanks.

Solution

The required usable oxidizer volume

$$V_o = \frac{12.78 \times 2 \times 410}{90.12} = 116.2 \text{ ft}^3$$

The oxidizer tank ullage volume

$$U_o = (V_o + T_o) \times 0.025 = 117.1 \times 0.025 = 2.9 \text{ ft}^3$$

From equation (8-1), the required design volume of the oxidizer tank

$$V_{to} = V_o + T_o + U_o = 116.2 + 0.9 + 2.9 = 120 \text{ ft}^3$$

The required usable fuel volume

$$V_f = \frac{10.65 \times 2 \times 410}{63.17} = 138.2 \text{ ft}^3$$

The fuel tank ullage volume

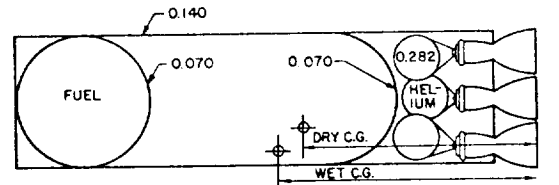
$$U_f = (V_f + T_f) \times 0.025 = 140 \times 0.025 = 3.5 \text{ ft}^3$$

From equation (8-1), the required design volume of the fuel tank

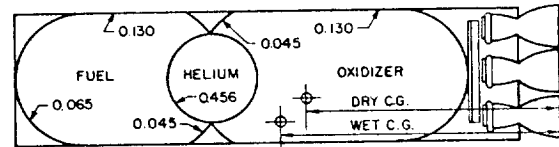
$$V_{tf} = V_f + T_f + U_f = 138.2 + 1.8 + 3.5 = 143.5 \text{ ft}^3$$

Propellant Tank Arrangement

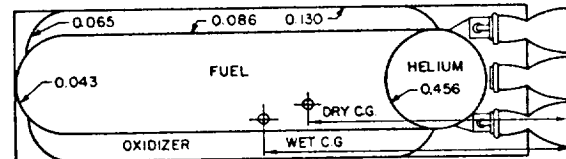
In most vehicle systems, the propellant tanks are arranged in tandem. Other arrangements are used for specific design reasons. Figure 8-4



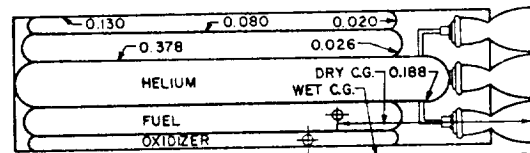
(a) TANDEM PROPELLANT TANKS WITH COMMON BULKHEAD AND SEPARATE HELIUM BOTTLES - TANKAGE WEIGHT, 100 PERCENT



(b) TANDEM PROPELLANT TANKS WITH INTEGRATED HELIUM BOTTLE IN THE MIDDLE - TANKAGE WEIGHT, 93 PERCENT



(c) CONCENTRIC PROPELLANT TANKS WITH INTEGRATED HELIUM BOTTLE AT AFT END - TANKAGE WEIGHT, 118 PERCENT



(d) MULTIPLE PROPELLANT TANKS AND HELIUM BOTTLE IN CLUSTER - TANKAGE WEIGHT, 162 PERCENT

Figure 8-4.—Various propellant tank arrangements of a typical vehicle system.

presents various propellant tank configurations for a typical vehicle system using helium for tank pressurization. A design analysis will determine the best solution for a given propellant storage volume and vehicle space envelope.

General considerations are:

- (1) Minimum overall weight
- (2) Maximum storage volume in a given envelope
- (3) Least possibility of propellant mixing
- (4) Clean aerodynamic vehicle shape
- (5) Ease of installation of ducts and lines
- (6) Ease of insulation
- (7) Ease of fabrication and handling
- (8) Minimum trapped (unusable) propellants

Arrangement (a) is taken as standard. Arrangement (b), combining tandem propellant tanks with an integrated helium bottle in between, results in lowest weight; however, it poses design problems in the routing of pneumatic lines and controls. Arrangement (c) with concentric tanks eases the installation of propellant ducts, but has the possibility of simultaneous puncture of both tanks (by bullets or from other causes), and subsequent mixing of the propellants. Arrangement (d) with multiple tanks has the highest weight, but is easier to fabricate and handle especially for very large vehicles.

Working Loads

The propellant tanks are structural members which must be designed to withstand a combination of the following probable working loads:

- (1) Internal pressure loads and their dynamic effects
- (2) Axial thrust loads and their dynamic effects
- (3) Bending moments due to vehicle transverse accelerations, wind loads, and shifting of the center of gravity
- (4) Aerodynamic forces
- (5) Thrust vector control forces
- (6) Vibration loads
- (7) Loads produced by mounting arrangement
- (8) Loads caused by thermal transients and gradients
- (9) Loads produced during ground handling

In most vehicle systems, internal tank pressure loads and axial thrust loads are the principal ones. Other loads require careful evaluation, including model tests or full-size experiments.

Safety Factors for Propellant Tank Designs

The recommended criteria for working loads presented in chapter II (eqs. 2-8 through 2-11) are generally applicable to propellant tank designs. However, when calculating allowable working stresses from tank internal pressure, the following correlations are recommended for various situations:

- (1) No hazard to personnel or vital equipment:

$$S_w = F_y \quad (8-2)$$

or

$$S_w = \frac{F_u}{1.25} \quad (8-3)$$

- (2) Special safety devices are provided for personnel (example: the booster for a manned upper stage which has an ejection device with an exceptionally high degree of reliability):

$$S_w = \frac{F_y}{1.1} \quad (8-4)$$

or

$$S_w = \frac{F_u}{1.35} \quad (8-5)$$

- (3) Hazard to personnel or vital equipment:

$$S_w = \frac{F_y}{1.33} \quad (8-6)$$

or

$$S_w = \frac{F_u}{1.65} \quad (8-7)$$

where

S_w = maximum allowable working stress, psi; i.e., the stress due to maximum tank working pressure under normal transient and steady operating conditions

F_y = yield strength, psi, of the tank construction material, at operating temperature conditions

F_u = ultimate strength, psi, of the tank construction material under operating temperature conditions

S_w is calculated for both F_y and F_u . The lower value should then be used. All propellant tanks are subjected to hydrostatic pressure tests prior to acceptance. For case (1), the proof test pressure equals maximum tank working pressure.

For case (2) and (3), the proof test pressures should be 110 percent of the maximum tank working pressure. For high-pressure inert gas, long-duration storage bottles, the following correlations are recommended:

No hazard to personnel:

$$S_w = \frac{F_y}{1.33} \quad (8-8)$$

Hazard to personnel:

$$S_w = \frac{F_y}{1.67} \quad (8-9)$$

Sample Calculation (8-2)

The start transient of a prepackaged storable liquid propulsion system for an aircraft-launched missile is programed not to reach main-stage level until the missile is at a specific distance from the aircraft.

Calculate the maximum allowable working stresses for the propellant tanks, if they are made of—

- (a) Aluminum alloy 6061-T6, $F_y = 35\,000$ psi, $F_u = 45\,000$ psi
- (b) Aluminum alloy 6066-T6, $F_y = 50\,000$ psi, $F_u = 57\,000$ psi

Solution

(a) *Tank made of aluminum alloy 6061-T6.*— Since the system involves personnel safety during start transient, equations (8-6) and (8-7) will be applied.

$$S_w = \frac{F_y}{1.33} = \frac{35\,000}{1.33} = 26\,300 \text{ psi}$$

or

$$S_w = \frac{F_u}{1.65} = \frac{45\,000}{1.65} = 27\,260 \text{ psi}$$

Thus, the maximum allowable working stress during start transient = 26 300 psi.

During mainstage operation, personnel are considered safe and equations (8-4) and (8-5) can be used:

$$S_w = \frac{F_y}{1.1} = \frac{35\,000}{1.1} = 31\,800 \text{ psi}$$

$$\text{or} \quad S_w = \frac{F_u}{1.35} = \frac{45\,000}{1.35} = 33\,360 \text{ psi}$$

The maximum allowable working stress for mainstage = 31 800 psi.

(b) *Tank made of aluminum alloy 6066-T6.*— During start transient

$$S_w = \frac{F_y}{1.33} = \frac{50\,000}{1.33} = 37\,600 \text{ psi}$$

or

$$S_w = \frac{F_u}{1.33} = \frac{57\,000}{1.65} = 34\,560 \text{ psi}$$

The maximum allowable working stress during start transient = 34 560 psi.

During mainstage operation

$$S_w = \frac{F_y}{1.1} = \frac{50\,000}{1.1} = 45\,400 \text{ psi}$$

or

$$S_w = \frac{F_u}{1.35} = \frac{57\,000}{1.35} = 42\,200 \text{ psi}$$

The maximum allowable working stress during mainstage = 42 200 psi.

Material and Fabrication Considerations in Propellant Tank Design

In addition to considerations of propellant compatibility and operational temperature ranges, selection of construction materials for propellant tanks is based on their strength-to-density ratio at a given temperature and on their ductility. For a given working pressure, the lightest tank structure will be the one made of the material with the highest ratio of ultimate strength to density. Most frequently used construction materials for propellant tanks are:

- (1) Aluminum alloys, such as 6061-T6, 6066-T6, and 2014-T6. Room temperature properties: Average density $\rho = 0.1$ lb/in³, F_y up to 60 000 psi, F_u up to 70 000 psi, $F_u/\rho = 70 \times 10^4$
- (2) Stainless steels, such as AISI 347 (for low-pressure tanks only), 17-7 PH and PH 15-7 Mo. Room temperature properties: Average density $\rho = 0.285$ lb/in³, F_y up to 200 000 psi, F_u up to 220 000 psi, $F_u/\rho = 77.2 \times 10^4$

- (3) Fiber glass, filament wound with an aluminum-alloy liner. Room temperature properties (fiber glass only): Average density $\rho = 0.08 \text{ lb/in}^3$, $F_u = 120\,000 \text{ psi}$. $F_u/\rho = 150 \times 10^4$

Aluminum alloys are compatible with most storable and cryogenic propellants, and may be used for working temperatures up to 350° F . Stainless steels are suitable for storable (limited duration) and cryogenic propellants, and are suitable for higher temperatures (800° F maximum). Fiber glass is limited to moderate temperature conditions (-60° to 160° F).

Fabrication methods for propellant tanks depend largely upon the type of material used. Most important considerations for tank fabrication are dimension control, heat treating, and welding. The lowest recommended wall-stock size for propellant tanks is about 0.010 inch for stainless steels and 0.020 for aluminum alloys. While tank stress calculations must consider the lower limit of wall-thickness variation, the upper limit is used for tank-weight calculation. The strength of a metal may fall into a band, too, the width of which depends on the heat-treating process. Stress calculation will be based on the minimum expected strength. The quality of the welding process or the efficiency of a welded joint may require extra stock added to the wall thickness as calculated from other working stresses. An assumed weld efficiency of 85 to 95 percent is a reasonable value for steels (50 to 65 percent for aluminum). To minimize weight penalties, build-up lands may be used at the welds (fig. 8-9) for an equivalent 100 percent weld efficiency. Figure 8-5 presents the construction of a welded propellant tank. Note the segmented tank end which is typical for large-size tanks.

Other Propellant Tank Design Problems

Many other design and analysis problems will have to be carefully considered before a successful propellant tankage can be produced. The relatively thin, highly stressed shells make it difficult to attach concentrated loads. The loads must be spread out in a suitable way to prevent localized overstresses. Cryogenic propellants may create thermal transient and gradient problems. While the empty portion of a tank may be

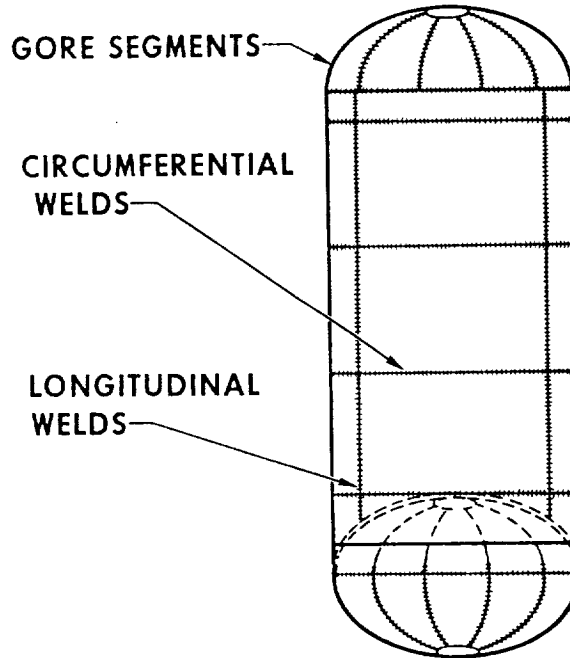


Figure 8-5.—Typical welded propellant tank construction.

subject to aerodynamic heating, the filled portion may be at a very low temperature. Additional thermal problems may arise in outer space, from solar heating of one tank side and radiation cooling of the other.

Also partly the tank designer's responsibility is the solution of certain problems associated with the management of the propellants within the tanks, such as:

- (1) Uniform dispersion of the entering tank pressurant
- (2) Sensing of propellant quantities (PU)
- (3) Prevention of propellant sloshing
- (4) Expulsion of the propellants under adverse conditions
- (5) Fill, drain, vent and pressure relief of the propellant tanks

8.3 STRUCTURAL DESIGN OF PROPELLANT TANKS

As a rule, the wall thickness of propellant tanks is first calculated from stresses caused by internal pressure loads and discontinuities. Then the design is checked for other loads. If the wall thickness of a pressure vessel is small compared to the radii of wall curvature ($t/r \leq 1/15$),

and offers no resistance to bending, the wall is subjected only to direct or hoop-membrane stresses, assumed to be uniformly distributed over the thickness. However, if any discontinuity is present along the wall, such as an abrupt change in radius of curvature or wall thickness, discontinuity and bending stresses are added. At a sufficient distance from the juncture between tank ends (sphere or ellipsoid) and cylindrical shell (where interaction does not occur), the maximum stress in the tank wall due to internal pressure is calculated using the hoop-membrane stress formula only.

Figure 8-6 identifies the major tank elements. In an optimum tank design, the wall thickness varies according to a combination of local membrane, bending, and discontinuity stresses. This is especially true for the spherical and ellipsoidal tank ends. The structural calculation methods for volume, wall thickness, wall surface area, and weight of various tank shapes will now be discussed. The following general terminology is used:

- p_t = maximum tank working pressure, psig
- S_w = maximum allowable working stress of the tank construction material, psi
- ρ = density of the tank construction material, lb/in³
- E = modulus of elasticity, psi
- ν = Poisson's ratio
- e_w = weld efficiency

Spherical Tanks

(1) Volume, in³:

$$V_s = \frac{4 \pi a^3}{3} \quad (8-10)$$

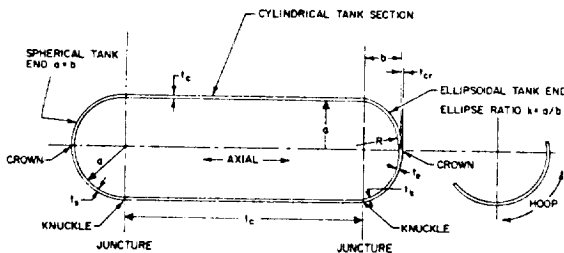


Figure 8-6.—Nomenclature of principal tank elements.

where a = nominal radius of the tank, in

(2) Wall thickness, in, required to withstand membrane stresses from internal tank pressure:

$$t_s = \frac{p_t a}{2 S_w e_w} \quad (8-11)$$

(3) Wall surface area, in²:

$$A_s = 4 \pi a^2 \quad (8-12)$$

(4) Weight, lb:

$$W_s = 4 \pi a^2 t_s \rho \quad (8-13)$$

(5) Critical pressure due to external loading, psi. When the external pressure is higher than the internal tank pressure, the pressure differential across the tank wall may cause the tank to buckle.

$$P_{cr} = \frac{2 E t_s^2}{a^2} \sqrt{3(1-\nu^2)} \quad (8-14)$$

Ellipsoidal and Spherical Tank Ends (fig. 8-6)

Note that the spherical end is a special case of ellipsoidal end, in which the major half-diameter, a , equals the minor half-diameter, b .

(1) Volume:

Ellipsoidal tank end volume, in³:

$$V_e = \frac{2 \pi a^2 b}{3} \quad (8-15)$$

Spherical tank end volume, in³:

$$V_s = \frac{2 \pi a^3}{3} \quad (8-16)$$

where

- a = elliptical tank end major half-diameter, in
- R = radius of the cylindrical tank section
- b = elliptical tank end minor half-diameter, in

(2) Wall thicknesses considering combined membrane, discontinuity, and local bending stresses caused by internal tank pressure p_t . An equivalent wall thickness, which is an average value of knuckle-and-crown thickness, may be

used to calculate the weight of the tank ends.

$$t_k = \frac{K p_t a}{S_w e_w} \quad (8-17)$$

$$t_{cr} = \frac{p_t R}{2 S_w e_w} \quad (8-18)$$

$$t_e = \frac{(t_k + t_{cr})}{2} = \frac{p_t a \left(K + \frac{k}{2} \right)}{2 S_w} \quad (8-19)$$

$$t_s = \frac{p_t a \left(K + \frac{1}{2} \right)}{2 S_w} \quad (8-20)$$

$$\frac{t_e}{t_s} = \frac{\left(K + \frac{k}{2} \right)}{\left(K + \frac{1}{2} \right)} \quad (8-21)$$

$$\frac{t_e}{t_c} = \frac{\left(K + \frac{k}{2} \right)}{2} \quad (8-22)$$

where

k = tank end ellipse ratio = a/b ; $k=1$ for a spherical end

R = tank end crown radius, in = ka ; $R=a$ for a spherical end

K = stress factor, a function of the ellipse ratio k . Figure 8-7 presents a K versus k curve for combined membrane, discontinuity, and local bending stresses

t_k = wall thickness at the knuckle, in

t_{cr} = wall thickness at the crown, in

t_e = equivalent wall thickness of an ellipsoidal tank end, in

t_s = equivalent wall thickness of a spherical tank end, in

t_c = wall thickness of a cylindrical tank section, in

(3) Wall surface area:

Ellipsoidal tank end surface area, in²:

$$A_e = a^2 + \frac{\pi b^2 \ln \left[\frac{(1+e)}{(1-e)} \right]}{2e} \quad (8-23)$$

Spherical tank end surface area, in²:

$$A_s = 2 \pi a^2 \quad (8-24)$$

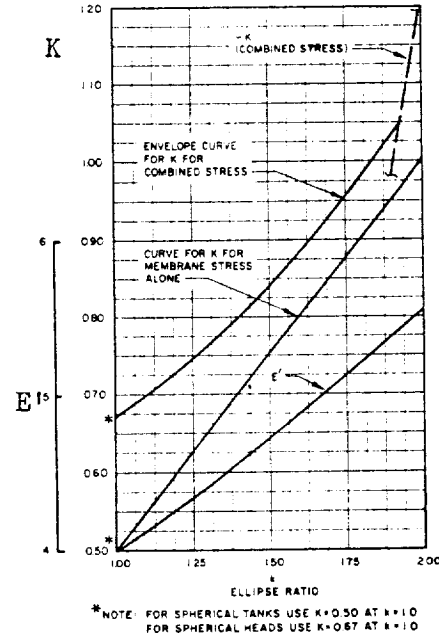


Figure 8-7.—Ellipse ratio k versus knuckle stress factor K , compression stress $-K$, and parameter E' . (From ARS paper, "Design Criteria and Analyses for Thin-Walled Pressurized Vessels and Interstage Structures," by T. J. Hart.)

where

$$e = \text{eccentricity} = \frac{\sqrt{a^2 - b^2}}{a} = \sqrt{1 - \frac{1}{k^2}}$$

(4) Weight:

Ellipsoidal tank end weight, lb:

$$W_e = \frac{\pi a^2 t_e E' \rho}{2k} \quad (8-25)$$

Spherical tank end weight, lb:

$$W_s = 2 \pi a^2 t_s \rho \quad (8-26)$$

where

$$E' = \text{design factor} = 2k + \frac{1}{\sqrt{k^2 - 1}} \ln \frac{k + \sqrt{k^2 - 1}}{k - \sqrt{k^2 - 1}}$$

(see fig. 8-7)

(5) Critical pressure due to external loading, psi:

For an ellipsoidal tank end, it may be approximated as

$$p_{cre} = \frac{C_b 2Et_e^2}{R^2} \quad (8-27)$$

For a spherical tank end

$$p_{crs} = \frac{0.342 Et_s^2}{a^2} \text{ (approximately)} \quad (8-28)$$

where

C_b = buckling coefficient, a function of R/t_e , ranging from 0.05 to 0.10

Cylindrical Tank Section

(1) Volume, in³:

$$V_c = \pi a^2 l_c \quad (8-29)$$

where

a = radius, in

l_c = length, in

(2) Wall thickness, in, required to withstand membrane stresses due to internal tank pressure:

$$t_c = \frac{p_t a}{S_w e_w} \quad (8-30)$$

(3) *Discontinuity stresses.*—The discontinuity at the juncture between the cylindrical tank section and the tank ends will cause bending and shear loads along the cylindrical circumference at the juncture, and the adjacent areas. These discontinuity stresses are superimposed upon the membrane stresses and comprise: (a) axial bending stress; (b) hoop bending stress; (c) additional hoop stress due to the shear load; (d) shear stress. Discontinuity stresses fade out rapidly, so that they become negligibly small a short distance from the juncture. Detail analyses of discontinuity stresses can be found in standard textbooks. In general, buildup of wall thickness of less than $0.5 t_c$, near the juncture, will suffice for most designs, with only small weight penalty.

(4) Wall surface area, in²:

$$A_c = 2 \pi a l_c \quad (8-31)$$

(5) Weight, lb:

$$W_c = 2 \pi a l_c t_c \rho \quad (8-32)$$

(6) External loading critical pressure, psi:
For a short tank (i.e., $l_c < 4.9 a \sqrt{a/t_c}$):

$$p_{crc} = 0.807 \frac{Et_c^2}{l_c a} \sqrt[4]{\left(\frac{1}{1-\nu^2}\right)^3 \frac{t_c^2}{a^2}} \quad (8-33)$$

For long tanks (i.e., $l_c \geq 4.9 a \sqrt{a/t_c}$):

$$p_{crc} = \frac{Et_c^3}{4(1-\nu^2)a^3} \quad (8-34)$$

where E = modulus of elasticity.

Sample Calculation (8-3)

The following design data are specified for the A-4 stage propulsion system, which employs a cylindrical propellant tank section with ellipsoidal ends (preliminary layout shown in fig. 3-10).

Required design volume of the oxidizer tank,
 $V_{to} = 120 \text{ ft}^3$

Maximum oxidizer tank working pressure,
 $p_{to} = 180 \text{ psia}$

Required design volume of the fuel tank,
 $V_{tf} = 143.5 \text{ ft}^3$

Maximum fuel tank working pressure, $p_{tf} = 170 \text{ psia}$

Internal radius of the cylindrical tank section,
 $a = 41 \text{ in}$

Tank construction material, aluminum alloy
6066-T6: $F_y = 50\,000 \text{ psi}$; $F_u = 57\,000 \text{ psi}$;
 $\rho = 0.101 \text{ lb/in}^3$; $E = 10.4 \times 10^6 \text{ psi}$; $\nu = 0.36$

Weld efficiency, $e_w = 100 \text{ percent}$.

Determine the following:

(a) Required internal tank dimensions

(b) Required thickness of the tank walls at various sections, considering internal pressure loads, discontinuity, and local bending stresses

(c) Approximate weight of the tankage

(d) Critical external loading pressures, using a buckling coefficient, $C_b = 0.10$ for the tank ends

Solution

(a) Since the oxidizer tank consists of two ellipsoidal ends without a cylindrical section, equation (8-15) may be applied:

$$V_{to} = \frac{2 \times 2 \pi a^2 b}{3}$$

We rearrange to obtain the minor elliptical half-diameter of the tank ends:

$$b = \frac{3 \times V_{to}}{2 \times 2 \pi a^2} = \frac{3 \times 120 \times 1728}{4 \times \pi \times (41)^2} = 29.4 \text{ in}$$

The tank end ellipse ratio:

$$k = \frac{a}{b} = \frac{41}{29.4} = 1.395$$

Since we use an ellipsoidal end of the same proportion at the fuel tank top, the fuel tank volume may be treated as the volume of a cylindrical tank section with the length l_c . From equation (8-29), the volume of the fuel tank:

$$V_{tf} = \pi a^2 l_c$$

$$l_c = \frac{V_{tf}}{\pi a^2} = \frac{143.5 \times 1728}{\pi \times (41)^2} = 46.9 \text{ in}$$

To summarize the internal dimensions of the tankage:

$$a = 41 \text{ in}, \quad b = 29.4 \text{ in}, \quad k = 1.395, \quad l_c = 46.9 \text{ in}$$

(b) We assume that certain missions of the A-4 vehicle require it to be man rated. From equations (8-6) and (8-7), the maximum allowable working stresses are derived:

$$S_w = \frac{F_y}{1.33} = \frac{50\,000}{1.33} = 37\,600 \text{ psi}$$

$$S_w = \frac{F_u}{1.65} = \frac{57\,000}{1.65} = 34\,560 \text{ psi}$$

We use the lower value of 34 560 psi.

From figure 8-6, the tank end stress factor K of the combined stresses is 0.80 for an ellipse ratio k of 1.395. From equation (8-17), the re-

quired wall thickness at the knuckle of the oxidizer tank end

$$t_{ko} = \frac{K p_t a}{S_w} = \frac{0.80 \times 180 \times 41}{34\,560} = 0.171 \text{ in}$$

From equation (8-18), the required wall thickness at the crown of the oxidizer tank end

$$t_{cro} = \frac{p_t R}{2 S_w} = \frac{180 \times 1.395 \times 41}{2 \times 34\,560} = 0.149 \text{ in}$$

From equation (8-19), the equivalent wall thickness of the oxidizer tank end

$$t_{eo} = \frac{(t_{ko} + t_{cro})}{2} = \frac{(0.171 + 0.149)}{2} = 0.16 \text{ in}$$

NOTE: In some designs, weight has been saved by taking advantage of the fact that the bulkhead common to both tanks is subject to a relatively small differential pressure in operation. Such systems, however, require more elaborate pressurization and loading systems including interlocks. In case of malfunction, the common bulkhead may suffer serious damage.

The required wall thickness at the knuckle of the fuel tank end:

$$t_{kf} = \frac{t_{ko} p_{tf}}{p_{to}} = \frac{0.171 \times 170}{180} = 0.162 \text{ in}$$

The required wall thickness at the crown of the fuel tank end:

$$t_{crof} = \frac{t_{cro} p_{tf}}{p_{to}} = \frac{0.149 \times 170}{180} = 0.141 \text{ in}$$

The equivalent wall thickness of the fuel tank end:

$$t_{ef} = \frac{(t_{kf} + t_{crof})}{2} = \frac{(0.162 + 0.141)}{2} = 0.152$$

From equation (8-30), the required wall thickness of the cylindrical tank section:

$$t_c = \frac{p_{tf} a}{S_w} = \frac{170 \times 41}{34\,560} = 0.202 \text{ in}$$

Provide a buildup of $0.4 t_c$ on the cylindrical tank section wall near the juncture to allow for discontinuity stresses:

$$t_{cj} = t_c + 0.4t = 0.202 + 0.4 \times 0.202 = 0.283 \text{ in}$$

To summarize:

$$\begin{aligned} t_{ko} &= 0.171 \text{ in}, & t_{cro} &= 0.149 \text{ in}, & t_{eo} &= 0.16 \text{ in} \\ t_{kf} &= 0.162 \text{ in}, & t_{crf} &= 0.141, & t_{ef} &= 0.152 \text{ in} \\ t_c &= 0.202 \text{ in}, & t_{cj} &= 0.283 \text{ in} \end{aligned}$$

(c) From equation (8-25), the weight of the oxidizer tank end:

$$W_{eo} = \frac{\pi a^2 t_{eo} E' \rho}{2k}$$

From figure 8-7, E' is 4.56, for $k = 1.395$:

$$W_{eo} = \frac{\pi(41)^2 \times 0.16 \times 4.56 \times 0.101}{2 \times 1.395} = 139.5 \text{ lb}$$

The weight of the fuel tank end:

$$W_{ef} = \frac{W_{eo} t_{ef}}{t_{eo}} = \frac{139.5 \times 0.152}{0.16} = 132.8 \text{ lb}$$

From equation (8-32), the weight of the cylindrical tank section:

$$W_c = 2\pi a l_c t_c \rho = 2 \times 41 \times 46.9 \times 0.202 \times 0.101 = 246.4 \text{ lb}$$

Add 4 percent of overall tankage weight for local wall thickness buildups, to allow for welded joints, discontinuity stresses, etc., and for tolerances during fabrication.

Approximate overall weight of the tankage (less accessories):

$$\begin{aligned} W_t &= 1.04(2 \times W_{eo} + W_{ef} + W_c) \\ &= 1.04(2 \times 139.5 + 132.8 + 246.4) = 685 \text{ lb} \end{aligned}$$

(d) From equation (8-27), the critical external loading pressure for the oxidizer ends

$$\begin{aligned} p_{creo} &= \frac{C_b 2 E t_{eo}^2}{R^2} = \frac{0.10 \times 2 \times 10.4 \times 10^6 \times (0.16)^2}{(1.395 \times 41)^2} \\ &= 16.3 \text{ psi} \end{aligned}$$

The critical external loading pressure for the fuel tank end:

$$\begin{aligned} p_{cref} &= \frac{C_b 2 E t_{ef}^2}{R^2} = \frac{0.10 \times 2 \times 10.4 \times 10^6 \times (0.152)^2}{(1.395 \times 41)^2} \\ &= 14.7 \text{ psi} \end{aligned}$$

We find that $l_c < 4.9a\sqrt{a/t_c}$. Thus equation (8-33) applies, yielding an external loading critical pressure for the cylindrical tank section

$$\begin{aligned} p_{crc} &= \frac{0.807 \times 10.4 \times 10^6 \times (0.202)^2}{46.9 \times 41} \\ &\quad \times \sqrt[4]{\left(\frac{1}{1 - (0.36)^2}\right)^3 \left(\frac{0.202}{41}\right)^2} \\ &= 13.9 \text{ psi} \end{aligned}$$

Axial Compressive Loading on the Cylindrical Tank Section

In integrated propellant tank designs (figs. 8-2 and 8-3), the cylindrical tank section must withstand large axial compressive loads during vehicle handling and operation. If the tank is not pressurized, i.e., if tank pressure = ambient pressure, the critical axial compressive stress for an unstiffened cylindrical tank may be calculated as

$$S_c = \left[9 \left(\frac{t_c}{a} \right)^{1.6} + 0.16 \left(\frac{t_c}{l_c} \right)^{1.3} \right] E \quad (8-35)$$

where S_c = critical axial compressive stress, psi.
This is the axial compressive stress that will cause the tank to buckle

One method of increasing the axial load-carrying ability of a cylindrical tank section with minimum weight penalty is to pressurize the tank. This is known as pressure stabilization. Internal pressure will raise the critical buckling stress of a tank; or it may be used to counterbalance an axial compressive load F_a , lb, where

$$F_a = \pi a^2 p_t \quad (8-36)$$

Pressurization will also reduce tank failures from very large bending loads. However, if the pressure is ever permitted to drop below a value necessary to carry the axial and bending loads, the tank will collapse and the vehicle will probably be damaged beyond repair.

An alternative method of increasing the external load-carrying ability of a cylindrical tank is to make it self-supporting. This involves stiffening the cylindrical skin by means of longitudinal and circumferential members, or honeycomb structures. The members may be either separate stiffeners welded to the tank wall, or may be made integral with the wall by machining or chemically milling a thicker sheet.

Sample Calculation (8-4)

For the A-4 stage tankage, calculate:

- Critical axial compressive load of the cylindrical tank section with no internal pressure.
- Required internal tank pressure to offset an axial compressive load of 100 000 pounds with no compressive stress on the cylindrical tank section.

Solution

(a) From equation (8-35), the critical compressive stress of the cylindrical tank section:

$$S_c = \left[9 \left(\frac{0.202}{41} \right)^{1.6} + 0.16 \left(\frac{0.202}{46.9} \right)^{1.3} \right] \times 10.4 \times 10^6$$

$$= 20360 \text{ psi}$$

The critical axial compressive load of the cylindrical tank section:

$$F_c = S_c \times 2\pi a t_c = 20360 \times 2\pi \times 41 \times 0.202$$

$$= 1\,060\,000 \text{ lb}$$

From the results it is obvious that the A-4 stage tankage is capable of withstanding a substantial axial compressive load without internal pressurization.

(b) From equation (8-36), the required internal tank pressure:

$$p_t = \frac{F_a}{\pi a^2} = \frac{100\,000}{\pi \times (41)^2} = 18.95 \text{ psi}$$

Water Hammer Effects Due to Impact

When a loaded propellant tank is subject to an impact force, a water-hammer effect occurs within

the tank. This effect produces a surge of the tank internal pressure. For very short impacting times (less than 1.2×10^{-3} sec), the following correlations are established for cylindrically shaped propellant tanks:

$$p_s = \frac{c \dot{w}}{\pi a^2 g} \quad (8-37)$$

$$c = \frac{c'}{\sqrt{1 + \frac{2.5 E_p a (1 - 0.8 \nu)}{E t_c}}} \quad (8-38)$$

where

- p_s = pressure surge due to the impact, psi
- \dot{w} = equivalent flow rate of the propellant due to the impact, lb/sec
- a = radius of the cylindrical tank, in
- t_c = wall thickness of the cylindrical tank, in
- g = gravitational constant, 32.2 ft/sec²
- c = acoustic velocity of the restrained propellant, in/sec
- c' = free acoustic velocity of the propellant, in/sec
- E_p = compressive modulus of elasticity of the propellant, psi
- E = modulus of elasticity of the tank construction material, psi
- ν = Poisson's ratio of the tank construction material

In many prepackaged liquid applications, the propellant tankage is required to withstand certain impact loads, as specified by the height of the drop tests. The details of estimating tank pressure surges from a free-fall impact are illustrated by sample calculation (8-5).

Sample Calculation (8-5)

The following data are given for the cylindrical fuel tank of a prepackaged storable liquid propulsion system:

Fuel, N_2H_4

Fuel density, $\rho_p = 63.17 \text{ lb/ft}^3$

Compressive modulus of elasticity of the fuel,

$$E_p = 6.06 \times 10^5$$

Free acoustic velocity of the fuel, $c' = 80100 \text{ in/sec}$

Tank construction material, aluminum alloy 6066-T6

Modulus of elasticity of the tank construction material, $E = 10.4 \times 10^6$

Poisson's ratio of the tank construction material, $\nu = 0.36$

Radius of the cylindrical tank, $a = 4$ in

Length of the cylindrical tank, $l_c = 50$ in

Wall thickness of the cylindrical tank, $t_c = 0.167$ in

For a tank falling in direction of its longitudinal axis, estimate:

- (a) Tank pressure surge due to the impact after a 6-foot free drop
- (b) Tank pressure surge due to the impact after a 20-foot free drop

Solution

(a) For a 6-foot free drop the final velocity at impact:

$$V = \sqrt{2gh} = \sqrt{2 \times 32.2 \times 6} = 19.65 \text{ fps}$$

This yields an equivalent propellant flow rate due to impact of

$$\dot{w} = \rho_p \pi a^2 V = 63.17 \times \pi \times \left(\frac{4}{12}\right)^2 \times 19.65 = 434.5 \text{ lb/sec}$$

From equation (8-38), the acoustic velocity of the restrained fuel

$$c = \frac{80100}{\sqrt{1 + \left[\frac{2.5 \times 6.06 \times 10^5 \times 4(1 - 0.8 \times 0.36)}{10.4 \times 10^6 \times 0.167} \right]}}$$

$$= 43100 \text{ in/sec}$$

Impact time delay in the tank:

$$\frac{l_c}{c} = \frac{50}{43100} = 1.16 \times 10^{-3} \text{ sec (i.e., } < 1.2 \times 10^{-3} \text{ sec)}$$

Using equation (8-37), we obtain the tank pressure surge due to impact after a 6-foot free drop:

$$p_s = \frac{c\dot{w}}{\pi a^2 g} = \frac{43100 \times 434.5}{\pi \times (4)^2 \times 386} = 964 \text{ psi}$$

(b) After a 20-foot free drop, the final velocity at impact is

$$V = \sqrt{2gh} = \sqrt{2 \times 32.2 \times 20} = 35.9 \text{ fps}$$

The equivalent propellant flow rate due to impact:

$$\dot{w} = \rho_p \pi a^2 V = 63.25 \times \pi \times \left(\frac{4}{12}\right)^2 \times 35.9 = 792.5 \text{ lb/sec}$$

The tank pressure surge due to impact after a 20-foot free drop:

$$p_s = \frac{c\dot{w}}{\pi a^2 g} = \frac{43100 \times 792.5}{\pi \times (4)^2 \times 386} = 1765 \text{ psi}$$

8.4 DESIGN OF STORABLE LIQUID PROPELLANT TANKS

The design of tanks for storable liquid propellants uses the same general design practices applied to other propellant tanks, except in the area of compatibility. Most storable propellants will remain stable for long periods of time if stored in tanks constructed of materials compatible with the propellants. To minimize propellant decomposition and tank material corrosion, the surface of tank walls in contact with the propellants must be smooth and clean.

Tank Material Compatibility

Prior to final selection, a detail study is required to determine the compatibility of potential tank construction materials with the propellant combination involved. In this study, two major considerations should be kept in mind: (1) the expected storage life of the propulsion system, and (2) the credibility of the available data. For a required storage period of less than 3 years, the compatibility data for many materials with various propellants are generally reliable. However, for longer periods, such as a 10-year storage requirement, the design data are usually extrapolated from the results of relatively short-term testing. Figure 8-8 illustrates the typical extrapolated corrosion and passivity rate of aluminum alloy 6066-T6 exposed to the liquid phase of inhibited red fuming nitric acid (IRFNA).

Much of the available compatibility test data tend to contradict each other. This is the result of differing test methods, conditions, and criteria. It involves the risk that although a material may be acceptable for a relatively short exposure, it may fail when the exposure time to a particular

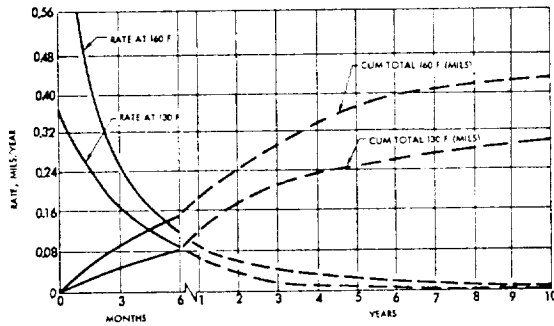


Figure 8-8.—Typical extrapolated corrosion and passivity rate of aluminum alloy 6066-T6 exposed to the liquid phase of IRFNA.

environment is increased. Whenever a discrepancy of material compatibility is observed, thorough verification of the test conditions is indicated. For most of the long-term storable propellant tankage, the aluminum alloys are used for best results. Austenitic and semiaustenitic stainless steels should be used only for rather short-term storage.

Tank Construction

One of the prime design objectives of storable propellant tankage is the elimination of maintenance during storage and prefiring activities. This may be accomplished by an all-welded, hermetically sealed construction. To achieve hermetic sealing, leakproof burst diaphragms are installed throughout the inlets and outlets of the tankage. Propellant fill ports are welded shut after tanking. Tandem tanks are favored over concentric tanks, since propellants are more positively separated during storage, transportation, and other adverse conditions. In some applications, the common bulkhead between two propellant tanks is designed to withstand a differential pressure in either direction that may result from inconsistent burst diaphragms. However, the burst diaphragm at the pressurant inlet to the oxidizer tank of the A-4 system is designed to a lower burst pressure than that of the pressurant inlet diaphragm for the fuel tank. This insures that the oxidizer tank pressure is always the higher.

Full-penetration welds should be used in the construction of all propellant tanks. This is especially important for storable propellants.

A full-penetration "100 percent" weld is one where complete fusion has taken place to the root of the joint. Unfused edges, oxide notch, or any concavity at the root indicate lack of full penetration. All full-penetration welds which cannot be visually examined on the reverse side must be X-rayed to assure full penetration. Figure 8-9 presents the design detail of a typical full-penetration, single-welded butt joint.

If possible, interpropellant welding (i.e., the fuel and oxidizer are separated by only one welded joint) should be avoided in tank designs. A double-weld design will prevent the mixing of propellants due to a single failure of welded joints. Figure 8-10 presents the design of a typical storable propellant tank with a forged one-piece common bulkhead. A double-weld design is used on the center-hold joint for the oxidizer duct.

Tank Wall Surface Requirements

The inner surfaces of the storable propellant tank wall must be relatively free of rust deposits

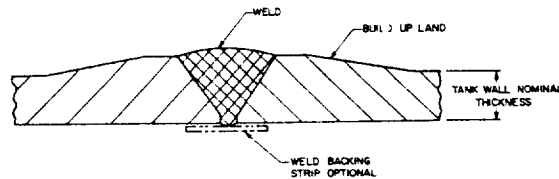


Figure 8-9.—Design detail of a typical full-penetration, single-welded butt joint for propellant tanks.

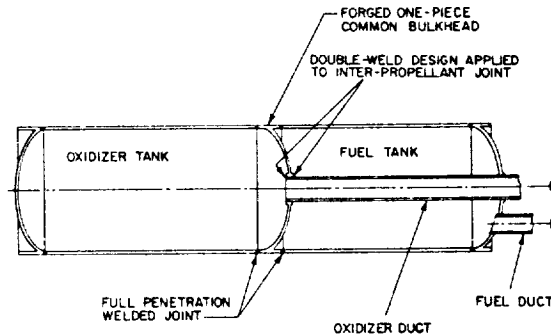


Figure 8-10.—Design of a typical storable propellant tank with a forged one-piece common bulkhead.

and tool marks. All welded joints should be ground to achieve a smooth dent-free contour. If an aluminum alloy is used for tank construction, anodizing of the inner surfaces is recommended. The tank should be cleaned and treated before use. The process rendering the surfaces inactive is known as passivation. Basically, passivation involves the cleaning of tank interior with solvents and, in some cases, the treatment with alkaline or acid solution. Passivation differs from conditioning or stability testing of a tank. Stability testing of a tank involves the application of a propellant rinse prior to propellant tanking.

8.5 DESIGN OF CRYOGENIC LIQUID PROPELLANT TANKS AND THEIR INSULATION

In the design of cryogenic propellant tanks, there are several potential problem areas which may affect proper functioning and reliability:

- (1) Properties of the tank construction materials at the cryogenic propellant service temperature range
- (2) Thermal stresses induced in the tank structure by temperature gradients
- (3) The relief of tank pressure caused by boiloff of the cryogenic propellants
- (4) Thermal insulation of the tank walls

The knowledge of the precise strength characteristics, degree of brittleness, and notch sensitivity of the tank construction materials at cryogenic temperatures (as low as -423°F for liquid hydrogen service) is a prerequisite for their selection. In general, most of the aluminum alloys, the austenitic and semiaustenitic stainless steels, possess good mechanical properties at cryogenic temperatures (also see ch. II). The thermal stresses can be analyzed by determining the temperature profile at various regions of the tank and may be minimized by discrete design approaches. The capacity of the tank relief valve should be based on the maximum anticipated propellant boiloff rate during ground hold and actual operation of the vehicle systems.

Among the cryogenic propellants, liquid hydrogen imposes the most serious tank design problems. This is mainly due to its very low service temperature and its relatively large specific volume. Design problems are especially

acute with the hydrogen tank insulation. It often becomes one of the most critical design factors in a hydrogen-fueled vehicle system. The difficulties arising in hydrogen systems in connection with heat transfer may be dramatically illustrated as follows:

Assume two tanks of equal size, subject to the same heat influx per unit time. One is filled with liquid oxygen, the other with liquid hydrogen. The ratio of heat of vaporization per unit weight $O/H = 0.48$, but the density ratio is $O/H = 14.3$. Thus the volume rate of vaporization in the hydrogen tank is 6.85 times faster than in oxygen. In reality, the heat influxes would not be equal for two uninsulated tanks, because of the higher temperature differential across the wall, and especially because of the greatly increased heat-transfer rate from air liquefaction on the hydrogen tank surface. This may further accelerate the hydrogen volume boiloff rate to approximately 70 times that of oxygen. In an actual oxygen/hydrogen system, operating at a weight mixture ratio $O/H = 5$, the tanked mixture ratio by volume is $H/O = 3.23$. Depending on the shape of the tanks (surface ratio), this may again double or triple the relative boiloff rate of hydrogen. The absolute necessity for insulation to drastically reduce heat influx into a hydrogen system becomes apparent.

Boiloff rates are not the only problem caused by the physical properties of hydrogen. Near the ambient boiling temperature, the gradient of vapor pressure is $2.4 \text{ psi}/^{\circ}\text{R}$, as compared to $0.78 \text{ psi}/^{\circ}\text{R}$ for liquid oxygen. Moreover, this gradient increases rapidly with increasing temperature, which would be experienced following tank pressurization. Figures 8-11 and 8-12 show the trend for both liquid oxygen and hydrogen. The data have great significance to pump NPSH. As may be seen, just one degree of liquid-hydrogen-temperature rise requires a 3-psi increase in tank pressure to maintain proper NPSH. In a large vehicle, the required increase in tank-wall thickness may affect payload capability noticeably. The situation is further aggravated by the high heat influx into hydrogen, for reasons mentioned in connection with boiloff. Even for relatively short boost periods, rapid warmup may create a problem more severe than boiloff, and places further emphasis on adequate insulation. The following discussion of tank insulations,

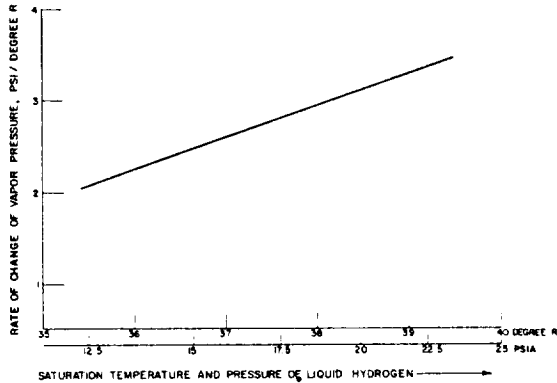


Figure 8-11.—Rate of change of saturation vapor pressure to temperature for liquid hydrogen.

therefore, is specially slanted to hydrogen service.

Insulation Requirements for the Cryogenic Propellant Tanks

Most vehicle missions include three distinct phases during which effective insulation for the cryogenic propellant tanks is essential: ground hold period, the boost phase, and coast flight in space. The propellant tank insulation design will primarily be based on flight performance criteria. However, propellant evaporative losses during long hold periods on the ground requiring continuous topping may also become a significant cost item. If long hold periods with a filled tank are anticipated, it may be indeed economical

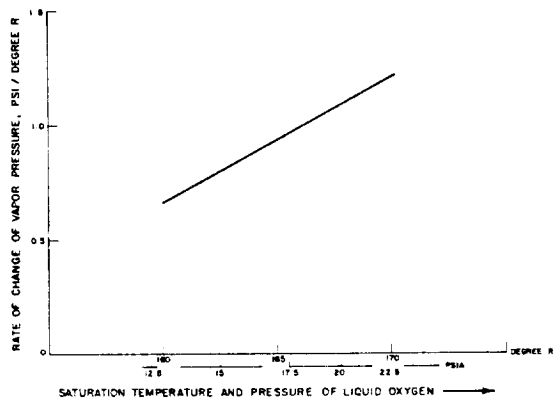


Figure 8-12.—Rate of change of saturation vapor pressure to temperature for liquid oxygen.

to provide an insulating blanket on the tanks, which is remotely removed just prior to liftoff. During the boost phase, high temperatures from aerodynamic heating, and large aerodynamic forces are encountered. Although of short duration, this phase dictates the structural elements of the insulation. During coast flight in space, the principal source of thermal energy is radiation from the Sun and the planets. By the use of radiation shields surrounding the basic tank insulation, the heat flux across the tank wall can be effectively controlled. The properties of the materials used in a solar shield are very important, such as the absorptivity and emissivity of the surface when subjected to various types of radiation and body temperatures. Magnesium oxide and silver are two materials showing promise for use in solar shields. These materials may be applied as coatings onto a lighter base material such as aluminum. The amount of shielding required depends on the duration of the coast flight and on optimization of shield weight versus propellant boiloff weight.

Basic Insulation Types

Major desirable design features of an insulation include: light weight, uniform and repeatable insulation characteristics, ease of application, low cost, low hazard, reasonable ruggedness, ease of repair, good reliability, and above all, low heat conductivity.

Excellent results can be achieved with a laminated-type insulation. This employs an aluminum foil and fiber-glass structure, often in multiple layers. The aluminum foils act as reflectors, effectively rejecting radiative heat, while the evacuated space in between prevents conductive heat transfer. This insulation can be applied to single-curved and to large-diameter, double-curved surfaces. The laminar insulation is sensitive to damage, however, possibly resulting in loss of vacuum due to cracks and to infiltration of leak gases. Application to airborne system thus has been infrequent.

For the latter, honeycomb-supported structures are finding wide application. Figure 8-13 shows the typical example of an externally applied hydrogen tank insulation of this type. A ½- to ¾-inch nominal-size plastic honeycomb is installed between an inner and outer facing

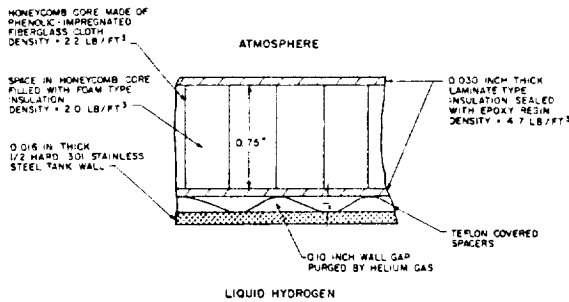


Figure 8-13.—Construction elements of a typical liquid hydrogen tank insulation design (external type).

sheet. The cells may or may not (weight!) be filled with an isocyanate-type foam. The foam bubbles or the properly sealed cells will form individual vacuum spaces when cold (cryopumping). However, because of the possibility of vacuum degradation by infiltration of air (outer insulation), or hydrogen (inside insulation), it is often preferred to purge the cells with helium, for which lateral passage ways must be provided. The purge also serves as a leak-detection device, in conjunction with gas analyzers, to detect contamination of the helium from leaks. In figure 8-13, a separate gap is purged with helium, rather than the honeycomb cells.

The thermal conductivity of the insulation shown is about 3.8×10^{-7} Btu-in/in²-sec-°F (0.2 Btu-in/ft²-hr-°F).

Thermal conductivities of various types of insulation vary from 0.05×10^{-7} to 6.0×10^{-7} Btu-in/in²-sec-°F. Their densities range from 2.0 to 20 lb/ft³. Since the quality of an insulation will affect cost and weight, an optimization study will have to be made, based on mission characteristics.

Sample Calculation (8-6)

Determine the heat-transfer rates in Btu/in²-sec across the tank insulation shown in figure 8-13 during—

- (a) *Ground hold.*—The temperature of the insulation surface near the tank wall is around -360° F and the outer surface is 70° F.
- (b) *Boost phase.*—The inner insulation surface temperature reaches -210° F and the outer insulation temperature reaches 800° F.

Solution

(a) During ground hold, the temperature differential across the insulation $\Delta T = 70 - (-360) = 430^\circ \text{ F}$. The overall thickness of the insulation $t = 2 \times 0.03 + 0.75 = 0.81 \text{ in}$. From equation (4-19), the heat transfer rate

$$q = \left(\frac{k}{t}\right)\Delta T = \left(\frac{3.8 \times 10^{-7}}{0.81}\right) \times 430 = 2.02 \times 10^{-4} \text{ Btu/in}^2\text{-sec}$$

(b) During the boost phase, $\Delta T = 800 - (-210) = 1010^\circ \text{ F}$. The heat-transfer rate

$$q = \left(\frac{k}{t}\right)\Delta T = \left(\frac{3.8 \times 10^{-7}}{0.81}\right) \times 1010 = 4.74 \times 10^{-4} \text{ Btu/in}^2\text{-sec}$$

Selection of Tank Insulation Designs

Many factors will influence the selection of a tank insulation design. The insulation may be located internal or external to the tank wall; it can be integral, or disposable during boost; i.e., it can be bonded in place or mechanically retained. Basically, any insulation applied to a tank must be justified with respect to advantages of performance and/or economy.

Locating the insulation inside of the propellant tank has the obvious advantage of protecting the insulation from handling damage. The tank structure is isolated from the severest low-temperature effects of the propellant and is thus subjected to only moderate thermal cycling from its source. Internal insulation also minimizes propellant loss when chilling the tank during filling. However, if a crack or leak should occur in internal insulation of a hydrogen tank, gaseous hydrogen would enter the crack and gradually increase the heat transfer. Other undesirable features of internal insulation are apparent, such as: difficulties in installation; in locating and repairing of leaks; and in cleaning the tank. Internal insulation is also subject to higher pressures and more severe temperature effects which tend to impair the insulation sealing.

External insulation has the advantage of isolating the tank structure from the extreme temperature of aerodynamic heating during boost. Installation, repair, and sealing of the external

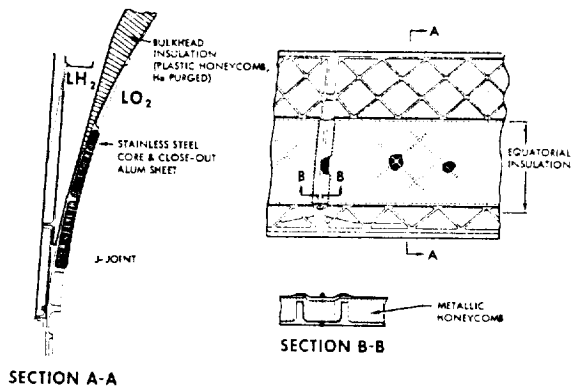


Figure 8-14.—Design of a typical insulated common bulkhead separating LH_2 and LO_2 tanks.

insulation can all be done without special consideration of access, ventilation, and curing techniques in closed areas. However, special consideration will be required for tank leak detection, especially with integrally insulated areas. If a crack does occur in the external insulation, liquefaction of air and cryopumping will occur resulting in a significant rise in heat transfer.

Insulation for Common Bulkheads

When a common bulkhead is used between propellant tanks and cryogenics are involved, insulation is required to prevent freezing of the propellant with the higher boiling point. Figure 8-14 shows the equatorial area of a typical insulated common bulkhead. A fiber-glass honeycomb is located between a forward and an aft facing sheet. In the equatorial area, where the facing sheets have to be faired into the cylindrical tank portion, they are reinforced by waffle grid ribs. This design also requires special insulation on the inside of the LOX tank in the equatorial region. No foam filler was used in this particular example.

8.6 DESIGN OF FIBER-GLASS FILAMENT-WOUND LIQUID PROPELLANT TANKS

Most of the pressure vessels which possess surfaces of revolution can be fabricated conveniently by the technique of filament winding. By this method a lightweight structural member can

be produced with mechanical precision and versatility of construction and materials. A strength-to-density ratio, F_u/ρ , can be obtained by filament winding and impregnating the fiber-glass roving with a suitable resin, which is higher than can be achieved by any other method or material. For instance, the strength-to-density ratio of a fiber-glass filament-wound resin-bonded structure (average $\rho = 0.08 \text{ lb/in}^3$, $F_u = 120\,000$, $F_u/\rho = 150 \times 10^4$) is about twice that of high-strength alloys.

Good reliability and close dimensional control of filament-wound pressure vessels is assured through the use of calibrated winding machines which orient the reinforcing fibers precisely. However, most of the liquid propellants are not compatible with resin-impregnated, fiber-glass structures. Therefore, an aluminum tank liner which is compatible with both propellants, must be used to separate the fiber glass from the liquid. It also provides a positive sealing barrier, since the resin-bonded fiber-glass material is pervious to both liquid and vapor over extended periods. Figure 8-15 presents a typical aluminum-lined, fiber-glass filament-wound liquid propellant tank.

Design and fabrication of fiber-glass filament-wound tanks with a thin aluminum liner is basically simple. However, a key problem arises from the fact that the modulus of elasticity of fiber-glass resin-bonded materials is about 5×10^6 psi, while that of aluminum is about 10×10^6 psi, and that the strength of the aluminum is usually no more than a third of that of the fiber glass. Since the geometry of the tanks usually imposes equal strain on aluminum liner and fiber glass as the tank is pressurized, the aluminum becomes loaded to its elastic limit long before the fiber glass reaches the level of its high-strength capability. Consequently, with a plain liner configuration, the aluminum is stretched far beyond its elastic limit and forced back to its original shape each time the tank is pressure cycled. Thus, the liner may experience fatigue failure after a small number of pressure cycles. The pressure-cycle life of a plain liner depends on amount of stretch beyond the elastic limit, type of aluminum, bonding between lines and fiber glass, weld joints, variation in thickness and contours, etc. A well-designed, plain-type tank liner should have a life of about 10 to 20 pressure cycles.

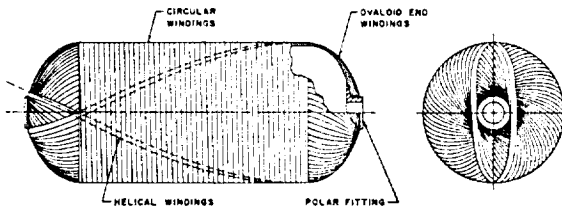


Figure 8-15.—A typical aluminum-lined, fiber-glass, filament-wound liquid propellant tank.

One design approach to extend cycle life is to use a corrugated liner. The corrugations have an effect equivalent to reducing the modulus of elasticity of the aluminum liner to a value less than that of the fiber glass. For instance, if the fiber glass is stressed to 100 000 psi and has a modulus of elasticity of 5×10^6 , its extension will be 2 percent. The corrugations of the liner then should be designed to permit the 2-percent extension so that the aluminum will not be stressed beyond its elastic limit.

8.7 DESIGN OF PROPELLANT TANK PRESSURANT DIFFUSERS

The main function of a pressurant diffuser is to introduce the pressurant gases evenly into the propellant tank at a desired direction and velocity. The gases are usually injected in a plane near the tank forward end, at a right angle to the tank and vehicle axes. This will minimize disturbances at the pressurant-propellant interface. Figure 8-16 presents some typical propellant tank pressurant diffuser designs. A radial-type diffuser, located at the tank axis, is used for the fuel tank. This arrangement permits a simple, lightweight diffuser design. However, the reversed ellipsoidal common bulkhead at the forward end of the oxidizer tank requires a ring-type diffuser, consisting of many individual diffusing nozzles located at the circumference of the tank.

The pressurant enters the tank at a temperature level depending on the source, such as a LOX heat exchanger. In some cases, this may not be the optimum temperature for critical struc-

tural members. In these cases, a separation tube (Hilsch tube) may be combined with the diffuser. Without moving parts, it operates on the principle of separating the higher energy molecules from those with lower energy. Temperature spreads of 100° F or more can be obtained, depending on construction and available pressure drop. Advanced configurations have been developed by the AiResearch Manufacturing Co. In a LOX/hydrogen system with common bulkhead, the device may be used to direct the cold stream toward the bulkhead, thus lowering the temperature differential and resultant heat transfer across it.

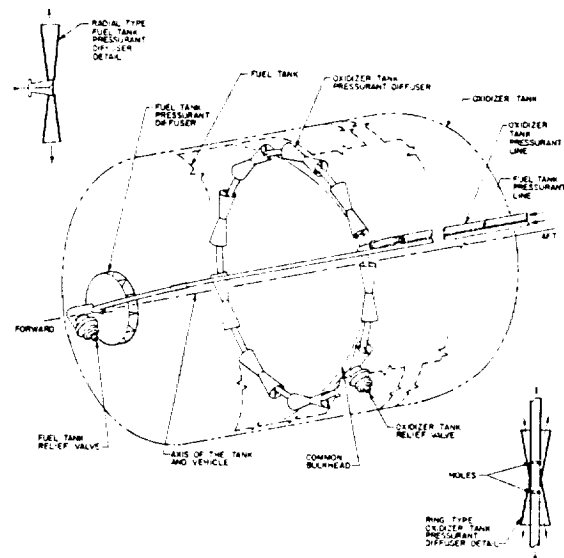


Figure 8-16.—Typical designs of propellant tank pressurant diffusers.

8.8 PROPELLANT EXPULSION UNDER ZERO GRAVITY OR OSCILLATORY G-LOADING CONDITIONS

Under zero or oscillatory g-loading conditions typical for many vehicle trajectories, fluid location in a propellant tank becomes uncertain and requires means to prevent gas pockets from interfering with propellant expulsion. The propellants must be either subjected to an acceleration force for settling immediately prior to usage, or they must be continuously confined in the tank. The two approaches can be defined as impulse settling and positive expulsion.

Impulse Settling

This method employs a small propulsive force directed axially, parallel to the vehicle center-line of thrust. This acceleration forces the propellant to cover the tank outlet prior to initiation of main engine operation. This approach is especially suitable for most space vehicles, because their low-thrust reaction control units can be used to perform the auxiliary function of providing the thrust required for propellant settling.

Although this method would eliminate the need for positive expulsion devices for the main propellant tanks, it would necessitate separate positive-expulsion propellant tank or tanks for the sole use of the reaction control system. The possible disadvantages of this impulse-settling method are (1) no control of vehicle center-of-gravity shifts, and (2) low thrust-to-weight ratio under these conditions, which may increase response times beyond tolerable limits.

For single-start upper stages, jettisonable short-duration solid settling rockets may also be applied to advantage.

Positive Expulsion

The other method of achieving proper fluid orientation within the propellant tanks is by continuously confining the propellant to the vicinity of the tank outlet. A positive expulsion propellant tank assembly usually consists of an outer tank shell and an inner movable expulsion device. Frequently used positive expulsion devices are: (1) metallic diaphragms, (2) elastomer diaphragms, and (3) moveable pistons. The design of the expulsion devices depends upon a number of considerations. Primary among these is the design configuration of the propellant tank. Another is the allowable shift of vehicle center of gravity during expulsion, which in many vehicle applications must be minimized to avoid instabilities induced by a pitch or yaw maneuver. A choice of construction materials capable of sustained contact with the pressurants and propellants must also be made.

Metal Expulsion Diaphragms

Metal expulsion diaphragms made of 1100-0 aluminum (0.010 to 0.020 inch thick) are desirable for long-term storage contact with storable

propellants and higher temperature pressurant gases. Figure 8-17 presents a concentric-circular, convoluted metal positive expulsion diaphragm used in a spherical tank. This system is unique for bipropellant systems because it allows both propellants to be stored in the same tank, as long as the volumetric mixture ratio does not deviate appreciably from unity. An expulsion efficiency above 97 percent (i.e., the percentage of the propellant which can be expelled from the tank) may be expected. This design also minimizes shift of center of gravity during the entire process of expulsion.

Figure 8-18 presents the corrugated metal positive expulsion diaphragm applied to a cylindrical tank. A center post is provided to support the diaphragm. The diaphragm is formed into a lobed corrugation capable of performing the required mechanical expansion. Transition sections are provided at both ends of the diaphragm for attachment to the tank ends. An expulsion efficiency of 97 to 98 percent may be achieved with this design. However, the utilization of

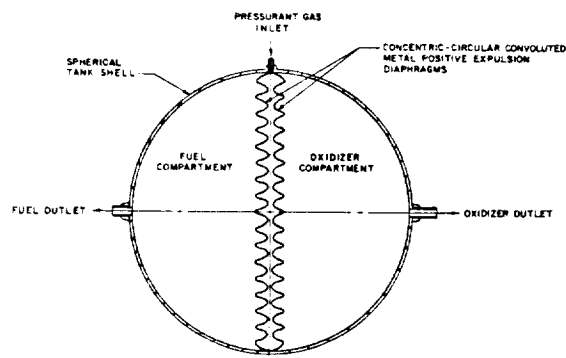


Figure 8-17.—Concentric-circular convoluted metal positive expulsion diaphragms used in a spherical-shape propellant tank.

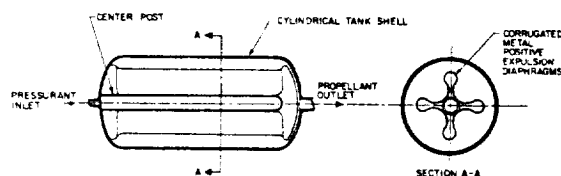


Figure 8-18.—Corrugated metal positive expulsion diaphragm used in a cylindrically shaped propellant tank.

tank volume is less efficient due to dimensional limitations (i.e., size of the center post compared to tank diameter). This design, too, minimizes shift of center of gravity.

One disadvantage of the metal diaphragms is that only one complete expulsion cycle is possible, because the metal probably will be cold worked. The cold working not only changes metal elastic properties and the Δp required for expulsion, but may cause fatigue failure.

Elastomer Expulsion Diaphragms

Elastomer-type diaphragms are applicable to most tank configurations and often offer a more efficient utilization of tank volume. One design approach takes advantage of the stretching properties of pure elastomer and uses the diaphragm as a bladder. Figure 8-19 presents the bladder-type elastomer positive expulsion diaphragm used in a spherical tank. As the bladder is pressurized and inflates, the propellant is displaced and positively expelled and uniformly confined during all phases of expulsion. By positioning the bladder in the geometric center of the tank, center-of-gravity shift during expulsion is virtually eliminated.

The initial unpressurized volume within the bladder can be utilized as the ullage volume. The elastomer diaphragm will produce an expulsion efficiency of up to 99 percent in many tank configurations. In addition, it is capable of many expulsion and refill cycles. An inherent

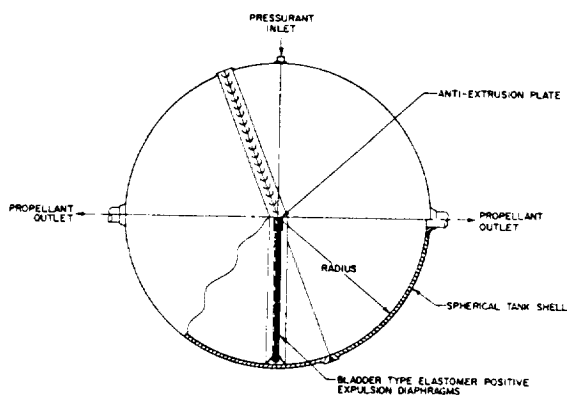


Figure 8-19.—Bladder-type elastomer positive expulsion diaphragms used in a spherically shaped propellant tank.

disadvantage of pure elastomers in storage contact with many storable propellants is tensile-strength degradation as a function of time. They are also incompatible with hot pressurant gases produced by gas generators.

Positive Expulsion By Movable Pistons

An alternate method of obtaining positive expulsion in cylindrical tanks is a movable piston actuated by pressurant gas. Positive attachment is required during storage to keep the piston in the proper position. To prevent leakage during operation, seals will be required. The seals may be piston-type rings or some type of metallic wiper seal. In either case, the dimension and surface finish of the tank inside diameter should be maintained relatively accurate and smooth. In some designs a concentric center post is utilized to guide the piston, requiring an additional seal. Figure 8-20 presents the design of a movable piston guided by a center post.

The pressure differential across the movable piston required to overcome friction during operation increases the required pressurant pressure and the tank structural pressure loads for a given propellant pressure at the tank outlet. It may be estimated by

$$\Delta p A_p = f_s F_n L_s \quad (8-39)$$

where

Δp = pressure differential across the piston, psi

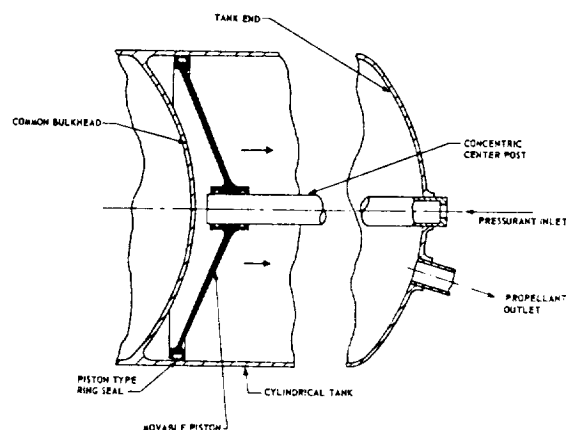


Figure 8-20.—Movable piston used in a cylindrical propellant tank for positive expulsion.

A_p = cross-sectional area of the piston, in²

f_s = coefficient of friction of the piston seals

F_n = unit normal force reacted by the piston seals on tank wall and guide post, lb/in of seal

L_s = total length of all piston seals, in

Estimate the pressure differential across the movable piston.

Solution

The cross-sectional area of the piston

$$A_p = \frac{\pi \times (20)^2}{4} - \frac{\pi \times (1.5)^2}{4} = 314.16 - 1.76 = 312.4 \text{ in}^2$$

The total length of piston seals:

$$L_s = \pi \times (20 + 1.5) = 67.54 \text{ in}$$

Substitute this into equation (8-39); the pressure differential across the piston

$$\Delta p = \frac{f_s F_n L_s}{A_p} = \frac{0.1 \times 500 \times 67.54}{312.4} = 10.8 \text{ psi}$$

Sample Calculation (8-7)

The following data are given for a cylindrical positive expulsion tank with a movable piston as shown in figure 8-20:

Inside diameter of the tank, 20 in

Diameter of the guide post, 1.5 in

Coefficient of friction of the piston seals,

$$f_s = 0.1$$

Unit normal force reacted by the seals, F_n
= 500 lb/in

Chapter IX

Design of Interconnecting Components and Mounts

9.1 THE PRINCIPAL INTERCONNECTING COMPONENTS AND MOUNTS

In section 1.4, we briefly introduced the principal interconnecting components and structures. Figure 9-1 shows these for a typical LH_2/LO_2 turbopump-fed engine system. A discussion of the most frequently used components follows. Design detail is presented in subsequent subchapters.

Propellant Supply Ducts

Among the principal interconnections between engine and vehicle are the propellant supply ducts. Since every psi of propellant tank pressure above the minimum required for proper engine performance results in additional weight of the tank walls and of the gas pressurants, it is desirable to keep the pressure losses between tank outlets and engine inlets to an absolute minimum.

The task of designing these ducts, or at least the flexible portion thereof immediately upstream of the engine, frequently falls to the engine designer. The designer must find an optimum balance between low pressure drop, by making the duct diameter as large as possible, and flexibility and structural integrity, which in general becomes more difficult with increasing diameters. The designer must further consider the fact that the ducts, because of their location off the engine gimbal center, are subjected to torsional loads, in addition to bending. Furthermore, the ducts are subjected to internal pressure, frequently in a stringent cryogenic and vibration environment. Because of the many forces acting upon the ducts, restrainers against buckling are frequently required. These may be located inside the ducts, thus adding to undesired pressure drop; or they may be applied externally, which

increases the duct envelope and may cause interference with other vehicle systems. Figure 9-2 shows a typical flexible propellant supply duct which has restraining linkages for stabilizing the bellows. At the vehicle end, these ducts will connect to longer or shorter vehicle ducts, the length of which depends on whether the forward or the rear tank is being connected. It is important that the engine designer not only inform the vehicle builder of connecting flange dimensions and types of gasket being used but also of the forces transmitted by the engine duct to the vehicle during gimbaling as well. In most pump-feed systems, the working pressure of propellant supply ducts usually does not exceed 50 psig. In upper stages, during lower stage boost, however, pressures may temporarily be substantially higher as a result of a combination of high accelerations and full tanks (100 psig and over).

Figure 9-3 shows the propellant ducting and mounting for a cluster of four storable propellant pressure-feed engines. The thrust mounts are of a box-type, beam construction. The propellant ducts, which consist of restrained bellows and rigid sections including flowmeters, connect the thrust chambers to the main propellant valves. The main valves, in turn, connect directly to the propellant tank ducts. Care has been taken in the design to keep the flow path and ducting volume constant between main valves and individual chambers. This arrangement also assures uniform pressure drops to all thrust chambers. Furthermore, all interconnecting components on the fuel side as well as on the oxidizer side are designed to be interchangeable. The valves used in this design include burst diaphragms. Thus, exposure to the propellants of all ducting downstream of the valves will occur only during engine firing. In most pressure-feed systems, the working pressure of the propellant ducts is less than 500 psia.

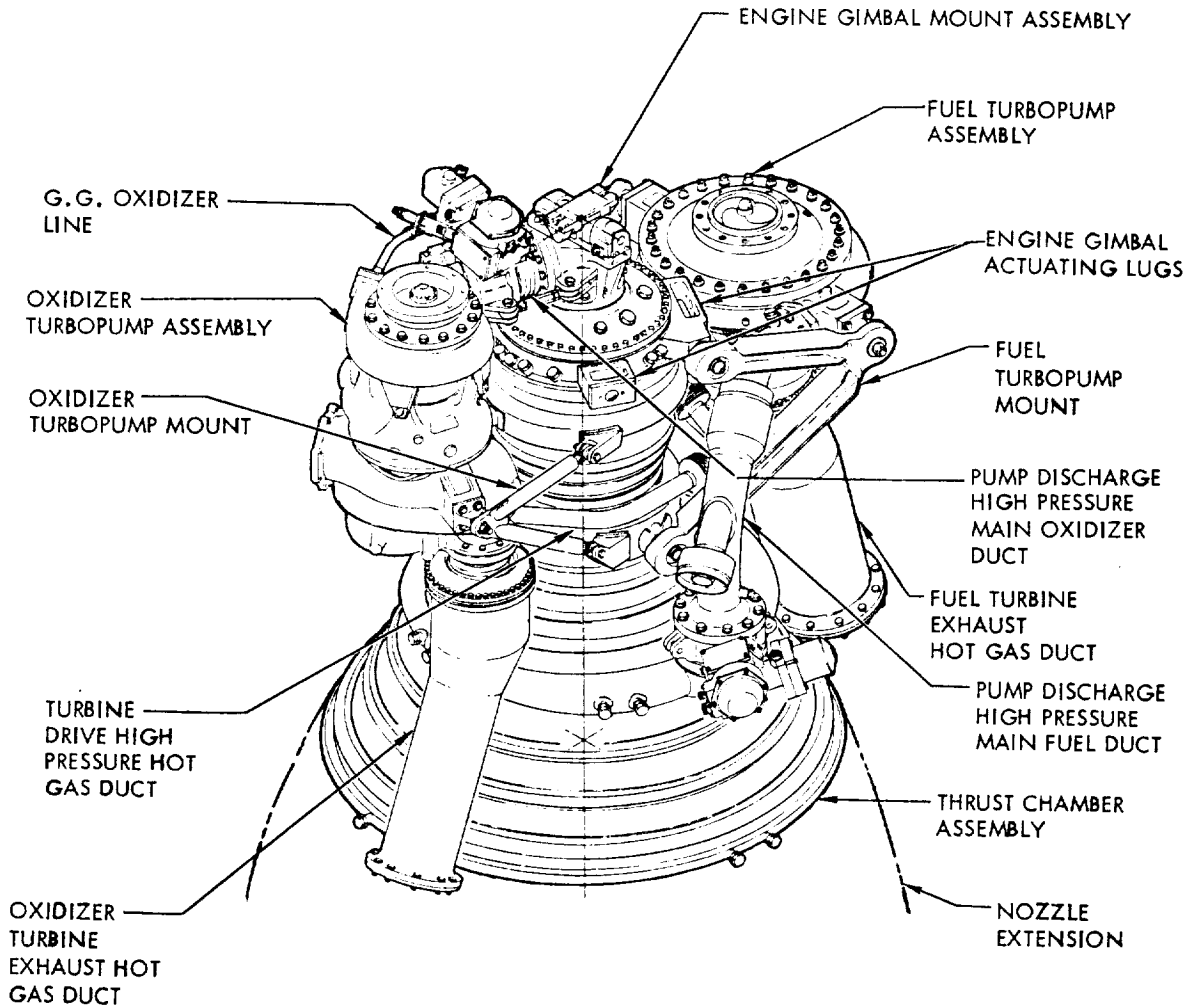


Figure 9-1.—Various interconnecting components and mounts in a typical LH_2/LO_2 pump feed engine system.

Pump-Discharge, High-Pressure Propellant Ducts

In turbopump-fed engines the pump-discharge high-pressure propellant ducts are designed to connect the oxidizer and fuel pump discharges to the main oxidizer and main fuel valves attached to the thrust chamber. The ducts contain bellows sections which permit the degree of movement required between thrust chamber and turbopump to accommodate tolerance buildups, misalignments, and motion due to temperature change and acceleration loads. However, in some engine designs rigid, in place welded ducts have been successfully applied. The working levels have been proposed. Therefore, the sepa-

rating pressure loads acting on the two components connected by a flexible member must be absorbed by restraining links attached to the bellows, or by other compensating means.

Figure 9-4 presents a typical pump-discharge, high-pressure propellant duct with external restraining links. It is used for the main oxidizer (LO_2) duct of the engine system shown in figure 9-1. Another typical pump-discharge, high-pressure propellant duct, used as the main fuel (LH_2) duct for the same engine system, is shown in figure 9-5. This duct has a unique end-load compensator which incorporates two bellows tied together by a restraining rod to limit bellows movements. One bellows opposes the other in

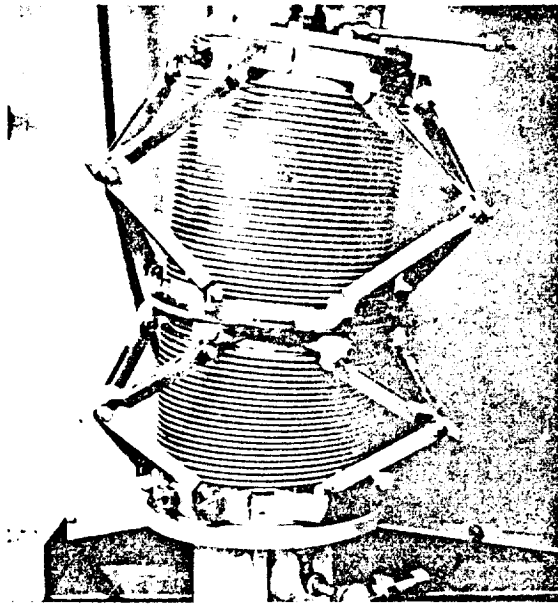


Figure 9-2.—Typical flexible propellant supply duct for a large turbopump-feed engine system. (Note: Duct is mounted in test fixture with fluid pressure connections.)

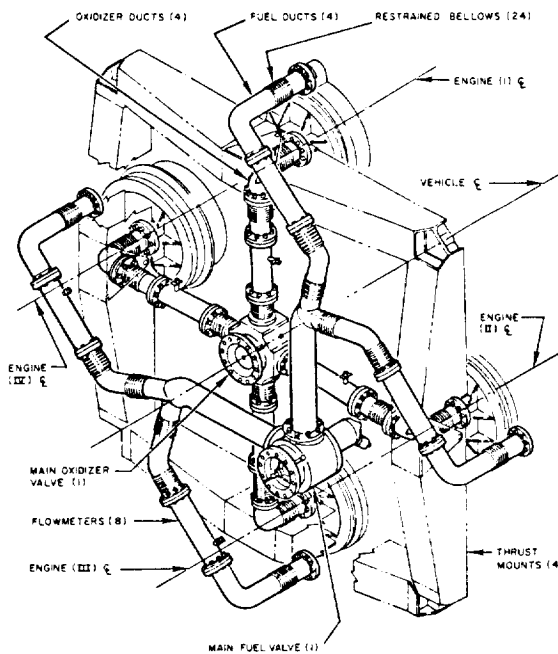


Figure 9-3.—Propellant ducting and mounting arrangements for a cluster of four storable-propellant pressure-feed engines.

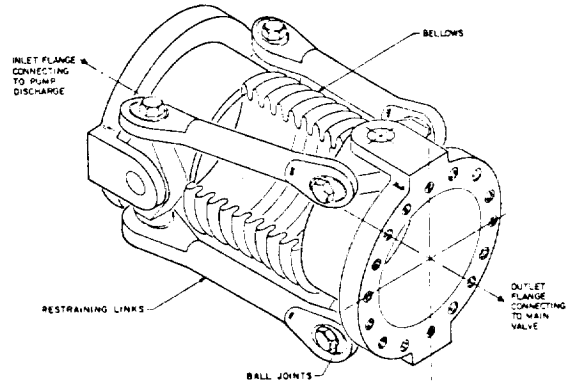


Figure 9-4.—Typical pump-discharge, high-pressure propellant duct with restraining links.

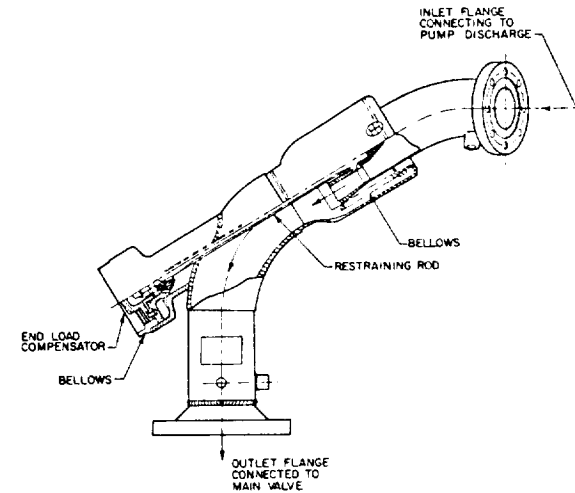


Figure 9-5.—Typical pump-discharge, high-pressure propellant duct with end-load compensator.

balancing the duct, thus reducing duct-separating loads by 90 percent.

The high-pressure propellant lines between pump discharge and gas generator usually can be made of wire-braided-type flexible hoses or tubing, because of their relatively small size (often less than 1 inch).

Propellant-Tank-Pressurization Lines

These lines are employed to connect the main propellant tanks to the pressurant sources such as stored pressurant gas systems (including

storage bottles, heat exchangers, pressure regulators), gas generators, cryogenic propellant heat exchangers, etc. High-pressure hoses and tubings are used.

Seal Drain Lines

It is difficult to achieve perfect dynamic sealing at the shafts or rods of turbopumps and other components. Therefore, seal drains are often provided between two dynamic seals placed in series. The required seal drain lines including flexible hoses and tubings are routed away and overboard. For LO₂/RP-1 systems, this can be done by routing the drain lines along the thrust chamber wall to the chamber exit. For propellant combinations which can form highly explosive mixtures, routing to sufficiently spaced vent ports at the vehicle periphery is required. Figure 9-6 presents a typical pump seal drain line schematic of an upper stage system. The seal drain lines are routed to the vehicle periphery during boost flight and to chamber exits during stage operation.

Pneumatic Supply Lines

Liquid rocket engines usually are equipped with one or more pressure vessels to supply pneumatic pressure for valve actuation, for turbine start, for sequenced purges, and possibly for other purposes. The vessels must be charged prior to test run or flight, requiring high-pressure flexible line connections to the vehicle, and disconnects at the vehicle periphery. Their design not only must consider the mating counterpart on the vehicle side but also the type of fluid and its temperature and pressure.

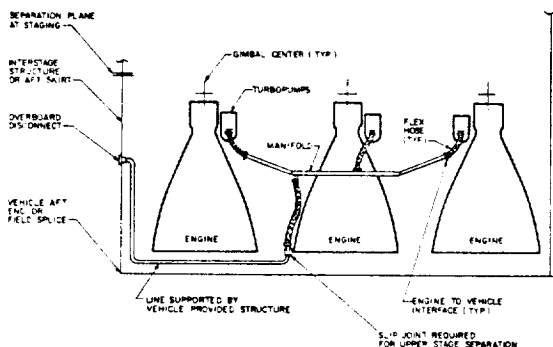


Figure 9-6.—Typical pump seal drain schematic.

Cryogenic Propellant Bleed Lines

Cryogenic propellant engine systems with turbopump feed may experience difficulties during start if the metal parts containing cryogenic fluid are at ambient or insufficiently low temperatures, and if the fluids in the volumes below the tank outlet are superheated and form gas pockets. Since the pressure upon opening of the main valves and start of the turbopumps will further reduce the static pressure at the pump inlet, accelerated gas production will result. This, in turn, may lead to pump cavitation and starving of the gas generator. To prevent this, a continuous bleed from a point farthest downstream from the pump inlet is applied until shortly before engine start. In this manner, fresh liquid at tank bulk temperature will continuously replace the warming fluid, and cool the containing metal parts. To avoid hazardous conditions at the launch site, the bleeds, particularly if they can form combustible or explosive mixtures, are ducted away. To make this possible, a line connection from the engine to the vehicle and beyond is required. The lines are generally made of wire-braided flexible hoses and tubings.

A special case is presented by cryogenic engines in upper stages which will not start until some time after the bleeds have been closed at liftoff, or which have to start after prolonged cruising periods. Here, a recirculation system which returns the fluids to the tanks rather than dumping them overboard is preferred. Lines across the interface between engine and vehicle are required. Bleed and recirculation flows can be minimized if the vehicle builder provides means, such as subcooling, insulation, avoidance of temperature stratification, maximum economic tank pressure to keep the temperature of the bulk sufficiently below the boiling temperature at operating tank pressures. In some cases, prechilling of metal parts exposed to cryogenic fluids may be advantageously accomplished by cooling media supplied from ground through a vehicle disconnect to the engine. Routing of all lines mentioned will be similar to drain lines (fig. 9-6).

Purge Lines

During the start and shutdown sequences, and for prerun and postrun servicing, inert gas purges

are frequently required to keep a system dry, to prevent combustible mixtures from forming, or to expel residual propellants. If they are continuous during ground hold, it is advantageous to feed them from ground to avoid increased flight weight. This requires connecting lines from the engine to the vehicle. It is strongly recommended that entirely separate purge systems for each propellant be employed to avoid backup of one fluid into the system of the other. Check valves are not considered as reliable as strict separation. For engine design we are concerned here only with those purges which connect directly to an inlet port of an engine part, such as the thrust chamber cooling jacket or injector manifold. From the viewpoint of the environment in which the engine must operate, the engine designer should additionally specify the purges to be provided by the vehicle builder to condition the engine compartment as needed. All purge lines can be made of wire-braided flexible hoses and tubings and may be routed as are the drain lines.

Hydraulic Lines

Various high-pressure hydraulic lines are used in a liquid rocket engine for hydraulic actuating, lubrication, etc. All lines must permit flexure and must be of the proper size and pressure rating. Most of the hydraulic lines are made of wire-braided flexible hoses and tubings.

Turbine-Drive, High-Pressure, Hot-Gas Ducts

In most turbopump-feed engines, the gas generator is connected directly to the turbine inlet; thus, there is no need for ducting. In some designs, however, high-pressure hot-gas ducts are required to connect between gas generator and turbines (in systems with two individual turbopumps), or between main thrust chamber bleedoff ports and turbines (tapoff gas-turbine-drive systems). These ducts usually consist of rigid and flexible sections made of stainless steels and nickel-based alloys, for service temperatures up to approximately 1700° F. The ducts must be capable of absorbing considerable deflections from thermal expansion, in addition to deflections due to misalignments and dynamic loads.

Turbine-Exhaust, Hot-Gas Ducts

The hot gases from the turbine exhaust may be ducted to near the main chamber nozzle exit or into a thrust chamber exhaust manifold. Most turbine-exhaust ducts are of welded stainless steel or nickel-alloy, sheet-metal construction. Bellows sections permit the degree of movement required by the system for thermal expansion, misalignments, and tolerances. In most cryogenic propellant systems, a heat exchanger is incorporated in the exhaust duct assembly to vaporize one of the propellants, usually LOX, for tank pressurization (fig. 5-7).

Thrust Mounts

The thrust mount transmits the thrust loads between engine and vehicle thrust frame. In some designs (fig. 2-4), the thrust mount also serves as the structural mount for many other major components of the engine system. Thrust mounts usually consist of truss members of tubular and box shape, made of aluminum alloy or alloy steels. In engine systems using fixed thrust mounts, thrust vector control is accomplished by swiveling the thrust chamber, or by other means such as jet vanes, secondary injection, or jetavators.

Gimbal Mount Assemblies

In most large turbopump-fed engine systems (figs. 3-2, 3-4, and 9-1), the complete engine assembly is gimbaled at a universal-joint-type gimbal mount assembly which connects the thrust chamber to the vehicle thrust structure.

Turbopump and Other Component Mounts

Turbopump mounts (fig. 9-1) are used to secure turbopumps to thrust chamber or other structural members, such as the thrust mount. They often consist of welded tubular trusses, forged structural members, and flexible end joints. In some designs, rigid-type, pump-discharge propellant ducts are used as members of the turbopump mounts. Most propellant valves are fastened directly to the thrust chamber or gas generator. Other control components and small storage vessels may be secured by aluminum-alloy sheet-metal brackets.

9.2 DESIGN OF TUBINGS AND TUBE FITTINGS

To interconnect fluid lines in rocket engines, high-quality, cold-finished seamless tubing of either aluminum alloys or austenitic stainless steels are frequently used. In rocket engine design practice, the term "tube" refers to lines up to 2 inches. Stated nominal tubing sizes refer to their outside diameters. For sizes of more than 3/4 inch, flanged joints should be used.

Two principal classes of tubing are distinguished: common pressure tubing and mechanical tubing. The latter is designed and manufactured with closer tolerances than the common tubing. It is more expensive, but may save much time when machining and chucking in automatic production machines is involved. Unless specified otherwise, pressure tubing is used in rocket engines for all purposes.

Tubing Design Working Pressures

Pressure tubes are supplied fully annealed and pressure tested. They fall into two major classifications: average wall and minimum wall. Average-wall pressure tubes are made with a wall thickness which may vary from the nominal size by plus or minus 10 percent. Minimum-wall tubes are made with a wall thickness that may not be less than that specified, but may be heavier by 20 to 40 percent, depending on the type of tubing. For lines carrying pressurized fluids, minimum-wall tubes should be used.

A factor of safety (i.e., the ratio of the ultimate strength of the tubing material to the maximum allowable working stress) of 4 may be used for general rocket engine applications. Higher values (6 to 8) should be used in applications involving hazard and excessive vibration. For high-pressure application, aluminum tubing should be avoided where possible. Allowable working pressures for a factor of safety of 4, for various stainless-steel and aluminum tubings, are presented in tables 9-1 and 9-2.

Tubing Installations in Engine Systems

Installations requiring bends must be accomplished with minimum distortion and constriction of the tubing. A satisfactory bend is one which

decreases tubing outside diameter less than 6 percent. Recommended minimum bend radii for stainless-steel and aluminum-alloy tubing are presented in table 9-3.

Tubing assemblies must be properly supported to prevent stresses and consequent weakening of the system under vibrating conditions. In addition, proper support minimizes the danger of recoil and live whip in the event of tube failure. Where tube fittings are employed, support spacing should be reduced by 20 percent to account for the added weight. Supports should be placed as close to each side of fittings, valves, and other components as practical. Overhang should be minimized by placing supports as close to bends as conditions allow. Table 9-4 presents the recommended maximum bracket spacing for common-size tubing assemblies in engine systems. Where tubes of different diameters are connected, average spacing may be used.

General design practice requires no detail drawings for tubing assemblies less than 3/8-inch size. They are to be shop fitted according to an engine mockup during the assembly of the engine system.

Tube-Fitting Designs

The three-piece AN flared tube fitting per AND10056 or MS33656 (fig. 9-7) is widely used as a standard in rocket engine designs.

The angle of flare of the fitting was established at 37° to give maximum flare contact and provide a nose sufficiently strong to resist crushing. The AN three-piece fitting consists of a coupling nut (AN818), a sleeve (AN819), and a connector. The sealing occurs between the nose of the fitting connector and the inside of the tube flare. The AN819 sleeve has an external shoulder against which the AN818 nut acts. This produces a locking effect on the nut, as the sleeve is slightly sprung upon proper torque. The sleeve is free to turn during initial assembly to allow for slight eccentricity of the tubing or the nose of the fitting connector.

Figure 9-8 illustrates a typical flareless tube fitting per MS33514, the Ermeto, manufactured by the Weatherhead Co. It is designed for use with flareless, heavy-walled tubing in high-pressure applications. The assembly of this fitting involves a preassembly to check for contact of the

TABLE 9-1.—Corrosion-Resistant Steel (18-8) Annealed (MIL-T-8504 ASG) Tubing
 [Allowable working pressures in psi at 100° F; safety factor of 4]

Maximum working pressure, 3000 psi									
Tube OD, in	1/4	3/8	1/2	5/8	3/4	1	1-1/4		
Wall thickness, in	0.022	0.035	0.042	0.058	0.065	0.083	0.109		
Maximum working pressure, 2400 psi									
Tube OD, in	1/4	3/8	1/2	5/8	3/4	1	1-1/4	1-1/2	
Wall thickness, in	0.020	0.028	0.035	0.049	0.058	0.072	0.095	0.109	
Maximum working pressure, 1500 psi									
Tube OD, in	1/4	3/8	1/2	5/8	3/4	1	1-1/4	1-1/2	2
Wall thickness, in	0.020	0.028	0.032	0.035	0.042	0.049	0.058	0.065	0.095

TABLE 9-2.—Aluminum Alloy, 5052 Round Seamless Drawn WW-T-78a Temper H34
 [Allowable working pressures in psi at 100° F; safety factor of 4]

Maximum working pressure, 1500 psi									
Tube OD, in	1/4	3/8	1/2	5/8	3/4	1	1-1/4		
Wall thickness, in	0.025	0.042	0.049	0.058	0.072	0.095	0.120		
Maximum working pressure, 750 psi									
Tube OD, in	1/4	3/8	1/2	5/8	3/4	1	1-1/4	1-1/2	2
Wall thickness, in	0.020	0.028	0.032	0.035	0.042	0.049	0.065	0.072	0.095

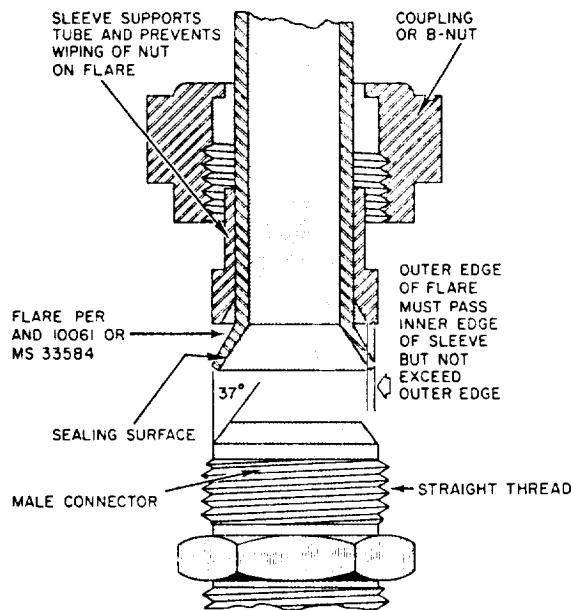


Figure 9-7.—3-piece AN flared-tube fitting per AND 10056 or MS33656.

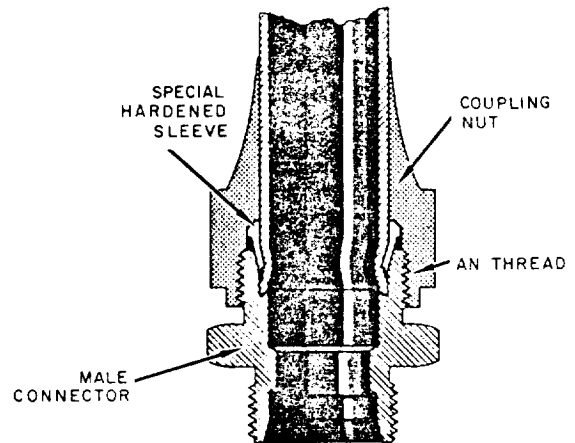


Figure 9-8.—Flareless tube fitting (Ermeto) per MS33514.

TABLE 9-3.—Minimum Bend Radii for Stainless-Steel and Aluminum-Alloy Tubing
[All measurements in inches]

Tube OD	Wall thickness	Inside bend radii	Radii to center of tube
3/16	Any	5/8	23/32
1/4	Any	3/4	7/8
5/16	Any	3/4	29/32
3/8	Through 0.022	1-1/2	1-11/16
	Over 0.022	1	1-3/16
1/2	Through 0.028	1-3/4	2
	Over 0.028	1-1/2	1-3/4
5/8	Through 0.028	2-1/2	2-13/16
	Over 0.028	1-3/4	2-1/16
3/4	Through 0.028	3	3-3/8
	Over 0.028	2-1/2	2-7/8
7/8	Through 0.035	3-1/4	3-11/16
	Over 0.035	2-3/4	3-3/16
1	Through 0.035	3-1/2	4
	Over 0.035	3	3-1/2
1-1/8	Through 0.035	4	4-9/16
	Over 0.035	3-1/4	3-13/16
1-1/4	Through 0.035	4-1/2	5-1/8
	Over 0.035	3-1/2	4-1/8
1-1/2	Through 0.035	6	6-3/4
	Over 0.035	4	4-3/4
1-3/4	Through 0.035	7	7-7/8
	Over 0.035	5	5-7/8
2	Through 0.035	7	8
	Over 0.035	6	7
2-1/2	Through 0.049	9	10-1/4
	Over 0.049	7	8-1/4
3	Through 0.049	11	12-1/2
	Over 0.049	9	10-1/2
4	Through 0.065	12	14
	Over 0.065	10	12

TABLE 9-4.—Recommended Support Bracket Spacing for Tubing Assemblies in Engine Systems

Tube size (OD), in	Maximum support spacing in inches	
	Aluminum alloy	Stainless steel
1/4 through 1/2	12	14
5/8 through 3/4	17	20
1 and over	21	24

special hardened sleeve, which cuts into the tube wall. Flareless tube fittings may be used optionally in engine designs.

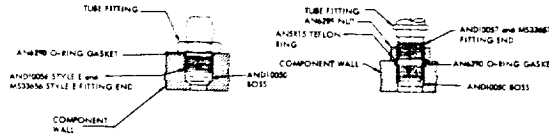


Figure 9-9.—Typical installations of tube fitting ends into AND10050 boss.

The tube fittings should be of the same material as the tubing. Fittings are designed to be as strong as the strongest tubing of like material used with the fitting. Design details and dimensions of tube fittings can be found from AND and MS specifications. In some cases, AN and MS parts are interchangeable.

The boss design for engine components, to connect AN tube fittings, is specified by AND10050. Figure 9-9 illustrates typical installation of tube fitting ends into the AND10050 boss.

9.3 DESIGN OF FLANGE JOINTS

The interconnecting lines of a rocket engine system must retain fluids at various pressures and temperatures. Each of these lines may have one or more mechanical joints requiring static seals to prevent leakage. The joint as an assembly must be capable of maintaining intimate conformance of seal and sealing surfaces throughout its operating life, regardless of all strains, loads, and thermal gradients. For line sizes of 3/4 inch or larger, bolted flange joints are generally used in rocket engine design. The design of these flange joints is also applicable to other components, such as thrust chamber injector dome flanges and turbopump and valve housing flanges.

Flange Joint Design Considerations

Figure 9-10 illustrates typical flange joints used in a propellant duct assembly. Most flange joints consist of three elements: the flanges, the fasteners (bolts and nuts), and the gasket. In addition to an effective gasket, a leaktight flange joint must have proper flanges and bolting. In flange joint structural design, the goal of optimum weight within safe stresses must consider the elastic behavior of the part.

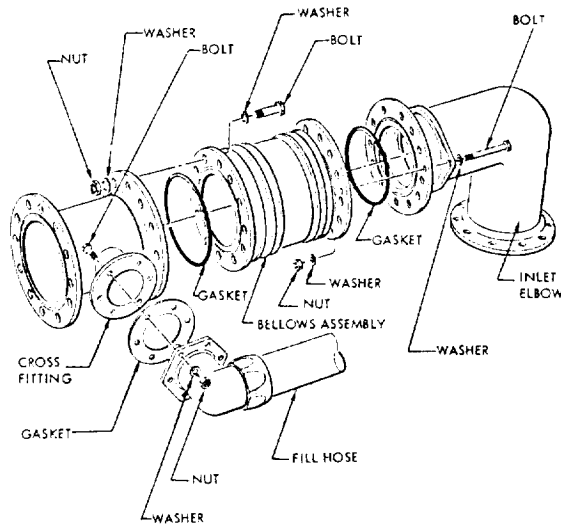


Figure 9-10.—Typical flange joints of a propellant duct assembly.

In addition to structural needs, other design considerations for flange joints are:

1. *Working temperature and pressure of the fluid.*—These greatly affect the type of seal design and material. The problems of maintaining a leaktight flange joint are greatly compounded by temperature effects. Temperature differentials at the flange joints of rocket engines are apt to be large, because of steep heating and flow transients. They introduce thermal stresses and strains which may disturb the sealing. When designing an elevated temperature (or subzero) flange joint, the temperatures of the various parts should be analyzed to assess their effect on the sealing load. Ideally, thermal effects should neither loosen nor tighten the joint. In actual design the flange joint must be sufficiently elastic, so that sealing loads are at least maintained within reasonable limits.

2. *Degree of sealing.*—For most applications it is sufficient to prevent mass flow as evidenced by liquid or gas tightness under soap bubble or immersion tests. When sealing the lighter gases (H_2 and He), diffusive flow through openings of molecular size may become significant.

3. *Gaskets.*—The function of a gasket is to seal effectively between two flange surfaces. It is usually made of a material which will readily conform to the surfaces, or which is coated with

a material so that when properly loaded, a barrier will be formed in depressed surface regions, preventing leakage of the contained fluid. Gaskets which damage the flange sealing surfaces are usually unsatisfactory, if the joint has to be repeatedly disassembled and reassembled. For these applications, gasket surfaces should always be softer than those of the flanges.

4. *Sealing surface condition.*—As a rule, leakage will occur when the internal fluid pressure begins to exceed the compressive stress which holds the gasket in contact with the sealing surface. Radial scratches on the flange sealing surface tend to induce a lower gasket local compressive stress along that radial path, resulting in leakage. Conversely, if the flange sealing surface consists of concentric serrations, higher local compressive stress will be induced circumferentially along the serrations, and will seal higher internal pressures for a given nominal compressive stress of the gasket. The required sealing-surface finish is a function of gasket design. Generally, it ranges from a microinch finish of 32 to 125 rms, with concentric tool markings.

5. *Gasket loading.*—The minimum requirement for good sealing of a flange joint is sufficient gasket precompression to close up all paths through which fluid flow could occur. Furthermore, the sealing load must be maintained so that a specific level of gasket compressive stress is induced to resist the internal fluid pressure.

6. *Seal drain.*—In some applications, positive sealing at the flange joint is required. Dual (series) seals and overboard drain line are then provided (fig. 9-15).

Flange Joint Structural Design

Figure 9-11 presents the structural design configuration of a typical flange joint as frequently used in rocket engines. The flange ring, under various working loads, is subject to bending as shown exaggeratedly by the dotted lines. The bending moments may become quite large; the resulting stresses reach their maximum at corner Z, where the flange joins the wall of the duct.

The basic approach to the design of a flange joint is to prestress the flange bolts in tension

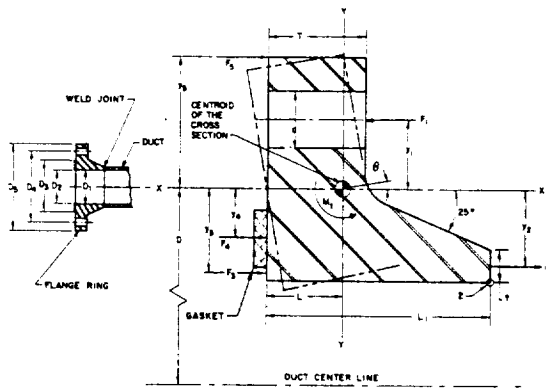


Figure 9-11.—Structural design configuration of a typical flange joint.

so that a gasket compressive stress is maintained to seal effectively against fluid leakage, under maximum working pressure and other loads. Defining a flange ring segment of unit length (i.e., 1 inch along the arc of a circle passing through the flange cross-section centroid) as a free body, the correlations between all forces acting on that segment, and the minimum required design flange bolt loading, are established as follows:

$$F_1 = F_2 + F_3 + F_4 + F_5 \quad (9-1)$$

$$F_2 = \left(\frac{pD_1^2}{4D} \right) + \frac{W_e}{\pi D} \quad (9-2)$$

$$F_3 = \frac{p(D_2^2 - D_1^2)}{4D} \quad (9-3)$$

$$F_4 = \frac{S_g(D_3^2 - D_2^2)}{4D} \quad (9-4)$$

$$S_g = mp \quad (9-5)$$

$$F_5 = nF_1 \quad (9-6)$$

$$W_b = F_1 \pi D \quad (9-7)$$

where (referring to fig. 9-11)

D = diameter of the circle passing through the centroid of the flange ring cross section, in

D_1 = inside diameter of the flange and duct, in

D_2 = inside diameter of the gasket, in

D_3 = outside diameter of the gasket, in

p = internal fluid pressure, psi (the maximum working pressure should be used)

F_1 = force per unit length of the flange ring from bolt loading, lb/in

F_2 = force per unit length of the flange ring from longitudinal tension of the duct, lb/in

F_3 = force per unit length of the flange ring from internal pressure p , lb/in

F_4 = force per unit length of the flange ring from gasket loading, lb/in

F_5 = force per unit length of the flange ring from compression load at the flange outside diameter, lb/in

S_g = required average gasket compressive stress, for proper seating against an internal fluid pressure p , psi

m = gasket factor, a function of gasket design and to be determined experimentally; design values range from 0.8 to 10

n = flange factor, a function of flange configuration and its rigidity; design values range from 0.1 to 0.8

W_e = end loads on the duct due to inertia and thermal effects (tension or compression), lb

W_b = minimum required design flange bolt loading, lb

Sample Calculation (9-1)

The following design data are given for the flange joint of the oxidizer-pump-discharge flexible duct of the A-1 stage engine:

Working pressure under normal steady operating conditions, 1505 psia

Maximum fluid working pressure under occasional transient conditions, 1750 psia

Inside diameter of the duct, $D_1 = 8$ in

Inside diameter of the gasket, $D_2 = 8$ in

Outside diameter of the gasket, $D_3 = 8.5$ in

End loads on the duct, due to thermal contraction, $W_e = 2400$ lb

Gasket factor, $m = 0.8$

Flange factor, $n = 0.3$

Determine the minimum required design bolt loading of the flange joint.

Solution

We will use a maximum working pressure $p = 1750$ psia

From equation (9-5), the required average gasket compressive stress:

$$S_g = mp = 0.8 \times 1750 = 1400 \text{ psi}$$

Combine equations (9-1) and (9-6):

$$F_1 = \frac{(F_2 + F_3 + F_4)}{(1 - n)}$$

Combine this and equations (9-2), (9-3), (9-4), and (9-7) to obtain the minimum required design bolt loading of the flange joint:

$$W_b = \frac{[p\pi D_1^2 + 4W_e + p\pi(D_2^2 - D_1^2) + S_g\pi(D_3^2 - D_2^2)]}{4(1 - n)}$$

$$W_b = \frac{[1750 \times \pi \times 8^2 + 4 \times 2400 + 1400 \times \pi(8.5^2 - 8^2)]}{4(1 - 0.3)}$$

$$= 141\,000 \text{ lb}$$

After the required design bolt loading has been determined, the number, size, and torque value of the bolts needed to produce that load must be chosen. Since tensile elasticity is advantageous, the use of small-diameter, high-strength bolts is desirable. Bolt spacing should be sufficiently close to insure a reasonably even distribution of the load around the gasket circumference. The following empirical correlation is recommended for maximum spacing to produce a tight joint:

$$P_s = 2d + T \quad (9-8)$$

where

P_s = maximum bolt spacing, in

d = nominal bolt dia, in

T = flange thickness, in

The general proportion of the flange ring may be determined by the following empirical equation (fig. 9-11):

$$T = At \quad (9-9)$$

$$L_1 = Bt \quad (9-10)$$

where

t = thickness of the duct wall, in, as determined by a hoop stress calculation

L_1 = overall axial length of the flange ring, in

A = design factor, ranging from 4 to 6

B = design factor, ranging from 10 to 14

A taper angle of 25° is generally used for the hub portion of the flange ring.

The stress and strain analysis of the flange ring may be treated as the twisting of a thick circular ring of uniform cross section under the influence of turning couples which are uniformly distributed along a circle passing through the centroid of the ring cross section. The following correlations approximate the maximum working stress and strain of a flange ring (refer to fig. 9-11):

$$M_t = F_1 y_1 + F_2 y_2 + F_3 y_3 + F_4 y_4 - F_5 y_5 \quad (9-11)$$

$$y_1 = \frac{(D_4 - D)}{2} \quad (9-12)$$

$$y_2 = \frac{(D - D_1 - t)}{2} \quad (9-13)$$

$$y_3 = \frac{(2D - D_2 - D_1)}{4} \quad (9-14)$$

$$y_4 = \frac{(2D - D_3 - D_2)}{4} \quad (9-15)$$

$$y_5 = \frac{(D_5 - D)}{2} \quad (9-16)$$

$$\theta = \frac{M_t D^2}{4EI_{y-y}} \quad (9-17)$$

$$S_z = \frac{M_t D^2 (L_1 - L)}{2D_1 I_{y-y}} \quad (9-18)$$

where

D_4 = diameter of the bolt circle, in

D_5 = outside diameter of the flange ring, in

y_1, y_2, y_3, y_4, y_5 = distances between the ring cross-section centroid and forces F_1, F_2, F_3, F_4 and F_5 , in

M_t = resultant twisting couple per unit length of flange ring, in-lb/in

I_{y-y}	= the moment of inertia of the ring cross section about the Y-Y axis, in ⁴
E	= modulus of elasticity of the flange material, psi
θ	= angular displacement of the flange ring under maximum working pressure and loads, rad
S_x	= flange ring maximum tensile stress, which occurs at the corner Z and is normal to the plane of figure 9-11, i.e., in the hoop direction

$$t = \frac{\text{Yield pressure} \times D_1}{2 \times F_y \times e_w} = \frac{2117 \times 8}{2 \times 170\,000 \times 0.75} = 0.066 \text{ in}$$

From equation (2-10), ultimate pressure = 1.5 × 1925 = 2887 psi.

Based on ultimate strength, the thickness of the duct wall

$$t = \frac{\text{Ultimate pressure} \times D_1}{2 \times F_u \times e_w} = \frac{2887 \times 8}{2 \times 200\,000 \times 0.75}$$

$$= 0.077 \text{ in}$$

We will use the higher value and round it to $t = 0.08$ inch, as the selected wall thickness of the duct.

Generally, based on given bolt size, gasket diameters, and duct dimensions, a proposed flange configuration may be derived simply from good design layout practice. Then the proposed design is checked for working stresses and strains. The flange thickness T may be adjusted accordingly. Assume flange design factors $A = 6$ and $B = 12.2$.

From equation (9-9), the flange thickness:

$$T = At = 6 \times 0.08 = 0.48 \text{ in}$$

From equation (9-10), the flange axial length:

$$L_1 = Bt = 12.2 \times 0.08 = 0.976 \text{ in, say } 0.98$$

Also, from a design layout, we obtained the following additional values:

$$D_4 = 9 \text{ in}$$

$$D_5 = 9.62 \text{ in}$$

$$L = 0.37 \text{ in (approximately)}$$

$$D = 8.6 \text{ in (approximately)}$$

$$I_{y-y} = 0.0273 \text{ in}^4 \text{ (approximately)}$$

From equation (9-7):

$$F_1 = \frac{W_b}{\pi D} = \frac{140\,400}{\pi \times 8.6} = 5200 \text{ lb/in}$$

From equation (9-2):

$$F_2 = \left(\frac{pD_1^2}{4D} \right) + \frac{W_e}{\pi D} = \left(\frac{1750 \times 8^2}{4 \times 8.6} \right) + \frac{2400}{\pi \times 8.6} = 3347 \text{ lb/in}$$

Sample Calculation (9-2)

With the data given in sample calculation (9-1), design the flange for the oxidizer pump discharge flexible duct of the A-1 stage engine, with the following recommended material and bolt data:

- Flange and duct material, Inco 718
- Minimum yield strength, $F_y = 170\,000$ psi
- Minimum ultimate strength, $F_u = 200\,000$ psi
- Modulus of elasticity, $E = 29.6 \times 10^6$ psi
- Duct weld efficiency, $e_w = 0.75$
- Bolt size and material, 5/16-24 A-286 (200 000 psi), stainless-steel bolt, 0.526 head dia
- Allowable ultimate bolt load, 10262 lb

Solution

Use the flange design and nomenclature shown in figure 9-11. From equation (2-8):

Design limit pressure

$$= 1.2 \times \text{steady operating pressure} = 1.2 \times 1505 \\ = 1806 \text{ psi}$$

or

Design limit pressure

$$= 1.1 \times \text{maximum transient pressure} = 1.1 \times 1750 \\ = 1925 \text{ psi}$$

From equation (2-9), yield pressure = 1.1 × 1925 = 2117 psi.

In accordance with standard practice, the thickness of the duct wall is determined as

CONFIDENTIAL

From equation (9-3):

$$F_3 = \frac{p(D_2^2 - D_1^2)}{4D} = 0$$

From equation (9-4):

$$F_4 = \frac{S_g(D_3^2 - D_2^2)}{4D} = \frac{1400(8.5^2 - 8^2)}{4 \times 8.6} = 336 \text{ lb/in}$$

From equation (9-6):

$$F_5 = nF_1 = 0.3 \times 5200 = 1560 \text{ lb/in}$$

From equation (9-12):

$$y_1 = \frac{(D_4 - D)}{2} = \frac{(9 - 8.6)}{2} = 0.2 \text{ in}$$

From equation (9-13):

$$y_2 = \frac{(D - D_1 - t)}{2} = \frac{(8.6 - 8 - 0.08)}{2} = 0.26 \text{ in}$$

From equation (9-15):

$$y_4 = \frac{(2D - D_3 - D_2)}{4} = \frac{(2 \times 8.6 - 8.5 - 8)}{4} = 0.175 \text{ in}$$

From equation (9-16):

$$y_5 = \frac{(D_5 - D)}{2} = \frac{(9.62 - 8.6)}{2} = 0.51 \text{ in}$$

From equation (9-11):

$$\begin{aligned} M_t &= F_1 y_1 + F_2 y_2 + F_3 y_3 + F_4 y_4 - F_5 y_5 \\ &= 5200 \times 0.2 + 3347 \times 0.26 + 336 \times 0.175 - 1560 \times 0.51 \\ &= 1174 \text{ in-lb/in} \end{aligned}$$

From equation (9-17), the angular displacement of the flange under maximum transient pressure condition:

$$\begin{aligned} \theta &= \frac{M_t D^2}{4 E I_{y-y}} = \frac{1174 \times (8.6)^2}{4 \times 29.6 \times 10^6 \times 0.0273} \\ &= 0.0268 \text{ rad or } 1.54^\circ \end{aligned}$$

From equation (9-18), the maximum working

stress under maximum transient pressure conditions:

$$\begin{aligned} S_z &= \frac{M_t D^2 (L_1 - L)}{2 D_1 I_{y-y}} = \frac{1174 \times (8.6)^2 \times (0.98 - 0.37)}{2 \times 8 \times 0.0273} \\ &= 121\,200 \text{ psi} \end{aligned}$$

From equations (2-8) and (2-9), the yield load stress = $121\,200 \times 1.1 \times 1.1 = 146\,600$ psi. This is smaller than the minimum yield strength $F_y = 170\,000$ psi of the material.

From equations (2-8) and (2-10), the ultimate load stress = $121\,200 \times 1.1 \times 1.5 = 200\,000$ psi.

Thus, the proposed flange configuration is satisfactory. We will now determine the number of bolts and, from equation (9-8), the maximum bolt spacing

$$P_s = 2d + T = 2 \times 0.312 + 0.48 = 1.104 \text{ in}$$

The required number of bolts:

$$\frac{\pi D_4}{P_s} = \frac{\pi \times 9}{1.104} = 25.6, \text{ say } 26$$

The required bolt loading W_b calculated in sample calculation (9-1) was based on the maximum transient pressure. Using equations (2-8) and (2-10), the required ultimate bolt loading:

$$W_b \times 1.1 \times 1.5 = 140\,400 \times 1.65 = 231\,800 \text{ lb}$$

Therefore, the ultimate loading on each bolt = $231\,800/26 = 8900$ lb. This is smaller than the allowable ultimate bolt load of 10 262 lb.

The required preload on each bolt:

$$\frac{W_b}{26} = \frac{140\,400}{26} = 5400 \text{ lb}$$

Sheet Gaskets for Flange Joints

Gasket materials consisting of asbestos fibers bonded with rubber or neoprene are readily available in flat sheets, from which the gasket may be cut to suit most requirements. Frequently used sheet gaskets range from 1/32 to 1/8 inch in thickness. At fluid pressures less than 50 psi, sheet gaskets can be used with flat faces at both flanges. For higher pressure applications, sheet gaskets can be secured in a flat,

concentric groove machined on one of the flanges, with the groove depth sized for proper preloading of the gasket. Preferably, the flange facing should be serrated concentrically. In rocket engine applications, sheet gaskets should be limited to pressure levels of less than 200 psi, and to temperatures in the range from -100° F to 900° F.

Elastomer and Metal O-Rings for Flange Joints

Elastomer O-rings have been used with good results for rocket engine flange joints in medium temperature service (-60° to 400° F). Satisfactory results have also been experienced at pressure levels as high as 3000 psi. Typical elastomer O-ring flange joint design data are presented in table 9-5 for use in groove-type flanges, as shown in figure 9-12. Table 7-3 may be used to select the hardness of the O-ring materials with respect to working pressures. Elastomer O-ring seals for various flange size may easily be made by cutting straight O-ring stock to a specific length, and cementing the ends together.

For low- and high-temperature services (-430° to 2000° F), and for sealing against very high pressures (up to 4000 psi), metal O-rings may be used in rocket engine flange joints, with proper detail design. Hollow stainless-steel O-rings, such as manufactured under the trade name "Toruseal" by the D.S.D. Co., have been used extensively in various services. They can be coated with Kel-F and Teflon for cryogenic service. One of the advantages of metal O-rings is that they require considerably less space than other seal types. However, the O-rings must have a good seal surface finish, and high compressive seal loads, to assure satisfactory re-

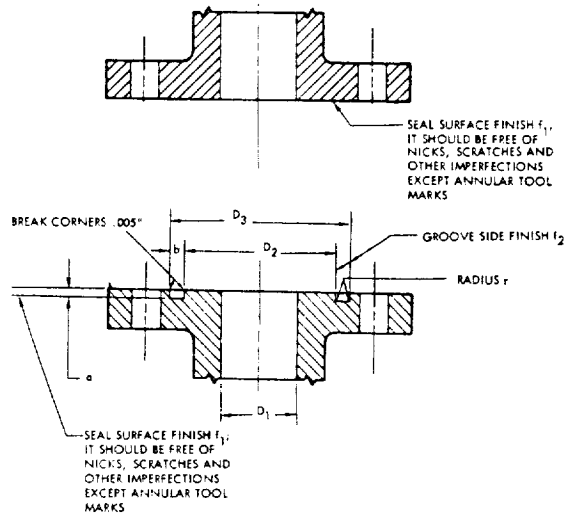


Figure 9-12.—Flange seal groove design.

sults. Metal O-rings can be used in a groove-type flange, as shown in figure 9-12. Table 9-6 presents typical design data for metal O-ring flange joints.

Spiral-Wound Gaskets for Flange Joints

Spiral-wound gaskets manufactured by the Flexitallic Gasket Co. have been used extensively in rocket engine flange joints for liquid oxygen and hot gas (up to 1600° F) services. Pressures are generally kept below 1000 psi. The gaskets (detail shown in fig. 9-13) are made of spiral-wound 304 stainless-steel ribbon, with a Canadian asbestos filler. It is not recommended that gasket widths of less than 3/16 inch

TABLE 9-5.—Typical Elastomer O-Ring Flange Joint Design Data^a
[All dimensions in inches]

Nominal O-ring cross section	Actual O-ring cross section	Minimum squeeze	Depth of groove, a	Width of groove, b	Bottom radius, r	Seal surface finish, f ₁	Seal surface finish, f ₂
1/16	0.070 ± 0.003	0.017	0.045 ± 0.005	3/32	1/64	64 rms	64 rms
3/32	.103 ± .003	.020	.075 ± .005	9/64	1/64		
1/8	.139 ± .004	.025	.105 ± .005	3/16	1/32		
3/16	.210 ± .005	.030	.170 ± .005	9/32	1/32		
1/4	.275 ± .006	.039	.225 ± .005	3/8	1/16		

TABLE 9-6.—Typical Metal O-Ring Flange Joint Design Data^a
[All dimensions in inches]

Nominal O-ring, OD	Actual O-ring size			Flange groove dimensions			
	Tube OD +0.005 -0	Tube OD +0.003 -0	Wall thickness	D_2 maximum	$D_3 + 0.005$ -0	$a + 0.005$ -0	t_1
1	1.000	0.061	0.009	0.867	1.005	0.042	32 rms
1-1/2	1.500	.061	.009	1.367	1.505	.042	
2	2.000	.061	.009	1.867	2.005	.042	
2-1/2	2.500	.061	.011	2.367	2.505	.042	
3	3.000	.061	.011	2.867	3.005	.042	
4	4.000	.094	.011	3.801	4.005	.075	
5	5.000	.094	.011	4.801	5.005	.075	
6	5.000	.094	.011	5.801	6.005	.075	
8	8.000	.124	.011	7.741	8.005	.105	
10	10.000	.124	.011	9.741	10.005	.105	
15	15.000	.124	.011	14.741	15.005	.105	
20	20.000	.124	.011	19.741	20.005	.105	
30	30.000	.124	.011	29.741	30.005	.105	

^aSee fig. 9-12 for flange design. Duct diameter D_1 may be equal to D_2 .

be used. These gaskets are made to various stiffnesses (spring rates) by varying the tension of the wrapping. The harder gaskets are recommended for the higher pressures.

The gaskets are used in groove-type flanges, as shown in figure 9-12. For optimum results, tool marks on sealing surfaces should be con-

centric. Typical design data for spiral-wound gasket flange joints are presented in table 9-7. Gaskets of this type require high compressive loads. The values range from 6000 to 25 000 psi. The amount of gasket compression is controlled by metal-to-metal contact of the flanges, with allowance for maximum tolerance buildup of

TABLE 9-7.—Typical Spiral-Wound Gasket Flange Joint Design Data^a
[All dimensions in inches]

Gasket dimensions			Approximate re- quired compressive load, lb at deflection		Flange groove dimensions				
A diameter ± 0.016	B diameter ± 0.032	Sealing area, sq. in.	0.025	0.035	D_2 ± 0.010	D_3 ± 0.010	a	r	t_1
1.000	1.375	0.442	8200	10 600	0.900	1.425	0.105 + 0.005 for fluid pressure below 200 psi -0 0.095 + 0.005 for fluid pressure above 200 psi -0	0.010 +0 -0.005	125 rms
1.500	1.875	.638	8300	11 500	1.400	1.925			
2.000	2.375	.835	9000	12 700	1.900	2.425			
2.500	2.875	1.031	9800	14 100	2.400	2.925			
3.000	3.375	1.227	10 800	15 600	2.900	3.425			
4.000	4.375	1.620	12 950	18 600	3.900	4.425			
5.000	5.500	3.056	23 000	32 400	4.875	5.560			
6.000	6.500	3.645	26 400	37 000	5.875	6.560			
8.000	8.500	4.832	33 600	43 000	7.875	8.560			
11.000	11.750	11.110	73 600	97 000	10.875	11.810			
15.000	15.750	15.040	98 600	122 500	14.860	15.820			
20.125	21.000	24.150	153 000	178 500	19.965	21.080			
25.000	25.875	29.900	186 500	206 000	24.840	25.955			

^aSee fig. 9-13 for seal design. See fig. 9-12 for flange design. Duct diameter D_1 may be equal to D_2 .

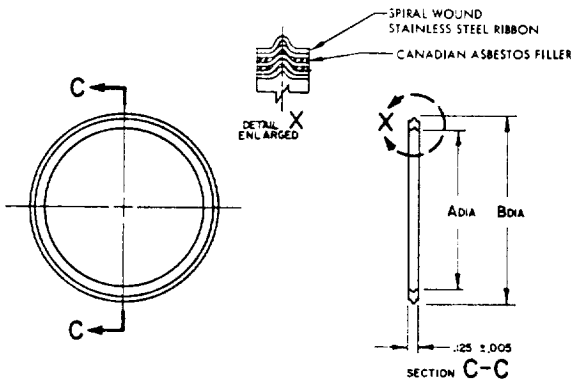


Figure 9-13.—Spiral-wound gasket for flange joints.

gasket thickness and groove depth. One difficulty with spiral-wound gaskets is the presence of erratic compression loads, due to thickness tolerances and variations in wrapping. Another is their tendency to indent the flange sealing surfaces, particularly when the flanges are of aluminum.

Pressure-Actuated Seals for Flange Joints

An ingenious approach toward attaining better seal deflection capabilities to accommodate deformations of the flange joint under working loads is the pressure-actuated type seal, shown in figure 9-14. The spring effect is achieved by a metal, circular seal having a U-shaped cross section. When such a seal is compressed between the surfaces of a flange joint, the high points at its open ends make contact with the flange surfaces. If properly designed, the spring-like legs flex to follow flange deflections.

The open end of the seal must always be oriented toward the inside of the flange joint. Thus the internal fluid pressure is utilized to generate a considerable portion of the seal contact load. Pressure-actuated seals are installed in a concentric groove cut into the flange joint. This limits the amount of total flange preload transmitted through the contact points of the seal. The following correlations are established for the seal design shown in figure 9-14 for the approximation of seal contact loads:

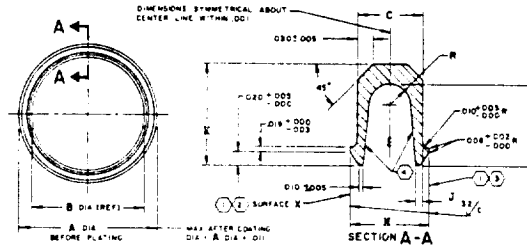
$$F_{s1} = \frac{EJ^3d}{8(H-0.02)^3C_1} \tag{9-19}$$

$$F_{s2} = F_{s1} + \frac{p(H-0.02)}{2} \tag{9-20}$$

where

- F_{s1} = seal contact load per inch of seal circumference without internal fluid pressure, lb/in
- F_{s2} = seal contact load per inch of seal circumference with internal fluid pressure, lb/in
- E = modulus of elasticity of the seal material, psi
- J = end thickness of the seal leg, in
- H = length of the seal leg, in
- d = seal deflection in the flange joint, in (i.e., the difference between initial seal width M and flange groove depth)
- p = internal fluid pressure, psi

MATERIAL - 4340 STEEL HEAT TREATED TO 160,000 - 180,000 PSI
 FINISH - ELECTROLESS NICKEL PLATE .0010 - .0012 INCH EMBRITTLEMENT RELIEVED
 TEFLON COAT .001 - .002 INCH



- ① THESE SURFACES TO BE FREE OF NICKS, BURRS, AND TOOL MARKS, EXCEPT ANNULAR TOOL MARKS
- ② FLAT WITHIN .0005 INCH PER INCH CIRCUMFERENCE
- ③ PARALLEL TO SURFACE X WITHIN .0005 INCH PER INCH CIRCUMFERENCE
- ④ THICKNESS OF TEFLON COATING ON THESE SURFACES OPTIONAL

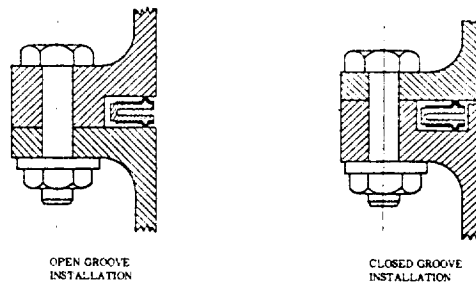


Figure 9-14.—Rocketdyne Naflex pressure-actuated seal design for flange joints.

C_1 = design factor. This is a function of seal leg configuration, its value ranging from 0.04 to 0.8

Generally, the contact surfaces of pressure-actuated seals are coated with a material of a lower elastic modulus than that of the material from which the seal is made. Thus the seal material can be utilized to achieve the spring-like properties required for maximum deflection capability, while the coating material provides the properties needed to establish the intimate contact required to prevent leakage between seal and flange surfaces. To prevent leakage, sufficient compressive stress must be developed in the coating to make it flow into imperfections on the flange surfaces. The required coating compressive stress may be determined by

$$S_c = \frac{E_c h}{t_c} \quad (9-21)$$

where

S_c = seal coating compressive stress, psi

E_c = modulus of elasticity of the coating material, psi

h = depth of the imperfections on the flange sealing surfaces, in

t_c = thickness of the coating, in

Many versions of pressure-actuated seals have been applied to rocket engines. Rocketdyne has developed the Naflex-type pressure-actuated seals, made of alloy steel and coated with a thin layer of Teflon. They are most effective for cryogenic (-430° F) and high-pressure (up to 4000 psi) services. Figure 4-32 illustrates a typical Naflex seal installation at the flange joint between thrust chamber and liquid oxygen dome. Design details and data for typical Naflex flange joints may be seen in figure 9-14. Also see table 9-8. For hot gas applications, up to approximately 1700° F, the seals may be coated with soft metals such as copper, aluminum, or gold.

For certain stringent applications, all propellant and turbine gas flanges in a rocket engine can be equipped with a Naflex-type dual static seal incorporating an intermediate cavity between high-pressure and low-pressure sealing areas. A seal drain line may be connected to the intermediate cavity, as shown in figure 9-15. This line can also be used to measure the seal leakage rate, if any. This arrangement may also be applied to pneumatic system flange joints, to monitor leakage.

TABLE 9-8.—Typical Design Data of Naflex Pressure-Actuated Seals and Flange Joints
[All dimensions in inches]

Seal dimensions								Flange groove dimensions				
A diameter +0 -0.005	B diameter (REF)	K +0 -0.005	J +0 -0.005	^a M +0 -0.003	R +0.004 -0	^a C +0 -0.003	H +0.005 -0	D ₂ +0 -0.010	D ₃ +0.010 -0	a +0.002 -0	r	f ₁
0.934	0.464	0.235	↑	0.155	↑	↑	0.190	0.433	0.948	↑	0.020 ± 0.005	32 rms
1.496	1.026	.235	↑	.155	↑	↑	.190	.995	1.510	↑		
2.058	1.548	↑	↑	↑	↑	↑	1.507	2.072	↑			
2.621	2.111	↑	0.018	↑	↑	0.139	2.070	2.635	0.148			
3.080	2.570	.255	↑	.160	↑	↑	2.529	3.094	↑			
3.620	3.110	↑	↑	↑	↑	.210	3.070	3.635	↑			
4.618	4.108	↑	↑	↑	0.037	↑	4.070	4.635	↑			
5.616	5.116	↑	↑	↑	↑	↑	5.070	5.635	↑			
6.614	6.114	↑	↑	↑	↑	↑	6.070	6.635	↑			
8.610	8.110	↑	↑	↑	↑	↑	8.070	8.635	↑			
10.606	10.106	.250	.017	.182	↑	.164	.205	10.070	10.635	.173		
15.596	15.096	↑	↑	↑	↑	↑	↑	15.070	15.635	↑		
20.870	20.370	↑	↑	↑	↑	↑	↑	20.320	20.885	↑		

^aDimension increases 0.009-inch maximum after nickel plating and Teflon coating.

- NOTES: 1. See fig. 9-14 for Naflex seal design.
2. See fig. 9-12 for flange design.
3. Duct diameter D_1 may be equal to D_2 .

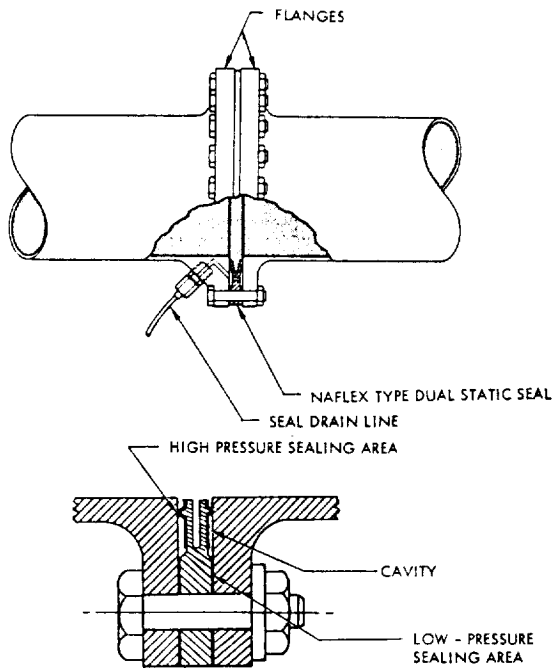


Figure 9-15.—Typical design of a flange joint with Naflex-type dual static seal and seal drain line.

Sample Calculation (9-3)

The following data are given for a Naflex seal represented by section A-A of figure 9-14: Design factor, $C_1 = 0.07$; $H = 0.205$ in; $J = 0.017$ in; $M = 0.187$ in. The seal material modulus of elasticity, $E = 30 \times 10^6$ psi. The flange seal groove depth, $a = 0.173$ in. The thickness of the Teflon coating, $t_c = 0.002$ in, with a modulus of elasticity, $E_c = 5 \times 10^4$ psi. Estimate the seal coating compressive stresses with and without an internal pressure, p , of 2000 psi. Also, determine the allowable depth of imperfections on the flange sealing surfaces.

Solution

The seal deflection

$$d = M - a = 0.187 - 0.173 = 0.014$$

From equation (9-19), the seal contact load without internal pressure

$$F_{s1} = \frac{30 \times 10^6 \times (0.017)^3 \times 0.014}{8(0.205 - 0.02)^3 \times 0.07} = 582 \text{ lb/in}$$

From figure 9-14, the seal land of contact = 0.019. Thus, the seal coating compressive stress without internal pressure

$$S_c = \frac{582}{1 \times 0.019} = 30\,600 \text{ psi}$$

From equation (9-20), the seal contact load with internal pressure

$$F_{s2} = 582 + \frac{2000(0.205 - 0.02)}{2} = 767 \text{ lb/in}$$

The seal coating compressive stress with an internal pressure of 2000 psi

$$S_c = \frac{767}{1 \times 0.019} = 40\,400 \text{ psi}$$

The allowable depth of imperfections on the flange sealing surfaces should be calculated from the initial coating compressive stress, using equation (9-21):

$$h = \frac{S_c t_c}{E_c} = \frac{30\,600 \times 0.002}{5 \times 10^4} = 0.0012 \text{ in}$$

9.4 DESIGN OF BRAZED JOINTS FOR ROCKET ENGINES

The best tube fitting or gasketed flange joint falls short of a good welded or brazed joint in reliability. Hence, every sealed joint on each rocket engine should be studied aiming at its elimination, or its replacement by a hermetically sealed joint, for increased overall system reliability. Specifically, certain sealed joints originally provided for convenience during the development phase of an engine system may no longer be needed as development approaches completion.

The brazed joint design shown in figure 9-16 may be utilized effectively to replace tube fittings and flange joints. A union sleeve with internal recesses for preplaced braze alloy foils connects the tube ends. The brazing can be accomplished by induction-heating coils, either in-place on the engine, or on the bench. Coax cables with low impedance losses have been developed, permitting a brazing fixture to be used in-place, even at great distances from the generator.

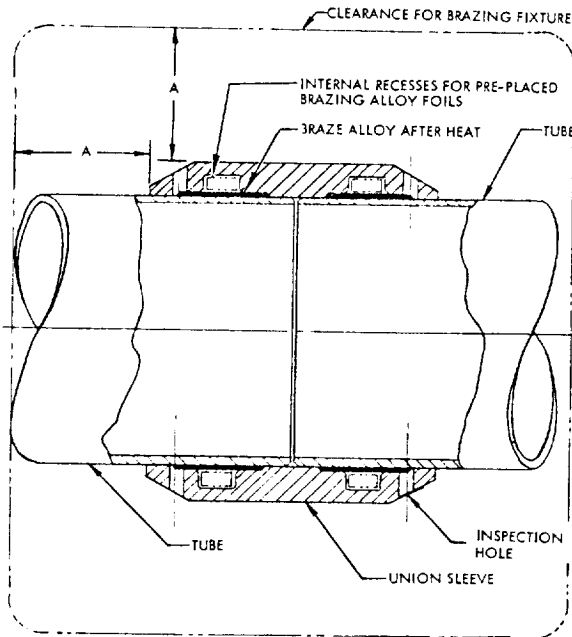


Figure 9-16.—Typical brazed joint design.

Pertinent design consideration and details of brazed joints for rocket engines are as follows:

Working Fluids, Pressures, and Temperatures Applicable to Brazed Joints

There are virtually no design limitations on the types of fluids that can be handled by brazed joints. Chemically active propellants such as fluorine, hydrazine, etc., have posed no problems to brazed joints. Similar satisfactory results have been obtained with brazed joints used in liquid hydrogen, liquid oxygen, hydraulic, and pneumatic lines.

Structurally, brazed joints are designed to be as strong as the strongest tubing or duct of like material. Brazed joints have demonstrated reliability at working fluid pressures as high as 4000 to 5000 psi. Generally, brazed joints are recommended to be limited to service temperatures of less than 1200° F. Allowance must be made for strength degradation of brazed joints used at elevated temperatures.

A typical brazed joint is illustrated in figure 9-16. The union sleeve can be used to join tube to tubes, tube to bellows, or tube to components. Line sizes as large as 6 inches (inside diameter) and walls as thin as 0.005 inch have been

successfully induction brazed. Tubes and sleeves for brazed joints can be made of aluminum alloys, austenitic and semiaustenitic steels, and nickel-base alloys such as Monel.

A preplaced braze alloy in the form of 0.001- to 0.003-inch-thick foil is snapped into recesses inside of the union sleeve. Diametrical clearances of 0.002-0.008 inch between sleeve and tubing are found to give satisfactory results. Holes are provided on the sleeve to permit visual joint inspection after brazing. The quality of the brazed joint can be also judged by the degree of external braze-alloy filleting at the outer edges of the sleeve. The recesses for the braze alloy are located midway between tube and sleeve ends. The length of the union sleeve can be determined by the braze bond shear strength and the effective bond area. Sleeve lengths range from 0.5 to 2 times the tube outside diameter.

Many types of brazing alloys can be used. A eutectic alloy of composition 71.8 percent silver, 28 percent copper, and 0.2 percent lithium, with a melting point of 1435° F, can braze without flux and permit in-place brazing.

System Applications of Brazed Joints

After an engine system has reached its production phase, the majority of the small- or medium-size sealed fittings and flange joints should be replaced by well-located brazed joints. These should be designed to facilitate in-place brazing, if possible. This requires a specific clearance around the joint for the brazing fixture. The minimum clearance *A* for the brazing fixture (fig. 9-16) is 5/8 inch for tube diameters of 1/4 to 5/8 inch; 3/4 inch for a 3/4-inch diameter; 7/8 inch for a 7/8-inch diameter; and 1 inch for 1- to 1-3/4-inch diameters. For repair of lines or servicing of components with brazed joints, a length of line may be cut out and a new length inserted and brazed in-place, with two union sleeves.

Figure 9-17 presents the in-place brazed joints applied to an upper stage propulsion system. About 80 percent of the original fittings and flanged joints were replaced by brazed joints, which eliminate considerable weight. In addition, it also permits the use of high-strength, thin-wall tubing, instead of the older heavy-wall tubing.

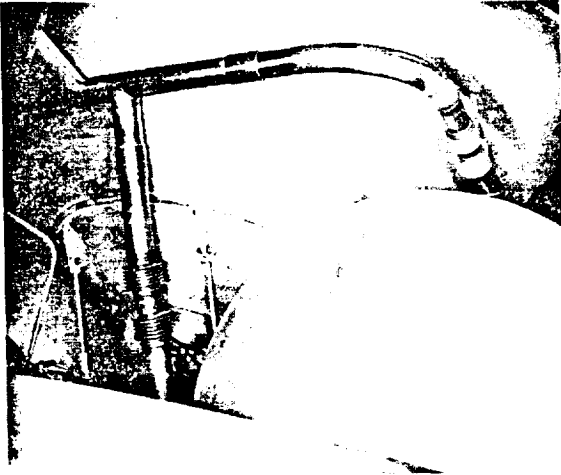


Figure 9-17.—In-place brazed joints applied in an upper stage propulsion system.

9.5 DESIGN OF DUCTS FOR ROCKET ENGINES

Basic Design Considerations

Primary design considerations for various ducts used on rocket engines are:

1. *Fluid flow rate and system pressure drop.*—The size of the duct is determined largely by the required flow rate and permissible pressure drop of the flow system. An optimization must be made considering duct weight, pressure drop, and space, before finalizing the duct size.

2. *Working temperature and pressure of the fluid.*—The selection of construction materials and structural design for ducts depends mainly on the working temperature and pressure level of the fluid, but also on chemical compatibility. Temperature also influences line flexibility and duct geometry.

3. *Duct joints.*—The number and type of joints in a duct system are usually determined by system assembly and servicing requirements. All mechanically sealed joints should be reviewed, at various engine design and development phases, for their possible elimination or replacement by in-place, induction-brazed or welded joints. (See secs. 9.3 and 9.4.)

4. *Line flexibility and geometry.*—The required degree of flexibility in a duct system is dictated by component tolerance buildups, misalignments, and required freedom of movement to

allow for temperature changes, dynamic loads, and engine gimbal effects, if any. This often determines the line geometry. In general, however, lines should be as short and straight as possible.

5. *Structural integrity.*—The structural design of a duct system may involve a number of complex problems. This is especially true with ducts for elevated or very low temperatures, and requiring a high degree of flexibility. The design and fabrication of metal bellows for application in ducts is a highly specialized technology.

Duct Design for Minimum Pressure Drop

Techniques for fluid-flow pressure drop determination have been discussed in chapter VII. Equation (7-7) may be used to estimate the pressure drop of a straight duct section. Either equation (7-7) or (7-9) can be utilized to predict the pressure drops of other shapes, for which some experimental data are available.

Besides avoiding excessive flow velocities at various sections of a duct system, basic requirements for minimum pressure drop are: constant flow area, smooth flow surfaces and path, minimum length, and few turns. In most duct designs, a certain number of turns is unavoidable. The design of these turns affects considerably the overall pressure drop of a duct system.

A turn may offer a large resistance to the flow if not carefully designed. Investigations show that the flow resistance in a bend with constant cross section is affected directly by its turning radius ratio R/D (where R = radius of curvature of the axis of the duct, D = diameter or width of the duct) (see fig. 7-21). By increasing the turning radius ratio, large reductions in pressure drop are possible. Bends with a circular section are better than those with a square section. However, the square section may be much improved by changing it to a rectangle, so that the turn is made on the short side; that is, the loss can be decreased by increasing the rectangle aspect ratio W/D (where W = width of the long side, D = width of the short side). For a duct with a rectangular section, therefore, a very efficient corner may be produced if the values of both the radius ratio and the aspect ratio are kept large.

This consideration should be applied in all cases where a sharp turning corner is unavoidable, such as the elbow-type turbopump inlet ducts shown in figure 6-15. Here, the loss around the sharp corner is due largely to the zero radius ratio. To reduce this pressure drop, guide vanes can be very effectively used. If the junctions of the duct walls on the diagonal are smoothed out and vanes added as shown in figure 9-18, the compartments so formed may be made to have a good radius ratio and a high aspect ratio. Since in most cases only a few vanes need to be added for high aspect ratios, the remaining problem is one of securing a good radius ratio.

The radius and aspect ratios of each compartment are increased as the gap/chord ratio S/C is reduced (fig. 9-18). Theoretically, then, the corner pressure drop will decrease as the ratio S/C is decreased. However, each additional vane adds more surface area and blockage, and consequently tends to increase losses. The S/C ratio can be optimized in tests and ranges from 0.25 to 0.45. Well-designed elbow-type sharp turns with guide vanes may have resistance coefficients K as low as 0.1 to 0.2 (see eq. 7-9).

Duct Design for Flexibility

For most interconnecting ducts between two engine components, the required flexibility such as for misalignments and temperature changes can be achieved by placing one or two bellows sections in the line (figs. 9-4 and 9-5). These may be either restrained or unrestrained, depending on structural loading considerations. In ducts connecting two components involving large relative movements, a minimum of three flexible sections is required. The longitudinal axis of at least two of the bellows sections should be positioned at a right angle to one another. Restrained bellows are preferred.

The duct systems shown in figure 9-3 illustrate a basic three-bellows arrangement as applied to gimballed clustered engines. Figure 9-19 presents one of the frequently used design approaches for a relatively short duct system to facilitate large movements during gimbaling of an engine system. The three flexible sections are kept in the plane of the engine gimbal point. This results in minimum displacements of the sections for a given engine movement. Bellows-type universal joints (fig. 9-20) may be conven-

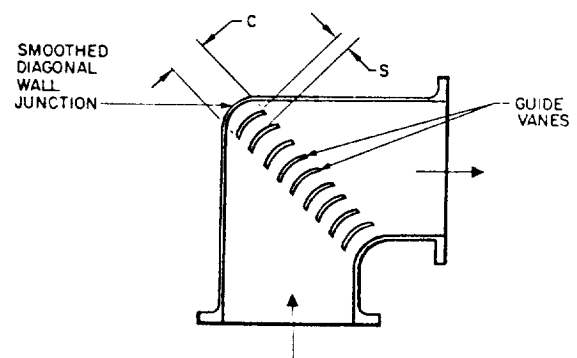


Figure 9-18.—Elbow-type sharp turning duct with guide vanes.

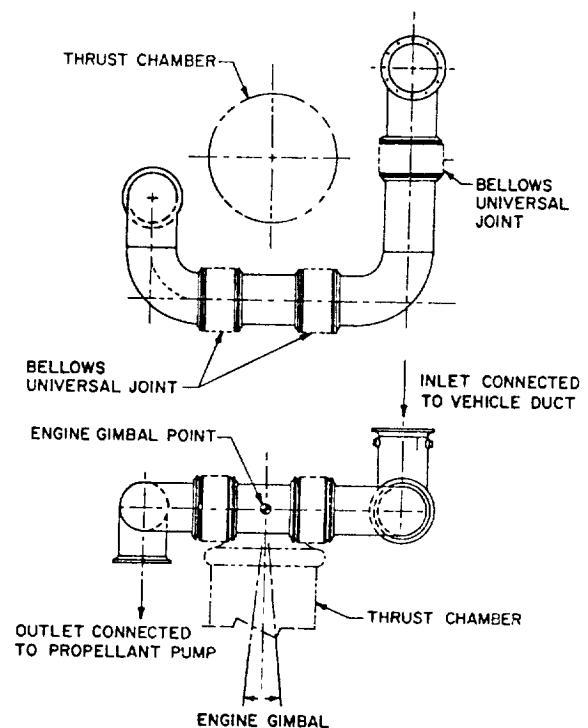


Figure 9-19.—Typical propellant supply duct designed for the flexibility required for engine gimbaling.

iently incorporated into this duct system by welding. These joints are made of stainless steel and will operate at cryogenic and elevated temperatures (up to 1000° F). The internal restraining mechanism is designed to give a smooth flow passage for low-pressure drop.

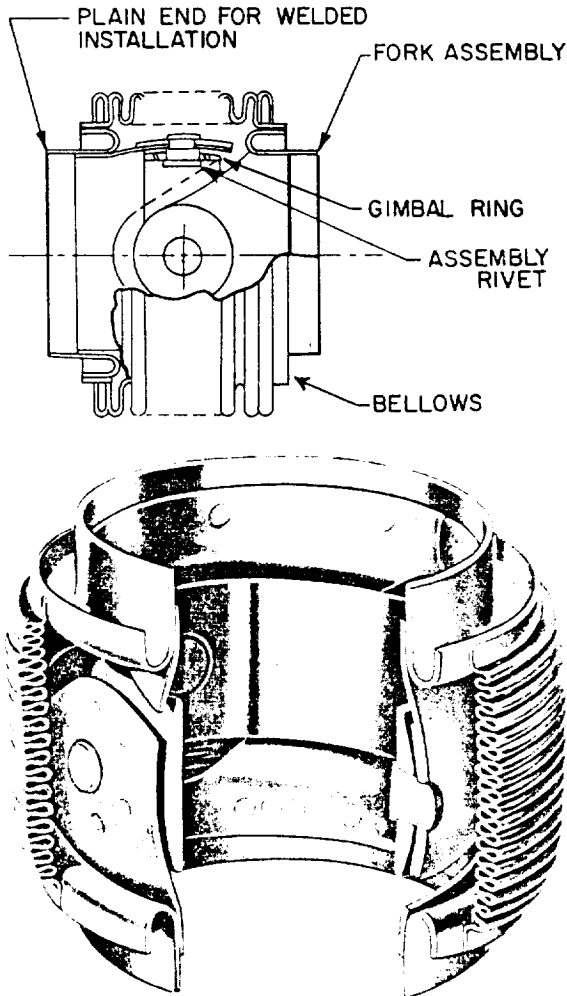


Figure 9-20.—Typical gimbal-ring-type bellows universal joint designed and manufactured by Marman Division of Aeroquip Corp.

For higher pressure applications (over 200 psi), external wire braids or links may be used to restrain the bellows section. The braids can be made of stranded stainless-steel wires, about 0.012-inch diameter. In extreme cases, more than one layer of braid should be used with regard to the high separation loads.

Structural Design of Bellows For Flexible Ducts

Most of the bellows used for flexible ducts in rocket engines are hydraulically formed by radi-

ally expanding thin-wall tubing, at spaced intervals along its axis, coincident with an axial compression, to a configuration as shown in figure 9-21. Our discussion will be confined to this type of bellows. The various structural characteristics and design correlations of bellows are presented using the following nomenclature (see figs. 9-21 and 9-22):

- C_t = bellows wall-thinning correction factor
- C_p = ply interreaction factor (1.00 for 1-ply bellows, 0.90 for 2-ply bellows, and 0.85 for 3-ply-or-more bellows)
- d_o = outside diameter of the bellows, in
- d_i = outside diameter of the convolution root of the bellows, in
- $d_m = \sqrt{(d_i^2 + d_o^2)/2}$ = root-mean-square diameter of the bellows, in
- d_d = mean duct diameter, in
- E = modulus of elasticity of the bellows material, psi
- e_a = axial deflection of the bellows, in
- e_b = equivalent axial deflection of the bellows due to pure bending, in
- e_p = equivalent axial deflection of the bellows due to parallel offset, in
- e_s = equivalent axial deflection of the bellows due to pure shear, in
- F_s = shear load, lb
- F_p = pressure separating load, lb
- G = shear modulus of elasticity of the bellows material, psi
- $h = (d_o - d_i)/2$ = mean convolution height, in
- L = pitch of the bellows (axial length of a convolution), in
- $L_a = (N_c - 0.5)L + N_p t$ = free axial length of the bellows, in
- N_c = number of bellows convolutions
- N_p = number of bellows plys
- t = thickness of the bellows wall, in
- L_b = axial length of the rigid duct section, in
- M = bending moment, in-lb
- p = internal (or external) fluid pressure, psi
- p_{cr} = critical stability pressure of the bellows, psi
- R_a = axial spring rate of the bellows, lb/in
- R_b = bending spring rate of the bellows, lb-in/degree
- R_p = parallel offset spring rate of the bellows, lb/in
- R_s = shear spring rate of the bellows, lb/in

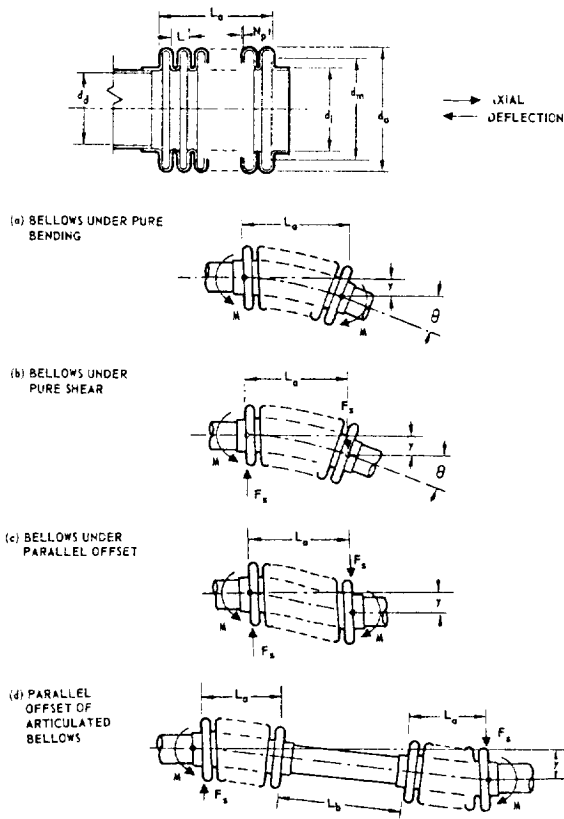


Figure 9-21.—Elements and various motions of bellows.

R_t = torsional spring rate of the bellows, lb-in/degree

S_b = bellows bulging stress, psi

S_h = bellows hoop stress, psi

S_m = bellows motion stress, psi

S_s = bellows shear stress, psi

S_t = bellows torsion stress, psi

T = torsional moment, in-lb

T_{cr} = critical stability torque of the bellows, psi

ν = Poisson's ratio of the bellows material, in

y = transverse deflection of the bellows, in

θ = bending angle of rotation, degrees

ϕ = torsional angle of rotation, degrees

1. *Thinning of the bellows wall.*—Hydraulic-formed bellows are usually made by starting with tubes of the same diameter as the bellows diameter at the root of convolution, d_i . The typical thinning profile of a bellows wall starts with the original material thickness at the root of the convolution, and tapers approximately linearly to

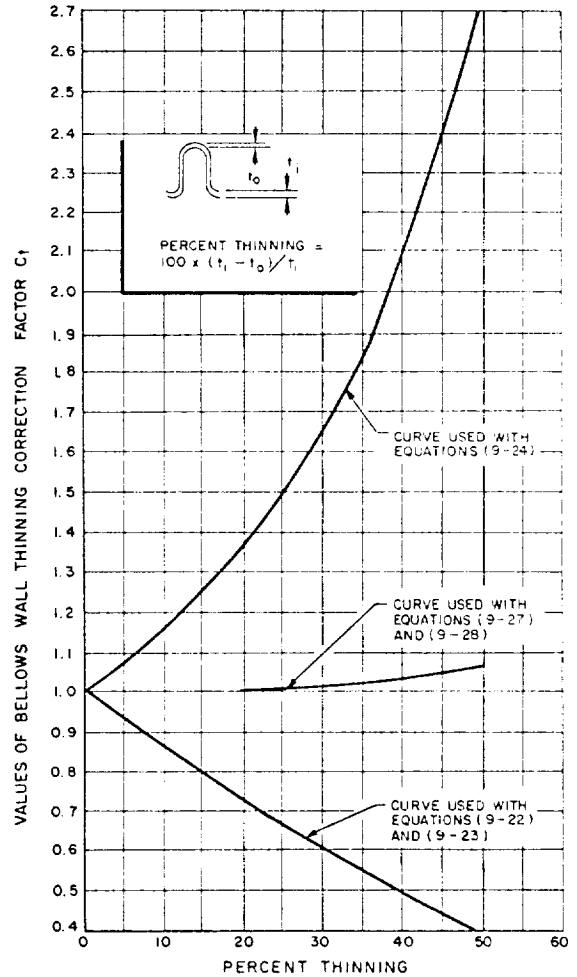


Figure 9-22.—Bellows wall thinning correction factor C_t versus percent thinning.

the minimum thickness at the convolution outside diameter (fig. 9-22). Amounts of thinning range from 10 to 40 percent. Effects of thinning are considered by applying the thinning correction factor C_t (fig. 9-22) to the bellows design.

2. *Bellows axial spring rate:*

$$R_a = \frac{1.49 C_t C_p N_p E d_i t^3}{N_c h^3}, \text{ lb/in}$$

(steel and nickel alloys) (9-22)

$$R_a = \frac{1.23 C_t C_p N_p E d_i t^3}{N_c h^3}, \text{ lb/in}$$

(aluminum alloys) (9-23)

3. *Bulging stresses.*—These are the radial bending stresses induced in the side walls of the bellows, by internal or external pressure. Bulging stresses should be kept below those listed in table 9-9:

$$S_b = \frac{C_t p h^2}{2 N_p t^2}, \text{ psi} \quad (9-24)$$

4. *Separating loads.*—Bellows are pressure loaded so that they experience a separating load, in addition to the normal duct axial force:

$$F_p = \frac{p(d_m^2 - d_d^2)\pi}{4}, \text{ lb} \quad (9-25)$$

5. *Hoop stresses.*—The bellows hoop stresses are calculated by using the total area per inch of bellows axial length of a tube of equivalent wall thickness. Hoop stresses should always be kept lower than the yield and ultimate strength of the bellows materials by a specified margin.

$$S_h = \frac{p d_m}{2 N_p t} \left[0.57 + \left(\frac{2h}{L} \right) \right], \text{ psi} \quad (9-26)$$

6. *Motion stresses due to axial deflections of the bellows.*—These are due to bending of the bellows side walls. Allowable motion stresses for bellows materials, with respect to design cycle life, are given in table 9-9:

$$S_m = \frac{1.40 C_t E t e_a}{N_c h^2}, \text{ psi} \quad (9-27)$$

(steel and nickel alloys)

$$S_m = \frac{1.78 C_t E t e_a}{N_c h^2}, \text{ psi} \quad (9-28)$$

(aluminum alloys)

All other types of bellows motions, such as angular and parallel offset, can be converted into an equivalent bellows axial deflection, and applied to equations (9-27) and (9-28) to calculate the corresponding motion stresses.

7. *Bellows under pure bending* (fig. 9-21a):

$$R_b = \frac{M}{\theta} = \frac{d_m^2 R_a}{458.4}, \text{ lb-in/degree} \quad (9-29)$$

$$e_b = \frac{d_m \sin \theta}{2}, \text{ in} \quad (9-30)$$

Motion stresses due to pure bending can be calculated by substituting e_b for e_a in equations (9-27) and (9-28).

8. *Bellows under pure shear* (fig. 9-21b):

$$R_s = \frac{F_s}{y} = \frac{3 d_m^3 R_a}{8 L_a^2}, \text{ lb/in} \quad (9-31)$$

$$\theta = \frac{229.2 F_s L_a}{R_a d_m^2}, \text{ degrees} \quad (9-32)$$

$$e_s = \frac{3 d_m y}{2 L_a}, \text{ in} \quad (9-33)$$

Motion stresses due to pure shear can be calculated by substituting e_s for e_a in equations (9-27) and (9-28).

9. *Bellows under parallel offset* (fig. 9-21c):

TABLE 9-9.—Yield Strength, Limiting Bulging Stresses, and Allowable Motion Stresses of Frequently Used Bellows Materials

Material	Yield strength, psi	Limiting bulging stresses, psi		Allowable motion stresses, psi		
		$t \leq 0.012$ in	$t \geq 0.013$ in	1000 cycles	10 000 cycles	100 000 cycles
321 and 347 stainless steels	39 000	140 000	120 000	208 000	150 000	92 000
19-9DL	88 000	140 000	120 000	208 000	150 000	92 000
A-286	180 000	190 000	150 000	160 000	150 000	138 000
Inco 718	170 000	190 000	150 000	160 000	150 000	138 000
Inconel X	98 000	190 000	150 000	160 000	150 000	138 000
6061-T6 aluminum alloy	40 000	65 000		106 000	68 000	28 000



$$R_p = \frac{F_s}{y} = \frac{3 d_m^2 R_a}{2 L_a^2}, \text{ lb/in} \quad (9-34)$$

$$M = \pm \frac{F_s L_a}{2} = \pm \frac{3 d_m^2 y R_a}{4 L_a^2}, \text{ in-lb} \quad (9-35)$$

$$e_p = \frac{3 d_m y}{L_a}, \text{ in} \quad (9-36)$$

Motion stresses due to parallel offset can be calculated by substituting e_p for e_a in equations (9-27) and (9-28).

10. *Parallel offset of articulated bellows* (fig. 9-21d):

$$R_p = \frac{F_s}{y} = \frac{3 d_m^2 R_a}{2 [4 L_a^2 + 6 L_a L_b + 3 L_b^2]}, \text{ lb/in} \quad (9-37)$$

$$M = \pm \frac{F_s (2 L_a + L_b)}{2} = \pm \frac{3 d_m^2 (2 L_a + L_b) y R_a}{4 (4 L_a^2 + 6 L_a L_b + 3 L_b^2)}, \text{ in-lb} \quad (9-38)$$

$$e_p = \frac{3 d_m (2 L_a + L_b) y}{(4 L_a^2 + 6 L_a L_b + 3 L_b^2)}, \text{ in} \quad (9-39)$$

e_p can be substituted for e_a in equations (9-27) and (9-28) to calculate motion stresses.

11. *Bellows torsion*.—The stress due to bellows torsion is given by the twist of a thin tube:

$$S_t = \frac{2 T}{N_p \pi d_i^2 t}, \text{ psi} \quad (9-40)$$

$$R_t = \frac{T}{\phi} = \frac{1.37 \times 10^{-2} G d_i t N_p}{(2 h + 0.57 L) N_c}, \text{ lb-in/degree} \quad (9-41)$$

12. *Bellows squirm due to internal pressure*.—When a restrained bellows is pressurized internally beyond a critical level, it experiences a stability failure of the same type as a buckling column:

$$p_{cr} = \frac{5.02 R_a}{L_a \left(\frac{d_o}{d_i} \right)}, \text{ psi} \quad (9-42)$$

13. *Bellows buckling due to external pressure*.—When a bellows is pressurized externally, it buckles in same manner as a thin cylinder:

$$p_{cr} = \frac{4 E t N_p h^3}{(1 - \nu^2) d_m^3 p_b}, \text{ psi} \quad (9-43)$$

14. *Bellows squirm due to torsion*.—When a bellows is loaded by pure torsion, it tends to buckle in some manner as with internal pressure squirm:

$$T_{cr} = \frac{\pi d_m^2 R_a}{2}, \text{ in-lb} \quad (9-44)$$

The values for p_{cr} and T_{cr} of bellows under angular and offset deflections will be reduced considerably. A correction factor which ranges from 0.2 to 0.9, as determined by experiments, should be applied.

15. *Allowable working stresses for bellows materials*.—Bellows generally operate in the plastic range. However, it has been the practice to calculate stresses on the basis of elastic deformation, and correlate the data on that basis. In reality, the calculated stresses are only index stresses, which define the plastic conditions of the bellows, under the influence of pressure and motion loading. The yield strength, limiting bulging stresses, and allowable stresses of frequently used bellows materials are presented in table 9-9.

16. *Bellows used at elevated temperatures*.—For applications at elevated temperatures allowable working stresses for bellows materials must be adjusted accordingly. Generally, an internal liner should be provided to protect the bellows against high-velocity, hot-gas flows.

17. *Bellows forming limits*.—Bellows designs are limited by how severely the material can be worked during forming. Generally, the following geometric limits should be used for bellows up to three plys:

$$\text{Maximum: } \frac{d_o}{d_i} = 1.35 \quad (9-45)$$

$$\text{Minimum: } L = (8 + 2 N_p) t, \text{ in} \quad (9-46)$$

Sample Calculation (9-4)

Design a bellows, as shown in figure 9-4, for the oxidizer pump discharge flexible duct of the A-1 stage engine, with the following data and requirements, in addition to those given in sample calculations (9-1) and (9-2).

Bellows material, Inco 718

Thinning of bellows wall, 20 percent

Outside diameter of the convolution root of the bellows, $d_i = 8$ in

Free axial length of the bellows, $L_a = 7$ in maximum

Required angular movement, $\theta = \pm 3^\circ$

Life, 10 000 cycles

In addition, determine the following:

Bellows axial spring rate, R_a

Bending or angular spring rate of the bellows, R_b

Bending moments of the duct at 3° angular motion, M

Required restraining link load at maximum working pressure

Solution

We will first use the limiting bulging stress of the bellows material to establish the ratio of convolution height h to wall thickness t . From figure 9-22, wall-thinning correction factor $C_t = 1.36$, for 20 percent thinning. From table 9-9, the limiting bulging stress for Inco 718 at $t > 0.013$ inch is 150 000 psi. From sample calculation (9-2) the design limit pressure of the duct is 1925 psi. Substitute all these into equation (9-24) for a three-ply bellows:

$$S_b = \frac{C_t p h^2}{2 N_p t^2}$$

$$\frac{h}{t} = \sqrt{\frac{2 N_p S_b}{C_t p}} = \sqrt{\frac{2 \times 3 \times 150\,000}{1.36 \times 1925}} = 18.5$$

For a reasonable value of h , in a bellows of this size, we arrive at a wall thickness t of 0.022 in (after several tries):

$$h = 18.5 \times 0.022 = 0.407 \text{ in, say } 0.410 \text{ in}$$

The bellows root-mean-square diameter and the equivalent axial deflection due to 3° angulation can now be found:

$$d_o = d_i + 2h = 8 + 2 \times 0.410 = 8.820 \text{ in}$$

$$d_m = \sqrt{\frac{(d_i^2 + d_o^2)}{2}} = \sqrt{\frac{(8^2 + 8.82^2)}{2}} = 8.42 \text{ in}$$

From equation (9-30), the equivalent axial deflection of a bellows, due to pure bending or angulation:

$$e_b = \frac{d_m \sin \theta}{2} = \frac{8.42 \times \sin 3^\circ}{2} = 0.22 \text{ in}$$

Table 9-9 lists, for Inco 718 and a life of 10 000 cycles, an allowable motion stress of 150 000 psi. It is good practice, however, to use a lower value for high-pressure bellows designed for improved stability. In our design, we use a value of 0.36 times the limiting bulging stress. Thus, the motion stress = $0.36 \times 150\,000 = 54\,000$ psi. Substitute this and e_b into equation (9-27):

$$S_m = \frac{1.40 C_t E t e_b}{N_c h^2}$$

$$N_c = \frac{1.40 C_t E t e_b}{S_m h^2} \text{ (from fig. 9-22, } C_t = 1 \text{ for 20 percent thinning)}$$

$$= \frac{1.40 \times 1 \times 29.6 \times 10^6 \times 0.022 \times 0.22}{54\,000 \times (0.410)^2} = 22.1, \text{ say } 22$$

From equation (9-46), the pitch of the bellows

$$L = (8 + 2 N_p) t = (8 + 2 \times 3) \times 0.022 = 0.308, \text{ say } 0.310 \text{ in}$$

Free axial length of the bellows:

$$L_a = (N_c - 0.5)L + N_p t$$

$$= (22 - 0.5) \times 0.310 + 3 \times 0.022$$

$$= 6.66 + 0.066 = 6.726 \text{ in (i.e., less than 7 in)}$$

From figure 9-22, the correction factor C_t for the axial spring rate at 20 percent thinning is 0.72. Substitute this into equation (9-22) to obtain the axial spring rate of the bellows:

$$R_a = \frac{1.49 C_t C_p N_p E d_i t^3}{N_c h^3}$$

$$= \frac{1.49 \times 0.72 \times 0.85 \times 3 \times 29.6 \times 10^6 \times 8 \times (0.022)^3}{22 \times (0.410)^3}$$

$$= 4550 \text{ lb/in}$$

From equation (9-42), the critical internal stability pressure for bellows without angulation:

$$p_{cr} = \frac{5.02 \times R_a}{L_a \left(\frac{d_o}{d_i} \right)} = \frac{5.02 \times 4550}{6.726 \left(\frac{8.82}{8} \right)} = 3080 \text{ psi}$$

Comparing this with the maximum working pressure of 1750 psi, a safety factor of $3080/1750 = 1.76$ remains to allow for bellows stability under conditions of angulation.

From sample calculation (9-2), the yield pressure = 2117 psi, and the ultimate pressure = 2887 psi. Substitute these into equation (9-26), to obtain the yield hoop stress of the bellows:

$$\begin{aligned} S_h &= \frac{pd_m}{2N_p t} \left[0.57 + \left(\frac{2h}{L} \right) \right] \\ &= \frac{2117 \times 8.42}{2 \times 3 \times 0.022} \times \left[0.57 + \left(\frac{2 \times 0.41}{0.31} \right) \right] \\ &= 42\,000 \text{ psi (less than 170\,000 psi)} \end{aligned}$$

The ultimate hoop stress of the bellows:

$$S_h = \frac{42\,000 \times 2887}{2117} = 57\,300 \text{ psi (less than 200\,000 psi)}$$

The bellows design configuration is now established:

$d_i = 8 \text{ in}$	$d_o = 8.82 \text{ in}$	$d_m = 8.42 \text{ in}$
$t = 0.022 \text{ in}$	$N_p = 3$	$h = 0.41 \text{ in}$
$N_c = 22$	$L = 0.31 \text{ in}$	$L_a = 6.726 \text{ in}$
$R_a = 4550 \text{ lb/in}$		

From equation (9-29), the angular spring rate of the bellows

$$R_b = \frac{d_m^2 R_a}{458.4} = \frac{(8.42)^2 \times 4550}{458.4} = 705 \text{ in-lb/degree}$$

The bending moment on the duct at 3° angulation

$$M = R_b \theta = 705 \times 3 = 2115 \text{ in-lb}$$

From equation (9-25), the bellows pressure separating load

$$F_p = \frac{p(d_m^2 - d_d^2)\pi}{4}$$

The required restraining link load at maximum working pressure, considering the normal axial force

$$\begin{aligned} F &= F_p + \frac{pd_d^2\pi}{4} = \frac{pd_m^2\pi}{4} = \frac{1750 \times (8.42)^2 \times \pi}{4} \\ &= 97\,500 \text{ lb} \end{aligned}$$

9.6 DESIGN OF GIMBAL MOUNTS

Gimbal Design Considerations

Primary design considerations for gimbal mounts are:

1. *Required pivotal movement of engine assembly or thrust chamber for thrust vector control.*—Generally ranging from $\pm 4^\circ$ to $\pm 10^\circ$.
2. *Required adjustment for thrust alignment and positioning.*
3. *Thrust level.*—This determines the structural and bearing design of the gimbal mounts.
4. *Required operational life.*—Generally 1000 cycles minimum.
5. *Minimum deformation of the bearing surface, prevention of bearing surface galling.*
6. *Propellant duct installation.*—Some designs require flow of one of the propellants through the center of the gimbal mount.
7. *Maintenance of the gimbal mount.*—This is largely affected by the lubrication requirement of the bearing surfaces. If possible, a gimbal boot should be provided to protect the bearing surfaces from dust, water, and foreign materials.
8. *Lightweight.*—High strength-to-weight materials should be used.

Ring-Type Gimbal Mounts

Figure 9-23 presents a typical gimbal mount designed for low-thrust, upper stage engine applications up to 20 000 pounds. The design is a closed-yoke, flowthrough-ring-type gimbal, utilizing plain bearing pivot joints. This configuration provides for the main oxidizer duct to pass through the assembly in the longitudinal axis to the thrust chamber dome. The gimbal mount is designed to connect the vehicle main oxidizer

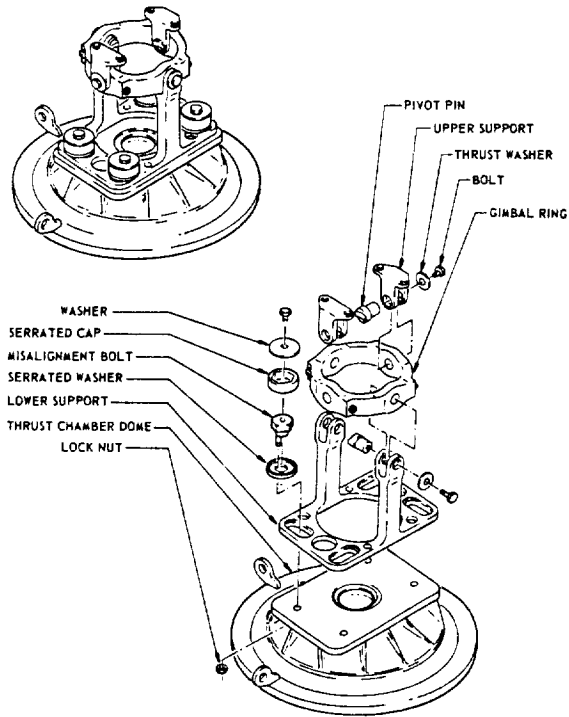


Figure 9-23.—Typical ring-type gimbal mount designed for low-thrust, upper stage engine applications.

duct and the top of the thrust chamber dome. The lower support of the gimbal mount provides an adjustment mechanism for thrust vector alignment. Except for the steel pivot pins and the alignment bolts, all other parts can be made of either aluminum or titanium alloys for minimum weight. The bearing surfaces of the pivot pins should be chromium or electroless nickel plated. Solid film dry lubricant coatings or grease may be applied to all bearing surfaces. The design bearing pressure of this gimbal type is about 10 000 psi of bearing projected area. The bearing coefficient of friction is around 0.08.

Cross-Type Gimbal Mounts

Figure 9-24 presents the design of a typical cross-type gimbal mount used on medium thrust engines (up to 200 000 lb), such as shown in figure 9-1. Here, the gimbal mount secures the engine assembly to the vehicle thrust frame, and is mounted to thrust chamber dome and elbow assembly. It consists of a cross-shaped unit

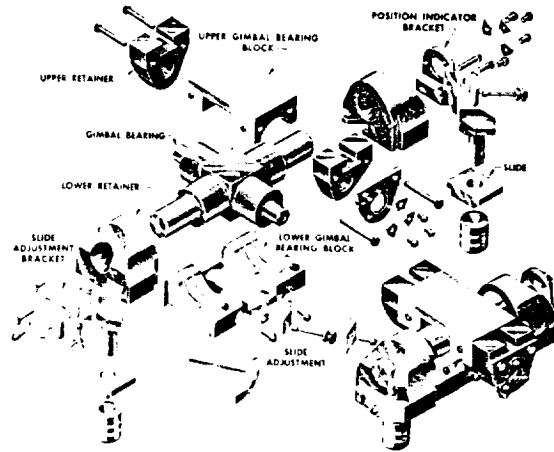


Figure 9-24.—Typical cross-type gimbal mount designed for medium-thrust engine applications.

incorporating bearing surfaces, upper and lower gimbal bearing blocks, upper and lower retainers, and thrust vector aligning slides. All parts of this design are made of 4340 alloy steel. The bearing surfaces of the cross unit are chromium or electroless nickel plated. The bearing surfaces are phosphate treated. Solid-film dry-lubricant coatings are applied to all bearing surfaces. The design bearing pressure of this type gimbal mount ranges from 15 000 to 20 000 psi of bearing projected area. The bearing coefficient of friction varies between 0.06 and 0.1.



Figure 9-25.—Typical socket-type gimbal mount designed for high-thrust engine applications.

Socket-Type Gimbal Mounts

Figure 9-25 presents a typical heavy-duty gimbal mount designed for high-thrust engine applications (up to several million pounds). This mount is also designed to secure the engine assembly to the vehicle thrust structure. The unit consists of integral upper and lower bearing blocks, and their retaining bar. All parts are made of alloy steel. The thrust load is carried by a socket-type spherical bearing located between two bearing blocks. The surface of the spherical socket has a Teflon-fiber-glass com-

position coating, which provides a dry, low-friction bearing surface.

The bearing surface on the sphere is electroless nickel plated. No lubrication or maintenance is required. For these gimbal mounts, design bearing pressures range from 24 000 to 28 000 pounds per square inch of bearing projected area. The bearing coefficient of friction is about 0.15.

Lateral adjustments for thrust alignment are accomplished using a tongue and groove arrangement between gimbal lower bearing block and thrust chamber dome.





Chapter X

Engine Systems Design Integration

10.1 SYSTEMS ENGINEERING

In the foregoing chapters the design of the major liquid rocket engine subsystems and their components has been discussed. By themselves, these subsystems cannot fulfill a useful purpose. Only when integrated into a whole will they function as a system and produce for what they were designed: thrust. While the engine designer thus must view the complete rocket engine as the system, he should not lose sight of the fact that, to the stage builder, the engine is again a subsystem. (In fact, to the launch vehicle systems engineer, the stage in turn becomes a subsystem, in addition to other stages, ground-support equipment, launch facilities, downrange stations, etc.)

In an earlier chapter the major engine parameters requiring optimization during implementation of rocket engine design were defined. It is apparent that the subsystems discussed will not form an optimized complete system unless they are designed for one another with this goal in mind from the beginning. The subsystems presented in the foregoing chapters have become highly specialized fields during recent years. Their designers and developers often have only a rather general feeling for the functions and peculiarities of the other subsystems. Their concentrated effort will not come about unless it is guided by an important function: systems engineering.

In most rocket engine projects this function is assigned to the "systems engineer," commonly called project engineer or project manager. In conformance with user requirements, he has the job of establishing all ground rules and performance parameters (ch. II) and to subsequently optimize them through complete integration of all subsystems during the entire design and development period.

Because of the previously discussed interaction of funding, time, and reliability, the project engineer must be a good manager, too, in addition to his engineering qualification. From his

superiors he needs adequate authority, commensurate with his responsibilities. He must have a broad and thorough understanding of the various disciplines governing the design and development of the subsystems. In view of the latter's high specialization, he cannot be expected to have a complete education in all these disciplines. However, in the words of Du Pont's Crawford H. Greenewalt, he must have "the ability to create a harmonious whole out of what the academic world calls dissimilar disciplines," and that in this respect his job may be compared to that of a "symphony conductor under whose hand a hundred or so highly specialized and very different talents become a single effort of great effectiveness."

The job of systems integration does not merely assure that all parts physically fit together, although this certainly is a first basic requirement. Wherever parts and subsystems join, an interface exists, a demarcation line between these systems. This may be a bolt hole pattern; a flow of fluid, heat, or electrical current; an exchange of forces, loads, or torques; or a complex dynamic interaction.

The importance of systems engineering is being recognized to an increasing degree. Figure 10-1 shows the final configuration of the engine for an early postwar ballistic missile. Comparing this to figure 2-4 we realize the progress made through good systems engineering. However, to have designed and developed a good-looking, perfectly functioning rocket engine is not enough.

It may appear superfluous to state that the design of rocket engines must also consider vehicle application. Yet in the daily grind of problem solving, engine detail design and development, this is easily forgotten. The rocket engine and component designer and developer who can think and converse in terms of vehicle application will be sought after indeed, and so will be the company he represents.

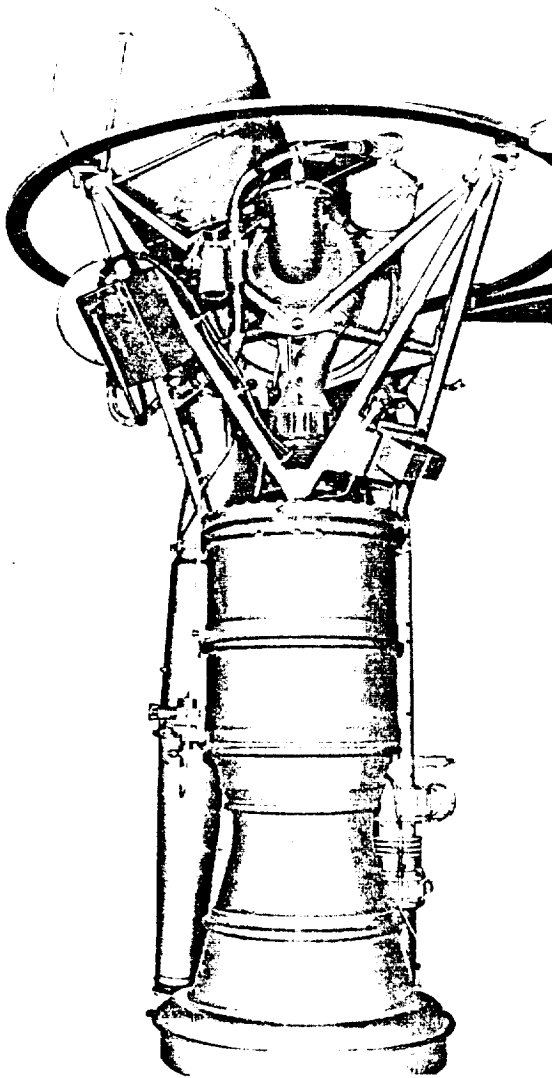


Figure 10-1.—Ballistic missile liquid rocket engine showing greatly improved simplicity.

Rocket engine design for vehicle application is a consideration not only for vehicle flight or for optimum mission performance. Long before the engine will fly, and after it has been designed and developed, it must be installed. The facets of engine installation in a vehicle range from more complex areas, such as guidance loop compliance and prestart conditioning to simple "nuts and bolts" problems, such as matching connecting fitting dimensions and attachment bolt sizes.

We can easily realize the importance of continuous and close communication between engine designer and vehicle builder. Complete and free exchange of correspondence, documentation and progress reports, frequent design reviews, and above all, prompt notification of changes is vital. During engine development, closest simulation of flight vehicle configuration, when performing static engine development tests, will materially reduce the possibility of later "surprises." Each vehicle type, according to its mission, will have somewhat different interface problems. Many of these occur, however, in almost any vehicle type.

10.2 ENGINE SYSTEM DESIGN INTEGRATION BY DYNAMIC ANALYSES

The Scope of Dynamic Analyses

Dynamic analyses are essential for optimum engine systems design integration, commensurate with vehicle mission requirements. Dynamic analyses may be grouped into two basic areas:

1. *Internal operating dynamics of the engine system.*—This refers to system schematic and control optimization, component optimization from a functional as well as system transient point of view, optimization of system start transients, minimization of cutoff impulse, determination of cutoff surges, etc.
2. *Engine-vehicle operating dynamics.*—This refers to vehicle tank pressurization systems design for adequate transient and steady-state engine performance, engine-vehicle structure and engine-guidance operating compatibility and stability, overall vehicle performance during special maneuvers, etc.

General Approach to the Analyses

The techniques and equations used, and the general approach taken by industry and Government agencies toward the solution of the various dynamic problems in rocket engine systems, are the result of many years of effort and experience in the areas of analysis, synthesis, and correlation of rocket engine operation. The philosophy governing this approach postulates that the relevant characteristics of any system depend on the characteristics of their components and physical

processes. By describing these components and processes in detail, as well as their interaction, the system can be described analytically with as much detail as is necessary. The complete set of equations then represents a mathematical model of the engine system.

Through the solution of the equations representing the mathematical model, the important characteristics of an engine system are studied, problem areas are defined, and improved component designs for the solution of these problems may be evaluated. Also, transient and steady-state engine systems operation, as affected by various component characteristics, may be simulated and checked by these dynamic analyses. If necessary, modifications will be incorporated prior to hardware testing.

Dynamic analyses, however, have their limitations, because not all of the physical processes involved in a given rocket engine system are immediately and/or thoroughly understood. As each of the processes becomes better defined functionally and quantitatively, confidence in the mathematical analyses increases.

Let us look at an example. The hydraulic head developed by a propellant pump is, as we know, a function of pump speed, flow rate, and geometry. We can write:

$$H = f(N, Q, r, A) \quad (10-1)$$

where

H = pump developed head, ft

N = pump speed, rpm

Q = pump flow rate, gpm

r = pump impeller radius, in

A = area normal to the meridional flow, in²

Correlations, such as equation (10-1), can be used to determine the interdependence of the many processes within an engine system.

Furthermore, equation (10-1) may be expressed as a specific form of function, as shown by equation (10-2), which is valid for a particular pump design only.

$$H = aN^2 + bNQ + cQ \quad (10-2)$$

When the numerical values of a , b , c are known, equation (10-2) becomes a quantitative description of a given pump design and a means to obtain the numerical solution of the operation of an engine system.

Some physical processes, such as thrust chamber combustion dynamics, are not always quantitatively fully understood. Rate of combustion is known to be a function of pressure, propellant type, mixture ratio, and combustion chamber geometry, but a specific quantitative expression for reliable use with rocket engine combustion chambers is not available. Certain system-start-transient analyses made with the aid of an engine model (set of equations like eq. (10-2)) have ideally assumed instantaneous combustion. Thus, combustion instability or thrust-chamber-feed-line, system-coupled instability is not described. This deficiency can be rectified by experimental systems evaluation.

Dynamic analyses can also be effectively used during the development-redesign phase of an engine system. Once test information is available, the predicted characteristics (with idealized assumptions) and the actual system operating characteristics can be compared. Differences can be noted and evaluated. This test-analysis cycle defines the limits of component performance and thus serves as a guide for the redesign of the components to be integrated into an optimum, final engine system. Similarly, from analyses of the engine-vehicle operating dynamics, and in conjunction with test results, the engine system and its components can be modified and improved.

Criteria for the Mathematical Model of an Engine System

The mathematical model of an engine system generally consists of a group of lumped parameters, and of linear or nonlinear algebraic and differential equations, which are formulated and then programmed for an analog or digital computer. Careful examination of an engine system schematic will be sufficient to determine whether a mathematical model will be possible for the system. This simply amounts to an observation of the many significant physical processes involved in the entire system which may be expressed mathematically. Some idealized assumptions are usually required to obtain a quantitative expression of the various equations. The physical significance of these assumptions must be understood before the mathematical model can become meaningful.

There are many ways to describe a rocket engine system mathematically. The choice will be based on the answers expected from the model. A model used to predict engine systems orificing requirements may call for high steady-state accuracy over a stated operating range, while the dynamic characteristics are of little consequence. A model used for the design integration of control components and subsystems may require good dynamic accuracy for intermediate frequencies (0.01-100 cycles/sec) and good static accuracy. A model needed to describe high-frequency effects (100-10 000 cycles/sec) may require little in the way of static accuracy, since the phenomena under study occur so rapidly that the system as a whole has no time to shift to new operating levels.

The mathematical model most frequently used is of the type employed for system main-stage operation and control design. This usually serves as the basic mathematical model of an engine system, with some modifications incorporated for other, special applications. In general, all mathematical descriptions of a basic model are for conditions around the systems design point, with the following assumptions:

- (1) All liquid propellant flows are incompressible and at constant temperature
- (2) All gas equations are based on perfect gas performance, where the gas properties are functions of composition
- (3) All vehicle-supplied parameters, such as main propellant tank discharge pressures, are constant.

Examples of Equations for a Mathematical Engine Model

The mathematical expressions and equations for the various physical processes and operating dynamics of a rocket engine may be derived from equations given in chapter I and in other chapters for the design of the various components. Here, we will present several typical examples to illustrate the application of these equations in a mathematical model.

1. *Pressure drop of fluid flow in a duct or component:*

$$p_1 - p_2 = a\dot{w}^2 + b\dot{w} - \rho h_{1-2} \quad (10-3)$$

$$a = \frac{K}{2g\rho A^2 R_a^2} \quad (10-4)$$

$$b = \frac{L}{Ag} \quad (10-5)$$

where

- p_1 = pressure at the inlet, psi
- p_2 = pressure at the outlet, psi
- a = design factor for turbulent flow pressure drop, $\text{sec}^2/\text{lb-in}^2$
- b = design factor for fluid inertia to changes in flow rate, sec^2/in^2
- \dot{w} = weight flow rate, lb/sec
- \dot{w} = change in weight flow rate, lb/sec^2
- h_{1-2} = gravity head of the fluid in the duct, in.
If the system is subject to an acceleration other than 1 g, this term must be modified
- ρ = fluid density, lb/in^3
- K = duct or component resistance coefficient, to be obtained from flow tests
- A = flow area of the duct, or flow area of the component at the design operating point, in^2
- R_a = component area ratio = component flow area/ A (at the design operating point, $R_a = 1$)
- L = length of the duct or component, in
- g = gravitational constant, $386.4 \text{ in}/\text{sec}^2$

2. *Combustion process and operating dynamics:*

Refer to figure 10-2, which describes schematically the combustion process. A transportation time delay is assumed, representing the time required for the propellants to pass through the injector and enter into the combustion process, and expressed as

$$\tau_o = \frac{\rho_o A_o (L_o + L_o')}{\dot{w}_o} \quad (10-6)$$

$$\tau_f = \frac{\rho_f A_f (L_f + L_f')}{\dot{w}_f} \quad (10-7)$$

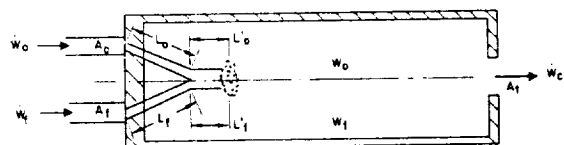


Figure 10-2.—Schematic description of the combustion process.

These can usually be indicated by the Laplace transformation operators $\rho^{-\tau o s}$ and $\rho^{-\tau f s}$. If we assume a homogeneous combustion gas, we can define the following correlations:

$$p_c = R' \left(\frac{T_c}{\mathfrak{M}} \right) \left(\frac{w_c}{V_c} \right) \quad (10-8)$$

$$w_c = w_o + w_f \quad (10-9)$$

$$R_o = \frac{w_o}{(w_o + w_f)} \quad (10-10)$$

$$w_o = \bar{w}_o + \int_0^t (\rho^{-\tau o s} \dot{w}_o - R_o \dot{w}_c) dt \quad (10-11)$$

$$w_f = \bar{w}_f + \int_0^t [\rho^{-\tau f s} \dot{w}_f - (1 - R_o) \dot{w}_c] dt \quad (10-12)$$

$$\dot{w}_c = \frac{A_t p_c g}{C^*} \quad (10-13)$$

$$\frac{T_c}{\mathfrak{M}} = f(R_o) \quad (10-14)$$

$$C^* = f(R_o) \quad (10-15)$$

where

- τ_o, τ_f = time required for oxidizer and fuel to pass through the injector and enter into the combustion process, sec
- ρ_o, ρ_f = density of oxidizer and fuel, lb/in³
- A_o, A_f = injector area, oxidizer and fuel, in²
- L_o, L_f = travel distance of injected oxidizer and fuel prior to impingement, in
- L_o', L_f' = travel distance of impinged oxidizer and fuel prior to combustion, in
- t = time period in consideration, sec
- \dot{w}_o, \dot{w}_f = injected flow rate of oxidizer and fuel, lb/sec
- \bar{w}_o, \bar{w}_f = weight of oxidizer and fuel stored in the combustion chamber volume, lb, at the beginning of time period t
- w_o, w_f = weight of oxidizer and fuel stored in the combustion chamber volume, lb, at the end of time period t
- s = complex operator in a Laplace transformation
- p_c = pressure of the combustion gas, psia
- T_c = temperature of the combustion gas, °R

- V_c = volume of combustion chamber from injector to throat, in³
- R' = universal gas constant, 18 528 in-lb/°R mole
- \mathfrak{M} = molecular weight of the combustion gas, lb/mole
- w_c = weight of the gas stored in the combustion volume, lb
- \dot{w}_c = flow rate of the gas emerging from the combustion chamber, lb/sec
- R_o = weight fraction of oxidizer stored in the combustion chamber
- A_t = throat area, in²
- g = gravitational constant, 32.2 ft/sec²
- C^* = characteristic velocity, ft/sec

These equations for the combustion process can be applied to engine main thrust chambers, gas generators, and other types of combustor.

3. Turbopump operating dynamics:

$$p_2 - p_1 = a N_p^2 \psi \quad (10-16)$$

$$a = \frac{4 \pi^2 r_p^2 \rho}{g} \quad (10-17)$$

$$\psi = f(\phi) \quad (10-18)$$

$$x = \frac{\phi \psi}{\eta_p} \quad (10-19)$$

$$T_p = b N_p^2 x \quad (10-20)$$

$$b = \frac{8 \pi^3 r_p^3 A_p \rho}{g} \quad (10-21)$$

$$N_t = R_g N_p \quad (10-22)$$

$$T_t = \frac{1485 \dot{w}_t \Delta H \eta_t}{N_t} \quad (10-23)$$

$$\Delta H = C_p T_o \left[1 - \left(\frac{1}{R_t} \right)^{\frac{\gamma-1}{\gamma}} \right] \quad (10-24)$$

$$I N_p = \int (R_g T_t - T_p) dt \quad (10-25)$$

Equation (10-25) is a torque-balanced equation for turbopumps. Any unbalanced torque between turbine and pump will initiate a change of shaft speed causing the integrand to seek zero.

where

- p_1 = pump inlet pressure, psia
 p_2 = pump discharge pressure, psia
 a = pump pressure rise design factor, lb-sec²/in²
 b = pump torque design factor, in-lb-sec²
 r_p = pump impeller radius, in
 A_p = pump flow area, in²
 ρ = density of the pumped fluid, lb/in³
 N_p = pump shaft speed, rev/sec
 N_t = turbine shaft speed, rev/sec
 R_g = speed ratio of the turbopump gear train
 T_p = torque at pump shaft, in-lb
 T_t = torque at turbine shaft, in-lb
 \dot{w}_t = turbine gas flow rate, lb/sec
 ΔH = available energy content of the turbine gas, Btu/lb
 C_p = turbine gas specific heat at constant pressure, Btu/lb-°F
 T_o = turbine gas total temperature at inlet, °R
 γ = turbine gas specific heat ratio
 R_t = turbine pressure ratio
 I = inertia of the gear train, referred to the main pump shaft, in-lb-sec²
 ψ = nondimensional pump head coefficient
 ϕ = nondimensional pump flow coefficient
 x = nondimensional pump torque coefficient
 η_p = pump overall efficiency
 η_t = turbine overall efficiency

Dynamic Analysis of Engine System Mainstage Operation

In general, engine design requirements at the mainstage level, as well as initial component and system specifications, can be determined with the aid of a mathematical model consisting of linearized descriptions of the complete engine system and a computer. Based on the static operating values at main stage (such as given in tables 3-2 to 3-5), the static design factors (such as a and b in eqs. 10-2, 10-3, 10-16, and 10-22) may be obtained. The primary dynamic analysis objectives for mainstage operation are:

- (1) Evaluation of the engine system schematic, with respect to mainstage operation
- (2) Evaluation of the dynamic characteristics, interactions, and the performance of various components at mainstage level.

This includes pressure drops in various flow passages, turbopump operating performance, and thrust chamber heat transfer and combustion characteristics

- (3) Optimization of engine system steady-state operation and performance, by properly calibrating and matching the design operating points of various components. (See sec. 10.3.)
- (4) Determination of engine system mainstage performance characteristics, including performance variations and engine influence coefficients. (See sec. 10.4.)
- (5) Evaluation of various engine control problems during main-stage operation, such as thrust and mixture ratio controls
- (6) Evaluation of various potential perturbations and their effects on mainstage operation

Once the basic mathematical model for the main-stage operation of an engine system is established, it can be utilized to study special problems with additional inputs. For example, a basic mathematical description of the 150 000-pound-thrust LO₂/RP-1 pump-fed rocket engine for an intermediate-range ballistic missile had been established on an analog computer. Following design of an additional engine-thrust-control subsystem, its electronics, main valves, and servovalve drive system were tied to an analog computer by suitable transducers to allow transient performance checkout and controller gain adjustment. An updated mathematical engine model, including the nonlinear perturbation, was then used for more detailed investigations of the thrust-control-loop dynamics.

Dynamic Analysis of Engine System Start and Cutoff Transients

The main objectives of dynamic analyses of engine system start transients are:

- (1) Investigation of the systems schematic for needed start-transient controls, such as type and quantity of control components, and sequencing and timing of their operation
- (2) Determination of thrust chamber ignition requirements
- (3) Estimation of start energy, time, and thrust buildup characteristics

- (4) Evaluation of component dynamic characteristics and interactions during start transients, such as combustion chamber ignition delays, gas generator temperature surges, and propellant pump stalling
- (5) Evaluation of system dynamic stability during the start transient. (The aim is to avoid prolonged operation at levels exhibiting system or thrust chamber instability.)
- (6) Evaluation of various potential perturbations and their effects on start transients, such as a start where the propellant-settling effects of gravitation are absent

For some engine systems, such as the LO_2/LH_2 turbopump-feed A-2 stage engine, dynamic analyses of its start transient become rather complex. They may include effects such as water hammer (wave equation) in the propellant feed systems, distribution of heat transfers and pressure drops throughout the high-pressure fuel feed system, choking of hydrogen gas in the chamber coolant passages, stall characteristics of the fuel pump, cavitation at the pump inlets, changes in fuel density in the pump caused by enthalpy changes from pumping, and many others. Because of this complexity, the equations of these mathematical models are usually programmed for a digital computer.

Figure 10-3 presents graphically the start transient model of a typical turbopump-feed engine system utilizing a gas generator for turbine drive. Valve timing, as well as pressure buildup characteristics of gas generator, propellant pumps, and main chamber are indicated. Other parameters, such as gas-generator combustion-gas temperature and propellant flow rates, can be included in the model.

Several alternate engine-start methods are usually simulated with the start model, in order to evaluate potential problem areas and to optimize systems start transient operation.

Important objectives of dynamic analyses of engine cutoff transients are:

- (1) Investigation of the systems schematic for needed cutoff transient controls, including operational sequencing and timing of various control valves
- (2) Evaluation of pressure surges and other adverse effects in propellant ducts and feed system components during the cutoff transient

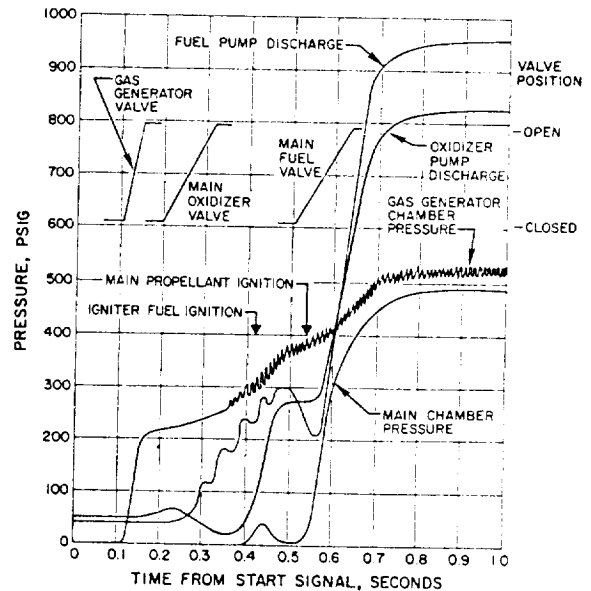


Figure 10-3.—Graphic presentation of the start transient model for a typical turbopump-feed engine system utilizing a gas generator for turbine drive.

- (3) Evaluation of possible temperature surges in main chamber or gas generator during the cutoff transient
- (4) Evaluation and optimization of total cutoff impulse, by minimizing cutoff time and improving repeatability
- (5) Evaluation of engine thrust decay characteristics

A series of cutoff sequences with modified shutoff timing of the control valves is usually simulated with the mathematical model. The various simulated cutoff runs are then analyzed to determine potential problem areas, and whether these problems are a function of the particular sequence used.

Figure 10-4 presents graphically the cutoff transient model of the typical engine of figure 10-3. The engine-thrust-decay characteristics are represented by the main chamber pressure decay curve. The integrated area under the chamber pressure versus time curve may be used to assess the engine cutoff impulse.

Dynamic Analysis of Engine-Vehicle Interactions

These analyses may be performed during the initial design phase of an engine system, as

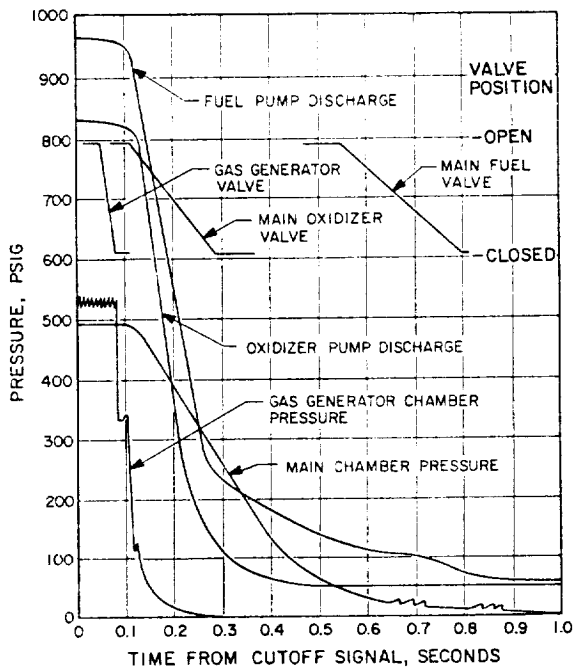


Figure 10-4.—Graphic presentation of the cutoff transient model of the typical engine of figure 10-3.

well as following development test firings. Areas of general interest to be analyzed may include, but should not be limited to—

- (1) Engine system operation and performance requirements from a vehicle mission point of view
- (2) Matching of engine propellant supply requirements with the vehicle propellant system, including dynamic evaluation of the vehicle propellant tank pressurization system, PU control system, vehicle acceleration and sloshing effects, and feed system-combustion coupled instabilities
- (3) Matching of the engine controls with the vehicle guidance system, including response of engine start, cutoff, thrust level, and vector controls to vehicle guidance commands
- (4) Simulation of interaction between engine systems operation and vehicle dynamics. (This may involve closed-loop coupling of an analog simulation of vehicle guidance and trajectory characteristics with an engine system during hot firing)

10.3 DESIGN INTEGRATION FOR ENGINE SYSTEM CALIBRATION

Design Requirements for the Calibration of an Engine System

Because of unavoidable mechanical tolerances, it may be expected that the operating characteristics and performance of the various engine system components will deviate somewhat from their nominal design value. A certain amount of calibration is always required for these components, as well as the engine system as a whole, to attain the desired engine performance characteristics within design specification. Therefore, provisions must be made in component and systems design to permit effective calibration during system integration.

The specific impulse I_s of an engine system is the ratio of thrust F to propellant weight flow rate \dot{w} . Thus, any deviations affecting F or \dot{w} will affect system performance. I_s also is a function of propellant mixture ratio. It is desirable, therefore, and beneficial to calibrate an engine system by adjusting its propellant feed system. Prior to complete engine system calibration, the pressure or pressure drop versus flow characteristics of each individual component should be calibrated and evaluated.

Hydraulic and pneumatic components, such as pressure and flow regulators, valves, flowmeters, ducts, and lines, can all be readily calibrated on flow benches. However, those components which operate at temperature extremes, such as thrust chamber assemblies, gas generators, and turbo-pumps, are best calibrated by combining the flow tests with actual hot firings. The characteristic propellant flow curve of an engine system is obtained by summing the pressure or pressure drop versus flow curves of the various components (figs. 10-5 and 10-6).

The general design approaches toward calibrating an engine system to attain its design thrust at design mixture ratio are:

- (1) The design operating point of each component should be kept within the relatively flat region of its pressure or pressure drop versus flow curve.
- (2) The mechanical tolerances and built-in adjustments of each component should be designed so that the random deviation

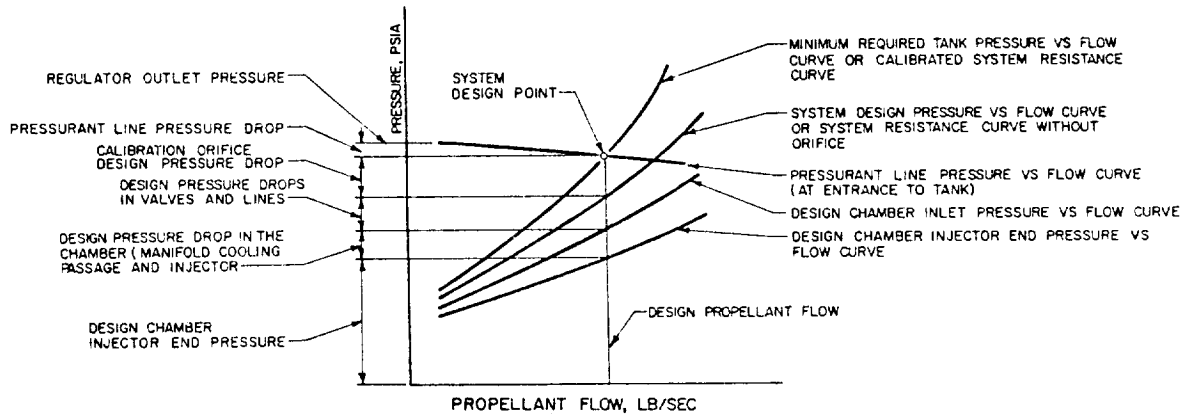


Figure 10-5.—Propellant flow design characteristics of a typical pressure feed engine system (oxidizer or fuel).

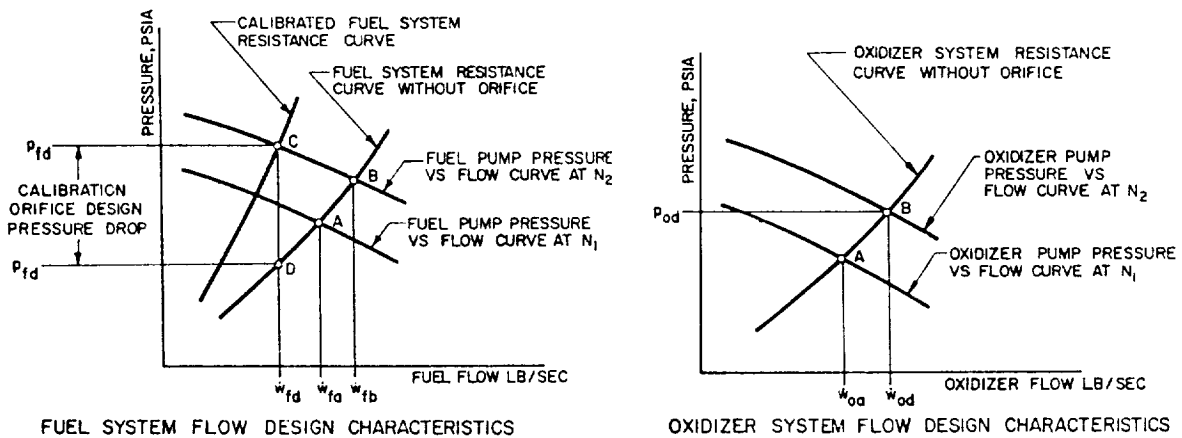


Figure 10-6.—Propellant flow design characteristics of the A-1 stage turbopump feed engine system.

of its flow characteristics from its design value will be kept within a reasonable limit, in order to facilitate systems calibration, and to keep other system components in their design operating region.

- (3) Sufficient pressure head should be set aside in each engine propellant feed system to compensate for contingencies due to component flow resistance deviations. The propellant feed system can then be calibrated by means of orifices or other adjusting means.

Design for Calibration of a Pressure Feed System

The first design step is the determination of the design flow rate of each propellant, as calculated from rated systems thrust, design mixture

ratio, and I_s (as verified by actual thrust chamber test firings). Based on these flow rates, the pressure drops of the various components at the design operating point can be estimated from previous design data, or as obtained from actual testing. Certain components may have to be newly designed for the specific design pressure drops allowed by the system.

The design pressure versus flow curve of either propellant flow system can be obtained by the summation of design chamber pressure versus flow and component design pressure drop characteristics, as shown in figure 10-5. In addition, an orifice is introduced in each propellant flow system for calibration. The minimum required tank pressure versus flow curve for each propellant is thus derived. In most pressure feed systems, the design orifice pressure drop for systems calibration determines the maximum

allowable cumulative pressure drop increase of the components above their nominal values. A suitable tank pressurization system can then be designed, compatible with minimum required tank pressure versus flow characteristics.

Sample Calculation (10-1)

The following data are available from analyses and component tests for the A-4 stage propulsion system, at rated thrust conditions:

Thrust chamber injector end pressure range required to maintain rated thrust = 110 ± 3 psia

Thrust chamber injector pressure drop range (both oxidizer and fuel) = 25 ± 2 psi

Thrust chamber oxidizer dome pressure drop = 3 ± 1 psi

Oxidizer line pressure drop = 5 ± 1 psi

Main oxidizer valve pressure drop (at the fully open position) = 4 ± 1 psi

Thrust chamber fuel manifold pressure drop = 4 ± 1 psi

Fuel line pressure drop = 4 ± 1 psi

Main fuel valve pressure drop (at the fully open position) = 4 ± 1 psi

Pressure allowance required for mixture ratio control by oxidizer valve vernier positioning (fig. 7-4) = ± 10 psi

Determine the design pressure drops of the calibration orifices, and the minimum required tank pressures for design flow rates.

Solution

The design pressure drop of a calibration orifice must be equal to the sum of the maximum pressure drop increases of components above their design values. Thus:

The design pressure drop of the oxidizer calibration orifice = $3 + 2 + 1 + 1 + 1 = 8$ psi.

The minimum required oxidizer tank pressure at the design flow rate = $110 + 25 + 3 + 5 + 4 + 8 + 10 = 165$ psia.

The design pressure drop of fuel calibration orifice = $3 + 2 + 1 + 1 + 1 = 8$ psi.

The minimum required fuel tank pressure at the design flow rate = $110 + 25 + 4 + 4 + 4 + 8 = 155$ psia.

Design for Calibration of a Turbopump Feed System

The propellant flow characteristics downstream of the pump discharges of a turbopump

feed system are similar to those of a pressure feed system. However, the difference in turbopump pressure or head versus flow characteristics from those of a pressurized system dictates a somewhat different approach to systems calibration. For mechanically coupled turbopump feed systems, such as the A-1 stage engine, systems calibration generally involves adjustment of the turbopump speed as well as the installation of an orifice in one of the propellant lines. For turbopump feed systems with dual turbine drive, such as the A-2 stage engine, the calibration can be accomplished by adjusting the speeds of both turbopumps.

The design principles for the calibration of mechanically coupled turbopump feed engine systems are best illustrated by a typical example, as shown in figure 10-6. Here, the propellant system resistance curves without orifices (representing conditions downstream of the pump discharges) are constructed based on the designs and test results of the components for the A-1 stage engine system. Next, the discharge pressure versus flow curves of both pumps are constructed from test data obtained with the A-1 stage engine turbopump, operated at speed N_1 . These pump curves intersect the corresponding system resistance curves at point A. At this speed, fuel flow rate \dot{w}_{fa} is above, and oxidizer flow rate \dot{w}_{oa} is below the required design flow rates, \dot{w}_{fd} and \dot{w}_{od} .

To achieve the design oxidizer pump flow \dot{w}_{od} , at a desired discharge pressure p_{od} , the design operating speed of the turbopump assembly must be raised to a required level N_2 by increasing the turbine gas flow. However, at this speed, the fuel pump, which is mounted on the same shaft as the oxidizer pump, would be delivering a flow rate \dot{w}_{fb} considerably above the required design flow rate \dot{w}_{fd} (point B in fig. 10-6). To reduce the fuel flow to \dot{w}_{fd} , a calibration orifice is placed in the fuel line. This amounts to increasing the fuel pump discharge pressure at constant speed N_2 to p_{fc} , where \dot{w}_{fd} is reached at point C. The pressure drop across the calibrating orifice is represented by $p_{fc} - p_{fd}$, where p_{fd} is the desired fuel pressure.

If fuel flow rate \dot{w}_{fa} is below and oxidizer flow rate \dot{w}_{oa} is above the required design flow rates, the calibrating process would be to speed up the turbopump to obtain the desired fuel flow,

and to place an orifice in the oxidizer line. However, it is generally desirable to place the orifice in the system of the propellant with the higher boiling point. In this situation, therefore, and also when the pressure drop across a calibrating orifice tends to become excessive, it is customary to trim the pump impeller so as to reduce the effective speed, and thus attain the required flow and pressure levels. In view of pump efficiency effects, it is desirable to trim the pump drawing the smaller horsepower, usually the one with the lower mass flow rate, except in cases of extreme density differences. The adjustment of the turbine gas flow rate, and thus the turbopump operating speed, can also be made by means of orifices in the turbine inlet gas line, or in the gas generator propellant lines.

In general, turbopump feed systems afford less stringent requirements for the various components regarding deviations from their design steady-state flow values, because the system is inherently more flexible. However, systems dynamic characteristics under transient conditions may restrict these deviations.

Sample Calculation (10-2)

The following design values and allowable deviations are given for the A-1 stage LOX/RP-1 engine system components, at rated thrust:

- Thrust chamber injector end pressure = 1095 ± 30 psia
- Thrust chamber injector pressure drop (both oxidizer and fuel) = 200 ± 20 psi
- Thrust chamber oxidizer dome pressure drop = 150 ± 10 psi
- Oxidizer line pressure drop = 25 ± 2 psi
- Main oxidizer valve pressure drop = 35 ± 3 psi
- Oxidizer pump specific speed, $N_s = 1980$ rpm
- Oxidizer pump suction pressure = 55 psia min
- Oxidizer pump discharge pressure at 7000 rpm and a design flow rate of 1971 lb/sec = 1505 ± 25 psia
- Thrust chamber fuel jacket and manifold pressure drop = 290 ± 20 psi
- Fuel line pressure drop = 10 ± 2 psi
- Main fuel valve pressure drop = 15 ± 2 psi
- Fuel pump specific speed, $N_s = 1090$ rpm
- Fuel pump suction pressure = 45 psia min
- Fuel pump discharge pressure at 7000 rpm and a design flow rate of 892 lb/sec = 1720 ± 25 psi

Determine the location of the calibration orifice, its nominal design pressure drop, and its expected range of adjustment.

Solution (see sample calculation (6-2))

The required oxidizer pressure head at the design point = 1095 + 200 + 150 + 25 + 35 = 1505 psia.

The required fuel pressure head at the design point = 1095 + 200 + 290 + 10 + 15 = 1610 psia.

Since the LOX pump discharge pressure is 1505 psia, but the fuel pump discharge pressure is 1720 psia, the calibration orifice must be located in the fuel system.

The nominal orifice design pressure drop = 1720 - 1610 = 110 psi.

From a detail analysis, we have found that the change of the fuel pump discharge pressure, as a function of turbopump speed increase or decrease, is a fraction of that of the oxidizer pump discharge pressure. Due to the effects of chamber pressure deviations, therefore, the maximum value of fuel calibration orifice pressure drop is required when the following conditions exist:

- (a) Thrust chamber injector end pressure is at its lower limit (1065 psia)
- (b) All pressure drops in oxidizer passages are at their higher limits
- (c) All pressure drops in fuel passages are at their lower limits
- (d) Oxidizer pump discharge pressure is 25 psi below its nominal value at the turbopump speed commensurate with the stated specific speed
- (e) Fuel pump discharge pressure is 25 psi above its nominal value, at the same speed

The equivalent required oxidizer pump discharge pressure under these conditions = 1065 + 220 + 160 + 27 + 38 + 25 = 1535 psia.

Required oxidizer pump developed head

$$H = \frac{144 \times (1535 - 55)}{71.38} = 2990 \text{ ft}$$

Oxidizer pump volumetric flow rate

$$Q = \frac{1971 \times 449}{71.38} = 12,420 \text{ gpm}$$

Substitute this into equation (6-7) to obtain the required pump speed

$$N = \frac{N_s H^{0.75}}{Q^{0.5}} = \frac{1980 \times (2990)^{0.75}}{(12420)^{0.5}} = 7190 \text{ rpm}$$

Fuel pump volumetric flow

$$Q = \frac{892 \times 449}{50.45} = 7950 \text{ gpm}$$

From equation (6-7), the fuel pump nominal developed head at 7190 rpm

$$H = \left(\frac{NQ^{0.5}}{N_s} \right)^{1.333} = \left[\frac{7170 \times (7950)^{0.5}}{1090} \right]^{1.333} = 4900 \text{ ft}$$

or

$$\frac{4900 \times 50.45}{144} = 1715 \text{ psi}$$

The equivalent fuel pump discharge pressure under these conditions would be $1715 + 45 + 25 = 1785$ psia.

The required pressure drop for the fuel line calibration orifice thus would be $1785 - 1065 - 180 - 270 - 8 - 13 = 249$ psi.

Similarly, a minimum fuel calibration orifice pressure drop is required when the following conditions exist:

- (a) Thrust chamber injector end pressure is at its higher limit (1125 psia), and conditions (b), (c), (d), and (e) above are reversed

The equivalent required oxidizer pump discharge pressure under these conditions = $1125 + 180 + 140 + 23 + 32 - 25 = 1475$ psia.

Required oxidizer pump developed head

$$H = \frac{144(1475 - 55)}{71.38} = 2870 \text{ ft}$$

Substitute this into equation (6-7); the required pump speed

$$N = \frac{1980 \times (2870)^{0.75}}{(12420)^{0.5}} = 6970 \text{ rpm}$$

From equation (6-7), the fuel pump nominal developed head

$$H = \left[\frac{6970 (7950)^{0.5}}{1090} \right]^{1.333} = 4730 \text{ ft}$$

or

$$\frac{4730 \times 50.45}{144} = 1666 \text{ psi}$$

The equivalent fuel pump discharge pressure under these conditions would be $1666 + 45 - 25 = 1686$ psia.

The required pressure drop of fuel line calibration orifice under these conditions would be $1686 - 1125 - 220 - 310 - 12 - 17 = 2$ psi.

Therefore the required range of adjustment for the pressure drop of the fuel line calibration orifice is from 2 to 216 psi.

10.4 ENGINE SYSTEM INTEGRATED PERFORMANCE CHARACTERISTICS

In the process of engine system design integration, an important task is the integration of engine system performance characteristics. These data are prepared and compiled by the rocket engine designer to provide the vehicle systems engineer with information necessary to integrate the propulsion system with the vehicle system. Where possible, a brief explanation of the data and its application should be included to provide clearer understanding and greater usefulness. The following are important aspects of integrated engine performance characteristics.

Nominal Engine Performance Values at Rated Conditions

These are usually prescribed by the engine model specification. These data are for engine system nominal steady-state operation, at rated conditions. Tables 3-2 to 3-5 are typical examples of nominal engine operating and performance parameters, which include nominal thrust, specific impulse, propellant combination, flowrates, mixture ratio, and various component operating data. Allowable deviations are specified for important parameters such as: thrust, ± 3 percent, and mixture ratio, ± 2 percent. Engine system specific impulse is usually specified at its minimum value. The performance of all deliverable engine systems must be above this minimum during acceptance tests.

In addition to tables for nominal engine performance parameters, nominal engine performance graphs such as chamber pressure versus engine thrust, and engine specific impulse versus engine thrust, are often included as additional monitoring aid. Figure 10-7 presents a typical performance graph for the A-1 stage engine system, of chamber pressure versus engine thrust at sea level.

Sample Calculation (10-3)

The following data were obtained from design analyses and component tests of the A-1 stage LOX/RP-1 engine system at nominal rated conditions; i.e., 750 000 pounds thrust at sea level:

Thrust chamber sea level specific impulse at 1000-psia nozzle stagnation pressure, and a mixture ratio of 2.35 O/F = 270 sec
Turbine exhaust gas specific impulse = 32.6 sec

Oxidizer pump developed head = 2930 ft
Oxidizer pump overall efficiency = 70.7 percent

Fuel pump developed head = 4790 ft
Fuel pump overall efficiency = 65.9 percent
Gas generator O/F mixture ratio = 0.408

Turbine gas available energy content = 359 Btu/lb

Turbine overall efficiency = 58.2 percent
Required auxiliary drive shaft power = 500 bhp

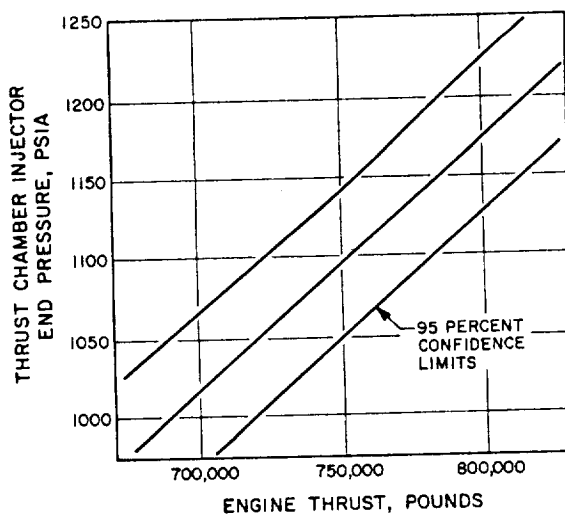


Figure 10-7.—Chamber pressure versus engine thrust at sea level for the A-1 stage engine.

Required oxidizer flow for vehicle tank pressurization = 3 lb/sec

Determine the following nominal performance values at rated conditions:

- Thrust generated by the turbine exhaust gas
- Thrust generated by the main thrust chamber
- Engine system propellant flow rates
- Engine system mixture ratio
- Engine system specific impulse

Solution

A trial-and-error method is used to solve this problem. Our first step is to approximate engine system and gas generator propellant flow rates. We substitute thrust chamber I_s into equation (1-28):

$$\dot{w} = \frac{F}{I_s} = \frac{750\,000}{270} = 2778 \text{ lb/sec}$$

The thrust chamber mixture ratio can now be used to approximate the corresponding oxidizer and fuel flow rates:

Engine oxidizer flow rate

$$\dot{w}_o = \frac{2778 \times 2.35}{(2.35 + 1)} = 1948 \text{ lb/sec}$$

$$\text{Oxidizer flow rate} = 1948 + 3 = 1951 \text{ lb/sec}$$

$$\text{Engine fuel flow rate } \dot{w}_f = 2778 - 1948 = 830 \text{ lb/sec}$$

From equations (6-12) and (6-13), the required oxidizer and fuel pump drive horse power for this approximation are:

$$\text{Oxidizer pump horsepower} = \frac{1951 \times 2930}{550 \times 0.706} = 14\,720 \text{ hp}$$

$$\text{Fuel pump horsepower} = \frac{830 \times 4790}{550 \times 0.659} = 10\,960 \text{ hp}$$

The corresponding turbine shaft horsepower:

$$T_{hp} = 14\,720 + 10\,960 + 500 = 26\,180 \text{ hp}$$

From equation (6-19), the corresponding turbine gas flow rate:

$$\dot{w}_t = \frac{0.707 \times 26180}{359 \times 0.582} = 88.4 \text{ lb/sec}$$

We use this value to start a new calculation cycle to separate main chamber and gas generator data.

The thrust generated by a turbine exhaust gas flow rate of 88.4 lb/sec = $88.4 \times 32.6 = 2880 \text{ lb}$.

Thus the main chamber thrust:

$$F_t = 750000 - 2880 = 747120 \text{ lb}$$

Thrust chamber flow rate

$$\dot{w}_{tc} = \frac{747120}{270} = 2769 \text{ lb/sec}$$

Oxidizer pump flow rate

$$= \frac{88.4 \times 0.408}{1 + 0.408} + \frac{2769 \times 2.35}{1 + 2.35} + 3$$

$$= 25.6 + 1942 + 3 = 1970.6 \text{ lb/sec}$$

Fuel pump flow rate

$$= (88.4 - 25.6) + (2769 - 1942) = 889.8 \text{ lb/sec}$$

Turbine shaft horsepower

$$T_{hp} = \frac{1970.6 \times 2930}{550 \times 0.706} + \frac{889.8 \times 4790}{550 \times 0.659} + 500 = 27090 \text{ hp}$$

Turbine gas flow rate

$$\dot{w}_t = \frac{0.707 \times 27090}{359 \times 0.582} = 91.7 \text{ lb/sec}$$

We use this value for another calculation trial:

The thrust generated by a turbine exhaust gas flow rate of 91.7 lb/sec = $91.7 \times 32.6 = 2980 \text{ lb}$.

Main chamber thrust $F_t = 750000 - 2980 = 747020 \text{ lb}$

Thrust chamber flow rate

$$\dot{w}_{tc} = \frac{747020}{270} = 2768 \text{ lb/sec}$$

Oxidizer pump flow rate

$$= \frac{91.7 \times 0.408}{1 + 0.408} + \frac{2768 \times 2.35}{1 + 2.35} + 3 = 1970.6 \text{ lb/sec}$$

Fuel pump flow rate

$$= (91.7 - 26.6) + (2768 - 1941) = 892.1 \text{ lb/sec}$$

Turbine shaft horsepower

$$T_{hp} = \frac{1970.6 \times 2930}{550 \times 0.706} + \frac{892.1 \times 4790}{550 \times 0.659} + 500$$

$$= 14850 + 11790 + 500 = 27140 \text{ hp}$$

Turbine gas flow rate $\dot{w}_t = \frac{0.707 \times 27140}{359 \times 0.582} = 92 \text{ lb/sec}$

This value closely confirms the assumptions for the last trial. Thus:

- (a) Nominal turbine exhaust gas thrust
= $92 \times 32.6 = 3000 \text{ lb}$
- (b) Nominal main thrust chamber thrust
= $750000 - 3000 = 747000 \text{ lb}$
- (c) Nominal thrust chamber propellant flow rate = $747000/270 = 2768 \text{ lb/sec}$
Nominal engine system propellant flow rate = $2768 + 92 = 2860 \text{ lb/sec}$
Nominal engine system oxidizer flow rate
= $\frac{92 \times 0.408}{1 + 0.408} + \frac{2768 \times 2.35}{1 + 2.35} = 1967.7 \text{ lb/sec}$
Nominal engine system fuel flow rate
= $(92 - 26.7) + (2768 - 1941) = 892.3 \text{ lb/sec}$
- (d) Nominal engine system O/F mixture ratio
= $1967.7/892.3 = 2.20$
- (e) Nominal engine specific impulse
= $750000/2860 = 262.4 \text{ sec}$

Engine Performance Variations Resulting From Off-Nominal Conditions

Engine performance characteristics at various off-nominal conditions must be available to the vehicle system engineer. They can be summarized in the graphic form such as figure 2-1 (engine thrust and specific impulse versus altitude curve), or by means of tabulated engine influence coefficients which will be discussed. The effects of off-nominal conditions of the following engine system performance parameters are considered vital for the design of a vehicle system:

- (1) Atmospheric pressure
- (2) Propellant densities
- (3) Pressures at the engine propellant inlets
- (4) Propellant mixture ratio and vehicle PU control
- (5) Vehicle acceleration
- (6) Throttling of the engine system

Engine Influence Coefficients

These are used to convert or correct steady-state, main-stage engine system performance parameters (dependent variables) from one condition to another of parameters (independent variables) such as atmospheric pressure, fuel temperature, oxidizer density, etc. This may be a correction to standard sea-level conditions (first-stage booster engine), or a conversion to other specified conditions. The coefficients are derived from the linearized solution of a set of steady-state differential equations which describe the performance of an engine system. These equations are solved by a digital computer and presented in tabular form, as shown in table 10-1 for the A-1 stage engine system. Each influence coefficient is expressed as a percentage and represents the change of a dependent engine variable, such as thrust, as produced by a 1-percent change in an independent variable, such as atmospheric pressure. A coefficient preceded by a positive sign (+) indicates that an increase of an independent variable produces an increase in the dependent variable. Conversely, a coefficient with a negative sign indicates a decrease in the dependent variable, as a result of independent variable increase. These influence coefficients are usually sufficiently accurate over the entire design operation range of an engine system.

Because the influence coefficients are linear, the total effects of several influences acting simultaneously on an engine system can be determined by summing the individual effects. For

example, the change of engine thrust for the A-1 stage engine system (without C* correction) can be expressed as:

$$\frac{(F - F_n)}{F_n} = \frac{C_1(p_a - p_{an})}{p_{an}} + \frac{C_2(\rho_o - \rho_{on})}{\rho_{on}} + \frac{C_3(\rho_f - \rho_{fn})}{\rho_{fn}} + \frac{C_4(p_{oi} - p_{oin})}{p_{oin}} + \frac{C_5(p_{fi} - p_{fin})}{p_{fin}} \quad (10-26)$$

where

- F, F_n = engine system thrust and its nominal value, lb
- p_a, p_{an} = atmospheric pressure and its nominal value, psia
- ρ_o, ρ_{on} = oxidizer density and its nominal value, lb/ft³
- ρ_f, ρ_{fn} = fuel density and its nominal value, lb/ft³
- p_{oi}, p_{oin} = oxidizer pump inlet suction pressure and its nominal value, psia
- p_{fi}, p_{fin} = fuel pump inlet suction pressure and its nominal value, psia
- C_1, C_2, C_3, C_4, C_5 = influence coefficients

Sample Calculation (10-4)

Estimate the thrust of the A-1 stage engine system operated at the following conditions, without considering the effects of C* correction:
 Atmospheric pressure, $p_a = 10.2$ psia
 Oxidizer density, $\rho_o = 71.00$ lb/ft³
 Fuel density, $\rho_f = 50.90$ lb/ft³
 Oxidizer pump inlet suction pressure, $p_{oi} = 65$ psia
 Fuel pump inlet suction pressure, $p_{fi} = 49$ psia

TABLE 10-1.—Influence Coefficient for the A-1 Stage Engine System

[Value of C* correction to be obtained from the C* correction versus mixture ratio curve shown in fig. 10-8]

A 1-percent increase of independent variables causes the following percentage change of dependent variables	Independent variables and nominal values					C* correction, 1.0000
	Atmospheric pressure, 14.696 psia	Oxidizer density, 71.38 lb/ft ³	Fuel density, 50.45 lb/ft ³	Oxidizer pump inlet suction pressure, 55 psia	Fuel pump inlet suction pressure, 45 psia	
Dependent variables and nominal values:						
Engine thrust, 750 000 lb	-0.1780	1.8750	-0.7420	0.0440	-0.0066	1.1030
Engine specific impulse, 262.4 sec	- .1780	.2650	- .0640	.0072	- .0150	1.1350
Engine mixture ratio, 2.200000	1.6420	-1.3650	.0270	- .0020	- .0260
Engine oxidizer flow, 1967.7 lb/sec.0000	2.0430	-1.1120	.0465	.0108	- .0632
Engine fuel flow, 892.3 lb/sec0000	.6530	.3120	.0207	.0045	.0094

Solution

From equation (10-26) and table 10-1:

$$\frac{(F - F_n)}{F_n} = \frac{(-0.178) \times (10.2 - 14.696)}{14.696} + \frac{1.875 \times (71.0 - 71.38)}{71.38} + \frac{(-0.742) \times (50.90 - 50.45)}{50.45} + \frac{0.044 \times (65 - 55)}{55} + \frac{(-0.0066) \times (49 - 45)}{45}$$

= 0.04531 or 4.531 percent

Engine system thrust of an altitude, where $p_a = 10.2$ psia:

$$F = 0.04531 \times F_n + F_n = 0.04531 \times 750\,000 + 750\,000 = 784\,000 \text{ lb}$$

Nonlinear Corrections

When the linear approximation is not sufficiently accurate, the usefulness of the engine influence coefficients can be extended by a technique which allows nonlinear corrections for certain parameters. An example of this method is the C^* correction. For instance, a plot of C^* correction versus engine mixture ratio change may be used in conjunction with a table of influence coefficients such as figure 10-8 and table

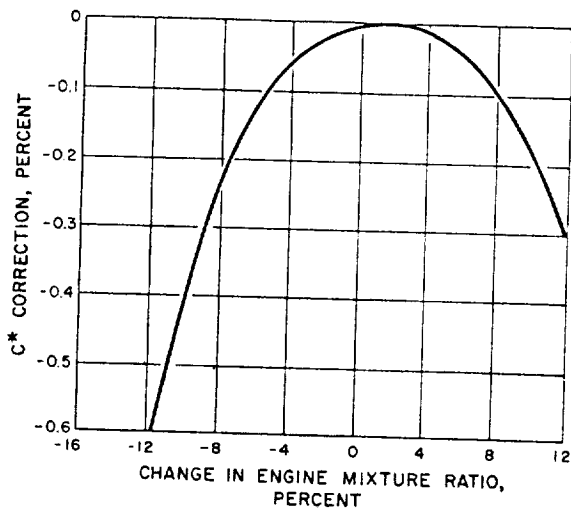


Figure 10-8.— C^* correction versus change in engine mixture ratio curve for the A-1 stage engine.

10-1, which are for the A-1 engine system. The change of engine mixture ratio is computed for changes in atmospheric pressure, propellant densities, etc., assuming the C^* correction first to be zero. For the resultant change in engine mixture ratio, the C^* correction is read from the graph. The value of C^* correction found is then used with other independent variables to compute the changes in the remaining dependent variables.

Sample Calculation (10-5)

Estimate the thrust of the A-1 stage engine system operated at the conditions listed for sample calculation (10-4), adding the effects of C^* correction. Also, for the same conditions, estimate the thrust assuming an additional mixture ratio error of +10 percent, due to faulty calibration.

Solution

By analogy with equation (10-26) and using table 10-1, the engine system mixture ratio change due to the conditions of sample calculation (10-4) are determined as

$$\frac{(MR - MR_n)}{MR_n} = \frac{1.642 \times (71.0 - 71.38)}{71.38} + \frac{(-1.365) \times (50.90 - 50.45)}{50.45} + \frac{0.027 \times (65 - 55)}{55} + \frac{(-0.002) \times (49 - 45)}{45} = -0.0162 \text{ or } -1.62 \text{ percent}$$

From figure 10-8, the C^* correction for a mixture ratio change of -1.62 percent is approximately -0.02 percent. From table 10-1, the influence coefficient for engine system thrust is 1.1030, for a 1 percent C^* correction. Thus

$$\begin{aligned} (\text{Percent change in } F) &= 4.531 + (-0.02) \times 1.103 \\ &= 4.509 \text{ percent} \end{aligned}$$

Therefore, engine system thrust considering effects of C^* correction:

$$F = 750\,000 \times (1 + 0.04509) = 783\,820 \text{ lb}$$

If the mixture ratio error of 10 percent is added, the total mixture ratio change = 10 - 1.62

= 8.38 percent. From figure 10-8, the C^* correction then is approximately -0.11 percent.

Thus

$$\begin{aligned} (\text{Percent change in } F) &= 4.531 + (-0.11) \times 1.103 \\ &= 0.441, \text{ or } 4.41 \text{ percent} \end{aligned}$$

Engine system thrust:

$$F = 750\,000 \times (1 + 0.0441) = 783\,080 \text{ lb}$$

10.5 MECHANICAL INTEGRATION OF ENGINE SYSTEMS

Basic Considerations

Besides combining all components and subsystems functionally and physically, the design for mechanical integration of an engine system must consider the overall envelope of the system and its weight. This includes the location of the system's center of gravity. Also, it should permit simplified maintenance and checkout practices. Judicious packaging design techniques should be applied to minimize the number of interconnecting hydraulic, pneumatic, and electrical lines, with their attendant fittings, connectors, joints, and other potential trouble spots. Welded and brazed joints should be used as much as possible. Problems introduced by vibration, high temperatures and pressures, leakage and space restrictions are thus more easily handled. Engine mechanical integration is a vital part of the system design concept; therefore, all factors related to integration and packaging of components and subsystems must receive careful consideration early in the preliminary design stage.

In general, a modular engine packaging approach should be selected such as used for the A-1 (fig. 3-2) and A-2 (fig. 3-4) stage engine systems, as well as for many advanced operational engine systems. This assures engine integrity from time of manufacture through vehicle launch. It also provides a compact package for ease of handling, transportation, and installation in the vehicle. Ease of checkout and component accessibility is also afforded by the packaging concept.

The engine should be completely assembled in the manufacturer's plant. Subsequent acceptance testing, air transportation, and installation

in the vehicle in the field should not require assembly of additional major components. Integrity of the propellant feed and hot-gas systems, once verified in a complete system during acceptance test, is not necessarily nullified by the need to temporarily disassemble the engine for shipment. The integrated engine package concept provides added assurance that static test-stand firing results have verified structural soundness of the package to a substantially greater degree, than is the case for a system where the vehicle provides portions of the engine structure.

An example of a special case of mechanical integration of a liquid propellant rocket engine is the prepackaged storable liquid rocket propulsion system shown in figure 8-1. This system is a completely integrated assembly of all-welded construction, consisting of thrust chamber assemblies, propellant tanks, pressurization system, and necessary controls. This provides maximum assurance of system integrity from the time of manufacture, which includes loading of the propellants, through delivery, vehicle assembly, and launch. Complete propellant separation until systems start is achieved by hermetically sealed burst diaphragms for maximum safety. Acceptance tests are conducted by taking sample units at random from the production line, and hot firing them. In addition, destructive tests of various types are performed.

Packaging of Rocket Engine Components

Most major rocket engine components, such as thrust chamber (fig. 4-1) and turbopump (fig. 6-14) assemblies, readily form a logical, independent mechanical unit by virtue of their function and their physical shape. However, in the case of minor components such as control valves, gas generators and igniters, packaging design principles can best be served by making them an integral part of a major component assembly, or to integrate them by grouping. A typical example is a gas generator assembly externally attached to a turbine inlet flange (fig. 3-2). Similarly, gas generator propellant valves and combustor can be integrated into one unit (fig. 4-51).

Certain types of hydraulic and pneumatic rocket engine control components lend themselves most conveniently to the packaging design. Here, one of the main objectives is to

reduce line runs, by combining all parts and passages into one housing. Such a housing (or mounting plate) is relatively leakproof, trouble areas now being limited to external line connections to other components. Furthermore, if components are packaged in this manner, reductions of weight and size are achieved through the use of common walls and through the elimination of extra mounting platforms, clamps, and fasteners. Since relatively few packages are required as compared to the usually large number of individual components, maintenance of such a system is greatly simplified. Integrated packages are about as easily removed and replaced as are the separate components making up each package. However, the packaged design is not necessarily desirable for every control system. Each case must be carefully studied.

As a rule, one or a combination of the following methods is used for packaging engine control components:

- (1) Bank packaging: A group of similar flat-sided component assemblies are bolted together in a bank or stack, with common porting through the mating surfaces from one unit to the next.
- (2) Subplate packaging: Attachment of two or more individually housed components to a subplate, so that all ports of the individual component housings lead into the subplate manifold, through their mating surfaces with the subplate, and on to the systems plumbing.
- (3) Cartridge packaging: Two or more components housed individually in cylindrical cartridges are in turn assembled in a common body with suitable manifolding to the systems plumbing.
- (4) Multiple-component packaging: Detail parts for two or more components are assembled in a normal fashion in a common housing or body.

Figure 10-9 presents a typical pneumatic control package for a large liquid propellant rocket engine. This package combines two pressure-regulator assemblies, two relief valves, a series of solenoid valves, filter units, and check valves. It controls the flow of helium gas to various engine components. When engine start is initiated, the helium control solenoid is energized allowing helium to flow through the main pres-

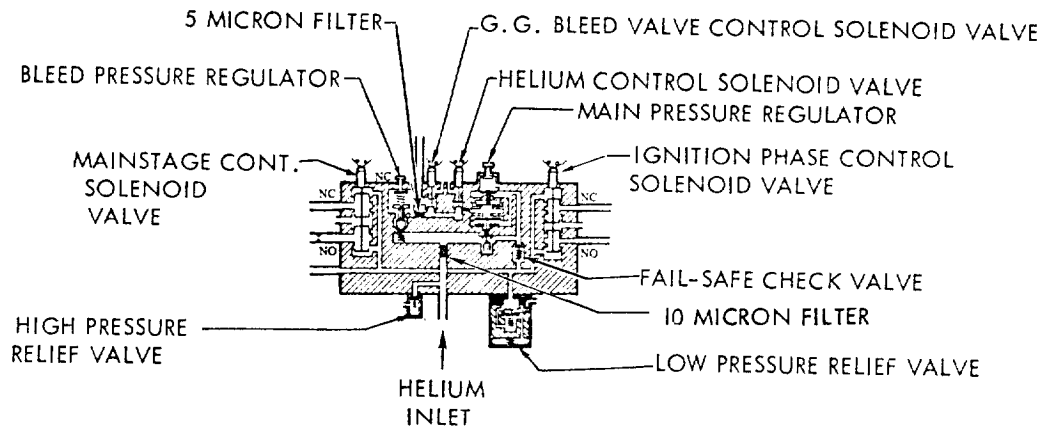
sure regulator to the control system. The helium is routed internally to the main control valves through a fail-safe check valve. This insures that the various engine propellant valves remain pressurized and thus open, should the helium gas supply system fail.

Packaging of Turbopump Feed Engine Systems

In earlier high-thrust rocket propulsion systems, some of which may still be in operational use, all major engine components were mounted into a cage-shaped thrust mount, which was bolted to the vehicle thrust frame by way of lugs. Figure 2-4 shows several typical examples. With these systems, vehicle steering was accomplished by means of carbon jet vanes protruding into the jet (V-2 and Redstone), or by swiveling the thrust chamber (Thor, Jupiter). In the latter case, the high-pressure feed lines between pumps and injector had to be much more flexible than for misalignments and thermal expansion/contraction alone.

Most advanced liquid rocket engines are tightly packaged. All major components are attached to the main thrust chamber, directly or by means of mounting structures, as shown in figures 3-2, 3-4, and 9-1. Here, the thrust chamber serves as the principal structural member of the entire engine system. For steering, the complete engine package is gimballed from a gimbal bearing which attaches directly to the thrust chamber dome. The other half of the bearing is attached to the vehicle thrust structure. The low-pressure propellant supply ducts must be sufficiently flexible to accommodate the gimbal motions. It is noted that vehicle steering through gimbaling of a single engine or chamber is effective only for the pitch and yaw planes. For roll control, at least two engines are required. For vehicles with a cluster of engines, therefore, this poses no difficulties. For single-engine vehicles, special roll-control devices are needed. These may be small auxiliary nozzles, possibly simultaneously used as vernier engines after main-engine cutoff. The use of the turbine exhaust for roll control has also been proposed.

Whether the engine attaches to the vehicle thrust structure by means of a thrust frame or a gimbal bearing, either device must be designed to be capable of transmitting the full thrust



PNEUMATIC CONTROL PACKAGE SCHEMATIC

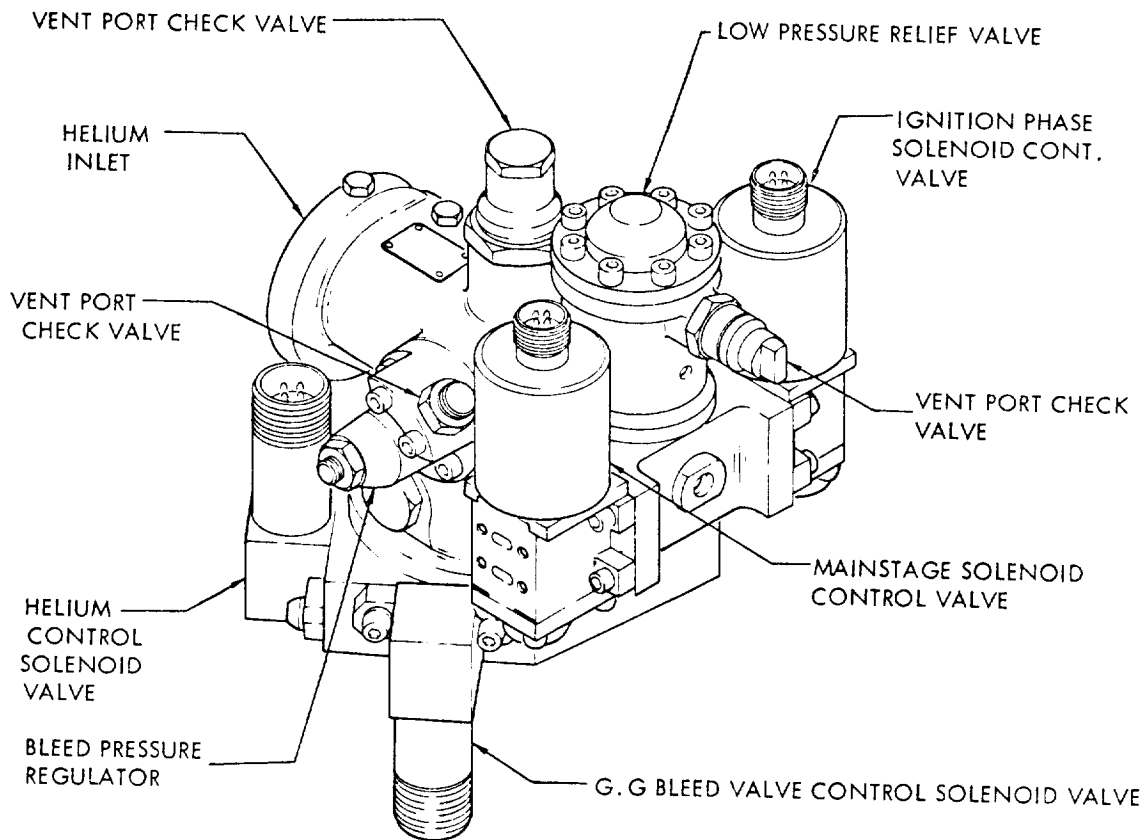


Figure 10-9.—Typical pneumatic control package design used in liquid propellant rocket engine systems.

forces at full gimballed deflection, including an adequate reserve for normal and for side loads. The bolt-hole pattern must permit adjustment for tolerance deviations. In general, engine and vehicle attachment halves must be designed for one another.

Figures 10-10 and 10-11 illustrate the packaging design details of a typical pump feed system. It is a $LO_2/ RP-1$, fixed-thrust engine with constant chamber pressure control. The basic engine package consists of the following sub-packages:

- (1) Gimballed main thrust chamber assembly (thrust chamber, injector, dome, oxidizer elbow, and gimballed mount)
- (2) Turbopump assembly (propellant pumps, turbine, gearbox, lube pump, electric heater, auxiliary drive)
- (3) Gas generator assembly (combustor, control valves, regulator and turbine inlet duct)
- (4) Main oxidizer duct assembly (including main oxidizer valve)
- (5) Main fuel duct assembly (including main fuel valve)
- (6) Turbine exhaust duct assembly (including heat exchanger)
- (7) Engine start subsystem (oxidizer and fuel tanks, control valves)
- (8) Turbopump lube subsystem (lube oil tank and fittings)
- (9) Pneumatic control package

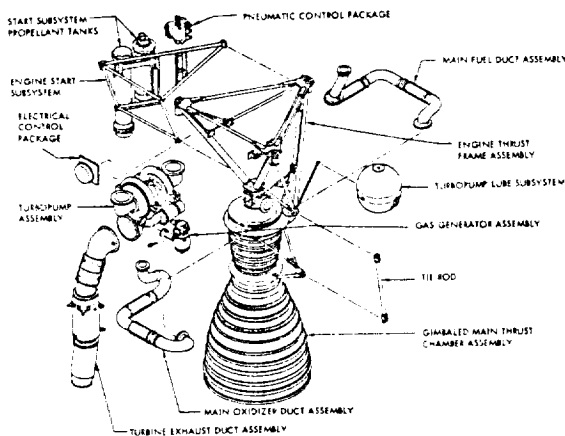


Figure 10-10.—Major component and subsystem packages of turbopump-fed liquid propellant rocket engine.

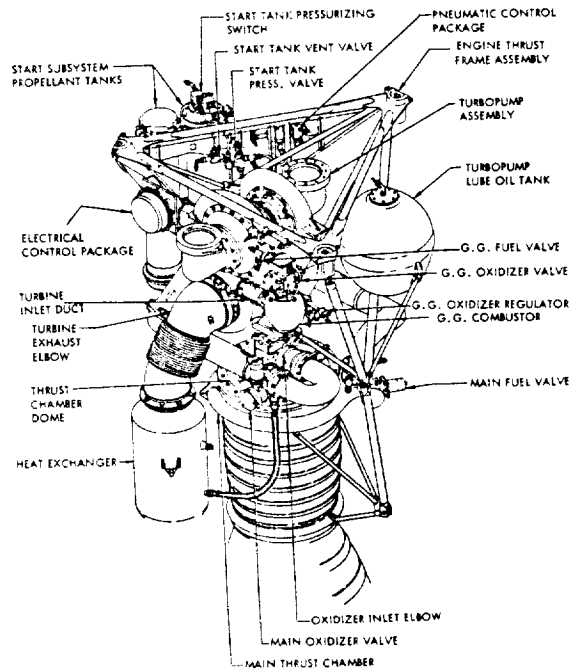


Figure 10-11.—System packaging design detail of the engine shown in figure 10-10.

- (10) Electrical control package
- (11) Engine thrust frame assembly

The majority of the major component and subsystem packages are installed within or at the periphery of the engine thrust frame assembly. The main thrust chamber assembly is attached to the thrust frame through a gimballed mount.

Mechanical Protection of Engine System Packages

It is normal that several years may elapse between the date a liquid propellant rocket engine is completed and accepted by the user, and its vehicle flight. Design, therefore, must consider means to protect the engine system package in transit or storage against moisture, dirt, and shock. These include simple closures, such as caps, plugs, and cover plates applied to valve and regulator vent holes, propellant inlets, and to other openings. Frequently, these closures contain desiccant bags and indicators which warn, through change of color, of undesired intrusion of moisture. Certain lines, however, may require communication with the ambient air

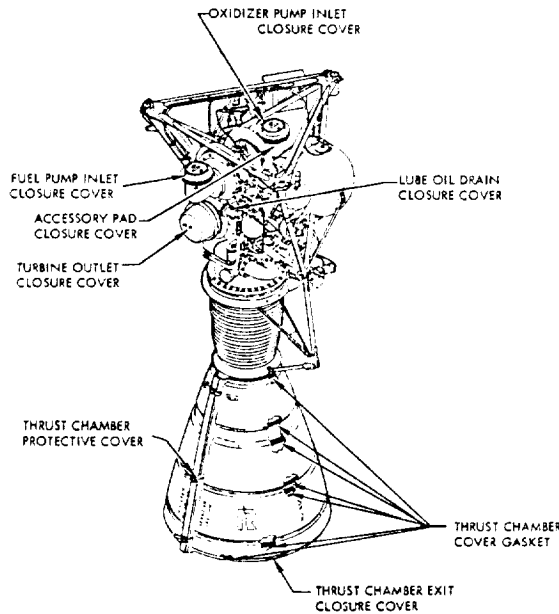


Figure 10-12.—Various protective closure covers for the engine shown in figure 10-10.

("breathing"). In this case, the closures may be equipped with desiccant filters to permit access of dry air only. Some of the covers must be removed for installation of engine to vehicle. Others will be left in place until the engine is actually operated. These must be readily accessible and clearly marked, such as with bright colors, to prevent their being left in place inadvertently. Figure 10-12 shows the location of various protective closures for the Rocketdyne LR79-NA-11 engine.

10.6 ELECTRICAL SYSTEM

All rocket engines depend on some type of electrical system for their operation. This is true for solid systems, where at least ignition is initiated electrically, as well as for liquid systems, in which the electrical system assumes numerous additional tasks. As with any common household device, electrical circuits in rocket engines have caused troubles, due to poor design, misapplication, abuse, poor maintenance, human errors, and wear. Properly applied, however, electrical circuits can substantially simplify the operation of a rocket engine, and will increase its usefulness and reliability. There

are many tasks, such as sequencing which can be accomplished much more effectively electrically than would be possible by mechanical means.

It is not possible nor necessary, in the framework of this book, to describe the physical laws and the general fundamentals of electrical circuitry. They are covered abundantly in the literature. Moreover, in contrast with most other basic liquid engine subsystems, the rocket engine designer will try to use commercially available "off the shelf" components for his electrical system. However, other cognizant members of the design team will have to provide the basic circuit diagram (schematic) and other data in support of the installation of the required electrical components. Characteristically, the electrical system of a rocket engine is one of the last subsystems to be "frozen" before production. This is because sequencing for start and stop represents one of the major engine development activities, often resulting in repeated modification of the electrical system as development progresses. Emphasis is therefore placed on the flexibility of electrical design. More recently, this process has been greatly aided by dynamic analyses (see sec. 10.2).

Electrical Schematic

The complete electrical schematic of a typical liquid rocket engine system, including its ground- and vehicle-based elements, fills a sizable drawing. With the aid of figure 10-13, which presents a portion of an earlier engine static-firing schematic, the basic features are discussed as follows. In ordinary wiring diagrams, such as that of a radio receiver, all the contacts of, for instance, a multiple switch or a tube are drawn to appear in the same location, as they do in reality. This requires numerous wire crossovers in the diagram. The number of crossovers would become prohibitive in a typical engine electrical schematic and may lead to confusion and errors. For rocket engine purposes it has long been found preferable to draw the basic diagram so as to show each circuit separately. In this "functional flow diagram," the various contacts of a relay, for instance, appear in different places, and often away from the circuit for the corresponding relay coil. The

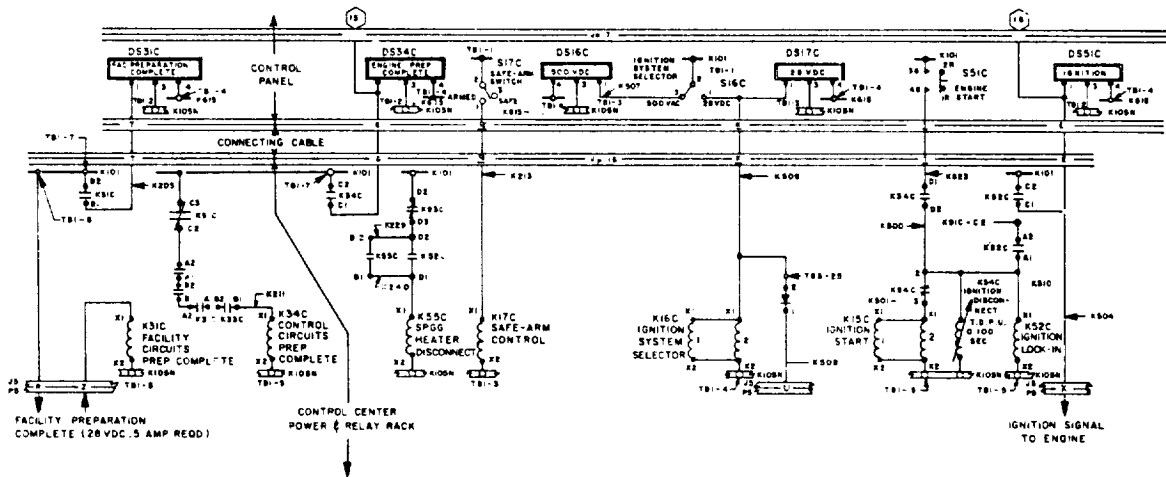


Figure 10-13.—Typical liquid rocket engine electrical diagram (partial).

drawing system also will materially simplify later troubleshooting. The diagram, of which figure 10-13 shows a portion, was drawn sequentially from left to right; i. e., circuits which are energized during test preparation and start are shown in the left portion, while those associated with the cutoff sequence appear on the right.

In the schematic, connectors are shown as continuous double lines, or portions thereof, running horizontally through the diagram (J16, P16 = receptacle 16 and plug 16, etc.).

Each of the contacts is called out by a letter (T, G, K, etc.). All wires are numbered, as indicated. Power buses, like connectors, are shown as horizontal lines, or portions thereof (heavy, single line = positive buses, usually shown near the top of the drawing; and double lines = negative or ground bus). The meaning of the remaining symbols becomes clear by following the circuit at the left of figure 10-13. Plug P5 is shown connected to the main power bus K101 at terminal TB1-8. If certain facility signal contacts are properly closed, such as those verifying "Cooling water OK," "Firex armed," "Observer on Station," and many more, power returns through plug P5, contact "Z," and is applied to relay coil K31C. The "B" contact of this relay closes a circuit to lamp DS31C, which lights up. The "A" contacts of the same relay are in the chain to the coil of K34C, together with the normally open contacts of several other relays, such as K29C, "Heater Power On," and

K28C, "Hypergol Cartridge Installed," as well as the normally closed contacts of cutoff relay K91C. If all contacts are properly closed, the "C" contacts of K34C will cause signal light DS34C to light up. Following selection of the ignition power source by means of switch S16C, ignition can now be initiated by means of push-button S51C, since the "D" contacts of K34C are now closed, and provided ignition disconnect timer K54C has not picked up (TDPU = time delayed pickup : 0.1 sec). In the diagram, several circuit elements appear which are part of other circuits not discussed. Note that in places two relays are used in parallel (e.g., K16C), if the number of contacts required is too large for one relay. The numbers shown in hexagonal frames refer to the channels of an inking sequence strip chart recorder or equivalent instrument. A special test bus K615 is provided which when energized makes all signal lights go on and thus permits spotting burnt-out bulbs.

In earlier engine designs, many of the elements shown in figure 10-13 were installed in an engine-mounted relay box. The trend has been to place as many parts of the electrical system on ground as possible. This is easier with first stages, which start while still connected to ground, or even held down mechanically until released, for brief periods following start, than it is with upper stages which must start and stop, and sometimes restart, some time after takeoff. Because of individual approach and of

preferences for the types of interlocks, safeguards required, and type of component used, two designers of a comparable engine may arrive at substantially different electrical diagrams. Specifically with respect to the number of interlocks and monitoring circuits applied, caution is advised, since these circuit elements by themselves are subject to malfunction and may do more harm than good.

The diagram discussed above employed relays, well-developed types of which continue to be used in several of today's rocket engines. In others, solid-state (transistorized) switches are being applied which fulfill a similar function. Solid-state switches have the advantage of requiring no moving parts and thus are much less sensitive to vibration effects. A circuit of this type is shown in figure 10-14. It functions as follows:

Transistor Q_2 is held in a "turned off" mode by maintaining the base at a higher voltage potential than the emitter. This is achieved by inserting a bias voltage, V_2 . As can be seen, as long as there is no appreciable current flow in R_4 , the base potential will be essentially V_0 , while that at the emitter is $V_0 - V_2$. Thus, Q_2 will remain off.

Transistor Q_1 is held in a "turned off" mode in a similar fashion, except that here the base

must be at a lower potential than the emitter. This is accomplished by inserting a bias voltage, V_1 , in the emitter leg, which raises the emitter potential V_1 volts above ground. Again, as long as no appreciable current flows through R_1 and R_2 , the base will essentially be at ground potential, and Q_1 will remain off.

When input voltage V_{in} is applied, current I_1 will flow. This raises the Q_1 base potential, until the combined Q_1 base-emitter voltage, (V_{be1}), plus bias voltage (V_1), is overcome. At this point, current will flow into the base (I_{b1}) causing the transistor to turn on. This occurs when

$$R_3(I_{cb01}) > (V_{be1} + V_1) \max \quad (10-27)$$

When Q_1 turns on, resistor R_4 is switched to ground, and current I_{C1} begins to flow. As I_{C1} increases, the potential at the base of Q_2 is lowered until it reaches the combined potential of V_2 and the Q_2 base-emitter voltage, V_{be2} . At this point, current I_{b2} flows out of the base of Q_2 and the transistor "turns on," thereby supplying current to the load. This occurs when

$$R_5(I_{cb01} + I_{cb02}) > (V_2 + V_{be2}) \max \quad (10-28)$$

The switch is turned off by either removing the input signal, V_{in} , or by using another static switch to ground the base of Q_1 .

Switch lock-in (to maintain output after input signal is removed) is accomplished by feeding the output voltage back to the input through a diode. In this case, shorting the base of Q_1 must be used to turn off the switch.

Figure 10-15 shows a typical solid-state switch module. Following assembly, a module is immersed in a potting compound. Overall module dimensions after potting are comparable to those of a matchbox.

Figure 10-16 shows a small portion of an engine-mounted sequence-controller diagram. The modules shown, together with the others required for engine operation, including connecting wiring and connectors, are housed in a hermetically sealed box or can.

Although the two diagrams are not related, the signal emitted at pin X of receptacle J-5 in figure 10-13 would be suitable to initiate engine start at contact A of plug P51 in figure 10-16. Similarly, the signal emitted from pin K of plug

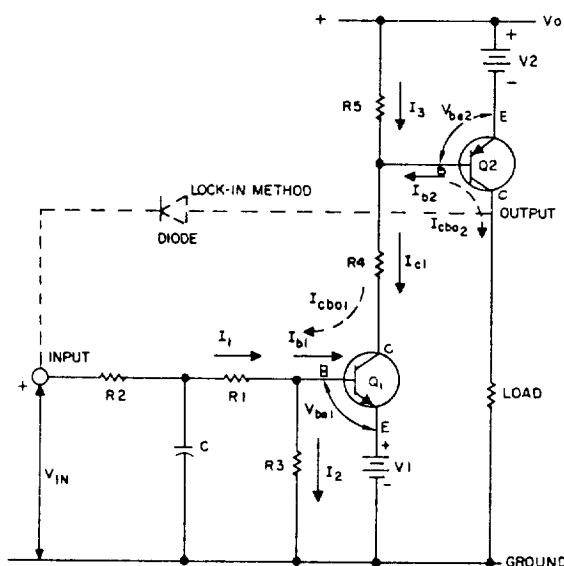


Figure 10-14.—Typical rocket engine solid-state switch circuit or "module" diagram.

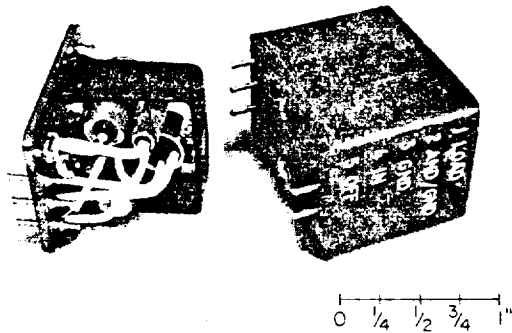


Figure 10-15.—Assembled solid-state switch module before and after potting.

P51 in figure 10-16, with the aid of an auxiliary relay, could be used to assure engine readiness in the chain leading to the coil of relay K34C in figure 10-13.

Electrical Components

To implement rocket engine electrical circuitry such as the one partially shown in figure 10-13, a number of components are required. These are:

Relays and Switches

Relays and, more recently, the solid state switches are used to receive usually low current command signals from the vehicle or ground control center and to translate them into properly sequenced actuation signals to igniters, control valves and other elements. In combination with interlocking relay contacts, bias voltages, valve position switches, continuity monitors, temperature sensors, spark plug monitors, voltage sensors, timers, and other devices, they form an engine-contained logic which will execute a sometimes elaborate starting sequence in response to only two external signals: start and stop. In practice many more signals are exchanged between engine and vehicle and/or

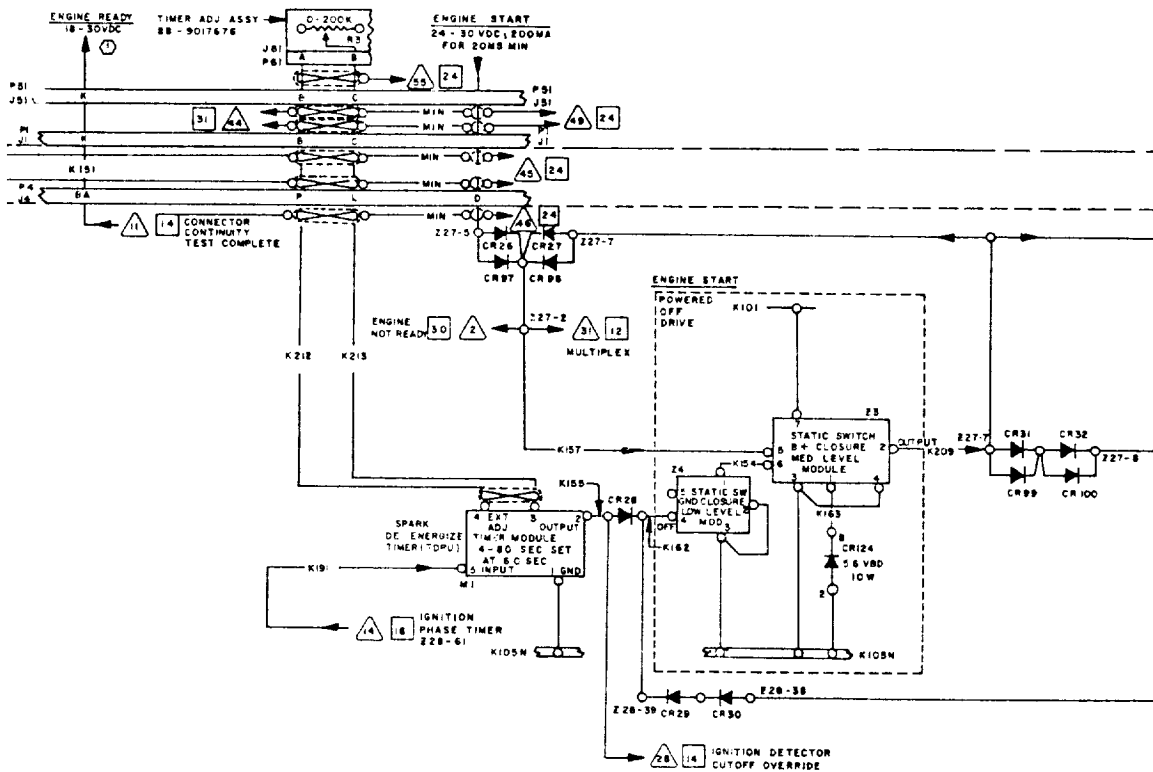


Figure 10-16.—Portion of a typical engine-mounted sequence controller diagram using solid-state switches.

ground control center, for checkout, monitoring, confirmation, instrumentation, telemetry and emergency reaction systems. Also, power supply connections are required.

The relays and switches, together with supporting circuitry elements such as resistors, capacitors, diodes, terminal strips, and connecting wiring, are best housed in a common box. This sequence controller is hermetically sealed and often includes temperature-conditioning provisions by means of electrical heaters (typical power requirement: 200 watts) or inert gas purges. The engine systems designer very likely will receive from the cognizant department merely a "black box" description of the sequence controller, giving external and mounting bracket dimensions, connector descriptions, and installation specifications, with all internal detail omitted. Because of miniaturization, relay boxes or sequence controllers have become very compact units. Figure 10-17 shows a typical can. Note brackets for engine attachment. In addition to approximately 30 modules, numerous diodes, resistors, timers, etc., the container shown

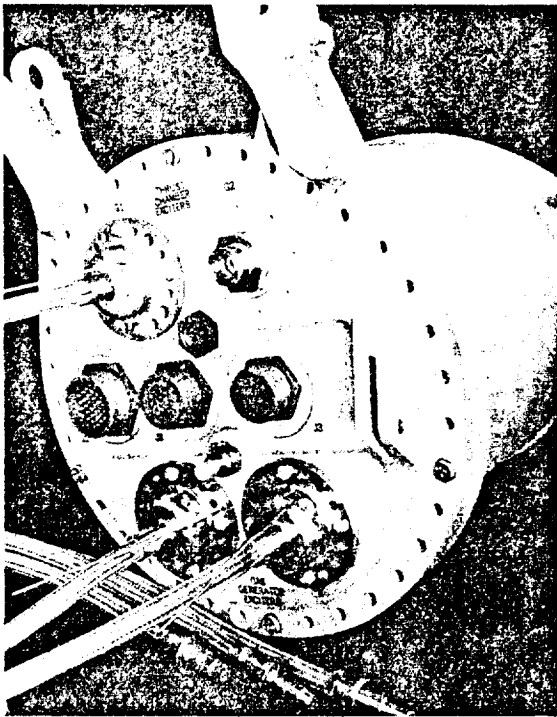


Figure 10-17.—Liquid rocket engine sequence controller.

houses 4 exciter coils for the spark plugs of thrust chamber and gas generator.

Position Indicators

To verify the position of a valve, or the proper installation of an igniter and similar mechanical conditions, position indicators are used. Most common types are:

Switches.—These are mainly used for "black and white" indications, such as "open" or "closed," "installed," "connection OK," etc. Numerous commercial products are qualified for rocket engine application and are available as compact, miniaturized, sealed units. They are part of the individual component designs and are described in other chapters. It will be the burden of the engine systems designer, however, to assure uniform standards, specifically for connectors. Position indicators of the switch type are instrumental for sequencing the start and stop of a liquid rocket engine.

Continuous indicators.—To know any intermediate position of a component, such as the angular position of a valve gate or the linear displacement of an actuator, continuously reading devices are required. Most widely used types are potentiometers and variable reluctance pickups. Potentiometers require a dc power source (typical: 5 volts), while inductive-type sensors require an ac power source (such as 400 cps, 28 volts). The output of both, often in combination with a bridge circuit, is fed to a telemetry and/or ground recording system. Indicators of the continuous type are predominantly used for instrumentation. It should be a goal to decrease their number as the development of the engine progresses.

Timers

During engine start and stop, timing devices are required for two principal reasons: correct sequencing of valve actuations and other events, and for monitoring the correctness of critical sequence times. In the latter case, they will inhibit progression of the sequence or initiate cutoff in case of malfunctions. A degree of timing can be accomplished by means of orifices and by sizing of volumes in the pneumatic or hydraulic activation system. All other timing must be provided by timers as part of the electrical system. For engine systems starting on

the ground, these timers are mostly located in the ground control system. Several types of timers are commercially available for this application. They may be motor driven or may use dashpots, springs, or other delaying devices for their function, usually with the capability for external adjustment within a specified range. If ground mounted, the timers' weight and size are of minor importance.

For systems starting at altitude, all timers required must be engine mounted (or at least stage provided). Here, weight and size do become important. Modifications of the solid-state switches described above, through addition of suitable capacitance/resistance circuits, have been successfully applied. As a rule, these timers are not adjustable once assembled, but require replacement of the entire module in case of timing changes.

Heaters

Ideally, all components of an engine system should be capable of operating reliably and unaided at all temperatures occurring during operation. In many applications, however, extreme temperature variations occur, due to the environment at high altitudes, or within an engine system, particularly within those using cryogenics. The development of components able to withstand these extremes without assistance would often be very costly or altogether impossible. Thus it is much simpler to reduce or eliminate the temperature extremes by suitable means. For some areas, mere insulation may be adequate. Others require heating (external means for cooling are rarely required for rocket engines, but are used for other vehicle systems). Bulk temperature conditioning is usually provided on static firing stands and within vehicles during standby by blowing preheated inert gases or air into the engine compartment. However, certain strategic components will require individual heating at all times after propellant loading. Of these, some may require this only through takeoff from a 28-volt dc ground source, if their heat capacity keeps them sufficiently warm for their relatively short period of operation following heater disconnect. Other components, particularly those which have to operate during extended periods following takeoff, will require supply from an airborne power source, which is usually the 28-V

main battery. Because of the relatively high power requirements for heaters airborne heating should be kept to a minimum. This can be accomplished by judicious placement of components away from areas of extreme cold, and by insulation and isolation. For instance, a hydraulic pump attached to the auxiliary drive of a LOX pump, or the actuator of a cryogenic valve (see fig. 10-18, near center) may require drastically reduced heating, or none at all, if a heat barrier (gasketlike wafer of suitable material) is placed between connecting flanges. Furthermore, in the hydraulic system of an engine, heating requirements may be completely avoided if the hydraulic fluid is continuously circulated during standby.

For cases where electrical heaters must be applied, a number of types are available. A common one is the blanket heater, which is applied externally as a sleeve or cover, formfitted for best efficiency, and equipped with a thermostat.

In other applications, an immersed heater, i.e., a Calrod-type heating element cast or embedded into the component metal, is used, for instance, to protect a cryogenic pump bearing.



Figure 10-18.—Wire harness installation for main valve position switches.

Power Sources; Batteries

For its operation, a rocket engine electrical system requires power which is almost always supplied by the vehicle or from the ground. The engine designer need not concern himself with the power supply, except for the specification of requirements and provisions for connection.

Frequently used voltages are:

- 28-volt dc for heaters, control solenoids, relays, switches, igniter spark excitors, certain instrumentation (typical peakload: 2000 watts per engine)
- 5-volt dc for instrumentation (potentiometers)
- 8-volt dc for spark monitors (see ch. IV, spark plugs)
- 115-volt, 400-cps ac for instrumentation

The required power is supplied directly from batteries for dc needs, or through converters for ac consumptions.

Miscellaneous Components

To complete an engine electrical system, a number of standard or special components are required: resistors, capacitors, diodes, terminal strips, connectors, and receptacles. All are commercially available, qualified for rocket engine use.

Connecting Wiring

The various subsystems of the engine electrical system must be connected by suitable wiring, which for proper mounting and clean routing is combined into one or several wire harnesses.

Figure 10-18 shows portion of a harness installed on a liquid rocket engine. For manufacture, the engine systems designer must supply certain information. This is best combined into a single drawing, which contains the following information (fig. 10-19):

- (1) *Wire list.*—This list calls out each harness wire by number and lists its length. It also specifies the wire routing between plugs and/or receptacles.
- (2) *Harness schematic.*—For clarity, the schematic repeats in pictorial form most of the information supplied in the wire list, together with additional information. It also calls out the total length of wire required for material procurement purposes.
- (3) *Physical routing diagram.*—This diagram

defines the branch points and their relative distance from the main plug or receptacle.

It is usually difficult to determine the exact length of individual wires and of some of the branches on the drawing board. It is customary to finalize these dimensions on a mockup engine. For this reason, certain dimensions in the physical routing diagram are left blank and the total cable length is specified "as required."

For proper design of a rocket engine wire harness, the following must be considered:

- Routing (minimum distance, weight, electrical resistance, interference)
- Secure clamping (safety, avoidance of wire chafing)
- Selection of attachment points (avoidance of special brackets)
- Adequate support (harness weight, vehicle acceleration)
- Moisture protection (potting, sheathing)
- Heat protection (routing, wrapping)
- Arcing protection (component selection, dryness)
- Flexibility (installation, stiffness versus gimbal load)

Connectors must have means to secure them to prevent accidental disconnect. This has been done with the connectors shown in figure 10-18 by means of threaded sleeves, further secured by safety wires. To prevent incorrect connections and/or damage to the connector pins, "clocking" by means of key and slot, of connectors and receptacles, is highly recommended.

In addition to the cabling required to interconnect the various engine electrical subsystems, other cables are required to link these systems to the vehicle systems. This includes wiring for power supply, controls (start and stop, PU, throttling, etc.), instrumentation and check-out circuits. To facilitate engine installation and line connections, these wires are combined into trunks, each terminating in connectors which must have, at the proper location, a mating counterpart on the vehicle. For the stage, a "J-Box" (junction box) is recommended, into which are plugged both the engine and the stage systems connectors. On the inside, the box permits easy and environment protected redistribution of incoming and outgoing wires to assigned connectors. Figure 10-20 shows a typical block

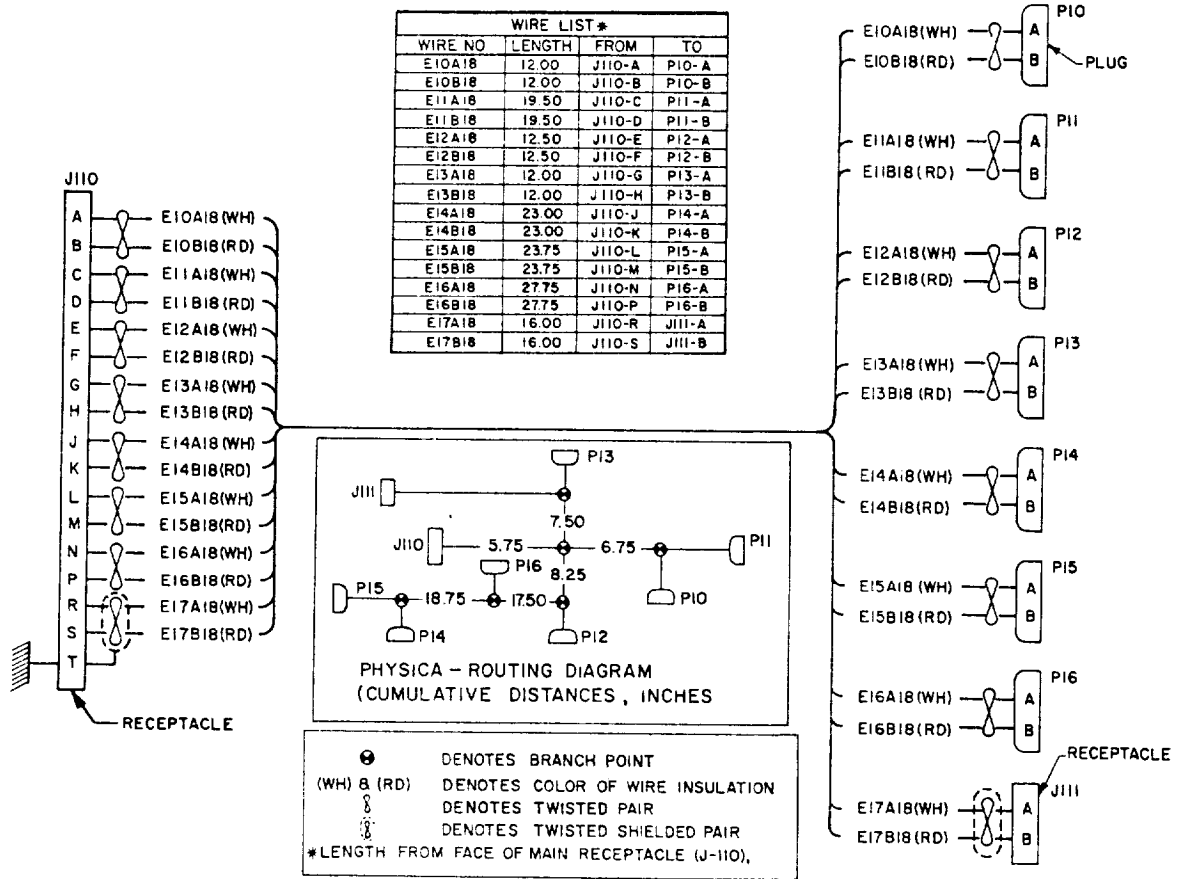


Figure 10-19.—Typical rocket engine wire harness diagram.

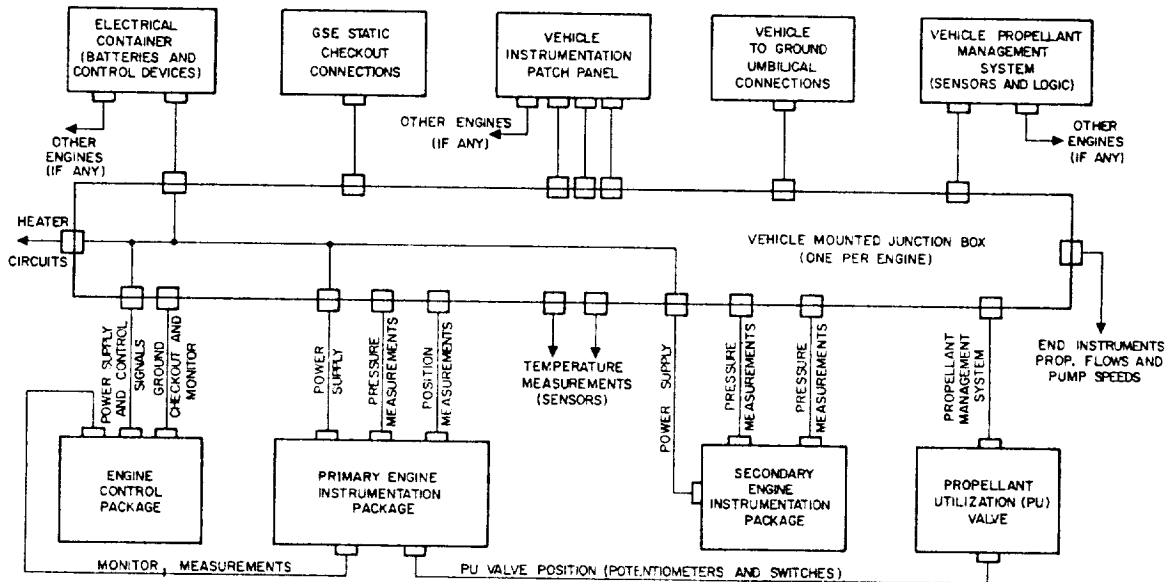


Figure 10-20.—Typical block diagram, engine to vehicle electrical connections.

diagram for the principal electrical connections between engine and vehicle. Flexibility of these trunks usually poses no problem in view of the relatively small engine deflection during gimbaling, but if heavy sheathing (armor) is used, care must be taken to avoid excessive loads to the gimbal actuators or damage to the cables.

10.7 ENGINE INSTRUMENTATION

To evaluate the quality of his design during and after test, to monitor progress, and finally to "sell" his engine to the customer, the designer needs recorded evidence of the engine's overall performance. These records may broadly be classified by two categories: visual inspection and measurements.

Visual inspections are self-explanatory. They consist, often after disassembly of a component, of an inspection for cracks, fractures, deformations, signs of overheating, etc. Surface discolorations may often be a sign of fluid leaks. In fact, minute amounts of a dye have been added to a number of propellants such as alcohol- and the kerosene-type fluids, which leave qualitative evidence at the leak spot. Visual checks assume a particularly important role in the event of serious malfunctions. As a rule, they do not require special preparations by the designer, except perhaps written instructions (drawing callouts) and forms.

By contrast, the second category, measurements, does require consideration during engine design. To make the required measurements, instruments are needed. Some of these may be simple devices such as gages, micrometers, and torque wrenches, which can only be used before and/or after test, and which will not be discussed here. However, for the majority of the instruments used for engine design and performance evaluation, particularly during test, the designer must provide adequate provisions for installation. Furthermore, the correct execution of command signals fed to the engine and the behavior of the major performance parameters must be transmitted back to the vehicle and from there to ground, either by hard wire (static tests) or by means of a radiating telemetry system (flight). The instrumentation of a liquid rocket propulsion system is a large field, and within the framework of this book we can merely point out

its significance. The engine designer must be fully cognizant of it, and must be sure to consult the development engineer and the instrumentation specialist at the very beginning of his design.

Principal Types of Instrumentation

Instrumentation signals to the vehicle are generated by engine-mounted end organs or transducers, with typical applications as follows:

Temperature gages.—Thermocouples or resistance bulbs are the principally used types. Their main application is for fluid-temperature measurement at the pump inlets for the determination of mass flow rates in combination with volume-reading flowmeters. Also, temperature measurements are made in other critical metal or fluid areas, such as at the gas generator, at the turbine inlet, at the gas storage vessels, and at solid propellant gas spinners, if such are employed.

Pressure switches.—A typical application would be a signal from the engine to the vehicle when thrust (chamber pressure) reaches a preset value during decay to initiate start of the next stage and separation of the spent one.

Pressure transducers.—A variety of types is available: strain gages, capacitance types, variable reluctance types, potentiometer types, piezoelectric types. Table 10-2 lists, among others, important pressures which can be expected to require monitoring and transmission to the vehicle and its telemetry system.

Accelerometers.—It is often important to measure the vibrations occurring in various locations of the engine system, and how these vary between static (tiedown) firing and flight. Accelerometers are used for this purpose and also, instead of pressure switches, to sense and signal thrust decay for staging.

Tachometers and flowmeters.—Small magnets mounted in a suitable manner to rotating parts of flowmeters or turbine wheels will induce periodic voltage pips in stationary coils. By counting the pips as a function of time, turbopump speed or volume flow rate can be determined.

Depending on the type of transducer used, a certain amount of signal conditioning will have to be provided at or near the transducer. Some of the latter give relatively weak signals (thermoelements, capacitance-type gages, tachometers, and flowmeters), which must be amplified

prior to transmission. In other cases, it may be desirable to convert a digital signal into an analog one, prior to transmission (tachometers, flowmeters). Small though the electronic (solid state) signal condition packages may be, room in a compatible environment must be provided for them on the engine. Under adverse conditions, it may be necessary to mount the conditioners on the vehicle near the engine.

Some transducers generate their own electric signal, such as the thermoelements, piezoelectric elements, and many of the flowmeters and tachometers. Most others, however, require an external electrical input which they modify as a function of the quantity sensed. Potentiometers, capacitors, inductances, and resistance temperature bulbs are examples. Resistance types can use ac or dc; capacitance and inductance types require ac. Typical instrumentation power supplies are 28 volts and 5 volts dc, and 115 volts ac, 400 cps. Certain transducers with built-in electronics receive 28 volts dc, chop, use and rectify it, and then return 5 volts (maximum) signals (dc-to-dc transducers). Strain gages and variable reluctance gages are typical examples.

Table 10-2 presents the basic static-firing measurement list for an engine of an A-1 stage. In practice, particularly during early development, this list may be expected to be augmented by special measurements, requiring additional instrumentation such as flowmeters, temperature gages, high-accuracy pressure gages, vibration pickups, and strain gages.

Instrumentation Installation

Some basic design considerations for correct installation of instrumentation end organs (pickups, sensors) will be briefly discussed.

1. Temperature Sensors

The most widely used temperature sensors are thermocouples. In rocket engine application, thermocouples are subject to certain measurement errors. Among these are:

Velocity errors.—Fluid friction may cause an excessive temperature reading, particularly at high fluid velocities. Suitable protection which does not affect the true measurement may have to be provided.

Conductive errors.—A heat leak may exist from probe to support. Figure 10-21 shows a

TABLE 10-2.—Basic Liquid Propellant Rocket Engine Measurement List
(A-1 Stage Engine)

Parameter	Range
Thrust	0-1×10 ⁶ lbs
Thrust chamber pressure (injector end)	0-1200 psig
Fuel pump inlet pressure	0-50 psig
Oxidizer pump inlet pressure	0-75 psig
Fuel pump outlet pressure	0-2000 psig
Oxidizer pump outlet pressure	0-2000 psig
Fuel injection pressure	0-1500 psig
Oxidizer injection pressure	0-1500 psig
Heat exchanger outlet pressure	0-1000 psig
Gas generator chamber pressure	0-1000 psig
Turbine inlet pressure	0-800 psig
Turbine discharge pressure	0-30 psig
Stored gas container pressure	0-3500 psig
Fuel pump inlet temperature	Ambient-100° F
Oxidizer pump inlet temperature	Ambient to -300° F
Cooling jacket inlet temperature	Ambient-100° F
Cooling jacket outlet temperature	Ambient-150° F
Turbine inlet temperature	Ambient-1500° F
Stored gas container temperature	-100°-+100° F
Fuel flow	0-10 000 gpm
Oxidizer flow	0-15 000 gpm
Turbopump speed	0-10 000 rpm
Electric bus voltage	20-35 volts dc
Spark igniter OK	On/off
Miscellaneous valve positions	On/off

thermocouple well proposed by B. N. Bose (ISA Journal, Sept. 1962) designed to offset this effect.

Carbon deposits.—In systems using kerosene-based fuels, carbon deposits may cause erratic thermoelectric and grounding effects. While certain electrical connections are possible to minimize this, regular cleaning and sometimes replacement of the probe is required. The engine designer must consider this need for easy accessibility of the instruments.

Installation of resistance thermometers or "bulbs" is governed by similar consideration.

2. Pressure Gages

Two principal types of pressure measurements are usually conducted during rocket engine testing: static and dynamic. As a rule static measurements are employed to record, with high accuracy, steady-state conditions or parameters varying only very slowly. Dynamic measurements are used where rapidly changing conditions

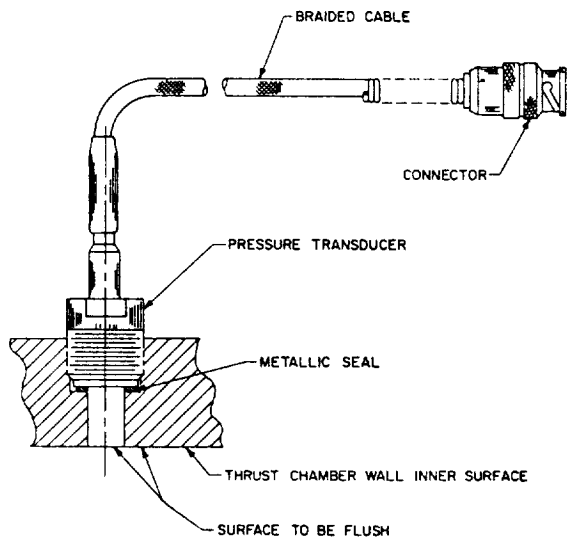
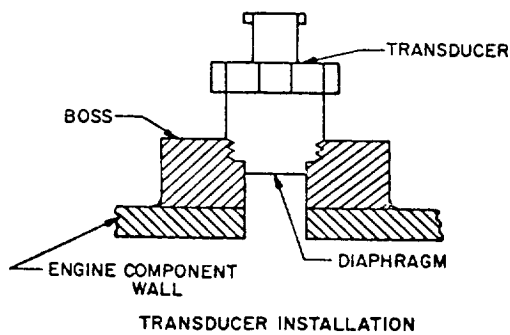


Figure 10-23.—Typical installation of a thrust chamber pressure transducer.



TRANSUCER INSTALLATION



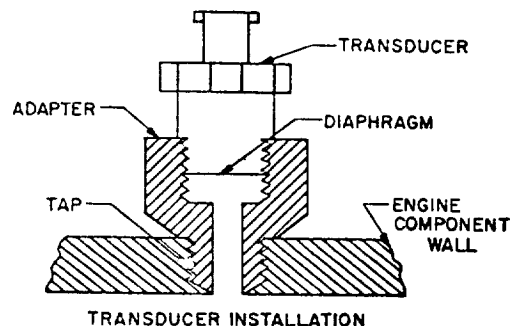
$$f_n = \frac{2n-1}{4} \left(\frac{C}{L} \right)$$

WHERE:

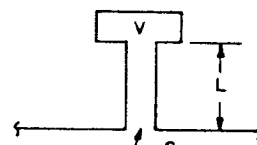
- n = ANY WHOLE NUMBER (1, 2, 3... etc)
- $n = 1$ FOR THE FUNDAMENTAL FREQUENCY
- C = ACOUSTIC VELOCITY OF THE MEDIUM (13,550 IN./SEC FOR AIR AT 68° F)
- L = LENGTH OF TUBE IN INCHES

ACOUSTIC EQUIVALENT

(A)



TRANSUCER INSTALLATION



$$f_n = \frac{C}{2\pi} \sqrt{\frac{S}{L'V}}$$

WHERE:

- C = ACOUSTIC VELOCITY
- S = CROSS-SECTIONAL AREA OF TUBE IN SQUARE IN.
- V = VOLUME OF CAVITY AT THE END OF THE TUBE IN CUBED IN.
- L' = EFFECTIVE LENGTH OF TUBE IN INCHES
- $L' = L + 1.7a$

WHERE: L = ACTUAL LENGTH
 a = RADIUS OF TUBE

ACOUSTIC EQUIVALENT

(B)

Figure 10-24.—Acoustic equivalents of pressure transducer mounting cavities.

of the frequency range of the measured parameter. Figure 10-24 shows two typical installations and associated equations to determine f_n . Figure 4-28 shows a typical tap arrangement for injector-end chamber pressure.

For still higher frequencies, above 2000 cps, transducers are installed so as to leave essentially no cavity at all (flush mounting). This poses problems with hot-gas measurements. Special water-cooled transducers have been developed for these applications. Needless to say, an effort toward high-frequency response at the pickup point is lost if the recording system is not capable of using it.

Flowmeters

Turbine-type flowmeters appear best suited to rocket engine installations. They are well developed and, as a rule, can be mounted in a simple fashion between available flanges in existing

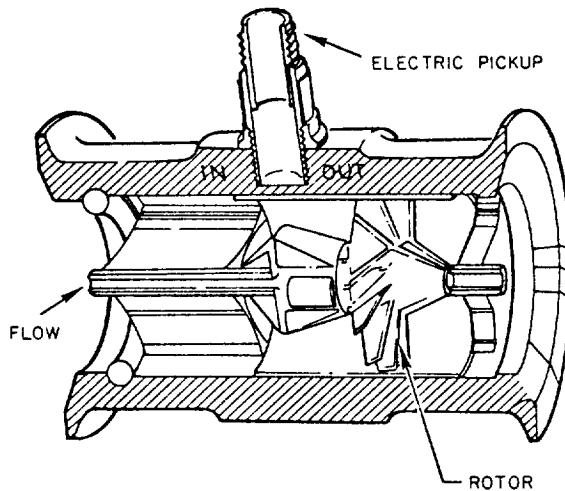


Figure 10-25.—Turbine-type flowmeter.

ducting (fig. 10-25). Turbine flowmeters are very sensitive to changes in upstream duct configuration. Once calibrated as installed, however, they exhibit a high degree of precision.

Accelerometers and Strain Gages

These are almost always applied externally, in connection with special measurement programs. At the time of engine systems design, no special consideration is usually required.

10.8 CLUSTERING OF LIQUID PROPELLANT ROCKET ENGINES

The idea of obtaining higher thrust levels expeditiously through combination of several smaller rockets probably is as old as rocketry itself. To today's liquid rocket vehicle and engine builders the topic of clustering still causes spirited debates, which reached a peak in March 1952 when Collier's published an article by Dr. von Braun in which a space vehicle was described as having a first stage powered by a cluster of 51 turbopump-fed rocket engines. The debates invariably hinge around the deceptively simple question: is higher overall reliability obtained through combination of a number of well-developed smaller engines, or through application of one large, specially developed unit. The answer is not simple. The failure probability of the smaller units may be low, but it increases with the number of units clustered.

For both large or small units, reliability is not a fixed value, but is a function of development time. A realistic analysis considering all factors may determine the appropriate choice. The absolute truth, however, may never be known, since the cost of going both routes for a given mission and of comparing final scores would be prohibitive.

Clustering of liquid rocket engines or, in other words, subdivision of vehicle thrust into smaller units may be accomplished in a number of ways. The choice for the most part will be based on vehicle considerations. Depending on the method chosen, however, engine design will be directly affected.

Some of the basic considerations of this topic which are specifically related to engine clustering and as they affect engine systems design and integration, are briefly reviewed.

There are no hard-and-fast rules which can be applied to determine optimum cluster configurations. With the aid of liquid engine clusters actually used in practice, however, we will present a number of considerations which may serve as a guide for future designs.

Earlier Cluster Configurations

Figure 10-26 shows the cluster of two experimental LOX/alcohol engines for a planned but discontinued ballistic missile. It consisted of two units of 120 000-pound thrust each. Both subunits included a tubular-wall, gimballed thrust chamber, and a geared turbopump. The turbines were powered in parallel from a single, common gas generator. The control system was also common for both units. Thus this propulsion system was not a true cluster, since it was not possible to develop and fire each unit independently. Several successful experimental flights were achieved with this engine.

Figure 10-27 shows another experimental cluster consisting of three units which, although never flown, achieved a remarkable reliability record during static firings at thrust levels up to 500 000 pounds. This cluster, too, used a common control and gas generating system for the three subunits. Most of its components were essentially the same as those used for the two-engine cluster, except that propellants were RP-1 and liquid oxygen.

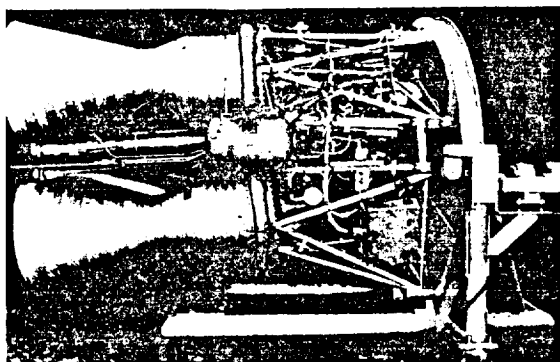


Figure 10-26.—Dual-engine cluster.

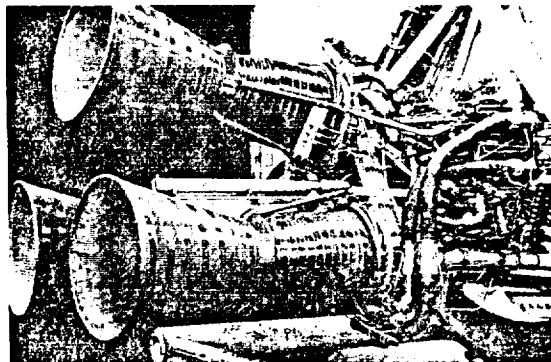


Figure 10-27.—Three-engine cluster.

Still another approach for ballistic missiles is the combination (clustering) of a pair of booster engines with a large-expansion-area sustainer engine. During flight, the booster engines may be jettisoned following the boost period, while the sustainer continues, fed from the same tanks. These configurations are also referred to as "One-and-one-half-stage vehicles."

Recent Cluster Design Trends

The first clustered engine vehicle, signifying the modern trend toward multipurpose engines, is NASA's S-1 first-stage booster for the Saturn I. It is powered by 8 LOX/RP-1 engines, the basic elements of which were transplanted with relatively minor modifications from earlier engines. The S-1 is noteworthy for its tank arrangement. Eight tanks from an earlier missile are clustered around a central larger tank. This "multicellular" design, which in the case of the S-1 permitted early availability of large tank capacity without major retooling, has been recommended by some vehicle designers for still larger vehicles. The eight engines of the S-1 are grouped into four fixed inner and four gimbaled outer engines. Except for the outer-engine actuators, all eight are identical, independent units, built and tested singly, and combined for the first time on the vehicle proper.

In the S-1, the number of engines was, no doubt, almost entirely governed by the availability of existing major engine components and tankage. For subsequent vehicles, such as the Saturn V three-stage vehicle, greater freedom existed, particularly with respect to the optimi-

zation of thrust and total impulse (propellant load).

To examine some of the considerations which govern engine cluster arrangements, we assume that payload and mission of a multistage vehicle are defined and that stage propellant loads (total impulse) and tank geometry (diameter) have been optimized. We further assume that engines are available and will not be redesigned, and that the optimum thrust for a typical stage suggests a range of from four to six engines. An analysis has shown that payload performance probably increases with the larger number of engines (fig. 10-28); however, there are other considerations.

One of the most influential considerations is "Engine Out Capability" for increased vehicle reliability (also see ch. II, "Thrust Level"). Specific engine provisions for engine-out (EO) are summarized in section 10.9. Capability of a vehicle to complete its mission with one engine inoperative always entails some performance losses. However, these losses decrease with increasing total number of engines, because less performance reserve is needed, and because less correcting thrust vector trim is required from the operating engines. Trim from engine-out is further affected by the diameter of the engine-mounting circle. The contribution to mission reliability by EO capability is substantial, with cluster failure potential reduced by more than half. In addition, absolute reliability values are a function of the number of engines in the cluster. This is most evident with no engine-out.

Figure 10-29 illustrates this at two points of time of engine overall development status. As the latter progresses, the difference between

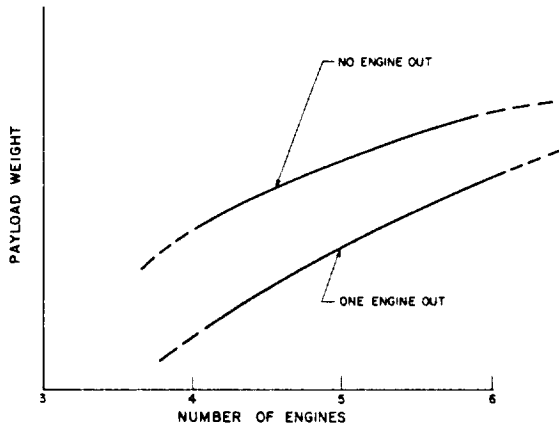


Figure 10-28.—Stage-payload weight as a function of number of engines in cluster.

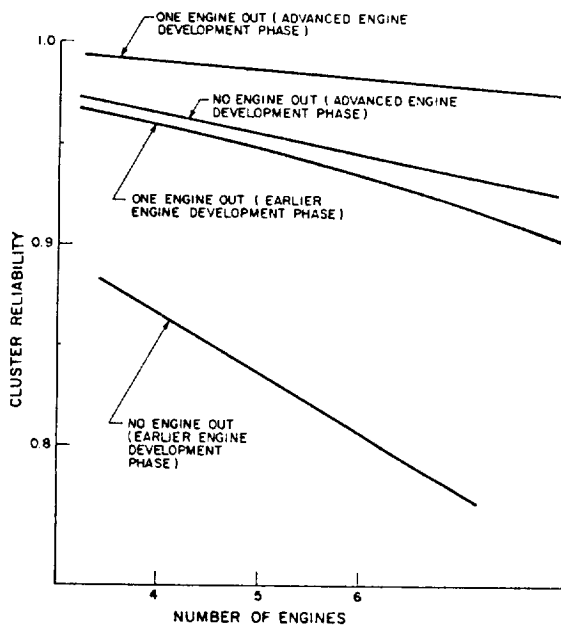


Figure 10-29.—Typical cluster reliability prediction as a function of number of engines in cluster and of development time.

engine-out and no engine-out narrows (see also table 2-2). It may be stated that for a given number of vehicle flights, the benefits of engine-out capability are the greater, the lower the single-engine reliability. Figure 10-28, in combination with figure 10-29, shows that simultaneous addition of one engine and inclusion of engine-out capability retain about the same pay-

load for a substantially higher cluster reliability at any single-engine reliability level.

Another important consideration is cluster diameter in relation to vehicle diameter. As will be discussed in section 10.9, it is mandatory that all engines fit into the interstages from which they must separate without interference. This restriction is not valid for the first stage, where engines may protrude beyond the tank profile. The degree of protrusion, however, must be balanced against drag losses.

Specific considerations for each chosen number of engines follow (fig. 10-30).

4-Engine Cluster

This configuration provides the lowest total thrust in the established band of 4 to 6 engines, but it is optimum for engine interchangeability. All four engines will be gimbaled. Only one installation is required: all inlet ducts and other engine to stage connections can be made identical. The thrust vector control mode is simplest: all engines deflect in pitch and yaw, and all actuators participate equally in roll control (fig. 10-30(a)).

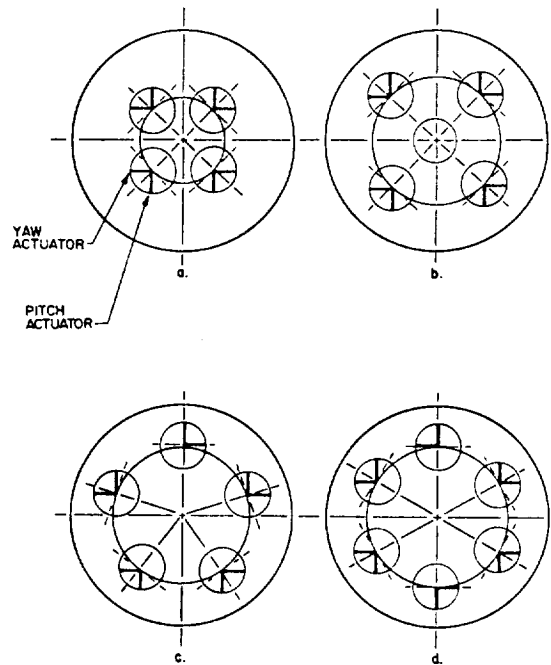


Figure 10-30.—Typical engine cluster arrangements.

5-Engine Cluster

This number provides greater thrust, but complicates matters in other respects. Two basic arrangements are possible, as shown in figure 10-30(b) and (c). The arrangement with center engine is preferred. The center engine is mounted fixed; i.e., stiff arms are installed in place of gimbal actuators. It is advisable to install the engine with complete gimbal bearing for standardization and ease of alignment. With the remaining four engines gimballed and grouped as in a 4-engine cluster, the same benefits are derived as with the latter. However, because of the center engine, two installations are required. Furthermore, two sets of inlet ducts are needed, their different length affecting pressure drop and fluid velocity profile (engine turbopump NPSH), water hammer from closure of valves (valve timing), trapped propellants, and possibly insulation requirements (weight penalties and complexity). Figure 10-31 shows a typical 5-engine installation with fixed center engine.

With all five engines arranged on a circle, the basic engine package may become more uniform, since all will be gimballed. However, three different installations are required (fig. 10-30(c)),

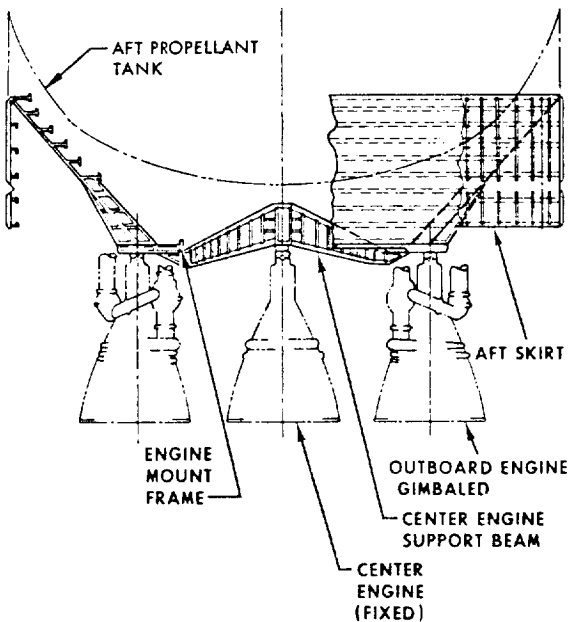


Figure 10-31.—Typical five-engine cluster configuration. Center engine fixed, four outer engines gimballed.

and systems thrust vector control response is seriously affected, due to roll and yaw coupling, particularly under malfunction conditions. As to mounting-circle diameter, the two 5-engine clusters are about equal.

6-Engine Cluster

This combination provides the highest thrust, at the expense of a larger mounting circle. This in turn increases the effects of one-engine-out on trim required and may compound interstage and interengine clearance problems. The control mode is comparable to the four engine cluster in simplicity. The 6-engine cluster requires two installations, with inlet and other effects similar to those discussed with the 5-engine configuration.

This cluster offers the potential of removing (not installing) 2 engines and still retaining a satisfactory 4-engine combination, which provides added flexibility at minimum scar weight (i.e., weight of components that cannot readily be removed along with the engines).

If at all possible, the engine designer should specify that the engine intended for cluster use be tested under conditions closely simulating vehicle installation. It may be expected that the vehicle builder will conduct a firing program of his own; however, this must be devoted to cluster behavior and performance evaluation, and should not deteriorate into continued single engine development. A major difference between single engine and cluster firing is in the *base conditions*, i.e., the heat and pressure environment of the engines, particularly at altitude. Flame radiation effects, backwash of combustion gases, and impingement may create much more severe conditions than are present during single-engine firing. The pressure environment produced by several engines firing together may create moments on the engines which must be accounted for in the design of the gimbal system. The engine designer should be familiar with these conditions so that his claim that the engine can be clustered remains valid after delivery.

Awareness by the engine designer of the considerations governing engine clustering, as presented here, will enable him to complete his systems integration with a broader view to application.

10.9 ENGINE-TO-VEHICLE INTERFACE

Throughout this book, references have been made to the ultimate purpose of rocket engine design and production: propulsion of a vehicle. Some of the principal engine-to-vehicle interfaces, such as thrust mount, and pneumatic, fluid, electrical and propellant lines, have been discussed in preceding chapters. In this section, we will summarize a number of vital engine-to-vehicle interfaces, of which the engine designer should also be cognizant.

Design Documentation

Adequate mechanical design data, vital for the physical integration of the engine into a vehicle system, must be properly documented by the engine systems designer. The following data are considered minimum requirements:

- (1) *Engine system general arrangement drawing.*—This drawing defines the engine space envelope and the locations and detail of various agreed-upon vehicle connect points, such as
 - Thrust or gimbal mount
 - Gimbal actuator attach points
 - Fuel and oxidizer inlet flanges
 - Hydraulic and pneumatic system connections
 - Electrical and instrumentation connections
- (2) Mechanical dimensions, tolerances, seals (if any), fasteners, and loads at the vehicle connect points listed
- (3) Engine system mass properties, as are shown in figure 2-6, which include engine weights, gimballed mass, center of gravity, and moment of inertia for the basic engine, including accessories
- (4) Engine performance data (as in fig. 3-1)
- (5) Engine functional description (as in ch. III)
- (6) Engine handling procedures and equipment, needed for installation and maintenance
- (7) Engine servicing needs

As a rule, this information is compiled in detailed handbooks, which will accompany the engines when delivered to the vehicle contractor. However, several years before the engines are delivered and handbooks become available, the

vehicle builder is in need of numerous engine design details in support of his stage design. An excellent source for this information is an "Engine Design Manual." It should be started during engine initial design and should be augmented as the design and, at a later date, the development progresses. Necessary revisions must be disseminated promptly.

Equally important is the early generation of an Interface Control Document. This defines each interface, for both mating sides, on one drawing.

Space Envelope

When installing an engine in a vehicle, it is not only necessary that it can be properly bolted to the vehicle thrust mount, but it is equally important that no other vehicle parts interfere. Space in the vehicle engine compartment must not only accommodate the engine envelope when in the neutral position, i.e., pointing straight aft, but when fully deflected in all directions as well. Typical maximum engine deflections range from 4° to 7°. For clusters, moreover, the possibility of faulty deflection of engines must be taken into account. Since space in the engine compartment of vehicles is usually limited, the need for the closest cooperation between engine and vehicle designer becomes apparent. This is especially true for upper stage clusters where large expansion area nozzles must be housed in minimum interstage structures.

Connect Panels

All engine-to-vehicle lines, which may amount to a dozen or more per engine, must be reliably connected for each engine installation, not only in the vehicle but in the static development and acceptance firing stands as well. It has been found beneficial to define this interface clearly by combining all lines in one or several terminal connecting panels (fig. 10-32). These panels, uniformly designed for all test locations, may be mounted on the vehicle (or test stand), or on the engine. For certain installations it may be advantageous to have matching panels on both: vehicle (or stand) and engine. Aligned a short distance apart, standardized jumper lines between pairs of panels will permit rapid and reliable connections. A possible disadvantage of

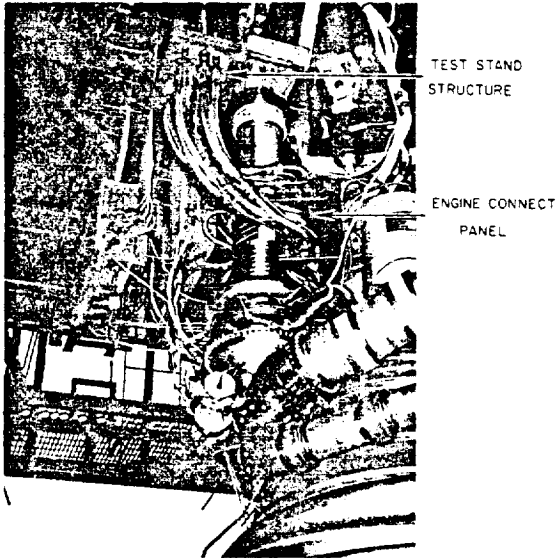


Figure 10-32.—Typical line connections on an experimental liquid rocket engine.

the panel method is that routing a line through the panels may result in additional line length, as compared to individual routing of each line. Through careful design and close coordination between engine and vehicle builder, considering optimum location, subdivision and orientation of the panels, advantages will, in most cases, far outweigh disadvantages.

Dynamic Interactions

The close coupling between propellant feed system, propulsion system, and vehicle structure may lead to undesired interactions. These have manifested themselves as longitudinal vehicle oscillations (also referred to as "Pogo Stick Effect," "Accordion Motion," or "Spring-Mass Effect") at frequencies from approximately 10 to 20 cps. They have led, in at least one instance, to vehicle destruction. The relationship of the contributing parameters is illustrated in figure 10-33 for a typical single-engine vehicle. The analyses and correction of these oscillations are extremely complex, particularly since they cannot be reliably reproduced during captive firings. It is believed, however, that any one of the contributing factors can modulate thrust at a frequency at which the vehicle is resonant at certain tank levels (flight time; fig. 10-34). Through

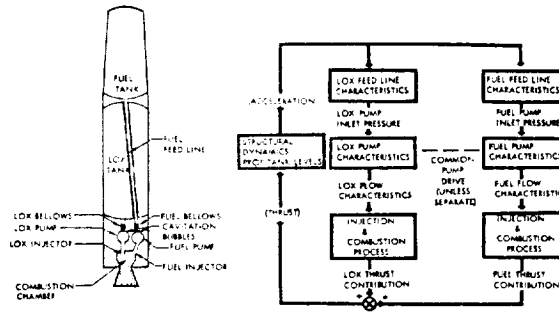


Figure 10-33.—Closed-loop coupling of propulsion system parameters and longitudinal vehicle mode.

acceleration, as a function of thrust, a powerful feedback exists. It has been demonstrated that the system can be detuned or uncoupled, through manipulation of propellant duct volumes, stiffening of structural members, and by other means. It is difficult if not impossible for the engine designer to predict analytically and prevent this problem, particularly since the vehicle configuration may not yet be firm. He may be called upon later for changes, however, if the problem shows up during flight.

Malfunction Reaction Systems

In chapter II we have discussed reliability and failure modes, as well as certain preventive measures. In the framework of engine-to-vehicle interfaces, some additional detail follows.

Engine Failure Sensing and Shutoff System (EFSS)

These systems have been in use since the early beginnings of liquid rocket engine application. They are specially important during engine

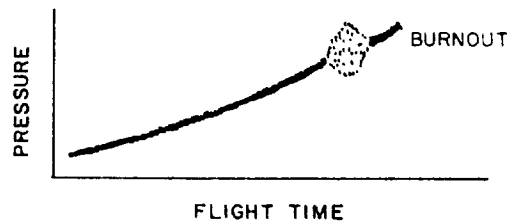


Figure 10-34.—Typical pump inlet pressure variation of a vehicle affected by longitudinal oscillations.

and early cluster development. Part of it may later become a portion of flight emergency detection systems (EDS) and engine-out systems (see ch. II). The following list of major engine-oriented malfunctions, which is not necessarily complete, should be considered:

- Pump inlet pressures below safe minimum
- Turbopump overspeed
- Turbopump bearing overheating
- Excessive turbopump leaks
- Turbine gas overtemperature
- Combustion instability
- Abnormal injection pressures
- Ignition failure
- Premature propellant depletion
- Electrical power failure
- Pneumatic pressure failure
- Improper valve positions
- Fires

Because of their potential sudden destructive effects, many of the malfunctions will be sensed and the signals used to initiate immediate automatic cutoff. For others which would not create an emergency within, say, fractions of a second, it is not uncommon to simply mark their allowable minimum and/or maximum values on an ink-recorder chart which is watched by an observer during test. If the recorder needle goes outside of the marked margin, the observer initiates cutoff manually.

For flight, a few selected highly critical parameters of the EFSS may be retained for automatic engine cutoff or mission abortion. In this case, if the engine failure sensing and shutoff system were called upon to shut down an engine, and the flight is continued with the remaining engines, a vehicle-mounted electronic logic must sense the shutdown and take certain actions.

These may include:

- Closure of emergency shutoff valves in the ducts to the defunct engine, but not those in the others.
- Disconnection of electric power to the defunct engine only.
- Resetting or disarming of backup cutoff timers, since the reduced number of engines will consume the available propellants over a longer period of time.
- Locking of the defunct engine in the neutral gimbal position.

Heat Protection

Rarely in our technology had lowest and highest temperatures to be handled so close together as in a liquid propellant rocket engine. Earlier we discussed the need for insulation, to maintain temperatures as low as -423°F in certain ducts, or for heaters to protect sensitive components against these temperatures. At the same time, in other areas at or around the engine, protection must be provided against the very high temperatures of the combustion process and the emerging gas jet, such as cooling of the thrust chamber. The exhaust jet, at sea level, usually is not a major problem, unless blowback occurs from the flame deflector. At higher altitudes with vacuum or near-vacuum pressures, however, which are experienced even by first stages for the last portion of their flight, a substantial portion of the thrust chamber gas jet expands sideways from the nozzle exit, forming a plume, creating considerable backwash and radiating powerfully back into the engine compartment. This endangers both engine and vehicle components. Surface temperatures of 1000°F or more may result unless heat protection is provided. In some cases it may be too cumbersome to provide individual insulation for each component. Also, excessive weight penalties may be incurred. A protective heat shield, forming a closeout diaphragm, may then be more effective (fig. 10-35). This shield may be supported from a stationary (center) engine, if available, or from a supporting structure.

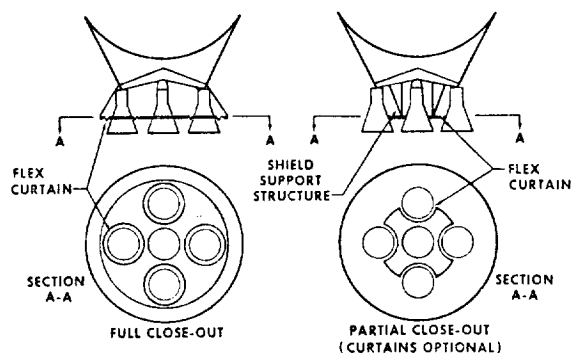


Figure 10-35.—Typical base heat protection concepts (center engine fixed, outer engines gimbaled).

Design and installation of the base heat shield requires closest cooperation between engine and vehicle designer. It must be determined, through special model tests, whether a partial or a full closeout is required. In most designs the shield connects to the engine nozzle. Suitable brackets must therefore be provided. During gimbaling the heat shield will resist the engine motion. The forces encountered must be considered in the power budget for the hydraulic actuators. Here it must be taken into account that the heat shield flex curtains may be quite cold prior to engine start and still remain relatively cool at the far side, as planned, during stage operation.

In addition to backwash and radiation, which are generally not harmful to the internally cooled engine nozzle itself, mutual gas jet impingement between engines may occur from extreme deflection during gimbaling. Unless a major control malfunction occurred, this should affect the nozzle only for very brief periods near the exit. However, the heat may affect chamber structural elements, such as stiffening bands, which are not internally cooled. A heat-protective strip, a few inches wide, of ablative or other suitable material applied to the nozzle should suffice in most cases (fig. 10-36). Obviously, this type of protection is not required for single-engine vehicles.

Engine Prestart Conditioning and Start

Functional conditions required within the engine to assure its readiness to start have been discussed earlier. When installed in the vehicle, the engine also requires external conditions which must be met by the vehicle builder. Provided that prelaunch checkouts have ascertained readiness with regard to absence of leaks, correct valve positions, etc., prestart conditioning of the engine essentially refers to temperature and pressure levels around the engine and at the pump inlets. For both, early cooperation between engine and vehicle designer to arrive at a mutually feasible solution is essential. Without it, the optimistic note in engine drawings "to be supplied by vehicle contractor" will accomplish little.

Certain engine subsystems, such as hydraulic components, control systems, and valve actua-

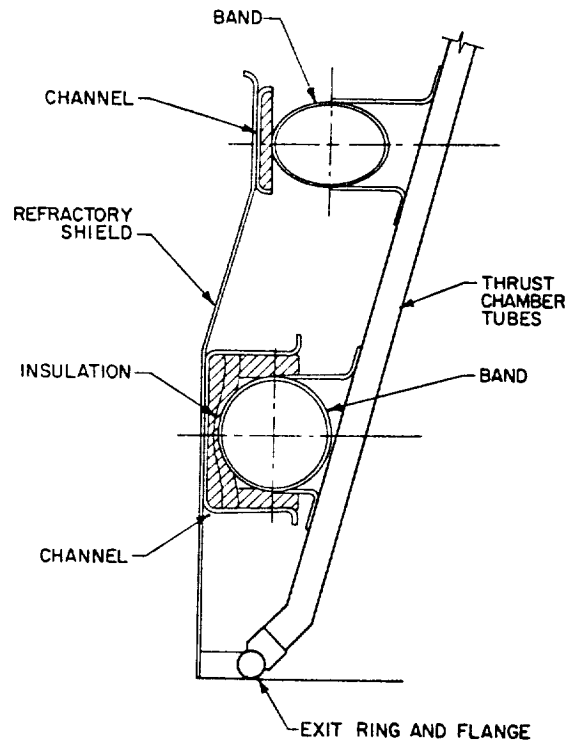


Figure 10-36.—Center-engine flame impingement shield.

tion mechanisms, can function properly only if they are within a specified temperature range. Engine systems not employing cryogenic propellants may be dependent on heating or cooling only if prolonged coasting times in space are involved. Engine systems which do use cryogenic propellants almost always need at least some heating. The cryogenic propellants within the engine following start of tanking, and the heat absorption of tank surfaces and lines may rapidly lower the air temperature surrounding the engine to several hundred degrees below 0° F.

Since most vehicle systems will specify an allowable hold period following tanking to allow for adjustments, checkout of other systems, to wait for optimum launch times (rendezvous missions), etc., severe subcooling of engine components may occur.

The temperature environment can be substantially improved by the vehicle builder through engine compartment purges with warm gases (fig. 10-37). If an inert gas is used, this has the

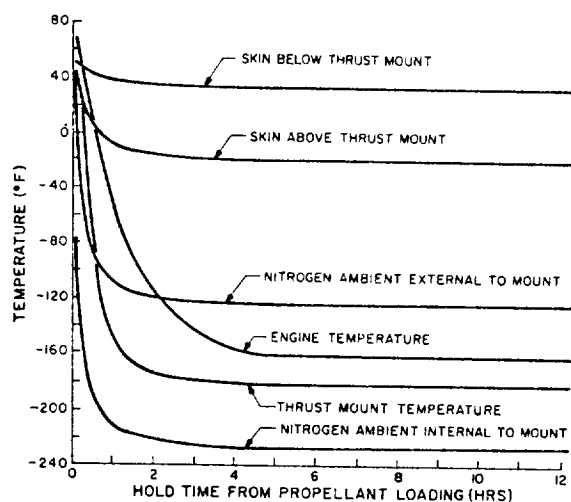


Figure 10-37.—Typical interstage temperature environment for an upper space vehicle stage using cryogenic propellants. 565 SCFM, (-100°F) nitrogen purge.

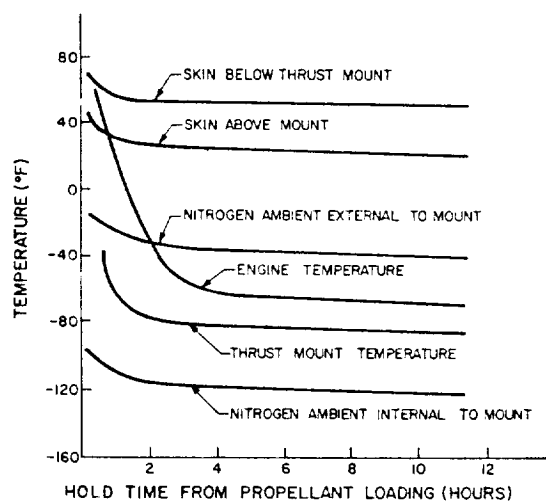


Figure 10-38.—Typical interstage environment for an upper space vehicle stage using cryogenic propellants. 4170 SCFM, (250°F) nitrogen purge.

additional advantage of counteracting the accumulation of combustible gas mixtures from minor leaks. However, the vehicle builder's possibilities of heating through use of compartment gas purges are definitely limited. Some of the limitations stem from the engine designer's own specifications, which require avoidance of elevated temperatures around components containing cryogenic fluids to minimize boiloff and to prevent formation of gas bubbles. Also, certain structural members must be kept below maximum temperatures because of their strength characteristics. Another limitation is established by the purge gas requirements and necessary heating provisions which would become prohibitive if it were attempted to raise compartment temperatures to above 32°F or even to 0°F . Figure 10-38 shows the effects of increased purge flow and temperatures over those of figure 10-37. The analyses on which the graphs are based have shown that a further increase of the purge rate to 12 000 SCFM (standard cubic feet per minute) and 250°F barely raises the interstage temperature above 0°F .

At the same time the propellant boiloff rates in exposed ducts increased tenfold over those under conditions of figure 10-37. The locations quoted are identified in figure 10-39.

For most applications the purges to the various areas are supplied from a ground source. Once preconditioned, affected components can

be expected to maintain their temperature within an allowable band after vehicle liftoff during the relatively short boost periods. Only stages with prolonged cruising times may require an onboard purge supply system which imposes payload penalties.

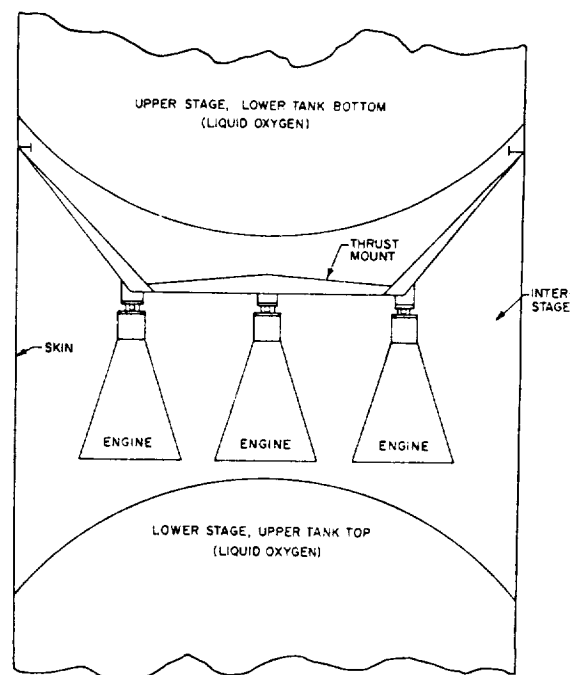


Figure 10-39.—Multistage vehicle interstage.

Literally a few inches away from the components requiring protection against low temperatures are others which must be protected against warmup due to influx of heat. Here again non-cryogenic propellants pose few problems. By contrast, cryogenic systems, in particular those including liquid hydrogen, are very sensitive to heat influx. The effects on pump NPSH, which includes the vapor pressure of the fluid pumped, were discussed in detail in section 8.5 in connection with tank insulation. For engine start, which involves the cryogenic fluids stored in the ducts immediately upstream of the engine and within the engine itself, insulation may become prohibitively complex. Continuous removal of superheated cryogenic fluids from the engine system and substitution of fresh liquid, therefore, has been widely used. This can be accomplished through continuous overboard bleeding or through recirculation back to the tank. In both cases, the liquids are tapped off at a point farthest away from the pump inlets and routed to the stage for overboard dumping or return to the tanks. A small auxiliary pump is often required to obtain the minimum flow rates required for adequate bleeding.

During engine development, and even during vehicle static firing programs, relatively favorable prestart conditions exist: the enclosing interstage is not in place, hold periods are under better control, cold lower stage tank surfaces are absent. There is thus the danger that what worked faultlessly under these conditions will fail in vehicle flight. A realistic recognition of this situation and close coordination between the two design teams in the early phases of engine and vehicle design and development is therefore vital.

For first-stage applications, the engine builder is relatively independent regarding start characteristics and sequence. The vehicle will not take off until thrust exceeds vehicle weight, gravity holds the propellants at the tank outlets, and all parameters are closely monitored from the ground control center. If a holddown period prior to vehicle release and takeoff is included, an additional safety margin exists.

For upper stage engine start, conditions become considerably more complicated. Absence of the propellant-settling effects of gravitation, the surrounding vacuum, altitude temperature

conditions, and remoteness from ground stations can only crudely be simulated in ground tests. Therefore, until first flights of a new vehicle have been accomplished, the engine in-flight start sequence, which is closely interwoven with the stage separation sequence, must be planned based largely on analytical work. Neither vehicle builder nor engine designer can do this without consideration of, and consultation with the other. The following principal relationships must be considered:

Starting of the upper stage engines while the lower stage is still at full-thrust level is difficult, mainly because of the problems of flame impingement and exhaust gas dissipation from the interstage. Therefore, engine start following stage separation is preferred. However, in this case propellant settling from acceleration effects of the lower stage is no longer assured. Auxiliary propellant settling (or "ullage") rockets (usually solid propellant type) are required instead during engine starts. These add weight and drag and reduce payload. The size of the weight penalty, in turn, depends on engine-start characteristics (thrust-buildup time). For engines with relatively protracted buildup times, advanced initiation (with respect to lower stage thrust decay and separation) of upper stage engine start may substantially reduce the penalties. A second lopped off the ullage rocket burning times may save hundreds of pounds of stage weight. The same amount of time added may not only reduce payload weight but pose serious control problems to the space vehicle which floats essentially "rudderless" after separation and prior to the start of its own engines. From the foregoing the need for thorough mutual understanding of this important vehicle-to-engine interface becomes apparent.

Vibration Environment

Even a normally or "smoothly" operating rocket engine generates a vibration pattern which is transmitted mechanically through the thrust mount, or acoustically through the ambient atmosphere, if present, to the vehicle structure. Neglect of these vibrations by the vehicle builder may lead to serious structural weakness or malfunction of vital control organs mounted to the vehicle structure. Means of reducing the normal engine vibrations are limited and hard to analyze.

~~CONFIDENTIAL~~

Rather, it is important that the engine developer establish as accurately as he can the existing acoustic and vibration pattern and inform the vehicle designer of his findings. Since the tie-down firing measurements cannot reliably predict free-flight conditions, a serious handicap exists. However, through his thorough understanding of the potential problems, and through specification in cooperation with the vehicle designer of static test and flight measurements, the engine designer can materially assist in reducing the incidence of serious problems.

Nozzle Expansion Area Ratio

From his own analyses, the engine designer may have selected a nozzle expansion area ratio which appears to be an optimum compromise between engine weight, engine performance, engine size, and producibility. When analyzed in the larger framework of vehicle performance, the selection may turn out not to be optimum. In reviewing the various influences, we will disregard single-engine first stages which are least affected. For stages with engine clusters, in particular, upper stages, the following must be considered:

Gimbal Angle

Following determination of the maximum gimbaling angle required for safe vehicle guidance, including consideration of actuation malfunctions, the nozzle exit diameter will determine the attachment point distances (mounting pattern) of the engines in a cluster.

Vehicle Diameter

When mounted for proper gimbaling capability, the envelope of the engine cluster must be in proper relationship to the vehicle diameter. If the cluster envelope is too large, the increase in vehicle dimensions may void all gains from a larger expansion area ratio. If engines are not permitted to protrude beyond the projected vehicle plane in neutral and/or in gimbaling position, an even more stringent situation exists.

Interstage Length

When mounted to the lower stage, the length of the upper stage engines will determine the length of the required interstage. For a vehicle of the Saturn V class, each additional inch of

interstage length will cost approximately 40 pounds. Thus, here too, the added interstage weight required to accommodate a longer, better performing nozzle may void the theoretical gains.

Stage Separation

When separating the stages of a space vehicle, three basic possibilities exist:

1. *Leaving the interstage with the lower stage.*—This requires the engines to pull out of the interstage cylinder during separation (fig. 10-40). If the clearance between engine skirts and interstage wall is marginal, complicated means may be required to avoid collisions between the separating stages. These may include a control system to tuck the engines inward, and then swing them out upon separation and start them. Any such system adds complexity, lowers reliability, and may add weight. A shorter nozzle skirt, of lesser diameter although somewhat lesser performance, may be better overall.

2. *Leaving the interstage with the upper stage.*—To avoid the problem of stage collisions, it may appear attractive to leave the interstage attached to the upper stage. However, this adds inert weight to the upper stage. This penalty may be considerably larger than the performance loss from a somewhat shorter nozzle. Also, a control problem may be incurred in that the engine nozzles, in their outward gimbaling deflection, still must clear the interstage wall. In joint optimization studies between engine and vehicle designer, the possibility of leaving part of the interstage with either stage may be considered.

3. *Leaving the interstage with the upper stage but dropping it in a second separation maneuver several seconds after first separation.*—In this dual-separation sequence, the second separation may consist of shedding the interstage as a complete ring, possibly in combination with guide rails, or of blowing it off to the side in segments. For either method, some form of actuation is required in addition to accurate timing. Also, while the interstage is still attached, a serious base-heating problem may develop. The means required to overcome any difficulties with this separation method again may increase complexity and reduce reliability and partially neutralize nozzle performance gains.

Whichever method is applied, the thrust-decay characteristics of the spent lower stage engines

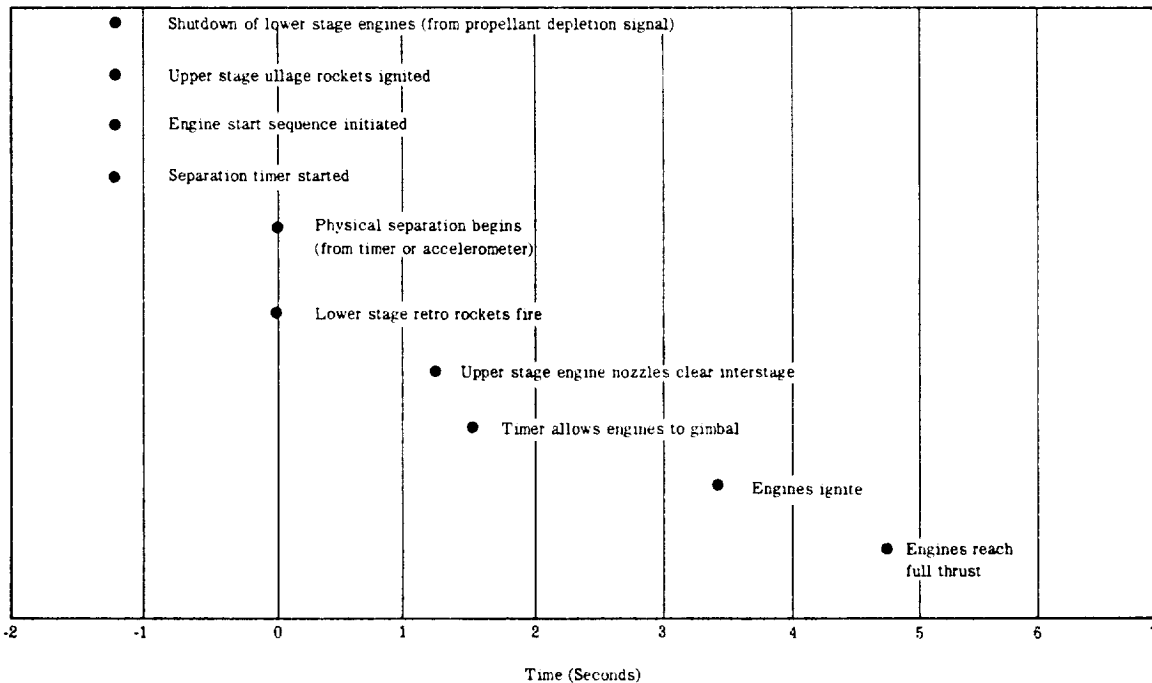


Figure 10-40.—Typical stage-separation sequence.

greatly affect the separation sequence and the clearances. To optimize these, the vehicle builder needs from the engine designer accurate information on thrust-decay characteristics and tolerances. This may be in the form of a graph, as shown in figure 10-41.

Flame Deflector Size

Although this is not entirely an engine-to-vehicle interface, it is pointed out that engine-nozzle size and arrangement on the vehicle, together with maximum gimbal angles, strongly influence the design of required flame deflectors on engine and stage static firing test stands, and of launcher flame deflectors. Here the problem is not so much one of optimizing vehicle performance, but of minimizing cost and of assuring the adequacy of these indispensable development tools.

Engine Handling, Installation, and Servicing Fixtures

For handling engine parts and assemblies during engine installation into development test

stands and for various servicing functions, the engine builder requires numerous fixtures commonly referred to as engine GSE (ground support equipment). Some of these fixtures can be used by the vehicle contractor as designed, others could be used if only a few minor changes or additions were made. The funding required for GSE in a typical vehicle program is substantial and approximates that of the flight hardware. Common use of as many of these fixtures as possible by engine and vehicle builders is strongly advised. To assure this the two must work together from the earliest design inceptions.

Standardization

The task of mating engine and vehicle will be substantially facilitated if the designers of both work to the same standards. This applies to national standards, Government standards, company standards, to terminology, mathematical symbols, and to the measuring system (metric or English, decimals or fractions, tolerances). Since several avenues are open, it is necessary, at the very outset, to agree on which one shall be pursued. This requires close cooperation and full documentation.

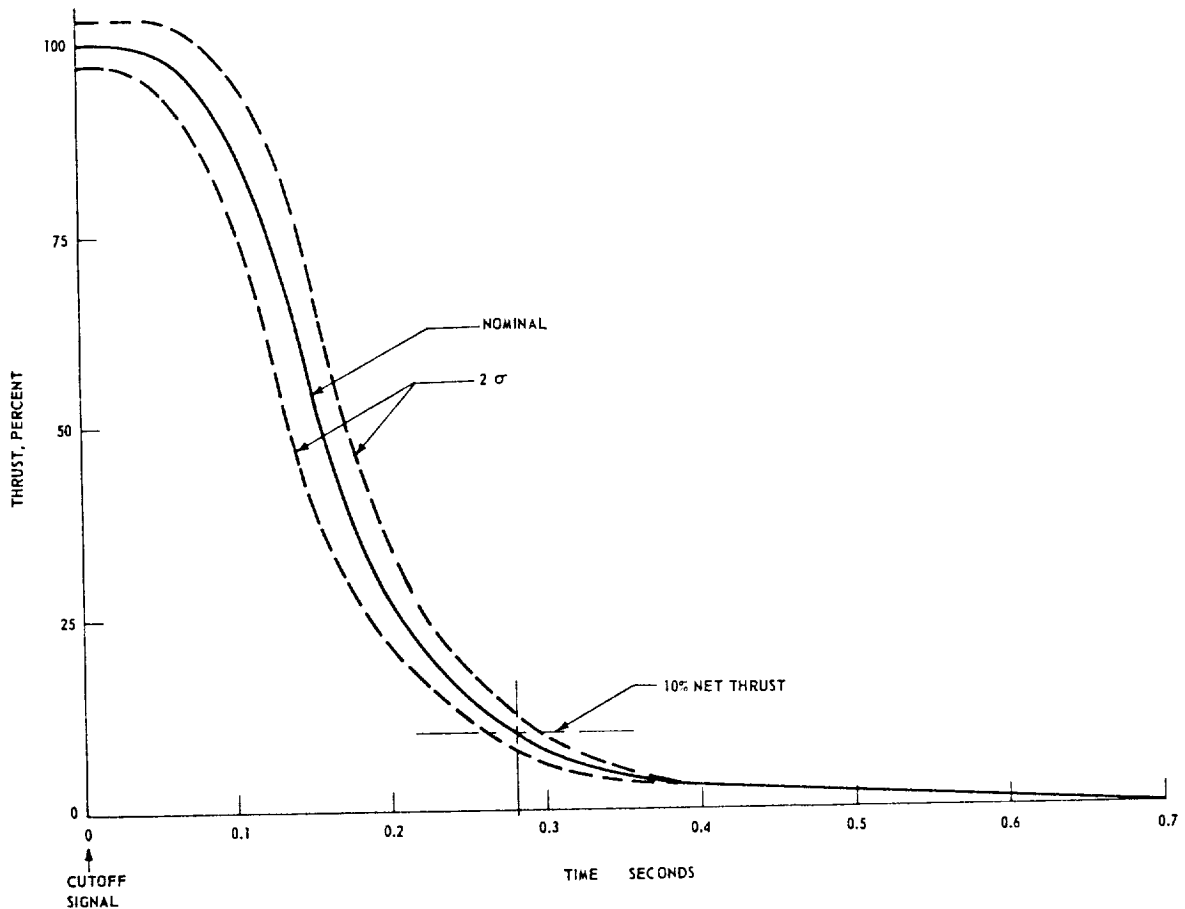


Figure 10-41.—Typical engine thrust decay deviations.

Delivery Schedules

For the vehicle builder to deliver his stage on time, complete and equipped with engines, the latter must be available to him with sufficient leadtime. If the engine builder is directly contracted by the vehicle contractor, this can be negotiated and followed up in a straightforward manner. In most cases, however, particularly with large liquid engines, these will be supplied to the vehicle contractor as Government-furnished equipment (GFE). The engine supplier, therefore, may not necessarily be fully cognizant of the detail vehicle needs. In either case, the engine designer and developer, to avoid sudden unexpected compression of his schedules, must make sure that his schedules for design, drawing release, manufacture, development, and engine delivery are in accord with the vehicle needs.

Maintenance and Logistics

Until reliable and economic methods are developed to recover and refurbish rocket vehicles, rocket engines will be used only once in flight, which will be preceded by a reasonable number of checkout and acceptance firings. The engine model specification will include the total prescribed run capability (lifetime) of the engine, usually expressed in multiples of the rated flight duration. A factor of, for instance, 6, which includes a reserve for repetition of checkout runs, is typical. Because of the stringent weight considerations in rocket vehicles, engine design attempts to assure this life expectancy, but no more. Although reasonable safety factors make it most unlikely that the engine would completely collapse shortly after the allowable maximum run time is exceeded, the statistical probability of

some engine part failing does increase. For this reason most engine specifications prescribe overhauls of a stated scope whenever this limit is exceeded.

Similarly, upper limits are set for storage times. If these are exceeded, routine replacement of certain engine parts will be made, notably of gaskets and seals. Rocket engine preservation and packaging methods are well developed, permitting storage periods from 3 to 5 years without overhaul.

During shipping, handling, installation, servicing, checkout, static firing, and launch preparation, damage of various types may be incurred by the engine because of parts failures, mishandling, oversights, or accidents. All incidents must be corrected by repair and/or parts replacements.

Any or all of the described maintenance action may be required while the engine is still with the engine builder, or following its delivery to the vehicle contractor. An accurate and effective maintenance or logistics plan must be worked out between the two contractors, or with their contracting agency, considering all handling needs at all test stations. This includes consideration of under what conditions engine return to the factory for overhauls, repairs, and parts replacements should be made. If return is not required, the correct handling fixtures and tools must be provided for each location. Above all, an adequate stock of spare parts must be planned. The engine designer will frequently be consulted for his advice in an effort to avoid both time losses due to lack of parts and costly overstocking.

Multiple-Engine Use

In view of the cost of rocket engine design, development, and procurement, common usage of a given engine for several vehicles, or for several stages of the same vehicle, is very desirable. Also logistics, handling, checkout, launch preparation, and instrumentation requirements can be substantially reduced or simplified. Caution must be exercised however, not to go "overboard," lest engine-to-vehicle interfaces become considerably more complicated.

Effort should be concentrated on the common usage of the major cost items and engine build-

ing blocks, such as turbopumps, injectors, combustion chambers, gas generators, valves, gimbal blocks, and high-pressure ducts. Peripheral equipment, such as instrumentation lines, servicing lines, inlet ducts, and wire connections, should be left flexible enough to adapt them to each vehicle without compromise. It is tempting to procuring agencies to warehouse just one engine model and ship "from the shelf" to wherever the need arises. This convenience, however, may cost substantially more than the expected savings: In mission compromises, reduced reliability, increased coordination effort between engine builder and vehicle builders, substantially increased possibility of oversights and communication gaps, and cost- and time-consuming retrofits. As always, a joint thorough and unbiased analysis considering all aspects, including that of the long-range future, will readily yield information about the point of diminishing returns.

Reserves and Safety Margins

In his negotiations with the engine user, i.e., "the customer," which quite likely is a Government agency, the engine designer, like the vehicle builder, will frequently find himself under pressure to compromise. This may be to cut weight, to accelerate schedules, or to maintain reliability with dwindling funds. It is then that he will be most in need of his top management's understanding and support. But it is here also where he will be most criticized if it is found that his analyses were incomplete, superficial, not optimized, or heavily biased by safety factor upon safety factor. To strike an optimum balance between high performance and adequate safety factors and reserves is one of the finest arts of engineering and is directly translatable into the degree of success. Once the designer is certain that he has achieved this balance, or if he is concerned that he may lose it, he should so go on record. If he does, he should also remember Edmund Berkeley's observation: "Thoughtful and tolerant disagreement is the finest climate for scientific progress."¹

¹Edmund C. Berkeley: Preface to "Giant Brains," John Wiley, 1949.

Chapter XI

Design of Liquid Propellant Space Engines

Liquid propellant space engines embody the same operating principles and general characteristics as the liquid propellant rocket systems previously discussed. However, their specific missions for the use in spacecraft require special design considerations, which will now be discussed.

11.1 PRINCIPAL SPACE ENGINE APPLICATIONS

By definition, space engines supply all those forms of rocket propulsion which a spacecraft requires for various maneuvers in space. This may include attitude control and stabilization, coplanar and interplanar orbit changes, trajectory corrections, rendezvous maneuvers, lunar and planetary landings and takeoffs, and retrofiring (reversed thrust for deceleration) during reentry into the Earth's atmosphere. The thrust of a space engine may be a fraction of a pound or many thousands of pounds. Besides a few solid propellant systems (used mainly for single-start, retrofiring rockets) and stored gas systems (used only in applications for thrust levels less than 1 pound, and for a total impulse of less than 5000 lb-sec), the great majority of the space engines are of the liquid propellant type. Because of their inherent operational advantages, liquid systems most likely will continue to dominate the space engine field, even when advanced nuclear and electrical propulsion systems become available.

Liquid propellant space engine systems may be divided into two basic groups: vehicle main propulsion systems and reaction control systems. These differ not only in function and thrust level but also in the type of propellant they use, the degree of required controllability and thrust variation, and system components. Common to virtually all of them is the requirement that they be able to start and operate reliably in the cold vacuum conditions of space.

Spacecraft Main Propulsion Systems

The main propulsion systems for most spacecraft are pressure-feed, storable hypergolic propellant systems, such as the A-4 stage propulsion system, with thrust levels up to about 25 000 pounds. These systems include propellant tanks and their pressurization system, control valves, main thrust chamber assembly or assemblies, and a gimbal mechanism or some other type of thrust vector control. Most main thrust chambers are ablatively cooled, while attached nozzle extension skirts are radiation cooled.

In a few cases, turbopump-feed systems have been used, such as the 50 000-pound thrust (sea level) turbopump-feed liquid oxygen/ammonia rocket engine produced by the Reaction Motors Division of the Thiokol Corp. for the North American X-15 research plane. As space missions become more ambitious, requiring increased total impulse and higher-energy cryogenic propellants, turbopump-feed systems will undoubtedly play an increasingly important role in spacecraft propulsion. Most space missions require multiple starts and a certain degree of thrust throttling. These requirements usually account for the principal differences between the main propulsion systems for spacecraft and those for booster vehicles.

Reaction Control System

These systems deviate more drastically from other liquid propellant rockets, because of their design arrangement and their thrust levels, which run from 1 pound up to 500 pounds, with most systems probably falling within the 1- to 100-pound range. The thrusts of these systems may be used to provide attitude control to properly position a spacecraft, to align a spacecraft for a midcourse corrective or terminal maneuver, and to stabilize the vehicle after separation from another stage or during Earth reentry.

As a rule, attitude-control engines are used in opposing pairs to produce pure couples about

an axis. They are mounted in clusters to simplify plumbing and wiring. Parallel pairs of engines, or individual units, are used for translational movements along the vehicle axis, as in rendezvous and docking maneuvers.

The reaction control engine systems are usually pressure fed, using monopropellants or storable hypergolic propellants. In all cases thrust level and duration must be very closely controllable. The thrust chambers may be ablatively cooled or radiation cooled, depending on the application.

Application Example

The application of various space engine systems may best be illustrated by typical examples, such as the spacecraft for the U.S. Apollo Moon-landing program. The space vehicle system to carry the Apollo aloft, the Saturn V, consists of the S-1C (five F-1 $\text{LO}_2/\text{RP-1}$ engines—total thrust, 7 500 000 pounds), the S-II (five J-2 LO_2/LH_2 engines—total thrust, 1.15 million pounds), and the S-IVB (one J-2 LO_2/LH_2 engine—thrust 230 000 pounds) stages (fig. 11-1). The Apollo spacecraft itself consists of the command, the service, and the lunar excursion modules.

The service module has a 21 900-pound, fixed-thrust restartable pressure feed $\text{N}_2\text{O}_4/50$ (UDMH)-50 (N_2H_4) engine as its main propulsion system. Its thrust chamber has a nozzle expansion area ratio of 60 to 1 and is gimballed for thrust vector control by a redundant electromechanical device. This engine system provides the thrust for mid-course correction as well as for entry into, and escape from, lunar orbit. It also serves as an abort system, if necessary, after the launch escape system has been jettisoned.

The service module's reaction control system is composed of four separate and interconnected pressure-feed engine systems utilizing the same propellants as the main propulsion system. The systems are mounted external to the forward skin of the service module at 90° intervals. Each engine system consists of four pulse-modulated, 100-pound thrust chamber assemblies with a 40-to-1 nozzle expansion area ratio. These provide the three-axis attitude control for the spacecraft during Earth orbit, lunar injection, lunar orbit, LEM docking and separation from the command module.

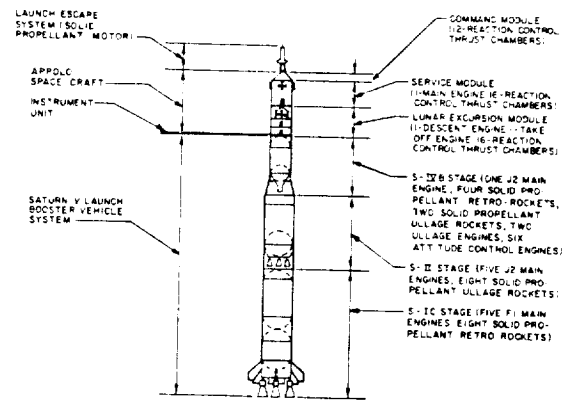


Figure 11-1.—The propulsion systems of the Saturn V for the U.S. manned Apollo flight to the Moon program.

The command module requires thrust only for three-axis attitude control during reentry into the Earth's atmosphere and to assist the service module's reaction control system during separation of the two modules. The command module reaction control system is made up of two separate, interconnected pressure feed $\text{N}_2\text{O}_4/\text{MMH}$ engine systems, either of which is capable of completing the Earth reentry mission. These engine systems are located in the aft equipment compartments. Each system consists of six pulse-modulated, 91-pound, thrust, chamber assemblies of a 9-to-1 nozzle expansion area ratio.

The lunar excursion module (LEM) has two main engine systems, one for the descent to the Moon's surface, and the other for takeoff from the Moon and injection into lunar orbit for rendezvous with the command and service modules. The LEM descent engine system has a nominal thrust level of about 10 500 pounds, which can be gimballed and throttled over a 10:1 range. The takeoff engine is a rigidly mounted, 3500-pound, fixed-thrust engine, which doubles as an abort engine in the early portion of the mission. The LEM also carries an attitude control system which uses 16 thrust-chamber assemblies. All are pressure fed, using a $\text{N}_2\text{O}_4/50$ (UDMH)-50 (N_2O_4) propellant combination.

11.2 GENERAL DESIGN CONSIDERATIONS

Prior to the actual design of a space engine system, it is necessary to examine the

basic engine parameters to determine their influence on the spacecraft's ability to perform its intended mission. Here, again, an overriding consideration is reliability. Typical space missions include the establishment of an orbit around a planet following a transfer from Earth which may last several months or years. The ability of a propulsion system to coast in space for these prolonged periods and then fire reliably is typical for many contemplated missions. It is one of the foremost considerations in the design of space engines. Based on mission, trajectory, and payload requirements, the following major design areas must be examined for the optimization of one or a group of propulsion systems:

- (1) Propellant type
- (2) Vehicle system operational requirements
- (3) Mission environmental effects

Several different designs (assuming various propellants, feed systems, chamber cooling methods, etc.) may be conducted simultaneously for a given space mission. These designs must be carried far enough to evaluate their relative merits such as reliability and performance, and to establish the advantage of one design over the other. An optimum system design should thus emerge.

Selection of Propellants

Various aspects of liquid rocket propellants have been discussed in section 1.4. Here we will discuss the characteristics which are pertinent to their selection for space engine application. The reliability and performance of a spacecraft will depend greatly on the propellants used. This is of paramount importance in establishing the optimum design criteria and final operational capabilities of a vehicle. For any planned space mission, the projected program time periods, as related to the anticipated state of the art and operational reliability of the propellants to be used, should be the first criterion for their selection. Propellants with undesirable characteristics and those that have no advantages over similar, more desirable types should be eliminated early in the studies. In addition, propellants are selected on the basis of the following:

1. *Specific impulse.*—The criterion of specific impulse is, perhaps, the most commonly used basis for comparison in nearly all propellant evaluations. For a given initial spacecraft

mass (limited by the payload capability of the launch vehicle) and required mission velocity increment, the mission payload capability is a function of the main engine system specific impulse and the spacecraft inert weight, as indicated by equation (2-1). Similarly, for a given spacecraft initial mass, inert weight, and payload, the mission velocity increment capability is directly proportional to the main engine system specific impulse. The specific impulse of a reaction control engine system affects directly its system package weight. A higher specific impulse will result in a lower system weight for a given total impulse requirement.

2. *Operating temperature.*—In an overall vehicle optimization study, the criterion of specific impulse must not be used as the only hard-and-fast rule for propellant selection, because the problem of maintaining the propellants at temperatures that permit effective use of the propulsion system after coast is an additional, major consideration in spacecraft design. The requirement for thermal control of the propellants during coast affects the selection of the propellants and the vehicle configuration. Heat transfer between propellants, and between propellants and other vehicle components, must be considered, as well as heat radiation out to space, in from the Sun, and between vehicle components. Studies have indicated the feasibility of insulating the propellants against excessive temperature changes, even during long coast periods in deep space missions. However, for the cryogenic propellants more insulation weight is required than for Earth-storable propellants. This difference becomes greater the longer the mission coast periods.

3. *Density.*—The bulk density of a propellant combination has a pronounced effect on vehicle payload. This can most easily be seen in the case of the $\text{LF}_2/\text{N}_2\text{H}_4$ combination, the specific impulse of which is comparatively low, as compared to LF_2/LH_2 or LO_2/LH_2 . However, its bulk density advantage may result in a higher ideal velocity increment for certain space missions.

4. *Ignition characteristics.*—Hypergolicity of the propellant combination used in space missions is always considered very desirable to effect a simpler and more reliable engine system, particularly for multiple starts.

5. *Cooling and other characteristics.*—Some propellants are excellent coolants (for regenerative or film cooling), while others have little cooling capability. The propellant combination will determine the combustion temperature and the gas constituents, which vary widely as to their compatibility with chamber materials, especially with ablative or refractory materials which are frequently used in space engines.

If possible, all propulsion systems in a spacecraft should use the same propellant combination. However, in some applications the reaction control engines are also used for propellant settling in the main system tanks. Thus they must be supplied by separate tanks equipped with positive expulsion devices. Different propellants may have to be used in this case. Characteristics of various propellants suitable for space engine applications are summarized in table 11-1. Characteristic trends of relative payload capabilities versus mission coast duration, for various propellants and engine systems, are shown in figure 11-2. It can be seen that for coast periods up to about 4300 hours (6 months), there is no significant change in payload capability.

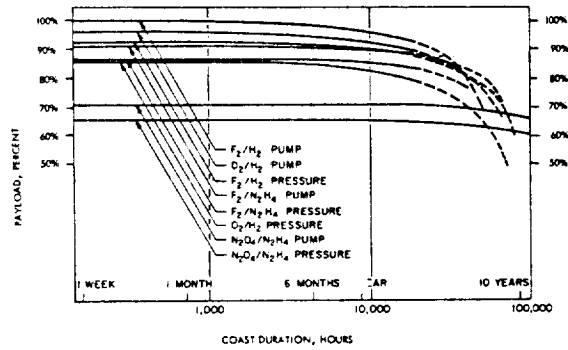


Figure 11-2.—Effect of mission coast duration on relative payload capabilities of various propellant engine systems for a given mission velocity increment.

Vehicle System Operational Requirements

After the vehicle system operational requirements have been analytically established for a given space mission, many design parameters and special considerations for the engine system or systems can be derived. Principal areas of consideration, in addition to propellant selection, are:

TABLE 11-1.—Comparison of Various Liquid Propellant Combinations for Space Engine Applications

Propellant combination	^a Specific impulse, seconds	Density impulse, sec-gm/cc	Freezing and boiling points °F, oxidizer/fuel (FP)(BP)/(FP)(BP)	Mixture ratio, O/F	Combustion temperature, °F	Remarks
F ₂ /H ₂	474	241	(-364)(-307)/(-435)(-423)	9.3	6440	Hypergolic
^b O ₂ /H ₂	456	143	(-362)(-298)/(-435)(-423)	4.7	5110	Nonhypergolic
OF ₂ /B ₂ H ₆	430	424	(-371)(-299)/(-265)(-135)	3.5	7010	Hypergolic
OF ₂ /B ₂ H ₆	420	357	(-371)(-299)/(-265)(-135)	2.15	5910	Hypergolic
F ₂ /N ₂ H ₄	419	551	(-364)(-307)/(35)(236)	2.4	7285	Hypergolic
OF ₂ /CH ₄	417	451	(-371)(-299)/(-300)(-260)	5.6	6700	Nonhypergolic
O ₂ /B ₂ H ₆	408	303	(-362)(-298)/(-265)(-135)	2.0	5960	Nonhypergolic
N ₂ H ₄ /B ₂ H ₆	402	254	(35)(236)/(-265)(-135)	1.2	4085	Nonhypergolic
N ₂ O ₄ /B ₂ H ₆	375	340	(11)(70)/(-265)(-135)	2.9	5710	Nonhypergolic
^b N ₂ O ₄ /N ₂ H ₄	341	409	(11)(70)/(35)(236)	1.23	5513	Hypergolic
^b MON/EMHF	341	407	(-23)(29)/(-76)(144)	2.2	5330	Hypergolic
^b MON/MMH	338	401	(-23)(29)/(-63)(189)	2.4	5370	Hypergolic
^b N ₂ O ₄ /50-50	339	408	(11)(70)/(18)(170)	2.1	5175	Hypergolic
^b N ₂ O ₄ /MMH	339	407	(11)(70)/(-63)(189)	2.3	5290	Hypergolic

Notes: MON = Mixed oxides of nitrogen, 85% N₂O₄-15% NO.

MMH = Monomethylhydrazine, CH₃ · N₂H₃, 50-50 = 50% UDMH, (H₃C)₂N₂H₂-50% N₂H₄.

EMHF = Eutectic mixture of hydrazine fuels = 87.6% MMH-12.4% N₂H₄.

^aBased upon theoretical shifting equilibrium at 150-psia nozzle stagnation chamber pressure and 40:1 nozzle expansion area ratio in the vacuum.

^bPropellant technology and application are well established.

1. *Engine system total impulse, design thrust level and run time.*—These are determined and optimized by analyses of the mission trajectory, considering spacecraft operating limitations such as acceleration loads. Typical liquid propellant rocket engine total impulse, thrust, and run times for various space missions are presented in figure 11-3. Required mission total impulse and engine thrust level influence, to a large extent, the choice between a pressure feed and a pump feed system.

2. *Engine system operating characteristics.*—This includes engine thrust throttling range, thrust as a function of time, number of starts and repetition rate, cutoff impulse and accuracy, and thrust vector control requirements. Most of these characteristics are determined by various projected spacecraft maneuvers. It may also be desirable for the same engine system to fulfill more than one type of maneuver, or to be reused on subsequent missions. Typical thrust-time histories for various spacecraft maneuvers are presented in figure 11-4.

3. *Engine system design.*—Experience has shown that multiple-start operation as required by most space engine systems has a more severe effect on a rocket engine than has continuous steady-state operation of comparable firing dura-

tion. This may be expected, considering that continuous operation involves a minimum of control components and actuations. Multiple starts, on the other hand, require that each component responds perfectly each time it is called upon. In addition, multiple starts require much longer periods of absolutely minimum propellant and pressurant leakage. Therefore, more rigorous approaches toward improved reliability, such as component or subsystem redundancies, must be considered in the design.

4. *Engine system component design.*—Besides mission environmental effects (to be discussed below), the detail design of the engine system components are directly affected by the spacecraft design configurations. For instance, the location of the system (internal in or external to the spacecraft) determines the feasibility of radiation cooling for the thrust chamber. Engine space envelope limitations affect the choice of nozzle type, allowable expansion area ratio, or even the feed system type. (In some applications a pump feed system affords a much higher

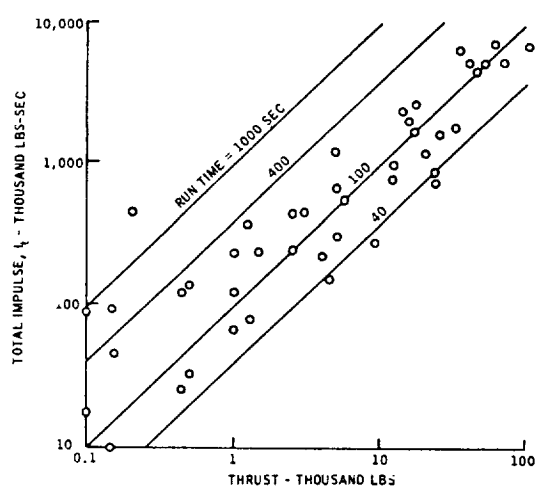


Figure 11-3.—Typical liquid propellant rocket engine total impulse, thrust, and run time for various space missions. (Coulbert, C. D., "Selecting Cooling Techniques for Liquid Rockets for Space Craft," J. Spacecraft and Rockets 1, 129-139, 1964.)

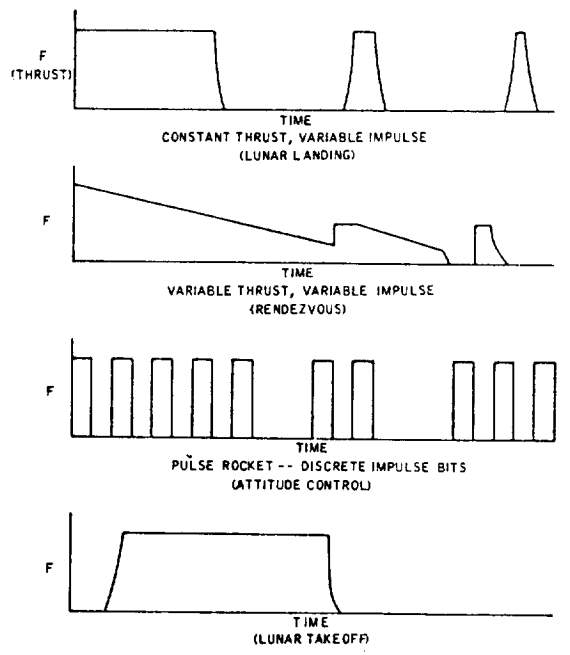


Figure 11-4.—Typical liquid propellant rocket engine thrust-time histories for various spacecraft maneuvers. (Coulbert, C. D., "Selecting Cooling Techniques for Liquid Rockets for Space Craft," J. Spacecraft and Rockets 1, 129-139, 1964.)

expansion area ratio for a given envelope.) The structural design of the system components is influenced by the maximum vehicle acceleration and by vibration loads.

Mission Environmental Effects

After the propellants have been selected and the basic propulsion system design established, with preliminary considerations of mission environmental effects, it is possible to examine the various engine subsystems in detail to determine which components or phase of system operation is still affected by the projected mission environment in space. The characteristics of this environment include the following:

1. *High vacuum.*—The low ambient pressures experienced in space missions may cause vaporization of metals and partial or complete removal of film or adsorbed gas layers at the surface of the material. Principal problems associated with high-vacuum conditions are:

- (a) Reduced ability of a component to perform its function, due to mass loss through material vaporization or bulk property changes.
- (b) Changes in the radiative heat transfer properties of the material, which could increase, to a destructive level, the bulk temperature of a component such as a radiation-cooled nozzle skirt.
- (c) Possibility of condensation of metallic vapor on electrical components, resulting in short circuiting.
- (d) Changes in the fatigue, frictional, and creep properties of materials, as well as the possibility of self-welding of metals.

Design remedies against high-vacuum effects include material selection and proper location of the components within the vehicle to take advantage of nonvacuum environments.

2. *Thermal environment.*—The thermal environment encountered in space missions, such as in Earth orbit or during the transfer phase in interplanetary flights, is an important consideration in the design of space propulsion systems, especially for the storage of the propellants. Three external sources of radiant energy must be considered when evaluating the thermal environment of a spacecraft. These are direct solar, albedo (solar energy reflected from a planet), and

planetary emitted radiation. Direct solar radiation is the largest external heat source. It is therefore advantageous to orient the spacecraft for maximum protection from direct solar radiation to the vulnerable subsystems such as propellant tanks. The quantitative evaluation of thermal radiation in space indicates that damage to some components may result from the excessive absorption of radiant energy, unless protective means are applied such as reflective surfaces or coatings. A very real problem with the prediction of the thermal properties of materials in the vacuum is the lack of knowledge about the effect of the ever-present oxide-metal surface film on heat transfer mechanisms.

3. *Nuclear radiation.*—The two most important effects of nuclear radiation in space on metals are the production of internal heat, and dislocation of the atoms within their crystalline structure. The nuclear particles of interest are fast neutrons, lower energy protons, alpha particles, electrons, and gamma rays. The fast neutrons present the most severe problem. It is known, however, that they do not exist to a great extent in space. Generally, the total radiative flux from all nuclear radiations is not sufficient to cause any appreciable damage to metals over a period less than 2 years.

4. *Meteoritic bombardment.*—Spacecraft will be exposed to the impact of meteoroids ranging in size from microscopic dust particles to bodies of asteroid dimensions with a wide distribution of kinetic energies. Collision of the spacecraft with these materials would result in surface erosion, punctures, or total destruction of the vehicle. The ideal protection for propulsion system components would be to locate them entirely within the vehicle. This, however, is usually not practical for parts such as the thrust chamber nozzle skirt. Therefore, adequate consideration must be given to the design of these parts with respect to the cited effects.

5. *Effects of gravity.*—The absence of acceleration forces, as well as the presence of large acceleration forces, should cause no mechanical design problems if proper provisions are made in the design phase. The main problem will be with the propellant feed system. This can be overcome by positive expulsion or by providing propellant settling rockets (which themselves would require a positive expulsion feed system).

11.3 DESIGN OF SPACECRAFT MAIN PROPULSION SYSTEMS

System Design

The reliability requirements for space missions have led to simple, stored inert gas pressure feed main propulsion systems (fig. 5-1), using conventional hypergolic Earth-storable propellants and redundant control components. For tube connections, the trend is to welded or brazed joints, with flexibility provided either by braided metal hoses or metal bellows. Integrated engine packages are preferred, consisting of thrust chamber and injector assembly, integrated propellant control valve package, and flight instrumentation. Besides meeting thrust and performance specifications, principal system design requirements for a spacecraft main engine are:

- (1) High reliability and crew safety (through redundancy in the control system; use of proven design concepts, materials, and fabrication techniques; and extended life and overstress testing)
- (2) High combustion stability rating with respect to perturbations during start and throttle transients
- (3) Capability of numerous starts, with repeatable cutoff impulse
- (4) Capability of deep throttling (optional, not required by all missions), with simple controls
- (5) Capability of propellant utilization and tank blowdown (ullage expansion)
- (6) One signal each, for start and cutoff
- (7) No purge, bleed, or lubrication equipment required
- (8) Effective isolation of the propellants from the system during long coast periods (use of propellant isolation valves)
- (9) System growth potential and flexibility to mission modifications
- (10) Sufficient protection against the effects of heat, nuclear radiation, and meteoric bombardment.

For missions involving intermittent propulsion system operation, during periods of more than a few months, the pressurization system design calls for special provisions, such as a completely sealed pressurant system. Pressuriza-

tion could be provided by several individual pressurant tanks of different size, each of which remains sealed by explosive-actuated valves (fig. 7-72) until needed. A sealed pressurization system would not require gas venting during any part of the mission, thus eliminating losses due to intentional venting, or because of leakage past the vent valves.

In some applications, the propulsion system can be operated on a propellant tank ullage gas blowdown principle during the latter portion of the mission. This could reduce the required amount of pressurant (and pressurant tank volume) by as much as one-half of that for a regulated, constant pressure system.

Ignition of the main thrust chamber is critical with any multiple-start space propulsion system. If hypergolic propellants are used, ignition devices such as spark plugs of ASI units are not needed. However, hypergolics suffer from ignition delays at low temperatures (such as are encountered in space). Under the peculiar conditions of vacuum starting, irregular transients may occur upon ignition, such as violent chamber pressure surges. These may not be destructive, but they could place a severe burden on the control system.

For nonhypergolic propellants, spark plugs or augmented spark igniters (ASI) may be used. Spark plugs have the disadvantage of corona-arcing and electrical leakage, even in a partial vacuum. However, injection of unburned propellants into the thrust chamber or ASI with attendant vaporization usually builds up sufficient chamber back pressure to allow the plugs to function. In some systems, this process may be augmented by purge gases. Certain propellant combinations tend to ionize the gas around the plug and thus quench the spark.

Various schemes have been considered and developed for the deep throttling often required by spacecraft main propulsion systems. For instance, the Apollo LEM descent engine is required to vary thrust continuously over a range from 1050 to 10500 pounds to permit hovering, selection of a landing site, and the landing itself. Two alternate approaches to throttling are being pursued. One calls for variation of the thrust level by main propellant line throttle valves, combined with aeration of the propellants with helium gas, as shown in figure 4-47(b).

Such aeration requires a surprisingly small proportion of gas by weight. The alternative approach is to vary combustion chamber injection area, as shown in figure 4-47(a). Other potential space engine throttling methods include use of throttlable propellant gasifiers or precombustors, or the subdivision of the injector manifolds into segments, each of which can be shut off by simple on-off valves.

Figure 11-5 presents the schematic of a typical pressure-feed spacecraft main propulsion system using hypergolic Earth-storable propellants. A smaller and a larger pressurant tank satisfy pressurization requirements before and after a long coast period. The propellant tanks are equipped with positive expulsion diaphragms and remain pressurized to mission completion. An integrated main valve package contains main propellant throttling and isolation valves, including redundant features. This redundancy is obtained by series-parallel connection of the mechanically linked main propellant valves and increases system reliability, virtually eliminating critical failures (see also fig. 2-8). Aeration of

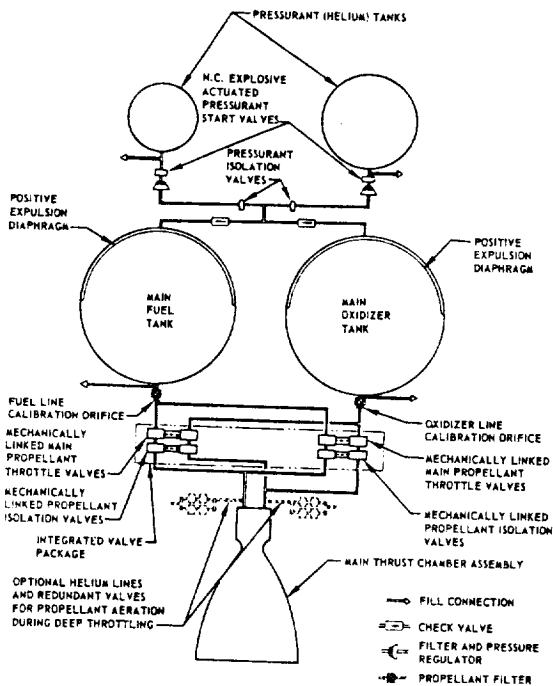


Figure 11-5.—Schematic of a typical pressure-feed spacecraft main propulsion system using hypergolic Earth-storable propellants.

propellants for deep throttling is provided by separate helium lines and redundant valves. If the system throttle requirements were removed, the main propellant throttling valves could be replaced by simple on-off types. Propellant filters are provided in both main propellant lines to minimize system line contamination with foreign particles.

The package design layout of the pressure-feed spacecraft main propulsion system schematically illustrated in figure 11-5 is shown in figure 11-6. The integrated main valve package is mounted directly to the main thrust chamber assembly, immediately upstream of the injector. The integrated engine assembly can be either rigidly mounted, or gimbal mounted, depending on requirements. Lightweight spherical propellant and pressurant tanks are secured by simple frames. An all-welded and brazed construction is employed for system assembly to prevent external leakage of pressurant gas or propellant.

In a complete space vehicle system, performance gains of the spacecraft stages will effect increasing weight savings for each succeeding lower booster stage, as indicated by equations (2-1) through (2-5). When planning future spacecraft missions, high-performance liquid propellants, such as LO_2/LH_2 and LF_2/LH_2 , thus definitely should be considered. For high mission total impulse requirements, these propellants, when used in turbopump-feed systems, tend to provide a considerable performance edge over pressure-feed systems (fig. 11-2). A turbopump-feed system for these applications must reliably supply high-pressure propellants to the combustion chamber, under vacuum and zero gravity conditions, and following extended coast

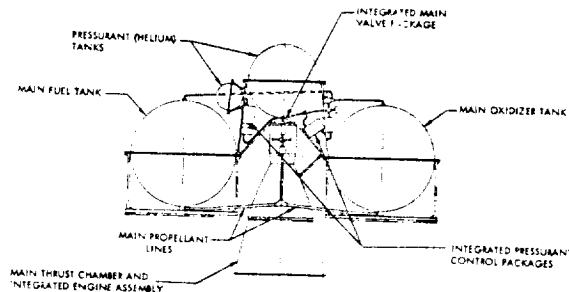


Figure 11-6.—Package design layout of a typical pressure-feed spacecraft main propulsion system using hypergolic Earth-storable propellants.

periods. All pumps must be fully primed prior to starting of the engine system to prevent delays in pump buildup and overspeeding. This may require ullage settling rockets, before and during main engine start, or positive propellant expulsion devices.

The well-proven turbopump subsystem designs and their operating concepts as established for large booster engine systems, and as discussed in preceding chapters, should be effectively applied to the design of turbopump-feed spacecraft main propulsion systems. In addition, the systems must be able to start an unlimited number of times (if possible from available tank pressure energy, without auxiliary starting devices) and to vary the thrust level (for some applications over a wide range). Major problem areas associated with turbopumps under space environmental conditions other than material considerations, are as follows:

- (1) Vacuum, temperature, and radiations effects on exposed high-speed bearings and dynamic seals
- (2) Micrometeorite penetration of fluid passages
- (3) Absence of the effects of gravitation on pump operation

Figure 11-7 presents the package design layout of a hypothetical turbopump-feed spacecraft main engine system using a LO_2/LH_2 or

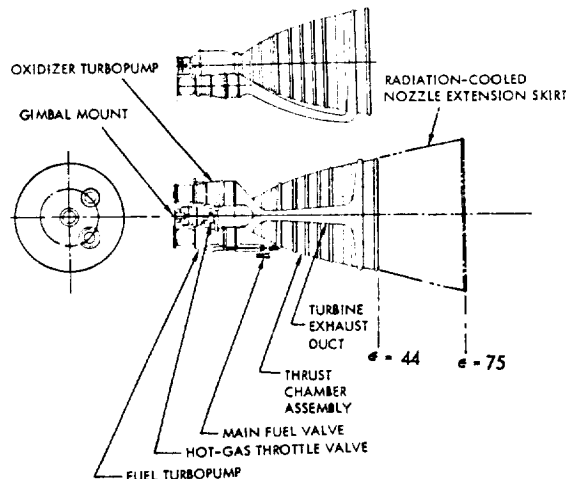


Figure 11-7.—Design layout of a hypothetical turbopump-feed spacecraft main engine system using a LO_2/LH_2 or LF_2/LH_2 propellant combination.

LF_2/LH_2 propellant combination. The main thrust chamber is regeneratively cooled by the fuel to a nominal nozzle expansion area ratio of 44:1. A radiation-cooled nozzle extension skirt may be added for certain missions to yield an overall expansion area ratio of 75:1. The propellants are supplied to the main chamber by two separate turbopump assemblies which are mounted to the thrust chamber body, resulting in an integral, compact engine. The turbines are driven by gases bled from the main combustion chamber in a parallel arrangement (fig. 6-13). A hot-gas throttle valve (such as shown in fig. 7-31) located upstream of the turbine inlets controls the turbine power, and thus the thrust level. A Y-type hot-gas duct is used to route the turbine exhausts into the main chamber nozzle. The entire engine package can be gimballed at the gimbal mount by linear gimbal actuators.

Main Thrust Chamber Design

In addition to the design elements presented in chapter IV, primary requirements for thrust chambers of spacecraft main propulsion systems are:

- (1) Optimum steady-state cooling methods, with due consideration of application in space
- (2) Ability to withstand postrun soakback, intermittent operation, and storage in the space environment
- (3) Ability to enter planetary atmospheres at high velocities

Many of the thrust-chamber-cooling techniques described in chapter IV are applicable to space engines. Especially the ablatively cooled thrust chambers, which offer the inherent advantage of simplicity, ruggedness, and independence of propellant coolant flows (including their pressure drops), and thus offset their limited total life and relatively heavy weight, are suitable for most pressure-feed space engine systems using Earth-storable propellants at chamber pressures of less than 150 psia. In some applications, ablatively cooling is supplemented by one or a combination of the following techniques:

- (1) Refractory throat inserts
- (2) Radiation-cooled nozzle extension skirts
- (3) Propellant film cooling

One of the problems associated with ablative cooling is the dimensional change of the chamber due to erosion. Nozzle throat erosion, if controlled and predictable, is acceptable for some engine systems and becomes proportionally less significant in larger thrust chamber units. For fixed-area injectors and fixed propellant supply pressures, propellant flow and engine thrust would increase with time, while specific impulse would decrease, due to throat enlargement. However, for a 40:1 expansion nozzle operated in vacuum, the specific impulse loss would be only 0.5 percent, for as much as 10 percent increase in throat area, if the aerodynamic characteristics of the nozzle contour did not deteriorate.

One remedy against excessive throat erosion is the use of a refractory throat insert. A ceramic, silicon carbide, has been used extensively for throat inserts in space engine applications. It has a high melting point (4400° F), excellent thermal shock characteristics, relatively high thermal conductivity (115 Btu/hr-ft²-°F/in), low coefficient of thermal expansion (2.4×10^{-6} in/in-°F), excellent oxidation resistance, and high abrasion resistance. Sometimes, a molybdenum backup sleeve is used when the silicon carbide insert cannot conduct heat sufficiently.

Another potential problem is the danger that the high-silica glass in the ablative material of the combustion chamber section becomes sufficiently fluid to be swept downstream and to be deposited in the throat section. This causes thrust variances and promotes an unsymmetrical velocity profile in this area. This phenomenon may be prevented by a liner of JTA (45 percent graphite, 45 percent zirconium diboride, and 10 percent silicon) inserted in the combustion zone. The liner is usually segmented, to provide a path for the gases from the pyrolyzed ablative (and reduce the Δp across the liner), and to prevent cracks that would develop in an expanding unsegmented liner.

Exclusively radiation-cooled thrust chambers would be subject to large stresses caused by the high temperatures in combustion zone and throat by the thrust transmission, and at the injector attachment points. By contrast, the radiation-cooled nozzle skirt is designed to accept and emit only the heat flux transmitted by the expanding gases, and some of the loads imposed by thrust transmission. Molybdenum alloys,

coated with molybdenum disilicide (MoSi_2) to prevent oxidation, are frequently used for nozzle skirt extensions (for skirts starting at $\epsilon = 8$ to 12) which operate at sustained temperatures around 2600°-2800° F. For nozzle skirts of higher expansion ratios (starting at $\epsilon = 40$ to 45), Hastelloy-X is sometimes used at operating temperatures around 2000°-2200° F. One potential disadvantage of radiation-cooled devices is their requirement to "see" space. A radiation-cooled skirt should face outboard and should not radiate undesirable heat to vehicle components. Radiation cooling appears unsuitable for clustered engines.

For exclusively ablative-cooled chambers used in LO_2/LH_2 or LF_2/LH_2 systems, analyses and tests have proven liquid hydrogen to be a very effective throat film coolant in low chamber pressure applications (less than 100 psia). As low as 0.1 percent of the total propellant flow used as the throat film coolant greatly reduces throat erosion for extended firing durations. The effect of such a small film coolant flow on system performance is so slight that it can be neglected. Ablative chambers with their throat film-cooled by liquid hydrogen, therefore, may be considered excellent prospects for future pressure-feed spacecraft main propulsion systems using LO_2/LH_2 or LF_2/LH_2 .

Following the firing of an ablative thrust chamber, the heat stored in the charred phenolic and silica reinforcement or in the throat insert refractory material soaks into the unburned virgin material. This postrun soakback propagates further thermal degradation, which might also be affected by the vacuum conditions, for 100 sec or more, until the mean temperature of the char is reduced to about 500° F. The weight of gas generated and expelled by soakback charring is about 15 percent of the weight of ablative material charred. It could cause a postrun residual impulse undesirably exceeding the desired minimum cutoff impulse. However, this effect is small for larger systems. For long-duration space missions, the temperature effects from solar radiation may cause vaporization of the ablative chamber material during coasting and should be prevented if possible.

Figure 11-8 shows the design of a typical thrust chamber for a pressure-feed spacecraft main propulsion system using hypergolic

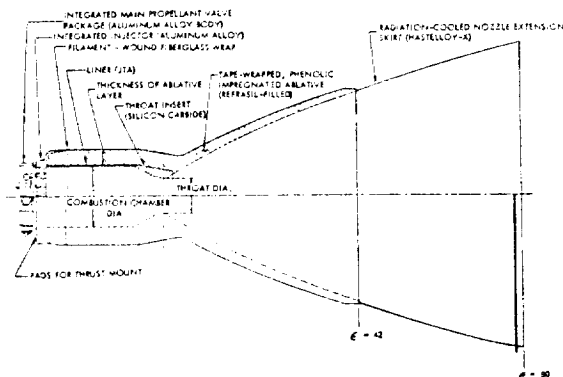


Figure 11-8.—Typical thrust chamber design details for a pressure-feed spacecraft main propulsion system using hypergolic Earth-storable propellants.

Earth-storable propellants at a chamber pressure of 125 psia. Refrasil-filled, phenolic-impregnated ablative materials are tape wrapped on a mandrel, at the combustion chamber and nozzle sections, up to an expansion ratio of 42. A JTA liner and a silicon carbide insert are provided for combustion chamber section and throat, respectively. The chamber outer wall is made of fiber-glass filament, wound to accept hoop stresses, and then wrapped longitudinally (helicallly) to contend with meridional stresses. An insulating layer, consisting of the basic or another ablative material such as asbestos or alumina silica, is wrapped around the basic ablative layer and cured to reduce the rate of heat flux to the structural fiber-glass outer wall. A radiation-cooled skirt made of 0.030-inch Hastelloy-X sheet is tape wrapped to the thrust chamber nozzle to provide the nozzle extension from an expansion ratio of 42:1 to 80:1. An integrated injector is attached to the end of the combustion chamber and is made of an aluminum-alloy forging. It is a conventional, fixed-orifice, single-ring, unlike-impinging doublet type.

Ablative thrust chambers for space engines, such as shown in figure 11-8, should be designed to permit many restarts. At the end of a specified total firing duration (design values: 400-2000 sec), sufficient insulation material must remain between char and fiber-glass shell to limit the outer wall temperature to a specified maximum value (design values: 400°-700° F). Any heat soakback during offtimes between fir-

ings should not affect total chamber duration. Equations (4-36) and (4-37) may be used to calculate the char depth. For Refrasil phenolic ablative thrust chambers operated at pressures around 100-125 psia, and using N_2O_4 and hydrazine type fuels, the following empirical equations may also be used to estimate char depth, including the effects of charring due to soakback:

- (1) For the combustion zone and the throat section (with or without liner and/or insert):

$$a = 0.0415 t^{0.5} \quad (11-1)$$

- (2) For nozzle sections downstream of the throat:

$$a = 0.0335 t^{0.5} e^{-0.0247\epsilon} \quad (11-2)$$

where

a = char depth, in

t = thrust chamber cumulative firing duration, sec

e = base of natural logarithms, 2.718

ϵ = nozzle expansion area ratio at the section under consideration

Once the char depth based on design duration, including effects of soakback, is determined, the thickness of the insulating layer required to keep the outer wall at the required temperature can be calculated.

For turbopump-feed space engine systems operated at relatively high chamber pressures, regeneratively cooled tubular-wall thrust chambers appear more suitable from heat transfer considerations. A possible disadvantage for space engine application is the response time from start signal to full thrust, which may be substantially increased if the propellant valve is located upstream of the coolant jacket. Relocating it to a point downstream of the jacket would reduce the response problem, but would introduce heat-transfer problems after shutdown, with the propellants trapped in the jacket.

Other potential problems are the heat-transfer characteristics during throttling. Also, tubular walls are more susceptible to meteoritic damage than are solid walls. In some applications, an optimum overall design may result from combining regenerative cooling with film cooling, and adding a radiation-cooled nozzle extension skirt.

Design of Control Components

The various aspects of control component design have been discussed in chapter VII. Pertinent considerations for the design of space main engine control components, in general and for propellant valves in particular, are:

- (1) Maximum reliability
- (2) Use of bellows for dynamic sealing in view of the need for long-term operating life in a vacuum environment
- (3) Combination hard and soft valve seats, for minimum leakage
- (4) Provision of a minimum of two seals and a vent between different propellants
- (5) Avoidance of sliding surfaces in components operating in a vacuum environment
- (6) Where possible, mechanical linkage of the propellant valve actuators by a mechanism that ensures positive, consistent, and synchronized opening and closing for smooth, repeatable ignition and thrust termination
- (7) Minimum electrical energy requirement for actuations

The basic design details for the various control components for space main engine systems, such as pilot valves, regulators, and vent valves, are quite similar to those for booster-stage applications. The mechanically linked, poppet-type dual-propellant valve arrangement shown in figure 11-9 is typical for main-propellant or propellant-isolation valves of space main engines using hypergolic Earth-storable propellants. In the valve shown, linked actuation is accomplished by locating the valve poppets in series, thus causing the oxidizer poppet motion to simultaneously move the fuel poppet. Complete separation of fuel and oxidizer is achieved by welded bellows seals located at both ends of the fuel poppet and at the connection end of the oxidizer poppet. Since valve actuation is provided by oxidizer fluid pressure, no bellows is required at the actuation chamber. The center vent chamber between valves sections is the critical area where propellant mixing must be prevented. However, both bellows would have to fail to cause this failure mode (reliability through redundancy). The design also incorporates all-welded static sealing joints, all-metal construction except for the Teflon dynamic poppet valve

seals, and hermetically sealed solenoids or torque motors.

The valve is spring loaded normally closed, and additionally pressure unbalanced closed when inlet pressure is applied. Actuation to open is achieved by allowing the oxidizer fluid to enter the actuation chamber at nominal oxidizer valve inlet pressure which, in turn, overcomes the closing forces on the poppets. For on-off and isolation valve applications, the full open or closed valve positions are effected by a three-way solenoid pilot valve which, when energized, pressurizes the valve actuation chamber to open, and which, when deenergized, vents the same chamber allowing the pressure unbalance and the springs to close the poppets.

In the applications as a dual-propellant throttling valve, the position of the linked main poppets is controlled by a servo pilot spool valve which meters the control fluid flow (oxidizer) to the main valve actuation chamber. The pilot spool valve, in turn, is proportionally positioned by a servo torque motor, as a function of the command signal current and its polarity supplied from a servo amplifier. By means of properly shaped valve poppet contours, the main throttling valves control the flow of oxidizer and fuel to the main thrust chamber at constant mixture ratio, and thus regulate the main chamber pressure (thrust).

System Design of Propellant Storage for Space Missions

As previously mentioned, the storage of propellants for space-system propulsion represents an important design area. Cryogenic propellants require protection against high temperatures, particularly for extended storage periods. Earth-storable propellants, by contrast, require protection against low temperatures, because of the danger of propellant freezing. There are two basic design approaches to propellant storage for space missions, the vented and the nonvented systems. The selection of the optimum system design depends on mission, propellants type, and type of engine feed system.

In a vented storage system, propellant pressure and temperature are maintained at a constant value. This system is mainly used for cryogenic propellants. Any heat input to the

propellants is absorbed by allowing a small percentage of boiloff. Since conditions will vary widely during travel, the net heat input to each propellant tank may be computed by a numerical integration process for the specific vehicle path, such as a complete orbit. This path can be

divided into a number of intervals. Equilibrium skin temperatures and net heat fluxes (considering both internal and external sources) to the propellant tanks are then determined for each orbit location. By algebraically adding the net heat inputs for each, the net heat input rate for

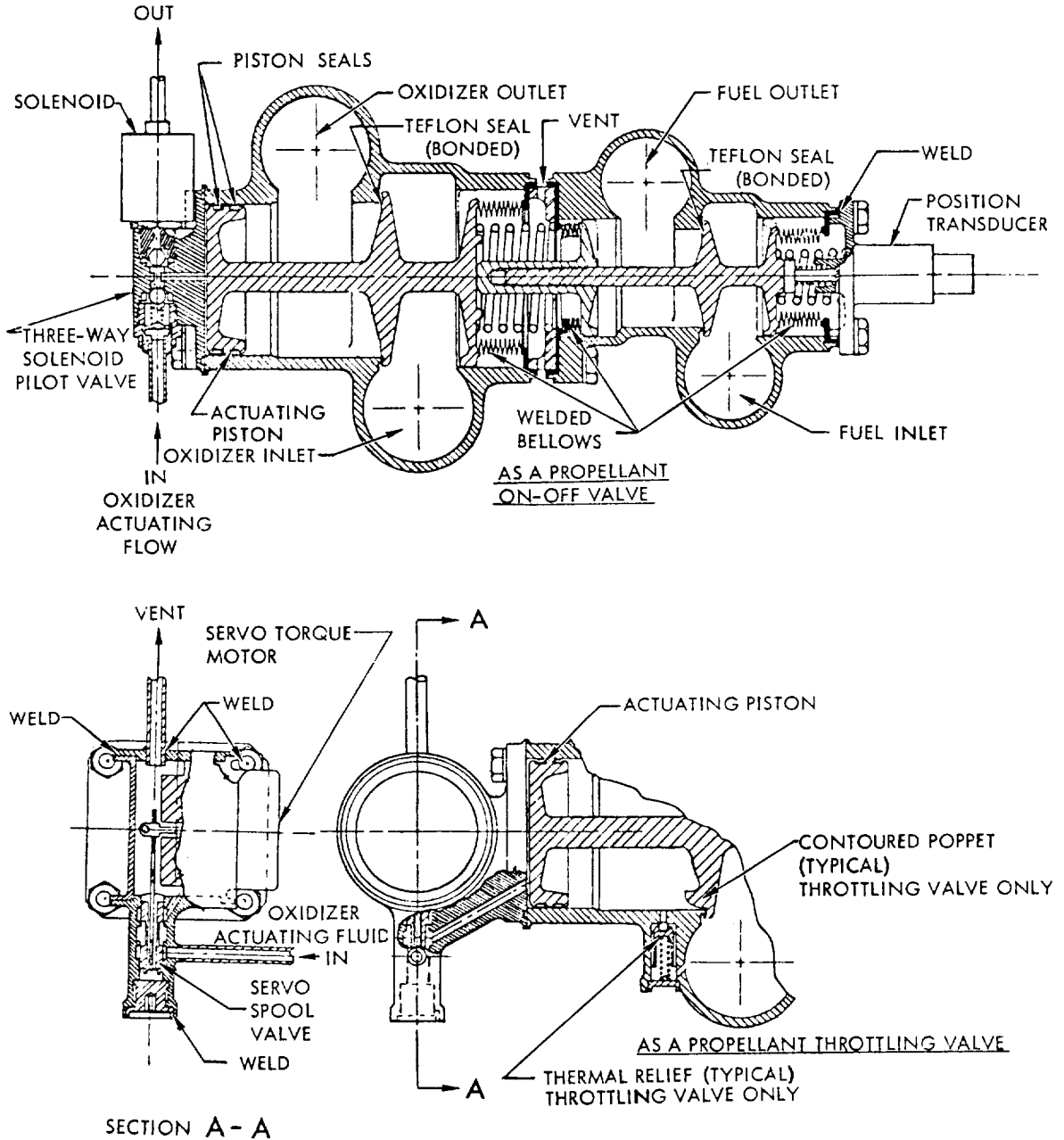


Figure 11-9.—Typical mechanically linked, poppet-type, dual-propellant on-off or throttling valve, for spacecraft main propulsion systems using hypergolic Earth-storable propellants.

one complete orbit can then be obtained and the amount of propellant boiloff per orbit calculated.

In a system without venting, any heat input to the propellant results in a propellant temperature rise and a corresponding increase in vapor pressure. This system can be applied to both cryogenic and Earth-storable propellants. The allowable pressure rise, and consequently the maximum heat input, is dictated by the allowable tank pressure. In this case, the storage analysis assumes an allowable vapor pressure rise during the mission, based on initial conditions. This permits determination of the final propellant temperature, expected changes in propellant density and ullage volume requirements, and pressure-dependent propellant tank weights. For cryogenics, it is usually assumed that the propellant experiences a uniform temperature rise. The maximum storage time is then computed by dividing the propellant heat capacity by the average rate of heat input. In this system, the storage weight penalties are composed of extra tank weight required to accommodate the pressure increase, the extra tankage required to allow for thermal expansion of the propellants, and the time-dependent insulation weight. For Earth storables, sufficient insulation is also required to prevent freezing.

11.4 DESIGN OF REACTION CONTROL ENGINE SYSTEMS

Spacecraft Attitude Control Requirements

Spacecraft attitude control requires the application of torques about the three axes (yaw, pitch, and roll) passing through the vehicle's center of mass. The problem of attitude control implies rotation and/or stabilization of the vehicle about these axes. Its operation consists of two main phases:

- (1) Rotation of the vehicle over a given angle, within a specified time
- (2) Stabilization of the vehicle in a required position, within acceptable tolerance limits

The position of a vehicle, if left uncontrolled, may not be the one required for efficient use of its main propulsion system. For example, a spacecraft may have to perform a series of tra-

jectory correction maneuvers, for which it must be oriented properly.

Another example is spacecraft separation from the launch vehicle, during which momentums may be imparted which require correction for proper orientation.

Ideally, when a spacecraft is oriented at some attitude, it should remain there indefinitely. This, however, is not the case, because the spacecraft is continuously subjected to small external and internal forces which will cause it to drift off the desired position. An attitude control system must function to counteract all disturbing torques. It could be of either a continuous, or of an on-off type. Practical considerations tend, in general, to favor the latter. The attitude control system itself contains certain nonlinearities and nonideal conditions. In actual operation these inherent nonlinearities cause the vehicle to settle in a periodic motion about a reference point. This motion is represented by a closed curve in the phase-plane and is termed the "limit cycle of operation."

The problem of attitude control, then, becomes twofold: (1) what is required to rotate the vehicle through a given angle to some new attitude, and (2) what is required to maintain the vehicle in this attitude. The energy requirement to accomplish these two basic maneuvers can be calculated, and total attitude control requirements for any space mission can be computed, by simply determining the total number of times that these two maneuvers occur.

Of the various attitude control systems, the reaction systems are the most versatile and provide a wide range of torque, up to high levels. They are universally applied to manned spacecraft and in large unmanned vehicles.

Operational Modes of Reaction Control Systems

If any reaction control system, the amount of thrust delivered on command must be very precisely controlled, if overshoot or undershoot and hunting are to be avoided. Three basic operational modes are available:

1. *On-and-off, or "bang-bang" control.*—This "multiple start" system operates intermittently as long as necessary at its rated thrust level. If the on-and-off command signals are given as a function of sensed position error only, the system would tend to be unstable because of the

timelags that are present in all real systems. This situation can be corrected through the use of control systems which utilize both position error and rate of error change to time the on and off command signals.

2. *Proportional control.*—The operating thrust of the reaction control system is varied according to the sensed error signals.

3. *Repetitive pulse control.*—This type of system needs only position error sensing and uses a system which delivers thrust in a continuous series of accurately reproducible impulse bits to assure orientation and stabilization of the vehicle. The optimum thrust pulse outline should be a square-wave. Control may be achieved by modulating pulse width, or the frequency of a fixed pulse width, or by combining both methods.

Selection of Reaction Control Engine Systems

For reaction control engine systems, both liquid monopropellants and bipropellants have been used. The selection of an optimum system for a given mission is based primarily on total systems weight (including propellants) versus total impulse. As mission time increases, so does the propellant and tankage portion of the total systems weight, while the weight of nozzles, valves, and plumbing remains fixed. A comparison of two reaction control systems of different fixed weight and specific impulse may show the lower fixed-weight system to have an overall weight advantage, despite a considerably lower specific impulse. However, sometimes the lower fixed-weight system cannot be used, simply because it has not enough thrust or cannot be operated more than a specific number of cycles.

If total impulse is the variable and total systems weight the evaluating criteria, a plot of total systems weight versus total impulse can be used to compare competitive systems. If thrust and number of restarts (operating cycles) are also factors, added dimensions in presenting the comparison are required. Based on the selection criteria of minimum total systems weight, the three major factors to be considered as independent variables for different space missions are total impulse, thrust level, and number of cycles. Selection of a reaction control engine system is largely dependent on these three requirements, in addition to reliability considerations. Other important factors are performance

tolerances, maximum impulse per cycle, space storage and environment, systems integration, and logistics.

For monopropellant reaction control systems, the system vacuum specific impulse varies from 140 to 165 seconds for 90 percent H_2O_2 , and from 200 to 230 seconds for N_2H_4 . For bipropellant systems using Earth storables or cryogenics, the system vacuum specific impulse may be estimated by applying an efficiency factor ranging from 90 to 94 percent for steady state, and from 80 to 86 percent for transient operation (less than 25 milliseconds pulse width), of the ideal specific impulse values given in table 11-1. The 90 percent H_2O_2 systems are applied up to a maximum total impulse of about 50 000 lb-sec and the N_2H_4 systems to the same or somewhat higher values. Beyond this level, the hypergolic Earth-storable bipropellant systems, which are in the majority, take over.

Optimization of Reaction Control System Operating Parameters

For most reaction control engine systems, a pressure-feed system using stored inert gas as pressurant is employed because of its simplicity and reliability. After the propellants and their feed system have been selected, parametric analyses of all engine system design variables are performed to establish the minimum weight system, within mission requirements, which still satisfies other important considerations. Major operating parameters affecting systems weight are: chamber pressure, pressurant storage pressure, mixture ratio, and nozzle expansion area ratio.

Chamber pressure and nozzle expansion area ratio are foremost optimization parameters, since the weight of major system components is directly related to and defined by them. Component weights considered in the analyses should include the pressurant and its storage tank, the fuel and oxidizer tanks, and the thrust chamber assemblies. Optimum values for chamber pressure range from 50 to 200 psia, and for nozzle expansion area ratios from 25:1 to 60:1. The optimum mixture ratio depends on propellant type and thrust chamber cooling method used. Optimum design values for inert gas pressurant storage pressure range from 3000 to 5000 psia (using 6 Al-4V titanium alloy forgings as tank material).

Basic System Design for Reaction Control Engines

For N_2H_4 and 90 percent H_2O_2 monopropellant systems, the propellant tanks can be pressurized by a stored inert gas system, as shown in figure 5-1. The propellant valves are located downstream of the propellant tanks and are used to control the propellant flow to the thrust chamber. In an H_2O_2 system, each thrust chamber has its own silver-mesh catalyst, similar to the one in the H_2O_2 gas generator shown in figure 4-50. When H_2O_2 comes in contact with the catalyst, a hot-gas mixture of steam and oxygen is produced, the temperature of which is a function of H_2O_2 concentration and its liquid temperature. For N_2H_4 monopropellant systems, some kind of ignition source is usually provided because the catalyst life with N_2H_4 is limited. The ignition source could be either an electrical heating element, or a continuously operated nuclear energy device. Frequently, to simplify ignition requirements in a N_2H_4 system, a common gas generator feeds several nozzles.

Since the liquid H_2O_2 is cool until it decomposes, the components upstream of the catalyst do not require high-temperature materials. However, feedback of heat from the catalyst chamber and the nozzle to other components must be prevented, since it would not only damage these components but could also initiate vaporization or even decomposition of the stored propellant. The H_2O_2 system has a temperature advantage (maximum temperature $1500^\circ F$) over a system using N_2H_4 , although the latter has a higher specific impulse. In the N_2H_4 system, the high operating temperature of $1800^\circ F$ requires suitable materials all the way from the generator to the nozzles.

Figure 11-10 illustrates the basic schematic of a typical reaction control system using hypergolic Earth-storable bipropellants and helium gas pressurization. Two redundant subsystems are provided, each of which is physically and functionally independent. Each subsystem is activated independently by an electrical command signal to the explosive-actuated pressurant-start valves located in the helium pressurization line, and to the various solenoid isolation valves. After passing through a micronic filter, different pressurant-isolation valves, pressure regulators, and the "quad" check-valve assemblies, the

helium at the required pressure level pressurizes the positive expulsion bladders in the oxidizer and fuel tanks. Opening of propellant isolation solenoid valves allows the pressurized propellants to flow through micronic filters, distribution lines, and line isolation solenoid valves to the normally closed injector solenoid valves which control the operation of the individual reaction control thrust chambers. The system is shut down by removal of the start signal. This closes the propellant-isolation valves and disconnects the reaction-control injector-valve solenoids from the command system.

A relief valve sealed with a burst diaphragm protects the pressurant tank against overpressurization. A high-pressure transducer monitors helium-tank pressure. In a hermetically sealed system, it could also be utilized to indicate the amount of propellants remaining in the tanks. A low-pressure transducer is located downstream of the helium pressure regulators to detect regulator malfunctions. Relief valves sealed with burst diaphragms are also provided for the propellant tanks to protect them against overpressurization.

Systems Redundancy in Reaction Control Systems

For reliable reaction control engine operation, redundancy may be provided in the following three areas:

1. *Redundancy within a subsystem.*—Several typical examples of redundancy within a subsystem are shown in figure 11-10. Two explosive-actuated pressurant start valves are used in parallel. Similarly, two pressure regulators are used in parallel, pilot selected by a three-way solenoid valve. In each propellant pressurant line, a "quad" check valve assembly is used to insure that propellants which may have permeated through the positive-expulsion bladders will not reverse-flow into the common pressurant line downstream of the pressure regulators. A similar "quad" check valve assembly is installed downstream of each propellant tank to prevent reverse flow of propellants from the other propellant subsystem, or from the main propulsion system.

2. *Redundancy between subsystems.*—Refer again to figure 11-10. Here, redundancy between two independent subsystems is provided by normally closed solenoid intersubsystem-propellant

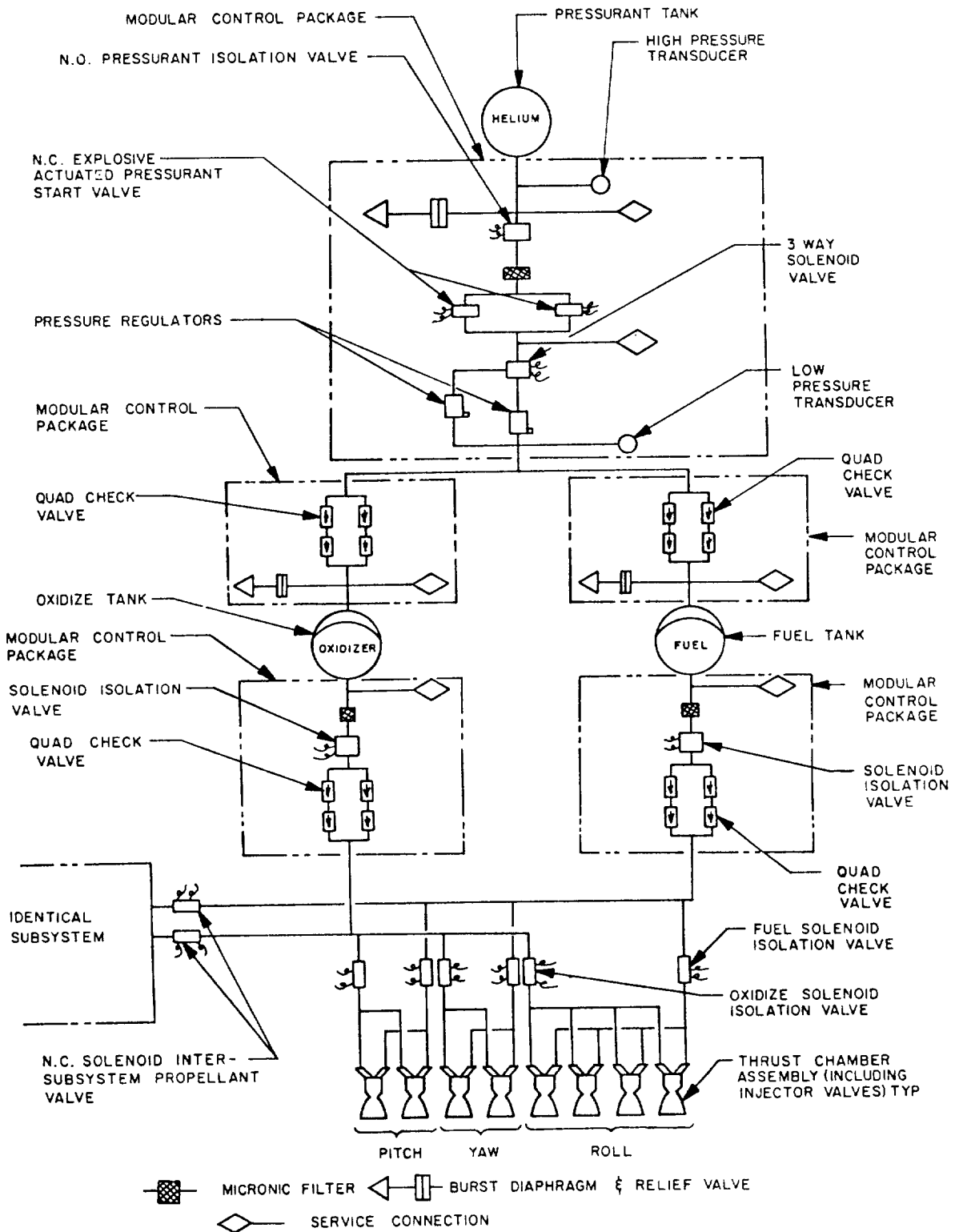


Figure 11-10.—Basic schematic of a typical reaction control system.

valves. If one propellant subsystem should fail, these valves open and connect to the propellant lines of the other subsystems. The distribution line solenoid isolation valves can isolate a group of thrust chambers (pitch, roll, or yaw) should an individual thrust chamber in the group malfunction.

3. *Redundancy outside the system.*—Redundancy outside the system may be provided by connecting to the pressurant and propellant system of the spacecraft main propulsion system, which must be capable of supplying one or both subsystems with pressurant and/or propellants.

Packaging and Installation of Reaction Control Engine Systems

As with spacecraft main propulsion systems, the control components of a reaction control engine system can be modular packaged. The modular packages will incorporate related control components within the same housing (forging or casting), as shown in figure 10-9. Typical modular control packages for reaction control systems are indicated schematically in figure 11-10. The thrust chamber injector propellant valves are frequently designed as an integral part of the thrust chamber assembly (fig. 11-13). All-welded and brazed construction is preferred to prevent pressurant and propellant external leakage.

Figure 11-11 presents the installations of the reaction control engine systems used on a typical manned spacecraft, the Gemini capsule. All

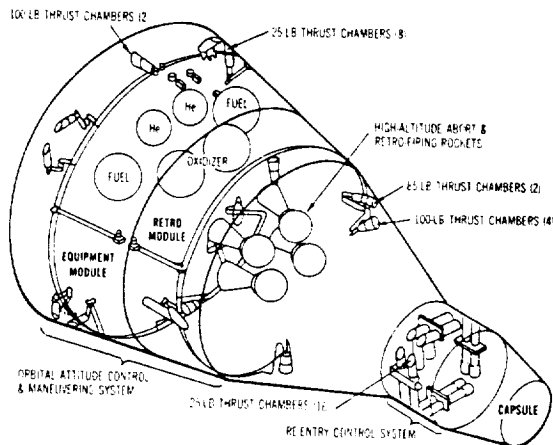


Figure 11-11.—Reaction control engine systems for the Gemini manned spacecraft.

systems are pressure fed and use a N_2O_4/MMH propellant combination. The tasks of the Gemini reaction control engine systems built by Rocketdyne are high-altitude abort trim, attitude control in orbit and during reentry, and rendezvous and docking control. In addition, four solid propellant engines built by Thiokol are used for high-altitude abort and reentry retrofiring.

The reaction control engine systems for the Gemini spacecraft (fig. 11-11) consist of—

- (1) Sixteen 25-pound thrust chambers for reentry control (also see fig. 11-14), consisting of two complete propulsion systems, with a pulsing requirement of 6 cycles/sec and a minimum impulse bit = 0.25 lb-sec
- (2) Eight 25-pound thrust chambers for orbital attitude control—pulsing requirement: 6 cycles/sec, minimum impulse bit = 0.25 lb-sec
- (3) Four 100-pound thrust chambers for translation control in rendezvous and docking maneuvers—pulsing requirement: 2 cycles/sec; minimum impulse bit = 26 lb-sec
- (4) Two 100-pound thrust chambers and two 85-pound thrust chambers for longitudinal propulsion—pulsing requirement: 2 cycles/sec; minimum impulse bit = 25 lb-sec

The Gemini control thrust chambers are all located inside the vehicle, with the nozzles trimmed flush with the outer skin. Thus, no radiation cooling can be used. All thrust chambers are ablatively cooled.

Design of Reaction Control Thrust Chambers

For systems using hypergolic Earth-storable bipropellants, the reaction control thrust chambers may be effectively cooled by one of the following methods:

- (1) Ablative cooling
- (2) Radiation cooling
- (3) Ablative cooling with radiation-cooled nozzle skirt
- (4) Ablative cooling supplemented by regenerative or film cooling

Other methods, such as regenerative cooling and film cooling, can probably be used successfully to a certain extent. However, none can compete

with ablative or radiation cooling in overall system simplicity, minimum system pressure drop, and minimum performance loss (film or transpiration cooling requires extra propellant flow). Also, the advancement of the state of the art of materials, and of analytical and design techniques, has made both ablative and radiation cooling, rather reliable and practical cooling methods for reaction control thrust chambers.

The design and construction principles for ablative-cooled reaction control thrust chambers are not basically different from those for main propulsion systems. However, the small physical sizes (from 1- to 100-pound thrust), and the operational modes (such as the pulse mode) of reaction control thrust chambers, require some special considerations.

For example, a typical roll control thrust chamber is designed to produce thrust ranging from 1.6 to 2.5 pounds at chamber pressures from 80 to 130 psia. The design throat area is 0.0120 in² (0.124-inch diameter). This throat diameter should be produced accurately and remain unaffected by erosion during firing. Generally, in small ablative rocket motors, the internal geometry remains essentially unchanged as ablation progresses. The thermal protection in this case is provided by the internal change from the pyrolysis or decomposition of the plastic resin. This yields a porous char layer without any significant dimensional changes. The transition zone between the virgin ablative and the char is referred to as the "char front." The ablation rate, in this case, is not governed by a surface regression, but rather by a regression of the interface between the virgin ablative and the char. However, if highest accuracy is required, throat inserts made of refractory ceramics, such as silicon carbide, and combustion chamber liners made of graphite or ceramics, will further reduce throat-size changes due to erosion and will prevent ablative fluid from being swept downstream from the combustion chamber and deposited in the throat section. Silicon carbide can be machined to rather close tolerances by grinding. The diameter of a throat can generally be maintained with a tolerance of ± 0.001 inch.

The methods of determining the char depth of ablative reaction control thrust chambers are similar to those of the larger size chambers. Semiempirical or empirical equations such as

equations (4-36), (4-37), (11-1), and (11-2) may be used. However, in the case of reaction control thrust chambers designed for repetitive pulse, or for intermittent operation, the heat-transfer conditions may be quite different. Many studies and experiments have been conducted in this area, and theoretical and empirical correlations have been generated.

A study by Lee and Hahn¹ indicates that for repetitive short-pulse operation, the char-front region in an ablative-cooled thrust chamber does not experience appreciable temperature fluctuations, because of the attenuating effect of the low thermal diffusivity of the char layer. The char front region therefore stays at the pyrolyzing temperature during the entire period of cycling. The char regression under pulse operation can, therefore, be treated as a case of continuous firing with effectively reduced gas-side heat transfer. The results show that the char depth based on equal cumulative firing time is a function of percentage of the firing time over the elapsed time. It increases with the decrease of the percentage of firing, to a maximum value several times that obtained with continuous firing. At low percentages of firing, i.e., below approximately 5 percent burn (pulse width/pulse cycle), the char depth drops again, because of the increasing proportion of radiation or convection losses from the outer skin surface of the chamber, to heat influx from the combustion gases. In fact, at some critical pulse mode, the char regression ceases after an equilibrium char depth is attained.

During intermittent, on/off, i.e., multiple-start firings, with off periods in between firings of relatively long durations, the temperature at the char front does not remain at the pyrolyzing temperature all the time. The char-depth progression for a typical multiple-start system is shown in figure 11-12. The ascending straight line represents char-depth progression for a continuous firing (100 percent burn). Assume that the first firing cycle was terminated at "a." Since the char layer at this time is at a higher temperature than the pyrolyzing temperature,

¹Lee, J. C., and Hahn, J. R., "Regression Rate of Char Front in Ablative-Cooled Rocket Motor Under Pulse Operation," AIAA Preprint 64-262.

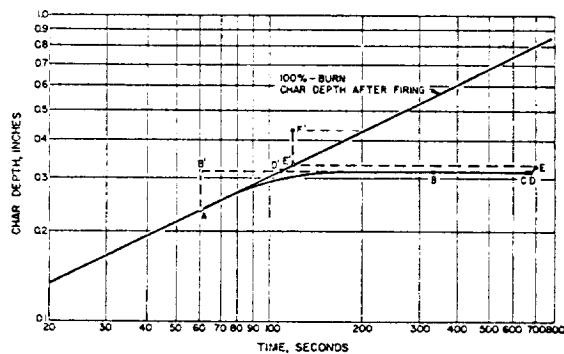


Figure 11-12.—Combustion chamber char depth versus cumulative firing time of a typical ablative-cooled reaction control thrust chamber.

ablation continuous until the temperature at the char front drops below the pyrolyzing temperature (point "b"). When the next cycle starts at "c," the char depth remains constant during warmup, until pyrolyzing resumes through shutoff at "e." The various events may be projected onto the 100-percent burn line for convenience. The line d'-e' in this case represents the soakback char depth following the second cycle. Subsequent cycles can be treated similarly. Note that in the short second cycle, soakback charring is a multiple of the charring during burning. In general, it can be seen from figure 11-12 that soakback usually consumes a large percentage of virgin ablative and does not contribute to the useful firing time. Even though some char preheating time is gained during the subsequent firing, it could hardly compensate for the loss of burn time which would have been available had the chamber been fired continuously. In this respect, it is desirable to minimize the number of soakbacks, particularly toward the last portion of the virgin ablative.

Combinations of repetitive pulsings and multiple starts can be treated in the same manner as described above, except that the "on" cycles composed of repetitive pulsings will effect a different gradient of the ablation curve, based on the particular percent-burn value, instead of the continuous firing or 100 percent curve.

Figure 11-13 presents the design details of a typical 100-pound-thrust, ablative-cooled, reaction control thrust chamber assembly for hypergolic Earth-storable bipropellants designed and manufactured by Rocketdyne. An optional regen-

eratively cooled jacket is provided for extra-long durations (up to 30 minutes). Fuel is used as the regenerative coolant to supplement the ablative cooling. A segmented JTA graphite liner is used in the combustion chamber section; the throat insert is made of silicon carbide. Ablative materials are oriented at 90° and 0° , respectively, at various regions according to structural requirements. Asbestos-phenolic is used for the outer insulation. The injector propellant valves are brazed to the injector, which forms an integral part of the thrust chamber assembly.

Figure 11-14 presents the 25-pound thrust chamber assembly for a reentry control system, also designed and manufactured by Rocketdyne. Its design details are similar to the thrust chamber shown in figure 11-13. However, no auxiliary regenerative cooling jacket is provided. Rather, a ceramic liner (silicon carbide) is used in the combustion chamber section. The nozzle exit is trimmed flush with the vehicle outer skin.

Total radiation cooling applied to reaction control thrust chambers may pose the following problems:

- (1) Difficulties when inboard-installation of the thrust chamber is required
- (2) Thermal shielding requirements for components surrounding the thrust chamber
- (3) Recrystallization of the chamber construction metals in multiple-start applications
- (4) Need for a larger thrust chamber, when operated at a relatively low chamber pressure

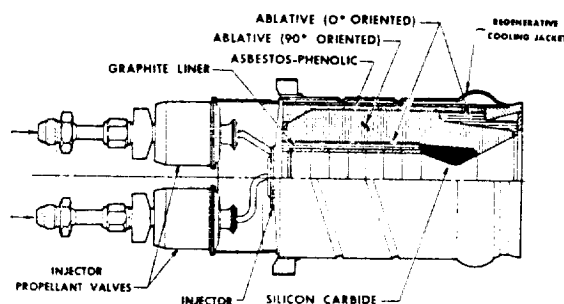


Figure 11-13.—Typical 100-pound-thrust, ablative-cooled, reaction control thrust chamber assembly for hypergolic Earth-storable bipropellants, designed and manufactured by Rocketdyne (regenerative cooling jacket optional).

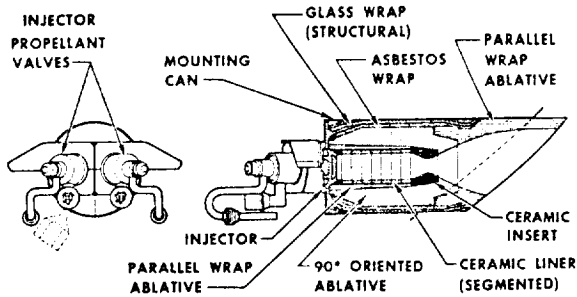


Figure 11-14.—25-pound thrust reentry control system thrust chamber assembly designed and manufactured by Rocketdyne.

A radiation-cooled thrust chamber, if properly designed and applied, is probably the simplest, lightest, and relatively most reliable. The required working temperature of a radiation-cooled thrust chamber wall could be as high as 3400°-3700° F for Earth-storable propellants operated at or near their optimum mixture ratio, and at chamber pressures of 100 psia. Advanced refractory materials such as the 90 percent tantalum-

10 percent tungsten alloy, electroplated with a cermet coating of chromium and zirconium diboride, could be used for the chamber. An alloy of molybdenum and 5 percent titanium, coated with $MoSi_2$, may also be used.

Figure 11-15 presents a typical, totally radiation-cooled reaction control thrust chamber assembly. It has an integral combustion chamber and nozzle, with a thick throat section. The injector plate can be either bolted as shown, or welded to the chamber. A heat shield is mounted aft of the injector to reduce radiant heat transfer to the injector propellant valves. The shield is shaped to minimize reflection back to the thrust chamber. The shield is attached to the mount structure and is thermally insulated by ceramic spacers.

The injectors for reaction control thrust chambers using hypergolic Earth-storable propellants are usually designed with a conventional fixed-orifice, single-ring, unlike-impinging doublet pattern. A splash plate is often utilized to improve performance.

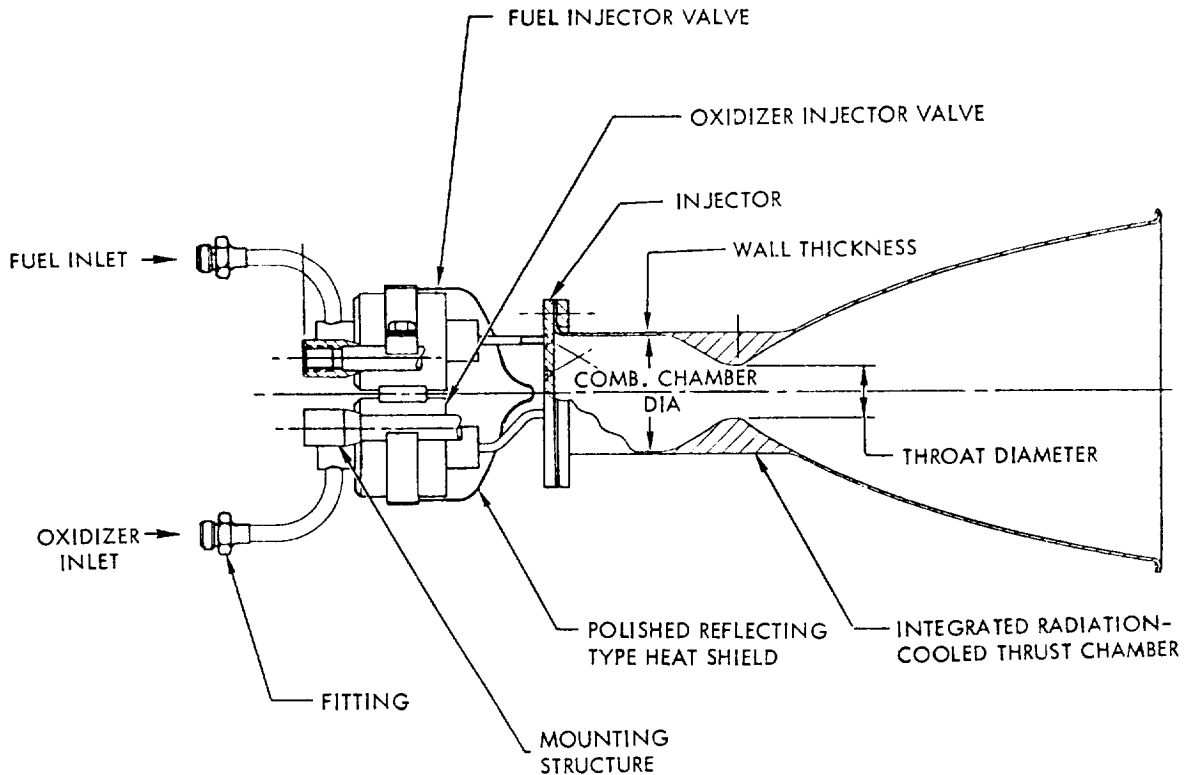


Figure 11-15.—Typical total radiation-cooled reaction control thrust chamber assembly.

Design of Control Components for Reaction Control Engine Systems

The various aspects of control component design for reaction control engine systems are similar to those for spacecraft main propulsion systems, except that propellant and pressurant flow rates are at much lower levels. For instance, the propellant flow rates of a typical roll control thrust chamber may be 0.0041 to 0.007 lb/sec (oxidizer), and 0.0021 to 0.0032 lb/sec (fuel), to produce a thrust range from 1.6 to 2.5 pounds. Besides the propellant injector valves, all other control components, such as pressure regulators, check valves, and vent valves, are similar to those of other systems.

In addition to high reliability and suitability for the space environment, pertinent design requirements for the injector propellant valves of reaction control engine systems are:

- (1) Fast (as short as 2 milliseconds) and precise response when opening or closing
- (2) Tight shutoff, with no afterdribble
- (3) Low power consumption

Most injector valves are solenoid operated. The needle-type propellant valve design shown in figure 7-43 is suitable for integral injector valve assemblies, with both valves actuated by a common solenoid.

Figure 11-16 shows another typical injector propellant valve, designed and manufactured by Rocketdyne. It is used with the reaction control

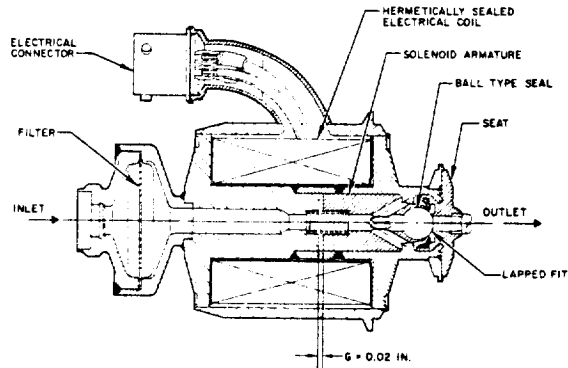


Figure 11-16.—Typical injector propellant valve used with reaction control thrust chambers in pulsing applications, designed and manufactured by Rocketdyne.

thrust chamber assemblies shown in figures 11-13 and 11-14 for pulsing applications. The valve is a fast-acting, solenoid-operated, direct-actuated type. The propellants flow through the solenoid core at nearly constant velocity, resulting in low-pressure drop. The valve incorporates a hermetically sealed electrical coil, and a metal-ball-type seal. The latter is crimped solidly into the nose of the armature and engages a conical metal seating surface. Positive seating is obtained by lapped fits. The inlet port contains a filter to protect against contaminants. The valve is capable of operating reliably in the temperature environment of space.

INDEX

- A-1 stage engine, 64, 65, 66, 67, 68, 86, 96, 102, 109, 110, 129, 130, 193, 201, 217, 218, 219, 222, 224, 249, 250, 261, 295, 296, 303, 364, 378, 391, 392, 393, 395, 397, 398, 399, 412
- alternate turbine design, 257
- assembly design layout, 261
- bellows, 378
- C* correction in performance, 398-399
- centrifugal pump, 224
- chamber pressure vs. engine thrust, 395
- chamber product gases of, values, 85, 86
- cutoff sequence, 68
- design values, 393
- engine performance diagram, 66
- general description, 64, 67
- ignition monitor valve, 303
- impulse turbine, 249, 250
- influence coefficient, 397-398
- injection momentum ratio, 129
- injection velocity, 130
- main oxidizer valve, 295-297
- oxidizer pump, 217-219, 222, 364
- packaging, 399
- preliminary layout for 750K, 67
- propellant flow design characteristics, 391
- starting sequence, 67
- static-firing measurement list, 412
- system operation, 67
- thermal conductance, 102
- thrust chamber, 95, 96, 109, 110
- turbopump, 193, 199, 201, 249, 392
- A-2 stage engine, 37, 38, 39, 68-72, 76, 96, 111, 112, 129, 131, 154, 165, 166, 199, 233, 236, 238, 269, 389, 392, 399
- accessory weight history, 37, 38, 39
- coaxial shell chamber design, 111, 112
- control of propellant, 269
- cutoff sequence, 72
- fuel pump, 233, 236, 238
- general description, 68-70
- injection momentum ratio, 129, 131
- injection velocity, 131
- injector data, 130
- nozzle expansion area ratio, 76
- operating parameters (150K), 69
- packaging, 399
- payload weight of, 38
- preliminary layout for 150K, 71
- schematic for tank pressurization of propellant, 165
- sequence diagram, 71
- A-2 stage engine (continued)
- starting sequence, 72
- steady state operation, data for, 166
- system operation, 70
- thermal conductance, 103
- thrust chamber configuration, 95, 96
- turbopump, 199, 389, 392
- venting, 166
- A-3 stage engine, 72, 73, 74, 75, 76, 86, 97, 156, 167
- chamber product gases, values for, 86
- engine and propulsion system operational sequence, 75
- general description, 72, 73
- helium system, 156
- preliminary design layout for 48K, 75
- system operation, 73, 74
- thrust chamber configuration, 95, 97
- thrust load, 76
- A-4 stage engine, 74, 75, 76, 77, 78, 95, 97, 121, 144, 154, 156, 158, 159, 163, 268, 269, 270, 324, 325, 338, 342, 344, 392
- burst diaphragm on oxidizer tank, 344
- chamber nozzle extension, 121
- chamber product gases, values for, 86
- comparison of various tank pressurization systems, 158, 159
- engine and propulsion schematic, 78
- engine mixture ratio control loop, 269
- estimated pressure drops in oxidizer tank, 158
- feed system, 320
- general description, 76
- helium system, 156
- internal configuration for thrust chamber, 97
- main-stage thrust throttle control loop, 268
- omission, 64
- operating parameters for 7.5K, 77
- operational sequence, 79
- oxidizer tank, 154
- propellant control system, 268
- propellant mixture ratio control loop, 269, 270
- propulsion system, 78, 338, 392
- relief valve, design data on, 324, 325
- storage pressure requirement, 159
- system operation, 76
- tankage, 342
- thrust chamber configuration, 95
- Ablative cooling, 118, 119, 448
- Acceleration, isentropic and nonisentropic, 13
- Accelerometers, 411, 415
- Accordion motion, 420

- Acoustic chamber liners, 149, 150
 Actuators for thrust vector control, 272-279
 Additives for propellants, 19
 Aerodynamic spike nozzle, 93
 AirResearch Manufacturing Co., 349
 ALBM, 26
 Alloys, 61-62
 aluminum, 61, 76, 118
 cobalt base, 62
 copper base, 62
 magnesium, 61
 nickel-base, high temperature, 61
 special, 61, 62
 Alpha vehicle, 4-stage, 63, 95
 Altitude control requirements, 442
 Altitude thrust coefficient, 17
 Alumina, palladium-impregnated, 141
 Aluminum-alloy tubing, minimum bend radii for, 360
 Aluminum alloys, 61, 76
 Aluminum on ablative liner, 118
 Ambient air pressure, effect on performance of, 1, 14
 Apollo LEM, 435
 Apollo moon-landing program, U.S., 430
 AR systems, 141
 Asbestos on ablative liner, 118
 ASI (augmented spark igniters), 140, 435
 Assurance of reliability, 43
Astronautics magazine, 127
 Atlas ICBM, 329
 Atlas Mercury, 64
 Atomization, evaluation of, 131
 Augmented spark igniters (ASI), 140, 435
 Axial pumps, multistage, 177-178
- B-10 life, 258
 Baffled injector, 122
 Baffles, combustion-chamber, 149
 Ball bearing centrifugal load DN limits, 259
 Ball-type valves, 298, 299
 Bang-bang control. *See* On-off type control
 Bartz calculation, 100, 101
 Bell nozzle, 90, 91
 Bellows, 292, 293, 375-379
 Berkeley, Edmund C., 428
 Bernoulli's energy equation, 280
 Beta angle, definition of, 128, 129
 Bipropellant combinations, 25-27
 Bipropellant gas generators, 134, 171, 181
 Bipropellant injector, 126
 Bipropellants, 19, 132, 138
 Bleed lines, cryogenic propellant, 356
 Bootstrap, 67
 Breadboard engines, 64
 British systems, 141
 Buddy plan, 45
 Burnout weight of engine, 35
 Burst diaphragms, 326
 Butterfly valves, 294-298
- C* correction, 398-399
 Calculations for 4 stages of Alpha vehicle, samples of, 63-79
 Catalysts, 141
 Catalytic bed of monopropellant gas generator, 133, 134
 Catastrophic failure, definition of, 44
 Cavitating inducers, 210
 Center of gravity, data sheet for typical, 39
 Centrifugal pumps, 176, 177, 196, 220-225
 Chamber, 4, 13, 14, 15, 149, 200
 Chamber wall cooling system, demands on, 34
 Change control, 51
 Char front, 447-448
 Char-rate analysis, 120
 Chemical reaction products, systems using, 167-171
 Chugging, 146
 Closed-loop mixture ratio control, 269-270
 Clustering of liquid propellant, 415-419
 Coaxial injector, 127
 Coaxial shell thrust chamber, 109
 Cobalt base alloys, 62
 Colburn calculation of gas-side heat-transfer coefficient, 100
Collier's magazine, 415
 Columbian, 62
 Combustion chambers, 4, 5, 123, 148, 149, 150
 baffles, 149
 design as factor in preventing triggering, 148
 disturbances, 150
 divergent wall gap, 149
 function, 5
 gas flow processes, 4
 gas flow through, 5
 heat protection, 123
 shape, 5
 velocity of liquid propellants at injection plane, 5
 Combustion devices, failures, definition, 47
 Combustion instability, 144-147
 design approaches toward control, 147
 German type, 144
 high-frequency, 145
 intermediate-frequency, 146
 low-frequency, 146
 types, 144
 Combustion product gases, 12, 197
 Combustion stability, 122, 147, 150
 injector, 122
 limits, 147
 rating, 150
 Combustion timelags, 146
 Complex redundancy, 46
 Components and mounts, interconnecting, 353-381.
 See also Interconnecting components and mounts
 Conax Corp., 327
 Confidence level, relation to reliability, 42
 Conical nozzle, 90
 Connectors, terminology for, 404, 405
 Conservation of energy, principle of, 4, 5
 Conservation of matter, principle of, 5
 Control of manufacturing and material defects, 48

- Control systems, 263-327
 - calibration, 266
 - checkout and test, 267
 - closed-loop, 263-265
 - cutoff, 265
 - dynamic seals for fluid-flow components, design for, 289-294
 - engine thrust level, 267-268
 - fixed-area-type regulators, design of, 307-309
 - fluid flow components, design for, 280-294
 - gas pressure regulators, design of, 315-321
 - liquid flow and pressure regulators, design of, 321-322
 - main stage duration, 265
 - miscellaneous valves, 325-327
 - open-loop, 263
 - orifice locations and sizes, 266
 - pilot valves, design for, 301-307
 - pressure relief valve, design for, 322-327
 - propellant-mixture ratio and utilization, 268-272
 - propellant valves, design of, 294-301
 - safety, 265
 - servovalves, design of, 309-315
 - start, 265
 - thrust vector actuators, 272-279
- Coolant side heat transfer, 105, 106, 107
- Cooling system for thrust chamber, 98-99, 100-102, 104-121
 - ablative, 119
 - circular tube wall of regenerative, 108
 - coaxial shell, 109
 - considerations in selecting, 99
 - coolant side-heat transfer, 105
 - correction factor, variation across boundary layer, 101
 - dump, 114
 - film, 115
 - gaseous film, 116, 117
 - gas-side heat transfer, 100
 - heat transfer schematic for regenerative, 104
 - liquid film, 115, 116
 - radiation, 120, 121
 - regenerative, 104-114
 - techniques and selection, 98
 - thermal resistance of carbon wall deposit, 102
 - transpiration, 117, 118
- Copper base alloys, 62
- Cost of vehicle design, 50
- Coulbert, C. D., 433
- Critical failure, definition, 44
- Critical pressure ratio between throat and chamber, 6
- Cryogenic propellants, 19, 68, 165, 166, 167, 187, 271, 279, 288, 291, 331, 332, 336, 345-348, 356, 422-424, 429, 440
- Curtis turbine, 180
- Cutoff impulse, 34

- Damping devices, 149
- Decay deviations, 427
- Deferred failure, definition of, 44

- De Laval nozzle, 6, 8, 89, 239
- Density impulse of propellant additives, 20
- Derivative pressure feedback (DPQ) valves, 273-274
- Derivative type control, 264
- Design change checkoff sheets, 51
- Design Check-Off Sheet, purpose of, 50
- Design integration of engine systems, dynamic analysis for, 384-390
- Design quality, importance of, 50, 51
- Design reviews, 49-50
- Diametral-squeeze-type O-ring seals, 290
- Directed nonexplosive gas flows, 150
- Discontinuity stresses, 339
- Divergent wall gap, chamber, 149
- DN value, 258
- Dome-loaded gas pressure regulator, 319-320
- Doublet injector, 125, 127
- Dry weight of engine, 35
- D.S.D. Co., 367
- Du Pont, 383
- Dual bipropellant gas generator system, 172
- Dual combustion, 181
- Dual shaft turbopump, 182
- Duct design, 373, 374
- Dump cooling, 114
- Dynamic analysis in engine system design integration, 384-390
- Dynamic seal, design, 258
- Dynamic stability, 148

- E-D (expansion-deflection) nozzle, 92, 93
- EDS. See Emergency detection system
- Elastomer rings, 366
- Electrical failures, definition of, 47, 48
- Electrical hydromechanical component analogies, 275
- Emergency detection systems (EDS), 45, 421
- Energy losses during pump operation, 194-195
- Engelhard Industries, Newark, N.J., 141
- Engels, D. A., 275
- Engine components, failure modes, 45
- Engine design, 1, 3-4, 16, 28, 31-62, 96-97, 181, 416, 419-421
 - A-1, A-2, A-3, A-4 stage, thrust chamber configurations for, 96-97
 - areas for increase in quality, 51
 - availability, 50
 - burnout weight, 35
 - departures from basic simplicity, 28
 - detailed procedures, 51-55
 - dry weight, 35
 - duration of run, 32-34
 - envelope (size), 42
 - flight run duration, 33
 - gas exhaust velocities, sea level and in space, sample calculation, 3-4
 - manual for, 419
 - parameters, major, 31-62
 - parameters, ranges of, 16
 - performance as function of altitude, 32
 - performance parameters, 32

- Engine design (continued)
 - quality, importance of, 50, 51
 - shape, most used laws and formulae for, 1
 - simplicity, 32, 43
 - stress analysis, 56
 - thrust in space, sample calculation to determine, 3-4
 - thrust level, 31-32
 - tools for improving quality, 51
 - typical sequence diagram, 55
 - wet gimbaled weight, 37
 - wet weight, 37
- Engine failure sensing and shutoff system (EFSS), 420-421
- Engine Out (EO) capability, 416
- Engine out, definition, 44
- Engine out source, 181
- Engine system, 1-30, 42, 43, 55, 59, 60, 63-79, 144, 148
 - A-1, A-2, A-3, A-4 stages for Alpha, 63-79
 - basic elements, 21
 - components, 28
 - function, 1
 - introduction, 1-30
 - low alloy steels, 60
 - model of thrust equation, 3
 - operating characteristics in prevention of triggering, 148
 - oscillations, effects of, 144
 - pressure environment as function of altitude, 2
 - reliability of design, 42, 43
 - selection of materials, 59
 - size, effects of, 42
 - thrust chamber nozzle, specific function of, 2
 - thrust equation (general), 2
 - thrust generation, momentum theorem in basic equation for, 1
 - typical pressurized gas feed, 28
 - typical schematic, 55
 - typical turbopump feed, 29
- Engine systems design integration, 383-428
 - calibration, 390-394
 - clustering of liquid propellant, 415-419
 - dynamic analysis, 384-390
 - electrical, 403-411
 - engine-to-vehicle interfaces, 383-384
 - instrumentation, 411-415
 - mechanical development, 399-403
 - performance characteristics, 394-399
 - simplicity, 383-384
- Engine-to-vehicle interfaces, actuator systems, 276-278
 - crossstalk and spring rate, 277
 - engine installation and alignment, 276
 - hydraulic system, 277, 278
 - loads, 276-277
 - performance evaluations, 279
 - secondary injection of matter, 279
- Envelope, definition, 42
- Environmental effects on stress, 56
- Enzian missile, 140
- Ermeto flareless tube fitting, 358
- Error, human, 49
- EWf (equivalent-weight factor), 187
- Expansion of gas, isentropic and nonisentropic, 13
- Failure, 44-48, 51, 58, 59
 - catastrophic, 44
 - combustion devices, 47
 - criteria, 59
 - critical, 44
 - deferred, 44
 - electrical, 47
 - fatigue, 46
 - functional, 45, 46
 - mission, 44
 - modes of, 44, 58
 - order of, 44, 45
 - reports, 51
 - unexplained, classification of, 48
- Failure modes of engine components, definition, 45
- Fatigue failure, definition, 46
- FBM, 26
- Feed system hydraulic capacitor, 149
- Feed system perturbations, 150
- Fiber-glass filament-wound propellant tanks, 348-349
- Film cooling of thrust chamber, 115
- Flame holding characteristic, 146
- Flame propagation velocity, 146
- Flange joints, design, 360-370
- Flexitallic Gasket Co., 367
- Flow (of propellant), 9-10
 - areas, computations for, 10
 - computations, 10
 - specific volumes, 9
 - static pressures, computation for, 9
 - temperatures, computation for, 9
 - velocities, computation for, 10
- Flowmeters, 271, 411, 414-415
- Fluid, ideal, basic flow characteristics of, 280
- Fluorine, in A-3 stage engine, 72
- Formula(s), 1, 7, 8, 13
 - design of shape and prediction of engine behavior, 1
 - effect of pressure on thrust, 13
 - ideal gas flow, 7, 8
- Fox Valve Development Co., 300
- Francis-type impeller, specific speeds, 190
- Frozen vs. shifting composition of gas flow, 21
- Fuel additive blender unit, 183, 184
- Fuel additive subsystem, 182, 184, 185
- Fuel characteristics, 34, 35
- Functional failures, definition, 45
- Fusible wire links, 142
- Gas constant, effect on performance of engine, 14, 15, 34
- Gas feed systems, 151, 167
- Gas flow, 4-8
 - combustion chamber, 4
 - formulas for ideal, 7, 8

- Gas flow (continued)
 parameters and terms applicable in thrust chamber, 4
 terms used in calculation, 5
 thrust chamber, ideal conditions, 4
- Gas flow orifices, 309
- Gas-generating devices, 131-136
 classification, 132
 design objectives, 131-132
 solid propellant, 132
- Gas generator igniter, 138
- Gas generators, 132-136, 171, 172
- Gas generators, liquid bipropellant, operating characteristics, 136
- Gas law, perfect, 4
- Gas pressure relief valves, 322-323
- Gaseous film cooling of thrust chamber, 116, 117
- Gaskets, 361
- Gate-type valves, 300-301
- Gears for turbines of turbopump, 260-261
- Gemini capsule, 446
- General Controls pilot valve, 302
- German A-4 engine (V-2), 138, 141, 142, 143, 156, 181
- German efforts, Peenemunde, 139
- German systems, 141. *See also* Catalysts
- German V-2 (1942), ratio of engine weight to thrust, 36
- GFE. *See* Government-furnished equipment
- Gimbal angle, 425
- Gimbal mounts, 379-381
- Government-furnished equipment (GFE), 427
- Gravity, effects of, 434
- Greenewalt, Crawford H., 383
- Ground support equipment (GSE), 267, 426
- Growth factor of single stage or multistage vehicle, 40
- GSE. *See* Ground support equipment
- Hahn, J. R., 447
- Hart, T. J., 338
- Hatch and Papell equation, 116
- Heat combustion chamber, protection, 123
- Heat exchanger propellant evaporation system, 165
- Heaters, 408
- Helium in A-3 stage engine, 73
- Helium in stored gas systems, 156-158
- Helium thrust chamber systems, 162
- H-F (horizontal-flow) nozzle, 92
- High-frequency instabilities, 145, 146
- High vacuum, characteristics of, 434
- Hilsch separation tube, 349
- H-Q curve, 189
- H-Q, efficiency, and required power curves of centrifugal pump, 196
- Human error, 49
- Hydraulic capacitor, feed system for, 149
- Hydraulic capacitor, schematic of isolation type, 149
- Hydraulic qualities of injector, 123
- Hydrazine, as a monopropellant, 133, 171
- Hydrazine-hydrate, 138, 141
- Hydrogen, 68, 107, 136, 167
 coolant properties, 107
 critical pressure considerations, 167
- Hydrogen (continued)
 drawbacks, 68
 gas tapoff systems, 136
- Hydrogen peroxide, 133, 138, 140. *See also* Catalysts
- Hypergolic fluid, 167
- Hypergolic ignition, 136, 138, 139, 140
- Hypergolic slug, 139
- Hypergolic vs. nonhypergolic, 432
- Hypergolics*, definition of, 19. *See also* Noeggerath and hypergolics, 138
- Iacobellis, S. F., 93
- ICBM, 26, 27, 33
- Igniters, 136, 137
- Ignition detection, 141
- Ignition devices, 136-143
 augmented spark, 140
 hypergolic, 138-140
 hypergolic slugs, 139
 igniters, 137
 indirect, 143
 optical, 142
 pressure-sensing, 143
 pyrotechnic, 137
 resistance wires, 143
 spark plugs, 139
 special designs, 140
 visual, 142
- Impeller, centrifugal pump, definition, 177
- Impeller rotor and stator, 236
- Impeller rotor, operation, 226
- Impellers for centrifugal turbopumps, 204-207, 230-231
- Impellers, specific speeds, 190-191
- Impulse, specific, 10
- Inducer, centrifugal pump, definition, 176
- Inducer, typical, 211
- Influence coefficients for engine, 397-398
- Inhibited red fuming nitric acid (IRFNA), 343, 344
- Injecting methods, throttleable, 128
- Injection pattern, 131
- Injection pressure drop, 128
- Injectors, 83, 113, 121-131, 123
 baffled-type, 122
 bipropellant, 126
 coaxial-type, 127
 concentric ring, 124
 configurations, 124-127
 doublet, 125, 127
 experimental evaluation, 131
 heat protection in combustion chamber, 123
 hydraulic qualities, 123
 impingement patterns, 125, 127
 integral face plate, 125
 manifold, 113
 objectives in design, 121-123
 parameters, 127-131
 premixing-type, 127, 128
 quintuplet-type, 125, 127
 ring-slot-type, 127
 self-impinging-type, 125, 127

- Injectors (continued)
 showerhead-type, 125, 127
 special requirements, 123
 splash plates, 127
 throttleable-type, 127
 thrust chamber, 83
 triplet-type, 125, 127
- Instability, 146, 147
- Instability of combustion. *See* Combustion instability
- Instrumentation of engine, additional elements, 48
- Insulation for cryogenic propellant tanks, 345-348
- Integral-type control, 264
- Interconnecting components and mounts, 353-381
 assemblies, 357
 brazed joints, 370-371
 cryogenic propellant bleed lines, 356
 ducts, 372-379
 flange joint, 360-370
 gimbal, 379-381
 hydraulic lines, 357
 pneumatic supply lines, 356
 propellant supply ducts, 353
 propellant-tank-pressurization lines, 355-356
 purge lines, 356-357
 seal drain lines, 356
 thrust, 357
 tubings and tube fittings, 358-360
 turbine-drive, high-pressure, hot-gas ducts, 357
 turbine-exhaust, hot gas ducts, 357
 turbopump and other, 357
- Interstage length, 425
- IRBM, 26, 27
- IRFNA (Inhibited red fuming nitric acid), 343, 344
- Isentropic flow process, relationship between any two points in, 5
- J-Box, 409
- J. Spacecraft and Rockets*, 433
- JTA liner, 438, 439, 448
- Jupiter rocket, 400
- Kaplan method of error triangles, 210
- Kinetic energy, conversion from thermal energy, 1
- L*. (characteristic length of combustion table), 87.
See also L-star
- L*, effect on c* value of thrust chamber, 87
- Laws, design and predict rocket behavior, 1-4
- Lee, J. C., 447
- LEM (lunar excursion module), 430
- Liquid bipropellant gas generator, 134-136
 operating characteristics, 136
 valve assembly, 134
- Liquid film cooling of thrust chamber, 115, 116
- Liquid flow regulators, 321-322
- Liquid hydrogen, selection of metals for use with, 60
- Liquid-hydrogen-fueled engines, operating regions of pumps, 226
- Liquid hydrogen tanks, 345-348
- Liquid monopropellant gas generators, 133
- Liquid propellant. definition, 18
- Liquid propellant rocket combustion chambers, gas flow through, 5, 9, 10
- Liquid Rocket Engine Design Check-Off Sheet, 52-54
- Lip seals, 291, 292
- Loads on rotor blades of turbine, 244
- Low-frequency instabilities, 146
- L-star (L*), 86, 87, 131, 134
- Magnesium alloys, 61
- Main propellant tank direct injection pressurization system, 172, 173
- Man Rating, definition, 44
- Manufacturing and material engine defects, control areas defined, 48
- Mark III turbopump gears and bearings, 184
- Mark V turbopump, 186
- Marman Division of Aeroquip Corp., 374
- Materials for engine part, selection of, 59, 60
- Messerschmitt Me-163, 141
- Messerschmitt rocket fighters, 140
- Metals, criteria for use with liquid hydrogen, 60
- Meteoric bombardment, 434
- Mission coast duration, effect, 432
- Mission failure, definition, 44
- Mission success, definition, 44
- Mixed-flow type impeller, specific speeds, 190, 210
- Mixture ratio of fuel, 34
- Moment of inertia, data sheet for typical, 39
- Momentum theorem, 1, 2
- Monergols. *See* Propellants, mono-
- Monopropellant gas generator schematic, 133, 181
- Monopropellants, 18, 19, 132, 133, 171
- Moody, L. F., diagram, 283, 284
- Multicellular design, 416
- Multiple-engine use, 428
- Multiple start, 442
- Multistage vehicle, growth factor equations, 40
- NASA, S-1 first stage booster for Saturn I, 416
- Needle-type valves, 301
- Newton's law of viscosity, 282
- Nickel-base alloys, 61, 76
- Noeggerath and hypergolics, 138
- Noncomplex redundancy, 46
- Noncryogenics, 167, 271
- Nonmetallic materials, uses, 62
- Nonpropellants, systems evaporating, 167
- North American Aviation, Rocketdyne Division, 136
- North American X-15, 429
- Nozzles, 2, 4, 6, 7, 8, 13, 14, 15, 89, 90, 92, 93, 94, 95, 97, 98, 239, 307
 aerodynamic spike, 93, 94
 annular, 92, 94, 95

- Nozzles (continued)
- area expansion ratio, effect on performance, 15
 - bell, 90, 91, 93, 98
 - conical, 89, 93
 - convergent section, 13, 14
 - De Laval type, 6, 7, 8, 89
 - divergent section, 14
 - E-D (expansion-deflection), 93
 - expansion area ratio, 89
 - gas flow through, 4, 6
 - incorrect length and jet separation, effect on thrust, 7
 - liquid flow through, 307
 - overexpanded, 6, 7
 - performance comparison, 94
 - pressure losses at inlet, 6
 - prime functions, 6
 - radial in-flow and out-flow, 92
 - reverse flow (R-F), 92
 - specific function in thrust chamber, 2
 - turbine, 239
- NPSH (net-positive suction head), 166, 176, 188, 192-194, 210, 346
- Nuclear radiation, 434
- Nusselt number, 100, 106
- Off-design characteristics of turbopump, 203
- Off-nominal conditions, engine performance variations, 396
- Offset turbopump, 182
- One-and-one-half stage vehicles, 416
- On-off type control, 264, 442
- Open-loop mixture-ratio control, procedures, 268-269
- Optical detection, 142
- Optoline, 140
- Order of failure, definition, 44, 45
- Orifices, liquid flow through, 307
- O-rings, 45, 83, 289-291, 292, 293, 300, 303
- correlations in design, 289, 290
 - flange joints, 366
 - friction, 290
 - poppet-type, 291
 - seal failure in, 45
 - selection, 290-291
 - squeeze-type, 291
 - surface finish, 290
 - valve seat, seals for, 291
- Over-stress and over-strain, definition, 47
- Oxidizer pump inducer, 215
- Packaging, 399-403
- Pancake turbopump, 182
- Parts list, rocket system, symbols, 28-29
- Payload, specific impulse effect on, 11
- Payload weight vs. growth factor, 40
- Peenemunde, 139, 140
- Perchlorate-type fuel, 138
- Perfect gas law, 4
- Performance, injector, 122
- Performance parameters for engine, 10, 15-18
- correction factors and magnitudes, 15, 16
 - measurement and dimensions, 10
 - sample calculation, 16, 17, 18
- Perturbations, feed system, 150
- PFRT. See Preliminary flight rating tests
- Pilot valves, control, design, 301-306
- Pneumatic pressure regulator, 317
- Pogo stick effect, 420
- Poiseuille's equation, 284
- Poisson's ratio, 108, 109, 110, 163, 209, 343, 375
- Poppet-type valves, 299
- Position indicators, 407
- Postwar engine, 36
- Potassium permanganate, 141. See also Catalysts
- Power sources, turbine, 181
- Prandtl-Meyer turning angle, 94
- Prandtl number, 100, 106, 118
- Preliminary flight rating tests, 32
- Pressurant requirements, 152-156
- Pressurant use factor, 153
- Pressure-compounded impulse turbine, 180
- Pressure drop, effective injector, 131
- Pressure environment as function of altitude, 2
- Pressure feedback (PQ) valves, 273
- Pressure, formula demonstrating effect on thrust of, 13
- Pressure gages, principal types of, 412-414
- Pressure losses at nozzle inlet, 6
- Pressure-sensing devices, 143
- Pressure switches and transducers, 411
- Pressurized-gas propellant-feed systems, 166-167, 170, 171, 173-174
- A-4 stage, 174
 - applications, 166-167
 - criteria for selecting, 173, 174
 - evaporating nonpropellants, 167
 - liquid propelled, 170, 171
 - using products of chemical reactions, 167
- Pressurizing gas turbulence, 152
- Programed mixture ratio control (PMR), 270
- Propellant combination, 129, 148
- Propellant evaporation systems, 165-167
- Propellant feed system, triggering prevention, 148
- Propellant feed system, centrifugal pumps, 176, 177
- Propellant feed system perturbations, 150
- Propellant flow design, pressure feed engine, 391
- Propellant fraction, definition of, 35
- Propellant management system, 270
- Propellant mass fraction of complete vehicle, definition of, 11
- Propellant storage, system design for, 440-442
- Propellant tanks, 329-352
- cryogenic, 345-348
 - design, basic, 329-331
 - design, general, 332-336
 - expulsion under zero gravity or oscillatory g loading, 349-352
 - fiber-glass filament-wound, 348-349
 - pressurant diffusers, 349
 - storable liquid, 343-345
 - structure, 336, 343

- Propellant utilization (PU), 268, 269, 270, 272, 311, 336, 393
- Propellant vaporization, 152
- Propellants, 18-20, 22-23, 188, 203, 431-432
- additives, 19, 20
 - bi-, 19, 26, 27
 - cooling and other characteristics, 432
 - cryogenic, 19, 24
 - density, 431
 - flow of, engine start, 203
 - fluid properties, 188
 - ignition characteristics, 431
 - mono-, 18, 25
 - operating temperature, 431
 - optimum mixture ratio for additives, 19, 20
 - performance and physical properties, 20
 - selection, 18-20
 - specific impulse in evaluation, 431
 - storable, 19, 22-23
- Propeller type impeller, specific speeds, 191
- Proportional-type control, 264, 443
- Propulsion system, definition, 28
- Pulses, 150
- Pump, cavitation, 192
- Pump developed head, 189
- Pump head coefficient, 189
- Pyrolytic graphite, 119
- Pyrometers, 142
- Pyrophoric fluid, 19
- Pyrotechnic igniters, 137, 138
- Qualification tests, 32
- Quality control, areas, 48
- Quintuplet injector, 125, 127
- Radial-flow impeller, minimum basic design elements, 208
- Radial in-flow nozzle, 92
- Radial out-flow nozzle, 92
- Radial-type impeller, specific speeds, 190
- Radiation cooling of thrust chamber, schematic, 120, 121
- Rannie equation, 118
- Rao, G. V. R., 91
- Rating stability, 150
- Rayleigh flow process, 6
- Reaction control system, 429-430
- Reaction Motors Division of the Thiokol Corp., 429
- Reaction turbine, 180
- Redstone rocket, 33, 34, 64, 141, 142, 400
- Redundancy, 46, 142, 444-446
- Refrasil-filled chambers, 119
- Regenerative cooling, 105-114
- Regulating devices, fixed-area, 307-309
- Regulators, gas pressure, 315-321
- Regulators, liquid flow, 321-322
- Relays and switches, 406-407
- Reliability, 42-49
- definition, 42
 - design reviews, 49
 - implements for obtaining highest, 43
 - pointers for obtaining, 42, 43
- Repetitive pulse control, 443
- Resins, pyrolysis, 118
- Resistance coefficients for fluid-flow control components, 286
- R-F (reverse-flow) nozzle, 92
- RF signals, 68, 138
- Ring slot injector, 127
- Rocket thrust, general, equation and model for, 2, 3
- Rocketdyne, 448, 449, 450
- Rocketdyne AR-1, 141
- Rocketdyne Atlas ICBM, 295
- Rocketdyne Division of North America, 37
- Rocketdyne LR79-NA-11 engine, 403
- Rocketdyne Naflex, 368-370
- Rotor blades of turbine, main loads, 244
- Rotor-stator assembly, centrifugal pumps, 176, 177
- RP fuel, 141
- RP-1 fuel, 64, 109
- Run duration, 32-34
- Safety features, disadvantages, 43
- Safety margins in design, 334-335, 428
- Sample calculations. See Calculations for 4 stages of Alpha vehicle, samples of
- Saturn I first stage (S-1) booster for, 416
- Saturn V, 329, 416, 425, 430
- Scheduling, availability of design in, 50
- Schmetterling AA rocket, 140
- Sealing, 361
- Secondary injection thrust vector control (SITVC), 279, 280
- Self-impinging injector, 125, 127
- Servovalve flapper, 319
- Servovalves, 309-315
- Shepard, Cdr., 141
- Showerhead injector, 125, 127
- Sieder-Tate equation, 106
- Simplicity of engine design, 32. See also von Kármán
- Single gas generator-helium system, 172
- Single gas generator system with injection cooling, 171
- Single-gear turbopump, 182
- Single-stage vehicle, growth factor equation, 40
- SITVC. See Secondary injection thrust vector control
- Skinner pilot valve, 302
- Solid propellant gas generators, 132, 133
- Solubility of pressurizing gas, 152
- Space engines, design, 429-450
- general applications, 430-434
 - main propulsion systems, 435-442
 - principal applications, 429-430
 - reaction control, 442-450
- Space system operational requirements, 433
- Spark plugs, 139, 140
- Special alloys, 61, 62

- Specific heat ratio, 9, 15
 effect on performance of, 15
 values for functions of, 9
- Specific impulse, 10, 11, 12
- Specifications improving engine design quality, 51
- SPGG. *See* Solid propellant gas generator
- Spike nozzle, 92
- Splash plates injector, 127
- Spool-type servovalves, 313, 314, 315
- Spring mass effect, 420
- Squeeze-type O-rings, 291
- Stage burnout velocity of single-stage vehicle, equations, 39, 40
- Stage separation, basic possibilities, 425-426
- Stainless steel in pressurant storage vessels, 162
- Stainless steel on ablative liner, 119
- Start (thrust buildup), characteristics, 33
- Stator, primary functions of, 177
- Stay time of burning gas in combustion chamber, 34
- Steels, stainless, 60, 61, 76, 119, 132, 162
- Stefan-Boltzmann radiation heat transfer constant, 121
- Stoichiometric mixture ratio, 34
- Storable liquid propellants, 19
- Stored gas systems, 156-165
 commonly used configurations, 156-157
 design of components, 162
 requirements of calculations, 157-162
- Strain gages, 415
- Stress analysis, 56-59
 experimental, 58, 59
 failure modes and criteria, 59
 selection of materials and dimensions, 58
 typical steps, 56
 working loads and environmental effects, 56, 57
- Structural integrity of injector, 123
- Suction specific speed, 192
- Sweeteners, 141
- Swing-gate-type check valve, 326
- Symbols for system parts, 28, 29
- System parts, symbols, 28, 29
- Systems using chemical reaction products, 167-171
- Tachometers, 411
- Taifun rocket, 140
- Tank wall temperature, 152
- Tanks, liquid hydrogen, 345-348
- Tanks, propellant. *See* Propellant tanks
- Tantulum, 62, 121
- Tapoff system, 136, 180
- Telemetry of engine, additional elements required, 48
- Temperature
 effect on low-alloy steels, 60
 chamber, calculation, 21
 gages, 411
 sensors, 412
 steels, low-alloy, effect, 60
- Thermal energy, conversion from chemical energy, 1
- Thermal energy, momentum caused by release of, 1
- Thermal environment, 434
- Thermocouples, errors in measuring by 412, 413
- Thiokol, 446
- Thoma parameters, 193, 194, 211
- Thor rocket, 64, 400
- Three-stage vehicle system, weight increase calculations, 41
- Throttleable injector, 127
- Thrust, 7, 12, 15, 31, 33, 34, 81-83, 181
 coefficient, 12
 decay, 34
 effect of incorrect nozzle length and jet separation, 7
 optimum, ambient pressure, 15
 total requirement, 31
- Thrust chamber
 assembly, 82
 basic cylindrical combustion in, 88
 basic elements, 81-83
 bleed, 181
 characteristic velocity, 83
 coaxial shell, 107, 109, 110
 coefficient, 84
 combustion data (theoretical), 84, 85
 configuration layout, 86
 cooling, 98-121
 deposits on walls, 101, 102, 103, 104
 designs, 13, 14
 film-cooled, 117
 gas tapoff systems, 136
 geometrical shapes, 88
 heat exchanger, 162
 ideal, data, 8
 injector, 82
 injector design, 121-131
 L*, effect on c* value, 87
 model of, 3
 nozzle expansion area ratio, 89
 nozzle, specific function of, 2
 nozzle shape, 89
 performance calculation, 84
 performance parameters, 83
 pressure, 144
 recommended combustion characteristic length (L*)
 for propellants, 87
 selecting cooling method, 99
 shape, 87, 131
 specific impulse, 11, 83
 thrust generated, 13, 14
 tubular wall, 107
- Thrust efficiency vs. bell nozzle length, 91
- Thrust vector control, 274-275
- Timers, 407-408
- Timoshenko, S., 209
- Titanium alloys, 121, 163
- Titanium-base alloys, 62, 121, 162
- Topping flow cycle, 200
- Topping systems, 181
- Transpiration cooling of thrust chamber, 117-118
- Triethyl aluminum and oxygen, 139
- Triggering processes, prevention of, 148-149
- Triplet injector, 125, 127
- Tubing, 358-360
- Tungsten, 119, 121

- Turbine gas flow rate, 186
- Turbines, 178-181
- Turbopump systems, 175, 181-189, 191-199, 200-261
 - axial-flow, design, 225-238
 - balancing axial thrust, 223-225
 - booster engine, 182, 183
 - calibration and off-design characteristics, 202, 203
 - cavitating inducers, 210-219
 - cavitation, 192
 - centrifugal, 204-225
 - cycle efficiency, 199, 200, 201
 - description of developed, 182-186
 - design layout, 261
 - design parameters, 187-202
 - drive arrangements, 181-182
 - elements, 176
 - envelope, 175
 - gear design, 260
 - heads and flow rates developed, 189
 - inlet suction pressure head, 186
 - operating ranges, 202
 - overall performance and operating efficiency, 196, 197
 - pump flow coefficient, 189
 - range of operation, 175
 - resistance and pump characteristic curves, 189
 - specific speeds, 190
 - trimming effects, 202
 - turbines, 238-257
 - variation of efficiency with speed, 195
 - variation of engine weight and flow ratios with chamber pressure change, 175
- Ullage gas compression, 152
- Valvair four-way solenoid pilot valve, 394
- Valves, 294-306
- Vapor condensation, 152
- Vascojet, 246
- VDI orifices, 307, 308
- Vehicle, definition, 21
- Vehicle, design, cost, 50
- Vehicle diameter, 425
- Vehicle performance, deviations, 35
- Vehicle range, effect, 35
- Vehicle reliability and flight safety, 44
- Vehicle system, three-stage, weight increase calculations, 41
- Velocity, characteristic, 12
- Velocity-compounded impulse turbine, 180
- Venting, 166
- Venturi-type valves, 299-300
- Vernier cutoff system, 34
- Von Braun, Wernher, 63, 415
- Von Kármán, 32
- V-2 rocket, 400
- Wasserfall anti-aircraft rocket, 140
- Weatherhead Co., 358
- Weight of payload, effect, 35-37
- Wet gimbaled weight of engine, 37
- Wet weight of engine, 37
- Wiring, connective, 409
- Working loads, 56-58
- World War II guided missiles, 140, 141
- Zucrow and Sellers equation, 115